

PREFACE

Nowadays, the investigation of any important scientific topic needs a broad interdisciplinary approach, which creates a cross-fertilization of different skills and competence. The conception of the book “Advanced Inorganic Fluorides: Synthesis, Characterization and Applications” was formulated in such a scope by bringing together specialists in inorganic chemistry, solid state chemistry, catalysis, material sciences and solid state physics.

A preceding book that appeared on this subject was “Inorganic Solid Fluorides”, edited by P. Hagenmuller in 1985. At that time the authors concluded that they expected fluorinated materials to become important targets for advanced applications. Fourteen years later their predictions proved to be correct. One should point out, for instance, the decisive importance of solid fluorides for the substitution of environmental pollutants such as CFCs by a new generation of HFCs, and their use as catalysts in numerous inorganic reactions. Furthermore, the use of fluorinated carbon materials for energy storage and the use of crystallized or glassy fluorides for optoelectronics is also important.

Therefore a wide range of scientists should be interested in this book, including those colleagues involved in inorganic and solid state chemistry, catalysis and organic reactions, physicists looking for new materials that exhibit outstanding properties or for materials that can be used as models, and generally speaking those who are concerned about important problems of the coming century, such as energy storage, the environment and industrial developments.

The editors would like to thank all the contributors for the marvellous work they did and for their brilliant co-operation on this project.

Tsuyoshi Nakajima
Alain Tressaud
Boris Žemva

List of Contributors

Dr Jean-Luc Adam

Laboratoire des Verre et Céramiques, Université de Rennes 1, Avenue du Général Leclerc, 35042, Rennes Cedex, France

Prof. Neil Bartlett

Department of Chemistry, University of California, Berkeley, CA 94720-1460, USA

Dr Horst Borrmann

Max-Planck-Institut für Chemische Physik fester Stoffe, Pirnaer Landstr. 176, D-01257 Dresden, Germany

Dr Christophe Cardinaud

Laboratoire des Plasmas et des Couches Minces, Institut des Matériaux de Nantes (IMN-CNRS), 2 rue de la Houssinière, BP 32229, 44322, Nantes Cedex 03, France

Dr Howard C.S. Clark

Department of Chemistry, University of Leicester, Leicester, LE1 7RH, UK

Dr Jacques Darriet

Institut de Chimie de la Matière Condensée de Bordeaux (ICMCB-CNRS), Université Bordeaux I, Avenue du Dr A Schweitzer, 33608, Pessac Cedex, France

Prof. Thomas A. O'Donnell

Department of Chemical Engineering, University of Melbourne, Parkville, Victoria, 3052, Australia

Prof. Gérard Férey

Institut de Réactivité, Electrochimie et Microporosité (UMR CNRS 173), Institut Lavoisier, Université de Versailles Saint-Quentin-en-Yvelines, 49 Avenue des Etats-Unis, 78035, Versailles Cedex, France

Dr Claude Fouassier

Institut de Chimie de la Matière Condensée de Bordeaux (ICMCB-CNRS), Université Bordeaux I, Avenue du Dr A. Schweitzer, 33608, Pessac Cedex, France

Dr Hiroyuki Fujimoto
Research & Development Department, Osaka Gas Co. Ltd., Torishima 6-19-9,
Konohana-ku, Osaka, 554-0051, Japan

Prof. Roland Georges
Institut de Chimie de la Matière Condensée de Bordeaux (ICMCB-CNRS),
Université Bordeaux I, Avenue du Dr A. Schweitzer, 33608, Pessac Cedex, France

Dr Michael Gerken
Department of Chemistry, McMaster University, Hamilton, Ontario L8S 4M1,
Canada

Prof. John H. Holloway
Department of Chemistry, University of Leicester, Leicester, LE1 7RH, UK

Dr Eric G. Hope
Department of Chemistry, University of Leicester, Leicester, LE1 7RH, UK

Dr Fuyuhiko Ishii
Fluorine Chemistry Laboratory, New Products Development Division, Kanto
Denka Kogyo Co. Ltd, 1497, Shibukawa, Gunma, 377-8513, Japan

Prof. Kiyoshi Kanamura
Department of Applied Chemistry, Graduate School of Engineering, Tokyo Metro-
politan University, 1-1 Minami-ohsawa, Hachioji, Tokyo, 192-0397, Japan

Prof. Erhard Kemnitz
Institut für Chemie, Humboldt-Universität zu Berlin, Hessische Str. 12, 0115, Berlin,
Germany

Dr Yasushi Kita
Fine Chemicals Department, Central Glass Co. Ltd, 7-1 Kanda-Nishikicho
3-chome, Chiyoda-ku, Tokyo, 101-0054, Japan

Prof. Marc Leblanc
Laboratoire des Fluorures, UPRES-A 6010, Université du Maine, 72085 Le Mans
Cedex, France

Dr Antoine Le Lirzin
Institut de Chimie de la Matière Condensée de Bordeaux (ICMCB-CNRS),
Université Bordeaux I, Avenue du Dr A Schweitzer, 33608, Pessac Cedex, France

Dr Thierry Loiseau

Institut de Réactivité, Electrochimie et Microporosité (UMR CNRS 173), Institut Lavoisier, Université de Versailles Saint-Quentin-en-Yvelines, 49 Avenue des Etats-Unis, 78035, Versailles Cedex, France

Dr Karel Lutar

Jožef Stefan Institute, Jamova 39, SI-1000 Ljubljana, Slovenia

Dr Toshiyuki Maeda

Research & Development Department, Osaka Gas Co. Ltd., Hirano-cho 4-1-2, Chuo-ku, Osaka, 541-0046, Japan

Dr Hélène P.A. Mercier

Department of Chemistry, McMaster University, Hamilton, Ontario L8S 4M1, Canada

Dr Dayal T. Meshri

Advance Research Chemicals Inc., 1110 W. Keystone Ave., Catoosa, OK 74015-3033, USA

Prof. Tsuyoshi Nakajima

Department of Polymer Chemistry, Graduate School of Engineering, Kyoto University, Sakyo-ku, Kyoto, 606-8501, Japan

Prof. Fujio Okino

Department of Chemistry, Faculty of Textile Science and Technology, Shinshu University, Ueda, 386-8567, Japan

Dr Didier Riou

Institut de Réactivité, Electrochimie et Microporosité (UMR CNRS 173), Institut Lavoisier, Université de Versailles Saint-Quentin-en-Yvelines, 49 Avenue des Etats-Unis, 78035, Versailles Cedex, France

Prof. Gary J. Schrobilgen

Department of Chemistry, McMaster University, Hamilton, Ontario L8S 4M1, Canada

Dr Alison M. Stuart

Department of Chemistry, University of Leicester, Leicester, LE1 7RH, UK

Prof. Masayuki Takashima

Department of Materials Science and Engineering, Faculty of Engineering, Fukui University, 3-9-1 Bunkyo, Fukui, 910-8507, Japan

Prof. Hidekazu Touhara
Department of Chemistry, Faculty of Textile Science and Technology, Shinshu
University, Ueda, 386-8567, Japan

Dr Alain Tressaud
Institut de Chimie de la Matière Condensée de Bordeaux (ICMCB-CNRS),
Université Bordeaux I, Avenue du Dr A. Schweitzer, 33608, Pessac Cedex, France

Prof. John M. Winfield
Department of Chemistry, University of Glasgow, Glasgow, G12 8QQ, UK

Prof. Boris Žemva
Jožef Stefan Institute, Jamova 39, SI-1000, Ljubljana, Slovenia

CHAPTER 1

Introductory Remarks

Neil Bartlett

*Department of Chemistry and the Chemical Sciences Division, Lawrence Berkeley National Laboratory,
University of California, Berkeley, CA 94720, USA*

This book reflects the achievements and challenges for the field of Fluorine Chemistry at the turn of the millennium. Many of the most active participants in that chemistry have contributed chapters on their particular specialties. These remarks can only give the slightest sketch of the overall situation. For an authoritative and accurate assessment of each aspect of the field, the reader must turn to the appropriate chapter

The small size and high electronegativity of the F-ligand, combined with the low bond energy in F_2 and the strong bonds that the ligand makes with most other atoms, are the fundamental characteristics that lie at the basis of the ready combustion of most of the elements in fluorine, often resulting in their oxidation to the highest known state of oxidation. Fluoride synthesis in the past, at least in its inorganic aspects, was often simply a matter of heating materials in F_2 (sometimes under pressure). Today's picture is changed dramatically.

Perhaps the ready availability of translucent fluorocarbon plastics such as FEP, which has remarkable kinetic stability to F_2 , has been the major technical factor in providing for low temperature synthesis of fluorides, especially in the highest attainable oxidation-states. The use of anhydrous liquid hydrogen fluoride, aHF, in such apparatus has provided not only an excellent ionizing solvent with a long liquid range, but also one that is remarkably robust oxidatively and reductively. In addition, the transparency of the FEP plastics to visible and near-UV light, has provided for the effective photo-dissociation of F_2 . A flux of F atoms generated in this way, in aHF made basic with good fluoride-ion donors (such as alkali fluorides), has provided high oxidation-state species, such as AgF_4^- and NiF_6^{2-} , at room temperature. From such salts as these, at temperatures below 20°C, AgF_3 , NiF_4 , NiF_3 , and other fluorides, thermodynamically unstable (but kinetically stable) with respect to loss of F_2 , have been prepared, and characterized. These have been used as potent fluorinating and oxidizing agents, e.g. cationic Ag(III) or Ni(IV) in aHF, at ~20°C, efficiently generate MF_6 ($M = Pt, Ru, Rh$) from MF_6^- .

Low-valent transition-element fluorides, especially those in which carbonyl and organo-ligands are incorporated, require other approaches, which are tailored to the element and the oxidation state. Here an inherent thermodynamic problem is imposed by the high C—F bond energy, which can exceed the M—F bond energy,

never-the-less an increased range of such materials is in prospect. Perfluorinated organic solvents evidently have a valuable role to play in this organo-metallic fluorine chemistry, where their redox and substitutional inertness are especially important.

The solvent aHF (because it is not easily reduced) is also likely to have an important role in the future in low oxidation-state chemistry. This solvent is a super-acid and in keeping with that character, low oxidation-state transition-metal cations, including carbonyl cations of such metals, can be prepared. Indeed, since the electronegativity of a given oxidation state must be higher in a cation than in the neutral or anionic relatives, it follows that low oxidation states are more likely to be achieved if oxidations (fluorinations) are carried out in solutions made acidic with strong fluoride-ion acceptors such as SbF_5 . Conversely, when the ionizing solvent (e.g. aHF) favors anion formation (as when alkali fluoride is present in aHF) high oxidation states result. So we see that oxidation of Pd metal with F_2 in acidified aHF gives a cationic Pd(II) solution from which PdF_2 may be precipitated, whereas Pd metal with F_2 in aHF containing alkali fluoride yields PdF_6^{2-} from which PdF_4 can be displaced with AsF_5 . The synthetic approaches discussed so far, however, are not efficiently applicable to oxyfluorides.

Efficient synthesis of an oxyfluoride often proceeds from an oxide with substitution of two F-ligands for one O-ligand. This requires a reagent which makes very strong bonds to oxygen. Especially useful are SF_4 , PF_5 , and XeF_6 . Since the last is not a reducing agent and can also be used as a solvent it is valuable in the generation of high oxidation-state oxyfluorides as exemplified by a variety of new technetium and rhenium oxyfluoro species. Good synthetic routes to main-group oxyfluorides, particularly those with OSO_2F , and OTeF_5 groups are presently of special interest as ligands of anions that have only very weak interaction with any cation (so-called *naked cation*). A variety of main-group and transition-element derivatives of the OTeF_5 group, are described here.

The strong bonding of the fluorine ligand to most other atoms has given rise to a major interest in fluoro-coatings for surfaces and this has in turn fostered much work on the effective use of plasmas in which SF_6 or CF_4 other kinetically inert (and hence rather safe reagents) are used as the source of F atoms. Such fluorocoatings can profoundly affect not only the susceptibility of the material to chemical attack but also the physical behavior, such as wettability and lubricity.

The need to replace chlorofluorocarbons and molecules related to them, because of the damage they do to the earth's protective ozone shield, has presented organo-fluorine chemists with the challenges of finding replacements for these widely used and economically important molecules. An aspect of the fluorination chemistry involved in the synthesis of substitutes, commonly involving the conversion of C1 and C2 compounds is the best choice of heterogeneous catalyst. Commonly such catalysts are fluorinated chromia or alumina. Their possible mechanistic roles have been investigated and point to ways in which fluorination specificity and efficiency might be improved.

As a consequence of the monovalence of fluorine, fluorides at the high oxidation-state limit are often at, or near, the coordination limit for that element,

with the result that such binary fluorides are easily volatile. This provides convenient gaseous sources for many metals (TiF_4 , WF_6 , MoF_6 , PtF_6 , are examples) some of which have already found applications in the semi-conductor industry. In lower oxidation states the commonly found six coordination is usually maintained, with an appropriate number of F-ligands symmetrically linking two metal centers. These μ -fluoro bridges usually have M—F interatomic distances that are ~ 0.2 Å longer than the non-bridging, but these are nevertheless strong enough to give many polymeric fluorides high thermal stability. Fluoride glasses and many other solid-state fluoro-materials derive their utility from such favorable bridge-bonding.

Fluoride glasses owe many of their optical properties to the high electronegativity of the F-ligand. An instance is the positioning of ligand-to-metal charge-transfer bands well into the UV. They have many potential applications, e.g. as lasers, optical fibers, waveguides, and optical amplifiers.

The luminescent properties of crystalline fluorides have also proved to be valuable, especially for certain lasers and scintillators.

The building of μ -fluoro bridged networks about removable template molecules has been known now for a number of years, most simply in the tungsten-bronze form trifluorides of the first transition series. This has motivated a synthetic program to combine this experience with the well known ability of oxides (particularly silicates) to form open frameworks, with resultant microporosity. Because silicates can generate SiF_4 in a fluorine rich environment, attention is particularly given to AlPO_4 and GaPO_4 based solids.

In addition to strong bonding, the M—F—M bridges also provide for moderately strong *antiferromagnetic* coupling of the magnetic centers at each M, unless the M—F—M angle is close to 90° . The antiferromagnetic coupling is *frustrated* when three M are linked in a ring. When the magnetic centers are inequivalent the antiferromagnetic coupling results in field dependence (*ferrimagnetism*). There is therefore a rich variety of magnetic behavior in transition-metal fluorides that is nicely illustrated by the *usovite* and *jarlite* relatives described here.

The electronegative character of fluorine invites its application, as an agent of energy storage, in combination with the electropositive element lithium. So far, the most useful approximations to this system have been via the lithium/graphite fluoride combination. Indeed, this has long been the basis of an important primary battery. It is evident that the lamella character of the graphite fluorides (whether they are flat carbon sheets, sp^2 , or puckered, sp^3) is probably crucial for the required facile migration of F from the graphite fluoride electrode to the electrolyte. Reconstitution of the graphite π system as F is removed could also be beneficial to the discharge process (and probably essential for a reversible electrode). There is an urgent need, for a secondary battery based on such lightweight high energy-density materials. This requires reversible lithium and fluorine source electrodes and a compatible electrolyte. Chapters in this volume address these difficult problems, and potential raw material sources for the graphite fluorides.

That the F-ligand can attach to the C atoms of graphite without affecting the sp^2 orbital hybridization has long been known, and it is now clear from the study of the fluorination products of the *fullerenes*, that attachment of F-ligand to the

C atoms of these molecules does not have profound influence on the C orbital hybridization either. The impact of fluorination on the physical and chemical properties of these new forms of carbon can now be seen.

Much of the work done in Fluorine Chemistry is financed or motivated from the economic benefits of industrial applications, many of which are outlined in the final two chapters of this volume. But, as we all know, the economic importance of what we fluorine chemists do cannot be easily foretold. What is important, is that the discoveries that are made should be related as firmly as possible to fundamental chemical and physical concepts. We see much of that kind of correlation in this book.

CHAPTER 2

Recent Developments in the Synthesis of Inorganic Fluorides

Karel Lutar,¹ Horst Borrmann² and Marc Leblanc³

¹*Jožef Stefan Institute, Jamova 39, SI-1000 Ljubljana, Slovenia;* ²*Max Planck Institut für Chemische Physik fester Stoff, Pirnaer Landstr. 176, D-01257 Dresden, Germany;* ³*Laboratoire des Fluorures, UPRES-A 6010, Université du Maine, 72085 Le Mans Cedex, France*

2.1 Introduction

The primary intention of this contribution is to show which synthetic methods have been most frequently used past 1985 in different fields of the broad area of preparative inorganic fluorine chemistry, emphasizing those routes which have had and still may have an impact on future progress. Attention is focused on developments that have led to actual or potential routes to new fluoride materials. It is the authors' wish that selected examples will help the reader in making his own choice of the most suitable synthetic approach to his desired compounds. It is, however, the authors' full responsibility if some interesting routes have been omitted, either due to lack of the available space or because the authors were not aware of them. Certain areas were intentionally omitted to stay within the limited space given, e.g. the broad field of compounds containing the SF₅ moiety or CF₃ compounds which are actually bridging from inorganic to organometallic and even organic fluorine chemistry. Main features of both topics have recently been reviewed [1,2].

The reader is referred to the second chapter "Preparative Methods" by J. Grannec and L. Lozano in "Inorganic Solid Fluorides", edited by P. Hagenmuller [3], for information on chemical syntheses and crystal growth techniques anterior to 1985, and for general instructions in major preparative techniques in the field of inorganic fluorine chemistry. Some excellent reviews of different topics in the field have been published past 1985 [4–9]. The wide synthetic possibilities of super-acidic media are described in T.A. O'Donnell's book [10]. Synthetic and characterization methods with emphasis on solid compounds have been summarized in a book edited by A.K. Cheetham and P. Day [11].

CAUTION: Work with elemental fluorine and highly reactive fluorides is demanding and potentially dangerous. Many of the syntheses discussed in this chapter require appropriate, mostly specific techniques and experienced personnel. Only original references should be consulted for any experimental work. It is strongly recommended not to start any of this chemistry on its own, but to join an experienced fluorine group for the first steps in this field.

2.2 Solid state reactions

The classical ceramic route is still widely used in the synthesis of complex fluorides and fluoride salts. A first step involves grinding and intimate mixing of the constituents, e.g. binary fluorides. After eventual cold pressing the mixture is heated for a prolonged length of time in order to promote interdiffusion between the individual grains and consequent reaction. A few recent examples are listed hereafter:

- fluorides Li_3AlF_6 [12], Li_4ZrF_8 [13], $\alpha\text{-MZr}_3\text{F}_{15}$ ($M = \text{Y, In, Ln, Tl}$) [14], NaMgF_3 [15], $\alpha\text{-BaTbF}_6$ [16]
- oxide fluorides $\text{Te}_2\text{O}_3\text{F}_2$ [17], $\text{Nd}_2\text{Eu}_2\text{O}_3\text{F}_6$ [18]
- fluoride salts $\text{Ln}_3(\text{BO}_3)_2\text{F}_3$ ($\text{Ln} = \text{Sm, Eu, Gd}$) [19], $\text{NaCa}_2(\text{SiO}_4)\text{F}$ [20].

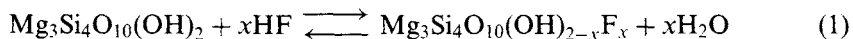
In some cases, but usually after prolonged heating close to the fusion temperature, small crystals suitable for X-ray structure determination may be selected from the products, e.g. $\text{Ba}_2\text{Mg}_3\text{F}_{10}$ [21], $\text{SmTh}_2\text{F}_{11}$ [22], $\text{Ba}_4\text{Cu}_2\text{Al}_3\text{F}_{21}$ [23]. Some emphasis within the field has clearly been on compounds with potential ion conductivity [24–26].

2.2.1 Influence of pressure

Pressure may be used in two quite different ways to influence solid state reactions or chemical reactions in general. One way is to apply mechanical pressure directly, either uniaxial or hydrostatically. To some extent, but with different intention, this is already done when a reaction mixture is pressed into pellets. A second way of using pressure as parameter in a reaction is the application of a gaseous reactant under increased pressure. Examples will be given in subsequent sections of this chapter.

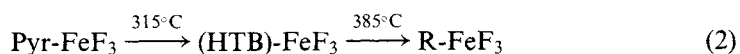
Only few direct pressure syntheses have been reported. LiTiMF_6 phases ($M = \text{Mn–Ni}$) were prepared from respective binary fluorides at $T = 700\text{–}1200^\circ\text{C}$ and 15–70 kbar [27]. The products crystallized in Na_2SiF_6 and PbSb_2O_6 type structures. On the other hand, pressure induced phase transitions are common, e.g. KMnF_3 transforms from cubic to tetragonal symmetry. However, in contrast to oxide containing perovskites, the transition temperature rises with increasing pressure [28].

An interesting application of pressure has been described in connection with fluoride substitution in the mineral talc. Fluorophlogopite $\text{KMg}_3\text{Si}_3\text{AlO}_{10}\text{F}_2$ (KFP) [29] and fluoride-substituted talc $\text{Mg}_3\text{Si}_4\text{O}_{10}(\text{OH})_{2-x}\text{F}_x$ [30] were recently studied for their potential coating properties of fibers used as reinforcement of ceramics. The synthesis is achieved in a sol–gel process, and after calcination the precursors are converted to KFP or $\text{Mg}_3\text{Si}_4\text{O}_{10}(\text{OH})_{2-x}\text{F}_x$, respectively, on heating under confined conditions. It was shown that the fluoride substitution rate in $\text{Mg}_3\text{Si}_4\text{O}_{10}(\text{OH})_{2-x}\text{F}_x$ depends on applied pressure: the limiting value was found at 71% substitution, with $T = 753^\circ\text{C}$ and $p = 1680$ bar. The substitution equilibrium may be simplified to:



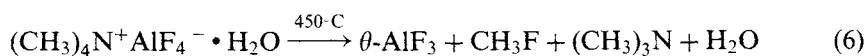
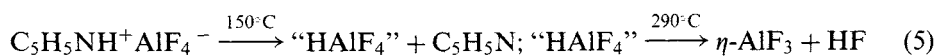
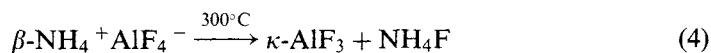
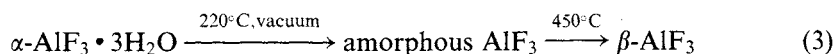
2.2.2 Influence of temperature

Polymorphism including also the formation of metastable and amorphous phases is widely observed. The properties of respective phases are strongly dependent on the particular structure and on temperature. Careful investigations of phase transitions may lead to a better understanding of the conditions necessary for the synthesis of new phases. A well-known example comes from the pyrochlore form of FeF_3 , which was first prepared in the pioneering days of what is nowadays called 'chimie douce'.



Upon heating, the metastable pyrochlore form (Pyr) is first converted to the hexagonal bronze-type modification (HTB), which is also metastable. Finally, transformation to the stable ReO_3 type structure (R) is observed [31]. The derived density of FeF_3 increases from 2.73 g/cm^3 , to 3.16 g/cm^3 and to 3.61 g/cm^3 with these transitions. Phase transitions have also been studied for the related AlF_3 [32], for the perovskites KMnF_3 (doped with Li^+ or Na^+) [33] and RbCaF_3 [34], as well as for rare earth trifluorides like SmF_3 [35].

In general, metastable phases are much more likely to form at rather low temperatures. Accordingly, the decomposition of hydrates [36–38], ammonium [39], organic cation [39], or hydrazinium [40–42] fluorides under mild conditions is much more suitable than sintering of binary fluorides. The large surface area of metastable phases renders them ideal candidates as catalysts. In connection with the problems associated with chlorofluorocarbons (CFCs) in the atmosphere, AlF_3 has been very thoroughly investigated (see 2.7.2. and Chapter 12).



Finally all these forms of AlF_3 directly and irreversibly transform to the stable $\alpha\text{-AlF}_3$ phase. Some parameters of the various phases are compared in Table 1.

Table 1

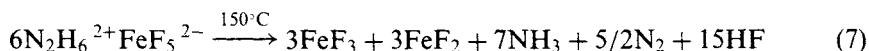
Selected properties of various forms of AlF_3

	T_{trans} ($^{\circ}\text{C}$)	VFU ^a (\AA^3)	Surface area (m^2/g)	Structure type	Ref.
$\eta\text{-AlF}_3$	450	55.7	58	Pyr ^b	[43]
$\beta\text{-AlF}_3$	660	49.8	30	HTB ^c	[37]
$\theta\text{-AlF}_3$	610	46.5	64		[44]
$\kappa\text{-AlF}_3$	640	46.1	19	TTB ^d	[39]
$\alpha\text{-AlF}_3$		43.6		ReO_3	

^a VFU = volume per formula unit; ^b Pyr = pyrochlore;^c HTB = hexagonal tungsten bronze; ^d TTB = tetragonal tungsten bronze.

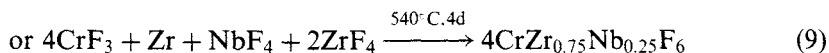
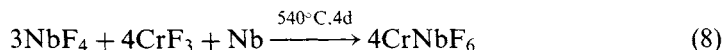
2.2.3 Influence of reducing or oxidising conditions

During the decomposition of precursors as mentioned above, additional reactions may occur. With hydrazinium compounds reduction may well take place [40]:



FeF_3 is thermally unstable and therefore products from reactions with FeF_3 at higher temperatures frequently contain some Fe^{2+} . In the same way thermal decomposition of CuF_2 leads to contamination with copper particles, due to the instability of CuF . However, Cu^+ may be trapped in appropriate host lattices. The doping of KMgF_3 is achieved via heating to 1050°C in the presence of CuF_2 [45]. Photoluminescence of Cu^+ is well documented when it is doped into NaF and KMgF_3 crystals.

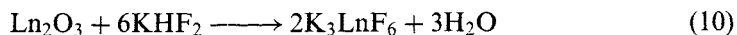
Contamination of reaction products with finely divided metal is a severe problem in reactions where metals are used to reduce higher oxidation state fluorides. For example, when CrF_2 is prepared from CrF_3 and Cr metal, the product often contains some Cr^{3+} . To avoid this problem reduction of Cr^{3+} to Cr^{2+} is better done in situ with further reaction [46,47]:



Reduction processes are frequently involved in doping of materials prepared for specific applications. $\text{Ba}_{1-\delta}\text{Sr}_{\delta}\text{MgF}_4$ ($\delta < 0.55$) was doped with Sm^{2+} by addition of Sm metal to the charge for crystal growth [48]. Eu^{2+} is the key ion in fluorescent lamp phosphors for emission of blue light. Respective reduction of Eu^{3+} is frequently achieved in H_2 atmosphere, but in alkaline earth fluoride phosphates, Sn^{2+} may act as reducing agent [49].

2.2.4 Influence of particle size

To enhance reactivity in ceramic reactions, intimate mixtures of small particles are preferred. Vigorous grinding, however, does not only reduce the particle size. Using high energy mills, considerable local pressures and temperatures may be achieved. So-called mechanochemical reactions are very rare with fluorides:



The latter reaction [50] proceeds at ambient temperatures for Ln = Lu, Yb, for Ln = Ho, Er, Tm at 200°C, and for Ln = Tb, Dy at the fusion temperature of KHF₂ (226°C). For the last two temperatures the mechanical influence is clearly diminished.

Finally, the influence of active surface area on fluorination is extremely well demonstrated by the various forms of Al₂O₃. The commercially available, activated Al₂O₃ reacts very vigorously with elemental fluorine and is a convenient active agent in absorption towers for fluorine and reactive fluorides. In contrast, tubes and crucibles made from sintered Al₂O₃ withstand fluorine up to several hundred degrees Celsius. Finally synthetic sapphire, which is actually crystalline Al₂O₃, is possibly the most inert material for use in fluorine chemistry.

2.3 Flow and pressure reactions

Considering the most basic approaches to the synthesis of fluorides, first of all direct fluorination, i.e. reaction of an element or of a suitable compound with elemental fluorine, diluted or undiluted, or with gaseous HF, or with another appropriate and available fluorinating agent will be considered. For an example like KAgF₄ there are several possibilities, e.g. [51]:

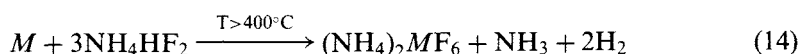
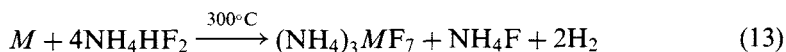


A major decision that must be made is whether to carry out the experiment in an open or, better, a flow system, or alternatively in a closed or pressure system. Both reactions are equally well suited to be carried out in a flow system, as solid and non-volatile starting compounds react with the fluorine gas to form the desired non-volatile product together with volatile by-products. The latter are swept away by excess fluorine. In case of a closed system example (Eqn. (11)) turns out less favorable, as ClF will react with F₂ to form ClF₃, which in turn may also compete for the potassium component to form KClF₄. Under these conditions therefore a pure product is not expected. No such complications are to be expected with the second reaction (Eqn. (12)), which results in a very clean product. This very simple example is intended to demonstrate that, although for many experiments a flow system or a closed reaction vessel are mutually exchangeable, characteristic

features of the two methods need to be carefully considered. In an open system volatile by-products are carried away with the excess of the fluorinating agent or by an inert gas which serves to dilute the agent. Obviously it is impossible to complete such a reaction with stoichiometric quantities of starting materials. In a closed system stoichiometric amounts of the reactants may be introduced, but, as volatile by-products are not removed, the reaction will be complete only in cases where the equilibrium is very much in favour of the products. Nevertheless, monitoring the pressure change offers an excellent way to follow the progress of the reaction. It also becomes evident, that equilibrium mixtures and by-products are easily analysed after removal from a closed vessel. Hence, for many reactions a closed vessel offers a clear advantage over a corresponding flow system. This tendency is reflected in recent years where closed systems have grown much more popular than the much older flow method. However, the latter still has distinct advantages in certain situations. Most important is the fact, that a flow system copes better with the considerable heat evolved in most fluorinations, which may result in sintering or even melting of the starting material, thus drastically reducing the active surface area. This frequently leads to incomplete reaction due to coverage with unreactive fluorides. On a larger scale, the evolved heat may even lead to the melting of the reaction vessel, making the closed system extremely dangerous. Therefore reactions designed to prepare several grams or more products should be carried out in flow systems. The proper scale-up of a closed system reaction may turn out to be very difficult. On a rather large scale as compared with laboratory measures, flow methods have been adapted for the fluorination of U_3O_8 with O_2F_2 at ambient temperatures [52], the synthesis of graphite fluoride, $(\text{CF})_n$, on the 100 g scale with diluted fluorine in a rotating reaction vessel [53], or the synthesis of $\text{S}_2\text{O}_6\text{F}_2$ yielding 100 g/h from a catalytic reaction [54]. Another important question to be considered is material of the reaction vessel or reaction tube. Nickel and Monel are able to resist almost any fluorinating agent, even at higher temperatures. At lower temperatures copper and stainless steel are also suitable, however, certain reagents, for example HF in combination with Lewis acids, results in serious corrosion problems with almost any metal. Under such conditions, aluminium seems to be quite resistant [55], but its mechanical properties hamper its wider use, especially under pressure. Synthetic sapphire is an excellent material for fluorine service, even under most severe conditions. Unfortunately, it is not possible to build pressure vessels entirely from sapphire, but tubes are commercially available. For flow reactions under the most severe conditions, there is certainly no better material, as sapphire is transparent in contrast to a metal.

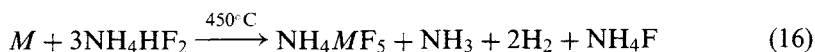
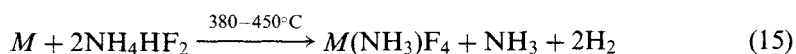
HF as a fluorinating agent for metals, halides, oxides, etc. has almost exclusively been used in flow systems at elevated temperatures. A major disadvantage of this technique is the corrosion of the reaction tube due to rather high temperatures used. Surprisingly, similar reactions in liquid HF seem to be very rare, although recent experiments demonstrate the method to be very useful at ambient temperature in Teflon FEP vessels [56]. As $\text{N}_2\text{H}_6\text{F}_2$, NH_4F , and especially NH_4HF_2 decompose at elevated temperatures with the formation of HF, they may be considered as stabilized HF, and are much more easily handled than HF itself. With the use

of these two versatile reagents a large variety of compounds were prepared. Hydrazinium- or ammonium-compounds are isolated which are subsequently decomposed at higher temperatures or used as reagents with other compounds. Depending on the actual reaction conditions, a variety of products may be obtained. Reactions aiming to produce SiNF as an analog of SiO₂ [57], and the respective reactions for Ge and Sn, were intensively studied, both in closed and open systems. From reactions with NH₄HF₂ under static conditions, two phases were isolated: (*M* = Si, Ge, Sn) [58–60]

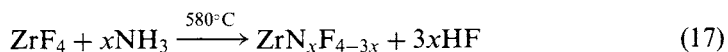


Subsequent treatment of (NH₄)₂MF₆ in a carefully dried stream of NH₃ affords stepwise release of NH₄F. Three intermediate phases were isolated so far, but in none of the cases was the respective nitride fluoride formed (Table 2).

Even more interesting than SiNF should be ZrNF as a close relative of the important ceramic material ZrO₂. In a closed reaction vessel two different products were isolated for *M* = Zr, Hf [61,62]:



Ammonolysis of ZrF₄ in a flow system revealed extreme sensitivity of the product even to traces of water, and to date no ZrNF has been isolated as a pure phase. Formulations given for the products range from Zr₉N₈F₁₂ to Zr₉N₇O₂F₁₁ [63]:



The large diversity available for zirconium compounds becomes evident when hydrazinium compounds are included, examples being (N₂H₅)₂ZrF₆ [64], N₂H₆ZrF₆

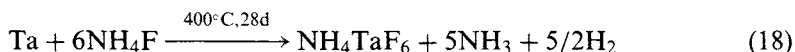
Table 2

Stepwise decomposition of (NH₄)₂MF₆ type compounds; crosses mark phases characterized

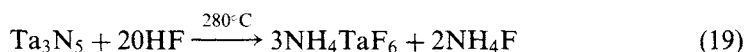
	(NH ₄) ₂ MF ₆ →	(NH ₄)M(NH ₃)F ₅ →	M(NH ₃) ₂ F ₄ →	M(NH ₂) ₂ F ₂ → MNF
Si	x	x	x	
Ge	x		x	
Sn	x	x	x	x

[65], and $(\text{N}_2\text{H}_6)_3\text{Zr}_2\text{F}_{13} \cdot \text{F}$ [66]. They are easily accessible from aqueous solution and usually decompose in a stepwise fashion.

With respect to ceramic materials, Ta seems of equal interest to Zr, but to date only reactions under static conditions have been studied. The fluorination of Ta metal with NH_4F requires rather severe conditions [67]:



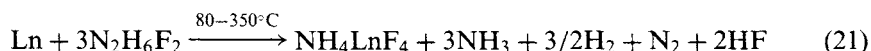
However, the product contains also $(\text{NH}_4)_4[\text{Ni}(\text{TaF}_6)_6]$, arising from attack of the Monel vessel by HF in combination with the Lewis acid TaF_5 . NH_4TaF_6 may be prepared under less severe conditions [68]:



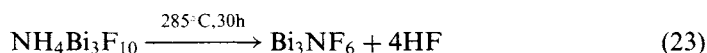
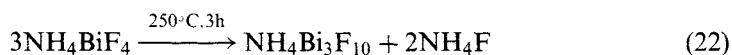
Even in the absence of Lewis acids, Ni is attacked by NH_4HF_2 [69]:



This problem also needs consideration with respect to the synthesis of ammonium fluoro metallates of the lanthanides, although some may be prepared at quite low temperatures [70], $\text{Ln} = \text{La} - \text{Dy}$:



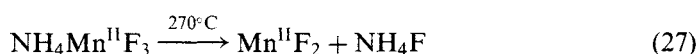
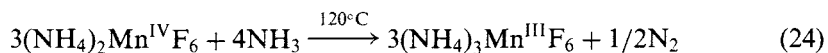
While reaction with the vessel is more severe in closed systems under pressure, avoidance of even traces of water is more difficult to achieve in flow systems. Only when NH_3 is rigorously dried with sodium metal, is Bi_3NF_6 obtained free of oxygen from a stepwise decomposition reaction in an NH_3 atmosphere [71]:



In the second reaction step BiF_3 is observed as an intermediate, however, direct ammonolysis of BiF_3 did not provide a pure product.

During the thermal decomposition of hydrazinium compounds reduction frequently occurs at the metal center. Although at higher temperatures NH_3 decomposes forming H_2 and N_2 , even at quite moderate temperatures an interesting

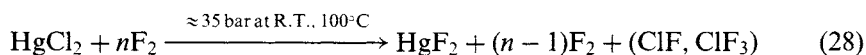
sequence of reduction steps has been observed [72]:



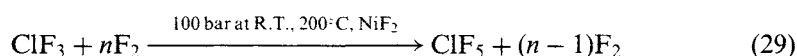
It should be mentioned, that in an N_2 atmosphere only $\text{NH}_4\text{Mn}^{\text{III}}\text{F}_4$ was observed as intermediate phase.

As may be seen from the previous examples, a combination of a flow system with a static pressure reaction frequently turns out to be the most effective. Accordingly, vigorous first reaction steps may be carried out under flow conditions, before the products are transferred to a pressure vessel, in order to bring the reaction to completion under more rigorous conditions. As examples, a new series of rare earth fluoroaurates may be mentioned, ranging from $\text{La}(\text{AuF}_4)_3$ [73], $\text{Ln}_2\text{F}(\text{AuF}_4)_5$ ($\text{Ln} = \text{La} - \text{Er}$) [74,75], to $\text{LnF}(\text{AuF}_4)_2$ ($\text{Ln} = \text{Tm} - \text{Lu}$) [76]. In all cases single crystals suitable for X-ray diffraction were obtained after pressure treatment. The same approach proved successful for PbF_4 [77] and for Cs_2CuF_6 [78], respectively.

In many fluorinations chlorides were used as convenient starting materials. For obvious reasons, reactions in closed vessels are offering great advantages if more than one volatile starting compound is to be used, but also in cases where desired products are volatile. An illustrative example is the fluorination of HgCl_2 resulting in the mild fluorinating agent HgF_2 and a mixture of ClF and ClF_3 as by-products [79]:

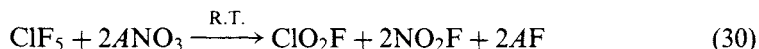


As ClF and ClF_3 are easily separated from excess F_2 , but also from one another via fractionating condensation, HgCl_2 will be transformed quantitatively into useful products. Under somewhat more severe reaction conditions and in the presence of NiF_2 as a catalyst, ClF_3 may be fluorinated further to form ClF_5 in almost 100% yield [80]:

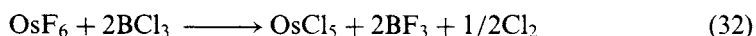


More unusual reactions are those aimed at substituting fluorine by oxygen or even

chlorine. Of course, for thermodynamic reasons such reactions are only possible if a more stable fluoride is formed as by-product. The most obvious case is the formation of HF during hydrolysis. For controlled replacement of two fluorine ligands by one double bonded oxygen atom, nitrates and sulfates of alkali metals (*A*) are very useful [81]. Nitrates convert ClF₅ directly into ClO₂F, because ClOF₃ as product of a first replacement step is more reactive towards nitrate than ClF₅ itself [82]:

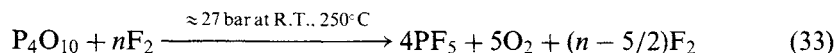


While this method has been used for a variety of compounds, replacement of F by N is very rare, although unusual compounds like the nitrenes OsF₅(NCl) [83] or ReF₅(NF) [84] have been isolated from such reactions. Even less favorable is fluorine replacement by Cl. Therefore this type of reaction is limited to very special but interesting cases [85,86]:



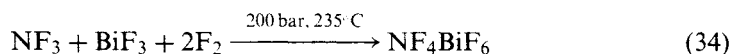
The driving force in both reactions is clearly the formation of CaF₂ and BF₃, respectively.

Nevertheless, reactions in ‘opposite’ direction like the replacement of O by F will remain much more common. Fluorination of P₄O₁₀ provides an instructive example [87]:



Special care needs to be taken at the beginning of this very exothermic reaction. Slightly higher temperatures are needed at the end of the reaction to ensure complete replacement of all oxygen atoms. This turns out to be a very general problem with fluorination of oxides. It is frequently quite tedious to remove the very last traces of oxygen. The method to prepare the weak Lewis acid PF₅ is also well suited for the strong Lewis acid AsF₅ using As₂O₃ as starting compound. The reaction is again very vigorous but still much less than the direct fluorination of elemental As. In this case it is more of a problem to convert all AsF₃ to AsF₅ than to remove last traces of oxygen. For larger amounts of these compounds a combination of flow and pressure method has to be preferred [88].

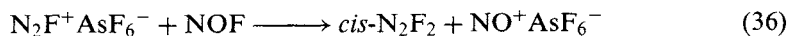
A further advantage of reactions in a closed vessel is offered with the possibility to prepare reactants in situ, i.e. in a first reaction step, one compound is formed which is finally used in a subsequent reaction without intervening isolation. An excellent example in this respect is the preparation of NF₄BiF₆ using commercially available BiF₃ instead of the extremely moisture sensitive BiF₅ as starting compound [89]:



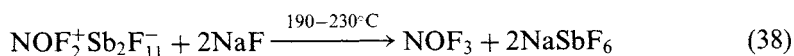
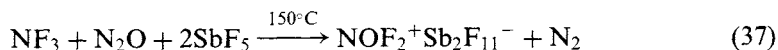
In reactions producing a gaseous product, the autoclave may conveniently be used for storage. For example, N_2F_2 exists in two isomers, *cis*- and *trans*-form. The *trans*-isomer is obtained from almost any synthetic reaction of N_2F_2 , but as the more stable isomer it is also less reactive, in particular, with strong Lewis acids it does not form N_2F^+ salts like the *cis*-form. As N_2F^+ salts happen to be useful oxidizers, a convenient source for *cis*- N_2F_2 was highly desirable. At elevated temperatures the *trans*-form may be converted to its *cis* relative, however, much of the material is lost due to decomposition. When N_2F_2 is gently heated in the presence of AsF_5 , any *cis*-isomer formed is immediately trapped as $N_2F^+AsF_6^-$, this way the *trans*-form is also converted [90]:



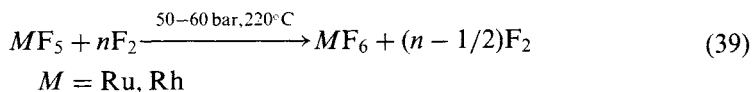
From the stable salt pure *cis*- N_2F_2 may be obtained via replacement by the stronger base NOF:



In a very similar approach NOF_3 may be prepared [91]:



In general, high reactivity of compounds is associated with high sensitivity. Thermally unstable fluorides may still be prepared under fluorine pressure, if their formation takes place already at moderate temperatures. Hexafluorides of the platinum metals are very strong oxidizers and volatile, but also thermally quite unstable, in particular those that are most reactive. Nevertheless, RuF_6 and RhF_6 were obtained via pressure fluorination of their respective pentafluorides [92]:



As the pentafluorides are easily prepared by fluorination of the metals, this method is ideally run as a two step process in the same autoclave. Utmost care needs to be taken to reduce the oxygen content of the system as much as possible. The metals should be reduced with hydrogen and subsequently be handled only in an inert atmosphere; the autoclave needs to be pretreated very carefully [93]. Any remaining trace of oxygen will contaminate the pentafluoride with oxidefluorides, mostly MOF_4 .

The fluorine dissociation pressure over thermally unstable fluorides increases exponentially with temperature. Accordingly, even in a rather narrow temperature

range, quite high pressures are necessary. The technique to reach 3 kbar pressure at 450°C was developed and its applicability reviewed recently [94]. It has proved useful to grow single crystals of labile compounds like many dioxygenyl salts, e.g. $\text{O}_2\text{Mn}_2\text{F}_9$. However, as also discussed in the review mentioned above, for the majority of unstable compounds, low-temperature methods such as photochemical or KrF_2 fluorination in solution are more suitable. These are described below.

2.4 Reactions in solution

It is probable that the majority of interesting new compounds reported during the last decade have been prepared in solution. One fascinating approach is the precipitation of binary fluorides in anhydrous HF (aHF) from anionic precursors by addition of a strong Lewis acid [95]. Using this method, very reactive and even thermodynamically unstable compounds can be isolated. A broad field of anion syntheses was opened up with a new but rather simple route to prepare highly pure $(\text{CH}_3)_4\text{NF}$, which is rather soluble in CH_3CN . Many strong oxidizers can be handled in such solutions [96]. Reactions in aqueous solution continue to be important, but emphasis is put now on optimizing conditions to achieve particular properties of the products. In this connection hydrothermal conditions are widely used.

2.4.1 Chemistry in aqueous media

Various fluorides may be precipitated from aqueous solution for use as constituent powders in solid state reactions. Co-precipitation offers very elegant access to intimate mixtures, but the actual products are strongly dependent on the fluoride ion activity within the solution but also on the stability constants of the respective metal complexes. Accordingly, not only anhydrous fluorides are obtained, but also hydrated fluorides or hydroxide fluorides, which may be very difficult to convert to pure fluorides. As noted already [3], reactive compounds, e.g. carbonates, acetates, oxalates, hydroxides etc., which quite easily dissolve in acidic HF solutions, are the preferred starting materials for fluoride syntheses. In contrast, many oxides which have been heated to rather high temperature are frequently unreactive and may not dissolve at all. To enhance reactivity but also improve crystallinity of the product, it has proved useful to perform reactions above the boiling point of water in adapting the hydrothermal method, which has already been shown to be useful in the recrystallisation of materials which are more or less insoluble at ambient temperatures and pressures. Up to about 240°C even PTFE vessels may be used. A number of selected examples with respective reaction conditions are listed in Table 3.

The synthesis of the compound $\text{Ba}_5\text{Nb}_3\text{O}_3\text{F}_{18}(\text{HF}_2)$ [101] is remarkable since the HF_2^- entity from the solution is maintained. One major advantage of the hydrothermal procedure is the range of usable reaction conditions. Gels, well known in zeolite synthesis, have been used successfully in the preparation of KAiPO_4F [104], while the addition of amines to the reaction mixture has provided access to microporous materials. Mesoporous and microporous materials as active materials

are discussed extensively in Chapter 7. In some cases organic templates like urea may decompose under the reaction conditions as exemplified by the preparation of $(\text{NH}_4)_2\text{TiOF}_4$ crystals [102]. Related compounds may also be prepared from solutions of ammonium or alkali fluorides. Representative examples are NaEuF_4 and NaHoF_4 prepared with uniform grain size ($0.5\ \mu\text{m}$) [98] (see Table 3).

Working at even higher temperatures does not provide any substantive new problems, but PTFE must be replaced by suitable container materials. Critical conditions for water ($T_c = 374^\circ\text{C}$, $p_c = 221\ \text{bar}$, $V_c = 55.3\ \text{cm}^3\text{mol}^{-1}$ or $\tau_c = 0.322$ = filling rate) are easily reached, and so for purposes of clarity, reactions in sub-critical or super-critical conditions are presented separately in Table 3. At sufficiently high temperatures anhydrous phases may be crystallized from aqueous solution. For example, in 1975 anhydrous FeF_3 crystals were grown from concentrated HF solution [121] at 380°C . Soon after, advantages of the method were realized and the method was used to obtain low temperature phases or mixed valence compounds and to prevent decomposition of ammonium salts etc.

In order to avoid corrosion of the autoclave, starting materials are sealed in ampoules made from gold or platinum tubing. Pressure build-up within the ampoule is compensated for by pressurizing the autoclave. Any remaining water within the autoclave will eventually react with the steel wall producing some hydrogen. Above 250°C H_2 starts to diffuse through the platinum, which may result in some reduction within the reaction mixture. Accordingly, reduction of Fe^{3+} to Fe^{2+} in critical water was observed and numerous mixed valence iron fluorides were prepared [108]. In contrast reduction of Cr^{3+} or V^{3+} was not observed.

In recent years interest has become focused on fluoride-containing salts rather than pure fluorides. For example:

- fluoride phosphates due to their open structures and their potential activity in catalysis;
- fluoride borates due to their optical behaviour (laser hosts, frequency doubling, extended UV transmission range) and fluoride carbonates. Trigonal ions like CO_3^{2-} or BO_3^{3-} showing large anisotropy in their electronic polarisability, favour non-linear optical properties;
- fluoride silicates because of their thermal stability.

Conditions for synthesis and crystallization of several compounds of these types are summarized in Table 3. An interesting modification of the hydrothermal method involves heating by microwaves, but to date, it has been used only in a few cases employing aqueous solutions or with other polar solvents. Its main advantage is that fast heating rates with thermally insulating vessels are possible. Oxides were obtained from quite short heating times [122], but fluoride carbonates are also accessible. For example, bastnaesite, LaCO_3F , was prepared from LaF_3 and K_2CO_3 in aqueous solution in a PTFE vessel within 2 h at 190°C under 12 bar pressure [123].

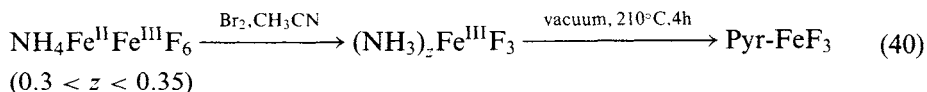
Quite fascinating was the observation some years ago, that some structures could be modified via cation exchange under mild conditions. While the method is now well

Table 3

Hydrothermal synthesis of selected fluorides and fluoride salts

	Material	Solvent	T(°C)	P(bar)	t(h)	Starting compounds	Ref.
Sub critical							
Fluorides	BaBeF ₄	0.5M NH ₄ HF ₂	140		96	Ba(OH) ₂ -BeF ₂	[97]
	NaHoF ₄	3M NH ₄ HF ₂	240		168	NaF-Ho ₂ O ₃	[98]
	α -Ba ₂ ZrF ₈	5M HF	200		72	BaF ₂ -ZrF ₄	[99]
	(H ₃ N(CH ₂) ₃ NH ₃)U ₂ F ₁₀ ·2H ₂ O	28M HF+15M H ₃ PO ₄	180		24	UO ₂ -amine	[100]
Mixed anions	Ba ₅ Nb ₃ O ₃ F ₁₈ (HF ₂)	5M HF	200		48	BaF ₂ -NbO ₂ F	[101]
	(NH ₄) ₂ TiOF ₄	28M HF	170		24	TiO ₂ -urea	[102]
	Ba ₇ Ga ₆ (F,OH) ₃₂ ·2H ₂ O	5M HF	200		48	BaF ₂ -Ga ₂ O ₃	[103]
	KAlPO ₄ F	0.2M KF	200		240	KOH-H ₃ PO ₄ -Al ₂ O ₃	[104]
	NH ₄ FePO ₄ F	5M HF	200		48	NH ₄ F-H ₃ PO ₄ -Fe ₂ O ₃ -HTMA	[105]
Supercritical							
Fluorides	K Y _{0.95} Er _{0.05} F ₄	3M KF	400	1500	400	Y ₂ O ₃ -Er ₂ O ₃	[106]
	NH ₄ CoAlF ₆	28M HF	400	3000	48	NH ₄ F-CoF ₂ -AlF ₃	[107]
	Fe ₃ F ₈ (H ₂ O) ₂	28M HF	450	2300	300	FeF ₃ -H ₂	[108]
	Sr ₂ Fe ₂ F ₁₀ ·H ₂ O	11M HF	700	1800	48	SrF ₂ -Fe ₂ O ₃	[109]
	Na ₂ Sr ₇ Al ₆ F ₃₄	28M HF	685	2000	24	NaF-SrF ₂ -AlF ₃	[103]
Mixed anions	NaVO ₂ F ₂	11M HF	550	1950	48	NaF-V ₂ O ₅ -BaF ₂	[110]
	Y(OH) _{3-x} F _x	(0.1-7)M KF	400	250	72	Y ₂ O ₃	[111]
	Co ₂ (PO ₄)F	15M H ₃ PO ₄	700	2000	30	CoF ₂	[112]
	K ₂ Cu ₃ Zn(PO ₄) ₃ F	LiF-KHF ₂	450	1000	24	ZnO-CuO-NH ₄ H ₂ PO ₄	[113]
	Sr ₂ Ga(HPO ₄)(PO ₄)F ₂	7M H ₃ PO ₄	700	1800	24	SrF ₂ -GaO(OH)	[114]
	Cs ₈ Fe ^{III} ₈ Fe ^{II} ₇ (PO ₄) ₁₂ F ₁₀	(NH ₄) ₂ HPO ₄	400	1000	24	CsF-Fe ₂ O ₃	[115]
	BaCu(CO ₃)F ₂	2.5M NaF	740	2000	20	BaCO ₃ -CuF ₂	[116]
	Na ₃ La ₂ (CO ₃) ₄ F	5M NaF	740	2000	20	Na ₂ CO ₃ -LaF ₃	[117]
	K ₄ Ln ₂ (CO ₃) ₃ F ₄	H ₂ O	740	2200	24	K ₂ CO ₃ -LnF ₃	[118]
	NaCa ₂ Lu(Si ₂ O ₇)F ₂	NaF+εH ₂ O	900-690	1700	33	Ca ₅ (PO ₄) ₃ OH-Lu ₂ O ₃ -CaF ₂ -SiO ₂	[119]
	Na ₂ MgGd ₂ (Si ₄ O ₁₂)F ₂	H ₂ O	700	1900	36	GdF ₃ -Na ₂ CO ₃ -Mg ₂ Si ₃ O ₈ ·5H ₂ O	[120]

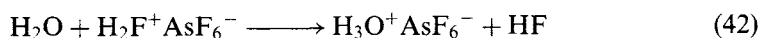
established as 'chimie douce', the first example was the synthesis of the pyrochlore (Pyr) FeF_3 [124]:



Though the composition changes dramatically, the structure of the starting compound is maintained throughout the elimination process.

Even more surprising was the observation that lithium ions may be inserted into the stable rhombohedral form of FeF_3 by electrochemical means [125]. In such reactions the final product is $\text{Li}_x\text{Fe}^{\text{III}}\text{F}_3$ with $x \leq 0.5$. Lithium insertion into $\text{Nb}_3\text{O}_7\text{F}$ [126] as well as NbO_2F [127,128] was also studied. On an even broader basis, exchange reactions were recently discovered in a new class of oxonium compounds of the lanthanide series [129]. In the phases $\delta\text{-(H}_3\text{O)Ln}_3\text{F}_{10} \cdot 2\text{H}_2\text{O}$, H_3O^+ may be replaced completely by Li^+ and Na^+ ions, but only partially by Cu^{2+} or Mn^{2+} . The new class of complex rare earth fluorides is characterized by open structures and has been prepared from the respective oxalates or via precipitation with HF solution from the solutions of binary oxides in concentrated nitric acid [130]. Phases $\delta\text{-KLn}_3\text{F}_{10} \cdot \text{H}_2\text{O}$ and $\delta\text{-RbLn}_3\text{F}_{10} \cdot \text{H}_2\text{O}$ are obtained only from direct synthesis but not via cation exchange. A similar co-precipitation technique has recently been applied to $\text{Na(Y}_{1-x-y}\text{Yb}_x\text{Pr}_y)\text{F}_4$ ($0 \leq x \leq 1$; $y \leq 0.05$) solid solutions [131].

Oxonium compounds are well known, especially in the field of super acids where traces of water are immediately converted to compounds like H_3OAsF_6 [132]. The formation of such salts is most easily understood as H_2O replacing the weaker base HF from H_2F^+ cations present in solutions of strong Lewis acids in anhydrous hydrogen fluoride (aHF).



Quite recently oxonium compounds of d-block transition metals and also closely related complexes of the lanthanides were isolated for the first time. In general, the solvent is aHF, and a strong Lewis acid, preferably AsF_5 , is added to the solution or suspension of an appropriate metal compound. Water may be introduced in various ways, e.g. using hydrated starting material, dissolution of metal oxides or even through the addition of H_3OAsF_6 . Some examples of reactions leading to new oxonium fluorometallates are collected in Table 4.

2.4.2 Chemistry in anhydrous hydrogen fluoride

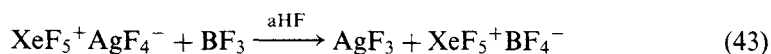
Anhydrous hydrogen fluoride (aHF) is a medium to good solvent for many fluorides in particular for those with polymeric structures. The solubility of ternary fluorides, especially those of transition metals, depends strongly on the counterion, for

Table 4

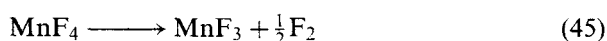
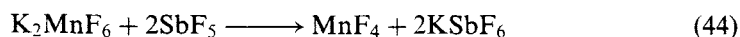
Synthesis of oxonium metallates in aHF at ambient temperatures

Reaction	Ref.
$3\text{H}_2\text{O} + 2\text{WF}_6 \longrightarrow \text{H}_3\text{OW}_2\text{O}_2\text{F}_9 + 3 \text{HF}$	[133]
$\text{H}_2\text{O} + \text{MF}_2 + 3\text{AsF}_5 \longrightarrow \text{H}_3\text{OM}(\text{AsF}_6)_3$ M = Mn, Co, Ni	[134]
$\text{H}_3\text{OAsF}_6 + \text{M}(\text{AsF}_6)_2 \longrightarrow \text{H}_3\text{OM}(\text{AsF}_6)_3$ M = Mn, Co, Ni	[134]
$\text{La}_2\text{O}_3 + 5 \text{H}_3\text{OAsF}_6 + 8\text{AsF}_5 \longrightarrow (\text{H}_3\text{O})_8\text{La}_2\text{F}(\text{AsF}_6)_{13}$	[135]

example XeF_5^+ salts are much more soluble than the respective alkaline metal salts, even at -60°C . Nevertheless, the alkali compounds have been used more frequently due to their easier availability and handling. Upon these observations a very versatile method for preparing binary fluorides has been developed, e.g. [95]:



Besides AgF_3 [136], also NiF_3 , NiF_4 [137], as well as a variety of other compounds have been prepared, thus proving the general applicability of this elegant method. Depending on the Lewis basicity of the starting compound, different Lewis acids, e.g. BF_3 , AsF_5 , SbF_5 , BiF_5 , or sometimes even the rather weak acid PF_5 , may be used. As the starting materials as well as the by-product are soluble in aHF, very pure products are usually obtained. The main strength of the method, however, comes from the fact that in majority of cases the highest oxidation state of a particular element is more easily achieved within an anion. Precipitation of the binary fluoride normally takes place without change in the oxidation state, thus providing access to high-oxidation state compounds which otherwise cannot be synthesized. Provided the respective ternary fluorides are available, binary fluorides with medium or even low oxidation states of the metal centre may be prepared, unless they themselves are solvolyzed by aHF. Using KBr and KI as reducing agents in aHF has afforded a whole series of ternary potassium salts in excellent purity and yield [138]. One drawback of the precipitation method discussed above, however, is the fact that the precipitated samples are frequently not well crystallized and may even be amorphous. In many cases this problem may be overcome by working at optimized reaction conditions. A definite highlight closely related to the approach described, was the first purely chemical synthesis of elemental fluorine [139]:



Both K_2MnF_6 and SbF_5 may be prepared without the use of elemental fluorine. The very broad potential of aHF as a reaction medium is apparent from the observation that even $Ag^I Ag^{III} F_4$ [140] may be isolated under carefully controlled conditions, although this formal isomer is much less stable than the well-known AgF_2 . The method also enables the preparation of Au^{II} -compounds [141]. The compounds just mentioned are selected representatives of a large variety of mostly ternary salts (Table 5).

In the presence of alkali fluoride even gold and platinum dissolve in aHF at ambient temperature when treated with elemental fluorine [143] (Table 6). While this provides easy access to anionic species of transition metals, replacing alkali fluorides by strong Lewis acids affords a route to the preparation of cationic species of almost any metal. Furthermore, reactions applying the strongest oxidizers KrF_2 , O_2F [150], AgF_3 , or NiF_3/NiF_4 are conveniently run in aHF at temperatures as low as $-70^\circ C$ (Table 7). By these reactions broad variety of compounds in the highest oxidation states of the particular element could be synthesized. The addition of a Lewis acid or Lewis base allows an increase or reduction, respectively, of the oxidizing potential with respect to neutral solutions, a nice example being Ag^{II} [151] (Table 8). The broad applicability of the method is demonstrated in the very effective fluorination of organic compounds using NiF_3 or NiF_4 in aHF under very mild conditions [152].

The combination of strong Lewis acids with aHF or other appropriate solvents, called 'super acids', provides access to various interesting cationic species like tetrahalocations of the pnictogens and related compounds (Table 9). Very remarkable in this connection is the isolation of $Xe_2^+ Sb_4 F_{21}^-$ which is possible only in the presence of HF besides SbF_5 [173]. Many cations mentioned are derived from molecules which have not been isolated so far, e.g. NF_5 , $NOCl_3$, PI_5 . All anions

Table 5

Reactions in aHF in presence of Lewis acids at ambient temperatures

Reaction	Ref.
$Au + 2SbF_5 + F_2 \longrightarrow Au(SbF_6)_2$	[141]
$Pd + 2AsF_5 + F_2 \longrightarrow Pd(AsF_6)_2$	[142]
$Pd + 2SbF_5 + F_2 \longrightarrow Pd(SbF_6)_2$	[143]
$In + BF_3 + HF \longrightarrow InBF_4 + 1/2H_2$	[144]
$NiF_2 + 2BiF_5 \longrightarrow Ni(BiF_6)_2$	[145]
$PdF_2 + 2AsF_5 \longrightarrow Pd(AsF_6)_2$	[142]
$LaF_3 + 3AsF_5 \longrightarrow La(AsF_6)_3$	[146]
$LnF_3 + 2AsF_5 \longrightarrow LnF(AsF_6)_2$	[146]
$Ln = Ce - Er$	
$2LnF_3 + 3AsF_5 \longrightarrow Ln_2F_3(AsF_6)_3$	[146]
$Ln = Tm - Lu$	
$AgF + 2WOF_4 \longrightarrow AgW_2O_2F_9$	[147]
$AgF_2 + 2WOF_4 \xrightarrow{F_2} AgFW_2O_2F_9$	[147]
$NF_4HF_2 + CrF_5 \longrightarrow NF_4CrF_6 + HF$	[148]

Table 6

Reactions in aHF in presence of Lewis bases at ambient temperatures

Reaction	Ref.
$\text{Au} + A\text{F} + 3/2\text{F}_2 \longrightarrow A\text{AuF}_4$ $A = \text{Li, K}$	[143]
$\text{M} + 2\text{LiF} + 2\text{F}_2 \longrightarrow \text{Li}_2\text{MF}_6$ $\text{M} = \text{Ru, Pd, Pt}$	[143]
$\text{M} + 2\text{KF} + 2\text{F}_2 \longrightarrow \text{K}_2\text{MF}_6$ $\text{M} = \text{Pd, Pt}$	[143]
$\text{Os} + \text{LiF} + 5/2\text{F}_2 \longrightarrow \text{LiOsF}_6$	[143]
$\text{M} + \text{KF} + 5/2\text{F}_2 \longrightarrow \text{KMF}_6$ $\text{M} = \text{Ru, Ir}$	[143]
$\text{M} + 2\text{NH}_4\text{F} + 2\text{F}_2 \longrightarrow (\text{NH}_4)_2\text{MF}_6$ $\text{M} = \text{Pd, Pt}$	[149]
$\text{M} + \text{NH}_4\text{F} + 5/2\text{F}_2 \longrightarrow \text{NH}_4\text{MF}_6$ $\text{M} = \text{Ru, Os, Ir}$	[149]

Table 7

Reactions with XeF_2 , XeF_6 , and KrF_2 in aHF at ambient temperatures unless stated otherwise

Reaction	Ref.
$2\text{CrO}_2\text{F}_2 + 2\text{KrF}_2 \longrightarrow 2\text{CrOF}_4 + 2\text{Kr} + \text{O}_2$	[153]
$\text{OsO}_4 + 2\text{KrF}_2 \longrightarrow \text{OsO}_2\text{F}_4 + 2\text{Kr} + \text{O}_2$	[154–156]
$\text{Tc}_2\text{O}_7 + \text{XeF}_6 \longrightarrow 2\text{TcO}_2\text{F}_3 + \text{Xe} + 3/2\text{O}_2$	[157]
$\text{TcO}_2\text{F}_3 + \text{KrF}_2 \longrightarrow \text{TcOF}_5 + \text{Kr} + 1/2\text{O}_2$	[158]
$\text{AgF}_2 + \text{KF} + 1/2\text{KrF}_2 \longrightarrow \text{KAgF}_4 + 1/2\text{Kr}$	[159]
$\text{AgF}_2 + \text{XeF}_6 + 1/2\text{KrF}_2 \longrightarrow \text{XeF}_5^+\text{AgF}_4^- + 1/2\text{Kr}$	[160,161]
$\text{XeF}_5^+\text{AuF}_4^- + \text{KrF}_2 \xrightarrow{\leq 0^\circ\text{C}} \text{XeF}_5^+\text{AuF}_6^- + \text{Kr}$	[161]
$\text{NiF}_2 + 4\text{XeF}_6 + \text{KrF}_2 \longrightarrow (\text{Xe}_2\text{F}_{11}^+)_2\text{NiF}_6^{2-} + \text{Kr}$	[162]
$\text{MnF}_4 + 2\text{KrF}_2 \xrightarrow{-45^\circ\text{C}} 2\text{KrF}_2 \cdot \text{MnF}_4$	[163]
$2\text{KrF}_2 \cdot \text{MnF}_4 \xrightarrow{-25^\circ\text{C}} \text{KrF}_2 \cdot \text{MnF}_4 + \text{Kr} + \text{F}_2$	[163]
$\text{MnF}_4 + \text{XeF}_2 \longrightarrow \text{XeF}_2 \cdot \text{MnF}_4$	[164]
$\text{AgAsF}_6 + 2\text{XeF}_2 \longrightarrow [\text{Ag}(\text{XeF}_2)_2]\text{AsF}_6$	[165]
$\text{HCNH}^+\text{AsF}_6^- + \text{KrF}_2 \xrightarrow{-60^\circ\text{C}} \text{HCNKrF}^+\text{AsF}_6^- + \text{HF}$	[166]
$\text{HCN} + \text{XeF}^+\text{AsF}_6^- \xrightarrow{-20^\circ\text{C}} \text{HCNXeF}^+\text{AsF}_6^-$	[167]
$\text{TeF}_5\text{NH}_2 + \text{XeF}^+\text{AsF}_6^- \xrightarrow{-33^\circ\text{C}} [\text{TeF}_5\text{N}(\text{H})\text{Xe}]^+\text{AsF}_6^- + \text{HF}$	[168]

derived from super acids are weakly coordinating and thus leave their counteranions coordinatively unsaturated, a topic which has been reviewed from a general standpoint [174]. Under 'super acidic' conditions many new carbonyl complexes have been isolated mainly of the platinum groups [175,176], Ag and Au [175–178], but also including Mn and Re [179]. Although it has been well established that the coordinating properties of PF_3 are very similar to CO [180], the number of PF_3 complexes

Table 8

Redox reactions of Ag^{II} species in aHF at ambient temperatures unless stated otherwise

Reaction	Ref.
AgF ₂ + AsF ₅ \longrightarrow AgFAsF ₆	[169]
AgF ₂ + BF ₃ \longrightarrow AgFBF ₄	[170]
4AgFAsF ₆ + 2Xe + AsF ₅ \longrightarrow Xe ₂ F ₃ AsF ₆ + 4AgAsF ₆	[171]
4AgFAsF ₆ + 2Xe \longrightarrow [Ag(XeF ₂) ₂]AsF ₆ + 3AgAsF ₆	[165]
2AgFBF ₄ + Xe \longrightarrow XeF ₂ + 2AgBF ₄	[171]
AgFAsF ₆ + O ₂ + AsF ₅ $\xrightleftharpoons[-60^{\circ}\text{C}]{-78^{\circ}\text{C}}$ O ₂ ⁺ AsF ₆ ⁻ + AgAsF ₆	[172]
AgOsF ₆ + F ₂ \longrightarrow AgF ₂ + OsF ₆	[172]
2LiIrF ₆ + Ag(SbF ₆) ₂ \longrightarrow IrF ₆ + AgIrF ₆ + 2LiSbF ₆	[172]

Table 9

Selected examples of interesting cations

Reaction	Ref.
HCl + SbF ₅ $\xrightarrow{\text{HF}, -78^{\circ}\text{C}}$ H ₂ F ⁺ SbClF ₅ ⁻	[184]
AsH ₃ + AsF ₅ $\xrightarrow{\text{HF}, -80^{\circ}\text{C}}$ AsH ₄ ⁺ AsF ₆ ⁻	[185]
AsCl ₃ + XeF ⁺ AsF ₆ ⁻ $\xrightarrow{\text{HF}, -78^{\circ}\text{C}}$ AsCl ₃ F ⁺ AsF ₆ ⁻ + Xe	[186]
Pt + AsF ₅ + 5/2F ₂ $\xrightarrow{\text{a}}$ AsF ₄ ⁺ PtF ₆ ⁻	[187]
^a no solvent	
NOCl + N ₂ F ⁺ AsF ₆ ⁻ $\xrightarrow{\text{CCl}_3\text{F}, -78^{\circ}\text{C}}$ NOClF ⁺ AsF ₆ ⁻ + N ₂	[188]
2NOCl + Cl ₂ + 3AsF ₅ $\xrightarrow{\text{SO}_2, -70^{\circ}\text{C}}$ 2NOCl ₂ ⁺ AsF ₆ ⁻ + AsF ₃	[189]
2NCl ₃ + Cl ₂ + 3AsF ₅ $\xrightarrow{\text{SO}_2, -78^{\circ}\text{C}}$ 2NCl ₄ ⁺ AsF ₆ ⁻ + AsF ₃	[190]
PI ₃ + I ₃ ⁺ AsF ₆ ⁻ $\xrightarrow{\text{CCl}_3\text{F}, 0^{\circ}\text{C}}$ PI ₄ ⁺ AsF ₆ ⁻ + I ₂	[191]
2AsBr ₃ + Br ₂ + 3AsF ₅ $\xrightarrow{-5^{\circ}\text{C}}$ 2AsBr ₄ ⁺ AsF ₆ ⁻ + AsF ₃	[192,193]
NF ₄ ⁺ SbF ₆ ⁻ + CsBrF ₄ $\xrightarrow{\text{BrF}_5, -31^{\circ}\text{C}}$ NF ₄ ⁺ BrF ₄ ⁻ + CsSbF ₆	[194]
2Sb(OTeF ₅) ₃ + 2X ₂ $\xrightarrow{\text{R.T.}}$ SbX ₄ ⁺ Sb(OTeF ₅) ₆ ⁻	[195]
X = Cl, Br	

is still comparatively small, in particular with respect to fluorine chemistry [181]. Protonation and fragmentation of transition metal carbonyls in aHF solution have been observed [182], while after addition of XeF₂, new fluoro complexes are formed [183].

2.4.3 Chemistry in other non-aqueous solvents

In addition to aHF, acetonitrile has proved to be an extremely useful solvent in fluorine chemistry. A major difference between both solvents is in the fact that CH₃CN is a much stronger ligand than HF and, accordingly, it frequently comprises an integral part of the isolated compounds. This is nicely demonstrated

by the reaction of NiF_2 with SbF_5 [196] or BiF_5 [145]. From solutions in aHF $\text{Ni}(\text{SbF}_6)_2$ or $\text{Ni}(\text{BiF}_6)_2$ is isolated, while attempts to recrystallize these materials from acetonitrile are leading to the solvated compound $[\text{Ni}(\text{CH}_3\text{CN})_6](\text{SbF}_6)_2$ [197] or its Bi relative, respectively. Beyond any doubt a major recent achievement was the development of a convenient synthesis of anhydrous $(\text{CH}_3)_4\text{N}^+\text{F}^-$ [96]. Solutions of this salt in CH_3CN but also in CHF_3 turned out to be an excellent source for the very strong fluorobase F^- , which is easily transferred to even very weak acids like the mono-anions of the strongest fluoro acids. This approach has facilitated the first time preparation of a group of anions characterized by unusually high coordination numbers and even some new dianions like SbF_7^{2-} and BiF_7^{2-} (see Table 10). One potential extension of the method is the use of larger cations and these have already been used with success in few cases [198]. Additional virtues of the method are the possibility of studying solutions by NMR spectroscopy and the isolation of well-crystallized pure products. Very recently, a number of tetramethylammonium salts have been prepared directly from $(\text{CH}_3)_3\text{N}$, CH_3F and the respective Lewis acid [199]. Another major achievement in CH_3CN solution was the first identification of a $\text{Xe}-\text{C}$ bond [200,201], followed by the isolation of single crystals from respective solutions [202]. This chemistry has been extended considerably [203].

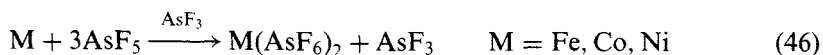
With respect to their coordination behavior, SO_2 and AsF_3 may be considered to fall between the very weakly coordinating solvent HF and the rather strong ligand CH_3CN . SO_2 coordinates a little more strongly than AsF_3 , while the latter is rather easily oxidized. However, this provides an elegant method of synthesizing

Table 10

Selected reactions in CH_3CN

Reaction			Ref.
$(\text{CH}_3)_4\text{N}^+\text{F}^- + (\text{CH}_3)_4\text{N}^+\text{IF}_4^-$	$\xrightarrow{-31^\circ\text{C}}$	$[(\text{CH}_3)_4\text{N}^+]_2\text{IF}_5^{2-}$	[204]
$2(\text{CH}_3)_4\text{N}^+\text{F}^- + \text{MF}_5$	$\xrightarrow{-31^\circ\text{C}}$	$[(\text{CH}_3)_4\text{N}^+]_2\text{MF}_7^{2-}$	[205]
M = Sb, Bi			
$(\text{CH}_3)_4\text{N}^+\text{F}^- + \text{IOF}_5$	$\xrightarrow{-31^\circ\text{C}}$	$(\text{CH}_3)_4\text{N}^+\text{IOF}_6^-$	[206–208]
$(\text{CH}_3)_4\text{N}^+\text{F}^- + \text{IF}_7$	$\xrightarrow{-31^\circ\text{C}}$	$(\text{CH}_3)_4\text{N}^+\text{IF}_8^-$	[206,209]
$(\text{CH}_3)_4\text{N}^+\text{F}^- + \text{TeF}_6$	$\xrightarrow{-40^\circ\text{C}}$	$(\text{CH}_3)_4\text{N}^+\text{TeF}_7^-$	[206,207]
$(\text{CH}_3)_4\text{N}^+\text{F}^- + (\text{CH}_3)_4\text{N}^+\text{TeF}_7$	$\xrightarrow{0^\circ\text{C}}$	$[(\text{CH}_3)_4\text{N}^+]_2\text{TeF}_8^{2-}$	[206]
$(\text{CH}_3)_4\text{N}^+\text{F}^- + \text{TeOF}_4$	$\xrightarrow{\text{R.T.}}$	$(\text{CH}_3)_4\text{N}^+\text{TeOF}_5^-$	[210]
$(\text{CH}_3)_4\text{N}^+\text{F}^- + (\text{CH}_3)_4\text{N}^+\text{TeOF}_5^-$	$\xrightarrow{-9^\circ\text{C}}$	$[(\text{CH}_3)_4\text{N}^+]_2\text{TeOF}_6^{2-}$	[211]
$(\text{CH}_3)_4\text{N}^+\text{F}^- + \text{CsClF}_4$	$\xrightarrow{\text{R.T.}}$	$(\text{CH}_3)_4\text{N}^+\text{ClF}_4^- + \text{CsF}$	[212]
$(\text{CH}_3)_4\text{N}^+\text{F}^- + \text{ClF}_5$	$\xrightarrow{-31^\circ\text{C}}$	$(\text{CH}_3)_4\text{N}^+\text{ClF}_6^-$	[213]
$(\text{CH}_3)_4\text{N}^+\text{F}^- + \text{XeOF}_4$	$\xrightarrow{\text{R.T.}}$	$(\text{CH}_3)_4\text{N}^+\text{XeOF}_5^-$	[214]
$(\text{CH}_3)_4\text{N}^+\text{F}^- + \text{XeF}_4$	$\xrightarrow{-40^\circ\text{C}}$	$(\text{CH}_3)_4\text{N}^+\text{XeF}_5^-$	[215]
$(\text{CH}_3)_4\text{N}^+\text{F}^- + \text{PF}_3$	$\xrightarrow{\text{R.T.}}$	$(\text{CH}_3)_4\text{N}^+\text{PF}_4^-$	[216]

hexafluoroarsenates from metals and AsF₅. This procedure is very clean as the reaction produces its own solvent [217]:



The isolated products crystallize with two solvent molecules per metal atom. Closely related products are obtained from reactions aiming at hexafluoroarsenates of the lanthanides. From reactions in SO₂ similar compounds were isolated in which AsF₃ is replaced by SO₂. Exchange reactions were consistent with SO₂ being the slightly stronger ligand. Although the experiments just described were performed quite recently, both solvents have been used with great success for many years in the synthesis of cations (see Table 11), and of poly-cations, mostly formed from halogens and/or chalcogens. Those recent experiments, however, should open up a wide field of complex type chemistry, as the loosely bounded solvent molecules may be easily replaced by stronger ligands. In connection with long-standing experiences in complex and even organometallic chemistry, this approach should allow for stepwise fine tuning of structural features and finally of particular properties related to potential applications.

Other important solvents are IF₅, BrF₅, and SO₂ClF. IF₅ has been used for many years because of its special properties. Although I^{III} as well as I^{VII} compounds are well known, IF₅ is rather inert with respect to redox reactions. It is a weaker fluoride

Table 11

Selected reactions in SO₂ and AsF₃

Reaction			Ref.
5I ₂ + 3AsF ₅	$\xrightarrow{SO_2, R.T.}$	2I ₅ ⁺ AsF ₆ ⁻ + AsF ₃	[218]
2I ₂ + 3AsF ₅	$\xrightarrow{SO_2, R.T.}$	I ₄ ²⁺ (AsF ₆ ⁻) ₂ + AsF ₃	[219]
2I ₂ + 4SbF ₅	$\xrightarrow{SO_2, R.T.}$	I ₄ ²⁺ (Sb ₃ F ₁₄ ⁻)(SbF ₆ ⁻)	[219]
2Se + 2I ₂ + 3AsF ₅	$\xrightarrow{SO_2, R.T.}$	Se ₂ I ₄ (AsF ₆) ₂ • SO ₂ + AsF ₃	[220]
6Se + I ₂ + 3AsF ₅	$\xrightarrow{SO_2, R.T.}$	Se ₆ I ₂ (AsF ₆) ₂ • 2SO ₂ + AsF ₃	[221]
2Se + 2I ₂ Sb ₂ F ₁₁	$\xrightarrow{SO_2, R.T.}$	Se ₂ I ₄ (Sb ₂ F ₁₁) ₂	[220]
S ₈ ²⁺ (MF ₆ ⁻) ₂ + AX	$\xrightarrow{SO_2, -55^\circ C}$	S ₇ X ⁺ MF ₆ ⁻ + AMF ₆ + 1/8S ₈	[222]
A = Na, K; X = F, Cl; M = As, Sb			
2CF ₃ SBr + Br ₂ + 3SbF ₅	$\xrightarrow{SO_2, 0^\circ C}$	2CF ₃ SBr ₂ ⁺ SbF ₆ ⁻ + SbF ₃	[223]
2Ln + 9AsF ₅	$\xrightarrow{SO_2, -25^\circ C}$	2 [Ln(SO ₂) ₃](AsF ₆) ₃ + 3AsF ₃	[224]
Ln = Y, La, Ce, Pr, Nd, Sm, Gd, Dy, Er, Yb			
W(CO) ₆ + Te ₄ (SbF ₆) ₂	$\xrightarrow{SO_2/AsF_3}$	[W(CO) ₄ Te ₃][SbF ₆] ₂ + ...	[225]
Sn(SbF ₆) ₂	$\xrightarrow{AsF_3, R.T.}$	Sn(SbF ₆) ₂ • 2AsF ₃	[226]
2Se + 3Cl ₂ + 3AsF ₅	$\xrightarrow{AsF_3, R.T.}$	2SeCl ₃ AsF ₆ + AsF ₃	[227]
1/2S ₈ + 6SbF ₅ + ^a	$\xrightarrow{AsF_3, R.T.}$	S ₄ ²⁺ (Sb ₂ F ₁₁ ⁻) ₂ + SbF ₃ • SbF ₅	[228]
2S ₈ + Br ₂ + 3AsF ₅	$\xrightarrow{AsF_3, R.T.}$	2S ₇ Br ⁺ AsF ₆ ⁻ + AsF ₃ + 1/4S ₈	[229]

^a traces of X₂ (X = Cl, Br, I)

ion acceptor than BrF_5 but shows remarkable ability to coordinate anions in quite surprising ways. For example, from CsF in excess BrF_5 crystalline CsBrF_6 is isolated [230], whereas the respective reaction with IF_5 leads to $\text{CsI}_3\text{F}_{16}$ [230]. The higher fluoride ion affinity of BrF_5 with respect to IF_5 is even more clearly demonstrated by the fact that attempts to recrystallize CsIF_6 from BrF_5 solution result in the formation of BrF_6^- besides $\text{I}_3\text{F}_{16}^-$ anions [231]. The latter anion may be described as three IF_5 molecules coordinated to a single fluoride ion. In this way IF_5 resembles the isoelectronic XeOF_4 molecule [232]. Experiments designed to isolate the IF_6^- anion have nicely demonstrated further influences of different solvents in combination with different counterions. Crystallization of the $(\text{CH}_3)_4\text{N}^+$ salt from CH_3CN solution afforded dimeric units [231] of IF_6^- , while with the small NO^+ cation tetramers were produced [231]. The great solvating properties of IF_5 were demonstrated with two other examples. Small amounts of HF , present in the experiments with CsIF_6 discussed above, resulted in the isolation of compounds like $\text{Cs}^+\text{H}_3\text{F}_4^- \cdot 3\text{IF}_5$ [233]. From solutions of N_2O_4 in IF_5 the complex $\text{NO}^+\text{NO}_3^- \cdot \text{IF}_5$ has been isolated [234]. It establishes one of the long discussed ionic forms of N_2O_4 .

BrF_5 and SO_2ClF have proved very useful as solvents in following experiments in solution by NMR spectroscopy, which have also led to the subsequent isolation of new species. While BrF_5 exhibits still some fluoride ion affinity, solvolysis is almost never observed with SO_2ClF . Both solvents are very weakly coordinating and are inert with respect to even the strongest oxidizers, thus complementing aHF very well. These special properties have led to the identification of the first $\text{Kr}-\text{N}$ bond [166] and many other new noble gas compounds, a topic which was reviewed quite recently [235]. Many of the compounds discussed therein are derived from rather large ligands whose group electronegativity is only slightly smaller than that of fluorine itself. However, in the anions $[\text{N}(\text{SO}_2\text{F})_2]^-$, $[\text{OTeF}_5]^-$, or $[\text{OIF}_4\text{O}]^-$ the negative charge is distributed over a rather large entity. In particular, the chemistry of the 'pseudofluoride' $[\text{OTeF}_5]^-$ has been intensively studied, extending considerably the field of superacids. In connection with transition metal compounds this topic was recently reviewed [236]. While larger cations like $(\text{CH}_3)_4\text{N}^+$ provide access to unstable anions, large anions like $\text{Sb}(\text{OTeF}_5)_6^-$ are equally effective in extending the field of unstable cations listed above (Table 9). However, as exemplified by the adduct $\text{AsOCl}_3 \cdot \text{AsF}_5$ [237], unstable molecules derived from such cations may be quite easily isolated in presence of a proper solvent. It is an interesting approach to use the strong Lewis acid AsF_5 and related compounds in the stabilization of unstable molecules. More surprising is the existence of the compounds $\text{ReF}_6^+\text{ReF}_7\text{MF}_6^-\text{MF}_5$ with $\text{M}=\text{Sb}, \text{Au}$, in which the very strong fluoro acids SbF_5 and AuF_5 co-exist with the weak base ReF_7 , but also alongside with the respective ions [238]. Rather peculiar also is the formation of the polynuclear anion $[\text{PO}_2\text{F}_2 \cdot 2\text{AsF}_5]^-$ without any indication of the expected formation of AsF_6^- units [239]. Equally unexpected are compounds characterized as $\text{Hg}_3(\text{NbF}_5)_2\text{SO}_4$ and $\text{Hg}_3(\text{TaF}_5)_2\text{SO}_4$, respectively, isolated from solution in SO_2 [240]. More detailed investigation of such fascinating compounds is highly desirable. Another candidate for stabilizing rather peculiar bonding situations is XeF_4 . Attempts to isolate the compound $\text{XeF}_5^+\text{CrF}_5^-$ have always yielded nicely crystalline

$(\text{XeF}_5^+\text{CrF}_5^-)_4 \cdot \text{XeF}_4$ besides mostly amorphous material. Removal of the XeF_4 from the complex turned out to be extremely difficult, indicating that it is stabilizing this phase in a very effective way [241]. In this connection a variety of reactions may be mentioned which have been undertaken in low-melting XeF_2 and XeF_6 [241–243] with both fluorides acting as reagent and as solvent simultaneously. Some products from such experiments have been successfully used as starting materials in other syntheses [244].

2.5 Photochemical reactions

Fluorine absorbs light in the visible and near UV regions, thus enabling photochemical activation for the preparation of fluorine compounds. As the bond in the fluorine molecule is easily cleaved, irradiation provides very convenient access to fluorine atoms, the strongest fluorinating agent known. Accordingly, photochemical reactions are most suitable for the synthesis of very reactive and thermally unstable fluorides. In contrast, activation by thermal methods frequently results in more side products not only due to thermal decomposition but also due to reactions with the vessel. For particular photochemical reactions, temperature, radiation wavelength and other conditions may be chosen in the most appropriate way. Well known are photosynthetic reactions to prepare binary noble gas fluorides. Unfortunately, the potential of photochemistry has not yet been realized in inorganic fluorine chemistry. Much remains to be done, as illustrated by a novel approach to high oxidation state complex metal fluorides via irradiation of elemental fluorine in fluorobasic aHF solution [245].

2.5.1 Photochemical reactions with elemental fluorine

As already mentioned, photochemistry is well established for the synthesis of the noble gas fluorides, XeF_2 , XeF_4 and KrF_2 , with the exception of radioactive RnF_2 . XeF_2 behaves as a moderately strong oxidant, which has some limited stability even in aqueous solution and may be stored indefinitely as a solid. These properties allow for its use in organic chemistry as a relatively mild, selective, and clean fluorinating agent. Accordingly, the synthesis of bigger quantities in a very pure form, particularly without any traces of XeF_4 and XeF_6 , has become important. The improved synthetic method [246] takes advantage of earlier findings that XeF_2 is best prepared by irradiation of a gaseous xenon-fluorine mixture at a mole ratio of 1:2. Addition of about 1% HF increases the rate of the reaction by about 4 times, however, as commercial fluorine contains up to 0.5% of HF, this parameter normally does not need special consideration. More importantly, the pressure within the reaction vessel should be carefully monitored in order to stop the reaction before all the Xe is consumed and XeF_4 begins to form. Using the procedure described in [246], about 2 g/h of pure XeF_2 in quantitative yield are obtained. Subsequently the preparation was scaled up from a 1.5 to a 10 ℓ photochemical reactor [247]. In this reactor up to 1 kg of XeF_2 has been prepared in a single batch. Infrared spectra of the products showed no indication of the bands characteristic for XeF_4 , whose absence is

absolutely vital as hydrolysis of XeF_4 (and also of XeF_6) leads to highly explosive XeO_3 .

An interesting approach is laser photolysis ($\lambda = 488 \text{ nm}$) of xenon-fluorine mixtures at -196°C in reactors made from 6 mm Teflon-FEP tubes with 0.5 mm wall thickness [248]. Only small amounts of XeF_2 but in 100% yield and free from XeF_4 are obtained. The virtue of this approach lies in its rather broad usability in the fluorination of various reagents dissolved in liquid fluorine (e.g. Kr, Xe, O_2 , UF_5).

Photosynthesis and photolysis of XeF_6 were also investigated [249] and proved the presence of a true photochemical equilibrium, though clearly towards XeF_4 :



These experiments were performed in nickel or copper reactors with sapphire windows and a 400 W medium pressure mercury lamp, radiating predominantly around $\lambda = 365 \text{ nm}$, was used as light source. As the photochemical dissociation of XeF_6 is rather fast and the equilibrium is shifted very much to the left-hand side, this reaction is an excellent method both for the synthesis of small quantities of very pure XeF_4 and also for the preparation of very pure elemental fluorine. XeF_4 and XeF_6 may easily be removed at liquid oxygen temperatures. Traces of XeF_6 may be removed from XeF_4 via reaction with AsF_5 . However, in general the direct photosynthesis catalyzed by NiF_2 is the preferred route [250] to synthesize XeF_4 , besides the thermal decomposition of Na_2XeF_8 [251].

KrF_2 is the strongest known oxidant which may be isolated as a pure compound, and many new synthetic routes in high oxidation state chemistry (see Chapter 4) are consequently based on this valuable reagent. Apart from the so-called 'hot-wire' reactor [252], the irradiation of Kr/ F_2 mixtures immersed in liquid nitrogen is by far the most widely used method for its preparation. After improvements in the original procedure [253], photosynthesis now enables the isolation of up to 10 g of pure KrF_2 in a single run [254]. In reference [255], photochemical and thermal dissociation processes involving KrF_2 are discussed in detail. One major advantage of the photochemical approach over the 'hot-wire' reactor is the much more versatile equipment which is also more easily operated and maintained.

O_2F_2 resembles KrF_2 in many respects, though, it is much less stable [255]. Investigations of the photolysis of O_2/F_2 mixtures at -183°C in the gas phase and at -196°C in liquid state clearly prove the latter conditions to be much more favorable in achieving a quantitative reaction [256]. Thermal instability, however, makes handling and storage of O_2F_2 much more difficult than that of KrF_2 [257]. O_2F_2 proved quite useful in the synthesis of XeF_4 at low temperatures (-155 to -120°C) [258]. Investigation into the system O_2/F_2 provided an excellent basis for the purification of elemental fluorine, O_2 being its most prominent impurity [256]. After irradiation, F_2 is distilled off at -183°C while O_2F_2 remains. In the course of most photochemical reactions involving O_2 and F_2 , O_4F_2 was observed at the beginning of the reaction, but it was never present in the O_2F_2 finally isolated [248,256].

Noble-gas chemistry originated with the synthesis of the first dioxygenyl salt $\text{O}_2^+\text{PtF}_6^-$. Compounds of this type may be prepared from O_2F_2 , however, photochemical treatment of O_2/F_2 mixtures in the presence of an appropriate Lewis acid is much more convenient. The original method for synthesis of $\text{O}_2^+\text{AsF}_6^-$, which works well even in sunlight [259], was optimized to provide easy access to this most valuable oxidizer [260]. In this way, up to 15 g of $\text{O}_2^+\text{AsF}_6^-$ may be prepared within 1 h in standard laboratory equipment. The decomposition of dioxygenyl salts in aHF provides a useful source of the very strong oxidizing/fluorinating agent O_2F , giving easy access to other high energy oxidizers [150] (see Chapter 4). In a closely related approach, the photodissociation of F_2 in the presence of basic aHF leads to oxidation of NiF_2 to NiF_6^{2-} salts [245] (see Chapter 4). These salts and the derived binary fluorides NiF_4 and NiF_3 provided an excellent opportunity to study the industrially important Simons process for conversion of organic compounds to perfluorinated derivatives. The main virtue of the new photochemical method in solution is the ease of recycling of the NiF_2 via fluorination with F_2 . The method has proved also its effectiveness with respect to Ag^{III} -compounds [261].

The technically important binary fluorides SF_6 and ClF_5 may also be prepared using photochemical methods. The photosynthesis of SF_6 from SF_4 and F_2 has been shown to be convenient at least on a laboratory scale [262]. The only by-product, S_2F_{10} , is safely removed via distillation at -110°C . At optimized conditions, 3 g/h of pure ClF_5 have been prepared from photolysis of ClF_3/F_2 mixtures in quantitative yield [263], this method being much easier and safer than the thermal process under pressure [80].

2.5.2 Photolysis of fluorine compounds

As already stated, photodissociation of XeF_6 is a convenient route to clean XeF_4 , and photodecomposition is also an effective tool elsewhere. A facile and high yield (99%) preparation of S_2F_{10} is achieved via photodecomposition of SF_5Br [264], in which the S-Br bond is easily cleaved by light from a halogen lamp:



After bromine is removed via treatment with mercury, very pure S_2F_{10} is obtained. Similarly the highest yield method (85%, based on SF_5OCl) for the preparation of SF_5OSF_5 from the readily available starting compounds is based on the photolysis of a mixture of SF_5OCl and SF_5Cl [265]. The main byproduct, $\text{SF}_5\text{O}_2\text{SF}_5$, is removed from the product by thermal decomposition in copper or Monel vessels.

$\text{CF}_2(\text{NO})_2$ was synthesized via photolysis of a mixture of CF_2I_2 and NO in the presence of mercury [266], a method well established for the synthesis of CF_3NO . The yield which depends on radiation time, however, never exceeded 10%. Though $\text{CF}_2(\text{NO})_2$ lacks thermal stability, separation of different by-products is reasonably straightforward.

2.6 Techniques for crystal growth

In previous sections the importance of aiming at crystalline material as the product of a synthetic reaction was frequently emphasized. One main reason for this aim certainly is in the fact that diffraction methods, in particular X-ray diffraction, on powders and even more on single crystals, have grown to be the most powerful analytical tools in wide areas of chemistry. Another, by no means less important reason comes from the experience, that well crystallized material generally turns out to be less sensitive to various handling procedures and influences. Crystallization is also well known as an important purification procedure for chemical substances. For these reasons, synthetic reactions are usually designed to produce crystalline material, unless other properties, e.g. large surface area or very small particles, are required. Accordingly, we discuss the hydrothermal method, which was originally developed as a crystal growth process, in connection with synthesis, as this method is now widely used as an excellent synthetic approach to crystalline material. In this section dedicated to crystal growth methods, those approaches will be emphasized, that lead to the larger crystals needed for detailed measurements of physical properties, especially where anisotropy is involved. Frequently this relates more or less directly to applications as exemplified by fluoride crystals and films, doped with Cr^{3+} or Ln^{3+} ions for use in optics. However, also rather new developments are included, such as molecular beam epitaxy or the extension of the hydrothermal method to solvents other than water under supercritical conditions. It should be noted that the borderline between crystal growth methods and synthetic methods is intentionally not clear-cut.

2.6.1 Crystallization from solution

Here shall be given some recent spots in a well-established area. Crystallization from solution, in particular from aqueous solution, is a very convenient method for growing large single crystals of compounds which show moderate to large solubility. Depending on conditions, solvated or anhydrous phases may be obtained. Least demanding with respect to setup and equipment is slow evaporation of the solvent. Quite large needle-like crystals of $\text{Cs}_2\text{WO}_2\text{F}_4$ were obtained this way and have been shown to exhibit efficient luminescence both under UV and X-ray excitation [267]. After slow evaporation from saturated solutions over quite a long period rather large crystals of $\text{KMnF}_4 \cdot \text{H}_2\text{O}$ were isolated and used in susceptibility measurements in defined orientation [268]. Presence of a properly pretreated drying agent facilitated for simultaneous crystal growth and replacement of H_2O by D_2O with $\text{CoSiF}_6 \cdot 6\text{H}_2\text{O}$ [269] and $\text{MgSiF}_6 \cdot 6\text{H}_2\text{O}$ [270]. Both, large crystal size and deuteration are prerequisites for successful experiments applying neutron diffraction. In cases of low solubility, slow diffusion of respective solutions of the starting compounds into one another may prove successful. As a nice example with improved setup, perovskite type KZnF_3 may be mentioned [271].

2.6.2 Crystallization from melts or fluxes

Crystallization from solution may be quite selective, making controlled doping of crystals very difficult to control or even impossible. In the melt this problem is much easier to handle and also much larger crystals may be grown. Because of their potential applications, various doped fluorides have been intensively studied:

- laser hosts for tunable femtosecond and UV pulse generation ($\text{LiSrAlF}_6\text{:Cr}^{3+}$ [272] and $\text{LiCaAlF}_6\text{:Ce}^{3+}$ [273]), for tunable mid-IR emission at 3400 nm ($\text{BaYb}_2\text{F}_8\text{:Dy}^{3+}$ [274]), and for upconversion at 456 nm, 551 nm or 639.5 nm wavelengths (LiYF_4 doped respectively with $\text{Tm}^{3+} + \text{Yb}^{3+}$ [275], $\text{Er}^{3+} + \text{Yb}^{3+}$ [276], $\text{Pr}^{3+} + \text{Yb}^{3+}$ [277]).
- radiation hard scintillators for high resolution γ -calorimetry and imaging. CeF_3 presents very attractive properties [278], together with other tysonite type compounds [279].

Fluoride salts with mixed anionic species present also interesting and specific features :

- extended UV transparency in fluoride borates. $\text{KBe}_2(\text{BO}_3)\text{F}_2$ (cut-off at 150 nm) is used for phase matched second harmonic generation [280].
- optically induced transitions (hole burning) in fluoride chlorides $\text{BaClF}\text{:Sm}^{2+}$ [281], and $\text{CaClF}\text{:Sm}^{2+}$ [282]. Interest in these alkaline earth chloride fluorides is high for data storage; moreover the relative bromide fluoride $\text{BaBrF}\text{:Eu}^{2+}$ is the active component in X-ray sensitive imaging plates [283].

Large crystals are grown by Czochralski, Bridgman–Stockbarger or VGF (Vertical Gradient Freezing) and flux methods preferentially, zone melting is less favorable. Accurate temperature regulation, with fluctuations less than 0.1°C from the target temperature, ensures good crystal quality.

Initially limited to congruently melting compounds, Czochralski and Bridgman–Stockbarger techniques are now adapted for use with non-congruently melting compounds; a variation in the temperature is imposed in order to follow the liquidus curve during crystallization. Supercooling of the melt allows for the direct crystallization of the low temperature form of BaY_2F_8 when an axial thermal gradient ($100^\circ\text{C}/\text{cm}$) is applied in the growth area [284,285].

Typical growth conditions are listed in Tables 12, 13 and 14.

2.6.3 Crystallization from supercritical fluids

The wide applicability of the hydrothermal method has already been stressed. The method was extended to other solvents in recent years and is now frequently characterized more generally as the solvothermal approach. Since it has been observed that even such inert materials like CO_2 or even Xe act as quite good solvents under supercritical conditions, an obvious extension was to evaluate fluorides such as NF_3 , SF_6 , AsF_5 , and, especially, HF under comparable conditions [322]. NF_3 was regarded as particularly interesting from a synthetic point of view, as it is chemically inert at ambient conditions, but above about 200°C it becomes a rather strong

Table 12

Examples of materials obtained by Czochralski growth or zone melting

	Material	Melt	Temperature (range) (°C)	Cooling rate (°C/h)	Rotation ω (rpm)	Translation v_p (mm/h)	Ref.
Czochralski							
Fluorides	YF ₃	0.8YF ₃ -0.2LiF	1050–850		30	1	[286]
	GdF ₃ : Nd ³⁺	1GdF ₃ -0.7LiF-0.04NdF ₃	850		30	0.5	[287]
	BaLiF ₃	0.43BaF ₂ -0.57LiF	830–780	0.5, 1, 2	10	1	[288]
	BaLiF ₃ :Ni ²⁺	0.4BaF ₂ -0.6LiF-0.03NiF ₂	820		10	1	[289]
	LiYF ₄	0.51LiF-0.49YF ₃	815–695		10	2.5	[290-292]
	LiYF ₄ :U ³⁺	0.51LiF-0.49YF ₃ -0.01UF ₄	815		10	2.5	[293]
	LiCaAlF ₆	LiCaAlF ₆	815		15	1	[294]
Zone melting							
Fluorides	LiSrAlF ₆	1.1LiF-SrF ₂ -1.1AlF ₃	780			2.67	[295]
	LiCaCrF ₆	LiCaCrF ₆	850			3.0	[296]

Table 13

Conditions of crystal growth of selected materials by Bridgman and slow cooling techniques

	Material	Melt	T (°C)	ΔT (°C/cm)	Displacement rate (mm/h)	Ref.
Bridgman						
Fluorides	CeF ₃	CeF ₃	1460	20	1.5	[278]
	KCaF ₃	KCaF ₃	1070	10	0.6	[297]
	K _{1-x} Rb _x AlF ₄	K _{1-x} Rb _x AlF ₄	600–400	15	0.6	[298]
	BaThF ₆ :Ce ³⁺	BaF ₂ -ThF ₄ -CeF ₃	1150	20	0.5	[279]
	Rb ₂ KInF ₆ :Ce ³⁺	Rb ₂ K(In _{1-x} Ce _x)F ₆	1100	25	0.15–1.5	[299]
	β -BaY ₂ F ₈	BaY ₂ F ₈	960	100	1	[285]
	Pb ₅ Al ₃ F ₁₉	72PbF ₂ -28AlF ₃	720–550	0.5		[300]
Mixed anions	K ₃ MoO ₃ F ₃	K ₃ MoO ₃ F ₃	860	20	1.0	[301]
	K ₃ TiOF ₅	TiOF ₂ -KF	750	20	1.0	[302]
Slow cooling						
Fluorides	BaZnF ₄	BaF ₂ -ZnF ₂	800	5		[303]
	LiInF ₄	LiInF ₄	670–200	3		[304]
	Na ₃ MnF ₆	3NaF-MnF ₃	850	20		[305]
	Ca ₂ YbF ₇	9CaF ₂ -5YbF ₃	1130–230	1		[306]
	Cs ₃ Ga ₂ F ₉	Cs ₃ GaF ₆ -GaF ₃	520	60		[307]
	ABa ₂ M ₂ F ₉ K,Rb-Co,Ni,Fe,Zn	AF-2BaF ₂ -2MF ₂	1000–400	10		[308]
	NaMnZr ₂ F ₁₁	NaF-MnF ₂ -2ZrF ₄	800	4		[309]
	PrZr ₂ F ₁₁	PrF ₃ -2ZrF ₄	850–700	5		[310]
	Ba ₂ CaCoFe ₂ F ₁₄	2BaF ₂ -CaF ₂ -CoF ₂ -2FeF ₃	850–680	1		[311]
Mixed anions	Bi ₇ O ₅ F ₁₁	5Bi ₂ O ₃ -11BiF ₃	800–280	5		[312]
	Ba ₁₀ (MnFeF _{11-x} Cl _x) ₃ F _x Cl _{2-x}	BaF ₂ -BaCl ₂ -MnF ₂ -FeF ₃	750	6		[313]
	LiSr ₂ (SiO ₄)F	2SrO-SiO ₂ -LiF	950–600	6		[314]
	KBe ₂ (BO ₃)F ₂	KBF ₄ -BeO	800	0.2		[280]

Table 14

Conditions of synthesis of selected materials by flux growth

	Material	Flux	Temperature range (°C)	Cooling rate (°C/h)	Ref.
Fluorides	NaSrAlF ₆	NaF-SrF ₂ -AlF ₃ -2.7NaCl-1.65ZnCl ₂	700	5	[315]
	Na ₂ Ca ₃ Al ₂ F ₁₄	10NaCl-5ZnCl ₂ -2CaCl ₂ -4NaF-2CaF ₂ -2AlF ₃	650-RT	5	[316]
	Ba _{5.24} Sr _{0.76} Mg ₇ F ₂₆	1.5BaF ₂ -0.5SrF ₂ -3MgF ₂ -6LiF	930-700	4.6	[317]
	Na ₂ Sr ₆ ZnFe ₆ F ₃₄	NaF-SrF ₂ -3FeF ₃ -5.85NaCl-3.6ZnCl ₂	650-RT	5	[103]
Mixed anions	CaClF:Sm ²⁺	40CaCl ₂ -60CaClF: Sm ²⁺	750-645	1	[282]
	Ba ₂ Mn ₂ ClF ₇	5ZnCl ₂ -NaF-ZnF ₂ -BaF ₂	550-RT	5	[318]
	K ₃ Ba ₇ Al ₆ Cl ₂ F ₃₃	KF-BaF ₂ -AlF ₃ -0.44KCl-1.67ZnCl ₂	650-RT	5	[319]
	Er ₃ (Si ₃ O ₁₀)F	ErF ₃ -Er ₂ O ₃ -9SiO ₂ -CsCl	700		[320]
	KEu ₂ (Si ₄ O ₁₀)F	EuSiO ₃ -KF	930-600		[321]

fluorinating agent. The use of HF, of course, presents tremendous problems with the container material, especially as corrosion becomes even more severe in the presence of Lewis acids. Nevertheless, single crystals of AgF_2 have resulted from early experiments in aHF [323]. Under optimized conditions suitable single crystals of TiF_4 , VF_4 , CrF_4 and MnF_4 have been obtained [94]. Further experiments should reveal, why for each of these simple tetrafluorides a different structure was determined. An exciting result comes from the first experiments in supercritical AsF_5 , from which $\text{La}(\text{HF})_2(\text{AsF}_6)_3$ as the first compound with HF molecules directly coordinated to a metal center has been isolated [324]. This result is particularly interesting as such a moiety was never obtained from solutions in aHF, although metal ions coordinated by HF molecules are definitely present in respective solutions [10]. Accordingly, the experiment in supercritical AsF_5 opens the way for exciting new compounds and materials.

2.6.4 Molecular beam and liquid phase epitaxy

Epitaxial growth of $\text{CaF}_2:\text{Ln}^{3+}$ layers has been demonstrated on (100) or (111) CaF_2 substrates. Nd^{3+} , Er^{3+} , Pr^{3+} doping or $\text{Er}^{3+}-\text{Yb}^{3+}$ codoping has been realised by simultaneous evaporation of LnF_3 and CaF_2 [325,326]. The growth rate and rare earth concentration are controlled by the temperature of the effusion cells: $0.5 \mu\text{m/h}$ and $0.05-6 \text{ mol}\%$ doping of Er^{3+} has been obtained with $T = 1210^\circ\text{C}$ for CaF_2 and $T = 800-1000^\circ\text{C}$ for ErF_3 . The substrate is maintained at $T = 450-600^\circ\text{C}$ and the layer thickness ($1.5-2.0 \mu\text{m}$) measured by profilometry. Active planar waveguides, useful for integrated optoelectronics, can be produced [327].

Active epitaxial layers of $\text{LiYF}_4:\text{Nd}^{3+}$ may be deposited by liquid phase epitaxy from LiF rich melts ($0.7\text{LiF}/0.3\text{YF}_3$) at 730°C . Deposition rate is high ($3 \mu\text{m/min}$), even in case of very low supersaturation [328,329]. Laser emission was achieved from a $40 \mu\text{m}$ thick layer on pure oriented ((100) or (110)) LiYF_4 substrate and with a ridge waveguide obtained by mechanical processing.

2.7 Techniques for preparation of solids with special properties

Once special properties of a fluoride have been detected, the main challenge comes from the necessity to prepare such a material in larger quantities at very confined conditions. Frequently very subtle changes in certain reaction parameters are providing for quite dramatic changes in properties. Hereafter few selected examples of interesting potential applications are given.

2.7.1 Films

Chemical sensors for gas detection are based on multi-layer systems which lead to the formation of three phase boundaries with the gas. As fluoride based solid electrolytes PbF_2 , PbSnF_4 , but especially LaF_3 were studied on quite a broad basis (see review by Fergus [330]). LaF_3 exhibits remarkable oxygen sensitivity even at ambient temperatures. Original setup used large single crystals of LaF_3 in connection with

porous Pt electrodes. While sensitivity of such cells is enhanced in replacing the Pt electrode by electrodes made from perovskite type oxides [331,332], a very interesting development comes from the replacement of the single crystal by a thin film of LaF_3 sputtered onto an oxidized Si substrate [333]. In this connection CaF_2 has also been very intensely investigated. Its ionic conductivity is enhanced via surface treatment with Lewis acids like SbF_5 or BF_3 [334]. Another interesting feature of alkaline-earth difluorides is their ability to act as protective and antireflective coating on glass optics. MgF_2 based films and composites have been obtained from an interesting combination of sol-gel and spin-coating methods leading to nanocrystalline MgF_2 [335]. Using reactive sputter deposition of Cr in an $\text{Ar}/\text{C}_2\text{F}_6$ plasma resulted in Cr/C/F thin films which turned out to be crystalline in electron diffraction experiments. Careful control of reaction parameters resulted in high reproducibility of film composition [336]. Applying another plasma based method, so-called plasma enhanced chemical vapour deposition (PECVD), polycrystalline silicon films have been obtained from SiF_4/H_2 mixtures at temperatures as low as 100°C [337]. An almost identical process has been used in the deposition of diamond films from CF_4/H_2 mixtures [338], but also CH_4/F_2 [339] and CF_4/F_2 [340] mixtures in connection with various activation methods to produce atomic fluorine have been investigated.

Closely related are successful experiments in deposition of tungsten films by the CVD method using WF_6 as precursor. One main advantage over organometallic precursors is the absence of impurities originating from decomposition products of the organic ligands. Further improvement of the process has come from the observation that addition of SiH_4 or GeH_4 as reducing agents lowered deposition temperature to 270°C [341,342].

2.7.2 Nanoparticles and catalysis

Small crystallites, whose size is measuring in the range of several nm, are commonly called nanocrystals or, more general, nanoparticles. Such small particles are frequently observed in connection with thin films as mentioned above, but have drawn considerable attention on a much broader basis. Chemical reactivity of nanocrystalline material is considerably enhanced with respect to bulk material. Consequently, sintering temperatures of ceramics are lowered remarkably. Outstanding properties of nanocrystalline alkali fluorides in comparison to other alkali halides have been described in an excellent review [343]. Very interesting are nanoparticles in connection with those physical properties, which are strongly connected to extended structures, e.g. ferromagnetism. NH_4MnF_3 has been prepared in the nanocrystalline state from microemulsion [344]. As NH_4MnF_3 is a well-known antiferromagnet, it should serve as a model substance to study the influence of particle size on a strongly cooperative effect like antiferromagnetism.

Calcium phosphate in the form of apatite is interesting in various fields, but especially in connection with substitutes for biomaterials like damaged bones or teeth [345]. Properties vary considerably with composition from hydroxyapatite to fluoroapatite, solid solutions of these two isostructural compounds being particu-

larly interesting. Nanosized material with composition identical to fluoroapatite has been isolated from ethanol solution and turned out to be amorphous as evidenced by X-ray powder diffraction. The amorphous material crystallized upon heating to 460°C forming very pure fluoroapatite. The high reactivity of this powder was evidenced by the active sintering process already starting at 500°C [346]. Increased surface area and reactivity of small particles makes such materials very interesting for catalytic processes. In connection with the production of more environmentally friendly hydrofluorocarbons (HFCs), alumina based aerogels doped with Cr or Cr and Ti have drawn remarkable attention. These very reactive aerogels have been fluorinated by CHF_3 , the final catalyst mostly consisting of doped $\alpha\text{-AlF}_3$ [347]. However, in similar experiments $\beta\text{-AlF}_3$ has been studied as catalyst, whose maximum in activity was reached after doping with 10–20 atom% Mg^{2+} [348]. The delicacy of such catalytic experiments was demonstrated with coprecipitates from $\text{Cr}^{3+}/\text{Fe}^{3+}$ or $\text{Cr}^{3+}/\text{Mg}^{2+}$ solutions in ethanol after addition to aqueous HF. Highest activity was clearly with the Fe-rich products identified as pseudo-hexagonal tungsten bronze type $\beta\text{-FeF}_3$, but also with materials rich in Mg [349]. This topic is discussed in detail in Chapter 12.

2.7.3 Oxide-based materials

Not yet widely exploited, but with quite some potential for fine-tuning of properties certainly is the stepwise fluorination of oxides. With LiCoO_2 cathode material for use in lithium secondary batteries, addition of small amounts of LiF considerably improved electrochemical properties [350]. However, further exploitation is needed to elucidate if improvements are due to improved particle size and crystallinity or also due to minor fluorine content of the material. Lithium batteries are discussed in consecutive Chapters 15 and 16.

A major challenge for fluorination of oxides was introduced with the discovery of high temperature superconducting copper oxides. For example, fluorination of Sr_2CuO_4 at ambient pressure brings about the same structural changes to induce superconductivity, which otherwise are only achievable at high pressures [351]. In the related oxidefluorides $\text{Sr}_2\text{Ca}_{n-1}\text{Cu}_n\text{O}_{2n+\delta}\text{F}_{2\pm y}$ ($n = 2, 3$) rather high transition temperatures ($T_c = -174^\circ\text{C}$ for $n = 2$, $T_c = -162^\circ\text{C}$ for $n = 3$) were observed after synthesis via solid state reactions at high pressures [352]. As analyzed in some detail with respect to strontium cuprate based materials, application of various fluorinating agents has resulted in quite different ways of fluorine incorporation [353–356]. Despite various claims there seem to be no reliable results yet to confirm an increase of superconducting transition temperature after fluorination. Moreover, a main obstacle is the formation of very stable alkaline earth fluorides at higher temperatures, but this has successfully and reproducibly been overcome through the use of soft chemistry or ‘chimie douce’ methods [357,358]. For future technological applications other results of fluorination may turn out very important. In particular, for $\text{YBa}_2\text{Cu}_3\text{O}_{7-\delta}$ considerable increase of stability with respect to degradation was observed after fluorination with XeF_2 [359]. The field of surface fluorination of inorganic materials is covered in Chapter 14.

2.8 Conclusions

Within previous two decades the tendency of exploiting mild reaction conditions has prevailed in comparison to methods involving quite drastic reaction conditions. Accordingly, remarkable progress has been made in solution chemistry. A new precipitation method has provided easy access even to unstable binary fluorides, in particular to a new class of very strong oxidizers. Their convenient use facilitates from the simple synthesis of well-known, but very versatile, compounds like PtF_6 to very clean reactions providing perfluorinated organic compounds in excellent yield. With the help of photochemical activation the method has gained even more potential. On the other hand, the use of truly anhydrous $(\text{CH}_3)_4\text{NF}$ in acetonitrile has proved extremely successful. Hopefully, this positive momentum will be carried on with already known cations like $[(\text{CH}_3)_2\text{N}]_3\text{S}^+$ (TAS^+) or $[(\text{CH}_3)_2\text{N}]_3\text{SO}^+$ (TAOS^+) [360], or some new ions may turn out even more useful.

With respect to solid state fluorine chemistry, the development of tunable, short pulse or UV lasers has strongly benefited from advances in crystal growth techniques. Accordingly, the search for planar or linear waveguides has become very active. The so-called rapid metathesis reactions certainly deserve more attention. So far, only few reactions involving fluorides have been studied, however, the results are very promising [361,362]. It remains still an open question, why Nb_6F_{15} happens to be an almost unique case of a fluoride containing metal-metal bonds [363], although respective compounds of the heavier halogens already form a quite mature field [364–366]. Some hope comes from a recently isolated Al-compound [367], showing an O-centered octahedron of Al atoms. All edges of the octahedron are bridged by fluorine ligands. Those are typical structural features of metal-rich compounds of d- and f-block elements.

In the introductory remarks of this chapter we mentioned vital importance of proper training before trying to do any kind of fluorine chemistry. At the very end, we like to stress few experiments demonstrating the importance of proper training and broad knowledge. T.A. O'Donnell and his coworkers at the University of Melbourne have done an outstanding job in developing industrial processes based on waste SiF_4 [368,369]. This way TiO_2 , titanium and zirconium metals may be produced in a very clean and environmentally friendly way.

Within this chapter we have tried to provide a sensible selection of synthetic reactions, spanning the broad and exciting field of inorganic fluorine chemistry. Several areas will be more deeply covered in consecutive, dedicated chapters of this monograph.

Acknowledgement

We are very grateful to Neda Hanc, Milenko Milojevič and Robert Moravec for excellent technical assistance. Two of us (K.L. and H.B.) appreciate continuous financial support by the Ministry of Science and Technology of the Republic of Slovenia; M.L. is very indebted to colleagues and coworkers for fruitful discussions.

References

- [1] R.D. Verma, R.L. Kirchmeier, J.M. Shreeve, In: *Advances in Inorganic Chemistry*, Vol. 41, A.G. Sykes (Ed.), Academic Press, Inc., San Diego, CA, 1994, p. 125.
- [2] E.F. Murphy, R. Murugavel, H.W. Roesky, *Chem. Rev.*, 97 (1997) 3425.
- [3] J. Grannec, L. Lozano, In: *Inorganic Solid Fluorides*, P. Hagenmuller (Ed.), Academic Press, Inc., Orlando, FL, 1985, Chapter 2.
- [4] *Inorganic Syntheses*, Vol. 24, J.M. Shreeve (Ed.), John Wiley & Sons, New York, NY, 1986, Chapter 1.
- [5] *Inorganic Fluorine Chemistry Toward the 21st Century*, J.S. Thrasher, S.H. Strauss (Eds.), ACS Symposium Series 555, Washington, DC, 1994.
- [6] *Synthetic Fluorine Chemistry*, G.A. Olah, R.D. Chambers, G.K.S. Prakash (Eds.), John Wiley & Sons, New York, NY, 1992.
- [7] G.R. Férey, In: *Encyclopedia of Inorganic Chemistry*, Vol. 3, R.B. King (Ed.), John Wiley & Sons, Chichester, 1994, p. 1207.
- [8] D.D. DesMarteau, C.W. Bauknight, Jr., T.E. Mlsna, In: *Encyclopedia of Inorganic Chemistry*, Vol. 3, R.B. King (Ed.), John Wiley & Sons, Chichester, 1994, p. 1223.
- [9] B. Žemva, In: *Encyclopedia of Inorganic Chemistry*, Vol. 5, R.B. King (Ed.), John Wiley & Sons, Chichester, 1994, p. 2660.
- [10] T.A. O'Donnell, *Superacids and Acidic Melts as Inorganic Chemical Reaction Media*, VCH Publishers, Inc., Weinheim, 1993.
- [11] *Solid State Chemistry — Techniques*, A.K. Cheetham, P. Day (Eds.), Clarendon Press, Oxford, 1988.
- [12] A.K. Tyagi, J. Köhler, *Mater. Res. Bull.*, 32 (1997) 1683.
- [13] P. Dugat, M. El-Ghozzi, J. Metin, D. Avignant, *J. Solid State Chem.*, 120 (1995) 187.
- [14] J.P. Laval, J.F. Gervais, L. Fournès, J. Grannec, P. Gravereau, A. Abaouz, A. Yacoubi, *J. Solid State Chem.*, 118 (1995) 389.
- [15] L. Topor, A. Navrotsky, Y. Zhao, D. J. Weidner, *J. Solid State Chem.*, 132 (1997) 131.
- [16] E. Largeau, V. Gaumet, M. El-Ghozzi, D. Avignant, J.C. Cousseins, *J. Mater. Chem.*, 7 (1997) 1881.
- [17] A. Ider, J.P. Laval, B. Frit, J. Carré, J.P. Bastide, *J. Solid State Chem.*, 123 (1996) 68.
- [18] M. Takashima, S. Yonezawa, K. Horita, K. Ohwaki, H. Takahashi, *J. Mater. Chem.*, 6 (1996) 795.
- [19] G. Corbel, R. Retoux, M. Leblanc, *J. Solid State Chem.*, 139 (1998) 52.
- [20] Ö. Andaç, F.P. Glasser, R.A. Howie, *Acta Crystallogr.*, C53 (1997) 831.
- [21] F. Gingl, *Z. Anorg. Allg. Chem.*, 623 (1997) 705.
- [22] A. Abaouz, A. Taoudi, J.P. Laval, *J. Solid State Chem.*, 130 (1997) 277.
- [23] N. Dupont, M. Samouël, P. Gredin, A. de Kozak, *Eur. J. Solid State Inorg. Chem.*, 35 (1998) 39.
- [24] S. Kyung-Soo, J. Senegas, J.M. Reau, P. Hagenmuller, *J. Solid State Chem.*, 93 (1991) 469.
- [25] G. Denes, Y.H. Yu, T. Tyliczszak, A.P. Hitchcock, *J. Solid State Chem.*, 91 (1991) 1.
- [26] P. Laborde, J.M. Reau, *J. Solid State Chem.*, 72 (1988) 225.
- [27] T. Sekino, T. Endo, T. Sato, M. Shimada, *J. Solid State Chem.*, 88 (1990) 505.
- [28] S. Åsbrink, A. Waskowska, *Eur. J. Solid State Inorg. Chem.*, 31 (1994) 747.
- [29] F.D. Duldulao, J.M. Burlitch, *Chem. Mater.*, 5 (1993) 1037.
- [30] F. Duldulao Perez, J.M. Burlitch, *Chem. Mater.*, 7 (1995) 2277.
- [31] G. Férey, J. Pannetier, *Eur. J. Solid State Inorg. Chem.*, 31 (1994) 697.

- [32] P. Daniel, A. Bulou, M. Rousseau, J. Nouet, J.L. Fourquet, M. Leblanc, R. Burriel, J. Phys.: Condens. Matter, 2 (1990) 5663.
- [33] A. Ratuszna, J. Phys.: Condens. Matter, 5 (1993) 841.
- [34] P. Daniel, M. Rousseau, J. Toulouse, Phys. Rev. B, 55 (1997) 6222.
- [35] K. Rotureau, P. Daniel, A. Desert, J.Y. Gesland, J. Phys.: Condens. Matter, 10 (1998) 1431.
- [36] A. Le Bail, H. Duroy, J.L. Fourquet, J. Solid State Chem., 98 (1992) 151.
- [37] A. Le Bail, C. Jacoboni, M. Leblanc, R. De Pape, H. Duroy, J.L. Fourquet, J. Solid State Chem., 77 (1988) 96.
- [38] U. Bentrup, Eur. J. Solid State Inorg. Chem., 28 (1991) 1347.
- [39] N. Herron, D.L. Thorn, R.L. Harlow, G.A. Jones, J.B. Parise, J.A. Fernandez-Baca, T. Vogt, Chem. Mater., 7 (1995) 75.
- [40] U. Bentrup, Z. Anorg. Allg. Chem., 619 (1993) 954.
- [41] S. Miličev, A. Rahten, Eur. J. Solid State Inorg. Chem., 28 (1991) 557.
- [42] D. Hanžel, A. Rahten, D. Hanžel, Eur. J. Solid State Inorg. Chem., 31 (1994) 381.
- [43] J.L. Fourquet, M. Riviere, A. Le Bail, M. Nygrens, J. Grins, Eur. J. Solid State Inorg. Chem., 25 (1988) 535.
- [44] U. Bentrup, Eur. J. Solid State Inorg. Chem., 29 (1992) 51.
- [45] T. Tsuboi, A. Scacco, J. Phys.: Condens. Matter, 10 (1998) 2787.
- [46] F. Goubard, J. Chassaing, D. Bizot, M. Quarton, Eur. J. Solid State Inorg. Chem., 31 (1994) 223.
- [47] F. Goubard, S. Llorente, D. Bizot, J. Chassaing, M. Quarton, J. Solid State Chem., 131 (1997) 231.
- [48] F. Kubel, H. Hagemann, H. Bill, Mater. Res. Bull., 32 (1997) 263.
- [49] R. Dafinova, A. Caralampydu, J. Phys.: Condens. Matter, 10 (1998) 6181.
- [50] B.N. Wani, U.R.K. Rao, J. Solid State Chem., 112 (1994) 199.
- [51] R. Hoppe, Z. Anorg. Allg. Chem., 292 (1957) 28.
- [52] L.B. Asprey, S.A. Kinkad, P.G. Eller, Nucl. Techn., 73 (1986) 69.
- [53] A. Zemljič, B. Družina, A. Šmalc, B. Žemva, Kem. Ind., 35 (1986) 441.
- [54] D. Zhang, C. Wang, F. Mistry, B. Powell, F. Aubke, J. Fluorine Chem., 76 (1996) 83.
- [55] M.F.A. Dove, M. Goodier, J. Fluorine Chem., 54 (1991) 23.
- [56] A. Turičnik, H. Borrmann, B. Žemva, unpublished results.
- [57] P. Woodward, T. Vogt, W. Weber, E. Schweda, J. Solid State Chem., 138 (1998) 350.
- [58] C. Plitzko, G. Meyer, Z. Kristallogr. — New Cryst. Struct., 213 (1998) 475.
- [59] C. Plitzko, G. Meyer, Z. Anorg. Allg. Chem., 623 (1997) 1347.
- [60] C. Plitzko, G. Meyer, Z. Anorg. Allg. Chem., 622 (1996) 1646.
- [61] C. Plitzko, M. Strecker, G. Meyer, Z. Anorg. Allg. Chem., 623 (1997) 79.
- [62] C. Plitzko, G. Meyer, Z. Anorg. Allg. Chem., 624 (1998) 169.
- [63] S. Schmid, R.L. Withers, J. Solid State Chem., 109 (1994) 391.
- [64] D. Gantar, A. Rahten, B. Volavšek, J. Fluorine Chem., 41 (1988) 335.
- [65] D. Gantar, A. Rahten, J. Fluorine Chem., 34 (1986) 63.
- [66] A. Rahten, I. Leban, S. Miličev, B. Žemva, J. Crystallogr. Spectr. Res., 20 (1990) 9.
- [67] R.A. Schöning, G. Meyer, Z. Anorg. Allg. Chem., 623 (1997) 1759.
- [68] C. Grimberg, J. Strähle, J.P. Laval, B. Frit, R. Sonntag, J. Ihringer, Eur. J. Solid State Inorg. Chem., 31 (1994) 449.
- [69] C. Plitzko, M. Strecker, G. Meyer, Z. Kristallogr. — New Cryst. Struct., 212 (1997) 3.
- [70] C. Plitzko, G. Meyer, Z. Anorg. Allg. Chem., 623 (1997) 1393.
- [71] M. Hofmann, E. Schweda, J. Strähle, J.P. Laval, B. Frit, M.A. Estermann, J. Solid State Chem., 114 (1995) 73.

- [72] S. Kaskel, J. Strähle, *Z. Anorg. Allg. Chem.*, 623 (1997) 1259.
- [73] O. Graudejus, B.G. Müller, *Z. Anorg. Allg. Chem.*, 622 (1996) 187.
- [74] E. Engelmann, B.G. Müller, *Z. Anorg. Allg. Chem.*, 589 (1990) 51.
- [75] E. Engelmann, B.G. Müller, *Z. Anorg. Allg. Chem.*, 618 (1992) 43.
- [76] E. Engelmann, B.G. Müller, *Z. Anorg. Allg. Chem.*, 619 (1993) 1661.
- [77] M. Bork, R. Hoppe, *Z. Anorg. Allg. Chem.*, 622 (1996) 1557.
- [78] D. Kissel, R. Hoppe, *Z. Anorg. Allg. Chem.*, 559 (1988) 40.
- [79] K. Lutar, D. Gantar, B. Frlec, *Vestn. Slov. Kem. Drus.*, 32 (1985) 337.
- [80] K. Lutar, A. Šmalc, B. Žemva, *Inorg. Synth.*, 29 (1992) 7.
- [81] K.O. Christe, W.W. Wilson, C.J. Schack, In: *Synthetic Fluorine Chemistry*, G.A. Olah, R.D. Chambers, G.K.S. Prakash (Eds.), John Wiley & Sons, New York, 1992, Chapter 2.
- [82] K.O. Christe, W.W. Wilson, R.D. Wilson, *Inorg. Chem.*, 28 (1989) 675.
- [83] R.W. Cockman, R.D. Peacock, *J. Fluorine Chem.*, 30 (1986) 469.
- [84] J. Fawcett, R.D. Peacock, D.R. Russell, *J. Chem. Soc. Dalton Trans.*, (1987) 567.
- [85] R. Minkwitz, H. Prenzel, *Z. Anorg. Allg. Chem.*, 548 (1987) 103.
- [86] R.C. Burns, T.A. O'Donnell, *Inorg. Chem.*, 18 (1979) 3081.
- [87] A. Jesih, B. Žemva, *Vestn. Slov. Kem. Drus.*, 33 (1986) 25.
- [88] A. Šmalc, personal communication.
- [89] W.W. Wilson, K.O. Christe, *J. Fluorine Chem.*, 40 (1988) 59.
- [90] K.O. Christe, R.D. Wilson, W.W. Wilson, R. Bau, S. Sukumar, D.A. Dixon, *J. Am. Chem. Soc.*, 113 (1991) 3795.
- [91] K.O. Christe, *J. Am. Chem. Soc.*, 117 (1995) 6136.
- [92] A.K. Bridson, P.J. Jones, W. Levason, J.S. Ogden, J.H. Holloway, E.G. Hope, G. Stanger, *J. Chem. Soc. Dalton Trans.*, (1990) 715.
- [93] W.J. Casteel, Jr., A.P. Wilkinson, H. Borrmann, R.E. Serfass, N. Bartlett, *Inorg. Chem.*, 31 (1992) 3124.
- [94] B.G. Müller, *Eur. J. Solid State Inorg. Chem.*, 34 (1997) 627.
- [95] B. Žemva, K. Lutar, A. Jesih, W.J. Casteel, Jr., N. Bartlett, *J. Chem. Soc. Chem. Commun.*, (1989) 346.
- [96] K.O. Christe, W.W. Wilson, R.D. Wilson, R. Bau, J.A. Feng, *J. Am. Chem. Soc.*, 112 (1990) 7619.
- [97] S. Feng, G. Li, C. Zhao, G. Wang, D. Wang, Y. Mao, *Proceedings of the 2nd International Conference on Solvothermal Reactions*, Takamatsu, Japan, 1996, p. 118.
- [98] X. Xun, S. Feng, J. Wang, R. Xu, *Chem. Mater.*, 9 (1997) 2966.
- [99] A. Le Bail, J.P. Laval, *Eur. J. Solid State Inorg. Chem.*, 35 (1998) 357.
- [100] R.J. Francis, P.S. Halasyamani, D. O'Hare, *Angew. Chem. Int. Ed. Engl.*, 37 (1998) 2214.
- [101] M.P. Crosnier-Lopez, H. Duroy, J.L. Fourquet, *J. Solid State Chem.*, 107 (1993) 211.
- [102] J. Patarin, F. Marcuccilli-Hoffner, H. Kessler, P. Daniels, *Eur. J. Solid State Inorg. Chem.*, 31 (1994) 501.
- [103] A. Hémon-Ribaud, M.P. Crosnier-Lopez, J.L. Fourquet, G. Courbion, *J. Fluorine Chem.*, 68 (1994) 155.
- [104] S.J. Kirkby, A.J. Lough, G.A. Ozin, *Z. Kristallogr. — New Cryst. Struct.*, 210 (1995) 956.
- [105] T. Loiseau, Y. Calage, P. Lacorre, G. Férey, *J. Solid State Chem.*, 111 (1994) 390.
- [106] Y. Le Fur, N.M. Khaidukov, S. Aléonard, *Acta Crystallogr.*, C48 (1992) 2062.
- [107] M.A. Subramanian, W.J. Marshall, R.L. Harlow, *Mater. Res. Bull.*, 31 (1996) 585.
- [108] M. Leblanc, G. Férey, R. De Pape, *Mater. Res. Bull.*, 19 (1984) 1581.

- [109] J.M. Le Meins, A. Hémon-Ribaud, G. Courbion, *Acta Crystallogr.*, C53 (1997) 1165.
- [110] M.P. Crosnier-Lopez, H. Duroy, J.L. Fourquet, M. Abrabri, *Eur. J. Solid State Inorg. Chem.*, 31 (1994) 957.
- [111] H. Nishizawa, K. Okumoto, T. Mitsushio, *J. Solid State Chem.*, 92 (1991) 370.
- [112] M. Leblanc, I. Collin-Fèvre, G. Férey, *J. Magn. Magn. Mat.*, 167 (1997) 71.
- [113] W. Massa, O.V. Yakubovich, O.V. Karimova, L.N. Dem'yanets, *Eur. J. Solid State Inorg. Chem.*, 35 (1998) 133.
- [114] J.M. Le Meins, A. Hémon-Ribaud, G. Courbion, *Eur. J. Solid State Inorg. Chem.*, 35 (1998) 117.
- [115] G. Frenzen, O.V. Yakubovich, O.K. Mel'nikov, *Acta Crystallogr.*, C52 (1996) 749.
- [116] N. Mercier, M. Leblanc, *Eur. J. Solid State Inorg. Chem.*, 30 (1993) 217.
- [117] N. Mercier, F. Taulelle, M. Leblanc, *Eur. J. Solid State Inorg. Chem.*, 30 (1993) 609.
- [118] N. Mercier, M. Leblanc, J. Durand, *Eur. J. Solid State Inorg. Chem.*, 34 (1997) 241.
- [119] M.E. Fleet, Y. Pan, *Can. Miner.*, 33 (1995) 879.
- [120] V. Maisonneuve, M. Leblanc, *Can. Miner.*, 36 (1998) 1039.
- [121] G. Férey, M. Leblanc, R. De Pape, M. Passaret, M.P. Bothorel-Razazi, *J. Cryst. Growth*, 29 (1975) 209.
- [122] S. Komarneni, *Proceedings of the 2nd International Conference on Solvothermal Reactions*, Takamatsu, Japan, 1996, p. 114.
- [123] V. Maisonneuve, personal communication.
- [124] R. De Pape, G. Férey, *Mater. Res. Bull.*, 21 (1986) 971.
- [125] H. Arai, S. Okada, Y. Sakurai, J. Yamaki, *Extended Abstracts of the 8th International Meeting on Lithium Batteries*, Nagoya, Japan, 1996, p. 540.
- [126] R.J. Cava, D.W. Murphy, S.M. Zahurak, *J. Electrochem. Soc.*, 130 (1983) 2345.
- [127] L. Permér, M. Lundberg, *J. Solid State Chem.*, 81 (1989) 21.
- [128] C. Bohnke, O. Bohnke, J.L. Fourquet, *Mol. Cryst. Liq. Cryst.*, 311 (1998) 23.
- [129] G. Courbion, personal communication.
- [130] J.J. Maguer, M.P. Crosnier-Lopez, G. Courbion, *J. Solid State Chem.*, 128 (1997) 42.
- [131] N. Martin, P. Boutinaud, R. Mahiou, J.C. Cousseins, M. Bouderbala, *J. Mater. Chem.*, 9 (1999) 125.
- [132] K.O. Christe, C.J. Schack, R.D. Wilson, *Inorg. Chem.*, 14 (1975) 2224.
- [133] B.F. Hoskins, A. Linden, T.A. O'Donnell, *Inorg. Chem.*, 26 (1987) 2223.
- [134] K. Lutar, B. Žemva, H. Borrmann, *Eur. J. Solid State Inorg. Chem.*, 33 (1996) 957.
- [135] Z. Mazej, H. Borrmann, K. Lutar, B. Žemva, *Abstracts of 15th International Symposium on Fluorine Chemistry*, Vancouver, Canada, 1997, no. Ba(1)C-5.
- [136] B. Žemva, K. Lutar, A. Jesih, W.J. Casteel, Jr., A.P. Wilkinson, D.E. Cox, R.B. Von Dreele, H. Borrmann, N. Bartlett, *J. Am. Chem. Soc.*, 113 (1991) 4192.
- [137] B. Žemva, K. Lutar, L. Chacón, M. Fele-Beuermann, J. Allman, C. Shen, N. Bartlett, *J. Am. Chem. Soc.*, 117 (1995) 10025.
- [138] W. Casteel, Jr., T. Horwitz, *Eur. J. Solid State Inorg. Chem.*, 29 (1992) 649.
- [139] K.O. Christe, *Inorg. Chem.*, 25 (1986) 3721.
- [140] W.J. Casteel, Jr., G.M. Lucier, B. Žemva, N. Bartlett, unpublished observations.
- [141] S.H. Elder, G.M. Lucier, F.J. Hollander, N. Bartlett, *J. Am. Chem. Soc.*, 119 (1997) 1020.
- [142] Z. Mazej, H. Borrmann, K. Lutar, B. Žemva, J. Darriet, J. Grannec, A. Tressaud, *Abstracts of the 12th European Symposium on Fluorine Chemistry*, Berlin, Germany, 1998, p. B20.
- [143] G. Lucier, S.H. Elder, L. Chacón, N. Bartlett, *Eur. J. Solid State Inorg. Chem.*, 33 (1996) 809.

- [144] H. Fitz, B.G. Müller, *Z. Anorg. Allg. Chem.*, 623 (1997) 579.
- [145] R. Bougon, P. Charpin, K.O. Christe, J. Isabey, M. Lance, M. Nierlich, J. Vigner, W.W. Wilson, *Inorg. Chem.*, 27 (1988) 1389.
- [146] M. Fele-Beuermann, K. Lutar, Z. Mazej, S. Miličev, B. Žemva, *J. Fluorine Chem.*, 89 (1998) 83.
- [147] Y. Katayama, R. Hagiwara, Y. Ito, *J. Fluorine Chem.*, 74 (1995) 89.
- [148] R. Bougon, W.W. Wilson, K.O. Christe, *Inorg. Chem.*, 24 (1985) 2286.
- [149] J.H. Holloway, E.G. Hope, C.D. Puxley, *Eur. J. Solid State Inorg. Chem.*, 33 (1996) 821.
- [150] G.M. Lucier, C. Shen, S.H. Elder, N. Bartlett, *Inorg. Chem.*, 37 (1998) 3829.
- [151] B. Žemva, *C.R. Acad. Sci. Ser. IIc*, 1 (1998) 151.
- [152] N. Bartlett, R.D. Chambers, A.J. Roche, R.C.H. Spink, L. Chacón, J.M. Whalen, *Chem. Commun.*, (1996) 1049.
- [153] K.O. Christe, W.W. Wilson, R.A. Bougon, *Inorg. Chem.*, 25 (1986) 2163.
- [154] K.O. Christe, R. Bougon, *J. Chem. Soc. Chem. Commun.*, (1992) 1056.
- [155] R. Bougon, B. Buu, K. Seppelt, *Chem. Ber.*, 126 (1993) 1331.
- [156] K.O. Christe, D.A. Dixon, H.G. Mack, H. Oberhammer, A. Pagelot, J.C.P. Sanders, G.J. Schrobilgen, *J. Am. Chem. Soc.*, 115 (1993) 11279.
- [157] H.P.A. Mercier, G.J. Schrobilgen, *Inorg. Chem.*, 32 (1993) 145.
- [158] N. LeBlond, G.J. Schrobilgen, *Chem. Commun.*, (1996) 2479.
- [159] K. Lutar, S. Miličev, B. Žemva, B.G. Müller, B. Bachmann, R. Hoppe, *Eur. J. Solid State Inorg. Chem.*, 28 (1991) 1335.
- [160] K. Lutar, A. Jesih, B. Žemva, *Rev. Chim. Min.*, 23 (1986) 565.
- [161] K. Lutar, A. Jesih, I. Leban, B. Žemva, N. Bartlett, *Inorg. Chem.*, 28 (1989) 3467.
- [162] A. Jesih, K. Lutar, I. Leban, B. Žemva, *Inorg. Chem.*, 28 (1989) 2911.
- [163] K. Lutar, A. Jesih, B. Žemva, *Polyhedron*, 7 (1988) 1217.
- [164] K. Lutar, H. Borrmann, B. Žemva, to be published.
- [165] R. Hagiwara, F. Hollander, C. Maines, N. Bartlett, *Eur. J. Solid State Inorg. Chem.*, 28 (1991) 855.
- [166] G.J. Schrobilgen, *J. Chem. Soc. Chem. Commun.*, (1988) 863.
- [167] A.A.A. Emara, G.J. Schrobilgen, *Inorg. Chem.*, 31 (1992) 1323.
- [168] J.M. Whalen, G.J. Schrobilgen, *J. Fluorine Chem.*, 71 (1995) 225.
- [169] D. Gantar, B. Frlc, D.R. Russell, J.H. Holloway, *Acta Crystallogr.*, C43 (1987) 618.
- [170] W.J. Casteel, Jr., G. Lucier, R. Hagiwara, H. Borrmann, N. Bartlett, *J. Solid State Chem.*, 96 (1992) 84.
- [171] B. Žemva, R. Hagiwara, W.J. Casteel, Jr., K. Lutar, A. Jesih, N. Bartlett, *J. Am. Chem. Soc.*, 112 (1990) 4846.
- [172] G. Lucier, C. Shen, W.J. Casteel, Jr., L. Chacón, N. Bartlett, *J. Fluorine Chem.*, 72 (1995) 157.
- [173] T. Drews, K. Seppelt, *Angew. Chem.*, 109 (1997) 264.
- [174] S.H. Strauss, *Chem. Rev.*, 93 (1993) 927.
- [175] F. Aubke, *J. Fluorine Chem.*, 72 (1995) 195.
- [176] C. Wang, A.R. Lewis, R.J. Batchelor, F.W.B. Einstein, H. Willner, F. Aubke, *Inorg. Chem.*, 35 (1996) 1279.
- [177] M. Adelhelm, W. Bacher, E.G. Höhn, E. Jacob, *Chem. Ber.*, 124 (1991) 1559.
- [178] P.K. Hurlburt, J.J. Rack, S.F. Dec, O.P. Anderson, S.H. Strauss, *Inorg. Chem.*, 32 (1993) 373.
- [179] K.D. Abney, K.M. Long, O.P. Anderson, S.H. Strauss, *Inorg. Chem.*, 26 (1987) 2638.

- [180] F.A. Cotton, G. Wilkinson, *Advanced Inorganic Chemistry*, 5th Edn, J. Wiley, New York, 1988, p. 64.
- [181] B. Bley, M. Bodenbinder, G. Balzer, H. Willner, G. Hägele, F. Mistry, F. Aubke, *Can. J. Chem.*, 74 (1996) 2392.
- [182] S.A. Brewer, J.H. Holloway, E.G. Hope, *J. Fluorine Chem.*, 70 (1995) 167.
- [183] K.S. Coleman, J.H. Holloway, E.G. Hope, *J. Chem. Soc. Dalton Trans.*, (1997) 1713.
- [184] R. Minkwitz, A. Kornath, H. Preut, *Z. Anorg. Allg. Chem.*, 620 (1994) 638.
- [185] R. Minkwitz, A. Kornath, W. Sawodny, H. Härtner, *Z. Anorg. Allg. Chem.*, 620 (1994) 753.
- [186] R. Minkwitz, W. Molsbeck, *Z. Anorg. Allg. Chem.*, 607 (1992) 175.
- [187] M. Broschag, T.M. Klapötke, I.C. Tornieporth-Oetting, *J. Chem. Soc. Chem. Commun.*, (1992) 446.
- [188] R. Minkwitz, D. Bernstein, H. Preut, P. Sartori, *Inorg. Chem.*, 30 (1991) 2157.
- [189] R. Minkwitz, D. Bernstein, W. Sawodny, H. Härtner, *Z. Anorg. Allg. Chem.*, 580 (1990) 109.
- [190] R. Minkwitz, D. Bernstein, W. Sawodny, *Angew. Chem. Int. Ed. Engl.*, 29 (1990) 181.
- [191] I. Tornieporth-Oetting, T. Klapötke, *J. Chem. Soc. Chem. Commun.*, (1990) 132.
- [192] T. Klapötke, J. Passmore, E.G. Awere, *J. Chem. Soc. Chem. Commun.*, (1988) 1426.
- [193] T. Klapötke, J. Passmore, *J. Chem. Soc. Dalton Trans.*, (1990) 3815.
- [194] K.O. Christe, W.W. Wilson, *Inorg. Chem.*, 25 (1986) 1904.
- [195] W.J. Casteel, Jr., P. Kolb, N. LeBlond, H.P.A. Mercier, G.J. Schrobilgen, *Inorg. Chem.*, 35 (1996) 929.
- [196] D. Gantar, I. Leban, B. Frlec, J.H. Holloway, *J. Chem. Soc. Dalton Trans.*, (1987) 2379.
- [197] I. Leban, D. Gantar, B. Frlec, D.R. Russell, J.H. Holloway, *Acta Crystallogr.*, C43 (1987) 1888.
- [198] A.R. Mahjoub, X. Zhang, K. Seppelt, *Chem. Eur. J.*, 1 (1995) 261.
- [199] R.Z. Gnann, R.I. Wagner, K.O. Christe, *J. Fluorine Chem.*, 83 (1997) 191.
- [200] H.J. Frohn, S. Jakobs, *J. Chem. Soc. Chem. Commun.*, (1989) 625.
- [201] D. Naumann, W. Tyrra, *J. Chem. Soc. Chem. Commun.*, (1989) 47.
- [202] H.J. Frohn, S. Jakobs, G. Henkel, *Angew. Chem. Int. Ed. Engl.*, 28 (1989) 1506.
- [203] H.J. Frohn, A. Klose, V.V. Bardin, A.J. Kruppa, T.V. Leshina, *J. Fluorine Chem.*, 70 (1995) 147.
- [204] K.O. Christe, W.W. Wilson, G.W. Drake, D.A. Dixon, J.A. Boatz, R.Z. Gnann, *J. Am. Chem. Soc.*, 120 (1998) 4711.
- [205] G.W. Drake, D.A. Dixon, J.A. Sheehy, J.A. Boatz, K.O. Christe, *J. Am. Chem. Soc.*, 120 (1998) 8392.
- [206] K.O. Christe, J.C.P. Sanders, G.J. Schrobilgen, W.W. Wilson, *J. Chem. Soc. Chem. Commun.*, (1991) 837.
- [207] A.R. Mahjoub, K. Seppelt, *J. Chem. Soc. Chem. Commun.*, (1991) 840.
- [208] K.O. Christe, D.A. Dixon, A.R. Mahjoub, H.P.A. Mercier, J.C.P. Sanders, K. Seppelt, G.J. Schrobilgen, W.W. Wilson, *J. Am. Chem. Soc.*, 115 (1993) 2696.
- [209] A.R. Mahjoub, K. Seppelt, *Angew. Chem. Int. Ed. Engl.*, 30 (1991) 876.
- [210] H.P.A. Mercier, J.C.P. Sanders, G.J. Schrobilgen, *J. Am. Chem. Soc.*, 116 (1994) 2921.
- [211] K.O. Christe, D.A. Dixon, J.C.P. Sanders, G.J. Schrobilgen, W.W. Wilson, *Inorg. Chem.*, 32 (1993) 4089.
- [212] W.W. Wilson, K.O. Christe, *Inorg. Chem.*, 28 (1989) 4172.
- [213] K.O. Christe, W.W. Wilson, R.V. Chirakal, J.C.P. Sanders, G.J. Schrobilgen, *Inorg. Chem.*, 29 (1990) 3506.

- [214] K.O. Christe, D.A. Dixon, J.C.P. Sanders, G.J. Schrobilgen, S.S. Tsai, W.W. Wilson, *Inorg. Chem.*, 34 (1995) 1868.
- [215] K.O. Christe, E.C. Curtis, D.A. Dixon, H.P. Mercier, J.C.P. Sanders, G.J. Schrobilgen, *J. Am. Chem. Soc.*, 113 (1991) 3351.
- [216] K.O. Christe, D.A. Dixon, H.P.A. Mercier, J.C.P. Sanders, G.J. Schrobilgen, W.W. Wilson, *J. Am. Chem. Soc.*, 116 (1994) 2850.
- [217] K. Lutar, H. Borrmann, A. Jesih, B. Žemva, Abstracts of the 11th European Symposium on Fluorine Chemistry, Bled, Slovenia, 1995, p. 38, *Acta Chim. Slov.*, 46 (1999) 213.
- [218] A. Apblett, F. Grein, J.P. Johnson, J. Passmore, P.S. White, *Inorg. Chem.*, 25 (1986) 422.
- [219] R. Faggiani, R.J. Gillespie, R. Kapoor, C.J.L. Lock, J.E. Vekris, *Inorg. Chem.*, 27 (1988) 4350.
- [220] W.A.S. Nandana, J. Passmore, P.S. White, C.M. Wong, *Inorg. Chem.*, 29 (1990) 3529.
- [221] J. Passmore, P.S. White, C.M. Wong, *J. Chem. Soc. Chem. Commun.*, (1985) 1178.
- [222] R. Minkwitz, J. Nowicki, *Inorg. Chem.*, 29 (1990) 2361.
- [223] R. Minkwitz, R. Lekies, H. Preut, *Z. Naturforsch.*, 42b (1987) 1227.
- [224] J. Petersen, E. Lork, R. Mews, *Chem. Commun.*, (1996) 2593.
- [225] R. Faggiani, R.J. Gillespie, C. Campana, J.W. Kolis, *J. Chem. Soc. Chem. Commun.*, (1987) 485.
- [226] A.J. Edwards, K.I. Khallow, *J. Chem. Soc. Chem. Commun.*, (1984) 50.
- [227] J. Passmore, T.S. Cameron, P.D. Boyle, G. Schatte, T. Way, *Can. J. Chem.*, 74 (1996) 1671.
- [228] M.P. Murchie, J. Passmore, G.W. Sutherland, R. Kapoor, *J. Chem. Soc. Dalton Trans.*, (1992) 503.
- [229] J. Passmore, G. Sutherland, T.K. Whidden, P.S. White, C.M. Wong, *Can. J. Chem.*, 63 (1985) 1209.
- [230] A.R. Mahjoub, A. Hoser, J. Fuchs, K. Seppelt, *Angew. Chem. Int. Ed. Engl.*, 28 (1989) 1526.
- [231] A.R. Mahjoub, K. Seppelt, *Angew. Chem. Int. Ed. Engl.*, 30 (1991) 323.
- [232] J.H. Holloway, V. Kaučič, D. Martin-Rovet, D.R. Russell, G.J. Schrobilgen, H. Selig, *Inorg. Chem.*, 24 (1985) 678.
- [233] A.R. Mahjoub, D. Leopold, K. Seppelt, *Eur. J. Solid State Inorg. Chem.*, 29 (1992) 635.
- [234] X. Zhang, K. Seppelt, *Z. Anorg. Allg. Chem.*, 624 (1998) 667.
- [235] G.J. Schrobilgen, In: *Synthetic Fluorine Chemistry*, G.A. Olah, R.D. Chambers, G.K.S. Prakash (Eds.), John Wiley & Sons, New York, 1992, Chapter 1.
- [236] F. Aubke, M.S.R. Cader, F. Mistry, In: *Synthetic Fluorine Chemistry*, G.A. Olah, R.D. Chambers, G.K.S. Prakash (Eds.), John Wiley & Sons, New York, 1992, Chapter 3.
- [237] J. Petersen, E. Lork, R. Mews, *Chem. Commun.*, (1996) 1897.
- [238] S.M. Yeh, N. Bartlett, *Rev. Chim. Min.*, 23 (1986) 676.
- [239] K.O. Christe, R. Gnann, R.I. Wagner, W.W. Wilson, *Eur. J. Solid State Inorg. Chem.*, 33 (1996) 865.
- [240] I.D. Brown, R.J. Gillespie, K.R. Morgan, J.F. Sawyer, K.J. Schmidt, Z. Tun, P.K. Ummat, J.E. Vekris, *Inorg. Chem.*, 26 (1987) 689.
- [241] K. Lutar, I. Leban, T. Ogrin, B. Žemva, *Eur. J. Solid State Inorg. Chem.*, 29 (1992) 713.
- [242] M. Fele-Beuermann, S. Miličev, K. Lutar, B. Žemva, *Eur. J. Solid State Inorg. Chem.*, 31 (1994) 545.
- [243] B. Družina, B. Žemva, *J. Fluorine Chem.*, 39 (1988) 309.
- [244] K. Lutar, H. Borrmann, B. Žemva, *Inorg. Chem.*, 37 (1998) 3002.
- [245] J.M. Whalen, G.M. Lucier, L. Chacón, N. Bartlett, *J. Fluorine Chem.*, 88 (1998) 107.

- [246] A. Šmalc, K. Lutar, *Inorg. Synth.*, 29 (1992) 1.
- [247] K. Lutar, A. Šmalc, *Kem. Ind.*, 38 (1989) 589.
- [248] M. Al-Mukhtar, J.H. Holloway, E.G. Hope, *J. Fluorine Chem.*, 59 (1992) 1.
- [249] K. Lutar, A. Šmalc, *Eur. J. Solid State Inorg. Chem.*, 27 (1990) 489.
- [250] K. Lutar, A. Šmalc, J. Slivnik, *Vestn. Slov. Kem. Drus.*, 26 (1979) 435.
- [251] K. Lutar, A. Šmalc, B. Žemva, *Inorg. Synth.*, 29 (1992) 4.
- [252] V.N. Bezmel'nitsyn, V.A. Legasov, B.B. Chaivanov, *Proc. Acad. Sci. USSR (Engl. Transl.)*, 235 (1977) 365.
- [253] J. Slivnik, A. Šmalc, K. Lutar, B. Žemva, B. Frlec, *J. Fluorine Chem.*, 5 (1975) 273.
- [254] A. Šmalc, K. Lutar, B. Žemva, *Inorg. Synth.*, 29 (1992) 11.
- [255] S.A. Kinkead, J.R. FitzPatrick, J. Foropoulos, Jr., R.J. Kissane, J.D. Purson, In: *Inorganic Fluorine Chemistry toward the 21st Century*, J.S. Thrasher, S.H. Strauss (Eds.), ACS Symposium Series 555, American Chemical Society, Washington, DC, 1994, Chapter 3.
- [256] K. Lutar, A. Šmalc, *Eur. J. Solid State Inorg. Chem.*, 28 (1991) 631.
- [257] K.D. Abney, P.G. Eller, M.P. Eastman, C.F. Pace, S.A. Kinkead, R.J. Kissane, W.H. Woodruff, *J. Fluorine Chem.*, 73 (1995) 137.
- [258] J.B. Nielsen, S.A. Kinkead, J.D. Purson, P.G. Eller, *Inorg. Chem.*, 29 (1990) 1779.
- [259] J. Shamir, J. Binenboym, *Inorg. Chim. Acta*, 2 (1968) 37.
- [260] A. Šmalc, K. Lutar, *Inorg. Synth.*, 29 (1992) 8.
- [261] G.M. Lucier, J.M. Whalen, N. Bartlett, *J. Fluorine Chem.*, 89 (1998) 101.
- [262] P.F. Aramendia, H.J. Schumacher, *J. Photochem.*, 28 (1985) 491.
- [263] A. Šmalc, K. Lutar, *Vestn. Slov. Kem. Drus.*, 37 (1990) 313.
- [264] R. Winter, P.G. Nixon, G.L. Gard, *J. Fluorine Chem.*, 87 (1998) 85.
- [265] S.H. Hwang, K. Naik, D.D. DesMarteau, *Inorg. Chem.*, 32 (1993) 2791.
- [266] E.O. John, R.L. Kirchmeier, J.M. Shreeve, *Inorg. Chem.*, 31 (1992) 329.
- [267] A.M. Srivastava, J.F. Ackerman, *J. Solid State Chem.*, 98 (1992) 144.
- [268] F. Palacio, M. Andres, C. Esteban-Calderon, M. Martinez-Ripoll, S. Garcia-Blanco, *J. Solid State Chem.*, 76 (1988) 33.
- [269] G. Chevrier, R. Saint-James, *Acta Crystallogr.*, C46 (1990) 186.
- [270] G. Chevrier, *J. Solid State Chem.*, 99 (1992) 276.
- [271] R.H. Buttner, E.N. Maslen, *Acta Crystallogr.*, C44 (1988) 1707.
- [272] G.J. Valentine, J.-M. Hopkins, P. Loza-Alvarez, G.T. Kennedy, W. Sibbett, D. Burns, A. Valster, *Opt. Lett.*, 22 (1997) 1639.
- [273] N. Sarukura, Z. Liu, H. Ohtake, Y. Segawa, M.A. Dubinskii, V.V. Semashko, A.K. Naumov, S.L. Korableva, R.Y. Abdulsabirov, *Opt. Lett.*, 22 (1997) 994.
- [274] N. Djeu, V.E. Hartwell, A.A. Kaminskii, A.V. Butashin, *Opt. Lett.*, 22 (1997) 997.
- [275] A. Knüpfer, E. Heumann, V. Ostroumov, G. Huber, V. Lupei, B. Chai, *J. Physique IV, Suppl. J. Physique III (C4)*, 4 (1994) 403.
- [276] P.E.-A. Möbert, E. Heumann, G. Huber, B.H.T. Chai, *Opt. Lett.*, 22 (1997) 1412.
- [277] T. Sandrock, E. Heumann, G. Huber, B.H.T. Chai, In: *Advanced Solid State Lasers*, Vol. 1 of OSA Trends in Optics, Photonics Series (Optical Society of America), Washington, DC, 1996, p. 550.
- [278] J.L. Allain, M. Couchaud, B. Ferrand, Y. Grange, B. Utts, C. Wyon, *Mater. Res. Soc. Symp. Proc.*, 348 (1994) 105.
- [279] J.P. Chaminade, P. Mesnard, A. Garcia, J. Grannec, M. Pouchard, C. Fouassier, C. Pédrini, A.N. Belsky, E.I. Zinin, *J. Cryst. Growth*, 179 (1997) 546.
- [280] L. Mei, X. Huang, Y. Wang, Q. Wu, B. Wu, C. Chen, *Z. Kristallogr.*, 210 (1995) 93.
- [281] A. Winnacker, R.M. Shelby, R.M. Macfarlane, *Opt. Lett.*, 10 (1985) 350.

- [282] J.P. Chaminade, A. Garcia, J.C. Vial, R.M. Macfarlane, *J. Cryst. Growth*, 128 (1993) 1031.
- [283] S.L. Issler, C.C. Torardi, *J. Alloys Comp.*, 229 (1995) 54.
- [284] L.H. Guilbert, J.Y. Gesland, A. Bulou, R. Retoux, *Mater. Res. Bull.*, 28 (1993) 923.
- [285] A.A. Kaminskii, A.V. Butashin, J. Hulliger, P. Egger, S.N. Bagayev, H.J. Eichler, J. Findeisen, B. Liu, U. Täuber, P. Peuser, S.N. Sulyanov, *J. Alloys Comp.*, 275–277 (1998) 442.
- [286] K. Rotereau, J.Y. Gesland, P. Daniel, A. Bulou, *Mater. Res. Bull.*, 28 (1993) 813.
- [287] J.M. Breteau, J.Y. Gesland, *Opt. Mater.*, 5 (1996) 267.
- [288] S.L. Baldochi, J.Y. Gesland, *Mater. Res. Bull.*, 27 (1992) 891.
- [289] M. Mortier, J.Y. Gesland, M. Rousseau, F. Auzel, D. Meichenin, *C. R. Acad. Sci. Paris, Ser. II*, 322 (1996) 233.
- [290] P. Rogin, J. Hulliger, *J. Cryst. Growth*, 172 (1997) 200.
- [291] L.E. Misiak, *Proc. SPIE Int. Soc. Opt. Eng.* 3178 (1997) 48.
- [292] M. Fornoni, A. Bulou, J.M. Breteau, J.Y. Gesland, M. Rousseau, *Appl. Optics*, 29 (1990) 1758.
- [293] M. Louis, E. Simoni, S. Hubert, J.Y. Gesland, *Opt. Mater.*, 4 (1995) 657.
- [294] D. Klimm, K. Seiranian, P. Reiche, A. Polity, R. Krause-Rehberg, *Proc. SPIE Int. Soc. Opt. Eng.* 3178 (1997) 35.
- [295] K.I. Schaffers, D.A. Keszler, *Acta Crystallogr.*, C47 (1991) 18.
- [296] B. Rupp, W.L. Kway, J. Wong, P. Rogl, P. Fischer, *J. Solid State Chem.*, 107 (1993) 471.
- [297] K. Idriss-Bey, P. Foucher, J.Y. Buzare, J. Nouet, C. Ridou, M. Rousseau, B. Hennion, P. Simon, *Ferroelectrics*, 107 (1990) 319.
- [298] M. Papin, A. Bulou, J. Nouet, *J. Phys.: Condens. Matter*, 5 (1993) 3177.
- [299] J.P. Chaminade, A. Garcia, T. Gaewdang, M. Pouchard, J. Grannec, B. Jacquier, *Radiation Effects, Defects in Solids*, 135 (1995) 137.
- [300] V. Andriamampianina, J. Ravez, J.P. Chaminade, F. Weill, P. Hagenmuller, S.C. Abrahams, *C. R. Acad. Sci. Paris, Ser. II*, 314 (1992) 1319.
- [301] M. Fouad, J.P. Chaminade, J. Ravez, A. Sadel, *J. Solid State Chem.*, 124 (1996) 123.
- [302] M. Fouad, J.P. Chaminade, J. Ravez, A. Sadel, *Adv. Mater. Res.*, 1–2 (1994) 469.
- [303] J. Lapasset, H.N. Bordallo, R. Almairac, J. Nouet, *Z. Kristallogr. New Cryst. Struct.*, 211 (1996) 934.
- [304] P. Gravereau, J.P. Chaminade, T. Gaewdang, J. Grannec, M. Pouchard, P. Hagenmuller, *Acta Crystallogr.*, C48 (1992) 769.
- [305] U. Englich, W. Massa, A. Tressaud, *Acta Crystallogr.*, C48 (1992) 6.
- [306] D.J.M. Bevan, M.J. McCall, S.E. Ness, M.R. Taylor, *Eur. J. Solid State Inorg. Chem.*, 25 (1988) 517.
- [307] A. de Kozak, Y. Mary, P. Gredin, J. Renaudin, G. Férey, D. Babel, *Eur. J. Solid State Inorg. Chem.*, 31 (1994) 115.
- [308] E. Herdtweck, S. Kummer, D. Babel, *Eur. J. Solid State Inorg. Chem.*, 28 (1991) 959.
- [309] M.H. Kettani, D. Avignant, J. Metin, *Acta Crystallogr.*, C51 (1995) 2207.
- [310] J.P. Laval, A. Abaouz, *J. Solid State Chem.*, 100 (1992) 90.
- [311] A. Le Lirzin, X. Quiang, J. Darriet, J.L. Soubeyroux, V. Kaiser, J. Pebler, D. Babel, *Eur. J. Solid State Inorg. Chem.*, 27 (1990) 791.
- [312] J.P. Laval, J.C. Champarnaud-Mesjard, B. Frit, A. Britel, A. Mikou, *Eur. J. Solid State Inorg. Chem.*, 31 (1994) 943.
- [313] J. Darriet, V. Nazabal, J. Fompeyrine, *J. Mater. Chem.*, 6 (1996) 1781.
- [314] A. Akella, D.A. Keszler, *Chem. Mater.*, 7 (1995) 1299.

- [315] A. Hémon, A. Le Bail, G. Courbion, *Eur. J. Solid State Inorg. Chem.*, 27 (1990) 905.
- [316] G. Courbion, G. Férey, *J. Solid State Chem.*, 76 (1988) 426.
- [317] F. Kubel, H. Hagemann, H. Bill, *Acta Crystallogr.*, C53 (1997) 1735.
- [318] J.-J. Maguer, G. Courbion, M.S. Schriewer-Pöttgen, J. Fompeyrine, J. Darriet, *J. Solid State Chem.*, 115 (1995) 98.
- [319] A. Le Bail, A. Hémon-Ribaud, G. Courbion, *J. Solid State Chem.*, 107 (1993) 234.
- [320] T. Schleid, H. Müller-Bunz, *Proceedings of the Jahrestagung der Deutschen Gesellschaft für Kristallographie*, Hamburg (1997), p. 134.
- [321] H. Jacobsen, G. Meyer, *Z. Kristallogr.*, 209 (1994) 348.
- [322] B. Žemva, A. Jesih, K. Lutar, In: *Chemical Processes, Reactions under Extreme or Non-classic Conditions*, J.L. Luche, C. Balny, S. Benefice, J.M. Denis, C. Pétrier (Eds.), European Commission, COST Action D6, 1996, p. 153.
- [323] A. Jesih, K. Lutar, B. Žemva, B. Bachmann, S. Becker, B.G. Muller, R. Hoppe, *Z. Anorg. Allg. Chem.*, 588 (1990) 77.
- [324] Z. Mazej, H. Borrmann, K. Lutar, B. Žemva, *Inorg. Chem.* 37 (1998) 5912.
- [325] E. Daran, R. Legros, A. Muñoz-Yagüe, C. Fontaine, L.E. Bausá, *J. Appl. Phys.*, 76 (1994) 270.
- [326] L.E. Bausá, A. Muñoz-Yagüe, *Appl. Phys. Lett.*, 59 (1991) 3511.
- [327] M.C. Marco De Lucas, E. Daran, B. Jacquier, C. Garapon, J. Mugnier, P. Pernas, A. Muñoz-Yagüe, *J. Appl. Phys.*, 83 (1998) 3345.
- [328] P. Rogin, J. Hulliger, *Opt. Lett.*, 22 (1997) 1701.
- [329] L. Douyset-Bloch, B. Ferrand, M. Couchaud, L. Fulbert, M.F. Joubert, G. Chadeyron, B. Jacquier, *J. Alloys Comp.*, 275-277 (1998) 67.
- [330] J.W. Fergus, *Sensors, Actuators*, B42 (1997) 119.
- [331] J.P. Lukaszewicz, N. Miura, N. Yamazoe, *Jpn. J. Appl. Phys.*, 28 (1989) L711.
- [332] J.P. Lukaszewicz, N. Miura, N. Yamazoe, *Sensors, Actuators*, B1 (1990) 195.
- [333] T. Katsube, M. Hara, I. Serizawa, N. Ishibashi, N. Adachi, N. Miura, N. Yamazoe, *Jpn. J. Appl. Phys.*, 29 (1990) L1392.
- [334] Y. Saito, J. Maier, *J. Electrochem. Soc.*, 142 (1995) 3078.
- [335] A.A. Rywak, J.M. Burlitch, *Chem. Mater.*, 8 (1996) 60.
- [336] M.J. O'Keefe, J.M. Rigsbee, *Mater. Lett.*, 18 (1994) 251.
- [337] B.Y. Ryu, J.I. Ryu, H.C. Kim, J. Jang, *Solid State Commun.*, 101 (1997) 17.
- [338] R.A. Rudder, G.C. Hudson, J.B. Posthill, R.E. Thomas, R.J. Markunas, *Appl. Phys. Lett.*, 59 (1991) 791.
- [339] J.L. Margrave, *Abstracts of 15th International Symposium on Fluorine Chemistry*, Vancouver, Canada, 1997, no. Ad. Mat. C-9.
- [340] R.A. Rudder, J.B. Posthill, R.J. Markunas, *Electronics Lett.*, 25 (1989) 1220.
- [341] M.J. Hampden-Smith, T.T. Kodas, *Chem. Vap. Deposition*, 1 (1995) 8.
- [342] A.A. Zinn, In: *The Chemistry of Metal CVD*, T.T. Kodas, M.J. Hampden-Smith (Eds.), VCH, Weinheim, 1994, Chapter 3.
- [343] R.L. Whetten, *Acc. Chem. Res.*, 26 (1993) 49.
- [344] M. Roth, R. Hempelmann, *Chem. Mater.*, 10 (1998) 78.
- [345] R. Kniep, S. Busch, *Angew. Chem. Int. Ed. Engl.*, 35 (1996) 2624.
- [346] P. Layrolle, A. Lebugle, *Chem. Mater.*, 8 (1996) 134.
- [347] T. Skapin, *J. Mater. Chem.*, 5 (1995) 1215.
- [348] I. Grohmann, A. Hess, E. Kemnitz, W. Fentrup, W.E.S. Unger, J. Wong, M. Rowen, T. Tanaka, M. Fröba, *J. Mater. Chem.*, 8 (1998) 1453.
- [349] B. Adamczyk, A. Hess, E. Kemnitz, *J. Mater. Chem.*, 6 (1996) 1731.
- [350] S. Yonezawa, T. Okayama, H. Tsuda, M. Takashima, *J. Fluorine Chem.*, 87 (1998) 141.

- [351] M. Al-Mamouri, P.P. Edwards, C. Greaves, M. Slaski, *Nature*, 369 (1994) 382.
- [352] T. Kawashima, Y. Matsui, E. Takayama-Muromachi, *Physica C*, 257 (1996) 313.
- [353] P.R. Slater, J.P. Hodges, M.G. Francesconi, C. Greaves, M. Slaski, *J. Mater. Chem.*, 7 (1997) 2077.
- [354] M.G. Francesconi, P.R. Slater, J.P. Hodges, C. Greaves, P.P. Edwards, M. Al-Mamouri, M. Slaski, *J. Solid State Chem.*, 135 (1998) 17.
- [355] F. Weill, B. Chevalier, M. Chambon, A. Tressaud, B. Darriet, J. Etourneau, G. VanTendeloo, *Eur. J. Solid State Inorg. Chem.*, 30 (1993) 1095.
- [356] M. Takashima, S. Yonezawa, S. Hirano, M. Iino, T. Unishi, A. Sumiyama, *J. Fluorine Chem.*, 72 (1995) 55.
- [357] E.E. Fadeeva, E.I. Ardashnikova, B.A. Popovkin, M.P. Borzenkova, *Russ. J. Inorg. Chem.*, 38 (1993) 363.
- [358] C. Greaves, M.G. Francesconi, *Current Opinion in Solid State and Materials Science*, 3 (1998) 132.
- [359] A. Šmalc, T. Skapin, *Acta Chim. Slov.*, 43 (1996) 285.
- [360] E. Lork, R. Mews, D. Viets, P.G. Watson, *Eur. J. Solid State Inorg. Chem.*, 33 (1996) 931.
- [361] P.R. Bonneau, R.K. Shibao, R.B. Kaner, *Inorg. Chem.*, 29 (1990) 2511.
- [362] E.G. Gillan, R.B. Kaner, *Chem. Mater.*, 8 (1996) 333.
- [363] H. Schäfer, H.G. Schnering, K.-J. Niehues, H.G. Nieder-Vahrenholz, *J. Less-Common Metals*, 9 (1965) 95.
- [364] J.D. Corbett, *J. Alloys Comp.*, 229 (1995) 10.
- [365] C. Perrin, S. Cordier, S. Ihmaine, M. Sergent, *J. Alloys Comp.*, 229 (1995) 123.
- [366] A. Simon, *J. Alloys Comp.*, 229 (1995) 158.
- [367] S.D. Waezsada, F.-Q. Liu, C.E. Barnes, H.W. Roesky, M.L. Montero, I. Usón, *Angew. Chem. Int. Ed. Engl.*, 36 (1997) 2625.
- [368] J. Besida, T.A. O'Donnell, T.K. Pong, D.G. Wood, *Abstracts of the 11th European Symposium on Fluorine Chemistry*, Bled, Slovenia, 1995, p. 21.
- [369] T.K. Pong, J. Besida, T.A. O'Donnell, D.G. Wood, *Ind. Eng. Chem. Res.*, 34 (1995) 308.

CHAPTER 3

Low Valent Transition Metal Fluorides

Howard C.S. Clark and John H. Holloway

Department of Chemistry, University of Leicester, Leicester, LE1 7RH, UK

3.1 Introduction

Although fluoride has generally been associated with high oxidation-state transition metal chemistry, there has been a gradually increasing interest in using fluoride as a ligand in low oxidation-state and organometallic systems. For the purpose of this Chapter we define 'low valent' metals as metals in +III oxidation state or lower.

There have been two valuable review articles on aspects of this topic area [1,2] and this Chapter seeks to summarise some of the main trends.

One of the principle problems that exists with the preparation of transition metal fluorides is the method of introducing the fluoride anion. There is no single reliable route that is applicable across the whole of the Periodic Table and the methodology required depends upon not only the metal in question but often also upon the coordination environment of the complex as a whole.

The most obvious synthetic route is via metathesis of an existing lower halide (chloride, bromide, iodide). Many such routes can be accomplished in a straightforward manner, using an alternative metal fluoride. Group 1 and 2 metal fluorides have been used extensively in conjunction with early transition metal fluorides in Groups 4–6 to give a variety of fluoride derivatives [1]. Apart from the low solubility of the alkali fluoride in many solvents, one of the major problems with this synthetic route is the incorporation of the fluorinating reagent into the final product. This makes separation of the compounds very difficult and, as a consequence, the use of excess of the fluorinating agent is ill-advised.

The use of silver fluoride rather than Group 1 and 2 fluorides is preferred for the fluorination of later transition metal species [2]. However, drying of this reagent is very difficult since it tends to coordinate water tenaciously, due to strong hydrogen bond interactions, often leading to the formation of hydroxy- and aquo-species. One route that is employed to overcome this has been to effectively prepare the silver fluoride in situ via the sequential addition of silver carbonate and ammonium fluoride. Similar chloride abstraction can also be achieved by use of other silver salts (AgOTf , AgBF_4) to generate cationic species which can react further with sources of fluoride such as TAS-F or $[\text{PPN}]\text{F}$.

An alternative fluorinating agent that has proved to be highly successful with Group 4–6 metal complexes, although of limited use with later groups, is Me_3SnF . This reagent, which has been developed and studied by Roesky and co-workers [1], has been described as an 'ideal fluorinating system', due to its low solubility and the high volatility of the generated trimethyl tin chloride, which enables facile removal of excess of reagent and by-product, whilst demonstrating a high tolerance for a range of ligands on the metal centre. If required, the trimethyltin fluoride can be regenerated by addition of either potassium or sodium fluoride to the trimethyltin chloride.

Protonolysis of metal-bound hydride and alkyl complexes with hydrofluoric acid provides another route into fluoride-containing species [1]. The metal–carbon bond is rapidly cleaved at low temperature by the action of the acid, yielding high purity forms of the desired metal fluoride. The major drawback of this technique is the need for extremely pure precursors since the presence of impurities, together with aHF, can often lead to rapid decomposition, and the requirement of special facilities to handle hydrofluoric acid, including all-metal vacuum lines and Teflon reaction vessels. This latter problem can be overcome by the use of the amine hydrofluoride salts, $\text{Et}_3\text{N} \cdot 3\text{HF}$ (TREAT-HF), $\text{C}_5\text{H}_2(\text{CH}_3)_3\text{N} \cdot 2\text{HF}$ (tmpy.2HF) and $\text{C}_5\text{H}_5\text{N} \cdot x\text{HF}$ (Olah's reagent). These reagents are mild enough to be used in glass reaction vessels without risk of etching.

Oxidative addition of metal centres with XeF_2 has led to the successful preparation of many metal fluorides. The choice of solvent can be rather critical to the reaction since, in dichloromethane, the XeF_2 exists as a discrete molecular entity whereas in HF, the adduct $[\text{F—Xe}]^+[\text{HF}_2]^-$ is formed, effectively polarising the F—Xe bond and creating a more reactive species. Unsurprisingly, the ratios of XeF_2 to complex are crucial since excess of the fluorinating reagent leads to the formation of by-products. Where the system allows, the XeF_2 can be substituted by fluorine gas (which is sparingly soluble in hydrofluoric acid and reacts at the solvent/gas interface), as, for example, in the fluorination of $[\text{Ir}_4(\text{CO})_{12}]$, in anhydrous HF, to *fac*- $[\text{IrF}_3(\text{CO})_3]$, since the use of an excess of XeF_2 leads to $[\text{XeF}][\text{IrF}_6]$ whereas, with fluorine gas, the reaction stops at $[\text{IrF}_3(\text{CO})_3]$ [3,4]. Other fluoride sources, such as EF_4 ($\text{E} = \text{S}, \text{Se}, \text{Te}$) and formyl fluoride can also be used to oxidatively add to the metal centre, providing alternative routes to metal bound fluorides.

The only other systematic route into metal fluorides is the use of metal fluoride starting materials and their subsequent substitution, such as in the reaction between $[\text{ScF}_3]$ and $[\text{NaCp}]$ or $[\text{MgCp}_2]$ to give a mixture including $[\{\text{ScF}(\text{Cp})_2\}_3]$ [5]. The clear restriction in this approach is the availability and isolation of appropriate starting materials.

The remaining routes into metal-bound fluorides really owe more to serendipity than to any systematic approach. C—F bond activation has led to several metal fluorides which are detailed extensively in a review article by Kiplinger, Richmond and Osterberg [6]. Decomposition of weakly coordinated anions can occur but frequently gives poor yields [7].

3.2 Group 3

Despite the obvious electronically compatible nature of the fluorine atom and the 'hard' Group 3 ion, there are remarkably few examples of Group 3 fluoride species. Presumably this can be attributed to the high air and moisture sensitivity displayed by complexes of this Group.

The reaction between either Cp_2Mg or CpNa with $[\text{ScF}_3]$ leads to a complex mixture of three compounds; an unidentified hexane-soluble species, a species characterised as $[\text{Cp}_3\text{Sc}]$ and a third toluene-soluble compound, identified as $[\{\text{ScF}(\text{Cp})_2\}_3]$, which has been crystallographically characterised [Fig. 1] [5]. The mixture was unaffected by variation of the ratio of the starting materials and, in solution, the fluoro complex exists as an equilibrium between the monomeric, dimeric and trimeric forms.

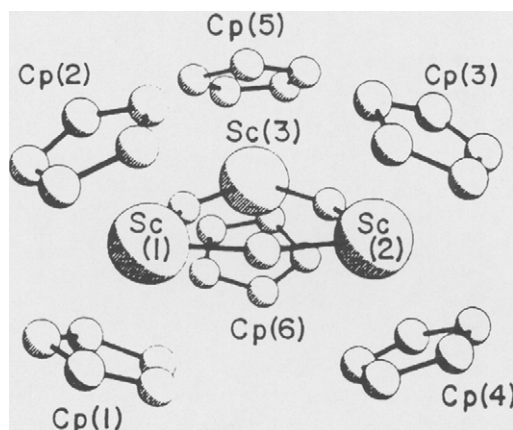


Fig. 1. The Molecular Structure of $[\{\text{ScF}(\text{Cp})_2\}_3]$ (Reproduced with permission from *J. Organomet. Chem.*, 291 (1985) 35–41. Copyright 1985 Elsevier).

The only other route to scandium fluoride derivatives has been via C—F bond activation of fluoro-alkenes with $[\text{ScR}(\text{Cp}^*)_2]$ ($\text{R} = \text{H}, \text{Me}$) to give $[\text{ScF}(\text{Cp}^*)_2]$ [1]. Very recent work has produced the first report of an organometallic yttrium fluoride. The reaction between $[(\text{C}_5\text{H}_5)_3\text{Y}]$ and Me_3NHF results in the isolation of $[\{(\text{C}_5\text{H}_5)_2\text{YF}(\text{THF})\}_2]$ which has been fully characterised by elemental analysis, infra-red, mass and NMR spectroscopies and X-ray diffraction [8].

3.3 Group 4

The area of Group 4 organometallic fluorides, which constitutes the vast bulk of the class of metal fluorides, has been comprehensively reviewed recently by Roesky and co-authors [1].

Recent Group IV chemistry has seen an upsurge in the number of amide derived species, and this has included fluoride derivatives. None of these compounds are of oxidation state +III or less, which are the subject of this review, but refer to titanium, zirconium or hafnium where the metal is the +IV state [1,9–12] and, consequently, not covered here.

3.4 Group 5

In general, Group 5 fluorides tend to adopt a preference for higher oxidation states, and as a consequence, over the past few years, there have been virtually no reported examples of low valent fluoro complexes of vanadium, niobium or tantalum.

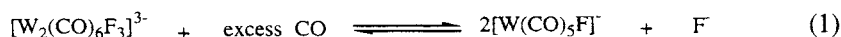
The reaction of $[\text{PEt}_4][\text{V}(\text{Cp})\text{I}(\text{CO})_3]$ with NaF under UV irradiation produces $[\text{PEt}_4][\text{V}(\text{Cp})\text{F}(\text{CO})_3]$, for which only the ^{51}V NMR and infrared spectral data were recorded [13].

The electrochemical reduction of $[(\text{EtCp}^*)_2\text{NbF}_2][\text{PF}_6]$ yields the paramagnetic complex, $[(\text{EtCp}^*)_2\text{NbF}_2]$, which produces a ten-line EPR spectrum with triplet hyperfine structure [14]. The complex is analogous to $[\text{Cp}_2\text{NbF}_2]$ (formed, in part, from the photolysis of $[\text{Cp}_2\text{NbH}_3]$ and $[\{\text{F}_3\text{CC}\}_2]$) and the extremely air-sensitive nature of both complexes precluded isolation [15].

3.5 Group 6

The preparation of fluoropentacarbonyl anions of chromium, molybdenum and tungsten, by reaction of the appropriate hexacarbonyl with salts such as KF, NEt_4F or $(\text{PPN})\text{F}$ is well established [16–19]. However, when the salt used was NMe_4F , the occurrence of dinuclear triplybridged anions $[\text{M}_2\text{F}_3(\text{CO})_6]^{3-}$ implied a more complex chemistry [20]. It has been noted [21] that, surprisingly, in the $[\text{M}(\text{CO})_5\text{X}]^-$ species reports, there was no indication of the expected enhanced CO lability of these complexes relative to that of other halide derivatives. This enhanced lability was predicted on the basis of the outcome of studies of the significant π -stabilisation of unsaturated derivatives by π -donor ligands, in which fluoride was reported to be a better π -donor than phenoxide [22,23]. In an effort to resolve this, the fluoride ligand in tungsten(0) carbonyl fluoride has been studied [21]. Addition of $[\text{W}(\text{CO})_5(\text{thf})]$ to one equivalent of anhydrous Et_4NF in tetrahydrofuran gave the dinuclear $[\text{Et}_4\text{N}]_3[\text{W}_2(\text{CO})_6\text{F}_3]$ which has been definitively characterised by infrared, ^{13}C NMR and X-ray crystallography [Fig. 2] [21].

It has been shown that the anion in this complex results from initial formation of $[\text{W}(\text{CO})_5\text{F}]^-$ which rapidly loses CO and dimerises with simultaneous incorporation of an additional fluoride ligand. This $[\text{W}_2(\text{CO})_6\text{F}_3]^{3-}$ anion reacts with CO in solution to give the fluoropentacarbonyl derivative (Eqn. (1)).



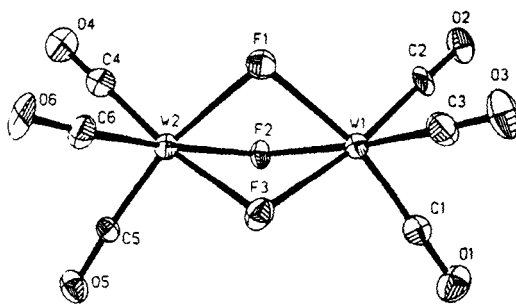


Fig. 2. The Molecular Structure of $[\text{W}_2(\text{CO})_6\text{F}_3]^{3-}$ Trianion (thermal ellipsoids are drawn at the 50% probability boundaries) (Reproduced with permission from *Inorg. Chem.*, 34 (1995) 4933–4934. Copyright 1995 American Chemical Society).

The average W—F distance in the complex is slightly longer than that observed in the related $[\{\text{W}(\text{CO})_2(\text{PMe}_2\text{Ph})_2\}_2(\mu\text{-F})_3][\text{BF}_4]$ [24] and the bond angles, F—W—F and W—F—W [21], compare with those of the phenoxide-bridged analogue $[\text{Et}_4\text{N}]_3[\text{W}_2(\text{CO})_6(\text{OPh})_3]$ [25,26]. However, $[\text{W}(\text{CO})_5\text{F}]^-$ is unstable in solution, reverting to the dinuclear complex in the absence of CO or, with prolonged exposure to CO, losing the fluoride ligand to form the hexacarbonyl [21].

Discussion of the reverse reaction of Eqn. (1) for other $[\text{W}(\text{CO})_5\text{X}]^-$ derivatives and the probability of possible hydrogen bonding of the fluoride ligand to methanol in the $[\text{W}(\text{CO})_5\text{F}]^-$ complex, prepared from $[\text{PPN}]\text{F}$ containing methanol, leads the authors to conclude that the fluoride ion in $[\text{W}(\text{CO})_5\text{F}]^-$ is as CO labilising as $[\text{OPh}]$, and perhaps more so [21].

Another route into the fluoropentacarbonyl anions and their relatives is via the reaction of silver fluoride with the anionic dimers, $[\text{M}_2(\text{CO})_{10}]$ ($\text{M} = \text{Cr}, \text{W}$) [26], the AgF acting, apparently, both as a source of fluoride and as an oxidising agent.

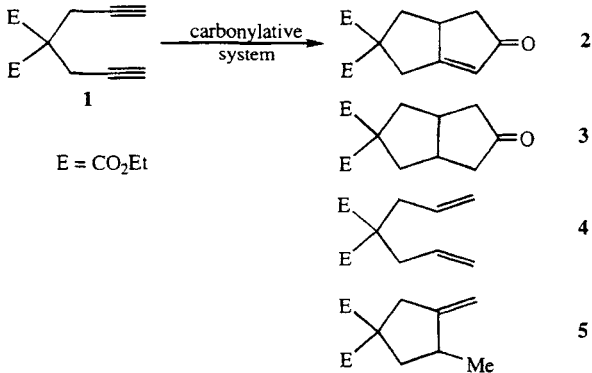
The role of fluoride ion in carbonylative insertion reactions in organic and organometallic enynes has been studied [27]. Whether it acts as a stabilising agent for the active ‘ $(\text{CO})_5\text{M}$ ’ fragments or as a carbonylation and/or insertion promoter is uncertain. However, it is evident from the results compared in Table 1 [27] and a related slower cycloaddition with organic enynes [28,29], thought to be triggered by thermal generation of $[\text{W}(\text{CO})_5(\text{thf})]$ in the absence of fluoride, that the fluoride system provides better control of the reaction product (cycloaddition rather than reduction) by modulation of the metal and counterion in shorter reaction times.

Other dinuclear, triply fluorine-bridged species, $[(\text{Ph}_3\text{P})_2(\text{CO})_2\text{M}(\mu\text{-F})_3\text{M}(\text{CO})_2(\text{PPh}_3)_2]^+[\text{BF}_4]^-$ ($\text{M} = \text{Mo}, \text{W}$) have been prepared by the reaction of $[\text{M}(\text{CO})_2(\text{PPh}_3)_2\text{Br}_2]$ with $[\text{AgBF}_4]$ [30].

Differences in the geometry of $[\text{Mo}(\text{CO})_2(\text{S}_2\text{CNEt}_2)_2(\text{tht})]$ ($\text{tht} = \text{SC}_4\text{H}_8$) and those of known $[\text{M}(\text{CO})_2(\text{S}_2\text{CNR}_2)_2\text{L}]$ structures ($\text{M} = \text{W}$; $\text{L} = \text{CO}$ [30], PPh_3 [31]) have prompted questions about whether this is due solely to the weak bonding of the tht to the metal or whether a stronger M—L bond to the seventh ligand might promote rearrangement to the mutually *cis*- $\text{M}(\text{CO})_2\text{L}$ unit observed for $\text{L} = \text{CO}$ and

Table 1

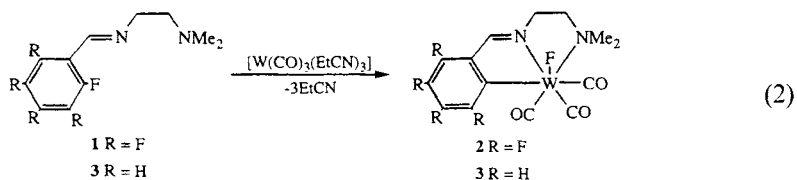
Reactions of different carbonylative systems with enyne (1)

 <p style="text-align: center;">$E = \text{CO}_2\text{Et}$</p>		
Carbonylative System	Yield of 2 (%)	Other products (yield %)
$\text{BU}_4\text{N}[(\text{CO})_5\text{WF}]$	56	3 (8), 4 (10), 5 (7)
$\text{BU}_4\text{N}[(\text{CO})_5\text{CrF}]$	10	4 (36)
$\text{K}(\text{DB18-C-6})[(\text{CO})_5\text{CrF}]$	59	traces
$\text{K}(\text{DB18-C-6})[(\text{CO})_5\text{WF}]$	52	traces
$[\text{Cr}(\text{CO})_5(\text{thf})]$	22 ^a	not detected

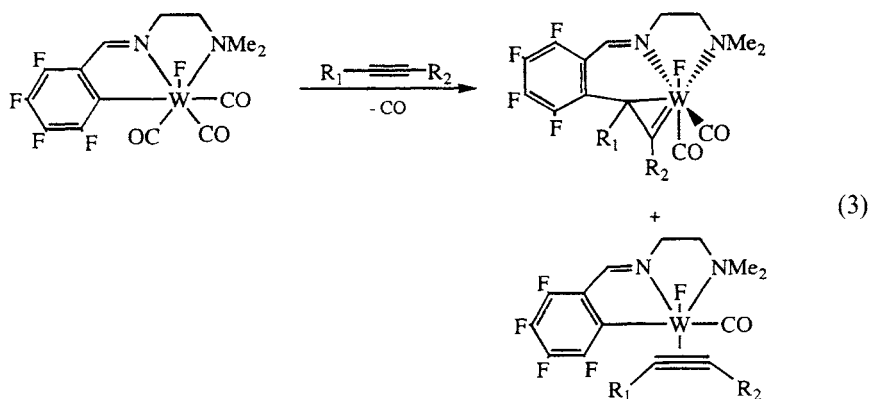
^a66% of the starting enyne was recovered

PPh_3 [32]. Preparation and structural investigation of the seven-coordinate $[\text{Et}_4\text{N}][\text{Mo}(\text{CO})_2(\text{S}_2\text{CNEt}_2)_2\text{F}]$ complex was carried out in order to try to answer these questions [33]. This has demonstrated that the idealised geometry of the seven-coordinate molybdenum carbonyl fluoride is that of a capped trigonal prism in which F occupies the capping site *trans* to both carbonyl groups. Extended Hückel calculations on $[\text{Mo}(\text{CO})_2(\text{S}_2\text{CNR}_2)_2]$, which has an OC-M-CO angle of 74.3° and the fluoride complex, which has a more acute angle (67.4°), have been carried out to probe factors that influence this [33].

The design of transition metal complexes capable of C—F bond activation for the functionalization of fluorocarbons has attracted attention recently. It has been known for several years that oxidative addition of an aromatic C—F bond takes place at tungsten(0) to yield stable tungsten(II) metallacycles, the cleaved carbon and fluorine atoms both finishing up bound to the metal centre (Eqn. (2)) [34–36].



More recently, a rare migration reaction of a highly fluorinated ligand at a tungsten(II) metal centre to give η^2 -vinyl compounds has been demonstrated (Eqn. (3)) [37]. A competitive reaction which involves the formation of four-electron donor alkyne complexes has been shown to be favoured for electron-rich alkynes [38,39]. Similar chemistry involving molybdenum(II) has also been outlined [40]. However, it has been shown that organonitriles do not take part in the migratory insertion reaction pathway outlined in Eqn. (3)



but rather π -bonded nitrile complexes in which the nitrile accesses both of its π orbitals for bonding are produced and this serves as a four electron donor ligand [6,41]. Now, a comparative study of η^2 -nitriles and η^2 -alkynes as four-electron donor ligands in tungsten(II) fluoride carbonyl systems has demonstrated that π -effects dominate the structures and reactivity of these systems. Both the alkyne and the nitrile ligands are orientated *cis* and parallel to the π -acid carbonyl ligand in these pseudooctahedral complexes and spectroscopic and X-ray crystallographic data show that the η^2 -nitrile ligand functions as a better π -acid/poorer base than the η^2 -alkyne ligand [42].

3.6 Group 7

The transition metal fluoro chemistry of manganese and rhenium up to the end of 1990 was comprehensively reviewed in 1991 [2]. Since then little has been published in this area. However, in their review Doherty and Hofman drew attention to the range of square planar d^8 complexes and the fact, that within such systems, halide affinity is greatest for fluoride ion when it is *trans* to a strong π acid [2]. They have now extended these studies to an octahedral d^6 system, [ReF(CO)₃(PPh₃)₂], which was selected on the basis of the stability of its heavier halo analogues and the fact that other [ReF(CO)₃L₂] derivatives and [MnF(CO)₃(PPh₃)₂] exist [43]. The *trans*-[ReF(CO)₃(PPh₃)₂] complex was prepared by reaction of *trans*-[ReCl(CO)₃(PPh₃)₂] with [Ag(SO₃CF₃)] followed by [N(PPh₃)₂F]. Both carbonyl exchange of the product with ¹³CO and its reaction with NCS⁻ was shown to

be far greater than for the chlorine-containing analogue. Also, reaction occurs with $[V(NSiMe_3)(OSiMe_3)_3]$ to give Me_3SiF and *trans*- $[(Me_3SiO)_3V=NRe(CO)_3(PPh_3)_2]$ whereas no reaction was observed for the chloro complex. This demonstrates the enhanced lability of the fluoro species and has provided the first example of condensation of a coordinatively saturated metal fluoro complex with a silylimido derivative [43].

In an effort to begin to understand how bulky pseudofluorides might influence the chemistry of low valent transition metals the reactions of metal carbonyl methyls with HF or HOTeF₅ have been investigated. This has shown that elimination of methane is a strong driving force in such reactions. The reaction of *cis*- $[Re(CO)_4(PPh_3)Me]$ with anhydrous HF gave *cis*- $[ReF(CO)_4(PPh_3)]$ and with HOTeF₅ produced the analogous teflate complex *cis*- $[Re(OTeF_5)(CO)_4(PPh_3)]$. The occurrence of these species also demonstrates that the $[OTeF_5]^-$ ligand and metal-bound methyl and triphenylphosphine ligands are mutually compatible [3b].

3.7 Group 8

In 1970 a product from the reaction of ruthenium pentafluoride with carbon monoxide was isolated and unambiguously characterized as $[Ru(CO)_3F_2]_4$ by X-ray crystallography [45]. Subsequently, it was shown that this could be reproducibly made by the controlled reaction of $[Ru_3(CO)_{12}]$ with XeF_2 in a molar ratio of 1:3 in 1,1,2-trichlorotrifluoroethane at room temperature and two other compounds, $[Ru(CO)_3F_3]$ and $[Ru(CO)_3F_2.RuF_5]_2$, were also reported [46]. A recent study of the reaction of $[Ru_3(CO)_{10}]$ with XeF_2 in anhydrous HF has allowed a detailed re-assessment of this work which has shown that, in solution, the major product of the reaction is *cis*- $[RuF_2(CO)_4]$ with $[RuF(CO)_5]^+$, $[Ru_2F_4(CO)_7]$, $[RuF(CO)_4]_2(\mu-F)^+$, *mer*- and *fac*- $[RuF_3(CO)_3]^-$, $[RuF_2(CO)_3]_n$ and $[RuF_2(CO)_3](\mu-F)[Ru(CO)_5]^+$ occurring as minor products [47]. All of these products were characterised by ^{13}C , ^{19}F and $^{13}C\{-^{19}F\}$ NMR spectroscopies. Removal of the solvent from any of the 3:1 molar ratio reaction mixtures yielded the pale yellow moisture-sensitive solid $[RuF_2(CO)_3]_4$ identified previously [45,46]. The polymerisation of the major, solution-stable, *cis*- $[RuF_2(CO)_4]$, with the loss of CO is paralleled by a very similar reaction with the analogous osmium system [48]. No evidence of $[Ru(CO)_3F_3]$ or $[Ru(CO)_3F_2.RuF_5]_2$ was observed [see Ref. 46]. In this case, reaction of $[Os_3(CO)_{12}]$ with XeF_2 in anhydrous HF gave *cis*- $[OsF_2(CO)_4]$ as the major product in solution, together with the minor products $[OsF(CO)_5]^+$, $[Os_2F_4(CO)_7]$ and $[OsF(CO)_4]_2(\mu-F)^+$. Again, all of these products were fully characterised by NMR spectroscopy and, again, removal of the HF solvent yielded the tetrameric $[Os(CO)_3F_2]_4$ species as a buff, moisture-sensitive powder [48]. Attention is drawn to the difference between this species and the heavier halide congeners which can all be isolated as monomers in the solid state and are polymerised to the halide-bridged dimers only at elevated temperatures. This implies that the fluoro complex has a greater carbonyl lability [48]. Interestingly, the latest results from our laboratory indicate that the same products can be formed by

the oxidation of the binary carbonyls with fluorine gas in anhydrous HF. This represents a more elegant and cleaner synthetic route to these complexes [49].

Having a reliable synthesis for pure $[\{\text{MF}_2(\text{CO})_3\}_4]$ ($\text{M} = \text{Ru}, \text{Os}$) has provided opportunities to investigate the chemistries of these species. Reaction of the tetramers with Lewis bases in organic solvents is a clean, high-yield route to air- and moisture-stable ruthenium and osmium(II) fluoride-containing coordination compounds, $[\text{MF}_2(\text{CO})_2\text{L}_2]$ [50].

The X-ray single crystal structures of three of these complexes, $[\text{OC-6-13}][\text{MF}_2(\text{CO})_2(\text{PR}_3)_2]$ [$\text{M} = \text{Ru}$, $\text{PR}_3 = \text{PEtPh}_2$; $\text{M} = \text{Os}$, $\text{PR}_3 = \text{PPh}_3$ or $\text{P}(\text{C}_6\text{H}_{11})_3$] have been determined and show that the geometry about the central metal atoms in all three is distorted pseudo-octahedral, and in each case the phosphine ligands are bent towards the fluoride ligands and exhibit intramolecular $\text{H}\cdots\text{F}$ interactions [47].

Further demonstration of the value of XeF_2 for the introduction of fluorine into low valent ruthenium and osmium is evidenced by the stepwise fluorination of neutral five-coordinate $[\text{M}(\text{CO})_3(\text{PPh}_3)_2]$ ($\text{M} = \text{Ru}$ or Os) via the metal fluoroacyl complexes, $[\text{MF}(\text{COF})(\text{CO})_2(\text{PPh}_3)_2]$, to give the low valent metal fluorides, $[\text{OC-6-13}][\text{MF}_2(\text{CO})_2(\text{PPh}_3)_2]$. In the ruthenium case the fluoroacyl complex decomposes by elimination of CO at room temperature but, for the analogous osmium complex, heating in solution for several hours is required [51]. The mechanism of the reaction, which has been probed by the addition of BF_3 , has been shown to involve oxidation of the metal centre by $[\text{XeF}]^+$ followed by nucleophilic attack at the coordinated CO by F^- . Here also, crystallographic characterisation of $[\text{OC-6-13}][\text{RuF}_2(\text{CO})_2(\text{PPh}_3)_2]$ has confirmed the *cis*-octahedral formation indicated by solution NMR data.

Recently, another approach to introducing fluoride ligands into organometallic and coordination compounds by the reaction of anhydrous HF with a metal hydride, with elimination of hydrogen gas has been tested [52]. Reaction of $[\text{OC-6-13}][\text{MH}_2(\text{CO})_2(\text{PPh}_3)_2]$ ($\text{M} = \text{Ru}$ or Os) with anhydrous HF with elimination of dihydrogen gives the previously known $[\text{OC-6-13}][\text{MF}_2(\text{CO})_2(\text{PPh}_3)_2]$. In the case of $[\text{OC-6-13}][\text{MF}_2(\text{CO})(\text{PPh}_3)_3]$, elimination of the H_2 is accompanied by loss of one phosphine ligand and aggregation to give a novel, triply fluorine-bridged, dinuclear cation in $[\text{M}_2(\mu\text{-F})_3(\text{CO})_2(\text{PPh}_3)_4][\text{HF}_2]$. Anion exchange with $\text{Na}[\text{BPh}_4]$ gave air-stable products which were characterised by mass spectrometry, NMR and metal-edge EXAFS to confirm their dinuclear structures [52]. The complexes $[\text{MF}_2(\text{CO})_2(\text{PR}_3)_2]$ also react with a variety of other reagents, such as MeLi to give $[\text{MMe}_2(\text{CO})_2(\text{PR}_3)_2]$ and BF_3 to yield $[\text{MF}(\text{CO})_2(\text{PR}_3)_2][\text{BF}_4]$. Trimethyl silyl reagents can also be employed resulting in elimination of trimethylsilyl fluoride and formation of either $[\text{OsF}(\text{X})(\text{CO})_2(\text{PR}_3)_2]$ or $[\text{RuX}_2(\text{CO})_2(\text{PR}_3)_2]$ ($\text{X} = \text{CN}^-$, NCO^-) and $[\text{M}\{\text{C}(\text{O})\text{CF}_3\}_2(\text{CO})_2(\text{PR}_3)_2]$ [53].

A ruthenium hydride fluoride, $[\text{RuHF}(\text{CO})\text{L}_2]$ ($\text{L} = \text{P}^i\text{Bu}_2\text{Me}$) has also figured in new chemistry of CF_2 as a ligand [54]. The complex was prepared by reaction of $[\text{RuHCl}(\text{CO})\text{L}_2]$ and anhydrous CsF in acetone. Compounds of the same general formula have also been used in detailed studies on reactivity and stereochemistry of ligands attached to ruthenium centres. Thus, the relative electron-donating ability

of X in the coordination complexes $[\text{RuHX}(\text{CO})(\text{P}^t\text{Bu}_2\text{Me})_2]$ ($\text{X} = \text{I}, \text{Br}, \text{Cl}, \text{F}, \text{OPh}, \text{OH}, \text{OCH}_2\text{CF}_3, \text{OEt}, \text{OCPh}_3, \text{OB}(\text{mesityl})_2, \text{OSiR}_3, \text{NHPh}, \text{SPh}$ or C_2Ph) has been evaluated based on the CO stretching frequency [55], and modulation of reactivity and stereochemistry of substrate binding by X in the complex $[\text{RuHX}(\text{CO})(\text{P}^t\text{Bu}_2\text{Me})_2]$ [56]. In the latter case, the reactivity of the complex with $\text{G}-\text{H}$ ($\text{G} = \text{H}, \text{SiR}_3$ or C_2Ph) occurs exclusively at the $\text{Ru}-\text{H}$ bond for $\text{X} = \text{Cl}$ and I . For fluoride or an oxygen-based X such as OCH_2CF_3 or OSiPh_3 , reactivity is dominated by cleavage of the $\text{Ru}-\text{X}$ bond. The reactivity of $[\text{RuHF}(\text{CO})(\text{P}^t\text{Bu}_2\text{Me})_2]$, however, is unique since this compound displays activity at both the $\text{Ru}-\text{H}$ and the $\text{Ru}-\text{F}$ bond [56].

Experiments in which introduction of bulky pseudofluorides to try to understand the way they might influence the chemistry of low-valent metals was described in Section 3.6 in respect of rhenium complexes. The same thinking has been applied in the case of osmium and the reaction of *cis*- $[\text{Os}(\text{CO})_4\text{Me}_2]$ with on the one hand, HF and on the other, HOTeF_5 have resulted in methane elimination and the formation of *cis*- $[\text{OsF}_2(\text{CO})_4]$ and *cis*- $[\text{Os}(\text{OTeF}_5)(\text{CO})_4\text{Me}]$ respectively [44]. This offers the promise that methane elimination from hydrides will be a useful route into other low-valent fluoro derivatives.

3.8 Group 9

3.8.1 Cobalt Fluorides

Due to the low solubility of cobalt(II) fluoride in most solvents, formation of cobalt fluoro N-donor complexes (which are the only low-valent cobalt fluorides which are reliably reported) features a variety of starting materials. A common theme that runs throughout this work has been the use of $[\text{Co}(\text{BF}_4)_2]$ as the fluoride source, and the subsequent ‘controlled’ decomposition to obtain a metal-bound fluoride. This has been done, for example, with tris- $\{(3,5\text{-dimethyl-pyrazol-1-yl})\text{methyl}\}$ amine (amtd) to give $[\text{M}_2(\text{amtd})_2\text{F}(\text{BF}_4)_3(\text{EtOH})_x(\text{H}_2\text{O})_y]$ ($\text{M} = \text{Co}, \text{Cu}, \text{Zn}; x = 0\text{--}1.5, y = 1\text{--}2$). The cobalt complex has been structurally characterised by X-ray diffraction [Fig. 3] [57]. Similarly, the combination of $[\text{M}(\text{BF}_4)_2]$ ($\text{M} = \text{Mn}, \text{Co}, \text{Ni}$), $[\text{M}(\text{NO}_3)_2]$, $\text{NH}_4(\text{NCS})$ and 3,5-diethyl-1,2,4-triazole (detrH) produces $[\text{M}_3(\text{detrH})_6(\text{NCS})_4\text{F}_2(\text{H}_2\text{O})_2]$, which has also been structurally characterised. This complex can also be prepared from MF_2 , detrH and $[\text{M}(\text{NCS})_2]$ [58]. This same preparative method has also been used with a variety of substituted triazole ligands to yield complexes of the form $[\text{M}_3\text{L}_4\text{F}_2(\text{NCS})_4(\text{H}_2\text{O})_x]$ ($\text{M} = \text{Co}, \text{Ni}$) [59].

Other starting materials have included $[\text{Co}(\text{OH})_2]$, together with hydrazine hydrate, 40% hydrofluoric acid and a variety of amine ligands to produce several cobalt(II) fluorides (e.g. $[\text{Co}(\text{N}_2\text{H}_4)_2\text{F}_2] \cdot 2\text{H}_2\text{O}$, $[\text{Co}(\text{dmpz})\text{F}_2(\text{H}_2\text{O})_2] \cdot 2\text{H}_2\text{O}$, $[\text{phenH}][\text{CoF}_3(\text{phen})] \cdot 8\text{H}_2\text{O}$ and $[\text{bipyH}][\text{CoF}_3(\text{bipy})] \cdot 6\text{H}_2\text{O}$) [60]. The dmpz complex has also been formed in situ from either $[\text{Co}(\text{acac})_2]$, F^- and $\text{N}_2\text{H}_4 \cdot 2\text{H}_2\text{O}$ or $[\text{CoF}_2(\text{N}_2\text{H}_4)_2]$, F^- and acacH_2 .

Finally, the addition of $[\text{AgBF}_4]$ to $[\{\eta^3\text{-HB}(3\text{-Bu}^t\text{pz})_3\}\text{MCl}]$ ($\text{M} = \text{Fe}, \text{Co}$) results in abstraction of F^- from the BF_4^- to give $[\{\eta^3\text{-HB}(3\text{-Bu}^t\text{pz})_3\}\text{MF}]$ [Fig. 4]. The

formation of the complex is accredited to the Lewis acidity of the generated cationic metal complex [61].

3.8.2 Rhodium and Iridium carbonyl fluorides

The study of Group 9 carbonyl fluoride derivatives in the +1 oxidation state has revolved solely around fluoro derivatives of Vaska's complex, $[\text{MF}(\text{CO})(\text{PR}_3)_2]$ ($\text{M} = \text{Ir}, \text{Rh}$). The preparation of $[\text{MF}(\text{CO})(\text{PPh}_3)_2]$ was originally the outcome

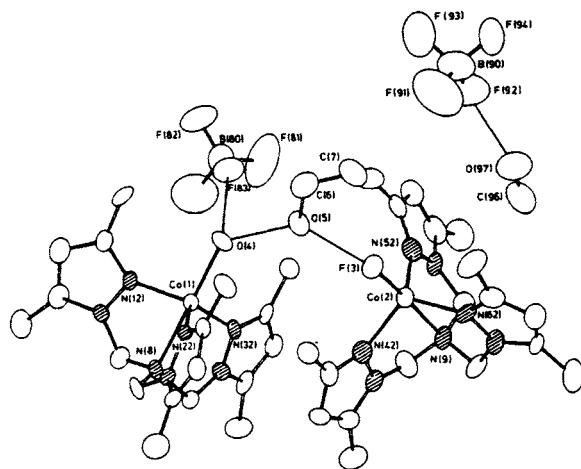


Fig. 3. The Molecular Structure of $[\text{Co}_2(\text{amtd})_2\text{F}(\text{BF}_4)_3(\text{EtOH})_x(\text{H}_2\text{O})]$ (hydrogen atoms are omitted) (Reproduced with permission from *Inorg. Chem.*, 24 (1985) 2919–2925. Copyright 1985 American Chemical Society).

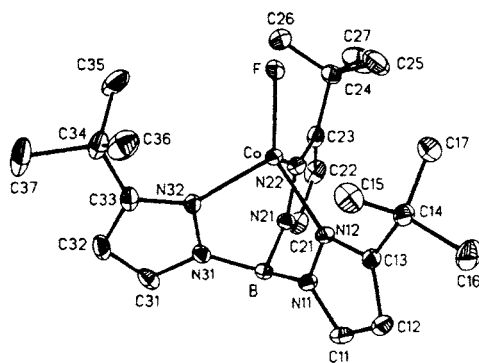


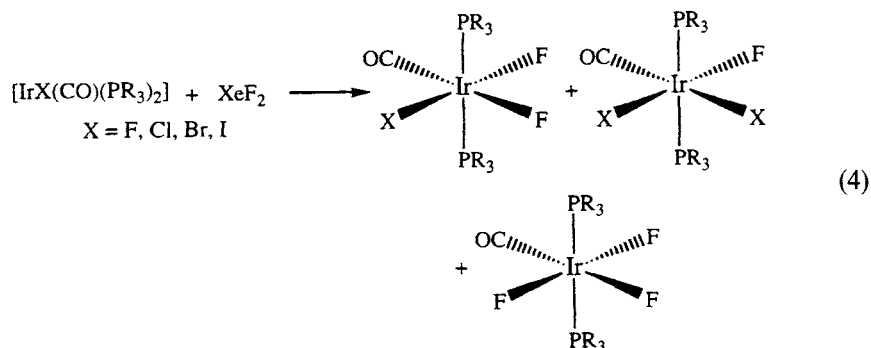
Fig. 4. The Molecular Structure of $[\eta^3\text{-HB}(3\text{-Bu}'\text{pz})_3\text{CoF}]$ (thermal ellipsoids are drawn at the 20% probability boundaries) (Reproduced with permission from *Inorg. Chem.*, 29 (1990) 2452–2456. Copyright 1990 American Chemical Society).

of a reaction between AgF and $[\text{MCl}(\text{CO})(\text{PPh}_3)_2]$ in boiling acetone, but this synthetic approach was limited solely to the triphenylphosphine, tris-*p*-tolylphosphine and triphenylarsine derivatives [62]. A more recent route has been the preparation of $[\text{M}(\text{Me})(\text{CO})(\text{PR}_3)_2]$ and subsequent addition of anhydrous hydrofluoric acid. This has led to the preparation of a wide range of fluoro Vaska's analogues, for $\text{PR}_3 = \text{PPh}_3, \text{PEt}_2\text{Ph}, \text{PEt}_3$ [4].

Contrary to the Pearson hard/soft acid/base predictions [63], the strength of the metal-halide bond in $[\text{MX}(\text{CO})(\text{PPh}_3)_2]$ ($\text{M} = \text{Rh}, \text{Ir}$) follows the trend $\text{X} = \text{F}^- > \text{Cl}^- > \text{Br}^- > \text{I}^-$ in anhydrous CH_2Cl_2 [64]. However, in protic solvents, the F^- anion becomes far more labile, presumably due to strong hydrogen bonding between the solvent and the uncomplexed F^- anion. This property has been utilised to prepare a wide range of derivatives, via metathesis of the F^- group in methanol [65].

Oxidative addition of a variety of 'small' molecules, such as $\text{O}_2, \text{I}_2, \text{MeI}, \text{HX}$ ($\text{X} = \text{F}, \text{Cl}, \text{Br}, \text{I}, \text{SH}$) to Vaska's style complexes has been extensively studied and reported in the literature, but has resulted in the formation of only a handful of poorly characterised fluoride species [2]. Since this work is generally outside the scope of this article, these compounds are not detailed here. However, the reader is directed towards a review article by Doherty and Hoffman for further information [2].

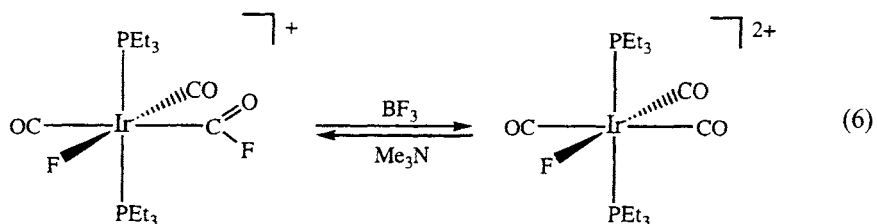
There have been a number of other well-documented iridium and rhodium carbonyl fluoride phosphines prepared via oxidative addition to an iridium or rhodium(I) metal centre that have been detailed recently [66]. A variety of iridium(III) fluorides can be prepared either by oxidative addition of a substrate to $[\text{IrF}(\text{CO})(\text{PPh}_3)_2]$ to give species such as $[\text{IrFI}_2(\text{CO})(\text{PPh}_3)_2]$ or $[\text{IrFI}_2(\text{CO})(\text{PPh}_3)_2]$, or by the use of a fluoride-containing substrate such as formyl fluoride with $[\text{IrCl}(\text{CO})(\text{PR}_3)_2]$, yielding $[\text{IrFClH}(\text{CO})(\text{PR}_3)_2]$ [66]. One of the simplest and cleanest methods of adding ' F_2 ' to an iridium(I) or rhodium(I) centre is using XeF_2 . Xenon difluoride oxidatively adds to $[\text{IrX}(\text{CO})(\text{PEt}_3)_2]$ ($\text{X} = \text{Cl}, \text{Br}, \text{I}$) to give the six coordinate iridium(III) species, $[\text{IrXF}_2(\text{CO})(\text{PEt}_3)_2]$, as the principle product, with minor contamination from both $[\text{IrFX}_2(\text{CO})(\text{PEt}_3)_2]$ and $[\text{IrF}_3(\text{CO})(\text{PEt}_3)_2]$. This work has now been extended to incorporate a range of different phosphine ligands and, in one case, the use of the iridium(I) fluoro starting material to yield the Ir(III)F_3 complex [Eqn. (4)] [4].



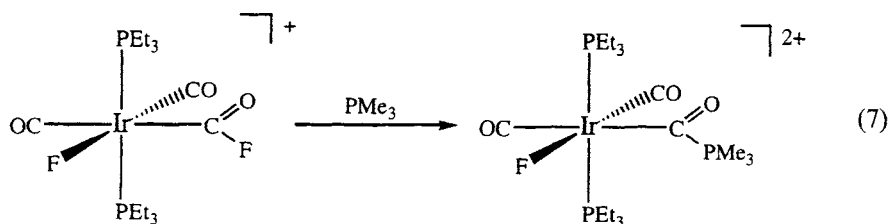
In a similar vein, the addition of XeF_2 to $[\text{Ir}(\text{CO})_3(\text{PR}_3)_2]^+$ results in addition of 'F₂' across an Ir—C bond to give the fluoroacyl derivative, $[\text{IrF}(\text{CO})_2\{\text{C}(\text{O})\text{F}\}(\text{PEt}_3)_2]^+$ [Eqn. (5)], which has been characterised by X-ray crystallography and multinuclear NMR spectroscopy [66]. The basicity of the phosphine is vital to this reaction. The use of the more basic phosphines (PMe_3 , PMe_2Ph , PEt_2Ph and PEtPh_2) all result in formation of the fluoroacyl derivative (although the PEtPh_2 complex is unstable at room temperature) whereas, when the phosphine is PPh_3 or PPh_2Me there is no evidence of reaction. The use of the highly basic PCy_3 also fails to yield a fluoroacyl product and this is believed to be a result of the steric bulk of the phosphine blocking the reaction [66].



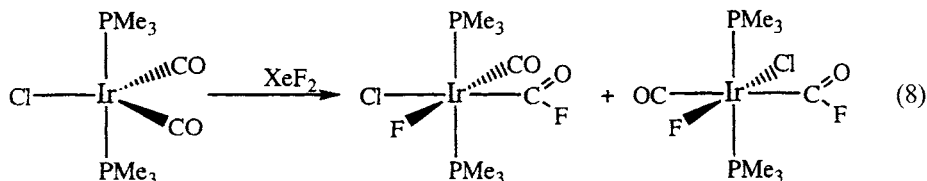
The fact that the fluoride on the acyl group is very reactive can be seen upon addition of SiH_3X ($\text{X} = \text{CN}, \text{NCO}, \text{NCS}$) where, even in the presence of excess of silyl reagent, the Ir—F bond remains intact whilst the acyl fluoride is substituted, concomitant with the formation of a silyl fluoride [66]. Similarly, addition of BF_3 cleanly abstracts the acyl fluoride to give the tris carbonyl dication, $[\text{IrF}(\text{CO})_3(\text{PEt}_3)_2]^{2+}$. The reverse reaction can also be achieved by addition of NMe_3 to form Me_3NBF_4 and regenerate the monocationic fluoroacyl species [Eqn. (6)] [66].



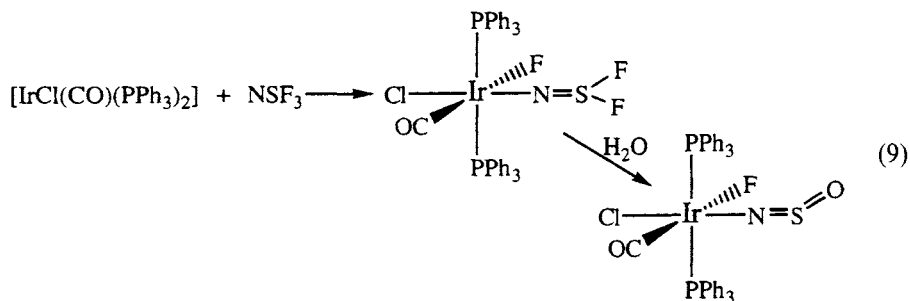
Use of an alternative Lewis base, namely PMe_3 , results in a very unusual reaction where, initially, the fluoroacyl species is reformed and then further reaction results in substitution of the acyl fluoride for PMe_3 to yield $[\text{IrF}(\text{CO})_2\{\text{C}(\text{O})\text{PMe}_3\}(\text{PEt}_3)_2]^+$ [Eqn. (7)] [66].



In a similar vein to that of the previous XeF_2 reaction, the product of the reaction between $[\text{IrCl}(\text{CO})_2(\text{PMe}_3)_2]$ and XeF_2 yields two isomeric forms of $[\text{IrClF}(\text{CO})\{\text{C}(\text{O})\text{F}\}(\text{PMe}_3)_2]$ [Eqn. (8)]. Overall, it appears that XeF_2 attacks the metal centre as XeF^+ and F^- , which would support the observation that the more basic phosphines facilitate reaction.



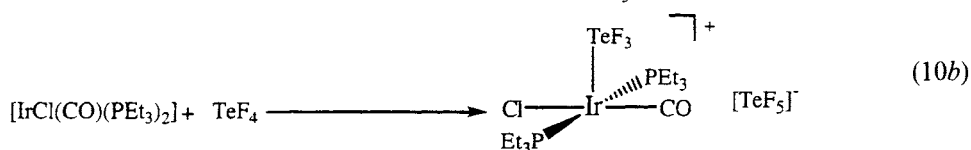
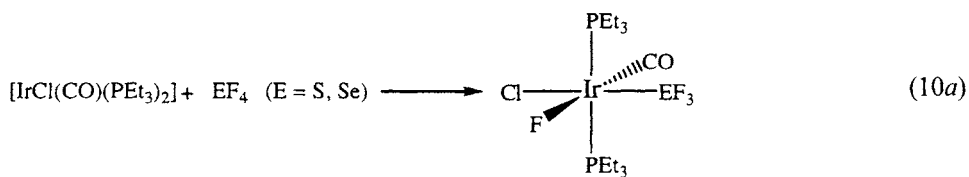
Other fluoride-containing species can be similarly utilised to oxidatively add to iridium or rhodium, transferring F^- to the metal centre in the process. Reaction of NSF_3 with $[\text{IrCl}(\text{CO})(\text{PPh}_3)_2]$ gives the novel thiazyl difluoride complex, $[\text{IrClF}(\text{CO})(\text{PPh}_3)_2(\text{NSF}_2)]$, which is the first example of thiazyl difluoride acting as a ligand [67]. The complex is extremely moisture sensitive and decomposes in the presence of water to the NSO complex, $[\text{IrClF}(\text{CO})(\text{PPh}_3)_2(\text{NSO})]$ [Eqn. (9)].



Oxidative addition across an $\text{S}-\text{F}$ bond can be observed in the reaction between SF_4 and $[\text{IrCl}(\text{CO})(\text{PEt}_3)_2]$ which yields the complex $[\text{IrClF}(\text{SF}_3)(\text{CO})(\text{PEt}_3)_2]$. This compound has been shown to be highly fluxional with at least two and maybe even three different exchange processes occurring. These are heavily influenced by the nature of the phosphine as well as the anionic ligand. Similar reactions have been carried out on the analogous rhodium complexes and the results are similar, although the final products tend to be less stable with the formation of isomeric products [66].

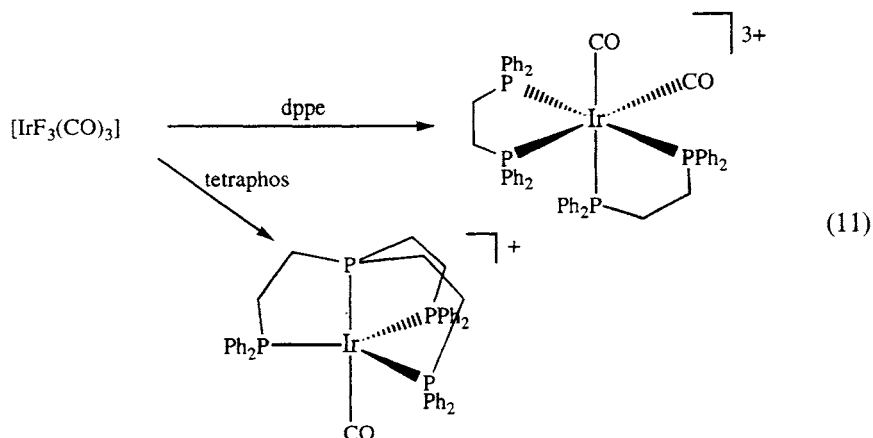
This reaction occurs with other chalcogen fluorides, such that the addition of SeF_4 to $[\text{RhX}(\text{CO})(\text{PEt}_3)_2]$ ($\text{X} = \text{Cl}, \text{Br}, \text{I}, \text{NCS}, \text{NCO}$) produces the complexes

$[\text{RhXF}(\text{SeF}_3)(\text{CO})(\text{PEt}_3)_2]$ [e.g. see Eqn. (10a)], which are less thermally stable than the sulfur analogues. In contrast, addition of TeF_4 to $[\text{RhCl}(\text{CO})(\text{PEt}_3)_2]$ produces $[\text{RhCl}(\text{CO})(\text{TeF}_3)(\text{PEt}_3)_2][\text{TeF}_5^-]$ [Eqn. (10b)]. Here, the excess of TeF_4 is a sufficiently strong Lewis acid to abstract fluoride from the metal centre. Similar reactions with SF_6 or NF_3 lead either to no reaction, in the case of the former, or to a multitude of products for the latter [66].

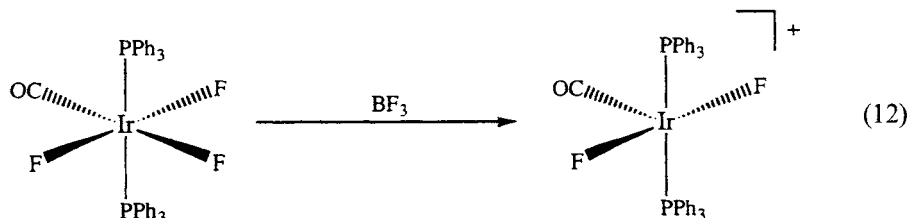


Instead of oxidative addition of XeF_2 to an Ir(I) centre, an alternative route into Ir(III) trifluoride chemistry is to begin with an Ir(III) fluorocarbonyl species and allow this to react with various Lewis bases. This is now possible following the reliable synthesis of *fac*- $[\text{IrF}_3(\text{CO})_3]$, which can be prepared by the reaction of $[\text{Ir}_4(\text{CO})_{12}]$, dissolved in aHF, with XeF_2 in a 1:6 ratio. This reaction has been repeated subsequently utilising F_2 gas rather than XeF_2 as the source of fluorine [4]. In both cases this yields a mixture of *mer*- and *fac*- $[\text{IrF}_3(\text{CO})_3]$ which, on removal of the solvent and then re-dissolution in aHF, yields only the *fac*-isomer, indicating that this is the preferred thermodynamic isomer [3]. Addition of an excess of XeF_2 results in elimination of COF_2 from the metal centre and ultimately the formation of $[\text{XeF}][\text{IrF}_6]$. The only previously reported iridium(III) carbonyl fluoride appears to have been incorrectly analysed as $[\text{IrF}_2(\text{CO})_{2.5}]$ [68] and is more probably correctly assigned as $[\text{IrF}_3(\text{CO})_3]$. Addition of a variety of monodentate alkyl and aryl phosphines to $[\text{IrF}_3(\text{CO})_3]$ results in the formation of complexes of the form, $[\text{IrF}_3(\text{CO})(\text{PR}_3)_2]$, where the phosphines are arranged in a *trans* configuration [69,70]. The greatest synthetic challenge in this reaction is the rigorous exclusion of all traces of water from the reaction mixture since *fac*- $[\text{IrF}_3(\text{CO})_3]$ is extremely moisture sensitive and contamination of the final product with hydroxyl-containing species is common. Addition of an excess of phosphine, in the case of the PMe_3 reaction, leads to formation of an impurity, namely $[\text{IrF}_4(\text{CO})\text{PMe}_3][\text{Ir}(\text{CO})\text{PMe}_4]$. The compounds NMe_3 and AsPh_3 can also be employed as the Lewis base to form the appropriate tris fluoride complexes. However, use of multi-dentate phosphines, for example dppe or tetrachos, results in elimination of F^- from the metal centre

to give iridium(I) or iridium(III) carbonyl phosphine cations respectively [Eqn. (11)] [70].



In a somewhat surprising result, addition of BF_3 to $[\text{Ir}(\text{CO})\text{F}_3(\text{PR}_3)_2]$ ($\text{R} = \text{Cy}, \text{Ph}$) results in abstraction of F^- from the metal. However, in contrast to previous work indicating that fluoride *trans* to a carbonyl ligand is a particularly stable arrangement, it is this fluoride and not the fluoride *trans* fluoride that is abstracted to form $[\text{IrF}_2(\text{CO})(\text{PR}_3)_2][\text{BF}_4]$ [Eqn. (12)] [4].



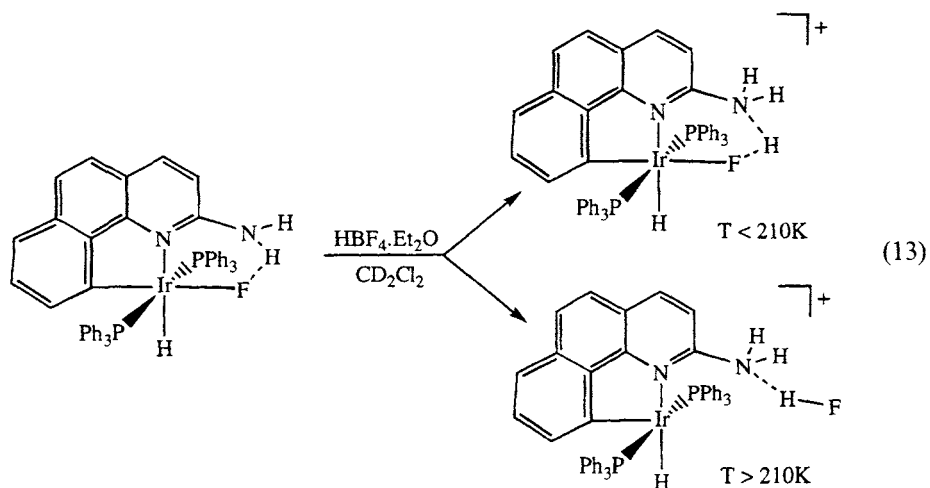
3.8.3 Rhodium and Iridium co-ordination chemistry

In the last thirteen years, despite the preparation of the potentially highly versatile fluorinated synthon, $[\text{RhF}(\text{C}_8\text{H}_{10})]_n$ and subsequent displacement of the olefin by both phosphine ligands and carbon monoxide to give a variety of compounds [70], there has been remarkably little interest in co-ordination compound fluoride derivatives of this Group. In particular, there has been no systematic research involving a variety of starting materials and fluoride sources. There are, however, a number of examples of reactions in which halide exchange in conjunction with displacement of olefinic ligands on the metal centre occurs. For example, the reaction between $[\{\text{RhCl}(\text{C}_2\text{H}_4)(\text{C}_2\text{F}_4)_2\}_2]$ and AgBF_4 , followed by addition of TAS-F, results in the formation of $[\{\text{RhF}(\text{C}_2\text{H}_4)(\text{C}_2\text{F}_4)\}_4]$ [72]. This tetramer can then undergo a series of reactions reminiscent of those of the $[\text{RhF}(\text{C}_8\text{H}_{10})]_n$ complex

in which addition of triphenylphosphine gives $[\text{RhF}(\text{C}_2\text{H}_4)(\text{PPh}_3)_2]$, subsequent addition of carbon monoxide yields $[\text{RhF}(\text{CO})(\text{PPh}_3)_2]$ and, finally, the fluoride can be exchanged at the metal centre for a triflate group by using trimethylsilyltriflate. This anion exchange was also observed again when the weak iridium fluoride bond in both $[\text{Ir}(\text{H})_2\text{F}(\text{P}^t\text{Bu}_2\text{Ph})_2]$ (prepared from the reaction between $[\text{Ir}(\text{H})_2\text{Cl}(\text{P}^t\text{Bu}_2\text{Ph})_2]$ and NMe_4F) and $[\text{IrHF}(\eta^2\text{-CH}_2\text{CMe}_2\text{P}^t\text{BuPh}) (\text{PtBu}_2\text{Ph})]$ was cleaved at room temperature by a variety of trimethylsilyl reagents, exchanging the fluoride for a large number of alternative anions (e.g. OTf , OPh , N_3 , NCO , NCS , SPh) [73,74].

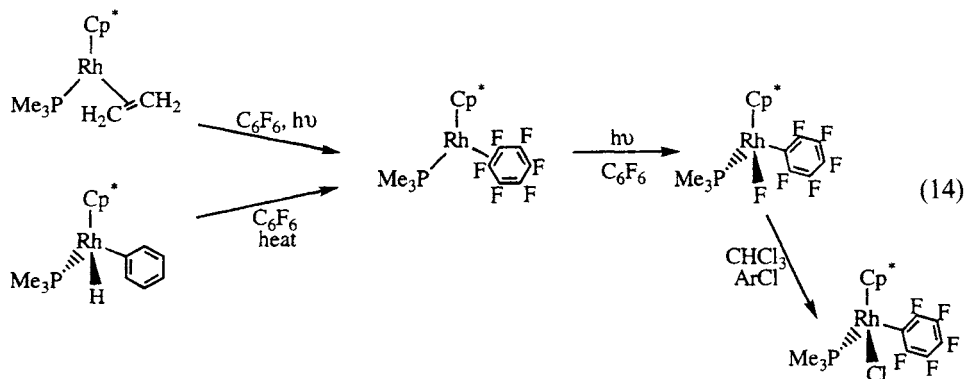
The displacement of cyclooctene or C_2H_4 from an iridium(I) centre by a variety of chiral phosphines (L) leads to the formation of $[\{(\text{L})\text{IrCl}\}_2]$ which, in conjunction with a source of F^- (phosphazanium fluoride), has been used for catalytic hydroamination of olefins. This combination leads to a 6.5 fold increase in the activity of the system and a total reversal in the enantioselectivity compared to that of the chloride analogue. There is no direct evidence of formation of a metal fluoride complex, but it is proposed that it may well form *in situ* and that this might explain these interesting results [75].

The value of the use of alkyl ammonium fluoride can also be seen in the reaction between $[\text{Ir}(2\text{-amino-7,8-benzoquinone})(\text{PR}_3)_2\text{H}(\text{OH}_2)]^+$ and $[\text{nBu}_4\text{N}]\text{F}$ which, at low temperature, gives an iridium(III) fluoride, as evidenced by ^1H NMR spectroscopic data. Protonolysis of the pendant NH_2 group at low temperature with HBF_4 leads to hydrogen bonding between the NH_3^+ group and the F^- anion and, as the complex warms above 210 K, the metal fluoride bond cleaves irreversibly to yield HF , co-ordinated to the amine group [Eqn. (13)] [76].

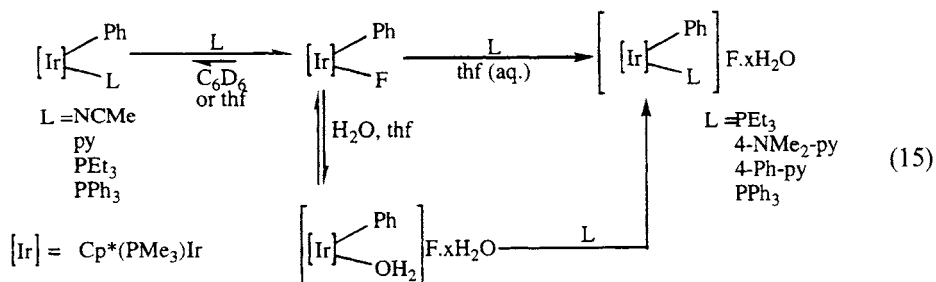


Some particularly elegant work by Perutz and co-workers has resulted in the co-ordination of hexafluorobenzene to a rhodium(I) centre to give $[\text{Rh}(\text{Cp}')(\text{PMe}_3)(\eta^2\text{-C}_6\text{F}_6)]$ ($\text{Cp}' = \text{Cp}, \text{Cp}^*$). Photolysis of this complex gives rise to insertion of the metal centre into one of the $\text{C}-\text{F}$ bonds to yield $[\text{RhCp}'(\text{F})(\text{C}_6\text{F}_5)(\text{PMe}_3)]$.

However, since the photolysis reaction is performed with the compound dissolved in C_6F_6 , it has proved impossible to determine whether this is an inter- or intra-molecular reaction. Exchange of the fluoride anion for chloride occurs rapidly in chloroform in the presence of $ArCl$ [77,78]. These reactions are summarised in Eqn. (14).



The labile nature of the Ir—F bond is also displayed in the displacement of F^- from $[IrCp^*F(PMe_3)(Aryl)]$ ($Aryl = Ph, p\text{-tolyl}$) by the addition of excess of phosphine. The complex $[IrCp^*F(PMe_3)(Aryl)]$ is prepared from the addition of TAS-F to $[IrCp^*OTf(PMe_3)(Aryl)]$ and, in the presence of excess of phosphine or amine (L), displacement of the fluoride anion from the metal centre gives $[IrCp^*(PMe_3)(Aryl)(L)]F$. These complexes are in equilibrium which lies over to the side of the uncharged species. The same reaction performed in wet solvent produces $[IrCp^*(PMe_3)(Ph)(OH_2)]F \cdot xH_2O$ very rapidly and is undoubtedly facilitated by strong hydrogen bonding between the water and the fluoride anion [see Eqn. (15)]. The anion can be similarly abstracted using BPh_3 to yield $[IrCp^*(PMe_3)(Aryl)(L)][BPh_3F]$ in which the vacant site created is readily filled by a Lewis base [79].

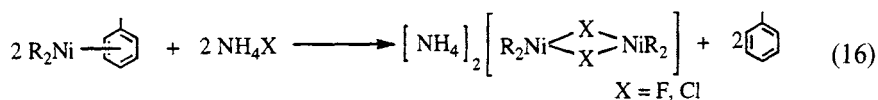


3.9 Group 10

3.9.1 Nickel

There are, in fact, very few reports of nickel(II) fluoride complexes in the literature over the past thirteen years. The formation of a nickel fluorine bond has been implied in two separate reports of organic couplings. However, there has been no characterising spectroscopic data and the suggested mechanisms which may give rise to the Ni—F bonds have been based only upon the products obtained [80,81].

In the handful of reports that can be confidently believed, there has been a surprisingly high proportion of crystal structures published. For example, the reaction between $[\text{NiR}_2(\eta^6\text{-arene})]$ ($\text{R} = \text{C}_6\text{F}_5$, SiCl_3) and NH_4X ($\text{X} = \text{Cl}$, F) leads to halide bridged dimeric species, $[\text{NH}_4]_2[\{\text{Ni}(\mu\text{-X})\text{R}_2\}_2]$ [Eqn. (16)], of which the fluorine containing species $[\text{NH}_4]_2[\{\text{Ni}(\mu\text{-F})(\text{C}_6\text{F}_5)_2\}_2]$, has been crystallographically characterised [82].

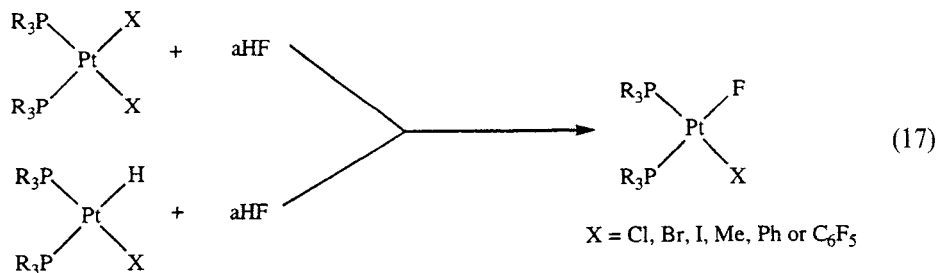


A crystal structure has also been obtained for the ultimate product from the reaction between $[\text{Ni}(\text{C}_{12}\text{H}_{18})]$, hydrofluoric acid and $\text{B}(\text{C}_6\text{F}_5)_3$. The $[\text{Ni}(\text{C}_{12}\text{H}_{18})]$ is initially protonated by the acid to give $[\text{Ni}(\text{C}_{12}\text{H}_{19})\text{F}]$, and the subsequent addition of $\text{B}(\text{C}_6\text{F}_5)_3$ results in partial abstraction of the fluoride anion from the metal centre. In addition to the structure, extensive NMR spectroscopic data have also been detailed. The complex has been used in the 1,4 *cis* polymerisation of butadiene, where it displays a fairly low activity but prolonged reaction lifetime [83]. Bridging fluoride species have been reported. These originate from the reaction between $[\text{Ni}_2(\eta\text{-OMe})_2\text{Me}_2(\text{PMe}_3)_2]$ and acetyl fluoride, which gives $[\text{Ni}_2(\eta\text{-F})(\eta\text{-X})\text{Me}_2(\text{PMe}_3)_2]$ ($\text{X} = \text{F}$, OMe) [2]. The difluoride can then be allowed to react with either $[\text{Ni}_2(\eta\text{-Cl})_2\text{Me}_2(\text{PMe}_3)_2]$ or $\text{Me}_3\text{SiNMe}_2$ to give the mixed fluoro-chloro or fluoro-amido dimer respectively. In contrast, the reports of reactions of $[\text{Ni}(\text{COD})(\text{PEt}_3)_2]$ with hexafluorobenzene or benzoyl fluoride to give, respectively *trans*- $[\text{NiF}(\text{C}_6\text{F}_5)(\text{PEt}_3)_2]$ and *trans*- $[\text{NiF}(\text{COC}_6\text{F}_5)(\text{PEt}_3)_2]$ must be viewed with some caution since they are formed in very low yields and analysed solely by infrared spectroscopy and elemental analysis [84].

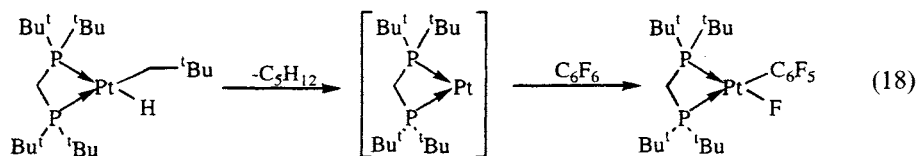
3.9.2 Palladium and platinum

Fluoride derivatives of palladium(II) and platinum(II), all of which are phosphine derivatives, can be most simply grouped into one of two subsections, namely neutral or cationic species. The neutral species are all of the form $[\text{MXF}(\text{PPh}_3)_2]$ ($\text{M} = \text{Pd}$, Pt) where X can be Cl , Br , I , H , methyl, phenyl and C_6F_5 . The synthetic route into these compounds involves either addition of HF to a metal phosphine dihalide or

hydride halide [Eqn. (17)] [2].

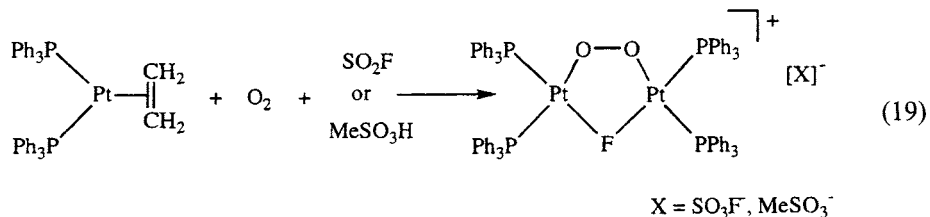


Formyl fluoride as a source of HF has been used in conjunction with $[\text{M}(\text{PPh}_3)_4]$ to form $[\text{MFH}(\text{PPh}_3)_2]$. Alternatively, simple halide metathesis of AgF with *trans*- $[\text{PtRCl}(\text{PPh}_3)_2]$ ($\text{R} = \text{Me, Ph}$) produces *trans*- $[\text{PtRF}(\text{PPh}_3)_2]$. This synthetic route has been utilised recently by Grushin and co-workers to prepare *trans*- $[\text{PdF}(\text{R})(\text{PPh}_3)_2]$ [85]. They have also demonstrated the synthesis of the same product via reaction between $[\text{Pd}_2(\text{R})_2(\mu\text{-OH})_2(\text{PPh}_3)_2]$, $\text{Et}_3\text{N} \cdot 3\text{HF}$ and PPh_3 . The complexes are very stable in air and take several hours to decompose in methanol. The NMR spectra display sharp peaks in dry solvents, but are much broadened in wet solvents. This is attributed to ionisation of the palladium-fluoride bond rather than hydrogen bonding between the fluoride anion and any water. The fluoride is rapidly abstracted from the metal centre by addition of $\text{BF}_3 \cdot \text{OEt}_2$ to give $[\text{PtPh}(\text{PPh}_3)_2][\text{BF}_4]$. However, other work, involving the displacement of the fluoride from the metal centre by either $[\text{Et}_3\text{NCH}_2\text{Ph}]\text{Cl}$ or $[\text{Ph}_3\text{P}=\text{N}=\text{PPh}_3]\text{Cl}$, yields a metal-chloride bond and formation of 'naked' fluoride. These reactions have been carried out in both CH_2Cl_2 and CHCl_3 , the former leading to the production of quantites of CH_2ClF and CH_2F_2 whilst use of the latter gives dichlorocarbene [86,87]. The formation of palladium(II) phosphine fluoride derivatives is complicated by the facile redox reaction between F^- and $\text{Pd}(\text{II})\text{-P}$ complexes in a variety of different solvents. The redox reaction tends to yield $\text{P-Pd}(0)$ and initially R_3PF_2 , which subsequently hydrolyses to phosphine oxide [88]. Insertion of a fourteen-electron platinum(0) centre into a C-F bond of hexafluorobenzene also provides a very elegant method of forming $\text{Pt}(\text{II})\text{-F}$ bonds [Eqn. (18)]. The metal complex $[\text{PtF}(\text{C}_6\text{F}_5)(\text{dbpe})]$, supported by a bulky chelating bisphosphine, has been fully characterised by elemental analysis and multinuclear NMR, and infrared spectroscopies [89].



Addition of a variety of different fluoride-containing species to platinum(0) olefin complexes has resulted in claims for the formation of several fluoride species. The reaction between $[\text{Pt}(\text{PhCH})_2(\text{PPh}_3)_2]$ and $\text{N}_2\text{C}(\text{CF}_3)_3$ produces $[\text{PtF}\{\text{C}(\text{CF}_3)_3\}]$

(PPh₃)₂] [90]; however, a lack of conclusive ¹⁹F NMR spectroscopic data, combined with difficulty in accounting for the origins of the traces of hydrofluoric acid invoked by the authors to account for the source of the metal bound fluoride, bring some doubt upon this claim. A similar absence of physical data also undermines the reliability of a report of [PtF₂(PPh₃)₂] prepared from XeF₂ and [Pt(C₂H₄)(PPh₃)₂] [2]. A more realistic, if somewhat surprising, result is the formation of a bridging, peroxy fluoro cation, [Pt₂F(O—O)(PPh₃)₄][X] (X = SO₃F, MeSO₃) from the reaction between [Pt(C₂H₄)(PPh₃)₂], O₂ and SO₂F₂ [Eqn. (19)] [91].



The reaction between [M(PPh₃)₄] and hydrofluoric acid produces different final products depending upon whether palladium or platinum metal is used. Use of [Pd(PPh₃)₄] is reported to give the bisphosphine fluoro-bridged dimer, [{PdF(PPh₃)₂}₂][2HF₂], on the basis of conductivity measurements and infrared spectroscopic data, whilst [Pt(PPh₃)₄] gives the triphosphine monofluoro cation, [PtF(PPh₃)₃]⁺ [2]. This species has been studied extensively in both wet and dry chlorinated solvents, and contrary to initial reports, appears to be stable almost indefinitely to F—Cl exchange. However, decomposition in the presence of water over a period of weeks yields initially the hydroxide species [Pt(OH)(PPh₃)₃]⁺, which in turn eliminates H₂O to give the orthometallated product, [Pt(C₆H₅PPh₂)(PPh₃)₂][SbF₆] [Fig. 5] [92].

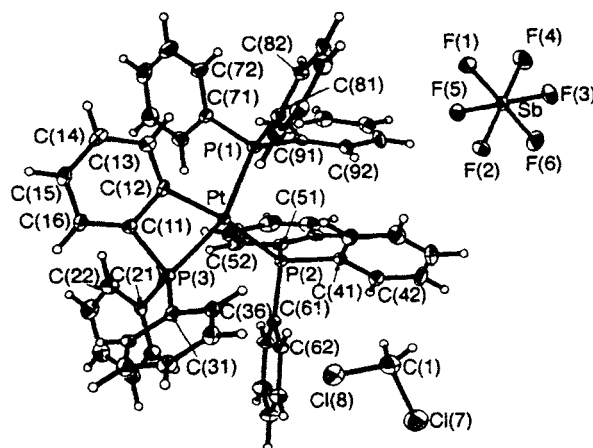


Fig. 5. The Molecular Structure of [Pt(PPh₃)₂(C₆H₄PPh₂)] [SbF₆]. CD₂Cl₂ (thermal ellipsoids are drawn at the 30% probability boundaries) (Reproduced with permission from J. Chem. Soc., Dalton Trans., (1998) 1249–1252. Copyright 1998 Royal Society of Chemistry).

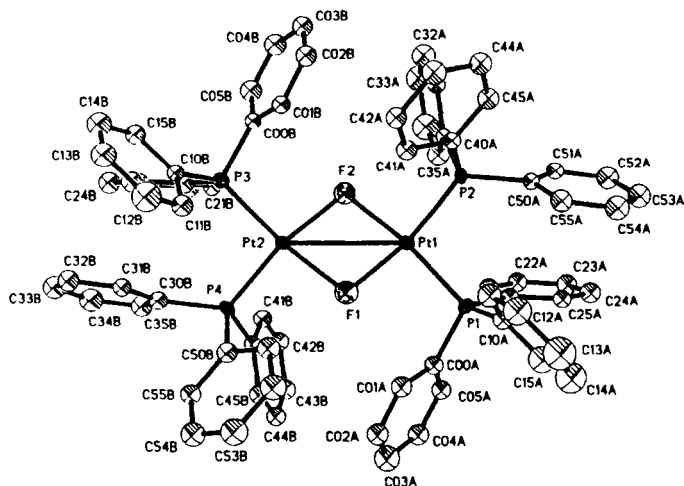


Fig. 6. The Molecular Structure of $[\{PtF(PPh_3)_2\}_2][HF_2]$ (thermal ellipsoids are drawn at the 30% probability boundaries) (Reproduced with permission from the copyright holders, H.C.S. Clark, J. Fawcett, J.H. Holloway, E.G. Hope, R. Nassar, L.A. Peck, G. Reid and D.R. Russell).

The $[HF_2]$ anion of $[PtF(PPh_3)_3]^+$ can be readily exchanged for other anions such as BF_4 , SbF_6 , PF_6 and BPh_4 by simple salt metathesis. However, use of $LiClO_4$ results in the displacement of one of the phosphines from the metal complex to give $[\{PtF(PPh_3)_2\}_2][ClO_4]$ [2]. In contrast, the simplest method of preparing the PEt_3 -supported trisphosphine monofluoro cation is via the metathesis reaction between AgF and $[PtCl(PEt_3)_3]^+$ and this product was the first of these complexes to have been crystallographically characterised. The cation is far less air sensitive than the PPh_3 analogue, but EXAFS analysis shows that the Pt-F bond lengths are identical for both, implying that any difference in reactivity is attributable to steric interactions rather than electronic influences [89].

An alternative route into the platinum bisphosphine fluoro-bridged dimer is via protonolysis of an alkyl group with anhydrous hydrofluoric acid. That is, reactions of $[PtMe_2(PR_3)_2]$ ($R = Me, Ph, p\text{-MeOPh}$) with aHF lead to the quantitative formation of the appropriate dimers, which, in the case of $R = Ph$, has been crystallographically characterised [Fig. 6]. Further work has shown that these dimers can be cleaved by subsequent addition of phosphines (PEt_3 , PPh_3 , PCy_3) to give mixed phosphine monofluoro cations [93].

3.10 Groups 11 and 12

Very little has been reported of the organometallic and co-ordination chemistry of Group 11 and 12 fluorides. The area of copper fluorides has been given the most attention, driven presumably, in part, by the role copper ions (and in particular

copper amine complexes) play in biological systems such as metalloenzymes, cofactors and metalloproteins.

Addition of a variety of monoamine and chelating diamines to CuF_2 in Teflon apparatus results in the formation of complexes of the form, $[\text{CuF}_2(\text{L})]$, where L is two mono-, or one bi- or tri-dentate ligand [94]. Many of these complexes have been analysed by X-ray structure determinations (as well as a variety of other techniques) and one notable feature common to all is the extensive hydrogen-bonding encountered between the metal-bound fluoride and any water incorporated into the crystal. This often leads to highly complex 3-D 'network' structures. One case where water is not trapped in the lattice, however, is when 3-methyl-4-ethyl-5-phenyl pyrazole is employed as the ligand, since the N—H bonds display a greater affinity for hydrogen bonding to the fluorides than the water does and, since intramolecular co-ordination is constrained due to the small 'bite' angle, then intermolecular co-ordination predominates leading to a polymeric structure [Fig. 7] [94].

Another source of ' CuF_2 ' is $[\text{Cu}(\text{BF}_4)_2]$ where use of pentamethyldiethylenediamine (pmdien) as the ligating amine, together with either 4,4'-bipyridine or trans-1,2-bis(pyridin-4-yl)ethene, leads to abstraction of F^- from the BF_4^- by the metal centre and formation of $[\{\text{CuF}(\text{pmdien})(\text{H}_2\text{O})\}_2][\text{BF}_4]_2$ [96].

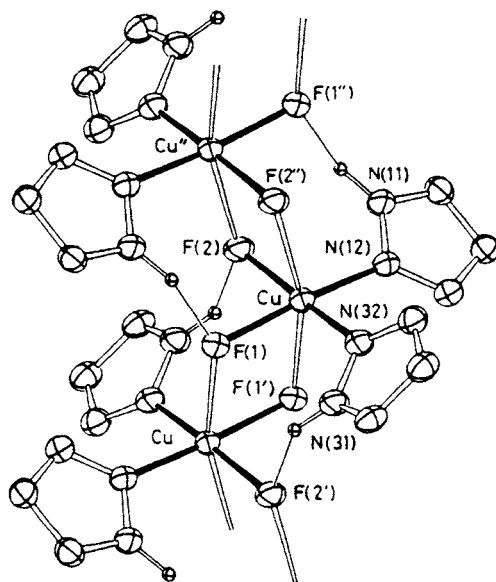


Fig. 7. The Molecular Structure of $[\text{CuF}_2(3\text{-methyl-4-ethyl-5-phenyl pyrazole})]$ showing the chain structure. The zig-zag chains consisting of two different CuF_2Cu units, lie along the b -axis. (Reproduced with permission from J. Chem. Soc., Chem. Commun., (1998) 423–424. Copyright 1998 Royal Society of Chemistry).

Phosphine-supported copper(II) fluorides are far rarer than their amine analogues, with the only reaction reported being the reduction of $\text{CuF}_2 \cdot 2\text{H}_2\text{O}$ with PPh_3 , in refluxing methanol, to produce initially $[\text{CuF}(\text{PPh}_3)_3] \cdot 4\text{PPh}_3 \cdot 4\text{MeOH}$. This simplifies upon recrystallisation to $[\text{CuF}(\text{PPh}_3)_3] \cdot 2\text{EtOH}$ [Fig. 8] [97]. The ^{19}F NMR spectrum yields a singlet at 9.6 ppm, apparently indicative of a highly ionic fluorine, whilst the ^{31}P NMR spectrum produces a broad singlet implying a fluxional process which has been determined to be the equilibrium between $[\text{CuF}(\text{PPh}_3)_3]$ and $[\text{CuF}(\text{PPh}_3)_2] + \text{PPh}_3$ [97].

Similar chemistry can be found in the reaction between ZnF_2 and ethylenediamine in refluxing methanol [95]. The product is $[\text{Zn}(\text{en})_3]\text{F}_2 \cdot 2\text{H}_2\text{O}$ with the three chelating diamine ligands arranged around the Zn centre in an octahedral form, whilst the F^- anions are strongly hydrogen bonded to the water molecules in a planar diamond cluster rather than the theoretically-anticipated tetrahedral form. This has been ascribed to an energetic preference to form four 2-centre hydrogen bonds rather than four 3-centre hydrogen bonds.

Another zinc fluoride has been prepared incorporating a pyrazolyl borate ligand. Reaction of $[\text{KHB}(3\text{-}R\text{-}5\text{-methylpyrazol-1-yl})]$ ($R = p\text{-tol}$) with $[\text{Zn}(\text{OAc})_2 \cdot 2\text{H}_2\text{O}]$ leads to the production of $[\text{Tp}^{\text{R,Me}}\text{ZnOAc}]$, which is transformed to the fluoride derivative upon addition of KF [99]. This compound has been structurally characterised. Use of $[\text{Zn}(\text{ClO}_4)_2]$ as the starting material in combination with $[\text{KHB}(3\text{-}t\text{Bu-}5\text{-methylpyrazol-1-yl})]$, followed by addition of KF leads to $[\text{Tp}^{t\text{Bu,Me}}\text{ZnF}]$. Further reaction of this compound at the fluoride anion leads to a variety of species. Abstraction of F^- by $\text{BF}_3 \cdot \text{solv.}$ ($\text{solv.} = \text{py}, \text{Et}_2\text{O}$) leads to $[\text{TpZn}(\text{solv.})][\text{BF}_4]$, whilst use of $[\text{HSiEt}_3]$ leads to formation of the hydride species,

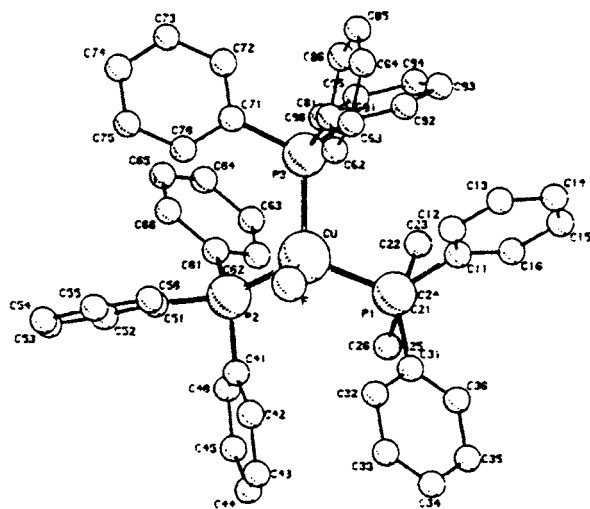
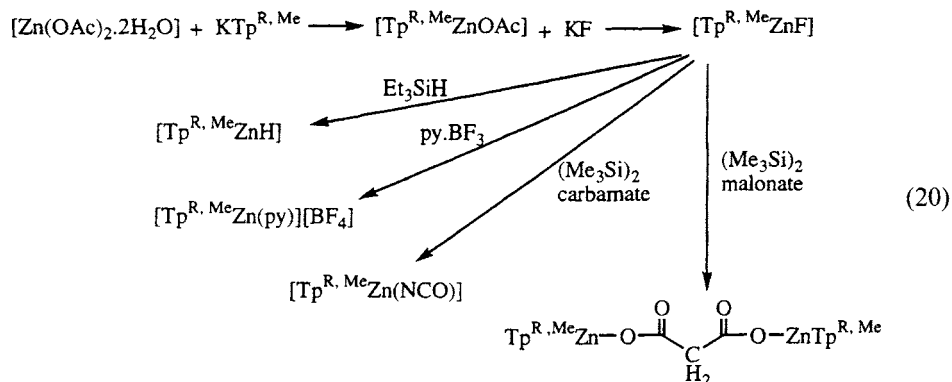
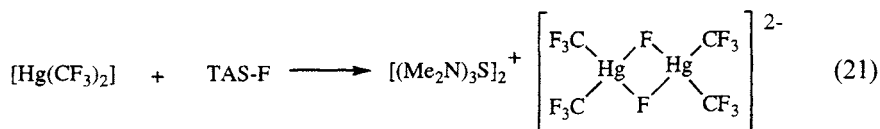


Fig. 8. The Molecular Structure of $[\text{CuF}(\text{PPh}_3)_3]$. (Reproduced with permission from *Inorg. Chim. Acta.*, 52 (1981) 153–159. Copyright 1981 Elsevier).

[TpZnH]. Other silyl reagents, bis(trimethylsilyl)malonate and bis(trimethylsilyl) carbamate, result in the formation of $[\{TpZnOC(O)\}_2CH_2]$ and $[TpZn(NCO)]$ respectively. This chemistry is summarised in Eqn. (20).



A mercury(II) fluoride has also been reported recently. Addition of TAS-F to $[Hg(CF_3)_2]$ produces $[TAS]_2[(CF_3)_2Hg(\mu-F)_2Hg(CF_3)_2]$ [Eqn. (21)] which has been analysed by X-ray diffraction studies [100]. Co-ordination of F^- to the metal centre results in surprising labilisation of the Hg—C bonds and stirring the complex in CH_3CN at $0^\circ C$ yields CF_3H . Similarly, addition of NSF_3 produces NSF_2CF_3 .



3.11 Conclusions

The growing interest in low valent transition metal fluorides, and their potential application in catalysis of organic fluorinations, assures for them a bright future over the next few years. The fact that, in some cases, air-stable species have been produced, notably $[MF_2(CO)_2(PR_3)_2]$ ($M = Ru, Os$) [50], means that these species need no longer remain the preserve of the specialised inorganic fluorine chemist.

References

- [1] E.F. Murphy, R. Murugavel, H.W. Roesky, Chem. Rev., 97 (1997) 3425 and references therein.
- [2] N.M. Doherty, N.W. Hoffman, Chem. Rev., 91 (1991) 553 and references therein.
- [3] (a) S.A. Brewer, J.H. Holloway, E.G. Hope, P.G. Watson, J. Chem. Soc., Chem. Commun., (1992) 1577; (b) S.A. Brewer, A.K. Bridson, J.H. Holloway, E.G. Hope, L.A. Peck, P.G. Watson, J. Chem. Soc., Dalton Trans., (1995) 2945.
- [4] J.H. Holloway, E.G. Hope, I.M. Smith, unpublished results.

- [5] F. Bottomley, D.E. Paez, P.S. White, *J. Organomet. Chem.*, 291 (1985) 35.
- [6] J.L. Kiplinger, T.G. Richmond, C.E. Osterberg, *Chem. Rev.*, 94 (1994) 373.
- [7] W. Beck, K. Sünkel, *Chem. Rev.*, 88 (1988) 1405.
- [8] Z. Xie, K. Chui, Q. Yang, T.C.W. Mak, J. Sun, *Organometallics*, 17 (1998) 3937.
- [9] S.A.A. Shah, H. Dorn, H.W. Roesky, E. Parisini, H.-G. Schmidt, M. Noltemeyer, *J. Chem. Soc., Dalton Trans.*, (1996) 4143.
- [10] S.A.A. Shah, H. Dorn, A. Voight, H.W. Roesky, E. Parisini, H.-G. Schmidt, M. Noltemeyer, *Organometallics*, 15 (1996) 3176.
- [11] D.R. Gauthier, Jr., E.M. Carreira, *Angew. Chem., Int. Ed. Engl.*, 35 (1996) 2363.
- [12] R.O. Duthaler, A. Hafner, *Angew. Chem., Int. Ed. Engl.*, 36 (1997) 43.
- [13] R. Talay, D. Rehder, *Inorg. Chim. Acta*, 77 (1983) L175.
- [14] H. Brunner, G. Gehart, W. Meier, J. Wachter, A. Riedel, S. Elkrami, Y. Mugnier, B. Nuber, *Organometallics*, 13 (1994) 134.
- [15] J. Sala-Pala, J. Amaudrut, J.E. Guerschais, R. Mercier, J. Douglade and J.G. Theobald, *J. Organomet. Chem.*, 204 (1981) 347.
- [16] W. Douglas, J.K. Ruff, *J. Organomet. Chem.*, 65 (1974) 65.
- [17] J.L. Cihonski, R.A. Levenson, *Inorg. Chem.*, 14 (1975) 1717.
- [18] E.C. Alyea, A. Malek, J. Malito, *Inorg. Chim. Acta.*, 101 (1985) 147.
- [19] R.N. Bagchi, A.M. Bond, R. Colton, D.L. Luscombe, J.E. Moir, *J. Am. Chem. Soc.*, 108 (1986) 3352.
- [20] S.J. White, M.F. Farona, *J. Organomet. Chem.*, 37 (1972) 119.
- [21] D.J. Darensbourg, K.K. Klausmeyer, J.H. Reibenspies, *Inorg. Chem.*, 34 (1995) 4933.
- [22] J.T. Poulton, K. Foltz, W.E. Streib, K.G. Caulton, *Inorg. Chem.*, 31 (1992) 3190.
- [23] K.G. Caulton, *New J. Chem.*, 18 (1994) 25.
- [24] D.M. Dawson, R.A. Henderson, A. Hills, D.L. Hughes, *J. Chem. Soc., Dalton Trans.*, (1992) 973.
- [25] D.J. Darensbourg, K.M. Sanchez, J.H. Reibenspies, *Inorg. Chem.*, 27 (1988) 3269.
- [26] D.J. Darensbourg, B.L. Muller, C. Bischoff, C.C. Johnson, K.M. Sanchez, J.H. Reibenspies, *Isr. J. Chem.*, 30 (1990) 369.
- [27] L. Jordi, A. Segundo, F. Camps, S. Ricart, J.M. Moretó, *Organometallics*, 12 (1993) 3795.
- [28] T.R. Hoyer, J.A. Suriano, *Organometallics*, 11 (1992) 2044.
- [29] T.R. Hoyer, J.A. Suriano, *J. Am. Chem. Soc.*, 115 (1993) 1154.
- [30] P. Rosendorfer, C. Robl, W. Beck, *Gazzet. Chim. Ital.*, 123 (1993) 145.
- [31] B.C. Ward, J.L. Templeton, *Inorg. Chem.*, 19 (1980) 1753.
- [32] B.C. Ward, J.L. Templeton, *J. Am. Chem. Soc.*, 103 (1981) 3743.
- [33] S.J.N. Burgmayer, J.L. Templeton, *Inorg. Chem.*, 24 (1985) 2224.
- [34] C.E. Osterberg, M.A. King, A.M. Arif, T.G. Richmond, *Angew. Chem., Int. Ed. Engl.*, 29 (1990) 888.
- [35] T.G. Richmond, *Coord. Chem. Rev.*, 105 (1990) 221.
- [36] B.L. Lucht, M.J. Poss, M.A. King, T.G. Richmond, *J. Chem. Soc., Chem. Commun.*, (1991) 400.
- [37] J.L. Kiplinger, T.G. Richmond, A.M. Arif, C. Dücker-Benfer, R. van Eldik, *Organometallics*, 15 (1996) 1545.
- [38] J.L. Kiplinger, M.A. King, A.M. Arif, T.G. Richmond, *Organometallics*, 12 (1993) 3382.
- [39] J.L. Kiplinger, M.A. King, A. Fechtenkötter, A.M. Arif and T.G. Richmond, *Organometallics*, 15 (1996) 5292.
- [40] J.L. Kiplinger, T.G. Richmond, *Polyhedron*, 16 (1997) 409.

- [41] (a) J.L. Kiplinger, T.G. Richmond, *J. Am. Chem. Soc.*, 118 (1996) 1805; (b) J.L. Kiplinger, T.G. Richmond, *J. Chem. Soc., Chem. Commun.*, (1996) 1115 and references therein.
- [42] J.L. Kiplinger, A.M. Arif, T.G. Richmond, *Organometallics*, 16 (1997) 246.
- [43] N.W. Hoffman, N. Prokopuk, M.J. Robbins, C.M. Jones, N.M. Doherty, *Inorg. Chem.*, 30 (1991) 4177.
- [44] S.A. Brewer, L.A. Bugghey, J.H. Holloway, E.G. Hope, *J. Chem. Soc., Dalton Trans.*, 1995, 2941.
- [45] C.J. Marshall, R.D. Peacock, D.R. Russell, I.L. Wilson, *J. Chem. Soc., Chem. Commun.*, (1970) 1643.
- [46] A.J. Hewitt, J.H. Holloway, R.D. Peacock, J.B. Raynor, I.L. Wilson, *J. Chem. Soc., Dalton Trans.*, (1976) 579.
- [47] K.S. Coleman, J.H. Holloway, E.G. Hope, *J. Chem. Soc., Dalton Trans.*, (1997) 1713.
- [48] S.A. Brewer, J.H. Holloway, E.G. Hope, *J. Chem. Soc., Dalton Trans.*, (1994) 1067.
- [49] K.C. Coleman, J.H. Holloway, E.G. Hope, Unpublished work.
- [50] K.S. Coleman, J. Fawcett, J.H. Holloway, E.G. Hope, D.R. Russell, *J. Chem. Soc., Dalton Trans.*, (1997) 3557.
- [51] S.A. Brewer, K.S. Coleman, J. Fawcett, J.H. Holloway, E.G. Hope, D.R. Russell, P.G. Watson, *J. Chem. Soc., Dalton Trans.*, (1995) 1073.
- [52] K.S. Coleman, J.H. Holloway, E.G. Hope, J. Langer, *J. Chem. Soc., Dalton Trans.*, (1997) 4555.
- [53] H.C.S. Clark, K.S. Coleman, J.H. Holloway, E.G. Hope, Unpublished work.
- [54] D. Huang, K.G. Caulton, *J. Am. Chem. Soc.*, 119 (1997) 3185.
- [55] J.T. Poulton, M.P. Sigalas, K. Folting, W.E. Sreib, O. Eisenstein, K.G. Caulton, *Inorg. Chem.*, 33 (1994) 1476.
- [56] J.T. Poulton, M.P. Sigalas, O. Eisenstein, K.G. Caulton, *Inorg. Chem.*, 32 (1993) 5490.
- [57] G.J. vanDriel, W.L. Driessen, J. Reedijk, *Inorg. Chem.*, 24 (1985) 2919.
- [58] F.J. Rietmeijer, G.A. van Albada, R.A.G. De Graaff, J.G. Haasnoot, J. Reedijk, *Inorg. Chem.*, 24 (1985) 3597.
- [59] F.J. Rietmeijer, J.G. Haasnoot, A.J. Den Hartog, J. Reedijk, *Inorg. Chim. Acta.*, 113 (1986) 147.
- [60] M.N. Bhattacharjee, M.K. Chaudhuri, M. Devi, *Polyhedron*, 11 (1992) 1523.
- [61] I.B. Gorrell, G. Parkin, *Inorg. Chem.*, 29 (1990) 2452.
- [62] L. Vaska, *Inorg. Synth.*, 11 (1968) 101.
- [63] R.G. Pearson, *J. Am. Chem. Soc.*, 85 (1963) 3533.
- [64] D. Forster, *Inorg. Chem.*, 11 (1972) 1686.
- [65] L. Vaska, J. Peone, Jr., *J. Chem. Soc., Chem. Commun.*, (1971) 418.
- [66] R.W. Cockman, E.A.V. Ebsworth, J.H. Holloway, H. Murdoch, N. Robertson, P.G. Watson, In: *Reaction of Non-metal Fluorides with some Platinum Metal Complexes*, J. Thrasher, S. Strauss (Eds.), ACS Symposium Series, ACS Books, 1994.
- [67] P.G. Watson, E. Lork, R. Mews, *J. Chem. Soc., Chem. Commun.*, (1994) 1069.
- [68] S. Misra, *Indian J. Chem. Sect (A)*, 19A (1981) 1191.
- [69] S. Brewer, PhD Thesis, Leicester University.
- [70] L.A. Peck, PhD Thesis, Leicester University.
- [71] H.L.M. Van Gaal, F.L.A. Van Den Bekerom, J.P.J. Verlaan, *J. Organomet. Chem.*, 114 (1976) C35.
- [72] R. R. Burch, R.L. Harlow, S.D. Ittel, *Organometallics*, 6 (1987) 982.
- [73] A.C. Cooper, J.C. Huffman, K.G. Caulton, *Inorg. Chim. Acta.*, 270 (1998) 261.
- [74] A.C. Cooper, K. Folting, J.C. Huffman, K.G. Caulton, *Organometallics*, 16 (1997) 505.

- [75] R. Dorta, P. Egli, F. Zürcher, A. Togni, *J. Am. Chem. Soc.*, 119 (1997) 10857.
- [76] B.P. Patel, R.H. Crabtree, *J. Am. Chem. Soc.*, 118 (1996) 13105.
- [77] W.D. Jones, M.G. Partridge, R.N. Perutz, *J. Chem. Soc., Chem. Commun.*, (1991) 264.
- [78] S.T. Belt, M. Helliwell, W.D. Jones, M.G. Partridge, R.N. Perutz, *J. Am. Chem. Soc.*, 115 (1993) 1429.
- [79] J.E. Veltheer, P. Burger, R.G. Bergmann, *J. Am. Chem. Soc.*, 117 (1995) 12478.
- [80] S. Park, D.M. Roundhill, *Inorg. Chem.*, 28 (1989) 2905.
- [81] C.G. Krespan, D.A. Dixon, *J. Org. Chem.*, 63 (1998) 36.
- [82] M.M. Brezinski, J. Schneider, L.J. Radonovich, K.J. Klabunde, *Inorg. Chem.*, 28 (1989) 2414.
- [83] R. Taube, S. Wache, J. Sieler, *J. Organomet. Chem.*, 459 (1993) 335.
- [84] D.R. Fahey, J.E. Mahan, *J. Am. Chem. Soc.*, 99 (1977) 2501.
- [85] S.L. Fraser, M.Y. Antipin, V.N. Khroustalyov, V.V. Grushin, *J. Am. Chem. Soc.*, 119 (1997) 4769.
- [86] M.C. Pilon, V.V. Grushin, *Organometallics*, 17 (1998) 1774.
- [87] V.V. Grushin, *Angew. Chem., Int. Ed. Engl.*, 37 (1998) 994.
- [88] M.R. Mason, J.G. Verkade, *Organometallics*, 11 (1992) 2212.
- [89] P. Hofmann, G. Unfried, *Chem. Ber.*, 125 (1992) 659.
- [90] J. Howard, P. Woodward, *J. Chem. Soc., Dalton Trans.*, (1973) 1840.
- [91] R. Gereke, H.-J. Plinta, R. Schmutzler, *Z. Anorg. Allg. Chem.*, 623 (1997) 1333.
- [92] H.C.S. Clark, J. Fawcett, J.H. Holloway, E.G. Hope, L.A. Peck, D.R. Russell, *J. Chem. Soc., Dalton Trans.*, (1998) 1249.
- [93] H.C.S. Clark, J. Fawcett, J.H. Holloway, E.G. Hope, R. Nassar, L.A. Peck, G. Reid, D.R. Russell, manuscript in preparation.
- [94] (a) J. Emsley, M. Arif, P.A. Bates, M.B. Hursthouse, *Inorg. Chim. Acta.*, 143 (1988) 25; (b) J. Emsley, N.M. Reza, H.M. Dawes, M.B. Hursthouse, *J. Chem. Soc., Dalton Trans.*, (1986) 313; (c) J. Emsley, M. Arif, P.A. Bates, M.B. Hursthouse, *J. Chem. Soc., Dalton Trans.*, (1987) 2397; (d) R.A. Jacobson, W.P. Jensen, *Inorg. Chim. Acta*, 52 (1981) 205.
- [95] F.S. Keij, R.A.G. De Graff, J.G. Haasnoot, A.J. Oosterling, E. Pedersen, J. Reedijk, *J. Chem. Soc., Chem. Commun.*, (1988) 423.
- [96] S.J. Barlow, S.J. Hill, J.E. Hocking, P. Hubberstey, W.-S. Li, *J. Chem. Soc., Dalton Trans.*, (1997) 4701.
- [97] (a) F.H. Jardine, L. Rule, A.G. Vohra, *J. Chem. Soc. (A)*, (1970) 238; (b) D.J. Gulliver, W. Levason, M. Webster, *Inorg. Chim. Acta.*, 52 (1981) 153; (c) P.C. Healy, J.V. Hanna, J.D. Kildea, B.W. Skelton, A.H. White, *Aust. J. Chem.*, 44 (1991) 427.
- [98] J. Emsley, M. Arif, P.A. Bates, M.B. Hursthouse, *J. Chem. Soc., Chem. Commun.*, (1989) 738.
- [99] W. Kläui, U. Schilde, M. Schmidt, *Inorg. Chem.*, 36 (1997) 1598.
- [100] D. Viets, E. Lork, P.G. Watson, R. Mews, *Angew. Chem., Int. Ed. Engl.*, 36 (1997) 623.

CHAPTER 4

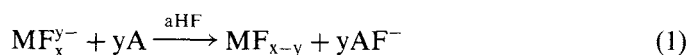
High Oxidation State Transition Metal Fluorides

Boris Žemva

Jožef Stefan Institute, Jamova 39, SI-1000, Ljubljana, Slovenia

4.1 Introduction

The purpose of this chapter is to describe a series of new binary fluorides of the transition metals in high oxidation states which were synthesized and characterized in the last ten years. These extensive new findings depended upon the invention of a general method for the synthesis of polymeric binary fluorides. This synthetic route is especially convenient for the syntheses of thermodynamically unstable binary fluorides [1]. The approach uses a strong acceptor fluoride, such as AsF₅, BiF₅, BF₃ etc., to abstract F[−] from anionic relatives of the binary fluoride, dissolved in anhydrous hydrogen fluoride (aHF). With properly chosen soluble salts the reaction temperature can be kept at 208 K or even lower. This synthetic route is generally applicable for the syntheses of high purity polymeric, aHF — insoluble fluorides, which have an anion stable in aHF.



A = AsF₅, BiF₅, BF₃

M = transition metal

The syntheses, structures, some properties and oxidizing capabilities of these new binary fluorides are described. In addition, some complex fluorides of these binary fluorides are also described if they have interesting properties, or they were used as starting materials for the preparation of new binary fluorides. Some new synthetic methods for the preparation of such complex fluorides with metals in high oxidation state are also described.

4.2 Binary and complex fluorides of silver

4.2.1 Introduction

In this section a new binary fluoride of silver(III), AgF₃, and two mixed valence silver fluorides Ag₃F₈ and Ag₂F₅ are described. In addition new synthetic methods are

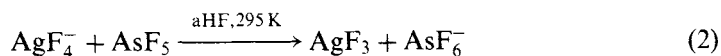
exemplified in the preparation of AgF_4^- salts of XeF_5^+ , K_5^+ and Li^+ . A new mixed valence $(\text{AgF})_2\text{AgF}_4\text{AsF}_6$ complex compound is also described. Syntheses of novel AgF^+ salts and Ag^{2+} salts are given together with their oxidizing capabilities, structures and magnetic properties. The first compound where XeF_2 is a ligand of a metal cation (Ag^+), is a product of the oxidation of xenon with cationic $\text{Ag(II)}_{(\text{solv})}$.

4.2.2 Binary fluorides of silver

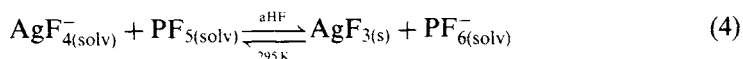
4.2.2.1 Synthesis and some properties of AgF_3

AgF_3 was first claimed by Bougon and Lance [2]. It was made by fluorination of silver metal or its mono- or difluoride in aHF by KrF_2 at room temperature. It was reported to be red brown highly reactive solid, weakly paramagnetic [3] and with X-ray powder diffraction pattern. The latter showed no relationship to that of AuF_3 [4]. Some years later, AgF_3 , was also claimed by Kiselev et al. [5] to be formed in the reaction of AgF_2 with O_2F_2 in ClF_5 . This material also was not isomorphous with AuF_3 .

Silver trifluoride, isomorphous with AuF_3 , and diamagnetic, when pure, was precipitated from solutions of AgF_4^- salts dissolved in aHF, as a bright red solid, when a Lewis acid was added to those solutions [1,6]. The strength and quantity of the applied fluoro acid was very important. Addition of excess AsF_5 (which is a strong F^- acceptor, and highly soluble in aHF) over that required for the precipitation of AgF_3 brought about dissolution of the AgF_3 in aHF and reduction of Ag(III) to Ag(II) .

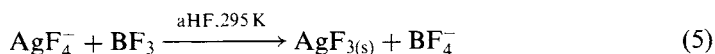


With such a soluble reagent as AsF_5 it is difficult to avoid the local excess of acid that brings about the reduction of the AgF_3 . With the weaker and much less aHF — soluble acids PF_5 or BF_3 , the reductive interaction was insignificant. PF_5 was able to precipitate AgF_3 from AgF_4^- in aHF when an overpressure of PF_5 was maintained over the solution. AgF_3 redissolved when the overpressure of PF_5 was released thus showing that AgF_3 and PF_5 are very close in acidity:

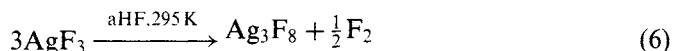


(The concentration of $\text{PF}_{5(\text{solv})}$ increases with pressure of the gas, and vice versa.)

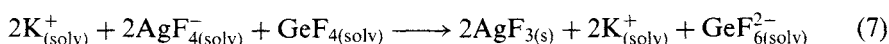
Boron trifluoride proved to be sufficiently superior acid to AgF_3 to quantitatively precipitate AgF_3 from its AgF_4^- solutions at low BF_3 partial pressure:



AgF_3 , freshly precipitated by BF_3 , is a bright red diamagnetic solid, and its X-ray powder diffraction pattern was entirely accounted for by an AuF_3 -like phase. Although the weaker fluoro acid BF_3 produced high purity AgF_3 it is necessary to remove aHF quickly from the AgF_3 , because AgF_3 is thermodynamically unstable and loses fluorine in aHF at 295 K according to Eqn. (6):



Although washing of the AgF_3 at 273 K diminishes Ag_3F_8 contamination it is desirable to minimize the need for extensive washing with aHF. This has been achieved by using fluoro acid GeF_4 which is strong enough to precipitate AgF_3 and which has a potassium salt, K_2GeF_6 , which is very soluble in aHF even at 273 K [7].



When dry, however, AgF_3 has considerable kinetic stability and can be kept in quartz capillaries for many weeks at 295 K. It has withstood high-intensity X-radiation from a synchrotron source for several hours.

It is clear now that under the preparative conditions given by Bougon et al. [2,3] or by Kiselev et al. [5] AgF_3 was not formed. Neither of the X-ray powder diffraction patterns, in those reports, corresponds with that of authentic AgF_3 given in Ref. [6]. There is a close matching of the data of Bougon et al. with that given for Ag_3F_8 in Ref. [6]. The data of Kiselev et al. also show a rough relationship to the Ag_3F_8 data.

4.2.2.2 Crystal structure of AgF_3

The structure of AgF_3 [6] is closely related to that of AuF_3 [4] and is illustrated in Figs 1 and 2.

The planar and approximately square MF_4 units ($\text{M}=\text{Ag}$ or Au) are almost isodimensional with differences which are not significant. These square MF_4 units are joined by the symmetrical sharing of cis F(1) ligands to generate the helical chains of 6_1 or 6_5 symmetry. The bridging angles $\text{M}-\text{F}(1)-\text{M}$ are close to 120° showing considerable covalency in the MF_4 unit bonding. The greatest difference in the two structures is in the interaction of the helical chains with one another (Fig. 2) where the F(2) ligands of one chain approach approximately normal to the square MF_4 unit of an adjacent chain. The elongation of the roughly octahedral arrangement is much greater for the AuF_6 unit than for the AgF_6 unit. In accordance with this feature is the difference in the formula unit volume (FUV) of AgF_3 and AuF_3 . The formula unit volume of AgF_3 is approximately 5 \AA^3 smaller than that of AuF_3 . A similar contraction of Ag(III) relatives to Au(III) is found in the primitive unit cell volumes of the XeF_5^+ and alkali-metal salts of MF_4^- and in their oxides.

These features both point out that the remaining valence electrons of Ag(III) $4d_{z^2}$ are more tightly bound than in the case of Au(III) $5d_{z^2}$. This is also in harmony with

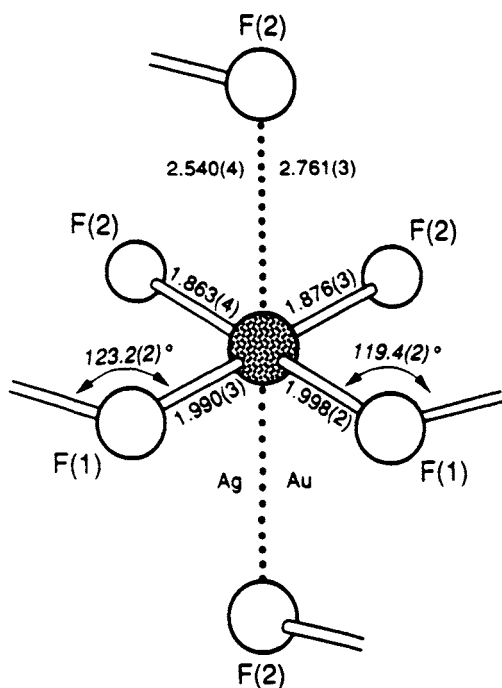


Fig. 1. Interatomic distances (Å) for the elongated octahedral F ligand arrangement about the metal atom in AgF_3 and AuF_3 (Reprinted with permission from J. Am. Chem. Soc., 113, May 1991, pp. 4192–4198. Copyright 1991 American Chemical Society.)

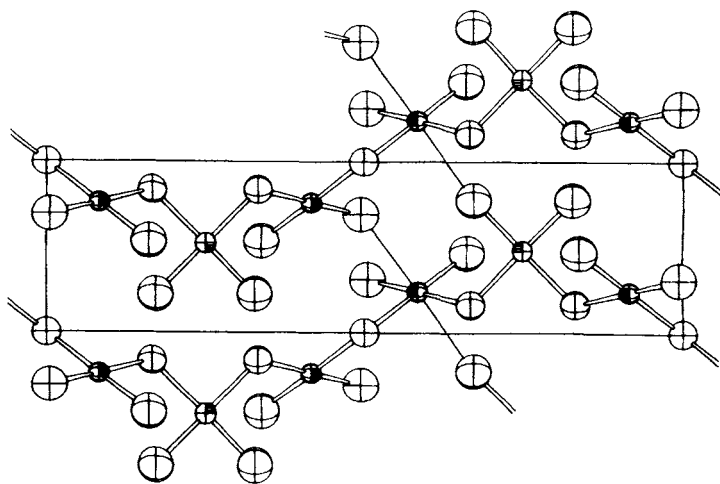
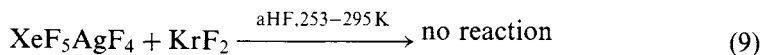
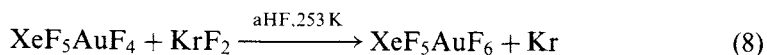


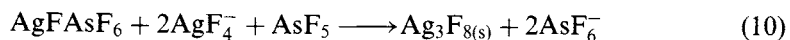
Fig. 2. View down a showing unit cell contents and the F(2) interchain bridging in AgF_3 and AuF_3 (Reprinted with permission from J. Am. Chem. Soc., 113, May 1991, pp. 4192–4198. Copyright 1991 American Chemical Society.)

the relative ease of oxidation of Au(III) to Au(V) [8], whereas the analogous oxidation of Ag(III) to Ag(V) does not proceed.

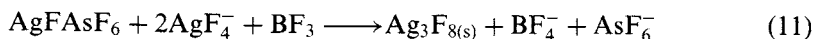


4.2.2.3 Synthesis and some properties of Ag_3F_8

The contamination of AgF_3 , by Ag_3F_8 [6], when precipitated by AsF_5 , is the consequence of the reductive interaction of AgF_3 with AsF_5 (see Eqn. (3)), and the further reaction of AgFAsF_6 with AgF_4^- ions in the acidic aHF.



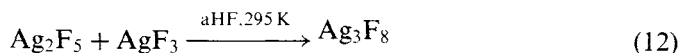
In a separate experiment AgFAsF_6 solution in aHF was mixed with exactly 2 mol equivalents of AgF_4^- solution in aHF and then treated with BF_3 . The red-brown solid, Ag_3F_8 , was obtained quantitatively:



The X-ray powder diffraction pattern of this solid was identical with that obtained after AgF_3 decomposed at room temperature in aHF (see Eqn. (6)). The formation of Ag_3F_8 by the interaction of 1 mol of Ag(II) and 2 mol of Ag(III) confirmed that Ag_3F_8 is a mixed valence material, $\text{Ag(II)Ag(III)}_2\text{F}_8$. Since AgF_4^- and AgF_3 are diamagnetic, a low spin d^8 configuration can be confidently expected for the two Ag(III) in Ag_3F_8 . The magnetic susceptibility of Ag_3F_8 closely obeys the Curie–Weiss law (Fig. 3). The small value of the Weiss constant ($\theta = -4.2(5) \text{ K}$) indicates that the material is magnetically dilute. The simple paramagnetism of Ag_3F_8 confirms this and shows that the Ag(II) species must be separated from one another by diamagnetic Ag(III) species, thus providing for only weak coupling between the Ag(II).

When the magnetic moment given by Bougon et al. [3] for their “ AgF_3 ” is recalculated for the formula Ag_3F_8 , it becomes $\mu_{\text{eff}} = 1.95(8) \mu_{\text{B}}$ which is in very good agreement with the magnetic moment measured for pure Ag_3F_8 $\mu_{\text{eff}} = 1.924(3) \mu_{\text{B}}$. This and the X-ray diffraction pattern establish that Bougon’s “ AgF_3 ” was really Ag_3F_8 .

Ag_3F_8 could be obtained also by the reaction between Ag_2F_5 (see Section 4.2.2.4) and AgF_3 in aHF in 1:1 molar ratio.



Easy formation of Ag_3F_8 and its much greater stability relative to AgF_3 indicate that the Ag(III) in this mixed valence compound is less electronegative than in AgF_3 . In

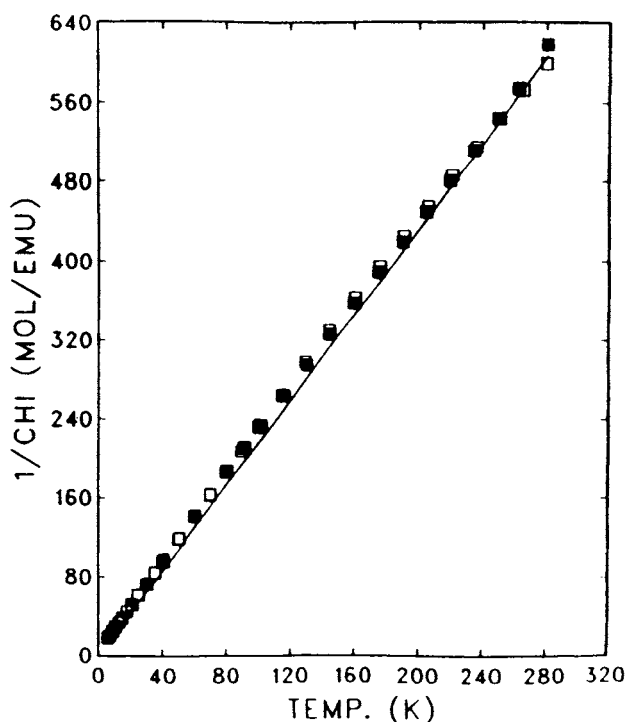


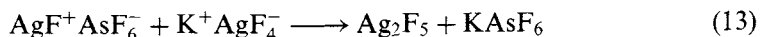
Fig. 3. Curie-Weiss plot for Ag_3F_8 □, 5 kG; ■, 40 kG (Reprinted with permission from J. Am. Chem. Soc., 113, May 1991, pp. 4192–4198. Copyright 1991 American Chemical Society.)

Ag_3F_8 , silver(III) resides in an electron rich species close in character to $[\text{AgF}_4^-]$. The salt formation $\text{Ag(II)[Ag(III)F}_4\text{]}_2$ fits the known fluoro base properties of AgF_2 and the fluoro acid character of AgF_3 .

4.2.2.4 Synthesis and some properties of Ag_2F_5

AgF_2 behaves also as a monofluoro base the first identified case [9,10] being that of $\text{AgF}^+\text{AsF}_6^-$. With the synthesis [11] of $\text{AgF}^+\text{BF}_4^-$ it appeared probable that the salt $\text{AgF}^+\text{AgF}_4^-$ would also exist. This material was sought because of the likelihood of the cation being a chain polymer, with linearly and symmetrically coordinated Ag(II) , as in $\text{AgF}^+\text{AsF}_6^-$ [10] and $\text{AgF}^+\text{BF}_4^-$ [12]. This structural conjecture has not been proved but the X-ray diffraction pattern of AgFAgF_4 is similar to that of AgFAuF_4 and the latter has been shown [12] to be isomorphous with the material $\text{CuF}^+\text{AuF}_4^-$ [13] in which a polymeric $(\text{CuF})_n^{n+}$ chain occurs. In the absence of definitive structural evidence for the salt formulation $\text{AgF}^+\text{AgF}_4^-$, the 1:1 complex of AgF_2 and AgF_3 is referred to as Ag(II)Ag(III)F_5 [6]. The compound Ag(II)Ag(III)F_5 was made by titration of a blue solution of $\text{AgF}^+\text{AsF}_6^-$ in aHF with an equimolar

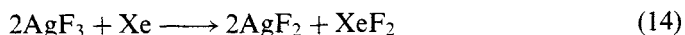
solution of K^+AgF_4^- to precipitate a maroon solid. The supernatant solution of aHF was colourless.



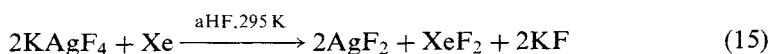
4.2.2.5 Oxidizing capability of Ag(III)

The superior fluoride ion affinity and greater aHF solubility of AsF_5 relative to BF_3 [14] is responsible for the difference in the reactivity of both acids with AgF_3 . The removal of F^- from Ag(III) should generate an exceptionally high electronegativity at silver in $[\text{AgF}_2]^+$ species [6]. Electron capture, with fluorine release, is to be expected for Ag(III) in $[\text{AgF}_2]^+$ since even cationic Ag(II) possesses extraordinary oxidizing power and is able to oxidize Xe to XeF_2 at room temperature [11]. The quantitative reduction of AgF_3 by AsF_5 in aHF suggested that the cation AgF_2^+ or some other cationic Ag(III) species could be the precursor to F_2 elimination.

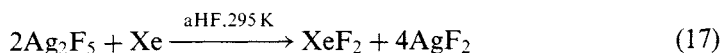
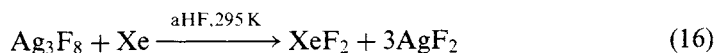
This high oxidating power of even neutral AgF_3 is demonstrated by its reaction, in suspension in aHF, with xenon gas at ordinary temperatures and pressures.



Thus, AgF_3 is a more effective fluorine atom source than molecular fluorine, with which xenon does not react at ordinary temperatures and pressures in the absence of catalyst. It is more surprising that even AgF_4^- is able to oxidize xenon since Ag(III) in the electron rich environment of an anion must be less electronegative than the Ag(III) in AgF_3 :



Also the mixed valence state fluorides, e.g. Ag_3F_8 and Ag_2F_5 are able to oxidize xenon:



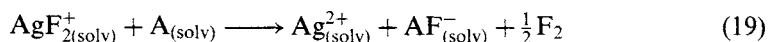
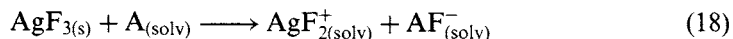
It is clear that Ag(III) in any fluoro ligand environment has a high enough electron affinity to take an electron from Xe and to be an effective source of fluorine atom ligands.

4.2.2.6 Cationic $\text{Ag(III)}_{(\text{solv})}$ species in aHF and its oxidizing capability

The instability of AgF_3 with respect to loss of fluorine in aHF was itself evidence of the greater electronegativity of this high-oxidation state in a neutral compound,

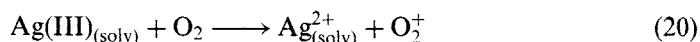
compared with this same state in the anion. It raised the possibility of even higher oxidizing potency for a cationic Ag(III) species derived from AgF₃, using strong F⁻ acceptors in aHF.

Stronger fluoro acids AsF₅, SbF₅ and BiF₅ (A) are sufficiently good F⁻ acceptors to cause AgF₃ to enter into solution in aHF first as Ag(III)_(solv) and finally as Ag_{g(solv)}²⁺ with liberation of fluorine.



It seems that Ag(III)_(solv) is a relatively long lived species in aHF under these conditions, since both PtF₆⁻ and RuF₆⁻ are oxidized to their neutral relatives in high yield (60% or better) [15]. Neither hexafluoride is generated by the action of fluorine on solutions of PtF₆⁻ or RuF₆⁻. The oxidizing species under the conditions used have to be cationic Ag(III) because of the strongly acidic conditions. Since it effectively removes the electron from PtF₆⁻ and RuF₆⁻, it is superior in that regard to KrF⁺. The salt KrF⁺PtF₆⁻ is known and is thermally stable at room temperature [16] when it decomposes the decomposition products are PtF₅, krypton and fluorine and not PtF₆. This indicates that unlike Ag(III)_(solv), the KrF⁺ is not able to take the electron from PtF₆⁻.

As anticipated, the dissolved Ag(III) species oxidizes oxygen in aHF at room temperature in high yield. (This is unlike Ag_{g(solv)}²⁺ which is only able to oxidize O₂ effectively in aHF [15] at or below 195 K).

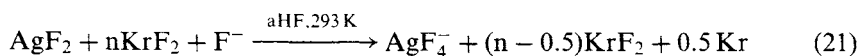


4.2.3 Complex fluorides of silver(III)

4.2.3.1 New synthetic routes to AgF₄⁻ salts

Potassium tetrafluoroargentate(III) was first described by Hoppe in 1957 [17]. It was synthesized by fluorination of mixtures of binary nitrates or halides. Hoppe and Homann [18] established from powder data that the interatomic distance in the square anion AgF₄⁻ is 1.90 Å. At approximately the same time Edwards et al. [19] also reported a preparation of KAgF₄ and their unit cell (also from the powder data), was in good agreement with that of Hoppe and Homann.

In the study of the catalytic influence of AgF₂ on the reaction between xenon and fluorine to form xenon fluorides [20] no evidence of interaction between AgF₂ and xenon(VI) fluoride was found, up to 393 K. The new synthetic approach to the synthesis of xenon(VI) fluoroargentate(III) was to use KrF₂ as a strong fluorinating agent in combination with XeF₆ as a moderately good fluoride-ion donor, in aHF as a solvent, at room temperature [21].



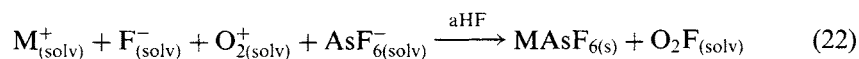
Using the same synthetic route, very pure KAgF_4 was also synthesized at room temperature, by making aHF basic with KF instead of XeF_6 .

XeF_5AgF_4 is a light yellow solid which is stable in thoroughly dried nickel, Teflon, FEP or even glass vessels. It is extremely sensitive to traces of moisture which rapidly turns it brown. It dissolves in aHF without decomposition. XeF_5AgF_4 is stable in a dynamic vacuum up to 343 K, when it begins to lose XeF_6 and fluorine. The final product is Ag_3F_8 as was shown by X-ray powder diffraction pattern. XeF_5AgF_4 is diamagnetic.

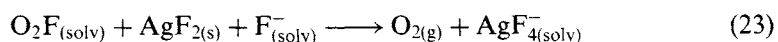
KAgF_4 is a yellow diamagnetic solid. It is stable in thoroughly dried nickel, Teflon, FEP or glass vessels. With traces of moisture it immediately turns brown. It is quite soluble in aHF (about 5 mmol per ml aHF). The concentrated solution in aHF is dark yellow orange.

The AgF_4^- salt can also be made, from AgF_2 or lower fluorides, in aHF solution made basic with good fluoride ion donors, by photodissociating F_2 with visible or UV light. LiAgF_4 was synthesized from the mixture of AgF_2 and LiF in molar ratio close to 1:1 at 293 K in aHF pressurised by about 2 atm of fluorine and UV irradiated for several hours [7]. The yield was low. A better yield was obtained by using excess of LiF (more basic aHF solution). Instead of UV irradiation also sunlight was used. The same method was used also for the preparation of KAgF_4 with practically quantitative yield. The obtained KAgF_4 was separated from KHF_2 (used in excess) by using the fluoro acid PF_5 to precipitate KPF_6 [7] to the first evidence of AgF_3 precipitation. (Here the similar fluoro acidity of PF_5 and AgF_3 was exploited).

Another synthetic route for the preparation of AgF_4^- salts is the use of $\text{O}_2\text{F}_{(\text{solv})}$ in aHF as an oxidizer [22]. Addition of alkali fluoride (MF) in solution in aHF to an O_2^+ salt solution (e.g. O_2AsF_6) at or below 223 K, usually produced a precipitate of alkali salt MAsF_6 and the oxidizer $\text{O}_2\text{F}_{(\text{solv})}$:



A particularly useful application of $\text{O}_2\text{F}_{(\text{solv})}$ is in the oxidation of fluorides that are themselves insoluble in aHF but the oxidized product being soluble; such an example is the oxidation of AgF_2 .



The oxidation of AgF_2 , both here, and in the photodissociated F_2 synthesis [7], could involve the formation of mixed valence state materials, such as Ag_2F_5 and Ag_3F_8 , at the AgF_2 surface.

4.2.3.2 Crystal structures of some AgF_4^- salts

4.2.3.2.1 Crystal structure of XeF_5AgF_4 . The crystal structure of XeF_5AgF_4 [8] confirms the earlier conclusion, based on Raman spectroscopy, that the material

is an essentially ionic assembly [21]. Each AgF_4^- interacts with two XeF_5^+ groups above and two below the layer of anions. This set of three strongly attracting layers ($\text{Xe} \cdots \text{F}(\text{Ag}) = 2.637(11) \text{ \AA}$) is fully charge compensated. The structure accommodates the bulky cations by arranging them head-to-tail in a close packed double layer as illustrated in the unit cell representation in Fig. 4. The axial F ligands of XeF_5^+ of one layer close-pack with the equatorial F ligands of the other layer. It is, perhaps, the lack of strong cohesion between these interpenetrating cation layers that explains the mica-like crystal habit of this material.

The interatomic distance $\text{Ag}-\text{F}$ is not significantly different from that given by Hoppe and Homann [18] for MAgF_4 ($\text{M} = \text{Na}, \text{K}$). The distance $\text{Ag(III)}-\text{F}$ of $1.902(11) \text{ \AA}$ is not significantly different from that of $1.915(3) \text{ \AA}$ [23] given for $\text{Au(III)}-\text{F}$ in KAuF_4 . Although the coordination of the cation to four anionic F ligands generates a capped-Archimedean-antiprism geometry (Fig. 5) like that

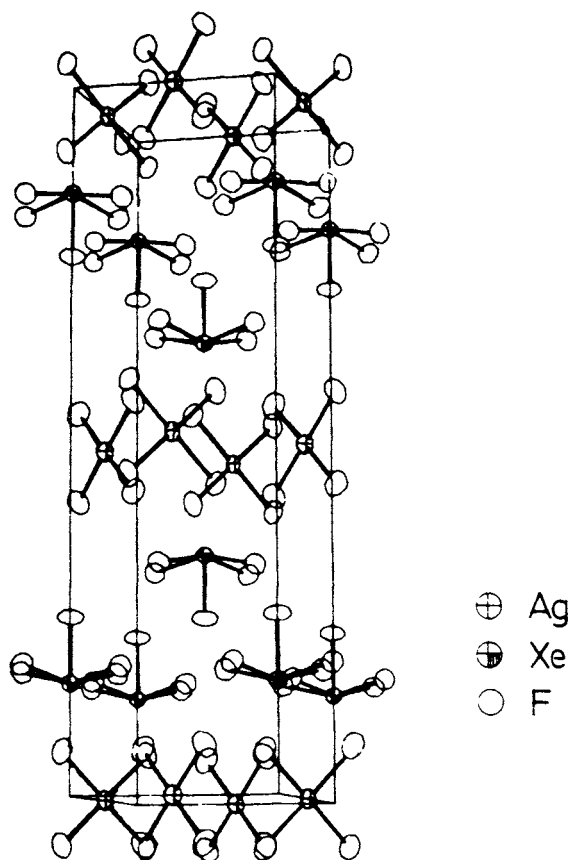


Fig. 4. Unit cell of XeF_5AgF_4 (Reprinted with permission from *Inorg. Chem.*, 28, September 1989, pp. 3467–3471. Copyright 1989 American Chemical Society.)

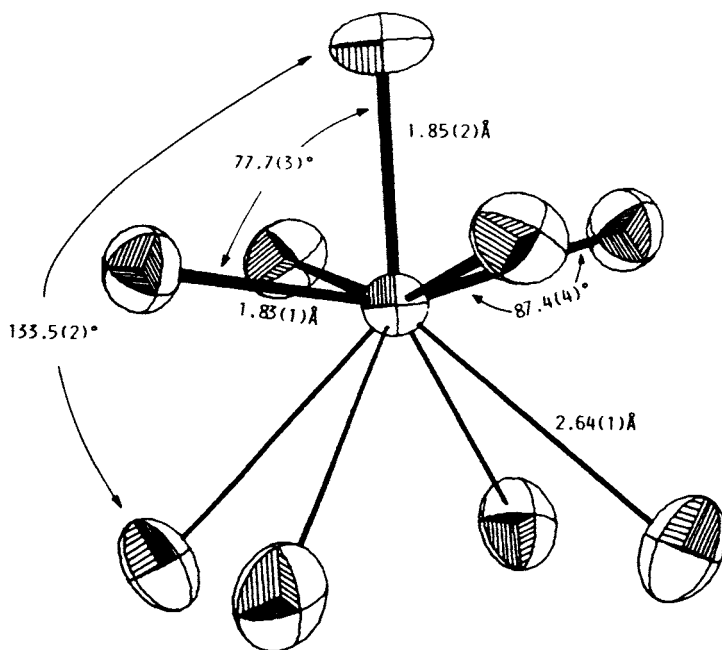


Fig. 5. XeF_5^+ cation in XeF_5AgF_4 (Reprinted with permission from *Inorg. Chem.*, 28, September 1989, pp. 3467–3471. Copyright 1989 American Chemical Society.)

observed in XeF_5MF_6 salts [24] with $\text{M} = \text{Pt}$ [25], Ru [26] and Nb [27], the cation shape exhibits some possible differences from the XeF_5^+ in the latter salts.

The apparent differences are that the axial bond $\text{Xe}-\text{F}_{\text{ax}}$ is longer, although not significantly so ($1.852(19) \text{ \AA}$) than $\text{Xe}-\text{F}_{\text{eq}}$ ($1.826(9) \text{ \AA}$), whereas the reverse usually holds; and the $\text{F}_{\text{ax}}-\text{Xe}-\text{F}_{\text{eq}}$ angle is smaller ($77.7(8)^\circ$), although again not significantly so, than the usual one of 80° . This angle reduction, taken together with the stretching of the $\text{Xe}-\text{F}_{\text{ax}}$ distance, suggests that the F ligand of the AgF_4^- interacts with the cation more strongly than in the XeF_5MF_6 salts. This is also in accord with the four shorter than usual cation-anion $\text{Xe}\cdots\text{F}$ distances in XeF_5AgF_4 (four at $2.64(1) \text{ \AA}$) which are to be compared with those in XeF_5RuF_6 , one at $2.55(1) \text{ \AA}$, another at $2.60(1) \text{ \AA}$ and two at $2.92(1) \text{ \AA}$. These differences can be attributed to greater charge for each F ligand in AgF_4^- compared with the MF_6^- ligands. The lower ligand number in the AgF_4^- anion is the major reason for this.

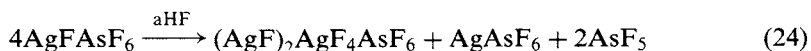
4.2.3.2.2 Crystal structure of KAgF_4 . The crystal structure of KAgF_4 [28] is the result of the interaction of potassium cations and essentially square planar AgF_4^- . Each AgF_4^- anion has its pseudo 4-fold axis perpendicular to the c axis. The AgF_4 plane of each anion is perpendicular to the AgF_4 planes of its four nearest neighbours. Each fluorine ligand of the AgF_4^- group interacts with two K^+ so that

each AgF_4^- interacts with four cations above and four cations below the layer of AgF_4^- . Potassium is therefore surrounded by eight fluorine atoms in a roughly cubic arrangement. The interatomic distance $\text{Ag(III)}-\text{F}$ is 1.889(3) Å which is not significantly different from the $\text{Ag(III)}-\text{F}$ in XeF_5AgF_4 of 1.902(11) Å [8].

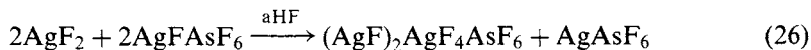
4.2.3.3 Synthesis of $(\text{AgF})_2\text{AgF}_4\text{MF}_6$ with $\text{M} = \text{As}, \text{Au}, \text{Sb}, \text{Pt}$

In many reactions in which Ag(II) or Ag(III) fluorides were involved in interaction with AsF_5 in aHF a black solid, of composition $(\text{AgF})_2\text{AgF}_4\text{MF}_6$ [29,30], was produced. Its X-ray powder photographs showed a clear relationship to those of rhombohedral binary trifluorides, notably that of RuF_3 .

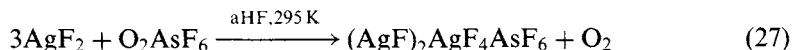
The black solid was produced in admixture with colourless AgAsF_6 in a disproportionation associated with solvolysis by aHF [31] when successive aliquots of aHF were added to AgFAsF_6 .



The black solid was also obtained by fluorination AgFAsF_6 in aHF or by interaction of AgF_2 with AgFAsF_6 in aHF.



It was also obtained in the reaction of AgF_3 with one equivalent of AsF_5 in aHF. Although it and its $(\text{AgF})_2\text{AgF}_4\text{MF}_6$ ($\text{M} = \text{Sb}, \text{Au}, \text{Pt}$) relatives are common products of oxidation and solvation of Ag(II) in aHF, their syntheses in high purity are more difficult to do. Very efficient synthesis of $(\text{AgF})_2\text{AgF}_4\text{AsF}_6$ was achieved via the interaction of AgF_2 and O_2AsF_6 in the molar ratio slightly less than 3:1. Although the solubility of AgF_2 is very low in aHF, the reaction is quantitative and facile:



Similar procedures are also effective for the preparation of $(\text{AgF})_2\text{AgF}_4\text{PtF}_6$, $(\text{AgF})_2\text{AgF}_4\text{AuF}_6$ and $(\text{AgF})_2\text{AgF}_4\text{SbF}_6$. In the case of gold and antimony the reactions are very slow. The reaction could be promoted by acidifying the aHF with BF_3 thus dissolving the AgF_2 to form AgFBF_4 which has greater solubility. Replacing AgF_2 by AgFBF_4 produces more crystalline products.



$\text{M} = \text{As}, \text{Au}, \text{Pt}, \text{Sb}$

The magnetic susceptibility of $(\text{AgF})_2\text{AgF}_4\text{AsF}_6$ [32] as a function of temperature show a small temperature independent paramagnetism at least down to 60 K when a Curie “tail” occurs which could represent small amounts of paramagnetic impurity. This magnetic behaviour, which is like that of a metallic system, is essentially identical in magnitude and in its temperature independence (above ~ 60 K) to that of the other known AgF^+ salts [12].

4.2.3.4 Crystal structure of $(\text{AgF})_2\text{AgF}_4\text{AsF}_6$

The structure consists of zigzag $(\text{AgF})_n^{n+}$ chains running along the c axis enclosing anion arrays of alternating inclined planar and octahedral anions AgF_4^- and AsF_6^- [29]. Therefore, the material should be formulated as $(\text{AgF}^+)_2\text{AgF}_4^-\text{AsF}_6^-$. The three Ag species are of two types: two Ag(II) and one Ag(III). The two Ag(II) are each linearly coordinated by two F ligands, each shared with an other Ag(II) atom, thus generating the $(\text{AgF})_n^{n+}$ chains. The Ag(III) is in an approximately square F ligand environment, as in the AgF_4^- anion. This anion is interacting with AsF_6^- above and below it at long $\text{Ag} \cdots \text{F}$ interatomic distances roughly perpendicular to the AgF_4^- plane. Although the AsF_6^- and AgF_4^- anions within one cation-chain cage, are in ordered alternating sequence along the c axis, like ordered stacks of anions, in neighbouring cells are not necessarily in registry. This renders all Ag(II), of the $(\text{AgF})_n^{n+}$ chains, equivalent to one another.

All the metal atoms are in pseudo-octahedral environments, with each fluorine ligand coordinated to only two metal atoms. This explains why the diffraction characteristics are so like those of a trifluoride. This rather closed packed structure probably gives these materials very favourable lattice energy, thus accounting for their relative ease of formation.

4.2.4 AgF^+ and Ag^{2+} salts

4.2.4.1 Syntheses of some novel AgF^+ salts and Ag^{2+} salts and their oxidizing capabilities

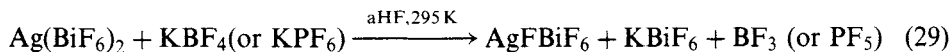
A series of AgF^+ salts (AgFMF_4 with $\text{M} = \text{B}, \text{Au}$ and AgFMF_6 with $\text{M} = \text{As}, \text{Au}, \text{Ir}, \text{Ru}, \text{Sb}, \text{Bi}$) have been prepared. The first was AgFAsF_6 [9] made by the interaction of AgF_2 with AsF_5 in aHF. They all have the weak, temperature independent paramagnetism indicative of a partially filled band and suggestive of metallic character [12]. In no case however has electrical conductivity of metallic type been demonstrated in any one of these solids. A wide variety of synthetic routes have been demonstrated for the preparation of $(\text{Ag}-\text{F})_n^{n+}$ salts.

AgFBF_4 was prepared by the reaction of AgF_2 and BF_3 in aHF [11] and by the reaction of AgBF_4 in aHF under pressure of BF_3 and elemental fluorine [12]. AgFAuF_4 was prepared by the reaction between AgFAsF_6 and KAuF_4 in aHF. The green precipitate formed on warming to room temperature was washed free of KAsF_6 and excess AgFAsF_6 by decantation and back distillation of aHF [12].

AgFAuF_6 was prepared by the reaction of KAuF_6 and AgFAsF_6 in aHF and subsequent washing of the product with aHF [12]. AgFMF_6 ($\text{M} = \text{Ir}, \text{Ru}, \text{Sb}, \text{Bi}$)

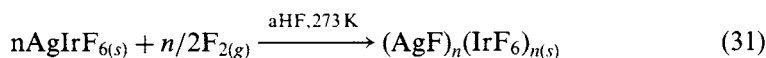
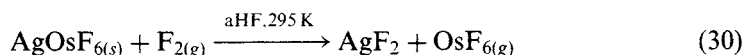
were prepared by the fluorination of the corresponding AgMF_6 compounds with elemental fluorine in aHF [33].

AgFBiF_6 was prepared also by the reaction:

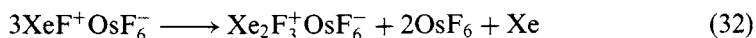


This synthesis nicely demonstrates the loss of F^- from a weak acid anion (BF_4^- or PF_6^-) to Ag^{2+} .

The low solubility of AgF^+ salts in aHF is in accord with the polymeric (one-dimensional) nature of the cation. The oxidizing power of the $(\text{AgF})_n^{n+}$ species is indicated by the following two reactions:



The immediate release of OsF_6 when AgOsF_6 is treated with elemental fluorine can be explained as electron capture by AgF^+ from OsF_6^- . This oxidation of OsF_6^- by $(\text{AgF})_n^{n+}$, is like that of $\text{XeF}^+\text{OsF}_6^-$ which decomposes [34]:



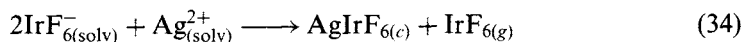
indicating that the $(\text{AgF})_n^{n+}$ has a comparable electron affinity to XeF^+ which has been estimated to be $1021 \pm 33 \text{ kJ mol}^{-1}$. On the other side $(\text{AgF})_n^{n+}(\text{IrF}_6)_n^{n-}$ is formed quantitatively under the same reaction conditions. The $(\text{AgF})_n^{n+}$ species has therefore an oxidizing potential in aHF which is greater than that of OsF_6 but less than that of IrF_6 (the electron affinities of the gases are, respectively, 5.7 and 6.7 eV).

The solvated $\text{Ag}_{(\text{solv})}^{2+}$ in aHF is stabilized by those MF_6^- that are very poor F^- donors (see below) but even AsF_5 stabilizes it in aHF since blue solutions are obtained by the reaction of AgFAsF_6 with an equimolar quantity of AsF_5 or when AgAsF_6 is oxidized by an equivalent of O_2AsF_6 [29] in aHF. Removal of aHF from such a solution of $\text{Ag}^{2+}(\text{AsF}_6^-)_2$ results in AsF_5 loss, even if the isolation is carried out at 213 K, because of the inadequate fluoro acidity of AsF_5 . Clearly, unsolvated Ag^{2+} is a sufficiently powerful fluoride ion acceptor to take F^- from AsF_6^- in $\text{Ag}^{2+}(\text{AsF}_6^-)_2$. The F^- affinity of gaseous AsF_5 has been evaluated to be at least 464 kJ mol^{-1} [14]. The following set of $\text{Ag}(\text{MF}_6)_2$ with $\text{M} = \text{Sb}$ [35], Nb [36], Ta [36] and Bi [33] is known. Recently also $\text{Ag}(\text{AuF}_4)_2$ [37] was structurally characterized as $\text{Ag}^{2+}(\text{AuF}_4^-)_2$ and since Ag_3F_8 [12] is isomorphous with that material, it is probable that it is also a Ag^{2+} salt. In an experiment designed to check if

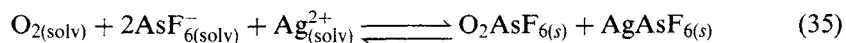
$\text{Ag}_{(\text{solv})}^{2+}$ in aHF is able to oxidize RuF_6^- the new Ag^{2+} salt with mixed anions was obtained $\text{AgRuF}_6\text{BiF}_6$ [33].



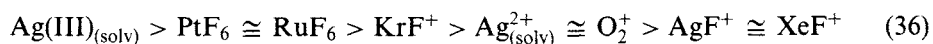
Not only is the Ag^{2+} species a stronger F^- acceptor than $(\text{AgF})_n^{n+}$ it is also a more potent oxidizer. This is demonstrated by the quick evolution of IrF_6 in the reaction of LiIrF_6 with $\text{Ag}(\text{SbF}_6)_2$.



$\text{Ag}_{(\text{solv})}^{2+}$ is able to oxidize Xe [11] at room temperature, and O_2 [15] (which is much less soluble in aHF than Xe) at 195 K. At 213 K the blue colour, characteristic of $\text{Ag}_{(\text{solv})}^{2+}$ is observable whereas the precipitated salts ($\text{O}_2^+ \text{AsF}_6^-$ and $\text{Ag}^+ \text{AsF}_6^-$) are colourless.



This big influence of temperature on the equilibrium is a consequence of the large change in translational entropy in going from reactants to products [15]. $\text{Ag}_{(\text{solv})}^{2+}$ is also able to oxidize perfluoroolefins such as perfluoropropene the ionization potential of which is much lower ($I = 10.62 \text{ eV}$) [29] than those of xenon or oxygen. The observed formation of perfluoropropane (quantitatively) is in accord with the cation being attacked by F^- , followed by a second one-electron oxidation and F^- attack. The hierarchy of powerful oxidizers could be written as follows (see also Sections 4.2.2.5 and 4.2.2.6).



4.2.4.2 Crystal structures of some AgF^+ salts

All AgF^+ salts that have been structurally characterized so far contain F-bridged $(\text{Ag}-\text{F})_n^{n+}$ chains or ribbons, with the Ag(II) linearly or square coordinated by F ligands, the MF_4^- tetrahedra or MF_6^- octahedra being cross-linked to these chains via F bridges.

The structure of AgFBF_4 [12] (either violet or bronze crystals) is illustrated in Fig. 6. (Crystals of roughly octahedral morphologie with a bronze luster were grown from the solutions of AgFBF_4 containing some AgF . Violet crystals were grown from the pure solutions of AgFBF_4).

Each linear $(\text{Ag}-\text{F})_n^{n+}$ chain, with two $\text{Ag}-\text{F} = 2.002(3)$, and $2.009(3) \text{ \AA}$ (violet AgFBF_4), is surrounded by four columns of linearly close-packed BF_4^- , and vice versa. Each Ag(II) atom in the chain is further coordinated by four F ligands of the anions in square array ($\text{Ag}-\text{F} = 2.330(2) \text{ \AA}$), each from one of the four surrounding BF_4^- anions. The Ag(II) is essentially in the same plane as these four

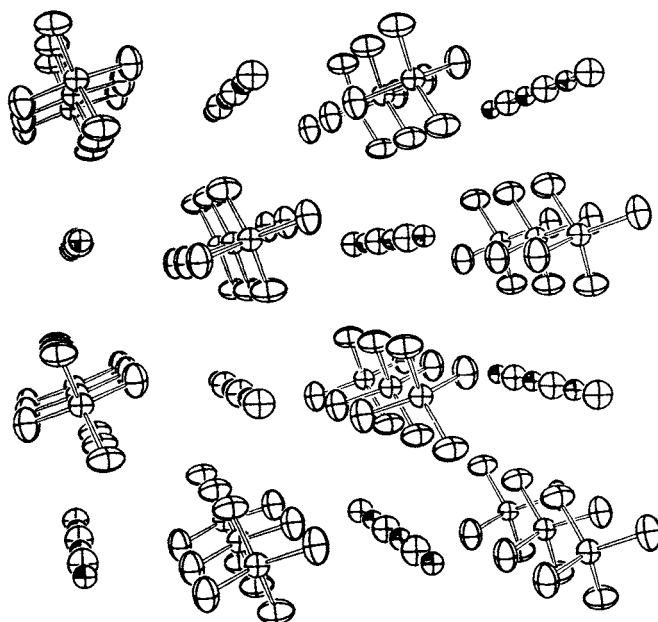


Fig. 6. The AgFBF_4 extended structure (Reproduced with permission of Academic Press from *J. Solid State Chem.*, 96, 1992, pp. 84–96.)

F ligands. The short Ag—F distances (those within the chain) must represent appreciable overlap of the valence-shell orbitals of the $4d$ and $5s$ of Ag(II) and the $2p$ of F.

The compound AgFAuF_4 [12] was found to be isostructural with CuFAuF_4 [13] in which a linear —Cu—F—Cu—F— chain had also been established [13].

The crystal structure of AgFAsF_6 [10] was the first structure determined for an $(\text{AgF})_n^{n+}$ salt. The structure consists of an infinite $(\text{AgF})_n^{n+}$ chain with Ag—F average $2.000(5)$ Å, F—Ag—F = $175.5(2)^\circ$ and kinked at F, with Ag—F—Ag = $143.3(3)^\circ$. AsF_6 octahedra are cross-linked to these chains via further F bridges. The Ag environment approximates to a pentagonal bipyramid with F ligands of the $(\text{AgF})_n^{n+}$ cation at each apex. The AsF_6 are distorted from octahedral symmetry because of their interaction with the cation. The nonbridging As—F distance is $1.677(7)$ Å while the bridging As—F distances are in the range $1.714(4)$ – $1.729(6)$ Å. The Ag—F distances with F ligands from the AsF_6 octahedra are in the range 2.394 – $2.439(6)$ Å.

The X-ray powder data for AgFAuF_6 [12] show that this salt is isostructural with AgFAsF_6 [10]. The interchain distances and the chain kinking have to be very similar to those observed in AgFAsF_6 , as has been established from a single-crystal structure of the iridium relative AgFIrF_6 salt [33].

Although the anion RuF_6^- is only ~ 0.3 Å³ smaller than IrF_6^- [33] the structure of AgFRuF_6 is different from that of AgFIrF_6 . The Ag(II) species in the AgFRuF_6 salt

is approximately square-coordinated by four F ligands (in this, resembling $\text{Ag}(\text{MF}_6)_2$ salts). $\text{Ag}(\text{II})$ species are brought close to one another by two *cis* related bridging F ligands, each nearly equidistant from two $\text{Ag}(\text{II})$ (2.007(3) and 2.018(2) Å). The nearly square F ligand array involves another two ligands, one from each of two RuF_6^- (2.140(3) and 2.158(3) Å). RuF_6^- octahedra are distorted. For those F ligands that make close contact with $\text{Ag}(\text{II})$ the Ru—F are 1.909(3) and 1.895(3) Å. Non-bridging Ru—F are in the range 1.812(3)–1.853(3) Å. Each RuF_6^- bridges two $\text{Ag}(\text{II})$. As shown in Fig. 7, all connected $\text{Ag}(\text{II})$ with their near-neighbour F ligands lie in a common plane. The $(\text{Ag}-\text{F})_n^{n+}$ cation is in this case a one-dimensional ribbon. This ribbon shows a striking resemblance to the coordination of $\text{Ag}(\text{II})$ in AgF_2 [38].

The X-ray powder diffraction photographs show that the salts AgFSbF_6 and AgFBiF_6 are isostructural with one another but not with the other known AgFMF_6 structures. The structure is not known.

The possible explanation for the two coordination of $\text{Ag}(\text{II})$ in AgFMF_6 ($\text{M} = \text{As}, \text{Ir}, \text{Au}$) AgFAuF_4 and AgFBF_4 and for the four coordination in AgFRuF_6 is associated with the negative charge on the fluorine ligands of the anion. Of course, the F ligand charge in BF_4^- and AuF_4^- is greater than in any of the MF_6^- considered in this chapter if for no other reasons than that there

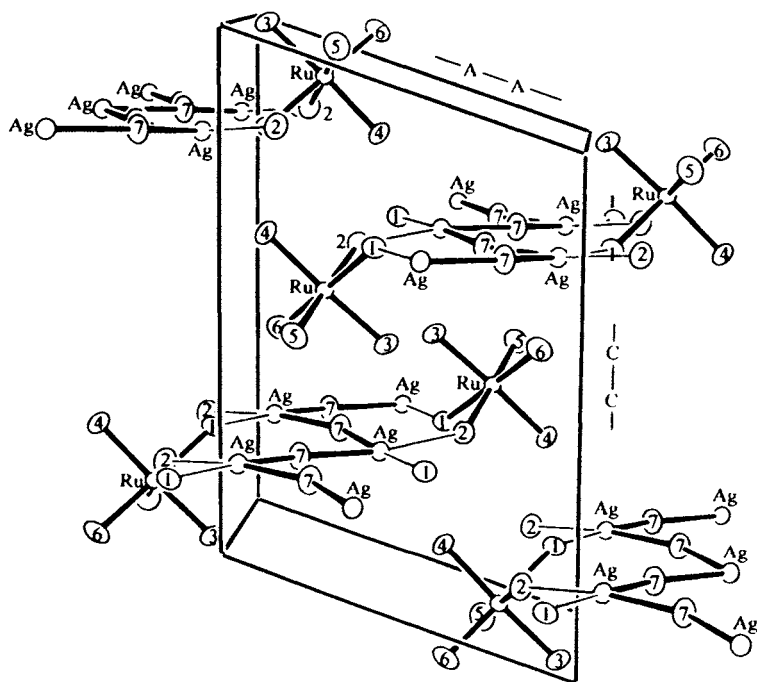


Fig. 7. Structure of AgFRuF_6 (Reprinted with permission from *Inorg. Chem.*, 34, May 1995, pp. 2692–2698. Copyright 1995 American Chemical Society.)

are only four F ligands for unit negative charge of BF_4^- or AuF_4^- . If the four coordination of Ag(II) in AgFRuF_6 is a consequence of low F ligand charge in the anion, the same would be expected for AgFSbF_6 and AgFBiF_6 . If so, it is possible that the anionic F ligands in the Ag(II) four-coordinate AgF_4 unit are placed *trans* rather than *cis* as in AgFRuF_6 .

4.2.4.3 Crystal structures of some Ag^{2+} salts

The first $\text{Ag}^{2+}(\text{MF}_6)_2$ salts of which the structures were determined (all are isostructural) were $\text{Ag}(\text{SbF}_6)_2$ [35], $\text{Ag}(\text{NbF}_6)_2$ [36] and $\text{Ag}(\text{TaF}_6)_2$ [36]. More recently also the structure of $\text{Ag}(\text{BiF}_6)_2$ has been described [33] and is illustrated in Fig. 8.

Ag^{2+} occupies an elongated octahedral site at the center of symmetry, in an approximately close-packed F ligand array provided by the anions. The distances in the approximately square F ligand array are: $2 \times \text{Ag}-\text{F} = 2.096(9) \text{ \AA}$ and $2 \times$ at $2.122(9) \text{ \AA}$. The two long bonds have $\text{Ag}-\text{F} = 2.440(10) \text{ \AA}$. The BiF_6^- octahedra are distorted. The Bi—F ligands that do not approach the Ag(II) have distances in the range $1.939(10)$ – $1.944(10) \text{ \AA}$, while those F that make close contact with the Ag(II) have Bi—F distances of $2.048(9)$ and $2.046(9) \text{ \AA}$. The long-bonded F

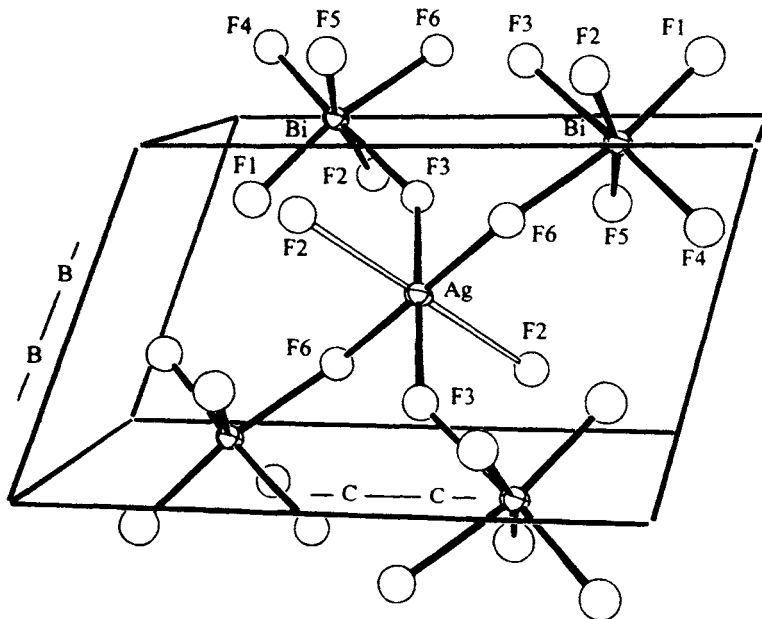


Fig. 8. Structure of $\text{Ag}(\text{BiF}_6)_2$ (Reprinted with permission from *Inorg. Chem.*, 34, May 1995, pp. 2692–2698. Copyright 1995 American Chemical Society.)

of the Ag(II) has $\text{Bi—F} = 1.966(9) \text{ \AA}$. Clearly, the shape of the BiF_6^- measures the strength of the individual F ligand interactions with the Ag^{2+} .

Recently also, the structure of $\text{Ag}[\text{AuF}_4]_2$ was determined [37]. In this compound the fluorine ligands around Ag^{2+} again form a tetragonally elongated octahedron with the Ag—F distances $2 \times 2.484 \text{ \AA}$, $2 \times 2.162 \text{ \AA}$ and $2 \times 2.072 \text{ \AA}$. The F of the elongated Ag—F are not perpendicular to the AgF_4 plane but are at an angle of $101.7\text{--}105.4^\circ$ to it. The distances (Au—F) in a square planar AuF_4 unit range from 1.899 to 1.946 \AA .

4.2.4.4 Magnetic properties of AgF^+ and Ag^{2+} salts

The nearly temperature independent magnetic susceptibility data for the AgFMF_6 compounds in the temperature range (from 50 to 280 K), shown on Fig. 9, indicate that the Ag(II) moments in the fluorine-bridged cations $(\text{AgF})_n^{n+}$ must be strongly coupled. All have small and approximately temperature independent magnetic susceptibility characteristic of partially filled band, typical of metals. It appears that the change in structure from coordination two to square coordination does not have a major influence on the magnetic properties since the magnetic data for AgFRuF_6 and AgRuF_6 indicate that the magnetic susceptibility of AgF^+ cation in AgFRuF_6 is also small and nearly temperature independent. This contrasts with the magnetic behaviour of Ag(II) in the salts $\text{Ag}(\text{MF}_6)_2$ of which $\text{Ag}(\text{BiF}_6)_2$ is typical. It obeys the Curie–Weiss law over the temperature range 35–280 K and has a room temperature moment, $\mu_{\text{eff}} = 2.1 \mu_{\text{B}}$ consistent with Ag^{2+} (a d^9 configuration) separated from one another by closed-shell BiF_6^- species.

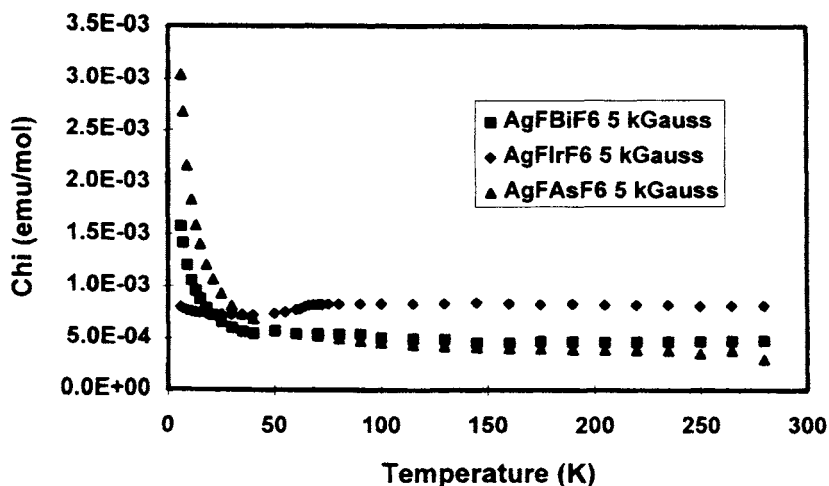
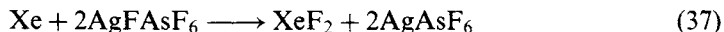


Fig. 9. Magnetic susceptibility of AgFMF_6 ($M = \text{Bi, Ir and As}$) (Reprinted with permission from Inorg. Chem., 34, May 1995, pp. 2692–2698. Copyright 1995 American Chemical Society.)

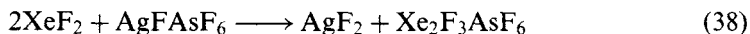
4.2.5 The first coordination compound of XeF_2 to a metal ion

4.2.5.1 Synthesis and some properties of $[\text{Ag}(\text{XeF}_2)_2]\text{AsF}_6$

Cationic $\text{Ag}(\text{II})$ in aHF oxidizes xenon at ordinary temperatures and pressures [11]. As long as there is enough fluoro acid AsF_5 present in aHF to generate the cationic blue $\text{Ag}(\text{II})$ species that solution will oxidize Xe to XeF_2 , or its derivatives.



As the XeF_2 concentration increases in aHF solution of the $\text{Ag}(\text{II})$, this strong base displaces the weaker and less soluble base, AgF_2 .



When all of cationic $\text{Ag}(\text{II})$ has been displaced, the oxidation of xenon ceases. Therefore fluoro acid must be supplied to neutralize the XeF_2 , if oxidation of Xe is to continue:



Additional acid ensures that $\text{Ag}(\text{II})$ remains in solution as cationic species (i.e. AgF_2 , which is insoluble in aHF, is not precipitated) and the xenon oxidation continues. Removal of aHF from a solution where additional fluoro acid was not provided for the neutralization of XeF_2 gave a mixture of AgF_2 , $\text{Xe}_2\text{F}_3\text{AsF}_6$ and $[\text{Ag}(\text{XeF}_2)_2]\text{AsF}_6$ [39].

The compound $[\text{Ag}(\text{XeF}_2)_2]\text{AsF}_6$ was also prepared in pure form both from an aHF solution of XeF_2 and AgAsF_6 and from a melt of AgAsF_6 in liquid XeF_2 . It represents the first example of XeF_2 acting as a ligand for a metal ion.

The high solubility of $[\text{Ag}(\text{XeF}_2)_2]\text{AsF}_6$ in aHF is in contrast to the relatively low solubility of AgAsF_6 . This may mean that the solvated complex cation $[\text{Ag}(\text{XeF}_2)_2]^+$ present in aHF solution is strongly hydrogen bonded to the free end of the XeF_2 ligand.

$[\text{Ag}(\text{XeF}_2)_2]\text{AsF}_6$ can be kept in a closed quartz vessel, but loses XeF_2 slowly in a dynamic vacuum at room temperature to yield finally AgAsF_6 .

The Raman spectrum of $[\text{Ag}(\text{XeF}_2)_2]\text{AsF}_6$ crystals is dominated by the ν_1 mode (symmetric stretch) of XeF_2 . The Raman active fundamentals, ν_1 , ν_2 and ν_5 of AsF_6^- are essentially the same as reported elsewhere. The peak splitting (501 , 508 cm^{-1}) and a slight shift to higher wave number for the ν_1 of XeF_2 , relative to that in crystalline XeF_2 (496 cm^{-1}), must be a consequence of the weak vibrational coupling of the XeF_2 molecules via the interaction with the Ag^+ ion.

4.2.5.2 Crystal structure of $[\text{Ag}(\text{XeF}_2)_2]\text{AsF}_6$

The Ag and As atoms are arranged in a NaCl type lattice. Two-dimensional sheets of that arrangement are preserved in $[\text{Ag}(\text{XeF}_2)_2]\text{AsF}_6$, with each Ag species surrounded by four AsF_6^- in the same plane and vice versa (Fig. 10). Each $\text{Ag}(\text{I})$ is coordinated via F ligands to four XeF_2 molecules in a square arrangement, which

is perpendicular to the AgAsF_6 sheet mentioned above. Each XeF_2 is coordinated through each of its F ligands to two Ag(I) 's. The distance $\text{Ag(I)} \cdots \text{F(Xe)} = 2.466 \text{ \AA}$. The other four F ligands about the Ag(I) are in the plane perpendicular to the plane of F ligands from XeF_2 and are from AsF_6 species, with a distance $\text{Ag(I)} \cdots \text{Feq(As)} = 2.732 \text{ \AA}$. The former distance is shorter than the latter probably as a consequence of a higher negative charge on F ligands from XeF_2 than on the F ligands from AsF_6 . Xenon has, besides its two ligands at the distance of $1.979(3) \text{ \AA}$, twelve surrounding fluorine atoms with distances ranging from 3.34 to 3.64 \AA . The AsF_6^- is a nearly regular octahedron with $\text{As}-\text{F}(\text{axial}) = 1.718(3) \text{ \AA}$ and $\text{As}-\text{F}(\text{equatorial}) = 1.712(3) \text{ \AA}$.

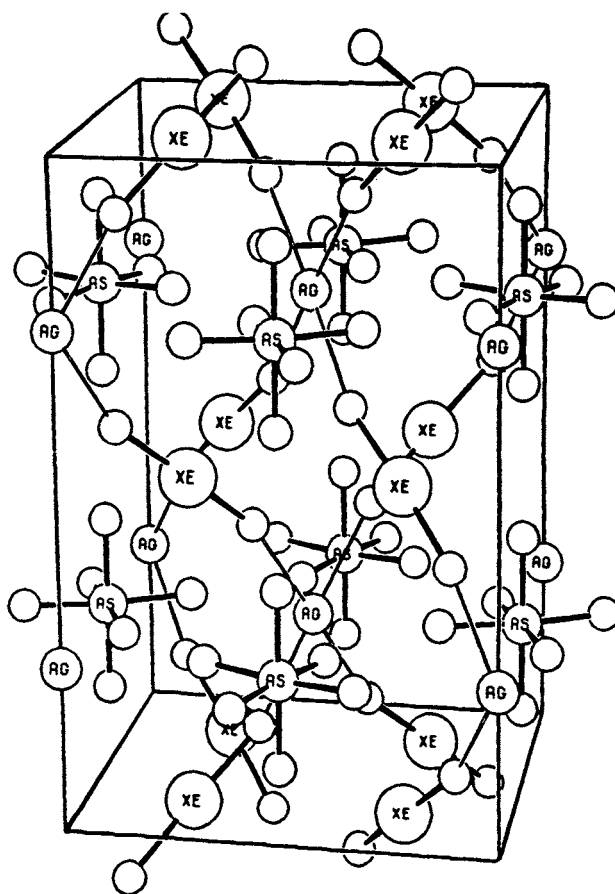


Fig. 10. The unit cell of $[\text{Ag}(\text{XeF}_2)_2]\text{AsF}_6$. (Reproduced with permission of Editions Scientifiques et Medicales Elsevier; 23, rue Linois, 75724 Paris cedex 15, from R. Hagiwara *et al.*, *Eur. J. Solid State Inorg. Chem.*, 28, 1991, pp. 855-866.)

4.3 Binary and complex fluorides of nickel

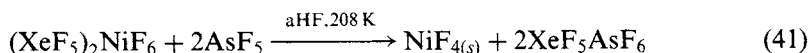
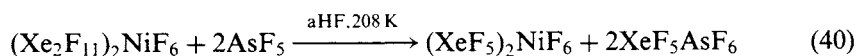
4.3.1 Introduction

The salts of NiF_6^{2-} have long been known [40] but the parent binary fluoride, NiF_4 , has not been described, although there had been efforts [41–43] to establish the existence of a higher binary fluoride than NiF_2 . The recent new synthetic method for the preparation of thermodynamically unstable fluorides [1] has, however, provided a route both to this and NiF_3 . In this chapter the syntheses of nickel(IV) fluoride and of nickel(III) fluorides are described. Three different crystallographic forms of NiF_3 have been established: rhombohedral NiF_3 (R— NiF_3), hexagonal tungsten bronze form (H— NiF_3) and pyrochlore form (P— NiF_3).

4.3.2 Binary fluorides of nickel

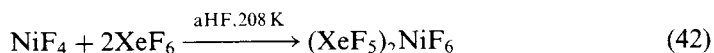
4.3.2.1 Synthesis and some properties of NiF_4

NiF_4 [44] was precipitated from the solution of $(\text{Xe}_2\text{F}_{11})_2\text{NiF}_6$ [45] or $(\text{XeF}_5)_2\text{NiF}_6$ [46] in aHF at 208 K by the fluoro acid AsF_5 or BF_3 .



This system provided for the easy removal of the side product, since XeF_5AsF_6 , is highly soluble in aHF even at 208 K. As AsF_5 was added to the solution of $(\text{Xe}_2\text{F}_{11})_2\text{NiF}_6$ in aHF at 208 K a tan precipitate was formed at the gas-solution interface but rapidly disappeared on agitation of the solution. At the point where nearly two equivalents of AsF_5 had been added this dissolution needed vigorous mixing and the next AsF_5 addition resulted in a permanent tan precipitate. With further addition of AsF_5 the red colour of the solution, characteristic of NiF_6^{2-} , paled, and at the point where four equivalents of AsF_5 had been added, the supernatant solution had a pale-straw colour, characteristic of solutions of XeF_5AsF_6 in aHF. Quenching the system to 77 K showed that there was no fluorine present. NiF_4 was separated from the XeF_5AsF_6 by repeated washing with aHF at 208 K. The dry NiF_4 was stable at 208 K. This powder did not lose fluorine up to 218 K.

Addition of base (e.g. XeF_6) in aHF at 208 K to the NiF_4 dissolved it. After 2 equivalents of XeF_6 were added all of the tan precipitate dissolved and a red solution was obtained, from which $(\text{XeF}_5)_2\text{NiF}_6$ was recovered.

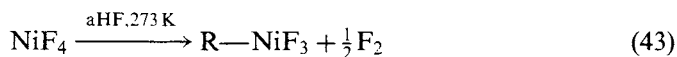


This established that the tan solid is NiF_4 and that it retains its integrity at 208 K, since NiF_2 does not interact with XeF_6 in aHF in the absence of other oxidizers.

The tan solid loses F_2 slowly at 218 K or higher. It is a powerful oxidizer and fluorinator. It dissolves in aHF in the presence of excess acid to (perhaps forming cationic Ni(IV) species) the solutions which are able to electron-oxidize PtF_6^- or RuF_6^- to form the neutral hexafluorides (see Section 4.3.2.6). The acidity of NiF_4 and AgF_3 are very close and not far from the acidity of PF_5 . This was shown by using PF_5 as a fluoro acid (see also Section 4.2.2.1). PF_5 was able to precipitate NiF_4 from NiF_6^{2-} solutions if there was an overpressure of PF_5 in the system. When the overpressure of PF_5 was released, the NiF_4 dissolved again.

4.3.2.2 Syntheses and some properties of R—, H— and P— NiF_3

The decomposition of NiF_4 in aHF at 273 K proceeds smoothly in several hours yielding a black solid, R— NiF_3 [44].



Suspensions of R— NiF_3 in aHF at 293 K slowly evolve fluorine over several days yielding yellow-brown NiF_2 . Rapid loss of fluorine at 293 K, with the assistance of HF occupancy of the lattice voids, may be reasons for the preference for the hexagonal tungsten bronze form of NiF_3 (H— NiF_3) [44] when the NiF_4 is decomposed at that temperature. The best synthetic method to ensure formation of pure R— NiF_3 is to use XeF_5^+ salts (e.g. $(XeF_5)_2NiF_6$) as the starting material for the preparation of NiF_4 . XeF_5AsF_6 is highly soluble in the aHF, even at lower temperatures, and unlike K^+ and smaller alkali cations XeF_5^+ is too big to fit in the hexagonal channels of the H— NiF_3 structure.

A simple and direct approach to the synthesis of NiF_3 is via the interaction of Ni^{2+} and NiF_6^- salts dissolved in aHF:

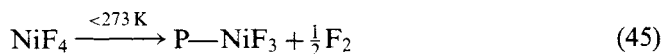


M = As, Sb, Bi

At 273 K R— NiF_3 is the main product, while at 293 K the dominant phase is H— NiF_3 . The relatively high solubility of $KBiF_6$, compared with $KSb(As)F_6$, eases the purification of the NiF_3 and especially recommends the use of $Ni(BiF_6)_2$.

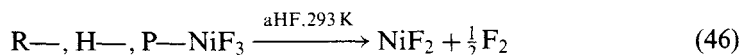
The hexagonal tungsten bronze form of NiF_3 (H— NiF_3) is formed when potassium salts are present in the aHF solution (as illustrated in Eqn. (44)) or when the NiF_4 prepared from K_2NiF_6 is decomposed near 293 K. Analytical data indicate that there is K^+ in the hexagonal tunnels of the structure, with a composition close to $K_{0.12}NiF_3$. Of course, this requires that an equivalent amount of Ni(II) should be present to compensate for the positive charge of K^+ . Loss of HF from the particles of solid H— NiF_3 , which is sufficiently vigorous to propel them in a dynamic vacuum, indicates that the channels are also occupied by HF, the latter probably acting as dielectric spacers between the K^+ . Both the HF and K^+ are similar in size to the fluorine which has been lost.

A pyrochlore form of NiF_3 (P— NiF_3) [44] is formed if *dry* NiF_4 is allowed to decompose at low temperatures.

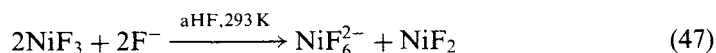


P— NiF_3 has a poorly packed structure perhaps as a consequence of the release of F_2 from the NiF_4 precursor without collapse of residual framework. Absence of solvent may have denied the possibility of recrystallization to a more thermodynamically stable form.

All forms of dry solid NiF_3 lose fluorine when they are warmed (R— $\text{NiF}_3 > 312$ K, H— $\text{NiF}_3 > 345$ K, and P— $\text{NiF}_3 > 411$ K). In suspension in liquid aHF at 293 K all forms of NiF_3 are observed to evolve fluorine over several days to form finally NiF_2 .



R— NiF_3 decomposes most rapidly and P— NiF_3 least. When a good F^- donor is available in aHF (e.g. KF , XeF_6) NiF_3 is partly converted (F_2 loss, as in Eqn. (46), also occurs) in disproportionation to NiF_2 and NiF_6^{2-} .



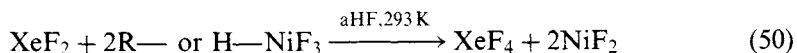
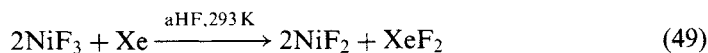
This reaction is slow and competes with the decomposition (Eqn. (46)).

4.3.2.3 Oxidizing properties of R—, H— and P— NiF_3

R— NiF_3 is able to oxidize xenon at 293 K in aHF to xenon(VI) fluoride which acts as a base in the disproportionation reaction mentioned in Eqn. (47).



When excess of xenon is used, all forms of NiF_3 yield XeF_2 , and both R— NiF_3 and H— NiF_3 also oxidize XeF_2 to XeF_4 .



Thermal decomposition of R— NiF_3 at 356 K yields a red-brown solid which has the same X-ray powder diffraction pattern as the product obtained when dry R— NiF_3 is reduced by xenon in the presence of aHF vapours. This compound is probably Ni_2F_5 and still possesses some oxidizing power in aHF.

The small K^+ content of both $H-NiF_3$ and $P-NiF_3$ requires incorporation of an equivalent quantity of $Ni(II)$ in each lattice. This evidently lowers the oxidizing power of these forms relative to $R-NiF_3$, which is the only fully stoichiometric NiF_3 . The K_xNiF_3 forms may also have a lower tendency to disproportionate, to $Ni(II)$ and $Ni(IV)$, than $R-NiF_3$ which could also diminish their oxidizing potential relative to $R-NiF_3$.

4.3.2.4 Structural features of $R-$, $H-$ and $P-NiF_3$

The $R-NiF_3$ represents the commonly available form of a transition metal trifluoride usually made under conditions which favour the thermodynamically preferred material. On the basis of X-ray powder diffraction data it was found that the structure consists of nearly closed-packed F-atom array with nickel atoms residing in octahedral holes but the F-atom positions and interatomic distances were not known with precision [44]. Neutron powder diffraction data were collected at 2 and 295 K on more crystalline material prepared from Li_2NiF_6 solutions in aHF (this is the least soluble of the alkali A_2NiF_6 salts). At 2 K, two distinct Ni—F bonds indicate that $R-NiF_3$ is a mixed valence material with composition $Ni(II)Ni(IV)F_6$ [47]. The long Ni—F bond of $R-NiF_3$ is 1.958(4) Å, the short Ni—F bond is 1.814(4) Å. The difference in length between the two Ni—F bonds is 0.144 Å at 2 K and only 0.078 Å at 295 K. The long distance Ni—F is compatible with the distance of Ni—F in NiF_2 (2.00(2) and 2.01(1) Å) [48], while the short Ni—F distance is compatible with Ni—F distance in K_2NiF_6 (1.776(8) Å) [49].

Mössbauer spectroscopy has shown that at 6 K, the nickel centres are non-equivalent [50], which is in harmony with the neutron structural analysis.

Although the Ni species in $R-NiF_3$ and $H-NiF_3$ are both octahedrally coordinated by F ligands and each F ligand is bridging two Ni species, the structures differ greatly. In the close-packed $R-NiF_3$, the octahedra are linked through bridging F ligands in eight membered Ni_4F_4 rings while Ni octahedra in $H-NiF_3$ are linked by corner sharing in the *ab* plane thus forming six-membered rings Ni_3F_3 . It is this trigonal grouping of the octahedra in $H-NiF_3$ that provides for the open channels that run parallel to *c*. These open channels have an effective inner diameter close to 2.6 Å. The change in structure from $R-NiF_3$ to $H-NiF_3$ results in a FUV increase of 8.3 Å³. This volume increase is associated with the open channels. This poorly packed arrangement probably arises from the advantageous lattice energy associated with incorporation of K^+ in the channels (which compensate for $Ni(II)$ in the nickel fluoride host). This $Ni(II)$ species is a result from the fast room temperature partial reduction of $Ni(III)$. HF is small enough to be intercalated in the channels too. When the particles of $H-NiF_3$ rapidly outgas, during the removal of aHF, the $H-NiF_3$ particles are propelled throughout the evacuated container.

The conductivity of $H-NiF_3$ is roughly $1 \times 10^{-6}(\Omega.cm)^{-1}$ in contrast of $R-NiF_3$ which is an insulator [47]. It is assumed that the conductivity associated with $H-NiF_3$ is due to mobility of the K^+ ions in the lattice of the hexagonal tungsten bronze structure.

Neutron powder diffraction data [47] for $H-NiF_3$ were collected at 2 K. Ni—F distances are in the range 1.847(12)–1.915(14) Å [47]. In $P-NiF_3$ the NiF_6 octahedra

are clustered tetrahedrally. Ni species are connected via F ligands to neighbouring Ni species in six membered rings. The FUV of $61.3(1) \text{ \AA}^3$ is close to that anticipated for a tetrafluoride. Open channels akin to those in H—NiF_3 run roughly at 109° to each other throughout this open structure.

4.3.2.5 Magnetic behaviour of R— , H— and P—NiF_3

In all three forms of NiF_3 , field dependence of the magnetic susceptibility is observed, but the ordering temperatures below which this occurs are very different for the different forms, being $\sim 250 \text{ K}$ in R—NiF_3 , $\sim 120 \text{ K}$ in H—NiF_3 and only $\sim 50 \text{ K}$ in P—NiF_3 [44]. This is very like the change in the three-dimensional ordering temperature observed by Ferey [51] in the case of R— , H— and P—FeF_3 .

The field dependence of the magnetic susceptibility in R—NiF_3 below 250 K [47] indicates superexchange between the nickel centers Ni(II) with the electron configuration $t_{2g}^6 e_g^{*2}$ and Ni(IV) with the electron configuration t_{2g}^6 . These two configurations being dominant ones as evidenced by the Ni—F bond distances at 2 K . The magnetic coupling between these configurations being very weak [52]. At higher temperatures the population of Ni(III) $t_{2g}^6 e_g^{*1}$ has increased because of charge transfer to a level at which antiferromagnetic and ferromagnetic coupling become important giving rise to the field dependence [47]. The essentially field-independent magnetic moment at room temperature is $2.1 \mu_B$ [47].

The magnetic susceptibility data for H—NiF_3 show marked field dependence below $\sim 150 \text{ K}$. This is probably a consequence of an antiferromagnetic coupling of Ni(II,III, or IV) species which (unlike R—NiF_3) can only occur along the c axis since the Ni_3F_3 connectivity in the ab plane frustrates any coupling in that plane. Reliable structural information is not yet available for this phase but a significant population of high spin Ni(III) ($t_{2g}^5 e_g^{*2}$) could be present, providing for the c axis antiferromagnetic coupling with like Ni(III) species or Ni(II) . The room temperature magnetic moment is $2.36 \mu_B$.

P—NiF_3 is a simple paramagnet with field dependence being apparent only below 50 K . This is in accord with the highly frustrated situation associated with antiferromagnetic coupling of Ni species in pyrochlore type structure. The magnetic frustration occurring in the ab planes of H—NiF_3 is present everywhere in the P—NiF_3 . This is a consequence of the tetrahedral clustering of the octahedra, since each Ni species is now linked to each of its six nearest Ni neighbours, as a component of a six-membered Ni_3F_3 ring.

4.3.2.6 Cationic $\text{Ni(IV)}_{\text{solv}}$ and its oxidizing capability

In the preparation of binary fluorides using the general method for the synthesis of polymeric binary fluorides [1] it was noted that when an excess of Lewis acid (beyond the stoichiometric amount) was added to binary fluorides in aHF , a coloured solution resulted without immediate loss of fluorine. This coloured solution contains solvated fluorospecies obtained by the action of excess of Lewis acid on the binary fluoride, probably by removal of F^- from it. In the case of NiF_4 the simplest cationic species would be $[\text{NiF}_3(\text{HF})_x]^+$ [15].

In acidic aHF, as has already been discussed for Ag(III), cationic species of high oxidation state metals are of high electronegativity and, as a consequence of this, very powerful oxidizers. Cationic Ni(IV)_{solv} is prepared by the addition of Lewis fluoro acid (BF₃, AsF₅, SbF₅) to a solution of K₂NiF₆ at 208 K [15]. Cationic Ni(IV)_{solv} is able to electron oxidize PtF₆⁻, RuF₆⁻, O₂ [15] but not AuF₆⁻ [47]. The oxidizing power of cationic Ni(IV)_{solv} is therefore comparable to the oxidizing capability of cationic Ag(III)_{solv}. Both these cationic species are stronger oxidizers than KrF⁺ and are the strongest oxidants known up to now [15].

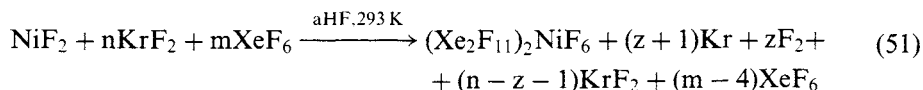
Attempts to characterize a cationic Ni(IV) species in the solid state were not successful. ¹⁹F NMR resonance studies [47] of cationic Ni(IV)_{solv} in aHF at 213 K have shown that the species in solution is not paramagnetic, in harmony with a low spin *d*⁶ configuration of Ni(IV). The resonance assigned to the cationic Ni(IV) (-235 ppm with respect to CFC₃ (external standard)) is significantly deshielded with respect to NiF₆²⁻ in aHF (-332 ppm) also at 213 K. This is in accordance with the removal of electron density from Ni(IV) in NiF₆²⁻ to cationic Ni(IV) [47].

Reaction of excess of fluoro acid with R— or H—NiF₃ in aHF give cationic species which are most probably cationic Ni(IV)_{solv} and not cationic Ni(III)_{solv}.

4.3.3 Complex fluorides of nickel (IV)

4.3.3.1 Room temperature syntheses of NiF₆²⁻ salts

Although in fluoronickelates the oxidation state 4+ is easily obtained [40], no evidence for the formation of a xenon(VI) fluoronickelate(IV) was found in the course of studies of the reaction between NiF₂, XeF₆ and fluorine under pressure [53]. It appeared that XeF₆ was not a sufficiently strong base to promote the formation of Ni(IV) at temperatures above 473 K where, with alkali fluorides, the oxidation of Ni(II) to Ni(IV) was known to occur [40]. With KrF₂ acting as oxidizing and fluorinating agent and XeF₆ as base in reactions at room temperature, in aHF as a solvent, there was however rapid and complete conversion of Ni(II) to Ni(IV) [45]. The reaction scheme is as follows (*n* ≥ 10, *m* ≥ 10, and *z* is the molar coefficient for the part of KrF₂ that thermally decomposes to the elements):



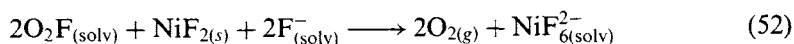
(Xe₂F₁₁)₂NiF₆ [45] is a red diamagnetic solid which loses XeF₆ slowly at room temperature in dynamic vacuum to form (XeF₅)₂NiF₆ [46].

Using the same synthetic route with KF exchanged for XeF₆ efficiently gives pure K₂NiF₆ and this could be extended to any of the alkali fluorides.

The atomization energy of KrF₂ (Δ*H*_{at} = 98 kJ/mol) is smaller than the dissociation energy of elemental fluorine (Δ*H*_{diss} = 158 kJ/mol) thus indicating that KrF₂ is closest in activity to atomic fluorine. The latter can however be generated from F₂ with visible or UV light. This provides a general low temperature route to NiF₆⁻ salts [47,54]. The reaction of NiF₂ with fluorine irradiated by visible or UV light in strongly basic aHF gives the NiF₆⁻ salts. Using this synthetic approach

K_2NiF_6 and the new lithium salt, Li_2NiF_6 , have been synthesized. Photodissociation of F_2 to F^\bullet atoms is a consequence of absorption of high energy photons. The F^\bullet atoms may be stabilized by formation of F_2^\bullet or its aHF solvates in strongly basic aHF ($\text{F}_2^\bullet\text{HF}$)⁻ or ($\text{F}_2^\bullet\text{nHF}$)⁻ [54]. These charged species are less likely than the neutral F^\bullet to quickly regenerate F_2 . These solvated F radicals are more effective sources of F atom than F_2 itself.

Another room temperature synthetic route for the preparation of NiF_6^{2-} salts has recently been demonstrated [22]. This uses $\text{O}_2\text{F}_{(\text{solv})}$ in aHF made basic with alkali fluoride, as the oxidizer:



The O_2F is generated from O_2^+ salts using alkali fluoride in aHF at ≤ 223 K. The oxidation of NiF_2 probably proceeds via the intermediacy of NiF_3 .

4.3.3.2 Crystal structures of some NiF_6^{2-} salts

4.3.3.2.1 Crystal structure of $(\text{Xe}_2\text{F}_{11})_2\text{NiF}_6$. As may be seen from Fig. 11, the structure analysis clearly defines an NiF_6 group and two Xe_2F_{11} groups in this salt. The Xe_2F_{11} group consists of two similar XeF_5 units linked by common fluorine atom. The cation $\text{Xe}_2\text{F}_{11}^+$ was crystallographically defined first in the compound $\text{Xe}_2\text{F}_{11}\text{AuF}_6$ [55]. The crystal structure of $(\text{Xe}_2\text{F}_{11})_2\text{NiF}_6$ [45] represents the first example of two $\text{Xe}_2\text{F}_{11}^+$ cations linked to the same anion. Comparison of $(\text{Xe}_2\text{F}_{11})_2\text{NiF}_6$ with $\text{Xe}_2\text{F}_{11}\text{AuF}_6$ reveals a greater interaction of the cation with the anion in the former. This is evident from comparison of the bridging $\text{Xe}-\text{F}-\text{Xe}$ angle of the complex cation in the two structures. It is $169.2(2)^\circ$ in the case of the gold compound and only $140.3(6)^\circ$ in the case of the nickel compound. The stronger cation-anion interaction in the nickel salt is probably a result of the large average negative charge on the fluorine ligands of NiF_6^{2-} . The NiF_6^{2-} anion is slightly distorted from octahedral symmetry as a consequence of its interaction with the Xe_2F_{11} cations. The average $\text{Ni}-\text{F}$ distance of $1.78(1)$ Å agrees well with the $\text{Ni}-\text{F}$ distance of $1.776(8)$ Å determined for K_2NiF_6 [49].

4.3.3.2.2 Crystal structure of $(\text{XeF}_5)_2\text{NiF}_6$. As may be seen from Fig. 12, the structure of this salt consists of XeF_5^+ and NiF_6^{2-} entities [46]. The anion is essentially octahedral, with an average $\text{Ni}-\text{F}$ bond distance of $1.77(2)$ Å which agrees well with the average $\text{Ni}-\text{F}$ distance in other Ni(IV) complexes: $1.78(1)$ Å in $(\text{Xe}_2\text{F}_{11})_2\text{NiF}_6$ [45], 1.78 Å in M_2NiF_6 ($\text{M} = \text{Rb}, \text{K}$) [56] and $1.776(8)$ Å in K_2NiF_6 [49].

The cations are close to C_{4v} symmetry with an averaged distances and angles as follows: $\text{Xe}-\text{F}_{\text{ax}} = 1.82(1)$ Å, $\text{Xe}-\text{F}_{\text{eq}} = 1.84(1)$ Å, and $\text{F}_{\text{ax}}-\text{Xe}-\text{F}_{\text{eq}} = 78.9(9)^\circ$. The structure of $(\text{XeF}_5)_2\text{NiF}_6$ is of most interest for the cation-anion interactions. As in $(\text{XeF}_5)_2\text{PdF}_6$ [57] each XeF_5^+ species of $(\text{XeF}_5)_2\text{NiF}_6$ is coordinated to three anion F ligands. The main difference between the analogous compounds is that in the case of palladium each xenon atom is coordinated to two PdF_6^{2-} groups thus

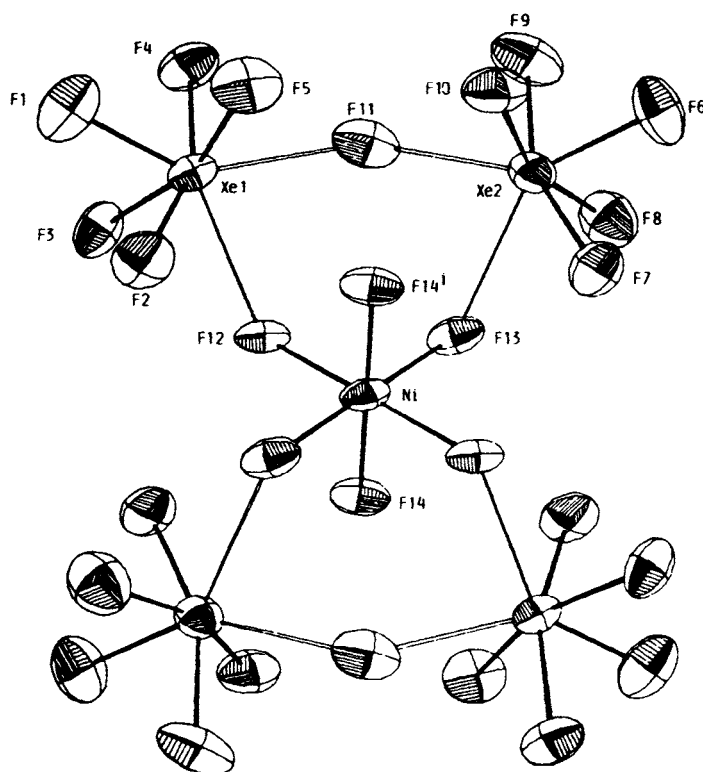


Fig. 11. Ortep diagram of $(\text{Xe}_2\text{F}_{11})_2\text{NiF}_6$. (Reproduced with permission from *Inorg. Chem.*, 28, July 1989, pp. 2911–2914. Copyright 1989 American Chemical Society.)

forming rings which are further linked to adjoining rings, whereas in the case of nickel single rings occur, because one XeF_5^+ is coordinated only to one NiF_6^{2-} and the other XeF_5^+ to two NiF_6^{2-} , thus forming isolated dimeric rings of unique structure.

4.3.4 Fluorination of organic compounds with nickel fluorides

Replacement of hydrogen by fluorine in a variety of organic compounds is accomplished with high efficiency in liquid aHF at room temperature or lower, using the unstable nickel fluorides NiF_4 and R-NiF_3 [58]. Each was prepared *in situ* from K_2NiF_6 and BF_3 [44]. The fluorination of organic substrates by these higher nickel fluorides was found to give products similar to those produced by the Simons Electrochemical Fluorination Process [59,60].

K_2NiF_6 in aHF is also useful for the fluorination of organic substrates. Its ability to fluorinate is probably enhanced by the negative charge carried by the NiF_6^{2-} oxidizer in solution especially so in the oxidation of cationic substrates [61].

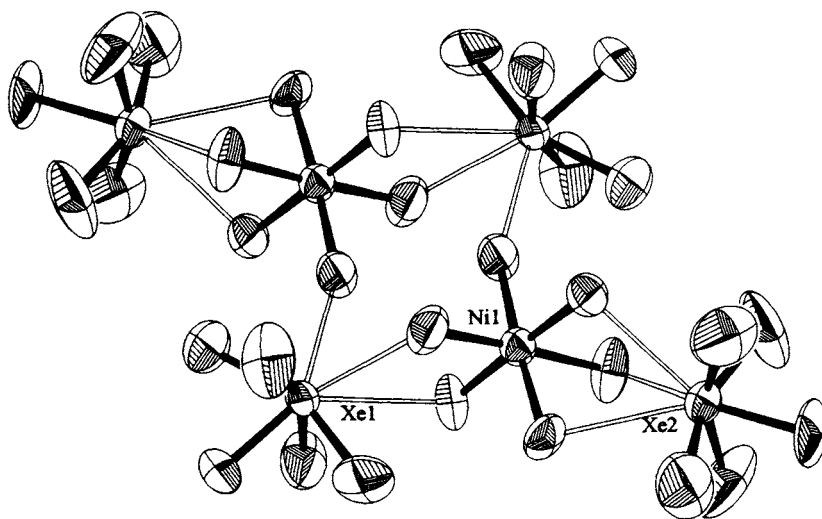
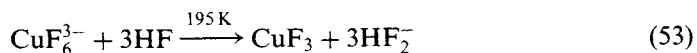


Fig. 12. Ortep diagram of dimeric ring in $(\text{XeF}_5)_2\text{NiF}_6$. (Reproduced with permission of Editions Scientifiques et Medicales Elsevier; 23, rue Linois, 75724 Paris cedex 15, from A. Jesih *et al.*, *Eur. J. Solid State Inorg. Chem.*, 28, 1991, pp. 829–840.)

4.4 Copper(III) and copper(IV) fluorides

4.4.1 Synthesis and some properties of CuF_3

CuF_6^{3-} salts have been known for a long time [40,62,63] but the parent binary fluoride, CuF_3 , was synthesized only recently [30,64]. CuF_6^{3-} salts solvolyze in aHF giving red CuF_3 at 195 K.



CuF_3 is stable only at temperatures up to 213 K and it has yet to be structurally and magnetically characterized. It has been shown that at 195 K it reacts with excess xenon immediately to form XeF_2 [64], the red colour of CuF_3 quickly disappearing.



CuF_3 loses F_2 at 233 K in KHF_2 rich aHF and if it is in excess oxidizes xenon to XeF_6 at 195 K [30].

Since CuF_6^{2-} salts have been claimed [65,66] it may be possible to isolate CuF_4 . That should be an even stronger oxidizer than NiF_4 or AgF_3 which presently represent the strongest oxidizers of the transition metal fluorides.

4.4.2 Synthesis and crystal structure of Cs_2CuF_6

Cs_2CuF_6 was prepared by the reaction between equimolar amounts of CsCl and CsCuCl_3 in a stream of fluorine gas at 523 K, following which the product was treated under high pressure with a mixture of fluorine and argon (3:2) at 350 bar, at 673 K. Cs_2CuF_6 is described as a pale orange solid, that is stable in glass ampoules at 273 K [66]. The magnetic properties (see below) imply an electron configuration for the Cu(IV) of $(\text{Ar})3d^7$ (low-spin configuration $t_{2g}^6 e_g^1$) that implies a Jahn–Teller distortion for the Cu(IV) . The structure of Cs_2CuF_6 has been described [66] as a tetragonal, pseudocubic variant of the antiferite $\text{K}_2[\text{PtCl}_6]$ type, and the following interatomic distances have been reported: $\text{Cu—F} = 1.750 \text{ \AA}$ ($4\times$) and $\text{Cu—F} = 1.772 \text{ \AA}$ ($2\times$). This represents a smaller difference than that anticipated for the Jahn–Teller effect of a low spin d^7 configuration. The Cu—F distances are slightly shorter than in NiF_6^{2-} where: (Ni(IV)—F) is 1.782 \AA in BaNiF_6 [67] (compare also other Ni(IV)—F distances in Ni(IV) salts). The CuF_6 octahedra are separated by Cs cations.

The magnetic susceptibility measurements of Cs_2CuF_6 were made in the temperature range 3.6 to 251.3 K and the data show it to be a simple paramagnetic, obedient to the Curie–Weiss law with $\theta = -1.4 \pm 2.2 \text{ K}$ and $\mu_{\text{eff}} = 1.77 \mu_B$ at 251.3 K. This is consistent with a low spin d^7 configuration for the Cu(IV) . The small Weiss constant shows that there are no significant magnetic interactions between the Cu(IV) centers separated by Cs cations.

4.5 Higher cobalt and iron fluorides

4.5.1 Synthesis and some properties of cobalt(IV) fluoride

Cobalt tetrafluoride has been detected only in the gas phase [68]. It was synthesized by the reaction between CoF_3 and excess of TbF_4 in a Knudsen-cell and detected by mass spectrometry. The reaction was performed at temperatures between 600 and 680 K. Under these reaction conditions, peaks of CoF_n^+ ($0 < n < 3$), F_2^+ , and CoF_4^+ were found. The peak for CoF_4^+ , $m/z = 135 \text{ g mol}^{-1}$ was present only when the CoF_3 and TbF_4 mixture was heated to 600 K. The bond dissociation enthalpy for the reaction $\text{CoF}_4 \longrightarrow \text{CoF}_3 + \text{F}$ was calculated to be $154 \pm 11 \text{ kJ mol}^{-1}$ and the standard molar enthalpy of the formation of $\text{CoF}_4(\text{g})$ was calculated to be $-630 \pm 30 \text{ kJ mol}^{-1}$. The electron affinity of $\text{CoF}_4(\text{g})$ was found to be $6.4 \pm 0.3 \text{ eV}$ [69].

4.5.2 Syntheses of fluorocobaltates(IV)

Oxidation state (IV) of cobalt is very difficult to stabilize with fluorine because the ligand field is usually not sufficiently large to provide a low spin electron configuration. Consequently there are two antibonding sigma electrons to weaken the CoF_6^{2-} bonds and render them labile. A_2CoF_6 has been obtained in a K_2PtCl_6 -type of structure where octahedra containing the cobalt atoms are completely isolated from one another, and each surrounded by a cube of cations (A). Bonding between fluorine and the alkali metal competes with that between fluorine and cobalt, therefore the synthesis of the A_2CoF_6 phase is facilitated by the larger

less polarizing alkali cations [70]. Use of fluorine under high pressure appears to be necessary for the synthesis of a A_2CoF_6 phase. CoF_6^{2-} salts are solvolyzed by aHF. In the case of Cs or Rb [71,72], A_2CoF_6 may be obtained under 60 bar, while in the case of K [73] a pressure of 250 bar of fluorine is necessary.

CoF_4 may be best prepared using low temperature solvolysis of A_2CoF_6 salts using aHF, as in the case of CuF_3 from CuF_6^{3-} (30).

4.5.3 Higher iron fluorides

Iron(IV) fluoride has not been prepared. Cs_2FeF_6 has been claimed from the reaction between Cs_2FeO_4 and elemental fluorine under a pressure of 40 bar at 423 K during 100 h [74] but it has not been satisfactorily characterized.

4.6 Higher manganese fluorides

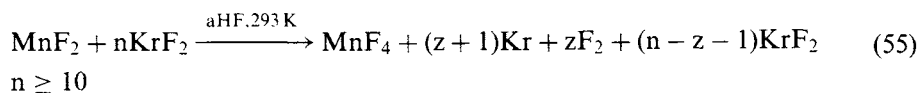
4.6.1 Introduction

The highest known binary manganese fluoride is still MnF_4 . Synthesis of higher fluorides, e.g. manganese(V) fluoride has long been a challenge in synthetics but opinion [75] is not optimistic that they will be found. The highest attainable oxidation states of any metal are normally found in their anions. This is especially true for fluorides. To the present time, not even fluoromanganates(V) have been isolated. Using the same synthetic strategy: as for $(Xe_2F_{11})_2NiF_6$ [45] or XeF_5AgF_4 [21] workers in these laboratories have not been able to prepare XeF_5^+ (or $Xe_2F_{11}^+$) salts of manganese(V), but only the $Xe_2F_{11}^+$ and XeF_5^+ salts of Mn(IV), that is $(Xe_2F_{11})_2MnF_6$ and $(XeF_5)_2MnF_6$ [76].

4.6.2 KrF_2 — MnF_4 adducts and the route to very pure MnF_4

The reaction between MnF_2 and an excess of KrF_2 in aHF as solvent yields an oily, dark red krypton difluoride — manganese tetrafluoride adduct [77]. After removal of the solvent, the curve of weight-loss versus time of pumping was recorded at 228 K. From the change in the slope of the curve it was concluded that the adduct $2KrF_2 \cdot MnF_4$ exists. It is unstable at this temperature and loses KrF_2 yielding $KrF_2 \cdot MnF_4$. The 1:1 adduct is stable at 248 K and is without measurable vapour pressure. This 1:1 compound decomposes to KrF_2 , Kr and F_2 , and MnF_4 above that temperature but at room temperature the decomposition is to Kr, F_2 and MnF_4 .

This reaction between manganese difluoride and excess KrF_2 in aHF at room temperature (after removal of Kr, F_2 , excess KrF_2 and aHF in a dynamic vacuum), yields pure deep blue manganese tetrafluoride (z is the molar coefficient for the part of KrF_2 that thermally decomposes to the elements).



This reaction represents the simplest route so far for the preparation of pure MnF_4 in

high yield but MnF_4 synthesized by this method is amorphous. Another approach to the synthesis of MnF_4 uses high pressure of fluorine (2–3 kbar) and high temperature (300–500°C) [78].

Magnetic susceptibility measurements [77] show that the MnF_4 obtained using KrF_2 follows the Curie–Weiss law (Weiss constant $\theta = 10$ K) with $\mu_{\text{eff}} = 3.85 \mu_{\text{B}}$ appropriate for three unpaired spins. Since the Weiss constant is small the super exchange coupling $\text{Mn(IV)}\text{—F—Mn(IV)}$ must be weak.

4.6.3 Crystal structure of MnF_4

Crystals of MnF_4 [79] have been obtained by the reaction between MnF_2 and elemental fluorine (3 kbar) at 650–670 K. The reaction was performed for 25–35 d. Traces of oxygen were essential to obtain crystalline MnF_4 . There exist two modifications: $\alpha\text{-MnF}_4$ and $\beta\text{-MnF}_4$. The structure of $\beta\text{-MnF}_4$ is still unknown in detail. The structure of $\alpha\text{-MnF}_4$ consists of $[\text{Mn}_4\text{F}_{20}]$ rings in which manganese octahedra are connected through *cis* fluorine bridges. These rings are further connected to generate a three dimensional network. The bridging Mn—F distances are in the range 1.845–1.948 Å while the non-bridging Mn—F distances are in the range 1.697–1.704 Å.

4.7 Higher palladium fluorides

PdF_4 was first prepared by the fluorination of PdSnF_6 and PdGeF_6 under pressure [80] but is now much more conveniently prepared in aHF from PdF_6^{2-} by the fluoro acid route [1]. No convincing evidence has been provided for any higher fluoride but a PdF_6^- salt has been claimed [81]. The preparation of O_2PdF_6 required 4.2 kbar of F_2/O_2 mixture at 593 K. Informative crystallographic information was not obtained but vibrational evidence was persuasive for the existence of O_2PdF_6 . More recently the synthesis of CsPdF_6 was reported [82]. It was obtained in aHF made basic with CsF using KrF_2 as oxidizer. Also in this case crystallographic information was missing but the vibrational evidence was in agreement with the reported spectra [81] of O_2PdF_6 . More recently a study [22] of the oxidizing and fluorination properties of O_2F in aHF has shown that in the reported O_2PdF_6 is most probably O_2PdF_5 . Also, further investigation of the products of the oxidation of Pd(IV) in basic aHF using KrF_2 have shown [83] that the previously claimed CsPdF_6 was probably just Cs_2PdF_6 and PdF_4 . The vibrational peak at 651 cm^{-1} which was assigned to ν_1 of CsPdF_6 belongs to PdF_4 .

Although the O_2F generated from O_2^+ salts [22] in aHF made basic with alkali fluoride at 223 K or below will oxidize Ag(II) to Ag(III), Au(III) to Au(V), Pt(IV) to Pt(V) and Ni(II) to Ni(IV) it does not oxidize Pd(IV). Also metathesis reactions in aHF yielded $(\text{O}_2^+)_2\text{PdF}_6^{2-}$ and although it proved to be highly soluble and long lived in aHF solution, at 273 K it fall to $\text{O}_2^+\text{Pd(IV)F}_5^-$ with loss of O_2 and F_2 as the solvent is removed. Photodissociation of F_2 in basic aHF has also failed to oxidize Pd(IV) to Pd(V) [84].

With KrF_2 , O_2F and atomic F failing to bring about the oxidation of PdF_6^{2-} to PdF_6^- in aHF there cannot now be much hope that this oxidation can be brought about in such solutions.

4.8 Higher fluorides of rhenium

4.8.1 Crystal and molecular structure of ReF_7

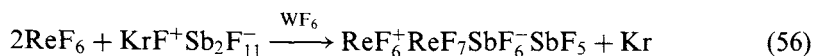
The presence of a phase transition in ReF_7 has prevented the growth of a single crystal of the low-temperature phase. Neutron diffraction of ReF_7 powder was used to determine the structure of ReF_7 at 1.5 K [85]. The lowest energy configuration of ReF_7 has symmetry $C_s(m)$ and is a distorted pentagonal bipyramid.

The molecular structure of ReF_7 is also that of a slightly distorted pentagonal bipyramid. The equatorial ring is puckered with a mean displacement of 0.17 Å from the ideal plane formed by the rhenium and equatorial fluorine atoms. The axial fluorines are not perpendicular to the equatorial plane and are not collinear. The average Re—F distance is 1.843 Å.

4.8.2 ReF_6^+ salts

ReF salts were first reported by E. Jacob and M. Föhnle [86] with vibrational spectroscopic evidence presented for $\text{ReF}_6^+\text{SbF}_6^-$.

$\text{ReF}_6^+\text{ReF}_7\text{SbF}_6^-\text{SbF}_5$ was prepared [87] by the reaction between ReF_6 dissolved in WF_6 and $\text{KrF}^+\text{Sb}_2\text{F}_{11}^-$

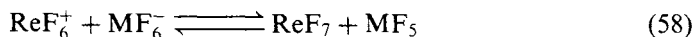


This material is also formed directly at 298 K from interaction of excess ReF_6 with $\text{KrF}^+\text{SbF}_6^-$ or $\text{KrF}^+\text{Sb}_2\text{F}_{11}^-$ or from mixture of SbF_5 with a molar excess of ReF_6 and F_2 photolyzed with a Xe-lamp. $\text{ReF}_6^+\text{ReF}_7\text{AuF}_6^-\text{AuF}_5$ was prepared by displacement of KrF_2 from AuF_6^- salts at 333 K. (Thermal decomposition of KrF_2 is not shown in the equation):



Raman spectra of these salts clearly show ReF_6^+ , ReF_7 , MF_6^- and monomeric MF_5 (M = Sb and Au).

ReF_7 is a weak fluoro base therefore it is reasonable to suppose that partial dissociation of $\text{ReF}_6^+\text{MF}_6^-$ might occur.



It appears that the neutral molecules and the ions are present in comparable concentration and it is possible that the neutral species in ordered array serve to screen like-charged species from one another. In such an ordered assembly each ion would

have only a tetrahedral arrangement of opposite ions about it, the neutrals serving as dielectric spacers. These materials are best represented by the general formula $\text{ReF}_6^+ \text{ReF}_7 \text{MF}_6^- \text{MF}_5$.

References

- [1] B. Žemva, K. Lutar, A. Jesih, W.J. Casteel, Jr., N. Bartlett, *J. Chem. Soc., Chem. Commun.*, (1989) 346.
- [2] R. Bougon, M. Lance, *C.R. Acad. Sci., Ser. 2*, 297 (1983) 117.
- [3] R. Bougon, T. Bui Huy, M. Lance, H. Abazli, *Inorg. Chem.*, 23 (1984) 3667.
- [4] F.W.B. Einstein, P.R. Rao, J. Trotter, N. Bartlett, *J. Chem. Soc. A*, (1967) 478.
- [5] Yu.M. Kiselev, A.I. Popov, A.A. Timakov, K.V. Bukharin, V.F. Sukhoverkhov, *Zh. Neorg. Khim.*, 33 (1988) 1252.
- [6] B. Žemva, K. Lutar, A. Jesih, W.J. Casteel, Jr., A.P. Wilkinson, D.E. Cox, R.B. Von Dreele, H. Borrmann, N. Bartlett, *J. Am. Chem. Soc.*, 113 (1991) 4192.
- [7] G.M. Lucier, J.M. Whalen, N. Bartlett, *J. Fluorine Chem.*, 89 (1998) 101.
- [8] K. Lutar, A. Jesih, I. Leban, B. Žemva, N. Bartlett, *Inorg. Chem.*, 28 (1989) 3467.
- [9] B. Frlec, D. Gantar, J.H. Holloway, *J. Fluorine Chem.*, 20 (1982) 385.
- [10] D. Gantar, B. Frlec, D.R. Russell, J.H. Holloway, *Acta Crystallogr.*, C43 (1987) 618.
- [11] B. Žemva, R. Hagiwara, W.J. Casteel, Jr., K. Lutar, A. Jesih, N. Bartlett, *J. Am. Chem. Soc.*, 112 (1990) 4846.
- [12] W.J. Casteel, Jr., G.M. Lucier, R. Hagiwara, H. Borrmann, N. Bartlett, *J. Solid State Chem.*, 96 (1992) 84.
- [13] B.G. Müller, *Angew. Chem., Int. Ed. Engl.*, 26 (1987) 688.
- [14] T.E. Mallouk, G.L. Rosenthal, G. Müller, R. Brusasco, N. Bartlett, *Inorg. Chem.*, 23 (1984) 3167.
- [15] G.M. Lucier, C. Shen, W.J. Casteel, Jr., L.C. Chacón, N. Bartlett, *J. Fluorine Chem.*, 72 (1995) 157.
- [16] R.J. Gillespie, G.J. Schrobilgen, *J. Chem. Soc., Chem. Commun.*, (1974) 90, *Inorg. Chem.*, 15 (1976) 22.
- [17] R. Hoppe, *Z. Anorg. Allg. Chem.*, 292 (1957) 28.
- [18] R. Hoppe, R. Homann, *Z. Anorg. Allg. Chem.*, 379 (1970) 193.
- [19] A.J. Edwards, R.G. Plevy, M.P. Stewart, *J. Fluorine Chem.*, 1 (1971) 246.
- [20] J. Levec, J. Slivnik, B. Žemva, *J. Inorg. Nucl. Chem.*, 36 (1974) 997.
- [21] K. Lutar, A. Jesih, B. Žemva, *Rev. Chim. Miner.*, 23 (1986) 565.
- [22] G.M. Lucier, C. Shen, S.H. Elder, N. Bartlett, *Inorg. Chem.*, 37 (1998) 3829.
- [23] U. Engelmann, B.G. Müller, *Z. Anorg. Allg. Chem.*, 598/599 (1991) 103.
- [24] B. Žemva, *Croat. Chem. Acta*, 61 (1988) 163.
- [25] N. Bartlett, F. Einstein, D.F. Stewart, J. Trotter, *J. Chem. Soc., A* (1967) 1190.
- [26] N. Bartlett, M. Gennis, D.D. Gibler, B.K. Morrell, A. Zalkin, *Inorg. Chem.*, 12 (1973) 1717.
- [27] B. Žemva, L. Golič, J. Slivnik, *Vestn. Slov. Kem. Drus.*, 30 (1983) 365.
- [28] K. Lutar, S. Miličev, B. Žemva, B.G. Müller, B. Bachmann, R. Hoppe, *Eur. J. Solid State Inorg. Chem.*, 28 (1991) 1335.
- [29] C. Shen, Ph.D. Thesis, University of California, Berkeley, 1992.
- [30] N. Bartlett, G.M. Lucier, C. Shen, W.J. Casteel, Jr., L.C. Chacón, J. Münzenberg, B. Žemva, *J. Fluorine Chem.*, 71 (1995) 163.
- [31] B. Žemva, N. Bartlett, unpublished results, 1992.

- [32] G.M. Lucier, unpublished results, U.C. Berkeley, 1992.
- [33] G.M. Lucier, J. Münzenberg, W.J. Casteell, Jr., N. Bartlett, *Inorg. Chem.*, 34 (1995) 2692.
- [34] F.O. Sladky, P.A. Bulliner, N. Bartlett, *J. Chem. Soc., A* (1969) 2179.
- [35] D. Gantar, I. Leban, B. Frlec, J.H. Holloway, *J. Chem. Soc., Dalton Trans.*, (1987) 2379.
- [36] B.G. Müller, *Angew. Chem., Int. Ed. Engl.*, 26 (1987) 689.
- [37] R. Fischer, B.G. Müller, *Z. Anorg. Allg. Chem.*, 623 (1997) 1729.
- [38] A. Jesih, K. Lutar, B. Žemva, B. Bachmann, St. Becker, B.G. Müller, R. Hoppe, *Z. Anorg. Allg. Chem.*, 588 (1990) 77.
- [39] R. Hagiwara, F. Hollander, C. Maines, N. Bartlett, *Eur. J. Solid State Inorg. Chem.*, 28 (1991) 855.
- [40] W. Klemm, E. Huss, *Z. Anorg. Allg. Chem.*, 258 (1949) 221.
- [41] T.L. Court, M.F.A. Dove, *J. Chem. Soc., Chem. Commun.*, (1971) 726.
- [42] T.L. Court, M.F. Dove, *J. Chem. Soc., Dalton Trans.*, (1973) 1955.
- [43] L. Stein, J.M. Neil, G.R. Alms, *Inorg. Chem.*, 8 (1969) 2472.
- [44] B. Žemva, K. Lutar, L.C. Chacón, M. Fele-Beuermann, J. Allman, C. Shen, N. Bartlett, *J. Am. Chem. Soc.*, 117 (1995) 10025.
- [45] A. Jesih, K. Lutar, I. Leban, B. Žemva, *Inorg. Chem.*, 28 (1989) 2911.
- [46] A. Jesih, K. Lutar, I. Leban, B. Žemva, *Eur. J. Solid State Inorg. Chem.*, 28 (1991) 829.
- [47] L.C. Chacón, Ph.D. Thesis, University of California, Berkeley, 1997.
- [48] J.W. Stout, S.A. Reed, *J. Am. Chem. Soc.*, 76 (1954) 5279.
- [49] J.C. Taylor, P.W. Wilson, *J. Inorg. Nucl. Chem.*, 36 (1974) 1561.
- [50] N. Jansen, D. Walcher, P. Gütlisch, D. Häussinger, B. Hannebauer, R. Kniep, K. Lutar, P.C. Schmidt, D. Sellmann, B. Žemva, *Il Nuovo Cimento*, 18D (1996) 231.
- [51] G. Ferey, R. de Pape, M. Leblanc, J. Pannetier, *Rev. Chim. Minerale*, 23 (1986) 474.
- [52] J.-M. Dance, A. Tressaud, In: *Inorganic Solid Fluorides*, P. Hagenmuller (Ed.), Academic Press, New York, 1985, Chapter 9.
- [53] B. Žemva, J. Slivnik, *J. Inorg. Nucl. Chem., Suppl.*, (1976) 173.
- [54] J.M. Whalen, G.M. Lucier, L.C. Chacón, N. Bartlett, *J. Fluorine Chem.*, 88 (1998) 107.
- [55] K. Leary, A. Zalkin, N. Bartlett, *Inorg. Chem.*, 13 (1974) 775.
- [56] R. Hoppe, Th. Fleischer, *J. Fluorine Chem.*, 11 (1978) 251.
- [57] K. Leary, D.H. Templeton, A. Zalkin, N. Bartlett, *Inorg. Chem.*, 12 (1973) 1726.
- [58] N. Bartlett, R.D. Chambers, A.J. Roche, R.C.H. Spink, L.C. Chacón, J.M. Whalen, *J. Chem. Soc., Chem. Commun.*, (1996) 1049.
- [59] J.H. Simons, *J. Electrochem. Soc.*, 95 (1949) 47.
- [60] *Fluorine Chemistry*, J.H. Simons (Ed.), Academic Press, N.Y. Vol. 1, 1950, p. 414.
- [61] J.M. Whalen, L.C. Chacón, N. Bartlett, *Electrochem. Soc. Proceedings*, 97-15 (1997) 1.
- [62] R. Hoppe, G. Wingefeld, *Z. Anorg. Allg. Chem.*, 519 (1984) 195.
- [63] D. Kissel, R. Hoppe, *Z. Anorg. Allg. Chem.*, 532 (1986) 17.
- [64] A. Jesih, K. Lutar, B. Žemva, unpublished results, 1991.
- [65] W. Harnischmacher, R. Hoppe, *Angew. Chem.*, 85 (1973) 590.
- [66] D. Kissel, R. Hoppe, *Z. Anorg. Allg. Chem.*, 559 (1988) 40.
- [67] B.G. Müller, R. Hoppe, *Z. Anorg. Allg. Chem.*, 498 (1983) 128.
- [68] M.V. Korobov, L.N. Savinova, L.N. Sidorov, *J. Chem. Thermodynamics*, 25 (1993) 1161.
- [69] J.V. Rau, N.S. Chilingarov, L.N. Sidorov, *Rapid Commun. Mass Spectrometry*, 11 (1997) 1977.
- [70] J. Grannec, A. Tressaud, P. Hagenmuller, *J. Fluorine Chem.*, 25 (1984) 83.
- [71] W. Klemm, W. Brandt, R. Hoppe, *Z. Anorg. Allg. Chem.*, 308 (1961) 179.

- [72] J.W. Quail, G.A. Rivett, *Can. J. Chem.*, 50 (1972) 2447.
- [73] J. Grannec, Ph. Sorbe, J. Portier, *C.R. Acad. Sci.*, 283 (1976) 441.
- [74] Yu.M. Kiselev, N.S. Kopelev, Yu.D. Perfilev, V.F. Sukhoverkhov, *Zh. Neorg. Khim.*, 35 (1990) 1704.
- [75] M.I. Nikitin, E.G. Rakov, *Zh. Neorg. Khim.*, 43 (1998) 375.
- [76] M. Bohinc, J. Grannec, J. Slivnik, B. Žemva, *J. Inorg. Nucl. Chem.*, 38 (1976) 75.
- [77] K. Lutar, A. Jesih, B. Žemva, *Polyhedron*, 7 (1988) 1217.
- [78] R. Hoppe, *Isr. J. Chem.*, 17 (1978) 48.
- [79] B.G. Müller, M. Serafin, *Z. Naturforsch.*, 42b (1987) 1102.
- [80] N. Bartlett, P.R. Rao, *Proc. Chem. Soc.*, 1964, 393.
- [81] W.E. Falconer, F.J. DiSalvo, A.J. Edwards, J.E. Griffiths, W.A. Sunder, M.J. Vasile, *J. Inorg. Nucl. Chem., Supplement*, (1976) 59.
- [82] K. Lutar, H. Borrmann, B. Žemva, *Proceedings of 15th International Symposium on Fluorine Chemistry*, Vancouver, Canada, 1997, p. Ba(1)IL-1
- [83] B. Žemva, K. Lutar, Z. Mazej, unpublished results.
- [84] O. Graudejus, S.H. Elder, G.M. Lucier, C. Shen, N. Bartlett, *Inorg. Chem.*, 38 (1999) 2503.
- [85] T. Vogt, A.N. Fitch, J.K. Cockcroft, *Science*, 263 (1994) 1265.
- [86] E. Jacob, M. Fähnle, *Angew. Chem., Int. Ed.*, 15 (1976) 159.
- [87] S.M. Yeh, N. Bartlett, *Rev. Chim. Miner.*, 23 (1986) 676.

CHAPTER 5

Syntheses and Structures of the Oxide Fluorides of the Main-Group and Transition Metal Elements

Michael Gerken, Hélène P.A. Mercier and Gary J. Schrobilgen

Department of Chemistry, McMaster University, Hamilton, Ontario L8S 4M1, Canada

5.1 Introduction

The goal of this Chapter is to summarize the syntheses and structural findings relating to the oxide fluorides that have been synthesized during the period 1985–1998. The excellent comprehensive reviews of Holloway and Laycock [1] relating to the main-group oxide fluorides, Christie [2] on the halogen oxide fluorides and Christie Wilson and Schack [3] on controlled replacement of fluorine by oxygen in fluorides and oxide fluorides should also be consulted. Physical properties, except those which are novel or of special interest have not been included in this Chapter. With the exception of the simple oxide fluorides of carbon, such as COF_2 , COF_3^- , CO_2F^- and $\text{CO}_2\text{F}_2^{2-}$, carbon derivatives and those in which carbon is coordinated to a main-group oxide fluoride group are not treated in this Chapter.

The replacement of fluorine atoms with oxygen atoms generally leads to the stabilization of higher oxidation states and the stabilization is further enhanced when the high-valent oxide fluoride occurs as an anion. This is illustrated by the stabilization of the highest oxidation state in the periodic table, +8. The tetroxides, RuO_4 , OsO_4 and explosive XeO_4 are all known as well as a host of notoriously stable perxenates, XeO_6^{4-} . While Ru^{VII} oxide fluorides are unknown, OsO_2F_4 and OsO_3F_2 are stable compounds and XeO_3F_2 and XeO_2F_4 have been prepared in small quantities from XeO_4 . In contrast, the highest oxidation state that can be attained in the binary fluorides of these elements is +6, e.g. XeF_6 , RuF_6 and OsF_6 .

5.2 The oxide fluorides of the main-group elements

5.2.1 Boron, Aluminum, Gallium, Indium and Thallium

The BOF_2^- anion and BOF have been generated and detected in the gas phase by ion cyclotron resonance spectrometry [4]. The BOF molecule has been established to have a fluoride affinity that is less than that of BF_3 .

The structure of the BOF_2^- anion has been determined for the first time in the crystal structure of $\text{cis-}\alpha\text{-[CoL(NO}_2)_2]^+\text{BOF}_2^-$ and resulted from the hydrolysis of the $\text{cis-}\alpha\text{-[CoL(NO}_2)_2]^+\text{BF}_4^-$ salt [5]. The BOF_2^- anion likely results from the dehydration of $\text{BF}_2(\text{OH})_2^-$ upon crystallization. The anion is planar but it is not possible to differentiate between oxygen and fluorine. A further serendipitous hydrolysis of the BF_4^- anion has been reported to lead to the cyclic $\text{B}_3\text{O}_3\text{F}_4^-$ anion. The anion was observed as the counterion in the crystal structure of the interstitial carbon compound, $[(i\text{-Pr}_3\text{PAu})_6\text{C}]^{2+}(\text{B}_3\text{O}_3\text{F}_4^-)_2 \cdot 3\text{CH}_2\text{Cl}_2$ [6]. However, the formulation of the anion as a six-membered ring of alternating boron and oxygen atoms with *exo*-B—F bonds is tentative as it was not possible to distinguish between fluorine and OH in the crystal structure.

The $\text{KF—KBF}_4\text{—B}_2\text{O}_3$ melt system leads to crystalline $\text{K}_3\text{B}_3\text{O}_3\text{F}_6$ in the temperature range 390–440°C [7]. The X-ray powder pattern has been indexed in the orthorhombic system. Infrared spectroscopy confirms that the anion is based on the trifluoroboroxole ring. A subsequent study reporting the synthesis of $\text{Na}_3\text{B}_3\text{O}_3\text{F}_6$ by the reaction of equimolar amounts of NaHF_2 and H_3BO_3 at 100°C for 3 h shows that the sodium compound indexes in the orthorhombic system with a cell that is slightly smaller than that of the potassium salt [8].

The reaction of the porphyrin ligand, TTP (tetra-*p*-tolylporphyrin) with $\text{BF}_3 \cdot \text{OEt}_2$ leads to the oxide fluoride complex, $\text{B}_2\text{OF}_2(\text{TTP})$ and the structure has been established using ^1H , ^{13}C , ^{11}B and ^{19}F NMR spectroscopy and FAB mass spectrometry [9]. The structure contains a B—O—B bridge in which each boron is bonded to fluorine and to a nitrogen of TTP. The structure of the diboron complex was confirmed by an X-ray crystal structure determination of the tetrakis-(*p*-chlorophenyl)porphyrin (TpClPP) derivative.

Crystalline $\text{K}^+\text{AlPO}_4^-$ [10] and $\text{H}_3\text{N}(\text{CH}_2)_3\text{NH}_3^{2+}\text{Ga}_3(\text{PO}_4)_3\text{F}_2^{2-} \cdot \text{H}_2\text{O}$ [11] have been synthesized by hydrothermal growth. The aluminum structure is formed by linking phosphate groups to four vertices of octahedrally coordinated aluminum atoms. The remaining two vertices of the Al coordination-octahedron are occupied by fluorine atoms which are bridged to two other AlO_4F_2 -octahedra. The three-dimensional structure of the gallium compound is built up from corner-linked $\text{Ga}_3(\text{PO}_4)_3\text{F}_2^{2-}$ units composed of three PO_4 tetrahedra, two GaO_4F trigonal bipyramids, in which the fluorine is in an axial position, and one *cis*- GaO_4F_2 octahedron. The compounds, $\text{Na}_5\text{MP}_2\text{O}_8\text{F}_2$ ($\text{M} = \text{Al, Ga}$), have been prepared by flux methods [12]. The group 13 metals in their crystal structures are octahedrally coordinated by four oxygen atoms of the PO_4 groups, used in bridging two different group 13 metals, and two *trans*-fluorine atoms.

Surface characterization by XPS, Auger spectroscopy and SEM of GaAs after reactive ion etching of the GeMoW contact in a radio frequency SF_6/O_2 plasma has led the first evidence for GaOF as a layer on GaAs [13].

The hexanuclear organogallium oxide fluoride, $\text{Mes}_6\text{Ga}_6\text{O}_4\text{F}_4$ (Mes = mesitylene) has been prepared by the reaction of Mes_2GaF with water in THF at ambient temperature [14]. The structure of $\text{Mes}_6\text{Ga}_6\text{O}_4\text{F}_4$, which crystallizes with a mole of THF, is a distorted octahedron of Ga atoms in which all eight faces are capped by O/F

atoms. The distortion of the Ga_6 octahedron arises because the Ga—O—Ga angles are larger than the Ga—F—Ga angles.

Direct solid state reactions have been used to prepare two new In^{III} oxide fluorides, $\text{Ba}_2\text{InO}_3\text{F}$ [15] and $\text{Ba}_3\text{In}_2\text{O}_5\text{F}_2$ [16]. The $\text{Ba}_2\text{InO}_3\text{F}$ structure has ordered anions producing a K_2NiF_4 superstructure with alternating layers of oxide and fluoride ions. The $\text{Ba}_3\text{In}_2\text{O}_5\text{F}_2$ structure also shows ordering of the oxide and fluoride ions, producing sheets of vertex-sharing indium–oxygen square pyramids separated by BaF layers. The electrosynthesis of the known compound, TlOF , has been reported from aqueous HF/TlF and TlOH/TlF solutions [17].

5.2.2 Carbon, Silicon and Tin

The previously accepted value for the heat of formation of COF_2 has been shown to be in error and has been revised, permitting re-analysis of the available kinetic and thermodynamic data on the energies of a number of other small fluorine-containing molecules, including the $\text{CF}_3\text{O}^\bullet$ radical, CF_3OF and CF_3OOCF_3 , resolving a number of discrepancies between previous calculated and experimental results [18].

The role of CF_3 radicals in stratospheric chemistry has been the subject of several experimental studies [19–21] and several products have been identified, e.g. CF_3O , CF_3O_2 and COF_2 . The reaction between $\bullet\text{CF}_3$ radical and $\bullet\text{NO}_2$ leads to COF_2 and NOF as the major products.

The compounds, $\text{TAS}^+\text{COF}_3^-$ ($\text{TAS}^+ = (\text{Me}_2\text{N})_3\text{S}^+$) [22] and $\text{N}(\text{CH}_3)_4^+\text{COF}_3^-$ [23] have been prepared by the reaction of TAS fluoride ($(\text{Me}_2\text{N})_3\text{S}^+\text{Me}_3\text{SiF}_2^-$) with COF_2 in THF and by the reaction of anhydrous $\text{N}(\text{CH}_3)_4^+\text{Cl}^-$ with CF_3OCl , respectively. Warming of $\text{N}(\text{CH}_3)_4^+\text{COF}_3^-$ to room temperature leads to the formation of COF_2 and $\text{N}(\text{CH}_3)_4^+\text{F}^-$ [23]. The crystal structure of $\text{TAS}^+\text{COF}_3^-$ has been determined and theoretical studies of the structure and bonding in COF_3^- have been carried out [22]. The COF_3^- anion, which is isoelectronic with NOF_3 , is distorted from its ideal C_{3v} symmetry in the crystal structure where the C—F bond lengths are found to be exceptionally long and the C—O bond quite short when compared to gas-phase experimental values for CF_2OX ($\text{X} = \text{F}, \text{Cl}, \text{CF}_3$). The FCF bond angles are also extraordinarily small. The unusual molecular structure of COF_3^- is largely attributed to negative hyperconjugation. A subsequent study showed that MCOF_3 ($\text{M} = \text{K}, \text{Rb}, \text{Cs}$) salts can be prepared by the reaction of MF and COF_2 in anhydrous CH_3CN [24]. Although the oxygen and fluorine atoms of the COF_3^- anion suffer a two-fold disorder in the ambient temperature crystal structures of the alkali metal salts, the positions are split at -150°C , providing reasonable estimates of the bond lengths which are somewhat longer for the C—O and shorter for the C—F bonds than in the TAS^+ salt [22].

Carbon dioxide behaves as a weak fluoride ion acceptor towards “naked” fluoride ion sources such as tetramethylammonium fluoride, neopentyl(trimethyl)-ammonium fluoride and piperidinium fluoride (pip^+F^-) in the absence of a solvent and in CH_2F_2 and $\text{CF}_3\text{CHFCF}_3$ solvents for pip^+F^- [25]. The CO_2F^- anion has been characterized in the solid state by $\{^1\text{H}\}^{13}\text{C}$ MAS NMR spectroscopy and

was prepared by the interaction of $^{13}\text{CO}_2$ with solid $\text{N}(\text{CH}_3)_4^+\text{F}^-$. The CO_2F^- anion is reported to be labile on the NMR time scale in CH_3CN solvent at an unspecified temperature. The vibrational spectrum of CO_2F^- has been obtained and the frequencies and assignments as well as the predicted C_{2v} geometry of the anion confirmed by theoretical calculations. No evidence was found for the $\text{CO}_2\text{F}_2^{2-}$ anion and ab initio calculations are reported to yield no minimum on the potential surface. An earlier matrix-isolation study reports the reactions of COF_2 with CsF and Ti_2O in an argon matrix to initially form $\text{Ti}^+\text{CO}_2\text{F}_2^{2-}$ which rapidly eliminated TiF to give $\text{Ti}^+\text{CO}_2\text{F}^-$ [26]. Attempts to synthesize BOF_3^{2-} in a matrix using a similar method were unsuccessful.

The thermodynamic study of the reaction of SiF_4 with SiO_2 to give Si_2OF_6 , in the temperature range 450–1015°C, has been investigated by mass spectrometry and the possibility of the existence of SiOF_2 has been discussed [27]. Ion cyclotron resonance studies have failed to show fluoride ion transfer from SiOF_3^- to SiF_4 or PF_5 , forming SiOF_2 [4].

The hydrolysis of SnF_2 in concentrated aqueous solution has resulted in the formation of the Sn^{II} oxide fluoride, Sn_4OF_6 , obtained by hydrolysis in aqueous systems [28] (the only other Sn^{II} oxide fluoride is $\text{Sn}_4\text{O}_2\text{F}_4$; B. Darriet and J. Galy, *Acta Crystallogr., Sect. B*, 33 (1977) 1489). The crystal structure of Sn_4OF_6 consists of a three-dimensional polymeric network of bridging fluorine and oxygen atoms. Tin is present in four distinct sites, one showing a tetragonal-based pyramidal geometry while the others show a trigonal-pyramidal geometry with a fourth long contact to a bridging fluorine atom. The non-bonding electrons are stereochemically active. A ^{119}Sn Mössbauer study of $\text{Sn}_4\text{O}_2\text{F}_4$ has been reported [29].

5.2.3 Nitrogen and Phosphorus

The formerly difficult synthesis of NOF_3 has now been achieved by the direct chemical oxygenation of NF_3 [30]. The interaction of NF_3 with N_2O in the presence of SbF_5 at 150°C leads to the quantitative formation of the previously known $\text{NOF}_2^+\text{Sb}_2\text{F}_{11}^-$ salt. Vacuum pyrolysis of $\text{NOF}_2^+\text{Sb}_2\text{F}_{11}^-$ at 190–230°C in the presence of excess NaF affords NOF_3 in high yield.

The mixed nitryl salts, $\text{NOClF}^+\text{AsF}_6^-$ and $\text{NO}(\text{CF}_3)\text{F}^+\text{AsF}_6^-$ have been prepared by oxidative fluorination of NOCl and NOCF_3 with $\text{N}_2\text{F}^+\text{AsF}_6^-$ [31]. An alternative method for the preparation of $\text{NOF}_2^+\text{MF}_6^-$ ($\text{M} = \text{As}, \text{Sb}$) was found involving the oxidative fluorination of NOF with $\text{XeF}^+\text{MF}_6^-$.

The formation of NO_2F by fluorination of alkali metal nitrates with COF_2 has been demonstrated [32]. The interaction of LiNO_3 or NaNO_3 with COF_2 at 85°C in stainless steel in the presence of 12 mol% CsF , an HF scavenger, resulted in near-quantitative yields of NO_2F . No reaction was observed between CsNO_3 and COF_2 both in the presence and absence of CsF , in agreement with thermochemical predictions.

The phosphorus analogue of nitrosyl fluoride, POF , is formed by the reaction between POFBr_2 and silver and has been characterized by matrix isolation infrared spectroscopy and by mass spectrometry [34]. Ab initio calculations and a normal

coordinate analysis showed the ground state to have a bent $F-P=O$ structure and is isoelectronic with the well known molecules SiF_2 and SO_2 . The heats of formation for $POFBr_2$ and POF_2Br have been determined mass spectrometrically [35] and the heat of formation for POF has been determined using the value derived for $POFBr_2$ [34]. The fluoride ion affinity of POF has been estimated and the POF_2^- anion has been formed by ion cyclotron resonance addition-elimination reactions [4].

The hydrolysis of PF_4^- has been studied by multi-NMR spectroscopy and vibrational spectroscopy [36,37]. An equimolar amount of water in a CH_3CN solution of $N(CH_3)_4^+PF_4^-$ leads to the formation of equimolar amounts of HPO_2F^- and HPF_5^- and in the presence of an excess of water, HPO_2F^- is the sole product. In the presence of a large excess of $N(CH_3)_4^+F^-$, the hydrolysis of PF_4^- with an equimolar amount of water produces POF_2^- . The resulting $N(CH_3)_4^+POF_2^-$ salt is the first example of a stable POF_2^- salt. The geometries and vibrational spectra of POF_2^- and HPO_2F^- have been calculated by ab initio methods and normal coordinate analyses have been carried out for POF_2^- , HPO_2F^- and the isoelectronic SOF_2 , HSO_2F and $ClOF_2^+$ species. The F^- affinities of POF , HPO_2 and related species and the reaction enthalpies of the hydrolysis reactions of PF_4^- and HPF_5^- have also been calculated by ab initio methods.

The tetrakis(difluorophosphonato)palladate(II) anion, $Pd(POF_2)_4^{2-}$, has been obtained as the $RPPH_3^+$ ($R = o\text{-}H_3CC_6H_4CH_2$) salt in the reaction of $Pd(PPh_3)_2Cl_2$ with $ROPF_2$ and the crystal structure of the complex confirmed that Pd^{II} is bonded to the POF_2 group through phosphorus as well as the square-planar geometry at palladium and tetrahedral geometry at phosphorus [38].

An improved synthesis of POF_3 from PF_5 and P_4O_{10} has been reported [39]. The microwave spectrum of $^{17}OPF_3$ has been investigated and the ^{17}O quadrupole coupling constant was determined and compared with several other phosphine oxides to characterize the π -bonding in these systems [40]. The structures of the difluorophosphino-oxo analogue of POF_3 , namely, $P'O'(OPF_2)_3$, have been determined in both the gas and solid phases [41]. The conformations in the gas and solid phases are considerably different. A flattening of the molecule is observed on going to the crystalline phase and is due to an increase in the $O-P'-O$ angle and changes in the $P'-O-P-F$ dihedral angles. There is also a lengthening of the $P'=O'$ bond which may be associated with short intermolecular $P'=O \cdots P$ contacts.

The oxygen coordinated POF_4^- anion has been characterized by single crystal X-ray diffraction in $Ru_2(PhNNNPh)_4OPF_4$ as a result of the serendipitous partial hydrolysis of PF_6^- [42]. The unstable POF_4^- anion (vide infra) exists in this compound by virtue of being strongly coordinated. The POF_4^- anion has been observed in the gas phase by ion cyclotron resonance spectrometry and has been shown to readily transfer fluoride ion to PF_5 , giving PF_6^- and POF_3 [4].

The uncoordinated POF_4^- has been characterized for the first time in solution and in the solid state and is formed from $N(CH_3)_4F$ and POF_3 in CHF_3 at $-140^\circ C$ and has been observed at this temperature by ^{19}F and ^{31}P NMR spectroscopy where it was shown to be fluxional [43]. The POF_4^- anion ultimately dismutates to $PO_2F_2^-$ and PF_6^- . The dismutation involves the reaction of POF_4^- with POF_3 between -140 and $-100^\circ C$ forming the $OF_2P-O-PF_5^-$ anion, which, at higher temperatures,

reacts with F^- ion to give $PO_2F_2^-$ and PF_6^- . In addition, the protonated form of $OF_2POPF_5^-$, i.e. HOF_2POPF_5 , has also been identified as a by-product in the study. The geometrical parameters, vibrational spectra, force field, NMR chemical shifts and dismutation energy of POF_4^- have been calculated by ab initio methods along with those of the closely related and known PF_4^- anion, POF_3 , PF_3 , SOF_4 and SF_4 molecules. Although the structures of the isoelectronic POF_4^- anion and SOF_4 exhibit the expected trigonal bipyramidal VSEPR (valence shell electron repulsion) geometry with the oxygen in the equatorial plane, and their dismutation energies are very similar, their dismutation behavior is strikingly different, with POF_4^- rapidly dismutating at low temperatures and SOF_4 kinetically stable toward dismutation to SO_2F_2 and SF_6 . The difference is attributed to the lack of a low activation energy barrier pathway for SOF_4 . Dismutation energy calculations for POF_4^- , SOF_4 and $ClOF_3$ revealed very large errors in the previously published thermodynamic data for the heats of formation of SO_2F_2 and SOF_4 and the dismutation energy of POF_4^- . The calculated energy barriers and the C_{4v} transition states for the Berry-style pseudorotation exchange of equatorial and axial fluorines in POF_4^- , SOF_4 , PF_4^- and SF_4^- account for the observation that on the NMR time scale the intramolecular exchange in PF_4^- and SF_4 can be frozen out at ca $-40^\circ C$, but in POF_4^- and SOF_4 it is still rapid at -140 and $-150^\circ C$, respectively. There is an erroneous report of the POF_4^- anion prepared by the hydrolysis of $AgPF_6$ in CD_2Cl_2 solvent at room temperature [44]. The reported ^{31}P chemical shift and $^{31}P-^{19}F$ scalar coupling are at considerable variance with those reported subsequently [43]. Moreover, the reported stability of the species at ambient temperature is not in agreement with the observed thermal instability of POF_4^- [43].

The $PO_2F_2^-$ anion has been observed in the gas phase by ion cyclotron resonance spectrometry and no evidence for the transfer of fluoride to PF_5 to give the neutral PO_2F molecule was observed [4]. The room temperature interaction of the $PO_2F_2^-$ anion (as the potassium salt) with excess AsF_5 in SO_2 solvent also fails to give PO_2F , but forms the oxygen bridged $[PO_2F_2 \cdot 2AsF_5]^-$ anion instead [39]. The anion is stable in SO_2 solution but reacts with CD_3CN to form the $CD_3CN \cdot AsF_5$ adduct and the $[PO_2F_2 \cdot AsF_5]^-$ anion. The analogous PF_5 adducts are also formed in the reaction of PF_5 with KPO_2F_2 at $-78^\circ C$ to give $K[PO_2F_2 \cdot 2PF_5]$ which decomposes upon warming to room temperature to the potassium salt of the previously known $[PO_2F_2 \cdot PF_5]^-$ anion and PF_5 [39].

The molecular structure of PF_2HO has been determined in the solid and gas phases [45] and the molecular parameters show that the greatest apparent differences between PF_2HO in the crystal and in the vapor are those involving the H atom, however, the estimated standard deviation for the X-ray value is so large that the difference from the gas-phase electron diffraction value is not significant. The P—H stretching frequencies for the gas and solid indicate an absence of substantial hydrogen bonding and there is no evidence for the P^{III} tautomeric form, $PF_2(OH)$, in the crystal.

An alternative synthesis, which provides HPO_2F_2 in high purity and yield, has been developed which involves the direct fluorination of PO_4^{3-} by HSO_3F [46]. The successive fluorination steps $PO_4^{3-} \rightarrow PO_3F^{2-} \rightarrow PO_2F_2^- \rightarrow POF_3$ were con-

firmed by ^{19}F and ^{31}P NMR and infrared spectroscopy. The fluorination of $\text{P}_2\text{O}_3\text{Cl}_4$ and POCl_3 in 40% aqueous HF also leads to the formation of HPO_2F_2 [47]. It has been shown that HPO_2Cl_2 , which is generated by the hydrolyses of $\text{P}_2\text{O}_3\text{Cl}_4$ and POCl_3 , occurs as an intermediate in the fluorination process to yield HPO_2F_2 .

Phosphorus-31 NMR spectroscopy has been used to monitor the formation of pure $\text{H}_2\text{PO}_3\text{F}$, which was obtained along with an equimolar amount of POF_3 when HPO_2F_2 was thermolyzed at 130°C [48]. The competing disproportionation of $\text{H}_2\text{PO}_3\text{F}$ to H_3PO_4 and POF_3 prevented yields of $\text{H}_2\text{PO}_3\text{F}$ greater than 50% from being achieved. The thermal decomposition of $\text{CaPO}_3\text{F} \cdot 2\text{H}_2\text{O}$ has been investigated by thermogravimetry leading to the elimination of H_2O , HF and POF_3 and to $\alpha\text{-Ca}_2\text{P}_2\text{O}_7$ at 360°C [49]. Solid state ^{31}P NMR studies have been carried out for the polycrystalline fluorophosphates $\text{K}_2\text{PO}_3\text{F}$, $\text{Na}_2\text{PO}_3\text{F}$, BaPO_3F and $\text{K}_2\text{P}_2\text{O}_5\text{F}_2$ [50]. The values of the ^{31}P shielding anisotropy and asymmetry parameters suggest that the covalent character of P—O bridge bonds is very similar to the terminal P—F bonds. On heating fluoride-containing urea melts with H_3PO_4 and H_3PO_3 , high yields of $\text{M}_2\text{PO}_3\text{F}$ and MPO_2F_2 ($\text{M} = \text{K}, \text{NH}_4$) are obtained [51]. The $(\text{NH}_4)_2\text{PO}_3\text{F} \cdot \text{H}_2\text{O}$ and $\text{K}_2\text{PO}_3\text{F}$ salts have also been obtained by the interaction of 88% H_3PO_4 and MHF_2 followed by precipitation with 95% ethanol [52]. The crystal structure of $\text{CoPO}_3\text{F} \cdot 3\text{H}_2\text{O}$, prepared by the aqueous reaction of $\text{Ag}_2\text{PO}_3\text{F}$ with CoCl_2 , comprises layers of PO_3F tetrahedra and CoO_6 octahedra held together by hydrogen bonding [53].

Difluorophosphate complexes $\text{M}(\text{O}_2\text{PF}_2)_2 \cdot \text{HPO}_2\text{F}_2$ ($\text{M} = \text{Mn}, \text{Fe}, \text{Co}, \text{Ni}$) and $\text{Cr}(\text{O}_2\text{PF}_2)_3$ [54] have been prepared by the direct reaction of the metals with an excess of HPO_2F_2 . Displacement of HBr and HCl in the reactions of CrBr_3 and FeCl_3 with an excess of HPO_2F_2 gave $\text{Cr}(\text{O}_2\text{PF}_2)_3 \cdot \text{HPO}_2\text{F}_2$ and $\text{Fe}(\text{O}_2\text{PF}_2)_3$, respectively. Single crystals of $\text{Co}(\text{O}_2\text{PF}_2)_2 \cdot 2\text{CH}_3\text{CN}$ [55] have been obtained by recrystallization of $\text{Co}(\text{O}_2\text{PF}_2)_2 \cdot \text{HPO}_2\text{F}_2$ [54] from CH_3CN . Crystalline $\text{Cu}(\text{O}_2\text{PF}_2)_2$ was obtained as hygroscopic blue needles by allowing copper metal to react with anhydrous HPO_2F_2 over a period of several weeks [55]. The crystal structures of $\text{Co}(\text{O}_2\text{PF}_2)_2 \cdot 2\text{CH}_3\text{CN}$ and $\text{Cu}(\text{O}_2\text{PF}_2)_2$ contain bridging PO_2F_2 groups. The octahedral Co^{II} coordination is achieved by monodentate coordination of four oxygen atoms of the bridging PO_2F_2 groups and two nitrogen atoms from *trans* oriented CH_3CN molecules. The copper compound has two independent Cu^{II} atoms, each with four near oxygen neighbors, and the distorted octahedral coordination is completed by two longer contacts to oxygen atoms of symmetry-related PO_2F_2 groups. The tridentate function for the PO_2F_2 group observed in the copper compound has not previously been observed.

The action of the anhydride, $\text{P}_2\text{O}_3\text{F}_4$, on UO_3 or UO_2NO_3 yields $\text{UO}_2(\text{O}_2\text{PF}_2)_2$ [56]. Infrared and Raman spectroscopic studies suggest a chain structure with O—P—O bridges. The monofluorophosphate, $\text{UO}_2(\text{PO}_3\text{F})$ was obtained by thermal decomposition of $\text{UO}_2(\text{O}_2\text{PF}_2)_2$. Difluorophosphate salts have also been prepared by the reaction of $\text{P}_2\text{O}_3\text{F}_4$ with fluorides (Ag^+ , Tl^+ , Hg_2^{2+} , NH_4^+ , Co^{3+}), oxides (Li^+ , Mg^{2+} , Ca^{2+} , Ba^{2+} , Zn^{2+} , Cd^{2+} , Hg^{2+} , Pb^{2+} , UO_2^{2+}), nitrates (K^+ , Na^+ , Mg^{2+} , Ca^{2+} , Ba^{2+} , Zn^{2+} , Cd^{2+} , Cu^{2+}) and Cs_2CO_3 [57]. Nitrilium salts of the fluorophosphate anions, $(\text{CH}_3\text{CNH}^+)_2\text{PO}_3\text{F}^{2-}$ and $\text{CH}_3\text{CNH}^+\text{PO}_2\text{F}_2^-$ result from the interaction

of NaPF_6 with wet CH_3CN and have been characterized by NMR spectroscopy [58]. The bis(nitrilium) salt, $(\text{CH}_3\text{CNH}^+)_2\text{PO}_3\text{F}^{2-}$, has been isolated from the reaction of CH_3CN with $\text{H}_2\text{PO}_3\text{F}$. Alkali metal hexafluorophosphates have been shown to fluorinate alkoxysilanes in polar and non-polar solvents to give $(\text{CH}_3\text{O})_2\text{FPO}$ and $(\text{CH}_3\text{O})\text{F}_2\text{PO}$ as by-products. Several further examples of transition metal compounds containing PO_2F_2^- coordinated or not coordinated to the metal are known [59–63]. The majority are derived from the intentional or fortuitous hydrolysis of the PF_6^- anion.

The first fluoroperoxophosphate, $(\text{NH}_4^+)\text{PO}_2(\text{O}_2)\text{F}\cdot\text{H}_2\text{O}$, has been prepared and characterized by vibrational spectroscopy [64]. The peroxide group is bonded in an end-on manner as encountered in simple monoperoxo-derivatives of sulfur and phosphorus.

5.2.4 Arsenic, Antimony and Bismuth

The AsOF_2^- anion has been detected by ion cyclotron resonance spectrometry and shown to transfer a fluoride ion to SiF_4 to give AsOF [4].

The complex antimony(III) glycinate, $\text{SbOF}\cdot(^+\text{NH}_3\text{CH}_2\text{COO}^-)$, has been prepared by the reaction of glycine with SbF_3 in aqueous HF [65]. The crystalline complex has been characterized by elemental analyses and infrared spectroscopy.

The oxide fluoride, $\text{Bi}_7\text{F}_{11}\text{O}_5$, has been prepared by the reaction of stoichiometric amounts of Bi_2O_3 and BiF_3 at 290°C for 12 h [66]. The bismuth atoms in the crystal structure are distributed over four sites and are seven- and eight-coordinated with a long range O/F order. The polyhedra are irregular and, in part, these irregularities are attributed to stereochemical activity of the $6s^2$ lone pair on Bi.

5.2.5 Oxygen and Sulfur

Dioxygen difluoride is one of the most potent oxidative fluorinating agents known. The synthesis of O_2F_2 from O_2 and F_2 by low-temperature UV photolysis, laser photolysis and by microwave (Ref. [67] and references therein) and thermal methods have been described [67,68]. The thermal and UV photolysis methods are capable of producing O_2F_2 in 5–30 g quantities. An electron diffraction study of O_2F_2 has been carried out which confirms an earlier microwave investigation and the non-planar structure of O_2F_2 [69].

The O_2F radical is a prominent species during the decomposition of gaseous O_2F_2 and is formed in the reaction of O_2 and O_2F_2 [70]. Like O_2F_2 , O_2F is thermodynamically unstable and a potent fluorinating agent having a room temperature half-life of a few seconds. The equilibrium among O_2F , O_2F_2 and O_2 has been studied in the temperature range 13 to -78°C [70e]. An activation energy of 13 kcal mol^{-1} was found for both the forward and reverse reactions. The equilibrium constant in the middle of the temperature range is 21.5 and the estimated heats of formation of O_2F and O_2F_2 are 2.6 and 4.5 kcal mol^{-1} , respectively. Although O_2F radical is a well-documented species in the decomposition of O_2F_2 , attempts to detect O_2F or its dimer, O_4F_2 , by electron diffraction have been unsuccessful [69].

EPR and FT-IR spectroscopy have been used to study the decomposition of O_2F_2 and O_2F in the gas phase by flow and stopped-flow methods [68].

Despite the reactivity of O_2F_2 and its short half life (seconds) at ambient temperature, its powerful oxidative fluorinating properties have been employed to quantitatively fluorinate low-valent actinide fluorides and oxide fluorides to their hexafluorides [71–77]. This is exemplified by the fluorination of aged PuF_4 with O_2F_2 at room temperature and forms the basis for the separation of involatile ^{241}Am fluorides from volatile $^{241}\text{PuF}_6$ [76]. Chlorine pentafluoride has been prepared in high purity and in quantitative yield by the fluorination of ClF_3 with O_2F_2 at -78°C [78].

Spark and negative corona discharges through SF_6 mixtures with O_2 , $\text{O}_2 + \text{H}_2\text{O}$, $\text{CF}_4 + \text{H}_2\text{O}$ lead to the formation of mixtures containing a range of sulfur oxide fluorides, including SOF_2 , SOF_4 , SO_2F_2 , S_2OF_{10} , $\text{S}_2\text{O}_2\text{F}_{10}$ and $\text{S}_2\text{O}_3\text{F}_6$ [79,80].

The fluoroxysulfate ion, O_3SOF^- , is formed by treatment of a 2 M aqueous solution of Cs_2SO_4 at -5 to -10°C with molecular fluorine (20% in nitrogen) [81]. The cesium salt is the easiest salt to prepare because the efficiency of the reaction is enhanced by the high solubility of the sulfate salt. Although CsSO_4F is not thermodynamically stable, it is kinetically stable at room temperature, undergoing rapid, but not violent, decomposition to CsSO_3F and O_2 at $\sim 100^\circ\text{C}$. The room temperature stable fluoroxysulfate ion contrasts with the long known isoelectronic chlorine analogue fluorine perchlorate, ClO_4F , a treacherously unstable gas. The SO_4F^- ion is a formidable oxidizer and fluorinating agent, with considerable potential as a synthetic and analytical reagent.

The interaction of SOF_2 with previously calcined $\gamma\text{-AlO}_2\text{F}_3$ has been studied using the radiotracer, ^{18}F [82]. The 1:1 molecular adducts between SOF_2 and SO_2F_2 and a wide variety of amines and oxygen-containing bases have been isolated and characterized in nitrogen matrices by infrared spectroscopy [83]. The crystal structures of SO_2F_2 and SO_2ClF have been determined at -147 and -150°C , respectively [84]. Neither structure could be correlated with close sphere packing.

The fluorosulfite, $\text{NH}_4\text{SO}_2\text{F}$, has been prepared from SO_2 and NH_4F and characterized by vibrational spectroscopy [85]. The assignments of the vibrational spectra of MSO_2F ($\text{M} = \text{K}, \text{Rb}, \text{Cs}, \text{NH}_4, \text{N}(\text{CH}_3)_4$) have been revised with the aid of ab initio calculations [86]. Although SO_2 reacts exothermically with CsF at room temperature forming CsSO_2F , and oxidation of CsSO_2F by SO_2 occurs at higher temperatures, the interaction under ultrasonic conditions leads to the formation of the trithionate, $\text{Cs}_2\text{S}_3\text{O}_6$, and SO_2F_2 [87]. The reaction of TAS fluoride ($(\text{Me}_2\text{N})_3\text{S}^+\text{Me}_3\text{SiF}_2^-$) with SO_2 (in liquid SO_2 solvent), and with NSF (isoelectronic with SO_2) and $\text{C}_2\text{F}_5\text{NSO}$ in CH_3CN solvent leads to $\text{TAS}^+\text{SO}_2\text{F}^-$, $\text{TAS}^+\text{NSF}_2^-$ and $\text{TAS}^+\text{C}_2\text{F}_5\text{NSOF}^-$ [88].

The solid state and gas-phase structures of the long-known sulfanuric fluoride, $(\text{NS}(\text{O})\text{F})_3$, which is known to exist in both the *cis*- and *trans*-isomeric forms by solution ^{19}F NMR spectroscopy, has been determined by X-ray crystallography and gas-phase electron diffraction [89]. Both structural studies are in close agreement and show chair conformations for the N_3S_3 -rings and *cis*-arrangements for the $\text{F}(\text{O})$ atoms of the SOF groups. Sulfanuric fluoride reacts with TAS fluoride in CH_3CN

below -30°C , forming $\text{TAS}^+ \{[\text{NS}(\text{O})\text{F}]_2[\text{NS}(\text{O})\text{F}_2]\}^-$ [90]. As in the molecular structure of sulfanuric fluoride, the crystal structure of the cyclic $[\text{NS}(\text{O})\text{F}]_2[\text{NS}(\text{O})\text{F}_2]^-$ anion also exhibits a chair conformation for the N_3S_3 -ring and a *cis*-arrangement for the four-coordinate sulfur atoms of the SOF groups. The unique five-coordinate sulfur atom has a trigonal bipyramidal arrangement of ligands with the doubly bonded oxygen and two nitrogen atoms in the equatorial plane and two fluorines in axial positions.

The conformation and gas-phase structure of difluorosulphenylimine, $\text{F}_2\text{S}(\text{O})\text{NCN}$, has been studied by vibrational spectroscopy [91] and electron diffraction [92]. Depending on the orientation of the cyano group relative to the $\text{S}=\text{O}$ bond, *cis*- and *trans*-conformers can occur in this compound. Both gas-phase studies conclude that the composition is 10% *cis* and 90% *trans* isomer.

The interaction of an excess of $\text{NSF}_2\text{NS}(\text{O})\text{F}_2$ with $[\text{Co}(\text{SO}_2)_n][\text{AsF}_6]_2$ in liquid SO_2 at room temperature results in the complex $[\text{Co}\{\text{NSF}_2\text{NS}(\text{O})\text{F}_2\}_4][\text{AsF}_6]_2 \cdot \text{SO}_2$ [93]. The crystal structure of the cation consists of a central Co^{2+} cation tetrahedrally coordinated to the nitrogens of the four NSF_2 groups. The bond distances are consistent with sulfur-nitrogen triple, double and single bonds, i.e. $[\text{Co}\{\text{N}\equiv\text{SF}_2-\text{N}=\text{S}(\text{O})\text{F}_2\}_4]^{2+}$.

5.2.5.1 Derivatives of the SO_2F group

The crystal structure of bis(fluorosulfonyl)imide, $\text{HN}(\text{SO}_2\text{F})_2$ has been determined [94]. The molecules are linked by hydrogen bonds, forming infinite chains. The previously reported salt, $\text{NH}_4\text{N}(\text{SO}_2\text{F})_2$, has been prepared from $\text{HN}(\text{SO}_2\text{F})_2$ dissolved in CFCl_3 and excess $\text{NH}_{3(\text{g})}$ and characterized by ^{19}F NMR and vibrational spectroscopy [95]. The salts, $\text{MN}(\text{SO}_2\text{F})_2$ ($\text{M}=(\text{C}_6\text{H}_5)_3\text{PH}$, 2,4,6-trimethyl pyridinium, $(\text{C}_6\text{H}_5)_3\text{C}$), have been prepared by the reaction of $\text{HN}(\text{SO}_2\text{F})_2$ with $(\text{C}_6\text{H}_5)_3\text{P}$ or 2,4,6-trimethyl pyridine and the metathesis reaction between $(\text{C}_6\text{H}_5)_3\text{CBr}$ and $\text{AgN}(\text{SO}_2\text{F})_2 \cdot \text{C}_6\text{H}_6$, respectively [96]. The crystal structures of the salts, $\text{MN}(\text{SO}_2\text{F})_2$ ($\text{M}=\text{K}$ [94], Cs [97], $(\text{C}_6\text{H}_5)_3\text{PH}$ [96]), $(\text{C}_6\text{H}_5)_3\text{CN}(\text{SO}_2\text{F})_2 \cdot \text{CHCl}_3$ [96] and $\text{AgN}(\text{SO}_2\text{F})_2 \cdot \text{C}_6\text{H}_6$ [98], contain isolated $\text{N}(\text{SO}_2\text{F})_2^-$ anions. In $\text{HN}(\text{SO}_2\text{F})_2$ [94] and $\text{MN}(\text{SO}_2\text{F})_2$ ($\text{M}=\text{Cs}$ [97], $(\text{C}_6\text{H}_5)_3\text{PH}$ [96], $(\text{C}_6\text{H}_5)_3\text{C}$ [96]), the $\text{N}(\text{SO}_2\text{F})_2$ group has a *trans*-conformation with the fluorine atoms on opposite sides of the plane defined by $\text{S}-\text{N}-\text{S}$ bonds while $\text{KN}(\text{SO}_2\text{F})_2$ [94] exhibits a *cis*-geometry. One oxygen and the fluorine equally occupy two positions in the SO_2F groups of $\text{AgN}(\text{SO}_2\text{F})_2 \cdot \text{C}_6\text{H}_6$ because of crystallographic disorder [98].

Crystalline $\text{CH}_2(\text{N}(\text{SO}_2\text{F})_2)_2$ has been obtained from the reaction of $\text{AgN}(\text{SO}_2\text{F})_2$ and CH_2Cl_2 in SO_2ClF and the structure shows a *trans*-conformation for the $\text{N}(\text{SO}_2\text{F})_2$ groups [99]. The reaction of ClSO_2NCO with SbF_3 produces FSO_2NCO [100]; vibrational data [100] for FSO_2NCO are consistent with the presence of the *gauche* conformer in the gaseous and liquid state which has been found by gas phase electron diffraction [101].

Several new imidodisulfonyl derivatives have been characterized by elemental analysis and NMR spectroscopy [97]. Transamination of $((\text{CH}_3)_3\text{Si})_2\text{NH}$ and $\text{HN}(\text{SO}_2\text{F})_2$ yields $(\text{CH}_3)_3\text{SiN}(\text{SO}_2\text{F})_2$; metathesis reactions between $\text{AgN}(\text{SO}_2\text{F})_2$ and MCl yield $\text{MN}(\text{SO}_2\text{F})_2$ ($\text{M}=(\text{C}_6\text{H}_5)_3\text{Si}$, $(\text{CH}_3)_3\text{Pb}$, $(\text{C}_6\text{H}_5)_3\text{Pb}$) and

$R_3SnN(SO_2F)_2$ ($R = CH_3, CH_3CH_2, CH_3CH_2CH_2, CH_3CH_2CH_2CH_2, C_6H_5$); solvolyses of $(CH_3)_4M$ ($M = Ge, Sn$) with $HN(SO_2F)_2$ yield $(CH_3)_3MN(SO_2F)_2$; and neutralization of $(C_6H_{11})SnOH$ with $HN(SO_2F)_2$ yields $(C_6H_{11})SnN(SO_2F)_2$. The crystal structure of $(CH_3)_3PbN(SO_2F)_2$ shows $N(SO_2F)_2$ groups with a *trans*-conformation coordinated through the nitrogen to one trigonal planar $(CH_3)_3Pb$ moiety and through one oxygen atom to a second $(CH_3)_3Pb$ moiety forming chains. Pyridine (py) and $(CH_3)_3SnN(SO_2F)_2$ form the coordination complex $[(CH_3)_3Snpy_2]^+[N(SO_2F)_2]^-$ which has a *trans*-trigonal bipyramidal geometry around Sn based on ^{119}Sn Mössbauer data [102].

The reaction of S_4N_4 with $S_2O_6F_2$ at $65^\circ C$ results in the formation of $(FSO_2)_2NSN(SO_2F)_2$ as a by-product in addition to the main product $S_4N_4(SO_2F)_2$ [103]. Extremely short S—O and S—F bond distances have been found in the crystal structure of $(FSO_2)_2NSN(SO_2F)_2$.

Addition of AsF_5 to $FXeN(SO_2F)_2$ followed by removal of AsF_5 at $-78^\circ C$ and room temperature yields $[XeN(SO_2F)_2][AsF_6]$ and $[F(XeN(SO_2F)_2)_2][AsF_6]$, respectively [104]. The reaction of $[F(XeN(SO_2F)_2)_2][AsF_6]$ with SbF_5 produces $[XeN(SO_2F)_2]Sb_3F_{16}$. All compounds have been ^{15}N -enriched and studied by ^{15}N , ^{19}F and ^{129}Xe NMR and Raman spectroscopy. The crystal structure of $XeN(SO_2F)_2Sb_3F_{16}$ consists of discrete $XeN(SO_2F)_2^+$ cations fluorine bridged to $Sb_3F_{16}^-$ anions in which Xe is bonded to the nitrogen of the $N(SO_2F)_2$ ligand.

Fluoride ion abstraction from the previously known $F_5SNSO_2F^-$ anion using AsF_5 yields the colorless liquid, F_4SNSO_2F , which was characterized by mass spectrometry, ^{19}F NMR and infrared spectroscopy [105,106], and reacts with CsF , HF and ClF to form CsF_5SNSO_2F , $HN(SO_2F)SF_5$ and $ClN(SO_2F)SF_5$, respectively [106]. The latter species reacts with ethylene to give $ClCH_2CH_2N(SO_2F)SF_5$. Addition of TAS fluoride to $F_2OS^{VI}NSO_2F$ [107], $F_2S^{IV}NSO_2F$ [107], $OS^{IV}NSO_2F$ [108] and $S^{II}NSO_2F$ [108] in CH_3CN yields the anions $F_3OSNSO_2F^-$, $F_3SNSO_2F^-$, $F(O)SNSO_2F^-$ and $FSNSO_2F^-$, respectively, which were characterized by low-temperature ^{19}F NMR spectroscopy and elemental analyses of the TAS^+ salts. The related $TAS^+RNS(O)F_3^-$ ($R = (CF_3)_2CF, SF_5$) [107] and $TAS^+R'NS(O)F^-$ ($R' = CF_3, (CF_3)_2CF, SF_5$) salts [108] have, in like manner, been synthesized from $RNSOF_2$ and $RNSO$, respectively, and characterized by low-temperature ^{19}F NMR spectroscopy.

The ^{15}N enriched $XeN(H)SO_2F^+$ cation was prepared from H_2NSO_2F and $XeF^+AsF_6^-$ in HF and from $[H_3NSO_2F^+AsF_6^-]$ and XeF_2 in BrF_5 and has been characterized by multi-NMR spectroscopy [109].

5.2.5.2 Derivatives of the SO_3F group

In addition to ionic bonding, the *pseudo*-tetrahedral fluorosulfate group exhibits four different coordination modes in the covalent bonding of its oxygen ligands: monodentate, *iso*-bidentate (bridging), *aniso*-bidentate (bridging) and tridentate (bridging) [110]. The reviews of Aubke [33,111–113] relating to main-group and transition metal fluorosulfate derivatives should be consulted.

Covalent fluorosulfates are often used as starting materials for trifluoromethyl sulfate derivatives. Complete degradation of SO_3F moieties by HSO_3CF_3 is the

reason for quantitative substitution of SO_3F by SO_3CF_3 , however, mechanistic understanding of the degradation reactions is still lacking [110].

Bis(fluorosulfonyl)peroxide, $\text{S}_2\text{O}_6\text{F}_2$, is a frequently used reagent for the preparation of main-group and transition metal fluorosulfates and its synthetic applications are discussed in the following sections.

5.2.5.2.1 The SO_3F^- anion. Previously reported CsSO_3F and its solvate, $\text{Cs}[\text{H}(\text{SO}_3\text{F})_2]$, have been characterized by single crystal X-ray diffraction [114]. Solutions of both compounds in HSO_3F only gave rise to a sharp singlet in the ^{19}F NMR spectra suggesting a rapid equilibrium between SO_3F^- and $\text{H}(\text{SO}_3\text{F})_2^-$, which is the fluorosulfate analogue of HF_2^- and $\text{H}(\text{OTeF}_5)_2^-$ (see Sec. 5.2.6.1.1).

Isolated SO_3F^- anions have also been found in the crystal structures of $\text{Se}_{10}(\text{SO}_3\text{F})_2$ [115] and $(\text{Se}_2\text{N}_2\text{S})_2(\text{SO}_3\text{F})_2$ [116]. Reaction of equimolar amounts of Se, Te and AsF_5 in SO_2 gave rise to an insoluble phase which was dissolved in 30% oleum, forming scarlet-red crystals of $\text{Se}_{10}(\text{SO}_3\text{F})_2$ [115]. The reaction of $\text{Se}(\text{NSO})_2$ with HSO_3F in SO_2 yields $(\text{Se}_2\text{N}_2\text{S})_2(\text{SO}_3\text{F})_2$ [116].

5.2.5.2.2 Main-group element derivatives of the SO_3F group. Metal bis(fluorosulfates), $\text{M}(\text{SO}_3\text{F})_2$ ($\text{M} = \text{Mn}, \text{Fe}, \text{Co}, \text{Ni}, \text{Cu}$) react with the strong fluorosulfate acceptor $\text{Sn}(\text{SO}_3\text{F})_4$ in HSO_3F at reaction temperatures of $25\text{--}70^\circ\text{C}$ to give bimetallic coordination polymers $\text{M}^{\text{II}}\text{Sn}^{\text{IV}}(\text{SO}_3\text{F})_6$ which were characterized by chemical analysis, infrared and ^{119}Sn Mössbauer spectroscopy [117]. Octahedral environments for both the tin and transition metal are suggested in all instances (except for possible Jahn–Teller distortions for Cu^{II}) with the $-\text{OSO}_2\text{F}$ groups strongly bonded to Sn^{IV} and coordinated more weakly to M^{II} through a second oxygen.

The $\text{Sn}(\text{SO}_3\text{F})_6^{2-}$ anion was also prepared in salts with the Hg^{2+} , Sn^{2+} , $(\text{CH}_3)_2\text{Sn}^{2+}$, $[(\text{CH}_3)_2\text{SnSO}_3\text{F}]^+$ cations from the corresponding bis(fluorosulfate) derivative and $\text{Sn}(\text{SO}_3\text{F})_4$ [118]. The polymeric $[(\text{CH}_3)_2\text{SnSO}_3\text{F}]^+$ cation has also been synthesized with the counter anion $\text{Pt}(\text{SO}_3\text{F})_6^{2-}$. The reaction of $(\text{CH}_3)_2\text{SnCl}_2$ and CsCl in a 1:2 ratio in HSO_3F produces $\text{Cs}_2[(\text{CH}_3)_2\text{Sn}(\text{SO}_3\text{F})_4]$. Tin-119 Mössbauer spectra of the dimethyl tin fluorosulfates $(\text{CH}_3)_2\text{Sn}(\text{SO}_3\text{F})_2$, $\text{Cs}[(\text{CH}_3)_2\text{Sn}(\text{SO}_3\text{F})_3]$, $\text{Ba}[(\text{CH}_3)_2\text{Sn}(\text{SO}_3\text{F})_4]$, $\text{M}_2[(\text{CH}_3)_2\text{Sn}(\text{SO}_3\text{F})_4]$ ($\text{M} = \text{Li}, \text{Cs}$) and $[(\text{CH}_3)_2\text{SnSO}_3\text{F}]_2[\text{Pt}(\text{SO}_3\text{F})_6]$ have been recorded [119].

Tin(II) bisfluorosulfate is prepared by the reaction of SnF_2 with HSO_3F and exhibits a three-dimensional framework of SO_3F groups acting as tridentate bridging ligands between tin atoms in the crystal structure [120]. The four short primary bonds around Sn^{II} have a disphenoidal geometry consistent with an AX_4E VSEPR arrangement of the electron lone pair and bond pair domains. Inclusion of two longer secondary bonds results in a distorted octahedral ($\text{AX}_4\text{Y}_2\text{E}$) geometry around tin. Chemical shift differences between the solid state and solution ^{119}Sn NMR spectra are consistent with partial ionization of $\text{Sn}(\text{SO}_3\text{F})_2$ in HSO_3F solutions. Addition of mesitylene to $\text{Sn}(\text{SO}_3\text{F})_2$ results in the formation of the adduct $\text{Sn}(\text{SO}_3\text{F})_2 \cdot \text{mes}$ [121]. The adduct was characterized by chemical analysis, infrared and ^{119}Sn Mössbauer spectroscopy. Infrared spectroscopy of $\text{Sn}(\text{SO}_3\text{F})_2 \cdot \text{mes}$

suggests that the SO_3F group is coordinated to tin, and is likely coordinated in a bidentate, possibly bridging manner.

Solvolysis of $(\text{CH}_3)_4\text{Ge}$ or $(\text{CH}_3)_3\text{GeCl}$ in HSO_3F leads to the formation of $(\text{CH}_3)_3\text{GeSO}_3\text{F}$ as a colorless liquid with tetracoordinated germanium and monodentate fluorosulfate groups [122].

The reactions of $(\text{C}_6\text{H}_5)_3\text{MO}$ ($\text{M} = \text{Sb}, \text{Bi}$) with $\text{S}_2\text{O}_5\text{F}_2$ in CH_2Cl_2 yield the fluorosulfates $(\text{C}_6\text{H}_5)_3\text{M}(\text{SO}_3\text{F})_2$, which have been characterized by elemental analyses, mass spectrometry, NMR and infrared spectroscopy [123]. The polymeric Sb^{III} fluorosulfates $[\text{SbF}_n(\text{SO}_3\text{F})_{3-n}]_x$, with $n = 0, 1, 2$, have been prepared from antimony metal and HSO_3F and $\text{S}_2\text{O}_6\text{F}_2$ [124,125]. The crystal structures of all three species contain asymmetric, tridentate bridging SO_3F groups. The reaction of equimolar amounts of Sb and CsSO_3F and excess $\text{S}_2\text{O}_6\text{F}_2$ in HSO_3F yield $\text{CsSb}^{\text{V}}(\text{SO}_3\text{F})_6$ which is stable up to 149°C [114,126]. The crystal structure contains the $\text{Sb}^{\text{V}}(\text{SO}_3\text{F})_6^-$ anion in which the monodentate SO_3F groups form a regular SbO_6 octahedron.

The complete vibrational spectra of the previously known $\text{EF}_5\text{OSO}_2\text{F}$ ($\text{E} = \text{S}, \text{Se}$ and Te) compounds have been studied and assigned [127].

Gas-phase and matrix-isolation infrared and solid state Raman spectra of XOSO_2F ($\text{X} = \text{F}, \text{Cl}$) have been recorded [128]. According to gas-phase electron diffraction, both derivatives prefer the *gauche* conformation [128,129]. The exothermic, sometimes explosive, reactions of FOSO_2F with SSF_2 , SeF_4 , AsF_3 and MoF_5 have been studied and the previously reported reactions with SF_4 , Br_2 and I_2 have been re-investigated [127]. Based on the by-products, thermal decomposition of FOSO_2F to $\text{O}_2 + \text{SO}_2\text{F}_2$ and $\text{F}_2 + \text{S}_2\text{O}_6\text{F}_2$ was suggested. The reaction of SO_3 with ClF provides a new, high-yield, synthetic route to ClOSO_2F [130]. Bromine(I) fluorosulfate can be used for the preparation of the *N*-bromo sulfonimides $(\text{CF}_3\text{SO}_2)_2\text{NBr}$ starting from $\text{Hg}(\text{N}(\text{SO}_2\text{CF}_3)_2)_2$ [131]. The crystal structure of $\text{I}(\text{OSO}_2\text{F})_2\text{I}$, which is related to that of $\text{I}(\text{OSO}_2\text{F})_2\text{Cl}$ (see Sec. 5.2.6.1.2), revealed a distorted T-shaped geometry (AX_3E_2 VSEPR arrangement) around the central I^{III} atom coordinated to two OSO_2F groups and the second I^{I} atom [132]. In addition to the primary $\text{I}-\text{I}$ bond, one OSO_2F group exhibits a long contact, through an oxygen, to I^{I} , giving a linear AXYE_3 arrangement.

5.2.5.2.3 Transition metal element derivatives of the SO_3F group. The tetrakis(fluorosulfate) species $\text{M}(\text{SO}_3\text{F})_4$ ($\text{M} = \text{Ti}, \text{Zr}, \text{Hf}$) have been prepared from the corresponding metal powder and $\text{S}_2\text{O}_6\text{F}_2$ in HSO_3F , yielding white solids for Zr^{IV} and Hf^{IV} and a greenish-yellow, resin-like material, which retains small amounts of HSO_3F , for the Ti^{IV} derivative [133]. The intrinsic SO_3F^- acceptor abilities of the tetrakis-derivatives were demonstrated by the formation of thermally stable (260°C) $\text{Cs}_2\text{M}(\text{SO}_3\text{F})_6$ upon addition of CsSO_3F to the metal/ $\text{S}_2\text{O}_6\text{F}_2$ / HSO_3F mixture. These salts have been characterized by vibrational spectroscopy.

The in situ oxidation of niobium and tantalum metals in HSO_3F by $\text{S}_2\text{O}_6\text{F}_2$ results in the formation of solvated Lewis acids, $\text{M}(\text{SO}_3\text{F})_5$ ($\text{M} = \text{Nb}, \text{Ta}$), which exhibit limited thermal stability [134]. The addition of one and two aliquots of CsSO_3F leads to the formation of $\text{CsM}(\text{SO}_3\text{F})_6$ and $\text{Cs}_2\text{M}(\text{SO}_3\text{F})_7$, respectively. The mixed

fluoride fluorosulfates, $\text{NbF}_2(\text{SO}_3\text{F})_3$ and $\text{TaF}_4(\text{SO}_3\text{F})$, have been obtained from a $\text{Nb/S}_2\text{O}_6\text{F}_2/\text{HSO}_3\text{F}$ mixture upon removal of the volatile materials, as a decomposition product of $\text{Nb}(\text{SO}_3\text{F})_5$, and from the ligand redistribution reaction of $\text{Ta}(\text{SO}_3\text{F})_5$ and TaF_5 in a 1:4 stoichiometry in HSO_3F solution, respectively [135]. The white, solid fluoride fluorosulfates appear to be polymeric with bridging SO_3F groups. Addition of MF_5 to a $\text{M/S}_2\text{O}_6\text{F}_2/\text{HSO}_3\text{F}$ reaction mixture yields $\text{Nb}_2\text{F}_9(\text{SO}_3\text{F})$, $\text{MF}_4(\text{SO}_3\text{F})$ and $\text{MF}_3(\text{SO}_3\text{F})_2$ which can be isolated by vacuum distillation without decomposition [137].

Oxidation of Mn by $\text{S}_2\text{O}_6\text{F}_2$ in HSO_3F in the absence or presence of $\text{M}'\text{SO}_3\text{F}$ ($\text{M}' = \text{K}, \text{Cs}$) yields $\text{Mn}^{\text{III}}(\text{SO}_3\text{F})_3$ and $\text{M}'_2\text{Mn}^{\text{III}}(\text{SO}_3\text{F})_5$, respectively [137]. Oxidation of $\text{Mn}_2(\text{CO})_{10}$ by $\text{S}_2\text{O}_6\text{F}_2$ also yields $\text{Mn}^{\text{III}}(\text{SO}_3\text{F})_3$. Solutions of $\text{M}'_2\text{Mn}^{\text{III}}(\text{SO}_3\text{F})_5$ in HSO_3F decompose at room temperature to polymeric $\text{Mn}(\text{SO}_3\text{F})_2$. The yellow oil, $\text{ReO}_2(\text{SO}_3\text{F})_3$, is produced from the reaction of Re or Re_2O_7 with $\text{S}_2\text{O}_6\text{F}_2$ [137] and is the fluorosulfate analogue of ReO_2F_3 (see Sec. 5.2.5.2.3) and $\text{ReO}_2(\text{OTeF}_5)_3$ (see Sec. 5.2.6.1.3). The metal carbonyl fluorosulfates $\text{M}(\text{CO})_5\text{SO}_3\text{F}$ ($\text{M} = \text{Mn}, \text{Re}$) have been obtained from the reaction of $\text{Mn}(\text{CO})_5\text{Br}$ and $\text{Re}(\text{CO})_5\text{Cl}$ with AgSO_3F in CH_2Cl_2 and pyrolysis of $\text{Mn}(\text{CO})_5\text{SO}_3\text{F}$ at 70°C affords $\text{Mn}(\text{CO})_4\text{SO}_3\text{F}$ [137].

The synthesis of $\text{M}(\text{SO}_3\text{F})_3$ ($\text{M} = \text{Rh}, \text{Os}$) can be accomplished by the oxidation of the metal with $\text{S}_2\text{O}_6\text{F}_2$ [138]. While the reaction with Os takes place at 60°C over a period of 3 d in the absence of a solvent, the reaction with Rh requires 130°C in a 1:1 mixture of $\text{S}_2\text{O}_6\text{F}_2$ and HSO_3F solvent and 21 d of reaction time.

Addition of CO to $\text{Ir}(\text{SO}_3\text{F})_3$ in HSO_3F results in the quantitative formation of $\text{Ir}(\text{CO})_3(\text{SO}_3\text{F})_3$ [139]. Raman, infrared and ^{19}F NMR spectroscopy indicate the presence of the *mer*- and *fac*-isomers in solution, however, in the solid state, when solvent removal was rapid, it was established by an X-ray structure and vibrational spectroscopy that only the *mer*- $\text{Ir}(\text{CO})_3(\text{SO}_3\text{F})_3$ isomer crystallized.

Reductive carbonylation of $\text{Pt}(\text{SO}_3\text{F})_4$ in HSO_3F at 80°C and 1–2 atm of CO yields $\text{Pt}(\text{CO})_2(\text{SO}_3\text{F})_2$ [140]. The Pd analogue is formed from $\text{Pd}^{\text{II}}\text{Pd}^{\text{IV}}(\text{SO}_3\text{F})_6$ at room temperature and 0.5 atm of CO. The nearly identical infrared and Raman spectra suggest a *cis*-square-planar arrangement as found in the crystal structure of yellow *cis*- $\text{Pd}(\text{CO})_2(\text{SO}_3\text{F})_2$ [141].

At 25°C , $\text{Pd}(\text{CO})_2(\text{SO}_3\text{F})_2$ undergoes a reductive decomposition in HSO_3F yielding red-orange $[\text{Pd}_2(\mu\text{-CO})_2](\text{SO}_3\text{F})_2$ [142]. The crystal structure of the latter species contains planar cyclic $[\text{Pd}_2(\mu\text{-CO})_2]^{2+}$ cations linked by bidentate-bridging fluorosulfate anions to form polymeric chains. The $\text{Pt}(\text{SO}_3\text{F})_6^{2-}$ anion has been prepared with the counter cations $(\text{CH}_3)_2\text{SnSO}_3\text{F}^+$ [118], $\text{Pt}(\text{CO})_4^{2+}$ [143] and Cs^+ [114]. The crystal structure of $\text{Cs}_2\text{Pt}(\text{SO}_3\text{F})_6$ shows a trigonally distorted PtO_6 environment [143].

Gold(III) tris(fluorosulfate) exists in the crystal as a dimer containing two symmetrically bridged bidentate and four terminal monodentate SO_3F ligands [144]. In HSO_3F solution, $\text{Au}^{\text{III}}(\text{SO}_3\text{F})_3$ reacts with CO, yielding linear $\text{Au}(\text{CO})_2^+_{(\text{solv})}$ cations [145]. Solvent removal in vacuo yields $\text{Au}^{\text{I}}(\text{CO})\text{SO}_3\text{F}$, which is thermally stable up to 190°C . Partial pyrolysis of $\text{Au}^{\text{III}}(\text{SO}_3\text{F})_3$ below 145°C produces Au^{2+} defects in the solid [146] and solvated Au^{2+} is obtained by reaction of $\text{Au}^{\text{III}}(\text{SO}_3\text{F})_3$ in

HSO_3F with Au powder at 65°C [147]. Both systems have been studied by EPR spectroscopy. A yellow solid isolated from the HSO_3F solutions of solvated Au^{2+} has been shown by vibrational spectroscopy and magnetic measurements to be $\text{Au}^{\text{I}}(\text{Au}^{\text{III}}(\text{SO}_3\text{F})_4)$ [147]. The X-ray structure of the $\text{Au}(\text{SO}_3\text{F})_4^-$ anion has been obtained as its Cs^+ salt in which Au^{III} is coordinated to four SO_3F groups in a square-planar fashion [114]. Solvolysis of $\text{Hg}(\text{SO}_3\text{F})_2$ in SbF_5 at 100°C and at 0.8–0.9 bar of CO yields $\text{Hg}(\text{CO})_2(\text{Sb}_2\text{F}_{11})_2$ containing linear $\text{Hg}(\text{CO})_2^+$ cations [148,149]. The corresponding Hg^{I} species $\text{Hg}_2(\text{CO})_2(\text{Sb}_2\text{F}_{11})_2$ is obtained by a similar procedure (60°C , 0.7 bar of CO), with the starting material produced by treatment of Hg_2F_2 with HSO_3F at 80°C .

5.2.5.3 Derivatives of the OSF_5 group and the SOF_4^- anion

Ion cyclotron resonance spectroscopy has shown that SO_3F^- efficiently transfers F^- to SOF_4 to yield the octahedral OSF_5^- anion which, in turn, is a relatively good fluoride donor towards SiF_4 in the gas phase [4].

High-yield syntheses of pure SF_5OSF_5 and SF_5OOSF_5 by the photolysis of SF_5Cl and SF_5OCl to give a mixture of SF_5OSF_5 and SF_5OOSF_5 have been reported [150]. The mixture was thermolyzed at 237°C for 2.5 h to give SF_5OSF_5 and small amounts of SO_2F_2 , SOF_4 and SF_6 . The reaction of SF_5OF and SOF_4 at 163 – 199°C affords high yields of SF_5OOSF_5 [150].

The pentafluorooxosulfate ion, OSF_5^- , has been synthesized from TAS fluoride and SOF_4 in CH_3CN [151]. The oxygen and fluorine atoms of the OSF_5^- anion in the crystal structure of $(\text{Me}_2\text{N})_3\text{S}^+\text{SOF}_5^-$ are disordered.

The gas-phase structure of FOSF_5 has been redetermined by electron diffraction [129,152]. The S—F and S—O bond lengths derived from this study are ca 2% longer than those reported previously with bond angles in excellent agreement. The mean S—F in FOSF_5 is shorter by 0.7 pm than in SF_6 .

The SOF_4^- anion has been generated by γ -irradiation of CsSOF_5 and characterized by its isotropic EPR spectrum at 27°C [153]. The SOF_4^- anion has a *pseudo*-octahedral structure of C_{4v} symmetry in which the equatorial positions are occupied by four equivalent fluorines, one axial position is occupied by a doubly bonded oxygen and the second axial position by the sterically active free valence electron. The structure and spin density of SOF_4^- have been analyzed by local density functional theory calculations and the isoelectronic POF_4^{2-} radical anion has also been calculated.

5.2.6 Selenium and Tellurium

Selenium oxide difluoride, SeOF_2 , is conveniently synthesized by the reaction of excess SeO_2 with SF_4 at 120°C for 12 h [154] and has been used to synthesize high-purity $\text{Xe}(\text{OSeF}_5)_2$ in its reaction with XeF_2 for 24 h at room temperature [154].

The alkali metal monofluoroselenites, prepared by direct fusion of MF ($\text{M} = \text{K}, \text{Rb}, \text{Cs}$) and SeO_2 , have been reinvestigated by single crystal X-ray diffraction [155]. The isolated SeO_2F^- anion exhibits the expected trigonal pyramidal geometry. The anions are bridged by long $\text{Se} \cdots \text{F}$ contacts resulting in infinite linear chains.

The first examples of Te^{IV} oxide fluorides have been prepared and characterized by single crystal X-ray diffraction [156,157]. The compound, $\text{Te}_2\text{O}_3\text{F}_2$, has been prepared by direct fusion of TeO_2 and TeF_4 at 250°C for 24 h [156] and by dissolution of TeO_2 in 40% aqueous HF followed by evaporation and heating of the residue to 200°C for 24 h [157]. The two Te atoms in the crystal structure [156] are four- and five-coordinate and their respective electron lone pairs are stereochemically active. The structure consists of exclusively oxygen-bridged TeO_3F and TeO_4F polyhedra sharing O—O edges to give $\text{Te}_2\text{O}_4\text{F}_2$ and $\text{Te}_2\text{O}_6\text{F}_2$ bipolyhedra, respectively, which, in turn, share corners to form independent sheets. The more highly fluorinated TeOF_2 has been prepared by heating an equimolar mixture of TeO_2 and TeF_4 at 140°C for 24 h and characterized by X-ray powder diffraction [156].

The TeOF_5^- anion has been shown to exhibit weak fluoride ion acceptor properties. The TeOF_6^{2-} anion has been isolated as its $\text{N}(\text{CH}_3)_4^+$ salt from solutions of $\text{N}(\text{CH}_3)_4\text{F}$ and $\text{N}(\text{CH}_3)_4\text{OTeF}_5$ in CH_3CN and characterized by vibrational spectroscopy, a normal coordinate analysis and ab initio calculations [158–160]. The anion is isoelectronic and isostructural with the IOF_6^- anion (see Sec. 5.2.7) and represents only the second known example of a pentagonal bipyramidal main-group element AX_5YZ species and the first multiply charged example of such a species. The mean amplitudes of vibration for TeOF_6^{2-} and IOF_6^- have also been calculated [161].

A polymeric Xe^{II} derivative has been reported resulting from the reaction of XeF_2 with *cis*-(HO) $_2\text{TeF}_4$, and is formulated as $(-\text{Xe}-\text{O}-\text{TeF}_4-\text{O}-)_n$ based on its Raman spectrum [162]. The reaction of *cis*-(HO) $_2\text{TeF}_4$ with $\text{Xe}_2\text{F}_3^+\text{AsF}_6^-$ affords a material corresponding to $\text{FXe}-\text{O}-\text{TeF}_4-\text{O}-\text{Xe}^+\text{AsF}_6^-$ on the basis of approximate mass balance and the Raman spectrum, although an Xe—F stretching mode has not been assigned. Dissolution of $\text{FXe}-\text{O}-\text{TeF}_4-\text{O}-\text{Xe}^+\text{AsF}_6^-$ in anhydrous HF and recrystallization has provided the crystal structure of *cis*- $\text{HO}-\text{TeF}_4-\text{O}-\text{Xe}^+\text{AsF}_6^- \cdot \text{HF}$.

5.2.6.1 Derivatives of the OTeF_5 group

A significant number of main-group and transition metal derivatives of the OTeF_5 group have been synthesized and structurally characterized since the synthesis of HOTeF_5 was first reported in 1964 [163]. The OTeF_5 group is highly electronegative [164], forming stable analogues of fluorides which are frequently the only fluoride analogues known [165,166]. The bonding of the oxygen atom to the central atom is generally more covalent than in the corresponding fluoride and is consistent with the overall lower electronegativity of OTeF_5 when compared with that of fluorine. Unlike fluorine, the OTeF_5 group has less tendency to participate in fluorine bridge formation, although several examples of bridge formation involving the OTeF_5 group in the solid state are now known (see Secs. 5.2.6.1.2 and 5.2.6.1.3).

The general reviews of Seppelt relating to OTeF_5 derivatives [165] and to xenon derivatives of the OSeF_5 and OTeF_5 groups [167] and that of Aubke [33] relating to OTeF_5 derivatives of the transition metals should also be consulted. A number of pentafluorotellurate(VI) anions such as $\text{B}(\text{OTeF}_5)_4^-$, $\text{Pn}(\text{OTeF}_5)_6^-$ ($\text{Pn} = \text{As}$,

Sb, Bi), $M(\text{OTeF}_5)_6^-$ ($M = \text{Nb, Ta}$) and $M'(\text{OTeF}_5)_6^{2-}$ ($M' = \text{Ti, Zr, Hf}$) have shown promise as weakly coordinating anions. A significant portion of this work has previously been reviewed [168,169].

The precursor for all OTeF_5 derivatives, HOTeF_5 , is prepared by the reaction of $(\text{HO})_6\text{Te}$ with a stoichiometric amount of HSO_3F , followed by separation from H_2SO_4 by fractional distillation [170].

5.2.6.1.1 The OTeF_5^- anion. Several salts of the OTeF_5^- anion have been investigated by infrared, Raman and ^{19}F NMR spectroscopy. Nitrosyl pentafluorotellurate(VI), $\text{NO}^+\text{OTeF}_5^-$, has been prepared from NOCl and $\text{Hg}(\text{OTeF}_5)_2$ [171]. Fluorine-19 NMR and vibrational spectroscopy show that the compound exhibits ionic behavior in the solid state and in CH_3CN solution. Gas-phase infrared spectroscopy shows that the compound is covalent in the gas phase and may be formulated as $\text{ON}-\text{OTeF}_5$. The salts, $\text{N}(n\text{-Bu})_4^+\text{OTeF}_5^-$ and $(\text{PS})\text{H}^+\text{OTeF}_5^-$ ($\text{PS} = \text{Proton Sponge; 1,8-bis(dimethylamino)naphthalene, C}_{14}\text{H}_{18}\text{N}_2$), have been prepared and investigated by vibrational spectroscopy [172]. The crystal structure of $(\text{PS})\text{H}^+\text{OTeF}_5^-$, which exists in two modifications [172,173], contains well-separated and non-disordered OTeF_5^- anions. A normal coordinate analysis of OTeF_5^- has been carried out using the geometry established from the crystal structure and spectroscopic data from ^{16}O and ^{18}O enriched samples of $\text{N}(n\text{-Bu})_4^+\text{OTeF}_5^-$. In a subsequent vibrational study of $\text{N}(\text{CH}_3)_4^+\text{OTeF}_5^-$ [160], the results of ab initio calculations and of a normal coordinate analysis of OTeF_5^- showed that six of the fundamental vibrations of OTeF_5^- that had been assigned [172] are incorrect.

The analogy between the OTeF_5 group and fluorine has been extended by the preparation of the OTeF_5 analogue of the bifluoride (HF_2^-) anion [174]. The compound, $\text{N}(n\text{-Bu})_4^+\text{H}(\text{OTeF}_5)_2^-$, was prepared by reaction of HOTeF_5 and $\text{N}(n\text{-Bu})_4^+\text{OTeF}_5^-$ in CH_2Cl_2 . Although the H position was not determined in the crystal structure of the $\text{H}(\text{OTeF}_5)_2^-$ anion, the long $\text{O} \cdots \text{O}$ distance showed that the hydrogen bond in $\text{H}(\text{OTeF}_5)_2^-$ is significantly weaker than in HF_2^- and this is confirmed by vibrational and ^{19}F NMR spectroscopy.

5.2.6.1.2 Main-group element derivatives of the OTeF_5 group. The strong Lewis acid, $\text{B}(\text{OTeF}_5)_3$, is one of the main precursors for the preparation of pentafluorotellurates(VI) and is employed in metathetical reactions with fluorides, leading to BF_3 elimination and element-oxygen bond formation. Tris[pentafluorotellurato(VI)]boron(III) is prepared by reaction of BCl_3 with a stoichiometric amount of HOTeF_5 at ca -60°C , followed by removal of HCl under vacuum at -112°C [170].

The suitability of $\text{B}(\text{OTeF}_5)_4^-$ as a counterion for the generation of weakly coordinated metal and metalloid cations has been extensively studied. The interaction of $\text{B}(\text{OTeF}_5)_3$ with AgOTeF_5 or TiOTeF_5 in the weakly coordinating solvents mesitylene, dichloromethane, 1,2-dichloroethane and 1,1,2-trichlorotrifluoroethane produces solutions of $\text{M}(\text{solv})_x^+\text{B}(\text{OTeF}_5)_4^-$ [175]. Unsolvated crystalline $\text{Ag}^+\text{B}(\text{OTeF}_5)_4^-$ has been isolated from 1,1,2-trichlorotrifluoroethane. The Ag^+ cat-

ion in the X-ray structure of $\text{Ag}^+\text{B}(\text{OTeF}_5)_4^-$ is weakly bonded to three $\text{B}(\text{OTeF}_5)_4^-$ anions through three Ag—O contacts and six Ag—F contacts. In the case of Tl^+ , the unsolvated $\text{Tl}^+\text{B}(\text{OTeF}_5)_4^-$ salt has been isolated from dichloroethane and from 1,1,2-trichlorotrifluoroethane. Both salts are thermally unstable, decomposing to the starting materials upon standing. Crystalline $\text{Tl}(1,2\text{-C}_2\text{H}_4\text{Cl}_2)^+\text{B}(\text{OTeF}_5)_4^-$ has been isolated from 1,2-dichloroethane and studied by X-ray crystallography [176]. The $\text{Tl}(1,2\text{-C}_2\text{H}_4\text{Cl}_2)^+$ cation comprises a five-membered chelate ring and the Tl^+ is weakly bonded to four $\text{B}(\text{OTeF}_5)_4^-$ anions with nine Tl—F interactions.

The compound, $\text{Tl}(\text{mes})_2^+\text{B}(\text{OTeF}_5)_4^-$ ($\text{mes} = 1,3,5\text{-(CH}_3)_3\text{C}_6\text{H}_3$), crystallizes from an equimolar mixture of TlOTeF_5 (vide infra) and $\text{B}(\text{OTeF}_5)_3$ in mesitylene [177]. The structure consists of chains of $\text{Tl}(\text{mes})_2^+$ cations in which Tl is η^6 -coordinated and the $\text{B}(\text{OTeF}_5)_4^-$ anions are connected by extremely weak $\text{Tl} \cdots \text{F}$ interactions (cf. $[\text{TlOTeF}_5(\text{mes})_2]_2 \cdot \text{mes}$; vide infra). It has been shown by ^{17}O NMR spectroscopy that the OTeF_5 groups in $\text{B}(\text{OTeF}_5)_4^-$ do not undergo rapid exchange with free OTeF_5^- , but rapidly exchange in the presence of Lewis acids such as H^+ , Ag^+ and $\text{B}(\text{OTeF}_5)_3$ [175]. The reactions of $\text{AgB}(\text{OTeF}_5)_4$ and $\text{TlB}(\text{OTeF}_5)_4$ with $\text{Fe}(\text{Por})\text{Cl}$ (Por = tetraphenylporphyrinate dianion or octaethylporphyrinate dianion) or Ph_3SiCl in dichloroethylene or mesitylene do not lead to the unsaturated $\text{Fe}(\text{Por})^+$ and Ph_3Si^+ cations, but produce $\text{B}(\text{OTeF}_5)_3$ and $\text{Fe}(\text{Por})\text{OTeF}_5$ or $\text{Ph}_3\text{SiOTeF}_5$, respectively. The reaction of $\text{Ph}_3\text{CB}(\text{OTeF}_5)_4$ with Ph_3SiH in dichloromethane also produces $\text{Ph}_3\text{SiOTeF}_5$ [175].

The syntheses and characterization of the first silver carbonyl complexes have been reported as the cationic silver(I) complexes $\text{Ag}(\text{CO})^+$ [178,179], $\text{Ag}(\text{CO})_2^+$ [179,180] and $\text{Ag}(\text{CO})_3^+$ [181]. The counterions used all contain the OTeF_5 moiety and include OTeF_5^- and the weakly coordinating anions $\text{B}(\text{OTeF}_5)_4^-$, $\text{Zn}(\text{OTeF}_5)_4^{2-}$, $\text{Nb}(\text{OTeF}_5)_6^-$ and $\text{Ti}(\text{OTeF}_5)_6^{2-}$ (also see Sec. 5.2.6.1.3). The crystal structures of $\text{AgCO}^+\text{B}(\text{OTeF}_5)_4^-$ [178,179] and $\text{Ag}(\text{CO})_2^+\text{B}(\text{OTeF}_5)_4^-$ [179,180] have been determined.

The compound, TlOTeF_5 , has been synthesized by direct interaction of TlF with HOTeF_5 and is soluble in toluene and mesitylene from which $[\text{TlOTeF}_5(\text{mes})_2]_2 \cdot \text{mes}$ crystallizes [177,182]. The crystal structure shows that the mesitylene ligands are η^6 -coordinated to the thallium atoms with two OTeF_5 groups bridging the two thallium atoms.

The OTeF_5 analogues of AsF_5 and BiF_5 have been synthesized by reaction of the pentafluorides with stoichiometric amounts of $\text{B}(\text{OTeF}_5)_3$. The synthesis of $\text{As}(\text{OTeF}_5)_5$ is carried out at room temperature in anhydrous liquid SO_2 followed by low temperature crystallization from liquid SO_2 [183], and $\text{Bi}(\text{OTeF}_5)_5$ has been synthesized in $\text{CClF}_2\text{CCl}_2\text{F}_2$ (Freon-114) at 0°C [184], and, like $\text{As}(\text{OTeF}_5)_5$, it is stable indefinitely at room temperature. All attempts to prepare pure $\text{Sb}(\text{OTeF}_5)_5$ have been unsuccessful and indicate that the compound is unstable above 0°C [184].

The weakly coordinating pnictogen anions, $\text{M}(\text{OTeF}_5)_6^-$ ($\text{M} = \text{As}, \text{Sb}, \text{Bi}$) have been synthesized as their tetraalkylammonium salts and structurally characterized by X-ray crystallography, ^{19}F , ^{75}As , $^{121,123}\text{Sb}$, ^{125}Te and ^{209}Bi NMR and Raman spectroscopy [184]. The $\text{As}(\text{OTeF}_5)_6^-$ anion had been previously characterized in

solution by ^{19}F , ^{75}As and ^{125}Te NMR spectroscopy as a counterion for the series of mixed Te^{IV} cations, $\text{Te}_n(\text{OTeF}_5)_{3-n}^+$ ($n=0-3$) (vide infra) [183]. The $\text{Cs}^+\text{As}(\text{OTeF}_5)_6^-$ salt had also been prepared by the reaction of $\text{Cs}^+\text{OTeF}_5^-$ with $\text{As}(\text{OTeF}_5)_5$ at 80°C [183,185]. The syntheses of the arsenic and bismuth salts were accomplished by the direct interaction of $\text{N}(\text{CH}_3)_4^+\text{OTeF}_5^-$ with $\text{As}(\text{OTeF}_5)_5$ and $\text{Bi}(\text{OTeF}_5)_5$ [184]. The instability of $\text{Sb}(\text{OTeF}_5)_5$ makes it inconvenient to use this compound for the synthesis of $\text{Sb}(\text{OTeF}_5)_6^-$ salts. One approach which yields a high purity product involves the reaction of $\text{NR}_4^+\text{OTeF}_5^-$ ($\text{R}=\text{CH}_3$, CH_3CH_2) with $\text{Sb}(\text{OTeF}_5)_3$ to give $\text{NR}_4^+\text{Sb}(\text{OTeF}_5)_4^-$ which is then oxidized to $\text{NR}_4^+\text{Sb}(\text{OTeF}_5)_6^-$ using an equimolar amount of $\text{Xe}(\text{OTeF}_5)_2$ [184]. A second approach involves the metathesis of AgOTeF_5 and a tetraalkylammonium salt of SbCl_6^- in CH_2Cl_2 or Freon-113 solvents [186]. The $\text{AsF}_5(\text{OTeF}_5)^-$ anion has been obtained as its NS^+ salt (vide infra) [187].

The $\text{Sb}(\text{OTeF}_5)_6^-$ anion has been used to stabilize the previously unreported SbBr_4^+ cation. The tetrahalonium salts $\text{SbCl}_4^+\text{Sb}(\text{OTeF}_5)_6^-$ and $\text{SbBr}_4^+\text{Sb}(\text{OTeF}_5)_6^-$ have been prepared by the oxidation of $\text{Sb}(\text{OTeF}_5)_3$ with Cl_2 and Br_2 , respectively [188]. Owing to the weakly coordinating nature of the $\text{Sb}(\text{OTeF}_5)_6^-$ anion, both salts are very soluble in SO_2ClF . The weak coordination of the $\text{Sb}(\text{OTeF}_5)_6^-$ to SbCl_4^+ and SbBr_4^+ has been confirmed by the crystal structures of these salts, in which the coordination is similar but weaker than in the previously known $\text{SbCl}_4^+\text{Sb}_2\text{F}_{11}^-$, $\text{SbCl}_4^+\text{Sb}_2\text{Cl}_{0.5}\text{F}_{10.5}^-$ and $\text{SbCl}_4^+\text{Sb}_2\text{Cl}_2\text{F}_9^-$ salts.

The gas-phase structure of $\text{F}_5\text{TeOOTeF}_5$, along with those of its sulfur and selenium analogues, has been determined by electron diffraction [189]. The O—O bond lengths are not well determined, and the M—F ($\text{M}=\text{S}$, Se , Te) bond lengths are similar to those in MF_6 whereas the M—O bonds are significantly longer than in the oxides F_5MOMF_5 owing to much smaller MOO bond angles when compared with the MOM angles of the oxides.

The structure of the previously known $\text{Te}(\text{OTeF}_5)_4$ molecule has been shown by X-ray crystallography to be a disphenoid with an AX_4E VSEPR geometry in which a lone electron pair and two OTeF_5 groups occupy the equatorial plane and two OTeF_5 groups occupy the axial positions of a trigonal bipyramid [190]. The structure provides an example of an OTeF_5 group that bridges through its fluorines and contrasts with oxygen bridging noted in several transition metal compounds that are subsequently described in this Chapter (see Sec. 5.2.6.1.3). Two secondary $\text{Te}^{\text{IV}}\cdots\text{F}$ contacts arising from two nearest neighbor $\text{Te}(\text{OTeF}_5)_4$ molecules give rise to a chain structure in which the coordination about Te^{IV} is best described as a distorted octahedral ($\text{AX}_4\text{Y}_2\text{E}$) VSEPR arrangement. The activation energy barrier to intramolecular exchange in the trigonal bipyramidal $\text{Te}(\text{OTeF}_5)_4$ molecule has also been derived from ^{19}F and ^{125}Te NMR studies in SO_2ClF solvent [183].

The compounds, $\text{F}_2\text{Te}(\text{OTeF}_5)_2$ and $\text{F}_2\text{Se}(\text{OTeF}_5)_2$, have been synthesized by ligand exchange between TeF_4 (SeF_4) and $\text{B}(\text{OTeF}_5)_3$ [191]. Both structures have been investigated by ^{77}Se and ^{125}Te NMR spectroscopy and show the expected trigonal bipyramidal structures with OTeF_5 ligands in the axial positions and fluorines in the equatorial positions. The molecule, $\text{F}_2\text{Te}(\text{OTeF}_5)_2$, cocrystallizes

with a trigonal bipyramidal $\text{Te}^{\text{IV}}\text{O}_2\text{F}_2$ arrangement in $\text{ReO}(\text{OTeF}_5)_4 \cdot \text{F}_2\text{Te}(\text{OTeF}_5)_2$ (see Sec. 5.2.6.1.3), but is unusual in that it adopts a *cis*-arrangement in which one fluorine and one OTeF_5 group occupy an equatorial and an axial position [192]. In contrast, solution studies and VSEPR arguments indicate that both fluorine atoms are in equatorial positions.

The interaction of $\text{N}(\text{CH}_3)_4^+\text{OTeF}_5^-$ with $\text{Te}(\text{OTeF}_5)_4$ has been shown to give rise to the $\text{Te}(\text{OTeF}_5)_5^-$ anion [190]. The anion geometry is analogous to the AX_5E VSEPR geometry of TeF_5^- and has been established in the solid state by an X-ray structure determination and in solution by ^{19}F and ^{125}Te NMR spectroscopy. The $\text{Te}(\text{OTeF}_5)_5^-$ and TeF_5^- anions were shown to undergo ligand redistribution and, with the exception of $\text{FTe}(\text{OTeF}_5)_4^-$, the intermediate $\text{F}_n\text{Te}(\text{OTeF}_5)_{5-n}^-$ anions were found to be labile on the NMR time scale. The OTeF_5^- donor properties of $\text{Te}(\text{OTeF}_5)_4$ in the presence of the strong Lewis acids AsF_5 and $\text{As}(\text{OTeF}_5)_5$ have been studied in SO_2ClF and SO_2 solvents and shown to give rise to the mixed $\text{Te}_n(\text{OTeF}_5)_{3-n}^+$ ($n=0-3$) cations and the neutral species, $\text{TeF}_n(\text{OTeF}_5)_{4-n}$ ($n=0-2$), and by solution ^{125}Te NMR spectroscopy [183]. The $\text{As}(\text{OTeF}_5)_6^-$ anion, identified for the first time in the course of this study, serves as a counterion (vide supra) and has been synthesized by the reaction of the $\text{N}(\text{CH}_3)_4^+\text{OTeF}_5^-$ with $\text{As}(\text{OTeF}_5)_5$.

Thiazyl pentafluorooxotellurate, NSOTeF_5 , has been prepared from NSF and $\text{B}(\text{OTeF}_5)_3$ at -35°C and from $\text{NS}^+\text{SbF}_6^-$ and CsOTeF_5 in liquid SO_2 at -35°C [187]. The compound is rather unstable, isomerizing rapidly to give OSNTeF_5 . The diimide, $\text{F}_5\text{TeNSNTeF}_5$, is formed from NSOTeF_5 in the BF_3 catalyzed elimination of SO_2 in the course of the reaction of NSF with $\text{B}(\text{OTeF}_5)_3$. The interaction of AsF_5 with NSOTeF_5 at -60°C leads to the thiazyl salt, $\text{NS}^+\text{AsF}_5(\text{OTeF}_5)^-$.

The compound, $\text{O}_2\text{BrOTeF}_5$, was prepared by the ozonization of BrOTeF_5 as a colorless solid (m.p. -20°C) and characterized by vibrational and ^{19}F NMR spectroscopy and a single crystal X-ray structure determination [193]. The structure has the expected pyramidal geometry at Br^{III} , consistent with an AX_3E VSEPR arrangement.

The compounds $\text{N}(\text{C}_4\text{H}_9)_4^+\text{I}(\text{OTeF}_5)_4^-$ and $\text{N}(\text{C}_4\text{H}_9)_4^+\text{OI}(\text{OTeF}_5)_4^-$ have been synthesized by the reaction of $\text{I}(\text{OTeF}_5)_3$ and $\text{I}(\text{OTeF}_5)_5$, respectively, with stoichiometric amounts of $\text{N}(\text{C}_4\text{H}_9)_4^+\text{OTeF}_5^-$ in CH_2Cl_2 [194]. Small amounts of $\text{N}(\text{C}_4\text{H}_9)_4^+\text{OI}(\text{OTeF}_5)_4^-$ were obtained as a fortuitous hydrolysis product in attempts to form $\text{I}(\text{OTeF}_5)_6^-$. The crystal structures of the anions show that they are based on AX_4E_2 and AX_4YE VSEPR arrangements corresponding to a square-planar IO_4 geometry for $\text{I}(\text{OTeF}_5)_4^-$ and a square-pyramidal IO_5 geometry for $\text{OI}(\text{OTeF}_5)_4^-$ in which the doubly bonded oxygen is in the axial position. The reaction of $\text{I}(\text{OTeF}_5)_3$ with CFCl_3 at room temperature resulted in the formation of $\text{Cl}-\text{I}(\text{OTeF}_5)_2$ [194]. The crystal structure shows that the molecule has a T-shaped arrangement of oxygens and the chlorine about iodine and is consistent with an AX_3E_2 VSEPR arrangement of lone pair and bond pair domains in which the less electronegative chlorine atom occupies the equatorial plane along with both lone pairs of electrons. The structure of $\text{Cl}-\text{I}(\text{OTeF}_5)_2$ closely resembles that of $\text{I}-\text{I}(\text{OSO}_2\text{F})_2$ [132; also see Sec. 5.2.5.2.2].

Krypton bis(pentafluoro-oxotellurate(VI)) provides the first example of a species containing a krypton-oxygen bond and has been prepared by the reaction of KrF_2 with natural abundance and ^{17}O -enriched $\text{B}(\text{OTeF}_5)_3$ at -90 to -112°C in SO_2ClF solvent [195]. The characterization of the thermally unstable $\text{Kr}(\text{OTeF}_5)_2$ molecule and its decomposition products has been achieved using ^{19}F and ^{17}O NMR spectroscopy. The detailed synthesis of $\text{Xe}(\text{OTeF}_5)_2$ by the reaction of an excess of HOTeF_5 with XeF_2 at room temperature has been described [170]. The reaction equilibrium is driven to near completion by periodic removal of HF under vacuum after small aliquots of HOTeF_5 are added and the medium has been fused near room temperature. The synthesis requires an approximate two-fold excess of HOTeF_5 . The synthesis of high-purity $\text{Xe}(\text{OTeF}_5)_2$ can also be achieved by the interaction of stoichiometric amounts of XeF_2 with $\text{B}(\text{OTeF}_5)_3$ in Freon-114 solvent between -78°C and room temperature [184].

The first OTeF_5 derivatives of XeOF_2 , $\text{XeO}(\text{OTeF}_5)_2$ and $\text{XeOF}(\text{OTeF}_5)$ have been generated in CH_3CN solution at -40°C by the interaction of $\text{N}(\text{CH}_3)_4^+\text{OTeF}_5^-$ and $\text{N}(\text{CH}_3)_4^+\text{F}^-$ with $\text{Xe}(\text{OTeF}_5)_4$ and characterized by ^{19}F and ^{129}Xe NMR spectroscopy at -40°C in CH_3CN [196]. The first solution evidence for XeOF_2 was also obtained in the course of this study (see Sec. 5.2.8).

The structure of the previously known compound, $\text{Xe}(\text{OTeF}_5)_4$, has been determined by X-ray crystallography [197] and comprises a planar XeO_4 arrangement and, like its isoelectronic $\text{I}(\text{OTeF}_5)_4^-$ analogue [194], it is based on an AX_4E_2 VSEPR arrangement of two electron lone pair domains and four bond pair domains in which the lone electron pairs are in the axial positions. The known compound, $\text{OXe}(\text{OTeF}_5)_4$, decomposes over a period of several months to $\text{F}_5\text{TeOTeF}_5$ and $\text{O}_2\text{Xe}(\text{OTeF}_5)_2$ [197], which had been previously characterized by ^{19}F and ^{129}Xe NMR spectroscopy [198]. The crystal structure of $\text{O}_2\text{Xe}(\text{OTeF}_5)_2$ shows that the molecular geometry is based on a trigonal bipyramidal $\text{AX}_2\text{Y}_2\text{E}$ arrangement in which the electron pair and both oxygen atoms occupy the equatorial plane and the OTeF_5 groups are in axial positions [197]. Interestingly, the $\text{O}-\text{Xe}-\text{O}$ angle appears to contradict the VSEPR formalism and is bent away from the electron lone pair.

Fluorine-19 and ^{129}Xe NMR studies of the solvolyses of $\text{Xe}(\text{OTeF}_5)_4$ and $\text{OXe}(\text{OTeF}_5)_4$ in the strong F^- and OTeF_5^- acceptor solvent, SbF_5 , have shown that OTeF_5/F ligand redistribution has occurred leading to the formation of two series of mixed xenon species, $\text{F}_n\text{Xe}(\text{OTeF}_5)_{3-n}^+$ and $\text{OXeF}_n(\text{OTeF}_5)_{3-n}^+$ ($n=0-2$) and $\text{O}_2\text{XeOTeF}_5^+$ [199]. The previously known XeF_3^+ , XeOF_3^+ and XeO_2F^+ cations were observed in addition to the mixed cations. The $\text{OXe}(\text{OTeF}_5)_3^+$ cation appears to be considerably less stable than $\text{OXeF}_n(\text{OTeF}_5)_{3-n}^+$ and was not observed in the $\text{OXe}(\text{OTeF}_5)_4/\text{SbF}_5$ systems. Problems of thermal instability were overcome by allowing $\text{OXe}(\text{OTeF}_5)_4$ and " $\text{Sb}(\text{OTeF}_5)_5$ " (vide supra) to react in SO_2ClF solvent at -60 to -80°C to give the $\text{OXe}(\text{OTeF}_5)_3^+$ cation. Owing to the complexity of the ^{19}F NMR spectra, the $\text{Sb}(\text{OTeF}_5)_6^-$ anion (vide supra), which was undoubtedly present, was not identified in this study.

5.2.6.1.3 Transition metal element derivatives of the OTeF_5 group. The pentakis-derivatives, $\text{Nb}(\text{OTeF}_5)_5$ and $\text{Ta}(\text{OTeF}_5)_5$, have been prepared by the

reaction of excess HOTeF_5 with NbCl_5 and TaCl_5 [200]. The interaction of $\text{M}(\text{OTeF}_5)_5$ ($\text{M} = \text{Nb}, \text{Ta}$) with an equimolar amount of $\text{A}^+\text{OTeF}_5^-$ ($\text{A} = \text{Cs}, \text{Et}_4\text{N}, \text{N}(n\text{-Bu})_4$) in HOTeF_5 solvent at room temperature has provided the corresponding $\text{A}^+\text{M}(\text{OTeF}_5)_6^-$ salts which have been characterized by ^{19}F NMR spectroscopy in CH_2Cl_2 or CH_3CN solution.

Several OTeF_5 derivatives of Mo^{VI} , W^{V} and W^{VI} are now known [201]. The interaction of excess ClOTeF_5 with MoCl_5 in CFCl_3 results in the formation of $\text{Mo}(\text{OTeF}_5)_6$ which decomposes over a period of seven days at 0°C to $\text{MoO}(\text{OTeF}_5)_4$. The reaction of WCl_5 with an excess of $\text{Xe}(\text{OTeF}_5)_2$ in CFCl_3 at room temperature yields $\text{W}(\text{OTeF}_5)_6$ and $\text{WO}(\text{OTeF}_5)_4$ was prepared by reaction of WOCl_4 with ClOTeF_5 at room temperature. The reaction of WCl_5 with ClOTeF_5 in CFCl_3 between -30°C and 0°C gives rise to $\text{W}(\text{OTeF}_5)_5$. The latter compound is unstable, decomposing to $\text{W}(\text{OTeF}_5)_6$ and $\text{WO}(\text{OTeF}_5)_4$. The crystal structures of $\text{Mo}(\text{OTeF}_5)_6$ and $\text{MO}(\text{OTeF}_5)_4$ ($\text{M} = \text{Mo}, \text{W}$) have been determined, and all three compounds crystallize in molecular lattices. The structure of $\text{Mo}(\text{OTeF}_5)_6$ comprises a regular MoO_6 octahedron of *pseudo*-octahedral OTeF_5 groups in which the $\text{Mo}-\text{O}-\text{Te}$ angles are non-linear. Similar features are observed for both $\text{MO}(\text{OTeF}_5)_4$ compounds which possess square pyramidal MO_5 moieties having the metal-oxygen double bond in an axial position. The coordination numbers of the metal atoms in $\text{MO}(\text{OTeF}_5)_4$ is increased to six by a long contact between the metal and a fluorine of an OTeF_5 group in a neighboring $\text{MO}(\text{OTeF}_5)_4$ molecule.

The compound, $\text{ReO}_2(\text{OTeF}_5)_3$, has been synthesized from the reaction of ReO_2F_3 with $\text{B}(\text{OTeF}_5)_3$ and structurally characterized in solution by ^{19}F and ^{125}Te NMR spectroscopy and in the solid state by Raman spectroscopy [202]. The spectroscopic findings are consistent with a trigonal bipyramidal arrangement in which the oxygen atoms and an OTeF_5 group occupy the equatorial plane and two OTeF_5 groups occupy the axial positions. The NMR spectra show that the axial and equatorial groups exhibit fluxional behavior consistent with intramolecular exchange by means of pseudorotation. The Lewis character of $\text{ReO}_2(\text{OTeF}_5)_3$ is exhibited in its reaction with $\text{N}(\text{CH}_3)_4^+\text{OTeF}_5^-$, forming the $\text{ReO}_2(\text{OTeF}_5)_4^-$ anion, which has been characterized in solution by ^{19}F and ^{125}Te NMR spectroscopy and in the solid state by Raman spectroscopy and single-crystal X-ray diffraction [202]. The coordination sphere about Re^{VII} in $\text{ReO}_2(\text{OTeF}_5)_4^-$ is *pseudo*-octahedral with the $\text{Re}-\text{O}$ double bonds *cis* to one another.

Both ReCl_5 and ReOCl_4 react with ClOTeF_5 to give blue, paramagnetic $\text{ReO}(\text{OTeF}_5)_4$ [192]. The reaction of ClOTeF_5 or $\text{Hg}(\text{OTeF}_5)_2$ with ReCl_5 also affords $\text{F}_2\text{Te}(\text{OTeF}_5)_2$ as a reduction product which crystallizes as $\text{ReO}(\text{OTeF}_5)_4 \cdot \text{F}_2\text{Te}(\text{OTeF}_5)_2$. In crystalline $\text{ReO}(\text{OTeF}_5)_4 \cdot \text{F}_2\text{Te}(\text{OTeF}_5)_2$, $\text{ReO}(\text{OTeF}_5)_4$ forms a square pyramid with the doubly bonded oxygen in the apical position. The sixth coordination site of the *pseudo*-octahedron around rhenium is occupied by a long contact with a fluorine bonded to tellurium(IV) in *cis*- $\text{F}_2\text{Te}(\text{OTeF}_5)_2$ (see Sec. 5.2.6.1.2). The OTeF_5 analogue of ReOF_5 has been prepared by oxidative addition of OTeF_5 to $\text{ReO}(\text{OTeF}_5)_4$ in $\text{ReO}(\text{OTeF}_5)_4 \cdot \text{TeF}_2(\text{OTeF}_5)_2$ and to ReCl_5 using $\text{Xe}(\text{OTeF}_5)_2$ as the oxidizing agent [192]. The crystal structure of $\text{ReO}(\text{OTeF}_5)_5$

shows the expected octahedral coordination about rhenium with one doubly bonded oxygen atom.

Iron(III) chloride reacts with ClOTeF_5 in SO_2ClF or $\text{C}_4\text{F}_9\text{SO}_2\text{F}$ forming $\text{Fe}(\text{OTeF}_5)_3$ [203]. Crystallization from SO_2ClF yields the adduct, $\text{Fe}(\text{OTeF}_5)_3 \cdot 3\text{SO}_2\text{ClF}$. The crystal structure shows that the $\text{Fe}^{\text{III}}\text{O}_6$ core has distorted octahedral coordination in which the three SO_2ClF and three OTeF_5 oxygen atoms provide a facial arrangement about iron. The large quadrupole splitting in the ^{57}Fe Mössbauer spectrum of solvent-free $\text{Fe}(\text{OTeF}_5)_3$ is consistent with trigonal planar coordination. The compound is extremely reactive towards bases and reacts with $\text{P}(\text{OC}_2\text{H}_5)_3$ in SO_2ClF solution to form $\text{P}(\text{OC}_2\text{H}_5)_4^+\text{Te}_2\text{Cl}_9^-$ and iron fluoride(s).

The five- and six-coordinate high-spin iron(III) porphyrin complexes, $\text{Fe}(\text{TPP})(\text{OTeF}_5)$ ($\text{TPP} = 5,10,15,20$ -tetraphenylporphyrinate dianion) and $\text{Fe}(\text{OEP})(\text{OTeF}_5)$ ($\text{OEP} = 2,3,7,8,12,13,17,18$ -octaethylporphyrinate dianion) have been prepared by treatment of $[\text{Fe}(\text{TPP})]_2\text{O}$ and $[\text{Fe}(\text{OEP})]_2\text{O}$ with excess HOTeF_5 in toluene [204]. The $\text{Fe}(\text{TPP})(\text{OTeF}_5)$ complex was also obtained by the metathesis reaction of $\text{Fe}(\text{TPP})\text{Cl}$ with $[\text{AgOTeF}_5(\text{CH}_3\text{CN})_2]_2$ in CH_2Cl_2 . Single-crystal X-ray diffraction of crystals obtained by recrystallization of $\text{Fe}(\text{TPP})\text{OTeF}_5$ from THF shows that the TPP complex crystallizes as $\text{Fe}(\text{TPP})(\text{OTeF}_5) \cdot \text{THF}$, and represents a rare example of a six-coordinate high-spin iron(III) porphyrin complex with different axial ligands.

The OTeF_5 /halide metathesis of AgOTeF_5 and PdCl_2 in CH_2Cl_2 or $1,2\text{-C}_2\text{H}_4\text{Cl}_2$ result in $\text{Ag}_2(\text{CH}_2\text{Cl}_2)_4\text{Pd}(\text{OTeF}_5)_4$ and $\text{Ag}_2(1,2\text{-C}_2\text{H}_4\text{Cl}_2)_4\text{Pd}(\text{OTeF}_5)_4$ whose crystal structures show that the OTeF_5 groups oxygen bridge the silver and palladium centers with silver again coordinated to the chlorocarbon in a bidentate fashion [205]. In the case of $\text{Ag}_2(\text{CH}_2\text{Cl}_2)_4\text{Pd}(\text{OTeF}_5)_4$, there is an additional long intramolecular contact between each silver and fluorine of the OTeF_5 group.

The metathesis of $\text{AgOTeF}_5(\text{tol})_2$ ($\text{tol} = \text{toluene}$) and $\text{PtCl}_2(\text{NBD})$ ($\text{NBD} = \text{norbornadiene}$) in CH_2Cl_2 leads to $\text{Pt}(\text{OTeF}_5)_2(\text{NBD})$ [206]. The crystal structure of $\text{Pt}(\text{OTeF}_5)_2(\text{NBD})$ contains a square-planar arrangement about the platinum defined by two OTeF_5 oxygens and the centroids of the double bonds of NBD.

The preparation of AgOTeF_5 from AgF and HOTeF_5 in CH_2Cl_2 leads to the formation of $[\text{Ag}(\text{CH}_2\text{Cl}_2)(\text{OTeF}_5)]_2$ which yields AgOTeF_5 under dynamic vacuum [205,207]. The interaction of AgOTeF_5 with $1,2\text{-C}_2\text{H}_4\text{Cl}_2$ results in $[\text{Ag}(1,2\text{-C}_2\text{H}_4\text{Cl}_2)(\text{OTeF}_5)]_2$ [205] and recrystallization of $[\text{Ag}(\text{CH}_2\text{Cl}_2)(\text{OTeF}_5)]_2$ from $\text{C}_6\text{H}_5\text{CH}_3$ yields $[\text{Ag}(\text{C}_6\text{H}_5\text{CH}_3)_2(\text{OTeF}_5)]_2$ [207]. The latter compound contains an Ag_2O_2 core comprised of two OTeF_5 groups bridging two silver atoms. Two $\text{C}_6\text{H}_5\text{CH}_3$ rings are coordinated in a η^2 -fashion to each silver atom. Spectroscopic data and the crystal structure show that $[\text{Ag}(1,2\text{-C}_2\text{H}_4\text{Cl}_2)(\text{OTeF}_5)]_2$ also contains a planar Ag_2O_2 core and that the OTeF_5 groups bridge the silver centers which are, in turn, each coordinated to a solvent molecule [205].

The only gold derivative of the OTeF_5 group that is presently known is $\text{Au}(\text{OTeF}_5)_3$, which has been prepared by the reaction of molten $\text{B}(\text{OTeF}_5)_3$ with AuF_3 at 60°C for 5 d [208]. The crystal structure of $\text{Au}(\text{OTeF}_5)_3$ consists of dimers containing both bridging and terminal OTeF_5 groups. Two OTeF_5 groups

oxygen bridge two gold atoms forming planar Au_2O_2 rings and the remaining two coordination sites of square planar Au^{III} are occupied by terminal OTeF_5 groups.

The compound, $\text{Zn}(\text{OTeF}_5)_2$, has been prepared in cyclopentane by the reaction of $\text{Zn}(\text{CH}_2\text{CH}_3)_2$ with HOTeF_5 and its interactions with the weakly coordinating solvents toluene, mesitylene, nitromethane, nitrobenzene, acetonitrile, acetone, diethyl ether and tetrahydrofuran have been studied by infrared and ^{19}F NMR spectroscopy, conductimetry and tensimetric titrations with solvent vapors [209]. The complexes, $[\text{Zn}(\text{OTeF}_5)_2(\text{PhNO}_2)_2]_2$ and $\text{Zn}(\text{OTeF}_5)_2(\text{PhNO}_2)_3$, have been structurally characterized by single crystal X-ray diffraction [210]. The structure of $[\text{Zn}(\text{OTeF}_5)_2(\text{PhNO}_2)_2]_2$ comprises planar Zn_2O_2 cores with each six-coordinate Zn coordinated to one terminal and two bridging OTeF_5 groups and to one monodentate and one bidentate nitrobenzene ligand, providing a ZnO_6 coordination sphere which is a distorted octahedron. Other than $\text{Au}(\text{OTeF}_5)_3$ (vide infra), this is the only structurally characterized compound containing both oxygen bridged and terminal OTeF_5 groups. The mononuclear complex, $\text{Zn}(\text{OTeF}_5)_2(\text{PhNO}_2)_3$ contains five-coordinate Zn coordinated to two terminal OTeF_5 ligands and three monodentate nitrobenzene ligands. The ZnO_5 coordination sphere is approximately trigonal bipyramidal. The $\text{Zn}(\text{OTeF}_5)_4^{2-}$ anion has been prepared as the Ag^+ salt and was shown by tensimetry and infrared spectroscopy to react with CO in a variety of organic solvents to give the AgCO^+ and $\text{Ag}(\text{CO})_2^+$ cations [179; also see Sec. 5.2.6.1.2].

The $\text{M}(\text{OTeF}_5)_6^-$ ($\text{M} = \text{Sb}, \text{Nb}$) and $\text{Ti}(\text{OTeF}_5)_6^{2-}$ anions have been prepared as their silver salts by reaction of MCl_5 and TiCl_4 with AgOTeF_5 in Freon-113 [186,211]. The $\text{Ag}_2\text{Zr}(\text{OTeF}_5)_6$ and $\text{Ag}_2\text{Hf}(\text{OTeF}_5)_6$ salts were prepared by the reaction of ZrCl_4 or HfCl_4 with AgOTeF_5 in CH_2Cl_2 [186]. The $\text{N}(n\text{-Bu})_4^+$ and Ph_3C^+ salts of the $\text{Sb}(\text{OTeF}_5)_6^-$, and $\text{Nb}(\text{OTeF}_5)_6^-$ anions and the $\text{N}(n\text{-Bu})_4^+$ salt have been prepared from AgOTeF_5 and $\text{N}(n\text{-Bu})_4^+\text{Cl}^-$ and $\text{Ph}_3\text{C}^+\text{Cl}^-$ in CH_2Cl_2 solution [186]. In general, these salts are highly soluble in weakly coordinating, low dielectric solvents such as chlorinated hydrocarbons and chlorofluorocarbons. Recrystallization of $(\text{Ag}^+)_2\text{Ti}(\text{OTeF}_5)_6^{2-}$ from CH_2Cl_2 resulted in $[\text{Ag}(\text{CH}_2\text{Cl}_2)_3]_2[\text{Ti}(\text{OTeF}_5)_6]$ [186,211]. Three CH_2Cl_2 solvent molecules are coordinated to each silver ion in a bidentate fashion and each silver ion has two additional very weak contacts with fluorines of the $\text{Ti}(\text{OTeF}_5)_6^{2-}$ anion.

Dissolution of $\text{Ag}^+\text{Nb}(\text{OTeF}_5)_6^-$ and $\text{Ag}^+\text{Sb}(\text{OTeF}_5)_6^-$ in CH_2Br_2 results in slow crystallization of $\text{Ag}(\text{CH}_2\text{Br}_2)_3^+\text{Nb}(\text{OTeF}_5)_6^-$ and $[\text{catena-poly}[\text{Ag}(1,2\text{-CH}_2\text{Br}_2)_2-\mu(1,2\text{-C}_2\text{H}_4\text{Br}_2)\text{-Br:Br}]]^+\text{Sb}(\text{OTeF}_5)_6^-$ [211]. The structure of $\text{Ag}(\text{CH}_2\text{Br}_2)_3^+\text{Nb}(\text{OTeF}_5)_6^-$ consists of discrete $\text{Ag}(\text{CH}_2\text{Br}_2)_3^+$ cations, in which the silver ion is coordinated to the bromines in a bidentate fashion, and $\text{Nb}(\text{OTeF}_5)_6^-$ anions. The structure of $[\text{catena-poly}[\text{Ag}(1,2\text{-CH}_2\text{Br}_2)_2-\mu(1,2\text{-C}_2\text{H}_4\text{Br}_2)\text{-Br:Br}]]^+\text{Sb}(\text{OTeF}_5)_6^-$ consists of single-strand polyatomic $[-(1,2\text{-C}_2\text{H}_4\text{Br}_2)_2\text{Ag-BrC}_2\text{H}_4\text{Br-}]_n^{n+}$ chains with two bidentate CH_2Br_2 molecules and two monodentate CH_2Br_2 molecules coordinated to the silver ion and discrete $\text{Sb}(\text{OTeF}_5)_6^-$ anions. Unlike $[\text{Ag}(\text{CH}_2\text{Cl}_2)_3]_2[\text{Ti}(\text{OTeF}_5)_6]$, there are no close contacts between the silver ion and the fluorines of the OTeF_5 groups in either structure.

A number of organometallic compounds are known in which the OTeF_5 group is coordinated to the organometal center. The reactions of HOTeF_5 with $\text{M}(\text{CO})_3(\text{PPh}_3)_2$ ($\text{M} = \text{Fe}, \text{Ru}, \text{Os}$) readily give the previously characterized octahedral protonated $[\text{HM}(\text{CO})_3(\text{PPh}_3)_2]^+$ cations hydrogen bonded to their OTeF_5^- counterions [212]. The $\text{Cp}_2\text{M}(\text{OTeF}_5)_2$ ($\text{M} = \text{Ti}, \text{Zr}, \text{Hf}, \text{Mo}$ or W ; $\text{Cp} = \eta^5\text{-C}_5\text{H}_5$) and $\text{Cp}_2\text{TiCl}(\text{OTeF}_5)$ complexes have been prepared by the reaction of Cp_2MCl_2 with HOTeF_5 in CH_2Cl_2 and characterized by infrared and NMR spectroscopy and mass spectrometry [213]. In the reactions of transition metal carbonyl methyls with HOTeF_5 , the elimination of methane has been shown to be a strong driving force. Methyl- OTeF_5 group metathesis routes have been used to prepare $\text{Mn}(\text{CO})_5(\text{OTeF}_5)$, $\text{Re}(\text{CO})_5(\text{OTeF}_5)$ and $\text{CpFe}(\text{CO})_2(\text{OTeF}_5)$ by the interaction of $\text{CH}_3\text{Mn}(\text{CO})_5$, $\text{CH}_3\text{Re}(\text{CO})_5$ and $\text{CpFe}(\text{CO})_2\text{CH}_3$ with HOTeF_5 [214]. The crystal structure of $\text{Mn}(\text{CO})_5(\text{OTeF}_5)$ has been determined. While the bond distances and angles within the $\text{Mn}(\text{CO})_5$ moiety are unexceptional, the short $\text{Te}-\text{O}$ bond length of the OTeF_5 group reflects the large degree of ionic character it possesses, in agreement with the spectroscopic findings. An analogous approach has been used to synthesize *cis*- $\text{Os}(\text{OTeF}_5)(\text{CO})_4(\text{CH}_3)$ and *cis*- $\text{Re}(\text{OTeF}_5)(\text{CO})_4(\text{PPh}_3)$ from *cis*- $\text{Os}(\text{CO})_4(\text{CH}_3)_2$ and *cis*- $\text{Re}(\text{CO})_4(\text{PPh}_3)\text{CH}_3$, which have been structurally characterized by ^{13}C , ^{19}F and ^{31}P NMR spectroscopy [215]. The unstable complexes $[\text{N}(n\text{-Bu})_4]^+[\text{M}(\text{CO})_5(\text{OTeF}_5)]^-$ ($\text{M} = \text{Mo}, \text{W}$) have been generated in solution by the photolysis of $\text{M}(\text{CO})_6$ in THF followed by the addition of excess $\text{N}(n\text{-Bu})_4^+\text{OTeF}_5^-$ [214].

5.2.7 Chlorine, Bromine and Iodine

Chloryl fluoride, ClO_2F , is the most common chlorine oxide fluoride and is commonly encountered in the reactions of the binary chlorine fluorides ClF , ClF_3 and ClF_5 with oxides and hydroxides. It is most conveniently prepared in high yield by the reaction of stoichiometric amounts of NaClO_3 and ClF_3 , yielding NaF , Cl_2 , O_2 and ClO_2F [216]. The chlorine fluorides ClF_5 , ClF_3 and ClF , when used in an excess, also undergo fluorine-oxygen exchange reactions with nitrate anion forming ClO_2F , unstable ClOF and ClONO_2 , respectively, as the primary products [217]. Although ClO_3F does not react with LiNO_3 at temperatures as high as 75°C , ClO_2F reacts with LiNO_3 or N_2O_5 to give ClONO_2 and O_2 in high yield. Chlorine nitrate slowly reacts with ClF to give NO_2F and Cl_2O as the primary products and a side reaction of Cl_2O with ClF gives Cl_2 and ClO_2F . Comparison of the NO_3^- - ClF_5 reactions with those of IF_5 and BrF_5 (vide infra) shows a noteworthy difference in that fluorine-oxygen exchange could be halted at the XOF_3 and XOF_4^- stages, whereas this is not possible for ClF_5 . The difference has been attributed to the extreme reactivity of ClOF_3 . The reaction of NaClO_3 with the mild fluorinating agent, COF_2 , yields ClO_2F , NaF and CO_2 [32]. Although thermodynamically favored, attempts to prepare ClO_3F from LiClO_4 and COF_2 at temperatures as high as 120°C failed.

The reactions of BrF_5 with MNO_3 ($\text{M} = \text{Na}, \text{K}, \text{Rb}, \text{Cs}$) provide one-step, high-yield syntheses of the corresponding BrOF_4^- salts and NO_2F [218]. The NaBrOF_4 and RbBrOF_4 salts have been prepared for the first time and characterized

by vibrational spectroscopy, DSC and X-ray powder diffraction. The reaction of LiNO_3 with an excess of BrF_5 does not result in LiBrOF_4 , but produces BrOF_3 in high yield, providing a one-step synthesis of BrOF_3 from commercially available starting materials.

The dinitramide anion, $\text{N}(\text{NO}_2)_2^-$, has been shown to be superior to NO_3^- as a reagent for the controlled, stepwise replacement of two fluorine ligands by a doubly bonded oxygen [219]. The salt, $\text{KN}(\text{NO}_2)_2$, readily reacts with BrF_5 at -45°C to give KBrOF_4 , N_2O and NO_2F in quantitative yield. An equimolar mixture of KClOF_4 and KClF_4 was obtained in the reaction of $\text{KN}(\text{NO}_2)_2$ with ClF_5 at -13°C . The formation of KClOF_4 is noteworthy because for most fluorine–oxygen exchange reagents such as NO_3^- (vide supra) the exchange cannot be arrested at the ClOF_4^- stage and yields ClO_2F as the only product. In the case of IF_7 , deoxygenation of the desired IOF_6^- product occurred resulting in the formation of KIF_6 .

The crystal structures of $\text{NO}^+\text{BrOF}_4^-$ and $\text{pip}^+\text{BrOF}_4^-$ ($\text{pip}^+ = 1,1,3,3,5,5$ -hexamethylpiperidinium) have been obtained in which the cations and anions are disordered [220]. The first example of a NF_4^+ salt with a halogen oxide fluoride anion, $\text{NF}_4^+\text{BrOF}_4^-$, was obtained by the metathetical reaction of CsBrOF_4 with NF_4SbF_6 in BrF_5 solvent [221]. The thermal decomposition at 25°C leads to NF_3 , F_2 and BrOF_3 . The NF_4^+ cation is not capable of fluorinating BrOF_4^- to either BrOF_5 or BrF_4OF , although NF_4BrF_4 does decompose to BrF_5 and NF_3 .

The crystal structure of BrO_2F has been determined, but exhibits a six-fold disorder with BrO_2F exhibiting the anticipated trigonal pyramidal geometry [193]. Fluorine–oxygen exchange reactions with BrF_5 and $(\text{Me}_3\text{Si})_2\text{O}$ or $[\text{F}_3\text{CC}(\text{O})_2]_2\text{O}$ in CH_2Cl_2 and CH_3CN result in the formation of BrO_2F and Me_3SiF and $\text{CF}_3\text{C}(\text{O})\text{F}$, respectively [222]. The reaction of BrF_5 with $\text{C}_6\text{F}_5\text{C}(\text{O})\text{OSiMe}_3$, leads to BrOF_3 and $\text{C}_6\text{F}_5\text{C}(\text{O})\text{F}$. The behavior of BrO_2F in organic solvents is apparently similar to that of BrF_3 , giving rise to fluorine-aryl substitution and is illustrated by the synthesis of $\text{C}_6\text{F}_5\text{BrO}_2$ from the reaction of BrO_2F and $\text{Cd}(\text{C}_6\text{F}_5)_2$ in CH_2Cl_2 . The reaction of $\text{C}_6\text{F}_5\text{BrF}_4$ with CsNO_3 leads to the formation of $\text{C}_6\text{F}_5\text{BrOF}_2$, NO_2F and CsF [222] and is analogous to the exchange behavior between BrF_5 and the NO_3^- ion, which has been studied previously (vide supra).

Phosphorus trifluoride oxide readily replaces two fluorine ligands in IF_7 by an oxygen, providing a convenient new synthesis for IOF_5 [223]. Ab initio and density functional theory calculations have been carried out for IOF_5 and, together with experimental and ab initio data for the isoelectronic TeOF_5^- anion, predict that the axial and equatorial I—F bonds of IOF_5 are of comparable lengths and the O—I—F_{eq} bond angle is close to 97.2° [224]. Using these two constraints and the previously published I^{16}OF_5 and I^{18}OF_5 microwave data, the structure of IOF_5 was determined. The finding that the axial I—F bond length is comparable to the equatorial one is also supported by its normal coordinate analysis and force field.

The IOF_5 molecule has been shown to be rather unreactive, and does not react with either LiF or CsF at 25 or 60°C or with LiNO_3 or CsNO_3 at 25°C but does react with LiNO_3 at 60°C , slowly losing oxygen with the IF_5 product reacting to yield LiIOF_4 [225]. The interaction of MF ($\text{M} = \text{Li}, \text{Na}, \text{Rb}, \text{NO}$), I_2O_5 and IF_5 in either CH_3CN or IF_5 as a solvent leads to MIOF_4 in high purity.

Although IOF_5 is a very weak fluoride ion acceptor, it reacts with “naked fluoride” forming the seven-coordinate IOF_6^- anion, which is the first example of a pentagonal bipyramidal AX_5YZ type species [158,160,226,227]. The anion has been prepared as its $\text{N}(\text{CH}_3)_4^+$ salt by the interaction of $\text{N}(\text{CH}_3)_4\text{F}$ with IOF_5 in CH_3CN solvent. The anion geometry has approximate C_{5v} symmetry with the oxygen atom in an axial position and the O—I—F_{ax} angle constrained by symmetry to 180° and the equatorial IF_5 plane puckered to alleviate its congestion. The mean O—I—F_{eq} bond angle is slightly larger than 90° due to the doubly bonded oxygen atom being more repulsive than the singly bonded axial fluorine ligand. Unlike IF_7 , the axial and equatorial fluorines of IOF_6^- do not undergo intramolecular exchange on the NMR time scale, although the puckering of the equatorial fluorines is shown to be dynamic.

Several xenon derivatives of the highly electronegative $\text{O=IF}_4\text{O}$ group have been synthesized. The xenon(II) derivatives FXeOIOF_4 and $\text{Xe}(\text{OIOF}_4)_2$ have been shown by ^{19}F and ^{129}Xe NMR spectroscopy to result from the reaction between IO_2F_3 and XeF_2 in SO_2ClF , CFCl_3 and BrF_5 solvents [228,229]. The $\text{O=IF}_4\text{O}$ groups are equilibrium mixtures of their *cis*- and *trans*-isomers and are oxygen bonded to xenon. The solid derivative, *cis,cis*- $\text{Xe}(\text{OIF}_4\text{O})_2$, has been isolated from the acid displacement reaction between $\text{Xe}(\text{OTeF}_5)_2$ and *cis/trans*- HOIF_4O and a mixture of *cis*- and *trans*- FXeOIF_4O has been prepared by the reaction of stoichiometric amounts of IO_2F_3 and XeF_2 in HF solvent. Both *cis/trans*- FXeOIF_4O and *cis,cis*- $\text{Xe}(\text{OIF}_4\text{O})_2$ have been characterized by ^{19}F and ^{129}Xe NMR spectroscopy and low-temperature Raman spectroscopy. The mixed species *cis/trans*- $\text{OF}_4\text{IOXeOSO}_2\text{F}$ is formed in the reaction of *cis/trans*- FXeOIF_4O with SO_2ClF and *cis/trans*- $\text{OF}_4\text{IOXeOTeF}_5$ has been observed for mixtures of $\text{Xe}(\text{OTeF}_5)_2$ and *cis,cis*- $\text{Xe}(\text{OIF}_4\text{O})_2$ by NMR spectroscopy. The effective group electronegativity order inferred from the ^{129}Xe chemical shifts of the Xe^{II} derivatives is $-\text{F} > -\text{OSO}_2\text{F} > \text{trans-OIF}_4\text{O} > \text{cis-OIOF}_4 > -\text{OTeF}_5$. The only Xe^{IV} derivative of the $-\text{OIF}_4\text{O}$ ligand reported to date is $\text{F}_3\text{XeOIF}_4\text{O}$, and was prepared by reaction of XeF_4 and IO_2F_3 in CFCl_3 [228].

5.2.8 Xenon

The review of Selig and Holloway [230] on noble-gas cations and anions and the general reviews of Holloway [231] and that of Schrobilgen and Whalen [232] on noble-gas compounds should also be consulted.

The previously known xenon(IV) oxide fluoride, XeOF_2 has been generated in CH_3CN solution by the reaction of H_2O with XeF_4 at -45°C to give a bright yellow solution which has been characterized by low-temperature ^{19}F and ^{129}Xe NMR spectroscopy [196].

Two convenient one-step syntheses of XeOF_4 have been published which significantly reduce the problem of XeO_3 formation that may be encountered in the preparation of XeOF_4 from the reactions of XeF_6 with H_2O or SiO_2 as well as the toxicity when prepared from the reaction of XeF_6 with SeO_2F_2 [233]. The reaction of XeF_6 and NaNO_3 leads to XeOF_4 , NaF and NO_2F [234]. The volatiles, XeOF_4

and NO_2F are trapped successively in -78 and -196°C traps, respectively. The synthesis avoids the possible formation of explosive XeO_3 , but may lead to XeO_2F_2 when XeOF_4 further reacts with NaNO_3 . An alternative approach involves the reaction of POF_3 with XeF_6 to give XeOF_4 and PF_5 [235]. Fractional condensation through two traps at -55 and -196°C separates XeOF_4 from PF_5 and POF_3 and affords pure XeOF_4 . If a slight excess of XeF_6 is used, the formation of XeO_2F_2 is avoided and purification is best accomplished by condensing the reaction products over NaF to complex PF_5 and XeF_6 as the NaXeF_7 adduct.

The reaction of an excess of XeF_6 with CsNO_3 yields XeOF_4 , NO_2F and CsXeF_7 in high yield [236]. With CsNO_3 in excess, the primary products are CsXeOF_5 and NO_2F , and after longer reaction times some CsXeO_2F_3 is also formed. The reaction of CsNO_3 with an excess of XeOF_4 produces NO_2F and XeO_2F_2 in quantitative yield in admixture with CsF and CsXeOF_5 . The reaction of N_2O_5 with an excess of XeOF_4 results in XeO_2F_2 and NO_2F , providing a new safe synthesis for XeO_2F_2 . Xenon dioxide difluoride forms an unstable adduct with NO_2F which has been characterized by Raman spectroscopy and formulated as $\text{NO}_2^+[\text{XeO}_2\text{F}_3 \cdot n\text{XeO}_2\text{F}_2]^-$ [236]. The vibrational spectra of CsXeO_2F_3 were recorded and assigned and it was shown that the oxygen atoms in XeO_2F_3^- are *cis* to each other and that the Raman spectrum previously assigned to CsXeO_2F_3 is that of the $\text{Cs}^+[\text{XeO}_2\text{F}_3 \cdot n\text{XeF}_2]^-$ adduct, where the XeF_2 arose from decomposition of XeO_2F_2 .

The crystal structure of the known $\text{XeOF}_3^+\text{SbF}_6^-$ salt has been determined [237]. The xenon has two close contacts with fluorines of SbF_6^- . The isolated XeOF_3^+ cation is consistent with the VSEPR rules and possesses an AX_3YE arrangement of the four bond pair domains and the lone pair domain, giving rise to a disphenoid-shaped cation having two longer $\text{Xe}-\text{F}_{\text{ax}}$ bonds and an $\text{Xe}-\text{O}$ bond which is coplanar with the shorter $\text{Xe}-\text{F}_{\text{eq}}$ bond. The fluoride ion acceptor properties of XeOF_4 have been reinvestigated leading to the characterization of the XeOF_5^- anion as its Cs^+ and $\text{N}(\text{CH}_3)_4^+$ salts. The Cs^+ salt was prepared by the direct interaction of XeOF_4 with CsF and characterized by Raman spectroscopy [238]. The $\text{N}(\text{CH}_3)_4^+$ salt was prepared by the interaction of $\text{N}(\text{CH}_3)_4\text{F}$ with XeOF_4 in CH_3CN and characterized by ^{19}F , ^{129}Xe NMR and vibrational spectroscopy and a C_{5v} symmetry for the XeOF_5^- anion in which the oxygen atom and electron lone pair on xenon are in axial position and the five fluorine atoms are in equatorial positions [239]. The proposed structure was confirmed by ab initio calculations [239] and a subsequent report of the X-ray crystal structure of $\text{NO}^+\text{XeOF}_5^-$. A single crystal of $\text{NO}^+\text{XeOF}_5^-$ was obtained in the course of a further investigation of the NO^+ salts of XeF_7^- and XeF_8^{2-} and resulted from the hydrolysis of one or both of the fluoro-anions [240]. The compound, $\text{NO}^+\text{XeOF}_5^-$, was also prepared in this study by direct interaction of NOF with XeOF_4 . The adduct, $\text{CsF} \cdot 3\text{XeOF}_4$ has been crystallized from an excess of XeOF_4 and shown by single crystal X-ray diffraction to consist of an $[(\text{XeOF}_4)_3\text{F}]^-$ polyanion in which the xenon atoms of the three XeOF_4 groups are bonded to a central fluorine atom to give an AX_3E VSEPR arrangement around this fluorine [238].

The previously known XeO_2F^+ cation has been characterized as its AsF_6^- salt from XeO_2F_2 and AsF_5 in anhydrous HF solvent [241]. On pumping or exposure

to a laser beam, $\text{XeO}_2\text{F}^+\text{AsF}_6^-$ loses AsF_5 to give $[\text{FO}_2\text{XeFXeO}_2\text{F}]^+\text{AsF}_6^-$. This salt was also obtained by the direct combination of XeO_2F_2 with AsF_5 in a 2:1 mole ratio in HF. Both XeO_2F_2 adducts were characterized by Raman spectroscopy. The XeO_2F^+ salt exhibits $\text{FO}_2\text{Xe}\cdots\text{FAsF}_5$ bridging and distortion of the AsF_6^- anion, whereas the anion-cation interaction in $[\text{FO}_2\text{XeFXeO}_2\text{F}]^+\text{AsF}_6^-$ is minimal.

5.3 The oxide fluorides of the transition metal elements

The preference of the *cis*-dioxo and *fac*-trioxo isomers over their respective *trans*-dioxo and *mer*-trioxo isomers in *pseudo*-octahedral d^0 transition metal oxide fluoride structures can be understood in terms of the spatial relationship of the strong π -donor oxygen atoms to the approximately $d_{t_{2g}}$ orbitals of the metal required for $p_\pi-d_\pi$ bonding [242 and references therein]. These arrangements have been observed as the exclusive arrangements for a considerable number of transition metal oxofluorides discussed in this section. This $p_\pi-d_\pi$ bonding effect is not observed for the IO_2F_4^- anion, which occurs as a kinetically determined mixture of *cis*- and *trans*-isomers [243]. Recently, the geometries of non-VSEPR molecules have been explained in terms of core electron distortions [244]. In this model, the preference for the *cis*-dioxo arrangement in d^0 transition metal complexes is attributed to non-spherical metal atom cores resulting from the distortion produced by the ligands. Calculation of the Laplacian of the electron density in these molecules reveals the formation of local concentrations of electron density in the outer shell of the core so that the geometry of a molecule is determined by the tendency of the more covalently bonded ligands to occupy sites facing regions of local charge depletion. For the dioxo d^0 transition metal complexes, it was determined that the oxygen ligands face larger depletions of charge in the *cis*-isomer than in the *trans*-isomer, rendering the *cis*-isomer more stable.

5.3.1 Titanium

The oxide fluoride $\text{Li}_3\text{TiO}_3\text{F}$ has been prepared by heating a mixture of Li_2CO_3 , TiO_2 and LiF at 900–1000°C for 10 h and has been characterized by X-ray powder diffraction and infrared spectroscopy [245]. The oxide fluoride was found to crystallize in the NaCl-type structure with a statistical distribution of the anions and cations in their corresponding sublattice.

Thermal decomposition of peroxide fluoride species provides a convenient route to titanium oxide fluorides [246]. Decomposition of $(\text{NH}_4)_3\text{Ti}(\text{O}_2)\text{F}_5$ and $\text{K}_3\text{Ti}(\text{O}_2)\text{F}_5$ at 640 and 450°C yields TiOF_2 and K_3TiOF_5 , respectively, which were identified by elemental analysis and vibrational spectroscopy.

Yellow crystals of $[\text{L}_2\text{Ti}^{\text{IV}}_2\text{O}_2\text{F}_2(\mu\text{-F})]^+\text{PF}_6^-$ have been obtained when the hydrolysis/oxidation reaction of $\text{LTi}^{\text{III}}\text{Cl}_3$ ($\text{L} = 1,4,7\text{-trimethyl-1,4,7-thiazacyclononane}$) was carried out in a $\text{H}_2\text{O}/\text{CH}_3\text{NO}_2$ mixture in the presence of NaF and NaPF_6 [247]. The crystal structure shows a dinuclear cation with distorted octahedral geometry around the Ti^{IV} and facial coordination of Ti^{IV} to the nitrogen atoms of the tridentate ligand. The terminal fluorine and oxygen ligands were not dis-

tinguishable by X-ray crystallography, however, the presence of one bridging fluorine, two terminal fluorines and two terminal oxygens per dinuclear cation has been established unambiguously by infrared and ^{19}F NMR spectroscopy.

The reaction of Cp^*TiF_3 ($\text{Cp}^* = \text{C}_5(\text{CH}_3)_5$) with $\text{O}(\text{SnBu}_3)_2$ affords tetranuclear, cyclic $[\text{Cp}^*\text{TiF}(\mu\text{-O})]_4$ upon Bu_3SnF elimination [248]. Single crystal X-ray analysis revealed the presence of an eight-membered, near-planar ring with bridging oxygen atoms and Cp^* groups which alternate above and below the plane of the ring.

Polycrystalline $\text{Pb}_5\text{Ti}_3\text{O}_3\text{F}_{16}$ has been produced by the reaction of 5PbF_2 and 3TiOF_2 at 502°C [249]. The compound was found to be tetragonal and is isostructural with $\text{Pb}_5\text{W}_3\text{O}_9\text{F}_{10}$.

The orange peroxide, $\text{K}_2\text{Ti}(\text{O}_2)\text{F}_4 \cdot \text{H}_2\text{O}$, loses its water of crystallization at 130°C to form yellow $\text{K}_2\text{Ti}(\text{O}_2)\text{F}_4$ which decomposes at 230°C to give K_2TiOF_4 as the main product [250]. The latter compound has been characterized by powder X-ray diffraction and the infrared spectrum of K_2TiOF_4 indicates the presence of —Ti—O—Ti—O— chains. Complete decomposition of K_2TiOF_4 takes place at 540°C forming the cryolite phase $\text{K}_{2.67}\text{TiO}_{0.67}\text{F}_{5.33}$ and TiO_2 . The decomposition of $\text{K}_2\text{Ti}(\text{O}_2)\text{F}_4 \cdot \text{H}_2\text{O}$ at pressures of 1–4 GPa and at 130 and 230°C yields $\text{K}_2\text{TiOF}_4 \cdot \text{H}_2\text{O}$ and K_2TiOF_4 , respectively [251]. The latter compound is a different modification when compared to the one prepared at atmospheric pressure and is stable at high pressure even above 600°C . X-ray diffraction studies and vibrational spectra of $\text{K}_2\text{TiOF}_4 \cdot \text{H}_2\text{O}$ show the presence of infinite chains of $[\text{TiF}_4\text{O}_{2/2}]^{2-}$ octahedra, linked by *trans*-bridging oxygen atoms, and the presence of non-coordinated water of crystallization. The structure of the high-pressure modification of K_2TiOF_4 was found to contain infinite chains of $[\text{TiOF}_3\text{F}_{2/2}]^{2-}$ octahedra, linked by *cis*-bridging fluorine atoms.

Hydrothermal syntheses were employed to prepare the titanium oxide fluorides, Ba_2TiOF_6 [252], BaTiOF_4 [253] and $(\text{NH}_4)_2\text{TiOF}_4$ [254]. The reaction of BaF_2 and TiOF_2 in aqueous HF solutions gave crystalline Ba_2TiOF_6 [252]. The crystal structure consists of infinite bent chains of *trans*- TiO_2F_4 octahedra sharing opposite oxygen atoms and independent fluoride ions. Single crystals of previously known BaTiOF_4 were obtained from aqueous HF solutions [253]. The crystal structure of BaTiOF_4 also contains infinite bent chains of oxygen bridged *cis*- TiO_2F_4 octahedra. The positions of the oxygen atoms in the structures of Ba_2TiOF_6 and BaTiOF_4 have been unambiguously assigned using the bond valence method. In contrast to BaTiOF_4 , the structure of $(\text{NH}_4)_2\text{TiOF}_4$ was found to consist of bent chains of oxygen bridged *trans*- TiO_2F_4 octahedra [254]. The ammonium oxide fluoride was prepared by heating an aqueous solution of H_2TiF_6 and urea, a pH buffer, at 170°C for 24 h.

Titanium peroxide fluorides have been synthesized from solutions of TiO_2 in mixtures of aqueous HF and H_2O_2 upon addition of MF/MF_2 or $\text{MOH}/\text{M}(\text{OH})_2$ ($\text{M} = \text{Ba}$ [255], K [256–259], Na [256,257], NH_4 [257]). The pH and $\text{M} : \text{Ti}$ ratio are important factors influencing the nature of the peroxide fluorides that are formed [256]. Bright yellow $\text{Ba}_3[\text{Ti}(\text{O}_2)\text{F}_5]_2 \cdot 2\text{H}_2\text{O}$ crystallizes from the system $\text{BaF}_2\text{—TiO}_2\text{—HF—H}_2\text{O}_2\text{—H}_2\text{O}$ at a pH of 1. The structure consists of isolated $\text{Ti}(\text{O}_2)\text{F}_5^{3-}$ anions having a geometry which can be viewed as a distorted

pentagonal bipyramid with three fluorine atoms and the peroxide group in the equatorial plane [255]. No evidence for the previously reported $\text{BaTi}(\text{O}_2)\text{F}_4$ salt has been found. The peroxide fluoride, $\text{Ba}_3[\text{Ti}(\text{O}_2)\text{F}_5]_2 \cdot 2\text{H}_2\text{O}$, decomposes at $180\text{--}200^\circ\text{C}$ directly to the previously known compound, $\alpha\text{-Ba}_3\text{Ti}_2\text{O}_2\text{F}_{10}$. Isolated $\text{Ti}(\text{O}_2)\text{F}_5^{3-}$ anions are also present in the crystal structure of $\text{K}_3\text{Ti}(\text{O}_2)\text{F}_5$ which forms from an aqueous $\text{HF}/\text{H}_2\text{O}_2$ solution of TiO_2 with excess K^+ cations over a pH range of 4.5–8 [256]. The compound, $\text{K}_3\text{Ti}(\text{O}_2)\text{F}_5$, crystallizes in the cubic system, consequently, the anion is severely disordered. A disorder model was employed that had been previously developed for the anion in $(\text{NH}_4)_3\text{Zr}(\text{O}_2)\text{F}_5$ (see Sec. 5.3.2). The $\text{Ti}(\text{O}_2)\text{F}_5^{3-}$ anion structure is based on a distorted octahedron with an apical O_2 group which is staggered with respect to the four equatorial fluorines. By varying the nature of the cation, $\text{Na}_3\text{Ti}(\text{O}_2)_2\text{F}_3$ and $\text{K}_2\text{NaTi}(\text{O}_2)_2\text{F}_3$ have been prepared and characterized by X-ray powder data and vibrational spectroscopy. The reaction of a solution of TiO_2 in 40% HF with an excess of 30% H_2O_2 and KOH , followed by the addition of aqueous HF to adjust the pH between 8 and 9 yielded $\text{KTi}(\text{O}_2)\text{F}_3 \cdot 3\text{H}_2\text{O}$ which was characterized by elemental analysis, and by infrared and Raman spectroscopy. Vibrational spectroscopy indicated that the peroxide ligand is bonded to the Ti center in a bidentate fashion giving local C_{2v} point symmetry [258]. The yellow peroxide fluorides $\text{M}_3\text{Ti}(\text{O}_2)\text{F}_5$ ($\text{M} = \text{Na}, \text{K}, \text{NH}_4$) have been synthesized from a solution of TiO_2 in 40% HF with 30% H_2O_2 at pH 6, maintained by addition of MOH [257]. Infrared and Raman spectroscopy also indicate a bidentate peroxide ligand and local C_{2v} point symmetry. The preparation of $\text{K}_3\text{Ti}(\text{O}_2)_2\text{F}_3$ at a pH of 9.5 follows the trend that the number of peroxide groups coordinated to the metal center increases with increasing pH [256]. The diperoxide difluorides, $\text{M}_2\text{Ti}(\text{O}_2)_2\text{F}_2$ ($\text{M} = \text{K}, \text{NH}_4$), have been synthesized from the reaction of a solution of TiO_2 in 40% HF with 30% H_2O_2 at pH 9 maintained by the addition of MOH [257]. The infrared and Raman spectra suggest that the peroxide groups are bonded to the titanium center in a bidentate manner to give local C_{2v} point symmetry.

The crystal structure of the yellow hemihydrate, $\text{K}_2\text{Ti}(\text{O}_2)\text{F}_4 \cdot \text{H}_2\text{O}$, contains the dimeric $[\text{Ti}_2(\text{O}_2)_2\text{F}_8]^{2-}$ anion which has previously been found in the structure of $\text{K}_2\text{Ti}(\text{O}_2)\text{F}_4$ [259]. The peroxide fluorides $\text{K}_2\text{Ti}(\text{O}_2)\text{F}_4 \cdot x\text{H}_2\text{O}$ ($x = 0, 1/2, 1$) have been characterized by infrared and Raman spectroscopy.

5.3.2 Zirconium and Hafnium

Zirconium oxide fluorides have been prepared from zirconium peroxide fluorides by thermal decomposition [246]. Decomposition of $(\text{NH}_4)_3\text{Zr}_2(\text{O}_2)_2\text{F}_7 \cdot 2\text{H}_2\text{O}$, $\text{K}_3\text{Zr}_2(\text{O}_2)_2\text{F}_7 \cdot 2\text{H}_2\text{O}$, $\text{K}_2\text{Zr}_2(\text{O}_2)_2\text{F}_6 \cdot 2\text{H}_2\text{O}$, $\text{Cs}_3\text{Zr}_2(\text{O}_2)_2\text{F}_7 \cdot 2\text{H}_2\text{O}$ and $\text{Cs}_2\text{Zr}_2(\text{O}_2)_2\text{F}_6 \cdot 2\text{H}_2\text{O}$ at 600, 375, 325, 300 and 275°C yields ZrOF_2 , $\text{K}_3\text{Zr}_2\text{O}_2\text{F}_7$, $\text{K}_2\text{Zr}_2\text{O}_2\text{F}_6$, $\text{Cs}_3\text{Zr}_2\text{O}_2\text{F}_7$ and $\text{Cs}_2\text{Zr}_2\text{O}_2\text{F}_6$, respectively, which were identified by elemental analysis and vibrational spectroscopy. The compound, $\text{K}_3\text{Zr}_2\text{O}_2\text{F}_7$, was shown by X-ray powder diffraction to crystallize in the cubic system [260].

The addition of the appropriate base to aqueous HF solutions of ZrO_2 produces $(1,10\text{-phenH}_2)\text{ZrOF}_4$, $(2,2'\text{-bipyH}_2)\text{ZrOF}_4$, $(\text{N}_2\text{H}_5)\text{Zr}_2\text{O}_2\text{F}_5 \cdot 4\text{H}_2\text{O}$, (enH_2)

$(\text{ZrOF}_3)_2 \cdot 5\text{H}_2\text{O}$, $(\text{pn}'\text{H}_2)(\text{ZrOF}_3)_2 \cdot 3\text{H}_2\text{O}$, $(\text{pnH}_2)(\text{ZrOF}_3)_2 \cdot 3\text{H}_2\text{O}$ and $(N,N'$ -dimen $\text{H}_2)(\text{ZrOF}_3)_2 \cdot 3\text{H}_2\text{O}$ (1,10-phen = 1,10-phenanthroline; 2,2'-bipy = 2,2'-bipyridyl; en = ethylenediamine; pn' = propylene-1,2-diamine; pn = propylene-1,3-diamine; N,N' -dimen = N,N' -dimethyl-ethylenediamine) [261]. The oxide fluorides were identified by elemental analysis. The presence of Zr—O—Zr chains in the oxide fluorides was suggested by infrared spectroscopy.

High-temperature synthesis, starting from a mixture of PbF_2 , 2ZrO_2 and ZrF_4 was employed to produce $\text{PbZr}_3\text{O}_4\text{F}_6$ [262]. X-ray powder data showed a three-dimensional framework of corner- and edge-sharing square antiprismatic ZrO_4F_4 -units. Analysis of the local balance of electrostatic valences and solid state ^{19}F NMR spectroscopic measurements of the second moment indicate that the oxygens are strictly localized on the eight corners of the cubic cavity of the $\text{Zr}_6\text{O}_8\text{F}_{24}$ group, i.e. on the anionic sites common to three square antiprisms.

Ammonolysis of $\beta\text{-ZrF}_4$ or $\text{ZrF}_4 \cdot \text{NH}_3$ yields ZrNF and $\text{Zr}_4\text{ON}_3\text{F}_5$ [263]. The structure of $\text{Zr}_4\text{ON}_3\text{F}_5$ was refined from neutron powder diffraction data and is based on an anion-excess fluorite structure containing four independent Zr coordination polyhedra; three square based polyhedra that are trigonally capped ($\text{ZrN}_2\text{O}_2\text{F}_3$, $2x \text{ZrN}_3\text{OF}_3$) in which three fluorines form the trigonal cap and the nitrogen and oxygen atoms occupy the square base, and one ZrN_4F_4 bicapped trigonal prism in which the four nitrogens form the uncapped square face.

Crystals of $(\text{NH}_4)_3\text{Zr}(\text{O}_2)\text{F}_5$ have been obtained from an aqueous $\text{HF}/\text{H}_2\text{O}_2$ solution of $\text{ZrO}_2 \cdot n\text{H}_2\text{O}$ at pH 6 adjusted using NH_3 [264]. The zirconium peroxide fluoride was characterized by vibrational spectroscopy and single crystal X-ray diffraction. A new disorder model for $(\text{NH}_4)_3\text{Zr}(\text{O}_2)\text{F}_5$, which crystallizes in a cubic space group, has been revised with respect to former proposals made for the isotypic Ti compound and has allowed the geometry of the $\text{Zr}(\text{O}_2)\text{F}_5^{3-}$ anion to be unambiguously determined. In the former model, the center of the O_2 group was on a unit cell edge, resulting in a pentagonal bipyramidal geometry. In the new split-atom model, the $\text{Zr}(\text{O}_2)\text{F}_5^{3-}$ anion is tilted along one diagonal, bisecting one unit cell angle with respect to the unit cell edge and gives rise to 24 anion orientations. The anion geometry is not derived from a pentagonal bipyramid because the O_2 group is rotated by 45° out of the pentagonal plane.

The reaction of $\text{ZrO}_2 \cdot \text{H}_2\text{O}$ with H_2O_2 and HF at pH 6 and 12 yields oxide peroxide fluorides containing zirconyl (ZrO^{2+}) centers, $\text{M}_2\text{ZrO}(\text{O}_2)\text{F}_2$ ($\text{M} = \text{Na}, \text{K}, \text{NH}_4$) and $\text{M}_3\text{ZrO}(\text{O}_2)_2\text{F}$ ($\text{M} = \text{Na}, \text{NH}_4$), respectively. The latter were characterized by chemical analysis and vibrational spectroscopy [265]. The μ -oxo species $\text{M}_4(\text{F}_4\text{ZrOZrF}_4)$ ($\text{M} = \text{Na}, \text{K}, \text{NH}_4$) have been isolated at pH 5. The complex $\text{ZrO}(\text{O}_2)\text{F}_2^{2-}$ ion reacts with SO_2 in aqueous medium to afford the ternary $\text{ZrO}(\text{SO}_4)\text{F}_2^{2-}$ complex through insertion of SO_2 into the O—O bond.

Crystals of $\text{K}_6\text{Zr}_3(\text{O}_2)_3\text{F}_{12} \cdot 2\text{H}_2\text{O}_2 \cdot 2\text{H}_2\text{O}$ were obtained from the $\text{ZrOCl}_2 \cdot 8\text{H}_2\text{O}$ — H_2O_2 — KF system and characterized by NMR, infrared and Raman spectroscopy and single crystal X-ray diffraction [266]. The structure is made up of isolated cyclic trinuclear $\text{Zr}_3(\text{O}_2)_3\text{F}_{12}^{6-}$ anions with the fluorines situated on the outer perimeter. The equivalent Zr environments are slightly distorted, bicapped trigonal prisms each having two capping fluorines and two edge-bonded

fluorines on one side and two edge-bonded peroxide groups. The peroxide groups of each trigonal prism, in turn, form the edge that joins an adjacent Zr polyhedron in the trimer.

After complete dehydration of $\text{HfF}_4 \cdot 3\text{H}_2\text{O}$, chemical reactions take place at 350 and 1227°C giving rise to the previously known compounds Hf_2OF_6 and $\text{Hf}_3\text{O}_2\text{F}_8$, respectively, which were identified from X-ray powder data [267].

5.3.3 Vanadium

Thermal decomposition of the previously known peroxide fluorides, $\text{K}_2\text{VO}(\text{O}_2)_2\text{F}$ and $\text{K}_2\text{V}_2\text{O}_3(\text{O}_2)_2\text{F}_2$, at 275°C and 325°C yields the oxide fluorides, $\text{K}_2\text{VO}_3\text{F}$ and $\text{K}_2\text{V}_2\text{O}_5\text{F}_2$, respectively, which were identified by infrared spectroscopy and elemental analysis [246]. Both $\text{K}_2\text{VO}_3\text{F}$ and $\text{K}_2\text{V}_2\text{O}_5\text{F}_2$ were shown by powder X-ray diffraction to crystallize in the hexagonal system [260].

Hydrothermal syntheses under autogeneous pressure at 180°C for 24 h yield $\text{V}_{14}\text{O}_{36}\text{F}_4 \cdot 4\text{N}_2\text{C}_6\text{H}_{18} \cdot 4\text{H}_2\text{O}$ from $\text{V}_2\text{O}_5/2\text{HF}/1.4$ 1,6-diaminohexane/80 H_2O and $\text{V}_{14}\text{O}_{36}\text{F}_4 \cdot 4\text{N}_2\text{C}_5\text{H}_{16} \cdot 8\text{H}_2\text{O}$ from $\text{V}_2\text{O}_5/2\text{HF}/0.8$ 1,5-diaminopentane/80 H_2O . Both compounds contain the $\text{V}_{14}\text{O}_{36}\text{F}_4^{8-}$ polyanion [268]. The latter anion is built up from two trimers of edge-sharing $\text{V}^{\text{V}}_{2/3}\text{V}^{\text{IV}}_{1/3}\text{O}_5\text{F}$ octahedra, two dimers of $\text{V}^{\text{V}}\text{O}_5$ square pyramids relating the two trimers by their basal plane, two $\text{V}^{\text{V}}\text{O}_4$ tetrahedra and two $\text{V}^{\text{V}}\text{O}_4\text{F}$ trigonal bipyramids.

Single crystals of NaVO_2F_2 were grown by hydrothermal synthesis from an aqueous HF solution of BaF_2 , NaF and V_2O_5 [269]. The bond valence method made it possible to unambiguously distinguish between the oxygen and fluorine atoms which was not possible solely on the basis of the X-ray crystal structure. The structure is very similar to that of NaMoO_3F (see Sec. 5.3.6) and consists of distorted *trans*- VO_4F_2 octahedra sharing two O—O edges forming infinite $\text{VOF}_2\text{O}_{3/3}^-$ double chains.

Isothermal evaporation of an aqueous solution of V_2O_5 and KF in H_2O_2 and HF at 5°C resulted in the successive formation of $\text{K}_3[\text{HV}_2\text{O}_2(\text{O}_2)_3\text{F}_4] \cdot 2\text{H}_2\text{O}$, $\text{K}_2[\text{VO}(\text{O}_2)_2\text{F}]$ and, ultimately, $\text{K}_{2n}(\text{VO}_2\text{F}_3)_n$ [270]. Light red crystals of $\text{K}_{2n}(\text{VO}_2\text{F}_3)_n$ containing infinite chains of *cis*-fluorine bridged octahedra were structurally identical with yellow crystals of $\text{K}_2(\text{VO}_2\text{F}_3)$, whose structure has been previously determined.

In previous reports on the $\text{VO}_2\text{F}_4^{3-}$ anion, infrared spectra have been interpreted in terms of a *cis*-dioxo arrangement while EPR spectroscopy of γ -irradiated polycrystalline $(\text{NH}_4)_3\text{VO}_2\text{F}_4$ and solution ^{19}F NMR spectra have been interpreted in terms of a *trans*-dioxo arrangement. The crystal structure of $(\text{NH}_4)_3\text{VO}_2\text{F}_4$ contains two independent $\text{VO}_2\text{F}_4^{3-}$ anions [271]. One is rotationally disordered and the fluorine and oxygen ligands cannot be distinguished, however, the second $\text{VO}_2\text{F}_4^{3-}$ anion is not disordered and exhibits a *cis*-dioxo arrangement.

The crystal structure of the previously known compound, $(\text{NH}_4)_3\text{V}_2\text{O}_4\text{F}_5$, contains dinuclear $\text{V}_2\text{O}_4\text{F}_5^{3-}$ anions consisting of two face-sharing octahedra [272]. Infrared spectroscopy showed the absence of bridging V—O—V units leaving four oxygens and two fluorines as terminal ligands in each anion. The crystallographic symmetry $\bar{6}$ determines a statistical distribution of the terminal oxide and fluoride

ligands. In order to reduce the symmetry, $(\text{NH}_4)_2\text{KV}_2\text{O}_4\text{F}_5 \cdot \text{H}_2\text{O}$ has been synthesized and its orthorhombic structure is closely related to the hexagonal structure of $(\text{NH}_4)_3\text{V}_2\text{O}_4\text{F}_5$ and also contains dinuclear $\text{V}_2\text{O}_4\text{F}_5^{3-}$ anions. The distribution of fluoride and oxide ligands in the terminal positions was determined on the basis of bond valence calculations and found to deviate considerably from statistics.

Hydrothermal synthesis was employed to prepare $\text{Ba}_3\text{V}_2\text{O}_4\text{F}_8$ from BaF_2 and V_2O_5 in aqueous HF [273]. The structure has been described in terms of isolated tetrameric $[\text{V}_4(\text{O},\text{F})_{20}]^{8-}$ anions comprised of corner sharing octahedra. Each vanadium is surrounded by one bridging oxygen, one bridging fluorine, one localized oxygen, one localized fluorine and two positions with statistical fluorine/oxygen occupation. Two fluoride anions in the crystal structure are not coordinated to a vanadium center. Orange crystals of Na_2VOF_5 have been obtained from a reaction mixture of V_2O_5 and NaF in a mixture of 30% H_2O_2 and dilute aqueous HF [270]. The *pseudo*-octahedral VOF_5^{2-} anion in Na_2VOF_5 is disordered with the oxygen atom randomly distributed over all corners. Mixing of V_2O_5 and NH_4HF_2 in a 1: 6 ratio at room temperature results in the formation of $(\text{NH}_4)_3\text{VOF}_6 \cdot 1.5\text{H}_2\text{O}$ [274]. X-ray powder diffraction was used to determine the completeness of the reaction. A DTA and TG study of $(\text{NH}_4)_3\text{VOF}_6 \cdot 1.5\text{H}_2\text{O}$ showed the presence of water of hydration and decomposition at $T = 350^\circ\text{C}$ to V_2O_5 .

The geometries of the vanadium oxide fluorides, $\text{VOCl}_{4-x}\text{F}_x^-$ ($x = 1-4$), $\text{VO}(\text{CF}_3\text{CO}_2)_{4-x}\text{F}_x^-$ ($x = 1-3$), VO_2ClF^- , $\text{VOClF}_2 \cdot n\text{CH}_3\text{CN}$, $\text{VOCl}_2\text{F} \cdot n\text{CH}_3\text{CN}$, $\text{VOF}_2(\text{NO}_3^-)$, $\text{VOF}(\text{NO}_3^-)$, VOF_3X ($\text{X} = \text{NO}_3^-$, CH_3SO_2^- , bipy, phen) have been studied by ^{51}V and ^{19}F NMR spectroscopy in organic solvents [275,276]. Two isomers of $\text{VOCl}_2\text{F}_2^-$ and $\text{VO}(\text{CF}_3\text{CO}_2)_2\text{F}_2^-$ have been observed indicating square-pyramidal geometries for these anions. A *pseudo*-octahedral geometry was tentatively assigned to VOF_3X where X is a bidentate ligand, NO_3^- , bipy, phen. All VOF_3Z ($\text{Z} = \text{NO}_3^-$, CF_3SO_3^- , Cl^- , CH_3SO_2^-) anions exhibit fluxional behavior in their ^{19}F NMR spectra. The vanadium monoxide fluoride species have been prepared from their respective $\text{N}(\text{C}_2\text{H}_5)_4^+$ salts or from the neutral ligand and VOF_3 in organic solvents.

The oxide fluoride complexes, $\text{M}(\text{N}(\text{CH}_3)_4)_2(\text{V}_3\text{O}_3\text{F}_{12})$ ($\text{M} = \text{Na}, \text{K}$), $\text{K}_2(\text{N}(\text{CH}_3)_4)(\text{V}_2\text{O}_2\text{F}_9) \cdot \text{H}_2\text{O}$, $\text{Cs}(\text{N}(\text{CH}_3)_4)(\text{V}_2\text{O}_2\text{F}_8(\text{H}_2\text{O}))$ and $(\text{N}(\text{CH}_3)_4)(\text{VOF}_4)$, have been crystallized from aqueous HF solutions of V_2O_5 and were characterized by vibrational spectroscopy and elemental analysis [277]. The crystal structure of $(\text{Na},\text{K})(\text{N}(\text{CH}_3)_4)_2(\text{V}_3\text{O}_3\text{F}_{12})$ contains a cyclic trimeric anion comprised of fluorine-bridged VOF_5 octahedra with their terminal oxygen atoms *trans* to the fluorine bridge atom. The dinuclear anion in $\text{Cs}(\text{N}(\text{CH}_3)_4)(\text{V}_2\text{O}_2\text{F}_8(\text{H}_2\text{O}))$ consists of fluorine bridged VOF_5 and $\text{VOF}_4(\text{H}_2\text{O})$ octahedra with the terminal oxygen of the VOF_5 octahedron *trans* to the fluorine bridge and the other terminal oxygen *cis* to the fluorine bridge and *trans* to the coordinated water molecule. The coordinated water found in the $\text{V}_2\text{O}_2\text{F}_8(\text{H}_2\text{O})^{2-}$ anion supports the previously suggested existence of $\text{VOF}_4(\text{H}_2\text{O})^-$ in aqueous solutions. X-ray diffraction of twinned crystals established that $\text{K}_2(\text{N}(\text{CH}_3)_4)(\text{V}_2\text{O}_2\text{F}_9) \cdot \text{H}_2\text{O}$ is isostructural with its Mo^{V} analogue (see Sec. 5.3.6) indicating the presence of fluorine bridged dimeric anions.

The reactions of VOF_3 with $\text{Ph}_3\text{P}=\text{NSi}(\text{CH}_3)_3$ and $\text{Ph}_2\text{S}=\text{NSi}(\text{CH}_3)_3$ yield $\text{VOF}_2(\text{N}=\text{PPh}_3)$ and $\text{VOF}_2(\text{N}=\text{SPh}_2)$, respectively [278]. The crystal structure of $\text{VOF}_2(\text{N}=\text{PPh}_3)$ shows that the compound is a monomer with a *pseudo*-tetrahedral environment around V in the solid state. Further treatment with $\text{Ph}_3\text{P}=\text{NSi}(\text{CH}_3)_3$ gives $\text{VOF}(\text{N}=\text{PPh}_3)_2$ which was characterized by elemental analysis, mass spectrometry, infrared and NMR spectroscopy.

The crystal structure of the oxide peroxide fluoride $\text{K}_3[\text{V}_2\text{O}_2(\text{O}_2)_3\text{F}_3] \cdot \text{HF} \cdot 2\text{H}_2\text{O}$ contains dinuclear anions comprised of two pentagonal bipyramidal $\text{VOF}_2(\text{O}_2)_2$ polyhedra sharing a face formed by a peroxide group and a fluorine atom [279]. The equatorial plane of the V^{V} polyhedron is formed by two peroxides and one fluoride ligand while the oxygen and the bridging fluorine are in the apical positions.

Blue vanadium peroxide fluorides, $\text{Cs}_2[\text{V}(\text{O}_2)_3\text{F}]$ and $(\text{NH}_4)_2[\text{V}(\text{O}_2)_3\text{F}]\text{H}_2\text{O}$, have been prepared from cold 15% H_2O_2 solutions of V_2O_5 and CsF (NH_4F) [280]. The latter compound is unstable at room temperature and exists as a tetragonal modification containing rotationally disordered anions. The crystal undergoes a phase transition to an orthorhombic modification in the range -91 to -100°C , resulting in differently oriented domains in the low-temperature modification. The X-ray data were, however, collected at -123°C giving a structure which consists of isolated $\text{V}(\text{O}_2)_3\text{F}^{2-}$ anions having a fluorine-capped, distorted trigonal prismatic geometry.

The reaction of a 1:1 mixture of V_2O_5 and V_2O_3 in aqueous HF with $\text{N}(\text{CH}_3)_4\text{F}$ yielded blue crystals of $[\text{N}(\text{CH}_3)_4][\text{VOF}_3(\text{H}_2\text{O})]$ [281]. The vanadyl ion VO^{2+} is coordinated to four fluorines and to one water molecule occupying a *cis* position relative to the vanadyl oxygen. These octahedra, in turn, share one F—F edge, forming discrete $[\text{V}_2\text{O}_2\text{F}_6(\text{H}_2\text{O})_2]^{2-}$ dimers that are connected by hydrogen bonds.

The blue vanadium oxide fluorides, Rb_2VOF_4 [282] and BaVOF_4 [283], have been synthesized by hydrothermal methods. Their crystal structures show infinite chains of VOF_5 octahedra linked by *cis*-bridging fluorine atoms. Despite an orientational disorder in Rb_2VOF_4 , clear evidence for a *trans* influence of the oxygen ligand could be established [282]. It was impossible to distinguish between oxygen and fluorine ligands in the X-ray structure of BaVOF_4 , but bond valence calculations revealed their relative positions [283].

Addition of methanolic $\text{N}(n\text{-C}_4\text{H}_9)_4\text{OH}$ to VO_2 dissolved in 40% HF with subsequent solvent evaporation and precipitation from DMF solution using $\text{N}(\text{CH}_3)_4\text{Cl}$ yielded turquoise green colored crystals of $[\text{N}(\text{CH}_3)_4]^+[\text{V}_2\text{O}_2\text{F}_7]^{3-}$ [272]. The $\text{V}_2\text{O}_2\text{F}_7^{3-}$ anion consists of two face-sharing octahedra with oxygen and fluorine ligands disordered over the terminal positions. The bridging atoms are three fluorine atoms, deduced from infrared spectroscopy.

5.3.4 Niobium and Tantalum

The high temperature reaction of a mixture of Li_2CO_3 , LiF , Nb_2O_5 [Ta_2O_5] at 800°C for 8 h and at 1100°C for 20 h [10 h] yields $\text{Li}_3\text{NbO}_4\text{F}$ [$\text{Li}_3\text{TaO}_4\text{F}$] which have been characterized by X-ray powder diffraction and infrared spectroscopy [245]. The

oxide fluorides were found to crystallize in the NaCl-type structure with statistical distribution of the anions and cations in their corresponding sublattice.

Thermal decomposition of the peroxide fluorides, $\text{K}_2\text{Nb}(\text{O}_2)\text{F}_5 \cdot \text{H}_2\text{O}$, $\text{K}_2\text{Ta}(\text{O}_2)\text{F}_5 \cdot \text{H}_2\text{O}$, $\text{Na}_3\text{Nb}(\text{O}_2)_2\text{F}_4$, $\text{K}_3\text{Nb}(\text{O}_2)_2\text{F}_4$, $\text{K}_3\text{Ta}(\text{O}_2)_2\text{F}_4$ and $(\text{NH}_4)_3\text{Nb}(\text{O}_2)_2\text{F}_4$ at 300, 300, 490, 400, 275 and 610°C leads to the oxide fluorides K_2NbOF_5 , K_2TaOF_5 , $\text{Na}_3\text{NbO}_2\text{F}_4$, $\text{K}_3\text{NbO}_2\text{F}_4$, $\text{K}_3\text{TaO}_2\text{F}_4$ and NbO_2F , respectively, which were identified by elemental analysis and vibrational spectroscopy [246]. X-ray powder diffraction studies showed that $\text{K}_3\text{NbO}_2\text{F}_4$ and $\text{K}_3\text{TaO}_2\text{F}_4$ are isomorphous with a cubic structure [260]. Similarly, K_2NbOF_5 and K_2TaOF_5 were found to be isomorphous, crystallizing in the tetragonal system.

The reaction of NbF_5 with SiO_2 (quartz vessel) at 310°C or with SiO_2 (Aerosil) at 180°C always leads to NbO_2F while the reaction with laboratory glass (Jenaer Glasgeräte) at 130°C leads to NbOF_3 [284]. Tantalum pentafluoride reacts with the quartz reaction vessel at 400°C forming TaO_2F , however, at 300 or 260°C , TaOF_3 is formed. The reactions of Nb_2O_5 and NbF_5 at 130°C and the reaction of Ta_2O_5 and TaF_5 at 260°C yield NbOF_3 and TaOF_3 , respectively. The compounds NbOF_3 and TaOF_3 were found to be isomorphous, decomposing at 280 and 375°C , respectively, to the corresponding pentafluoride and dioxide fluoride.

New mixed metal compounds, $(\text{pyH}^+)_2(\text{M}(\text{py})_4(\text{NbOF}_5)_2)^{2-}$ [285,286] and $\text{M}(\text{py})_4\text{NbOF}_5$ ($\text{M} = \text{Cu}, \text{Cd}$), have been synthesized from MO and Nb_2O_5 in $(\text{HF})_x \cdot \text{py}/\text{py}/\text{water}$ solutions at 150°C for 24 h under autogeneous pressures [285,287]. The $(\text{HF})_x \cdot \text{py}$ concentration has been shown to be the controlling factor in the crystal growth of the anionic versus the neutral species [285,287]. At high HF concentrations, the pyridine solvent is protonated, supplying pyridinium cations needed to crystallize $(\text{pyH}^+)_2(\text{M}(\text{py})_4(\text{NbOF}_5)_2)^{2-}$. As more water is added, less pyridine is protonated favoring the crystallization of $\text{M}(\text{py})_4\text{NbOF}_5$. The $(\text{M}(\text{py})_4(\text{NbOF}_5)_2)^{2-}$ anion consists of clusters of one $\text{M}(\text{py})_4\text{O}_{1/2}$ octahedron corner-shared with two $(\text{NbF}_5\text{O}_{1/2})^-$ octahedra [285,286]. The neutral species $\text{M}(\text{py})_4\text{NbOF}_5$ consists of infinite chains of alternating corner sharing $(\text{M}(\text{py})_4(\text{O}/\text{F})_{2/2})^{0.5+}$ and $(\text{NbF}_4(\text{O}/\text{F})_{2/2})^{0.5-}$ octahedra [285,287].

Heating a 1:6 mixture of Nb_2O_5 and NH_4HF_2 to 126°C results in the formation of $(\text{NH}_4)_3\text{NbOF}_6 \cdot 1.5\text{H}_2\text{O}$ which was identified by its X-ray diffraction pattern [274]. A thermolysis study of $(\text{NH}_4)_3\text{NbOF}_6 \cdot 1.5\text{H}_2\text{O}$ showed the presence of water of hydration with decomposition to NbO_2F occurring at 450°C .

The compounds, M_2NbOF_5 and MNbOF_4 ($\text{M} = \text{Li}, \text{Na}, \text{K}, \text{Rb}, \text{Cs}$), have been obtained from the reaction of Nb_2O_5 with MF in molten NH_4HF_2 which was monitored by infrared spectroscopy [288]. The analogous reactions with Ta_2O_5 yield hexafluorotantalates. Heating a $\text{Nb}_2\text{O}_5-6\text{NH}_4\text{HF}_2-2\text{MF}$ mixture to $200-280^\circ\text{C}$ resulted in the formation of $(\text{NH}_4)_3\text{NbOF}_6$. Raising the temperature to 350°C results in the formation of NbOF_5^{2-} and NbOF_4^- . At 400°C , only MNbOF_4 was present and was shown by infrared spectroscopy to possess an oxygen bridged chain structure as previously found in the crystal structure of the NH_4^+ salt. Infrared spectra of sintered $\text{Nb}_2\text{O}_5-6\text{NH}_4\text{HF}_2-4\text{LiF}$ mixtures show the successive formation of LiNbOF_4 and Li_2NbOF_5 with the latter produced at 450°C . Infrared spectroscopy

indicates the presence of isolated NbOF_5^{2-} anions in M_2NbOF_5 as previously observed in the crystal structure of the Na^+ salt. The thermal stabilities of the MNbOF_4 compounds increase along the alkali metal series from Li to Cs [289]. For $\text{M} = \text{Li}$, LiNbO_2F_2 and LiNbO_3 are decomposition products at 400 and 500°C, respectively. In addition to NaNbO_2F_2 and NaNbO_3 , Na_2NbOF_5 is the major decomposition product for the Na^+ salt. Decomposition products for $\text{M} = \text{K}$, Rb , Cs could not be unambiguously determined.

The NbF_6^- and NbOF_5^{2-} anions are in equilibrium in the system $\text{Nb}_2\text{O}_5\text{—HF—H}_2\text{O}$, with NbOF_5^{2-} being favored at lower HF concentrations [290]. The addition of ammonium or alkali metal fluorides to the $\text{Nb}_2\text{O}_5\text{—HF—H}_2\text{O}$ mixture shifts the equilibrium in the mother liquor in favor of NbOF_5^{2-} formation [291] and precipitation of MNbOF_4 as well as new phases having the reported composition “ $\text{M}_3\text{Nb}_2\text{OF}_{11}$ ” ($\text{M} = \text{NH}_4$, K , Rb) occur. The $\text{M}_3\text{Nb}_2\text{OF}_{11}$ phases and MNbOF_4 have been characterized by chemical analysis, infrared spectroscopy and X-ray powder diffraction. Crystals of one of the new phases have been obtained which have the composition $\text{Rb}_5\text{Nb}_3\text{OF}_{18}$ [292]. The structure contains infinite chains of oxygen bridged *trans*- NbO_2F_4 octahedra and isolated NbF_7^{2-} anions.

Single crystals of $\text{Ba}_3\text{Nb}_2\text{O}_2\text{F}_{12} \cdot 2\text{H}_2\text{O}$ [293], $\text{Ba}_4\text{Nb}_2\text{O}_3\text{F}_{12}$ [294], $\text{Ba}_5\text{Nb}_3\text{O}_3\text{F}_{18}(\text{HF}_2)$ [295], and $\text{Ba}_3\text{Ta}_2\text{O}_2\text{F}_{12}$ [296] have been grown by hydrothermal methods from aqueous HF solutions of BaF_2 and MO_2F ($\text{M} = \text{Nb}$, Ta). In all four structures, it was not possible to distinguish between oxygens and fluorines on the basis of X-ray diffraction data. The structures of the niobium species contain isolated pentagonal bipyramidal NbOF_6^{3-} anions and the relative fluorine and oxygen positions in the NbOF_6^{3-} anions could be assigned unambiguously on the basis of bond valence calculations. Complete ordering of the oxygen in the apical position of the NbOF_6^{3-} anion was found in $\text{Ba}_3\text{Nb}_2\text{O}_2\text{F}_{12} \cdot 2\text{H}_2\text{O}$ [293] and $\text{Ba}_4\text{Nb}_2\text{O}_3\text{F}_{12}$ [294], while the NbOF_6^{3-} anions in $\text{Ba}_5\text{Nb}_3\text{O}_3\text{F}_{18}(\text{HF}_2)$ exhibit a fluorine oxygen disorder over one apical and one equatorial position with an oxygen site preference for one apex [295]. In addition to the NbOF_6^{3-} anion, the structure of $\text{Ba}_4\text{Nb}_2\text{O}_3\text{F}_{12}$ contains well-separated $(\text{Nb}_4\text{O}_7\text{F}_{14})^{8-}$ anions comprised of blocks of four *cis*-oxygen linked distorted octahedra ($2 \times \text{cis-NbO}_2\text{F}_4$ and $2 \times \text{fac-NbO}_3\text{F}_3$) [294]. In contrast to the niobium species, a monocapped trigonal prismatic TaOF_6^{3-} anion was found in the structure of $\text{Ba}_3\text{Ta}_2\text{O}_2\text{F}_{12}$ [296]. Bond valence calculations indicate an oxygen/fluorine disorder over the four positions of the capped face.

During the phase analysis studies of the $\text{PbO—PbF}_2\text{—M}_2\text{O}_5\text{—MO}_2\text{F}$ ($\text{M} = \text{Nb}$, Ta) systems, the compounds $\text{Pb}_3\text{M}_4\text{O}_{12}\text{F}_2$ ($\text{M} = \text{Nb}$, Ta) were prepared and shown to be isostructural [297]. The crystal structure of $\text{Pb}_3\text{Nb}_4\text{O}_{12}\text{F}_2$ may be described as a framework of NbX_6 octahedra having the general composition Nb_4X_{13} into which three Pb atoms and one extra X ($\text{X} = \text{O}$, F) atom are inserted. Bond valence calculations suggest that some of the anion sites are occupied predominantly by fluorine. Heating a mixture of PbF_2 , M_2O_5 and MO_2F to 1002°C for several hours gave rise to $\text{Pb}_2\text{Nb}_4\text{O}_7\text{F}_5$, which has a layered, ReO_3 -type structure having the net anion composition $\text{Nb}_4\text{O}_7\text{F}_5^{2-}$, separated by $\text{Pb}_2\text{F}_2^{2+}$ layers [298].

The peroxo-compound, $\text{K}_2\text{Nb}(\text{O}_2)\text{F}_5 \cdot \text{H}_2\text{O}$, has been structurally characterized by X-ray crystallography and EPR spectroscopy of a γ -irradiated single crystal [299].

The geometry around the hepta-coordinated niobium atom in the $\text{Nb}(\text{O}_2)\text{F}_5^{2-}$ anion has been viewed as a distorted monocapped octahedron with one oxygen capping an octahedral face. The EPR spectroscopic results indicate that the unpaired electron in the $\text{Nb}(\text{O}_2)\text{F}_5^-$ radical anion resides in the non-bonding orbital of the peroxide group; this was further supported by EHMO calculations done on the precursor.

By addition of NaF to the extensively studied $\text{Na}_2\text{O}-\text{Nb}-\text{Nb}_2\text{O}_5$ system, it is possible to vary the number of electrons available for Nb—Nb bond formation by varying the O/F ratio [300]. The compound, $\text{NaNb}_3\text{O}_5\text{F}$ has been prepared by high temperature synthesis. The structure contains chains of NbX_6 octahedra ($\text{X}=\text{O}, \text{F}$), which are *trans*-edge-linked to two octahedra and vertex-linked to two other octahedra to form folded layers. Differentiation of oxygens and fluorines, however, was not possible. Rows of Nb atoms are inserted between the layers in such a way that Nb_2X_8 units are formed, yielding the shortest known Nb—Nb distance.

5.3.5 Chromium

Convenient methods for the preparation of CrO_2F_2 , a violet-red solid, involve the reaction between CrO_3 and COF_2 at 185°C [301] and the reaction of KCrO_4 with an excess of a mild fluorinating agent such as HF or IF_5 at room temperature or with IF_5 at a non-specified elevated temperature [302]. Chromium difluoride dioxide was structurally characterized by chromium K-edge EXAFS and infrared spectroscopy of the solid at -263°C showing that CrO_2F_2 exists as a molecular monomer in the solid state [303].

Chromium tetrafluoride oxide can be prepared in high yield and purity from CrO_2F_2 and KrF_2 in HF solution [304]. The reaction of CrO_2F_2 with excess F_2 and small quantities of CsF at 200°C for 62 h and subsequent removal of all volatile compounds at -60°C yields dark red CrOF_4 in 90% yield [305]. Vibrational spectroscopy confirmed a monomeric, square-pyramidal structure for gaseous, matrix-isolated, and dissolved CrOF_4 and a fluorine-bridged polymeric structure for solid CrOF_4 [304]. Chromium isotope fine structure and relative intensity estimates from the infrared spectra of CrOF_4 in nitrogen matrices suggest a bond angle of $\text{ca } 106 \pm 6^\circ$ for $\text{O}-\text{Cr}-\text{F}$ [306]. Data from an electron diffraction study of gaseous CrOF_4 at $42-45^\circ\text{C}$ are consistent with a molecule of C_{4v} symmetry, but small deviations from that symmetry cannot be ruled out [305].

Excess KrF_2 is unable to replace the second oxygen of CrO_2F_2 to yield CrF_6 but forms an unstable 1:1 CrOF_4 adduct in the solid state which is completely dissociated in SO_2ClF solution at -120°C [304]. The vibrational spectra of solid $\text{CrOF}_4 \cdot \text{KrF}_2$ indicate an essentially covalent structure containing a $\text{Kr}-\text{F} \cdots \text{Cr}$ bridge.

The reaction of equimolar amounts of CrOF_4 and CsF at 100°C yields orange-brown $\text{Cs}^+\text{CrOF}_5^-$, which was characterized by infrared spectroscopy [306]. Chromium tetrafluoride oxide combines with NOF in a 1:1 mole ratio to yield the stable, pink solid adduct $\text{NO}^+\text{CrOF}_5^-$ which was characterized by vibrational spectroscopy [304]. Controlled pyrolysis of $\text{NO}^+\text{CrOF}_5^-$ yields a mixture of $\text{NO}^+\text{CrOF}_5^-$ and $\text{NO}^+\text{CrOF}_5^- \cdot n\text{CrOF}_4$ [304]. The infrared spectrum of this mixture

exhibits a CrF_4 stretching frequency for $\text{NO}^+\text{CrOF}_5^-\cdot n\text{CrOF}_4$ which is in the range found for $\text{Cs}^+\text{CrOF}_5^-$.

No stable adduct of CrOF_4 with AsF_5 is formed at temperatures as low as -78°C [304]. When combined with an excess of SbF_5 in HF and subsequent removal of excess SbF_5 at 55°C , CrOF_4 forms a dark red, crystalline 1:1 adduct with SbF_5 [307]. Single crystal X-ray diffraction analysis failed because of twinning or disorder. However, based on its low-temperature Raman spectrum, $\text{CrOF}_4\cdot\text{SbF}_5$ has a predominantly covalent, fluorine-bridged structure.

Heating CrO_2F_2 with XeF_2 at temperatures up to 278°C produces deep purple CrOF_3 in 88% yield [308]. The crystal structure obtained by this new preparative route consists of an infinite three-dimensional array of corner-shared CrOF_5 octahedra.

5.3.6 Molybdenum

Cooling of a mixture of MoO_3 and NaF just below its fusion point (460°C) has yielded NaMoO_3F which has a crystal structure built up of isolated double chains of MoX_6 ($\text{X} = \text{O}, \text{F}$) and $\text{MoO}_2\text{FO}_{3/3}$ octahedra sharing two edges [309,310]. Raman and ^{19}F NMR spectroscopy, electrostatic energy and site potential calculations in conjunction with bond valence calculations were used to establish an ordered model for the anion [310].

Single crystals of $\text{Ba}_4\text{Mo}_2\text{O}_5\text{F}_7(\text{HF}_2)_3\cdot\text{H}_2\text{O}$ were grown by hydrothermal synthesis from aqueous HF solutions of MoO_3 and BaF_2 upon heating to 180°C for 3 d [311]. Molybdenum exhibits distorted *fac*- MoO_3F_3 octahedral coordination, comprised of two octahedra, linked by an oxygen corner to form isolated $\text{Mo}_2\text{O}_5\text{F}_7^{4-}$ anions.

The reaction of MoO_3 with equivalent amounts of HF and KOH produced $\text{K}_6[\text{Mo}_8\text{O}_{26}\text{F}_2]\cdot 6\text{H}_2\text{O}$ [312]. The crystal structure contains difluorooctamolybdate anions which consist of eight centrosymmetrically condensed edge-sharing octahedra having 16 terminal positions. Of these 16 positions, 14 are occupied by oxygen atoms and two by fluorine atoms.

Five phases have been identified in the system $\text{PbF}_2\text{—MoO}_3$, i.e. cubic $\text{Pb}_{1-x}\text{Mo}_x\text{O}_{3x}\text{F}_{2-2x}$ with $x < 0.15$, orthorhombic $\text{Pb}_3\text{MoO}_3\text{F}_6$, tetragonal and closely related α - and β - $\text{Pb}_5\text{Mo}_3\text{O}_9\text{F}_{10}$, which are isostructural with $\text{Pb}_5\text{W}_3\text{O}_9\text{F}_{10}$ (see Sec. 5.3.7), and tetragonal PbMoO_3F_2 [249]. The oxide fluorides decompose at elevated temperatures by formation of volatile MoO_2F_2 .

Crystal structures of Lewis acid-base adducts of MoO_2F_2 have been obtained with the bases, THF [313] and 2,2'-bipyridine [314]. Both adducts, MoO_2F_2 (2,2'-bipyridyl) [313] and $\text{MoO}_2\text{F}_2(\text{THF})_2$ [314], contain *cis*-dioxo arrangements with the Lewis bases, THF and 2,2'-bipyridine, coordinated *trans* to the oxygens.

Addition of $\text{N}(\text{CH}_3)_4\text{Cl}$ and KCl, $\text{N}(\text{CH}_3)_4\text{Cl}$ or $\text{N}(\text{CH}_2\text{CH}_3)_4\text{Cl}$ to aqueous HF solutions of MoO_3 and subsequent evaporation of the solvent and cooling has yielded crystals of $\text{K}(\text{N}(\text{CH}_3)_4)_2(\text{Mo}_3\text{O}_6\text{F}_9)$, $(\text{N}(\text{CH}_3)_4)_2(\text{Mo}_2\text{O}_4\text{F}_6(\text{H}_2\text{O}))$ and $(\text{N}(\text{CH}_2\text{CH}_3)_4)_2(\text{Mo}_2\text{O}_4\text{F}_6)$, respectively [315]. Since X-ray camera techniques showed that $\text{K}(\text{N}(\text{CH}_3)_4)_2(\text{Mo}_3\text{O}_6\text{F}_9)$ is isotypic with $\text{M}(\text{N}(\text{CH}_3)_4)_2(\text{V}_3\text{O}_3\text{F}_{12})$ ($\text{M} = \text{Na}, \text{K}$) (see Sec. 5.3.3), it was concluded that the $\text{Mo}_3\text{O}_6\text{F}_9^{3-}$ anion is a cyclic

fluorine-bridged trimer with *cis*-dioxo groups in the molecular plane. The crystal structure of $[\text{N}(\text{CH}_3)_4]_2[\text{Mo}_2\text{O}_4\text{F}_6(\text{H}_2\text{O})]$ contains the dimeric fluorine-bridged $\text{Mo}_2\text{O}_4\text{F}_6(\text{H}_2\text{O})^{2-}$ anion with *cis*-dioxo groups and the water ligand *trans* to one oxygen. Two *cis*- $\text{MoO}_2\text{F}_2\text{F}_{2/2}$ octahedra in the anion of $[\text{N}(\text{CH}_2\text{CH}_3)_4]_2[\text{Mo}_2\text{O}_4\text{F}_6]$ share an edge occupied by fluorine ligands. However, detailed structural parameters could not be determined because of disorder.

Controlled hydrolysis of MoF_6 in HF solvent only yields MoOF_4 without any evidence for anion formation which is in contrast to the hydrolysis of WF_6 [316; also see Sec. 5.3.7].

Yellow crystals of $(\text{NH}_4)_2[\text{MoOF}_2(\text{O}_2)_2]$ have been obtained from an aqueous H_2O_2 solution of NH_4F and $(\text{NH}_4)_6\text{Mo}_7\text{O}_{24}$ by adding several drops of HF followed by solvent evaporation [317]. The molybdenum atom in the $\text{MoOF}_2(\text{O}_2)_2^{2-}$ anion is surrounded by a pentagonal-bipyramidal arrangement of ligand atoms in which two side-on bonded peroxide groups and a fluorine atom form the equatorial plane while one fluorine atom and a doubly bonded oxygen atom occupy the apical positions with the molybdenum atom displaced from the equatorial plane towards the oxygen double bond.

Recrystallization of $(\text{NH}_4)_2[\text{MoOF}_2(\text{O}_2)_2]$ in 6% H_2O_2 yielded $(\text{NH}_4)_3[\text{F}\{\text{MoOF}_2(\text{O}_2)_2\}_2]$ [318]. The crystal structure of $(\text{NH}_4)_3[\text{F}\{\text{MoOF}_2(\text{O}_2)_2\}_2]$ contains a dinuclear anion which is composed of two identical corner-sharing pentagonal bipyramids. The bridging fluorine and the doubly bonded oxygen atom occupy the apical positions.

Crystals of $(\text{NH}_4)_3\text{F}[\text{MoOF}_4(\text{O}_2)]$ were obtained from an aqueous HF/ H_2O_2 solution of NH_4F and $(\text{NH}_4)_2\text{MoO}_4$ [319]. The $\text{MoOF}_4(\text{O}_2)^{2-}$ anion has a pentagonal-bipyramidal geometry with the peroxide group in the equatorial plane and the molybdenum atom displaced out of the plane towards the doubly bonded oxygen atom. Crystals of $\text{K}_2[\text{MoOF}_4(\text{O}_2)] \cdot \text{H}_2\text{O}$ were obtained upon addition of a KOH solution to an aqueous HF/ H_2O_2 solution of MoO_3 and subsequent evaporation of the solvent and recrystallization from water [320]. The crystal structure also shows the pentagonal-bipyramidal $\text{MoOF}_4(\text{O}_2)^{2-}$ anion. The single-crystal EPR spectrum of γ -irradiated pure $\text{K}_2[\text{MoOF}_4(\text{O}_2)] \cdot \text{H}_2\text{O}$ was also determined.

Electrochemical anodic dissolution of molybdenum metal in aqueous HF followed by addition of KF provides a single-step synthesis of the previously known $\text{K}_2\text{Mo}^{\text{V}}\text{OF}_5$ as a green microcrystalline precipitate which was characterized by elemental analysis and infrared spectroscopy [321].

Pale blue crystals of $\text{K}_2(\text{N}(\text{CH}_3)_4)[\text{Mo}_2\text{O}_2\text{F}_9] \cdot \text{H}_2\text{O}$ have been obtained from an aqueous HF solution of $\text{N}(\text{CH}_3)_4\text{Cl}$ and KCl followed by evaporation of the solvent [315]. The crystal structure shows the presence of the dinuclear fluorine-bridged $\text{Mo}_2\text{O}_2\text{F}_9^{3-}$ anion with the oxygen atoms *trans* to the bridging fluorine and *cis* to the terminal fluorines.

5.3.7 Tungsten

Polycrystalline $\text{Ba}_2\text{WO}_3\text{F}_4$ was prepared by high-temperature synthesis from BaF_2 and WO_3 [322]. Single crystals were obtained hydrothermally in an HF solution.

The structure contains chains of distorted *cis*-W^{VI}O₄F₂ octahedra that share opposite oxygen corners. Individual octahedra are alternately tipped giving a zig-zag pattern along the chain.

The crystal structure of LiW₃O₉F contains the trinuclear W₃O₉F[−] anion [310]. Using Raman and ¹⁹F NMR spectroscopy, electrostatic energy and site potential calculations in conjunction with bond valence considerations, the anion geometry was found to consist of three edge sharing WX₆ (X = O, F) octahedra where all the terminal atoms are oxygens while the fluorine and one oxygen are disordered between the two bridging sites.

Crystals of the lead tungsten oxide fluoride, Pb₅W₃O₉F₁₀, which was investigated because of its ferroelectric properties, have been obtained from the reaction of PbF₂ and WO₃ at 502°C [249,323]. The crystal structure contains isolated *fac*-WO₃F₃^{3−} anions and infinite linear chains of alternating oxygen bridged W^{VI}O₆ and *trans*-W^{VI}O₂F₄ octahedra.

High-temperature synthesis yields the complex oxide fluoride WTh₈Zr₁₈F₄O₅₃ upon heating a mixture of WO₃, 18ZrO₂, 6.5ThO₂ and 1.5ThF₄ at 1200°C for 2 d [324]. The crystal structure contains WOF₅ octahedra, ZrO₈ square antiprisms, ZrO₇ bicapped trigonal prisms, ZrO₈ polyhedra, which are intermediate between a bicapped trigonal prism and a distorted cube, and ThO₉F polyhedra.

The reaction of K₂WO₄ with IF₅ at 120°C for 20 h has produced a material having a Raman spectrum consistent with the formation of WO₂F₂ [302]. High temperature oxidation of tungsten with a 6:1 O₂/F₂ mixture in a Knudsen cell yielded WO₂F₂ as the dominant product, which was detected by mass spectrometry [325].

During attempts to grow crystals of WOF₄·bipy, colorless crystals of WO₂F₂·bipy were obtained [326]. Discounting accidental hydrolysis, a solvent-assisted dismutation of WOF₄·bipy yielding WO₂F₂·bipy and WF₆·bipy was considered, which was supported by NMR spectroscopic studies. The structure of WO₂F₂·bipy contains a *cis*-dioxo group with the nitrogen atoms of the 2,2'-bipyridyl coordinated *trans* to the oxygen atoms.

Accidental partial hydrolysis of (Na-15-crown-5)WF₇, which was formed upon ligand exchange from (Na-15-crown-5)WSF₅, yielded colorless crystals of (Na-15-crown-5)₂(WO₂F₃)₂·2CH₃CN [327]. The crystal structure of (Na-15-crown-5)₂(WO₂F₃)₂·2CH₃CN contains (WO₂F₃)₂^{2−} anions composed of two *cis*-W^{VI}O₂F₄ octahedra sharing an edge occupied by two fluorine atoms.

Mixing WO₃ and CsF in aqueous HF and dissolution of Cs₂WO₄ in aqueous HF produce Cs₂WO₂F₄ upon evaporation of the solvent [328]. The crystal structure of Cs₂WO₂F₄ showed the presence of isolated WO₂F₄^{2−} octahedra, however, the fluorine and oxygen atoms were completely disordered. The crystal structure of Na₂WO₂F₄ contains isolated *cis*-WO₂F₄^{2−} anions in which the oxygen and fluorine ligands were indistinguishable; the *cis*-dioxo arrangement was arrived at by Raman and ¹⁹F NMR spectroscopy, electrostatic energy and site potential calculations in conjunction with bond valence considerations [310].

As a modification of a previous synthetic method, WOF₄ can be prepared using quartz wool and excess WF₆ in HF [329]. The use of stoichiometric amounts of SiO₂

and WF_6 leads to the formation of some $\text{H}_3\text{O}^+\text{WOF}_5^-$ and $\text{H}_3\text{O}^+\text{W}_2\text{O}_2\text{F}_9^-$ as by-products that are difficult to separate from WOF_4 .

Controlled hydrolysis of WF_6 in HF yields only $\text{H}_3\text{O}^+\text{W}_2\text{O}_2\text{F}_9^-$ even with excess WF_6 [316]. Raman spectra of the solid and of the HF solution were characteristic of the $\text{W}_2\text{O}_2\text{F}_9^-$ anion. A previous report that hydrolysis of WF_6 in the presence of excess WF_6 yields only WOF_4 and that the products $\text{H}_3\text{O}^+\text{WOF}_5^-$ and $\text{H}_3\text{O}^+\text{W}_2\text{O}_2\text{F}_9^-$ only result when excess water is used could not be verified. The crystal structure of $\text{H}_3\text{O}^+\text{W}_2\text{O}_2\text{F}_9^-$ consists of discrete fluoro-bridged dinuclear $\text{W}_2\text{O}_2\text{F}_9^-$ anions with the oxygens *trans* to the bridging fluorine atom. Accidental hydrolysis of a mixture of WF_6 and 2,2'-bipyridyl in CD_2Cl_2 produced crystals of $[\text{WF}_4(\text{bipy})_2]^{2+}[\text{W}_2\text{O}_2\text{F}_9^-]_2 \cdot 0.25\text{HF}$ [330]. The structure of the $\text{W}_2\text{O}_2\text{F}_9^-$ anion in $[\text{WF}_4(\text{bipy})_2]^{2+}[\text{W}_2\text{O}_2\text{F}_9^-]_2 \cdot 0.25\text{HF}$ is similar to that of the anion in $\text{H}_3\text{O}^+\text{W}_2\text{O}_2\text{F}_9^-$ and ^{19}F NMR spectroscopy indicated the presence of the $\text{W}_2\text{O}_2\text{F}_9^-$ anion in CD_2Cl_2 solutions of $[\text{WF}_4(\text{bipy})_2]^{2+}[\text{W}_2\text{O}_2\text{F}_9^-]_2 \cdot 0.25\text{HF}$. Single crystals of $[\text{HOS}_3(\text{CO})_{12}]^+[\text{W}_2\text{O}_2\text{F}_9^-]$ were obtained upon accidental hydrolysis during the treatment of $[\text{Os}_3(\text{CO})_{12}]$ dissolved in anhydrous HF with WF_6 [331]. The terminal equatorial fluorine atoms bonded to one of the two W atoms in the $\text{W}_2\text{O}_2\text{F}_9^-$ anion exhibited large thermal parameters and were subsequently refined on two distinct sites.

A 1:2 mixture of AgF and WOF_4 in anhydrous HF gave the ivory colored solid $\text{Ag}^+\text{W}_2\text{O}_2\text{F}_9^-$, which was identified by vibrational spectroscopy, whereas a 1:1 ratio of AgF and WOF_4 in anhydrous HF followed by slow evaporation of the solvent resulted in the formation of $\text{Ag}^+\text{WOF}_5^-$, which was identified by vibrational spectroscopy [332]. The dark purple product of the reaction of AgF_2 with WOF_4 in 1:1 and 1:2 stoichiometries and the product of the oxidation of $\text{Ag}^+\text{W}_2\text{O}_2\text{F}_9^-$ with F_2 in anhydrous HF were found to be the 1:2 salt $\text{Ag}^{2+}\text{F}^-\text{W}_2\text{O}_2\text{F}_9^-$ which was characterized by X-ray powder diffraction. The solid, $\text{Ag}^{2+}\text{F}^-\text{W}_2\text{O}_2\text{F}_9^-$, reacts with xenon in HF over a period of 24 h at room temperature to give $\text{XeF}_2 \cdot \text{WOF}_4$, which was identified by Raman spectroscopy, and AgF_2 and $\text{Ag}^+\text{W}_2\text{O}_2\text{F}_9^-$ which were identified by X-ray powder diffraction.

The reactions of WOF_4 with excess or stoichiometric amounts of pyridine in CH_2Cl_2 yield the Lewis acid-base adducts $\text{WOF}_4 \cdot 2\text{py}$ and $\text{WOF}_4 \cdot \text{py}$, respectively [333]. The adducts were characterized by elemental analysis, X-ray powder data, vibrational and NMR spectroscopy and single crystal X-ray diffraction. The tungsten atom in $\text{WOF}_4 \cdot \text{py}$ is surrounded by a distorted octahedron of ligands with the nitrogen of the pyridine ligand *trans* to the oxygen atom. The crystal structure of $\text{WOF}_4 \cdot 2\text{py}$ established the pentagonal bipyramidal coordination around tungsten. On the basis of a comparison of the stretching vibrations in similar compounds, $\text{WOF}_4 \cdot 2\text{py}$ was refined with two nitrogen atoms of the pyridine ligands, one oxygen atom and two fluorine atoms forming a regular pentagon around W and two fluorine atoms located in the apical positions. On the basis of low-temperature ^{19}F NMR spectroscopy of a CD_2Cl_2 solution of $\text{WOF}_4 \cdot 2\text{py}$ showing an A_2MX spin system, the structural solution was reconsidered [334]. At temperatures higher than 0°C , only $\text{WOF}_4 \cdot \text{py}$ and py were observed as a reversible dissociation product of $\text{WOF}_4 \cdot 2\text{py}$ in CD_2Cl_2 solution. A model in accord

with the low-temperature ^{19}F NMR spectrum has the oxygen atom and one fluorine atom disordered at the apical positions while the equatorial plane is made up of the two nitrogen atoms of the coordinated pyridine molecules, two equivalent fluorine atoms and a fourth unique fluorine atom. Using 2-fluoropyridine (F-py) as a Lewis base, only the mono-adduct $\text{WOF}_4 \cdot \text{F-py}$ has been obtained from a CH_2Cl_2 solution of WOF_4 and F-py [335]. The adduct was characterized by X-ray powder diffraction, vibrational and NMR spectroscopy and single crystal X-ray diffraction. The tungsten atom in $\text{WOF}_4 \cdot \text{F-py}$ is surrounded by a distorted octahedron of ligands with the nitrogen atom *trans* to the oxygen atom.

The Lewis acid-base adduct $\text{WOF}_4 \cdot \text{bipy}$ was prepared from the reaction of WOF_4 with 2,2'-bipyridyl in the melt or in solutions of CH_2Cl_2 or CH_3CN [336]. The adduct, which is not moisture sensitive at room temperature, was characterized by elemental analysis, X-ray powder diffraction and vibrational spectroscopy. Attempts to grow single crystals resulted in dismutation to $\text{WO}_2\text{F}_2 \cdot \text{bipy}$ and $\text{WF}_6 \cdot \text{bipy}$. The reactions of WOF_4 with 1,8-naphthyridine (napy) and 2,7-dimethyl-1,8-naphthyridine (dmnapy) in CH_2Cl_2 yield the adducts $\text{WOF}_4 \cdot \text{napy}$ and $\text{WOF}_4 \cdot \text{dmnapy}$, respectively. Both adducts were characterized by elemental analysis, X-ray powder analysis and infrared spectroscopy. The negligible solubility of both adducts in the usual organic solvents prevented NMR spectroscopic elucidation of the molecular structure.

Addition of aqueous H_2O_2 to aqueous HF solutions of $(\text{NH}_4)_2\text{WO}_4$ adjusted to $\text{pH} = 3-4$ using NH_3 yielded $(\text{NH}_4)_3\text{F}[\text{WO}(\text{O}_2)\text{F}_4]$ [319]. The crystal structure contains the $\text{WO}(\text{O}_2)\text{F}_4^{2-}$ anion with pentagonal-bipyramidal coordination in which the peroxide group bonded side-on in the equatorial plane and the tungsten atom is displaced out of the equatorial plane towards the apical doubly bonded oxygen atom.

The potassium salts of $[\text{W}_{18}\text{O}_{56}\text{F}_6\text{NaH}_2]^{7-}$ and $[\text{ZnW}_{17}\text{O}_{56}\text{F}_6\text{NaH}_2]^{9-}$ have been prepared and found to be isomorphous [337]. Multi-NMR spectroscopy, ^{22}Na -exchange studies and the unpublished crystal structure of the NH_4^+ salt of the latter anion suggest Dawson structures for the anions with a non-labile Na^+ ion enclosed in the center of the complex and coordinated to a trigonal-prismatic arrangement of six fluorine atoms. A Zn-substituted isomorph is known in which Zn replaces W in one WO_6 octahedron. The ammonium salts of $[\text{CoW}_{17}\text{O}_{56}\text{F}_6\text{NaH}_4]^{9-}$ [338], $[\text{FeW}_{17}\text{O}_{56}\text{F}_6\text{NaH}_4]^{8-}$ [338], and $[\text{InW}_{17}\text{O}_{56}\text{F}_6\text{NaH}_4]^{8-}$ [339] have been prepared from aqueous HF solutions of $\text{Na}_2\text{WO}_4 \cdot 2\text{H}_2\text{O}$ and a corresponding metal salt and shown to be isomorphous. The crystal structure of $(\text{NH}_4)_8(\text{FeW}_{17}\text{O}_{56}\text{F}_6\text{NaH}_4) \cdot 8\text{H}_2\text{O}$ shows the Dawson structure for the heteropolyanion [338].

5.3.8 Manganese, Technetium and Rhenium

Dark green, shock-sensitive MnO_3F can be prepared from KMnO_4 and excess IF_5 and purified by transfer onto an excess of KMnO_4 at 0°C , reportedly with little or no danger of explosion [302], contrasting with an earlier claim that detonations occur in the presence of excess KMnO_4 . Pure MnO_3F , in any

quantity, should be handled with the proper safety precautions and it should be noted that greater than 0.2 g quantities have been reported to detonate violently [302]. Further fluorination of MnO_3F using IF_5 and temperatures as high as 100°C was unsuccessful. Manganese fluoride trioxide is a product of the reactions of KMnO_4 with IF_7 , XeF_2 or HF and of K_2MnO_4 or K_3MnO_4 with HF or IF_5 . Infrared and UV/VIS spectra of matrix-isolated MnO_3F have been reported [340] and Mn K-edge EXAFS data have been obtained for MnO_3F at -263°C [303].

High-temperature fluorination of partially oxidized technetium metal using fluorine in a Knudsen cell reportedly yields the technetium oxide fluorides, TcO_3F , TcOF_4 and TcO_2F_3 , in the gas phase which were proposed from the detection of their cations in the mass spectrum [325]. The synthesis of pure yellow TcO_2F_3 was accomplished by the reaction of XeF_6 and Tc_2O_7 in a 3:1 molar ratio in anhydrous HF solution [341]. Technetium trifluoride dioxide was characterized by Raman spectroscopy and single crystal X-ray diffraction. The structure consists of open chains of fluorine bridged *cis*- TcO_2F_4 units in which the bridge fluorines are *trans* to the oxygens. The use of excess XeF_6 does not result in further fluorination of TcO_2F_3 but yields $\text{XeF}_5^+\text{TcO}_2\text{F}_4^-$, which is soluble in HF and was observed by NMR spectroscopy [242,341].

Technetium trifluoride dioxide behaves as a Lewis acid towards the fluoride ion and CH_3CN forming $\text{M}^+\text{TcO}_2\text{F}_4^-$ [$\text{M} = \text{Li}, \text{Cs}, \text{N}(\text{CH}_3)_4$] salts and $\text{TcO}_2\text{F}_3 \cdot \text{CH}_3\text{CN}$ [242,342]. Fluorine-19 NMR spectroscopy established that the TcO_2F_4^- anion has a *cis*-dioxo geometry in CH_3CN , which also has been found in the crystal structure of $\text{Li}^+\text{TcO}_2\text{F}_4^-$. The Raman spectra of $\text{M}^+\text{TcO}_2\text{F}_4^-$ [$\text{M} = \text{Li}, \text{Cs}, \text{N}(\text{CH}_3)_4$] and $\text{TcO}_2\text{F}_3 \cdot \text{CH}_3\text{CN}$ were assigned under C_{2v} and C_s point symmetries, respectively.

Krypton difluoride reacts with TcO_2F_3 in anhydrous HF at room temperature to yield the last member of the Tc^{VII} oxide fluoride series, TcOF_5 [343]. The compound is yellow-orange in color and highly volatile. Fluorine-19 and ^{99}Tc NMR and Raman spectroscopic studies are in agreement with a *pseudo*-octahedral C_{4v} geometry.

Contrary to a previous report, KReO_4 and IF_5 do not react even at temperatures as high as 200°C [302]. However, when a trace of HF is added to the reaction mixture, ReO_3F formation occurs at 100°C . The reaction between KReO_4 and XeF_2 in $\text{CF}_3\text{CH}_2\text{Cl}$ solution is slow, yielding ReO_3F . The adduct, $\text{ReO}_3\text{F}(\text{CH}_3\text{CN})_2 \cdot \text{CH}_3\text{CN}$, was obtained by hydrolysis of $\text{ReO}_2\text{F}_3 \cdot \text{CH}_3\text{CN}$, and was shown by X-ray crystallography to have a facial arrangement of oxygen atoms on rhenium with the nitrogens of the CH_3CN molecules coordinated *trans* to oxygens in the *pseudo*-octahedral $\text{ReO}_3\text{F}(\text{CH}_3\text{CN})_2$ complex [344].

Fluorination of partially oxidized Re with fluorine in a Knudsen cell at 350°C results in the vapor phase oxide fluorides, ReO_3F , ReO_2F_3 and ReOF_4 which have been proposed on the basis of the cations detected in the mass spectrum [325]. The oxide fluorides, ReO_3F , ReO_2F_3 , ReOF_5 and ReOF_4 have been studied by infrared and UV/VIS spectroscopy in inert-gas matrices [340].

The reaction of Re_2O_7 with XeF_6 in anhydrous HF provides a convenient route to high purity ReO_2F_3 [344]. The structure of ReO_2F_3 in $\text{K}^+\text{Re}_2\text{O}_4\text{F}_7^- \cdot 2\text{ReO}_2\text{F}_3$ shows polymeric open chains containing fluorine-bridged *cis*- ReO_2F_4 units with the fluor-

ine bridges *trans* to the oxygens, which was anticipated based on the analogous TcO_2F_3 structure. The vibrational spectrum of the ReO_2F_3 monomer has now been reassigned using density functional theory calculations [345].

The Lewis base properties of ReO_2F_3 have been investigated leading to the formation of $\text{M}^+\text{ReO}_2\text{F}_4^-$ [$\text{M} = \text{Li}, \text{Na}, \text{Cs}, \text{N}(\text{CH}_3)_4$], $\text{K}^+\text{Re}_2\text{O}_4\text{F}_7^-$, $\text{K}^+\text{Re}_2\text{O}_4\text{F}_7^- \cdot 2\text{ReO}_2\text{F}_3$, $\text{Cs}^+\text{Re}_3\text{O}_6\text{F}_{10}^-$ and $\text{ReO}_2\text{F}_3 \cdot \text{CH}_3\text{CN}$ [342,344]. The ReO_2F_4^- , $\text{Re}_2\text{O}_4\text{F}_7^-$ and $\text{Re}_3\text{O}_6\text{F}_{10}^-$ anions and the $\text{ReO}_2\text{F}_3 \cdot \text{CH}_3\text{CN}$ adduct have been characterized by Raman spectroscopy and the structures of $\text{Li}^+\text{ReO}_2\text{F}_4^-$, $\text{K}^+\text{Re}_2\text{O}_4\text{F}_7^-$, $\text{K}^+\text{Re}_2\text{O}_4\text{F}_7^- \cdot 2\text{ReO}_2\text{F}_3$ and $\text{Cs}^+\text{Re}_3\text{O}_6\text{F}_{10}^-$ have been determined by X-ray crystallography. The structure of ReO_2F_4^- consists of a *cis*-dioxo arrangement of $\text{Re}=\text{O}$ double bonds in which the $\text{Re}-\text{F}$ bonds *trans* to the oxygen atoms are significantly lengthened. The $\text{Re}_2\text{O}_4\text{F}_7^-$ and $\text{Re}_3\text{O}_6\text{F}_{10}^-$ anions and ReO_2F_3 are open chains containing fluorine-bridged *cis*- ReO_2F_4 units with the fluorine bridges *trans* to the oxygens. Fluorine-19 NMR spectra show that ReO_2F_4^- , $\text{Re}_2\text{O}_4\text{F}_7^-$ and $\text{ReO}_2\text{F}_3 \cdot \text{CH}_3\text{CN}$ also have *cis*-dioxo arrangement in CH_3CN solution.

Although previously reported, the ReOF_6^- anion has only recently been characterized crystallographically as the $\text{Cs}^+\text{ReOF}_6^-$ and $\text{NO}_2^+\text{ReOF}_6^-$ salts which have been prepared by the reaction of ReOF_5 with CsF at 60°C and by the reaction of ReF_7 with NO_2F , followed by slow accidental hydrolysis [346]. A pentagonal bipyramidal ReOF_6^- anion with the oxygen in the apical position was found in both crystal structures and gave rise to an AB_5 spin system in the room temperature ^{19}F NMR spectrum of CH_3CN solutions of $\text{Cs}^+\text{ReOF}_6^-$ and $\text{NO}_2^+\text{ReOF}_6^-$. Hydrolysis of ReF_6 in HF affords a mixture of ReOF_4 and $\text{H}_3\text{O}^+\text{Re}_2\text{O}_2\text{F}_9^-$, which were characterized by Raman spectroscopy [316]. The stepwise hydrolyses of rhenium penta- and tetrafluorides have been studied, leading to the isolation of ReO_2F and ReOF_2 and their characterization by infrared spectroscopy [347]. Rhenium oxide difluoride disproportionates at 600°C to Re , $\text{Re}^{\text{VII}}\text{O}_3\text{F}$ and $\text{Re}^{\text{VI}}\text{OF}_4$, while $\text{Re}^{\text{VO}}_2\text{F}$ disproportionates at 500°C to Re , $\text{Re}^{\text{VII}}\text{O}_3\text{F}$ and $\text{Re}^{\text{IV}}\text{OF}_2$.

Rhenium oxide tetrafluoride and rhenium oxide pentafluoride can be used as selective fluorination agents reacting with CH_2Cl_2 by chlorine-fluorine exchange with $>90\%$ selectivity and, in the case of ReOF_5 , subsequent decomposition of the unstable Re^{VII} chloride species results in ReOCl_4 [348].

5.3.9 Iron and Nickel

Successive additions of iron(II) oxalate and H_2O_2 to an aqueous solution of KHF_2 has resulted in the isolation of $\text{K}_4\text{HFe}^{\text{III}}_2\text{OF}_9$; the structure was postulated on basis of magnetic measurements and an incomplete infrared spectroscopic study and by analogy with structure of $\text{Fe}_2\text{OCl}_6^{2-}$ [349]. The salts, $\text{Ba}_5(\text{Fe}_2\text{OF}_9)_2 \cdot 2\text{H}_2\text{O}$, $(\text{Co}(\text{NH}_3)_6)_4\text{H}_3(\text{Fe}_2\text{OF}_9)_3 \cdot 2\text{H}_2\text{O}$ and $(\text{Coen}_3)_4\text{H}_3(\text{Fe}_2\text{OF}_9)_3 \cdot 8\text{H}_2\text{O}$ have been isolated by treating aqueous solutions of $\text{K}_4\text{HFe}_2\text{OF}_9$ with the appropriate Cl^- salt. All four solids are believed to contain the $\text{Fe}_2\text{OF}_9^{5-}$ anion with hexacoordination around each iron atom.

The oxide fluorides, $\text{Li}_2\text{FeO}_2\text{F}$ and LiNiOF , have been prepared by heating a $\text{Li}_2\text{CO}_3/\text{Fe}_2\text{O}_3/\text{LiF}$ and a LiF/NiF_2 mixture at $900\text{--}1100^\circ\text{C}$ and 1000°C for 40

h, respectively, and have been characterized by X-ray powder diffraction and infrared spectroscopy [245]. The oxide fluorides were found to crystallize in the NaCl-type structure with a statistical distribution of the anions and cations in their corresponding sublattice.

5.3.10 Ruthenium and Osmium

The fluorination of RuO_4 with KrF_2 in anhydrous HF produced RuOF_4 [350]. Fluorine was not found to be a powerful enough fluorinating agent to react with RuO_4 in HF solution at room temperature. Ruthenium oxide tetrafluoride was prepared by the reaction of RuF_5 with glass at ca 300°C and was characterized by mass spectrometry and matrix-isolation infrared spectroscopy [351]. Infrared peak intensities and isotope fine structure have been used to estimate the O—Ru—F angle of the C_{4v} molecule.

The species RuOF_4 and RuF_n ($n = 4, 5, 6$) have been identified as the fluorination products in earlier studies of the direct fluorination of RuO_2 , with RuOF_4 found to be the primary product. The fluorination of RuO_2 with 100 kPa of F_2 at various temperatures has been investigated and a reaction sequence has been proposed [352]. The solid residue from the fluorination at $300\text{--}320^\circ\text{C}$ was found to be the previously unknown RuOF_3 which was characterized by chemical analysis and Raman spectroscopy. In the proposed reaction sequence, RuOF_3 is assumed to be the product of the reaction between RuO_2 and RuF_6 .

Osmium tetroxide reacts with CsF or RbF in water forming $\text{M}_2[\text{OsO}_4\text{F}_2] \cdot \text{H}_2\text{O}$ ($\text{M} = \text{Cs}, \text{Rb}$) which were characterized by elemental analysis, X-ray powder diffraction, infrared spectroscopy and thermogravimetric analysis [353]. Based on vibrational spectroscopy, the $\text{OsO}_4\text{F}_2^{2-}$ anion is considered to possess a *cis*-difluoro arrangement. Osmium L_{III} EXAFS data have been obtained for $\text{Cs}_2[\text{OsO}_4\text{F}_2]$ giving values for the $\text{Os}=\text{O}$ and $\text{Os}-\text{F}$ bond distances [354].

An improved preparation of OsO_3F_2 results from the room temperature reaction of OsO_4 and ClF_3 and subsequent removal of Cl_2 , O_2 and OsOF_5 by-product (ca 15%) at -10°C [355]. The generation of the higher fluorinated osmium oxide fluoride, *cis*- OsO_2F_4 , has been observed during this reaction which is thought to be an intermediate in the formation of OsOF_5 since *cis*- OsO_2F_4 is slowly converted to OsOF_5 in ClF_3 solution [356]. The slow reaction of OsO_4 and BrF_5 yields OsO_3F_2 at ambient temperature without the formation of OsOF_5 , however, the conversion is complete only after 14 d. Osmium trioxide difluoride has been characterized by matrix-isolation infrared and UV/VIS spectroscopy [357], EXAFS data [354], and single crystal X-ray diffraction of the low-temperature monoclinic phase [355]. The crystal structure reveals a polymeric chain structure with fluorine-bridged *fac*- OsO_3F_3 moieties. The Os L_{III} EXAFS data accurately reproduced the $\text{Os}=\text{O}$ and $\text{Os}-\text{F}$ bond lengths [354]. Values for the $\text{Os}=\text{O}$ and $\text{Os}-\text{F}$ bond lengths of the OsO_3F_3^- anion, which has previously been shown to have a facial configuration based on vibrational spectroscopy, have been obtained by an Os L_{III} -edge EXAFS study of KOsO_3F_3 [354].

The purple osmium(VIII) oxide fluoride obtained from the reaction of KrF_2 and OsO_4 in anhydrous HF solution, and originally identified as OsOF_6 [358], was shown by quantitative material balance [359,360], gas-phase electron diffraction [360], and NMR and vibrational spectroscopy [360] to be *cis*- OsO_2F_4 [355]. The ^{19}F NMR spectrum of *cis*- OsO_2F_4 exhibits a characteristic A_2X_2 spin pattern flanked by natural abundance (1.64%) ^{187}Os satellites [360]. Observation of ^{187}Os satellites made it possible to detect the ^{187}Os chemical shift for *cis*- OsO_2F_4 from its $^{19}\text{F}\{^{187}\text{Os}\}$ inverse correlation spectrum. A single crystal X-ray structure determination exhibited positional disorder between the fluorine and oxygen atoms [355].

Osmium dioxide tetrafluoride, *cis*- OsO_2F_4 , reacts with the strong fluoride ion acceptors AsF_5 and SbF_5 in HF and SbF_5 solutions to form orange salts [345]. Raman spectra are consistent with the formation of the fluorine-bridged diosmium cation $\text{Os}_2\text{O}_4\text{F}_7^+$, as the AsF_6^- and $\text{Sb}_2\text{F}_{11}^-$ salts, respectively. The crystal structure of $\text{Os}_2\text{O}_4\text{F}_7^+\text{Sb}_2\text{F}_{11}^-$ consists of discrete fluorine-bridged $\text{F}(\text{cis}\text{-OsO}_2\text{F}_3)_2^+$ cations that are isoelectronic with the $\text{Re}_2\text{O}_4\text{F}_7^-$ anion and in which the fluorine bridge is *trans* to oxygen atoms. The OsO_2F_3^+ cation, which is isoelectronic with the ReO_2F_3 monomer, was characterized by ^{19}F NMR and Raman spectroscopy in neat SbF_5 solution but was not isolable in the solid state. The NMR and Raman spectroscopic findings are consistent with a trigonal bipyramidal cation in which the oxygen atoms and a fluorine atom occupy the equatorial plane and two fluorine atoms are in axial positions. Attempts to prepare the OsOF_5^+ cation by oxidative fluorination of *cis*- OsO_2F_4 with $\text{KrF}^+\text{AsF}_6^-$ in HF proved unsuccessful leading to $\text{Os}_2\text{O}_4\text{F}_7^+\text{AsF}_6^-$ [345].

The vapor phase species produced by heating solid OsO_2F_3 in vacuo have been isolated in low-temperature matrices and studied by matrix-isolation infrared spectroscopy and by mass spectrometry [361]. Both studies indicate a complex mode of decomposition, and in addition to the identification of OsOF_4 (C_{4v}) and OsO_3F_2 (D_{3h}), the infrared spectra show two additional features assigned to the OsO_2F_3 molecule with D_{3h} point symmetry.

Contrary to previous work, no ^{19}F NMR signal could be observed assignable to paramagnetic OsOF_5 in HF or WF_6 solutions [362]. Well-resolved EPR spectra of OsOF_5 were obtained in WF_6 , Freon-113a and SO_2 at -196°C . Hyperfine coupling to ^{189}Os and to four equivalent equatorial fluorines was observed, but no coupling to the axial fluorine was observed.

The osmium oxide fluorides, OsO_3F_2 , OsO_2F_3 and OsOF_5 react with CH_2Cl_2 as selective fluorinating agents upon chlorine-fluorine exchange with >90% selectivity, affording unstable high oxidation state chloride species which decompose to chlorine and an intractable lower oxidation-state osmium oxide [348].

5.3.11 Cadmium

Polycrystalline Cd_4OF_6 was prepared by high temperature synthesis from a stoichiometric mixture of CdO and CdF_2 at 620°C [363]. The structure of Cd_4OF_6 has been solved from X-ray powder data using the Rietveld method and consists

of a three-dimensional network of edge- and corner-sharing CdOF_6 polyhedra which derive from cubes having one corner missing.

References

- [1] J.H. Holloway, D. Laycock, *Adv. Inorg. Chem. Radiochem.*, 27 (1983) 157.
- [2] K.O. Christe, *Inorganic Reactions, Methods*, Verlag Chemie, Vol.3 (1989) 39.
- [3] K.O. Christe, W.W. Wilson, C.J. Schack, In: *Synthetic Fluorine Chemistry*, R.D. Chambers, G.A. Olah, G.K.S. Prakash, (Eds.), New York: John Wiley & Sons, 1992, Chapter 2, pp. 31–42.
- [4] J.W. Larson, T.B. McMahon, *Inorg. Chem.*, 26 (1987) 4018.
- [5] I. Bernal, J. Cetrullo, J. Cai, R.A. Geanangel, J.H. Worrel, *J. Chem. Soc., Dalton Trans.*, (1995) 99.
- [6] H. Schmidbaur, B. Brachthäuser, O. Steigelmann, H. Beruda, *Chem. Ber.*, 125 (1992) 2705.
- [7] A.A. Andriiko, N.I. Parkhomenko, A.N. Antishko, *Zh. Neorg. Khim.*, 33 (1988) 729; *Russ. J. Inorg. Chem.*, 33 (1988) 410.
- [8] N.N. Babich, B.F. Dmitruk, G.N. Novitskaya, *Zh. Neorg. Khim.*, 37 (1992) 1443; *Russ. J. Inorg. Chem.*, 37 (1992) 729.
- [9] W.J. Belcher, P.D.W. Boyd, P.J. Brothers, M.J. Liddell, C.E.F. Rickard, *J. Am. Chem. Soc.*, 116 (1994) 8416.
- [10] S.J. Kirkby, A.J. Lough, G.A. Ozin, *Z. Kristallogr.*, 210 (1995) 956.
- [11] T. Loiseau, R. Retoux, P. Lacorre, G. Férey, *J. Solid State Chem.*, 111 (1994) 427.
- [12] D.M. Poojary, A. Clearfield, V.A. Timofeeva, S.E. Sigaryov, *Solid State Ionics*, 73 (1994) 75.
- [13] A. Campo, Ch. Cardinaud, G. Turban, C. Dubon-Chevallier, V. Amarger, J. Etrillard, *J. Vac. Sci. Technol.*, A11 (1993) 2536.
- [14] B. Neumüller, F. Gahlmann, *Angew. Chem.*, 105 (1993) 1770; *Angew. Chem. Int. Ed. Engl.*, 32 (1993) 1701.
- [15] R.L. Needs, M.T. Weller, *J. Chem. Soc., Chem. Commun.*, (1995) 353.
- [16] R.L. Needs, M.T. Weller, *J. Chem. Soc., Dalton Trans.*, (1995) 3015.
- [17] G.A. Tsirlina, O.A. Petrii, *J. Electroanal. Chem.*, 401 (1996) 33.
- [18] W.F. Schneider, T.J. Wallington, *J. Phys. Chem.*, 98 (1994) 7448.
- [19] F. Caralp, R. Lesclaux, A.M. Dognon, *Chem. Phys. Lett.*, 129 (1986) 433.
- [20] K.C. Clemitshaw, J.R. Sodeau, *J. Phys. Chem.*, 93 (1989) 3552.
- [21] P. Pagsberg, J.T. Jodkowski, E. Ratajczak, A. Sillesen, *Chem. Phys. Lett.*, 286 (1998) 138.
- [22] W.B. Farnham, B.E. Smart, W.J. Middleton, J.C. Calabrese, D.A. Dixon, *J. Am. Chem. Soc.*, 107 (1995) 4565.
- [23] R. Minkwitz, R. Bröchler, M. Berkei, *Z. Anorg. Allg. Chem.*, 622 (1996) 1749.
- [24] J. Arlt, M. Jansen, *Chem. Ber.*, 124 (1991) 321.
- [25] X. Zhang, U. Gross, K. Seppelt, *Angew. Chem.*, 107 (1995) 2019; *Angew. Chem. Int. Ed. Engl.*, 34 (1995) 1858.
- [26] S.J. David, B.S. Ault, *Inorg. Chem.*, 24 (1985) 1238.
- [27] M. Shinmei, T. Imai, T. Yokokawa, C.R. Masson, *J. Chem. Thermodynamics*, 18 (1986) 241.
- [28] I. Abrahams, S.J. Clark, J.D. Donaldson, Z.I. Khan, J.T. Southern, *J. Chem. Soc., Dalton Trans.*, (1994) 2581.

- [29] L. Fournes, J. Grannec, C. Mirambet, B. Darriet, P. Hagenmuller, *Z. Anorg. Allg. Chem.*, 601 (1991) 93.
- [30] K.O. Christe, *J. Am. Chem. Soc.*, 117 (1995) 6136.
- [31] R. Minkwitz, D. Bernstein, H. Preut, P. Sartori, *Inorg. Chem.*, 30 (1991) 2157.
- [32] C.J. Schack, K.O. Christe, *Inorg. Chem.*, 27 (1988) 4771.
- [33] F. Aubke, M.S.R. Cader, F. Mistry, In: *Synthetic Fluorine Chemistry*, R.D. Chambers, G.A. Olah, G.K.S. Prakash, (Eds.), New York: John Wiley & Sons, 1992, Chapter 3, pp. 43–86.
- [34] R. Ahlrichs, R. Becherer, M. Binnewies, H. Borrmann, M. Lakenbrink, S. Schunck, H. Schnöckel, *J. Am. Chem. Soc.*, 108 (1986) 7905.
- [35] M. Binnewies, H. Borrmann, *Thermochim. Acta*, 103 (1986) 401.
- [36] K.O. Christe, W.W. Wilson, H.P.A. Mercier, J.C.P. Sanders, G.J. Schrobilgen, D.A. Dixon, *J. Fluorine Chem.*, 71 (1995) 205.
- [37] K.O. Christe, D.A. Dixon, J.C.P. Sanders, G.J. Schrobilgen, W.W. Wilson, *Inorg. Chem.*, 33 (1994) 4911.
- [38] H.-J. Plinta, R. Gereke, A. Fischer, P.G. Jones, R. Schmutzler, *Z. Naturforsch.*, 48B (1993) 737.
- [39] K.O. Christe, R. Gnann, R.I. Wagner, W.W. Wilson, *Eur. J. Solid State Inorg. Chem.*, 33 (1996) 865.
- [40] E.R. Bittner, J. Matos, K.W. Hillig II, R.L. Kuczkowski, *Z. Naturforsch.*, 42A (1987) 1415.
- [41] D.W.H. Rankin, A.J. Blake, M.J. Davis, E.A.V. Ebsworth, A.J. Welch, *J. Chem. Soc., Dalton Trans.*, (1989) 223.
- [42] F.A. Cotton, M. Matusz, *Chimia*, 43 (1989) 167.
- [43] K.O. Christe, D.A. Dixon, G.J. Schrobilgen, W.W. Wilson, *J. Am. Chem. Soc.*, 119 (1997) 3918.
- [44] R. Fernández-Galán, B.R. Manzano, A. Otero, M. Lanfranchi, M.A. Pellinghelli, *Inorg. Chem.*, 33 (1994) 2309.
- [45] A.J. Blake, E.A.V. Ebsworth, A.J. Welch, *Acta Crystallogr., Sect. C* 44 (1988) 949.
- [46] P. Vast, A. Semmoud, A. Addou, G. Palavit, *J. Fluorine Chem.*, 27 (1985) 319.
- [47] A. Semmoud, A. Benghalem, A. Addou, *J. Fluorine Chem.*, 46 (1990) 1.
- [48] P. Vast, A. Semmoud, G. Palavit, *J. Fluorine Chem.*, 34 (1986) 229.
- [49] K. Heide, D.-H. Menz, C. Schmidt, L. Kolditz, *Z. Anorg. Allg. Chem.*, 520 (1985) 32.
- [50] U. Haubenreisser, U. Sternberg, A.-R. Grimmer, *Mol. Phys.*, 60 (1987) 151.
- [51] U. Schülke, R. Kayser, *Z. Anorg. Allg. Chem.*, 600 (1991) 221.
- [52] M. Bhattacharjee, M.K. Chaudhuri, *J. Chem. Soc., Dalton Trans.*, (1987) 477.
- [53] P.J. Durand, L. Cot, M. Berraho, M. Rafiq, *Acta Crystallogr., Sect. C* 43 (1987) 611.
- [54] M.F.A. Dove, R.C. Hibbert, N. Logan, *J. Chem. Soc., Dalton Trans.*, (1985) 707.
- [55] M.J. Begley, M.F.A. Dove, R.C. Hibbert, N. Logan, M. Nunn, D.B. Sowerby, *J. Chem. Soc., Dalton Trans.*, (1985) 2433.
- [56] P. Vast, A. Semmoud, *J. Fluorine Chem.*, 27 (1985) 47.
- [57] P. Vast, A. Semmoud, A. Addou, G. Palavit, *J. Fluorine Chem.*, 38 (1988) 297.
- [58] O. Farooq, *J. Fluorine Chem.*, 86 (1997) 189.
- [59] G. Bruno, S.L. Schiavo, P. Piraino, F. Faraone, *Organometallics*, 4 (1985) 1098.
- [60] D.L. Reger, M.F. Huff, L. Lebioda, *Acta Crystallogr., Sect. C* 47 (1991) 1167.
- [61] S. Kitagawa, S. Kawata, Y. Nozaka, M. Munakata, *J. Chem. Soc., Dalton Trans.*, (1993) 1399.
- [62] M.A. Bennet, A.C. Willis, L.Y. Goh, W. Chen, *Polyhedron*, 15 (1996) 3559.
- [63] T. U. Fessler, R. Hübener, J. Strähle, *Z. Anorg. Allg. Chem.*, 623 (1997) 1367.

- [64] M. Bhattacharjee, M.K. Chaudhuri, *J. Chem. Soc., Dalton Trans.*, (1988) 2005.
- [65] R.L. Davidovich, V.B. Logvinova, L.A. Zemnukhova, A.A. Udovenko, I.P. Kondratyuk, *Sov. J. Coord. Chem.*, 17 (1991) 709; *Koord. Khimiya*, 17 (1991) 1342.
- [66] J.-P. Laval, J.-C. Champarnaud-Mesjard, B. Frit, A. Britel, A. Mikou, *Eur. J. Solid State Inorg. Chem.*, 31 (1994) 943.
- [67] T.R. Mill, *J. Fluorine Chem.*, 52 (1991) 267.
- [68] K.D. Abney, P.G. Eller, M.P. Eastman, C.F. Pace, S.A. Kinkead, R.J. Kissane, W.H. Woodruff, *J. Fluorine Chem.*, 73 (1995) 137.
- [69] L. Hedberg, K. Hedberg, P.G. Eller, R.R. Ryan, *Inorg. Chem.*, 27 (1988) 232.
- [70] (a) K.C. Kim, G.M. Campbell, *J. Mol. Struct.*, 129 (1985) 263; (b) K.C. Kim, G.M. Campbell, *Appl. Spectrosc.*, 39 (1985) 625; (c) K.C. Kim, G.M. Campbell, *Chem. Phys. Lett.*, 116 (1985) 236; (d) G.M. Campbell, *J. Mol. Struct.*, 189 (1988) 301; (e) G.M. Campbell, *J. Fluorine Chem.*, 46 (1989) 357; (f) J.L. Lyman, R. Holland, *J. Phys. Chem.*, 92 (1988) 7232.
- [71] J.G. Malm, P.G. Eller, L.B. Asprey, *J. Am. Chem. Soc.*, 106 (1984) 2726.
- [72] L.B. Asprey, P.G. Eller, S.A. Kinkead, *Inorg. Chem.*, 25 (1986) 670.
- [73] L.B. Asprey, S.A. Kinkead, P.G. Eller, *Nucl. Tech.*, 73 (1986) 69.
- [74] L.B. Asprey, P.G. Eller, S.A. Kinkead, *J. Less. Comm. Met.*, 121 (1986) 653.
- [75] P.G. Eller, L.B. Asprey, S.A. Kinkead, B.I. Swanson, *Abs. of papers of the ACS* (1989) 197.
- [76] T.R. Mills, L.W. Reese, *J. Alloys Comp.*, 213 (1994) 360.
- [77] P.G. Eller, L.B. Asprey, S.A. Kinkead, B.I. Swanson, R.J. Kissane, *J. Alloys Comp.*, 269 (1998) 63.
- [78] S.A. Kinkead, L.B. Asprey, P.G. Eller, *J. Fluorine Chem.*, 29 (1985) 459.
- [79] C. Pradayrol, A.M. Casanovas, A. Hernoune, J. Casanovas, *J. Phys. D: Appl. Phys.*, 29 (1996) 1941.
- [80] C. Pradayrol, A.M. Casanovas, C. Aventin, J. Casanovas, *J. Phys. D: Appl. Phys.*, 30 (1997) 1356.
- [81] E.H. Appelman, In: *Inorganic Syntheses*, John Wiley & Sons, Inc., 1986, Vol. 24, p. 22.
- [82] A. Bendada, G. Webb, J.M. Winfield, *Eur. J. Solid State Inorg. Chem.*, 33 (1996) 907.
- [83] C.S. Sass, B.S. Ault, *J. Phys. Chem.*, 89 (1985) 1002.
- [84] D. Mootz, A. Merschenz-Quack, *Acta Crystallogr., Sect. C44* (1988) 924.
- [85] K.-H. Moock, D. Sülzle, P. Klæboe, *J. Fluorine Chem.*, 47 (1990) 151.
- [86] A. Kornath, F. Neumann, R. Ludwig, *Inorg. Chem.*, 36 (1997) 5570.
- [87] A. Kornath, F. Neumann, *Inorg. Chem.*, 36 (1997) 2708.
- [88] W. Heileman, R. Mews, *Chem. Ber.*, 121 (1988) 461.
- [89] R. Haist, H. Oberhammer, E. Lork, R. Mews, *J. Fluorine Chem.*, 89 (1998) 51.
- [90] E. Lork, R. Mews, *J. Chem. Soc., Chem. Commun.*, (1995) 1113.
- [91] R.M.S. Alvarez, E.H. Cutin, H.-G. Mack, O. Sala, C.O. Della Védova, *J. Mol. Struct.*, 328 (1994) 221.
- [92] E.H. Cutin, C.O. Della Védova, H.-G. Mack, H. Oberhammer, *J. Mol. Struct.*, 354 (1995) 165.
- [93] R. Hoppenheit, E. Lork, J. Petersen, R. Mews, *J. Chem. Soc., Chem. Commun.*, (1997) 1659.
- [94] Z. Žák, A. Růžicka, Ch. Michot, *Z. Kristallogr.*, 213 (1998) 217.
- [95] A. Růžicka, L. Zatloukalová, *Z. Chem.*, 27 (1987) 227.
- [96] O. Hiemisch, D. Henschel, P.G. Jones, A. Blaschette, *Z. Anorg. Allg. Chem.*, 622 (1996) 829.

- [97] O. Hiemisch, D. Henschel, A. Blaschette, P.G. Jones, *Z. Anorg. Allg. Chem.*, 623 (1997) 324.
- [98] M.J. Begley, D.B. Sowerby, R.D. Verma, A. Vig, *J. Organomet. Chem.*, 481 (1994) 243.
- [99] Z. Žák, A. Růžicka, *Z. Anorg. Allg. Chem.*, 549 (1987) 67.
- [100] R.M.S. Alvarez, E.H. Cutin, H.-G. Mack, C.O. Della Védova, *J. Mol. Structure*, 323 (1994) 29.
- [101] C.O. Della Védova, E.H. Cutin, H.-G. Mack, H. Oberhammer, *J. Mol. Structure*, 380 (1996) 167.
- [102] A. Vij, S. Singh, R.D. Verma, *J. Fluorine Chem.*, 58 (1992) 43.
- [103] A. Haas, C. Klare, P. Betz, J. Bruckmann, C. Krüger, Y.H. Tsay, F. Aubke, *Inorg. Chem.*, 35 (1996) 1918.
- [104] R. Faggiani, D.K. Kennepohl, C.J.L. Lock, G.J. Schrobilgen, *Inorg. Chem.*, 25 (1986) 563.
- [105] T. Meier, R. Mews, *J. Fluorine Chem.*, 42 (1989) 81.
- [106] T. Meier, R. Mews, *Chem. Ber.* 126 (1993) 2437.
- [107] W. Heileman, R. Mews, *Eur. J. Solid State Inorg. Chem.*, 29 (1992) 799.
- [108] W. Heileman, R. Mews, *J. Fluorine Chem.*, 52 (1991) 377.
- [109] J.M. Whalen, G.J. Schrobilgen, *J. Fluorine Chem.*, 71 (1995) 225.
- [110] S.P. Mallela, J.R. Sams, F. Aubke, *Can. J. Chem.*, 63 (1985) 3305.
- [111] F. Aubke, In: *Inorganic Fluorine Chemistry, Toward the 21st Century*, ACS Symposium Series 555, J. Thrasher, S.H. Strauss (Eds.), 1994, Chapter 22, pp. 350–365.
- [112] F. Aubke, *J. Fluorine Chem.*, 72 (1995) 195.
- [113] H. Willner, F. Aubke, *Angew. Chem.*, 109 (1997) 2506; *Angew. Chem. Int. Ed. Engl.*, 36 (1997) 2402.
- [114] D.L. Zhang, S.J. Rettig, J. Trotter, F. Aubke, *Inorg. Chem.*, 35 (1996) 6113.
- [115] M.J. Collins, R.J. Gillespie, J.F. Sawyer, G.J. Schrobilgen, *Acta Crystallogr.*, C42 (1986) 13.
- [116] A. Haas, J. Kasproski, M. Pryka, *Chem. Ber.*, 125 (1992) 789.
- [117] S.P. Mallela, K. Lee, P.F. Gehrs, J.I. Christensen, J.R. Sams, F. Aubke, *Can. J. Chem.*, 65 (1987) 2649.
- [118] S.P. Mallela, S.T. Tomic, K. Lee, J.R. Sams, F. Aubke, *Inorg. Chem.*, 25 (1986) 2939.
- [119] S.P. Mallela, S. Yap, J.R. Sams, F. Aubke, *Inorg. Chem.*, 25 (1986) 4327.
- [120] D.C. Adams, T. Birchall, R. Faggiani, R.J. Gillespie, J.E. Vekris, *Can. J. Chem.*, 69 (1991) 2122.
- [121] D.Y. Gin, M.S.R. Cader, J.R. Sams, F. Aubke, *Can. J. Chem.*, 68 (1990) 350.
- [122] S.P. Mallela, S. Tomic, S. Lee, S. Karunanithy, H.A. Cartier, J.R. Sams, F. Aubke, *J. Fluorine Chem.* 44 (1989) 309.
- [123] D.G. Niyogi, S. Singh, R.D. Verma, *J. Fluorine Chem.*, 70 (1995) 237.
- [124] W.V. Cicha, D. Zhang, F. Aubke, *J. Fluorine Chem.*, 71 (1995) 203.
- [125] D.L. Zhang, S.J. Rettig, J. Trotter, F. Aubke, *Inorg. Chem.*, 34 (1995) 3153.
- [126] D.L. Zhang, S.J. Rettig, J. Trotter, F. Aubke, *Inorg. Chem.*, 34 (1995) 2269.
- [127] H. Willner, F. Mistry, F. Aubke, *J. Fluorine Chem.*, 59 (1992) 333.
- [128] F. Aubke, B. Casper, H.S.P. Müller, H. Oberhammer, H. Willner, *J. Mol. Struct.*, 346 (1995) 111.
- [129] B. Casper, H.-G. Mack, H. Oberhammer, *J. Fluorine Chem.*, 71 (1995) 215.
- [130] C.J. Schack, R.R.D. Wilson, *Adv. Inorg. Synth.*, 24 (1986) 6.
- [131] S. Singh, D.D. DesMarteau, *Inorg. Chem.*, 25 (1986) 4596.
- [132] T. Birchall, G. Denes, R. Faggiani, C.S. Frampton, R.J. Gillespie, R. Kapoor, J.E. Vekris, *Inorg. Chem.*, 29 (1990) 1527.

- [133] F. Mistry, F. Aubke, *J. Fluorine Chem.*, 68 (1994) 239.
- [134] W.V. Cicha, F. Aubke, *J. Am. Chem. Soc.*, 111 (1989) 4328.
- [135] W.V. Cicha, F. Aubke, *J. Fluorine Chem.*, 47 (1990) 317.
- [136] D. Zhang, F. Aubke, *J. Fluorine Chem.*, 58 (1992) 81.
- [137] S.P. Mallela, F. Aubke, *Inorg. Chem.*, 24 (1985) 2969.
- [138] P.C. Leung, G.B. Wong, F. Aubke, *J. Fluorine Chem.*, 35 (1987) 607.
- [139] C.Q. Wang, A.R. Lewis, R.J. Batchelor, F.W.B. Einstein, H. Willner, F. Aubke, *Inorg. Chem.*, 35 (1996) 1279.
- [140] G. Hwang, C. Wang, M. Bodenbinder, H. Willner, F. Aubke, *J. Fluorine Chem.*, 66 (1994) 159.
- [141] C.Q. Wang, H. Willner, M. Bodenbinder, R.J. Batchelor, F.W.B. Einstein, F. Aubke, *Inorg. Chem.*, 33 (1994) 3521.
- [142] C.Q. Wang, M. Bodenbinder, H. Willner, S. Rettig, J. Trotter, F. Aubke, *Inorg. Chem.*, 33 (1994) 779.
- [143] G. Hwang, M. Bodenbinder, H. Willner, F. Aubke, *Inorg. Chem.*, 32 (1993) 4667.
- [144] H. Willner, S.J. Rettig, J. Trotter, F. Aubke, *Can. J. Chem.*, 69 (1991) 391.
- [145] H. Willner, F. Aubke, *Inorg. Chem.*, 29 (1990) 2195.
- [146] F.G. Herring, G. Hwang, K.C. Lee, F. Mistry, P.S. Phillips, H. Willner, F. Aubke, *J. Am. Chem. Soc.*, 114 (1992) 1271.
- [147] H. Willner, F. Mistry, G. Hwang, F.G. Herring, M.S.R. Cader, F. Aubke, *J. Fluorine Chem.*, 52 (1991) 13.
- [148] H. Willner, M. Bodenbinder, C.Q. Wang, F. Aubke, *J. Chem. Soc., Chem. Commun.*, (1994) 1189.
- [149] M. Bodenbinder, G. Balzer-Jöllenbeck, H. Willner, R.J. Batchelor, F.W.B. Einstein, C. Wang, F. Aubke, *Inorg. Chem.*, 35 (1996) 82.
- [150] S.H. Hwang, K. Naik, D.D. DesMarteau, *Inorg. Chem.*, 32 (1993) 2791.
- [151] W. Heilemann, R. Mews, S. Pohl, W. Saak, *Chem. Ber.*, 122 (1989) 427.
- [152] E. Jaudas-Prezel, D. Christen, H. Oberhammer, S.P. Mallela, J.M. Shreeve, *J. Mol. Struct.*, 248 (1991) 415.
- [153] K.O. Christe, D.A. Dixon, I.B. Goldberg, C.J. Schack, B.W. Walther, J.T. Wang, F. Williams, *J. Am. Chem. Soc.*, 115 (1993) 1129.
- [154] K. Seppelt, D. Lentz, G. Klöter, In: *Inorganic Syntheses*, John Wiley & Sons, Inc., 1986, Vol. 24, p. 27.
- [155] C. Feldmann, M. Jansen, *Chem. Ber.*, 127 (1994) 2173.
- [156] A. Ider, J.P. Laval, B. Frit, J. Carré, J.P. Bastide, *J. Solid State Chem.*, 123 (1996) 68.
- [157] A. Ider, B. Frit, J.P. Laval, J. Carré, P. Claudy, J.M. Létoffé, *Thermochim. Acta*, 258 (1995) 117.
- [158] K.O. Christe, J.C.P. Sanders, G.J. Schrobilgen, W.W. Wilson, *J. Chem. Soc., Chem. Commun.*, (1991), 837.
- [159] K.O. Christe, D.A. Dixon, J.C.P. Sanders, G.J. Schrobilgen, W.W. Wilson, *J. Am. Chem. Soc.*, 32 (1993) 4089.
- [160] K.O. Christe, E.C. Curtis, D.A. Dixon, H.P.A. Mercier, J.C.P. Sanders, G.J. Schrobilgen, W.W. Wilson, In: *Inorganic Fluorine Chemistry, Toward the 21st Century*, ACS Symposium Series 555, J. Thrasher, S.H. Strauss (Eds.), 1994, Chapter 5, pp. 66–89.
- [161] E.J. Baran, *An. Asoc. Quim. Argent.*, 83 (1995) 207.
- [162] L. Turowsky, K. Seppelt, *Inorg. Chem.*, 29 (1990) 3226.
- [163] A. Engelbrecht, F. Sladky, *Angew. Chem.*, 76 (1964) 379; *Angew. Chem., Int. Ed. Engl.*, 3 (1964) 383.

- [164] T. Birchall, R.D. Myers, H. de Waard, G.J. Schrobilgen, *Inorg. Chem.*, 21 (1982) 1068.
- [165] K. Seppelt, *Accounts Chem. Res.*, 12 (1979) 211.
- [166] K. Seppelt, *Angew. Chem.*, 94 (82) 890; *Angew. Chem. Int. Ed. Engl.*, 21 (1982) 877.
- [167] K. Seppelt, D. Lentz, *Progress in Inorg. Chem.*, 29 (1982) 167.
- [168] S.H. Strauss, *Chem. Rev.*, 93 (1993) 927.
- [169] K. Hurlburt, D.M. Van Seggen, J.J. Rack, S.H. Strauss, In: *Inorganic Fluorine Chemistry, Toward the 21st Century*, ACS Symposium Series 555, J. Thrasher, S.H. Strauss (Eds.), 1994, Chapter 21, pp. 338–349.
- [170] F. Sladky, In: *Inorganic Syntheses*, John Wiley & Sons, Inc., 1986, Vol. 24, p. 33.
- [171] J.S. Thrasher, K. Seppelt, *Z. Anorg. Allg. Chem.*, 529 (1985) 85.
- [172] P.K. Miller, K.D. Abney, A.K. Rappé, O.P. Anderson, S.H. Strauss, *Inorg. Chem.*, 27 (1988) 2255.
- [173] P.J. Kellet, O.P. Anderson, S.H. Strauss, K.D. Abney, *Can. J. Chem.*, 67 (1989) 2023.
- [174] S.H. Strauss, K.D. Abney, O.P. Anderson, *Inorg. Chem.*, 25 (1986) 2806.
- [175] D.M. Van Seggen, P.K. Hurlburt, M.D. Noirot, O.P. Anderson, S.H. Strauss, *Inorg. Chem.*, 31 (1992) 1423.
- [176] P.K. Hurlburt, O.P. Anderson, S.H. Strauss, *Can. J. Chem.*, 70 (1992) 726.
- [177] M.D. Noirot, O.P. Anderson, S.H. Strauss, *Inorg. Chem.*, 26 (1987) 2216.
- [178] P.K. Hurlburt, O.P. Anderson, S.H. Strauss, *J. Am. Chem. Soc.*, 113 (1991) 6277.
- [179] P.K. Hurlburt, J.J. Rack, J.S. Luck, S.F. Dec, J.D. Webb, O.P. Anderson, S.H. Strauss, *J. Am. Chem. Soc.*, 116 (1994) 10003.
- [180] P.K. Hurlburt, J.J. Rack, S.F. Dec, O.P. Anderson, S.H. Strauss, *Inorg. Chem.*, 32 (1993) 373.
- [181] J.J. Rack, B. Moasser, J.D. Gargulak, W.L. Gladfelter, H.D. Hochheimer, S.H. Strauss, *J. Chem. Soc., Chem. Commun.*, (1994) 685.
- [182] S.H. Strauss, M.D. Noirot, O.P. Anderson, *Inorg. Chem.*, 25 (1986) 3850.
- [183] M.J. Collins, G.J. Schrobilgen, *Inorg. Chem.*, 24 (1985) 2608.
- [184] H.P.A. Mercier, J.C.P. Sanders, G.J. Schrobilgen, *J. Am. Chem. Soc.*, 116 (1994) 2921.
- [185] M.J. Collins, U.R.K. Rao, G.J. Schrobilgen, *J. Magn. Reson.*, 61 (1985) 137.
- [186] D.M. Van Seggen, P.K. Hurlburt, O.P. Anderson, S.H. Strauss, *Inorg. Chem.*, 34 (1995) 3453.
- [187] R. Hoppenheit, R. Mews, *Chem. Ber.*, 118 (1985) 4276.
- [188] W.J. Casteel, Jr., P. Kolb, N. LeBlond, H.P.A. Mercier, G.J. Schrobilgen, *Inorg. Chem.*, 35 (1996), 929.
- [189] P. Zylka, H. Oberhammer, K. Seppelt, *J. Mol. Struct.*, 243 (1991) 411.
- [190] H.P.A. Mercier, J.C.P. Sanders, G.J. Schrobilgen, *Inorg. Chem.*, 34 (1995) 5261.
- [191] R. Damerius, D. Lentz, P. Huppmann, K. Seppelt, *J. Fluorine Chem.*, 29 (1985) 33.
- [192] L. Turowsky, K. Seppelt, *Z. Anorg. Allg. Chem.*, 590 (1990) 37.
- [193] I.C. Hwang, R. Kuschel, K. Seppelt, *Z. Anorg. Allg. Chem.*, 623 (1997) 379.
- [194] L. Turowsky, K. Seppelt, *Z. Anorg. Allg. Chem.*, 602 (1991) 79.
- [195] J.C.P. Sanders, G.J. Schrobilgen, *J. Chem. Soc., Chem. Commun.*, (1989) 1576.
- [196] G.J. Schrobilgen, Final Technical Report: Contract F04611-91-K-0004, Phillips Laboratory, Propulsion Directorate, U.S. Air Force Materiel Command, Edwards Air Force Base, CA 93524-7001; Report No. PL-TR-93-3007; Feb., 1993; Vol. 1, Part IV.
- [197] L. Turowsky, K. Seppelt, *Z. Anorg. Allg. Chem.*, 609 (1992) 153.
- [198] G.A. Schumacher, G.J. Schrobilgen, *Inorg. Chem.*, 23 (1984) 2923.
- [199] R.G. Syvret, K.M. Mitchell, J.C.P. Sanders, G.J. Schrobilgen, *Inorg. Chem.*, 31 (1992) 3381.

- [200] K. Moock, K. Seppelt, *Z. Anorg. Allg. Chem.*, 561 (1988) 132.
- [201] L. Turowsky, K. Seppelt, *Z. Anorg. Allg. Chem.*, 590 (1990) 23.
- [202] W.J. Casteel, Jr., D.M. MacLeod, H.P.A. Mercier, G.J. Schrobilgen, *Inorg. Chem.*, 35 (1996) 7279.
- [203] T. Drews, K. Seppelt, *Z. Anorg. Allg. Chem.*, 606 (1991) 201.
- [204] P.J. Kellett, M.J. Pawlik, L.F. Taylor, R.G. Thompson, M.A. Levstik, O.P. Anderson, S.H. Strauss, *Inorg. Chem.*, 28 (1989) 440.
- [205] M.R. Colman, T.D. Newbound, L.J. Marshall, M.D. Noirot, M.M. Miller, G.P. Wulsberg, J.S. Frye, O.P. Anderson, S.H. Strauss, *J. Am. Chem. Soc.*, 112 (1990) 2349.
- [206] M.R. Colman, M.C. Manning, O.P. Anderson, S.H. Strauss, *Inorg. Chem.*, 26 (1987) 3958.
- [207] S.H. Strauss, M.D. Noirot, O.P. Anderson, *Inorg. Chem.*, 24 (1985) 4307.
- [208] P. Huppmann, H. Hartl, K. Seppelt, *Z. Anorg. Allg. Chem.*, 524 (1985) 26.
- [209] J.J. Rack, P.K. Hurlburt, P.J. Kellett, J.S. Luck, O.P. Anderson, S.H. Strauss, *Inorg. Chim. Acta*, 242 (1996) 71.
- [210] P.K. Hurlburt, P.J. Kellett, O.P. Anderson, S.H. Strauss, *J. Chem. Soc., Chem. Commun.*, (1990) 576.
- [211] D.M. Van Seggen, P.K. Hurlburt, M.D. Noirot, O.P. Anderson, S.H. Strauss, *J. Am. Chem. Soc.*, 114 (1992) 10995.
- [212] L.A. Bugey, E.G. Hope, *J. Fluorine Chem.*, 76 (1996) 109.
- [213] M.C. Crossman, E.G. Hope, G.C. Saunders, *J. Chem. Soc., Dalton Trans.*, (1996) 509.
- [214] K.D. Abney, K.M. Long, O.P. Anderson, S.H. Strauss, *Inorg. Chem.*, 26 (1987) 2638.
- [215] S.A. Brewer, L.A. Bugey, J.H. Holloway, E.G. Hope, *J. Chem. Soc., Dalton Trans.*, (1995) 2941.
- [216] K.O. Christe, R.D. Wilson, C.J. Schack, In: *Inorganic Syntheses*, John Wiley & Sons, Inc., 1986, Vol. 24, p. 3.
- [217] K.O. Christe, W.W. Wilson, R.D. Wilson, *Inorg. Chem.*, 28 (1989) 675.
- [218] W.W. Wilson, K.O. Christe, *Inorg. Chem.*, 26 (1987) 916.
- [219] K.O. Christe, W.W. Wilson, *J. Fluorine Chem.*, 89 (1998) 97.
- [220] X.Z. Zhang, K. Seppelt, *Z. Anorg. Allg. Chem.*, 623 (1997) 491.
- [221] K.O. Christe, W.W. Wilson, *Inorg. Chem.*, 25 (1986) 1904.
- [222] W. Breuer, H.J. Frohn, *Z. Anorg. Allg. Chem.*, 619 (1993) 209.
- [223] C.J. Schack, K.O. Christe, *J. Fluorine Chem.*, 49 (1990) 167.
- [224] K.O. Christe, E.C. Curtis, D.A. Dixon, *J. Am. Chem. Soc.*, 115 (1993) 9655.
- [225] K.O. Christe, W.W. Wilson, R.D. Wilson, *Inorg. Chem.*, 28 (1989) 904.
- [226] A.R. Mahjoub, K. Seppelt, *J. Chem. Soc., Chem. Commun.*, (1991) 840.
- [227] K.O. Christe, D.A. Dixon, A.R. Mahjoub, H.P.A. Mercier, J.C.P. Sanders, K. Seppelt, G.J. Schrobilgen, W.W. Wilson, *J. Am. Chem. Soc.*, 115 (1993) 2696.
- [228] R.G. Syvret, G.J. Schrobilgen, *J. Chem. Soc., Chem. Commun.*, (1985) 1529.
- [229] R.G. Syvret, G.J. Schrobilgen, *Inorg. Chem.*, 28 (1989) 1564.
- [230] H. Selig, J.H. Holloway, *Top. Curr. Chem.*, 124 (1984) 33.
- [231] J.H. Holloway, *J. Fluorine Chem.*, 33 (1986) 149.
- [232] G.J. Schrobilgen, J.M. Whalen, Helium-Group Gases, Compounds. In: *Kirk-Othmer Encyclopedia of Chemical Technology*, 4th Edn, New York: John Wiley & Sons, Inc., 1994, Chapter 13, pp. 38–53.
- [233] K. Seppelt, H.H. Rupp, *Z. Anorg. Allg. Chem.*, 409 (1974) 331.
- [234] K.O. Christe, W.W. Wilson, *Inorg. Chem.*, 27 (1988) 1296.
- [235] J.B. Nielsen, S.A. Kinkead, P.G. Eller, *Inorg. Chem.*, 29 (1990) 3621.
- [236] K.O. Christe, W.W. Wilson, *Inorg. Chem.*, 27 (1988) 3763.

- [237] H.P.A. Mercier, J.C.P. Sanders, G.J. Schrobilgen, S. Tsai, *Inorg. Chem.*, 32 (1993) 386.
- [238] J.H. Holloway, V. Kaučič, D. Martin-Rovet, D.R. Russell, G.J. Schrobilgen, H. Selig, *Inorg. Chem.*, 24 (1985) 678.
- [239] K.O. Christe, D.A. Dixon, J.C.P. Sanders, G.J. Schrobilgen, S.S. Tsai, W.W. Wilson, *Inorg. Chem.*, 34 (1995) 1868.
- [240] A. Ellern, K. Seppelt, *Angew. Chem.*, 107 (1995) 1772; *Angew. Chem. Int. Ed. Engl.*, 34 (1995) 1586.
- [241] K.O. Christe, W.W. Wilson, *Inorg. Chem.*, 27 (1988) 2714.
- [242] W.J. Casteel, Jr., D.A. Dixon, N. LeBlond, H.P.A. Mercier, G.J. Schrobilgen, *Inorg. Chem.*, 37 (1998) 340.
- [243] K.O. Christe, R.D. Wilson, C.J. Schack, *Inorg. Chem.*, 20 (1981) 2104.
- [244] R.J. Gillespie, I. Bytheway, T.H. Tang, R.F. Bader, *Inorg. Chem.*, 35 (1996) 3954.
- [245] A.I. Agulyanskii, V.A. Bessonova, V.Ya. Kuznetsov, V.T. Kalinnikov, *Russ. J. Inorg. Chem.*, 31 (1986) 1547; *Zh. Neorg. Khim.*, 31 (1986) 2683.
- [246] J.K. Ghosh, G.V. Jere, *J. Fluorine Chem.*, 35 (1987) 669.
- [247] A. Bodner, P. Jeske, T. Weyhermüller, K. Wieghardt, E. Dubler, H. Schmalle, B. Nuber, *Inorg. Chem.*, 31 (1992) 3737.
- [248] H.W. Roesky, I. Leichtweis, M. Noltemeyer, *Inorg. Chem.*, 32 (1993) 5102.
- [249] A. Arquis-Canouet, J. Ravez, J.P. Chaminade, P. Hagenmuller, S.C. Abrahams, P. Marsh, *J. Appl. Phys.*, 60 (1986) 357.
- [250] G. Pausewang, R. Schmidt, *Z. Anorg. Allg. Chem.*, 523 (1985) 213.
- [251] M. Schabert, G. Pausewang, *Z. Anorg. Allg. Chem.*, 559 (1988) 143.
- [252] M.P. Crosnier, J.L. Fourquet, *J. Solid State Chem.*, 99 (1992) 355.
- [253] M.P. Crosnier, J.L. Fourquet, *Eur. J. Solid State Chem.*, 29 (1992) 199.
- [254] J. Patarin, F. Marcuccilli-Hoffner, H. Kessler, *Eur. J. Solid State Inorg. Chem.*, 31 (1994) 501.
- [255] R. Schmidt, G. Pausewang, *Z. Anorg. Allg. Chem.*, 575 (1989) 197.
- [256] R. Schmidt, G. Pausewang, *Z. Anorg. Allg. Chem.*, 537 (1986) 175.
- [257] M.K. Chaudhuri, B. Das, *Inorg. Chem.*, 25 (1986) 168.
- [258] M.K. Chaudhuri, B. Das, *Polyhedron*, 4 (1985) 1449.
- [259] R. Schmidt, G. Pausewang, *Z. Anorg. Allg. Chem.*, 559 (1988) 135.
- [260] J.K. Ghosh, G. Ghosh, *J. Fluorine Chem.*, 38 (1988) 183.
- [261] A.K. Sengupta, U. Bhattacharyya, *J. Fluorine Chem.*, 46 (1990) 229.
- [262] A. Mikou, J.-P. Laval, B. Frit, J. Senegas, *Rev. Chim. Min.*, 22 (1985) 115.
- [263] R. Schlichenmaier, E. Schweda, J. Strähle, T. Vogt, *Z. Anorg. Allg. Chem.*, 619 (1993) 367.
- [264] R. Schmidt, G. Pausewang, W. Massa, *Z. Anorg. Allg. Chem.*, 535 (1986) 135.
- [265] C.R. Bhattacharjee, M. Bhattacharjee, M.K. Chaudhuri, S. Choudhury, *Polyhedron*, 9 (1990) 1653.
- [266] B.H. Chernyshov, N.A. Didenko, B.V. Bukvetskii, A.V. Gerasimenko, V.Ya. Kavun, S.S. Sergienko, *Russ. J. Inorg. Chem.*, 34 (1989) 1594; *Zh. Neorg. Khim.*, 34 (1989) 2786.
- [267] M.C. Caracoche, J.A. Martínez, P.C. Rivas, A.R. López Garia, *Hyperfine Interact.*, 23 (1985) 221.
- [268] C. Ninclaus, D. Riou, G. Férey, *J. Chem. Soc., Chem. Commun.*, (1997) 851.
- [269] M.P. Crosnier-Lopez, H. Duroy, J.L. Fourquet, M. Abrabri, *Eur. J. Solid State Inorg. Chem.*, 31 (1994) 957.
- [270] R. Stomberg, *Acta Chem. Scand.*, A40 (1986) 325.
- [271] M. Leimkühler, R. Mattes, *J. Solid State Chem.*, 65 (1986) 260.

- [272] N. Buchholz, M. Leimkühler, L. Kiriazis, R. Mattes, *Inorg. Chem.*, 27 (1988) 2035.
- [273] M.P. Crosnier-Lopez, H. Duroy, J.L. Fourquet, *Z. Anorg. Allg. Chem.*, 619 (1993) 1597.
- [274] U.R.K. Rao, K.S. Venkateswarlu, B.N. Wani, *J. Fluorine Chem.*, 31 (1986) 29.
- [275] R.C. Hibbert, *J. Chem. Soc., Chem. Commun.*, (1985) 317.
- [276] R.C. Hibbert, *J. Chem. Soc., Dalton Trans.*, (1986) 751.
- [277] M. Hilbers, M. Leimkühler, R. Mattes, *Z. Naturforsch.*, B44 (1989) 383.
- [278] H.W. Roesky, M. Zimmer, H.G. Schmidt, M. Noltemeyer, *Z. Naturforsch.*, B43 (1988) 1490.
- [279] A.E. Lapshin, Y.I. Smolin, Y.F. Shepelev, P. Schwendt, D. Gyepesova, *Acta Crystallogr.*, C46 (1990) 1753.
- [280] K. Westermann, M. Leimkühler, R. Mattes, *J. Less Comm. Met.*, 137 (1988) 181.
- [281] J. Darriet, Q. Xu, A. Tressaud, *Acta Crystallogr.*, 43C (1987) 224.
- [282] M. Schabert, G. Pausewang, *Z. Naturforsch.*, B40 (1985) 1437.
- [283] M.P. Crosnier-Lopez, H. Duroy, J.L. Fourquet, *Z. Anorg. Allg. Chem.*, 620 (1994) 309.
- [284] H.-G. Nieder-Vahrenholz, H. Schäfer, *Z. Anorg. Allg. Chem.*, 544 (1987) 122.
- [285] P.S. Halasyamani, M.J. Willis, C.L. Stern, P.M. Lundquist, G.K. Wong, K.R. Poeppelmeier, *Inorg. Chem.*, 35 (1996) 1367.
- [286] P.S. Halasyamani, M.J. Willis, K.R. Heier, C.L. Stern, K.R. Poeppelmeier, *Acta Crystallogr.*, C52 (1996) 2491.
- [287] P.S. Halasyamani, K.R. Heier, A.J. Norquist, C.L. Stern, K.R. Poeppelmeier, *Inorg. Chem.*, 37 (1998) 369.
- [288] A.I. Agulyanskii, E.L. Tikhomirova, V.Ya. Kuznetsov, V.T. Kalinnikov, *Russ. J. Inorg. Chem.*, 33 (1988) 47; *Zh. Neorg. Khim.*, 33 (1988) 85.
- [289] A.I. Agulyanskii, E.L. Tikhomirova, V.T. Kalinnikov, *Russ. J. Inorg. Chem.*, 33 (1988) 654; *Zh. Neorg. Khim.*, 33 (1988) 1155.
- [290] D.V. Tsikaeva, S.D. Nikitina, A.I. Agulyanskii, V.T. Kalinnikov, *J. Gen. Chem. USSR*, 57 (1987) 866; *Zh. Obsh. Khim.*, 57 (1987) 974.
- [291] D.V. Tsikaeva, A.I. Agulyanskii, Yu.I. Balabanov, V.Ya. Kuznetsov, V.T. Kalinnikov, *Russ. J. Inorg. Chem.*, 34 (1989) 1740; *Zh. Neorg. Khim.*, 34 (1989) 3046.
- [292] A.I. Agulyanskii, V.E. Zavodnik, V.Ya. Kuznetsov, N.V. Sidorov, S.Yu. Stefanovich, D.V. Tsikaeva, V.T. Kalinnikov, *Inorg. Mater.*, 27 (1991) 880; *Izv. Akad. Nauk SSSR, Neorg. Mat.*, 27 (1991) 1055.
- [293] M.P. Crosnier-Lopez, J.L. Fourquet, *J. Solid State Chem.*, 105 (1993) 92.
- [294] M.P. Crosnier-Lopez, J.L. Fourquet, *J. Solid State Chem.*, 103 (1993) 131.
- [295] M.P. Crosnier-Lopez, H. Duroy, J.L. Fourquet, *J. Solid State Chem.*, 107 (1993) 211.
- [296] M.P. Crosnier-Lopez, Y. Laligand, J.L. Fourquet, *Eur. J. Solid State Inorg. Chem.*, 30 (1993) 155.
- [297] Ö. Sävborg, M. Lundberg, *J. Solid State Chem.*, 57 (1985) 135.
- [298] Ö. Sävborg, *J. Solid State Chem.*, 57 (1985) 143.
- [299] R. Geetha, P.S. Rao, V. Babu, S. Subramanian, *Inorg. Chem.*, 30 (1991) 1630.
- [300] J. Köhler, A. Simon, *Angew. Chem.*, 98 (1986) 1011; *Angew. Chem., Int. Ed. Engl.*, 25 (1986) 996.
- [301] G.L. Gard, *Inorg. Synth.*, 24 (1986) 67.
- [302] A.K. Brisdon, J.H. Holloway, E.G. Hope, *J. Fluorine Chem.*, 89 (1998) 35.
- [303] W. Levason, J.S. Ogden, A.K. Saad, N.A. Young, A.K. Brisdon, P.J. Holliman, J.H. Holloway, E.G. Hope, *J. Fluorine Chem.*, 53 (1991) 43.
- [304] K.O. Christe, W.W. Wilson, R.A. Bougon, *Inorg. Chem.*, 25 (1986) 2163.
- [305] J.F. Huang, K. Hedberg, J.M. Shreeve, S.P. Mallela, *Inorg. Chem.*, 27 (1988) 4633.

- [306] E.G. Hope, P.J. Jones, W. Levason, J. S. Ogden, M. Tajik, J.W. Turff, *J. Chem. Soc., Dalton Trans.* (1985) 529.
- [307] W.W. Wilson, K.O. Christe, *J. Fluorine Chem.*, 35 (1987) 531.
- [308] M. McHughes, R.D. Willett, H.B. Davis, G.L. Gard, *Inorg. Chem.*, 25 (1986) 426.
- [309] J-M. Moutou, J-P. Chaminade, M. Pouchard, P. Hagenmuller, *Rev. Chim. Min.*, 23 (1986) 27.
- [310] J.P. Chaminade, J.M. Moutou, G. Villeneuve, M. Couzi, M. Pouchard, P. Hagenmuller, *J. Solid State Chem.*, 65 (1986) 27.
- [311] J.L. Fourquet, H. Duroy, M.P. Crosnier-Lopez, *Z. Anorg. Allg. Chem.*, 623 (1997) 439.
- [312] B. Kamenar, B. Kaitner, N. Strukan, *Acta Crystallogr.*, C46 (1990) 2249.
- [313] M. Rhiel, S. Wocadlo, W. Massa, K. Dehnicke, *Z. Anorg. Allg. Chem.*, 622 (1996) 1195.
- [314] I. Sens, H. Stenger, U. Müller, K. Dehnicke, *Z. Anorg. Allg. Chem.*, 610 (1992) 117.
- [315] M. Leimkühler, N. Buchholz, R. Mattes, *Z. Naturforsch.*, B44 (1989) 389.
- [316] B.F. Hoskins, A. Linden, T.A. O'Donnell, *Inorg. Chem.*, 26 (1987) 2223.
- [317] R. Stomberg, *J. Cryst. Spec. Res.*, 18 (1988) 659.
- [318] R. Stomberg, *J. Less Comm. Met.*, 144 (1988) 109.
- [319] R. Stomberg, *Acta Chem. Scand.*, A42 (1988) 284.
- [320] G. Ramakrishna, P.S. Rao, S. Subramanian, *J. Chem. Soc., Dalton Trans.*, (1991) 3185.
- [321] M.C. Chakravorti, D. Bandyopadhyay, *Polyhedron*, 7 (1988) 1135.
- [322] C.C. Torardi, L.H. Brixner, *Mat. Res. Bull.*, 20 (1985) 137.
- [323] S.C. Abrahams, P. Marsh, J. Ravez, *J. Chem. Phys.*, 87 (1987) 6012.
- [324] J.P. Laval, A. Taoudi, *J. Solid State Chem.*, 115 (1995) 283.
- [325] J.K. Gibson, *J. Fluorine Chem.*, 55 (1991) 299.
- [326] L. Arnaudet, R. Bougon, B. Ban, P. Charpin, J. Isabey, M. Lance, M. Nierlich, J. Vigner, *Can. J. Chem.*, 68 (1990) 507.
- [327] R. Wollert, E. Rentschler, W. Massa, K. Dehnicke, *Z. Anorg. Allg. Chem.*, 596 (1991) 121.
- [328] A.M. Srivastava, J.F. Ackerman, *J. Solid State Chem.*, 98 (1992) 144.
- [329] W.W. Wilson, K.O. Christe, *Inorg. Synth.*, 24 (1986) 37.
- [330] L. Arnaudet, R. Bougon, B. Ban, M. Lance, A. Navaza, M. Nierlich, J. Vigner, *J. Fluorine Chem.*, 59 (1992) 141.
- [331] M.C. Crossman, J. Fawcett, E.G. Hope, D.R. Russell, *J. Organomet. Chem.*, 514 (1996) 87.
- [332] Y. Katayama, R. Hagiwara, Y. Ito, *J. Fluorine Chem.*, 74 (1995) 89.
- [333] L. Arnaudet, R. Bougon, B. Ban, P. Charpin, J. Isabey, M. Lance, M. Nierlich, J. Vigner, *Inorg. Chem.*, 28 (1989) 257.
- [334] L. Arnaudet, R. Bougon, B. Buu, *J. Fluorine Chem.*, 74 (1995) 223.
- [335] L. Arnaudet, R. Bougon, B. Buu, M. Lance, M. Nierlich, J. Vigner, *Inorg. Chem.*, 32 (1993) 1142.
- [336] L. Arnaudet, R. Bougon, B. Ban, M. Lance, W.C. Kaska, *J. Fluorine Chem.*, 53 (1991) 171.
- [337] T.L. Jorris, M. Kozik, L.C.W. Baker, *Inorg. Chem.*, 29 (1990) 4584.
- [338] S.H. Wasfi, C.E. Costello, A.L. Rheingold, B.S. Haggerty, *Inorg. Chem.*, 30 (1991) 1788.
- [339] S.H. Wasfi, S.A. Tribbitt, *Inorg. Chim. Acta*, 268 (1998) 329.
- [340] A.K. Brisdon, J.H. Holloway, E.G. Hope, P.J. Towson, W. Levason, J.S. Ogden, *J. Chem. Soc., Dalton Trans.*, (1991) 3127.

- [341] H.P.A. Mercier, G.J. Schrobilgen, *Inorg. Chem.*, 32 (1993) 145.
- [342] W.J. Casteel, Jr., N. LeBlond, P.E. Lock, H.P.A. Mercier, D.M. MacLeod, G.J. Schrobilgen, *J. Fluorine Chem.*, 71 (1995) 181.
- [343] N. LeBlond, G.J. Schrobilgen, *J. Chem. Soc., Chem. Commun.*, (1996) 2479.
- [344] W.J. Casteel, Jr., D.A. Dixon, N. LeBlond, P.E. Lock, H.P.A. Mercier, G.J. Schrobilgen, *Inorg. Chem.*, 38 (1999) 2340.
- [345] W.J. Casteel, Jr., D.A. Dixon, H.P.A. Mercier, G.J. Schrobilgen, *Inorg. Chem.*, 35 (1996) 4310.
- [346] S. Giese, K. Seppelt, *Angew. Chem.*, 106 (1994) 473; *Angew. Chem., Int. Ed. Engl.*, 33 (1994) 461.
- [347] Y.A. Politov, V.D. Butskii, O.G. Ellert, V.S. Pervov, *Russ. J. Inorg. Chem.*, 32 (1987) 290; *Zh. Neorg. Khim.*, 32 (1987) 520.
- [348] J.H. Holloway, E.G. Hope, P.J. Townson, R.L. Powell, *J. Fluorine Chem.*, 76 (1996) 105.
- [349] S. Ghosh, A.K. Sengupta, B.B. Bhaumik, *J. Fluorine Chem.*, 76 (1996) 125.
- [350] L. Meublât, M. Lance, R. Bougon, *Can. J. Chem.*, 67 (1989) 1729.
- [351] A.K. Brisdon, E.G. Hope, J.H. Holloway, W. Levason, J.S. Ogden, *J. Fluorine Chem.*, 64 (1993) 117.
- [352] E.G. Rakov, A.V. Dzhalyan, *Russ. J. Inorg. Chem.*, 32 (1987) 477; *Zh. Neorg. Khim.*, 32 (1987) 853.
- [353] B.N. Ivanov-Emin, N.A. Nevskaya, Y.N. Medvedev, B.E. Zaitsev, I.V. Lin'ko, *Russ. J. Inorg. Chem.*, 31 (1986) 1088; *Zh. Neorg. Khim.*, 31 (1986) 1889.
- [354] S.A. Brewer, A.K. Brisdon, J.H. Holloway, E.G. Hope, W. Levason, J.S. Ogden, A. K. Saad, *J. Fluorine Chem.*, 60 (1993) 13.
- [355] R. Bougon, B. Buu, K. Seppelt, *Chem. Ber.*, 126 (1993) 1331.
- [356] R. Bougon, W.V. Cicha, J. Isabey, *J. Fluorine Chem.*, 67 (1994) 271.
- [357] E.G. Hope, W. Levason, J.S. Ogden, *J. Chem. Soc., Dalton Trans.* (1988) 61.
- [358] R. Bougon, *J. Fluorine Chem.*, 53 (1991) 419.
- [359] K.O. Christe, R. Bougon, *J. Chem. Soc., Chem. Comm.* (1992) 1056.
- [360] K.O. Christe, D.A. Dixon, H.G. Mack, H. Oberhammer, A. Pagelot, J.C.P. Sanders, G.J. Schrobilgen, *J. Am. Chem. Soc.*, 115 (1993) 11279.
- [361] E.G. Hope, W. Levason, J.S. Ogden, *J. Chem. Soc., Dalton Trans.*, (1988) 997.
- [362] J.H. Holloway, E.G. Hope, J.B. Raynor, P.T. Townson, *J. Chem. Soc., Dalton Trans.*, (1992) 1131.
- [363] A. Aftati, J.-C. Champarnaud-Mesjard, B. Frit, *Eur. J. Solid State Inorg. Chem.*, 30 (1993) 1063.

CHAPTER 6

Oxide Fluorides of Rare Earth Elements

Masayuki Takashima,

*Department of Materials Science and Engineering, Faculty of Engineering, Fukui University, 3-9-1
Bunkyo, Fukui 910-8507 Japan*

6.1 Introduction

The rare earths are the general term for 17 elements including Sc, Y and the lanthanides (Ln), La, Ce, Pr, Nd, [Pm], Sm, Eu, Gd, Tb, Dy, Ho, Er, Tm, Yb and Lu. Ln is the general symbol for the lanthanides; however, in this chapter Sc and Y will be also written as Ln. The lanthanides are referred to as the inner-transition elements because, after lanthanum with the outermost electronic configuration of $5d^1 6s^2$, the additional electrons occupy more readily the inner and well-shielded 4f level than the 5d. The seven 4f orbitals, each with a capacity of two electrons, are filled before additional 5d electrons appear. Fourteen elements from cerium to lutetium are in the 4f inner-transition group. It can be seen that the rare earths have very similar chemical properties determined by the common outer electronic configuration of Sc^{3+} with $3s^2 3p^6$, Y^{3+} with $4s^2 4p^6$ and Ln^{3+} with $5s^2 5p^6$. The small differences in the properties arise principally from the so-called lanthanide contraction. As shown in Table 1, the contraction is quite regular in Ln^{3+} ions. On the basis of size relationships alone, we should expect a decrease in the basicity of Ln^{3+} ions. Therefore, the electron affinity of Ln^{3+} ions, except for Sc^{3+} and Y^{3+} , tends to be enhanced with increasing atomic number. This affects chemical properties such as the pyro-hydrolysis of lanthanide fluorides and the stability of complexes, $\text{Ln}^{3+}[\text{EDTA}][1]$. This contraction is also reflected in decreasing values for the standard redox potential. The stable ionic charge throughout the rare earths is trivalent. The La^{3+} ($4f^0$), Gd^{3+} ($4f^7$) and Lu^{3+} ($4f^{14}$) ions are invariable. The lower charge of the Ln^{2+} ion occurs with Sm, Eu, Tm and Yb. Regarding the higher, Ce^{4+} , Tb^{4+} and Pr^{4+} exist stably in CeO_2 , Tb_4O_7 and Pr_6O_{11} . Nd^{4+} has been presumed to be possible. The chemical properties of the early members of the series are similar to those of calcium, and with increasing atomic number, other properties more like those of aluminum appear.

The rare earths are the key elements in producing useful materials among which are alloys, intermetallics and large numbers of nonmetallic compounds such as oxides, chalcogenides and halides. These materials have been widely used as func-

Table 1

Oxidation states, ionic size of Ln^{3+} and redox potential of rare-earth elements

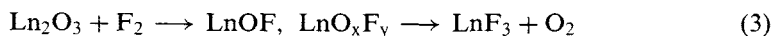
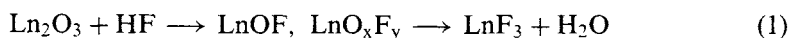
Atomic number	Element	Electronic configuration				Crystal radius r, nm (Ln^{3+})	Standard redox potential, $E^\circ_{273\text{ K}}$, Volt $\text{Ln}^{3+}(\text{aq.}) + 3\text{e} = \text{Ln}(\text{s})$
		Ln	Ln^{2+}	Ln^{3+}	Ln^{4+}		
21	Sc	$3\text{d}^1 4\text{s}^2$		$3\text{s}^2 3\text{p}^6$		0.068	-2.08
39	Y	$4\text{d}^1 5\text{s}^2$		$4\text{s}^2 4\text{p}^6$		0.088	-2.37
57	La	$5\text{d}^1 6\text{s}^2$		$5\text{s}^2 5\text{p}^6$		0.104	-2.52
58	Ce	$4\text{f}^2 6\text{s}^2$		$4\text{f}^1 5\text{s}^2 5\text{p}^6$	$5\text{s}^2 5\text{p}^6$	0.102	-2.48
59	Pr	$4\text{f}^3 6\text{s}^2$		$4\text{f}^2 5\text{s}^2 5\text{p}^6$	$4\text{f}^1 5\text{s}^2 5\text{p}^6$	0.100	-2.47
60	Nd	$4\text{f}^4 6\text{s}^2$		$4\text{f}^3 5\text{s}^2 5\text{p}^6$	$(4\text{f}^2 5\text{s}^2 5\text{p}^6)$	0.099	-2.44
61	[Pm]	$4\text{f}^5 6\text{s}^2$		$4\text{f}^4 5\text{s}^2 5\text{p}^6$		0.098	-2.42
62	Sm	$4\text{f}^6 6\text{s}^2$	$4\text{f}^6 5\text{s}^2 5\text{p}^6$	$4\text{f}^5 5\text{s}^2 5\text{p}^6$		0.097	-2.41
63	Eu	$4\text{f}^7 6\text{s}^2$	$4\text{f}^7 5\text{s}^2 5\text{p}^6$	$4\text{f}^6 5\text{s}^2 5\text{p}^6$		0.096	-2.41
64	Gd	$4\text{f}^7 5\text{d}^1 6\text{s}^2$		$4\text{f}^7 5\text{s}^2 5\text{p}^6$		0.094	-2.40
65	Tb	$4\text{f}^9 6\text{s}^2$		$4\text{f}^8 5\text{s}^2 5\text{p}^6$	$4\text{f}^7 5\text{s}^2 5\text{p}^6$	0.092	-2.39
66	Dy	$4\text{f}^{10} 6\text{s}^2$		$4\text{f}^9 5\text{s}^2 5\text{p}^6$		0.091	-2.35
67	Ho	$4\text{f}^{11} 6\text{s}^2$		$4\text{f}^{10} 5\text{s}^2 5\text{p}^6$		0.089	-2.32
68	Er	$4\text{f}^{12} 6\text{s}^2$		$4\text{f}^{11} 5\text{s}^2 5\text{p}^6$		0.087	-2.30
69	Tm	$4\text{f}^{13} 6\text{s}^2$	$4\text{f}^{13} 5\text{s}^2 5\text{p}^6$	$4\text{f}^{12} 5\text{s}^2 5\text{p}^6$		0.086	-2.28
70	Yb	$4\text{f}^{13} 6\text{s}^2$	$4\text{f}^{14} 5\text{s}^2 5\text{p}^6$	$4\text{f}^{13} 5\text{s}^2 5\text{p}^6$		0.085	-2.27
71	Lu	$4\text{f}^{14} 5\text{d}^1 6\text{s}^2$		$4\text{f}^{14} 5\text{s}^2 5\text{p}^6$		0.084	-2.25

tional substances with magnetic, optic, electro-optic, ferroelectric, super-electronic and -ionic conductive, nuclear properties and so on. Almost all of these functional materials of the rare earths used practically are complex oxides with the structures of perovskite, garnet, pyrochlore, fluorite and glass [2-4]. Except for oxides, rare-earth fluorides have been utilized in the optical devices [5]. These useful properties of the functional metal oxides would originate from the partial covalency of the M—O bond and the variety of crystal structures. It is expected that the bond character and the coordination structure would be controlled by introducing the mainly ionic M—F bond into the metal oxides and that we can obtain interesting materials with quite new properties. Similar in size to the fluoride ion, the oxide ion would be substituted to form the oxide-fluoride compounds with various compositions under the condition that the electrical neutrality of the overall system must be achieved. So far, two reviews of the crystallograph and the crystal chemistry of the simple rare-earth oxide fluorides (Ln—OF) have been prepared [6,7]. Recently, the binary rare-earth oxide fluorides, $\text{Ln}_2\text{Ln}'_2\text{O}_3\text{F}_6$, in which Ln and Ln' are different rare earths, have been reported to be applicable as an oxide ion-conducting solid electrolyte with much higher conductivity than that of stabilized zirconia [8]. In this chapter, first the preparation and the crystal studies of the simple rare-earth oxide fluorides are briefly summarized, and then the electrical properties and the crystal chemistry of binary rare-earth oxide fluorides ($\text{Ln}_2\text{O}_3\text{—Ln}'\text{F}_3$ system) and rare-earth fluoride-stabilized zirconia ($\text{LnF}_3\text{—ZrO}_2$ system) are reviewed.

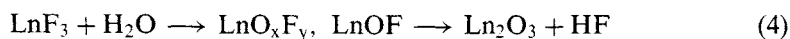
6.2. Preparative methods of rare earth oxide fluorides

The rare-earth oxide fluorides have been prepared using several techniques by the following reactions:

1. Fluorination of rare-earth oxides,

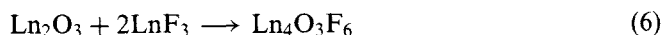


2. Pyro-hydrolysis of rare-earth fluorides,

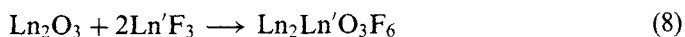
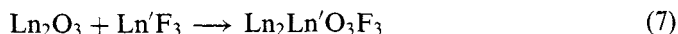


3. Solid-state reaction between rare-earth oxide and rare-earth fluoride,

(a) Single metal system,



(b) Binary metal system,



The rare-earth oxide fluorides have been encountered as contaminants in the preparation of rare-earth trifluorides by reactions (1) [9]. The hydrolysis of metal trifluorides, reaction (2), has been studied by thermo-gravimetric and crystallographic analyses [10–13]. When rare-earth fluorides are kept at a temperature of approximately 800°C in an atmosphere of low humidity, they slowly lose weight. The hydrolysis proceeds until the fluoride is completely converted to oxide. On the weight loss curve vs. heating time, there are two definite breaks corresponding to the conversion of LnF_3 to LnOF and of LnOF to Ln_2O_3 . The kinetic studies of the direct fluorination using elementary fluorine, by reaction (3), have been carried out [14,15]. La_2O_3 , Pr_6O_{11} and Tb_4O_7 violently react with fluorine under a pressure of 2.7×10^4 Pa at room temperature to form trifluorides. The other twelve rare-earth oxides begin to react at ca. 260°C. CeO_2 , Nd_2O_3 , Sm_2O_3 and Eu_2O_3 are completely converted to trifluoride up to 550°C, but the fluorination of sesquioxides of Y, Gd and Dy through Lu is not completed by holding them at 550°C, yielding mixtures of LnF_3 with LnO_xF_y as shown in Fig. 1 and Table 2. That is, in case of a solid-gas reaction such as reaction (1) or (2), the reaction must proceed heterogeneously from the surface of the starting metal oxide, and the simple rare-earth oxide fluoride is formed as an intermediate compound. In addition, the formed rare-earth oxide fluoride is very readily hydrolyzed to the corresponding oxide at a temperature above ca. 700°C even under low humidity as shown in Fig. 2 and Table 3. It is, therefore, very difficult to obtain a rare-earth oxide fluoride separately as a single phase using these solid-gas reactions. In order to prepare the rare-earth oxide fluoride as a single compound in an anhydrous reaction system, the solid-state reactions of Eqns (5–8) should be applied. In the solid state reaction between oxide and fluoride of the same rare-earth metal, simple rare-earth compounds LnOF and $\text{Ln}_4\text{O}_3\text{F}_6$ are formed according to Eqns (5) and (6) [16–18]. From the solid-state reaction systems of Ln-oxide and Ln'-fluoride, where Ln and Ln' are different rare-earths, the binary rare-earth compounds, $\text{LnLn}'\text{O}_3\text{F}_3$ and $\text{Ln}_2\text{Ln}'_2\text{O}_3\text{F}_6$ are synthesized as given by Eqns (7) and (8) [19]. Both the rare-earth fluorides as starting materials and the produced oxide fluorides are easily hydrolyzed at a high temperature above 800°C by residual moisture even in an inert atmosphere; therefore, the reaction system

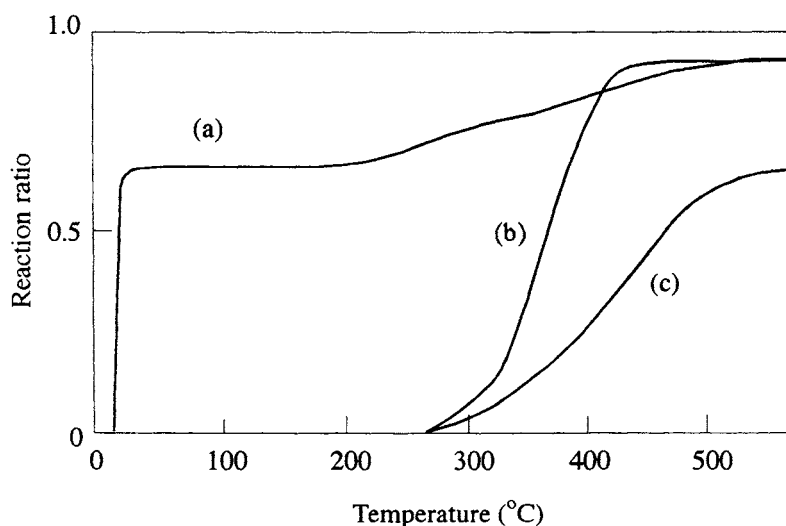


Fig. 1. TG curves for the reactions between rare-earth oxides and elementary fluorine. TG measurement was performed under the fluorine pressure of 2.7×10^4 Pa at the heating rate of 2°C min^{-1} (a) La_2O_3 , Pr_6O_{11} , Tb_4O_7 ; (b) CeO_2 , Nd_2O_3 , Sm_2O_3 , Eu_2O_3 ; (c) Y_2O_3 , Gd_2O_3 , Dy_2O_3 , Ho_2O_3 , Er_2O_3 , Tm_2O_3 , Yb_2O_3 , Lu_2O_3 (reproduced with permission from Eur. J. Solid State Inorg. Chem. 29 (1992) 691 [14]).

Table 2

Reactions between rare earth oxides and fluorine¹

Oxide	Reaction Beginning Temperature °C	Products
Y_2O_3	275	$\text{YF}_3 + \text{Y—OF}$ (Tetra.)
La_2O_3	RT	LaF_3
CeO_2	175	$\text{CeF}_3 + \text{Ce—OF}$
Pr_6O_{11}	RT	PrF_3
Nd_2O_3	265	NdF_3
Sm_2O_3	265	$\text{SmF}_3 + \text{Sm—OF}$
Eu_2O_3	260	EuF_3
Gd_2O_3	255	GdF_3
Tb_4O_7	RT	TbF_3
Dy_2O_3	260	DyF_3
Ho_2O_3	260	$\text{HoF}_3 + \text{Ho—OF}$ (Tetra.)
Er_2O_3	265	$\text{ErF}_3 + \text{Er—OF}$ (Tetra.)
Tm_2O_3	265	$\text{TmF}_3 + \text{Tm—OF}$ (Tetra.)
Yb_2O_3	260	$\text{YbF}_3 + \text{Yb—OF}$ (Tetra.)
Lu_2O_3	255	$\text{LuF}_3 + \text{Lu—OF}$ (Tetra.)

¹Heating rate, 2°C/min ; Fluorine pressure, 27 kPa. Products when heating to 550°C .

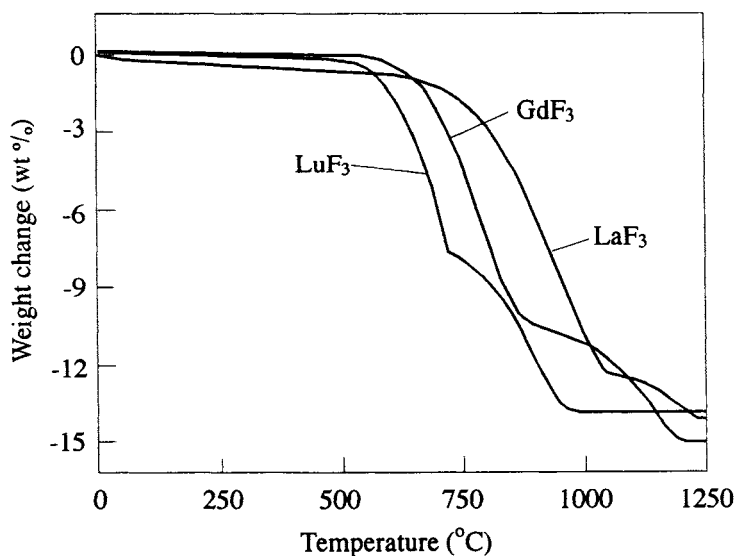


Fig. 2. TG curves for pyro-hydrolysis of rare-earth fluorides in an ordinary atmosphere. TG measurement was performed under the water vapour pressure of 1.8×10^3 Pa at the heating rate of 5°C min^{-1} .

Table 3

Pyro-hydrolysis of rare earth fluorides¹

Fluoride	Reaction Beginning Temperature $^\circ\text{C}$	Products
YF ₃	700	YOF (Rhomb.)
LaF ₃	770	LaF ₃ + La—OF (Tetra.)
CeF ₃	515	CeO ₂
PrF ₃	720	PrOF (Rhomb.)
NdF ₃	695	NdOF (Rhomb.)
SmF ₃	675	SmOF (Rhomb.)
EuF ₃	665	EuOF (Rhomb.) + Eu ₂ O ₃
GdF ₃	670	GdOF (Rhomb.) + Gd ₂ O ₃
TbF ₃	670	TbOF (Rhomb.) + TbO _x
DyF ₃	650	DyOF (Rhomb.) + Dy ₂ O ₃
HoF ₃	645	HoOF (Rhomb.) + Ho ₂ O ₃
ErF ₃	645	ErOF (Rhomb.) + Er ₂ O ₃
TmF ₃	630	TmOF (Rhomb.) + Tm ₂ O ₃
YbF ₃	615	YbOF (Hexa.) + Yb ₂ O ₃
LuF ₃	625	Lu ₂ O ₃

¹Heating rate, 5°C/min ; H₂O pressure, 1.8 kPa. Products when heating to 1000°C .

must be kept under a highly dried atmosphere in order to prepare the single phase oxide fluoride without contamination.

6.3. Crystal chemistry and properties of the simple rare-earth metal oxide fluoride

The ionic radii of trivalent rare-earth ions range from Lu^{3+} : 0.084 nm to La^{3+} : 0.104 nm except for Sc^{3+} : 0.068 nm. On the other hand, those of O^{2-} and F^- are 0.120 nm and 0.127 nm, respectively. From the rule of ionic radius ratio for the packing of cation and anion, the coordination number is known to be 8 in the crystal lattice of LnOF. The structure is based on simple cubic packing for the anions and face-centered packing of the cations occupying all sites of the center of the cube. The common octa-coordinated MX_2 structure is the fluorite structure. In the simple rare-earth metal oxide fluorides with fluorite-related structures, three crystal phases of rhombohedral, tetragonal and cubic structure have been identified. The relationships between crystal phases and chemical compositions of rare-earth oxide fluorides have been systematically investigated by several research groups. The first report was on the system of La_2O_3 — LaF_3 [20]. The rhombohedral phase was found to have a stoichiometric composition, LnOF [16,17]. The unit lattice consists of two molecules of LnOF and the space group is $R\bar{3}m$ [16]. ScOF has a monoclinic structure ($P2_1/c$, Cell contents: 4ScOF) [21]. The tetragonal phases were observed as a single phase in the fluorine-rich composition range. The chemical composition of the phase can be written by the general formula $\text{LnO}_x\text{F}_{3-2x}$. The composition ranges, in which the tetragonal phase existed stably as a single phase, were reported to be Y: $x = 0.7$, La: $x = 0.7$, Ce: $x = 0.75$, Nd: $0.73 \leq x \leq 0.85$, Sm: $x = 0.75$, Eu: $x = 0.77$, Gd: $0.75 \leq x \leq 0.83$, Dy: $0.75 \leq x \leq 0.82$, Ho: $0.75 \leq x \leq 0.83$, Er: $0.75 \leq x \leq 0.84$, Tm: $x = 0.75$, and Yb: $x = 0.75$ [18]. The stoichiometric compound, $\text{Ln}_4\text{O}_3\text{F}_6$ (when $x = 0.75$), is formed by the reaction of 2 mol: LnF_3 with 1 mol: Ln_2O_3 . This composition contains an excess fluorine over the amount which can be accommodated in a fluorite structure of MX_2 : $\text{Ln}_4\text{O}_3\text{F}_5$. The excess fluorine must occupy interstitial sites. The arrangement of anions not only in the rhombohedral but also in the tetragonal forms of LnOF was believed to be ordered [22]. The cubic phase, in which the arrangement of anions must be disordered, was reported to be the phase at a high temperature [23]. The structure transition from both rhombohedral (SmOF) and tetragonal ($\text{Sm}_4\text{O}_3\text{F}_6$) phases to the cubic phase was observed after quenching from a high temperature around 1200°C [13,24]. The cubic NdOF was reported to be obtained by quenching after the reaction between 1 mol: NdF_3 and 1 mol: Nd_2O_3 at 1250°C [24]. The transition temperatures from the rhombohedral to the cubic for various LnOF materials were measured to be ca. 500°C for EuOF as the lowest and ca. 600°C for GdOF as the highest [13,25]. It was, however, difficult to determine the accurate phase diagram for the LnF_3 — Ln_2O_3 system because the transition temperature cannot be measured clearly by differential thermal analysis [17,18]. Before around 1970, some efforts were made to determine the crystal structures of ScOF and YOF [26–28], but it was not clear how to prepare a single crystal. There was no report on the growth of single crystals of the simple rare-earth metal oxide

fluorides. The lattice parameters of rhombohedral LnOF and tetragonal $\text{LnO}_x\text{F}_{3-2x}$ are summarized in Table 4.

To date, only a little has been known about the physical properties of rare-earth oxide fluorides. About the functional properties of the simple rare-earth metal oxide fluorides, there are only a couple of reports on the catalytic and fluorescence properties. The catalytic properties of LaOF for oxidative coupling with methane were investigated [29]. The LaOF catalyst was assumed to have ample stoichiometric defects and to generate active sites suitable for the methane dehydrogenation [29]. The cubic NdOF obtained by quenching from 1250°C was reported to be electro-catalytically active for both hydrogen oxidation and oxygen reduction [25]. The fluorescence properties arising from UV-excitation of LaOF and YOF activated by doping with 5% Tb^{3+} were studied [30]. Both oxide fluorides showed a maximum quantum efficiency of 40–45%, but their radiant efficiencies were too low (less than 1% under 20 kV UV-excitation) [29]. Solid solutions of YOF with ThO_2 or HfO_2 were applicable as a refractory for molten reactive metals such as titanium, niobium and zirconium [31]. The magnetic susceptibilities of LnOF compounds except for La, Sm and Lu were shown to depend on the Curie–Weiss law [32].

6.4. Preparation and properties of the binary rare-earth oxide fluoride

6.4.1 Formation reaction

As mentioned in section 6.2, binary rare-earth oxide fluorides, $\text{LnLn}'\text{O}_x\text{F}_y$, where Ln and Ln' are different rare-earth elements coming respectively from Ln_2O_3 and $\text{Ln}'\text{F}_3$

Table 4

Lattice parameters of the rhombohedral LnOF and the tetragonal $\text{LnO}_x\text{F}_{3-2x}$, ($0.7 \leq x \leq 0.75$) [16–18]

LnOF	a_o (nm)	α (degree)	$\text{LnO}_x\text{F}_{3-2x}$	a_o (nm)	c_o (nm)
YOF	0.6697	33.20	$\text{YO}_{0.7}\text{F}_{1.6}$	0.393	0.546
LaOF	0.7132	33.01	$\text{LaO}_{0.7}\text{F}_{1.6}$	0.4098	0.5840
CeOF	0.7075	33.00	$\text{CeO}_{0.75}\text{F}_{1.5}$	0.577	0.574
PrOF	0.7018	33.03	$\text{PrO}_{0.75}\text{F}_{1.5}$	0.571	0.5758
NdOF	0.6953	33.04	$\text{NdO}_{0.74}\text{F}_{1.56}$	0.5676	0.572
SmOF	0.6863	33.10	$\text{SmO}_{0.75}\text{F}_{1.5}$	0.5643	0.5602
EuOF	0.6828	33.05	$\text{EuO}_{0.75}\text{F}_{1.5}$	0.5623	0.5574
GdOF	0.6801	33.05	$\text{GdO}_{0.75}\text{F}_{1.5}$	0.5595	0.5527
TbOF	0.6751	33.09	$\text{TbO}_{0.75}\text{F}_{1.5}$	0.5575	0.5491
DyOF	0.6719	33.02	$\text{DyO}_{0.75}\text{F}_{1.5}$	0.5559	0.5456
HoOF	0.6687	33.02	$\text{HoO}_{0.75}\text{F}_{1.5}$	0.5539	0.5414
ErOF	0.6639	33.10	$\text{ErO}_{0.75}\text{F}_{1.5}$	0.5524	0.5379
TmOF	0.6604	33.06	$\text{TmO}_{0.75}\text{F}_{1.5}$	0.5513	0.5355
YbOF	0.6569	33.04	$\text{YbO}_{0.75}\text{F}_{1.5}$	0.5498	0.5323
LuOF	0.6536	33.05	$\text{LuO}_{0.75}\text{F}_{1.5}$	0.5482	0.5308

as starting materials, are obtained only by the solid-state reaction between Ln_2O_3 and $\text{Ln}'\text{F}_3$ at a temperature of more than 1000°C [19]. The anhydrous sesquioxides and trifluorides of rare earths, CeO_2 , Pr_6O_{11} and Tb_4O_7 , are commercially available in a purity of 99.9–99.99%. Because both rare-earth fluoride starting materials and oxide fluoride products are very moisture-sensitive at a temperature higher than 700°C , in addition to sufficient dehydration of starting materials, all the preparative operations such as powdering, mixing and firing must be carried out in an atmosphere as dry as possible. The solid-state reaction path examined by X-ray powder diffraction is shown in Fig. 3. In the solid-state reaction, the anion exchange reaction between Ln_2O_3 and $\text{Ln}'\text{F}_3$ begins to take place even at 200°C and proceeds up to around 600°C until two simple rare-earth oxide fluorides of rhombohedral LnOF and tetragonal $\text{Ln}'_{2-x}\text{O}_{3+x}\text{F}_{3(2-x)}$ are formed as intermediates. At a temperature higher than around 900°C , the mutual diffusion of rare-earth cations between both simple rare-earth oxide fluorides occurs to form the binary rare-earth oxide fluoride. Figure 4 shows the examples of X-ray powder diffraction patterns of the products prepared by the reaction between 1 mol: Nd_2O_3 and 2 mol: EuF_3 at various temperatures [33]. The product obtained at 1000°C shows the diffraction profile of a mono-phase which is identified to be a tetragonal structure, as indicated by the Miller indices given in Fig. 4. Because the decrease in the mass of the starting mixture due to pyro-hydrolysis can be controlled to be negligible during the sample firing at

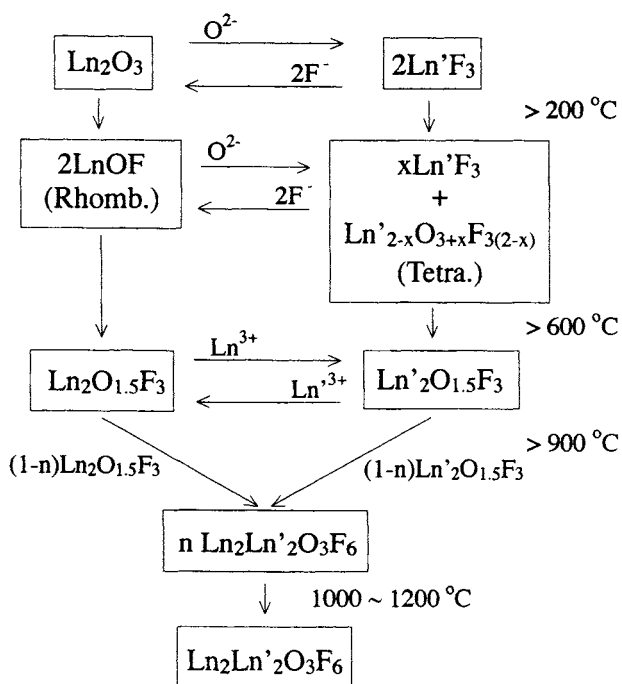


Fig. 3. The route of formation reaction of binary rare-earth oxide fluorides, $\text{Ln}_2\text{Ln}'_2\text{O}_3\text{F}_6$.

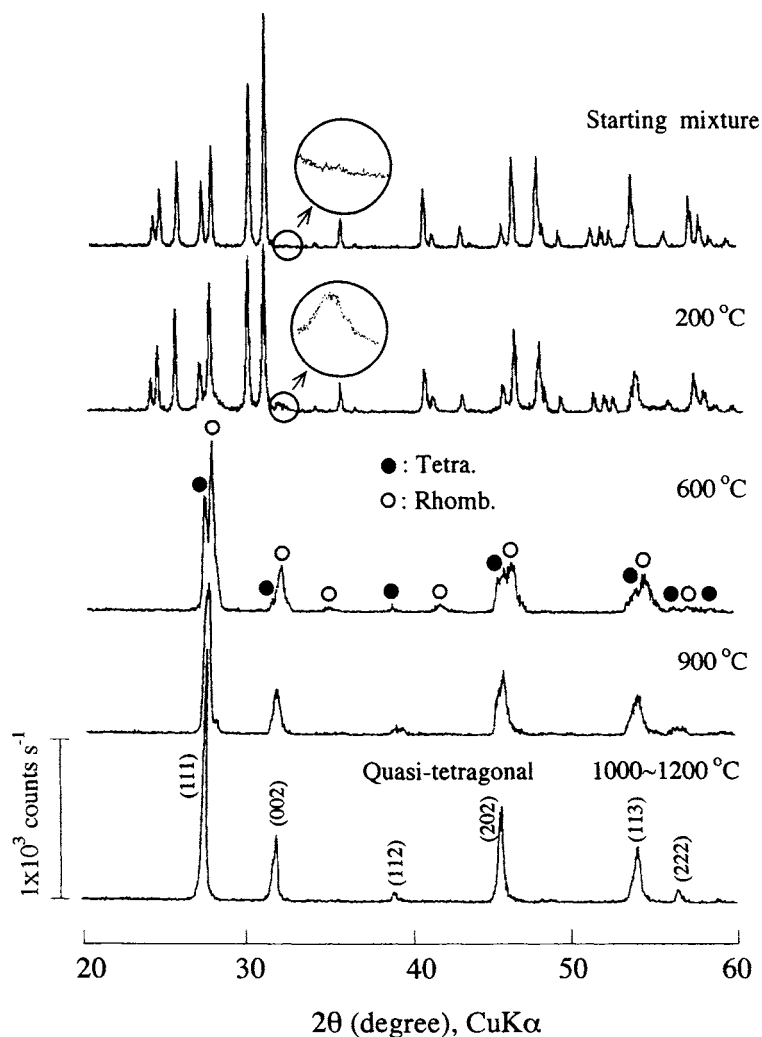


Fig. 4. X-Ray diffraction profiles of products obtained at various temperatures from the mixture of 1 mol: Nd_2O_3 and 2 mol: EuF_3 .

1000°C by processing under a highly dried atmosphere, $\text{Nd}_2\text{Eu}_2\text{O}_3\text{F}_6$ is considered to be produced stoichiometrically from the 1 mol: Nd_2O_3 to 2 mol: EuF_3 system. The phase regions in the products prepared from various systems of Ln_2O_3 and $\text{Ln}'\text{F}_3$ are illustrated against the nominal composition of $\text{Ln}'\text{F}_3$ (Fig. 5). Two mono-phases of the rhombohedral and the tetragonal exist in the binary rare-earth oxide fluorides in the same way as in the simple rare-earth oxide fluorides. The rhombohedral mono-phase appears within a narrow composition range around 50 mol% $\text{Ln}'\text{F}_3$. This suggests that the rhombohedral mono-phase is a stoichiometric compound, $\text{Ln}_2\text{Ln}'\text{O}_3\text{F}_3$. On the other hand, the tetragonal mono-phase appears over a wide

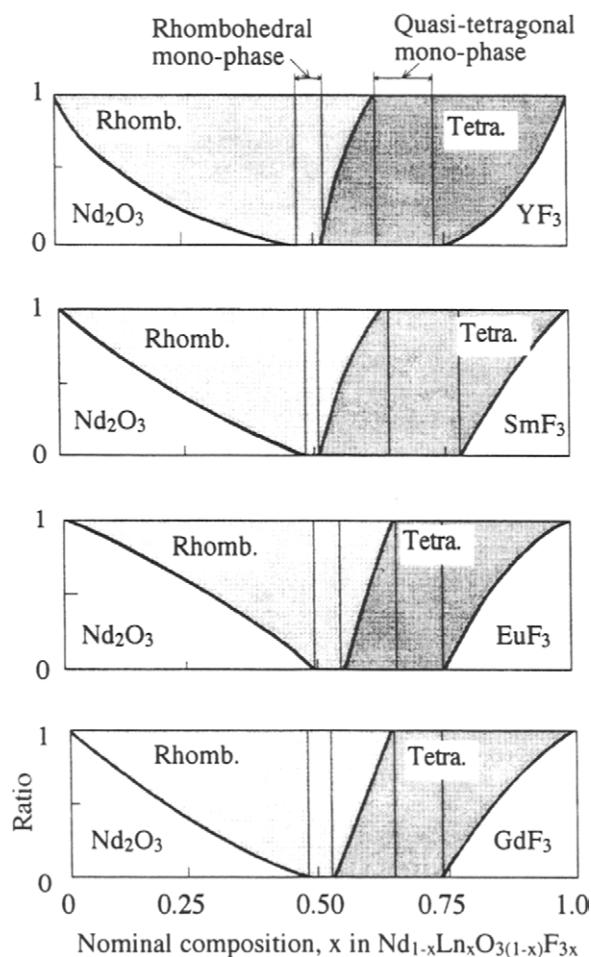


Fig. 5. Phase regions of rhombohedral and tetragonal $\text{Nd}_{1-x}\text{Ln}_x\text{O}_{3(1-x)}\text{F}_{3x}$.

composition range from 65 to 78 mol% $\text{Ln}'\text{F}_3$. $\text{Ln}_2\text{Ln}'_2\text{O}_3\text{F}_6$ is synthesized as a stoichiometric compound from a mixture of 1 mol Ln_2O_3 and 2 mol $\text{Ln}'\text{F}_3$.

6.4.2 Electrical conductivity

The electrical conductivity of rare-earth oxide fluorides was first investigated for the development of a binary anion conductive solid electrolyte. As a result, it was found that the binary rare-earth oxide fluorides exhibited oxide ion conductivity. Among them, the conductivity of neodymium europium oxide fluoride, $\text{Nd}_2\text{Eu}_2\text{O}_3\text{F}_6$, was reported to be much higher than that of yttria-stabilized zirconia, YSZ, practically used as an oxygen sensor [34]. The electrical conductivities of the binary rare-earth oxide fluorides vary not only with the combination of Ln_2O_3 with $\text{Ln}'\text{F}_3$

but also with the composition of the products. Figure 6 shows the relationship between the electrical conductivity and the nominal composition of $\text{Ln}'\text{F}_3$ for the products obtained from several Ln_2O_3 — $\text{Ln}'\text{F}_3$ systems. In any system, the electrical conductivity steeply increases in the composition range from 50 to 60 mol% LnF_3 where the phase changes from the rhombohedral to the tetragonal. It is important to consider the electrical conduction mechanism in connection with the crystal structure. The electrical conductivity of the tetragonal phase is at least one hundred times higher than that of the rhombohedral phase. The electrical conductivities of all 210 binary rare-earth compounds, $\text{Ln}_2\text{Ln}'_2\text{O}_3\text{F}_6$, and 15 simple rare-earth compounds, $\text{Ln}_4\text{O}_3\text{F}_6$, are summarized in Fig. 7 except for the Sc compound [19]. Figure 8 shows plots of the conductivities vs. the species of Ln for $\text{Ln}_2\text{Y}_2\text{O}_3\text{F}_6$ and $\text{Nd}_2\text{Ln}'_2\text{O}_3\text{F}_6$ as a typical example extracted from Fig. 7. Most of the compounds displaying electrical conductivities of more than $1.0 \times 10^{-1} \text{ Sm}^{-1}$ contain La, Ce, Pr, Nd, Sm or Eu. Among others, neodymium containing compounds, $\text{Nd}_2\text{Ln}'_2\text{O}_3\text{F}_6$, except for compounds of Ln': Nd, Yb and Lu, show the much higher electrical conductivities of around 1.0 Sm^{-1} . It is worth noting for these elements that these trivalent ions are larger than the limiting size (around 0.09 nm in radius) permitting octa-coordination to both fluoride and oxide anions, and can vary to divalent and/or tetravalent ions except for La^{3+} . The electrical conductivities of

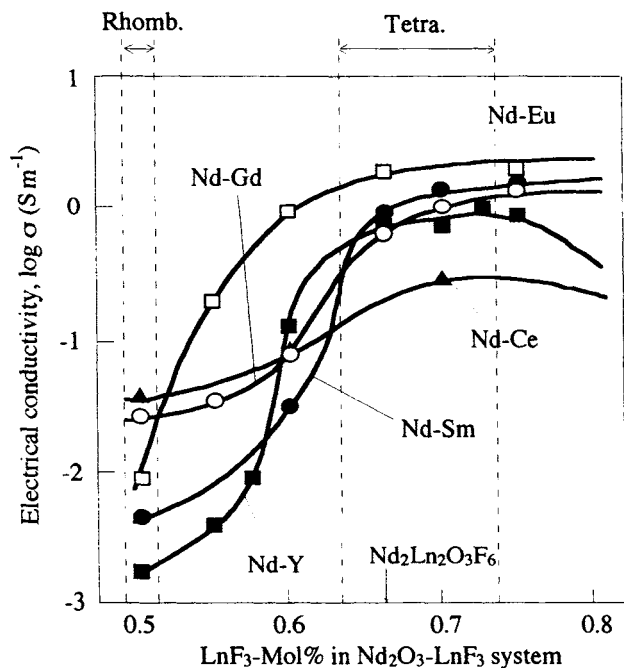


Fig. 6. Relationship between the electrical conductivities of the products obtained from various Nd_2O_3 — LnF_3 systems and nominal compositions of LnF_3 . The electrical conductivity was measured at 650°C under an oxygen partial pressure of 0.13 Pa.

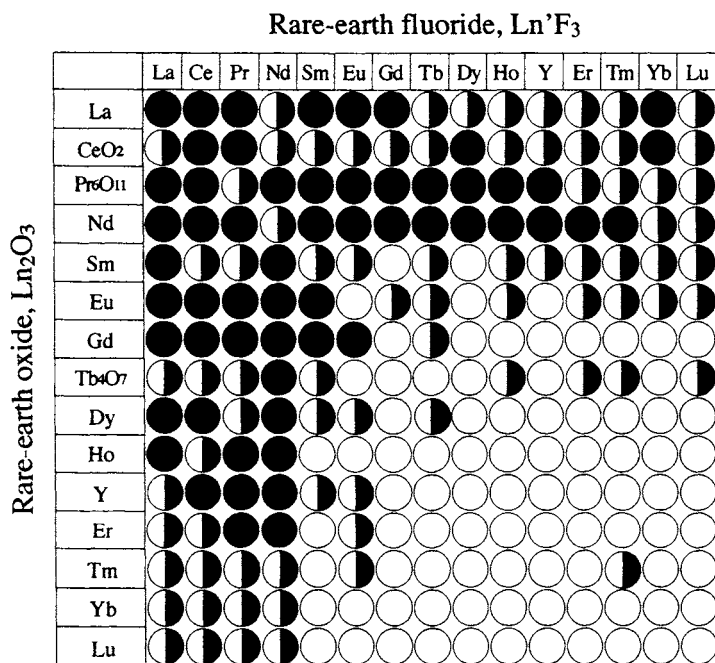


Fig. 7. The electrical conductivities of binary rare-earth oxide fluorides, $\text{Ln}_2\text{Ln}'_2\text{O}_3\text{F}_6$, measured at 650°C under an oxygen partial pressure of 1.33×10^{-1} Pa. ●, more than 1 S m^{-1} ; ◐, $0.1\text{--}1 \text{ S m}^{-1}$; ○, less than 0.1 S m^{-1} (reproduced with permission from Solid State Ionics, 23 (1989) 99 [19]).

$\text{Nd}_4\text{O}_3\text{F}_6$ which is $\text{Ln}_2\text{Ln}_2\text{O}_3\text{F}_6$ (Ln: Nd) is, however, much lower than the others as shown in Fig. 8. In the case of the simple oxide fluoride, there would be no reason to form a special arrangement of anions in the crystal lattice to generate an easy path for the oxide ion conduction as mentioned in Sec. 6.4.5. Those of the compounds, $\text{Ln}_2\text{Ln}'_2\text{O}_3\text{F}_6$, of Gd through Lu are less than $10 \times 10^{-2} \text{ S m}^{-1}$. The electrical conductivities of various compounds of $\text{Nd}_2\text{Ln}_2\text{O}_3\text{F}_6$ (Ln: Y, Ce, Sm, Eu, Gd) and yttria-stabilized zirconia, YSZ-11: $(\text{ZrO}_2)_{0.89}(\text{Y}_2\text{O}_3)_{0.11}$, measured in dried air evacuated to 1.33×10^{-1} Pa are shown in Fig. 9 in the form of Arrhenius plots. As is evident from this figure, the conductivities of $\text{Nd}_2\text{Ln}'_2\text{O}_3\text{F}_6$ (Ln: Y, Sm, Eu, Gd) are higher than that of YSZ. Remarkably, $\text{Nd}_2\text{Eu}_2\text{O}_3\text{F}_6$ shows much higher conductivity than the others; the value at 650°C reaches 5.0 S m^{-1} which corresponds to the conductivity of YSZ-11 at 900°C . The activation energies calculated from the slope of the linear plots [$\sigma = \sigma_0 \exp(\Delta E/kT)$] are 70 kJ mol^{-1} for $\text{Nd}_2\text{Ln}_2\text{O}_3\text{F}_6$ (Ln: Sm, Eu) and 100 kJ mol^{-1} for $\text{Nd}_2\text{Ln}_2\text{O}_3\text{F}_6$ (Ln: Y, Ce, Gd) and YSZ-11. The difference in the activation energies among $\text{Nd}_2\text{Ln}_2\text{O}_3\text{F}_6$ compounds may be due to the variation of the ionic arrangement in the crystal lattice. The charge-carrying species can be identified using an electrolysis method involving a simple cell, for example, as shown in Fig. 10 [33]. If the fluoride ion is mobile in the sample compound, the anode mixture should be converted by electrolysis to fluorine-containing nickel

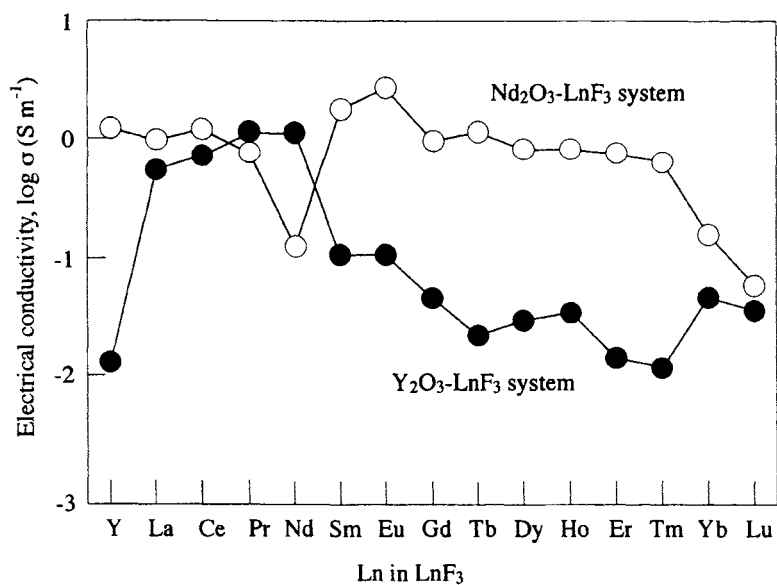


Fig. 8. The electrical conductivities of binary rare-earth oxide fluorides, $\text{Ln}_2\text{Ln}'_2\text{O}_3\text{F}_6$ produced from Nd_2O_3 - LnF_3 and Y_2O_3 - LnF_3 systems. The electrical conductivity was measured at 650°C under an oxygen partial pressure of 3.3×10^{-1} Pa.

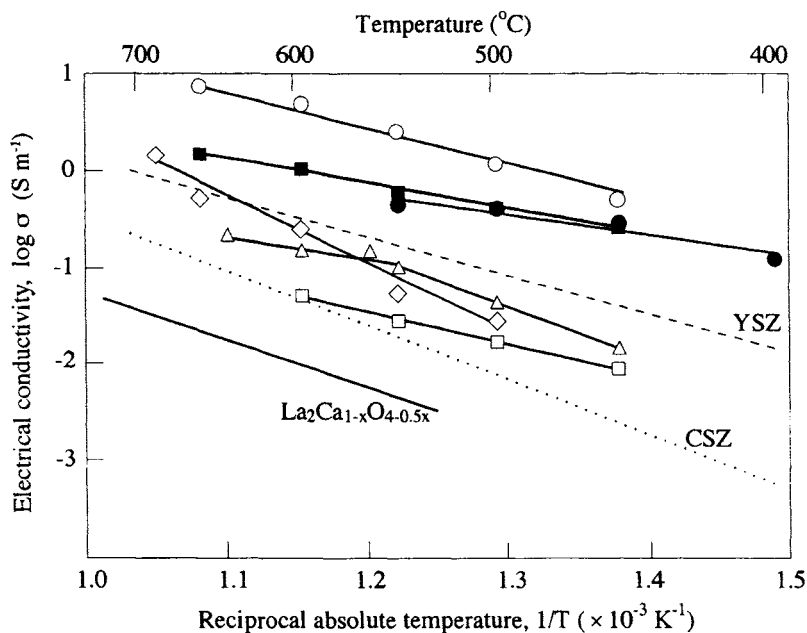


Fig. 9. The electrical conductivities of several binary rare-earth oxide fluorides, $\text{Ln}_2\text{Ln}'_2\text{O}_3\text{F}_6$. \circ , $\text{Nd}_2\text{Eu}_2\text{O}_3\text{F}_6$; \square , $\text{Nd}_2\text{Ce}_2\text{O}_3\text{F}_6$; \triangle , $\text{Nd}_2\text{Gd}_2\text{O}_3\text{F}_6$; \diamond , $\text{Nd}_2\text{Y}_2\text{O}_3\text{F}_6$; \bullet , $\text{La}_2\text{Eu}_2\text{O}_3\text{F}_6$; \blacksquare , $\text{Nd}_2\text{Sm}_2\text{O}_3\text{F}_6$ (reproduced with the permission from J. Fluorine Chem., 87 (1988) 229 [39]).

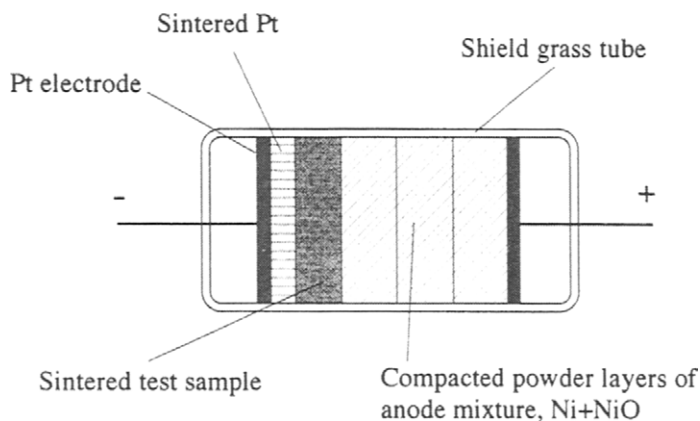


Fig. 10. Electrolysis cell to examine the charge carrier.

compounds. On the other hand, if the oxide ion is the charge carrier, consumption of nickel metal in the anode mixture must be detected. The experimental results indicate that only the oxide ion is mobile, that is, $\text{Nd}_2\text{Ln}_2\text{O}_3\text{F}_6$ can be called an oxide ion-conducting solid electrolyte. As shown in Fig. 11, the oxide ion transport number of $\text{Nd}_2\text{Ln}_2\text{O}_3\text{F}_6$ (Ln: Y, Ce, Sm, Gd) decreases as the temperature falls. $\text{Nd}_2\text{Ce}_2\text{O}_3\text{F}_6$ is noted because both the oxide ion and electron transport numbers became 0.5 at around 600°C . This is suitable for an electrode used for water vapor electrolysis. On the other hand, $\text{Nd}_2\text{Eu}_2\text{O}_3\text{F}_6$ has an oxide ion transport number of more than 0.9 at $500\text{--}700^\circ\text{C}$. The electron transport number of this compound has been measured to be less than 0.05 by a DC polarization method [35]. Most of the complex metal oxides having oxide ion conductivity also have semiconducting properties which depend on the oxygen partial pressure. The total electrical conductivity is generally expressed by the equation, $\sigma_{\text{total}} = \sigma_i + \sigma^{\text{e}}(\text{PO}_2)^{-1/n} + \sigma^{\text{h}}(\text{PO}_2)^{1/n}$, where σ_i is the oxide ion conductivity, $\sigma^{\text{e}}(\text{PO}_2)^{-1/n}$ and $\sigma^{\text{h}}(\text{PO}_2)^{1/n}$ are the conductivities due to electrons and positive holes. The oxide ion conductivity is not influenced by the oxygen partial pressure [36]. Figure 12 shows the relationship between the electrical conductivity of $\text{Nd}_2\text{Eu}_2\text{O}_3\text{F}_6$ at 400 and 500°C and the partial pressure of oxygen. Because the electrical conductivity is determined to be constant under an oxygen partial pressure of more than 0.4 Pa, the electrical conduction is seen to be due to only the oxide ion. The performance of $\text{Nd}_2\text{Eu}_2\text{O}_3\text{F}_6$ as the oxide ion-conducting solid electrolyte is regarded to reach an applicable level for use in an oxygen sensor and/or a fuel cell which can be operated even at 450°C .

6.4.3 Chemical stability

When the binary rare-earth oxide fluorides are utilized in a solid-state fuel battery, they must often withstand at a high temperature of around 1000°C to exhibit sufficient oxide ion mobility, i.e. to supply appropriate electrical current. These

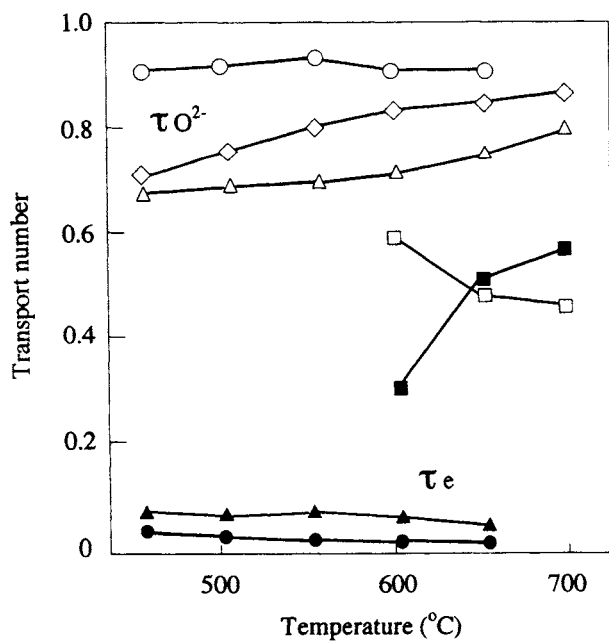


Fig. 11. The transport number of various $Nd_3Ln'_2O_3F_6$ compounds.

Oxide ion transport number, $\tau_{O^{2-}}$: \circ , $Nd_2Eu_2O_3F_6$; \square , $Nd_2Ce_2O_3F_6$; \triangle , $Nd_2Gd_2O_3F_6$;

Electron transport number, τ_e : \bullet , $Nd_2Eu_2O_3F_6$; \blacksquare , $Nd_2Ce_2O_3F_6$; \blacktriangle , $Nd_2Gd_2O_3F_6$ (reproduced with permission from J. Fluorine Chem., 87 (1998) 229 [39]).

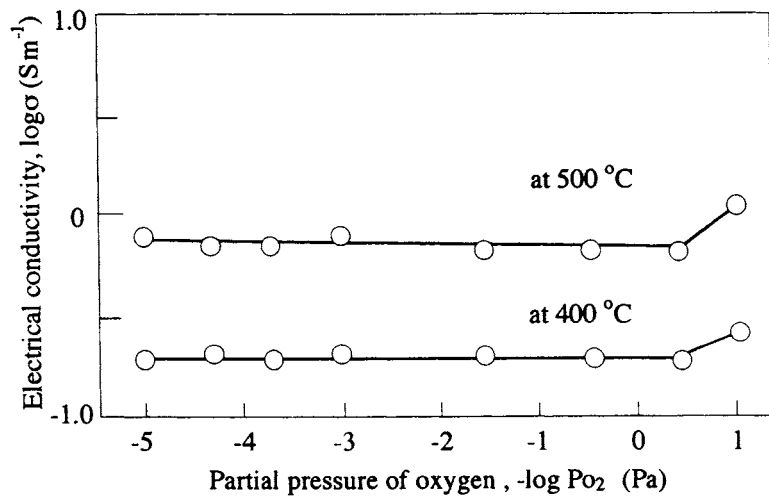


Fig. 12. Relationship between electrical conductivity and partial pressure of oxygen (reproduced with permission from J. Fluorine Chem., 87 (1998) 229 [39]).

compounds have been proven to be chemically stable up to 650°C even in a moist atmosphere but begin to undergo pyro-hydrolysis at ca. 700°C. $\text{Nd}_2\text{Eu}_2\text{O}_3\text{F}_6$ is stable indeed at 650°C, and is gradually converted to NdEuO_3 (monoclinic) at 1200°C through a quasi-stable intermediate with the composition of NdEuO_2F_2 (rhombohedral) (Fig.13). The kinetics of the hydrolysis is expressed by Jander's equation, $1 - (1 - x)^{1/3} = [(2DC)^{1/2}/r_0] t^{1/2}$, where x : reaction ratio, D : diffusion constant, C : concentration of reaction gas, r_0 : radius of solid reactant and t : reaction time [37]. The electrical conductivity largely falls with decreasing fluorine content due to the pyro-hydrolysis. The conductivity of the final product NdEuO_3 is less than one thousandth of that of $\text{Nd}_2\text{Eu}_2\text{O}_3\text{F}_6$ (Table 5). This is worth noting for the crystal structure investigations because the fluoride ion must play an important role in generating the oxide ion conduction in $\text{Nd}_2\text{Eu}_2\text{O}_3\text{F}_6$. Some attempts to improve the thermal stability have been carried out. Addition of a small amount

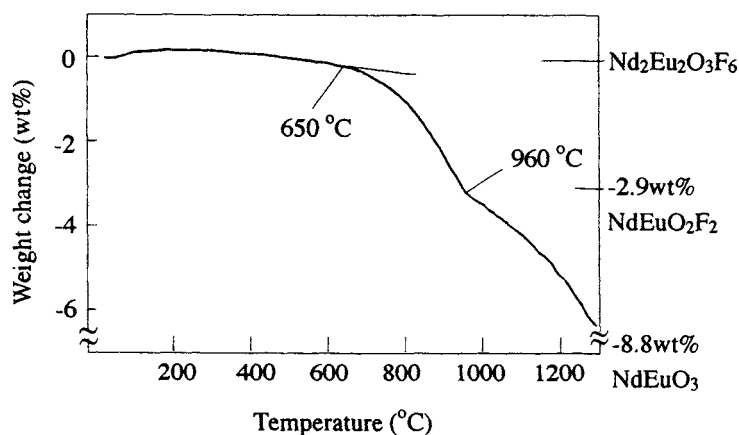


Fig. 13. TG curve for the pyro-hydrolysis of $\text{Nd}_2\text{Eu}_2\text{O}_3\text{F}_6$ in the air.

Table 5

Change in properties of $\text{Nd}_2\text{Eu}_2\text{O}_3\text{F}_6$ due to pyro-hydrolysis in an ordinary atmosphere

Treatment condition		Weight decrease (wt%)	Composition	Crystal type	Electric conductivity (S m^{-1})
temperature (°C)	time (h)				
—	—	—	$\text{Nd}_2\text{Eu}_2\text{O}_3\text{F}_6$	Monocl.	5.250
800	10	3.04	$\text{Nd}_2\text{Eu}_2\text{O}_{4.04}\text{F}_{3.92}$	Rhomb.	0.026
900	10	4.56	$\text{Nd}_2\text{Eu}_2\text{O}_{4.56}\text{F}_{2.88}$	Rhomb., Monocl.	0.013
1300	30	8.51	$\text{Nd}_2\text{Eu}_2\text{O}_{5.92}\text{F}_{0.17}$	Monocl.	0.001

of In_2O_3 or V_2O_5 was found to be effective in elevating the beginning temperature of pyro-hydrolysis without a decline in the electrical conductivity [38].

6.4.4 XPS spectra of $\text{Ln}_2\text{Ln}'_2\text{O}_3\text{F}_6$

Figure 14 shows the XPS spectra of the O1s electron in $\text{Nd}_2\text{Eu}_2\text{O}_3\text{F}_6$, Eu_2O_3 and Nd_2O_3 [33]. Every spectrum could be separated into two peaks as shown by the dashed line. The peak at higher binding energy is due to a rare-earth hydroxide formed at the sample surface, because the surfaces of rare-earth oxides are easily hydrolyzed by exposure to ordinary atmosphere. The peak at lower binding energy

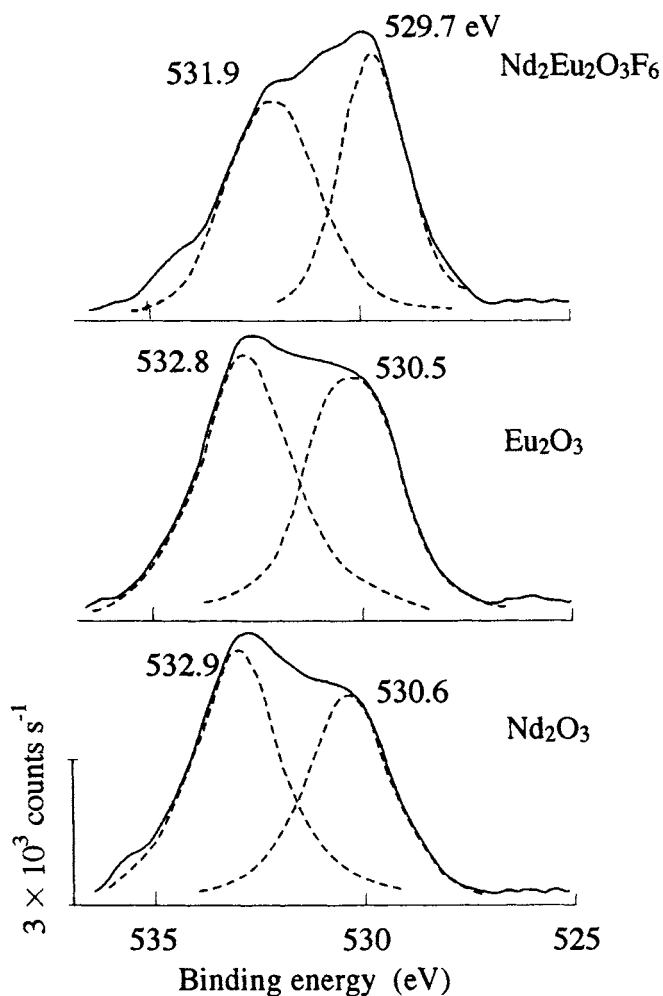


Fig. 14. XPS spectra for the O1s electrons of $\text{Nd}_2\text{Eu}_2\text{O}_3\text{F}_6$, Eu_2O_3 and Nd_2O_3 (reproduced with permission from J. Mater. Chem., 6 (1996) 795 [33]).

corresponds to the O1s electron in metal–oxygen bonding. The peak for $\text{Nd}_2\text{Eu}_2\text{O}_3\text{F}_6$ is found at a slightly lower binding energy than those of Eu_2O_3 and Nd_2O_3 , that is, the oxide ion in $\text{Nd}_2\text{Eu}_2\text{O}_3\text{F}_6$ tends to be more negative than in both oxides. This shows that the covalency in the bond between the metal ion and the oxide ion in $\text{Nd}_2\text{Eu}_2\text{O}_3\text{F}_6$ becomes weaker than in Eu_2O_3 or Nd_2O_3 . The shifts in binding energy of the F1s electron from the standard energy of 689 eV for all $\text{Nd}_2\text{Ln}_2\text{O}_3\text{F}_6$ compounds are summarized in Fig. 15. All energy shifts for $\text{Nd}_2\text{Ln}_2\text{O}_3\text{F}_6$ compounds are smaller than those in rare-earth fluorides. This indicates that the bond between the fluoride ion and the rare-earth ion in $\text{Nd}_2\text{Ln}_2\text{O}_3\text{F}_6$ is stronger than that in rare-earth fluorides, i.e. the ionic interaction of the oxide ion with the rare-earth ion becomes weaker, and the mobility of the oxide ion increases.

6.4.5 Crystal structures of binary rare-earth oxide fluorides

Because no single crystal of any binary rare-earth oxide fluoride has been obtained to date, computational efforts such as Rietveld analysis have been carried out to determine the crystal structure by means of X-ray and neutron powder diffraction. While

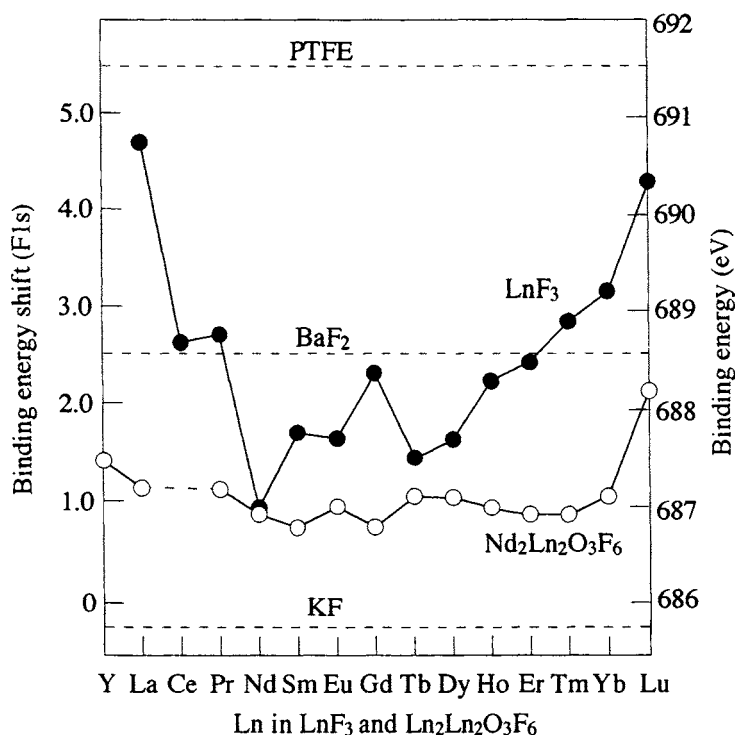


Fig. 15, Binding energy shifts of the F1 s electron from the standard (686 eV) for all compounds of $\text{Nd}_2\text{Ln}_2\text{O}_3\text{F}_6$ (Ln: Y–Ln) (reproduced with permission from J. Mater. Chem., 6 (1996) 795 [33]).

binary rare-earth oxide fluorides exhibit oxide ion-conduction as mentioned in Sec. 6.4.2, the structural aspects resulting in the oxide ion conduction have been considered as the background information essential to a simulation of the crystal structure. Two stoichiometric compounds, $\text{Ln}_2\text{Ln}'\text{O}_3\text{F}_3$ and $\text{Ln}_2\text{Ln}'_2\text{O}_3\text{F}_6$, have been analyzed compared with the simple rare-earth oxide fluorides such as rhombohedral LnOF and tetragonal $\text{Ln}_4\text{O}_3\text{F}_6$ mentioned in Sec. 6.3. The structure of $\text{Ln}_2\text{Ln}'\text{O}_3\text{F}_3$ can be determined based on the analogy of LnOF with a rhombohedral lattice. In Table 6, the lattice parameters of several $\text{Nd}_2\text{Ln}'\text{O}_3\text{F}_3$ compounds are listed. Details of the structure of $\text{Nd}_2\text{Ln}'\text{O}_3\text{F}_3$ such as the order-disorder arrangement of anions have not been investigated yet.

6.4.6 Crystal structures of $\text{Nd}_2\text{Eu}_2\text{O}_3\text{F}_6$

The analysis of the crystal structure of $\text{Nd}_2\text{Eu}_2\text{O}_3\text{F}_6$ is the main interest here because this compound shows the highest level of oxide ion conductivity as a solid electrolyte. The primitive cell was shown to have a tetragonal lattice referring to $\text{Ln}_4\text{O}_3\text{F}_6$. The cell constants were determined to be $a_0 = 0.563$ nm and $c_0 = 1.132$ nm by computation using the 9 largest peaks between 10° and 70° on the X-ray diffraction profile [39]. In view of the rule of ionic radius ratio $[(r\text{Nd}^{3+} + r\text{Eu}^{3+})/(r\text{O}^{2-} + r\text{F}^-)]$ is ca. 0.9] for the packing of ions, both cations in $\text{Nd}_2\text{Eu}_2\text{O}_3\text{F}_6$ require a coordination number of 8 like that of Ca in fluorite. The density of $\text{Nd}_2\text{Eu}_2\text{O}_3\text{F}_6$ was determined to be 6.98×10^3 kg m⁻³ using a helium gas displacement pycnometer. The molecular number Z is 2 in a cell; therefore, the theoretical density is calculated to be 7.02×10^3 kg m⁻³ which is close to the measured value. The crystal structure of $\text{Nd}_2\text{Eu}_2\text{O}_3\text{F}_6$ was estimated to be constructed of two units of the simple fluorite structure. Because the general formula of a fluorite structure is written as MX_2 , $\text{Ln}_2\text{Ln}'_2\text{O}_3\text{F}_6$ can be expressed by " $\text{Ln}_2\text{Ln}'_2\text{O}_3\text{F}_5 + \text{F}$ " or " $\text{Ln}_2\text{Ln}'_2\text{O}_2\text{F}_6 + \text{O}$ ". Therefore, one extra anion of fluoride or oxide ion in each case must occupy the interstitial site in the lattice such as the extra oxide ions in UO_{2+x} [40]. As mentioned already, among simple rare-earth oxide fluorides, the tetragonal compounds written as $\text{LnO}_x\text{F}_{3-2x}$ ($0.7 \leq x \leq 0.75$), had been considered to have the extra fluoride ion occupying the interstitial site in the lattice derived from the fluorite structure. That is, tetragonal $\text{Ln}_4\text{O}_3\text{F}_6$ ($x = 0.75$) was analyzed as " $\text{Ln}_4\text{O}_3\text{F}_5 + \text{F}$ " [22]. Rietveld analysis

Table 6

Cell constants of rhombohedral $\text{Nd}_2\text{LnO}_3\text{F}_3$ compounds

Ln in $\text{Nd}_2\text{LnO}_3\text{F}_3$	a_0 (nm)	α (degree)
Y	0.688	33.10
Ce	0.695	33.09
Sm	0.693	33.08
Eu	0.681	34.32
Gd	0.688	33.18

for the several arrangements of cations and anions indicated that the crystal system of $\text{Nd}_2\text{Eu}_2\text{O}_3\text{F}_6$ is not the tetragonal derived from the disordered arrangement but the monoclinic (slightly distorted tetragonal) in which cations and anions were highly ordered. In fact, it is very difficult to determine the arrangement of oxide and fluoride ions in the crystal structure even by precise XRD measurement. The special ordered arrangement of ions to form an oxide ion mobile structure is, however, required. The refined crystal data are shown in Table 7, and the metal coordination polyhedrons are shown in Fig. 17(a). There is no contradiction in assuming an ordered structure in which fluoride and oxide ions occupy the respective sites in the lattice. The lattice constants of $\text{Nd}_2\text{Eu}_2\text{O}_3\text{F}_6$ derived as " $\text{Ln}_2\text{Ln}'_2\text{O}_3\text{F}_5 + \text{F}$ " were calculated to be $a_0 = 0.3961$ nm, $b_0 = 1.132$ nm and $c_0 = 0.5632$ nm, $\beta = 134.87^\circ$ [$R_F = 3.80$]. The molecular number, Z , was calculated to be one from the density data (measured: 6.98×10^3 kg m $^{-3}$; calculated: 7.00×10^3 kg m $^{-3}$). The valencies of neodymium and europium in this structure are estimated from the anionic surroundings of each metal to be +3.5 and +2.5, respectively. $\text{Nd}^{+3.5}$ and $\text{Eu}^{+2.5}$ are not improbable considering the electronic configuration of neodymium and europium (Table 1). In fact, the XPS results suggested the variance in the valency state of $\text{Nd}^{+(3+\delta)}$ and $\text{Eu}^{+(3-\delta)}$ in $\text{Nd}_2\text{Eu}_2\text{O}_3\text{F}_6$. There are oxide ion-conductible sites (2f site) at which the site occupancy is 0.5. However, fluoride ions also ought to be mobile in this lattice because the site occupancy of fluoride ion at the 2e sites is also 0.5. A little evidence of fluoride ion conduction has been observed in $\text{Nd}_2\text{Ln}'_2\text{O}_3\text{F}_6$ compounds. The transport number of the fluoride ion was determined to be less than 0.05 for $\text{Nd}_2\text{Eu}_2\text{O}_3\text{F}_6$. It can be seen that " $\text{Ln}_2\text{Ln}'_2\text{O}_3\text{F}_5 + \text{F}$ " is not likely to be adopted for $\text{Nd}_2\text{Eu}_2\text{O}_3\text{F}_6$ in contrast to

Table 7

Crystallographic data for $\text{Nd}_2\text{Eu}_2\text{O}_3\text{F}_6$ derived as $\text{Nd}_2\text{Eu}_2\text{O}_3\text{F}_5 + \text{F}$
 Cell parameters; $a_0 = 0.3961$ nm, $b_0 = 1.1325$ nm,
 $c_0 = 0.5632$ nm, $\beta = 134.87^\circ$,
 Cell volume = 1.790×10^{-28} m 3 ,
 X-ray density 6.997×10^3 kg m $^{-3}$,
 Space group; $P1\ 2/c1$ (No. 13), Cell contents; 1 $\text{Nd}_2\text{Eu}_2\text{O}_3\text{F}_6$

Atomic parameters					
atom	site	x	y	z	occupancy
Nd	2e	0	0.111	0.25	1.0
Eu	2e	0	0.614	0.25	1.0
O	2f	0.5	0.012	0.75	0.5
O	2f	0.5	0.273	0.75	1.0
F	2f	0.5	0.526	0.75	1.0
F	2f	0.5	0.747	0.75	1.0
F	2e	0	0.838	0.25	0.5
F	2e	0	0.377	0.25	0.5

$\text{Nd}_4\text{O}_3\text{F}_6$. On the other hand, the result of Rietveld refinement with the parameters derived from " $\text{Nd}_2\text{Eu}_2\text{O}_2\text{F}_6 + \text{O}$ " is shown in Table 8 [$R_F = 3.33$], and the unit lattice and the metal coordination polyhedron are shown in Figs 16 and 17(b). In this structure, the Eu atom is closely surrounded with eight fluoride ions (2f sites) as is Ca in fluorite. Three oxide ions occupy the six corners of an octahedron (2e sites) which correspond to the interstitial sites in the fluorite lattice and which surround a fluorite-like cluster consisting of EuF_2 . The oxide ion occupancy at the 2e sites is 0.5. The octa-coordinating cluster containing Nd can be written as $\text{NdO}_{0.5}\text{F}$. Therefore, four corners of the 2f sites surrounding Nd are occupied by four fluoride ions, and two oxide ions occupy the other four corners (2f sites, $y = 0.012$) with an occupancy of 0.5. The occupancy of the fluoride ion at the 2f sites is unit. Therefore, only the oxide ion in $\text{Nd}_2\text{Eu}_2\text{O}_3\text{F}_6$ can be transported via the vacant sites (2f) lying in the $y = 0.012$ plane and the 2e sites at which the site occupancy of O^{2-} is 0.5. In addition, the valency of neodymium required from the anionic surroundings is

Table 8

Crystallographic data for $\text{Nd}_2\text{Eu}_2\text{O}_3\text{F}_6$ derived as $\text{Nd}_2\text{Eu}_2\text{O}_3\text{F}_6 + \text{O}$

Cell parameters; $a_0 = 0.396$ nm, $b_0 = 1.1325$ nm,

$c_0 = 0.5632$ nm, $\beta = 134.84^\circ$

Cell volume $= 1.790 \times 10^{-28} \text{ m}^3$

X-ray density $6.997 \times 10^3 \text{ kg m}^{-3}$

Space group; $P1\ 2/c1$ (No. 13), Cell contents; 1 $\text{Nd}_2\text{Eu}_2\text{O}_3\text{F}_6$

Atomic parameters					
atom	site	x	y	z	occupancy
Nd	2e	0	0.111	0.25	1.0
Eu	2e	0	0.611	0.25	1.0
O	2f	0.5	0.012	0.75	0.5
F	2f	0.5	0.275	0.75	1.0
F	2f	0.5	0.480	0.75	1.0
F	2f	0.5	0.775	0.75	1.0
O	2e	0	0.832	0.25	0.5
O	2e	0	0.325	0.25	0.5

Inter-atomic distance (nm)			
Nd—O 0.2290	Nd—F 0.2364	Eu—O 0.2503	Eu—F 0.2346
Nd—O 0.2421	Nd—F 0.2729	Eu—O 0.2901	Eu—F 0.2359
Nd—O 0.2423		Eu—O 0.2908	Eu—F 0.2364
Nd—O 0.2882		Eu—O 0.3239	Eu—F 0.2727
Nd—O 0.2889			
Nd—O 0.3160			
Nd—Eu 0.4219	Nd—Nd 0.3770	Eu—Eu 0.3770	

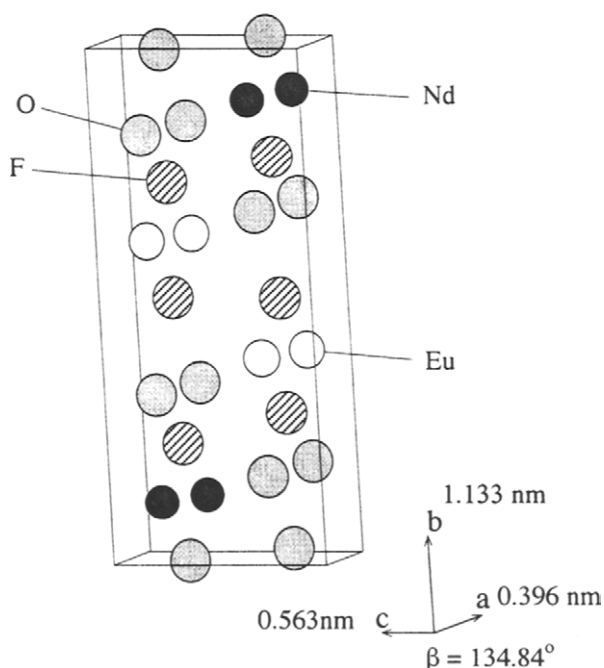


Fig. 16. The unit lattice of $\text{Nd}_2\text{Eu}_2\text{O}_3\text{F}_6$.

trivalent and that of europium as well. Consequently, it is concluded that the structure based on " $\text{Nd}_2\text{Eu}_2\text{O}_3\text{F}_6 + \text{O}$ " rather than " $\text{Nd}_2\text{Eu}_2\text{O}_3\text{F}_5 + \text{F}$ " is useful to explain the properties of $\text{Nd}_2\text{Eu}_2\text{O}_3\text{F}_6$. Figure 18 shows the linkage of the metal coordination polyhedrons (a) and its projection in the direction of $[100]$ (b), respectively. As shown in Figs 18(a) and (b), the oxide ions of which the site occupancy is 0.5 form continuous layers and can be transported easily in the layer. The crystal structure parameters of various compounds of $\text{Nd}_2\text{Ln}_2\text{O}_3\text{F}_6$ are listed in Table 9. The configurations of anions and cations in $\text{Nd}_2\text{Ln}_2\text{O}_3\text{F}_6$ seem to vary with the Ln species. The differences in the electrical conductivities among $\text{Nd}_2\text{Ln}_2\text{O}_3\text{F}_6$ compounds can be seen based on the configurations.

6.4.7 Crystal structure of NdEuO_2F_2

As mentioned in Sec. 6.4.3, $\text{Nd}_2\text{Eu}_2\text{O}_3\text{F}_6$ is gradually converted to NdEuO_3 at a temperature of around 1200°C . By calcination of $\text{Nd}_2\text{Eu}_2\text{O}_3\text{F}_6$ at around 800°C in an ordinary atmosphere, NdEuO_2F_2 with rhombohedral structure can be obtained as the intermediate compound by pyro-hydrolysis. The structure conversion from monoclinic $\text{Nd}_2\text{Eu}_2\text{O}_3\text{F}_6$ to rhombohedral NdEuO_2F_2 can be understood using the tetragonal expression instead of the monoclinic lattice of $\text{Nd}_2\text{Eu}_2\text{O}_3\text{F}_6$. The monoclinic lattice of $\text{Nd}_2\text{Eu}_2\text{O}_3\text{F}_6$ can be illustrated as the slightly distorted tetragonal as shown in Fig. 19. In the rhombohedral lattice, there is no space through

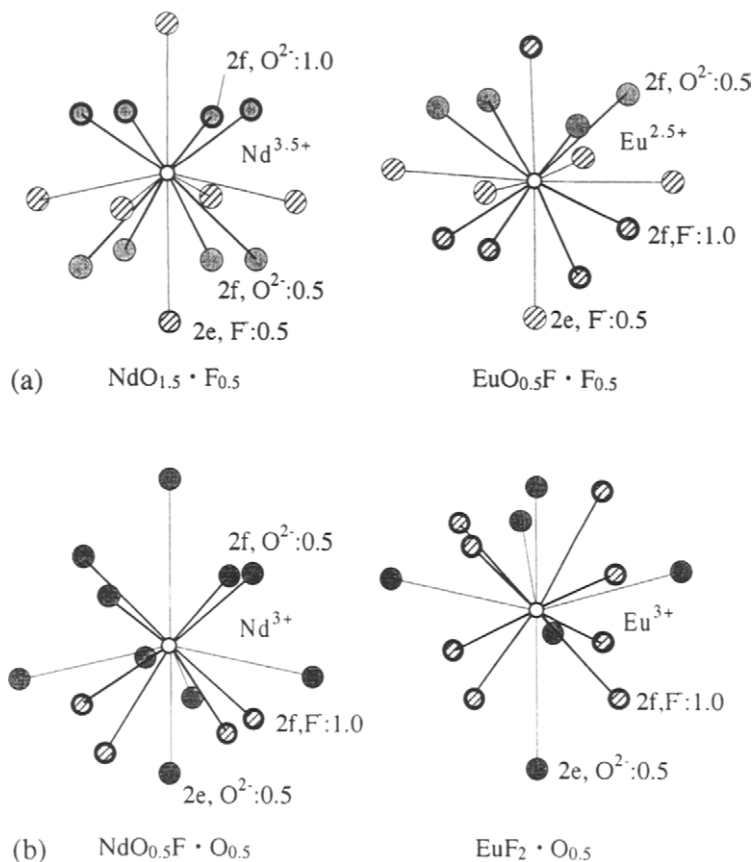


Fig. 17. The metal coordination polyhedron in $\text{Nd}_2\text{Eu}_2\text{O}_3\text{F}_6$; (a) derived as $\text{Nd}_2\text{Eu}_2\text{O}_3\text{F}_6 + \text{F}$ and (b) derived as $\text{Nd}_2\text{Eu}_2\text{O}_3\text{F}_6 + \text{O}$.

which either an oxide ion or a fluoride ion can be transported; therefore, the electrical conductivity of $\text{Nd}_2\text{Eu}_2\text{O}_3\text{F}_6$ falls due to pyro-hydrolysis.

6.5 Rare-earth fluoride stabilized zirconia, LnFSZ

Zirconium oxide, ZrO_2 , is one of most important materials in ceramic technology. So-called stabilized zirconia is well-known as an oxide ion-conducting solid electrolyte used in solid state fuel cells and oxygen sensors [34] and attracted special interest in toughened zirconia ceramics [41]. Pure zirconia exhibits a transformation from monoclinic to tetragonal at 1150°C with a volume change of several percent. To avoid thermal cracking of a sintered zirconia ceramic due to the phase transformation, alkaline earth or rare-earth oxides can be used to stabilize the fluorite

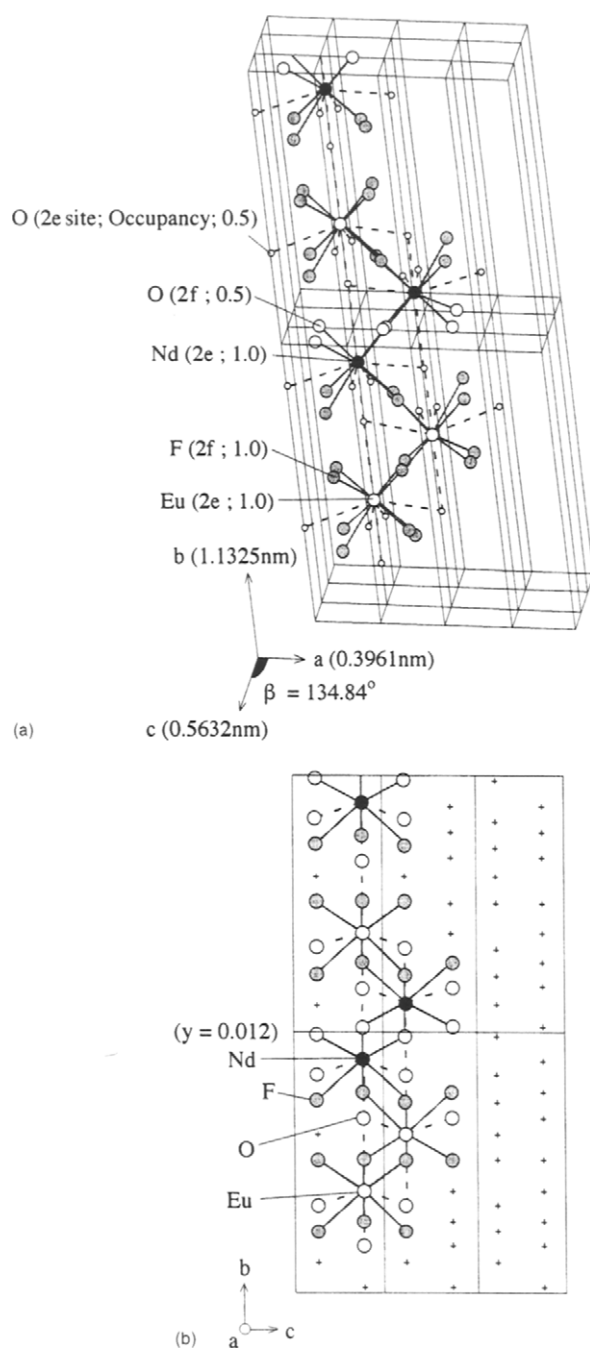


Fig. 18. (a) The space lattice and linkage of metal coordination polyhedrons; (b) The projection of the linkage of the metal coordination polyhedrons in the directions of [100].

Table 9

Lattice parameters and electrical properties of several $\text{Ln}_2\text{Ln}'_2\text{O}_3\text{F}_6$ compounds

$\text{Ln}_2\text{Ln}'_2\text{O}_3\text{F}_6$	Color	Lattice parameters				Cell volume $\times 10^{-28} (\text{m}^3)$	Density $\times 10^3 (\text{kg m}^{-3})$	
		$a_0 (\text{nm})$	$b_0 (\text{nm})$	$c_0 (\text{nm})$	$\beta (^\circ)$		Calcd.	Measd.
$\text{La}_2\text{Eu}_2\text{O}_3\text{F}_6$	white	0.4032	1.1377	0.5723	135.23	1.85	6.68	6.75
$\text{Nd}_2\text{Y}_2\text{O}_3\text{F}_6$	light blue	0.3945	1.1117	0.5587	134.73	1.74	5.99	6.01
$\text{Nd}_2\text{Ce}_2\text{O}_3\text{F}_6$	light gray	0.4019	1.1478	0.5689	134.97	1.86	6.54	6.60
$\text{Nd}_2\text{Sm}_2\text{O}_3\text{F}_6$	light blue	0.3961	1.1330	0.5627	134.81	1.79	6.96	7.02
$\text{Nd}_2\text{Eu}_2\text{O}_3\text{F}_6$	light blue	0.3961	1.1325	0.5632	134.84	1.79	7.00	6.99
$\text{Nd}_2\text{Gd}_2\text{O}_3\text{F}_6$	light blue	0.3973	1.1228	0.5595	134.75	1.77	7.17	7.04

$\text{Ln}_2\text{Ln}'_2\text{O}_3\text{F}_6$	Electrical ¹ conductivity (S m^{-1})	Oxide ion ¹ transport number
$\text{La}_2\text{Eu}_2\text{O}_3\text{F}_6$	—	—
$\text{Nd}_2\text{Y}_2\text{O}_3\text{F}_6$	0.3	0.8
$\text{Nd}_2\text{Ce}_2\text{O}_3\text{F}_6$	0.05	0.3
$\text{Nd}_2\text{Sm}_2\text{O}_3\text{F}_6$	1.1	0.8
$\text{Nd}_2\text{Eu}_2\text{O}_3\text{F}_6$	5.2	0.9
$\text{Nd}_2\text{Gd}_2\text{O}_3\text{F}_6$	0.2	0.7

¹; Measured at 600°C.

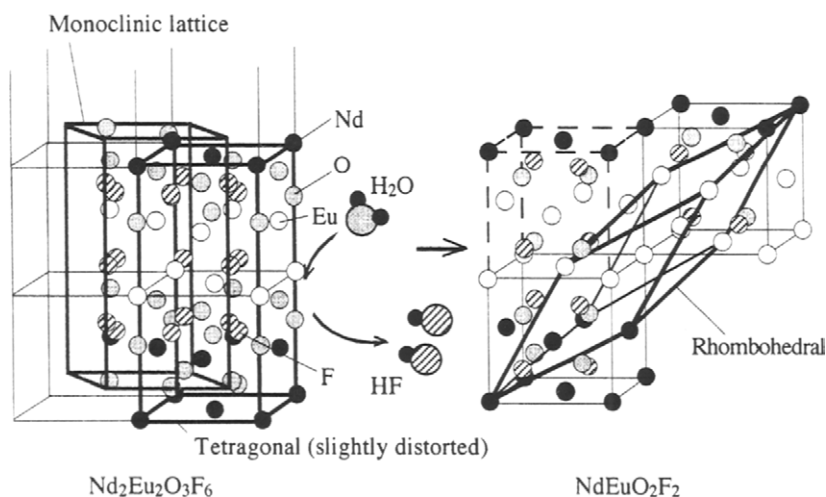


Fig. 19. Transformation of the crystal structure of $\text{Nd}_2\text{Eu}_2\text{O}_3\text{F}_6$ due to pyro-hydrolysis.

phase in zirconia. The stabilizing treatment then results in oxide ion conductivity because oxide ion defects are formed in the crystal structure of zirconia due to substitution of M^{2+} or Ln^{3+} ion for Zr^{4+} . The stabilizing treatment is usually performed at a high temperature of more than 1600°C . It was reported that, by using rare-earth fluorides as stabilizing reagents, stabilized zirconia with a cubic structure (cubic-LnFSZ) was formed at around 1100°C which was much lower temperature than that in the case of metal oxides [42].

6.5.1 Formation reaction of rare-earth fluoride stabilized zirconia

The formation reaction of LnFSZ is endothermic. The formation temperature depends on the Ln^{3+} crystal radius. The temperature is around 1100°C when the radius is less than ca. 0.09 nm and rises steeply to 1400°C with increasing radius ranging from 0.09 nm to 0.1 nm as shown in Fig. 20. The reaction no longer occurs with LnF_3 in which the Ln^{3+} radius is larger than 0.1 nm. This can be seen to be based on the ionic size of the cation able to substitute at the zirconium site, 0.093 nm. The reaction begins at around 600°C . The initial reaction is assumed to be pyro-hydrolysis of the rare-earth fluoride because the fluoride is very sensitive to even a small amount of water remaining in the reaction system filled with dry inert gases according to Eqn. (9). Hydrogen fluoride produced by pyro-hydrolysis reacts promptly with ZrO_2 , and zirconium tetrafluoride and water are formed, Eqn. (10). ZrF_4 leaves from the reaction system by subliming readily at the formation temperature of LnFSZ (1100°C), and the vacant sites of Zr^{4+} are produced in the vicinity of the rare-earth fluoride. Inevitably, rare-earth ions can easily occupy the vacant sites, and consequently, stabilized zirconia is formed with a decrease in sample weight due to the sublimation of ZrO_2 as the total reaction (11). That is, a small amount of water

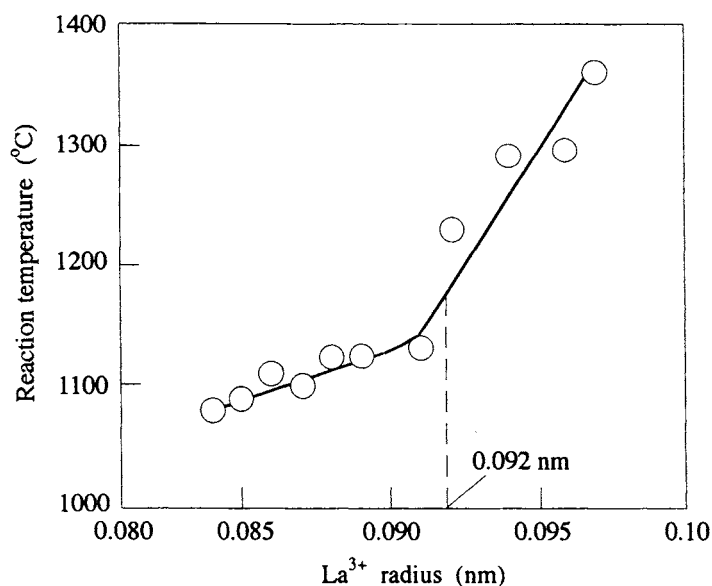
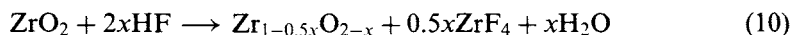
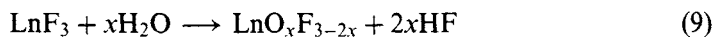


Fig. 20. Relationship between the solid-phase reaction temperature of $\text{ZrO}_2\text{—LnF}_3$ system and Ln^{3+} radius. The solid-phase reaction temperature was measured by DTA in an argon flow at a heating rate of $15^\circ\text{C min}^{-1}$.

remaining in the reaction system would be considered to act as a catalyst. This reaction cannot proceed even at 1100°C if the volatile product, ZrF_4 , cannot exit the reaction system such as the case of reaction in a sealed alumina tube.



The mono-phase of cubic stabilized zirconia was obtained in the nominal compositions of 13–25 mol% YF_3 , 22–30 mol% EuF_3 , 22–30 mol% GdF_3 , 24–35 mol% ErF_3 or 22–30 mol% HoF_3 [43–45]. In Table 10, the reaction conditions, the composition and lattice constants of the products obtained by calcination in argon flow are summarized. The reaction conditions for the systems of Sm through Lu are optimum conditions to prepare cubic-LnFSZ with higher electrical conductivity in the respective systems. Because the compositions of Ln_2O_3 and LnF_3 in all cubic-LnFSZ are almost equimolar, the composition of LnFSZ may be expressed as $(\text{ZrO}_2)_x(\text{LnO})_y$. In fact, LnOF is detected before the cubic-LnFSZ is formed.

Table 10

Reaction conditions, compositions and lattice constants of cubic rare-earth fluoride stabilized zirconia

Reaction conditions					Products			
System	LnF ₃ mol%	Temp. (°C)	Time (h)	Weight loss (wt%)	LnFSZ	Lattice const. <i>a</i> ₀ (nm)	Composition (ZrO ₂) _z (Ln ₂ O ₃) _y (LnF ₃) _x	
ZrO ₂ —LaF ₃	25	1400	3	2.2	LaOF+ZrO ₂	—	—	—
ZrO ₂ —CeF ₃	25	1400	3	5.1	CeOF+ZrO ₂	—	—	—
ZrO ₂ —PrF ₃	25	1400	3	3.8	PrOF+ZrO ₂	—	—	—
ZrO ₂ —NdF ₃	25	1400	9	11.3	NdF ₃ SZ+NdOF+ZrO ₂	—	—	—
ZrO ₂ —SmF ₃	25	1300	3	17.0	SmFSZ	0.518	0.80	0.13
ZrO ₂ —EuF ₃	25	1300	3	12.7	EuFSZ	0.518	0.79	0.10
ZrO ₂ —GdF ₃	25	1300	3	13.5	GdFSZ	0.518	0.78	0.09
ZrO ₂ —TbF ₃	25	1300	3	13.2	TbFSZ	0.518	0.78	0.10
ZrO ₂ —DyF ₃	20	1200	3	12.0	DyFSZ	0.516	0.84	0.08
ZrO ₂ —HoF ₃	25	1200	3	13.3	HoFSZ	0.516	0.78	0.10
ZrO ₂ —YF ₃	25	1200	3	14.4	YFSZ	0.516	0.78	0.09
ZrO ₂ —ErF ₃	25	1200	3	12.0	ErFSZ	0.515	0.78	0.09
ZrO ₂ —TmF ₃	25	1200	3	13.5	TmFSZ	0.515	0.79	0.10
ZrO ₂ —YbF ₃	25	1100	3	13.0	YbFSZ	0.514	0.79	0.10
ZrO ₂ —LuF ₃	25	1100	3	13.2	LuFSZ	0.514	0.79	0.09

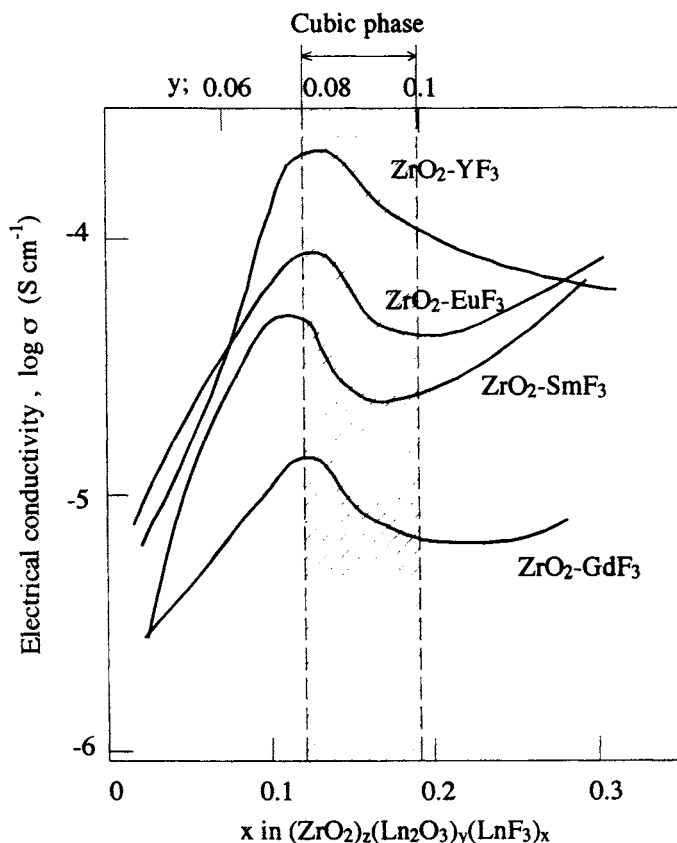


Fig. 21. Relationship between the composition and electrical conductivities measured at 650°C under an oxygen pressure of 0.7 Pa for the products of several $\text{ZrO}_2\text{—LnF}_3$ systems.

6.5.2 Electrical conductivity

As expected, LnFSZ exhibits oxide ion conductivity [43–45]. The relationships between the composition and the electrical conductivity at 650°C for some LnFSZ compounds are given in Fig. 21. The maximum conductivity is obtained at a composition at the zirconia-rich end of the composition range forming stabilized zirconia. At this composition, the activation energy of electrical conduction becomes minimum. The electrical conductivity of several LnFSZ compounds measured in dried air evacuated to 1.33×10^{-1} Pa is shown in Fig. 22 in the form of Arrhenius plots. The conductivities of YbFSZ ($2.0 \times 10^{-1} \text{ S m}^{-1}$) and EuFSZ ($3.5 \times 10^{-1} \text{ S m}^{-1}$) are comparable to those of yttria-stabilized zirconia (YSZ) and calcia (CSZ). Plots for any of the compounds show a linear relationship in parallel with those of YSZ and CSZ. The activation energies were calculated to be 100–120 kJ mol^{-1} . As shown in Fig. 23, the oxide ion transport number of EuFSZ is larger than 0.9 even at 450°C.

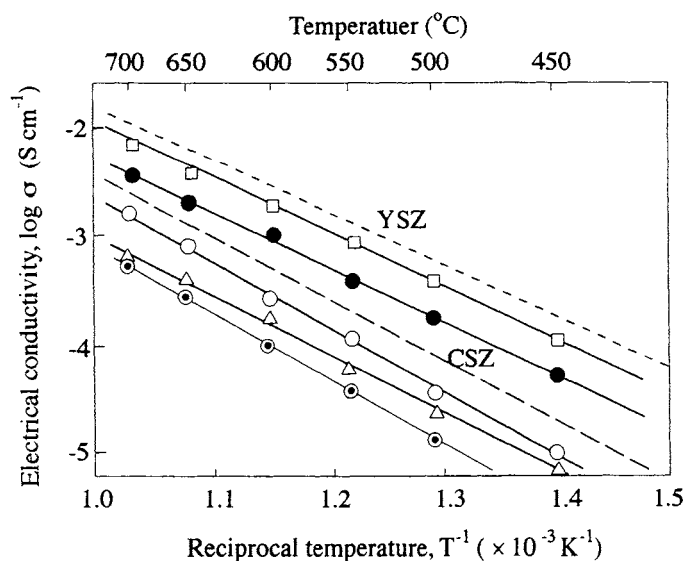


Fig. 22. Arrhenius plots of the electrical conductivities of several rare-earth fluoride stabilized zirconias measured under an oxygen partial pressure of 1.33×10^{-1} Pa.

○, $(\text{ZrO}_2)_{0.79} (\text{Y}_2\text{O}_3)_{0.10} (\text{YF}_3)_{0.11}$; ⊙, $(\text{ZrO}_2)_{0.79} (\text{Sm}_2\text{O}_3)_{0.10} (\text{SmF}_3)_{0.11}$;
 ●, $(\text{ZrO}_2)_{0.83} (\text{Eu}_2\text{O}_3)_{0.06} (\text{EuF}_3)_{0.11}$; △, $(\text{ZrO}_2)_{0.83} (\text{Ho}_2\text{O}_3)_{0.07} (\text{HoF}_3)_{0.10}$;
 □, $(\text{ZrO}_2)_{0.78} (\text{Yb}_2\text{O}_3)_{0.10} (\text{YbF}_3)_{0.12}$.

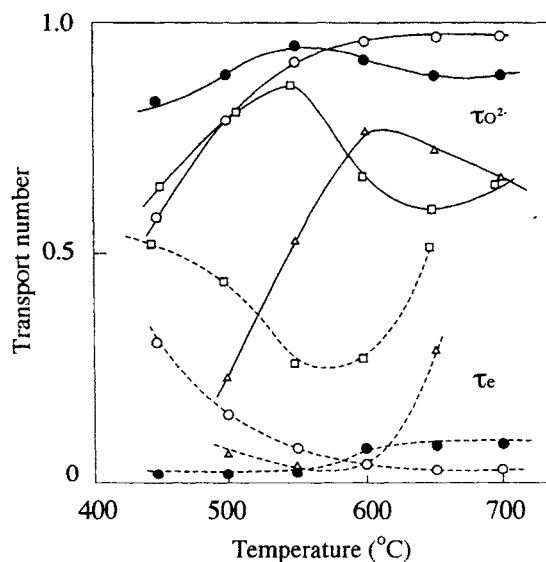


Fig. 23. The transport number of various rare-earth fluoride stabilized zirconias.

Oxide ion transport number, $\tau_{\text{O}^{2-}}$ —; Electron transport number, τ_e - - -;

○, $(\text{ZrO}_2)_{0.79} (\text{Y}_2\text{O}_3)_{0.1} (\text{YF}_3)_{0.11}$; ●, $(\text{ZrO}_2)_{0.78} (\text{Eu}_2\text{O}_3)_{0.1} (\text{EuF}_3)_{0.12}$;
 □, $(\text{ZrO}_2)_{0.84} (\text{Gd}_2\text{O}_3)_{0.08} (\text{GdF}_3)_{0.08}$; △, $(\text{ZrO}_2)_{0.83} (\text{Ho}_2\text{O}_3)_{0.07} (\text{HoF}_3)_{0.1}$.

References

- [1] J.E. Powell, In: Handbook on the Physics and Chemistry of Rare Earths, K.A. Gschneider, Jr., L. Eyring (Eds.), North-Holland Physics Publishing, Amsterdam, 1979, Chapter 22.
- [2] J.F. Collins, V.P. Calkins and J.A. McGurty, In: The Rare Earths, F.H. Spedding, A.H. Daane (Eds.), Robert E. Krieger Publishing Co. Ltd., Huntington, NY, 1971, Chapter 20, M.M. Woyski, W.J. Silvernail, *ibid*, chapter 21, W.K. Anderson, *ibid*, Chapter 22.
- [3] T. Takahashi, In: Physics of Solid Electrolytes, edited by J. Hladik (Eds.), Academic Press, London, 1972, Chapter 24.
- [4] C.P. Khattak, F.E.Y. Wang, In: Handbook on the Physics and Chemistry of Rare Earths, K.A. Gschneider, Jr., L. Eyring (Eds.), North-Holland Physics Publishing, Amsterdam, 1979, Chapter 29.
- [5] Fluoride Glasses, A.E. Comyns (Ed.), John Wiley & Sons, NY 1989.
- [6] D.J.M. Bevan, E. Summerville, In: Handbook on the Physics and Chemistry of Rare Earths K.A. Gschneider, Jr., L. Eyring (Eds.), North-Holland Physics Publishing, Amsterdam, 1979, Chapter 28.
- [7] B.L. Chamberland, In: Inorganic Solid Fluorides, P. Hagenmuller (Eds.), Academic Press, Inc., Orland, 1985, Chapter 5.
- [8] M. Takashima, G. Kano, Solid State Ionics, 23 (1987) 99.
- [9] The Rare Earth, F. H. Spedding, A. H. Daane (Eds.), Robert E. Krieger Publishing Co. Inc., Huntington, NY 1970.
- [10] A.I. Povov, G.K. Kunudson, J. Am. Chem. Soc., 76 (1954) 3921.
- [11] W.H. Zachariasen, Acta Cryst., 4 (1951) 231.
- [12] F. Kutek, J. Ruusi, Inorg. Chem., 9 (1964) 1500.
- [13] D.B. Shinn, H.A. Eick, Inorg. Chem., 8 (1968) 232.
- [14] M. Takashima, Y. Nosaka, T. Unishi, Eur. J. Solid State Inorg. Chem., 29 (1992) 691.
- [15] M. Takashima, S. Fukami, Y. Nosaka, T. Unishi, J. Fluor. Chem., 57 (1992) 131.
- [16] W.H. Zachariasen, Acta Cryst, 4 (1951) 231.
- [17] K. Niihara, S. Yajima, Bull. Chem Soc. Jpn., 44 (1971) 653.
- [18] K. Niihara, S. Yajima, Bull. Chem Soc. Jpn., 45 (1972) 20.
- [19] M. Takashima, G. Kano, Solid State Ionics, 23 (1987) 99.
- [20] W. Klemm, H.A. Klein, Z. Anorg. Allg. Chem. 248 (1941) 2367.
- [21] B. Holmberg, Acta Chem. Scand., 20 (1966) 1082
- [22] A.F. Weels, Structural Inorganic Chemistry, 4th Edn, Clarendon Press, Oxford, 1975.
- [23] C.W.F.T. Pistorius, J. Less-Common Met, 31 (1973) 119.
- [24] M. Takashima, G. Kanoh, H. Konishi, Nippon Kagaku Kaishi, 1982, 1896.
- [25] R.G. Bedford, E. Cataland, J. Solid State Chem., 2 (1970) 585.
- [26] N.C. Baenziger, J.R. Holdenand, G.E. Knudson, A.I. Popov, J. Amer. Chem. Soc., 76 (1954) 4734.
- [27] B. Holmberg, Acta Chem. Scand., 20 (1966) 1082.
- [28] A.W. Mann, D.J.M. Bevan, Acta Cryst., B26 (1970) 2129.
- [29] C.T. Au, Y.Q. Zhang, C.F. Ng, H.L. Wan, Catalysis Letters, 23 (1994) 377.
- [30] G. Blasse, A. Bril, Philips Res. Repts, 22 (1967) 481.
- [31] R.B. Waldron, U.S. Patent 4,014,736 (1977).
- [32] F.S. Karapetyan, V.E. Adamyan, A.A. Davtyan, Izv. Akad. Nauk Arm. SSR, Fiz., 13 (1978) 390.
- [33] M. Takashima, S. Yonezawa, K. Horita, K. Owaki, H. Takahashi, J. Mater. Chem., 6 (1996) 795.

- [34] K.S. Goto, W. Pluschkell, In: *Physics of Electrolytes*, J. Hladik (Eds.), Academic Press, London, 1972, Chapter 13.
- [35] C. Wagner, *Adv. Electrochem. Eng.*, 4 (1966) 1.
- [36] A. Kvist, In: *Physics of Electrolytes*, J. Hladik (Ed.), Academic Press, London, 1972, Chapter 8.
- [37] W. Jander, *Z. Anorg. Allgem. Chem.*, 163 (1927) 1.
- [38] M. Takashima, G. Kano, K. Hirano, Y. Hibino, *Nippon Kagaku Kaishi*, 1987, 1779.
- [39] M. Takashima, S. Yonezawa, Y. Ukuma, *J. Fluor. Chem.*, 87 (1998) 229.
- [40] M.T. Weller, *Inorganic Materials Chemistry*, Oxford Univ. Press, NY, 1994.
- [41] R.C. Garvie, R. H. Hannik, R. T. Pascoe, *Nature (London)*, 258 (1975) 703.
- [42] M. Takashima, G. Kano, *J. Fluor. Chem.*, 40 (1988) 375.
- [43] M. Takashima, G. Kano, M. Kawase, *Denki Kagaku*, 53 (1985) 119.
- [44] M. Takashima, G. Kano, N. Tabota, K. Higashimoto, *Denki Kagaku*, 55 (1987) 706.
- [45] M. Takashima, G. Kano, H. Uno, N. Kondo, *Denki Kagaku*, 57 (1989) 718.

CHAPTER 7

Oxyfluorinated Open Frameworks

G rard F rey, Thierry Loiseau and Didier Riou

*Institut Lavoisier (UMR CNRS 8637), Universit  de Versailles Saint Quentin en Yvelines, 45, Avenue des
Etats Unis, 78035. VERSAILLES Cedex, France*

7.1 Historical introduction

The concept of porous solids originates from the discovery by Cr nstedt [1], during the XVIIIth century, of the zeolitic properties of the mineral stilbite. Many natural zeolites were discovered later, but the importance of this family increased when chemists were able to synthesize them. The first success was due to Sainte Claire Deville as soon as 1862 [2] and most of the syntheses required organic molecules as templates.

Zeolites are hydrated alkaline or alkaline earth aluminosilicates with the general formula $M^{n+}_{x/n}[(AlO_2)_x(SiO_2)_y]^{x-}, w H_2O$, where x indicates the number of M^{n+} cations which are necessary to compensate the negative charge of the framework, and w the number of water molecules. From the structural point of view, zeolites exhibit a three dimensional network of corner sharing TO_4 tetrahedra ($T = Al, Si$) which delimits interconnected tunnels or cages in which water molecules and M ions are inserted. The elimination of the water molecules keeps intact the framework and the solid becomes porous.

At this stage of the paper, it is already necessary to distinguish porous solids and solids with an open framework. There is often confusion between these two terms in the literature. In these types of compounds, the initial structure can be divided in two parts: the skeleton and the occluded species (or templates). The skeleton itself is the open framework, even when the templates are present in the cavities. The solid becomes porous when the template has left the structure without modification of the skeleton. Therefore, in the following, solids will be generally considered as open frameworks. The term porous will only be applied when the solids exhibit chemical and/or physical properties related to voids in the corresponding solid.

The porosity, which is usually quantified structurally by the number of polyhedra surrounding the pore, was first used over forty years ago for molecular sieves requirements in gas separation, and quasi simultaneously, for catalytic purposes. These types of applications have now an incidence on the economic growth of developed countries. They represent in the world a turnover of 1000 billions dollars per

year and ca 25% of the Gross Domestic Product [3]. The concerned industries are chemicals, petrochemicals, oil refining, fine chemicals, pharmaceutical, separation and environmental technologies. A detailed overview of the field of zeolites is given in [4-6]. Today, more than one hundred different types of tetrahedron-based topologies are known.

There is now an increasing demand for new porous materials with higher selectivity in separation technologies, higher rates of conversion in fine chemicals and catalysis industry. That means a strategy for designing new compounds with new structures and enhanced performances.

The first breakthrough was provided by Flanigen et al. [7] who, playing on the similarity $2\text{Si}^{4+} \leftrightarrow \text{Al}^{3+} + \text{P}^{5+}$, synthesized microporous aluminophosphates (hereafter noted AlPOs) with structures related to those of zeolites. The structural studies [8] showed however a striking difference between the two families. As already mentioned, the framework of zeolites is built up exclusively from connected tetrahedra which can accept small amounts (<10% of substitution) of other metals, whereas in aluminophosphates and homologous gallophosphates, Al and Ga polyhedra can adopt five and sixfold coordinations, which change [9] the connectivity of the framework, and therefore the shape of the windows.

The second important change was provided by Guth et al. [10] in Mulhouse (France) who introduced the fluoride method in the synthesis of microporous solids. The fluoride ion is a mineralizing agent but can also participate to the reaction and the structure for providing new topologies as shown mainly by Kessler and Férey's groups [11,12]. It is this point which will be developed in this Chapter.

The third breakthrough concerns the mesoporous compounds [13,14] with pore sizes in the 20–100 Å range by using surfactant micellar templates. Very recently, the concept of microporous frameworks, which was primarily reserved to inorganic skeletons took a new dimension by the discovery of porous mixed inorganic–organic frameworks [15].

However, despite the increasing number of new compounds, a description of the mechanism of formation of these phases is always missing and prevents a rational design of compounds with an open framework, necessary to answer to the increasing demand of the concerned industries. This needs a systematic study of some systems and a careful characterization of the phases to engage this way. The only attempts, described below, concern exclusively fluorinated phosphates with an open framework. This short review presents the state of the art in this domain. It is limited to new solids and excludes zeolites and mesoporous compounds for which a dedicated literature already exists [4-6,16]. After a short history of the synthesis of these materials (Sec. 7.2), the paper will present the results of a detailed study of some systems (Sec. 7.3) which lead to the proposal of a mechanism (Sec. 7.4). Its experimental study and its consequences (Sec. 7.5) for the evidence of new families of porous solids are then described. After the description of some very recent features (Sec. 7.6), the critical analysis of this mechanism and the limitations that it provides lead to a new strategy for the design of new solids whose first results are given in the last part of the paper.

7.2 Synthesis of solids with an open framework

It generally requires hydrothermal conditions. The first synthetic zeolites discovered in the systems $M_2O-Al_2O_3-SiO_2-H_2O$ (M = alkaline ion) were obtained from the gels arising from the mixture at temperatures higher than 200°C under pressures of ca 100 bars. Further, the reagents in the autoclaves were submitted to lower temperatures ($100-180^\circ\text{C}$) under autogenous pressures (10–30 bars), using either inorganic or organic (amines or tetraalkylammoniums) bases as templates [17,18]. The resulting strongly basic medium explains the low coordination of aluminium in zeolites.

The alumino and gallophosphates were formed [7] in the systems amine- $Al(Ga)_2O_3-P_2O_5-H_2O$ using the same way of the synthesis and the same range of temperatures and pressure. However, the introduction of phosphoric acid in the synthesis lowered the pH of the solutions to a neutral or weakly acidic medium which favours higher coordinations for aluminium and gallium ions. The combined effect of pH and of the shape of the amines lead to ca two hundred structure types.

The introduction of fluoride ions (via fluorhydric acid) in these systems [10–12], using the same range of temperature and pressure, strongly modifies the conditions of synthesis. These ions have first a well known mineralizing role. The lowering of crystallization kinetics that they induce indeed gives more homogeneous and better crystallized phases. However, until the end of the seventies, their effect was scarcely used in molecular sieve syntheses. The first clear example was the crystallization of silicalite I in the presence of F^- by Flanigen and Patton [19]. Moreover, the presence of HF implies an acidic medium. The latter can play a role on the coordination polyhedra of the cations which can be fluorinated complexes. Then, the resulting solid can include fluoride ions in the framework [11,12]; the charge and the electronegativity of F^- may have an influence on the topology of the skeleton.

According to the experience of Guth et al. [20,21] in Mulhouse and ours in Versailles [12], one can define for F^- four main effects in the synthesis of open framework solids:

- (i) F^- is a *mineralizer* if it makes the formation of a more stable solid phase from a less stable solid phase possible through a dissolution/crystallization process. It allows the formation of a solution, generally from a gel, super-saturated in polycondensable species. It also increases the dissolution rate. Like a catalyst, the mineralizer is normally not consumed during the transformation;
- (ii) F^- is a *structure directing agent* if its presence in the reaction mixture is found to be necessary for forming a given material. This does not necessarily imply its incorporation into the final solid;
- (iii) F^- is a *template* if it is incorporated in the cavities of the open framework and stabilizes specific configurations around F^- ;
- (iv) F^- is a *ligand* if it belongs to the coordination polyhedra of the metallic species of the skeleton. It can be bridging or terminal.

The fluoride route of synthesis seems very rich and already provided four among the six most open frameworks described up to now in the literature in the category of microporous compounds ($\phi < \text{\AA}$): VSB-1 [22] cloverite [11], ULM-5 [23] and ULM-16 [24] with tunnels limited by 24, 20, 16 and 16 polyhedra respectively. These four solids are really porous, the porosity being generated by the elimination of the template either by thermal or chemical methods which preserve the inorganic framework.

Beside this classical synthesis, which involves exclusively inorganic frameworks, a supramolecular approach, based on the predictions of J.M. Lehn [25], begins to appear [26] for the designed construction of three-dimensional network solids from distinct and soluble molecular components. These syntheses use room temperature or hydrothermal conditions for the elaboration of the metal organic solids. Finally, organic synthesis can lead to microporous solids [15,27] in which the skeleton is exclusively based on organic species, with the alternation of covalent and hydrogen bonding to ensure the three-dimensional character.

As already mentioned, most of the syntheses use hydrothermal synthesis. The reaction takes place in the autoclave, which acts as a 'black box' for the understanding of the mechanism of formation of the solids which are finally isolated. Nothing was known about the interaction between organic and inorganic species. This needed to choose appropriate systems for the study of the pertinent chemical parameters, to carefully characterize the compounds and use in situ measurements to collect informations able to shed some light on the steps of formation of these solids. Such an approach has been initiated only on oxyfluorinated species, and shall be developed in the following.

7.3 Chemical parameters and structures of fluorinated open frameworks

In the fluoride route, which was primitively applied to silica based and AlPO_4 and GaPO_4 materials, the first chemical parameter is the nature of the metallic species, since the reactivity of Si toward F^- is completely different from that of Al or Ga.

7.3.1 Silica based solids

This work was essentially done by the group of Kessler (see Refs [20,21] and refs therein). In this family of silicates and aluminosilicates, fluoride ions play the three first roles noted above, with a priority to the mineralizing effect. The structural types FER, BEA, LEV, MOR are obtained with different templating agents at low Si/Al ratio, while MFI, MTW, AST, NU1, MTN are formed for high values of this ratio. *(The reader is informed that the zeolitic structural types (with only tetrahedral coordinations) are labelled by three letters by the International Zeolite Association; their structural characteristics have been collected in a special issue of Zeolites [28]).* The structure directing effect was evidenced for the AST type. The templating effect is encountered in the structure types MFI, TON, MTT, AST and MTN. In these cases, F^- is incorporated, as ion pairs, with the organic cation. In the AST type,

it is located (Fig. 1) at the center of a cube of tetrahedra, called double 4-rings and noted D4R in the nomenclature of the structure of zeolites [28].

These D4R are connected via isolated tetrahedra to ensure the three dimensional network of AST and can be considered as the building blocks (named SBU for secondary building units in [28]) of the structure. In MFI type, F^- is between two five-membered rings. According to our definitions, in these two examples, the fluoride ion has a templating effect. This situation, rather scarce in the crystal chemistry of dense inorganic fluorides, will be encountered many times in the following. The ^{19}F solid state NMR chemical shift (δ : -70 ppm/ $CFCl_3$) of templated F^- strongly differs from what is observed when F^- is linked to the metal (δ : -100 – 120 ppm/ $CFCl_3$). This will be seen below during the study of the gallophosphates.

7.3.2 $AlPO_4$ and $GaPO_4$ based solids

This family has been widely studied for seven years. Besides individual results, that mainly played on the nature of the template, only one systematic study correlating chemistry and structure has been undertaken by my group since 1992 in order to try to understand what happens in the 'black box', and to find a possible mechanism of formation with the long term aim of a 'tailor made' design of new solids with an open framework. This work, which combines chemistry, structures, NMR studies and in situ measurements in hydrothermal conditions, was primitively made in the system M_2O_3 ($M = Al, Ga$)- P_2O_5 -HF-amine- H_2O with a range of ratios 1–2; 1–4; 1–3; 1–10; 100–200. The corresponding series of compounds was labelled ULM- n . It mainly illustrates the fourth role of fluorine as a ligand of the metals in the open framework.

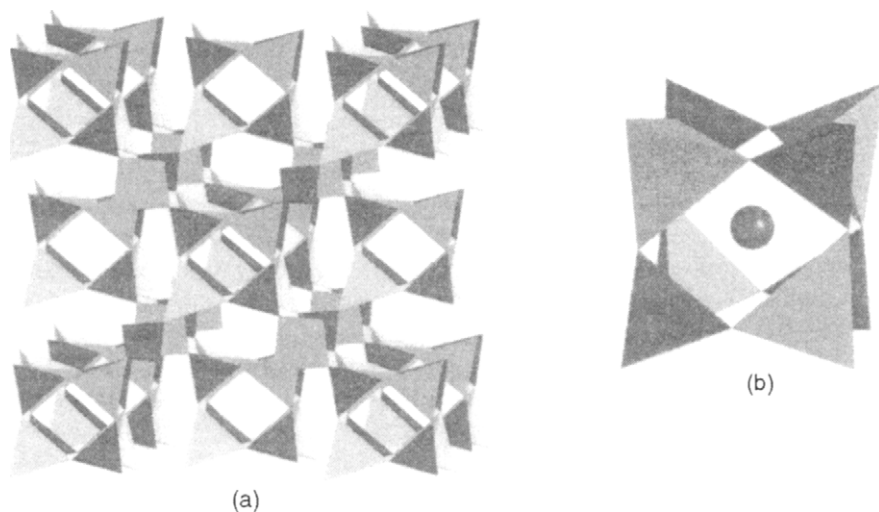


Fig. 1. Perspective view of AST structure type built from D4R units (see text) (a). For sake of clarity, fluorine (black sphere) has been represented only in the isolated D4R unit (b).

7.3.2.1 Chemical nature and concentrations of the constituents

In a first step, the physical parameters were kept constant (180°C, 24 h, autogenous pressure). Different studies proved first that if NH_4F is used instead of HF as a source of F^- , only one structure type, called CJ2 or $\text{NH}_4\text{AlPO}_4(\text{OH})_{0.3}\text{F}_{0.7}$, appears whatever the nature of the amine in the system. Attempts with other alkaline fluorides provide open frameworks without incorporated fluorine [29]. This explains that HF was used in the following.

The structure of CJ2 (Fig. 2) is however of interest [30] since it can be described from the connection of tetrameric units, called SBU-4 (for secondary building units) according to the notation of Meier and Olson [28]. These SBU are formed by two PO_4 tetrahedra, one MX_6 octahedron and one MX_5 trigonal bipyramid. In the octahedron, one fluorine, which is terminal, is strongly hydrogen bonded to NH_4^+ groups; the other fluorine, in statistical distribution with OH groups, is shared between the octahedron and the bipyramid. In addition, NMR shows that the NH_4^+ groups are partially substituted by H_3O^+ in the structure (12% for Al and 7% for Ga). The substitution occurs only on the ammonium site which is close to the fluorine site partially substituted with OH^- , thus giving detailed information on the ammonium-SBU interaction.

The source of phosphorus can be either P_2O_5 or H_3PO_4 . If it has no incidence on the final product, however, the use of P_2O_5 leads to intermediary phases which further transform in the stable solid. This point will be discussed in detail in Sec. 7.4.2, relative to in situ studies.

The concentration of the amines also plays a major role. If it is very high compared to the concentrations of the other species, the amine acts as a ligand of the metallic species instead of its usual templating role as shown by $\text{AlF}(\text{HPO}_4)$,

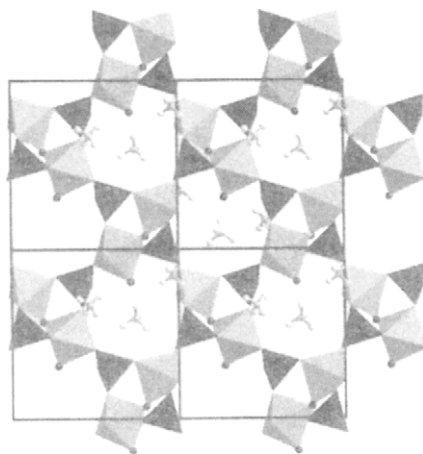


Fig. 2. [001] projection of CJ2 which shows the corner sharing linkage of SBU-4 incorporating ammonium ions. The PO_4 tetrahedra are in black and the aluminium polyhedra in grey. Black spheres in the skeleton are fluorine atoms.

$\text{NH}_2\text{—CH}_2\text{—CH}_2\text{—NH}_2$ [31]. Moreover, it seems that a medium amine/Ga and P ratios (2–8 range) favours the templating role of fluorine toward its ligand effect. Indeed, some solids, synthesized after 1991 in these conditions, are all built up from the connection of D4R units occluding fluorine.

The most famous example is provided by cloverite [11], a fluorinated gallophosphate templated with quinuclidine, which has for a long time been the most open framework with cages of 30 Å diameter. Each cage can be accessed through six 20-membered rings clover-shaped pores, making the material's pore system three dimensional. This material is really porous, quinuclidine being evolved at 350°C without change of the diffraction pattern up to 500°C. The structure (Fig. 3(a)) is built exclusively from F^- -centered D4R units, linked by vertices, the large cages

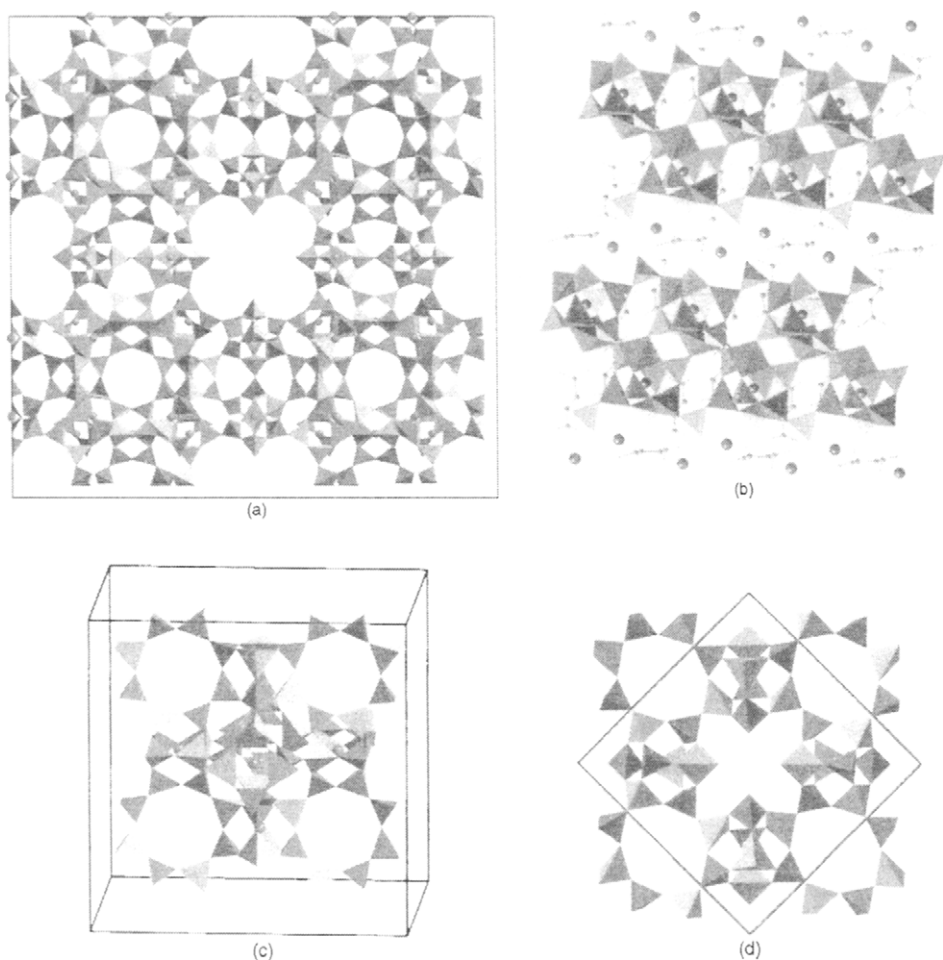


Fig. 3. Polyhedral representation of cloverite (a), ULM-18 (b), LTA (c) and Mu-2 (d) structures based on F^- -centered D4R units. Fluorine atoms are black spheres.

being initially occupied by water molecules and quinuclidinium ions. When the cages become empty, it is possible to introduce host species like XSnR_3 organometallic complexes [32] or liquid crystals [33]. It has been also proposed to use them as nanoreactors, but no data are up to now available. A nice paper [34] explores the possibilities of the supercage for advanced materials science applications. In particular, cloverite has been proved to be an excellent catalyst for the gas phase formation of methyl *tert*-butyl ether [35].

Beside this famous example, the structures of some new solids are built from these D4R units including fluorine: GaPO_4 -AST type [36], GaPO_4 -LTA type [37], M_U -2 [38] and ULM-18 [39] (Fig. 3(b)–(d)). All of them present a signal in ^{19}F solid state NMR with a chemical shift at $\delta = -70$ ppm/ CFCl_3 , which is now the signature of fluorine in a D4R cage. From a careful recent analysis of the different structures containing F^- -D4R units [39] combining X-ray diffraction and all the new possibilities of solid state NMR, it seems that the occluded species are not really F^- but $\text{H}^+ + \text{F}^-$.

If all compounds presented in this chapter are synthesized using one amine as template, an exception must be mentioned here. The oxyfluorophosphate TREN-GaPO [40] uses two templating amines: tris-(2-aminoethyl)amine (TREN) and pyridine. In the three-dimensional structure, TREN molecules occupy 12-ring channels while the pyridine molecules reside in 8-ring tunnels.

7.3.2.2 Influence of pH

It was illustrated by the system using 1,3-diaminopropane (1,3-DAP), in which the pH variations ($1 \leq \text{pH} \leq 10$) were induced by playing on the concentrations of P_2O_5 and 1,3-DAP, keeping the contents of the other species fixed. In these conditions, three compounds are isolated ([12] and refs therein) beside Ga_2O_3 above pH 9 and α - GaPO_4 in very acidic medium. In all of them, the amines are diprotonated. ULM-3 [41,42], or $\text{Ga}_3(\text{PO}_4)_3\text{F}_2$, $\text{H}_3\text{N}(\text{CH}_2)_3\text{NH}_3$, H_2O is stable in the range $5 \leq \text{pH} \leq 9$, and the structure shows that the water molecule is fixed to the amine and not to the skeleton. ULM-4 [43–44] or $\text{Ga}_3(\text{PO}_4)_3\text{F}_2$, $\text{H}_3\text{N}(\text{CH}_2)_3\text{NH}_3$ exists between pH 2 and 4. At $\text{pH} \leq 1$, triclinic ULM-6 [45] $\text{Ga}_4(\text{PO}_4)_4\text{F}_2(\text{H}_2\text{O})$, $\text{H}_3\text{N}(\text{CH}_2)_3\text{NH}_3$ is formed.

The structures of ULM-3 and ULM-4 are built up with the same hexameric SBU-6, also encountered with TREN-GaPO [40]. It contains three PO_4 tetrahedra, two GaO_4F trigonal bipyramids and one GaO_4F_2 octahedron (Fig. 4). The two types of gallium polyhedra are linked together via the fluorine atoms. Within the SBU, two of the three tetrahedra are linked by corners to one octahedron and one bipyramid, whereas the third connects the three Ga polyhedra. The signal of the bridging fluorine atoms in ^{19}F solid state NMR has a chemical shift at $\delta = -100$ ppm/ CFCl_3 .

The corner sharing between SBU-6 is different in ULM-3 and ULM-4, but creates 10-membered tunnels in both cases: ‘fer de lance’ shaped in ULM-3, and rectangular in ULM-4. The difference is due to the volume of the template: 1,3-DAP is hydrated in ULM-3 and not in ULM-4, and it seemed that the ‘structure-direction’ concept could apply in this case. It is also the contrast between the shapes of the two different amines in TREN-GaPO which creates 12- and 8-channels and a third topology of

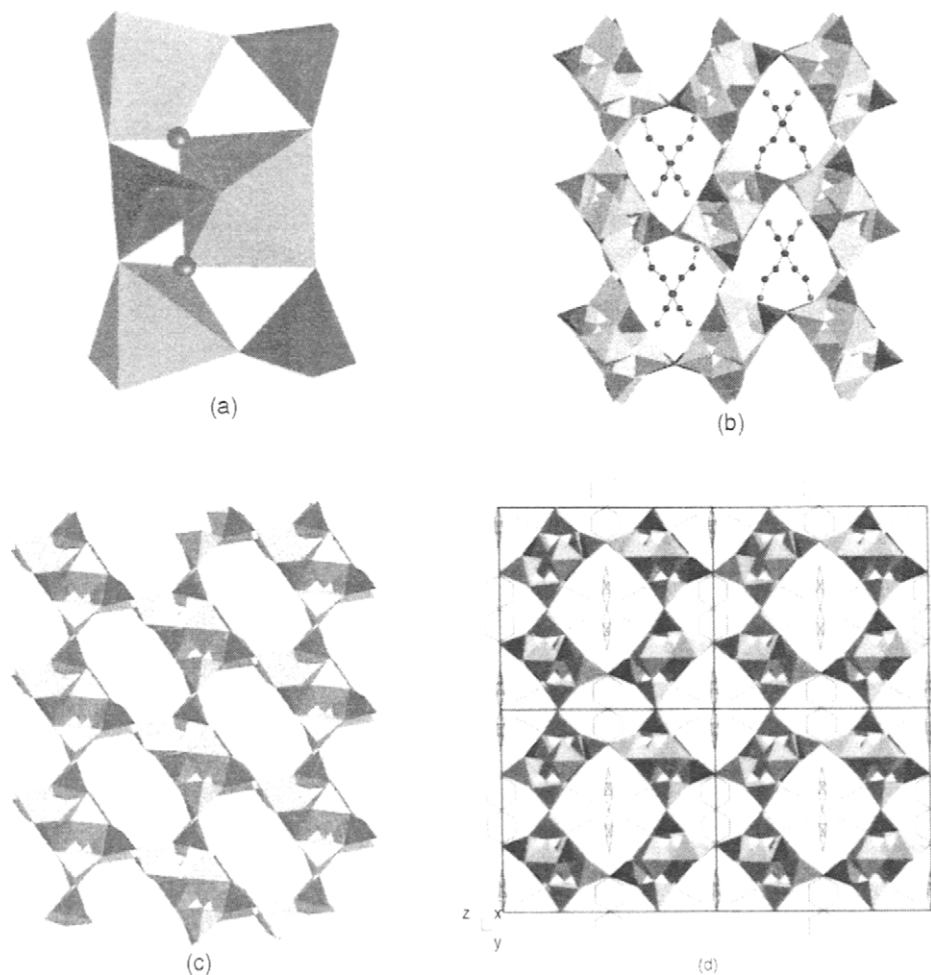


Fig. 4. Topologies based on SBU-6 clusters. (a) Perspective view of SBU-6 with bridging fluorine atoms represented as dark spheres and PO_4 tetrahedra in black; (b) [100] projection of ULM-3; (c) [010] projection of ULM-4; (d) [100] projection of TREN-GaPO (see text).

SBU-6, different from the two others. However, here and in all the phases isolated in these systems, the diprotonated amines point toward the fluoride ions of the framework.

It is also the case for ULM-6, obtained at very low pH, but the structure contains now octameric SBU-8 in which, this time, gallium octahedra share corners and edges.

This study exemplifies the complex role of pH: it influences the nature of the phases, the hydration of the amine (at high pH), the nature and the kind of linkage of the polyhedra around the metallic atoms (corner shared tetrahedra in basic

medium, both bipyramids and octahedra at medium pH, corner and edge shared octahedra at low pH); finally, the size of the SBU increases with lowering pH.

7.3.2.3 Nature of the amine

Beside the effect of pH, the difference between ULM-3 and ULM-4 showed that the volume of the amine also plays a role on the nature of the observed solids. Consequently, a careful analysis of the structural evolution in the system using different amines was required. Two parameters are important: the shape of the amine (either spherical or linear) and its correlated ability to be protonated. Indeed, there is a relation between their shape and their acidobasic characteristics. Their acidity constants are very different and, if the pK_a of aliphatic diamines lies in the 7–10 range, for spherical amines, it is only in the range 4–6. That means that both the volume, the anisotropy and the charge will influence the structure of the solid and therefore the shape of the cavities.

For the linear amines, the systematic study of the system $\text{Ga}_2\text{O}_3\text{—P}_2\text{O}_5\text{—HF—1,}n\text{ diamino}(n)\text{ane—H}_2\text{O}$ with $n \leq 8$ in the pH range corresponding to that of ULM-3 described above shows that for $n=2$, the ULM-4 topology prevails. For $n=3\text{--}5$, the topology of ULM-3 [46] is preserved (Fig. 5). For $n=4$, water has evolved the structure and is replaced by one NH_3 group of the protonated amine in the cavity. For $n=5$, the torsion of the aliphatic chain is important and indicates a higher internal pressure within the cavity.

This explains why a new structure appears for $n=6\text{--}8$: ULM-5 [47] or $\text{Ga}_{16}(\text{PO}_4)_{14}(\text{HPO}_4)_2\text{F}_7(\text{OH})_2$, $[\text{H}_3\text{N}(\text{CH}_2)_6\text{NH}_3]_4$, $6\text{H}_2\text{O}$. The three-dimensional network (Fig. 6) contains the same SBU-6 as encountered before but also an octameric one $\text{Ga}_4(\text{PO}_4)_4$, with the D4R type already encountered above in silica based materials forming a cube of corner linked GaO_4 and PO_4 tetrahedra, which encapsulates a fluorine atom. This is the first example of both bonding and encapsulated F^- in the same structure with very different NMR chemical shifts ($\delta \approx -100$ ppm and -63.5 ppm/ CFCl_3 respectively). The framework delimits 16- and 6-membered ring channels along [100] and 8-membered ones along [010]. The diprotonated amines are inserted in the 16-membered oval channels, whose free aperture is 12.20×8.34 Å. The water molecules are in the 6-membered tunnels. Very recently, $\text{M}_U\text{-5}$ structure type [48] provided a second case of both bonding and

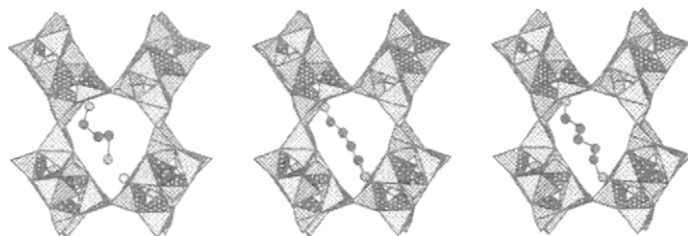


Fig. 5. Schematic disposition of the diamino-propane (left), butane (centre) and pentane (right) in the ULM-3 topology (C, N, H_2O : black, grey and empty spheres respectively).

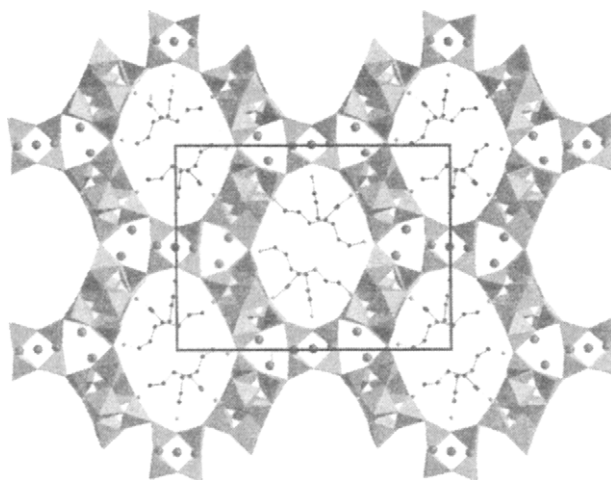


Fig. 6. Perspective view along [100] of ULM-5 showing the free aperture (12.20×8.34 Å) of the 16-membered tunnels formed by four SBU-6 and two D4R, and occupied by 1,6-diaminohexane.

encapsulated F^- in the same structure; the ligating F^- being this time terminal ($\delta \approx -192$ and -204 ppm/ $CFCl_3$) on one Ga trigonal pyramid of the D4R. The encapsulated F^- exhibits a signal at -70 ppm, in the usual range of chemical shifts already observed.

Spherical amines like DABCO (1,4 diazabicyclo[2.2.2] octane) lead to different structure types with cages rather than tunnels for the pores. For instance, ULM-1 [49], or $(Ga_3(PO_4)(HPO_4)_2F_3(OH), C_6N_2H_{14}), 0.5 H_2O$) exhibit cages formed by the connection of two types of tetrameric SBU-4; the first is close to that of $AlPO_4$ -CJ2, except that the trigonal bipyramid is replaced by an octahedron, the bridging vertex being a OH^- group; in the second, the two octahedra share an edge instead of a corner.

7.4 Hypothesis for an approach of the mechanism of formation

The understanding of the formation has always been a challenge. For zeolites, two contradictory hypotheses for the crystallization were proposed: the first [50] supposed the reorganization of the initial gel, and implied a diffusion of ionic species in the solid phases; in the second [51,52], the diffusion occurs in the liquid phase, and the crystallization occurs after a progressive dissolution of the gel, and the dissolved species would aggregate around the organic molecule (template) to give the final solid. The role of the organic part (often an amine) remains also mysterious. If the above hypotheses were true, one amine would lead specifically to one structural type, which is not verified. Davis proposed then three different roles of the template according to the flexibility and the geometry of the pores [53]. If the structure is flexible, the template acts only as a space-filling agent; on the other hand, when

the shape of the template and the framework are correlated, the template is said structure-directing. If the pore geometry strictly fits with the organic molecule, it is a true template effect.

The improvement of the understanding of the formation of oxyfluorinated compounds with an open structure needed the systematic study including chemistry, structures and NMR characteristics described above on the ULM-*n* (University of Le Mans) system M_2O_3 ($M = Al, Ga$)- P_2O_5 -HF-amine- H_2O .

7.4.1 *The hypothesis*

The chemical and structural knowledge on this system sheds some light on a possible mechanism of formation of these phases. It is first necessary to take into account that the hydrothermal conditions imply a lowering of dielectric constant and of the polarizing power of the solvent. Moreover, in aqueous solutions, cations like Al^{3+} or Ga^{3+} form hydrated complexes which, in the presence of phosphates give rise to cationic monophosphate complexes in the solution [54]. On the other hand, the above structural results show three general features: (i) in all the structures, the amine is diprotonated and points toward the fluoride ions of the inorganic skeleton; (ii) all the structures present well identified SBU: tetramers M_2P_2 (in $AlPO_4$ -CJ2 and ULM-1), hexamers M_3P_3 (in ULM-3, ULM-4 and ULM-5) and octamers M_4P_4 in ULM-5 and ULM-6, whose formal charge is always -II, whatever the size of the SBU; and (iii) all the structures can be described from a very small number of SBU whose configuration is not at first glance strongly dependent of the nature of the amine chosen for the synthesis.

The mechanism must explain the transition from the cationic monophosphate complexes in the initial solution to the anionic SBU in the final solid. The hypothesis therefore proposes the existence of these SBU in the solution and implies three steps for the condensation of the final solid: first, in the solution, an oligomeric condensation of the monophosphate complexes, during which these SBU might be formed in an identical way, despite the fact that the amines are different; the second and the third steps should correspond to the formation of zero-charged ammonium-SBU associations (hereafter called MBU) and the edification of the solid framework from the infinite condensation of these neutral MBU, respectively.

Starting from precursors in the solution, it is well known that the formation of a solid, i.e. the infinite condensation, mostly periodic, of these precursors, occurs when the condensing units correspond to neutral species, allowing the mutual approach of the entities without electrostatic repulsion [55]. This rules out that the monophosphate complexes are neutral species since, in such a case, one should find them in the resulting solid, instead of the observed anionic SBU. The size of the latter, larger than that of the primitive monocomplexes, also shows that the charge density of the complex was too high. The anionic condensation mechanism is therefore driven by the lowering of the charge density of the condensed species, in agreement with the previous conclusions of Henry [55]. From this viewpoint, it is the charge density of the species which controls the structure. For the anionic species,

this density will be lowered for SBU with large size, or for the same size of SBU, when the coordination of aluminium and gallium decreases.

Coming back to the conditions of syntheses, the amine is the only fixed parameter with its shape and its pK_a , and, after its choice, its charge density is fixed in a wide pH range. As already noted, the spherical amines, which have a pK_1 close to 5, are much less basic than the linear amines whose pK_a varies in the range 8–10. Their positive charge density is therefore higher than that of the linear amines, the charge density of which decreases when the length of the chain increases. In this classification, NH_4^+ plays a special role since, despite a high pK_a , its small size leads to a high charge density. The charge density of the amine controls the importance of the oligomeric condensation and therefore the size of the SBU, up to the equalization of the electronegativities of the organic and the inorganic groups. In such an hypothesis (Fig. 7), a high positive charge density (case of DABCO in ULM-1 and NH_4^+ in CJ2) will be associated with small SBU (SBU4). This explains why (i) $AlPO_4$ -CJ2 is always obtained whatever the amine used in the synthesis: NH_4^+ having a higher charge density than the amines governs the formation of the SBU4 entities; (ii) the increase of the size of the linear amine (weaker charge density) leads to SBU6 rather than SBU4 to reduce the charge density (ULM-3 and ULM-4); and (iii) ULM-5, which contains SBU6-6 and SBU4-4, appears with the longest chains.

The oligomeric condensation implies olation and oxolation reactions which transform the cationic monophosphate complexes into anionic SBU. It stops when the electronegativities of the organic and the inorganic groups become equal. Both the lower solvating properties of water in hydrothermal conditions and the strong interaction between the amine and the fluoride ions in the final solid allow to propose at this stage the formation of a tight ammonium-SBU association which can be compared to a neutral cation-anion pair. These MBU pairs present the zero-charge characteristics which allow the infinite condensation. They have two specificities: (i) they contain the inorganic SBU which bear the functions which will condense; and (ii) they have a topology and a steric occupancy which will determine the nature and the characteristics of the resulting structural forms (size and shape of the cavities, connection mode of the SBU).

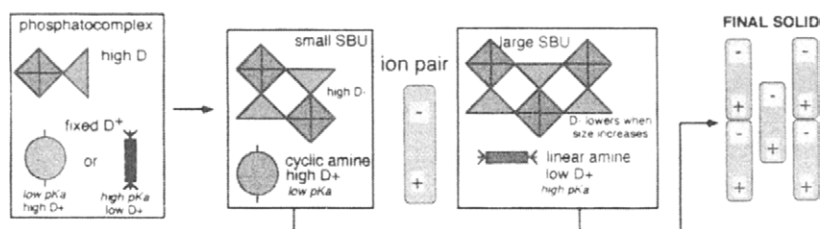


Fig. 7. Scheme of the steps of the formation of the solid from the phosphatocomplexes in solution (left) to the final solid (right) via the oligomeric condensation whose extent depends on the charge density of the amine, linear (rectangle) or cyclic.

In this way, the notion of 'template' must be revisited. It is not the SBU which 'arrange' around the 'templates' represented by the amines, but all the neutral pairs which form the structure corresponding to the lowest lattice energy satisfying the constraints imposed by the size, shape and plasticity of the SBU-ammonium association, as illustrated by the ULM-3 type with diaminopropane, butane and pentane. This assessment supposes that, if there is an intermediate solid, it possesses the same pairs as the final one.

The amine is the driving force in such an hypothesis. It is the principal parameter which governs the formation of the different phases: (i) the introduction of a given amine in the reaction medium, owing to its pK_a , its form and its length, experimentally imposes a known charge density in a system in which all the other species are variable; (ii) it will determine the evolution in size and charge of the SBU until the latter reaches a charge density and an electronegativity equal to that of the considered amine; (iii) it is at the origin of the creation of the neutral ammonium-SBU pair which allow the infinite condensation; and (iv) when the pair is formed, the steric effects and the flexibility of the amine fix the adopted structure type.

7.4.2 First in situ investigations in hydrothermal conditions

As already mentioned at the end of Sec. 7.2, autoclaves in hydrothermal synthesis are 'black boxes', and all the attempts to explain the formation of the porous solids originated from ex situ experiments. The above hypothesis concerns reactions within the autoclave and requires for its analysis in situ measurements in hydrothermal conditions which were never performed so far. These experiments must give information both on the solution and on the solid. Moreover, in the systems chosen for such studies, the kinetics of formation must be adapted to the possibilities of observation of the chosen technique. Two of them are particularly useful for this purpose: in situ diffraction studies using synchrotron radiation (SR) and in situ NMR (liquid and solid state).

In the first, a special autoclave with a heating device [56], is put in the SR beam. The power of the latter allows us to collect data every 60 s. and therefore observe both the induction time for crystallization of the solid and its nature and evolution with time. Experiments performed on ULM-5 [57,58] show an interesting chemical feature, already evoked without details above, which could not be predicted when the chemical parametrization of the systems was performed. When H_3PO_4 is used as the phosphorus source in the synthesis, ULM-5 is directly formed and appears very quickly after 15 mn of induction, the crystallization being complete after 40 mn at 180°C. However, if P_2O_5 is the starting product, an intermediary phase appears after 5 mn of induction, with a maximum yield after 15 mn, after which ULM-5 begins to form with a concomitant decrease of the intermediate (Fig. 8). The transformation is much slower than both the initial formation of the intermediate and the formation of ULM-5 when orthophosphoric acid is used as a starting material, taking over 2 h to go to completion. This illustrates the unexpected influence of the chemical nature of the reagents on the reaction pathways leading to

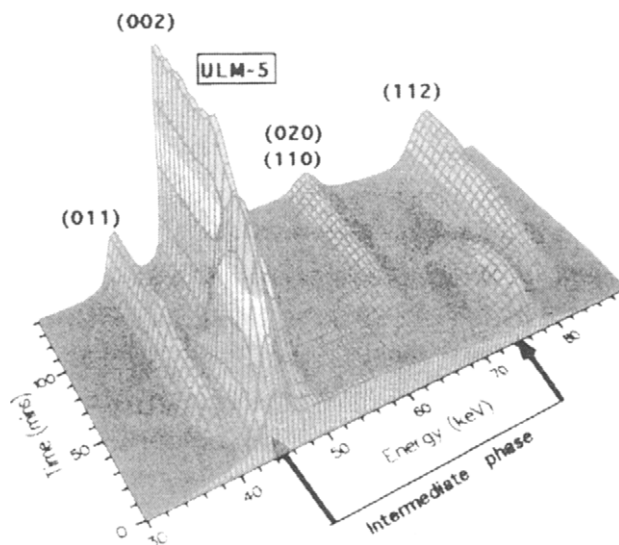


Fig. 8. Time evolution of the energy dispersive X-ray powder diffraction of the solid formed when P_2O_5 is used as phosphorus source during the synthesis at 180°C of ULM-5. The intermediate phase is characterized by two peaks at the beginning of the reaction. The (hkl) indices are those of ULM-5.

the porous solid. Similar studies on CJ2, ULM-3 and ULM-4 are on the way and confirm this phenomenon.

The second in situ technique is NMR. An autoclave fitting with the NMR cavity was designed by Gérardin et al. [59] and allows to follow the evolution of many parameters of the synthesis via the NMR characteristics of the different nuclei versus temperature and reaction time. The first measurement that can be reached now is the absolute value of the pH in hydrothermal conditions and the quantitative evolution of the concentration of protons in the bomb with the parameters of the synthesis [60]. They proved that ^{14}N NMR chemical shifts of well chosen amine compounds (imidazole and DABCO which possess complementary pK_a s) are precise pH indicators in aqueous solutions from room temperature to 475 K. Use of both amines permit to cover a wide range of about 9 pH units, with a precision of 0.1 pH unit.

As fluorinated aluminos and gallophosphates of the ULM-*n* series present attractive nuclei (^{31}P , ^{27}Al , ^{71}Ga , ^{19}F , ^{14}N , ^{13}C , ^1H), with most of them with high natural abundances, allowing rapid acquisitions for real time investigations during the synthesis, it is possible to follow the evolution of all the species during the reaction, correlated with the evolution of pH in hydrothermal conditions. The first study concerned $\text{AlPO}_4\text{—CJ2}$ ($\text{NH}_4\text{AlPO}_4(\text{OH})_{0.3}\text{F}_{0.7}$), which has only one type of SBU-4 with two different ^{27}Al sites (five- and six-fold coordinations with different NMR signatures) and two different ^{19}F sites (one terminal on $^{\text{VI}}\text{Al}$ site and one bridging the two Al units). It represented the best kinetics compromise, and allowed, using the ^{31}P , ^{27}Al , ^{19}F , ^{14}N data, a quantitative analysis in relation with mass transfers and formation process of $\text{AlPO}_4\text{—CJ2}$ [61].

The results of in situ ^{14}N NMR study of the reaction vs time at 150°C (Fig. 9(a)) in the presence of imidazole and DABCO show a pH increase from 3.2 to 6 in the first 2 h of the reaction and then an almost constant value of 6 during the rest of the synthesis. This value, which indicates quasi neutral conditions since pK_a is 11.5 at 150°C , is precious when considering speciation, protonation of ligands and coordination of Al atoms.

Both the evolution of the atomic fractions in the solution and of the chemical shift of all species (Fig. 9(b)–(e)) allow four steps in the formation of $\text{AlPO}_4\text{—CJ2}$: induction, dissolution, nucleation and crystal growth. During the induction period, a constant amount of Al atoms in the solution is observed during the set up of the pH synthesis. The dissolution step, which is quasi simultaneous with the induction period, is characterized by an increase of the amount of Al species in the solution (Fig. 9(b)–(c)). During this period, the different NMR results show the development of the right solution composition for the formation of soluble reactive species, the development of supersaturation conditions (with an increase of the soluble species concentration) and the formation of the solution species involved in the crystallization.

From the evolution of the two ^{27}Al NMR signals with time and temperature, the authors claim a solution speciation first with primary monophosphate ^{VI}Al complexes units (Fig. 10(a)) which loose one water molecule at higher temperature, giving a fivefold coordination to Al. Then prenucleation clusters form in the solution by dimerization of these 5-coordinated complexes (Fig. 10(b)) which will be involved in the nucleation and crystallization steps.

The latter are characterized by a decrease of the Al atomic fraction in the solution. From this decrease, it is postulated that the nucleation involves the condensation of prenucleation clusters and formation of nucleites. The two main signals decrease in intensity and their chemical shifts change with time (Fig. 9(e)). After about 17 h, the remaining peak, which does not change any longer in intensity and chemical shift, and indicates that the crystal growth is over, is then the signature of the clusters in the solution. It is suggested that the Al—F—Al bridge within the final SBU occurs during the condensation of the clusters. As for synchrotron experiments, similar studies are on the way on ULM-3 and ULM-4.

7.5 Consequences of the hypothesis. Magnetic materials with an open structure

The experimental support for the verification of the hypothesis will require a long time. For testing it, another way is to suppose that it is true and examine its implications [12]. Three points were considered. If it is true (i) for given experimental conditions, the use of diamines, too large for ensuring the three dimensional connection of the SBU, must lead to lamellar solids, the sheets being built up from the connection of the expected SBU. This was realized with ULM-8 [62]; (ii) with a proper choice of the geometry, the acidobasic characteristics and the reactivity of an amine, it may be possible to synthesize ‘tailor-made’ solids. The first success concerned ULM-16 [24] which used two amines, one for structure

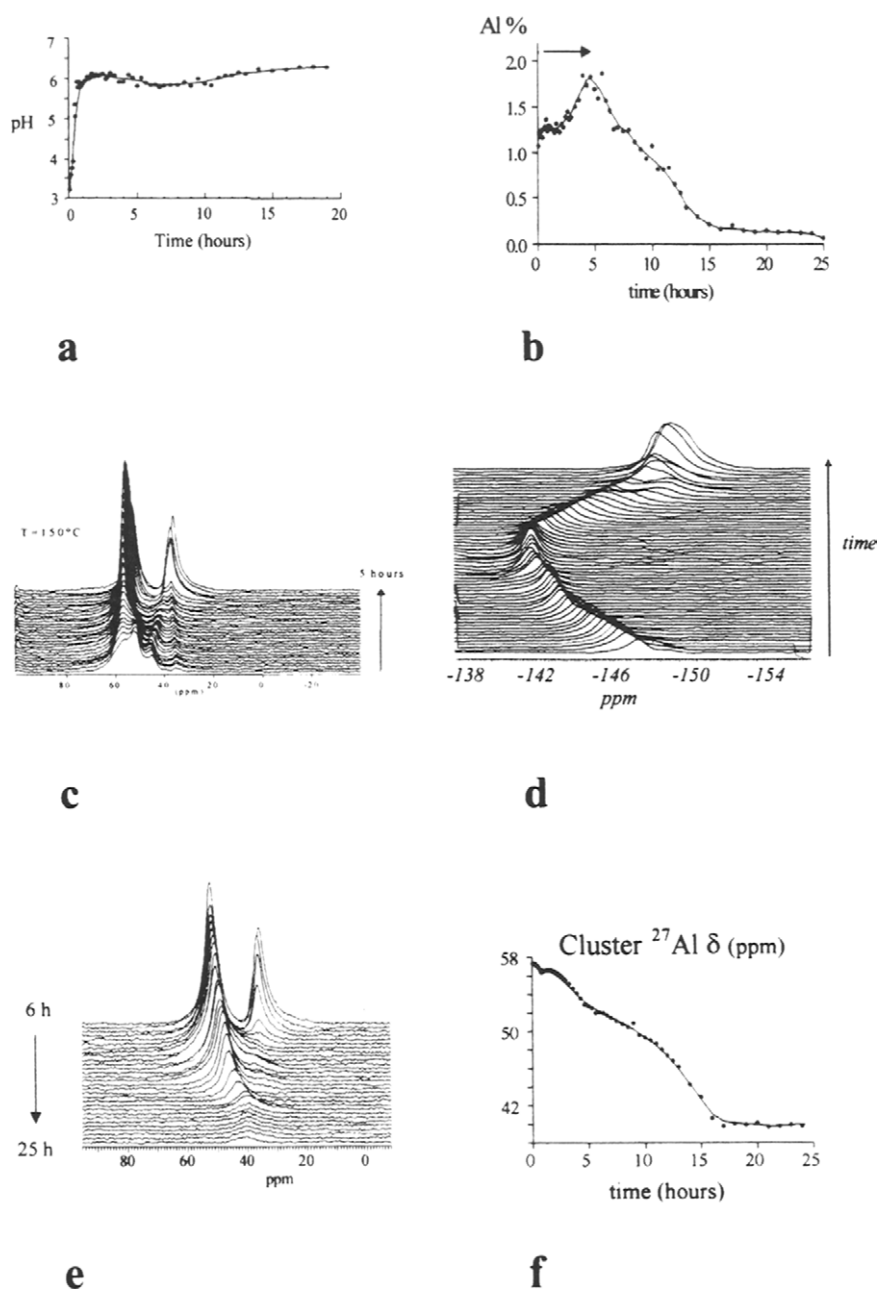


Fig. 9. Evolution with time of the NMR characteristics of $\text{AlPO}_4\text{-CJ2}$. (a) pH variation at 150°C from ^{14}N NMR; (b) Al atomic fraction in solution versus time at 150°C ; (c) in situ ^{27}Al NMR spectra during the first 5 h of synthesis at 150°C ; (d) in situ ^{19}F at 150°C ; (e) in situ ^{27}Al NMR spectra during nucleation and growth; (f) chemical shift evolution of the prenucleation cluster peak vs time (with courtesy of C. In Gérardin and F. Taulelle).

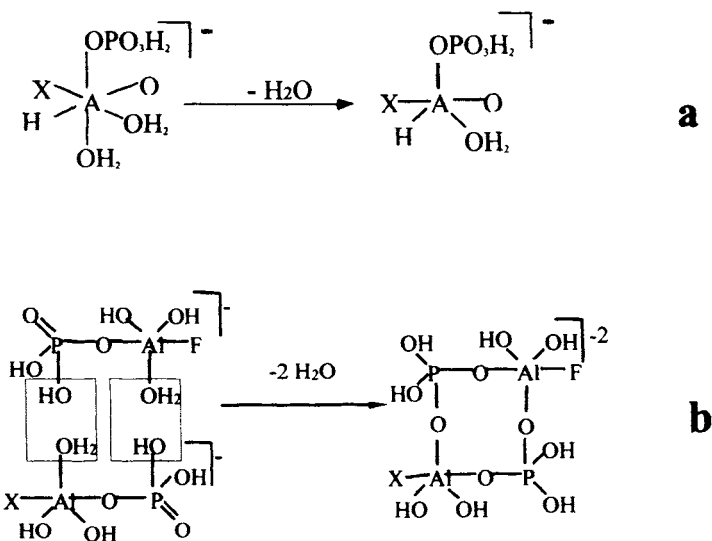


Fig. 10. (a) Dehydration of the hexacoordinated Al complex ($\text{X} = \text{OH}, \text{F}$) and (b) their dimerization for forming (see text) the prenucleation clusters (with courtesy of C. In G  rardin and F. Taulelle).

direction purposes and the other, unreactive, for adjusting the pH in a range suitable with SBU-6 oligomers. This lead to a solid with pores (Fig. 11) limited by 16 polyhedra and a free aperture of $10 \text{ \AA} \times 10 \text{ \AA}$ for the corresponding tunnels; (iii) the hypothesis is in agreement with the existence of porous solids containing transition metal ions instead of aluminium and gallium, and able to lead to significant magnetic properties. Up to now, only molybdenum and vanadium phosphates were described, but with magnetic ordering temperatures close to 4 K ([63] and Refs therein).

The strategy developed before for the systems containing Al and Ga was first applied by us to the $\text{V}_2\text{O}_5\text{--P}_2\text{O}_5\text{--HF--diamine--H}_2\text{O}$ [64] and lead to $\text{V}_2\text{PO}_8\text{F}$, *en*, the first fluorovanadophosphate with an open structure. In the systems $\text{Fe}_2\text{O}_3\text{--P}_2\text{O}_5\text{--HF--diamine--H}_2\text{O}$. Cavellec et al. isolated for the first time porous fluorinated iron(III) phosphates. Beside the well known ULM-3 and ULM-4 structure types, they characterized three new ones ULM-12 [65] or $\text{Fe}_4(\text{PO}_4)_4\text{F}_2(\text{H}_2\text{O})_3$, DABCO, its anhydrous variant ULM-19 [66] $\text{Fe}_4(\text{PO}_4)_4\text{F}_2$, DABCO, and ULM-15 [67] $\text{Fe}_4(\text{PO}_4)_4(\text{HPO}_4)_4\text{F}_3(\text{H}_2\text{O})_4$, $\text{H}_3\text{N}(\text{CH}_2)_3\text{NH}_3$. Most of these structures are built from SBU-6, except ULM-15 (Fig. 12) which exhibits a very original structure with chains and dimers of iron(III) octahedra.

All these compounds are the first porous antiferromagnets, with N  el temperatures in the range 37–12 K as confirmed by magnetic measurements and M  ssbauer spectrometry. Regarding to their structures, these magnetic ordering temperatures are relatively high since the iron sublattice exists as clusters linked by phosphate groups. Despite the relatively long distance between the clusters, strong magnetic interactions exist and let hope that, in the future, magnetic porous solids with high

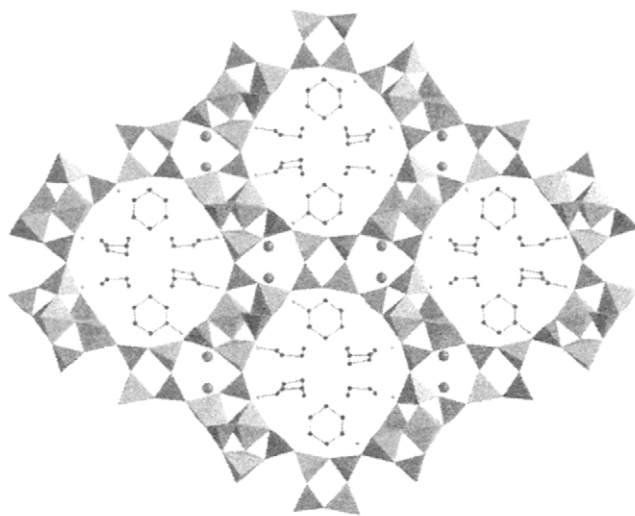


Fig. 11. Projection of the structure of ULM-16, synthesized with cyclohexylamine as structure-directing agent.

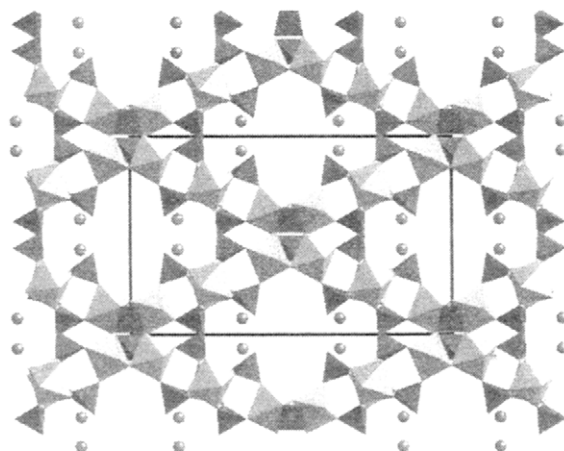


Fig. 12. Projection of the structure of ULM-15, an iron fluorophosphate with an open framework. The PO₄ tetrahedra are the darkest polyhedra.

magnetic ordering temperatures can be isolated, particularly ferromagnetic compounds.

After this discovery, Lii ([68] and Refs therein) and Haushalter [69] isolated very recently new iron oxyphosphates with an open structure, working in very acidic medium and a large excess of phosphoric acid. At variance to ours, but in agreement with our previous observations concerning the increasing size of the SBU with pH

decrease, their structures are built up from D4R close to those observed in Cloverite and ULM-5 (see Fig. 1). Finally, in the field of porous solids including transition metals, it is noteworthy the works initiated by Chippindale [70] and Stucky [71] on zeolite-like alumino and gallophosphates in which some extent of Al(Ga) is replaced by Co(II) in tetrahedral coordination, but with no fluorine in the structure.

If it becomes easy now to obtain open structures with di and trivalent transition metals, the litterature is very poor concerning tetravalent cations. However, very recently, two zirconium [72,73] and two titanium [74,75] fluorophosphates were evidenced. The titanium family provides the first example [74], of a mixed valence compound, $\text{Ti}^{\text{III}}\text{Ti}^{\text{IV}}\text{F}(\text{PO}_4)_2 \cdot 2 \text{H}_2\text{O}$ (Fig. 13) in the series of oxyfluorinated solids with an open framework.

7.6 Limits and future

All the above results confer some credibility to the hypothesis and allow a continuation of the research in this field, but the increasing knowledge of the mechanism of formation shows also the limits for obtaining 'tailor made' microporous compounds with given shape and size of the pores using this way. Indeed, if the amine is the driving force for the synthesis of microporous compounds, it is also the major limiting factor for fluorinated phosphates. Its charge induces strong electrostatic interactions with the framework and makes difficult its extraction after the synthesis. Its charge density, which controls the extent of the oligomeric condensation of the SBU, is not so variable and give rise to limited sizes for these oligomers whose

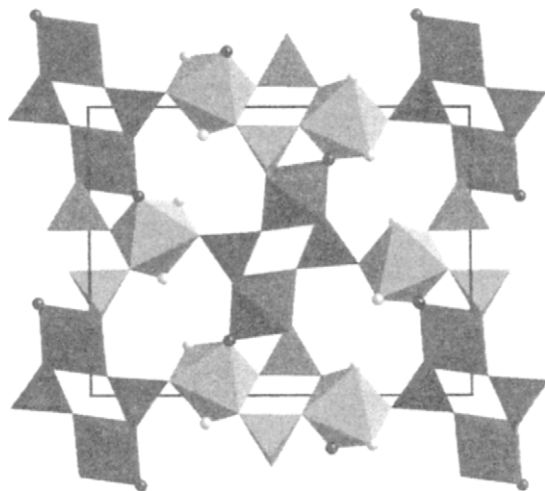


Fig. 13. Projection along [001] of $\text{Ti}^{\text{III}}\text{Ti}^{\text{IV}}\text{F}(\text{PO}_4)_2 \cdot 2 \text{H}_2\text{O}$ showing the two types of SBU-4: $\text{Ti}^{\text{III}}_2\text{P}_2$ (light grey SBU) and $\text{Ti}^{\text{IV}}_2\text{P}_2$ (darker SBU). Black and grey spheres represent bridging fluorine atoms and water molecules fixed on Ti^{III} octahedra.

number of polyhedra seems to be limited at eight. The ratio of the sizes of the SBU and the amine in the neutral pair limits also the possibilities for having three-dimensional networks. Very rapidly, the increasing size of the amine prevents from the connection of the SBU in the three directions and leads to layered compounds. All these reasons show that, if this way of synthesis is suitable for having pores in a limited size range, say 10–15 Å, it does not allow wide possibilities for having a large range for the modulation of the porosity. It is the reason why many researches are currently devoted to the study of new templates such as metallic complexes, polyanions, micelles for obtaining new open frameworks. Mesoporous compounds illustrate this tendency.

Another limiting factor is the use of phosphates. Within the SBU, it acts as a chelating agent toward the metallic ions, and shares its oxygen at least with three cations to give the three-dimensional network. In the scope of having larger pores, its small size is a handicap. In this way, the concept of SBU must be revisited. Instead of considering the SBU as the association of polyhedra, it may be described (Fig. 14) as assemblies of metallic clusters linked by chelating agents, and among the latter,

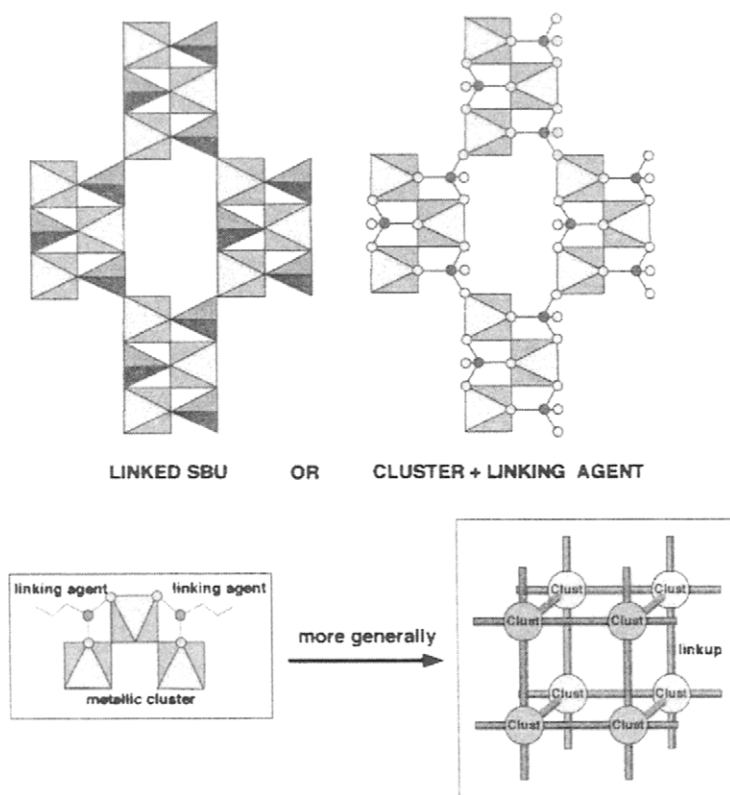


Fig. 14. From SBU to metallic clusters linked by chelating organic molecules.

phosphate is surely the worst since it does not offer any variability for the building of the framework.

Using this approach leads to replace phosphates by other chelating agents. The first attempts concerned phosphonates and were developed by Alberti and Clearfield ([76] and Refs therein) in the early seventies. These authors showed that phosphonates could replace phosphates in a lot of syntheses, but this way was essentially devoted to layered compounds in order to increase the distance between the layers, and not with the aim of obtaining porous compounds. They mainly used monophosphonates, but some further attempts with diphosphonates or functionalized monophosphonates lead to pillared compounds which sometimes offer frameworks with an open structure. Using this way, we recently characterized [77] a porous vanadium(IV) diphosphonate $(\text{NH}_4)_2(\text{H}_2\text{O})_2(\text{VO})(\text{VO}(\text{H}_2\text{O}))_2(\text{O}_3\text{P}-\text{CH}_2-\text{PO}_3)_2$ or MIL-2 (for Materials of Institut Lavoisier) in which the channels are occupied with water molecules and ammonium ions (Fig. 15 (left)).

This method is not restricted to phosphonates but opens the way for many porous hybrid organic-inorganic frameworks in which the organic part belongs to the skeleton and ensures the three dimensional connection of inorganic oligomers or chains and leaves pores which are occupied by easily removable water molecules. The flexibility of the organic chelates, their variability in lengths and shapes allow now to consider the possibility of a real modulation of the pores. For example, we recently characterized zeolithic lanthanide glutarates (Fig. 15 (right)) in which chains of lanthanide polyhedra are linked in the two other directions by glutarate chains [78]. The free aperture is 5 Å, the pores being occupied by water molecules which reversibly evolve the structure at 80°C [79].

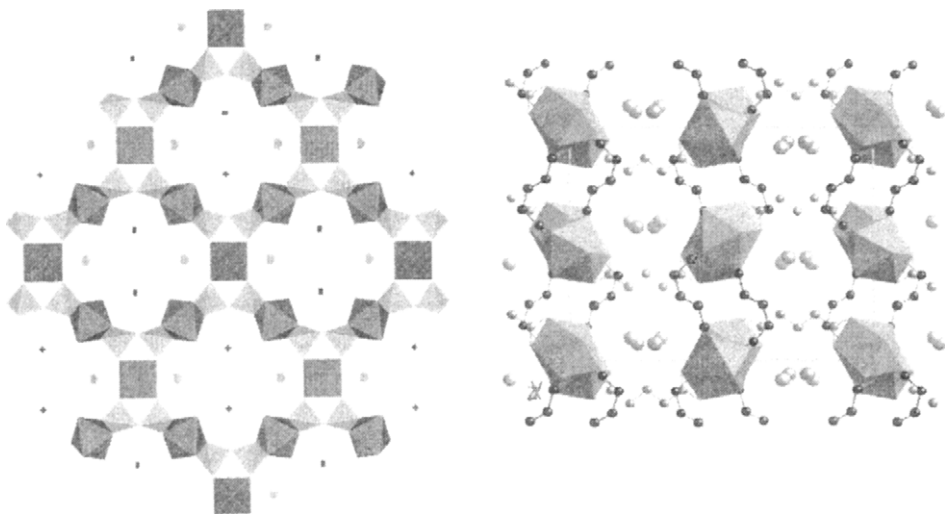


Fig. 15. Projection of the structures of the vanadium phosphonate MIL-2 (left) and of a lanthanide glutarate (right), two hybrid inorganic-organic open frameworks.

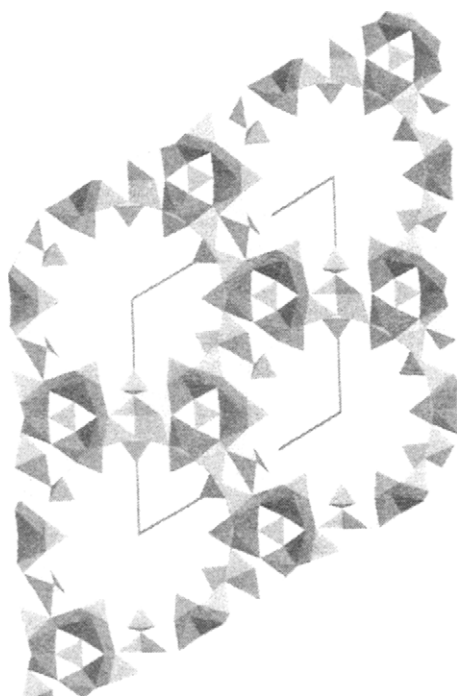


Fig. 16. [001] projection of VSB-1, a nickel fluorophosphate with 24-rings tunnels.

Even if the thermal stability of these compounds will not be very high, they offer a flexible way for obtaining porous compounds with a modulable and predictable size of the pores; this approach seems to be one of the ways to follow in the future for obtaining 'tailor made' porous solids.

Another way to explore comes from a new result recently evidenced in our group, which was just cited in the introduction. It concerns VSB-1 (for Versailles Santa Barbara), a nickel oxyfluorophosphate [22] which is together porous, magnetic and ion exchanger, and which exhibits the largest pores ever discovered with synthetic solids. Indeed the tunnels are 24-rings (Fig. 16). Beside its structural characteristics, it provides also one of the rare examples of a porous solid with only water as template. If one remembers that the largest known pores exist in the mineral Cacoenite [80], and that these pores are filled only by water molecules, this probably represents a new field of research in this area.

Finally, a question obviously arises at the end of this chapter on oxyfluorinated open frameworks. Does open frameworks exist with only fluoride anions? The recent discovery of two-dimensional uranium fluorides templated by alkyldiamines by O'Hare et al. [81,82] is a first answer to the question, and no doubt that in a few years, the discovery of purely fluorinated solids with an open framework will be claimed.

Acknowledgements

The authors are very grateful to their young colleagues of Institut Lavoisier and, for the in situ studies, to the groups of F. Taulelle (UMR 50 Strasbourg) and D.O'Hare (ICL Oxford).

References

- [1] A.F. Cronstedt, *Akad. Handl. Stockholm*, 17 (1756) 120.
- [2] H. de Sainte Claire Deville, *C.R. Acad. Sci.*, 54, (1862) 324.
- [3] M.E. Davis, I.E. Maxwell, *Current Opinion in Solid State & Materials Science*, 1 (1996) 55.
- [4] D.W. Breck, *Zeolite Molecular Sieves: Structure, Chemistry and use*, J.Wiley & Sons., NY, 1974.
- [5] P. Venuto, *Microporous Mater.*, 2 (1994) 297.
- [6] A.K. Cheetham, H. Inokuchi, J.M. Thomas, *Current Opinion in Solid State & Materials Science*, 1 (1996) 55.
- [7] S.T. Wilson, B.M. Lok, C.A. Messina, T.R. Cannan, E.M. Flanigen, *J. Am. Chem. Soc.*, 104 (1982) 1146.
- [8] J.V. Smith, *Chem. Rev.*, 88 (1988) 149.
- [9] J.B. Parise, *Inorg. Chem.*, 24 (1985) 4312
- [10] J.L. Guth, H. Kessler, R. Wey, *Stud. Surf. Sci. Catal.*, 28 (1986) 121.
- [11] M. Estermann, L. McCusker, Ch. Baerlocher, A. Merrouche, H. Kessler, *Nature*, 352 (1991) 320.
- [12] (a) G. Férey, *J. Fluorine Chem.*, 72 (1995) 187; (b) G. Férey, *C.R. Acad. Sci. Série C*, 1 (1998) 1.
- [13] C.T. Kresge, M.E. Leonowicz, W.J. Roth, J.C. Vartuli, J.S. Beck, *Nature*, 359 (1992) 710.
- [14] J.S. Beck, J.C. Vartuli, W.J. Roth, M.E. Leonowicz, C.T. Kresge, *J. Am. Chem. Soc.*, 114 (1992) 10835.
- [15] J.S. Moore, *Nature*, 374 (1995) 495.
- [16] J.S. Beck, J.C. Vartuli, *Current Opinion in Solid State & Materials Science*, 1 (1996) 76.
- [17] R.M. Milton, US Patents, 2882243 and 2882244 (1959).
- [18] R.M. Barrer, P.J. Denny, *J. Chem. Soc.*, (1961) 971.
- [19] E.M. Flanigen, R.L. Patton, US Patent, 4073865 (1978)
- [20] J.L. Guth, H. Kessler, P. Caullet, J. Hazm, A. Merrouche, J. Patarin, *Proc. 9th International Zeolite Conference, Montreal, 1993*, p. 215.
- [21] E. Klock, L. Delmotte, M. Soulard, J.L. Guth, *Proc. 9th International Zeolite Conference, Montreal, 1993*, p. 223.
- [22] N. Guillou, Q. Gao, R. Morris, M. Hervieu, M. Nogues, A.K. Cheetham, G. Férey, *C.R. Acad. Sci. série C* (in press).
- [23] T. Loiseau, D. Riou, F. Taulelle, G. Férey, *Stud. Surf. Sci. Catal.*, 84A (1994) 395.
- [24] T. Loiseau, G. Férey, *J. Mat. Chem.*, 6 (1996) 1073.
- [25] J.M. Lehn, *Angew. Chem., Int. Ed. Engl.*, 27 (1988) 89.
- [26] O.M. Yagui, Z. Sun, D.A. Richardson, T.L. Groy, *J. Am. Chem. Soc.*, 116, (1994) 807.
- [27] D. Venkataraman, G.B. Gardner, S. Lee, J.S. Moore, *J. Am. Chem. Soc.*, 117, (1995) 11600.

- [28] W.M. Meier, D.H. Olson, Ch Baerlocher, Atlas of Zeolite Structure Types, 4th Edn, Elsevier, 1996.
- [29] D.E. Akporiaye, H. Fjellvag, E.N. Halvorsen, T. Haug, A. Karlsson, K.P. Lillerud, Chem. Comm., (1996) 1553.
- [30] G. Férey, F. Taulelle, T. Loiseau, P. Lacorre, J. Solid State Chem., 105 (1993) 179.
- [31] D. Riou, T. Loiseau, G. Férey, J. Solid State Chem., 102 (1993) 4.
- [32] M. Adachi, J. Corker, H. Kessler, F. Lefebvre, J.M. Basset, Microporous and Mesoporous Materials, 21 (1998) 81.
- [33] H.L. Zubowa, H. Kosslick, H.E. Carius, S. Frunza, L. Frunza, H. Landsmesser, M. Richter, E. Schreier, U. Steinike, R. Fricke, Microporous and Mesoporous Materials, 21 (1998) 467.
- [34] R.L. Bedard, C.L. Bowes, N. Coombs, A.J. Holmes, T. Jiang, S.J. Kirkby, P.M. Macdonald, A.M. Malek, G.A. Ozin, S. Petrov, N. Plavac, R.A. Ramik, M.R. Steele, D. Young, J. Am. Chem. Soc., 115 (1993) 2300.
- [35] M. Richter, H.L. Zubowa, R. Eckelt, R. Fricke, Microporous. Mesoporous Mat., 7 (1996) 119.
- [36] J.M. Bennett, R.M. Kirchner, Zeolites, 11 (1991) 502.
- [37] A. Simmen, J. Patarin, Ch. Baerlocher, Proc. 9th International Zeolite Conference Montreal, 1993, p. 433.
- [38] P. Reinert, B. Marler, J. Patarin, Chem. Comm., (1998) 1769.
- [39] F. Taulelle, A. Samoson, T. Loiseau, G. Férey, J. Phys. Chem., B102 (1998) 8588.
- [40] S. Weigel, S.C. Weston, A.K. Cheetham, G.D. Stucky, Chem. Mater., 9 (1997) 1293.
- [41] T. Loiseau, R. Retoux, P. Lacorre, G. Férey, J. Solid State Chem., 111 (1994) 427.
- [42] X. Yin, L. Nazar, J. Chem. Soc. Chem. Comm., (1994) 2349.
- [43] M. Cavelllec, D. Riou, G. Férey, Eur. J. Solid State Inorg. Chem., 31 (1994) 583.
- [44] T. Loiseau, F. Taulelle, G. Férey, Microporous. Mat., 9 (1997) 83.
- [45] T. Loiseau, N. Simon, G. Férey, J. Chem. Soc. Dalton Trans 7 (1999) 1147.
- [46] T. Loiseau, F. Taulelle, G. Férey, Microporous Mat. 5 (1996) 365.
- [47] T. Loiseau, G. Férey, J. Solid State Chem., 111 (1994) 403.
- [48] T. Wessels, L.B. McCusker, Ch. Baerlocher, P. Reinert, J. Patarin, Microporous Mesoporous Mater., 23 (1998) 67.
- [49] T. Loiseau, G. Férey, J. Chem. Soc., Chem. Comm., (1992) 1197.
- [50] D.W. Breck, E.M. Flanigen, Molecular Sieves Soc. Chem. London, (1968) 47.
- [51] R.M. Barrer, J.W. Baynham, F.W. Bultitude, W.M. Meier, J. Chem. Soc., (1959) 195.
- [52] S.P. Zhdanov, Adv. Chem. Ser., 101 (1971) 20–27.
- [53] M.E. Davis, R.F. Lobo, Chem. Mater., 4 (1992) 756.
- [54] R.F. Mortlock, A.T. Bell, C.J. Radke, J. Phys. Chem., 97 (1993) 767.
- [55] M. Henry, J.P. Jolivet, J. Livage, Structure and Bonding, 77 (1992) 153
- [56] (a) J.S.O. Evans, R.J. Francis, D. O'Hare, S.J. Price, S.M. Clarke, J. Flaherty, J. Gordon, A. Nield, C.C. Tang, Rev. Sci. Instr., 66 (1995) 2442; (b) R.J. Francis, D. O'Hare, J. Chem. Soc. Dalton Trans., (1998) 313; (c) A.K. Cheetham, C.F. Mellot, Chem. Mater., 9 (1997) 2269.
- [57] R.J. Francis, S.J. Price, S. O'Brien, A.M. Fogg, D. O'Hare, T. Loiseau, G. Férey, Chem. Comm., (1997) 521
- [58] R.J. Francis, S.J. Price, S. O'Brien, A.M. Fogg, D. O'Hare, T. Loiseau, G. Férey, J. Am. Chem. Soc., 121 (1999) 1002.
- [59] C. In-Gézardard, M. In, F. Taulelle, J. Chim. Phys., 92 (1995) 1877.
- [60] C. Gérardard, M. In, L. Allouche, M. Haouas, F. Taulelle, J. Chem. Mater. 11 (1999) 1285.

- [61] M. Haouas, C. Gérardin, F. Taulelle, C. Estournes, T. Loiseau, G. Férey, *Colloids and Surfaces A.*, (1999) in press.
- [62] F. Serpaggi, T. Loiseau, D. Riou, M.W. Hosseini, G. Férey, *Eur. J. Sol. State Inorg. Chem.*, 31 (1994) 583.
- [63] G. Bonavia, R.C. Haushalter, J. Zubieta, *J. Solid State Chem.*, 126 (1996) 292.
- [64] D. Riou, G. Férey, *J. Solid State Chem.*, 111 (1994) 422.
- [65] M. Cavellec, D. Riou, J.M. Grenèche, G. Férey, In: *MRS series: Microporous and Macroporous Compounds*, 431 (1996) 57.
- [66] M. Cavellec, D. Riou, J.M. Grenèche, G. Férey, *Microporous Mesoporous Mater.*, 20 (1998) 45.
- [67] M. Cavellec, D. Riou, J.M. Grenèche, G. Férey, *Microporous Mater.*, 8 (1997) 103.
- [68] K.H. Lii, Y.F. Huang, *J. Chem. Soc. Dalton Trans.*, (1997) 2221.
- [69] R.C. Haushalter, private communication.
- [70] A.R. Cowley, A.M. Chippindale, *J. Chem. Soc. Chem. Comm.*, (1996) 673.
- [71] P. Feng, X. Bo, G.D. Stucky, *Nature*, 388 (1997) 735.
- [72] E. Kemnitz, M. Wloka, S. Trojanov, A. Stiewe, *Angew. Chem., Intl. Ed. Engl.*, 35 (1996) 2677.
- [73] M. Wloka, S. Trojanov, E. Kemnitz, *J. Solid State Chem.*, 135 (1998) 293.
- [74] C. Serre, N. Guillou, G. Férey, *J. Mater. Chem.*, 9 (1999) 1185.
- [75] C. Serre, G. Férey, *J. Mater. Chem.*, 9 (1999) 579.
- [76] A. Clearfield, *Current Opinion in Solid State & Materials Science*, 1 (1996) 268.
- [77] D. Riou, O. Roubeau, G. Férey, *Microporous Mesoporous Mat.*, 23 (1998) 23.
- [78] F. Serpaggi, G. Férey, *J. Mater. Chem.*, 8 (1998) 2737.
- [79] F. Serpaggi, T. Luxbacher, A.K. Cheetham, G. Férey, *J. Solid State Chem.*, 145 (1999) 580.
- [80] P.B. Moore, J. Shen, *Nature*, 306 (1983) 356.
- [81] R.J. Francis, P.S. Malasyamani, D. O'Hare, *Chem. Mater.*, 10 (1998) 3131.
- [82] R.J. Francis, P.S. Malasyamani, D. O'Hare, *Angew. Chemie, Intl. Ed. Engl.*, 37 (1998) 2214.

CHAPTER 8

Optical Properties and Applications of Fluoride Glasses

Jean-Luc Adam

Laboratoire des Verres & Céramiques, UMR-CNRS 6512, Université de Rennes 1, Campus de Beaulieu, 35042 Rennes Cedex, France

8.1 Introduction

For two decades, fluoride glasses have generated a growing interest due to exceptional optical properties combined with a relative ease of preparation. Based on heavy metals such as zirconium, barium, indium or gallium and on fluorine anions, the fundamental vibration modes of fluoride glasses are at lower frequencies than that of silica glass. This results in an extended optical transmission domain up to 6–10 μm in the infrared, depending on the glass composition. Another major consequence is the lower probability of non-radiative mechanisms in rare-earth-doped fluoride glasses. Thus, several radiative emissions of rare-earth ions, which are weak or absent in silica, can be observed in fluoride glasses.

This paper reviews the optical properties of undoped and activated fluoride glasses for the period 1985–1998. First, the infrared transmission, Rayleigh scattering, and refractive indices of several fluoride glasses are given and discussed. For the sake of completeness, fundamental physical characteristics such as thermo-mechanical properties are also given, although they may have been published before this period.

Then, the spectroscopic properties of rare-earth-activated fluoride glasses are extensively reviewed with emphasis on radiative transitions specific to low-phonon-energy materials. The various preparation methods of fluoride glass fibers are detailed and the characteristics of more than thirty fiber lasers are given. Rare-earth-doped fluoride glass lasers operate at discrete wavelengths from the UV (381 nm) to the mid-IR (3.9 μm). From a practical point of view, several visible lasers can be pumped via efficient up-conversion processes by means of commercially available laser diodes. In the long-wavelength side, lasing is reported in the eye-safe domain, above 1.4 μm , and in transparency domains of the atmosphere, around 2 μm and in the 3–5 μm window. Fluoride glass optical amplifiers for the three telecommunication windows, at 0.8, 1.3 and 1.55 μm , receive special attention, especially praseodymium and erbium-doped amplifiers.

Finally, the most recent results on fluoride glass channel waveguides are presented. Channel waveguides are a promising technology for low-cost integrated optics and appear as complementary components of optical fibers. The physical vapor deposition and ionic exchange techniques are detailed in this paper together with a demonstration of optical amplification with neodymium ions.

8.2 General physical properties of fluoride glasses

The chemical compositions of fluoride glasses mentioned in this review are given in Table 1. Based essentially on zirconium fluoride, ZBLAN, ZBLA and ZBL glasses are referred to as fluorozirconate glasses. In addition to indium fluoride, fluoroindate glasses usually contain appreciable amounts of gallium fluoride and barium fluoride. BIG glass is one of them. A large number of different fluorozirconate and fluoroindate glass compositions are actually used worldwide, and only most representative glasses are listed in Table 1.

PZG is characterized by a high lead content, which results in a high refractive index for that glass. ZnSB, with 80–90% Zn—Sr—Ba, is an example of divalent fluoride glass. CNBZn and CNBK are chlorofluoride glasses, which contain 22 and 33 mol% CdCl_2 in addition to divalent and monovalent fluorides.

The glass transition temperature, T_g , of fluoride glasses is in the 300°C range, and melting occurs at temperatures T_m between 450 and 600°C, depending on the glass composition. An estimation of the glass stability is given by the Hruby factor — $H_r = (T_x - T_g) / (T_m - T_x)$ where T_x is the crystallization temperature — which must be as large as possible. On this basis, ZBLAN appears very stable against devitrification. In addition, thermal analysis curves show a weak crystallization peak for that glass. These favorable conditions are confirmed experimentally by a better ability of ZBLAN for fiber drawing, as compared to other fluoride glasses.

Because of the presence of chlorine ions, which form lower energy bonds with the glass forming cations, CNBZn and CNBK present low glass transition and melting temperatures. Typically, these temperatures are equal to 150°C and 300°C, respectively. Therefore, both glasses are quite stable against devitrification on the one hand and sensitive to hydrolysis on the other hand. The corrosion is due to a preliminary ionic exchange between OH^- and Cl^- at the glass surface followed by the diffusion of the hydroxyl groups inside the glass.

The densities (d), refractive indices at sodium D-line (n_D) and linear expansion coefficients (α) are also given in Table 1, for information. One should remark the higher refractive indices measured for glasses containing highly polarizable elements such as Pb or Cl.

8.3 Passive optical properties of fluoride glasses

8.3.1 Transmission of fluoride glasses

Optical transmission is an essential physical characteristic of halide glasses in the sense that, except for beryllium-based fluoride glass, this property differentiates

Table 1

Chemical compositions and physical properties of fluoride glasses

Glass	Composition (mol%)	T_g ($\pm 2^\circ\text{C}$)	T_x ($\pm 2^\circ\text{C}$)	T_m ($\pm 3^\circ\text{C}$)	$d(\pm 0.02)$ (g cm^{-3})	n_D (± 0.002)	α ($\pm 6 \cdot 10^{-7} \text{ K}^{-1}$)
ZBLAN	53ZrF ₄ —20BaF ₂ —4LaF ₃ —3AlF ₃ —20NaF	262	352	455	4.34	1.498	200
ZBLA	57ZrF ₄ —34BaF ₂ —5LaF ₃ —4AlF ₃	305	388	545	4.58	1.512	187
BIG	30BaF ₂ —18InF ₃ —12GaF ₃ —20ZnF ₂ — 10YbF ₃ —6ThF ₄ —4ZrF ₄	332	460	576	5.44	1.505	171
PZG	35.3PbF ₂ —23.5ZnF ₂ —34.3GaF ₃ — 4.9YF ₃ —2AlF ₃	270	325	547	≈ 5.5	≈ 1.59	170
ZnSB	47ZnF ₂ —24SrF ₂ —10BaF ₂ —5CdF ₂ — 6InF ₃ —4GaF ₃ —2LaF ₃ —2NaF	303	377	615	4.87	1.498	227
CNBZn	18CdF ₂ —22CdCl ₂ —30NaF—20BaF ₂ — 10ZnF ₂ —	158	259	—	4.45	1.570	276
CNBK	17CdF ₂ —33CdCl ₂ —34NaF—13BaF ₂ —3KF	137	249	296	4.00	1.650	215

easily halide glasses from traditional oxide glasses. It is because of their broad transmission in the mid-infrared that heavy-metal fluoride glasses, such as those based on zirconium fluoride, were first investigated.

Fluoride glasses usually start transmitting around 250 nm in the UV, which corresponds to an energy gap of ≈ 5 eV. For comparison, pure silica shows a better UV transparency with an energy gap of ≈ 8 eV ($\lambda \approx 160$ nm). In the infrared, fluoride glasses (except BeF_2 -based glasses) are transparent at wavelengths greater than or equal to $5 \mu\text{m}$, depending on the nature of the main cation in the glass. Glasses with large, heavy and lightly-charged elements will possess lower phonon energies and a consequent extended infrared transparency. The IR multiphonon edge may attain $10 \mu\text{m}$ for ZnF_2 -based glasses.

Infrared transmission spectra are shown in Fig. 1 for typical tetravalent-, trivalent-, and divalent-based fluoride glasses. With a refractive index of ≈ 1.5 at sodium D-line, fluoride glasses show a nearly constant transmission of $\approx 92\%$ throughout the visible and near infrared. The loss is due primarily to 4% reflection at each end-face of the glass sample.

For ZBLAN, the IR edge is in the $5\text{--}8 \mu\text{m}$ range with a 50% transmission located at $\approx 7.1 \mu\text{m}$ (1400 cm^{-1}) for a 2 mm-thick sample. This is to be compared with silica glass whose transparency starts decreasing at $\approx 3 \mu\text{m}$. The IR edge is due to multiphonon absorption processes related to the fundamental vibration frequencies

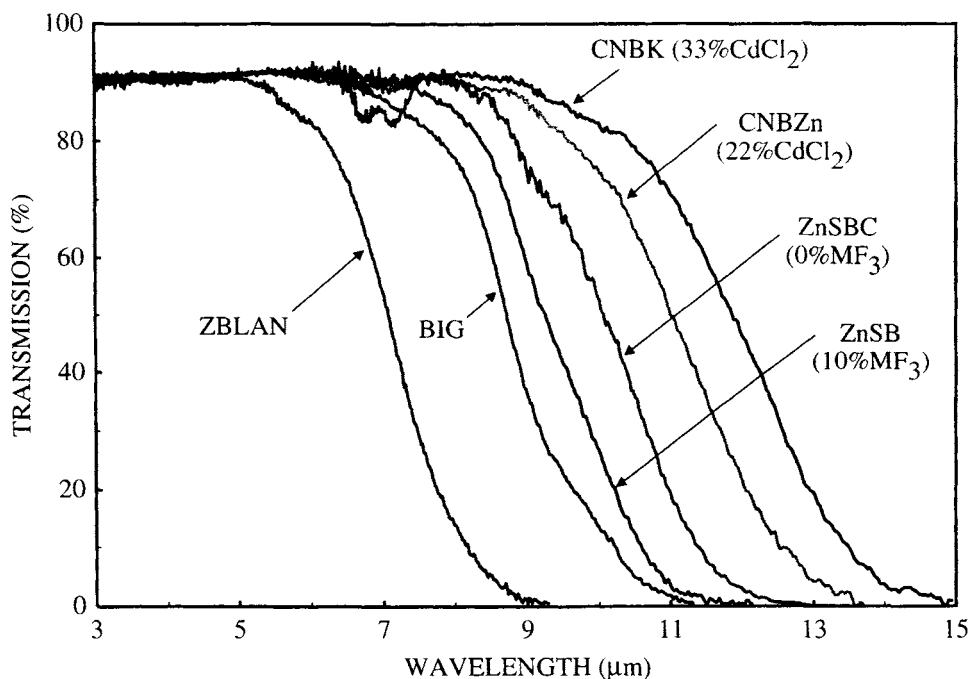


Fig. 1. Infrared transmission spectra of fluoride glasses. M = trivalent metal ions.

of the host. For ZBLAN, Zr—F vibrations around 580 cm^{-1} account for the multiphonon absorption, while, for silica, the position of the IR edge is due to Si—O vibrations at 1100 cm^{-1} .

When substituting hafnium for zirconium, the larger atomic weight of the former results in fundamental vibrations with lower frequencies and, consequently, with an IR edge shifted towards longer wavelengths. The IR edges of several ZrF_4 , HfF_4 , or ThF_4 -based fluoride glasses can be found in Refs [1–4]. For all compositions, the presence of AlF_3 has a detrimental effect on transmission. This is due to the high fundamental frequency of Al—F bonds, typically 650 cm^{-1} .

Fluoride glasses based on trivalent metals belong essentially to two families with distinct optical properties: $\text{InF}_3/\text{GaF}_3$ -based glasses and AlF_3 -based glasses. IR transmission for a typical $\text{InF}_3/\text{GaF}_3$ glass, referred to as BIG, is given in Fig. 1. A shift by more than $1.5\text{ }\mu\text{m}$ in the IR is observed as compared to standard ZBLAN glass [5–7]. This is due to the lower frequency of In—F bonds ($\approx 510\text{ cm}^{-1}$) with respect to Zr—F. The detrimental effect of aluminum shifts the IR transparency of AlF_3 -based glasses down to $6\text{--}7\text{ }\mu\text{m}$ [8,9], to be compared with $8\text{ }\mu\text{m}$ for an Al-free BIG glass.

Except for BeF_2 , glasses based on divalent fluorides show a broader IR transparency than glasses based on indium or zirconium, as reported for ZnSB and ZnSBC in Fig. 1 [10]. They exhibit a full transparency up to $9\text{ }\mu\text{m}$ for the former and $10\text{ }\mu\text{m}$ for the latter which is a pure MF_2 fluoride glass containing Zn, Sr, Ba, and Cd.

BeF_2 glass shows a special behavior, as far as optical transmission is concerned. Although it is a pure divalent glass, the light and small beryllium cation induces a narrow IR transmission with a cut-off wavelength in the $4\text{--}5\text{ }\mu\text{m}$ range, comparable to most silica glasses [11]. Ohno et al. [12] have studied the influence of BeF_2 content on AlF_3 -based glasses. The IR edge shifts dramatically from $\approx 7\text{ }\mu\text{m}$ (50% T) with 0% BeF_2 down to $\approx 5\text{ }\mu\text{m}$ with only 25 mol% BeF_2 .

8.3.2 Intrinsic light scattering in fluoride glasses

The knowledge of intrinsic scattering losses is of prime importance for determining the theoretical minimum loss of halide glass fibers. In addition to multiphonon absorption and, in a lesser extent, to UV absorption, intrinsic scattering contributes to the total intrinsic attenuation of optical fibers [13]. Of course, extrinsic losses due to light-absorbing impurities, Mie scattering due to defects whose size is similar to the wavelength and wavelength independent scattering due to larger scattering centers add to the intrinsic contribution.

The Rayleigh scattering loss (α_{RS}) is simply given by:

$$\alpha_{\text{RS}} = A/\lambda^4, \quad (1)$$

where A is the Rayleigh scattering coefficient expressed in $(\text{dB km}^{-1}\text{ }\mu\text{m}^4)$, with λ in μm units.

Rayleigh scattering includes true intrinsic light scattering from microscopic density and composition fluctuations, and scattering due to sub-micron particles, whose intensity varies with the nature of the glass and the conditions of its preparation. Both processes obey a λ^{-4} dependence, and constitute globally most of the published results on *intrinsic* scattering. Raman and Brillouin scattering mechanisms, which are typically one or two orders of magnitude smaller than Rayleigh scattering are not considered here.

The Rayleigh scattering coefficient was estimated theoretically for some fluoride glasses by means of the following equation:

$$A = 8/3 \pi^3 n^8 p^2 \beta k_B T_g \quad (2)$$

where n is the refractive index of the glass, p is the average photoelastic constant, β is the isothermal compressibility, T_g is the glass transition temperature, and k_B is the Boltzmann's constant. Theoretical Rayleigh coefficients as low as ≈ 0.11 and $0.4 \text{ dB km}^{-1} \mu\text{m}^4$ were calculated for two distinct ZrF_4 -based glasses [14,15]. This compares favorably with the coefficient of $0.65 \text{ dB km}^{-1} \mu\text{m}^4$ reported for SiO_2 glass.

Attaining the theoretical level of intrinsic Rayleigh scattering necessitates, at first, stringent glass preparation conditions. Especially, the melting conditions play an important role. In order to avoid the particle contamination associated with the use of crucibles for glass melting, Lopez and Baniel have developed a containerless gas film levitation technique [16,17]. They obtained a Rayleigh coefficient of $0.66 \text{ dB km}^{-1} \mu\text{m}^4$ for a ZBLAN bulk glass. This is the lowest value reported to date for that glass. Moreover, the Rayleigh scattering loss is comparable to that of silica. It is, however, still a factor of 6 higher than the theoretical limit determined for zirconium-based fluoride glasses [14].

The results presented above were obtained at wavelengths in the visible. However, since the minimum loss of heavy-metal fluoride glasses is at about $2.5 \mu\text{m}$, it is desirable to know the experimental values of Rayleigh scattering in the infrared. Thus, Tran et al. measured the scattering losses for a fluorozirconate glass at six wavelengths ranging from 2.4 to $3.2 \mu\text{m}$ [18]. The experimental light scattering losses obeyed a typical Rayleigh λ^{-4} behavior and were lower, by nearly 30%, than that of silica at $2.5 \mu\text{m}$ extrapolated from results in the visible.

Scattering measurements were performed for optical fibers as well, and a typical λ^{-4} dependence was observed [19]. Considering the thermal history of fiber glass, which experiences critical re-heating between T_g and T_x during preform casting and drawing, a pure Rayleigh behavior must be considered as a great achievement. This result shows that fluoride fibers with particles no greater than the sub-micron scale can be obtained.

Day and France found that the addition of lead fluoride to ZBLAN fibers caused, however, a marked increase of the Rayleigh coefficient ($A = 1.12 \text{ dB km}^{-1} \mu\text{m}^4$) [20], [21]. Very likely, this is due to an increase of the concentration of submicron crystallites related to the lower stability of ZBLAN-Pb glass, as compared to pure ZBLAN.

8.3.3 Refractive index of fluoride glasses

8.3.3.1 Glass composition dependence

Most fluoride glasses show refractive indices of about 1.5 at sodium D-line. However, this parameter has to be accurately controlled for the realization of fluoride glass fibers whose core index must be significantly larger than that of the cladding glass. Usually, the increase is obtained by addition of heavy, highly-polarizable ions such as Pb^{2+} or Cl^- . Substitution of 4 mol% PbF_2 for BaF_2 in both BIG and ZBLAN glasses is sufficient to increase the refractive index by 10^{-2} , the minimum value required to ensure light guiding in the fiber [22]. Some applications such as optical amplification at $1.3 \mu\text{m}$ necessitate optical fibers with high numerical aperture, that is with high refractive index difference. This is achieved by addition of higher content of lead fluoride [23]. However, this is detrimental to the glass thermal stability towards devitrification.

Typical of sodium-containing glasses such as ZBLAN or BIG-Na, another way to increase the refractive index is to substitute Li^+ for Na^+ ions, despite the lower polarizability of lithium ions because of their small size. Actually, Li^+ ions are so small that they induce a local collapse of the glassy network resulting in an increase of the densification and of the refractive index [10,24,25]. This property is utilized for the elaboration of fluoride glass planar waveguides by ionic exchange, as described in Sec. 5.3.

On the other hand, a significant decrease of the refractive index can be obtained by substitution of alkali ions or aluminum ions for Ba^{2+} in both ZBLAN and BIG glasses [22,25], or by substitution of hafnium for zirconium in ZBLA [2].

8.3.3.2 Dispersion

The knowledge of refractive index variations with wavelength is essential for determining accurately the potential of optical devices based on glass fibers and bulks. Thus, the refractive index dispersion has been studied in various fluoride glasses such as fluorozirconates [2,26,27], fluoroindates [28] and fluoroaluminates [29] for wavelengths ranging from the visible to $5 \mu\text{m}$ in the infrared. The results, obtained at room temperature, obey the following dispersion formula:

$$n(\lambda) = A/\lambda^4 + B/\lambda^2 + C + D\lambda + E\lambda^4 \quad (3)$$

The parameters A, B, C, D, and E are listed in Table 2 for ZBLAN and BIG glasses. Typically, the refractive index drops rapidly with increasing wavelengths in the $0.4\text{--}1 \mu\text{m}$ region and, then, decreases moderately at longer wavelengths. Fleming et al. have studied the dispersion of beryllium-based fluoride glasses [30].

8.4 Active optical properties of rare-earth-doped fluoride glasses

Fluoride glasses are hosts of prime interest for rare-earth spectroscopy. They show low phonon energies, which induce high quantum efficiencies of rare-earth

Table 2

Room temperature coefficients of refractive index dispersion curves

Glass	A (μm^4)	B (μm^2)	C	D (μm^{-2})	E (μm^{-4})	Ref.
ZBLAN	$13.5123 \cdot 10^{-6}$	$2.94780 \cdot 10^{-3}$	1.48965	$-1.30933 \cdot 10^{-3}$	$-3.23335 \cdot 10^{-6}$	[27]
BIG	$4.6485 \cdot 10^{-5}$	$3.0267 \cdot 10^{-3}$	1.499700	$-9.6782 \cdot 10^{-4}$	$0.1010 \cdot 10^{-5}$	[28]

emissions. Thus, a number of transitions, which can not be detected in silica-based rare-earth-doped glasses, are observed in fluoride glasses.

8.4.1 General properties

Extensive research including the study of radiative and non-radiative properties of rare-earth ions has been carried out. Especially, the Judd–Ofelt theory has been applied to most rare-earth — fluoride-glass combinations. Typical Judd–Ofelt parameters are reported in Table 3 for ZBLAN glass [31–34]. An exhaustive list of such parameters for glasses and crystals can be found in Ref. [35].

In most cases, the Judd–Ofelt parameters are calculated with good confidence considering that results from various laboratories are convergent. They are found to adequately predict the radiative properties — lifetimes and branching ratios — of several transitions especially for Ho^{3+} , Er^{3+} , and Tm^{3+} ions in ZBLAN as well as in fluoroindate glasses.

The Judd–Ofelt parameterization accounts fairly well for the properties of Nd^{3+} in fluoride glasses, although the calculated radiative lifetime of the $^4\text{F}_{3/2}$ level is quite systematically overestimated, as compared to the experiment. For instance, for fluorozirconate glasses, the experimental lifetime is in the 400–450 μs range, to be compared with 450–500 μs for the calculated one [36].

Table 3

Judd–Ofelt parameters Ω_t ($t = 2, 4, 6$) of rare-earth ions in ZBLAN fluoride glasses

Rare-earth ion	Ω_2 (10^{-20} cm^2)	Ω_4 (10^{-20} cm^2)	Ω_6 (10^{-20} cm^2)	Ref.
Pr^{3+}	1.60	5.06	4.79	[31]
Nd^{3+}	2.20	2.82	3.94	[31]
Sm^{3+}	2.06	2.55	1.63	[32]
Eu^{3+}	2.89	3.87	2.88	[33]
Gd^{3+}	3.35	—	2.81	[34]
Tb^{3+}	0.03	1.88	2.48	[32]
Dy^{3+}	3.03	1.32	2.06	[32]
Ho^{3+}	2.14	2.22	2.05	[33]
Er^{3+}	2.67	1.41	1.02	[31]
Tm^{3+}	2.21	1.71	0.92	[32]

Special care must be taken when applying the Judd–Ofelt theory to Eu^{3+} ions. At room temperature, absorption occurs not only from the $^7\text{F}_0$ ground state, but also from the thermalized $^7\text{F}_1$ level located $\approx 300\text{ cm}^{-1}$ above. Thus, the respective population of both levels must be considered to properly apply the theory [37,38]. Very good agreement between experiment (4 ms) and calculation (4.2 ms) was obtained for the $^5\text{D}_0$ lifetime of Eu^{3+} in a fluorophosphate glass [38].

Just like in other hosts, the Judd–Ofelt approach is not satisfactory for Pr^{3+} ions in fluoride glasses because of possible mixing effect between 4f and 5d electrons. In addition, in most cases, the strong hypersensitive $^3\text{P}_2$ absorption band has to be suppressed from the fitting procedure to obtain a positive Ω_2 parameter. For ZBLAN, the Judd–Ofelt parameterization is found to fairly predict the radiative lifetime and branching ratios for the $^3\text{P}_0$ emitting level, while only branching ratios can be evaluated for $^1\text{D}_2$. Depending on the authors, the computed radiative lifetime of the $^1\text{G}_4$ level is given between 2 and 3.8 ms.

Several solutions were proposed to improve the standard Judd–Ofelt theory in the case of Pr^{3+} . Thus, Medeiros Neto et al. [39] have described a modified Judd–Ofelt theory based on a 4-phenomenological-parameter fitting procedure. This modified theory leads to a significant improvement of the quality of the fit and a consequent acceptable agreement between experimental and calculated lifetimes for the $^1\text{D}_2$ level. Other techniques derived from the Judd–Ofelt approach incorporate the measured fluorescence branching ratios [40] or take into account a relative deviation between experimental and calculated oscillator strengths [41].

One of the main spectroscopic properties that differentiate fluoride glasses from silica-based glasses is the low multiphonon emission rate. These non-radiative relaxations that may strongly compete with radiative processes in rare-earth ions are nearly three orders of magnitude lower in ZBLAN glass than in silicate, as shown in Fig. 2. This property is directly related to the fundamental vibration modes of the host and, therefore, varies basically in the same manner as the infrared absorption edge.

Raman spectroscopy or far-IR spectroscopy can determine the fundamental vibration frequencies of the host. However, these methods give information about the whole glass matrix and do not account for the local nature of electron-phonon interactions. So, the fundamental frequencies are preferably determined by recording the phonon-side bands (PSB) of rare-earth transitions or by studying the temperature-dependence of multiphonon relaxations [42,43]. The phonon energies determined by PSB spectroscopy, which is the most direct method, are usually lower (400 cm^{-1} in ZBLAN) than those measured by other methods ($\approx 500\text{ cm}^{-1}$) suggesting that weak M–F bonds are coupled to the rare-earth [43].

In cadmium chloro-fluoride glass, the highest phonon energy is around 370 cm^{-1} which corresponds to Cd–F vibrations [44]. This results in low multiphonon emission rates for CNBK glass, as shown in Fig. 2.

8.4.2 Praseodymium (Pr^{3+})

The optical properties of Pr^{3+} ions have been studied in various fluoride glasses based on zirconium [31,43,45–47], on indium [31,43,48,49] or on zinc fluorides [48,50].

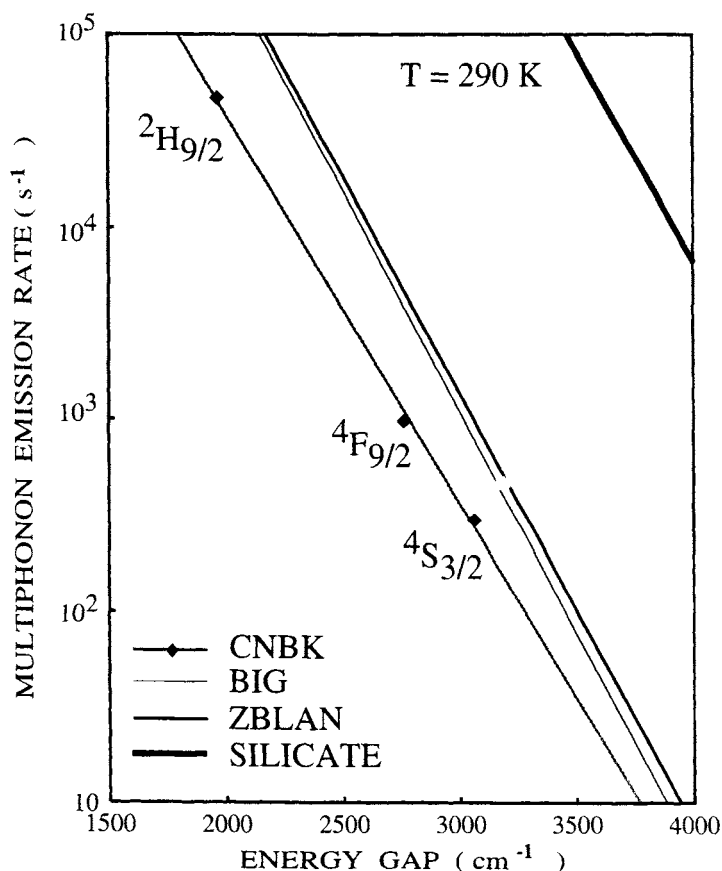


Fig. 2. Multiphonon emission rates of rare-earth ions in silicate, fluoride and chlorofluoride glasses. The position of three levels of Er^{3+} ions are indicated, with respect to the energy gap to the next-lower level (reproduced with permission from Eur. J. Solid State Inorg. Chem., 31 (1994) 337 [44]).

Pr^{3+} -doped fluoride glasses are efficient emitters in the visible with strong emissions in the blue, green and red domains from the ($^3\text{P}_0$, $^3\text{P}_1$) levels as shown in Fig. 3. These levels can be excited by various up-conversion mechanisms. When exciting at 588 nm, that is into the $^1\text{D}_2$ level, a cross-relaxation process involving two neighboring ions promotes one electron up to the $^3\text{P}_2$ level — right above ($^3\text{P}_0$, $^3\text{P}_1$) — while the other one is down to $^1\text{G}_4$. This process, which is concentration-dependent, results in the characteristic $^3\text{P}_0 \rightarrow ^3\text{H}_4$ blue emission of Pr^{3+} ions [51]. Remillieux et al. demonstrated excitation of the $^3\text{P}_0$ level via non-resonant 2-photon ESA or energy transfer up-conversion mechanisms [52]. Single-wavelength excitation was used at 919 nm, 883 nm or 796 nm.

Visible emissions can also be obtained by means of 2-step excited state absorption (ESA) mechanisms involving two different wavelengths [53,54] and a single ion. Pr^{3+} ions are first excited into the $^1\text{G}_4$ level with 1010 nm light and then a second pump

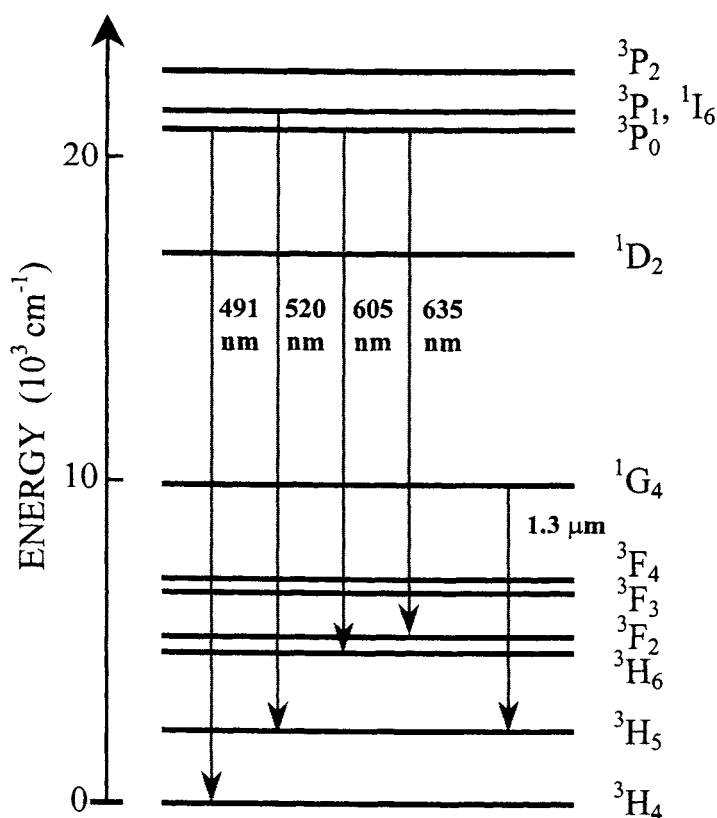


Fig. 3. Energy level diagram and selected emissions of Pr^{3+} ions in fluoride glasses.

laser at either 916 nm or 835 nm promotes the electrons into $^3\text{P}_0$ or $^3\text{P}_1$, respectively. It is to be noted that the second process, which can take advantage of existing laser diodes for pumping, offers a realistic combination for generating blue light. Blue light is also obtained with a direct two-930-nm-photon absorption in Pr^{3+} -singly-doped fluorozirconate fibers [53] or by energy transfer up-conversion in Yb^{3+} , Pr^{3+} -codoped glasses [55].

The 1.3 μm emission of Pr^{3+} ions has been extensively studied because of its suitability for optical amplification in the second telecommunication window. This emission, which occurs from the $^1\text{G}_4$ excited state to the $^3\text{H}_5$ level, peaks at 1.31 μm as shown in Fig. 4. Because of an energy gap of about 3000 cm^{-1} between $^1\text{G}_4$ and $^3\text{F}_4$, this transition is observed exclusively in low-phonon energy materials such as fluorides, chlorides, sulfides and so on. It shows a favorable branching ratio of nearly 0.65 in fluoride glasses [31] and ESA of the emission wavelength, located in the long-wavelength side of the band [56,57], is by far not as severe as for the 1.3 μm emission of Nd^{3+} ions (see Sec. 4.3). A main drawback is the weak oscillator strength of the $^3\text{H}_4 \rightarrow ^1\text{G}_4$ absorption which results in poor pumping conditions.

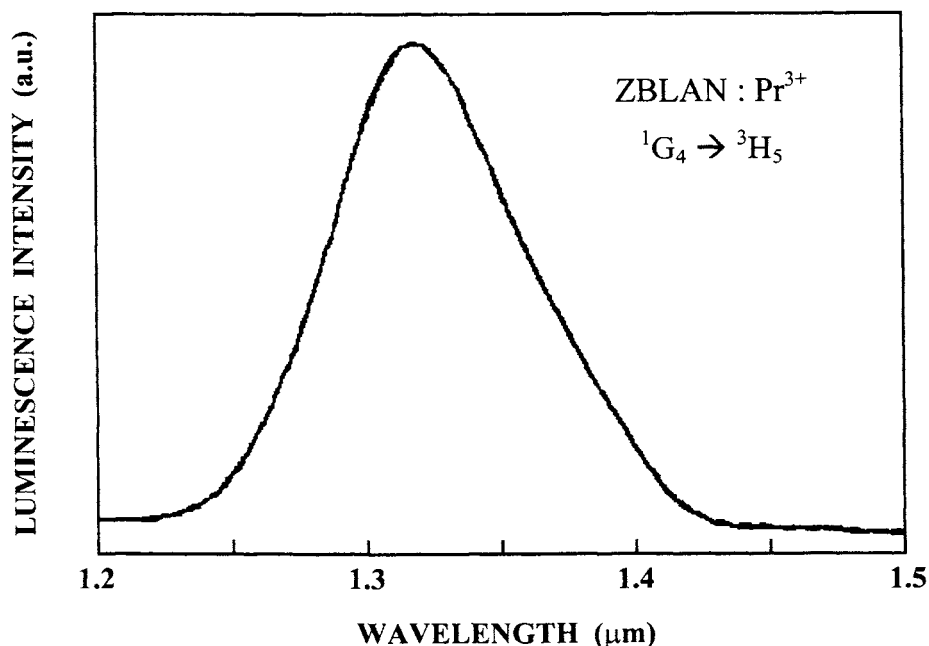


Fig. 4. 1.3 μm emission of Pr^{3+} ions in ZBLAN fluoride glasses.

This can possibly be improved by codoping with Yb^{3+} whose $^2\text{F}_{5/2}$ level coincides with $^1\text{G}_4$ [58,59].

Recently, researchers at Corning Inc. have demonstrated 1.3 μm emission in a Pr^{3+} -doped oxyfluoride glass ceramic [60–62]. A relatively high quantum efficiency of 8–9% was found, to be compared with 3% in ZBLAN glass. This indicates that Pr^{3+} ions are embedded in a crystalline fluoride environment. With such oxyfluoride vitroceramics, one takes advantage of the good mechanical properties of oxide materials, of easier shaping of glasses, and of better emission efficiencies of rare-earth ions in crystallized fluoride environment.

8.4.3 Neodymium (Nd^{3+})

Nd^{3+} ions are by far the most widely investigated ions in all types of materials, essentially because of the ideal, 4-level, 1.06 μm laser transition from $^4\text{F}_{3/2}$ to $^4\text{I}_{11/2}$ shown in Fig. 5. Thus, the spectroscopic properties of Nd^{3+} ions are reported for a large number of different compositions of fluorozirconate, fluoroindate, fluorohafnate, fluoroaluminate and other kinds of fluoride glasses [31,36,63–69].

A classical mean to excite the $^4\text{F}_{3/2}$ level is to take advantage of energy transfer processes between Cr^{3+} ions and Nd^{3+} ions in codoped glasses. Excitation energy is efficiently absorbed via the strong $^4\text{A}_2 \rightarrow ^4\text{T}_2$ absorption of Cr^{3+} before being transferred to the ($^4\text{F}_{5/2}$, $^2\text{H}_{9/2}$) and $^4\text{F}_{3/2}$ levels of Nd^{3+} . This transfer is found

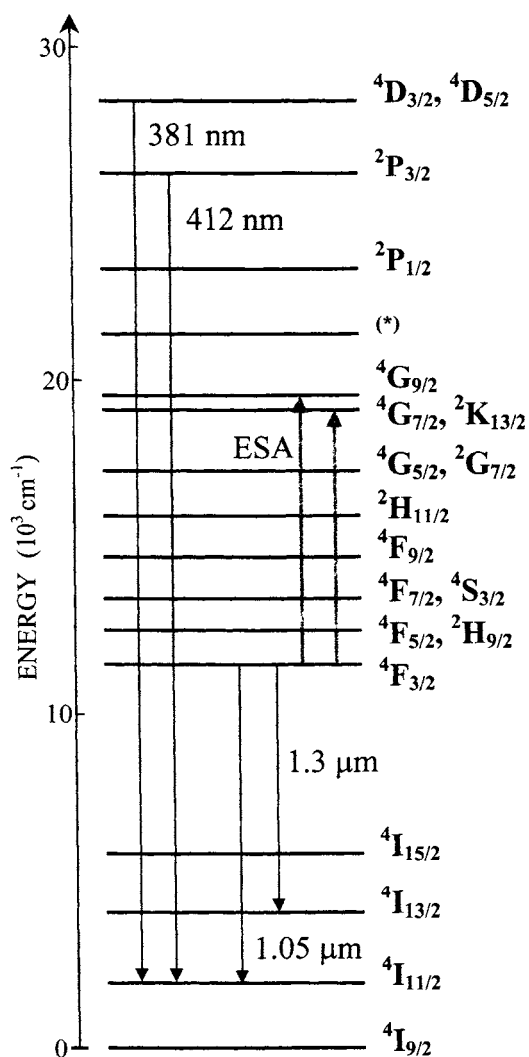


Fig. 5. Energy level diagram and selected transitions of Nd^{3+} ions in fluoride glasses. (*): $^2\text{D}_{3/2}$, $^2\text{G}_{9/2}$, $^4\text{G}_{11/2}$, and $^2\text{K}_{15/2}$ levels.

to be efficient essentially at low temperatures (77 K) because non-radiative relaxations from $^4\text{T}_2$ down to $^4\text{A}_2$ are predominant in Cr^{3+} at room temperature [66,70].

Lasing has been demonstrated at $1.06 \mu\text{m}$ in Nd^{3+} -doped ZBLAN and BIG fluoride glass rods pumped by an alexandrite laser and xenon flashlamps, respectively [71,72]. Fig. 6 shows the $1.06 \mu\text{m}$ laser output energy out of Nd^{3+} -doped and Cr^{3+} : Nd^{3+} -codoped fluorindate glass rods of $\sim 40 \text{ mm}$ length. In presence of Cr^{3+} ions, which are efficient absorbers of excitation light from flashlamps,

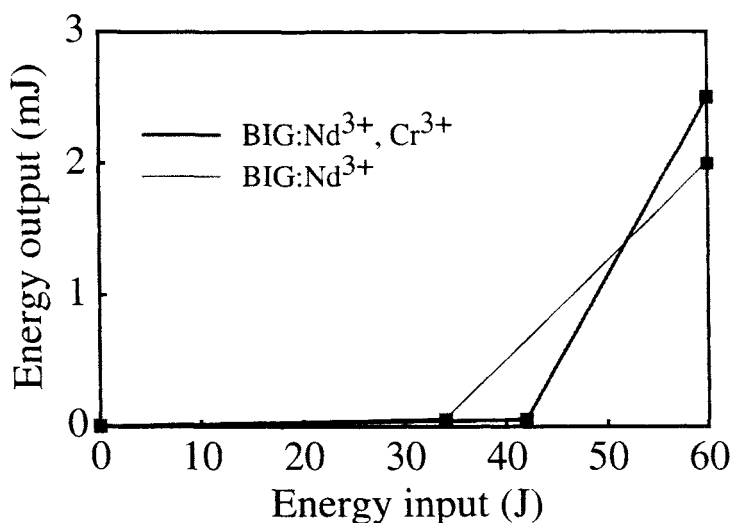


Fig. 6. 1.06 μm laser output energy as a function of lamp discharge energy in $\text{Nd}^{3+}(1\%)$ -doped and $\text{Cr}^{3+}(0.1\%)$; $\text{Nd}^{3+}(1\%)$ codoped fluorindate glass rods.

the slope efficiency is significantly higher. Thus, despite a higher threshold, the maximum output of 2.5 mJ is measured out of the codoped rod with the greatest available discharge of 60 J.

Thanks to the low phonon energy of fluoride glasses, some high energy levels of Nd^{3+} ions can be efficiently populated leading to emissions at several wavelengths ranging from the UV to the red. These emitting high-energy levels are indicated in the diagram in Fig. 5 with the two most intense transitions ${}^4\text{D}_{3/2} \rightarrow {}^4\text{I}_{11/2}$ at 381 nm and ${}^2\text{P}_{3/2} \rightarrow {}^4\text{I}_{11/2}$ at 412 nm. These levels can be pumped by up-conversion processes involving 2 photons of 532 nm from a doubled Nd:YAG laser [73]. The first photon excites the ${}^4\text{G}_{7/2}$ level and, after relaxation down to ${}^4\text{F}_{3/2}$, a second photon promotes the electrons to the upper levels. Three-step up-conversion of 866 nm light leading to emission from ${}^4\text{D}_{3/2}$ and ${}^2\text{P}_{3/2}$ is demonstrated in Nd^{3+} -doped fluorindate glass [74].

Up-converted UV and visible emissions occur also from lower-lying levels such as ${}^2\text{P}_{1/2}$, (${}^2\text{D}_{3/2}$ ${}^2\text{G}_{9/2}$ ${}^4\text{G}_{11/2}$ ${}^2\text{K}_{15/2}$), ${}^4\text{G}_{7/2}$ and ${}^4\text{G}_{5/2}$ with excitation at 532 nm or 801 nm [75,76]. Excitation of ${}^4\text{D}_{3/2}$ requires a 3-step process with 801 nm pumping. Due to the predominance of multiphonon relaxations from these levels, experimental lifetimes are very short, in the tens of nanosecond range.

With an emission at 1.3 μm , Nd^{3+} is a potential candidate for optical amplification in the second telecommunication window. However, optical gain remains limited because of amplified spontaneous emission at 1.05 μm and also because of strong ESA at 1.3 μm . This ESA process, which takes place from ${}^4\text{F}_{3/2}$ to (${}^4\text{G}_{7/2}$, ${}^2\text{K}_{13/2}$) and to ${}^4\text{G}_{9/2}$ as shown in Fig. 5, is so probable that no gain is achieved around 1.3 μm in silica fibers. In ZBLAN fluoride fibers, gain is achieved at 1.34

μm , too far away from the $1.31\ \mu\text{m}$ wavelength required for telecommunication [77]. A new pump-probe technique was recently developed to investigate ESA processes directly from bulk samples [78], with no measurements on optical fibers whose preparation is difficult and time-consuming. The gain and ESA profiles determined by this technique for ZBLAN bulk glass are shown in Fig. 7.

The stimulated-emission spectrum is calculated by the Fuchtbauer–Ladenburg equation. The excited-state absorption bands in the $1.3\ \mu\text{m}$ region are obtained by subtracting the calculated stimulated emission profile from the recorded spectrum. The short-wavelength component, around $1230\ \text{nm}$, corresponds to the ${}^4\text{F}_{3/2} \rightarrow {}^4\text{G}_{9/2}$ transition. Despite its intensity, this band is not broad enough to alter the ${}^4\text{F}_{3/2} \rightarrow {}^4\text{I}_{13/2}$ stimulated emission. Conversely, the long-wavelength ESA component, around $1320\ \text{nm}$ (${}^4\text{F}_{3/2} \rightarrow ({}^2\text{K}_{13/2}, {}^4\text{G}_{7/2})$), coincides with the maximum of the stimulated emission peak, resulting in a negative signal at wavelengths below $1310\ \text{nm}$ for ZBLAN. For BIG fluoroindate glasses, a higher stimulated emission cross-section results in an increase of the signal at $1320\ \text{nm}$, as compared to ZBLAN [79]. It must be mentioned that these results are in excellent agreement with those reported for fibers in terms of ESA profiles, and in terms of overall excited-state spectrum as compared to optical gain response [77]. This indicates that gain profiles in rare-earth-doped fibers can efficiently be predicted by means of excited-state spectroscopy applied to simple parallel-plate samples.

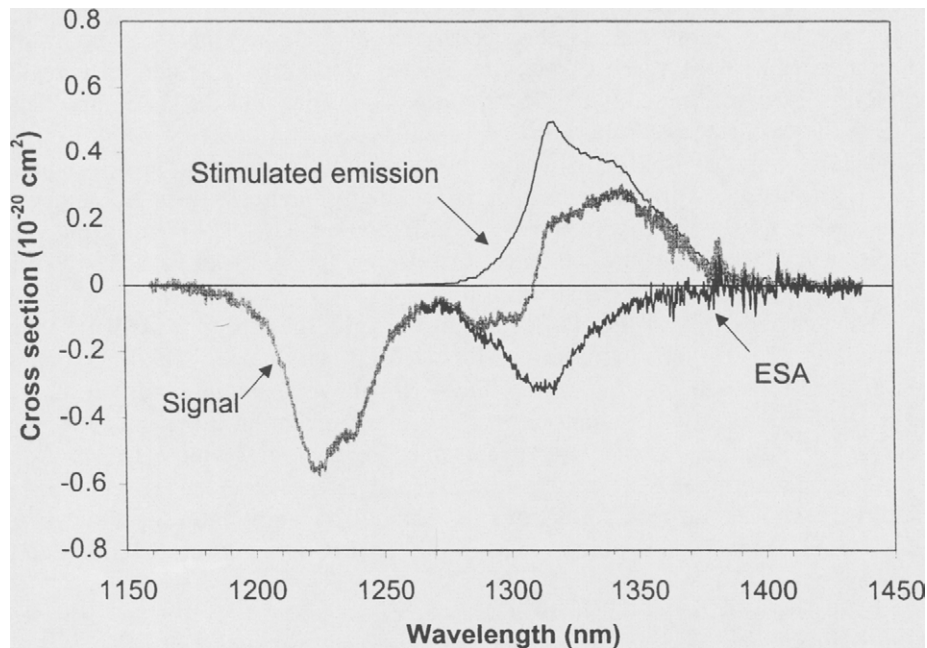


Fig. 7. Excited state absorption in the $1.3\ \mu\text{m}$ region in ZBLAN:Nd³⁺ glass.

8.4.4 Europium (Eu^{3+})

When excited with UV light, Eu^{3+} ions luminesce in the red, green, blue and even violet spectral domains [37,80–83]. Such a broad spectrum can be observed in low-phonon-energy materials only. Thus, the short-wavelength transitions originate from the higher-lying $^5\text{D}_3$ and $^5\text{D}_2$ levels which are phonon-energy sensitive. The $^5\text{D}_3 \rightarrow ^7\text{F}_{0,1,2}$ blue emissions are found to increase with decreasing europium concentration. This is because of the absence of energy transfer processes via cross-relaxation at low concentration. At higher concentrations, these processes contribute to depopulate $^5\text{D}_3$ for the benefit of $^5\text{D}_2$, $^5\text{D}_1$, and $^5\text{D}_0$, resulting in enhanced green and red emissions [37].

Several studies have been performed with fluoride glasses containing Eu^{3+} as probe ions for structural investigations. Site-selective spectroscopy has been carried out with fluorozirconate [80,84–87], fluoroindate [84] and chlorofluorozirconate glasses [88]. The $^5\text{D}_0$ emitting level of europium is a singlet, and, therefore, the interpretation of band profiles is more straightforward than for transitions between multiplets. Thus, the measurements were carried out by monitoring the $^5\text{D}_0 \rightarrow ^7\text{F}_1$ and the $^5\text{D}_0 \rightarrow ^7\text{F}_2$ emissions under resonant excitation. All measurements show a similar spectral evolution, that is a broadening of $^5\text{D}_0 \rightarrow ^7\text{F}_1$ with decreasing excitation wavelength which reflects the variety of sites in glasses. Moreover, additional components show up in the $^5\text{D}_0 \rightarrow ^7\text{F}_1$ profile when excitation is in the high-energy side of the $^7\text{F}_0 \rightarrow ^5\text{D}_0$ absorption band. Deconvolution of the spectra shows that six components are present, while only three Stark components are expected for $^5\text{D}_0 \rightarrow ^7\text{F}_1$. A controversy exists about the interpretation of these six-component spectra. Some teams explain the occurrence of six components as being due to two non-equivalent types of sites connected by energy transfer as revealed by time-resolved spectroscopy [80,84,88]. Others consider that the six-component profile is the result of the superposition of emission from one type of sites only and emission from the whole distribution of sites excited via the phonon-side band (PSB) [85–87]. This new approach, even though quite satisfactory, raises some new questions such as the relatively narrow width of the $^5\text{D}_0 \rightarrow ^7\text{F}_1$ transition via PSB excitation. PSB excitation, which is not selective, should lead to a broad emission spectrum due to the large distribution of sites.

The spectroscopy of the $^5\text{D}_0$ level is also a valuable tool to investigate the point symmetry of Eu^{3+} ions in materials. It is well-known that the $^5\text{D}_0 \rightarrow ^7\text{F}_2$ transition is electric-dipole in nature, while $^5\text{D}_0 \rightarrow ^7\text{F}_1$ shows a magnetic-dipole character. $^5\text{D}_0 \rightarrow ^7\text{F}_2$ is totally forbidden in presence of an inversion center and it is allowed in the opposite case. Usually, in vitreous phases, where the symmetry is low, electric dipolar transitions exhibit the strongest intensity. The fluorescence spectra displayed in Fig. 8 show that both transitions have about the same intensity indicating that Eu^{3+} ions are in high-symmetry sites in fluorozirconate glasses, relatively to oxide glasses.

Comparison of glass and crystals spectra suggests that the site symmetry in fluorozirconates is close to the 8-coordinate bicapped trigonal prism in EuZrF_7 . The similarity is confirmed by lifetime measurements [80] and by photoluminescence

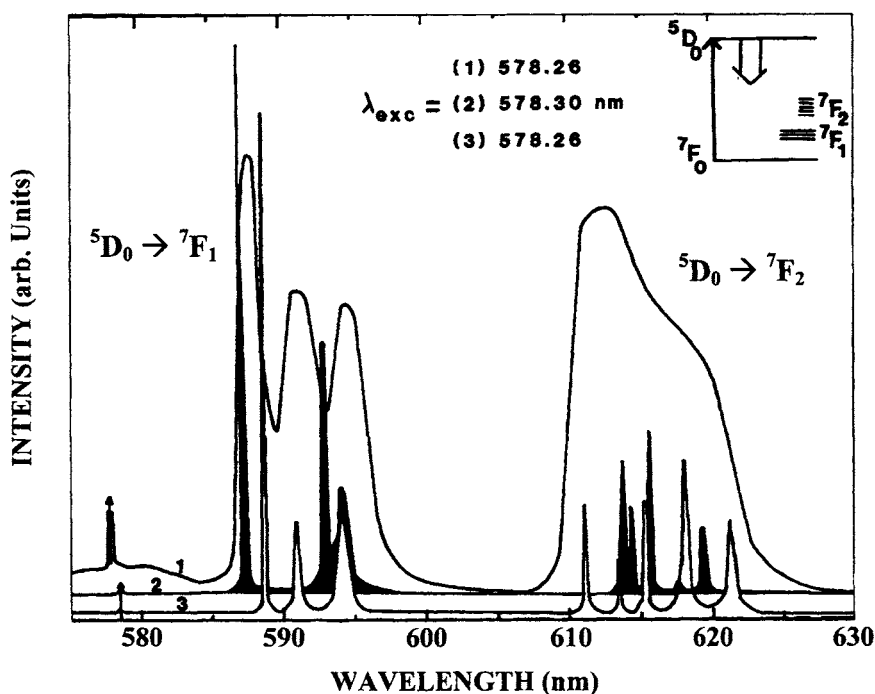


Fig. 8. Fluorescence spectra of Eu^{3+} ions in (1) fluorozirconate glass; (2) EuF_3 ; and (3) EuZrF_7 crystals at 4.4 K (reproduced with permission from J. Non-Cryst. Solids 91 (1987) 191 [80]).

of devitrified samples [87]. The preferential coordination number of 8 is also confirmed by molecular dynamics simulation [86].

8.4.5 Holmium (Ho^{3+})

Due to its numerous radiative emissions in the visible and the IR, holmium has been extensively studied in various fluoride glasses [89–92].

Several transitions are of special interest, namely ($^5\text{S}_2$, $^5\text{F}_4$) \rightarrow $^5\text{I}_8$ around 540 nm, $^5\text{I}_7 \rightarrow ^5\text{I}_8$ at 2 μm and $^5\text{I}_5 \rightarrow ^5\text{I}_6$ at 3.9 μm . These transitions are shown in the energy level diagram in Fig. 9. Emission in the visible can be obtained with excitation in the IR, via up-conversion processes. Thus, blue and green emissions are observed with excitation at 647 nm in Ho^{3+} singly-doped fluorozirconate and fluoroaluminate glasses [93,94]. The process involves two photons according to the following pumping schemes: ($^5\text{I}_8 \rightarrow ^5\text{F}_5$) + ($^5\text{I}_6 \rightarrow ^5\text{G}_5$ and $^5\text{I}_7 \rightarrow ^5\text{F}_3$). The populations of the intermediate levels, $^5\text{I}_6$ and $^5\text{I}_7$, dominate the up-conversion efficiency. In other words, up-conversion is more efficient in low-phonon-energy fluorozirconate glasses than in fluoroaluminates. Cross-relaxation processes are found to account for the concentration dependence of up-conversion. Thus, the $^5\text{I}_7$ lifetime is found to increase with increasing Ho^{3+} concentration (up to 8 mol% in fluoroaluminate glass) which results in a higher up-conversion efficiency.

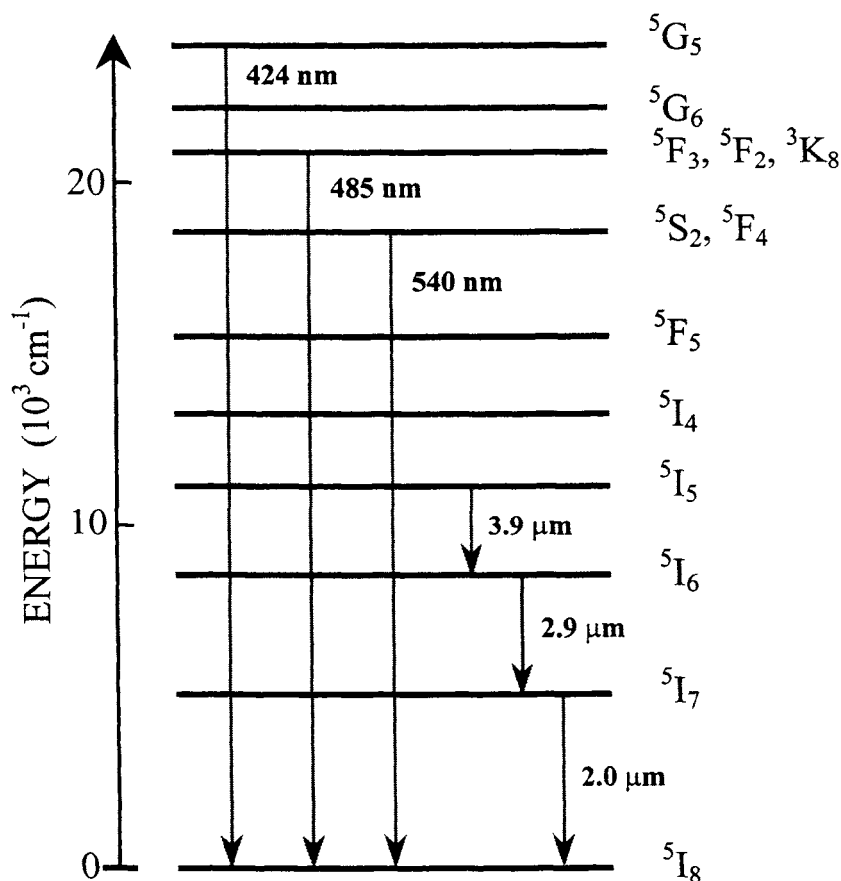


Fig. 9. Energy level diagram and selected emissions of Ho^{3+} ions in fluoride glasses.

The green emission from $^5\text{S}_2$ can also be observed in (Yb, Ho) codoped glasses [95,96]. This is due to a 2-step energy-transfer up-conversion mechanism with excitation around 980 nm, that is in the strong $^2\text{F}_{7/2} \rightarrow ^2\text{F}_{5/2}$ absorption band of Yb^{3+} ions. The first transfer from Yb^{3+} to Ho^{3+} ($^5\text{I}_6$) is non-resonant necessitating the dissipation of an energy of about 1600 cm^{-1} in the lattice. The second transfer promotes the electrons from $^5\text{I}_6$ to $^5\text{S}_2$. Due to a more efficient first-step transfer, fluoroaluminates show more intense up-converted green light, as compared to fluorozirconates.

The $2\text{-}\mu\text{m}$ emission from $^5\text{I}_7$ to $^5\text{I}_8$ was observed in bulk Ho^{3+} -fluoride glasses. This transition could be enhanced by appropriate co-doping with Yb^{3+} or (Er^{3+} , Tm^{3+}) [97]. The $3.9 \mu\text{m}$ transition shows very weak branching ratio and quantum efficiency, so that it is observed only at liquid-nitrogen temperature, in fiber configuration. More details are given in Sec. 8.5.1.2.

8.4.6 Erbium (Er^{3+})

Erbium ions in fluoride glasses possess several radiative transitions from the violet to the mid-IR ($3.45\ \mu\text{m}$) as shown in Fig. 10. Their spectroscopic parameters such as radiative lifetimes and branching ratios were determined for several types of glasses based on zirconium, indium, aluminum or even zinc fluoride [31,98–100].

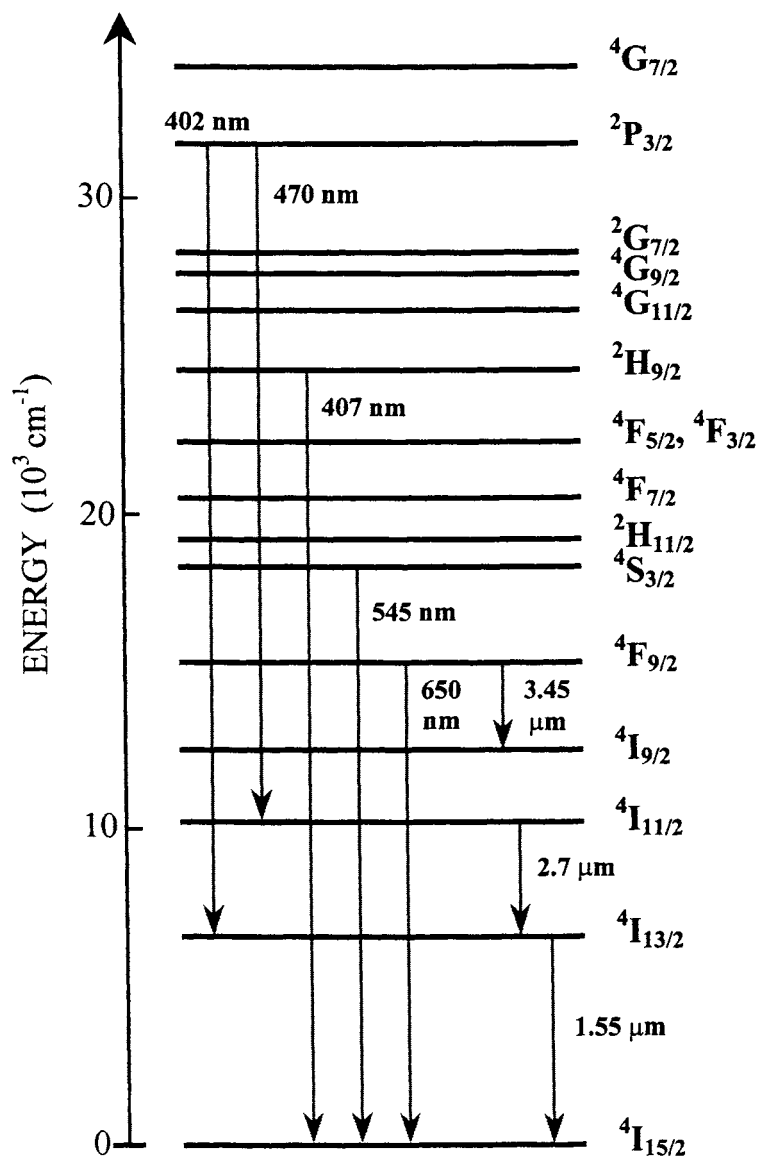


Fig. 10. Energy level diagram and selected emissions of Er^{3+} ions in fluoride glasses.

High-energy levels can be pumped efficiently by various up-conversion processes. Thus, Takahashi et al. showed that strong green emission from $^4S_{3/2}$ and weaker red emission from $^4F_{3/2}$ could be observed in an Er^{3+} -doped fluorozirconate glass with excitation at 800 nm, into $^4I_{9/2}$ [101]. The mechanism involved two photons via ($^4I_{15/2} \rightarrow ^4I_{9/2}$) + ($^4I_{11/2} \rightarrow ^4F_{3/2}$ and $^4I_{13/2} \rightarrow ^4S_{3/2}$), the energy in excess being absorbed by the phonons of the host. While the green emission is essentially due to an ESA process, additional energy transfer governs the red emission, as suggested by the increase of the red to green intensity ratio with Er^{3+} concentration. Energy transfer is possible through several cross-relaxation mechanisms: ($^4S_{3/2} \rightarrow ^4F_{9/2}$; $^4I_{9/2} \rightarrow ^4F_{9/2}$), ($^4S_{3/2} \rightarrow ^4I_{11/2}$; $^4I_{13/2} \rightarrow ^4F_{9/2}$), and ($^4I_{9/2} \rightarrow ^4I_{13/2}$; $^4I_{11/2} \rightarrow ^4F_{9/2}$) [101,102]. Cho et al. have shown that Tm^{3+} -codoping results in a significant increase of up-conversion efficiencies with 786 nm pumping [103]. This is explained by three successive energy transfer steps involving the $^3H_4 \rightarrow ^3F_4$ transition in Tm^{3+} and ($^4I_{15/2} \rightarrow ^4I_{13/2}$, $^4I_{13/2} \rightarrow ^4I_{9/2}$, $^4I_{9/2} \rightarrow ^2H_{11/2}$) in Er^{3+} .

Pumping around 800 nm can also initiate 3-step up-conversion mechanisms leading to violet emission at 407 nm from $^2H_{9/2}$ [104]. The third step originates either from $^4F_{9/2}$ or $^4I_{9/2}$.

The violet, green and red emissions of Er^{3+} ions in fluoride glasses can also be obtained with excitation at 650 nm and 1.48 μm , which are other spectral domains where laser diodes are commercially available. Violet and green emissions are obtained through a 2-step 650 nm up-conversion process, while four and three steps are required with 1.48 μm pumping [105,106]. Excitation at 980 nm into $^4I_{11/2}$ may initiate two-step up-conversion and consequent green and red emissions [107].

Three-fold up-conversion of 637 nm light results in excitation of the $^2P_{3/2}$ level via ($^4I_{15/2} \rightarrow ^4F_{9/2}$) + ($^4I_{13/2} \rightarrow ^4F_{5/2}$) + ($^4S_{3/2} \rightarrow ^4G_{7/2}$), each step being followed by multiphonon relaxations. Efficient blue (470 nm) and violet (402 nm) emissions occur from that level together with weak UV emission at 320 nm down to the $^4I_{15/2}$ ground state [108].

Two-fold energy-transfer up-conversion occurs in (Yb, Er) codoped fluoride glasses with excitation at 980 nm into Yb^{3+} ions. Energy transfer takes place from the $^2F_{5/2}$ level of a first Yb^{3+} ion to the quasi-resonant $^4I_{11/2}$ level of Er^{3+} . Then, transfer from a second Yb^{3+} ion promotes the electrons to $^4F_{7/2}$ (Er^{3+}) and, after successive multiphonon relaxations, green and red emissions from $^4S_{3/2}$ and $^4F_{9/2}$ are observed [109–111]. Enhanced green and red emissions are obtained with two-fold excitation at 800 nm into erbium ions through an $Er \rightarrow Yb \rightarrow Er$ energy transfer mechanism [112]. In an oxyfluoride vitroc ceramic, three-step energy-transfer up-conversion is observed, promoting the violet emission from $^2H_{9/2}$ [113].

The $^4I_{13/2} \rightarrow ^4I_{15/2}$ infrared emission band of Er^{3+} ions in fluorozirconate glass is displayed in Fig. 11. The band maximum is located at 1.53 μm and the width at half-maximum is as broad as 60 nm, which favors the use of this transition for optical amplification in the third telecommunication window. In bulk geometry, 1.6 μm CW-laser action is reported for a Cr, Yb, Er-codoped fluoroaluminate glass slab pumped by a krypton laser [114].

Further in the infrared, lasing at 2.7 μm was obtained with Er^{3+} in bulk fluorozirconate glasses [115,116]. Glass samples were slabs with a few-mm thickness

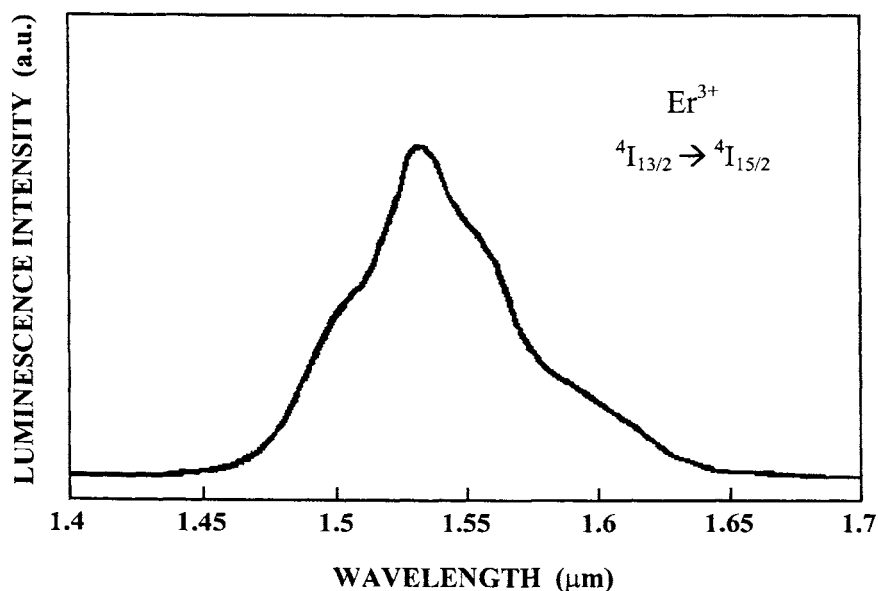


Fig. 11. 1.55 μm emission of Er^{3+} ions in ZBLAN fluoride glasses.

and high rare-earth concentration (4–8 mol%). Pulsed lasing was obtained with flashlamp pumping while CW lasing was achieved with excitation at 514.5 nm from an argon laser. Both systems were operated at room temperature.

8.4.7 Thulium (Tm^{3+})

Fundamental properties of Tm^{3+} ions, such as spontaneous emission probabilities and radiative lifetimes, have been established in fluorozirconate [117,118], and in fluoroindate [119] glasses. The emission spectrum of Tm^{3+} is especially rich with transitions ranging from the UV to the IR as shown in the energy level diagram in Fig. 12. One should note the blue emissions occurring from the $^1\text{G}_4$ and $^1\text{D}_2$ levels, and the IR emission at 1.47 μm from $^3\text{H}_4$ to $^3\text{F}_4$ suitable for amplification between the second and third telecommunication windows. Ultra-violet and blue emissions are also reported from the high-energy $^1\text{I}_6$ level located at nearly $35,000\text{ cm}^{-1}$ (not shown).

Tm^{3+} ions in fluoride glasses are capable of emitting strong blue light with excitation in the red, around 650 nm. The $^1\text{D}_2$ level is populated via the 2-step ($^3\text{H}_6 \rightarrow ^3\text{F}_2 + ^3\text{H}_4 \rightarrow ^1\text{D}_2$) up-conversion mechanism with intermediate non-radiative relaxations from $^3\text{F}_2$ to $^3\text{H}_4$. It must be noted that additional non-radiative and radiative decays occur from $^3\text{H}_4$ to the $^3\text{F}_4$ level whose lifetime is long enough to permit absorption of a second 650-nm photon up to $^1\text{G}_4$. Thus, blue emission can also be obtained from that level by 2-step up-conversion pumping [120–122].

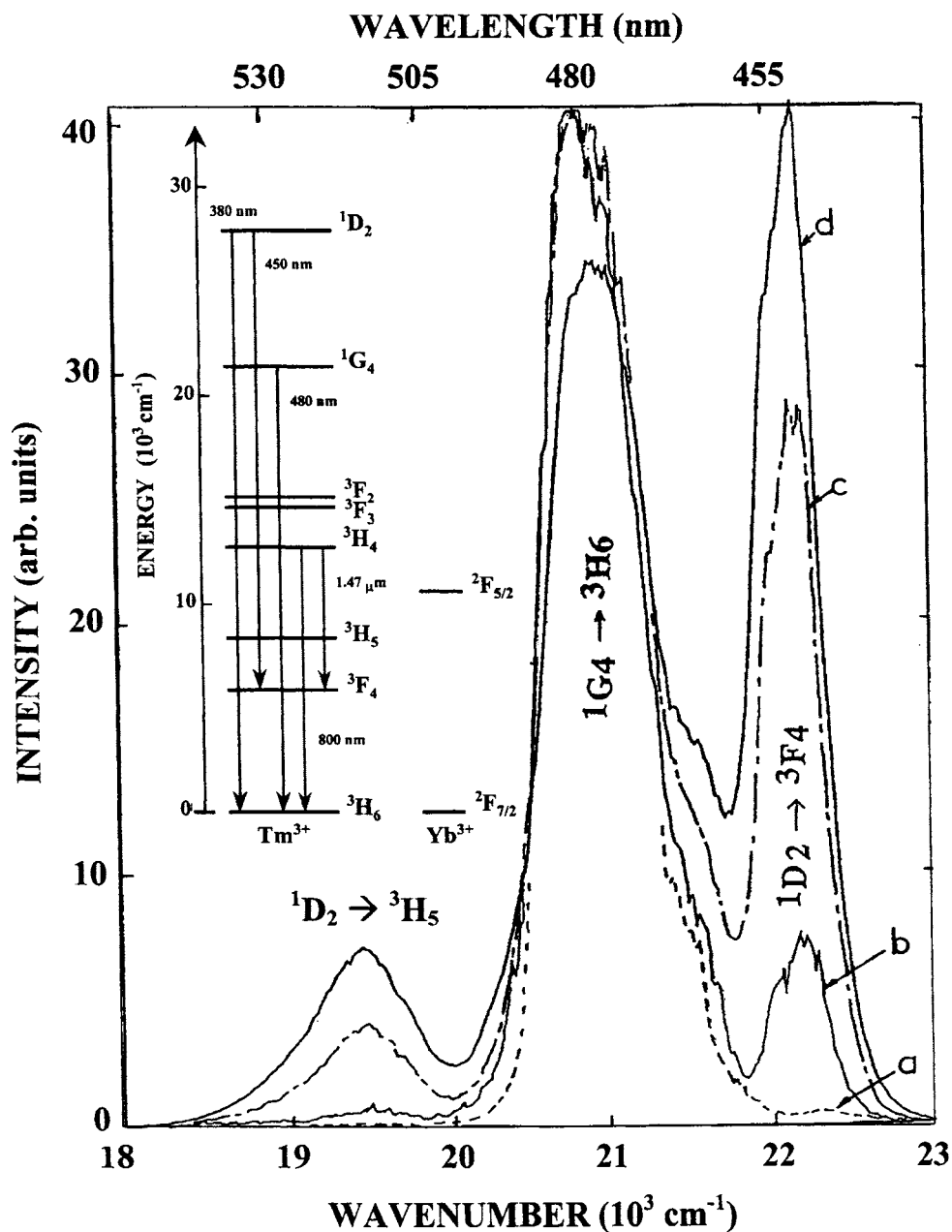


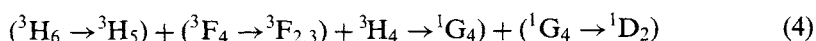
Fig. 12. Room-temperature blue-green emissions spectra of BIG:Yb, Tm (1%) fluoride glass and energy level diagram of Tm^{3+} and Yb^{3+} ions. Excitation is at 975 nm, into the Yb absorption band, for various pumping densities: (a): 0.06; (b) 0.5; (c) 2; (d): 6, in kW cm^{-2} units (reproduced with permission from Adv. Mat. Res., 1-2 (1994) 101 [133]).

Kishimoto et al. have demonstrated that both processes are strongly host dependent [123]. Basically, the up-conversion fluorescence intensity increases with decreasing phonon energy, that is with longer fluorescence lifetimes for the intermediate levels, $^3\text{H}_4$ and $^3\text{F}_4$.

The ($^3\text{H}_4 \rightarrow ^3\text{F}_4$; $^3\text{H}_6 \rightarrow ^3\text{F}_4$) cross-relaxation is an efficient energy transfer mechanism for Tm^{3+} concentration greater than 0.1 mol% in indium-based fluoride glasses [124]. Therefore, the intermediate $^3\text{F}_4$ level can be populated not only by successive multiphonon relaxations from $^3\text{F}_3$, but also through this cross-relaxation process [125].

Co-doping with Yb^{3+} ions results in less effective up-conversion of 650 nm light into 450 nm radiation because of ($^3\text{F}_3 \rightarrow ^3\text{F}_4$; $^2\text{F}_{7/2} \rightarrow ^2\text{F}_{5/2}$) cross-relaxation between Tm^{3+} and Yb^{3+} [123]. This energy transfer process, however, is responsible for the increase of the 480 nm transition because of a larger population of the $^3\text{F}_4$ level and consequent higher probability for absorption of a second 650-nm photon via $^3\text{F}_4 \rightarrow ^1\text{G}_4$ [126]. On the other hand, Eu^{3+} codoping in fluorozirconate fiber leads to enhanced blue emission at 450 nm from $^1\text{D}_2$ and reduced emission at 480 nm from $^1\text{G}_4$ [127]. This is because the $^3\text{F}_4$ level of Tm^{3+} is depopulated by energy transfer to the $^3\text{F}_6$ level of Eu^{3+} . This results in a significant decrease of the $^3\text{F}_4$ fluorescence lifetime. Thus, the $^1\text{D}_2 \rightarrow ^3\text{F}_4$ transition whose terminal level is depleted, is favored, while the $^1\text{G}_4 \rightarrow ^3\text{H}_6$ transition, whose second excitation step originates from $^3\text{F}_4$, is strongly decreased. The effect of other codopants such as Tb^{3+} , Dy^{3+} , Pr^{3+} , Sm^{3+} , and Co^{2+} on $^3\text{F}_4$ depletion was systematically investigated. Theoretical considerations suggest that Tb^{3+} is the most appropriate ion for quenching the thulium $^3\text{F}_4$ lifetime [128].

Blue transitions are also observed with IR excitation at $1.064\ \mu\text{m}$ in Tm^{3+} -doped fluorozirconate fibers. Depending on the pumping power, different up-conversion pathways are identified. For low pumping powers, a four-fold up-conversion process leads to excitation of $^1\text{D}_2$:



with non-radiative decays from $^3\text{H}_5$ and from $^3\text{F}_{2,3}$. With high pump powers, two steps are sufficient for reaching $^1\text{D}_2$. The first step promotes the electrons to $^3\text{F}_4$, possibly to $^3\text{H}_5$ that can be saturated for the highest powers. The second step is believed to be an energy transfer by cross-relaxation between two nearby Tm^{3+} ions: ($^1\text{G}_4 \rightarrow ^3\text{H}_6$; $(^3\text{F}_4, ^3\text{H}_5) \rightarrow ^1\text{D}_2$) [129].

Similarly to Er^{3+} ions, Tm^{3+} ions in fluoride glasses are very efficiently excited by energy transfer from Yb^{3+} ions. Up-conversion processes have been demonstrated in (Yb, Tm) codoped fluorozirconate [130,131], fluorozirconaluminate [96,132], fluoroindate [55,133,134] and thorium-based fluoride glasses [135]. The strong blue emissions observed with excitation at 975 nm in a codoped fluoroindate glass is shown in Fig. 12. For low-power pumping, the $^1\text{G}_4 \rightarrow ^3\text{H}_6$ transition at 480 nm is predominant. The upper level is populated by a 3-step up-conversion mechanism similar to the first three transitions of process (4). With higher pump powers, the $^1\text{D}_2 \rightarrow ^3\text{F}_4$ transition increases dramatically. This phenomenon is interpreted

as being due to a higher population of the 3F_4 level for high pump powers, resulting in excited-state absorption of 480 nm light from 1G_4 and consequent excitation of the 1D_2 level.

The 800 nm transition from 3H_4 to 3H_6 has been extensively studied because of its suitability for optical amplification in the first telecommunication window. With a branching ratio of 90%, this transition is not perturbed by amplified spontaneous emission of competing transitions. The 1.47 μm emission from 3H_4 to 3F_4 is also of special interest for optical amplification between the second and third telecommunication window. Both transitions arise from the 3H_4 level, which can be excited directly at 800 nm with a laser diode. This level can also be pumped by 2-step up-conversion, either from a mini-YAG:Nd at 1.06 μm or from a laser diode at 975 nm, in (Yb, Tm) codoped glasses. Details on these applications are given in Sec. 8.5.2.

Energy transfer processes between Ho^{3+} and Tm^{3+} have been investigated. When Tm^{3+} ions are excited at 800 nm, two different cross-relaxation mechanisms take place: [$^3H_4 \rightarrow ^3F_4$ (Tm); $^3H_6 \rightarrow ^3F_4$ (Tm)] and [$^3H_4 \rightarrow ^3F_4$ (Tm); $^5I_8 \rightarrow ^5I_7$ (Ho)]. Once the 3F_4 and 5I_7 levels are populated, efficient transfer and backtransfer occur, leading to a thermal equilibrium between these two levels [124].

$\text{Er}^{3+} \rightleftharpoons \text{Tm}^{3+}$ energy transfers have been studied as well, in fluorindate [136] and in fluorozirconaluminate glasses [137]. With 790 nm excitation, the introduction of Tm^{3+} ions quenches the green up-conversion fluorescence from the $^4S_{3/2}$ level of Er^{3+} ions. This is due to an efficient cross-relaxation process: [$^4I_{13/2} \rightarrow ^4I_{15/2}$ (Er); $^3H_6 \rightarrow ^3F_4$ (Tm)] which causes a decrease of the population of $^4I_{13/2}$ and reduces consequently the probability for absorption of a second 790-nm photon through $^4I_{13/2} \rightarrow ^4S_{3/2}$ (Er). Conversely, the red emission from $^4F_{9/2}$ (Er) is favored by Tm^{3+} codoping because of [$^3F_4 \rightarrow ^3H_6$ (Tm); $^4I_{11/2} \rightarrow ^4F_{9/2}$ (Er)] cross-relaxation.

8.4.8 Other rare-earth ions: Sm^{3+} , Sm^{2+} , Gd^{3+} , Tb^{3+} , Dy^{3+} , Yb^{3+}

In the last few years, only a few studies have been devoted to the optical properties of Sm^{3+} ions in fluoride glasses [138,139]. The main result concerns the excitation of the $^4G_{5/2}$ level by a three-fold up-conversion process including a direct two-photon absorption mechanism. Izumitani et al. have succeeded in stabilizing divalent samarium in fluoroaluminate and fluorohafnate glasses [140]. Absorption spectra reveal a strong $4f \rightarrow 5d$ transition whose maximum is located around 320 nm. Emission of Sm^{2+} ions in fluoroaluminate glass occurs in the red, between 680 nm and 810 nm, from the 5D_0 excited state to the 7F_J ($J=0, 1, 2, 3, 4$) levels.

Gd^{3+} ion possesses high energy levels located in the UV. Absorption spectra of Gd^{3+} -doped fluoride glasses show several peaks in the 240–320 nm range. They correspond to transitions from the $^8S_{7/2}$ ground state to the 6P , 6I , and 6D excited states. Judd–Ofelt parameters and experimental lifetimes have been determined for Gd^{3+} -doped fluorozirconate [34,141], and fluorindate glasses [142]. X-ray excitation of both glasses leads to radiative emission from all excited states: 6P , 6I ,

and ${}^6\text{D}$ together with a broad emission band in the 350–400 nm region attributed to electron-hole recombination [143].

There has been no reliable results published recently on Tb^{3+} ions in pure fluoride glasses. However, extensive investigations have been conducted in strontium fluorophosphate [144] and sodium fluorophosphate glasses [145]. As far as phonon energies are concerned, fluorophosphate glasses behave essentially like phosphates, rather than fluorides. The recording of phonon sidebands associated with europium emission shows phonon energies of nearly 1100 cm^{-1} in strontium fluorophosphates, to be compared with bands at 1160 and 1300 cm^{-1} in pure phosphate glasses. Thus, a large number of rare-earth emissions can not be observed in fluorophosphate glasses. However, the ${}^5\text{D}_4$ level of Tb^{3+} , which is located $15\,000\text{ cm}^{-1}$ above its next lower level, is not phonon-sensitive and still emits strongly in the visible in fluorophosphate glasses. By monitoring the dominant ${}^5\text{D}_4 \rightarrow {}^7\text{F}_5$ green emission, it is found that the theoretical and experimental lifetimes are similar, around 3.5 ms, confirming the absence of multiphonon relaxations.

It is well-known that concentration quenching of the ${}^5\text{D}_4$ luminescence is not observed in usual glasses whose rare-earth concentration is limited to a few atomic percent. In some sodium fluorophosphate glasses, whose terbium concentration is as high as 35 atm%, ${}^5\text{D}_4$ luminescence quenching is found to occur at concentration of 20 atm% ($3.3 \times 10^{21}\text{ ions cm}^{-3}$) and greater [145].

A two-step up-conversion process involving 982-nm photons is capable of exciting the ${}^5\text{D}_4$ level of Tb^{3+} ions in (Yb, Tb) co-doped fluorophosphate glasses. This is due to a cooperative effect between two Yb^{3+} ions which transfer their energy to one Tb^{3+} ion. The process leads to the characteristic ${}^5\text{D}_4 \rightarrow {}^7\text{F}_5$ green emission. In absence of terbium, the cooperative effect between Yb^{3+} ions still occurs leading to a short-lifetime blue emission [146].

The Judd–Ofelt parameters, radiative properties, and emission spectra of Dy^{3+} ions have been investigated in several fluoride glasses, namely fluorozirconates [147,148], PZG [149], fluorozincate [150], and fluorindate glasses [65]. Excitation in the UV results in visible emissions from the ${}^4\text{F}_{9/2}$ level. One of the main interest of Dy^{3+} ions is the $1.3\text{ }\mu\text{m}$ emission from (${}^6\text{F}_{11/2} + {}^6\text{H}_{9/2}$) to the ground state, which could be utilized for optical amplification in telecommunication. However, with an energy gap to the next lower level of 1900 cm^{-1} , this group of levels cannot emit in any of the glasses listed above. Four phonons only are required for spanning the energy gap, which makes the multiphonon relaxation very probable. In sulfide glasses, whose phonon energy is around 350 cm^{-1} , the $1.3\text{ }\mu\text{m}$ emission of Dy^{3+} is observed [150].

Little basic research has been devoted to Yb^{3+} ion itself which possesses only one excited state [151]. However, as shown previously, this ion is of special interest for a number of energy transfer and up-conversion processes, which take advantage of the strong ${}^2\text{F}_{7/2} \rightarrow {}^2\text{F}_{5/2}$ absorption band of Yb^{3+} . In addition, efficient lasing around $1.02\text{ }\mu\text{m}$ can be obtained with this ion and laser cooling effects have been observed. These points are developed in the next section devoted to applications of rare-earth-doped fluoride glasses.

8.5 Fluoride glass applications and devices

Because of their unique properties, in terms of fluorescence efficiency and broad spectral domain, rare-earth-doped fluoride glasses generate a great deal of interest for fiber laser and optical amplifier applications. Lasing is achieved in fluoride glass fibers at discrete wavelengths ranging from the UV to the mid-IR. In addition, Pr^{3+} fluoride glass fibers are, for the moment, the only realistic components for optical amplification at 1.3 μm .

8.5.1 Fluoride glass fiber lasers

While very few fluoride glass lasers exist in bulk configuration (see Secs 8.4.3 and 8.4.6), more than thirty lasers have been demonstrated in fiber configuration, in the last ten years. This is because the optical fiber geometry is more appropriate than that of bulk material for attaining high optical density and for releasing the heat generated by possible non-radiative processes concomitant to lasing. Optical confinement necessitates the use of single-mode optical fibers with, in several cases, high numerical aperture. Numerical aperture as large as 0.4 can be obtained by adequately modifying the core/clad glass compositions (see Sec. 8.3.3.1).

8.5.1.1 Preparation of single-mode fibers

Various techniques may be employed for the preparation of fluoride fibers and preforms [152]. The basic steps involved in the fabrication of preforms suitable for singlemode fiber are summarized in Fig. 13.

In a first step, two tubes made of cladding glass are cast in a brass mold by emptying the central part of the melt. An alternative to this step is to form tubes by rotational casting which consists in a fast rotation of the mold containing the cladding glass melt [13]. Whatever the method, the core glass, whose refractive index is higher than that of the cladding, is then poured into the first tube, forming a preform. At this stage, the preform is drawn into a small diameter rod — a few millimeters — before being jacketed by the second tube [153,154]. After a final drawing, the new preform that shows a high cladding/core diameter ratio, gives a singlemode fiber whose core diameter is in the 3–10 μm range. Depending on the tube diameter, several jacketing steps may be required to achieve small-core fibers.

Either the traditional built-in casting or the rotational method causes the cladding glass to cool below T_g . So, when pouring the core melt, the inner-part of the tube is reheated well above T_g , which creates favorable conditions for crystal growth at core/clad interface and increases the risk of optical loss by light scattering. Another drawback is the risk of contamination at the interface from the environment. Thus, several methods are developed to improve the built-in casting technique. The tubular-crucible technique, the shutter-mold technique, and the suction-casting method are all based on the principle that the core melt must replace the cladding melt in the central part of the preform before solidification of the cladding is complete. Technical details may be found in References [155–157]. Combined with

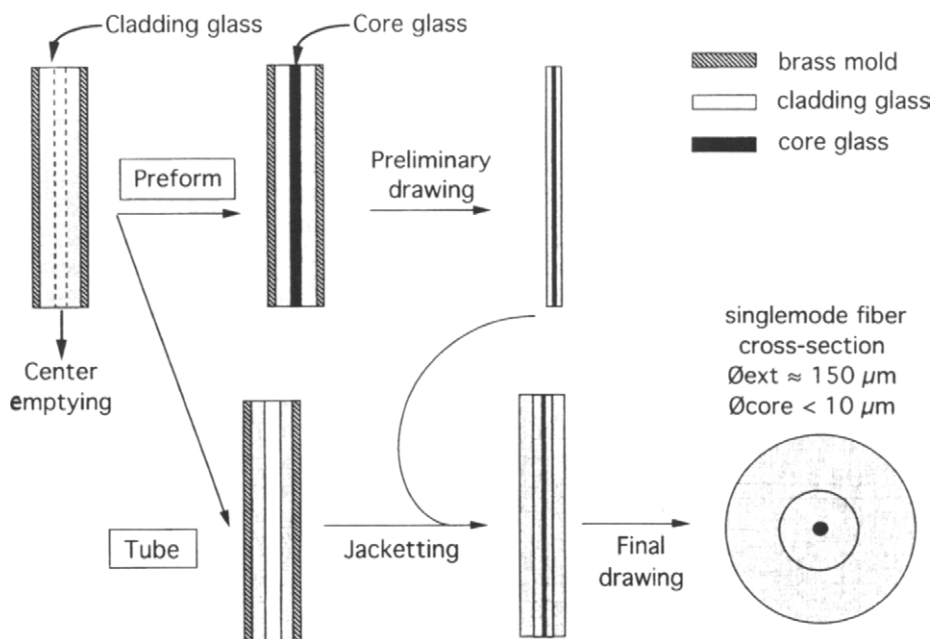


Fig. 13. Preparation of single-mode fluoride glass optical fibers by the jacketing technique (reproduced with permission from *Annales Chim.* 20 (1995) 261, Gauthier-Villars, Paris).

jacketing, the suction method is successfully applied to fluorozirconate and fluoroindate glasses leading to single-mode fibers suitable for *real-world* applications such as lasers and amplifiers.

Whatever the method employed for making the initial preform, one or several jacketing steps are then required to reduce the core/clad ratio. Recently, a single-step procedure was proposed for the fabrication of the final preform [158]. The method necessitates the preliminary elongation of a core-glass rod into a pseudo-fiber. Then, this pseudo-fiber is rapidly inserted into the solidifying cladding glass right before solidification is complete. Pseudo-fibers of $150\ \mu\text{m}$ diameter are successfully inserted that way. However, high optical losses, in the dB/m range, are measured for core/clad fibers pulled from these preforms. They are imputable to impurities in the starting chemicals and drawing-induced defects.

Another technique suitable for fluoride glass preform fabrication is extrusion. This technique consists in the preparation of preforms with the help of pressure (5 MPa) under moderate temperature (410°C). This is a high-viscosity process with less favorable conditions for crystal growth. Losses of $6\ \text{dB km}^{-1}$ are obtained with multimode fluorozirconaluminate fibers drawn from extruded preforms [159,160].

Fluoride glasses are known for being prone to hydrolysis and devitrification. Therefore, whatever the procedure, great care must be taken during all the stages of optical fiber preparation in terms of chemical purity of the starting materials, environment control and heating procedures.

The loss mechanisms in fluoride glass fibers are due to both intrinsic and extrinsic parameters. Intrinsic factors that limit the transparency of the material are the multiphonon absorption process in the long-wavelength side of the spectrum, and the Rayleigh scattering, essentially, in the short-wavelength side. Combining both the absorption and scattering contributions leads to an estimated total intrinsic attenuation of 0.02 dB km^{-1} at $2.5 \mu\text{m}$ for ZBLAN fibers. For comparison, silica fibers show a theoretical attenuation of 0.16 dB km^{-1} at $1.55 \mu\text{m}$, level that was experimentally attained in the late 1970s.

Extrinsic losses include MIE scattering, wavelength-independent scattering and extrinsic absorption. The first process is due to scattering centers whose diameter is of the same order of magnitude as the wavelength. They originate mainly from a partial devitrification of the glass. Larger defects, such as large crystals and bubbles, are responsible for the second process, and the latter one is because of the presence of impurities such as transition metals, undesired rare earths, and hydroxyl ions. Besides OH^- , it has been shown that Fe^{2+} , Co^{2+} , Ni^{2+} , and Cu^{2+} , as well as Pr^{3+} , Nd^{3+} , Sm^{3+} , Eu^{3+} , Tb^{3+} , and Dy^{3+} , are the species absorbing most in the mid-infrared region. [161,162]. Because of these extrinsic factors, one of the lowest attenuation ever achieved with ZBLAN fluoride glass was $0.45 \pm 0.15 \text{ dB km}^{-1}$ at $2.35 \mu\text{m}$, measured for a 60-meter fiber [163]. That is more than one order of magnitude higher than the theoretical value. Detrimental for long distance applications, such level of optical losses is compatible with fiber lasers and amplifiers applications, which require short lengths of fiber only, typically a few meters.

8.5.1.2 Lasing characteristics of rare-earth-doped fluoride fibers

Because of the exceptional guiding properties and confinement provided by optical fibers, lasing has been obtained for a large number of rare-earth transitions, including several three-level systems that hardly lase in bulk configuration. The suitable fiber structure for most applications is close to single mode, that is a core radius in the $2\text{--}10 \mu\text{m}$ range for an outside fiber diameter around $150 \mu\text{m}$. The rare-earth concentration in the core of the fiber is typically $100\text{--}1000 \text{ ppm}$, possibly 1% . Usually, the length is from a few centimeters to several meters. A fiber laser scheme is given in Fig. 14.

The numerous lasing wavelengths that have been observed with fluoride glass fibers are shown in Table 4. Each of them is characterized by the highest output power reported to date, and by the pumping conditions, either direct or through up-conversion.

The development of up-conversion fiber lasers, especially in the visible, is assisted by the availability of intense semiconductor lasers and mini-crystal lasers for pump sources. The various energy levels involved in pumping and lasing transitions are detailed in Sec. 8.4 and in related energy level diagrams.

Room-temperature lasing has been demonstrated in the ultraviolet at 381 nm and in the violet at 412 nm with Nd^{3+} -doped ZBLAN fibers of about 40 cm in length [164,165]. The transitions involved are $^4\text{D}_{3/2} \rightarrow ^4\text{I}_{11/2}$ and $^2\text{P}_{3/2} \rightarrow ^4\text{I}_{11/2}$, as depicted in Fig. 5. Excitation of the $^4\text{D}_{3/2}$ and $^2\text{P}_{3/2}$ levels is obtained by a two- 590 nm -photon up-conversion process. Output powers are equal to $74 \mu\text{W}$ and $500 \mu\text{W}$, with 320

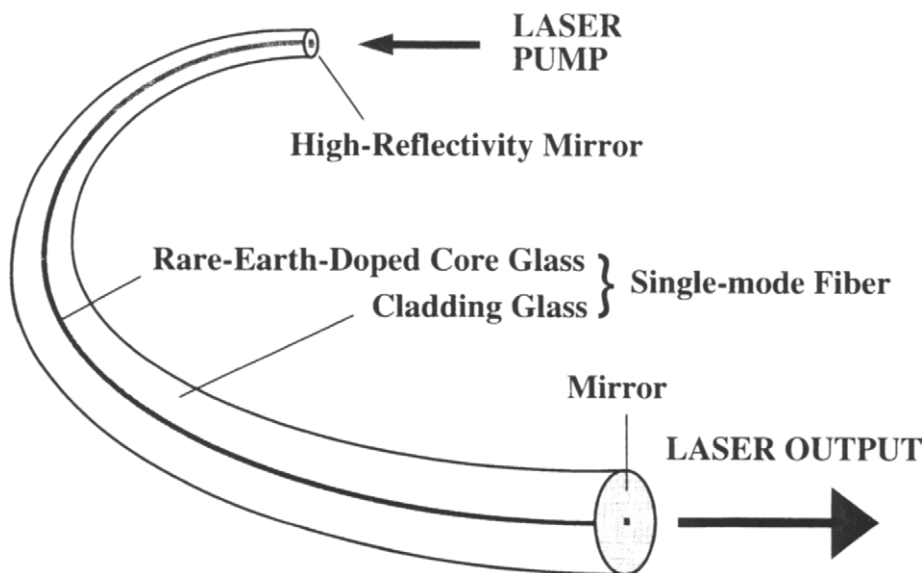


Fig. 14. Glass fiber laser. (Reproduced with permission from *Annales Chim.* 20 (1995) 261, Gauthier-Villars, Paris).

mW and 275 mW pumping powers, respectively [166]. This new UV up-conversion system provides access to applications for which high photon energy and compactness of the laser are of primary importance.

The generation of coherent blue light is a crucial point for application to high-density optical data storage, color displays, laser printing, and medical diagnostics [167]. Blue lasing in fluoride glass fibers was demonstrated at 455 nm and 481 nm with Tm^{3+} ions [168,169], and at 492 nm with Pr^{3+} [170]. Transitions are from the $^1\text{D}_2$ and $^1\text{G}_4$ levels of thulium and $^3\text{P}_0$ of praseodymium as shown in Figs 3 and 12. The highest output of 230 mW is obtained with Tm^{3+} at 481 nm with 1.6 W pump power at 1123 nm from a mini-YAG: Nd. However, at these high pump powers, the laser performances degrade rapidly because of the presence of color centers. Sanders et al. have demonstrated up-conversion lasing with a Tm^{3+} -doped ZBLAN fiber pumped directly by two high-power laser diodes [171]. With a blue output of 106 mW at 482 nm and a 12% overall conversion efficiency from IR to blue radiation, this system shows promise for powerful, small-size, all-solid-state blue laser source. Diode-pumped Pr^{3+} blue fiber laser shows more modest output powers of ≈ 1 mW [172]. These systems all require dual-pumping, as shown in Table 4, or three-step up-conversion pumping. Alternatives include co-doped systems such as Yb^{3+} : Pr^{3+} [173] and Nd^{3+} : Pr^{3+} [174] which combine two-step up-conversion with single-wavelength pumping.

Green coherent light has been obtained as well. Up-conversion of 801 nm light from a single laser diode leads to 3 mW of 544 nm light at the output of an Er^{3+} -doped ZBLAN fiber [175]. Higher output powers are attained with large pump

Table 4

Characteristics of rare-earth-doped ZBLAN fluoride glass fiber lasers. (i): incident, (l): launched, and (a): absorbed pump powers, (uc): up-conversion pumping

λ (μm)	Rare-earth	Output power	Pump characteristics	Ref.
0.381	Nd	74 μW	590 nm (uc); 275 mW (i)	[164]
0.412	Nd	500 μW	590 nm (uc); 320 mW (i)	[165]
0.455	Tm	3 mW	(645+1064) nm (uc); (600+230) mW (i)	[168]
0.481	Tm	230 mW	1123 nm (uc); 1.6 W (i)	[169]
0.492	Pr	22 mW	(1017+835) nm (uc); (250+42) mW (l)	[170]
0.520	Pr	2 mW	476 nm; 500 mW (i)	[178]
0.546	Er	23 mW	801 nm (uc); 780 mW (a)	[176]
0.549	Ho	38 mW	643 nm (uc); 280 mW (a)	[177]
0.605	Pr	150 mW	476 nm; 800 mW (i)	[178]
0.635	Pr	250 mW	476 nm; 800 mW (i)	[178]
0.715	Pr	50 mW	476 nm; 770 mW (i)	[182]
0.753	Ho	2 mW	647 nm (uc); 370 mW (i)	[93]
0.810	Tm	130 mW	1053 nm (uc); 800 mW (a)	[183]
0.850	Er	60 mW	801 nm (uc); 360 mW (a)	[184]
0.980	Er	10 mW	647 nm; 300 mW (i)	[185]
1.02	Yb	85 mW	911 nm; 200 mW (l)	[186]
1.05	Nd	50 mW	795 nm; 110 mW (l)	[189]
1.298	Pr	50 mW	1047 nm; 900 mW (i)	[193]
1.345	Nd	30 mW	795 nm; 110 mW (l)	[194]
1.47	Tm	1 W	1064 nm (uc); 3.6 W (l)	[195]
1.72	Er	9 mW	791 nm (uc)	[196]
1.88	Tm	115 mW	780 nm; 320 mW (l)	[197]
1.925	Tm	90 mW	790 nm; 300 mW (l)	[198]
1.963	Tm	8 mW	791 nm; 230 mW (l)	[199]
2.024	Ho	250 mW	826 nm; 500 mW (l)	[201]
2.35	Tm	40 mW	790 nm; 300 mW (l)	[198]
2.71	Er	158 mW	791 nm; 800 mW (l)	[196]
2.9	Ho	12 mW	640 nm; 500 mW (a)	[204]
3.45	Er	2.5 mW	650 nm; 300 mW (a)	[205]
3.9	Ho	11 mW (77 K)	885 nm; 900 mW (l)	[206]

sources such as Ti-sapphire lasers which permit 23 mW output at 546 nm with Er^{3+} ions [176]. With an Ar^+ -pumped dye laser, 38 mW are achieved at 549 nm with Ho^{3+} -doped fibers [177].

Powerful compact, all-solid-state red lasers around 635 nm are also demanded for color displays. To date, high-power lasing in this region has been demonstrated with Pr^{3+} -doped ZBLAN fibers pumped at 476 nm with an argon laser [178]. Similarly to blue lasers, compactness of red-emitting systems may be achieved by using Yb^{3+} : Pr^{3+} or Nd^{3+} : Pr^{3+} codoped fibers which can be pumped by a single wavelength

— 850 nm or 796 nm, respectively — via up-conversion mechanisms [174,179,180]. Red lasing at 635 nm with 4.5 mW output power is achieved in a $\text{Yb}^{3+}:\text{Pr}^{3+}$ ZBLAN fiber pumped by a single laser diode at 860 nm [181]. The incident pump power is 170 mW.

Several fiber lasers are demonstrated in the 700–1050 nm spectral domain as shown in Table 4 [93,182–187]. One should note the 130 mW thulium laser at 810 nm, a spectral domain where cheap silicon detectors can operate. Pulses as short as 380 ps are generated at that wavelength. In addition, the laser can be tuned from 805 to 820 nm [188]. Lasing with ytterbium-doped fluoride glass fiber is achieved at 1.02 μm with 85 mW output power. The system shows a high slope efficiency of 56% with respect to launched pump power. Neodymium-doped ZBLAN fibers are found to lase at 1.05 μm with quite good efficiency, as expected. A threshold of only 22 mW and a slope efficiency of nearly 60% are reported [189]. Recently, ultrashort pulses from 9 ps to 320 fs were generated in the 1.047–1.060 μm spectral range with an average output of 4 mW from a diode pumped neodymium fluoride glass fiber [190]. Besides optical fibers, CW lasing was demonstrated in Nd^{3+} -doped fluoride glass microspheres whose diameter ranges from 30 μm to 500 μm . The system was pumped at 800 nm with Ti:sapphire laser and lased at 1.05 μm and 1.33 μm [191,192].

In fiber configuration, two ions are susceptible to lase in the 1.3 μm region: Pr^{3+} at 1.298 μm and Nd^{3+} at 1.345 μm . The highest output power reported for the former is 50 mW with a pump threshold and slope efficiency of 300 mW and 8%, respectively [193]. The latter produces 30 mW output power with only 60 mW threshold and a fairly high slope efficiency of 57% [194].

Laser transitions above 1.4 μm belong to the so-called *eye-safe* spectral domain. In this infrared domain, the light is absorbed by the cornea and the lens of the eye, avoiding irreversible damage of the retina. However, it must be borne in mind that these wavelengths still damage both the cornea and the lens, although it is less detrimental from a biological point of view than retinal burns. Thulium and erbium ions provide several laser transitions in the 1.4–2.0 μm spectral range [195–199]. The most significant result, in terms of output power, concerns a Tm^{3+} -doped fluoride fiber that delivers 1 W, continuous-wave, at 1.47 μm . Pumping is at 1.064 μm from a laser-diode-pumped Nd:YAG. The threshold and slope efficiency are 175 mW and 29%, respectively, and wavelength tunability is from 1.445 to 1.51 μm . More recently, 250 mW output was achieved with 200 mW threshold and a high slope efficiency of 59% [200]. Powerful 1.47- μm lasers are of interest for pumping erbium-doped fiber amplifiers with high gains and high output powers.

Because of the wide transmission range and low phonon energies of fluoride glasses, the observation of numerous rare-earth laser lines is possible at wavelengths beyond 2 μm , where the transmission of silica fibers is extremely poor. Laser sources around 2 μm are of special interest because they belong, not only to the *eye-safe* spectral domain, but also to an optical transparency window of the atmosphere. Two fluoride glass fiber lasers have been demonstrated in that region. First, a Ho^{3+} laser with the $^5\text{I}_7 \rightarrow ^5\text{I}_8$ transition at 2.024 μm which delivers 250 mW with 60%

slope efficiency [201]. The ZBLAN fiber is actually codoped with thulium ions in order to take advantage of efficient energy transfer from the 3F_4 (Tm) level to 5I_7 (Ho) when pumping at 826 nm from a Ti : sapphire laser. Efficient lasing with 150 mW output power is also demonstrated with a codoped aluminozirco-fluoride fiber of only 25-mm in length [202]. The 2.35 μm transition of Tm^{3+} ions, from 3H_4 to 3H_5 is also within the optical transparency domain of the atmosphere [198]. Like the Ho^{3+} laser at 2.024 μm , this Tm^{3+} fiber laser is susceptible to find applications in lidar technologies and in surgery.

The 2.71 μm laser with Er^{3+} ions and 2.9 μm laser with Ho^{3+} can also be applied in surgery as well as in dermatology and dental drilling. These transitions take place between the $^4I_{11/2}$ and $^4I_{13/2}$ levels of erbium and from 5I_6 to 5I_7 in Ho^{3+} , as depicted in Figs 9 and 10. The highest output power is reported for the erbium fluoride glass laser with a value of 158 mW, the slope efficiency being 22% [196]. Pumping is at 791 nm, a wavelength domain where laser diodes are available. Lasing at 2.7 μm can also be obtained with pumping at 650 nm or 980 nm into the $^4F_{9/2}$ or $^4I_{11/2}$ levels [203]. Even though more modest in terms of output power (12 mW), the Ho^{3+} fluoride glass laser provides broad tunability from 2.83 to 2.95 μm . With 640-nm pumping, the threshold lies at about 65 mW and the slope efficiency is equal to $\approx 3\%$ with respect to absorbed pump power [204].

The only glass lasers ever achieved at wavelengths greater than 3 μm , are a 3.45 μm Er^{3+} -doped fluoride fiber laser [205], and a 3.9 μm Ho^{3+} laser [206]. They correspond to the $^4F_{9/2} \rightarrow ^4I_{9/2}$ and $^5I_5 \rightarrow ^5I_6$ transitions shown in Figs 9 and 10, and are pumped at 650 nm and 885 nm, respectively. An output power of 2.5 mW is obtained in CW mode at 3.45 μm . The position of the lasing wavelength is found to be temperature-dependent. So, tuning can be achieved from 3.456 μm at 5°C up to 3.478 μm at 29°C. This laser line is in the absorption range of various hydrocarbon groups, the C—H absorption being typically located around 3.5 μm . This opens possibilities for the monitoring of trace gases and common pollutants.

Contrary to all the laser lines reported in Table 4, lasing at 3.9 μm with ZBLAN: Ho^{3+} fiber is achieved at liquid-nitrogen temperature. CW output power of 11 mW is obtained with 900 mW launched pump power at 885 nm. It must be noted that such lasers are of prime importance for military and space applications because they lie within an atmospheric window transparent from 3 μm to 5 μm . Very few lasers exist in this spectral region.

All the results above were obtained with set-ups of the Fabry–Perot type with two external mirrors butted against the fiber input and output ends. More sophisticated systems will take advantage of Bragg gratings written directly inside fluoride glass optical fibers. Permanent Bragg gratings can be photo-induced in cerium-doped fluorozirconate glass plates and fibers by means of conventional holographic interferometry of 246-nm light from a pulsed UV laser [207,208]. Refractive index changes up to $4 \cdot 10^{-4}$ and reflectivity of nearly 100% are achieved. Similar experiments have been conducted with Eu^{2+} and Ce^{3+} -doped PZG thin films illuminated by a CW laser at 244 nm. Photo-induced modifications of the refractive index were as high as $1.3 \cdot 10^{-2}$ and $3.9 \cdot 10^{-3}$, respectively [209].

8.5.2 Fluoride glass optical amplifiers

Optical amplifiers are essential components for the development of high capacity telecommunication networks based on silica optical fibers. Silica fibers are characterized by three optical windows at 0.8 μm , 1.3 μm and 1.55 μm . While amplification at 1.55 μm is commonly achieved with Er^{3+} -doped silica fibers, amplification at 0.8 μm with Tm^{3+} or at 1.3 μm with Pr^{3+} requires the use of materials with lower phonon energy than silica. High gain optical amplification was demonstrated in the three telecommunication windows with rare-earth-doped fluoride glass fibers. *Real-world* amplifiers have been constructed and commercialized. With an estimated lifetime of more than 25 years in normal conditions, state-of-the-art fluoride fibers are now compatible with long-term applications such as telecommunications [210]. The most significant performances of fluoride glass amplifiers are listed in Table 5.

Strictly speaking, 0.8 μm is not a telecommunication window since silica fibers do not possess a minimum loss in that region. However, inexpensive components such as sources and detectors are available at 0.8 μm and an optical amplifier at that same wavelength will be useful for short distance communications, inside a building for instance. Percival et al. have constructed a fully connectorized amplifier operating at 806 nm [211]. The amplifying medium was a Tm^{3+} -doped, 9-meter-long, ZBLAN-type fiber pumped by a single laser diode at 780 nm. Up to 26 dB small signal gain was achieved for 17 mW launched pump power, which resulted in a 2.4 dB/mW gain efficiency. Amplification at 850 nm was demonstrated with Er^{3+} -doped fibers pumped at 792 nm with small signal gain in excess of 25 dB [212].

Neodymium, with the ${}^4\text{F}_{3/2} \rightarrow {}^4\text{I}_{13/2}$ transition at 1.3 μm , was the first ion to be investigated for potential fluoride glass amplifiers operating in the second telecommunication window. Although the emitting level can easily be populated by means

Table 5

Characteristics of fluoride glass optical amplifiers. All fibers are ZBLAN-based glass except when otherwise indicated. (LD): laser diode; (*) gain obtained with two amplification units.

λ (μm)	RE ion	max. Gain (dB)	Pump characteristics	Ref.
0.806	Tm	26	780 nm 17 mW (LD)	[211]
1.3	Pr	29	1.047 μm 670 mW (Nd:LYF)	[215]
1.3	Pr	40.6*	1.047 μm 650 mW (Nd:LYF)	[216]
1.3	Pr	30.5	1.017 μm 500 mW (MOPA)	[223]
1.3	Pr	20	1.012 μm 100 mW (MOPA)	[231]
	(Pb/In glass)			
1.54	Er	33	1.48 μm 50 mW (LD)	[235]
<hr/>				
1.47	Tm	28	1.064 μm 200 mW (Nd:YAG)	[200]
1.658	Tm	35	1.22 μm 140 mW (LD)	[243]
2.7	Er	35	642 nm 250 mW	[244]

of 800-nm pumping, neodymium amplifiers face two major drawbacks. First, amplified spontaneous emission (ASE) of predominant transitions at 1.05 μm and 880 nm limits drastically the gain in the 1.3 μm region. The highest optical gain reported to date is equal to 10 dB only, with a 2-meter-long fiber pumped forward and backward with 100 mW and 60 mW powers at 820 nm [213]. Modeling of neodymium amplifiers predicts that optical gain can be tripled if adequate filtering of ASE is achieved [214]. The second detrimental effect is excited state absorption (ESA), as described in Sec. 8.4.3. Because of ESA, amplification is shifted towards longer wavelengths, typically 1.34 μm , which is too far away from the ideal wavelength of 1.31 μm . In addition, ESA in Nd^{3+} contributes to decrease significantly the amplified signal. From this point of view, no improvement is to be expected with other glass hosts such as fluoroindates or sulfides [79].

Praseodymium-doped ZBLAN glass fiber appears to be the best compromise for 1.3 μm amplification. High-gain, low-noise Pr^{3+} -doped fluoride fiber amplifier modules (PDFA) have been developed by several laboratories around the world. The best performances of first generation PDFAs, in terms of small-signal gain, were achieved by British Telecom Laboratory and Nippon Telegraph and Telephone [215,216]. The amplifier characteristics listed in Table 5 show that these modules utilize a high-power Nd : LYF pump source at 1.047 μm . The highest gain of 40.6 dB is attained by means of two amplification units. However, these PDFAs show low gain coefficients as revealed by the high pump powers required to operate the amplifiers (> 650 mW). One reason for such high pump powers is that Nd : LYF emission does not correspond rigorously to the maximum of the $^1\text{G}_4$ absorption band. Much higher gain coefficients of 0.1–0.2 dB/mW were demonstrated with systems pumped by Ti : sapphire lasers tuned at a more appropriate wavelength around 1020 nm [217,218]. For practical and efficient devices, high power InGaAs laser diodes were developed for pumping Pr^{3+} fluoride glass fibers at 1017 nm [219,220]. With these second-generation PDFAs, gains in excess of 20 dB and efficiencies of 0.1–0.2 dB/mW were achieved with launched pump powers of about 300 mW from either InGaAs laser diodes or a MOPA (master oscillator power amplifier) [221,222]. Taking advantage of better pumping conditions, Yamada et al. have constructed a MOPA-pumped PDFa module whose Pr^{3+} fiber is only 10 m in length. This is to be compared with the 20-m fiber length needed in an equivalent module pumped by Nd : LYF. Gain of 30 dB with 500 mW launched pump power was achieved in this configuration [223]. A high gain coefficient of 0.4 dB/mW was demonstrated with a double-pass configuration and only one laser diode [224]. However, if an amplifier with high output power rather than maximum small-signal gain is needed, then a single-pass configuration is preferred [225]. PDFAs have been successfully implemented in test systems for local communication such as multichannel CATV for example [226–229].

Besides the issue of pump wavelength adequacy, the low quantum efficiency of the 1.3 μm transition of Pr^{3+} ions accounts for the relatively small gain coefficients and high pump powers of PDFAs. This transition is highly phonon-dependent, so its quantum efficiency can be increased by employing glass hosts with phonon energies lower than that of ZBLAN. Thus, lead-fluoroindate glasses were developed [230]

and more efficient PDFAs are now available with 20 dB net gain at only 100 mW pump power from a 1015-nm MOPA [231]. Gain coefficient as high as 0.36 dB/mW is reported for single-pass amplification. A compact, plug-in type module pumped by laser diodes was developed [232]. The system is capable of delivering 24 dB small-signal gain. Recently, lead-fluorindate PDFAs have been successfully utilized for data transmission at 2.5 Gb/s rate over more than 100 Km [233]. High gain coefficient of 0.81 dB/mW has been achieved with a sulfide-glass-based amplifier [234]. However, refractive index compatibility between this sulfide glass and silica remains to be solved for real devices.

A net optical gain of 33 dB was achieved with Er^{3+} -doped ZBLAN optical amplifiers for the third telecommunication window at 1.54 μm [235]. This gain was obtained with only 50 mW pump power at 1.48 μm , which resulted in gain efficiency of 0.86 dB/mW. These fundamental characteristics are not as good as those reported for silica erbium-doped fiber amplifiers (EDFA). However, compared with silica amplifiers, fluoride EDFAs remain of practical interest because they possess a flat and broad gain bandwidth as a function of signal wavelength [236,237]. This property, which is fundamental for wavelength division multiplexing (WDM), is depicted in Fig. 15. This figure shows the optical spectrum of 16 channels at the output of four cascaded fluoride and silica EDFAs without any spectral filtering [238]. One may note that all channels, which range from 1533.7 to 1558.2 nm, are quasi-equally amplified by fluoride EDFAs with a maximum gain variation of 3 dB only. With silica EDFAs on the other hand, large discrepancies are observed as shown in Fig. 15(b). The gain variation between minimum and maximum amplified channels is as high as 23 dB in that case. Consequently, spectral filtering has to be added to silica EDFAs in practical systems, contrary to fluoride EDFAs. Laboratory tests have demonstrated the transmission of such 16 channels at 10 Gbits/s over 531 Km with seven fluoride EDFAs [239].

Because of the growing demand for high-speed and high-capacity telecommunication networks, intensive research is devoted to ultra-broadband amplifiers in the 1.55 μm domain. Several systems that include fluoride-based EDFAs are proposed. Thus, an amplifier unit, composed of three silica-based EDFAs and one fluoride-based EDFA in parallel/cascade configuration, shows flat amplification from 1530 to 1560 nm and from 1576 to 1600 nm. Within these bands, an optical gain of 30 dB is achieved with a maximum fluctuation of less than 1.7 dB [240,241]. Combination of a fluoride-based EDFA with a fiber Raman amplifier leads to a 75-nm bandwidth amplifying unit that operates from 1531 to 1606 nm. Maximum gain fluctuation is equal to 3 dB [242].

Following the same logic of expanding capability of telecommunication, optical amplification has been demonstrated at wavelengths located outside the usual three communication windows. Thus, a Tm^{3+} -doped ZBLAN up-conversion amplifier was demonstrated with a maximum gain of 28 dB at 1.47 μm . Gains in excess of 10 dB were measured between 1.44 and 1.51 μm [200]. Optical amplifiers have been developed also at wavelengths greater than 1.55 μm . Besides silica-based erbium amplifiers operating at 1.6 μm , amplification was demonstrated at 1.65 μm with fluoride glass amplifiers. In that system, the ZBLAN-based fiber consisted

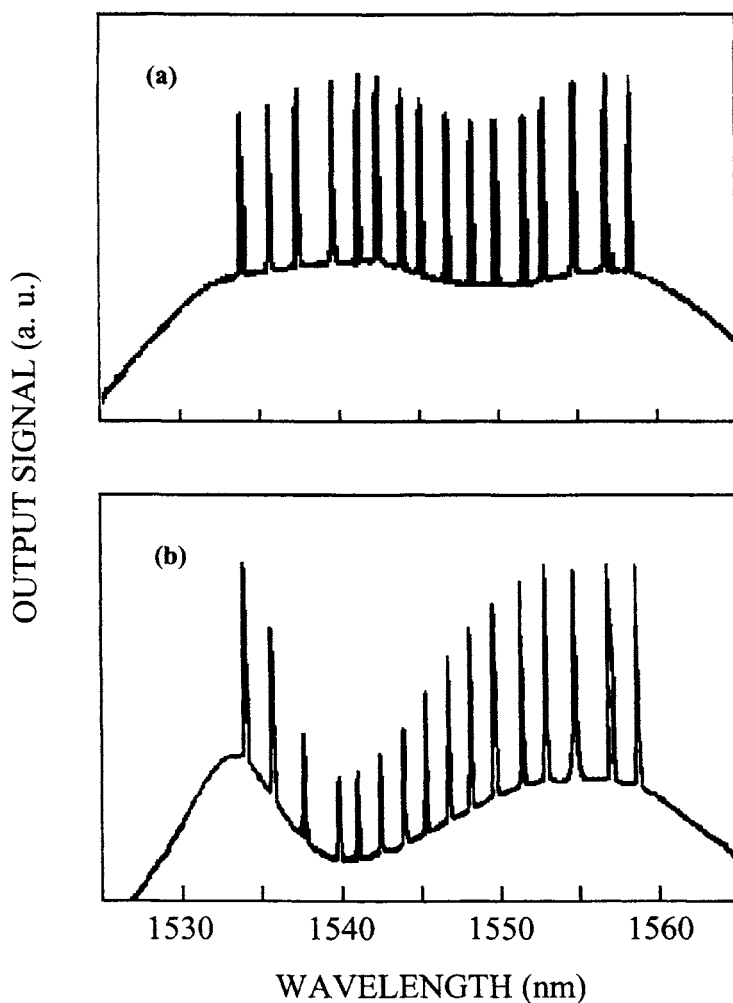


Fig. 15. Optical spectrum of 16 channels at the output of four cascaded EDFAs: (a) fluoride amplifier; (b) silica amplifier (reproduced with permission from *Electron. Lett.*, 30 (1994) 586 [238]).

of a Tm^{3+} -doped core and a Tb^{3+} -doped cladding which role was to suppress the amplified spontaneous emission at $1.75\text{--}2.0\text{ }\mu\text{m}$. A signal gain of 35 dB was achieved for a pump power of 140 mW from a $1.22\text{ }\mu\text{m}$ laser diode [243].

In the early 1990s, when intensive research was still pursued on ultra-low-loss fibers, amplifiers were developed for the minimum attenuation region of fluoride glasses located around $2.5\text{ }\mu\text{m}$. Amplification was achieved with the $^4\text{I}_{11/2} \rightarrow ^4\text{I}_{13/2}$ transition of Er^{3+} ions at $2.7\text{ }\mu\text{m}$ in ZBLAN fluoride glass fibers. Up to 35 dB optical gain was obtained with 250 mW pump power at 642 nm [244]. Gains of 20 dB were available over a 90-nm wavelength from 2.72 to $2.81\text{ }\mu\text{m}$ [245].

8.5.3 Fluoride glass channel waveguides

Because of the similarities with optical fibers, in terms of light guiding and confinement, planar waveguides are a very promising technology for realizing integrated, all-solid-state laser sources and optical amplifiers. The feasibility of such guiding structures has been demonstrated with fluoride glasses by means of two techniques: physical vapor deposition and ionic exchange.

Physical vapor deposition techniques have been successfully applied to PZG fluoride glass [246]. The fundamental reason for this success is that the main components of PZG — PbF_2 , ZnF_2 , and GaF_3 — show similar vapor pressures, contrary to ZBLAN and BIG glasses. Thus, a congruent vaporization of PZG melts is possible, and thin films with a given glass composition can be obtained after deposition of the vapor phase on an appropriate substrate (e.g. ZBLAN or CaF_2). Planar waveguides are the result of successive deposition of three PZG layers, a few microns thick. The adequate refractive index difference between the core and cladding is realized by adjusting the PbF_2 concentration within the glass (n_D may vary from 1.57 up to 1.64). The central active layer is obtained by evaporating simultaneously the core glass composition and a given rare-earth fluoride. Infrared ($\lambda = 1.55 \mu\text{m}$) luminescence together with blue ($\lambda = 410 \text{ nm}$) and green ($\lambda = 550 \text{ nm}$) up-converted emissions are observed at room temperature with an erbium-doped PZG planar — two-dimensional — waveguide pumped at 980 nm by a Ti : sapphire laser [247]. Intense up-converted luminescence is also observed with a Nd^{3+} -doped waveguide deposited on a CaF_2 substrate and pumped at 797 nm [248].

Optical confinement can be achieved in channel configurations. These one-dimensional structures are obtained by evaporation of PZG glass, as described above, onto an etched ZBLAN substrate showing strips with 60–120 μm width [249]. Typically, PZG films of 3- μm thickness are deposited within 20-min evaporation time. Depending on evaporation time and temperature, thickness from 0.5 to 100 μm can be achieved. Near-field measurements show that multimode light propagation is observed in the channel waveguide formed at the top of the strips, not in the valleys between the strips.

Various ionic exchange mechanisms have been investigated with ZBLAN and BIG glasses in order to create planar waveguides. Successful results were first obtained by immersing ZBLAN or a BIG-Na glass in a lithium-containing organic melt during several hours. The partial replacement of sodium by lithium results in a gradual increase of the refractive index at the glass surface. Four guided modes at 633 nm were observed in this configuration [250].

Fluoride glass planar waveguides were also obtained via anionic exchange mechanisms. The controlled pyrohydrolysis of fluoride glasses results in F^-/OH^- interdiffusion and a consequent graded-index is created at the glass surface. A similar effect is obtained with F^-/OD^- interdiffusion. Both exchange mechanisms are quite efficient, so that up to 10 guided modes could be observed at a wavelength of 633 nm [251].

Of course, the presence of hydroxyl groups in the waveguide is detrimental to the luminescence of rare-earth ions, especially Pr^{3+} at 1.3 μm . As a result, F^-/Cl^-

exchange techniques were investigated. The best results are obtained with optically-polished ZBLA fluoride glasses treated by a gas flow composed of a mixture of argon and HCl. The samples are maintained in this reactive atmosphere for several hours, depending on the desired number of guided modes, at a temperature below the glass transition temperature [252]. Chlorine ions were found to partially substitute for fluorine down to a depth of 10 μm from the glass surface after a 10-h treatment at 250°C. The chlorine concentration profile is constant from the surface down to 1 μm depth, and then, obeys a normal diffusion profile. Five propagation modes at 632.8 nm were measured for such sample. Channel waveguides are prepared by, first, creating a silica mask at the fluoride glass surface by using photolithography techniques. Then, the guide is formed by ionic exchange as described above, and the silica mask is removed by reactive ion etching (RIE). The optical quality of the guiding structure is given by a near-field analysis at the output of the channel waveguide with 830-nm light from a laser diode. The result, obtained for a 1-cm long, 3- μm wide waveguide, indicates that propagation is single-mode at that wavelength. Measurement of the intensity profiles leads to a horizontal mode-width of 2.1 μm and a vertical one of 1.4 μm [253].

Optical amplification was demonstrated with a Nd^{3+} -doped ZBLA channel waveguide prepared by F^-/Cl^- ionic exchange [254]. The guide was multimode, 40- μm wide. Up to 2.7 dB/cm internal gain was measured at a signal wavelength of 1.047 μm . The absorbed pump power was 7 mW. Amplification at about the same wavelength (1.064 μm) was obtained in a Nd^{3+} -doped ZBLAN bulk glass optically coupled to a borosilicate glass waveguide. In this configuration, the Nd^{3+} ions are excited by evanescent waves from light propagating in the adjacent waveguide [255]. A gain of 0.45 dB was measured at the output of this optically-induced fluoride glass waveguide.

Another very promising fabrication process of fluoride glass channel waveguides has been investigated by Davis et al. [256]. This process is based on the possibility to create photo-induced modification of the refractive index by a focused, femtosecond IR laser beam. Linear, transparent and colorless marks were formed in the inside of the glass sample translated relatively to the laser beam. Similar experiments were conducted with UV irradiation of PZG fluoride glass thin films [257].

8.5.4 Other applications of rare-earth-doped fluoride glasses

Rare-earth-doped fluoride glasses are suitable for some other specific applications that require laser transitions at wavelengths greater than 2 μm , efficient up-conversion mechanisms or ultra-high quantum efficiencies.

Some studies were devoted to Tm^{3+} -doped fluoride fibers for hydrocarbon gas sensing, especially CH_4 with respect to safety issues. A special laser cavity was designed in order to take maximum advantage of the broad tunability of the $^3\text{H}_4 \rightarrow ^3\text{H}_5$ transition of Tm^{3+} around 2.3 μm . A flat laser output power could be achieved over the 2.3–2.4 μm range where methane shows two strong absorption peaks. The sensor, whose principle is based on the direct absorption of laser light

by CH_4 , presents a high sensitivity of 150 ppm.m, which is higher than the requirements for safety applications [258].

Other sensing applications include water sensing by direct absorption of the $^3\text{H}_4 \rightarrow ^3\text{F}_4$ transition of Tm^{3+} at $1.47 \mu\text{m}$ [259] and alcohol sensing by evanescent wave in undoped fluoride glass fibers [260].

The exceptional efficiency of up-conversion mechanisms in fluoride glasses has been utilized for realizing three-dimensional solid-state color displays. The blue, green and red colors are obtained with Tm^{3+} , Er^{3+} and Pr^{3+} ions, respectively. Each color is created by pumping from two infrared laser diodes operating at different wavelengths. The two beams intersect inside the glass volume producing a luminescent point. Finally, the 3D-effect is obtained by monitoring the position of the luminescent point by means of fast-scanning mirrors [261,262].

Laser-induced cooling is another domain of application for fluoride glasses, because of their low-phonon energy. The fundamental principle of laser-induced cooling is anti-Stokes luminescence, that is luminescence that occurs at a wavelength shorter than that of the pump laser. The energy mismatch is then provided by absorption of phonons from the glass host, which results in a cooling of that host. The cooling efficiency is quite low, so radiative transitions with quantum efficiencies near unity are to be used. From this point of view, the best combination is obtained with Yb^{3+} ions in ZBLAN-type fluoride glasses. Cooling by 21 K starting from room temperature was demonstrated in a Yb^{3+} (1 wt%)-doped ZBLAN fiber in vacuum. The fiber was pumped by a Ti : sapphire laser with 1360 mW power at 1015 nm [263].

8.6 Conclusion

On the basis of the properties reviewed in this paper, it can be concluded that rare-earth-doped fluoride glasses are excellent materials for active integrated optics, in either optical fiber or planar waveguide configurations. A large number of laser emissions can be obtained with fluoride fibers. They may find applications in systems where compact solid-state laser sources emitting at wavelengths ranging from the blue to the mid-infrared are needed. The fact that permanent Bragg gratings could be induced in ZBLAN optical fibers is a definite advantage for future developments of compact, all-solid-state fluoride glass fiber lasers. We have shown that fluoride glass channel waveguides can be realized, opening new prospects in active fluoride glass research and developments.

From a material point of view, amplification at $1.3 \mu\text{m}$ and up-conversion processes will benefit from the use of glasses with lower phonon energies than fluorides. As far as rare-earth spectroscopy is concerned, sulfide glasses are for the moment the most promising materials. However, significant improvements are still to be made with sulfides in terms of glass chemical purity and fiber drawing processes.

References

- [1] J. Qiu, K. Maeda, R. Terai, *Phys. Chem. Glasses*, 36 (1995) 70.
- [2] D.C. Tran, G.H. Sigel, B. Bendow, *J. Lightw. Technol.*, LT-2, (1984) 566.

- [3] Y.L. Page, G. Fonteneau, J. Lucas, *Rev. Chim. Min.*, 21 (1984) 589.
- [4] J.L. Adam, In: Properties, processing and applications of glass and rare-earth doped glasses for optical fibres, D. Hewak (Ed.), EMIS Datareviews Series Vol 22, Chap. C1.1 INSPEC, London, UK, 1998.
- [5] N. Rigout, J.L. Adam, J. Lucas, *J. Non-Cryst. Solids*, 161 (1993) 161.
- [6] I. Chiaruttini, G. Fonteneau, J. Lucas, P.S. Christensen, S. Mitachi, *Mater. Sci. Forum*, 67–68 (1991) 245.
- [7] Y. Messaddeq, A. Delben, M.A. Aegerter, *J. Mater. Res.*, 8 (1993) 885.
- [8] T. Iqbal, M.R. Shahriari, G. Merberg, G.H. Sigel, *J. Mater. Res.*, 6 (1991) 401.
- [9] J.M. Jewell, E.J. Friebele, I. Aggarwal, *J. Non-Cryst. Solids*, 188 (1995) 285.
- [10] C. Henriel-Ricordel, J.-L. Adam, B. Boulard, C. Sourisseau, *Eur. J. Solid State Inorg. Chem.*, 34 (1997) 125.
- [11] J. Lucas, J.-L. Adam, *Glass Techn. Ber.*, 62 (1989) 422.
- [12] H. Ohno, N. Igawa, Y. Ishii, N. Umesaki, M. Tokita, *J. Nucl. Mater.* 191–194 (1992) 525.
- [13] J. Lucas, J.L. Adam, In: Optical properties of glass, D.R. Uhlmann, N.J. Kreidl (Eds.), American Ceramic Society, Westerville, USA, 1991,
- [14] S. Shibata, M. Horiguchi, K. Jinguji, S. Mitachi, T. Kanamori, T. Manabe, *Electron. Lett.*, 17 (1981) 775.
- [15] H. Poignant, *Electron. Lett.*, 17 (1981) 973.
- [16] P. Baniel, C. Belouet, *J. Non-Cryst. Solids*, 203 (1996) 143.
- [17] A. Lopez, P. Baniel, P. Gall, J. Granier, *J. Non-Cryst. Solids*, 203 (1996) 143.
- [18] D.C. Tran, M.J. Burk, K.H. Levin, C.F. Fisher, P. Hart, L. Busse, G. Lu, G.H. Sigel, *Mater. Sci. Forum*, 5 (1985) 339.
- [19] H. Hattori, T. Kanamori, S. Sakaguchi, Y. Ohishi, *Appl. Opt.*, 26 (1987) 650.
- [20] C.R. Day, P.W. France, S.F. Carter, M.W. Moore, J.R. Williams, *S.P.I.E.*, 799 (1987) 94.
- [21] P.W. France, S.F. Carter, M.W. Moore, J.R. Williams, *Mater. Sci. Forum*, 19–20 (1987) 381.
- [22] N. Rigout, J.L. Adam, J. Lucas, *Eur. J. Solid State Inorg. Chem.*, 30 (1993) 997.
- [23] K. Fujiura, T. Kanamori, Y. Ohishi, Y. Terunuma, K. Nakagawa, S. Sudo, K. Sugii, *Appl. Phys. Lett.*, 67 (1995) 3063.
- [24] C. Charron, G. Fonteneau, J. Lucas, *J. Non-Cryst. Solids* 122 (1993) 213.
- [25] D.R. MacFarlane, P.J. Newman, Z. Zhou, J. Javorniczky, *J. Non-Cryst. Solids*, 161 (1993) 182.
- [26] S. Mitachi, T. Miyashita, *Appl. Opt.*, 22 (1983) 2419.
- [27] L. Wetenkamp, T. Westendorf, G. West, A. Kober, *Mater. Sci. Forum*, 32–33 (1988) 471.
- [28] G. Fonteneau, I. Chiaruttini, S. Mitachi, J. Lucas, *J. Non-Cryst. Solids*, 140 (1992) 340.
- [29] K. Jinguji, M. Horiguchi, S. Shibata, T. Kanamori, S. Mitachi, T. Manabe, *Electron. Lett.*, 18 (1982) 164.
- [30] J.W. Fleming, W.H. Grodkiewicz, S.A. Modugno, L.G.V. Uitert, *Mater. Sci. Forum*, 5 (1985) 361.
- [31] J.-L. Adam, N. Rigout, E. Dénoue, F. Smektala, J. Lucas, *S.P.I.E.*, 1581 (1991) 155.
- [32] J. McDougall, D.B. Hollis, M.J.P. Payne, *Phys. Chem. Glasses*, 35 (1994) 258.
- [33] K. Binnemans, In: On the coordination effects in rare-earth spectra, PhD Thesis, Katholieke Universiteit Leuven, Heverlee, Belgium, 1996.
- [34] K. Binnemans, C. Görrler-Walrand, J.-L. Adam, *Chem. Phys. Lett.*, 280 (1997) 333.

- [35] C. Görller-Walrand, K. Binnemans, In: Handbook on the Physics and Chemistry of Rare Earths, Vol. 25, K.A. Gschneidner, L. Eyring (Eds.), Elsevier Science B.V., Amsterdam, The Netherlands, 1998.
- [36] A. Tesar, J. Campbell, M. Weber, C. Weinzapfel, Y. Lin, H. Meissner, H. Toratani, *Opt. Mater.*, 1 (1992) 217.
- [37] M. Dejneka, E. Snitzer, R. E. Riman, *J. Luminesc.*, 65 (1995) 227.
- [38] R. Balda, J. Fernandez, J.L. Adam, M.A. Arriandiaga, *Phys. Rev.*, B 54 (1996) 12076.
- [39] J.A. Medeiros Neto, D.W. Hewak, H. Tate, *J. Non-Cryst. Solids*, 183 (1995) 201.
- [40] R.S. Quimby, W.J. Miniscalco, *J. Appl. Phys.*, 75 (1994) 613.
- [41] P. Goldner, F. Auzel, *J. Appl. Phys.*, 79 (1996) 7972.
- [42] R. Cases, M.A. Chamarro, *J. Solid State Chem.*, 90 (1991) 313.
- [43] W. Seeber, E.A. Downing, L. Hesselink, M.M. Fejer, D. Ehrh, *J. Non-Cryst. Solids*, 189 (1995) 218.
- [44] J.-L. Adam, M. Matecki, H. L'Helgoualch, B. Jacquier, *Eur. J. Solid State Inorg. Chem.*, 31 (1994) 337.
- [45] J.-L. Adam, W.A. Sibley, *J. Non-Cryst. Solids*, 76 (1985) 267.
- [46] M. Eyal, E. Greenberg, R. Reisfeld, N. Spector, *Chem. Phys. Lett.*, 117 (1985) 108.
- [47] A. Remillieux, B. Jacquier, C. Linares, C. Lesergent, S. Artigaud, D. Bayard, L. Hamon, J.L. Beylat, *J. Phys. D – Appl. Phys.*, 29 (1996) 963.
- [48] A.B. Arauzo, R. Cases, R. Alcalá, *Phys. Chem. Glasses*, 35 (1994) 202.
- [49] A. Florez, O.L. Malta, Y. Messaddeq, M.A. Aegerter, *J. Non-Cryst. Solids*, 213-214 (1997) 315.
- [50] M.A. Bunuel, R. Cases, M.A. Chamarro, R. Alcalá, *Phys. Chem. Glasses*, 33 (1992) 16.
- [51] L.E.E. de Araujo, A.S.L. Gomes, C.B. de Araujo, Y. Messaddeq, A. Florez, M.A. Aegerter, *Phys. Rev.*, B 50 (1994) 16219.
- [52] A. Remillieux, B. Jacquier, *J. Luminesc.*, 68 (1996) 279.
- [53] K. Hirao, M. Higuchi, N. Soga, *J. Luminesc.*, 60-61 (1994) 115.
- [54] R.G. Smart, D.C. Hanna, A.C. Tropper, S.T. Davey, S.F. Carter, D. Szebesta, *Electron. Lett.*, 27 (1991) 1307.
- [55] B. Jacquier, C. Linares, R. Mahiou, J.-L. Adam, E. Dénoue, J. Lucas, *J. Luminesc.*, 60-61 (1994) 175.
- [56] R.S. Quimby, B. Zheng, *Mater. Res. Soc. Symp. Proc.*, 244 (1992) 169.
- [57] R.S. Quimby, B. Zheng, *Appl. Phys. Lett.*, 60 (1992) 1055.
- [58] P. Xie, T.R. Gosnell, *Electron. Lett.*, 31 (1995) 191.
- [59] T. Iqbal, M.R. Shahriari, P. Hajcak, G.H. Sigel, L.R. Copeland, W.A. Reed, *Appl. Opt.*, 33 (1994) 965.
- [60] P.A. Tick, N.F. Borelli, L.K. Cornelius, M.A. Newhouse, *J. Appl. Phys.*, 78 (1995) 6367.
- [61] R.S. Quimby, P.A. Tick, N.F. Borelli, L.K. Cornelius, *J. Appl. Phys.*, 83 (1998) 1649.
- [62] P.A. Tick, *Extended Abstr. of the 11th Int. Symp. on Non-Oxide, New Optical Glasses*, Sheffield, UK, 1998 p. 214.
- [63] R. Reisfeld, M. Eyal, *J. Less Common Met.*, 126 (1986) 187.
- [64] A.A. Tesar, *J. Quant. Spectrosc. Radiat. Transfer*, 46 (1991) 425.
- [65] R. Cases, M.A. Chamarro, R. Alcalá, V.D. Rodriguez, *J. Luminesc.*, 48-49 (1991) 509.
- [66] M.J. Elejalde, R. Balda, J. Fernandez, E. Macho, J.-L. Adam, *Phys. Rev.*, B 46 (1992) 5169.
- [67] E. Macho, R. Balda, M.J. Elejalde, J. Fernandez, J.-L. Adam, *J. Non-Cryst. Solids*, 161 (1993) 245.

- [68] R. Balda, J. Fernandez, A. Mendioroz, J.-L. Adam, B. Boulard, *J. Phys. — Cond. Matter*, 6 (1994) 913.
- [69] K. Binnemans, D. Verboven, C. Görller-Walrand, J. Lucas, N. Duhamel-Henry, J.L. Adam, *J. Non-Cryst. Solids*, 204 (1996) 178.
- [70] M.D. Shinn, A.A. Tesar, *J. Luminesc.*, 51 (1992) 189.
- [71] R.R. Petrin, M.L. Kliewer, J.T. Beasley, R.C. Powell, I.D. Aggarwal, R.C. Ginther, *IEEE J. Quant. Electron.*, 27 (1991) 1031.
- [72] J. Azkargorta, I. Iparraguirre, R. Balda, J. Fernandez, E. Dénoue, J.-L. Adam, *IEEE J. Quant. Electron.*, 30 (1994) 1862.
- [73] L.H. Acioli, J.T. Guo, C.B. Dearaujo, Y. Messaddeq, M.A. Aegerter, *J. Luminesc.*, 72–74 (1997) 68.
- [74] L.D.S. Menezes, C.B. de Araujo, G.S. Maciel, Y. Messaddeq, M.A. Aegerter, *Appl. Phys. Lett.*, 70 (1997) 683.
- [75] T.T. Basiev, A.Y. Dergachev, Y.V. Orlovskii, A.M. Prokhorov, *J. Luminesc.*, 53 (1992) 19.
- [76] A.T. Stanley, E.A. Harris, T.M. Searle, J.M. Parker, *J. Non-Cryst. Solids*, 161 (1993) 235.
- [77] J.E. Pedersen, M.C. Brierley, S.F. Carter, P.W. France, *Electron. Lett.*, 26 (1990) 329.
- [78] P. Le Boulanger, In: *Mesures d'absorption dans les états excités de l'ion Er³⁺ dans les matériaux solides*, Thèse de l'Université de Caen, Caen, France, 1998.
- [79] J.-L. Adam, J.-L. Doualan, L. Griscom, S. Girard, R. Moncorgé, *Extended Abstr. of the 11th Int. Symp. on Non-Oxide and New Optical Glasses*, Sheffield, UK, 1998, p. 405.
- [80] J.-L. Adam, V. Ponçon, J. Lucas, G. Boulon, *J. Non-Cryst. Solids*, 91 (1987) 191.
- [81] G.J. Quarles, A. Suchocki, R.C. Powell, *J. Appl. Phys.*, 63 (1988) 861.
- [82] K. Soga, H. Inoue, A. Makishima, *J. Luminesc.*, 55 (1993) 17.
- [83] S.L.J. Ribeiro, R.E.O. Diniz, Y. Messaddeq, L.A. Nunez, M.A. Aegerter, *Chem. Phys. Lett.*, 220 (1994) 214.
- [84] R. Balda, J. Fernandez, H. Eilers, W.M. Yen, *J. Luminesc.*, 59 (1994) 81.
- [85] M.T. Harrison, R.G. Denning, S.T. Davey, *J. Non-Cryst. Solids*, 184 (1994) ???
- [86] M.T. Harrison, R.G. Denning, *J. Luminesc.*, 69 (1996) 265.
- [87] V. Lavin, D. Rodriguez, R. Martin, R. Rodriguez-Mendoza, *J. Luminesc.*, 72–74 (1997) 437.
- [88] K. Soga, M. Uo, H. Inoue, A. Makishima, S. Inoue, *J. Amer. Ceram. Soc.*, 78 (1995) 129.
- [89] K. Tanimura, M.D. Shinn, W.A. Sibley, M.G. Drexhage, R.N. Brown, *Phys. Rev.*, B 30 (1984) 2429.
- [90] M. Eyal, R. Reisfeld, C.K. Jørgensen, B. Bendow, *Chem. Phys. Lett.*, 139 (1987) 395.
- [91] B. Villacampa, V.M. Orera, R.I. Merino, R. Cases, P.J. Alonso, R. Alcalá, *Mater. Res. Bull.*, 26 (1991) 741.
- [92] K. Binnemans, C. Görller-Walrand, J. Lucas, N. Duhamel, J.L. Adam, *J. Alloys and Comp.*, 225 (1995) 80.
- [93] J.Y. Allain, M. Monerie, H. Poignant, *Electron. Lett.*, 26 (1990) 261.
- [94] X. Zou, H. Toratani, *J. Non-Cryst. Solids*, 201 (1996) 37.
- [95] A. Shikida, H. Yanagita, H. Toratani, *J. Opt. Soc. Amer.*, B11 (1994) 928.
- [96] X. Zou, H. Toratani, *J. Non-Cryst. Solids*, 181 (1995) 87.
- [97] J.-L. Adam, C. Guéry, J. Lucas, J. Rubin, B. Moine, G. Boulon, *Mater. Sci. Forum*, 19–20 (1987) 573.

- [98] A. Florez, Y. Messaddeq, O.L. Malta, M.A. Aegerter, *J. Alloys and Comp.*, 227 (1995) 135.
- [99] S. Tanabe, K. Takahara, M. Takahashi, Y. Kawamoto, *J. Opt. Soc. Amer.*, B12 (1995) 786.
- [100] J. McDougall, D.B. Hollis, M.J.P. Payne, *Phys. Chem. Glasses*, 37 (1996) 73.
- [101] M. Takahashi, M. Shojiya, R. Kanno, Y. Kawamoto, K. Kadono, T. Ohtsuki, N. Peyghambarian, *J. Appl. Phys.*, 81 (1997) 2940.
- [102] E.W.J.L. Oomen, P.M.T. Le Gall, A.M.A. Van Dongen, *J. Luminesc.*, 46 (1990) 353.
- [103] W.J. Cho, M.W. Kim, J.C. Jo, S.S. Choi, S.J. Park, *Jpn. J. Appl. Phys.*, 33 (1994) L1527.
- [104] T. Catunda, L.A.O. Nunez, A. Florez, Y. Messaddeq, M.A. Aegerter, *Phys. Rev.*, B 53 (1996) 6065.
- [105] R. Reiche, L.A.O. Nunez, C.C. Carvalho, Y. Messaddeq, M.A. Aegerter, *Solid State Commun.*, 85 (1993) 773.
- [106] C.B. de Araujo, L.S. Menezes, G.S. Maciel, L.H. Acioli, A.S.L. Gomes, Y. Messaddeq, A. Florez, M.A. Aegerter, *Appl. Phys. Lett.*, 68 (1996) 602.
- [107] K. Soga, M. Tsuda, S. Sakuragi, H. Inoue, S. Inoue, A. Makishima, *J. Non-Cryst. Solids*, 222 (1997) 272.
- [108] C.L. Pope, B.R. Reddy, S.K. Nash-Stevenson, *Opt. Lett.*, 22 (1997) 295.
- [109] D.C. Yeh, W.A. Sibley, M. Suscavage, M.G. Drexhage, *J. Appl. Phys.*, 62 (1987) 266.
- [110] D.C. Yeh, W.A. Sibley, I. Schneider, R.S. Afzal, I. Aggarwal, *J. Appl. Phys.*, 69 (1991) 1648.
- [111] I. Martin, D. Rodriguez, Lavin, R. Rodriguezmendoza, *J. Luminesc.*, 72 (1997) 954.
- [112] S. Inoue, A. Nukui, K. Soga, A. Makishima, *J. Amer. Ceram. Soc.*, 77 (1994) 2433.
- [113] X. Wu, J.P. Denis, G. Özen, P. Goldner, F. Pellé, *Solid State Commun.*, 85 (1993) 351.
- [114] E. Heumann, M. Ledig, D. Ehrhart, W. Seeber, *Appl. Phys. Lett.*, 52 (1988) 255.
- [115] S.A. Pollack, M. Robinson, *Electron. Lett.*, 24 (1988) 320.
- [116] F. Auzel, D. Meichenin, H. Poignant, *Electron. Lett.*, 24 (1988) 1463.
- [117] J. Sanz, R. Cases, R. Alcalá, *J. Non-Cryst. Solids*, 93 (1987) 377.
- [118] J. McDougall, D.B. Hollis, M.J.P. Payne, *Phys. Chem. Glasses*, 36 (1995) 139.
- [119] C. Guéry, J.-L. Adam, J. Lucas, *J. Luminesc.*, 42 (1988) 181.
- [120] E.W.J.L. Oomen, *J. Luminesc.*, 50 (1992) 317.
- [121] S. Tanabe, K. Tamai, K. Hirao, N. Soga, *Phys. Rev.*, B47 (1993) 2507.
- [122] S. Tanabe, T. Hanada, *J. Appl. Phys.*, 76 (1994) 3730.
- [123] S. Kishimoto, K. Hirao, *J. Appl. Phys.*, 80 (1996) 1965.
- [124] A. Brenier, C. Pédrini, B. Moine, J.-L. Adam, C. Pledel, *Phys. Rev.*, B41 (1990) 5364.
- [125] K. Hirao, K. Tamai, S. Tanabe, N. Soga, *J. Non-Cryst. Solids*, 160 (1993) 261.
- [126] A. Kermaoui, G. Özen, P. Goldner, J.P. Denis, F. Pellé, *J. Phys. Chem. Solids*, 55 (1994) 677.
- [127] G. Tohmon, H. Sato, J. Ohya, T. Fujita, *J. Appl. Phys.*, 73 (1993) 1528.
- [128] E.W.J.L. Oomen, E.J. Lous, *Philips Journal of Research*, 46 (1992) 157.
- [129] A.S.L. Gomes, G.R. Boyer, G. Demouchy, A. Mysyrowicz, H. Poignant, M. Monerie, *Opt. Commun.*, 95 (1993) 246.
- [130] K.W. Bennet, R. Pafchek, A. Elyamani, G.H. Sigel, E. Snitzer, *Ceram. Trans.*, 28 (1992) 321.
- [131] A. Kermaoui, J.P. Denis, G. Özen, P. Goldner, F. Pellé, B. Blanzat, *Opt. Commun.*, 110 (1994) 581.
- [132] B. Peng, T. Izumitani, *Opt. Mater.*, 4 (1995) 701.
- [133] B. Jacquier, R. Mahiou, J.-L. Adam, J. Lucas, *Adv. Mater. Res.*, 1–2 (1994) 101.

- [134] V.D. Rodríguez, I.R. Martín, R. Alcalá, R. Cases, *Rad. Effects & Defects Sol.*, 135 (1995) 129.
- [135] D.C. Yeh, W.A. Sibley, M.J. Suscavage, *J. Appl. Phys.*, 63 (1988) 4644.
- [136] C.Y. Chen, R.R. Petrin, D.C. Yeh, W.A. Sibley, J.-L. Adam, *Opt. Lett.*, 14 (1989) 432.
- [137] X. Zou, A. Shikida, H. Yanagita, H. Toratani, *J. Non-Cryst. Solids*, 181 (1995) 100.
- [138] V.D. Rodríguez, I.R. Martín, R. Alcalá, R. Cases, *J. Luminesc.*, 54 (1992) 231.
- [139] C.X. Bo, C.J. Kai, *Opt. Commun.*, 97 (1993) 69.
- [140] T. Izumitani, S.A. Payne, *J. Luminesc.*, 54 (1993) 337.
- [141] P.J. Alonso, V.M. Orera, R. Cases, R. Alcalá, V.D. Rodríguez, *J. Luminesc.*, 39 (1988) 275.
- [142] Y. Messaddeq, S. Inoue, C.T.M. Ribeiro, L.A.O. Nunes, *J. Non-Cryst. Solids*, 213–214 (1997) 179.
- [143] L. Brixner, M. Crawford, J.-L. Adam, J. Lucas, *C.R. Acad. Sci. Paris*, 309 (1989) 1541.
- [144] H. Ebendorff-Heidepriem, D. Ehrhart, *J. Non-Cryst. Solids*, 208 (1996) 205.
- [145] N. Duhamel-Henry, J.-L. Adam, B. Jacquier, C. Linarès, *Opt. Mater.*, 5 (1996) 197.
- [146] J.-L. Adam, N. Duhamel-Henry, J.Y. Allain, *J. Non-Cryst. Solids*, 213–214 (1997) 245.
- [147] J.-L. Adam, A.-D. Docq, J. Lucas, *J. Solid State Chem.*, 75 (1988) 403.
- [148] V.M. Orera, P.J. Alonso, R. Cases, R. Alcalá, *Phys. Chem. Glasses*, 29 (1988) 59.
- [149] R. Reisfeld, M. Eyal, C. Jacoboni, C.K. Jørgensen, *Chimia*, 42 (1988) 145.
- [150] S. Tanabe, T. Hanada, M. Watanabe, T. Hayashi, N. Soga, *J. Amer. Ceram. Soc.*, 78 (1995) 2917.
- [151] D.C. Yeh, W.A. Sibley, M. Suscavage, M.G. Drexhage, *J. Non-Cryst. Solids*, 88 (1986) 66.
- [152] P.A. Tick, *S.P.I.E.*, 2287 (1994) 47.
- [153] W.J. Cho, M.W. Kim, J.C. Jo, T.S. Hahn, S.S. Choi, K.H. Chung, *J. Mater. Sci. Lett.*, 10 (1991) 241.
- [154] W. Andrews, D. Coulson, G. Rosman, *J. Non-Cryst. Solids*, 140 (1992) 281.
- [155] N. Norimatsu, Y. Noda, T. Nakai, O. Shinbori, Y. Mimura, *IOOC'89 Techn. Digest*, 4 (1989) 44.
- [156] K. Clarke, Y. Ito, *J. Non-Cryst. Solids*, 140 (1992) 265.
- [157] Y. Ohishi, S. Sakaguchi, S. Takahashi, *Electron. Lett.*, 22 (1986) 1034.
- [158] A.R. Kortan, N. Kopylov, E. Özdas, *J. Non-Cryst. Solids*, 213–214 (1997) 90.
- [159] K. Miura, I. Masuda, K. Itoh, T. Yamashita, *Mater. Sci. Forum*, 67–68 (1991) 335.
- [160] K. Itoh, K. Miura, I. Masuda, M. Iwakura, T. Yamashita, *J. Non-Cryst. Solids*, 167 (1994) 112.
- [161] P.W. France, S.F. Carter, J.M. Parker, *Phys. Chem. Glasses*, 27 (1986) 32.
- [162] Y. Ohishi, S. Mitachi, S. Shibata, T. Manabe, *Jpn. J. Appl. Phys.*, 20 (1981) L191.
- [163] D. Szebesta, S.T. Davey, J.R. Williams, M.W. Moore, *J. Non-Cryst. Solids*, 161 (1993) 18.
- [164] D.S. Funk, J.W. Carlson, J.G. Eden, *Electron. Lett.*, 30 (1994) 1859.
- [165] D.S. Funk, J.W. Carlson, J.G. Eden, *Opt. Lett.*, 20 (1995) 1474.
- [166] D.S. Funk, J.G. Eden, *IEEE J. Select. Topics in Quant. Electron.*, 1 (1995) 784.
- [167] M.C. Brierley, J.F. Massicott, T.J. Whitley, C.A. Millar, R. Wyatt, S.T. Davey, D. Szebesta, *Opt. Network Technol.*, 5 (1995) 242.
- [168] M.P. Le Flohic, J.Y. Allain, G.M. Stéphan, G. Mazé, *Opt. Lett.*, 19 (1994) 1982.
- [169] R. Paschotta, N. Moore, W.A. Clarkson, A.C. Tropper, D.C. Hanna, G. Maze, *IEEE J. Sel Top Quantum Electr.*, 3 (1997) 1100.
- [170] Y. Zhao, S. Fleming, S. Poole, *Opt. Commun.*, 114 (1995) 285.
- [171] S. Sanders, G. Waarts et al., *Appl. Phys. Lett.*, 67 (1995) 1815.

- [172] Y. Zhao, S. Fleming, *Electron. Lett.*, 32 (1996) 1199.
- [173] D.M. Baney, G. Rankin, K.W. Chang, *Appl. Phys. Lett.*, 69 (1996) 1662.
- [174] S.C. Goh, R. Pattie, C. Byrne, D. Coulson, *Appl. Phys. Lett.*, 67 (1995) 768.
- [175] J.F. Massicott, M.C. Brierley, R. Wyatt, S.T. Davey, D. Szebesta, *Electron. Lett.*, 29 (1993) 2119.
- [176] T.J. Whitley, C.A. Millar, R. Wyatt, M.C. Brierley, D. Szebesta, *Electron. Lett.*, 27 (1991) 1785.
- [177] D.S. Funk, S.B. Stevens, S.S. Wu, J.G. Eden, *IEEE J. Quant. Electron.*, 32 (1996) 638.
- [178] R.G. Smart, J.N. Carter, A.C. Tropper, D.C. Hanna, S.T. Davey, S.F. Carter, D. Szebesta, *Opt. Commun.*, 86 (1991) 333.
- [179] J.Y. Allain, M. Monerie, H. Poignant, *Electron. Lett.*, 27 (1991) 1156.
- [180] D. Piehler, D. Craven, N. Kwong, H. Zarem, *Electron. Lett.*, 29 (1993) 1857.
- [181] D.M. Baney, L. Yang, J. Ratcliff, K.W. Chang, *Electron. Lett.*, 31 (1995) 1842.
- [182] J.Y. Allain, M. Monerie, H. Poignant, *Electron. Lett.*, 27 (1991) 189.
- [183] L.M. Yang, D.T. Walton, J. Nees, W.H. Weber, *Electron. Lett.*, 32 (1996) 658.
- [184] C.A. Millar, M.C. Brierley, M.H. Hunt, S.F. Carter, *Electron. Lett.*, 26 (1990) 1871.
- [185] J.Y. Allain, M. Monerie, H. Poignant, *Electron. Lett.*, 25 (1989) 1082.
- [186] J.Y. Allain, M. Monerie, H. Poignant, *Electron. Lett.*, 28 (1992) 988.
- [187] M.C. Brierley, C.A. Millar, *Electron. Lett.*, 24 (1988) 438.
- [188] R.G. Smart, J.N. Carter, A.C. Tropper, D.C. Hanna, *S.P.I.E.*, 1581 (1991) 167.
- [189] M.C. Brierley, M.H. Hunt, *S.P.I.E.*, 1171 (1989) 157.
- [190] M. Wegmüller, M. Schürch, W. Hodel, H.P. Weber, *IEEE J Quantum Electron*, 34 (1998) 14.
- [191] K. Miura, K. Tanaka, K. Hirao, *J. Mater. Sci. Lett.*, 15 (1996) 1854.
- [192] K. Miura, K. Tanaka, K. Hirao, *J. Non-Cryst. Solids*, 213–214 (1997) 276.
- [193] H. Döring, J. Peupelmann, F. Wenzel, *Electron. Lett.*, 31 (1995) 1068.
- [194] C.A. Millar, S.C. Fleming, M.C. Brierley, M.H. Hunt, *IEEE Photon. Technol. Lett.*, 2 (1990) 415.
- [195] Y. Miyajima, T. Komukai, T. Sugawa, *Electron. Lett.*, 29 (1993) 660.
- [196] M. Pollnau, C. Ghisler, G. Bunea, M. Bunea, W. Lüthy, H.P. Weber, *Appl. Phys. Lett.*, 66 (1995) 3564.
- [197] R.M. Percival, D. Szebesta, S.T. Davey, *Electron. Lett.*, 28 (1992) 1866.
- [198] R.M. Percival, D. Szebesta, S.T. Davey, *Electron. Lett.*, 28 (1992) 671.
- [199] R.G. Smart, J.N. Carter, A.C. Tropper, D.C. Hanna, *Opt. Commun.*, 82 (1991) 563.
- [200] T. Komukai, T. Yamamoto, T. Sugawa, Y. Miyajima, *IEEE J. Quant. Electron.*, 31 (1995) 1880.
- [201] R.M. Percival, D. Szebesta, S.T. Davey, N.A. Swain, T.A. King, *Electron. Lett.*, 28 (1992) 2231.
- [202] M. Doshida, M. Obara, *Jpn. J. Appl. Phys.*, 34 (1995) 6079.
- [203] J. Schneider, D. Hauschild, C. Frerichs, L. Wetenkamp, *Int. J. Infrared Millimeter Waves*, 15 (1994) 1907.
- [204] L. Wetenkamp, *Electron. Lett.*, 26 (1990) 883.
- [205] H. Többen, *Electron. Lett.*, 29 (1993) 667.
- [206] J. Schneider, C. Carbonnier, U.B. Unrau, *Appl Opt.*, 36 (1997) 8595.
- [207] T. Taunay, P. Niay, P. Bernage, E.X. Xie, H. Poignant, S. Boj, E. Delevaque, M. Monerie, *Opt. Lett.*, 19 (1994) 1.
- [208] H. Poignant, S. Boj, E. Delevaque, M. Monerie, T. Taunay, P. Niay, P. Bernage, W.X. Xie, *Electron. Lett.*, 30 (1994) 1339.

- [209] W.X. Xie, P. Bernage, D. Ramecourt, M. Douay, T. Taunay, P. Niay, B. Boulard, Y. Gao, C. Jacoboni, A. Da Costa, H. Poignant, M. Monerie, *Opt. Commun.*, 134 (1997) 36.
- [210] K. Fujiura, Y. Nishida, T. Kanamori, Y. Terunuma, K. Hoshino, K. Nakagawa, Y. Ohishi, S. Sudo, *IEEE Photonic Technol Lett.*, 10 (1998) 946.
- [211] R.M. Percival, D. Szebesta, J.R. Williams, R.D.Y. Lauder, A.C. Tropper, D.C. Hanna, *Electron. Lett.*, 30 (1994) 1598.
- [212] B. Sridhar, H.R.D. Sunak, B.R. Strauss, S.P. Bastien, *IEEE Photon. Technol. Lett.*, 8 (1996) 215.
- [213] T. Sugawa, Y. Miyajima, T. Komukai, *Electron. Lett.*, 26 (1990) 2042.
- [214] M. Øbro, B. Pedersen, A. Bjarklev, J.H. Povlsen, *Electron. Lett.*, 27 (1991) 470.
- [215] T.J. Whitley, *J. Lightw. Technol.*, 13 (1995) 744.
- [216] M. Yamada, M. Shimizu, T. Kanamori, Y. Ohishi, Y. Terunuma, K. Oikawa, H. Yoshinaga, K. Kikushima, Y. Miyamoto, S. Sudo, *IEEE Photon. Technol. Lett.*, 7 (1995) 869.
- [217] Y. Miyajima, T. Sugawa, Y. Fukasaku, *Electron. Lett.*, 27 (1991) 1706.
- [218] T. Whitley, R. Wyatt, D. Szebesta, S. Davey, *IEEE Photon. Technol. Lett.*, 4 (1993) 401.
- [219] W.J. Gignac, J.J.S. Major, W.E. Plano, D.W. Nam, D.F. Welch, D. Scifres, *Electron. Lett.*, 28 (1992) 1232.
- [220] M. Yamada, M. Shimizu, Y. Ohishi, J. Temmyo, M. Wada, T. Kanamori, M. Horiguchi, S. Takahashi, *IEEE Photon. Technol. Lett.*, 4 (1992) 994.
- [221] M. Shimizu, T. Kanamori, J. Temmyo, M. Wada, M. Yamada, Y. Terunuma, Y. Ohishi, S. Sudo, *IEEE Photon. Technol. Lett.*, 5 (1993) 654.
- [222] S. Sanders, K. Dzurko, R. Parke, S. O'Brien, D.F. Welch, S.G. Grubb, G. Nykolak, P.C. Becker, *Electron. Lett.*, 32 (1996) 343.
- [223] M. Yamada, T. Kanamori, Y. Ohishi, M. Shimizu, Y. Terunuma, S. Sato, S. Sudo, *IEEE Photon. Technol. Lett.*, 9 (1997) 321.
- [224] M. Yamada, M. Shimizu, Y. Ohishi, J. Temmyo, T. Kanamori, S. Sudo, *Electron. Lett.*, 29 (1993) 1950.
- [225] V. Morin, E. Taufflieb, *IEEE J. Sel. Top Quantum Electr.*, 3 (1997) 1112.
- [226] K. Nakazato, C. Fukuda, M. Onishi, M. Nishimura, *Electron. Lett.*, 29 (1993) 1600.
- [227] N. Tomita, K. Kimura, H. Suda, M. Shimizu, M. Yamada, Y. Ohishi, *IEEE Photon. Technol. Lett.*, 6 (1994) 258.
- [228] K. Kikushima, T. Whitley, R. Cooke, K. Stalley, M. Fake, E. Lawrence, *Electron. Lett.*, 30 (1994) 1431.
- [229] H. Yoshinaga, M. Yamada, M. Shimizu, T. Kanamori, *Electron. Lett.*, 30 (1994) 2042.
- [230] Y. Nishida, T. Kanamori, T. Sakamoto, Y. Ohishi, S. Sudo, *J. Non-Cryst. Solids*, 221 (1997) 238.
- [231] Y. Nishida, M. Yamada, T. Kanamori, K. Kobayashi, J. Temmyo, S. Sudo, Y. Ohishi, *IEEE J Quantum Electron.*, 34 (1998) 1332.
- [232] Y. Nishida, M. Yamada, J. Temmyo, T. Kanamori, Y. Ohishi, *IEEE Photonic Technol. Lett.*, 9 (1997) 1096.
- [233] K. Isshiki, M. Kubota, Y. Kuze, S. Yamaguchi, H. Watanabe, K. Kasahara, *IEEE Photonic Technol. Lett.*, 10 (1998) 1112.
- [234] H. Tawarayama, E. Ishikawa, K. Itoh, H. Aoki, H. Yanagita, K. Okada, K. Yamanaka, Y. Matsuoka, H. Toratani, *Extended Abstr. of the Techn. Digest of Topical Meet. on Opt. Amplif. & Their Applications*, Victoria, Canada, 1997, p. PDP1.
- [235] Y. Miyajima, T. Komukai, T. Sugawa, T. Yamamoto, *Opt. Fiber Technol.*, 1 (1994) 35.

- [236] H. Ibrahim, D. Ronarc'h, L. Pophillat, A. Madani, J. Moalic, M. Guibert, J.L. Roch, P. Jaffre, *IEEE Photon. Technol. Lett.*, 5 (1993) 540.
- [237] M. Yamada, T. Kanamori, Y. Terunuma, K. Oikawa, M. Shizimu, S. Sudo, K. Sagawa, *IEEE Photon. Technol. Lett.*, 8 (1996) 882.
- [238] B. Clesca, D. Bayart, L. Hamon, J.L. Beylat, C. Coeurjolly, L. Berthelon, *Electron. Lett.*, 30 (1994) 586.
- [239] S. Artigaud, M. Chbat, P. Nouchi, F. Chiquet, D. Bayart, L. Hamon, A. Pitel, F. Goudeseune, P. Bousselet, J.-L. Beylat, *Electron. Lett.*, 32 (1996) 1389.
- [240] M. Yamada, H. Ono, T. Kanamori, S. Sudo, Y. Ohishi, *Electron. Lett.*, 33 (1997) 710.
- [241] M. Yamada, H. Ono, T. Kanamori, T. Sakamoto, Y. Ohishi, S. Sudo, *IEEE Photon. Technol. Lett.*, 8 (1996) 620.
- [242] S. Kawai, H. Masuda, K. I. Suzuki, K. Aida, *Electron. Lett.*, 34 (1998) 897.
- [243] T. Sakamoto, M. Shimizu, M. Yamada, T. Kanamori, Y. Ohishi, Y. Terunuma, S. Sudo, *IEEE Photon. Technol. Lett.*, 8 (1996) 349.
- [244] D. Ronarc'h, M. Guibert, F. Auzel, D. Mechenin, J.Y. Allain, H. Poignant, *Electron. Lett.*, 27 (1991) 511.
- [245] T. Yamamoto, T. Komukai, Y. Miyajima, *Jpn. J. Appl. Phys.*, 32 (1993) L62.
- [246] C. Jacoboni, O. Perrot, B. Boulard, *J. Non-Cryst. Solids*, 184 (1995) 184.
- [247] M. F. Joubert, A. Remillieux, B. Jacquier, J. Mugnier, B. Boulard, O. Perrot, C. Jacoboni, *J. Non-Cryst. Solids*, 184 (1995) 341.
- [248] M.C. Marco de Lucas, C. Garapon, B. Jacquier, J. Mugnier, O. Frezza, O. Perrot, B. Boulard, C. Jacoboni, *Opt. Mater.*, 10 (1998) 19.
- [249] Y. Gao, O. Perrot, B. Boulard, J.E. Broquin, R. Rimet, C. Jacoboni, *J. Non-Cryst. Solids*, 213–214 (1997) 137.
- [250] E. Fogret, G. Fonteneau, J. Lucas, R. Rimet, *Opt. Mater.*, 5 (1996) 79.
- [251] E. Fogret, G. Fonteneau, J. Lucas, *Eur. J. Solid State Inorg. Chem.*, 33 (1996) 879.
- [252] E. Josse, G. Fonteneau, J. Lucas, *Mater. Res. Bull.*, 32 (1997) 1139.
- [253] E. Josse, J.E. Broquin, E. Lebrasseur, G. Fonteneau, R. Rimet, B. Jacquier, J. Lucas, *S.P.I.E.*, 2996 (1997) 74.
- [254] E. Lebrasseur, B. Jacquier, M.C.M. De Lucas, E. Josse, J.L. Adam, G. Fonteneau, J. Lucas, Y. Gao, B. Boulard, C. Jacoboni, J.E. Broquin, R. Rimet, *J. Alloys Compounds*, 277 (1998) 716.
- [255] T. Ohtsuki, S. Honkanen, N. Peyghambarian, M. Takahashi, Y. Kawamoto, J. Ingenhoff, A. Tervonen, K. Kadono, *Appl. Phys. Lett.*, 69 (1996) 2012.
- [256] K.M. Davis, K. Miura, N. Sugimoto, K. Hirao, *Opt. Lett.*, 21 (1996) 1729.
- [257] B. Boulard, L. Brilland, H. Poignant, *Electron. Lett.*, 34 (1998) 267.
- [258] F.J. McAleavey, J. O'Gorman, J.F. Donegan, B.D. MacCraith, J. Hegarty, G. Mazé, *IEEE J. Sel. Top Quantum Electr.*, 3 (1997) 1103.
- [259] F.J. McAleavey, B.D. MacCraith, *Electron. Lett.*, 31 (1995) 1379.
- [260] B.D. MacCraith, V. Ruddy, S. McCabe, *S.P.I.E.*, 1587 (1991) 310.
- [261] E.A. Downing, L. Hesselink, J. Ralston, R.M. Macfarlane, *Science*, 273 (1996) 1185.
- [262] T. Honda, T. Doumuki, A. Akella, L. Galambos, L. Hesselink, *Opt. Lett.*, 23 (1998) 1108.
- [263] X. Luo, M.D. Eisaman, T.R. Gosnell, *Opt. Lett.*, 23 (1998) 639.

CHAPTER 9

Magnetic Properties of Usovite and Jarlite Derivative Compounds

Jacques Darriet, Antoine Le Lirzin and Roland Georges

Institut de Chimie de la Matière Condensée de Bordeaux (ICMCB), CNRS, Avenue A. Schweitzer, 33608 PESSAC, Cedex, France

9.1 Introduction

Large interest in the thermodynamics of one-dimensional (1D) systems has been stimulated by the engineering of new materials of this type, as for instance ferrimagnetic chains made up of two unequal spin sublattices spreading in a 1D network. Very often, their peculiar topological features allow an accurate theoretical description of their behavior, so that one can hope to get fundamental insights into the underlying physics of magnetic phenomena. Here we present some results of different bimetallic chains encountered in Usovite and Jarlite compounds. Despite the large differences between the sizes of the alternating sites offered, some compounds are disordered, making irrelevant any description in terms of regularly alternating chains. New theoretical treatments are suggested in order to account for the magnetic behavior.

9.2 Jarlites

In the structure of the natural jarlite $\text{Sr}_6\text{Na}_2\text{MgAl}_6\text{F}_{32}(\text{OH})_2$ (monoclinic, S.G. C2/m) 1, three successive AlF_6 octahedra share edges to form linear trimers, these later being bound together by $\text{MgF}_4(\text{OH})_2$ octahedra to form chains of rings running along the b -axis (Fig. 1). The same structure was independently determined in the synthetic compounds $\text{Ba}_7\text{CuFe}_6\text{F}_{34}$ and $\text{Ba}_7\text{CuV}_6\text{F}_{34}$ [2–3], where Cu^{2+} and $\text{Fe}^{3+}(\text{V}^{3+})$ occupy respectively the sites of Mg^{2+} and Al^{3+} in the natural compound; the Sr^{2+} and Na^+ ions of this later are as for them replaced by the Ba^{2+} ions, a vacancy being left in one of the Na sites to ensure electroneutrality.

A rather exhaustive survey of the possible substitutions in this structure showed the $\text{Ba}_7\text{M}^{II}\text{Fe}_6\text{F}_{34}$ phases to form only for a few M^{2+} ions ($\text{M}^{2+} = \text{Cu}^{2+}, \text{Mn}^{2+}, \text{Fe}^{2+}$) [2,4], all of them magnetic ones, a 1D magnetic behavior being therefore observed in all cases; the creation of isolated Fe^{3+} trimers was nevertheless possible in $\text{Ba}_7\text{LiNaFe}_6\text{F}_{34}$ [5], where the Li^+ ion occupies the M^{2+} site, whereas an Na^+ is

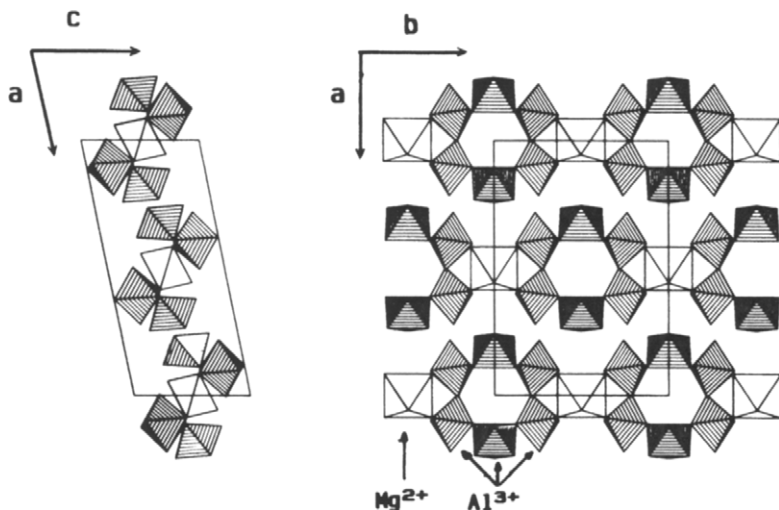


Fig. 1. Structure of jarlite, $\text{Sr}_6\text{Na}_2\text{MgAl}_6\text{F}_{32}(\text{OH})_2$.

reintroduced for charge compensation in the site it occupies in the natural jarlite, which is empty in the synthetic $\text{Ba}_7\text{M}^{\text{II}}\text{Fe}_6\text{F}_{34}$ compounds. These later will be treated first.

9.2.1 The chains of rings: $\text{Ba}_7\text{MnFe}_6\text{F}_{34}$, $\text{Ba}_7\text{FeFe}_6\text{F}_{34}$ and $\text{Ba}_7\text{CuFe}_6\text{F}_{34}$

9.2.1.1 Magnetic properties in the ordered state

Below their respective Curie temperatures, ($T_C = 27.0, 30.0$ and 12.0 K), these three compounds order ferrimagnetically, as shown by the appearance of a spontaneous magnetization at zero-field. Their magnetic structures, solved from neutron diffraction data recorded in the magnetically ordered state, are very similar: describing at first the magnetic structure of $\text{Ba}_7\text{MnFe}_6\text{F}_{34}$, we will then show how it transforms in $\text{Ba}_7\text{FeFe}_6\text{F}_{34}$ and $\text{Ba}_7\text{CuFe}_6\text{F}_{34}$.

In $\text{Ba}_7\text{MnFe}_6\text{F}_{34}$ [5], the magnetic lines can be indexed in the crystallographic unit cell; on refinement, best results ($R_{\text{nucl}} = 9.97\%$, $R_{\text{mag}} = 6.42\%$ for 104 hkl triplets in the $2 < \Theta > 80^\circ$ range, using 2.52 \AA thermal neutrons) are obtained when considering strictly parallel moments for all symmetry related ions. Within this hypothesis, the moments do not show any significant component along the b and c axes, the remaining component along a refining to: $4.19 (3) \mu_B$ for Mn, $+3.73 (3) \mu_B$ for FeI and $-3.56 (3) \mu_B$ for Fe2 (Fig. 2(a)): this disposition accounts well for the overall ferrimagnetism of the compound, as, due mostly to the unequal number of 'up' and 'down' moments it contains, each MnFe_6 unit carries a non-zero magnetic moment ($2.6 (2) \mu_B$) which then adds to the others when the whole crystal is considered; besides, it also corresponds to a strictly antiparallel orientation of any two adjacent ions in the chain, as expected in a system mostly governed by antiferromagnetic exchange interactions.

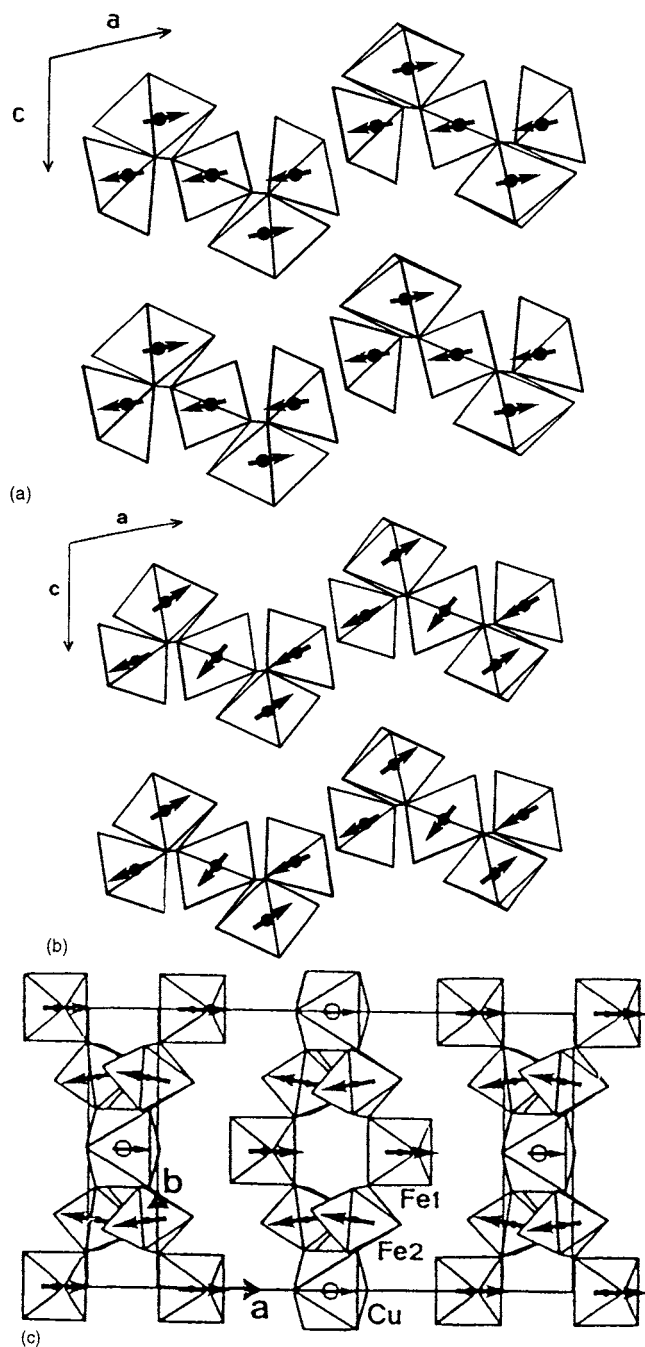


Fig. 2. Magnetic structures of (a) $\text{Ba}_7\text{MnFe}_6\text{F}_{34}$ ($[010]$ projection; the b components are all 0); (b) $\text{Ba}_7\text{FeFe}_6\text{F}_{34}$ ($[010]$ projection; the b components are all 0); (c) $\text{Ba}_7\text{CuFe}_6\text{F}_{34}$ ((001) projection; all the components along c are positive).

For decisive they might be within a chain, these exchange interactions are, as far as they remain isotropic, unable to explain either the interchain ferromagnetic coupling or the direction of the moments with respect to the crystal lattice; among the possible sources of anisotropy required to explain these last features, the magnetic dipolar interactions seem by far the most probable one: to study their role, one needs at first to check if, for the observed magnetic symmetry, the observed spin direction corresponds effectively to the one calculated when considering the dipolar interactions; then, to compare the minimum energies attained for various magnetic symmetries.

Such a screening has been performed for $\text{Ba}_7\text{MnFe}_6\text{F}_{34}$, considering various collinear magnetic structures defined by a vector u giving the common spin direction, and by the $+$ or $-$ signs associated to each moment; in such a case, the magnetic dipolar energy is obtained as $E_{\text{dip}} = u \cdot [E] \cdot u$, $[E]$ being a 3×3 tensor whose lower eigenvalue and associated principal axis give the preferred spin orientation and the corresponding energy. Results are given in Table 1 for various hypotheses in which the ferrimagnetic structure of each chain is preserved, whereas the relative orientations of the moments from chain to chain varies according to Fig. 3: as it may be seen, the minimum dipolar energy is effectively reached for ferromagnetic interchain interactions; more, the calculated spin direction corresponds within ten degrees to the observed one. The magnetic structure of $\text{Ba}_7\text{MnFe}_6\text{F}_{34}$ seems therefore to be fully explainable by the joint effects of the intrachain exchange couplings and of the interchain magnetic dipolar interactions.

These considerations do not apply longer for the magnetic structure of $\text{Ba}_7\text{FeFe}_6\text{F}_{34}$ ($R_{\text{nucl}} = 5.81\%$, $R_{\text{mag}} = 3.16\%$ for 104 hkl triplets for the parameters given in Table 2) [5]: in this compound indeed, the overall symmetry of magnetic structure is preserved (strict parallelism of the moments of symmetry related atoms), but the moments of unequivalent ions are no longer parallel, their direction varying now in the a - c plane (Fig. 2(b)); these changes are probably related to the single ion anisotropy of Fe^{2+} , but this lone factor cannot explain the departure of collinearity as far as no other anisotropy source acts on the remaining ions; as single ion or exchange anisotropy are unprobable in the $(\text{Fe}^{\text{III}})_3$ subunits, it seems more

Table 1

Values of the magnetic dipolar energy reported to one MnFe_6 unit in $\text{Ba}_7\text{MnFe}_6\text{F}_{34}$, as calculated over a sphere of radius 75 \AA for various possible structures

Symmetry (referred to Fig. 3)	Lower eigenvalue of the magnetic dipolar tensor	Preferred spin direction: angle with axes:		
		<i>a</i>	<i>b</i>	<i>c</i>
1	-0.502 cm^{-1}	8	90	86
2	-0.345 cm^{-1}	35	90	67
3	-0.378 cm^{-1}	15	90	63
4	-0.388 cm^{-1}	23	90	79

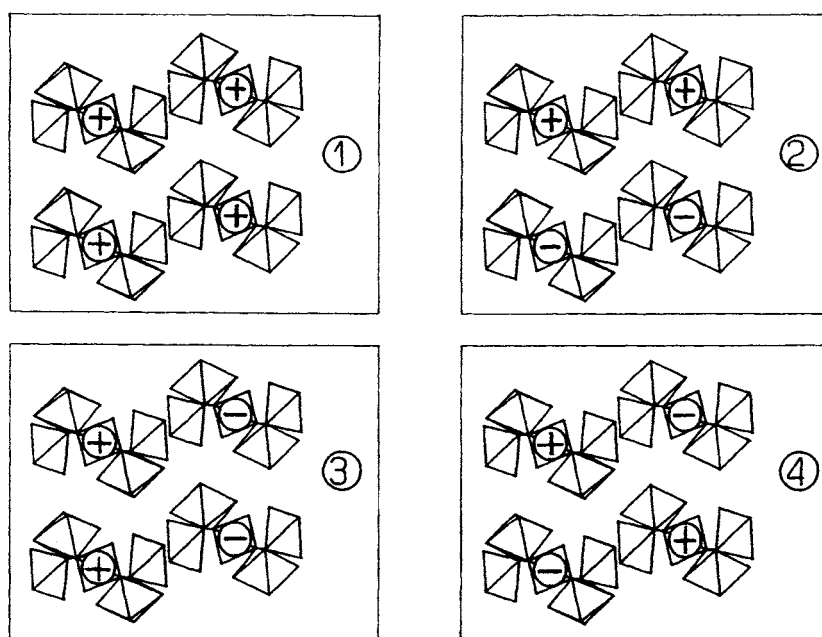


Fig. 3. Definition and numbering of the magnetic symmetries whose magnetic dipolar energies are given in Table 1.

Table 2

Coordinates of the magnetic moments in the $\text{Ba}_7\text{M}^{\text{II}}\text{Fe}_6\text{F}_{34}$ phases

M^{2+}	Atom	$\text{Ma}(\mu_{\text{B}})$	$\text{Mb}(\mu_{\text{B}})$	$\text{Mc}(\mu_{\text{B}})$	$\text{M}(\mu_{\text{B}})$
Mn^{2+}	Mn0	4.19(3)	0.0	0.0	4.19(3)
	Fe1	3.73(3)	0.0	0.0	3.73(3)
	Fe2	3.56(3)	0.0	0.0	3.56(3)
Fe^{2+}	Fe0	2.7(3)	0.0	-2.7(6)	4.3(4)
	Fe1	3.1(3)	0.0	-1.1(3)	3.5(2)
	Fe2	-3.5(3)	0.0	1.8(2)	4.2(3)
Cu^{2+}	Cu0	0.71(2)	0.0	0.15(3)	0.69(3)
	Fe1	3.5(1)	0.0	0.4(2)	3.4(2)
	Fe2	-3.54(9)	-1.1(1)	0.8(1)	3.9(1)

reasonable to consider this slightly canted structure as resulting from a competition between the exchange interactions and the magnetic dipolar ones.

In $\text{Ba}_7\text{CuFe}_6\text{F}_{34}$ [6], whose magnetic structure was solved with a far better resolution than the previous ones ($R_{\text{nucl}} = 7.0\%$, $R_{\text{mag}} = 8.7\%$ for 683 hkl triplets in the $10^\circ < \Theta < 128^\circ$ range, using 1.909 \AA thermal neutrons), a significant non-zero b-component was refined on the Fe2 ion adjacent to the copper (Table 2 and

Fig. 2(c)); its sign is reversed on application of the crystallographic symmetry operator m . Such a component remains symmetry-forbidden on the two other magnetic ions which lie on the mirror plane. The moments, as previously mainly directed along the a -axis, depart from collinearity from as much as 28° , but no explanation is proposed for this canting.

9.2.1.2 Magnetic properties in the paramagnetic state

The high temperature behaviors of $\text{Ba}_7\text{MnFe}_6\text{F}_{34}$ (Fig. 4) and $\text{Ba}_7\text{FeFe}_6\text{F}_{34}$ are extremely similar; in the high temperature limit, both follow a Curie-Weiss law $\chi = C/(T - \theta)$ with Curie constants of 30.5 and 31.9, and θ parameters of -152.0 and -163.5 K respectively. Their $\chi T = f(T)$ curves show around 60 K the minimum expected for ferrimagnetic systems and, at lower temperatures, a divergence when approaching T_C .

Due to the nature of the magnetic ions involved, both having a 6A_1 fundamental term, the magnetic chains of $\text{Ba}_7\text{MnFe}_6\text{F}_{34}$ are likely to be well described by an isotropic classical spin model, similar in principle to the one developed by Fisher [7] for the simple chain. This later uses however the recurrence relation (written here with trivial notations):

$$\langle S_i^z \cdot S_0^z \rangle = \langle S_i^z \cdot S_{i-1}^z \rangle \langle S_{i-1}^z \cdot S_0^z \rangle$$

which implicitly supposes that the only correlation pathway between S_i and S_0 passes through S_{i-1} . Now, no similar relation can longer be written for the chains of rings of $\text{Ba}_7\text{MnFe}_6\text{F}_{34}$ (Fig. 5), where two spins belonging to the same ring interact through 2 different pathways, one along each branch of the ring: the core of the problem is that

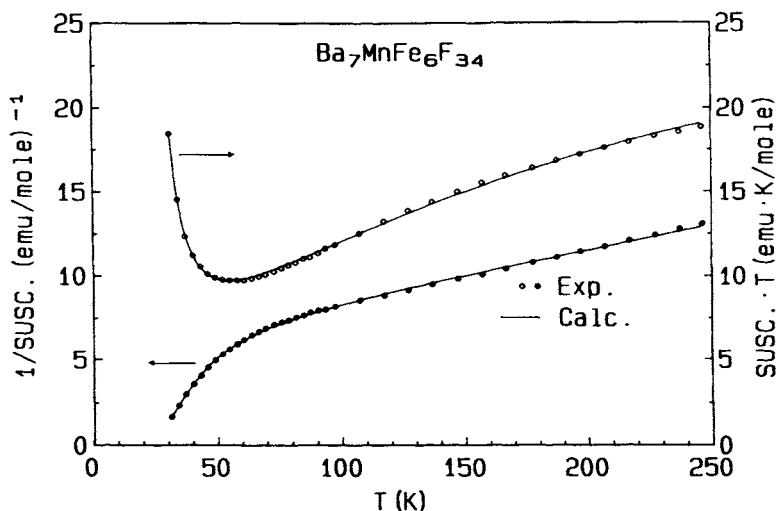


Fig. 4. Magnetic susceptibility on powder of $\text{Ba}_7\text{MnFe}_6\text{F}_{34}$.

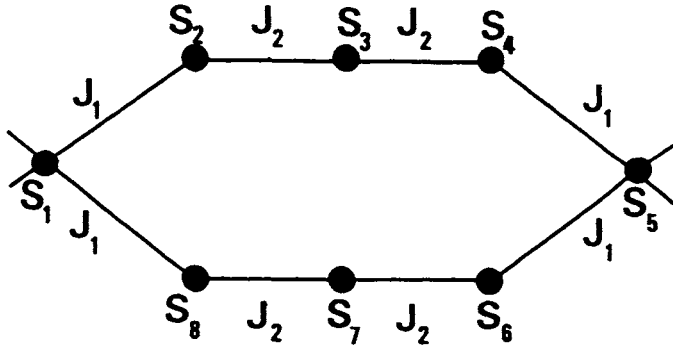


Fig. 5. Schematic representation of the magnetic unit of the chains of $\text{Ba}_7\text{MnFe}_6\text{F}_{34}$.

the ring closure condition $S_0 = S_N$ cannot be introduced in such a recurrence relation.

The key-point in solving this problem [8] is the development on the spherical harmonics of the partition function of a single ring (and of its derivatives with respect to the field), using the relation:

$$\exp(-JS_1 \cdot S_2) = \sum_{l=0}^{\infty} A_l(J/k_B T) \sum_{m=-1}^{m=1} Y_l^m(S_1) Y_l^{m*}(S_2)$$

thus replacing the subsequent integrations on the $\Theta_{i-1,i}$ angles between S_{i-1} and S_i by separate integrations on S_{i-1} and S_i : no more difficulties are then encountered when identifying the first and the last spin to express the ring closure, and the intraring correlations are obtained in a straightforward manner; they are finally extended to the whole chain using the nodal spins shared by two consecutive rings as 'relays' on which a recursive relation may be written.

The susceptibility rapported to an MnFe_6 unit is then obtained as:

$$\chi = (1/3k_B T)(A + 2B/C)$$

with:

$$\begin{aligned} A &= \sum g_u g_v \langle S_u \cdot S_v \rangle \\ B &= (\sum g_u \langle S_u \cdot S_5 \rangle)(\sum g_v \langle S_1 \cdot S_v \rangle) \\ C &= 1 - \langle S_1 \cdot S_5 \rangle, \end{aligned}$$

where the summations on u and v run over just one ring [8]. Within it, the correlations $\langle S_u \cdot S_v \rangle$ between two spins correlated through respectively m and n J_1 and J_2 exchange interactions (and alternatively by $m' = 4 - m$ and $n' = 4 - n$ J_1 and J_2

exchange interactions along the other branch of the ring) are given by:

$$D_{m,n} = \frac{\sum_{l=0}^8 (l+1) \left[A_l^m(z_1) A_l^n(z_2) A_{l+1}^{m'}(z_1) A_{l+1}^{n'}(z_2) + A_{l+1}^m(z_1) A_{l+1}^n(z_2) A_l^{m'}(z_1) A_l^{n'}(z_2) \right]}{\sum_{l=0}^{\infty} (2l+1) A_l^4(z_1) A_l^4(z_2)}$$

using the following notations:

$$z_i = J_i S(S+1)/k_B T \quad A_l(z_i) = 2\pi \int_{-1}^1 P_l(t) \exp(-tz_i) dt$$

where $P_l(t)$ is the Legendre polynomial of degree l in t .

Combined with a mean field correction for the effects of the interchain interactions n_j' [9], this expression allows a fine fit (Fig. 4) of the experimental curve for:

$$J_1/k_B = -8.1 \text{ K}; \quad J_2/k_B = -3.7 \text{ K}; \quad n_j'/k_B = 2.5 \text{ K},$$

both g -factors being fixed to 2.0 [4,5].

9.2.2 The isolated linear trimers: $\text{Ba}_7\text{LiNaFe}_6\text{F}_{34}$

The replacement of the M^{2+} ion of the $\text{Ba}_7\text{M}^{\text{II}}\text{Fe}_6\text{F}_{34}$ series by Li^+ in $\text{Ba}_7\text{LiNaFe}_6\text{F}_{34}$ was unambiguously confirmed by neutron diffraction data recorded on powders [5]; as said before, such a substitution is allowed by the simultaneous insertion of an Na^+ ion in an octahedral site which, although occupied in the natural jarlite, remains vacant in the synthetic $\text{Ba}_7\text{M}^{\text{II}}\text{Fe}_6\text{F}_{34}$ phases. From a magnetostructural point of view, this transformation chiefly splits the $[\text{M}^{\text{II}}\text{Fe}_{6\infty}]$ magnetic chains into discrete $(\text{Fe}^{\text{III}})_3$ linear trimers.

Experimentally, this splitting mainly results in a drastic lowering of the 3D ordering temperature, no substantial evolution of the neutron diffraction spectra being seen on lowering temperature even down to 1.5 K: this points out the crucial role of extended 1D correlations in the 3D ordering phenomena of quasi-1D ferrimagnets, as already emphasized in Refs [10] and [11]. Indeed, the more collectively behave the moments of a chain, the more likely are weak interchain short-range interactions, as the dipolar one, to act efficiently toward magnetic ordering, their effects being enabled to sum constructively over large chain portions. Thus, passing from $\text{Ba}_7\text{MnFe}_6\text{F}_{34}$ to $\text{Ba}_7\text{LiNaFe}_6\text{F}_{34}$ naturally results in a lowering of the transition temperature, the splitting of the chains in the later preventing obviously the spreading of 1D correlations on cooling. From this point of view, $\text{Ba}_7\text{CuFe}_6\text{F}_{34}$, with its ordering temperature of only 12 K, could correspond to intermediate values of the intrachain correlations.

$\text{Ba}_7\text{LiNaFe}_6\text{F}_{34}$ also provides a tempting testing field for the isotropic classical spin model used to refine the susceptibility of $\text{Ba}_7\text{MnFe}_6\text{F}_{34}$: its susceptibility may indeed be described for either considering linear trimers of Fe^{3+} and using the Van Vleck's formula [12], either considering chains of rings and using the

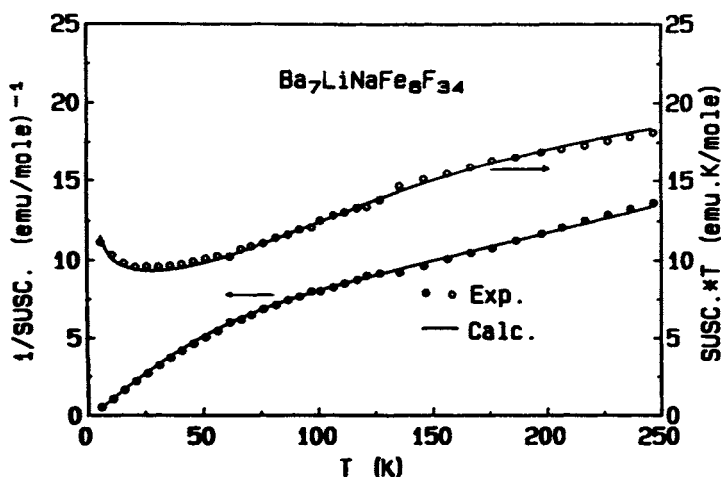


Fig. 6. Magnetic susceptibility on powder of $\text{Ba}_7\text{LiNaFe}_6\text{F}_{34}$.

corresponding theoretical model, just setting both g_{Li} and $J_{\text{Fe-Li}}$ to 0; the results obtained in the first way are shown in Fig. 6, for the final refined values:

$$J_2/k_B = -23.1 \text{ K}; \quad zj'/k_B = 0.5 \text{ K};$$

when on the other hand the second approach is used, a fit of similar quality is reached for the refined values:

$$J_2/k_B = -24.1 \text{ K}; \quad zj'/k_B = 0.5 \text{ K},$$

the g-factors being in both cases fixed to 2.0: comparison between these two results shows that the approximation level inherent to the use of a classical spin description does not exceed 5% in our case.

9.3 Usovites

The usovite structure proved to be an exceptionally rich vein of original 1-dimensional (1D) systems: the ability of the parent compound usovite $\text{Ba}_2\text{CaMgAl}_2\text{F}_{14}$ to undergo cationic substitutions allowed indeed to prepare a wide series of magnetic compounds presenting various magnetic dimensionalities, ranging from isolated ions to magnetic planes. Between those extremes, the ferrimagnetic chains also obtained in this structure revealed to be almost as many challenges for the theoretician, and various theoretical models considering partly disordered ion distribution, or exotic topological configurations, had to be developed to account for their properties. We will at first present the usovite structure and the way to use it to form the compounds we are interested in; then, summarizing the experimental

results obtained on their magnetic properties, we shall also try to explain the bases on which, within some approximations, a mathematical expression for their zero-field susceptibilities has been obtained.

The natural usovite $\text{Ba}_2\text{CaMgAl}_2\text{F}_{14}$ [13] crystallizes in the $C2/c$ space group (monoclinic); as it may be seen in Fig. 7, its structure presents layers $[(\text{CaMgAl}_2\text{F}_{14})^{4-}]_{\infty}$ the (100) plane, separated by Ba^{2+} ions. In these layers, Mg^{2+} and Al^{3+} occupy octahedral sites, whereas Ca^{2+} is 8-fold coordinated, its surrounding fluoride ions forming roughly a square-antiprism.

The same structure was independently fully redetermined for the synthetic ternary fluorides BaMnAlF_7 and BaMnGaF_7 [14–16], in which the trivalent ions occupy the site of Al^{3+} in the natural usovite, whereas the manganese splits up between the octahedral site of Mg^{2+} and the 8-fold coordinated site of Ca^{2+} : this initiated a successful quest for isostructural synthetic compounds $\text{Ba}_2\text{M}^{\text{II}}\text{M}'^{\text{II}}\text{M}''^{\text{III}}_2\text{F}_{14}$ [15,17], where the different sizes of M^{II} and M'^{II} would induce a selective repartition of the divalent ions between the square-antiprism site and the octahedral one.

A survey of the usovite phases obtained up to now [5,15,18] shows that Al^{3+} , Ga^{3+} and all the 3D trivalent ions from V^{3+} to Fe^{3+} readily occupy the M''^{3+} site; all the 3D divalent ions from Mn^{2+} to Cu^{2+} can be used as M'^{2+} ; as for M^{2+} , it may be Ca^{2+} , Cd^{2+} or Mn^{2+} : almost every combination of choices in these three series of possibilities will allow to obtain an usovite for the stoichiometry $\text{Ba}_2\text{MM}'\text{M}''_2\text{F}_{14}$ (with however some exceptions as BaMnFeF_7 [19]). The correctness of the original structure determination has now been confirmed by several full X-ray structure refinements on single crystals and by Rietveld profile analyses on powder neutron diffractograms, so that this structural type is now firmly established and may be seen as rather common among fluorides.

From the magnetic point of view, the exceptional ability of usovites to undergo cationic substitutions offers a nice building game to the magnetochemist: taking for example only one paramagnetic ion among M^{2+} , M'^{2+} and M''^{3+} , and letting

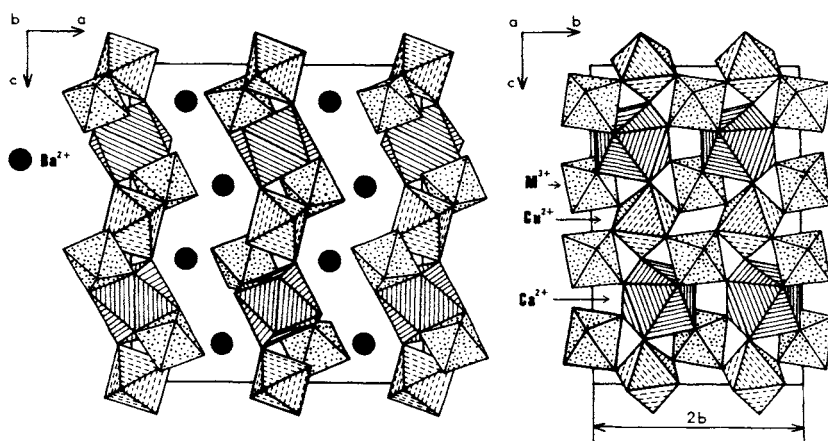


Fig. 7. Polyhedral representation of the usovite structure.

the two others be diamagnetic, there will be no pathway for superexchange interactions between the magnetic species, and the overall behavior will be typical of isolated paramagnetic centers: to this category belong, among many others, BaCdFeF_7 and $\text{Ba}_2\text{CdMnAl}_2\text{F}_{14}$. On the contrary, and although no compound of this type seems to have been actually prepared, if all the three ions are paramagnetic, exchange interactions will couple all ions within a same layer, so that a 2D system should be observed.

More interesting are the fields open by the two possibilities shown in Fig. 8; they may be described as follow:

- $\text{M}^{\prime\prime 3+}$ diamagnetic, M^{2+} and M'^{2+} paramagnetic: in this case, the magnetic ions form simple alternating chains $[\text{MM}'\text{F}_{12}]_\infty$ directed along the c -axis;
- M^{2+} diamagnetic, M'^{2+} and $\text{M}^{\prime\prime 3+}$ paramagnetic: this other type of compounds shows complex chains $[\text{M}'\text{M}''2\text{F}_{14}]_\infty$, build up of concatenated lozenges sharing one spin with each of their two neighbours, and running along the b -axis.

9.3.1 The homometallic chains: BaMnAlF_7 and BaMnGaF_7

The Rietveld profile analysis of the neutron powder diffractogram [18] of BaMnAlF_7 at room temperature (Fig. 9) confirms that the manganese ions form chains along the c -axis, where they occupy alternatively 8- and 6-fold coordinated sites, in agreement with the original X-ray structural determinations [14–16]. On lowering temperature,

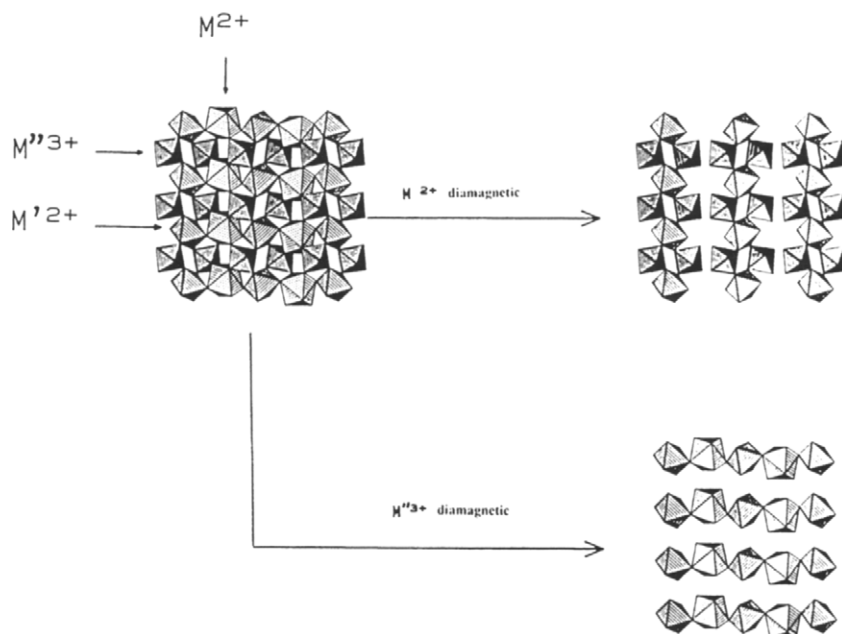


Fig. 8. The two types of 1D systems obtainable in the usovite structure.

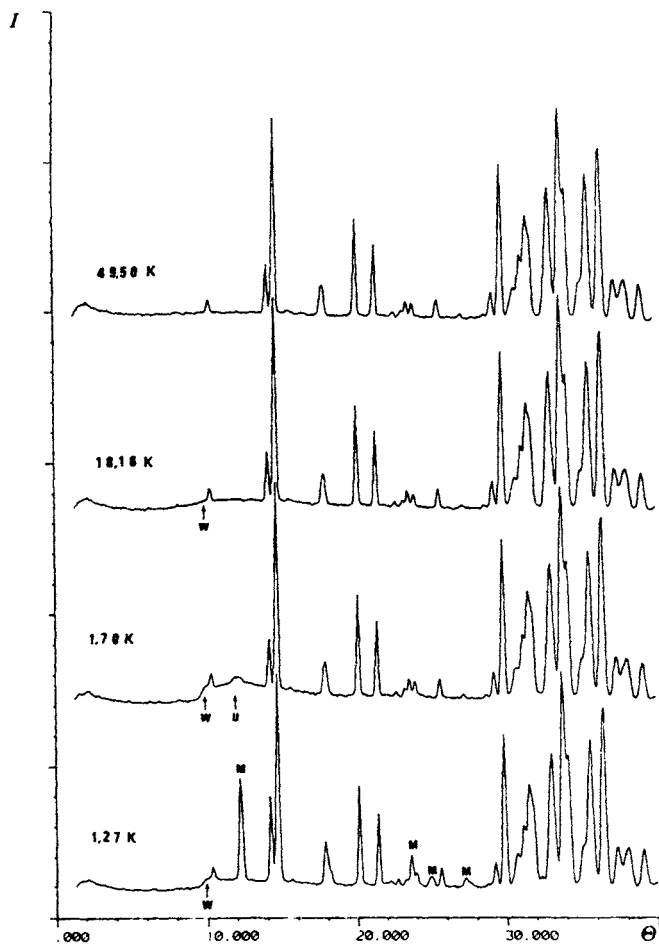


Fig. 9. Neutron powder diffractogram ($\lambda = 2.52 \text{ \AA}$) of BaMnAlF₇.

the rise of a Warren front [20] (denoted by W in Fig. 9) characterizes the spreading of 2D correlations below 20 K: its position corresponds to a spacing of $c/2$, i.e. to the distance between parallel spins in the chain. Further cooling ultimately leads to the 3D magnetic ordering at $T = 1.65 \text{ K}$, as indicated by the appearance of magnetic Bragg peaks: they may be indexed when doubling the crystallographic cell along the a and b axes ($Q = (1/2, 1/2, 0)$), but no refinement of the magnetic structure was attempted.

In the paramagnetic state, the susceptibility curves of BaMnAlF₇ (Fig. 10) and BaMnGaF₇ are extremely similar, obeying in most of the temperature range a Curie-Weiss law $\chi = C/(T - \theta)$ with Curie constants of 4.4 for both compounds and θ values respectively equal to -35 and -31 K . Both are nicely fitted using

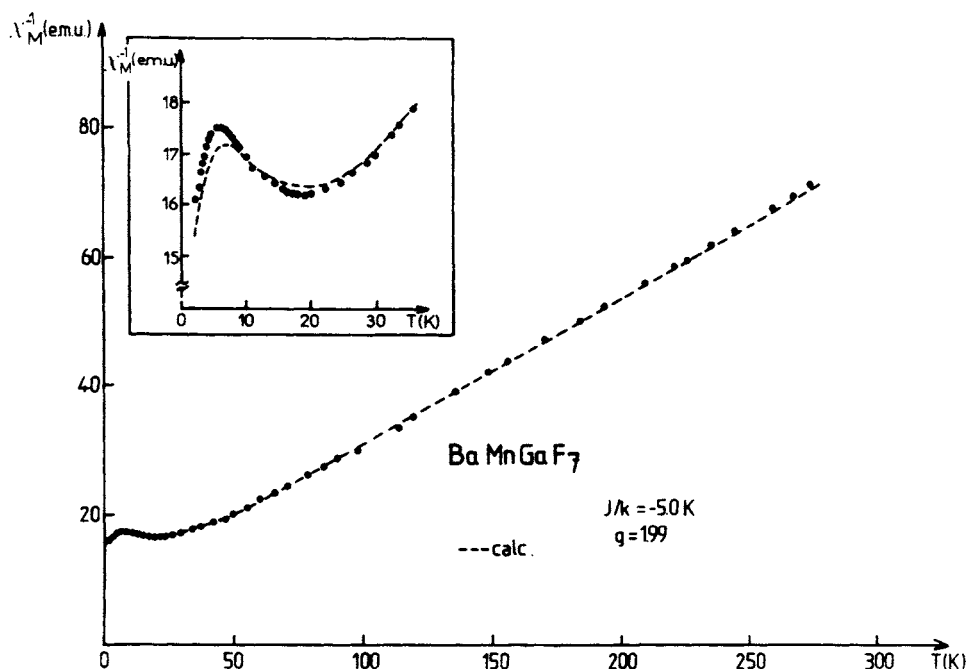


Fig. 10. Magnetic susceptibility on powder of BaMnAlF₇.

Fisher's expression for isotropic chains of classical spins [7]:

$$\chi T = \frac{NG^2\mu_B^2}{3k_B T} \left[\frac{1 + u(z)}{1 - u(z)} \right]$$

where $z = JS(S+1)/k_B T$, $G = g_{Mn} \sqrt{S(S+1)}$ and $u(z) = \coth z - 1/z$; best fits are obtained for $J/k_B = -4.8$ K in BaMnAlF₇ and $J/k_B = -5.0$ K in BaMnGaF₇, both g factors being fixed to 2.0 [18,21].

Further comment is needed on the low temperature variations of the susceptibilities of these compounds, showing both an abrupt increase below 5 K: such a behavior remains unaccounted for by Fisher's model, which expects the susceptibility of an antiferromagnetic chain to tend monotonously to some finite limit when approaching absolute 0. This discrepancy may be ascribed: (i) to the limits of the classical spin approximation when the z parameter becomes too large; (ii) to the interchain correlations, which were shown by neutron diffraction to be already present at $T = 20$ K; (iii) to some finite chain effects due to crystal defects. Using Fisher's correction for this last phenomenon, a better description of this part of the curve could be obtained (Fig. 10 (insert)) for mean chain lengths of ~ 100 and ~ 70 atoms in BaMnAlF₇ and BaMnGaF₇ respectively [18], but the significance of such improvement remains questionable.

9.3.2 The bimetallic chains: $Ba_2MnFeAl_2F_{14}$, $Ba_2MnCuAl_2F_{14}$ and $Ba_2MnCoAl_2F_{14}$ and their solid solutions with $BaMnAlF_7$

In the $Ba_2MnM^{II}Al_2F_{14}$ compounds ($M^{2+} = Fe^{2+}, Cu^{2+}, Co^{2+}$), the magnetic ions form bimetallic simple chains $[MnM^{II}]$ running along the c-axis; ideally, they should show a regular alternance of 8-fold coordinated Mn^{2+} and 6-fold coordinated M^{2+} , but experimentally, strong deviations from this ideal repartition are observed, at least in the powder samples obtained by solid state synthesis, on refinement of the neutron diffraction data for the Cu and Co compounds [5,22], or by Mössbauer spectroscopy in the Fe one [18]. The Mössbauer spectrum of this later is given in Fig. 11: its deconvolution is possible only when considering two different types of Fe^{II} in the sample, characterized by isomeric shifts and quadrupolar splittings of respectively 1.37 and 2.25 mms^{-1} for the most abundant one C.N.6, and 1.45 and 2.76 mms^{-1} for the other C.N.8, their atomic ratio being 84/16. This disorder is even stronger in the Cu and Co phases, the C.N.6/C.N.8 ratios for M^{2+} reaching 81/19 and 76/24 respectively.

As a consequence, any theoretical description of the susceptibility curves of the $Ba_2MnM^{II}Al_2F_{14}$ compounds shall have to deal with disordered cationic distributions. To appreciate how strongly it may affect the properties of the chains, one may consider a simple bimetallic $MaMb$ antiferromagnetically coupled chain, for two limiting repartitions of the ions on the two + and - magnetic sublattices: if Ma and Mb regularly altern, their succession corresponds to the alternance of + and - sites in the chain; the two magnetic sublattices are then unequivalent,

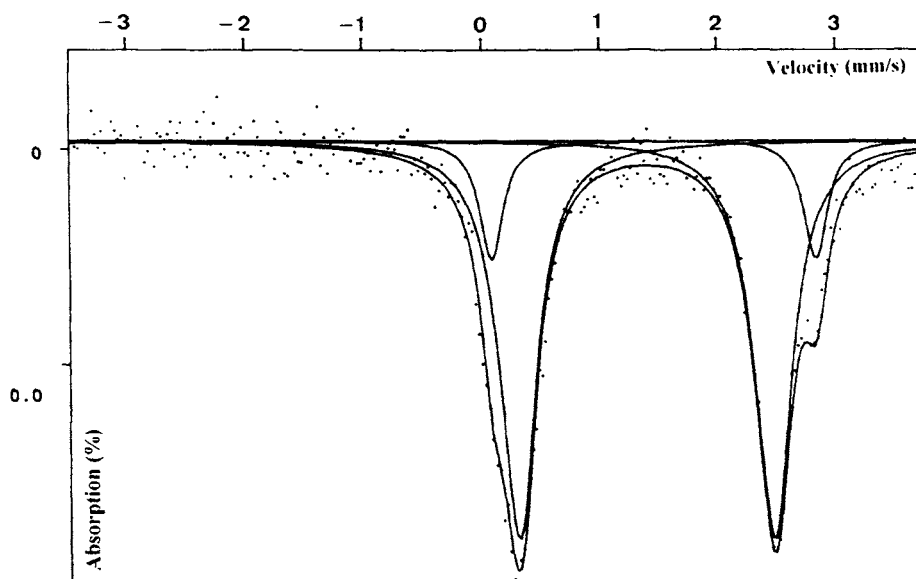


Fig. 11. Mössbauer spectrum of $Ba_2MnFeAl_2F_{14}$.

and a typical ferrimagnetic behavior may be expected, including a divergence of the χT curve when approaching absolute zero; on the contrary, any difference between the magnetic sublattices vanishes if each type of ion is equally spread between them: in such a case, the chain will behave antiferromagnetically, the limit of its χT product at $T=0$ K remaining finite. Intermediate values of the order parameter, as in the $\text{Ba}_2\text{MnM}^{\text{II}}\text{Al}_2\text{F}_{14}$ phases, will correspond to a progressive evolution between these two limiting cases, with continuous changes in the position and the depth of the χT minimum.

Beyond these general considerations, the magnetic behavior of these three compounds show great individual variations, as expectable from the very distinct magnetic properties of Cu^{2+} , Co^{2+} and Fe^{2+} , so that each case will be described separately.

9.3.2.1 $\text{Ba}_2\text{MnCuAl}_2\text{F}_{14}$ and $\text{Ba}_2\text{Mn}_{1.5}\text{Cu}_{0.5}\text{Al}_2\text{F}_{14}$

At low temperatures, a three dimensional magnetic ordering is revealed by the rise of a very few magnetic peaks in the neutron diffraction pattern at 2.8(5) K; the magnetic lines cannot be indexed even when doubling the crystallographic parameters, so that it was not attempted to solve the magnetic structure [5,22].

Above its ordering temperature, $\text{Ba}_2\text{MnCuAl}_2\text{F}_{14}$ behaves as a typical ferrimagnetic chain (Fig. 12), showing a minimum of χT at about 40 K and a negative paramagnetic Curie temperature ($\theta = -21.0$ K); the obvious presence of rather strong couplings in the chain is well explained by the structural data obtained on refinement of the neutron diffractograms, since the orientation of the $\text{dx}^2\text{-y}^2$

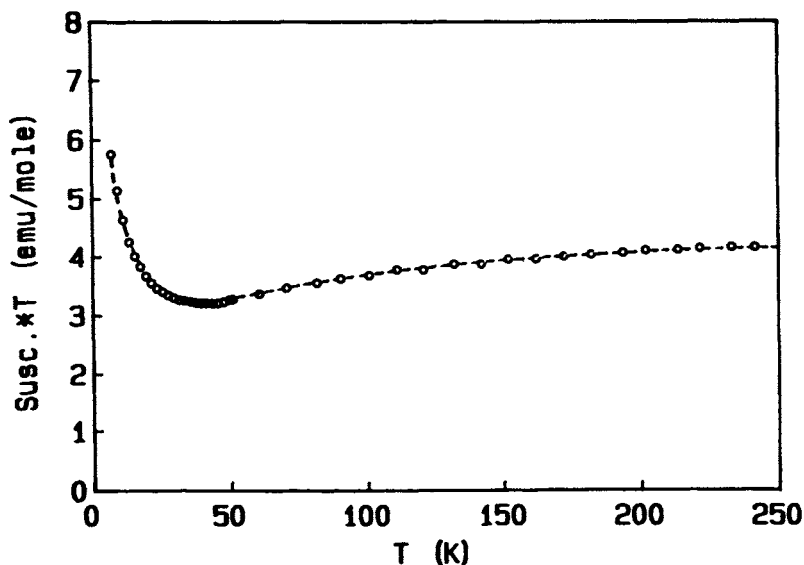


Fig. 12. Magnetic susceptibility on powder of $\text{Ba}_2\text{MnCuAl}_2\text{F}_{14}$

magnetic orbital of the Cu^{2+} , as deduced from the Jahn–Teller distortion of its octahedral site, makes possible rather large overlaps with Mn^{2+} around the bridging fluorine F7 (Fig. 13) [22]

Theoretical expressions for the susceptibility of such systems have already been proposed in the two particular cases of the regularly alternating chain Mn—Cu—Mn—Cu [23] and of the Mn chain randomly doped with Cu [24]; in both cases, the $S=5/2$ spin of the manganese is described within the classical approximation, whereas the one of the copper conserves its quantum mechanical character, taking the two values $s=\pm 1/2$ on the quantization axis defined by its neighbours. Strikingly, both models establish at first the correlations between classical spins as a ‘skeleton’ from which the classical–quantum and quantum–quantum spins correlations can be obtained: this reflects the fact that the possible states of a quantum spin s_i are defined by its neighbours S_{i-1} and S_{i+1} , so that the correlation $\langle S_{i-1}, s_i \rangle$ can be obtained only once $\langle S_{i-1}, S_{i+1} \rangle$ is known. Thus, denoting by u the correlation $\langle S_i, S_{i+1} \rangle$ between two adjacent classical spins, and by f the correlation $\langle S_i, S_{i+2} \rangle$ if these two spins are separated by a quantum one s_{i+1} , it may be written:

$$\langle S_i, S_0 \rangle = P(S_{i-1}) u \langle S_{i-1}, S_0 \rangle + P(s_{i-1}) P(S_{i-2}) f \langle S_{i-2}, S_0 \rangle \dots$$

where $P(S_{i-1})$ (resp. $P(s_{i-1})$) denotes the probability to find a classical spin (resp. a quantum one) in the $(i-1)$ th site. Further terms could be added to take into account the possible successions $S_i - s_{i-1} - s_{i-2} - S_{i-3}$, $S_i - s_{i-1} - s_{i-2} - s_{i-3} - S_{i-4}$ etc., but they were neglected according to their weak probabilities; in practice, this sets to zero all couplings between adjacent quantum-spins, without appreciable effect on the final result if the Cu–Cu pairs are rare enough.

In the usovite phases, where the probability to find either a classical or a quantum spin depends on the nature \triangleright (CN6) or \square (CN8) of the site considered, this recursion relation takes different forms as S_i occupies a \triangleright or a \square in the first case for example, the relation is written down as:

$$\langle S_{i\triangleright}, S_0 \rangle = u P(S_{i-1}, \square) \langle S_{i-1\square}, S_0 \rangle + f P(s_{i-1}, \square) P(S_{i-2}, \triangleright) \langle S_{i-2\triangleright}, S_0 \rangle,$$

where the regular alternance of sites \triangleright (i and $i-2$) and \square ($i-1$) in the chain is easily recognized. A system of coupled recursion relations is then obtained, whose solution

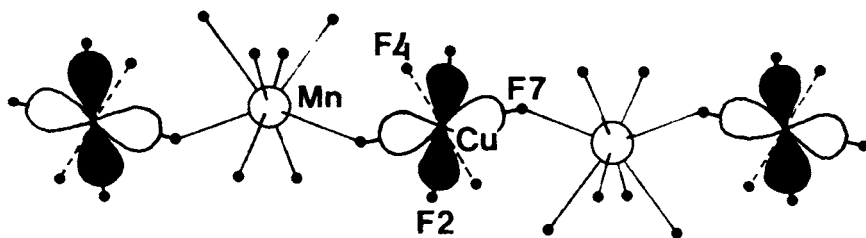


Fig. 13. Schematic representation of the orientation of the magnetic orbital $d_{x^2-y^2}$ of the copper in $\text{Ba}_2\text{MnCuAl}_2\text{F}_{14}$.

provides the 'skeleton' of classical-classical correlations. The other ones are then derived straightforwardly, and the susceptibility can be obtained under a closed form; its final expression remains however somewhat lengthy, so that it will not be reported here: the interested readers are referred to Refs [5] and [22].

As it neglects the Cu—Cu couplings, this model fairly inadequate to describe $\text{Ba}_2\text{MnCuAl}_2\text{F}_{14}$ where the pairs of adjacent Cu represent 16% of the total number of ion pairs; it was instead used to fit the powder susceptibility of a solid solution $\text{Ba}_2\text{Mn}_{1.5}\text{Cu}_{0.5}\text{Al}_2\text{F}_{14}$ between the parent compound and BaMnAlF_7 , where the copper is more diluted; with g factors fixed to 2.0 and 2.2 for Mn^{2+} and Cu^{2+} respectively, satisfying results are obtained (Fig. 14) for $J_{\text{Mn—Mn}}/k_B = -5.7$ K, $J_{\text{Mn—Cu}}/k_B = -17.6$ K, the order parameter $\delta = 2[\text{Cu}_b]/([\text{Cu}_b + \text{Cu}_\square]) - 1$ refining to 0.68, close to the value measured by neutron diffraction in $\text{Ba}_2\text{MnCuAl}_2\text{F}_{14}$ [22].

9.3.2.2 $\text{Ba}_2\text{MnCoAl}_2\text{F}_{14}$ and $\text{Ba}_2\text{Mn}_{1.5}\text{Co}_{0.5}\text{Al}_2\text{F}_{14}$

New lines appear in the neutron diffractograms of $\text{Ba}_2\text{MnCoAl}_2\text{F}_{14}$ [5,22] when the temperature is lowered below 9.0(5) K, but, as precedently, they do not allow to solve the magnetic structure; the ordered state is found to be antiferromagnetic on magnetization measurements, these later revealing also a metamagnetic transition near $H = 7$ kG (Fig. 15): this transition most probably arises from the single ion anisotropy of Co^{2+} in octahedral sites, and could proceed according to the same mechanism as the similar transition observed in $\text{Ba}_2\text{CaCoFe}_2\text{F}_{14}$ [18,26], discussed in more detail hereafter.

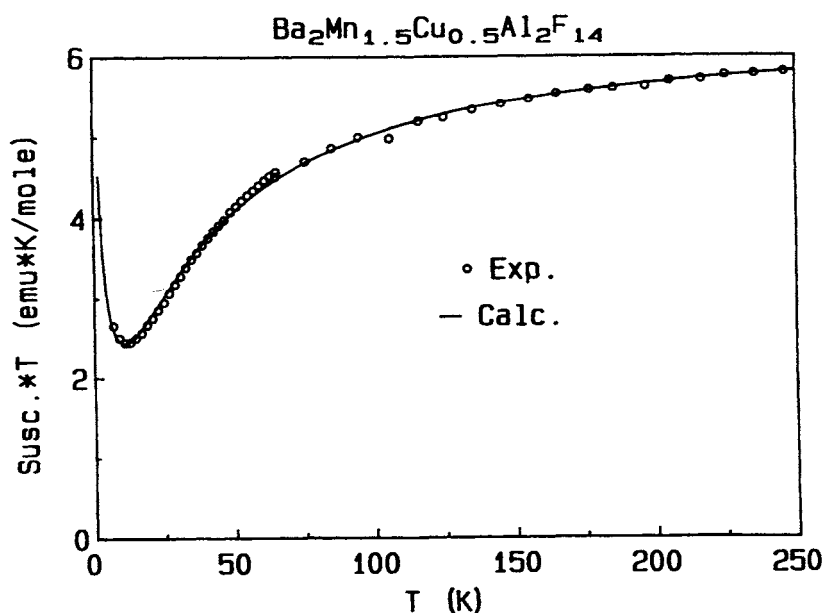


Fig. 14. Magnetic susceptibility on powder of $\text{Ba}_2\text{Mn}_{1.5}\text{Cu}_{0.5}\text{Al}_2\text{F}_{14}$.

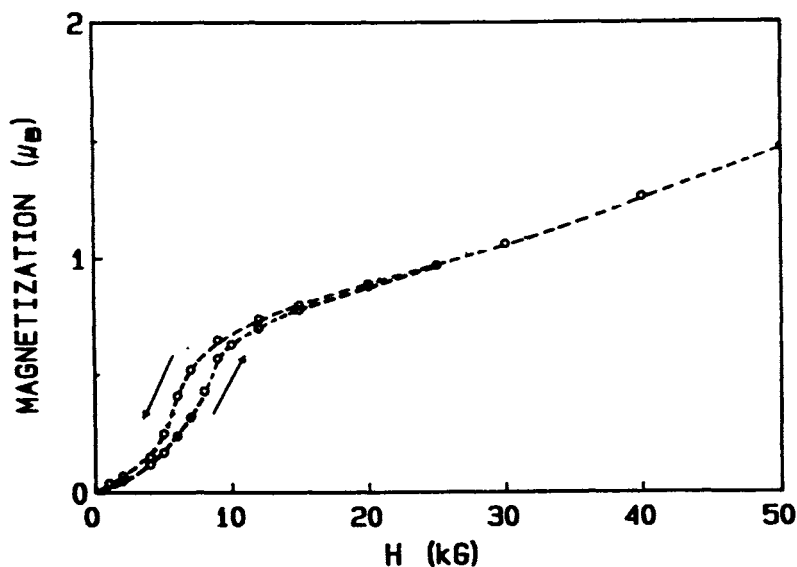


Fig. 15. Magnetization curve on powder of $\text{Ba}_2\text{MnCoAl}_2\text{F}_{14}$.

The magnetic characteristics of the Co^{2+} ions were precised by E.P.R. studies on a sample of $\text{Ba}_2\text{CaMg}_{0.95}\text{Co}_{0.05}\text{Al}_2\text{F}_{14}$: at room temperature, where the octahedrally coordinated Co^{2+} are expected to be E.P.R. silent, the spectrum shows an isotropic signal centered at $g = 2.01$ (Fig. 16(a)), which probably arises from the 8-coordinated Co^{2+} ; on lowering temperature down to 12 K, supplementary contributions appear (Fig. 16(b)), from which the signal of the octahedrally coordinated Co^{2+} is obtained by subtraction (Fig. 16(c)), leading to $g_z = 7.96$, $g_y = 2.66$, $g_x = 2.15$ and $A_z = 422.10^{-4} \text{ cm}^{-1}$ for the parallel component of the hyperfine tensor: already looking toward modelization, these characteristics show that the Ising model will be adapted for the cobalt in octahedral sites, whereas the classical spin approximation will apply to the 8-coordinated one.

The powder susceptibility of $\text{Ba}_2\text{MnCoAl}_2\text{F}_{14}$ is given in Fig. 17: no minimum can be seen on the $\chi T = f(T)$ curve, the divergence expected when approaching zero being probably hidden by the spreading of 3D correlations in the vicinity of T_N . The 1D-ferrimagnetic character of the compound is nevertheless confirmed by the negative sign of $\theta = -35.5 \text{ K}$ and the rather low ratio $T_N/\theta = 0.25$. The Curie constant, 7.9, furnishes a somewhat high contribution of 3.5 for the cobalt, rather unexplainable as the presence of 8-coordinated cobalt is expected to lower the Curie constant with respect to the values observed for pure octahedral coordination. Susceptibility measurements on a single crystal of composition $\text{Ba}_2\text{Mn}_{1+x}\text{Co}_{1-x}\text{Al}_2\text{F}_{14}$ ($x = 0.5$) revealed a weak axial anisotropy of the susceptibility along the c -axis (Fig. 18), but since these measurements were only performed along the crystallographic axes, this direction could be only approximate.

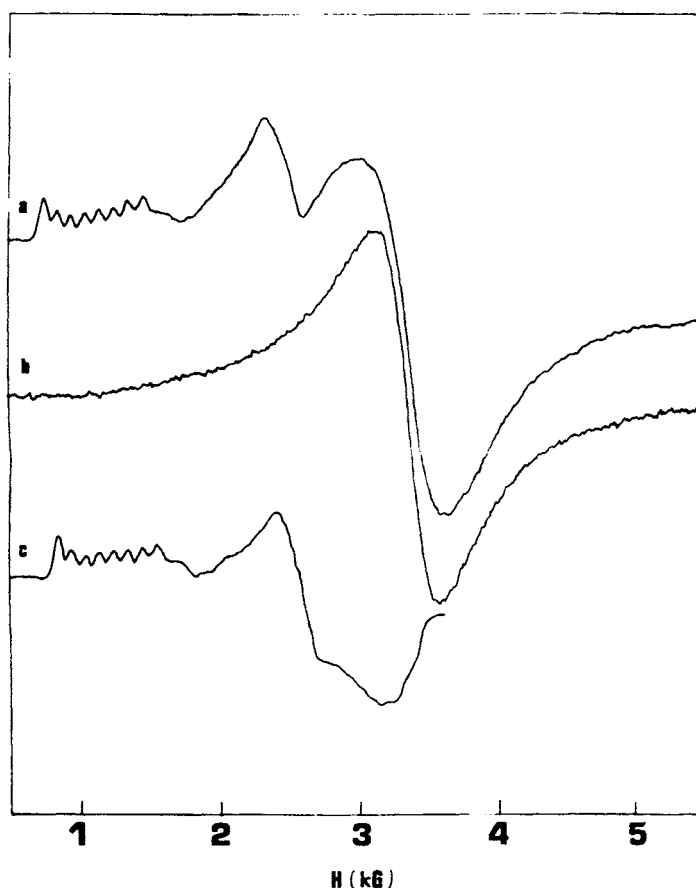


Fig. 16. ESR spectrum of a powder of $\text{Ba}_2\text{CaMg}_{0.95}\text{Co}_{0.05}\text{Al}_2\text{F}_{14}$.

The parallel susceptibility of this crystal was modeled [5,22] considering the octahedrally coordinated Co^{2+} ion as an Ising spin taking only the two values $\varepsilon = \pm 1/2$ along its anisotropy axis, and using besides the classical approximation for the manganese and the 8-fold coordinated cobalt; then, each chain was described as a succession of Ising spins $\varepsilon_0 \dots \varepsilon_n$, each ε_i being separated from the following ε_{i+1} by a variable number η_{i+1} of Heisenberg coupled classical spins. Now, it is possible to divide the partition function of a chain segment running from ε_0 to ε_n into two parts Z_n^+ and Z_n^- , one corresponding to a summation over all the states ending by $\varepsilon_n = +1/2$, the other to a summation over the states ending by $\varepsilon = -1/2$. The recursion relation between Z_n and Z_{n-1} is then written using a transfer matrix:

$$\begin{bmatrix} Z_n^+ \\ Z_n^- \end{bmatrix} = \begin{bmatrix} a_n & b_n \\ b_n & a_n \end{bmatrix} \begin{bmatrix} Z_{n-1}^+ \\ Z_{n-1}^- \end{bmatrix}$$

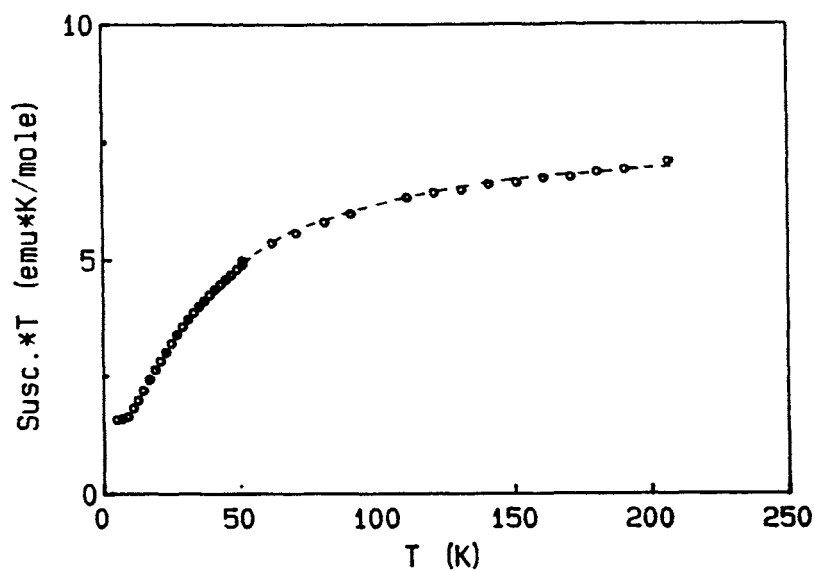


Fig. 17. Magnetic susceptibility on powder of $\text{Ba}_2\text{MnCoAl}_2\text{F}_{14}$.

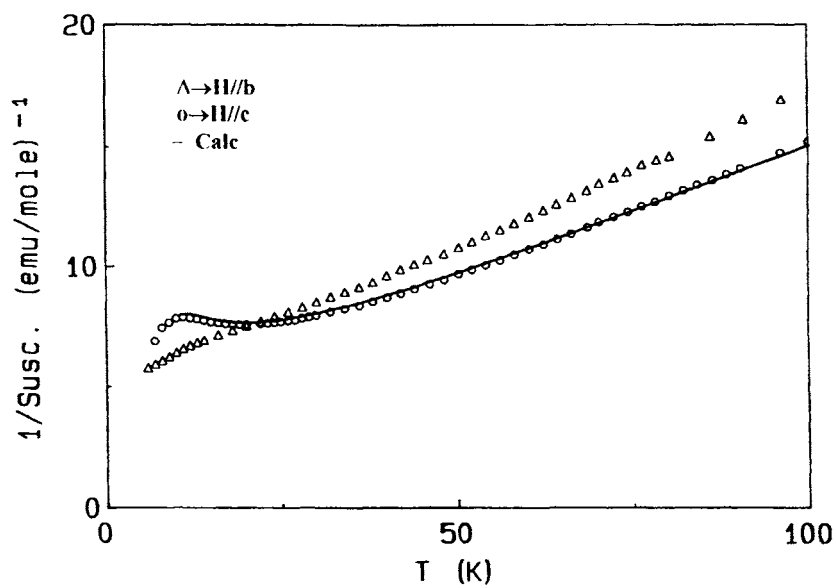


Fig. 18. Magnetic susceptibility of a single crystal of $\text{Ba}_2\text{Mn}_{1.5}\text{Co}_{0.5}\text{Al}_2\text{F}_{14}$ for H parallel (●) and perpendicular (○) to c .

where the coefficients a_n b_n depend on η_n and are obtained by integration over all the possible orientations of the classical spins separating ε_n and ε_{n-1} . These integrations can be performed only using developments into infinite series of spherical harmonics, a fact easily understandable if one realizes that these later implicitly define a polar axis, which is taken conveniently along the anisotropy axis of the Ising spins. The final expression is too complex to be given here, but it is worth saying that it is expressed as a function of the weighted mean values $\langle a \rangle$ and $\langle b \rangle$ of the a_i and b_i coefficients (and of their derivatives) over the various possible values of η_i .

This expression allows a good description of the experimental results (Fig. 18) of the following parameters [22]:

$$J_{\text{Mn-Mn}}/k_B = -5.8 \text{ K}; \quad J_{\text{Mn-Co}}/k_B = -14.1 \text{ K}; \quad \mu(\text{Co}^{2+}) = 3.6 \mu_B; \quad \delta = 1$$

(the value of $J_{\text{Mn-Co}}$ is expressed considering a fictive spin 1/2 for the cobalt in octahedral sites). Noteworthy, the refined value of $J_{\text{Mn-Mn}}/k_B$ is consistent with the results obtained on BaMnAlF_7 , BaMnGaF_7 and $\text{BaMn}_{1.5}\text{Cu}_{0.5}\text{Al}_2\text{F}_{14}$; the moment refined for the cobalt, though a bit too small, remains in rough agreement with the E.S.R. results; more suspicious is the refined order parameter, whose astonishingly high value contrasts with the strong disorder evidenced from the neutron diffraction spectra. This discrepancy is possibly just an artefact caused by the many approximations on which is based the modelization; but, possibly also, it could reflect significantly the differences in the cationic repartition observed in other usovites between the single crystals grown from melts and the powders prepared by sintering, as discussed below. Anyway, beyond these uncertainties, this calculation shows how satisfyingly the basic characteristics of the behavior of such a very complex system can be reproduced by theoretical models.

9.3.2.3 $\text{Ba}_2\text{MnFeAl}_2\text{F}_{14}$

The susceptibility curve of $\text{Ba}_2\text{MnFeAl}_2\text{F}_{14}$ [18] is given in Fig. 19. Above 50 K, the behavior is paramagnetic, the Curie constant $C = 8.2$ allowing to calculate a contribution of 3.8 for the divalent iron.

This curve could be parametrized using a classical model developed for disordered bimetallic chains. The susceptibility is derived from the fluctuation relation:

$$\chi T = (1/3k_B) \mu_B^2 \sum_i \sum_j g_i g_j \langle S_i \cdot S_j \rangle,$$

the correlations $\langle S_i \cdot S_j \rangle$ being calculated according to Fisher [7], applying recursively the relation:

$$\langle S_i \cdot S_{i+1} \rangle = u(z_i) = \coth z_i - 1/z_i \text{ with } z_i = J_{i,i+1}/k_B T$$

Now, since $J_{i,i+1}$ can take three different values in $\text{Ba}_2\text{MnFeAl}_2\text{F}_{14}$ (namely $J_{\text{Mn-Mn}}$, $J_{\text{Mn-Fe}}$ and $J_{\text{Fe-Fe}}$), the correlations between two distant spins S_i and S_j will actually depend on the repartition of the different ions in the segment of chain separating them, and be written as:

$$S_i \cdot S_j = u(z_i) \cdot u(z_{i+1}) \cdot \dots \cdot u(z_{j-1}),$$

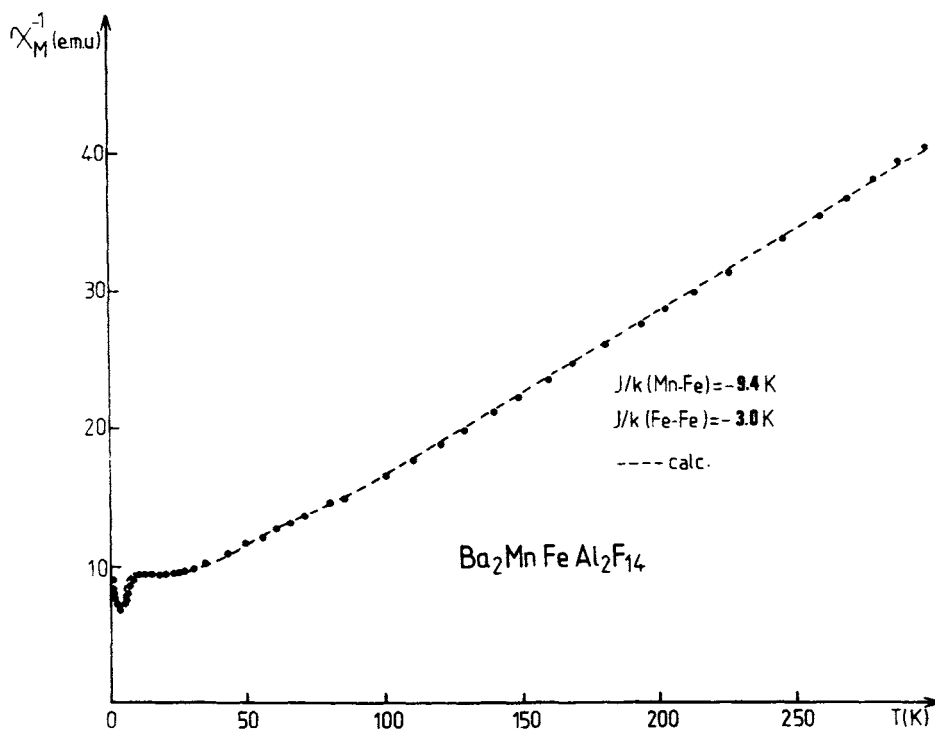


Fig. 19. Magnetic susceptibility on powder of $\text{Ba}_2\text{MnFeAl}_2\text{F}_{14}$

where each of the z_k will take one of three different values according to the nature of the ions present in the sites k and $k + 1$. Averaging this expression over the possible successions of z_k , it is possible to get a closed form expression for the susceptibility of the disordered chain [18].

Although this model inadequately describes the Fe^{2+} ion as an isotropic one, it allows to reach a good fit (Fig. 19) of the experimental curve down to 6 K for:

$$J_{\text{Fe-Fe}} = -3.0 \text{ K}; J_{\text{Mn-Fe}} = -9.4 \text{ K and } g_{\text{Fe}^{2+}} = 2.33,$$

$J_{\text{Mn-Mn}}$ being kept to -4.8 K , its value refined in BaMnAlF_7 , and the disorder parameter being fixed to the value obtained from the Mössbauer data.

9.3.3 The lozenge chains: $\text{Ba}_2\text{CaMnFe}_2\text{F}_{14}$ and $\text{Ba}_2\text{CaCoFe}_2\text{F}_{14}$

In these two compounds, Ca^{2+} was expected to occupy the 8-coordinated site, leaving the magnetic ions Mn^{2+} (Co^{2+}) and Fe^{3+} occupy as for them the octahedral ones, forming then an uncommon type of chains of concatenated lozenges.

This idealistic description had to be tempered by the observation of some cationic disorder between Ca^{2+} and Mn^{2+} (Co^{2+}), similar to the one already encountered in the $\text{Ba}_2\text{MnM}^{\text{II}}\text{Al}_2\text{F}_{14}$ compounds. In $\text{Ba}_2\text{CaMnFe}_2\text{F}_{14}$, this disorder was evidenced

by refinement of the neutron diffraction powder patterns; the reported structural parameters consider an actual formula $\text{Ba}[\text{Ca}_{1-x}\text{Mn}_x]_{\square}[\text{Mn}_{1-x}\text{Ca}_x]_{\triangleright}\text{Fe}_2\text{F}_{14}$, with x amounting to 0.16 [25]. This value was probably strongly reduced in the powder sample used for the susceptibility measurements, which had been annealed further at low temperature and showed an ordering temperature of 22 K instead of 26 K for the neutron sample. In the case of $\text{Ba}_2\text{CaCoFe}_2\text{F}_{14}$, no data are available on the amount of disorder in the neutron sample; on the contrary, the single crystals grown for the magnetic measurements were also used for a full X-ray structure determination. A careful examination of the bond lengths around Ca^{2+} and Co^{2+} led to propose a cobalt-deficient formulation $\text{Ba}_2\text{Ca}_{\square}[\text{Ca}_{1-x}\text{Co}_x]_{\triangleright}\text{Fe}_2\text{F}_{14}$ with $x = 0.07$ [26]; noteworthy, all the subsequent X-ray structural refinements on single crystals of the calcium containing usovites led to similar formulations.

Experimental data seem up to now too scarce to delineate definitive rules on the problem of cationic repartition in the usovite phases, and to know if the actual type of disorder in the samples depends on their preparation, i.e. sintering for the neutron powder samples vs melting for the X-ray single crystals. Whatever the definitive answer should be, it is worth noticing that any $\text{Ca}/\text{M}^{\text{II}}$ disorder affects the magnetic dimensionality of the system, splitting the chains into fragments if only Ca^{2+} substitution for M^{2+} occurs, or even crosslinking these fragments together if also M^{II} substitution for Ca takes place. The 1D approach seems nevertheless to work fairly well for these compounds also, as evidenced by the successful description of the magnetic behavior of $\text{Ba}_2\text{CaMnFe}_2\text{F}_{14}$ by a purely monodimensional model.

9.3.3.1 Magnetic properties in the ordered state

The magnetic structures of $\text{Ba}_2\text{CaMnFe}_2\text{F}_{14}$ and $\text{Ba}_2\text{CaCoFe}_2\text{F}_{14}$ could be refined from neutron powder diffractograms recorded below their 3D ordering temperatures (respectively 26 and 30 K) [18,25–26]. Both structures can be described with the same magnetic symmetries (Table 3), the transformations of the S_b component being

Table 3
Symmetries of the magnetic structures of $\text{Ba}_2\text{CaMnFe}_2\text{F}_{14}$ and $\text{Ba}_2\text{CaCoFe}_2\text{F}_{14}$

Position	Moment
x, y, z	S_x, S_y, S_z
$-x, -y, -z$	S_x, S_y, S_z
$-x, y, 1/2 - z$	$S_x, -S_y, S_z$
$x, -y, 1/2 + z$	$S_x, -S_y, S_z$
$1/2 - x, 1/2 + y, 1/2 - z$	$-S_x, S_y, -S_z$
$1/2 + x, 1/2 - y, 1/2 + z$	$-S_x, S_y, -S_z$
$1/2 + x, 1/2 + y, z$	$-S_x, -S_y, -S_z$
$1/2 - x, 1/2 - y, -z$	$-S_x, -S_y, -S_z$

however irrelevant for $\text{Ba}_2\text{CaMnFe}_2\text{F}_{14}$, in which no component could be seen along this axis; the refined values of the magnetic moments are listed in Table 4.

In $\text{Ba}_2\text{CaMnFe}_2\text{F}_{14}$, whose structure is drawn in Fig. 20(a), the magnetic moments of two adjacent ions in a same chain are antiparallel within experimental error, summing nevertheless to a non-zero resulting magnetic moment mostly due to the unequal number of ions in the two magnetic sublattices; they are also perpendicular to the chain direction [010], an orientation corresponding to the minimization of the magnetic dipolar interactions in antiferromagnetically coupled linear systems. The other basic features of this structure may be summarized as follow: chains belonging to the same $[(\text{CaMnFe}_2\text{F}_{14})^{4-}]_\infty$ layer are coupled ferromagnetically, their resulting moments being parallel; on the contrary, the coupling between adjacent layers is antiferromagnetic, making thus any spontaneous magnetization vanish on the macroscopic scale.

Almost the same structure is obtained for $\text{Ba}_2\text{CaCoFe}_2\text{F}_{14}$ (Fig. 20(b)), the moments of the magnetic ions having however an appreciable moment along the b -axis (Table 4). Within the chains, the magnetic moments are as previously (anti-)parallel, but those carried by two adjacent chains in the b - c plane have now opposite components along the b -axis, creating then a canting in the $[(\text{CaCoFe}_2\text{F}_{14})^{4-}]_\infty$ layers whose net moment lies therefore in the a - c plane. When considering finally the whole crystal, this later cancels due to the interlayer antiferromagnetic coupling, making the canting remain hidden.

The differences between the magnetic structures of $\text{Ba}_2\text{CaMnFe}_2\text{F}_{14}$ and $\text{Ba}_2\text{CaCoFe}_2\text{F}_{14}$ may be explained by the joint effects of the crystal symmetry and of the well-known anisotropy of Co^{2+} in octahedral sites: in the $[(\text{CaM}^{\text{II}}\text{Fe}_2\text{F}_{14})^{4-}]_\infty$ layers, two adjacent chains deduce one from the other by a c -glide plane; on such symmetry operation, the b -component of any single ion anisotropy tensor is reversed. In $\text{Ba}_2\text{CaMnFe}_2\text{F}_{14}$, in which no strong spin-lattice coupling is expected, this has no visible effect on the magnetic structure, which remains essentially determined by the exchange interactions and the magnetic dipolar couplings. On the contrary, with a very anisotropic ion like Co^{2+} , this situation induces a canting between adjacent chains as soon as the preferred axes differ from the b -axis, as it apparently happens in $\text{Ba}_2\text{CaCoFe}_2\text{F}_{14}$. Understandably, the direction of the moments of the rather isotropic Fe^{3+} will be in this case mostly

Table 4

Coordinates of the magnetic moments in the $\text{Ba}_2\text{CaM}^{\text{II}}\text{Fe}_2\text{F}_{14}$ phases ($\text{M}^{2+} = \text{Mn}^{2+}, \text{Co}^{2+}$)

M^{2+}	Atom	Ma(μ_B)	Mb(μ_B)	Mc(μ_B)	M(μ_B)
Mn^{2+}	Mn0	4.28	0.0	1.85	4.6(1)
	Fe1	-4.06	0.0	-1.57	4.32(7)
Co^{2+}	Co0	1.5(2)	1.6(1)	3.66(7)	4.22(8)
	Fe1	-1.6(1)	-1.80(5)	-4.24(6)	4.84(7)

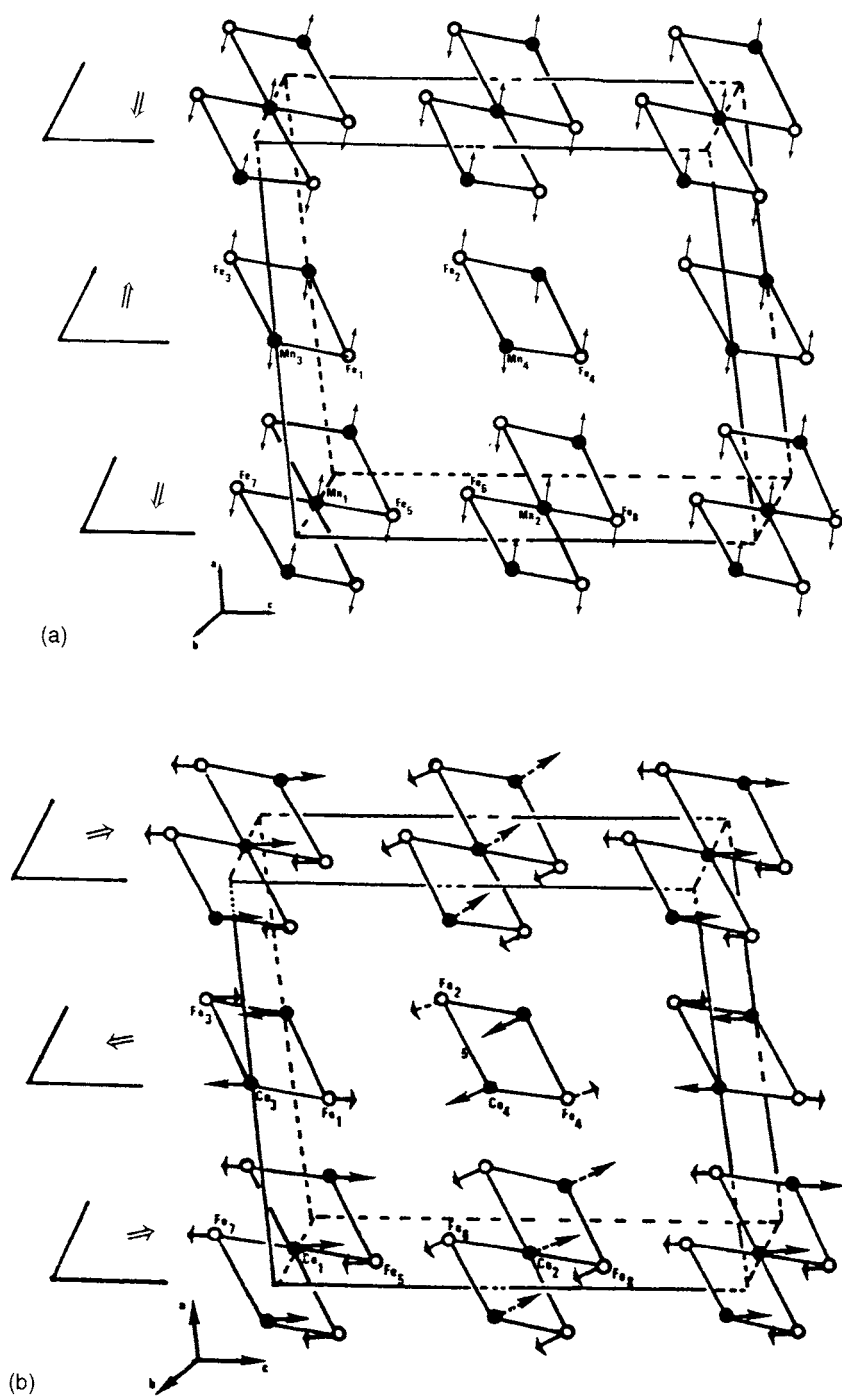


Fig. 20. Representation of the magnetic structures of $\text{Ba}_2\text{CaMnFe}_2\text{F}_{14}$ (a) and $\text{Ba}_2\text{CaCoFe}_2\text{F}_{14}$ (b).

determined by the exchange interactions with the neighbouring cobalts, differing then also from chain to chain.

The anisotropy of Co^{2+} also results in a metamagnetic transition at $H = 11$ kG for a field parallel to the c -axis (Fig. 21) [26]. The saturation value of the magnetization, $5.2 \mu_B$, can be accounted for supposing that the net moments of the $[(\text{CaCoFe}_2\text{F}_{14})^{4-}]_\infty$ layers are now parallel, in which case a value of $5.1 \mu_B$ can be calculated from the results of Table 2. This metamagnetic transition could then correspond to a collective reversal of all the spins in one half of the layers, and be a first step toward the saturation, the last one being the complete alignment of all the atomic moments: further increase of the field up to 60 kG does not allow however to observe this second transition, confirming the 1D character of the magnetism in this compound.

9.3.3.2 Magnetic susceptibilities

Above their respective Néel temperatures ($T_N = 26$ and 30 K), $\text{Ba}_2\text{CaMnFe}_2\text{F}_{14}$ (Fig. 22) and $\text{Ba}_2\text{CaCoFe}_2\text{F}_{14}$ behave as expected for ferrimagnetic chains, their $\chi T = f(T)$ curves on powders showing both a broad minimum around 60 K, tending then, down to T_N , to diverge on the low-temperature side. In the high-temperature range, they follow a Curie–Weiss law; from the value (11.95) of the Curie constant of the Cobalt compound, the contribution of the Co^{2+} in octahedral site may be estimated to 3.2, a figure commonly encountered among fluorides.

The isotropic classical spin model for chains of rings already used for $\text{Ba}_7\text{MnFe}_6\text{F}_{34}$ could be applied successfully to $\text{Ba}_2\text{CaMnFe}_2\text{F}_{14}$ [18,25] considering now the basic magnetic unit drawn in Fig. 23. The special role devoted to the nodal

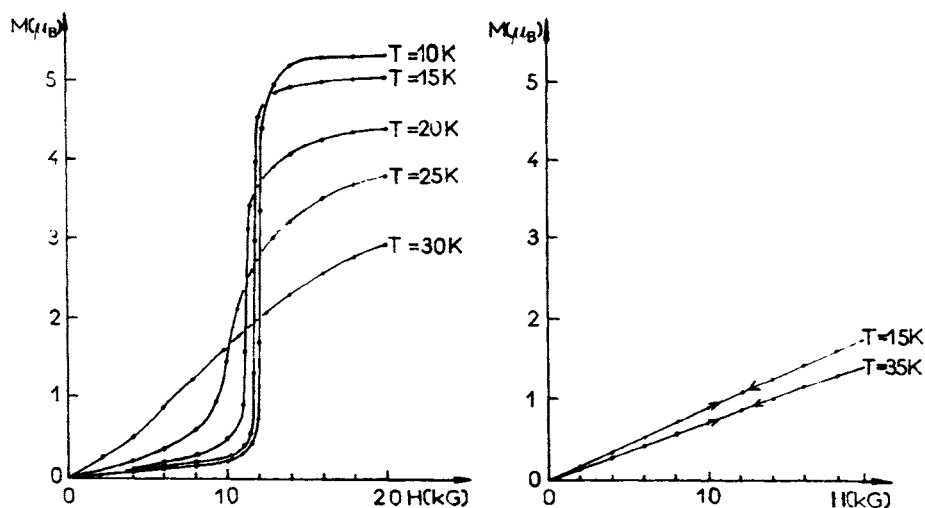


Fig. 21. Magnetization measurements on a single crystal of $\text{Ba}_2\text{CaCoFe}_2\text{F}_{14}$ for H applied parallel (left) and perpendicularly (right) to the c -axis.

spins S_1 and S_5 in the former case is now assumed by S_1 and S_3 , and the quantities m' and n' are now respectively $2-m$ and $2-n$; both g-factors being fixed to 2.0, a very satisfying agreement (Fig. 22) between theory and experiment is obtained down to T_N for the following parameters:

$$J_1/k_B = -6.7 \text{ K}; J_2/k_B = -2.7 \text{ K};$$

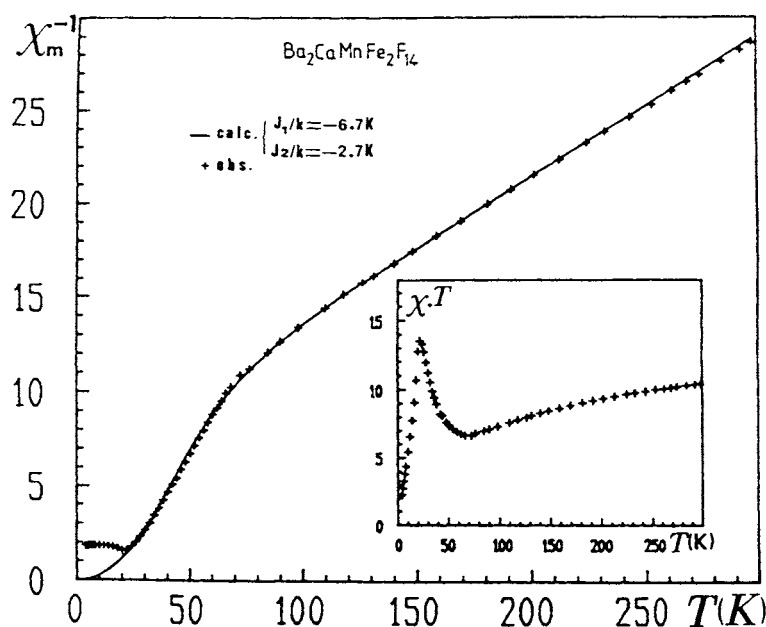


Fig. 22. Magnetic susceptibility on powder of $\text{Ba}_2\text{CaMnFe}_2\text{F}_{14}$.

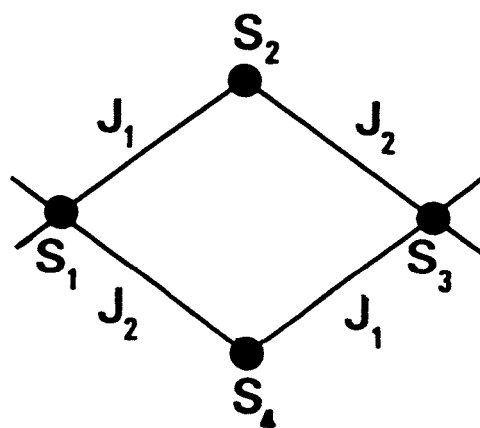


Fig. 23. Schematic representation of the magnetic unit of the chains of $\text{Ba}_2\text{CaMnFe}_2\text{F}_{14}$.

Obviously, such an isotropic model does not apply longer to $\text{Ba}_2\text{CaCoFe}_2\text{F}_{14}$, where the presence of Co^{2+} ions in octahedral sites causes the susceptibility tensor to remain anisotropic even above T_N , as it may be seen on the single crystal susceptibility measurements given in Fig. 24 [26].

9.3.4 The copper-containing usovites $\text{Ba}_2\text{CaCuM}^{III}_2\text{F}_{14}$ ($M = \text{V}, \text{Cr}, \text{Mn}$ and Fe)

Although presenting the same repartition of magnetic ions as the two previous compounds, the copper-containing usovites must be classified separately, since the Jahn–Teller effect around Cu^{2+} causes the dimension of the magnetic lattice to drop from 1 to 0. These usovites are then described in terms of isolated trimers rather than in terms of magnetic chains, passing therefore slightly beyond the scope of this chapter. For this reason, among the members of this group ($\text{M}^{3+} = \text{V}^{3+}$ [27], Cr^{3+} [18,28], Mn^{3+} [5] and Fe^{3+} [18,28]), only the last one will be briefly treated here, as a typical example of the whole series.

In spite of their poor resolution, the Rietveld profile refinements of the neutron powder spectra of $\text{Ba}_2\text{CaCuFe}_2\text{F}_{14}$ show that the copper lies in a distorted octahedron (Fig. 25), the Cu—F4 distances ($2 \times 2.4 \text{ \AA}$) being significantly higher than the Cu—F2 and the Cu—F7 ones (2×2.0 and $2 \times 1.9 \text{ \AA}$ respectively). The orientation of the magnetic orbital $d_{x^2-y^2}$ of the copper can then be deduced (Fig. 25) and shown to be unfavourable to any significant superexchange interaction through the fluorine F4. As a consequence, the Cu—Fe magnetic interactions are likely to occur mostly along the Cu—F2—Fe pathways, lining up isolated Fe—Cu—Fe clusters rather than

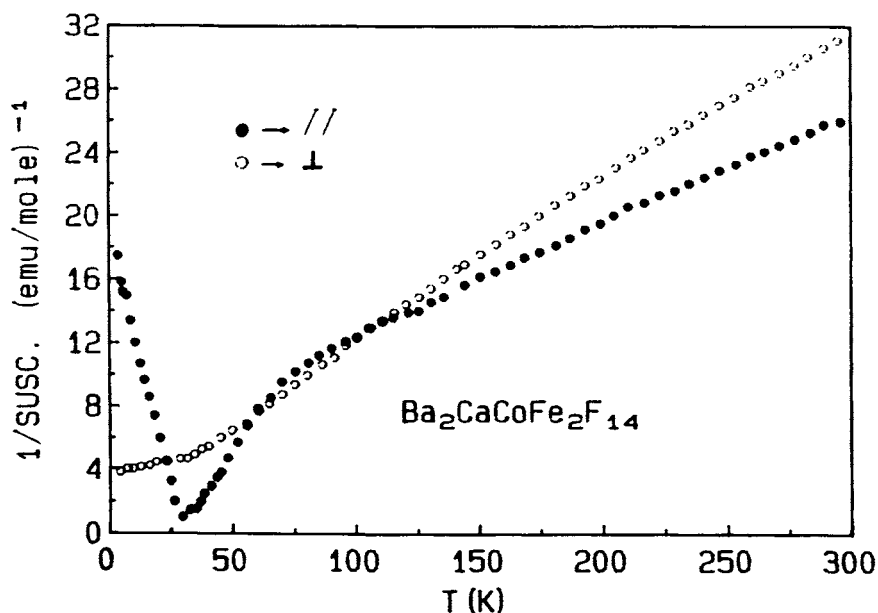


Fig. 24. Magnetic susceptibility of a single crystal of $\text{Ba}_2\text{CaCoFe}_2\text{F}_{14}$.

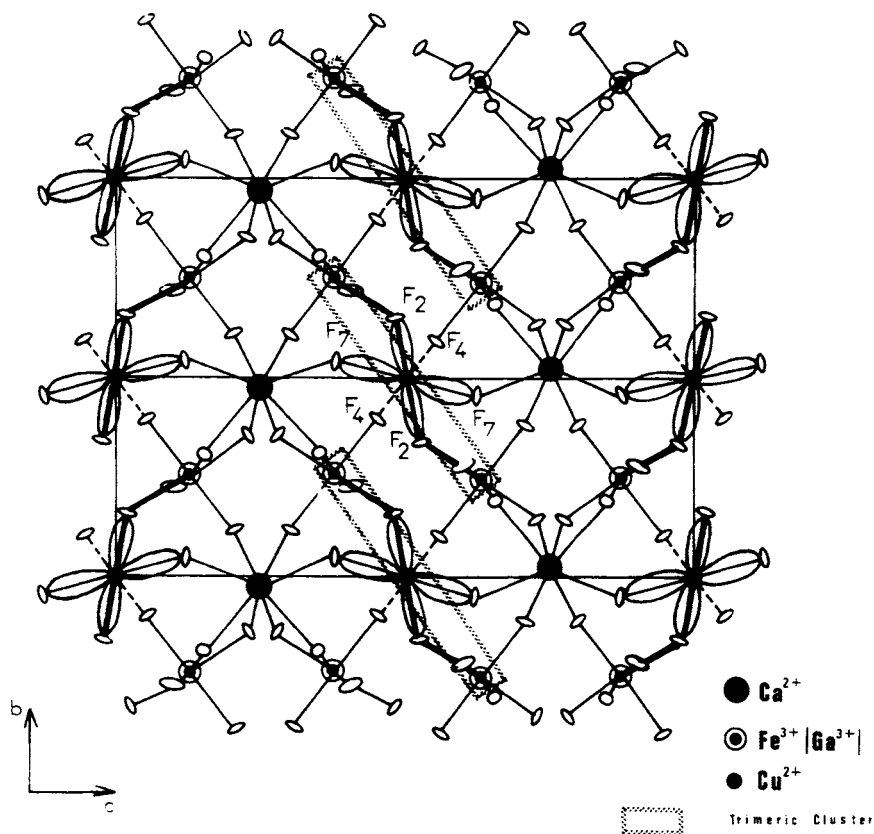


Fig. 25. Schematic representation of the orientation of the magnetic $d_{x^2-y^2}$ orbital of the copper in $\text{Ba}_2\text{CaCuFe}_2\text{F}_{14}$.

$[\text{CuFe}_2]$ infinite chains. Following the Kanamori–Goodenough rules [29–30], the intracluster couplings are most probably antiferromagnetic: this later point is evidenced by the value of the saturated magnetization at 1.8 K ($8.5 \mu_B$, Fig. 26), which is in fair agreement with the $8.9\text{--}9.0 \mu_B$ calculated for an $S=9/2$ ground state.

The susceptibility curve of $\text{Ba}_2\text{CaCuFe}_2\text{F}_{14}$, given in Fig. 27, is well described down to 25 K by a model considering discrete CuFe_2 ferrimagnetic trimers: the exchange interactions are simply described by an Heisenberg hamiltonian, but more troubles are encountered for the Zeeman hamiltonian which must account for the g-factor anisotropy of Cu^{2+} ; it is then written down as:

$$\begin{aligned}
 H_z = & -g_{\text{Fe}} \mu_B H \left[\sin \theta \left(\frac{S_{\text{Fe}_1}^+ + S_{\text{Fe}_1}^- + S_{\text{Fe}_3}^+ + S_{\text{Fe}_3}^-}{2} \right) + \cos \theta (S_{\text{Fe}_1}^z + S_{\text{Fe}_3}^z) \right] \\
 & - \mu_B H \left[\sin \theta g_{\text{Cu}\perp} \left(\frac{S_{\text{Cu}}^+ + S_{\text{Cu}}^-}{2} \right) + \cos \theta g_{\text{Cu}\parallel} S_{\text{Cu}}^z \right]
 \end{aligned}$$

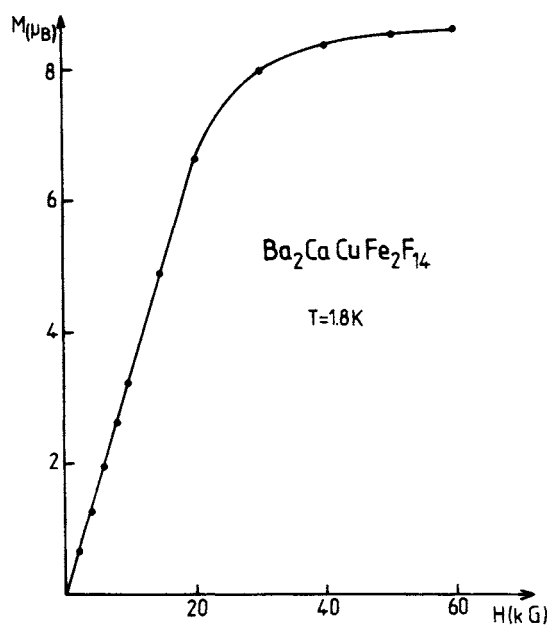


Fig. 26. Magnetization curve on powder of $\text{Ba}_2\text{CaCuFe}_2\text{F}_{14}$.

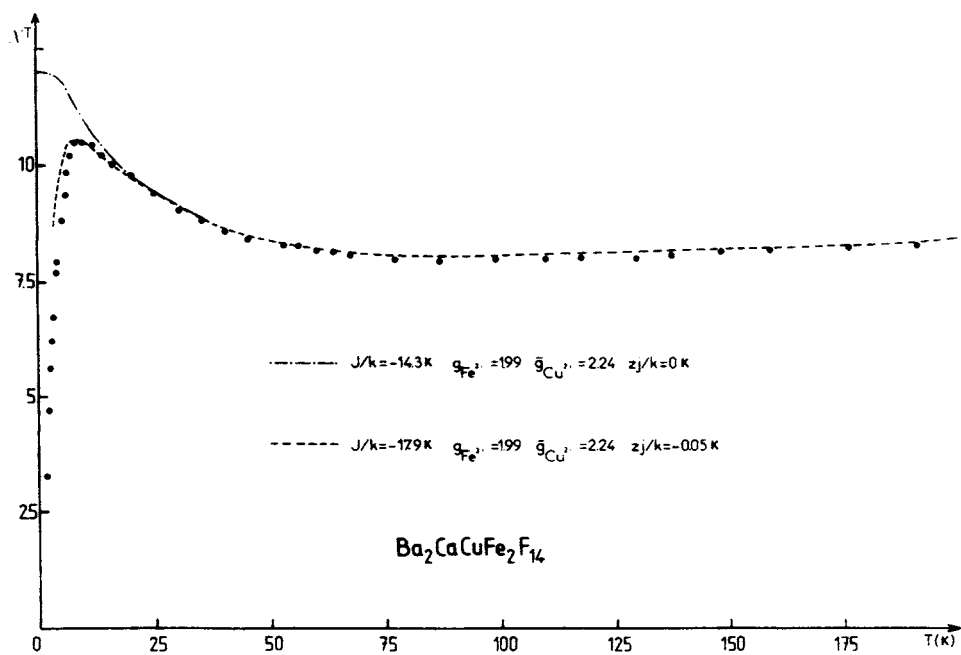


Fig. 27. Susceptibility curve on powder of $\text{Ba}_2\text{CaCuFe}_2\text{F}_{14}$.

where θ represents the angle between the external field H and the anisotropy axis of the g -factor of the copper. The calculation of the susceptibility proceeds therefore through the diagonalization of the resulting matrix, giving ultimately the result shown in Fig. 27 (upper curve) for:

$$g_{\text{Fe}} = 2.0, g_{\text{Cu}\perp//} = 2.5, g_{\text{Cu}\perp} = 2.1 \text{ and } J/k_{\text{B}} = -14.3 \text{ K}$$

(the g -factors are kept fixed, the values for g_{Cu} being taken from the E.S.R. data reported for $\text{Ba}_2\text{CaCuGa}_2\text{F}_{14}$ [15]). As expectable for a ferrimagnetic trimer, this calculated curve tends to a finite limit when T approaches 0, in plain disagreement with the experimental one which tends to 0 below 15 K. The decrease of this later is probably due to the rise of intercluster interactions, as confirmed by the appearance of Warren peaks in the neutron powder diffractogram below 12 K. These interactions can be modeled using a mean field approach according to:

$$-2zj'S_i \cdot S_j = -2zj'S_\theta \langle S_\theta \rangle$$

the resulting implicit equation in S_θ being solved using the density matrix. This correction greatly improves the agreement with the experimental data (Fig. 27, lower curve) for:

$$g_{\text{Fe}} = 2.0, g_{\text{Cu}\perp//} = 2.5, g_{\text{Cu}} = 2.1, J/k_{\text{B}} = -17.9 \text{ K and } zj'/k_{\text{B}} = -0.05 \text{ K.}$$

References

- [1] F.C. Hawthorne, *Can. Miner.*, 21 (1983) 553.
- [2] J. Renaudin, G. Férey, A. de Kozak, M. Samouël, *Rev. Chim. Miner.*, 24 (1987) 295.
- [3] M. Samouël, A. de Kozak, J. Renaudin, G. Férey, *J. Less Com. Met.*, 143 (1988) 93.
- [4] A. le Lirzin, J. Darriet, A. Tressaud, P. Hagenmuller, *C.R. Acad. Sci. Paris*, 308 (1989) 713.
- [5] A. le Lirzin, PhD thesis, Université de Bordeaux-I, Bordeaux, France, 1990.
- [6] J. Renaudin, G. Férey, M. Drillon, A. de Kozak, M. Samouël, *C.R. Acad. Sci. Paris*, 308 (1989) 1217.
- [7] M.E. Fisher, *Am. J. Phys.*, 32 (1964) 343.
- [8] Xu Q., J. Darriet, R. Georges, *J. Magn. Magn. Mat.*, 73 (1988) 379.
- [9] A.P. Ginsberg, M.E. Lines, *Inorg. Chem.*, 11 (1972) 2289.
- [10] J. Villain, J.M. Loveluck, *J. Phys. Lett. (Paris)*, 38 (1977) L77.
- [11] A. Caneschi, D. Gatteschi, P. Rey, R. Sessoli, *Inorg. Chem.*, 30 (1988) 3936.
- [12] J.H. van Vleck, *Electric and Magnetic Susceptibilities*, Oxford University Press, 1932.
- [13] A.T. Litvin, A.A. Petrunina, S.S. Ostapenko, A.S. Povarennykh, *Dopov Akad. Nauk Ukr. RSR*, ser B, 3 (1980) 47.
- [14] A. de Kozak, M. Samouël, *Rev. Chim. Miner.*, 18 (1981) 255.
- [15] H. Holler, PhD thesis, Philipps Universität, Marburg, Germany, 1987.
- [16] H. Holler, D. Babel, M. Samouël, A. de Kozak, *Rev. Chim. Miner.*, 21 (1984) 358.
- [17] H. Holler, J. Pebler, D. Babel, *Z. Anorg. Allg. Chem.*, 522 (1985) 189.
- [18] Xu Q., PhD thesis, Université de Bordeaux-I, Bordeaux, France, 1990.
- [19] H. Holler, D. Babel, *Z. Anorg. Allg. Chem.*, 491 (1982) 137.
- [20] A.J.C. Wilson, *Acta Cryst.*, 2 (1949) 245.
- [21] J. Darriet, Xu Q., A. Tressaud, R. Georges, J.L. Soubeyroux, *Phase Trans.*, 13 (1988) 49.

- [22] A. le Lirzin, J. Darriet, R. Georges, J.L. Soubeyroux, *J. Magn. Magn. Mat.*, 109 (1992) 47.
- [23] J. Seiden, *J. Phys. Lett. (Paris)*, 44 (1983) 947.
- [24] P.M. Richards, *Phys. Rev. B*, 14 (1976) 1239.
- [25] Xu Q., J. Darriet, J.L. Soubeyroux, R. Georges, *J. Magn. Magn. Mat.*, 14 (1988) 219.
- [26] A. le Lirzin, Xu Q., J. Darriet, J.L. Soubeyroux, V. Kaiser, J. Pebler, D. Babel, *Eur. J. Solid State Inorg. Chem.*, 27 (1990) 791.
- [27] A. le Lirzin, V. Kaiser, J. Darriet, D. Babel, unpublished results.
- [28] Xu Q., J. Darriet, A. Tressaud, J.L. Soubeyroux, P. Hagenmuller, *Mat. Res. Bull.*, 23 (1988) 637.
- [29] J. Kanamori, *J. Phys. Chem. Solids*, 10 (1959) 87.
- [30] J.B. Goodenough, *Magnetism and the Chemical Bond*, Wiley Interscience, NY, 1963.

CHAPTER 10

Luminescent Properties of Fluorides

Claude Fouassier

Institut de Chimie de la Matière Condensée de Bordeaux. CNRS, Avenue A. Schweitzer, 33608 Pessac cedex, France

10.1 Introduction

Due to the high optical quality of crystals and their wide transmission range, fluorides are well suited for the study of spectroscopic properties. They have brought a major contribution to the knowledge of luminescence processes.

This chapter deals with luminescent properties of crystalline fluorides. Luminescent properties of glassy materials are presented in Chapter 8.

Fluorides possess specific characteristics which influence luminescent properties. They are recalled in Sec. 2 with examples of peculiar luminescences to which they give rise. In Secs 3, 4, 5 and 6 are reviewed four domains which have attracted considerable attention in recent years:

- laser crystals. Because of the wide transmission range and the high number of emitting levels, consequence of the low phonon energies, a considerable amount of laser emissions have been obtained from fluoride crystals with wavelength ranging from 285 nm in the ultraviolet to 4.34 μm in the infrared.
- scintillator crystals. Because under excitation by X or γ radiations or particles, the number of emitted photons decreases with increasing bandgap, fluorides have lower efficiencies than oxides or other halides. However the high optical quality, chemical stability and radiation hardness make them well suited for application in fast detectors for high-energy particles.
- ionization processes, hole burning. Ionization processes have been investigated in detail. Photoionization is responsible for the quenching of the luminescence of cations with reducing character in some lattices and two-step ionization affects the efficiency of lasers. Ionization can be used for obtaining high capacity optical memories (hole burning).
- energy storage phosphors. Much work has been devoted to photostimulable phosphors for digital X-ray imaging systems. Most of them contain halides and in particular fluorine which brings the chemical stability required for application.

10.2 Specific characteristics of fluorides

Fluorides have specific characteristics which allow peculiar luminescent properties.

Wide bandgap The wide bandgap makes possible emission from high-energy levels. For instance for Nd^{3+} , Er^{3+} and Tm^{3+} an allowed $5d \rightarrow 4f$ emission has been observed in various fluorides around 170 nm in the vacuum UV [1,2].

It allows the existence of the scintillating properties of BaF_2 crystals: a wide forbidden band is necessary for avoiding reabsorption of the ultraviolet $2pF \rightarrow 5pBa$ emission produced when holes are formed in the $5pBa$ core levels by X-rays or γ -rays (cross-luminescence) [3].

Low nephelauxetic effect and moderate crystal field splitting Because of its high electronegativity fluorine is the element inducing the lowest nephelauxetic effect (lowering of the energy levels with respect to their positions in the free ion caused by a decrease in interelectronic repulsions with increasing covalency). The crystal field in fluorides is lower than in oxides but stronger than in other halides. In oxides the nephelauxetic effect and crystal field splitting strongly displace the position of levels formed from external orbitals. In fluorides the higher energy of the first $5d$ level of lanthanide ions allows the existence of line emissions from $4f$ levels usually located in the $5d$ bands. So in fluorides with high coordination number such as BaLiF_3 , BaY_2F_8 , BaSiF_6 , Eu^{2+} substituted for barium shows an emission from the first excited $4f^7$ level (${}^6P_{7/2}$) instead of the usual $5d \rightarrow 4f$ band [4]. Similarly in LaF_3 , YF_3 and $\alpha\text{-NaYF}_4$ excitation in the $5d$ states of Pr^{3+} leads to population of the upper $4f^2$ level (1S_0) at $46,700\text{ cm}^{-1}$ (214 nm) [5]. $\text{YF}_3 : \text{Pr}$ has the peculiarity to exhibit a visible luminescence from this level with a quantum efficiency exceeding 1: a two-photon emission occurs by a cascade process (${}^1S_0 \rightarrow {}^1I_6$, followed after non radiative decay to 3P_0 by ${}^3P_0 \rightarrow {}^3H_J, {}^3F_J$) [6].

Long lifetimes of excited levels of nd^N and $4f^N$ configurations Electric dipole transitions are allowed if the initial and final states are made up of orbitals of opposite parity ($\Delta l = 1, 3$; l : orbital angular momentum quantum) and if the spin remains unchanged ($\Delta S = 0$). However parity-forbidden transitions can occur as a result of mixing with states of opposite parity. Because of the ionicity of the bonds formed by fluorine, the probability of the $nd \rightarrow nd$ transitions of transition element ions and $4f \rightarrow 4f$ transitions of lanthanide ions are lower than in oxides. This results in lower absorption properties and longer lifetimes of excited states ($\tau = 1/p_{\text{rad}}$, p_{rad} : sum of the radiative rates of transitions from the excited state). The lifetime of the ${}^4F_{3/2}$ Nd^{3+} state from which the $1.06\text{ }\mu\text{m}$ laser emission originates, amounts to $700\text{ }\mu\text{s}$ in LaF_3 , compared to $260\text{ }\mu\text{s}$ in Y_2O_3 , $220\text{ }\mu\text{s}$ in LaCl_3 and $60\text{ }\mu\text{s}$ in $\gamma\text{-La}_2\text{S}_3$. Long lifetimes are favourable for up-conversion processes which are used for instance for infrared-to-visible conversion.

Low phonon energies The thermal stability of luminescence depends on the energy of the emitting level, the change in equilibrium cation-anion distance induced by the electronic transition and phonon energies [7,8]. In fluorides phonon energies are lower than in oxides and higher than in other halides. Typically for most host lattices the highest phonon energies lie in the $400\text{--}500\text{ cm}^{-1}$ range (CaF_2 : 465 cm^{-1} , LiYF_4 : 490 cm^{-1}). The relatively low phonon energies in fluorides are favourable

for a high stability. Quenching of the $5d \rightarrow 4f$ emission of Ce^{3+} in LiYF_4 ($\lambda_{\text{max}} = 320 \text{ nm}$) starts only at about 900 K [9].

The probability of non-radiative transitions between the 4f levels of lanthanide ions (multiphonon transitions) diminishes with increasing gap with the next lower level and decreasing phonon energies. A comparison between the multiphonon emission rates of Er^{3+} levels in silicate and fluoride glasses is given in Sec. 8.4.1. Typically the probability for non-radiative decay becomes negligible when the energy gap exceeds 4–5 times the highest phonon energies of the host [10]. Because of the lower phonon energy and smaller crystal field splitting of J levels, in fluorides for Ln^{3+} ions with closely spaced levels such as Ho^{3+} and Er^{3+} this condition is filled for various levels which in oxides decay essentially non radiatively. This is the case of the green emitting level $^4S_{3/2}$ of erbium which is separated from the next-lower level by 3000 cm^{-1} [11]. The highest efficiencies for conversion of infrared radiation to visible (up-conversion) have been obtained with YF_3 and NaYF_4 doped with Yb^{3+} and Er^{3+} [12,13]: the energy of two IR photons ($\lambda = 970 \text{ nm}$) absorbed by ytterbium is transferred to an erbium ion which is excited into the $^2H_{11/2}$, $^4S_{3/2}$ states.

10.3 Laser crystals

10.3.1 Lasers emitting in the infrared

The high optical quality of fluoride crystals make them attractive for laser applications. Because of low nonlinear index, they can sustain high peak powers without causing beam distortion. $\text{LiYF}_4:\text{Nd}$ ($\lambda = 1.053 \text{ }\mu\text{m}$) is used as amplifiers in high power lasers. It also has significant advantage over $\text{YAG} : \text{Nd}^{3+}$ for diode-pumped systems [14].

Because of the low probability of non-radiative transitions and the transparency up to long wavelengths resulting from the relatively low phonon energies, fluorides are appropriate matrices for obtaining laser emissions at long wavelength in the infrared. The development of laser sources emitting in the 3–5 μm wavelength range is of interest for hazardous chemical detection and remote atmospheric sensing applications. Various trivalent lanthanide ions possess levels whose separation corresponds to this wavelength range. Laser emissions have been obtained at 3 μm with $\text{BaY}_2\text{F}_8 : \text{Dy}$ ($^6H_{13/2} \rightarrow ^6H_{15/2}$) [15], 3.41 μm with $\text{LiYF}_4:\text{Er}$ ($^4F_{9/2} \rightarrow ^4I_{9/2}$) [16], 3.91 μm with $\text{LiYF}_4 : \text{Ho}$ ($^5I_5 \rightarrow ^5I_6$) [17] and 4.34 μm with $\text{LiYF}_4 : \text{Dy}$ ($^6H_{11/2} \rightarrow ^6H_{13/2}$) [18].

For 3d ions such as V^{2+} , Co^{2+} , Ni^{2+} the energy gap between the ground state and first excited state corresponds to wavelengths in the near infrared. Because an electron is transferred from a t_{2g} to an e_g orbital, there is a strong modification of the equilibrium cation-anion distance. Consequently these ions show broad-band fluorescence. Tunable laser operation around 1 μm has been demonstrated for V^{2+} in MgF_2 and KMgF_3 [19]. Tunable emissions at low temperature had been obtained around 1.7 μm with Ni^{2+} in MgF_2 [20] and 2 μm with Co^{2+} in MgF_2 and KZnF_3 [20,21]. BaLiF_3 doped with Ni^{2+} substituted for Li^+ has favourable characteristics for operation at room temperature [22].

The possibility of using the $6s \rightarrow 6p$ emission of Pb^{+} centres in the perovskite-type fluorides $KMgF_3$ and $BaLiF_3$ for obtaining tunable lasers in the near-infrared is also investigated [23,24]. Pb^{+} centres are generated by high-energy electron irradiation of the Pb^{2+} -doped crystals.

An "ultrabroadband" infrared laser oscillation has been obtained at 300 K with F_2^{+} colour centres in LiF [25]. Its wavelength range, 850–1040 nm, is almost comparable to the bandwidth of the F_2^{+} luminescence spectrum. Ultrabroad band laser oscillation is of interest in laser spectroscopy and photochemistry.

10.3.2 Lasers emitting in the visible

In recent years much work has been devoted to the development of lasers emitting at short wavelength. Compact continuous wave solid-state lasers are of interest for high-density data storage and display applications. Laser emissions in the visible can be obtained by up-conversion. This was demonstrated for the first time with BaY_2F_8 as the matrix: an infrared-pumped stimulated emission in the red (670 nm) and green (551 nm) was produced at 77 K for doping respectively with Yb, Er and Yb, Ho [26]. In the last decade laser emissions have been obtained in the green (551 nm) at 300 K with $LiYF_4:Er$ [27] and the blue (450 nm) at 70 K with $LiYF_4:Tm$ [28]. Also laser operation at 413 nm was achieved at 30 K with $LiYF_4:Nd$ ($^3P_{3/2} \rightarrow ^4I_{11/2}$ transition) [29]. Up-conversion lasers have also been obtained with glass fibers (Sec. 8.5).

10.3.3 Lasers emitting in the ultraviolet

There is also an increasing interest on lasers operating in the ultraviolet and more particularly on solid-state lasers which can be tuned continuously in a wavelength domain [30]. They have found applications in the fields of medicine and biology (cornea shaping, angioplasty, measurements of ADN sequences) and environmental sciences. Because of the low crystal field splitting of 5d levels (Sec. 10.2), the $5d \rightarrow 4f$ emission band of Ce^{3+} in fluorides usually lies in the ultraviolet. Two difficulties occur for obtaining a laser radiation with this ion: losses are caused by the excited-state absorption phenomenon, colour centres can be generated by the pump radiation (solarization). The first laser emission was reported for $LiYF_4:Ce$ at 325 nm [31]. In recent years tunable emission has been obtained with several cerium-doped fluorides: $LiCaAlF_6$ and $LiSrAlF_6$ between about 285 and 300 nm [32], $LiLuF_4$ around the peaks of the two emission band components caused by the spin-orbit splitting of the ground state, 307–313 nm and 324–328 nm [33].

The possibility of using the $nd^9(n+1)s \rightarrow nd^{10}$ transitions of Cu^{+} or Ag^{+} doped alkaline earth fluorides for obtaining a tunable UV laser emission (ex. $SrF_2:Ag^{+}$: $\lambda_{max} = 315$ nm) is also investigated [34,35].

10.4 Scintillator crystals

10.4.1 Physical processes

Scintillators are materials which convert the energy of ionizing radiation such as X-rays, γ -rays, charged particles or neutrons into light. They are used in a variety of applications including medical imaging, measuring equipments used in scientific research (high energy physics, astrophysics), industrial control, security inspection and geophysical exploration. The physical processes occurring in scintillators are:

- absorption of the ionizing radiation, resulting in the transfer of electrons from the valence to conduction band of the material;
- transfer from the electron-hole recombination energy to the luminescent centre;
- emission process.

A strong absorption generally requires a high density. Because of their high fluorine content, fluorides are less dense than the homologous oxides. Consequently more voluminous crystals are required for absorbing the ionizing radiation. The number of electron-hole pairs created by one ionizing particle decreases as the forbidden band increases. The incident particle and the created charge carriers also lose part of their energy by generation of phonons [36]. Even though the lower phonon energies in fluorides are a favourable characteristic, because of their wide bandgap they cannot compete with oxides as regards the number of emitted photons. Nevertheless fluorides have some interesting characteristics. Their low melting point makes easier the growth of crystals. Ionization energies are greater than in oxides so that for ions like Ce^{3+} having a reducing character fluorides offer a larger variety of host lattices: for instance in LaF_3 and YF_3 Ce^{3+} luminesces efficiently while in La_2O_3 and Y_2O_3 its luminescence is quenched by electron transfer from the excited 5d state to the conduction band [37]. With respect to other halides, fluorides present the interest of a high chemical stability. So for some applications fluorides show the most appropriate characteristics. This is in particular the case for the detection of high-energy particles because a large number of electron-hole pairs is generated in the crystal so that a high light yield is not crucial.

A fast decay is necessary for particle discrimination. It is crucial for positron emission tomography [38].

10.4.2 Cerium scintillators

The allowed $5d \rightarrow 4f$ emission of Ce^{3+} shows a fast decay. Because of the weak nephelauxetic effect and small crystal field splitting of 5d states the emission lies generally in the UV range which is favourable for fast decay because the radiative rate increases with the transition energy. Typical decay times at 300 K are 20–40 ns [9]. During the last decade a considerable amount of research has been devoted to the study of the crystal growth and scintillation processes of cerium fluoride. CeF_3 has a density of 6.16 g/cm^3 . The $5d \rightarrow 4f$ emission band peaks at 285 nm. A favourable characteristic of this material is the absence of concentration quenching. Often luminescent ions must be diluted among ions devoid of electronic transitions in the emission wavelength range like La^{3+} or Y^{3+} with as a consequence a reduction

of the probability of transfer of the energy released in the lattice by the ionizing radiation. The light yield is 4500 photons/meV. In oxides yields of the order of 15,000 photons/meV have been obtained for yttrium aluminates and 25,000 photons/meV for the dense but costly lutetium silicate Lu_2SiO_5 [38]. As shown by the initial fast component of the decay, under excitation by ionizing particles the luminescence of CeF_3 is affected by non-radiative processes. From a comparison of decay curves obtained for γ -ray and laser excitation, it has been concluded that losses are the result of interactions between excited Ce^{3+} ions [39]. With increasing temperature the contribution of the fast component to the decay lessens and intensity increases due to higher mobility of localized excitations resulting in larger separations [40].

The probability of excitation of Ce^{3+} ions from the matrix is often higher in gadolinium compounds than in lanthanum or yttrium materials. Because of the high gadolinium concentration the recombination energy of electron-hole pairs created by the ionizing particle can be efficiently transmitted to Gd^{3+} ions. After energy migration among the latter, energy transfer to a Ce^{3+} ion can occur if the $4f \rightarrow 5d$ absorption bands of the latter extend to the wavelength of the emission from the first excited Gd^{3+} level (${}^6P_{7/2}$), 312 nm. This condition is less frequently fulfilled than in oxides because of the lower crystal field splitting of 5d levels. $\text{Gd}^{3+} \rightarrow \text{Ce}^{3+}$ transfer occurs in CsGd_2F_7 whose light yield (7600 photons/MeV) markedly exceeds that of $\text{CsY}_2\text{F}_7 : \text{Ce}$ but the decay time is considerably lengthened because of the too low $\text{Gd}^{3+} \rightarrow \text{Ce}^{3+}$ transfer rate resulting from insufficient absorption of cerium at 312 nm [41].

Denser cerium-activated crystals have been obtained with BaThF_6 ($d = 6.68 \text{ g/cm}^3$) [42] and LuF_3 ($d = 8.3 \text{ g/cm}^3$) [43]. For a cerium content of only 0.04% in LuF_3 a light yield of 8000 photons/MeV has been obtained.

10.4.3 Crystals doped with other trivalent lanthanides showing a $5d \rightarrow 4f$ emission: Pr^{3+} , Nd^{3+} , Er^{3+} , Tm^{3+}

In some lattices, Pr^{3+} , Nd^{3+} , Er^{3+} , Tm^{3+} exhibit a $5d \rightarrow 4f$ emission. Because the stability of the $4f^N$ configurations increases with the number of electrons with parallel spins, the emission lies at shorter wavelengths than for Ce^{3+} ($4f^1$).

In the energy scheme of $4f^2$ levels of Pr^{3+} a large gap separates the highest level, 1S_0 , located at $46,700 \text{ cm}^{-1}$ (214 nm) and the next-lower level, 3P_2 , at $23,000 \text{ cm}^{-1}$ (435 nm). A $4f \rightarrow 5d$ emission can occur if the lowest 5d level lies below 1S_0 . Because of the strong crystal field generated by a cubic environment, such an emission has been observed in Pr^{3+} -doped CaF_2 and BaF_2 [44].

The $5d \rightarrow 4f$ emission around 160–170 nm obtained with Nd^{3+} , Er^{3+} , Tm^{3+} is of interest for detection by photosensitive gases or photocathodes sensitive to VUV photons only. Because of the high energy of the transition, the emission decays rapidly: τ is of the order of 5 ns [2,45].

10.4.4 BaF_2 . Cross-luminescence scintillators

The discovery of the fast emission of BaF_2 [46,47] has brought about a large activity in the field of cross-luminescence materials. The cross-luminescence (CL) (or

core-valence luminescence) mechanism is represented in Fig. 1 in the case of BaF_2 [3]. An electron is transferred from the upper core band (5p Ba) to the conduction band. The hole relaxes rapidly to the uppermost core level and is annihilated by an electron from the valence band formed by 2p fluorine orbitals with emission of an UV photon. A condition for CL is that the separation between the valence band and the upper core levels is lower than the width of the forbidden band. The CL is very fast: $\tau = 0.8$ ns for BaF_2 . The hole formed in the valence band is afterwards annihilated by the electron transferred into the conduction band (self-trapped exciton (STE) luminescence). The STE luminescence lies at longer wavelength than the cross-luminescence and has a slower decay: $\tau = 600$ ns.

The wide bandgap of fluorides is therefore favourable for the existence of a CL. Such a luminescence has been observed in binary or ternary fluorides containing K, Rb, Cs and Ba [3]. Even when the emission is not affected by thermal quenching, the light yield is relatively small: 1400 and 2000 photons/MeV for BaF_2 and CsF respectively. The probability that a hole is produced in the upper core band by a X-ray or γ -ray photon appears relatively low. BaF_2 ($d = 4.88$ g/cm³) is used in applications requiring very fast decay. It is non-hygroscopic and large crystals can be grown.

In order to increase the efficiency and suppress the slow excitonic luminescence, the effect of the incorporation of Ce^{3+} in BaF_2 has been examined, the presence of the Ce^{3+} $4f \rightarrow 5d$ absorption bands in the wavelength range of the excitonic luminescence allowing energy transfer [48,49].

10.5 Photoionization. Hole burning

10.5.1 Photoionization processes

In halides lower oxidation states are more stable than in oxides. In most oxide lattices europium and ytterbium are the only lanthanide ions which, because of

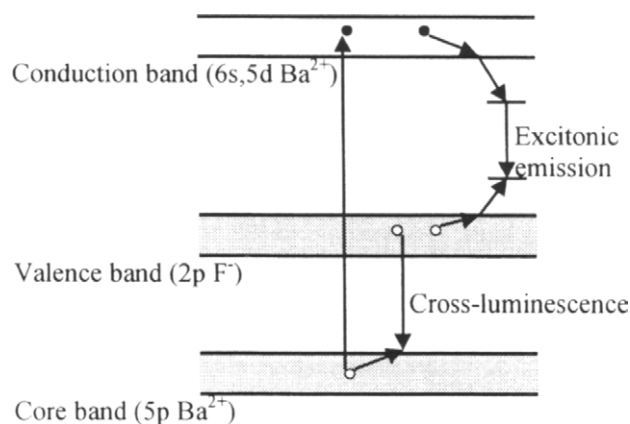


Fig. 1. Mechanisms of the luminescence of BaF_2 (reproduced with permission from J. Lumin., 60-61 (1994) 936 [3]).

the stability of the half-filled shell ($4f^7$) and filled shell ($4f^{14}$) configurations, can exist in the divalent state. In fluorides such as CaF_2 , SrF_2 and BaF_2 most lanthanides can be obtained in the divalent state. Photoionization processes in these lattices have been investigated in detail. While in CaF_2 and SrF_2 Eu^{2+} shows an usual $5d \rightarrow 4f$ emission in the blue, in BaF_2 for excitation in the $4f \rightarrow 5d$ absorption bands it exhibits an anomalous emission in the yellow range [50]. As a result of the large Stokes shift the emission is characterized by a large bandwidth and a strong temperature quenching. In the three alkaline earth fluorides Yb^{2+} shows such an 'anomalous emission' [50]. Recently it has been shown that despite the small magnesium size a small amount of Eu^{2+} and Yb^{2+} can be incorporated in MgF_2 [51,52]. Both ions show a $5d \rightarrow 4f$ emission in this lattice. Photoconductivity measurements have allowed the determination of the nature of the 'anomalous emission'. Because of the low stability of the divalent state the ground state is only a few eV below the conduction band. Excitation in a $5d$ state located in the conduction band results in an ionization which induces a current if an electric field is applied. The Eu^{2+} $5d$ state is split into E_g and T_{2g} states. For $\text{CaF}_2:\text{Eu}^{2+}$ and $\text{SrF}_2:\text{Eu}^{2+}$ the photoconductive threshold is at higher energy than the $4f \rightarrow 5d$ (E_g) transitions [53,54]. Consequently the ion returns to the ground state by a radiative $5d \rightarrow 4f$ transition. In BaF_2 all the Eu^{2+} excited states are in the conduction band of the crystal [54]. This is confirmed by the broadening of the absorption spectrum resulting from the coupling of the $5d$ states with the conduction band (Fano resonance) [55,56]. The anomalous emission is ascribed to a trapped exciton with the hole at the europium site and the electron held on the next-neighbour barium atoms in the Coulomb field of the Eu^{3+} ion. The probability of the excitonic emission is low (radiative rate $(1/\tau)$ for $\text{BaF}_2:\text{Eu}$: 7900 s^{-1}). A weak broad absorption band at lower energy than the first $4f \rightarrow 5d$ band has been ascribed to the formation of the exciton [54]. The large variation in europium-fluorine distances induced by the change in oxidation state accounts for the large Stokes shift of the emission. Similar results have been obtained for $\text{SrF}_2:\text{Yb}$ [57].

The ionization energy is equal to the difference between the third ionization potential and the electrostatic potential at the cationic site in the crystal (local distortions due to the size difference between the lanthanide ion and the substituted ion and the electron affinity of the host also must be taken into consideration). For Eu^{2+} [54], Tm^{2+} and Yb^{2+} [57] it has been found that the ionization energies vary with the nature of the substituted ion in the order $\text{Ca} > \text{Sr} > \text{Ba}$. The ionization energy can be increased by substituting the divalent lanthanide ion for a monovalent ion. While in the alkaline earth fluorides MF_2 the Yb^{2+} emission is completely quenched at room temperature, in NaMgF_3 and KMgF_3 crystals this ion shows a violet or blue $5d \rightarrow 4f$ emission with high quenching temperature [58]. The absence of photoionization is ascribed to the effective positive charge of Yb^{2+} substituted for the alkali ion.

10.5.2 Hole burning

In CaF_2 and BaF_2 all the excited states of Sm^{2+} belonging to the $4f^5 5d$ configuration lie in the conduction band [59,60]. Photoionization of Sm^{2+} allows the possibility of

making optical memories with high capacity based on “hole burning”. In the latter, information is stored not just by means of a photoinduced modification of the material at a given spatial location but a wavelength domain is used as an additional dimension by burning multiple ($\sim 10^3$) spectral holes in an absorption line. When Sm^{2+} substitutes for an alkaline earth ion, the absorption lines are inhomogeneously broadened because, due to the difference in size with the substituted ion, Sm^{2+} ions have slightly different environments. By irradiation with a laser a hole can be created at a specific wavelength in an absorption line by converting the ions absorbing at this wavelength into Sm^{3+} ions. Hole burning has been obtained at low temperature with CaF_2 , SrF_2 , SrClF , BaClF as host lattices [61,62]. In CaF_2 because of the large crystal field splitting of 5d levels the first excited states belong to the $4f^55d$ configuration while in SrF_2 , SrClF and BaClF the first excited $4f^6$ levels (3D_0 , 5D_1) lie below the $4f^55d$ states. In the latter case hole burning in the transition to 5D_0 occurs in two steps: electrons of atoms excited to 5D_0 are transferred to the conduction band by a second photon. Capacities of 10^{11} bits/cm² can be achieved. The absorption lines can be inhomogeneously broadened by incorporating Sm^{2+} in solid solutions containing different alkaline earth or halide ions [63,64]. Hole burning has been achieved at room temperature in $\text{SrBr}_{0.5}\text{Cl}_{0.5}\text{F} : \text{Sm}$ [65,66] and fluorite-type crystals obtained in the systems $\text{MF}_2\text{—AF—LnF}_3$ ($\text{M} = \text{Ca, Sr, A} = \text{Na, K, Rb, Ln} = \text{La, Y}$) [67].

10.6 Energy storage phosphors

Energy storage phosphors are materials in which an irradiation induces ionization of some ions followed by capture of the extracted electrons by vacancies, forming colour centres, or oxidizing cations. By irradiation in the absorption bands of the centres so created (photostimulation) or temperature rise, the trapped electrons can be released and the recombination energy with holes transferred to a luminescent ion.

10.6.1 Photostimulable phosphors for X-ray imaging

Much research has been carried out in recent years on photostimulable materials for digital X-ray imaging systems. Such systems offer a number of advantages compared with conventional films, in particular are a high sensitivity and a high dynamical range (10^5). Moreover the electronic transmission of digitized X-ray images is expected to become a necessity in the medical world. Photostimulated materials are also used in detectors for nondestructive testing and X-ray diffraction.

A schematical representation of the process is shown in Fig. 2. Under X-ray irradiation of a material containing a luminescent ion, electrons are transferred from the valence to conduction band and trapped at anion vacancies. The absorption bands of the formed colour centres have high oscillator strengths. The photostimulable screen is scanned by a laser beam whose wavelength is located in their absorption range. Transfer of the electron-hole recombination energy induces excitation of the luminescent ion. The amount of light emitted from each

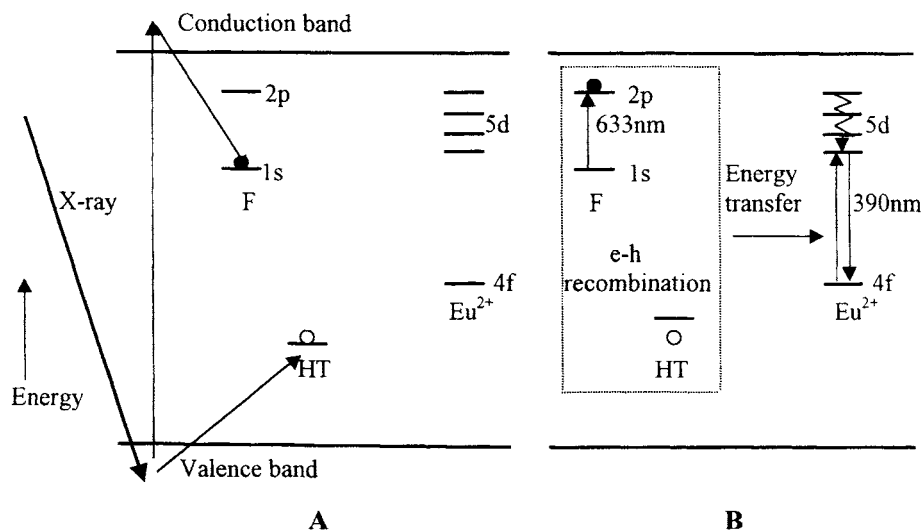


Fig. 2. Schematic representation of the mechanism of photostimulated luminescence in BaBrF : Eu. (A) Formation of a colour centre (F) under X-ray irradiation by trapping of an electron in a bromine vacancy with trapping of the hole formed in the valence band by a hole trapping centre (HT) in the vicinity; (B) Release of the trapped electron by laser irradiation and transfer of the electron-hole recombination energy to Eu²⁺. Relaxations after electron transfers have not been represented.

location of the screen is proportional to the absorbed X-ray dose [68]. A photostimulable material must fulfil several conditions, in particular:

- strong absorption of X-rays;
- a high density of stable colour centres with absorption bands extending at longer wavelengths than the emission range of the luminescent ion;
- a fast luminescence decay in order to have short scan time.

Halides can form colour centres with absorption bands in the visible range. Doped with europium whose decay time of the allowed $5d \rightarrow 4f$ transition is of the order of $1 \mu\text{s}$, they are the most appropriate materials. Because of the presence of fluorine, only BaClF:Eu and BaBrF:Eu have a high enough chemical stability for screens fabrication. The highest efficiencies of photostimulated luminescence have been obtained with the fluorobromide ($\lambda_{\text{max}} = 390 \text{ nm}$).

The mechanisms of the photostimulated luminescence of Eu²⁺-doped fluorohalides have been extensively studied. In BaBrF:Eu an excess of fluorine favours the formation of F centres in bromine sites. This results in a red shift of the absorption induced by X-rays which increases the luminescence yield for stimulation by a He—Ne laser at 633 nm [69]. Various interpretations have been proposed both about the nature of the hole-trapping centre and the electron-hole recombination mechanism [70]. It was initially assumed that holes are trapped by Eu²⁺, leading to the formation of Eu³⁺ [71]. However after long X-ray irradiation no change in the EPR signal of Eu²⁺ was observed and the luminescence of Eu³⁺

could not be detected. It has been demonstrated that the presence of oxygen enhances the formation of colour centres [70]. Oxygen substitutes mainly for fluorine with formation of a bromine vacancy in the vicinity. Below 120 K holes are trapped by bromine ions forming V_k (Br_2^-) centres. Above 120 K the V_k centres become mobile and the hole is transferred to oxygen ions, forming O_F^- centres [70]. From the time dependence of the luminescence and conductivity during photostimulation at various temperature, most authors conclude that the trapped electron recombines with a hole mainly via tunneling and not via the conduction band [72,73]. It was therefore proposed that photostimulated luminescence occurs within triple aggregates between F centres, hole centres and Eu^{2+} ions. Photostimulation of the Eu^{2+} luminescence in the near-infrared absorption bands of aggregates of F centres in BaClF and BaBrF has also been investigated [74,75]. Stimulation in this wavelength range would allow use of semiconductor lasers instead of He-Ne lasers.

Two new fluorine-rich barium fluororochlorides, $\text{Ba}_{12}\text{Cl}_5\text{F}_{19}$ and $\text{Ba}_7\text{Cl}_2\text{F}_{12}$, have been recently obtained [76,77]. While in BaF_2 the Eu^{2+} $5d \rightarrow 4f$ emission is quenched by ionization processes (Sec. 10.5.1), in these fluorochlorides Eu^{2+} shows an intense emission. Only part of chlorine can be substituted by bromine. The efficiency of the photostimulated luminescence after X-ray irradiation increases with the bromine content. The new fluorohalides have higher chemical stability and are denser than $\text{BaClF}:\text{Eu}$ and $\text{BaBrF}:\text{Eu}$.

A photostimulated luminescence emission ($\lambda_{\text{max}} = 358 \text{ nm}$) has been recently obtained with Ce^{3+} incorporated in the elpasolite Cs_2NaYF_6 [70]. The decay time, 42 ns, is identical to that obtained by direct excitation.

10.6.2 Energy storage materials based on change in the oxidation states of two cations

In the elpasolite Rb_2KInF_6 Ce^{3+} ions, located in indium sites, yield a blue-green $5d \rightarrow 4f$ emission ($\lambda_{\text{max}} = 480 \text{ nm}$). Steady UV excitation in the first $5d \rightarrow 4f$ transition (315 nm) causes a decrease of this emission while simultaneously a new emitting centre exhibiting a red emission is formed [78]. The initial state can be optically or thermally regenerated. The origin of the phenomenon is ascribed to electron transfers from Ce^{3+} to In^{3+} resulting in the formation of In^+ ions emitting in the red. The high stability of the $(\text{Ce}^{4+}, \text{In}^+)$ state is appropriate for optical storage data.

10.7 Conclusions

Because of the optical quality and chemical stability of crystals, the low probability of non radiative processes and the wide transmission range, fluorides are the most appropriate materials for solid state lasers with specific wavelengths. Thus the $4f \rightarrow 4f$ line emissions of lanthanide ions have been used in order to obtain infrared laser radiation up to $4.34 \mu\text{m}$ and blue or green radiation by up-conversion pumping. Tunable laser operation in the ultraviolet has been demonstrated using the broad $5d \rightarrow 4f$ emission of Ce^{3+} . Tunable lasers in the UV or IR ranges have also been experimented using Ag^+ , Pb^+ , $3d$ ions.

Fluoride crystals are also well suited for fast detectors for high-energy radiation. Scintillators based on the Ce^{3+} emission have been particularly investigated. The discovery of the very fast cross-luminescence of BaF_2 has led to the investigation of the luminescence of fluorides containing K, Rb, Cs and Ba under excitation by ionizing radiation.

Fluorides or fluorine-rich compounds are of particular interest for data storage. In 1985 it was shown that persistent spectral holes could be produced in the inhomogeneous band of Sm^{2+} in CaF_2 . Research on samarium-doped fluorides or fluorohalides has led in recent years to materials with broad inhomogeneous band and permanent hole burning at room temperature. In the 80s digital radiography systems based on the storage properties of BaBrF:Eu have been developed. Since then much work has been performed in order to improve the knowledge of the mechanisms and find new materials with improved performance.

References

- [1] K.H. Yang, J.A. De Luca, *Appl. Phys. Lett.*, 29 (1976) 499.
- [2] J. Becker, J.Y. Gesland, N.Y. Kirikova, J.C. Krupa, V.N. Makhov, M. Runne, M. Queffelec, T.V. Uvarova, G. Zimmerer, *J. Lumin.*, 78 (1998) 91.
- [3] C.W. van Eijk, *J. Lumin.*, 60–61 (1994) 936.
- [4] C. Fouassier, B. Latourrette, J. Portier, P. Hagenmuller, *Mat. Res. Bull.*, 11 (1976) 933.
- [5] W.A. Hargreaves, *J. Phys.: Condens. Matter.*, 4 (1992) 6141.
- [6] W.W. Piper, J.A. De Luca, F.S. Ham, *J. Lumin.*, 8 (1974) 344.
- [7] C.W. Struck, W.H. Fonger, *J. Lumin.*, 10 (1975), 1.
- [8] K.C. Bleijenberg, G. Blasse, *J. Sol. State Chem.*, 28 (1979) 303.
- [9] L.-J. Lyu, D.S. Hamilton, *J. Lumin.*, 48–49 (1991) 251.
- [10] G. Blasse, *Mater. Chem. Phys.*, 16 (1987) 201.
- [11] M.J. Weber, *Phys. Rev.*, 157 (1967) 262.
- [12] F. Auzel, D. Pecile, *J. Lumin.*, 8 (1973) 32.
- [13] A. Bril, J.L. Sommerdijk, A.W. de Jager, *J. Electrochem. Soc.*, 122 (1975) 660.
- [14] M. Pollnau, P.J. Hardman, W.A. Clarkson, D.C. Hanna, *Opt. Commun.*, 147 (1998) 203.
- [15] L.F. Johnson, H.J. Guggenheim, *Appl. Phys. Lett.*, 23 (1973) 96.
- [16] J.F. Pinto, G.H. Rosenblatt, L. Esterowitz, *Electron. Lett.*, 30 (1994) 1596.
- [17] L. Esterowiz, R.C. Eckardt, R.E. Allen, *Appl. Phys. Lett.*, 35 (1979) 236.
- [18] N.P. Barnes, R.E. Allen, *IEEE J. Quant. Electron.*, 27 (1991) 277.
- [19] R. Moncorgé, T. Benyattou, *Phys. Rev.*, 37 (1988) 9177.
- [20] P.F. Moulton, A. Mooradian, *Appl. Phys. Lett.*, 35 (1979) 838.
- [21] W. Künzel, W. Knierim, D. Dürr, *Opt. Commun.*, 36 (1981) 383.
- [22] M. Mortier, J.-Y. Gesland, M. Rousseau, F. Auzel, D. Meichenin, *C.R. Acad. Sci. II*, 322 (1996) 233.
- [23] G. Horsch, H.J. Paus, *Opt. Commun.*, 60 (1986) 69.
- [24] L. Prado, N.D. Vieira, S.L. Baldochi, S.P. Morato, J.P. Denis, N. Tercier, B. Blanzat, *J. Phys. Chem. Soc.*, 57 (1996) 413.
- [25] V.V. Ter-Mikirtychev, T. Tsuboi, *Opt. Commun.*, 137 (1997) 74.
- [26] L.F. Johnson, H.J. Guggenheim, *Appl. Phys. Lett.*, 19 (1971) 44.

- [27] F. Heine, E. Heumann, T. Danger, T. Schweizer, G. Huber, B. Chai, *Appl. Phys. Lett.*, 65 (1994) 383.
- [28] T. Hebert, R. Wannemacher, R.M. Macfarlane, W. Lenth, *Appl. Phys. Lett.*, 60 (1992) 2592.
- [29] W. Lenth, R.M. Macfarlane, *J. Lumin.*, 45 (1990) 346.
- [30] N. Sarukura, M.A. Dubinskii, Z. Liu, V.V. Semashko, A.K. Naumov, S.L. Koableva, R.Y. Abdulsabirov, K. Edamatsu, Y. Suzuki, T. Itoh, Y. Segawa, *IEEE J. Quantum Electron.*, 1 (1995) 792.
- [31] D.J. Ehrlich, P.F. Moulton, R.M. Osgood, *Opt. Lett.*, 4 (1978) 184.
- [32] M.A. Dubinskii, V.V. Semashko, A.K. Naumov, R.Y. Abdulsabirov, S.L. Korableva, *J. Mod. Phys.*, 40 (1993) 1.
- [33] P. Rambaldi, R. Moncorgé, J.P. Wolf, C. Pedrini, J.Y. Gesland, *Opt. Commun.*, 146 (1998) 163.
- [34] C. Pedrini, B. Moine, H. Bill, *J. Phys. Condens. Matter*, 4 (1992) 1615.
- [35] P. Boutinaud, H. Bill, *J. Phys. Chem. Sol.*, 57 (1996) 55.
- [36] D.J. Robbins, *J. Electrochem. Soc.*, 127 (1980) 2694.
- [37] G. Blasse, W. Schipper, J.J. Hamelink, *Inorg. Chim. Acta*, 189 (1991) 77.
- [38] G. Blasse, B.C. Grabmaier, *Luminescent Materials*, Chapter 9, Springer-Verlag, Berlin, 1994.
- [39] M. Nikl, J.A. Mares, M. Dusek, P. Lecoq, I. Dafinei, E. Auffray, G.P. Pazzi, P. Fabeni, J. Jindra, Z. Skoda, *J. Phys. : Condens. Matter*, 7 (1995) 6355.
- [40] C. Pedrini, B. Moine, D. Bouttet, A.N. Belsky, V.V. Mikhailin, A.N. Vasil'ev, *Chem. Phys. Lett.*, 206 (1993) 470.
- [41] D.R. Schaart, P. Dorenbos, C.W. van Eijk, R. Visser, C. Pedrini, B. Moine, N.M. Khaidukov, *J. Phys.: Condens. Matter*, 7 (1995) 3063.
- [42] J.P. Chaminade, P. Mesnard, A. Garcia, J. Grannec, M. Pouchard, C. Fouassier, C. Pédrini, A.N. Belsky, E.I. Zinin, *J. Cryst. Growth*, 179 (1997) 546.
- [43] B. Moine, C. Dujardin, H. Lautesse, C. Pedrini, C.M. Combes, A. Belsky, P. Martin, J.Y. Gesland, *Mater. Sci. Forum*, 239-241 (1997) 245.
- [44] C. Pedrini, D. Bouttet, C. Dujardin, B. Moine, H. Bill, *Chem. Phys. Lett.*, 220 (1994) 433.
- [45] P. Schotanus, C.W. van Eijk, R.W. Hollander, *Nucl. Instr. Methods A*, 272 (1988) 913.
- [46] N.N. Ershov, N.G. Zakharov, P.A. Rodnyi, *Opt. Spectrosc.*, 53 (1982) 51.
- [47] M. Laval, M. Moszynski, R. Allemand, E. Cormoreche, P. Guinet, R. Odru, J. Vacher, *Nucl. Instrum. Methods*, 206 (1983) 169.
- [48] E.N. Melchakov, P.A. Rodnyi, M.A. Terekhin, *Opt. Spectroc.*, 69 (1990) 634.
- [49] R. Visser, P. Dorenbos, C.W. van Eijk, A. Meijerink, G. Blasse, H.W. den Hartog, *J. Phys.: Condens. Matter*, 5 (1993) 1659.
- [50] E.G. Reut, *Opt. Spectrosc.*, 40 (1976) 55.
- [51] S. Lizzo, A.H. Velders, A. Meijerink, G.J. Dirksen, G. Blasse, *J. Lumin.*, 65 (1996) 303.
- [52] S. Lizzo, A. Meijerink, G.J. Dirksen, G. Blasse, *J. Lumin.*, 63 (1995) 223.
- [53] C. Pedrini, F. Rogemond, F. Gaume, D.S. McClure, *J. Less Com. Met.*, 112 (1985) 103.
- [54] B. Moine, C. Pedrini, B. Courtois, *J. Lumin.*, 50 (1991) 31.
- [55] R. Fuller, D.S. McClure, *J. Lumin.*, 38 (1987) 193.
- [56] C. Dujardin, B. Moine, C. Pedrini, *J. Lumin.*, 54 (1993) 259.
- [57] B. Moine, B. Courtois, C. Pedrini, *J. Phys. Fr.*, 50 (1989) 2105.
- [58] S. Lizzo, A. Meijerink, G.J. Dirksen, G. Blasse, *J. Phys. Chem. Solids*, 56 (1995) 959.
- [59] C. Pedrini, F. Rogemond, D.S. McClure, *J. Appl. Phys.*, 59 (1986) 1196.
- [60] R.L. Fuller, D.S. McClure, *J. Lumin.*, 45 (1990) 354.

- [61] R.M. Macfarlane, R.S. Meltzer, *Opt. Commun.*, 52 (1985) 320.
- [62] A. Winnacker, R.M. Shelby, R.M. Macfarlane, *Opt. Lett.*, 10 (1985) 350.
- [63] L. Zhang, J. Yu, S. Huang, *J. Lumin.*, 45 (1990) 301.
- [64] F. Kubel, H. Hagemann, H. Bill, *Mat. Res. Bull.*, 30 (1995) 405.
- [65] R. Jaaniso, H. Bill, *Europhys. Lett.*, 16 (1991) 569.
- [66] N. Umez, T. Asatsuma, Y. Takemoto, M. Kaneko, *J. Lumin.*, 64 (1995) 195.
- [67] N. Kodama, S. Hara, Y. Inoue, K. Hirao, *J. Lumin.*, 64 (1995) 181.
- [68] M.K. Crawford, L.H. Brixner, *J. Lumin.*, 48-49 (1991) 37.
- [69] W. Zao, M.Z. Su, *Mat. Res. Bull.*, 28 (1993) 123
- [70] J.M. Spaeth, Th. Hangleiter, F.K. Koschnick, Th. Pawlik, *Rad. Eff. Defects Solids*, 135 (1995) 1.
- [71] Y. Iwabuchi, C. Umemoto, K. Takahashi, S. Shionoya, *J. Lumin.*, 48-49 (1991) 481.
- [72] Y. Dong, M.Z. Su, *J. Lumin.*, 65 (1995) 263.
- [73] H. von Seggern, T. Voigt, W. Knüpfer, G. Lange, *J. Appl. Phys.*, 64 (1988) 1405.
- [74] W. Zao, Y. Mi, M.Z. Su, Z. Song, Z. Xia, *J. Electrochem. Soc.*, 143 (1996) 2346.
- [75] W. Chen, Z. Wang, L. Lin, M.Z. Su, *J. Phys. Chem. Sol.*, 59 (1998) 49.
- [76] F. Kubel, H. Hagemann, H. Bill, *Z. Anorg. Allg. Chem.*, 622 (1996) 343.
- [77] B. Es-Sakhi, P. Gravereau, C. Fouassier, *Powd. Diffract.*, 13 (1998) 152.
- [78] J.P. Chaminade, A. Garcia, T. Gaewdang, M. Pouchard, J. Grannec, B. Jacquier, *Rad. Eff. Defects Solids*, 135 (1995) 137.

CHAPTER 11

Superacidic Reaction Media

Thomas A. O'Donnell

Department of Chemical Engineering, University of Melbourne, Parkville, Victoria, 3052, Australia

11.1 Introduction

A convention adopted generally by chemists is to refer to all protonic reaction media more acidic than 100% sulfuric acid as being “superacidic”. Historically, most early chemical investigations in superacidic media involved syntheses and study of reaction mechanisms in H_2SO_4 itself or in oleums, i.e. in H_2SO_4 made more acidic by addition of SO_3 . In that early work much more effort was devoted to elucidation of the nature of organic reactions than of inorganic systems.

Those synthetic and mechanistic studies led inevitably to investigation of the complex ionisation processes in H_2SO_4 and the oleums and thence to characterisation of speciation of solutes in these media. This work has been reviewed by R.J. Gillespie [1] who led much of the pioneering work on inorganic and physico-chemical investigation of H_2SO_4 — SO_3 solvent systems and of later superacid systems.

The three fluoro-acids HF , HSO_3F and $\text{CF}_3\text{SO}_3\text{H}$ have proved to be fruitful and **essential** media for preparation of many compounds of ionic species of transition metals in unusually high or low oxidation states and of cations of non-metallic elements in fractional oxidation states.

The primary thrust of the material in this chapter will be to indicate to researchers not already familiar with the details of superacid chemistry that, for the synthesis of many inorganic fluorides and other compounds containing fluorine, a favourable reaction medium can frequently be found by careful selection of an appropriate superacid, by deliberate control of the acidity or basicity of that medium and by use of suitable redox and other reactants and precipitants.

11.1.1 Choice of superacidic media — physical and chemical properties

Concentrating initially only on the physical and chemical nature of the four superacids in common use, it can be shown that, for most synthetic purposes, the fluorine-containing superacids, fluorosulfuric acid (HSO_3F), trifluoromethylsulfuric or “triflic” acid ($\text{CF}_3\text{SO}_3\text{H}$) and hydrogen fluoride (HF) offer far more

favourable physical properties, chemically simpler reaction media and greater scope for tight control of acidity and basicity than is the case for H_2SO_4 and oleums.

Pure H_2SO_4 is an extremely viscous liquid, melting at 10.371°C and boiling with decomposition at about 300°C . It can be manipulated in glass apparatus but, for purposes of inorganic syntheses, it presents experimental problems not associated with the fluoro-acids in that it is difficult to remove from a reaction by distillation because of its high boiling point and, further, decantation and filtration of solids are made very difficult because of its viscosity.

H_2SO_4 is the least acidic of these four superacids, as indicated by measured values of the Hammett Acidity Function, H_0 , which are -11.9 for 100% H_2SO_4 , -14.3 for $\text{CF}_3\text{SO}_3\text{H}$ and -15.1 for both HSO_3F and HF . The Hammett Acidity Scale does not have the thermodynamic rigor of the pH scale used for aqueous solutions, but it appears to be the most reliable and useable of several acidity scales developed for superacidic media, providing reliable comparisons between superacids and between levels of acidity and basicity in any one superacid. Experimentally, H_0 values are determined spectrophotometrically, using a similar procedure to that which can be used for measuring pH values in aqueous solutions, by measuring the ratio of concentrations of protonated and non-protonated forms of extremely weakly basic indicators, such as nitroanilines and nitro- and halo-nitroaromatic compounds with measured pK_a values. Discussion of the basis of Hammett Function measurements is available from several sources [2,3(a),4(a)].

It should be stressed that it is not the relatively small difference between the H_0 value for pure H_2SO_4 and the values for the three fluoro-acids that limits the effectiveness of the H_2SO_4 system as a superacidic medium for syntheses that require controlled acidity or basicity of the medium. Very complex ionisation processes occur in H_2SO_4 , particularly if small amounts of SO_3 or of H_2O or other bases are present. This leads to buffering with relatively small change in acidity or basicity for relatively large additions of acid or base. Figure 1 shows minimal change in acidity and basicity of H_2SO_4 for additions of 0.5 mol% of acid or base, whereas moderate changes occur for HSO_3F and $\text{CF}_3\text{SO}_3\text{H}$ with large changes for HF . Even 5 mol% addition of acid or base changes the acidity of H_2SO_4 by only about one H_0 unit. By comparison, for HSO_3F and $\text{CF}_3\text{SO}_3\text{H}$, 0.5% addition of acid or base causes H_0 changes of about 2 units and for HF the change is about 6 units, the latter being similar to pH changes in aqueous solutions.

As is the case for pH curves showing the addition of acid or base to water, the slope of the curve for H_0 values for HF near the neutral point is so steep that minute traces of impurities can markedly change the value of H_0 for the solvent. As shown in Sec. 11.2.2, the most likely impurity, H_2O , is fully protonated in dilute solution causing a very large increase in concentration of the base, F^- , relative to the residual proton concentration. Consequently, working solutions of HF , even after distillation, have directly measured H_0 values of about -11 . Even protonation of indicators causes increase in basicity of the HF . Therefore "single value" determinations of Hammett Functions conducted only on the parent acid itself are likely to give H_0 values less negative than those for the 100% acid. Gillespie [2] developed a procedure for obtaining reliable values of H_0 for the pure superacids

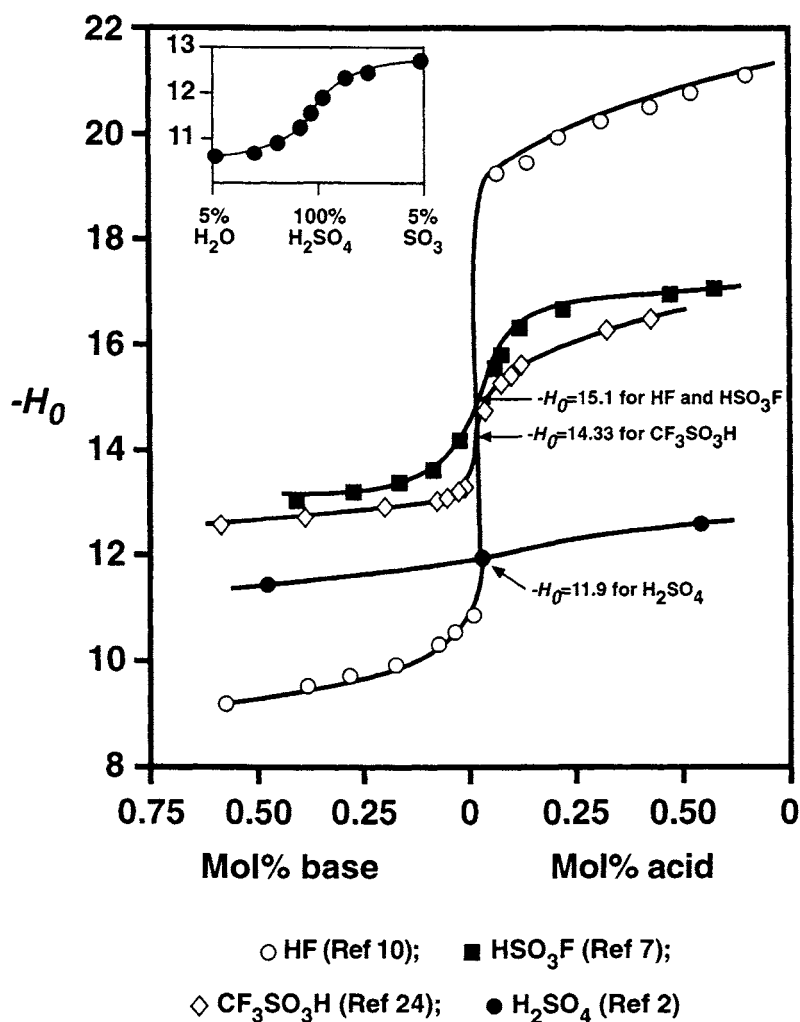
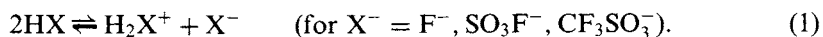


Fig. 1. Dependence of H_0 values on acidity and basicity for H_2SO_4 , CF_3SO_3H , HSO_3F and HF [5].

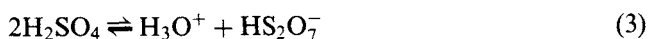
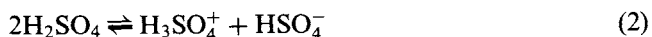
by determining H_0 values in solutions to which significant concentrations of strong acid or base had been added. This had the effect of "swamping" the effects of minor impurities. The point of inflection of the resulting sigmoidal curve (see Fig. 1) was then taken as the value of H_0 for the pure superacid.

The shapes of the H_0 plots in Fig. 1 reflect, of course, the nature and extent of ionisation processes in the four superacids themselves. The three fluoro-acids undergo simple autoprotolysis which can be represented as:



This representation is over-simplified, each of the ions being further solvated in each acid. Autoprotolysis constants have been reported as $3 \times 10^{-13} \text{ mol}^2 \text{ kg}^{-2}$ (0°C) for HF[6], 3.8×10^{-8} (25°C) for HSO_3F [7] and 7.9×10^{-7} (25°C) for $\text{CF}_3\text{SO}_3\text{H}$ [8]. Protonic media are made more acidic by addition of an entity which increases the proton concentration. Superacids are themselves so very weakly basic that very few, if any, compounds can act as Brønsted acids to donate protons to the solvent directly. Lewis acids combine with X^- to shift the autoprotolysis equilibria to increase the proton concentration. Superacids are rendered basic by direct addition of the X^- species, the base of the system, (e.g. from an alkali metal compound MX) or by addition of compounds which accept protons from the medium, increasing the concentration of the base X^- .

The simple autoprotolysis reactions for the three fluoro-acids contrast markedly with the complexity of ionisation processes in H_2SO_4 which include the self-ionisation equilibria in Eqns (2) and (3):



for which equilibrium constants at 25°C are 2.7×10^{-4} and 5.1×10^{-5} . However the two most likely impurities in supposedly pure H_2SO_4 are H_2O and SO_3 and each of these enormously enhances the extent of ion formation. Equilibrium constants of 1.4×10^{-2} and 1 are quoted for Eqns (4) and (5):



If H_2SO_4 were to be used as a superacidic medium in which tight control of acidity or basicity was necessary, the interrelated ionic equilibria, complicated still further by the formation of ionic species resulting from the addition of reactants, could lead to a buffered system which would militate against adequate acidity/basicity control. However the simple and relatively small autoprotolyses allow quite precise control of levels of acidity or basicity in the three fluoro-acids, as will be discussed in Sec. 11.2.

Values of Hammett Acidity Functions and some physical properties relevant to vacuum manipulation and physico-chemical investigation of the three fluoro-acids are given in Table 1. The three acids have viscosities comparable with that of water, allowing easy decantation and filtration and they have high dipole moments making them good solvents for ionic compounds or species which are chemically compatible with the solvent. The boiling points of HSO_3F and $\text{CF}_3\text{SO}_3\text{H}$ allow relatively easy separation of excess solvent from reaction mixtures. HF lends itself particularly well to solvent removal and manipulation in a vacuum system, having a vapour pressure

Table 1

Properties of fluoro-acids

	Hammett Function H_0	Melting Point (°C)	Boiling Point (°C)
HF	-15.1	-83.55	19.51
HSO ₃ F	-15.1	-89	162.7
CF ₃ SO ₃ H	-14.3	-	162

of about 1 atmosphere at ambient temperatures and being easily condensed by liquid nitrogen or at convenient cold bath temperatures.

The low freezing points of the fluoro-acids have been used to advantage to obtain vastly improved resolution of NMR spectra resulting from the slowing of exchange reactions at temperatures near the freezing point. It will be shown in Sec. 11.3.5 that use of reduced reaction temperatures can allow successful synthesis of compounds expected to be thermally unstable at higher reaction temperatures or even at ambient temperature.

HSO₃F, when freed from small amounts of HF usually present in the commercially-available acid, and CF₃SO₃H can be handled in glass apparatus, preferably with greaseless valves and other vacuum system components. HF cannot be handled in glass as it reacts to form gaseous SiF₄, providing potentially explosive experimental conditions. However, techniques have been developed over many years for vacuum manipulation of the pure acid and of solutions in HF as well as for the many reactive volatile fluorides used in HF solution studies. The **separate*** volatile components can be handled in stainless steel or nickel vacuum lines, constructed from commercially-available vacuum valves, connecting unions, storage bulbs etc. HF and volatile fluorides can be condensed to form solutions in reaction tubes or cells constructed from fluoropolymers, such as FEP, Kel-F and Teflon, or from synthetic sapphire. Quantitative filtration units, electrochemical (conductance, potentiometric, voltammetric) and spectroscopic (UV-vis, infra-red, Raman, NMR, ESR) cells have been fabricated from fluoropolymers with platinum and mercury electrodes and synthetic sapphire windows where appropriate.

The three fluoro-acids have one significant chemical advantage over H₂SO₄ which in the pure state is a moderately strong oxidant. Addition of SO₃ to increase the acidity of H₂SO₄ greatly enhances the oxidant strength, so that study of species in highly reduced oxidation states, which are favored in highly acidic media, is not possible. HSO₃F is in equilibrium with very small concentrations of HF and SO₃ at elevated temperatures, so that its potential oxidant strength cannot be ignored under these conditions. CF₃SO₃H can undergo cleavage of the C—S bond under strongly oxidising or reducing conditions. As with all protonic media, solvated

*See Sec. 11.3.4.1 for necessity of separate additions.

protons in HF oxidise strongly electropositive metals. Otherwise HF has virtually no oxidant strength in working solutions. HF can be reduced electrolytically to H_2 and oxidised to F_2 . The useable potential range for HF has been shown to be about 4.5 volt. This can be compared with a useable potential range of about 2 volt, depending on pH, for H_2O . HF can sustain solutes in much lower and higher oxidation states than CF_3SO_3H , HSO_3F and H_2SO_4 or, of course, H_2O .

11.1.2 Summary

Because of their extreme acidity, superacids have a great avidity for water which, as shown in Sec. 11.2.1, increases their basicity. Consequently, for reliable experimental procedures, they should not be handled in the presence of atmospheric moisture. Normal experimental practice is to handle them in vacuum systems or, less frequently, under inert atmospheres.

Unless there are particular specific reasons for using H_2SO_4 and oleums as superacidic reaction media for inorganic syntheses or other purposes, the three fluoro-acids HF, HSO_3F and CF_3SO_3H provide more reliable and controllable reaction media for inorganic solutes than does H_2SO_4 . They are much less viscous, allowing easier separation of solids and liquids, and are more volatile, allowing easier handling in vacuum systems and easier removal of solvent from reaction mixtures.

As Fig. 1 shows, CF_3SO_3H , HSO_3F and HF provide progressively more acidic media than H_2SO_4 , particularly as their acidity is increased by addition of Lewis acids. Control of acidity and basicity is far superior, as will be indicated in Secs 11.2 and 11.3. Also, it will be shown in Secs. 11.3.4 and 11.3.5 that highly reduced or oxidised species which would disproportionate in H_2O or reduce it to H_2 or oxidise it to O_2 can be generated and form stable solutions in the fluoro-acids, particularly HF.

HF has proved to be a very fruitful medium for generation, characterisation and investigation of species in solution and for synthesis of solid fluorides and fluoro-complexes. Its acidity and basicity can be adjusted and controlled quite precisely covering a range of acidity far exceeding those of the other protonic acids. Its major disadvantage is that its reactions cannot be studied in glass; but appropriate materials of construction and design of reaction cells or electrochemical and spectroscopic cells are now available to overcome this problem.

The main use of CF_3SO_3H in synthetic inorganic chemistry reported to date has been in preparation of binary compounds which are themselves triflates or of complexes derived from those triflates. HSO_3F has been used similarly in the generation of fluorosulfates and of fluorosulfato-complexes; but it has also been the medium of choice, particularly when coupled with the oxidant $S_2O_6F_2$, in the generation and characterisation of many homopolyatomic cations and transition metal carbonyl cations, as will be shown in Sec. 11.3.4.

It will be seen in the examples given in Sec. 11.3 that a much broader range of binary and complex compounds in a wide range of oxidation states has been synthesised in HF than in the other two fluoro-acids. However, it can be assumed that, with appropriate modifications and with account taken of the differences in acidity levels of the three acids, many of the strategies developed for synthesis of compounds

in HF as described in Secs 11.3.4 and 11.3.5 could be applied with equal potential to studies in $\text{CF}_3\text{SO}_3\text{H}$ and HSO_3F solutions.

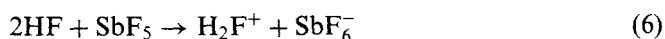
11.2 Enhancement of acidity and basicity in fluoro-acids

11.2.1 Introduction

Superacids have extremely low basicity and therefore have little or no tendency to accept protons from formal Bronsted acids. In fact virtually all compounds which act as Bronsted acids in aqueous solution are protonated to a greater or less extent in these fluoro-acids. The converse of this situation is that, because superacids are such strong proton donors, a vast range of compounds act as Bronsted bases in superacidic media. Most acids of the water system undergo protonation, e.g. carboxylic acids, H_3PO_4 and HNO_3 are protonated in HF to $\text{RC}(\text{OH})_2^+$, $\text{P}(\text{OH})_4^+$ and H_2NO_3^+ initially. $\text{P}(\text{OH})_4^+$ is then solvolysed to a series of oxofluorophosphoric acids and H_2NO_3^+ is solvolysed to NO_2^+ and H_2O followed, in turn, by protonation of H_2O to H_3O^+ . Similar behaviour has been reported for HSO_3F . Weak bases of the water system, e.g. NH_3 and amides, are fully protonated in superacids.

Protonation by superacids of solutes such as these displaces the self-ionisation of the superacids causing enhancement of concentration of the base of the superacid system, F^- , SO_3F^- or CF_3SO_3^- . This may be a disadvantageous situation when acidity/basicity control is required for synthetic purposes. If controlled increase of basicity is required, the simplest procedure is by direct addition of the conjugate base of the parent acid, i.e. by addition of F^- , SO_3F^- or CF_3SO_3^- as indicated in Sec. 11.2.3.

In the absence of effective Bronsted acids, enhancement of acidity in superacidic media is achieved by use of Lewis acids. For example in the HF system, SbF_5 acts as a Lewis acid by accepting F^- to form SbF_6^- , as represented in highly idealised form in Eqn. (6):



The self-ionisation equilibrium (Eqn. (1)) is displaced, increasing the proton concentration effectively quantitatively in the case of relatively dilute solutions of SbF_5 . Weaker Lewis acids such as AsF_5 and BF_3 , which will be described in Sec. 11.2.3.1, cause partial displacement of the equilibrium.

11.2.2 Bronsted acids and bases

As stated in the Introduction to this section, the basicity of the three fluoro-acids is so low that there is virtually no evidence for any compound exhibiting significant Bronsted acidity towards the solvents. Gut and Gautschi [9] used a hydrogen electrode to monitor potentiometric titrations of NaF against Lewis acids in HF to determine comparative Lewis acid strengths. In that work they reported that HSO_3F and $\text{CF}_3\text{SO}_3\text{H}$ acted as non-electrolytes in HF; addition of these solutes to fluoride-containing HF solutions did not change pF values. Gillespie and Liang [10]

reported H_0 values of -11 to -12 for solutions of HSO_3F in a “neat” working solution of HF . Unavoidable traces of impurities and use of indicators in Hammett Acidity Function measurements cause the working solvent to have H_0 values in this region for the reasons given in Sec. 11.1.2. So the acidity of the working solution was not changed by addition of HSO_3F . Since both HSO_3F and HF have H_0 values of -15.1 in the pure state, it is to be expected that neither will act as a Bronsted acid towards the other. $\text{CF}_3\text{SO}_3\text{H}$ with a value of -14.3 for H_0 might be expected to be an extremely weak proton acceptor from either HF or HSO_3F , but there are no experimental observations to support this.

The converse of lack of Bronsted acid activity towards the three highly acidic fluoro-acids is that there is a vast range of compounds which act as Bronsted bases — i.e. they are protonated by the superacids. As indicated in the Introduction, carboxylic and many other oxo-acids are protonated and/or solvolysed. Compounds having coordinately unsaturated O, S, N or P atoms, e.g. alcohols, aldehydes, esters, ketones, amines, amides, etc, are Bronsted bases in the superacids. H_2O is a case requiring special emphasis because it is a likely impurity in the solvent, especially for HF and $\text{CF}_3\text{SO}_3\text{H}$. Protonation of H_2O causes enhancement of the concentration of the conjugate base of the solvent, so that H_0 values for the “neat” acid can be much less than that for the pure solvent.

Compounds which are vanishingly weakly basic in H_2O , such as nitro-anilines, nitro-aromatic or halo-nitro-aromatic compounds are protonated to a greater or less extent in superacids, allowing them to be used as indicators in Hammett Acidity Function measurements. Cl^- which has essentially zero base strength in H_2O is protonated by the superacids to HCl , which being monomolecular is expelled as a gas from the highly associated solvents. This provides a commonly-used important route to synthesis of anhydrous fluorides, fluorosulfates and triflates.

11.2.3 Lewis acids and bases

The Lewis bases for each of the superacid systems are the conjugate bases of the acids themselves, namely F^- , SO_3F^- and CF_3SO_3^- . If enhanced basicity of one of the acids is required for specific speciation of a solute in a synthetic reaction, for example, it is easily achieved by direct quantitative addition of the base F^- , SO_3F^- and CF_3SO_3^- as the appropriate alkali metal cation or ammonium salts which dissociate completely in these media of high dielectric constant.

By comparison with Lewis bases in superacids, there is a greater diversity of Lewis acids and of relative strengths of the acids in the three fluoro-acids under consideration. Each of the three acids will be presented separately in the remainder of this section. HF will be considered first because higher acidities occur in HF than in HSO_3F and $\text{CF}_3\text{SO}_3\text{H}$ and easier control of acidity can be achieved.

11.2.3.1 Hydrogen fluoride

Despite the experimental difficulties to be overcome in undertaking solution studies in HF , there has been extensive investigation of several fluorides as Lewis acids of the system, with SbF_5 and AsF_5 receiving special attention.

11.2.3.1.1 Antimony Pentafluoride. Equation (6), which represents the behaviour of SbF_5 as the strongest Lewis acid of the HF system in a reaction that goes virtually to completion except in concentrated solutions, was described as being idealised because under normal working conditions each of the ions, as well as being solvated, can be more complex than as written in the equation. H_2F^+ has been shown [11] to be the dominant cationic species only in very concentrated SbF_5 solutions (greater than 40 mol%). Solvated H_3F_2^+ is the dominant cation in more dilute solutions.

Conversely, monomeric SbF_6^- is the anionic species only in dilute solutions. Cryoscopic measurements on SbF_5 -HF solutions [12] gave a value of $v=2$, indicating the presence of two moles of particles per mole of SbF_5 up to 0.4 molal, the same behaviour as for the solutes KF and Et_4NSbF_6 which are assumed to be completely dissociated in HF. In order to rationalise their own and earlier observations that the electrical conductance of SbF_5 -HF solutions reached a maximum at about 8 mol% SbF_5 and then decreased, reaching very low values at about 50 mol%, Gillespie and Moss [13] proposed that, as the concentration of SbF_5 in HF was increased, polymeric anions formed at the expense of SbF_6^- . From about 10 mol% SbF_5 , the dominant anionic species was $\text{Sb}_2\text{F}_{11}^-$, followed by $\text{Sb}_3\text{F}_{16}^-$ and, at high concentrations, $\text{Sb}_n\text{F}_{5n+1}^-$.

They supported this hypothesis by recording NMR spectra for SbF_5 -HF solutions at low temperatures, about -60°C . The ^{19}F spectrum for a 2 mol% solution gave a single peak attributable to SbF_6^- in addition to the solvent peak. However in 20 mol% solution they observed three additional peaks with relative areas 1:2:8 and each with some fine structure. This is consistent with the spectrum expected for a dimeric anion in which each of the two Sb atoms is hexacoordinated by F atoms, with one F bridging the two Sb atoms. The fine structure of the peaks was consistent with a unique bridging F atom, two terminal Fs *trans* to the bridging F and eight F atoms in equivalent positions to complete the 6-coordination of each Sb. Subsequently NMR evidence was obtained for the $\text{Sb}_3\text{F}_{16}^-$ anion and both the dimeric and trimeric anions were identified by X-ray diffraction crystallography in $\text{I}_2^+\text{Sb}_2\text{F}_{11}^-$, $\text{Br}_2^+\text{Sb}_3\text{F}_{16}^-$ and several other compounds.

SbF_5 has been shown [10] to be the strongest Lewis acid of the HF system. A relatively dilute solution (0.5 mol%) of SbF_5 increases the acidity of HF by nearly six H_0 units (see Fig. 2). When it is to be used to increase the acidity of a reaction medium, account should be taken of the potential oxidant strength of Sb(V). It is not a strong oxidant in relatively dilute solution because it is present effectively as fluoro-antimonate(V) anions. However evidence is presented in Sec. 11.3.4.2, in discussing the oxidation of Ti(II), that in more concentrated solutions there appears to be sufficient molecular SbF_5 present to warrant consideration of its possible oxidant strength. Another drawback in the use of SbF_5 in syntheses in HF is that recovery of a reaction residue by removal of solvent is made very difficult because, as the more volatile HF is removed, the fluoroantimonates polymerise to give an extremely viscous liquid.

11.2.3.1.2 Arsenic Pentafluoride. Early conductimetric investigations of dilute solutions (up to 0.1 molal) of AsF_5 in HF indicated that AsF_5 was a weaker Lewis acid

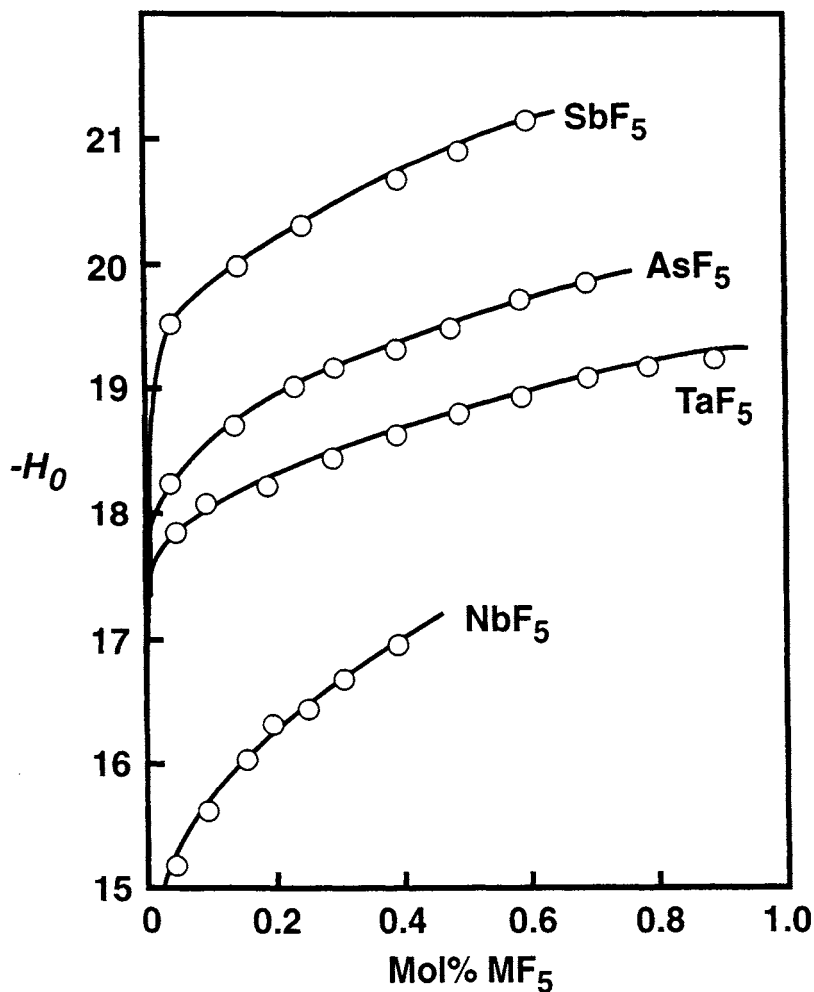


Fig. 2. H_0 values for pentafluorides in HF [5].

in HF than SbF_5 , specific conductances at 0°C being 30–40% of those for SbF_5 –HF. Cryoscopy, which had indicated $\nu = 2$ for SbF_5 , gave a value of $\nu = 1$ for AsF_5 [12] which could have been interpreted as showing that AsF_5 exists in HF as the molecular, non-ionised entity. However AsF_5 solutions at 0°C had been shown to be conducting. Conductivities for both pentafluorides measured at -83.6°C gave values for AsF_5 at almost exactly one-half of those for SbF_5 [12]. The interpretation, which was essentially correct for solutions at -83.6°C was that, whereas in dilute SbF_5 solutions, the ionic species were H_2F^+ and SbF_6^- , AsF_5 at these low temperatures existed in solution as H_2F^+ and $\text{As}_2\text{F}_{11}^-$, accounting adequately for cryoscopic and low-temperature conductivity data, two AsF_5 molecules producing two ionic particles.

In synthetic work AsF_5 -HF solutions are usually at or near ambient temperatures where, as was shown in subsequent Melbourne work [14], speciation is more complex than near the freezing point of HF. Raman spectra of a solution 0.1 molal in AsF_5 demonstrated the presence at ambient temperature of peaks for each of the species in the following equation:



In more concentrated solutions (2 to 6 molal) there was no significant Raman evidence for AsF_6^- and the peak for AsF_5 grew to be comparable with that for $\text{As}_2\text{F}_{11}^-$.

The Melbourne group [14] recorded Raman spectra for an HF solution 0.18 molal in AsF_5 at 20° , 0° and -20°C and demonstrated a temperature-dependent shift in the equilibrium in Eqn. (7). A sharp peak for AsF_5 at 20°C was not detectable at -20°C and the small AsF_6^- peak was diminished on cooling. Gillespie and colleagues [12] were correct in stating that $\text{As}_2\text{F}_{11}^-$ is the predominant species at very low temperatures (-60 to -80°C) but much free AsF_5 and some AsF_6^- are in equilibrium with $\text{As}_2\text{F}_{11}^-$ at ambient temperatures. Conductance measurements at 0°C [14] support the findings from Raman spectroscopy.

Hammett Acidity Function measurements for AsF_5 -HF solutions [10], as shown in Fig. 2, indicate that AsF_5 is a moderately strong Lewis acid of the HF system, being well over one H_0 unit weaker than SbF_5 in 0.5 mol% solution, but considerably stronger than TaF_5 .

There are several conflicting factors to be taken into consideration if AsF_5 is to be used for syntheses in HF. While AsF_5 can be useful as a moderately strong acid, note must be taken of its oxidant strength because of the presence of large concentrations of molecular AsF_5 which is a much stronger oxidant than AsF_6^- or $\text{As}_2\text{F}_{11}^-$. When present as a counter ion, AsF_6^- generally provides solutions of high concentration. Being much more volatile than SbF_5 , AsF_5 is easily volatilised from solution and residues tend to contain monomeric AsF_6^- anions rather than the polymers left by SbF_5 . Solids containing AsF_6^- anions are more easily thermally decomposed to yield residual fluorides than are fluoro-antimonates.

11.2.3.1.3 Pentafluorides of tantalum, niobium and phosphorus. Figure 2 shows that TaF_5 and NbF_5 are progressively weaker acids in HF than SbF_5 and AsF_5 . TaF_5 cannot be reduced to a lower oxidation state fluoride and so has particular value as a moderately strong acid where non-oxidising conditions are required, e.g. in HF solutions containing or designed to produce highly reducing species. Compared with SbF_5 and AsF_5 , NbF_5 and TaF_5 frequently give compounds of low solubility containing $\text{Nb}_2\text{F}_{11}^-$ and $\text{Ta}_2\text{F}_{11}^-$ as anionic species.

The available physico-chemical evidence suggests that PF_5 is a vanishingly weak Lewis acid in HF. It was shown in Sec. 11.1.2 that the value of -15.1 for H_0 for pure HF was obtained by interpolation between measured values of H_0 for HF solutions of strong Lewis acids and for HF containing strong base. "Neat" HF, the working solvent after distillation, usually gives experimentally measured H_0 values of about -11 , because of the presence of very small traces of water

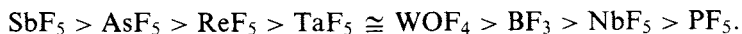
and other impurities. Gillespie and Liang [10] obtained H_0 values from -11.34 to -12.02 for HF containing PF_5 from 0.02 to 0.5 mol%. Even for the weak acid NbF_5 their values ranged from about -15 to about -17 over the same concentration range, while the very strong acid SbF_5 gave values from about -19.5 to -21 . Whereas SbF_5 and even NbF_5 "swamp" the basicity resulting from the protonation of impurities, PF_5 appears to be such a weak acid that it does not completely remove the very small amounts of F^- resulting from protonation of impurities in the solvent.

The relatively small role for PF_5 in synthetic procedures would appear to be its ability to reduce the basicity of an HF solution to being nearly neutral.

11.2.3.1.4 Boron trifluoride. Hammett Acidity Function measurements which are based on spectrophotometry have not been carried out on BF_3 -HF solutions. So direct quantitative comparisons of the Lewis acidity of BF_3 with those of the pentafluorides presented above cannot be made. However there are two sources of potentiometric evidence that BF_3 is a weak Lewis acid of the HF system. Gut and Gautschi [9] used a hydrogen electrode to monitor potentiometric titrations of F^- against Lewis acids and calculated pF values of HF solutions containing the buffers TaF_5/TaF_6^- , BF_3/BF_4^- , NbF_5/NbF_6^- and PF_5/PF_6^- . Devynck, Trémillon and co-workers [15] used the tetrachloroquinone electrode — a redox system in which the position of redox equilibrium is dependent on the proton concentration of the medium — to measure the acidity of similar buffer systems based on BF_3 and the pentafluorides and showed, as did Gut and Gautschi, that BF_3 is intermediate in strength between TaF_5 and NbF_5 and considerably stronger than PF_5 .

BF_3 has an advantage over several of the stronger Lewis acids for synthetic work in that it is non-oxidising. However, like PF_5 , its solubility in HF is low. It can be used to hold an HF solution somewhat on the acid side of neutrality, whereas PF_5 should, in principle, provide a solution slightly on the basic side. In general tetrafluoroborates are quite soluble in HF. If, after removal of solvent, products are isolated as tetrafluoroborates they are very easily thermally decomposed to the corresponding fluorides.

11.2.3.1.5 Summary. There is now ample physico-chemical evidence for the ordering of the relative strengths of the fluorides presented in Secs 11.2.3.1.1 to 11.2.3.1.4 as Lewis acids in HF. There has been much less quantitative investigation of other pentafluorides and oxidefluorides, such as ReF_5 and WOF_4 , but the information that is available [4(b)] indicates an order:



However there would usually be no need to use fluorides other than the ones discussed in detail in this section to fix the acidity or basicity of HF to establish a controlled medium for synthetic purposes. NaF can be used to adjust the basicity of HF from H_0 values of about -10 (0.1 molal NaF) to about -12 (0.001 molal). On the acidic side of neutrality NbF_5 , TaF_5 and SbF_5 cover H_0 values from about -15 to beyond -22 . There could be advantages in using BF_3 or even the weaker

acids PF_5 , SiF_4 or GeF_4 to adjust reaction medium acidities to values close to those for neutral HF.

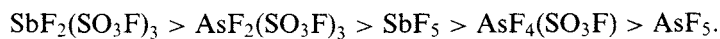
11.2.3.2 Fluorosulfuric acid

As with the other superacids, the basicity of HSO_3F is most easily adjusted quantitatively by direct addition of the conjugate base SO_3F^- in the form of the alkali metal cation or ammonium salts. Less directly, the basicity is increased by proton acceptors, e.g. H_2O and a vast range of Bronsted bases. Such an increase in basicity is frequently an unwanted result of protonation of solutes or of reaction products but must be taken into account in considering the final level of acidity in any reaction mixture.

This is no reliable evidence of any solute acting as a Bronsted acid in HSO_3F . So enhancement of acidity has always been achieved by addition of Lewis acids. The first potential acids investigated in HSO_3F were binary fluorides. As discussed immediately below in Sec. 11.3.2.1, addition of SO_3 to fluorides dissolved in HSO_3F was subsequently found to enhance acidity due to insertion of SO_3 into the metal-fluorine bond. More recently, Lewis acids of the **HSO_3F system**, i.e. binary fluorosulfates, have been studied.

11.2.3.2.1 Fluorides and derived fluorosulfates. Gillespie and co-workers at McMaster University used conductance measurements in the first survey of the relative strengths of binary fluorides as Lewis Acids in HSO_3F [16] where it was shown that SbF_5 was the most acidic binary fluoride with BiF_5 , AsF_5 , TiF_4 , NbF_5 and PF_5 much weaker and in that order. Addition of SO_3 to the more strongly acidic systems $\text{AsF}_5\text{--HSO}_3\text{F}$ and $\text{SbF}_5\text{--HSO}_3\text{F}$ increased the conductivities markedly, trebling for $\text{SO}_3\text{:AsF}_5$ in the ratio 1:1 and increasing more than seven-fold for $\text{SO}_3\text{:AsF}_5$, 3:1. Addition of a three-fold excess of SO_3 to SbF_5 in HSO_3F caused greatly enhanced conductivity relative to $\text{SbF}_5\text{--HSO}_3\text{F}$ for similar concentrations of SbF_5 ; but $\text{SO}_3\text{:AsF}_5$ ratios greater than 3:1 had little effect on conductances.

It was assumed, and later demonstrated experimentally, that in the cases of 1:1 and 3:1 additions of SO_3 to pentafluorides, the active Lewis acids were $\text{AsF}_4(\text{SO}_3\text{F})$, $\text{AsF}_2(\text{SO}_3\text{F})_3$ and $\text{SbF}_2(\text{SO}_3\text{F})_3$ in equilibrium with $[\text{AsF}_4(\text{SO}_3\text{F})_2]^-$, $[\text{AsF}_2(\text{SO}_3\text{F})_4]^-$ and $[\text{SbF}_2(\text{SO}_3\text{F})_4]^-$ in solution, with consequent displacement of the self-ionisation of HSO_3F to increase the proton concentration to a greater or less degree. The observed order of Lewis acid strengths based on conductance measurements was:



The McMaster group sought to maximise HSO_3F acidity through the pentafluorosulfates of As and Sb; but attempts to prepare them were fruitless. They reported that these compounds “do not appear to be stable”.

They then embarked on Hammett Acidity Function measurements [7] of several of the solutes previously studied by conductance measurements. Their results are summarised in Fig. 3. SO_3 is a very weak acid, increasing the acidity of HSO_3F by less than 0.5 units beyond the H_0 value of -15.07 for the “pure” acid. As in

HF, NbF_5 is a weak acid with AsF_5 and TaF_5 of medium strength, increasing the acidity by one to two H_0 units. As expected, SbF_5 is the strongest acid of the binary fluorides. $\text{SbF}_2(\text{SO}_3\text{F})_3$ is stronger again by about one H_0 unit over a reasonable concentration range, providing media with H_0 values more negative than -19 in moderately concentrated solutions, namely at about 5 mol%.

11.2.3.2.2 Binary Fluorosulfates. As reported in the section above, the McMaster group, seeking increasingly strong Lewis acids in HSO_3F , attempted unsuccessfully to prepare pentafluorosulfates of As and Sb. Recently, Aubke and colleagues [17] at the University of British Columbia crystallised $\text{Cs}[\text{Sb}(\text{SO}_3\text{F})_6]$ from HSO_3F after oxidising Sb with the strong oxidant, $\text{S}_2\text{O}_6\text{F}_2$, in the presence of CsSO_3F and the quest for $\text{Sb}(\text{SO}_3\text{F})_5$ has been renewed. Earlier, Lee and Aubke had synthesised several noble metal fluorosulfates by reaction of bis(fluorosulfonyl)peroxide, $\text{S}_2\text{O}_6\text{F}_2$, with the appropriate metal in HSO_3F . In the reaction, $\text{S}_2\text{O}_6\text{F}_2$ is reduced to SO_3F^- , the conjugate base of the solvent system. Lee and Aubke prepared $\text{Au}(\text{SO}_3\text{F})_3$ [18] and $\text{Pt}(\text{SO}_3\text{F})_4$ [19] and showed by conductimetric titration against SO_3F^- that they accepted the base SO_3F^- to form $[\text{Au}(\text{SO}_3\text{F})_4]^-$ and $[\text{Pt}(\text{SO}_3\text{F})_6]^{2-}$ [19]. Conductance studies showed that the consequent increase in acidity of HSO_3F

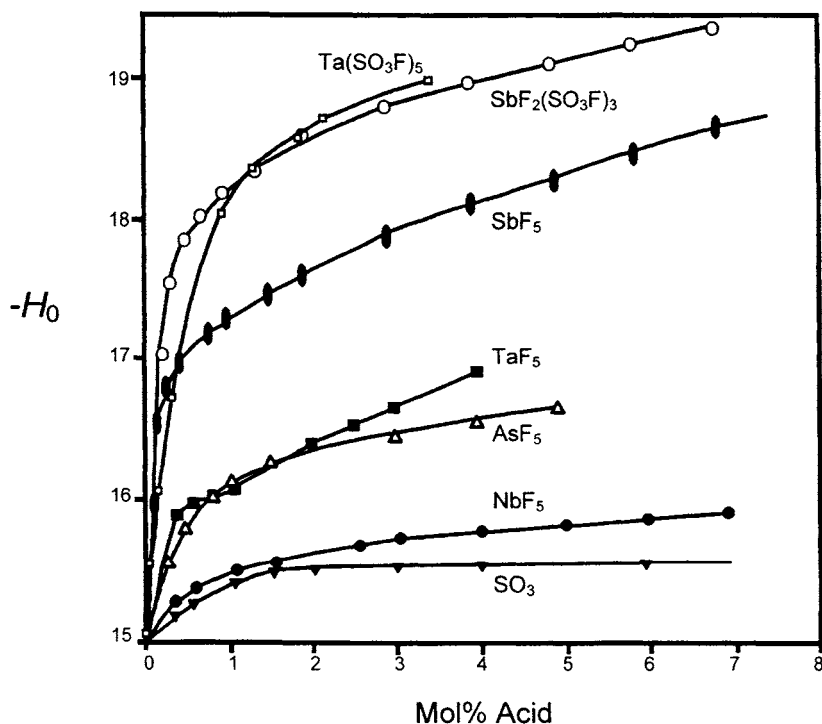
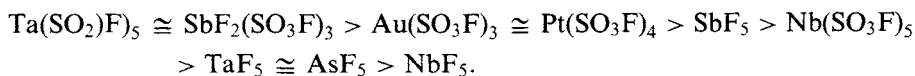


Fig. 3. H_0 values for Lewis acids in HSO_3F [5].

was very similar for both $\text{Au}(\text{SO}_3\text{F})_3$ and $\text{Pt}(\text{SO}_3\text{F})_4$, considerably greater than for SbF_5 and a little less than for $\text{SbF}_2(\text{SO}_3\text{F})_3$. They also prepared binary and ternary fluorosulfates of Pd and Ir; but, for reasons of solubility and thermal stability in HSO_3F solution, these were not studied as Lewis acids.

Cicha and Aubke [20] prepared $\text{Nb}(\text{SO}_3\text{F})_5$ and $\text{Ta}(\text{SO}_3\text{F})_5$ *in situ* in HSO_3F by oxidation of the metals with $\text{S}_2\text{O}_6\text{F}_2$ and showed by conductance measurements that $\text{Nb}(\text{SO}_3\text{F})_5$, while stronger than NbF_5 , is a weaker acid than SbF_5 . Subsequently they measured Hammett Functions for $\text{Ta}(\text{SO}_3\text{F})_5$ in HSO_3F [21] and showed that, for concentrations up to about 0.4 mol%, $\text{Ta}(\text{SO}_3\text{F})_5$ is a weaker acid than $\text{SbF}_2(\text{SO}_3\text{F})_3$ or SbF_5 . At 0.5 mol%, $\text{Ta}(\text{SO}_3\text{F})_5$ is stronger than SbF_5 but weaker by about 0.5 H_0 unit than $\text{SbF}_2(\text{SO}_3\text{F})_3$, while at concentrations a little beyond 1 mol%, $\text{Ta}(\text{SO}_3\text{F})_5$ appears to be marginally more acidic than $\text{SbF}_2(\text{SO}_3\text{F})_3$. Its H_0 value is more negative than that for $\text{SbF}_2(\text{SO}_3\text{F})_3$ by about 0.05 of a unit, as indicated in Fig. 3.

11.2.3.2.3 Summary. Combination of conductance and Hammett Acidity Function measurements suggests an order of Lewis acid strength in HSO_3F as:



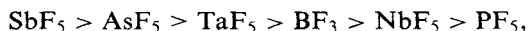
If required, the level of basicity of HSO_3F can be controlled easily by addition of alkali metal cation or ammonium fluorosulfates. For adjustment of levels of acidity, the readily available fluoro-acids $\text{SbF}_2(\text{SO}_3\text{F})_3$, TaF_5 and NbF_5 appear to provide adequate control over the H_0 range -15.07 to -19 or so. The inconvenience of preparing the binary fluorosulfates, $\text{Au}(\text{SO}_3\text{F})_3$, $\text{Ta}(\text{SO}_3\text{F})_5$ etc, could be outweighed if compounds for synthesis might be expected to be complexed or precipitated by free F^- arising from the more readily available acids or if oxidising conditions needed to be avoided. The noble metal fluorosulfates have proved to be effective acidic precursors to preparation of transition metal carbonyl cations, as presented in Sec. 11.3.4.3.

11.2.3.3 Trifluoromethylsulfuric ("triflic") acid

Only four compounds have been studied as Lewis acids in triflic acid, namely boron triflate, $\text{B}(\text{OSO}_2\text{CF}_3)_3$, and the pentafluorides of Sb, Ta and Nb. Engelbrecht and Tschager [22] generated $\text{B}(\text{OSO}_2\text{CF}_3)_3$ *in situ* in triflic acid and published H_0 values over a range of concentrations. Liang [23] compared spectrophotometric and NMR chemical shift methods for determining H_0 values for SbF_5 in $\text{CF}_3\text{SO}_3\text{H}$. Recently, Adrien [24] measured H_0 values spectrophotometrically for $\text{B}(\text{OSO}_2\text{CF}_3)_3$, the strongest known acid of the $\text{CF}_3\text{SO}_3\text{H}$ system, and for SbF_5 , TaF_5 and NbF_5 which, as shown in Fig. 4, show the same order of acid strength as in other superacids. As in HSO_3F , the pentafluorides MF_5 accept the base to form species such as $[\text{F}_5\text{MOSO}_2\text{CF}_3]^-$ to increase the solvated proton concentration in the acid.

11.2.4 Summary

The order of acidity of the binary fluorides most commonly used as Lewis acids is the same in the three fluoro-acids which have been studied in detail:



with $\text{SbF}_2(\text{SO}_3\text{F})_3$ and $\text{Ta}(\text{SO}_3\text{F})_5$ much stronger than SbF_5 in HSO_3F and $\text{B}(\text{OSO}_2\text{CF}_3)_3$ stronger than SbF_5 in $\text{CF}_3\text{SO}_3\text{H}$. Many other acids have been studied, e.g. ReF_5 and WOF_4 in HF and $\text{Au}(\text{SO}_3\text{F})_3$, $\text{Pt}(\text{SO}_3\text{F})_4$ and $\text{Nb}(\text{SO}_3\text{F})_5$ in HSO_3F ; but adequate control of acidity and basicity appears feasible for most synthetic purposes using the common Lewis acids or the conjugate base of each solvent system. However, particular circumstances could call for use of other acids. For example, if minimal oxidising conditions were to be necessary, TaF_5 which cannot be reduced in HF would be preferable to AsF_5 or, in HSO_3F , $\text{Ta}(\text{SO}_3\text{F})_5$ would be superior to $\text{SbF}_2(\text{SO}_3\text{F})_3$ or SbF_5 and TaF_5 to AsF_5 .

To provide a suitable reaction medium for syntheses, acidity and basicity can be adjusted over a much wider range in HF than is possible for HSO_3F and $\text{CF}_3\text{SO}_3\text{H}$. H_0 values for 0.4 mol% solutions for the bases F^- , SO_3F^- and CF_3SO_3^- in the appropriate acids are -9.63 , -13.24 and -12.80 respectively. Solutions of 0.4 mol% of SbF_5 , $\text{SbF}_2(\text{SO}_3\text{F})_3$ and $\text{B}(\text{OSO}_2\text{CF}_3)_3$ in HF , HSO_3F and $\text{CF}_3\text{SO}_3\text{H}$ respectively have H_0 values of -20.64 , -17.71 and -16.51 . That is, the ranges of H_0 units for solutions containing from 0.4 mol% of base to 0.4 mol% of acid are 11.01, 4.47 and 3.71 for HF , HSO_3F and $\text{CF}_3\text{SO}_3\text{H}$ respectively.

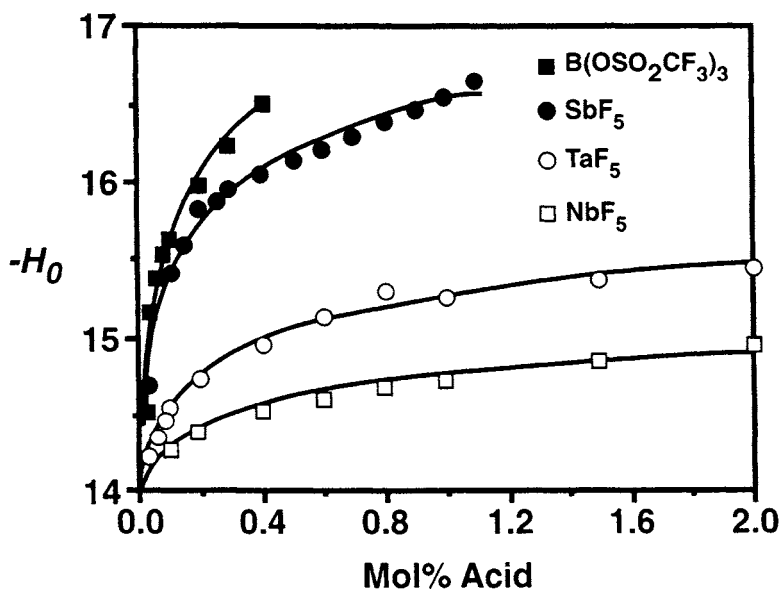


Fig. 4. H_0 values for Lewis acids in $\text{CF}_3\text{SO}_3\text{H}$ [5].

By far, HF provides the most acidic media. Even in very dilute solution (0.05 mol%), $\text{SbF}_5\text{-HF}$ has a value for H_0 of -19.53 , "greater" than values of -18.94 and -19.35 for 10 mol% $\text{SbF}_5\text{-HSO}_3\text{F}$ and 7 mol% $\text{SbF}_2(\text{SO}_3\text{F})_3\text{-HSO}_3\text{F}$. H_0 values, based on kinetic studies, of about -25 to -30 have been reported for concentrated solutions (10–50%) of SbF_5 in $\text{HF}[3(b)]$. These concentrated $\text{SbF}_5\text{-HF}$ solutions have been used in the study of mechanisms of organic reactions; but being moderately strong oxidants and providing very viscous media, their use appears to be very limited in inorganic syntheses.

Wide acid-base control can be achieved using dilute solutions of Lewis acids and bases in HF. It will be shown in Sec. 11.3.4.4 that Besida and O'Donnell used dilute solutions (<0.5 molal) of NaF , NbF_5 , TaF_5 and SbF_5 to progressively control the levels of basicity and acidity between the H_0 limits of -9.95 and -20.65 in monitoring the dependence on acidity levels of the stability and disproportionation of polyatomic cations of iodine. Similar control over narrower ranges could be achieved in HSO_3F and $\text{CF}_3\text{SO}_3\text{H}$ using readily-available Lewis acids.

11.3 Species dissolved in or derived from superacids

11.3.1 Introduction

This section will provide brief accounts of some representative synthetic procedures for preparation of solutes in superacidic media and of compounds which are derived from superacids and which owe their peculiar properties to their formation and stability under extremely weakly or strongly basic conditions. A large proportion of the examples will, of necessity, be drawn from studies using HF^* as solvent or reactant. This is because, in the case of HF, somewhat more inorganic chemistry has been published, to date, on acid-base properties of the solvent itself, on the nature of solutes, on unusual solutions produced in the solvent or on compounds derived from the solvent than is the case for HSO_3F , with even less available for $\text{CF}_3\text{SO}_3\text{H}$.

The major disadvantage in studying HF solutions is that special materials of construction must be used in the development and use of research components. This is offset somewhat by the fact that HF and reactants such as many of the Lewis acids have favourable physical properties for vacuum manipulation. Of more fundamental importance is the fact that HF has a much larger acid-base range than HSO_3F and $\text{CF}_3\text{SO}_3\text{H}$ and also has a larger useable potential range. As a result, generation of highly reduced species, which are stable in very acidic media, or of highly oxidised species, which require very basic conditions for stability, has proved to be more widely achievable in HF than in the other two superacids. However, the general synthetic approaches developed to date for HF chemistry have been shown to be applicable to the HSO_3F and $\text{CF}_3\text{SO}_3\text{H}$ systems with due regard being taken

*A convention adopted in most of the literature cited here is to refer to anhydrous HF as aHF (or AHF), as distinct from hydrofluoric acid which is an aqueous solution of HF. Since aqueous HF will not be referred to in this section, the symbol HF will be used on all occasions to describe anhydrous HF.

for smaller acid-base ranges and for somewhat greater oxidant strengths of the solvents themselves.

A very wide range of cationic species, many in unusually low oxidation states, can be generated in superacids. However there is a dearth of anionic speciation, with most of it related to the solvents themselves.

11.3.2 Anionic species in superacids

As was indicated in Sec. 11.2.2, most of the familiar anions of aqueous chemistry, e.g. the oxo-anions and halide ions are protonated and/or solvolyzed in superacidic media – even the conjugate Brønsted acids of the oxo-anions are protonated. The anions which have been shown to have separate existence in the three superacids are the three conjugate bases F^- , SO_3F^- and $CF_3SO_3^-$ and the complex anions resulting from the interaction of these bases with Lewis acids of each system, as exemplified in Eqn. (6). Some representative examples of these complex anions are SbF_6^- , $Sb_2F_{11}^-$, AsF_6^- and BF_4^- for the HF system, $[F_5Sb(OSO_2F)]^-$, $[F_2Sb(OSO_2F)_4]^-$, $[Au(SO_3F)_4]^-$ and $[Ta(SO_3F)_6]^-$ in HSO_3F and $[F_5Sb(OSO_2CF_3)]^-$ and $[B(OSO_2CF_3)_4]^-$ in CF_3SO_3H .

These complex anions are very weakly basic, i.e. of very low nucleophilicity, and have been used deliberately as counter-ions in the isolation of solid compounds where the cation is highly electrophilic and subject to disproportionation or other reaction with species of reasonable base strength. Relative basicities of anions can be of great importance in isolating such compounds. An example which will be discussed in detail in Sec. 11.3.4.6 involved attempts to synthesise solid compounds of I_2^+ and Br_2^+ . These were unsuccessful when the counter-ion was fluorosulfate, because of disproportionation of the halogen cations, whereas the cations were stable in the presence of less basic fluoro-antimonates.

An extremely important class of fluoro-anions will be presented in Sec. 11.3.5 where it will be shown that it is possible to generate fluoro-anions of transition metals in unusually high oxidation states, e.g. $Mn^{IV}F_6^{2-}$, $Ag^{III}F_4^-$ and $Ni^{IV}F_6^{2-}$ and to isolate the corresponding binary fluorides from HF solutions of these anions.

11.3.3 Solubility of binary solids in superacids

11.3.3.1 Ionic solids

The alkali metal cation and ammonium fluorides all have high solubilities at ambient temperatures in HF (5–10 molal, except for LiF which is about 4 molal). As expected on lattice energy grounds, the alkaline earth fluorides are much less soluble, particularly MgF_2 and CaF_2 . Solubilities of the alkali metal cation and ammonium fluorosulfates in HSO_3F are of the same magnitude as for the fluorides in HF and the corresponding triflates have high solubilities in CF_3SO_3H . These high solubilities allow easy basicity control in the three superacids.

11.3.3.2 Molecular solids

The volatile molecular hexafluorides MoF_6 , WF_6 , UF_6 , OsF_6 , and ReF_6 , as well as ReF_7 , all have reasonable solubilities (0.5–3 molal), without ionisation, in HF at

ambient temperature. Surprisingly, when compared with NbF_5 and TaF_5 , VF_5 , although very soluble (3.3 molal), gives a non-conducting solution. XeF_2 and XeF_4 exhibit little, if any, ionisation in HF ; but XeF_6 , which is an aggregate of fluoride-bridged XeF_5^+ units in the solid state, gives a highly conducting 8.6 molal solution. The transition metal pentafluorides are all tetramers or infinite chains with $\text{M}-\text{F}-\text{M}$ bridging and, to greater or less extent, as already indicated in Sec. 11.2.3.1, behave like SbF_5 in interacting with the conjugate base to form MF_6^- or polymeric anions $\text{M}_n\text{F}_{5n+1}^-$. Other molecular fluorides such as the gases AsF_5 , BF_3 , SiF_4 , GeF_4 , PF_5 and AsF_3 are also potential fluoride-acceptors, ranging from being moderately strong to vanishingly weak.

In an extensive and critical review of the synthesis and properties of transition metal fluorosulfates and triflates, Aubke, Cader and Mistry [25] state that the only known molecular structure amongst the fluorosulfates is the dimeric $\text{Au}(\text{SO}_3\text{F})_3$, the rest being associated solids.

In studies of $\text{B}(\text{OSO}_2\text{CF}_3)_3$ as a Lewis acid in triflic acid [22,24] the compound was prepared *in situ* by reaction of BCl_3 with the acid. By reacting the appropriate chlorides or bromides with $\text{CF}_3\text{SO}_3\text{H}$ in SO_2ClF or Freon-113 at -78°C , Olah and colleagues [26] have synthesised $\text{B}(\text{OSO}_2\text{CF}_3)_3$ as a relatively volatile monomeric molecular compound and have produced the formal counterparts $\text{Al}(\text{OSO}_2\text{CF}_3)_3$ and $\text{Ga}(\text{OSO}_2\text{CF}_3)_3$ as relatively high melting, associated solids.

11.3.3.3 Polymeric solids

In discussing the states of aggregation of solid fluorides as solutes, there is some overlap between the structures of the transition metal pentafluorides, discussed above, and those of corresponding tetra-, tri- and difluorides of *d*- and *f*-transition metals. The intermediate and lower fluorides of the transition metals are fluorine-bridged polymeric lattices, whereas the alkali metal and alkaline earth fluorides are essentially ionic and the non-metal fluorides are molecular.

Aubke, Cader and Mistry [25] report that fluorosulfates have been prepared for virtually all of the transition metals and they outline generalised approaches to synthesis of them. One of the neatest and most effective routes that they have used is direct oxidation by $\text{S}_2\text{O}_6\text{F}_2$ of the metal in HSO_3F to the fluorosulfate. They comment that the ability of the fluorosulfate group to act as a mono-, bi-, or tridentate ligand leads to the formation of polymeric solids. They also list synthetic methods that have been used for preparation of the smaller number of transition metal trifluoromethylsulfates which, again, are associated solids.

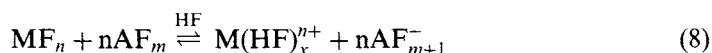
As a generality, electrostatically neutral polymeric solutes exhibit minimum solubility in the near-neutral superacid solvents unless they have significant Lewis acid strength. However, their solubility is markedly increased — frequently by orders of magnitude — by increasing the acidity of the medium, leading to formation of cationic species derived from the solute (see Sec. 11.3.4.1). When the neutral polymeric solutes are sufficiently amphoteric, increase in basicity of the solvent gives anionic species resulting from interaction of the neutral solid with the base of the solvent (see Sec. 11.3.5).

11.3.4 Cationic species in superacidic solutions

In aqueous solutions transition metals are characterised by their ability to provide aquo-cations in varying oxidation states and, as a convention, we can regard those oxidation states that are stable in water as being “normal”. Further, many of the metals can be stabilised in the solid state or in non-aqueous media in oxidation states in which they would reduce or oxidise water and we can, again as a convention, regard these oxidation states as being “unusual”.

11.3.4.1 Transition metal cations in “normal” oxidation states

Until the late 1970s, there had been little study of transition metal cations in HF because of the very low solubility of the di-, tri- and tetrafluorides of the *d*- and *f*-elements in HF. Use of counter-anions other than fluoride was precluded because the anions were protonated or solvolysed leading to formation of insoluble metal fluorides. The problem was overcome by treating the insoluble fluoride (MF_n) in HF with an appropriate Lewis acid (AF_m):



Reduction of $[\text{F}^-]$ in equilibrium with sparingly soluble MF_n led to dissolution. UV-vis spectra of many of the cations of the First Row *d*-transition metals, of virtually all the lanthanides and of some actinides were recorded.

BF_3 acidified HF sufficiently to dissolve the difluorides of the *d*-transition metals and the trifluorides of the lanthanides, while trifluorides of *d*-transition metals and tetrafluorides required SbF_5 -HF or AsF_5 -HF for dissolution. Many of the metals dissolved readily in acidified HF. Evolution of H_2 from BF_3 -HF solutions indicated oxidation of the metals by H_2F^+ . SbF_5 -HF solutions usually oxidised metals without H_2 evolution, Sb(V) being reduced to Sb(III), a factor which can adversely affect recovery of fluorides or fluorocomplexes from these solutions because of the relatively low volatility of Sb(III) fluorocompounds.

Examples of published spectra were for Ni^{2+} and Co^{2+} [27], Mn^{2+} and Cr^{3+} [28] and Pr^{3+} and Nd^{3+} [27]. In all cases comparison of HF solution spectra with those in acidic aqueous solutions indicated that the extent of solvation by HF was identical for each cation with that by H_2O . Spectra of cationic species in HF, usually $[\text{M}(\text{HF})_6]^{n+}$, are simpler than those in water where many species such as Cl^- can enter the coordination sphere to form, in the simplest case, $[\text{M}(\text{H}_2\text{O})_5\text{Cl}]^{(n-1)+}$. The only anions other than F^- in HF are the conjugate anions of the Lewis acids, e.g. BF_4^- , SbF_6^- , etc, which coordinate extremely weakly and have not been observed spectroscopically in the coordination sphere of metal cations in HF solutions.

Metallic Pu and Am, PuCl_3 and AmO_2 were dissolved in SbF_5 -HF and in SbF_5 - HSO_3F and UV-vis spectra recorded in each solution [29]. Comparison with the known aqueous spectra for Pu(III) and Am(III) indicated the presence in both superacid media of $\text{Pu}_{(\text{solv})}^{3+}$ and $\text{Am}_{(\text{solv})}^{3+}$. Am(IV) in AmO_2 was reduced to Am(III) in the superacids.

The small amount of inorganic solution chemistry that has been done in $\text{CF}_3\text{SO}_3\text{H}$ is enough to indicate that transition metals provide solvated cations in $\text{CF}_3\text{SO}_3\text{H}$ acidified with appropriate Lewis acids. Adrien [24] dissolved metallic Co and Ni in both $\text{SbF}_5\text{--CF}_3\text{SO}_3\text{H}$ and $\text{B(OSO}_2\text{CF}_3)_3\text{--CF}_3\text{SO}_3\text{H}$ and obtained spectra very similar to those for cations in acidified H_2O , HF and HSO_3F .

The dissolution of fluorides and of metals by superacids with enhanced acidity has implications for the manipulation of such acid mixtures in metal apparatus, e.g. in the metal manifold of a vacuum system. Ni and Ni-based alloys can be used to handle **separately** HF vapour and many individual volatile fluorides because of formation of a cohering surface layer of metal fluoride which passivates the metal against further attack. For example anhydrous HF vapor and AsF_5 individually can be handled in a metal vacuum system. If, however, a mixture of HF and AsF_5 were to be introduced into a metal vacuum system, even as the mixed vapors, the passivating film of metal fluoride would be dissolved as in Eqn. (8) and the underlying metal would be attacked. In Sec. 11.1.2 it was stated in a very brief account of procedures for experimental manipulation of HF and related fluorides that volatile fluorides **must be handled separately**. HF and AsF_5 together have been observed to cause gross contamination of reaction mixtures with fluorides of the metals of construction in very short time periods.

11.3.4.2 Transition metal cations in low oxidation states

Superacids with enhanced acidity have proved to be fruitful media for generation and stabilisation of a wide range of cations of elements in unusually low and fractional oxidation states. These highly electrophilic species require for stability media of high proton acidity which is further increased by Lewis acids, having high electron pair acceptor strength, to provide conjugate bases of low nucleophilicity or electron pair donor ability.

The first transition metal cation which is unstable in water but which can be generated as a stable entity in HF was U^{3+} [30]. It was formed by oxidation of the metal by protons in a $\text{BF}_3\text{--HF}$ solution which is non-oxidising and relatively weakly acidic. The UV-vis spectrum of the lilac-colored solution was virtually identical with that observed for an acidified aqueous solution in which the uranium solution was under continuous electrolytic reduction to maintain U(III) as the aquo-cation.

Subsequent reactions between metallic Cr and V in $\text{BF}_3\text{--HF}$ yielded solutions containing Cr(HF)_6^{2+} and V(HF)_6^{2+} [31] characterised by comparison of spectra with those of acidic aqueous solutions of $\text{Cr(H}_2\text{O)}_6^{2+}$ and $\text{V(H}_2\text{O)}_6^{2+}$. Metallic Ti was found to be unreactive towards $\text{BF}_3\text{--HF}$ but yielded green-blue solutions in the more acidic $\text{AsF}_5\text{--HF}$. These solutions had complex spectra, suggesting the presence of Ti(III) . The strongly acidic medium 3M $\text{SbF}_5\text{--HF}$ provided a stable orange solution [31] having the UV-vis spectrum shown in Fig. 5(a) and believed to contain Ti(II) . Since Ti(II) cannot exist in H_2O , no $\text{Ti(H}_2\text{O)}_6^{2+}$ spectrum was available for comparison. The spectrum in Fig. 5(b) is that for TiCl_2 formed *in situ* in molten AlCl_3 [32]. It has been proposed [4(c)] that this melt contains the very weakly solvated cation Ti^{2+} . The solid state spectrum in Fig. 5(c) is of crystalline NaCl, in which the coordination number of the cations is six, and which had been “doped” at

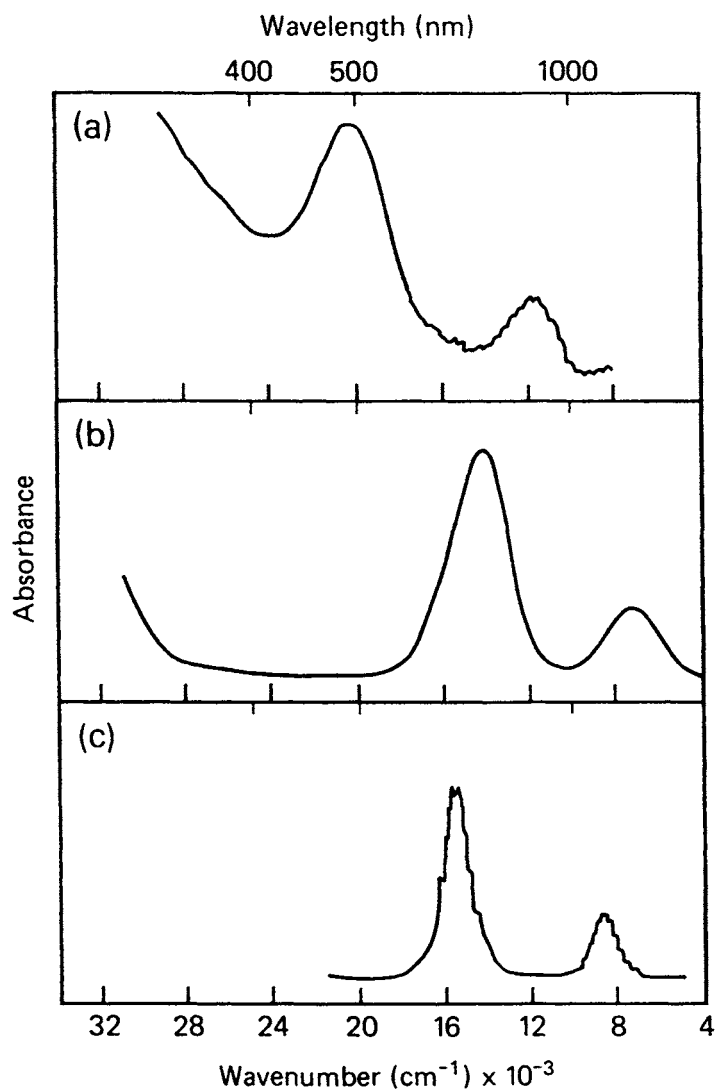


Fig. 5. Spectra of titanium(II) in (a) $\text{SbF}_5\text{--HF}$; (b) molten AlCl_3 at 500 K; and (c) crystalline NaCl at 10 K (doped at 1% level) [5].

the 1% level by adding TiCl_2 to molten NaCl before crystallisation [33]. Comparison of the three spectra in Fig. 5 indicates the presence of Ti(II) in the $\text{SbF}_5\text{--HF}$ solution and suggests very strongly that it is the six coordinate cation Ti(HF)_6^{2+} . Ti(II) was oxidised to solutions or solids containing Ti(III) in HF solutions considerably stronger in SbF_5 than 3 M. It was proposed [31] that, even though the greater acidity of such solutions should favor stabilisation of Ti(II) , these solutions contain sufficient free SbF_5 in equilibrium with fluoroantimonates to oxidise Ti(II) . SbF_5 is

a considerably stronger oxidant than either SbF_5^- or more complex fluoroantimonates.

Direct reaction between "neat" HF and the three very electropositive lanthanide elements, Eu, Yb and Sm, gave H_2 evolution and yielded solutions containing Eu^{2+} , Yb^{2+} and Sm^{2+} [34], characterised by comparison with aqueous spectra obtained, in the case of Yb^{2+} and Sm^{2+} , while the lanthanide(III) solutions were being continuously reduced electrolytically. These dipositive cations were stable in basic HF, i.e. containing excess F^- as a result of reduction of H_2F^+ to H_2 , whereas the dipositive *d*-transition element cations required acidic HF for stability. Also, as is consistent with the greater ionic radii of the Ln(II) cations, the LnF_2 compounds were more soluble than those of the *d*-transition elements. They have solubilities like those of CaF_2 and SrF_2 . All three Ln^{2+} cations were precipitated from HF solutions as LnGeF_6 compounds when the solutions were saturated with the very weak Lewis acid GeF_4 . Despite the highly reducing nature of Sm^{2+} , SmGeF_6 proved to be a very stable solid, reasonably resistant to oxidation in a normal moist atmosphere. Details of its characterisation have been reported [35].

No stable aquo-cation Au^+ exists in water. Typical of the few Au(I) species to exist in aqueous solution are the anions $\text{Au}(\text{CN})_2^-$ and AuCl_2^- . Chain polymeric solids $(\text{AuX})_n$ are formed with the halogens. The chemistry of Au(II) is also very limited. Solids that formally contain Au(II), such as Au_4Cl_8 , are mixed oxidation state compounds containing Au(I) and Au(III). Aubke and co-workers [36] prepared the first solution containing stable solvated Au^{2+} in HSO_3F of enhanced acidity by reacting a working excess (2.42:1) of $\text{Au}(\text{SO}_3\text{F})_3$, previously shown by them to be a strong Lewis acid, with metallic Au. The excess $\text{Au}(\text{SO}_3\text{F})_3$ ensured enhanced acidity of the HSO_3F . Over a period of 24 h, the gold dissolved completely to give a clear brown solution that gave an ESR signal characteristic of Au^{2+} . Over a period of 3 d, a yellow diamagnetic precipitate formed which had the overall composition $\text{Au}(\text{SO}_3\text{F})_2$, but was identified as the mixed oxidation state compound $\text{Au}^{\text{I}}[\text{Au}^{\text{III}}(\text{SO}_3\text{F})_4]$. $\text{Au}_{(\text{solv})}^{2+}$ had disproportionated to Au(I) and Au(III). The necessity for increased acidity in the reaction medium to form Au^{2+} is indicated by their report that attempts to oxidise metallic Au in HSO_3F with $\text{Cs}[\text{Au}(\text{SO}_3\text{F})_4]$, which is basic in HSO_3F , left the gold unreacted, regardless of stoichiometric ratio of reactants, temperature or time duration of the experiments [36].

Subsequently Au^{2+} was generated in acidic HF and crystallised as $\text{Au}(\text{SbF}_6)_2$ which was then the subject of crystallographic structure determination [37]. Metallic Au and SbF_5 , in the ratio 1:1.62, were subjected to controlled oxidation with elemental F_2 in HF. The reaction was stopped while there was still metallic gold left in the reaction mixture, as well, presumably, as residual SbF_5 not neutralised by F^- from reduction of the F_2 . Extended fluorination and exhaustion of the SbF_5 led to formation of a mixed oxidation state compound $\text{Au}^{\text{II}}(\text{SbF}_6)_2 \cdot \text{Au}^{\text{II}}(\text{Au}^{\text{III}}\text{F}_4)_2$. This is consistent with the reported observation that under basic or near basic conditions, namely $\text{KF}:\text{Au}(\text{SbF}_6)_2$, 2:1 in HF, $\text{Au}(\text{SbF}_6)_2$ disproportionated to Au^0 and $\text{Au}^{\text{II}}(\text{Au}^{\text{III}}\text{F}_4)_2$. Again in HF, as in HSO_3F , it was demonstrated that increased acidity of the medium is required to stabilise Au^{2+} .

The fact that $\text{CF}_3\text{SO}_3\text{H}$ and its solutions are significantly less acidic than for HF and HSO_3F is reflected in the relative stabilities of low oxidation state cations in the different media, as found in a survey by Adrien [24]. Whereas metallic Ti was oxidised to Ti^{2+} in $\text{SbF}_5\text{--HF}$, a 2.5 m $\text{B}(\text{OSO}_2\text{CF}_3)_3$ solution in $\text{CF}_3\text{SO}_3\text{H}$ gave Ti^{3+} . For Cr , a solution initially containing both Cr^{2+} and Cr^{3+} contained only Cr^{3+} after standing for several days. This latter observation possibly reflects the instability of $\text{B}(\text{OSO}_2\text{CF}_3)_3$ in HSO_3F .

Adrien also found that metallic U reacted with 0.4 m $\text{B}(\text{OSO}_2\text{CF}_3)_3\text{--CF}_3\text{SO}_3\text{H}$ to produce $\text{U}_{(\text{solv})}^{3+}$ but, with a solution containing 0.4 m TaF_5 , the spectrum indicated the presence of $\text{U}_{(\text{solv})}^{4+}$. This is consistent with the fact that 0.4 m $\text{TaF}_5\text{--CF}_3\text{SO}_3\text{H}$ is less acidic by about two H_0 units than 0.4 m $\text{B}(\text{OSO}_2\text{CF}_3)_3\text{--CF}_3\text{SO}_3\text{H}$. None of the lanthanide metals reacted with “neat” $\text{CF}_3\text{SO}_3\text{H}$, whereas they did so with “neat” HF . However $\text{CF}_3\text{SO}_3\text{H}$ acidified with $\text{B}(\text{OSO}_2\text{CF}_3)_3$ and with TaF_5 reacted with Yb to yield Yb^{2+} but with Sm gave solutions of the more stable Sm^{3+} rather than Sm^{2+} .

These superacidic solutions of *d*- and *f*-transition element cations can provide a controllable low-temperature route to compounds containing transition metals in unusually low oxidation states. Also they are perceived as the precursors to transition metal carbonyl cations, as indicated in Sec. 11.3.4.3 immediately below.

11.3.4.3 Transition metal carbonyl compounds and carbonyl cations

During the 1970s there were several reports of the preparation in HF of transition metal carbonyl fluorides of Mo and Re involving redox reactions between fluorides and carbonyls of transition metals, metathetical conversion of metal carbonyl chlorides to carbonyl fluorides and oxidation of metal carbonyls by XeF_2 in HF . Holloway and co-workers prepared a range of rhenium compounds including $\text{Re}(\text{CO})_5\text{F}$, the fluorine bridged compound $[\text{F}_3\text{Re--F--Re}(\text{CO})_5]$ and $[\text{Re}(\text{CO})_6]^+[\text{Re}_2\text{F}_{11}]^-$ and they provided a systematic summary of this and related work in 1978 [38]. The preparation and structures of these and other metal carbonyl fluorides prepared in HF have been reviewed somewhat later [39]. More recently, the Holloway group have used XeF_2 in HF to oxidise $\text{Ir}_4(\text{CO})_{12}$ to the *mer*- and *fac*-isomers of $\text{Ir}(\text{CO})_3\text{F}_3$ [40] and $\text{Os}_3(\text{CO})_{12}$ to *cis*- $[\text{Os}(\text{CO})_4\text{F}_2]$ in solution with tetrameric $[\{\text{Os}(\text{CO})_3\text{F}_2\}_4]$ as the residue after removal of the HF solvent [41].

Since about 1990, Aubke and colleagues have used HSO_3F as a medium for synthesis of a very wide range of compounds containing carbonyl cations of transition metals in association with extremely weakly basic anions.

Seeking initially to prepare the formyl cation HCO^+ , they applied CO to HSO_3F containing $\text{Au}(\text{SO}_3\text{F})_3$ which had previously been shown by them to be a strong Lewis acid in HSO_3F . $\text{Au}(\text{III})$ was reduced to $\text{Au}(\text{I})$ and they used infra-red and Raman spectroscopy to characterise the linear cation $\text{Au}(\text{CO})_2^+$ in solution [42]. Their attempt to isolate this cation in a solid compound by removal of the solvent was unsuccessful because the base of the solvent, SO_3F^- , is comparable in base strength with CO . One CO ligand was displaced from the cation and the solid isolated was $\text{Au}(\text{CO})\text{SO}_3\text{F}$ — a compound thermally stable to 190°C . They proceeded to prepare the solid $[\text{Au}(\text{CO})_2]^+[\text{Sb}_2\text{F}_{11}]^-$, which is stable to 130°C , by

applying CO to $\text{Au}(\text{CO})\text{SO}_3\text{F}$ dissolved in a large excess of SbF_5 [43]. Under these conditions the cation $\text{Au}(\text{CO})_2^+$ was stable in the solid state because of the extremely weak basicity of the counter-ion $\text{Sb}_2\text{F}_{11}^-$, the less basic SO_3F^- being displaced.

In subsequent related work [44], the less thermally stable solid compound $[\text{Au}(\text{CO})_2]^+[\text{UF}_6]^-$ was prepared quantitatively by oxidation of elemental Au with UF_6 in HF under a pressure of CO. UF_6^- , the reduction product of UF_6 , is, presumably, just sufficiently weakly basic to stabilise the bis(carbonyl) cation, whereas the more weakly basic $\text{Sb}_2\text{F}_{11}^-$ gave a thermally stable compound.

Aubke developed a general synthetic procedure based originally on reactions in HSO_3F to prepare many stable compounds containing carbonyl cations of transition metals. Typically, these are thermally stable in the 100–200°C region. He oxidised several metals, initially electron-rich noble metals, with $\text{S}_2\text{O}_6\text{F}_2$ in HSO_3F to prepare the corresponding fluorosulfates which acted as Lewis acids in HSO_3F . Application of quite low pressures of CO (typically 0.5–2 atm) to those solutions generated carbonyl cations in solution. Removal of solvent gave essentially covalent metal carbonyl fluorosulfates as for $\text{Au}(\text{CO})\text{SO}_3\text{F}$, which, when carbonylated in “neat” SbF_5 , gave the essentially ionic analogues of $[\text{Au}(\text{CO})_2]^+[\text{Sb}_2\text{F}_{11}]^-$.

Aubke has rationalised this approach by postulating that under superacidic conditions highly reactive, extremely electrophilic “naked” or very weakly solvated cations of low charge are formed (as shown in Sec. 11.3.4.2) and that they function as strong Lewis acids towards CO to form metal carbonyl cations in solution. Aubke and Wang [45] reviewed synthesis and spectroscopic characterisation of several of the compounds described briefly below.

Having demonstrated earlier that $\text{Pt}(\text{SO}_3\text{F})_4$ acts as a strong Lewis acid in HSO_3F , Aubke’s group showed that partial reduction and carbonylation of $\text{Pt}(\text{SO}_3\text{F})_4$ yielded $[\text{Pt}(\text{CO})_2(\text{SO}_3\text{F})_3]$ and complete reduction gave *cis*- $[\text{Pt}(\text{CO})_2(\text{SO}_3\text{F})_2]$. They formulated $[\text{Pt}(\text{CO})_2(\text{SO}_3\text{F})_3]$ as $[\text{Pt}(\text{CO})_4][\text{Pt}(\text{SO}_3\text{F})_6]$. Carbonylation of $[\text{Pt}(\text{CO})_2(\text{SO}_3\text{F})_2]$ in excess SbF_5 yielded $[\text{Pt}(\text{CO})_4][\text{Sb}_2\text{F}_{11}]_2$ which contains the square planar cation $[\text{Pt}(\text{CO})_4]^{2+}$. Reductive carbonylation of $\text{Pd}[\text{Pd}(\text{SO}_3\text{F})_6]$ in HSO_3F gave the solid $\text{Pd}(\text{CO})_2(\text{SO}_3\text{F})_2$ which on further carbonylation in SbF_5 gave $[\text{Pd}(\text{CO})_4][\text{Sb}_2\text{F}_{11}]_2$. The reaction mixture which had yielded $\text{Pd}(\text{CO})_2(\text{SO}_3\text{F})_2$ underwent reductive decomposition on long standing at ambient temperature to give $\text{Pd}(\text{CO})\text{SO}_3\text{F}$. Crystallographic investigation showed that it contained the cyclic planar, binuclear carbonyl-bridged cation $[\text{Pd}_2(\mu\text{-CO})_2]^{2+}$.

Subsequently, Aubke simplified his experimental approach to syntheses of this type by direct carbonylation of the fluorosulfates of Hg(I) and Hg(II) in neat SbF_5 to produce $[\text{Hg}_2(\text{CO})_2][\text{Sb}_2\text{F}_{11}]_2$ and $[\text{Hg}(\text{CO})_2][\text{Sb}_2\text{F}_{11}]_2$ as the first compounds containing carbonyl cations of post-transition elements [46]. This direct synthesis of “naked” cations in SbF_5 has proved a fruitful area of research and has been reviewed by Aubke, Willner and their colleagues [47]. In addition to being able to produce those carbonyl cations originally generated in HSO_3F , they report direct synthesis of variously-charged cations such as $[\text{Mn}(\text{CO})_6]^+$, $[\text{Re}(\text{CO})_6]^+$, $[\text{Fe}(\text{CO})_6]^{2+}$, $[\text{Ru}(\text{CO})_6]^{2+}$, $[\text{Os}(\text{CO})_6]^{2+}$ and $[\text{Ir}(\text{CO})_6]^{3+}$, all isolated in association with the anion $\text{Sb}_2\text{F}_{11}^-$.

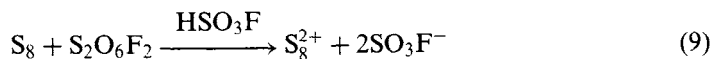
In a recent comprehensive review Willner and Aubke [48] have set the range of syntheses of transition metal carbonyl cations in superacidic media within the general context of synthesis of these types of cations by all known methods. They have presented the available spectroscopic and crystallographic evidence for the structures of the cations and have discussed the nature of bonding in the carbonyl complexes.

11.3.4.4 Homopolyatomic cations in fractional oxidation states

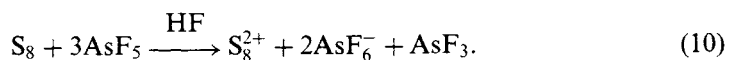
Even though much of the pioneering study of polyatomic cations of the non-metallic elements was done by Gillespie and his colleagues at McMaster University in the 1960s, this area will be presented in some detail here because a semi-quantitative basis can now be provided to define the experimental conditions leading to generation, stabilisation and disproportionation of many of these cations.

As early as 1804 solutions of non-metals such as sulfur and iodine in oleums were reported to produce highly colored solutions but the nature of the solutes was unknown. From the mid 1960s, Gillespie's group adduced reliable evidence to indicate that solutions such as these and others in HSO_3F and HF contained the polyatomic halogen cations I_2^+ , I_4^{2+} , I_3^+ , I_5^+ , Br_2^+ and Br_3^+ and the chalcogen cations listed in Table 2.

The methods of preparation of these species in superacid solution and the structures of many of the cations in association with very weakly basic anions were reviewed by Gillespie and Passmore [49]. Typical generation of the cations in solution involved oxidation of the appropriate element with bis(fluorosulfonyl) peroxide, $\text{S}_2\text{O}_6\text{F}_2$, in HSO_3F to yield the cation and SO_3F^- which is both the reduction product of the oxidant and the base of the solvent:



or, less frequently, oxidation in HF by AsF_5 or SbF_5 , both strong Lewis acids and strong oxidants:



The structure of S_8^{2+} was determined from the crystalline compound $\text{S}_8(\text{AsF}_6)_2$, isolated under "naked" ion conditions (see Sec. 11.3.4.5).

Stability of polyatomic cations in solution depends on acidity levels of the reaction media (as indicated below by values of the Hammett Acidity Function, H_0), on cationic charge and on the atomic number of the element. I_2^+ is quite stable in $\text{SbF}_5\text{-HSO}_3\text{F}$ ($H_0 \cong -18$) but only marginally stable in slightly basic HSO_3F ($H_0 \cong -13.8$), whereas I_3^+ is stable at $H_0 \cong -13.8$. Br_2^+ is only marginally stable in $\text{SbF}_2(\text{SO}_3\text{F})_3\text{-HSO}_3\text{F}$ ($H_0 \cong -19$) whereas Br_3^+ is stable at $H_0 \cong -19$ and marginally stable at -13.8 . So, for the species X_n^+ , higher acidities are required for stabilisation in solution when $\text{X} = \text{Br}$ than for $\text{X} = \text{I}$ and, for each element, stabilisation of species with smaller values of n requires higher acidity than for larger

values of n . It is consistent with these trends that no cations of chlorine have been generated in solution. Cl_2^+ has not been observed in solution or in the solid state. Cl_3^+ occurs in an unstable solid but not in solution.

For each element, there is a greater attenuation of the single positive charge over X_3^+ than over X_2^+ . X_3^+ is less electrophilic than X_2^+ ; that is, X_3^+ can exist with a greater availability of nucleophilic base, either in solid compounds or in solution, than X_2^+ . For a particular value of n , X_n^+ is more electrophilic for $\text{X}=\text{Cl}$ than for $\text{X}=\text{Br}$ and I in turn. That is, Cl_n^+ would react more readily than Br_n^+ and I_n^+ with bases such as SO_3F^- or F^- in solution or in solids. Such reaction in solution leads to disproportionation, as discussed below.

Table 2 shows that high fractional charge-to-element ratios occur in stable cations of Te. There are no known X_6^{4+} cations for Se and S nor does Te exhibit a fractional oxidation state of 0.25 or less, while very low ratios occur for S cations. Listed in Table 2 are lower threshold value of the acidity (H_0 values) for media in which each of the cations was generated in a range of H_2SO_4 -based media from acidic $\text{SO}_3\text{--H}_2\text{SO}_4$ (H_0 from -14.1 to -12.7), through H_2SO_4 itself ($H_0 = -11.9$) to basic $\text{HSO}_4^-\text{--H}_2\text{SO}_4$ ($H_0 = -10$). The H_0 values show that a higher acidity level, that is a lower availability of base, is necessary to stabilise S_4^{2+} than for S_8^{2+} and that, for the series X_4^{2+} , progressively less acidity is required in proceeding from S to Te cations. A full set of H_0 values was not available for stabilisation of these cations in HSO_3F . However, the data that do exist show the same trends.

The implicit strategy behind Gillespie's preparation of non-metal cations in solution was to use media of sufficient acidity that the cations sought would be stable and then to use an appropriate oxidant stoichiometry. For example $\text{I}_2\text{:S}_2\text{O}_6\text{F}_2$ at 3:1 and 5:1 in HSO_3F gave I_3^+ and I_5^+ . This strategy is effective if a powerful oxidant, such as $\text{S}_2\text{O}_6\text{F}_2$ in HSO_3F or F_2 in HF , is used. If, however, a mild oxidant (or reductant) is used, it is the level of acidity or basicity of the medium alone which determines cation speciation, as indicated immediately below.

Table 2

Stability of homopolyatomic cations of chalcogen elements in superacid media

General Formula	X_6^{4+}	X_4^{2+}	X_8^{2+}	$\text{X}_n^{2+} (n > 8)$
Oxidation State	0.67	0.5	0.25	< 0.25
Tellurium	Te_6^{4+} (-13.8)*	Te_4^{2+} (-11)	—	—
Selenium	—	Se_4^{2+} (-11.9)	Se_8^{2+} (-11.9)	Se_{10}^{2+} (-10)
Sulfur	—	S_4^{2+} (-14.1)	S_8^{2+} (-13.2)	S_{19}^{2+} (-12.7)

*Numbers in parentheses are values of the Hammett Acidity Function (H_0) calculated on the basis of the reported experimental preparative conditions and represent approximate acidity thresholds above which the particular species are stable in solution.

Using UV-vis and Raman spectroscopy to monitor the iodine species in solution, Besida and O'Donnell [50] have delineated quite sharply the threshold levels of acidity and basicity that determine the different equilibria that exist between the cations I_2^+ , I_3^+ and I_5^+ and the final disproportionation products of those cations, namely I_2 and IF_5 . Two sets of experiments were conducted. In the first, excess I_2 in HF was treated with controlled amounts of F_2 in a series of solutions from basic (NaF) through weakly acidic (NbF₅) to strongly acidic (TaF₅ and SbF₅). I_2 in excess over the amount of F_2 was used in this series because if excess of the oxidant F_2 were to be used in acidic HF most of the cations formed would be determined by the $F_2:I_2$ stoichiometry regardless of the level of acidity of the medium. In the second set, the mild oxidant IF_5 , shown by Raman spectroscopy to be the major high oxidation state disproportionation product of the iodine cations, was maintained in ten-fold excess over the reductant I_2 , the other disproportionation product, as the acidity-basicity levels were fixed.

Table 3 summarises the results from the first set of experiments. I_2^+ is the only species detectable spectroscopically at H_0 values more negative than -16.20 . An extremely acidic HF solution (5 molal in SbF₅, $H_0 \cong -22$) showed no spectral peaks other than those for I_2^+ . There was no suggestion of formation of I^+ . With reduction of acidity to $H_0 = -16.05$, the first disproportionation product I_3^+ appeared in equilibrium with I_2^+ which was present only in trace amounts at $H_0 = -15.65$. With further reduction in acidity I_3^+ and I_5^+ , the next disproportionation product, were in equilibrium until in basic solutions, at H_0 values less negative than -10.95 , the final dis-

Table 3

Dependence of formation of iodine cations on the level of acidity of hydrogen fluoride^a

HF acidity-basicity (solute, molality)	$-H_0^b$	Species in solution
NaF, 0.1	9.95 ^c	$I_2 + IF_5$
NaF, 0.01	10.80 ^c	$I_2 + IF_5$
NaF, 0.0075	10.95 ^d	$I_5^+ + I_3^+$
NaF, 0.001	11.80 ^d	$I_5^+ + I_3^+$
NbF ₅ , 0.05	15.65 ^c	$I_3^+ + \text{trace } I_2^+$
NbF ₅ , 0.075	15.90 ^c	$I_3^+ + I_2^+$
NbF ₅ , 0.091	16.05 ^e	$I_3^+ + I_2^+$
NbF ₅ , 0.11	16.20 ^e	I_2^+
TaF ₅ , 0.4	19.20 ^c	I_2^+
SbF ₅ , 0.2	20.65 ^c	I_2^+

^aExcess I_2 was reacted with controlled amounts of F_2 under the conditions listed.

^bValues rounded to 0.05 unit.

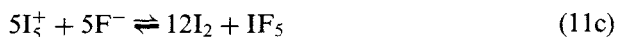
^cExperimentally determined values from Ref. [10].

^dCalculated from experimental values from Ref. [10], an autoprotolysis constant of 5×10^{-13} , and a value of -15.10 for H_0 for pure HF.

^eObtained by interpolation between experimental values from Ref. [10].

proportionation products I_2 and IF_5 were formed. There was Raman spectroscopic evidence for a very small amount of IF_3 in the disproportionation products.

The stepwise disproportionation that would occur if F^- were to be added gradually to an acidic HF solution containing I_2^+ can be represented as:



These lead to an overall reaction:



Small increases in the amount of base available cause disproportionation of I_2^+ to I_3^+ and to I_5^+ . When the *available* F^- is comparable with or somewhat greater than the concentration of I_2^+ , total disproportionation will occur to elemental iodine and an essentially covalent compound of iodine in a higher oxidation state than in the parent cation, in this case mainly IF_5 with a small equilibrium concentration of IF_3 .

The second set of experiments involved conproportionation reactions with controlled acidity. A ten-fold excess of the mild oxidant IF_5 was added to a solution of I_2 in basic HF and the acidity was gradually increased by quantitative stepwise additions of SbF_5 . The same general features emerged as for the first set of experiments. IF_5 and I_2 co-existed in basic HF. Increase in acidity led to equilibrium formation firstly of I_5^+ and I_3^+ , then of I_3^+ and I_2^+ and, in strongly acidic HF, I_2^+ was the only species present other than excess IF_5 .

An important aspect of this work is that it shows that, as long as an extremely strong oxidant like F_2 is **not present in excess**, the nature of the species present is determined by the level of acidity or basicity of the medium. Presence of the mild oxidant IF_5 in vast excess over I_2 in the second set of experiments led to formation of I_5^+ , I_3^+ and I_2^+ in turn as the acidity thresholds were reached.

Adrien [24] demonstrated the dependence of iodine cation speciation on acidity levels in triflic acid. He conproportionated ICl_3 and I_2 , with each in ten-fold excess in different experiments, in triflic acid solutions that were made progressively more acidic using TaF_5 , SbF_5 and $B(OSO_2CF_3)_3$. He showed I_3^+ to be dominant, with a trace of I_2^+ , in TaF_5 solutions. Increase in concentration and strength of the other two Lewis acids led to I_2^+ gradually becoming the dominant cationic species.

In their review Gillespie and Passmore [49] describe homopolyatomic cations of metallic elements such as Bi, Hg, Cd and Zn and these have been discussed more recently [4(d)]. Many of these were isolated initially as “naked” cations from molten salt mixtures by reacting the metal with its normal chloride directly or in a host melt. The cation Hg_2^{2+} has been known for 100 years. It was not then so surprising when

reaction of a 1:2:2 mixture of HgCl_2 , Hg and AlCl_3 yielded yellow $\text{Hg}_3(\text{AlCl}_4)_2$, characterised spectroscopically and polarographically in molten NaCl-AlCl_3 mixtures. Gillespie and colleagues [51] generated Hg_3^{2+} essentially under “naked” conditions by oxidising metallic Hg with AsF_5 and with SbF_5 in solution in SO_2 . They isolated yellow solids $\text{Hg}_3(\text{AsF}_6)_2$ and $\text{Hg}_3(\text{Sb}_2\text{F}_{11})_2$. The solvent SO_2 and the reduction products AsF_3 and SbF_3 are so weakly basic that Hg_3^{2+} was stable towards disproportionation under these conditions.

Molten salt reactions between Bi and BiCl_3 showed the existence of the cations Bi_5^{3+} , Bi_9^{5+} and Bi_8^{2+} . Burns et al. [52] reacted Bi with several potential oxidants in SO_2 . With AsF_5 they isolated the stable compound $\text{Bi}_5(\text{AsF}_6)_3 \cdot 2\text{SO}_2$ which decomposed slowly in 100% H_2SO_4 . In contrast, Besida and O'Donnell [53] produced in HF acidified with the weak acid BF_3 a solution which was stable for several months containing Bi_5^{3+} , identified by comparison of its UV-vis spectrum with that of a freshly prepared solution of $\text{Bi}_5(\text{AsF}_6)_3$ in H_2SO_4 .

There has been little reported study of preparation of polyatomic cations of metals in superacids. The very limited experience with Bi_5^{3+} in weakly acidic HF suggests that this may be a fertile field for research. For example, Hg_4^{2+} , which was found to disproportionate in SO_2 [51], should be stable in protonic superacids or in acidic media such as “neat” SbF_5 . Similarly, bismuth cations other than Bi_5^{3+} should be stable in media of controlled acidity.

Note added in proof: Very recently Christie and colleagues [53a] have provided a spectacular example of a stable homopolyatomic cation in N_5^+ , the third known all-nitrogen entity after N_2 itself and the familiar azide ion, N_3^- . It was generated in superacidic medium and stabilised as a solid by the weakly basic anion AsF_6^- . They reacted $\text{N}_2\text{F}^+\text{AsF}_6^-$, formed by direct reaction of *cis*- N_2F_2 and AsF_5 , with HN_3 in anhydrous HF at -78°C and isolated the product $\text{N}_5^+\text{AsF}_6^-$, which is marginally stable at ambient temperature but stable indefinitely at -78°C , even though its enthalpy of formation has been calculated as being about 1470 kJ mol^{-1} . There is some indirect chemical evidence that the acidity of the HF medium was enhanced by availability of free AsF_5 formed during the synthesis.

11.3.4.5 “Naked” cations in unusual oxidation states

Archetypal “naked” cations have been formed by stoichiometric reaction of compounds in the molten state. Thus, when I_2 , ICl and AlCl_3 were melted in the stoichiometric ratios 1:1:1 and 2:1:1, the products were $\text{I}_3^+\text{AlCl}_4^-$ and $\text{I}_5^+\text{AlCl}_4^-$. The anion AlCl_4^- produced in the reaction was sufficiently weakly basic for the cations I_3^+ and I_5^+ to be formed without disproportionation in the neutral melt.

Oxidation of I_2 in SbF_5 produces a reaction mixture which is deep blue, characteristic of the cation I_2^+ . However, in acting as an oxidant, SbF_5 is reduced to SbF_3 which interacts with SbF_5 to form complex anions of low volatility, making isolation of a pure compound containing I_2^+ impossible. Gillespie modified this approach by reacting I_2 and SbF_5 in liquid SO_2 as a non-interacting solvent [54]. SbF_3 , insoluble in SO_2 , was removed and $\text{I}_2^+\text{Sb}_2\text{F}_{11}^-$ was crystallised from the solution, allowing X-ray

crystallographic structure determination. SO_2 is sufficiently weakly basic that disproportionation of I_2^+ is not induced.

As their review [49] shows, Gillespie, Passmore and co-workers have isolated I_4^{2+} , I_3^+ , I_5^+ and many cations of S, Se, Te and Hg as solids in this general way. They used the weaker oxidant AsF_5 to produce homopolyatomic cations of Se, Te and Hg in SO_2 , the reduction product AsF_3 being weakly basic. On occasions they used liquid AsF_3 as the reaction solvent.

Modifications of this general approach have been used by Gillespie to produce heteropolyatomic cations containing chalcogen elements, e.g. $\text{Te}_2\text{Se}_8^{2+}$, $\text{Te}_3\text{Se}_3^{2+}$, $\text{Te}_2\text{Se}_2^{2+}$ [55] S_4N_4^+ , S_6N_2^+ and $\text{S}_6\text{N}_4^{2+}$ [56]. Passmore has reported the preparation of heterocations containing halogens and sulfur using SO_2 and AsF_3 as reaction media and has provided experimental details for these syntheses [57].

It was shown in Sec. 11.3.4.3 that Aubke, Willner and colleagues [47] recently carbonylated transition metal fluorosulfates and other compounds in "neat" SbF_5 to generate "naked" transition metal carbonyl cations in association with the very weakly basic anion $\text{Sb}_2\text{F}_{11}^-$.

11.3.4.6 Base-induced disproportionation of cations

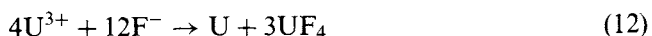
In the sections above there has been frequent reference to base-induced disproportionation of transition metal cations in low oxidation states (Sec. 11.3.4.2), of carbonyl cations of transition metals (Sec. 11.3.4.3) and of polyatomic cations of non-metals in fractional oxidation states (Sec. 11.3.4.4). In the last-named section, disproportionation of polyiodine cations was presented and discussed in considerable detail; but a similar rationale can be applied to stability of all cations — metallic or non-metallic — in unusually low or fractional oxidation states, whether produced in non-aqueous ionising media or as "naked" cations.

Thus, disproportionation occurs when a highly electrophilic polyatomic non-metal cation interacts with a nucleophilic base to form, in the first instance, a polyatomic cation of lower charge per non-metal atom (lower fractional oxidation state) and a compound, essentially covalent, formed between the base and the non-metal of the cation, with that non-metal now in a higher oxidation state than in the parent cation. For example I_2^+ disproportionates to I_3^+ and IF_5 . With greater availability of base, the polyatomic cation first formed will disproportionate to a lower-charge polyatomic cation and ultimately to the free element from which the parent cation was formed. Similar patterns differing in detail, are observed for metallic polyatomic cations, monatomic transition metal cations in low oxidation states and for all "naked" electrophilic cations.

A report from Aubke et al. [58] on improved synthetic procedures for preparing $[\text{I}_2^+][\text{Sb}_2\text{F}_{11}^-]$ and $[\text{Br}_2^+][\text{Sb}_3\text{F}_{16}^-]$ provides a good example of the dependence of disproportionation and conproportionation on basicity and acidity of reaction media and shows the reversibility of these processes. They equilibrated exactly stoichiometric (2:1) mixtures of I_2 and of Br_2 with $\text{S}_2\text{O}_6\text{F}_2$, stoichiometries designed to produce the compounds $[\text{I}_2^+][\text{SO}_3\text{F}^-]$ and $[\text{Br}_2^+][\text{SO}_3\text{F}^-]$. Instead they isolated the disproportionation products for each compound, namely $[\text{I}_3^+][\text{SO}_3\text{F}^-]$ and ISO_3F and a mixture of Br_2 and BrSO_3F . They then treated each reaction mixture with a

vast excess of SbF_5 and isolated $[\text{I}_2^+][\text{Sb}_2\text{F}_{11}^-]$ and $[\text{Br}_2^+][\text{Sb}_3\text{F}_{16}^-]$, the SO_3F moiety being removed as volatile $\text{Sb}_2\text{F}_9(\text{SO}_3\text{F})$. A comproportionation reaction had occurred. In the presence of SO_3F^- each diatomic cation was unstable towards disproportionation, whereas each was stable when associated with fluoroantimonate anions which are more weakly basic than fluorosulfate. Further, it is significant that, whereas I_2^+ is stable in the solid state with $\text{Sb}_2\text{F}_{11}^-$ as the counter ion, the more electrophilic cation Br_2^+ required the more weakly basic $\text{Sb}_3\text{F}_{16}^-$ anion for stability. The difference in electrophilicity of the two cations also accounts for the different nature of the disproportionation products in each case — a pattern previously observed.

When a solution of NaF in HF was added gradually to the stable lilac-colored solution of U^{3+} in $\text{BF}_3\text{--HF}$ (Sec. 11.3.4.2) a precipitate was observed which was green UF_4 “flecked” with black particles of metallic U and the supernatant solution was colorless, i.e. it contained no U(III) or U(IV) species. Under favorable experimental conditions some of the metallic uranium was deposited as a bronze-colored mirror on the walls of the “synthetic sapphire” reaction tube, as shown in the original reference [59]. Base-induced disproportionation had occurred.



Besida and O'Donnell [53] showed that addition of NaF--HF to the yellow-orange solutions of Ti^{2+} in $\text{SbF}_5\text{--HF}$ produced mixed precipitates of blue TiF_3 , white TiF_4 and black metallic Ti and the supernatant solution was colorless. A complex pattern of disproportionation of Ti(II) to the element and to both Ti(III) and Ti(IV) simultaneously had occurred because of the insolubility of TiF_3 in near-neutral HF .

Reference was made in Sec. 11.3.4.2 to disproportionation of $\text{Au}_{(\text{solv})}^{2+}$ to Au(I) and Au(III) in HSO_3F which was not sufficiently acidic to stabilise the cation. In similar context, the more highly reduced cation Au(CO)_2^+ could be formed at the expense of Au(CO) when the basicity of the medium was decreased (Sec. 11.3.4.3).

The usual reversibility of disproportionation reactions with increase in acidity provides an effective general route to synthesis of cations in low or fractional oxidation states, as was shown for preparation of Au^{2+} in Sec. 11.3.4.3 and for iodine cations in Sec. 11.3.4.4.

11.3.5 High oxidation state anions and derived compounds

In all media, preparation of compounds containing elements in unusually high oxidation states is favored by oxidation reactions in basic solvents, producing complex anions of the element with the base of the solvent as ligands (solvo-anions). A common example from aqueous chemistry is $\text{Mn}^{\text{VII}}\text{O}_4^-$, prepared by oxidation of Mn(II) in alkaline solution. An extremely high oxidation state for Pu is exhibited in $\text{Pu}^{\text{VII}}\text{O}_5^{3-}$ which is produced by oxidation with ozone in strongly alkaline solutions.

Solid ternary fluorides prepared by high temperature, high-pressure fluorination of mixed salts have been known for a long time. Examples, relevant to the discussion

below, of such compounds in HF are M_2NiF_6 , M_2MnF_6 and $MAGF_4$, where M is an alkali metal, its fluoride produced *in situ* providing a basic medium.

Basic HF has proved to be a fruitful medium for synthesis of fluoro-anions containing metals in high oxidation states from which binary and ternary solid compounds in corresponding oxidation states can be isolated. In 1964 $Ni^{IV}F_6^{2-}$ was generated in strongly basic HF (0.5 to 1.5 M in KF) by electrolytic oxidation of a Ni electrode [60]. In synthesising salts containing the NF_4^+ cation and fluoro-anions of transition metals in very high oxidation states, Christie [61] carried out a metathetical reaction in HF between NF_4SbF_6 and Cs_2NiF_6 , previously prepared by fluorination of CsF and $NiCl_2$. $CsSbF_6$ precipitated from solution and $(NF_4)_2NiF_6$ was recovered by recrystallisation from HF. $(NF_4)_2MnF_6$ was prepared in similar fashion [62].

Žemva et al. treated AgF_2 and NiF_2 with the extraordinarily powerful oxidant KrF_2 in the presence of XeF_6 in HF to generate the anions $Ag^{III}F_4^-$ [63] and $Ni^{IV}F_6^{2-}$ [64]. XeF_6 ionises extensively in HF to form XeF_5^+ and F^- (as discussed in Sec. 11.3.3.2), providing **both** a basic solution and the counter-cations XeF_5^+ and $Xe_2F_{11}^+$ with which the fluoro-anions were isolated from the solution as the solids $[XeF_5^+AgF_4^-]$ and $[(Xe_2F_{11}^+)_2(NiF_6^{2-})]$.

Very recently Bartlett has shown that NiF_2 and AgF_2 can be oxidised quantitatively to NiF_6^{2-} [65] and AgF_4^- [66] **at room temperature**, using ultra violet- or sunlight-irradiated F_2 in strongly basic HF, i.e. in solutions containing excess alkali metal fluorides ($KF:HF \cong 1:4$). The anions were isolated as the solid compounds M_2NiF_6 and $MAGF_4$ with the alkali metal (M) cations.

Žemva, Bartlett and colleagues reported a general approach to synthesis from HF of polymeric binary fluorides [67] which has a major advantage over many of the synthetic routes used to date. Some of these fluorides are thermodynamically unstable or marginally stable at ambient temperature. Earlier attempts to prepare some of these compounds at elevated temperatures had proved unsuccessful or had led to contaminated products. Some reported synthetic procedures for transition metal tetrafluorides, for example, involving reduction by the metal of the stable pentafluoride at elevated temperature have resulted in products contaminated to greater or lesser extent with the trifluoride or with the metal.

High purity RuF_4 and OsF_4 were obtained quantitatively by precipitation on controlled addition of the gaseous acid AsF_5 to solutions of K_2RuF_6 and K_2OsF_6 in basic HF. The polymeric fluorides are insoluble in nearly neutral HF as discussed in Sec. 11.3.3.3. Full experimental details of this preparation of RuF_4 and its crystallographic structure determination have been reported later [68]. Bartlett has shown that many potential precursors to these types of binary compounds can be synthesised readily by room temperature oxidation with F_2 of the metals, Au, Ru, Os, Ir, Pt and Pd, to give solutions of AuF_4^- , RuF_6^{2-} , RuF_6^- , OsF_6^- , IrF_6^- , PtF_6^{2-} and PdF_6^{2-} in HF made basic with alkali metal fluorides [69]. The appropriate binary fluorides can be isolated and characterised crystallographically.

The great power of the general synthetic procedure proposed by Žemva, Bartlett et al. lies in the ability to prepare marginally thermally stable and even thermodynamically unstable fluorides at low temperatures. Originally [67], they

reported preparation of AgF_3 , which loses F_2 slowly on standing in HF at room temperature, and of NiF_4 , which loses F_2 from the solid above -55°C , by addition of AsF_5 to solutions in HF of $\text{XeF}_5\cdot\text{AgF}_4$ and $(\text{XeF}_5)_2\text{NiF}_6$.

Subsequently they published crystallographic data and details of more refined experimental procedures for recovery of the two binary fluorides from the HF reaction media. For AgF_3 [70] they demonstrated that when the moderately strong Lewis acid AsF_5 was used to cause precipitation from the solution of AgF_4^- in HF, the initial precipitate lost F_2 in HF to be reduced to $\text{Ag}^{\text{II}}[\text{Ag}^{\text{III}}\text{F}_4]_2$, i.e. Ag_3F_8 . They observed that when the much weaker acid BF_3 was used, they achieved good recovery of AgF_3 . Later again Bartlett [66] found that use of the very weak Lewis acid GeF_4 led to isolation of AgF_3 with minimum contamination by Ag_3F_8 .

It seems likely that the strong acid AsF_5 , in addition to abstracting F^- from AgF_4^- , could also combine with F^- of HF to enhance the proton concentration of the medium, particularly in local concentrations before the solution was made homogeneous. Whereas high F^- concentrations favor high oxidation states in HF, increased acidity favors lower oxidation states. Reduction of $\text{Ag}(\text{III})$ to $\text{Ag}(\text{II})$ with loss of F_2 would lead to formation of the more stable solid compound $\text{Ag}^{\text{II}}[\text{Ag}^{\text{III}}\text{F}_4]_2$. BF_3 and GeF_4 , being progressively weaker acids, would be less prone to provide reducing conditions.

A secondary experimental advantage in using GeF_4 is that GeF_6^{2-} , formed by the interaction of GeF_4 with excess F^- , is reported [66] to be more soluble in HF in the presence of K^+ than the anions AsF_6^- and BF_4^- and so is more easily washed from the solid product, making the AgF_3 less susceptible to loss of F_2 on prolonged standing in HF. It may well be that there is a small threshold level of F^- concentration necessary to stabilise AgF_3 in HF and that washing with 0.001 M NaF or NH_4F ($H_0 \cong -12$) or 0.01 M fluoride ($H_0 \cong -11$) could enhance the stability of AgF_3 during the recovery process.

Žemva, Bartlett and colleagues [71] reported formation of a tan precipitate believed to be the unstable NiF_4 on introduction of BF_3 to a solution of K_2NiF_6 in HF at -65°C ; but separation of the reaction products was difficult. Identification of the tan precipitate as NiF_4 was made indirectly after using another synthetic route. $(\text{Xe}_2\text{F}_{11})_2\text{NiF}_6$, prepared in HF using KrF_2 and XeF_6 [64] as described earlier, was dissolved in HF. AsF_5 , measured tensimetrically, was added slowly to the red solution at -65°C . Addition of exactly 4 equivalents of AsF_5 neutralised the XeF_6 molecules of the two cationic moieties $\text{Xe}_2\text{F}_{11}^+$ and abstracted two fluorides from NiF_6^{2-} to produce a tan precipitate and a pale-straw colored solution, typical of solutions of $\text{XeF}_5^+\text{AsF}_6^-$ in HF. $\text{XeF}_5^+\text{AsF}_6^-$ was washed from the precipitate which was shown to be NiF_4 by adding two equivalents of XeF_6 to a suspension of the precipitate in HF. This gave a red solution from which $(\text{XeF}_5)_2\text{NiF}_6$ was recovered. The paper [71] describes decomposition of NiF_4 to various forms of highly reactive NiF_3 by thermal decomposition of the solid above -55°C or of its solution in HF at 0°C .

Subsequently Bartlett and colleagues [72,73] made detailed studies of the oxidant strengths of the anions AgF_4^- and NiF_6^{2-} , of the neutral binary fluorides AgF_3 and NiF_4 , derived from the anions by action of Lewis acids in HF, and of cationic

species of Ag(III) and Ni(IV), obtained by treating the neutral binary fluorides suspended in HF with Lewis acids.

This work showed that, while acidification with BF_3 of a solution of KAgF_4 in HF causes precipitation of AgF_3 , without dissolution in excess BF_3 -HF, the stronger Lewis acids AsF_5 , SbF_5 and BiF_5 cause dissolution of AgF_3 with decomposition to soluble Ag^{2+} and F_2 , i.e. reduction in oxidation state occurs in strongly acidic solution. However they state that "it appears that there is a relatively long-lived Ag^{III} species present under these conditions, since both PtF_6^- and RuF_6^- are oxidised to their neutral relatives in high yield ($\sim 60\%$ or better)". They suggest that the effective oxidant is $\text{Ag}_{(\text{solv})}^{\text{III}}$, which is probably cationic in view of the strongly acidic conditions that prevail, since neither PtF_6^- nor RuF_6^- is oxidised in HF by F_2 , which is a product of the dissociation of AgF_3 . The dissolved Ag^{III} species oxidises O_2 in HF at ambient temperatures to O_2^+ , which Ag^{2+} , the other dissociation product, cannot do.

Even the weak acid BF_3 causes dissolution of NiF_4 in HF to provide solutions which probably contain cationic species NiF_{4-x}^{x+} which oxidise PtF_6^- and RuF_6^- to their neutral counterparts. The authors [73] describe the species $\text{Ag}_{(\text{solv})}^{\text{III}}$ and $\text{Ni}_{(\text{solv})}^{\text{IV}}$ as being "oxidisers of unsurpassed power", of greater strength than PtF_6 and RuF_6 , as indicated above, greater than O_2^+ , which is formed by electron oxidation of O_2 by PtF_6 and RuF_6 , and greater again than several other potent oxidisers, which they discuss in detail. They summarise a large study of the oxidising properties of these types of compounds by saying [72,73] that cationic $\text{Ag}_{(\text{solv})}^{\text{III}}$ and $\text{Ni}_{(\text{solv})}^{\text{IV}}$ are oxidants of comparable strength, greater than the neutral binary fluorides and greater again than their anionic counterparts.

The syntheses cited in this section have all involved attainment of high oxidation states in transition metal fluoro-anions, and thence in binary fluorides and in cationic species, by oxidation with F_2 or other fluoro-oxidants in HF of metals or of compounds in lower oxidation states. A couple of examples are offered of syntheses of new fluoro-oxo-compounds involving fluorination of oxides already in high oxidation states with rare gas fluorides in HF. The ratio of F:O in the ligands of these new compounds is greater than in the related compounds already reported.

The only oxo-fluoride of technetium reported until recently was TcO_3F , prepared by direct fluorination of TcO_2 or, more importantly in this context, by solvolysis of TcO_4^- in HF. Reaction between XeF_6 and Tc_2O_7 in a 3:1 ratio in HF yielded the product TcO_2F_3 , with a higher F:O ratio [74]. Reaction of KrF_2 with OsO_4 in a 2:1 ratio in HF gave *cis*- OsO_2F_4 quantitatively, Kr and O_2 being the other products [75]. Increasing the KrF_2 : OsO_4 ratio gave no further oxygen-fluorine exchange, excess KrF_2 being recovered unreacted.

11.4 Summary

Synthesis of inorganic triflates has been restricted almost entirely to metathetical or solvolysis reactions [25] and only a very small number of ionic inorganic species has been generated in $\text{CF}_3\text{SO}_3\text{H}$ [24]. Many more binary fluorosulfates and several

ternary compounds have been produced by similar interactions with HSO_3F . However an important additional approach to synthesis of fluorosulfates lies in the use of $\text{S}_2\text{O}_6\text{F}_2$ as a controlled oxidant, reacting directly with either the elements or compounds or in HSO_3F [25].

Controlled oxidation by $\text{S}_2\text{O}_6\text{F}_2$ of non-metallic elements in HSO_3F led to rigorous studies of polyatomic non-metal cations in fractional oxidation states (Sec. 11.3.4.4). Fluorosulfates have proved useful precursors to compounds generated in the less basic "neat" SbF_5 to produce many new carbonyl cations of transition metals (Sec. 11.3.4.3). Conproportionation of Au and $\text{Au}(\text{SO}_3\text{F})_3$ in acidic HSO_3F gave the low oxidation state cation Au^{2+} [36]. Many other "naked" or weakly coordinated cations in low oxidation states were generated in HSO_3F en route to preparation of carbonyl cations.

For synthetic purposes, HF provides a broader range of acidity and basicity and a larger useable potential range than is available in the other two fluoro-acids and many more syntheses have been reported in this medium. In addition to the vast number of solid binary and ternary fluorides produced from HF, many species have been produced in solution from the highly reducing $\text{Ti}_{(\text{solv})}^{2+}$ [31] and $\text{Sm}_{(\text{solv})}^{2+}$ [34] to $\text{Ag}_{(\text{solv})}^{\text{III}}$ and $\text{Ni}_{(\text{solv})}^{\text{IV}}$ described as "oxidants of unsurpassed power" [73].

References

- [1] R.J. Gillespie, E.A. Robinson, In: *Advances in Inorganic Chemistry and Radiochemistry*, Vol. 1, H.J. Emeléus, A.G. Sharpe (Eds.), Academic Press, 1959, p. 385.
- [2] R.J. Gillespie, T.E. Peel, E.A. Robinson, *J. Am. Chem. Soc.*, 93 (1971) 5083.
- [3] G.A. Olah, G.K. Surya Prakash, J. Sommer, *Superacids*, Wiley-Interscience, 1985, (a) pp. 11–14; (b) pp. 49–50.
- [4] T.A. O'Donnell, *Superacids and Acidic Melts as Inorganic Chemical Reaction Media*, VCH, New York, 1993, (a) pp. 38–41; (b) pp. 73–78; (c) 168, 139–145; (d) pp. 117–128.
- [5] Reprinted from Ref. [4] by permission of John Wiley and Sons, Inc.
- [6] R. Gut, *J. Fluorine Chem.*, 15 (1980) 163.
- [7] R.J. Gillespie, T.E. Peel, *J. Am. Chem. Soc.*, 95 (1973) 5173.
- [8] B. Carre, J. Devynck, *Anal. Chem. Acta*, 159 (1984) 149.
- [9] R. Gut, K. Gautschi, *J. Inorg. Nucl. Chem.*, Supplement (1976) 95.
- [10] R.J. Gillespie, J. Liang, *J. Am. Chem. Soc.*, 110 (1988) 6053.
- [11] (a) I. Gennick, K.M. Harmon, M.P. Potvin, *Inorg. Chem.*, 16 (1977) 2033; (b) D. Mootz, D. Boenigk, *Z. Anorg. Allg. Chem.*, 544 (1987) 159.
- [12] P.A.W. Dean, R.J. Gillespie, R. Hulme, D.A. Humphreys, *J. Chem. Soc. (A)*, (1971) 341.
- [13] R.J. Gillespie, K.C. Moss, *J. Chem. Soc. (A)*, (1966) 1170.
- [14] C.G. Barraclough, J. Besida, P.G. Davies, T.A. O'Donnell, *J. Fluorine Chem.*, 38 (1988) 405.
- [15] J. Devynck, A.B. Hadid, P.L. Fabre, B. Trémillon, *Anal. Chem. Acta*, 100 (1978) 343.
- [16] R.J. Gillespie, K. Ouchi, G.P. Pez, *Inorg. Chem.*, 8 (1969) 63.
- [17] D. Zhang, S.J. Rettig, J. Trotter, F. Aubke, *Inorg. Chem.*, 35 (1996) 6113.
- [18] K.C. Lee, F. Aubke, *Inorg. Chem.*, 18 (1979) 389.
- [19] K.C. Lee, F. Aubke, *Inorg. Chem.*, 23 (1984) 2124.

- [20] W.V. Cicha, F. Aubke, *J. Am. Chem. Soc.*, 111 (1989) 4328.
- [21] W.V. Cicha, D. Zhang, F. Aubke, *J. Fluorine Chem.*, 89 (1998) 117.
- [22] A. Engelbrecht, E. Tshager, *Z. Anorg. Allg. Chem.*, 433 (1977) 19.
- [23] J. Liang, PhD Thesis, McMaster University, 1976.
- [24] R. Adrien, PhD Thesis, University of Melbourne, 1992.
- [25] F. Aubke, M.S.R. Cader, F. Mistry, In: *Synthetic Fluorine Chemistry*, G.A. Olah, R.D. Chambers, G.K. Surya Prakash (Eds.), John Wiley and Sons, Inc., 1992, p. 43.
- [26] G.A. Olah, O. Farooq, S. Morteza, F. Farnia, J.A. Olah, *J. Am. Chem. Soc.*, 110 (1988) 2560.
- [27] C.G. Barraclough, R.W. Cockman, T.A. O'Donnell, *Inorg. Chem.*, 16 (1977) 673.
- [28] C.G. Barraclough, R.W. Cockman, T.A. O'Donnell, M. Snare, *Inorg. Chem.*, 27 (1988) 4504.
- [29] S.A. Kinkad, K.D. Abney, T.A. O'Donnell, In: *Handbook on the Physics and Chemistry of Rare Earths*, Vol. 18 – Lanthanides/Actinides: Chemistry, K.A. Gschneidner Jr., L. Eyring, G.R. Choppin, G.H. Lander (Eds.), Elsevier Science B.V., 1994, p. 507.
- [30] M. Baluka, N. Edelstein, T.A. O'Donnell, *Inorg. Chem.*, 20 (1981) 3279.
- [31] C.G. Barraclough, R.W. Cockman, T.A. O'Donnell, W.S.J. Schofield, *Inorg. Chem.*, 21 (1982) 2519.
- [32] H.A. Øye, D.M. Gruen, *Inorg. Chem.*, 3 (1964) 836.
- [33] D.H. Brown, A. Hunter, W.E. Smith, *J. Chem. Soc., Dalton Trans.* (1979) 79.
- [34] C.G. Barraclough, R.W. Cockman, T.A. O'Donnell, *Inorg. Chem.* 30 (1991) 340.
- [35] C.G. Barraclough, R.W. Cockman, T.A. O'Donnell, *Inorg. Chem.*, 30 (1991) 343.
- [36] F.G. Herring, G. Hwang, K.C. Lee, F. Mistry, P.S. Phillips, H. Willner, F. Aubke, *J. Am. Chem. Soc.*, 114 (1992) 1271.
- [37] S.H. Elder, G.M. Lucier, F.J. Hollander, N. Bartlett, *J. Am. Chem. Soc.*, 119 (1997) 1020.
- [38] D.M. Bruce, J.H. Holloway, *Transition Met. Chem.*, 3 (1978) 217.
- [39] N.M. Doherty, N.W. Hoffman, *Chem. Rev.*, 91 (1991) 553.
- [40] S.A. Brewer, J.H. Holloway, E.G. Hope, P.G. Watson, *J. Chem. Soc., Chem. Commun.*, (1992) 1577.
- [41] S.A. Brewer, J.H. Holloway, E.G. Hope, *J. Chem. Soc., Dalton Trans.*, (1994) 1067.
- [42] H. Willner, F. Aubke, *Inorg. Chem.*, 29 (1990) 2195.
- [43] H. Willner, J. Schaebs, G. Hwang, F. Mistry, R. Jones, J. Trotter, F. Aubke, *J. Am. Chem. Soc.*, 114 (1992) 8972.
- [44] A. Adelhelm, W. Bacher, E.G. Höhn, E. Jacob, *Chem. Ber.*, 124 (1991) 1559.
- [45] F. Aubke, C. Wang, *Coord. Chem. Rev.*, 137 (1994) 483.
- [46] M. Bodenbinder, G. Balzer-Jöllenbeck, H. Willner, R.J. Batchelor, F.W.B. Einstein, C. Wang, F. Aubke, *Inorg. Chem.*, 35 (1996) 82.
- [47] C. Wang, G. Hwang, S.C. Siu, F. Aubke, B. Bley, M. Bodenbinder, C. Bach, H. Willner, *Eur. J. Solid State Inorg. Chem.*, 33 (1996) 917.
- [48] H. Willner, F. Aubke, *Angew. Chem., Int. Ed. Engl.*, 36 (1997) 2402.
- [49] R.J. Gillespie, J. Passmore, In: *Advances in Inorganic Chemistry and Radiochemistry*, Vol. 17, H.J. Emeléus, A.G. Sharpe (Eds.), Academic Press, 1975, p. 49.
- [50] J. Besida, T.A. O'Donnell, *Inorg. Chem.*, 28 (1989) 1669.
- [51] B.D. Cutforth, C.G. Davies, P.A.W. Dean, R.J. Gillespie, P.R. Ireland, P.K. Ummat, *Inorg. Chem.*, 22 (1983) 1344.
- [52] R.C. Burns, R.J. Gillespie, W.-C. Luk, *Inorg. Chem.*, 17 (1978) 3596.
- [53] J. Besida, T.A. O'Donnell, unpublished observations.

- [53a] K.O. Christie, W.W. Wilson, J.A. Sheehy and J.A. Boatz, *Angew. Chem.*, 38 (1999) 2004.
- [54] C.G. Davies, R.J. Gillespie, P.R. Ireland, J.M. Sowa, *Can. J. Chem.*, 52 (1974) 2048.
- [55] P. Boldrini, I.D. Brown, M.J. Collins, R.J. Gillespie, E. Maharajh, D.R. Slim, J.F. Sawyer, *Inorg. Chem.*, 24 (1985) 4302.
- [56] R.J. Gillespie, J.P. Kent, J.F. Sawyer, *Inorg. Chem.*, 20 (1981) 3784.
- [57] M.P. Murchie, J. Passmore, C.-M. Wong, In: *Inorganic Syntheses*, Vol. 27, A.P. Ginsberg (Ed.), John Wiley and Sons, 1990, p. 332.
- [58] W.W. Wilson, R.C. Thompson, F. Aubke, *Inorg. Chem.*, 19 (1980) 1489.
- [59] T.A. O'Donnell, *Chem. Soc. Rev.*, 16 (1987) 1.
- [60] L. Stein, J.M. Neil, G.R. Alms, *Inorg. Chem.*, 8 (1969) 2472.
- [61] K.O. Christie, *Inorg. Chem.*, 16 (1977) 2238.
- [62] K.O. Christie, W.W. Wilson, R.D. Wilson, *Inorg. Chem.*, 19 (1980) 3254.
- [63] K. Lutar, A. Jesih, B. Žemva, *Revue de Chimie Minérale*, 23 (1986) 565.
- [64] A. Jesih, K. Lutar, I. Leban, B. Žemva, *Inorg. Chem.*, 28 (1989) 2911.
- [65] J. Whalen, G.M. Lucier, L. Chacón, N. Bartlett, *J. Fluorine Chem.*, 88 (1998) 107.
- [66] G.M. Lucier, J.M. Whalen, N. Bartlett, *J. Fluorine Chem.*, 89 (1998) 101.
- [67] B. Žemva, K. Lutar, A. Jesih, W.J. Casteel Jr., N. Bartlett, *J. Chem. Soc., Chem. Commun.*, (1989) 346.
- [68] W.J. Casteel Jr., A.P. Wilkinson, H. Borrmann, R.E. Serfass, N. Bartlett, *Inorg. Chem.*, 31 (1992) 3124.
- [69] G. Lucier, S.H. Elder, L. Chacón, N. Bartlett, *Eur. J. Solid State Inorg. Chem.*, 33 (1996) 809.
- [70] B. Žemva, K. Lutar, A. Jesih, W.J. Casteel Jr., A.P. Wilkinson, D.E. Cox, R.B. Von Dreele, H. Borrmann, N. Bartlett, *J. Am. Chem. Soc.*, 113 (1991) 4192.
- [71] B. Žemva, K. Lutar, L. Chacón, M. Fele-Beuermann, J. Allman, C. Shen, N. Bartlett, *J. Am. Chem. Soc.*, 117 (1995) 10025.
- [72] N. Bartlett, G. Lucier, C. Shen, W.J. Casteel Jr., L. Chacón, J. Munzenberg, B. Žemva, *J. Fluorine Chem.*, 71 (1995) 163.
- [73] G. Lucier, C. Shen, W.J. Casteel Jr., L. Chacón, N. Bartlett, *J. Fluorine Chem.*, 72 (1995) 157.
- [74] H.P.A. Mercier, G.J. Schrobilgen, *Inorg. Chem.*, 32 (1993) 145.
- [75] K.O. Christie, D.A. Dixon, H.G. Mack, H. Oberhammer, A. Pagelot, J.C.P. Sanders, G.J. Schrobilgen, *J. Am. Chem. Soc.*, 115 (1993) 11279.

CHAPTER 12

Fluoride Catalysts: Their Application to Heterogeneous Catalytic Fluorination and Related Processes

Erhard Kemnitz^a and John M. Winfield^b

^a *Institut für Chemie, Humboldt-Universität zu Berlin, Hessische Str. 1–2, 10115, Berlin, Germany*

^b *Department of Chemistry, University of Glasgow, Glasgow, G12 8QQ, UK*

12.1 Introduction

‘A catalyst is by definition a substance that increases the rate of approach to equilibrium of a chemical reaction without being substantially consumed in the reaction’ [1] and the concept of catalysis is thus ubiquitous throughout all branches of chemistry, fluorine chemistry being no exception. Fluoride anion is possibly the most widely used fluorine-containing catalyst, certainly for laboratory syntheses, since depending on the counter-cation, it is capable of high catalytic activity. Less widely appreciated, but nevertheless important, is the promotion of the Brønsted and/or Lewis acidity of a metal oxide surface by pre-treatment with NH_4F or a volatile, covalent fluoride, prior to its use as a catalyst or catalyst support material. An important sub-set of reactions within the latter application is catalytic fluorination, reactions in which carbon–halogen (normally chlorine) bonds are converted to carbon–fluorine using anhydrous hydrogen fluoride as the fluorinating agent. Reactions may be performed under homogeneous conditions using HF as the solvent and reactant or under heterogeneous (gas–solid) conditions depending on the organic substrate involved. Antimony(V) chloride has been a widely used catalyst-precursor for homogeneous work, while fluorinated γ -alumina or chromia have normally been the catalysts of choice for use under heterogeneous conditions.

In this chapter, recent advances in our understanding of catalytic fluorination under heterogeneous conditions are surveyed from the standpoint of catalyst properties, including developments based on the use of mixed metal fluorides having different structural types, and reaction mechanisms. Much of the newer work has been the result of the need to replace chlorofluorocarbons (CFCs) by alternatives, hydrofluorocarbons (HFCs) or, more controversially, hydrochlorofluorocarbons (HCFCs), following adoption of the Montreal and successor Protocols [2,3]. Where relevant, aspects of catalytic hydrogenolysis, where fluorides have been used as replacement supports in the conventional palladium/carbon catalysts, and isomerization reactions are included.

12.1.1 The situation prior to the mid 1980s

The well established routes for the large scale production of CFCs such as CCl_2F_2 (CFC-12) and $\text{CCl}_2\text{FCClF}_2$ (CFC-113) involved homogeneous catalytic fluorination of the chlorocarbons CCl_4 and C_2Cl_6 (or a $\text{C}_2\text{Cl}_4, \text{Cl}_2$ mixture). Heterogeneous catalytic fluorination using chromia or γ -alumina based catalysts was used to prepare more highly fluorinated members of the ethane series, particularly $\text{C}_2\text{Cl}_2\text{F}_4$ isomers (CFC-114 and 114a) and CClF_2CF_3 (CFC-115). These processes were profitable and there was little apparent need to develop new catalysts or to understand the mechanisms of catalysis. Investigation of the fundamentals of heterogeneous catalytic fluorination was therefore a somewhat esoteric research activity but was pursued actively by a few groups.

Replacement of C—Cl by C—F bonds in the C_2 series characteristically leads to mixtures of compounds and under heterogeneous conditions, even when an excess of HF is used, highly chlorinated CFCs are always byproducts from reactions designed to produce highly fluorinated products such as $\text{CClF}_2\text{CClF}_2$ or CClF_2CF_3 . In one of the early, classic, studies of the catalytic $\text{C}_2\text{Cl}_6 + \text{HF}$ reaction, the distribution of products obtained was rationalized by postulating that even in the presence of a large excess of surface fluoride on the catalyst, sufficient catalytically active surface chloride was present, for catalytic chlorination to be significant [4]. In an alternative rationalization advanced a little later [5,6], it was suggested that catalytic fluorination was accompanied by dismutation and isomerization of chlorofluoroethanes on the catalyst surface, therefore the distribution of compounds isolated within the series $\text{C}_2\text{Cl}_{6-n}\text{F}_n$ would depend critically upon the interplay among quite different surface processes, fluorination, for example $\text{CCl}_2\text{FCClF}_2 \rightarrow \text{CClF}_2\text{CClF}_2$, dismutation, for example $2\text{CCl}_2\text{FCClF}_2 \rightarrow \text{CCl}_3\text{CClF}_2 + \text{CClF}_2\text{CClF}_2$, and isomerization, for example $\text{CCl}_2\text{FCClF}_2 \rightarrow \text{CCl}_3\text{CF}_3$ [5–9]. Although the behaviour of $\text{CCl}_2\text{FCClF}_2$ on chromia/carbon catalysts in the absence of HF is consistent with the importance of isomerization and dismutation [10], the evidence for the model is essentially circumstantial, being based purely on analyses of product distributions.

Direct evidence for a combination of catalytic fluorination and chlorination [4] was obtained from radiotracer studies in which fluorinated chromia catalysts were labelled with the short-lived ($t_{1/2} = 110$ min) β^+ emitting isotope fluorine-18 [11]. Using this isotope it was possible to probe the interactions between HF and various fluorinated chromia catalysts more directly than had been possible hitherto. Three types of surface F-containing species were differentiated, weakly adsorbed HF which was easily removed by an inert gas flow, non-labile F, believed to be bound directly to surface Cr^{III} , and catalytically active F which could be incorporated into the organic products [12]. The controversy between dismutation (concerted F-for-Cl and Cl-for-F transfers) and non-concerted halogen exchange processes has been resolved more recently and the evidence is described later in the chapter. What is clear from this early work however, is the importance of aluminium and chromium(III) oxides as catalyst precursors. Fluorination of the surfaces of these oxides is slow (cf [12]) and although there are many references to alu-

minium and chromium(III) fluoride catalysts, particularly in the patent literature, in these early studies there was no real evidence for complete fluorination of the surface. We return to this point later.

Possibly because of the importance of homogeneous catalytic fluorination for C_1 compounds, less attention was paid to catalytic fluorination of CCl_4 under heterogeneous conditions. However, in an important early study of the $HF + CCl_4$ reaction over an aluminium fluoride catalyst, the effect of strongly adsorbed HF on the catalyst surface was demonstrated [13]. Dismutation of CF_3Cl on a mixed alumina/chromia catalyst was also shown to occur, the mixed oxide being more active than either component alone [14]. Also during this period, the heterogeneous non-catalytic fluorination of CH_2Cl_2 at 773 K by a NaF/KF mixture was reported, the products being CH_2ClF and CH_2F_2 [15]. Kinetic studies of the heterogeneous fluorination of CCl_4 vapour by Group 1 fluorides or the tertiary fluorides $KFeF_4$ and K_3FeF_6 , laid the basis for future kinetic studies of catalytic reactions leading to HCFCs, by emphasising the importance of equilibria involving adsorbed states and the effect on the reaction of the chlorine-containing phases formed [16].

12.1.2 Some consequences of the Montreal protocol

The challenge for manufacturers of CFCs and their bromine-containing analogues (Halon) was straightforward, to devise economically viable syntheses of molecules that would have the desirable properties of CFCs without the long atmospheric lifetimes characteristic of these compounds. Much defensive research had already been carried out by CFC producers and it was recognised that hydrofluorocarbons represented the most obvious candidates with hydrochlorofluorocarbons (HCFCs) being a possibility for use as transitional compounds [2,3]. It was recognized also that the market for CFC alternatives would be significantly smaller than for CFCs, since many applications of the latter, for example aerosol and foam blowing agents, cleaning agents for electronic components, would be fulfilled in completely different ways. Attention has therefore been concentrated on refrigerants, the 'market leader' being 1,1,1,2-tetrafluoroethane, CF_3CH_2F (HFC-134a) which is a drop-in alternative to the widely used CFC, CCl_2F_2 [2,3].

In contrast to the situation for C_2 CFCs, there was no single obvious route to CF_3CH_2F . Three of the most attractive, starting from the feedstocks trichloroethene, tetrachloroethene/ Cl_2 ($=C_2Cl_6$) or tetrachloroethene alone, involve (i) hydrofluorination of $CCl_2=CHCl$ followed by a series of F-for-Cl replacement steps; (ii) a series of F-for-Cl and isomerization steps leading to CF_3CCl_2F followed by its hydrogenolysis; and (iii) hydrofluorination of C_2Cl_4 , a series of F-for-Cl replacement steps leading to CF_3CHClF , followed by its hydrogenolysis. The types of reactions that are relevant to the synthesis of CF_3CH_2F are summarised in Table 1.

Heterogeneous catalysis is important in all cases. The catalytic fluorination steps (F-for-Cl replacement) either use existing chlorofluoroethane methodology or new methodology for the catalytic fluorination of the C_2 HCFCs. Development of new catalysts was particularly important for the conversion of CF_3CH_2Cl to

Table 1

Types of catalytic reaction relevant to the synthesis of $\text{CF}_3\text{CH}_2\text{F}$

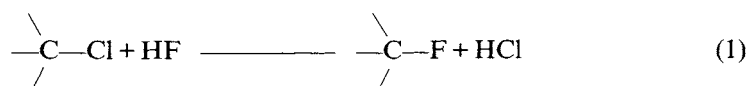
Reaction type	Examples
Hydrofluorination	$\text{CHCl}=\text{CCl}_2 + \text{HF} \rightarrow \text{CH}_2\text{ClCCl}_2\text{F}$ $\text{CCl}_2=\text{CCl}_2 + \text{HF} \rightarrow \text{CHCl}_2\text{CCl}_2\text{F}$
Fluorination	$\text{CH}_2\text{ClCCl}_2\text{F} + 2\text{HF} \rightarrow \text{CH}_2\text{ClCF}_3 + 2\text{HCl}$ $\text{CH}_2\text{ClCF}_3 + \text{HF} \rightarrow \text{CH}_2\text{FCF}_3 + \text{HCl}$ $2\text{C}_2\text{Cl}_6 + 4\text{HF} \rightarrow \text{CClF}_2\text{CClF}_2 + \text{CCl}_2\text{FCF}_3 + 4\text{HCl}$ $\text{CHCl}_2\text{CCl}_2\text{F} + 2\text{HF} \rightarrow \text{CHCl}_2\text{CF}_3 + 2\text{HCl}$ $\text{CHCl}_2\text{CF}_3 + \text{HF} \rightarrow \text{CHClFCF}_3 + \text{HCl}$
Isomerization	$\text{CClF}_2\text{CClF}_2 \rightarrow \text{CCl}_2\text{FCF}_3$ $\text{CCl}_2\text{FCClF}_2 \rightarrow \text{CCl}_3\text{CF}_3$
Hydrogenolysis	$\text{CCl}_2\text{FCF}_3 + \text{H}_2 \rightarrow \text{CH}_3\text{FCF}_3 + 2\text{HCl}$ $2\text{CHClFCF}_3 + \text{H}_2 \rightarrow 2\text{CH}_2\text{FCF}_3 + 2\text{HCl}$

$\text{CF}_3\text{CH}_2\text{F}$, a reaction which is limited thermodynamically. Hydrogenolysis of $\text{CF}_3\text{CCl}_2\text{F}$ (and its isomer $\text{CClF}_2\text{CClF}_2$) is traditionally carried out using palladium catalysts supported on carbon, the asymmetric isomer being more reactive to replacement of C—Cl by C—H [17]. However, in contrast to the hydrogenolysis and hydrogenation of hydrocarbons, halocarbon behaviour with respect to these processes has received relatively little attention. In very early work [18,19] it was established that lower members of an homologous CFC series undergo hydrogenolysis with greater difficulty than the higher members, that F is more difficult to replace by H than is Cl and that, in halo-olefins, Cl is replaced by H *before* hydrogenation of C=C occurs. Later mechanistic work [20], extrapolating from mechanisms postulated originally for the hydrogenolysis of chlorocarbons [21], led to the conclusions that hydrogenolysis of C—F occurs most readily in compounds that contain no more than one F per C atom (hydrogenolysis of a CF_3 -group is very rare) and that hydrogenation of C=C is faster than hydrogenolysis of C—F [20]. However much work in the area of catalytic hydrogenolysis remains to be done, the most important problem being to produce catalysts with longer lifetimes than that of Pd/C, where deactivation is relatively rapid.

In this section the two major challenges that follow from the introduction of $\text{CF}_3\text{CH}_2\text{F}$ as an alternative refrigerant have been introduced. The remainder of the chapter traces some of the recent progress that has been made in the development of new catalytic materials potentially of use in the fluorination of hydrochlorofluorocarbons and catalyst supports for Pd in the hydrogenolysis of CFCs. The rational design of new catalysts is aided by an understanding of mechanisms, therefore recent work in this area is surveyed. Inevitably these two aspects of catalytic chemistry merge to some extent.

12.2 Chromia and alumina based fluorination catalysts

As described above, the non-oxidative substitution of chlorine by activated fluorine is one of the most important synthetic routes from the industrial point of view. In these reactions, a C—Cl is replaced by a C—F bond using an appropriate fluorinating agent such as HF. Among all technically-relevant catalysed halogen exchange reactions, synthesis of chlorofluorocarbons, hydrochlorofluorocarbons, and hydrofluorocarbons performed according Eqn. (1) are doubtless the most important processes.



Although the first technical plants for CFC manufacturing used the Swarts catalyst exclusively, heterogeneously catalysed processes are competitive in the situations described above. Metal(III) oxides, especially chromia and alumina, are frequently used as solid catalysts. Moreover, they have often been used mixed with traces of other, usually metal(II), oxides, to prepare catalysts that have perceived advantages.

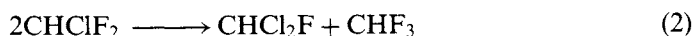
The public pressure for replacing CFCs by HFCs resulted in a strong boost for fundamental research on the action of heterogeneous fluorination catalysts and on the mechanism of halogen exchange reactions at the catalyst surface. However, as will be demonstrated, highly fluorinated phases, formed at the oxide surface as a result of the interaction of the solid with the fluorine containing gas phase reagent, most probably act as the catalytically active phases.

12.2.1 Fluorinated chromia

The catalytic properties of chromia have attracted considerable attention and only a few metal oxides, for example silica and alumina, have been more extensively studied than chromia. It is established as an excellent heterogeneous catalyst for fluorination reactions. Chromia and fluorinated chromia catalysts have been cited in numerous patents during the last ten years, e.g. [22–28], because chromia related compounds exhibit enhanced catalytic activity and improved selectivity in comparison with alumina. Chromia belongs to the group of *n*-type semiconducting ceramics occurring with the structure of the corundum type in which the cations occupy distorted octahedral sites surrounded by six O ligands. The (0001) surfaces have been extensively investigated [29]. It has been concluded from ion scattering spectroscopic measurements [30] as well as from LEED-I/V analysis [31,32] that the volume terminated surface structures [33–35] are the result of a reconstruction resulting in a surface where only half of the expected Cr atoms are present and are nearly completely imbedded in the oxygen layer [32]. In contrast, under ordinary conditions, uncalcined, newly prepared chromia contains large quantities of water and hydroxyl groups which saturate the metal sites that remain at the surface. Consequently, activation of chromia involves a dehydration of the surface, resulting

in coordinatively unsaturated Cr(III) which can act as active sites. These hydroxyl groups play a key role in the necessary activation step of chromia to be used as a fluorination catalyst. It is well known that a metal oxide catalyst requires activation for a certain time either in HF and/or a CFC/HFC gas stream until it becomes catalytically active [7]. Thus, chromia catalysts used for halogen exchange require an activation procedure in order to achieve high activity [14,36]. Although chemical analysis indicates significant uptake of halogen by the solid, X-ray diffraction commonly does not provide any evidence for change of the bulk composition [5,6,37].

The changes occurring during the initial activation stage of chromia are illustrated in Fig. 1 on the basis of coupled thermal analysis mass spectrometry measurements for the dismutation reactions of CHClF_2 and CHCl_2F , Eqns (2) and (3).



Under dynamic-thermal conditions [38], the onset temperature at which the reaction between the solid and the gas phase starts, detected by a sudden increase in weight

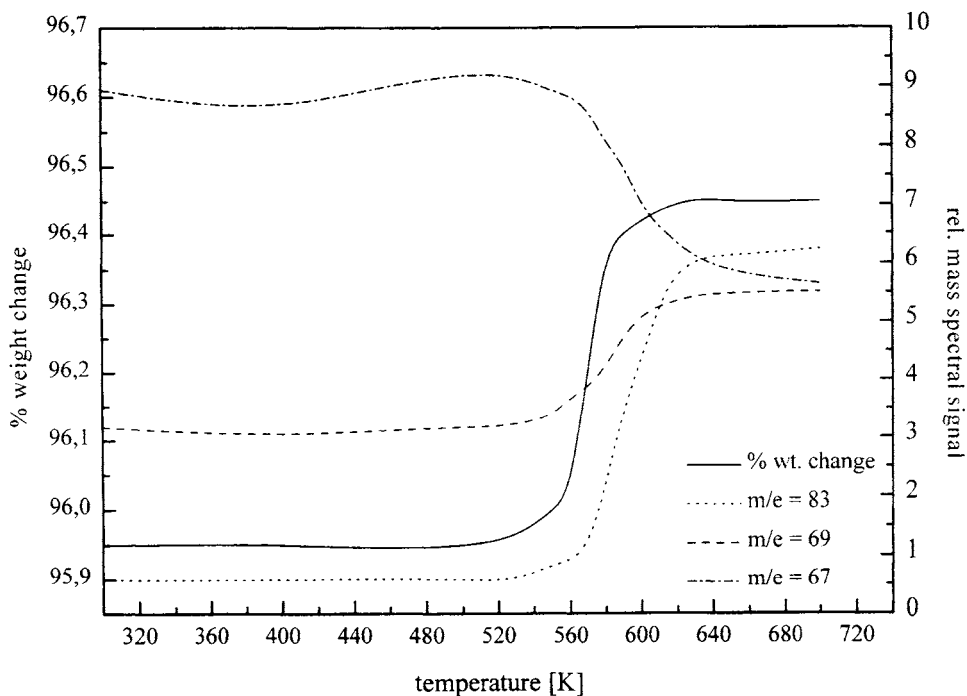
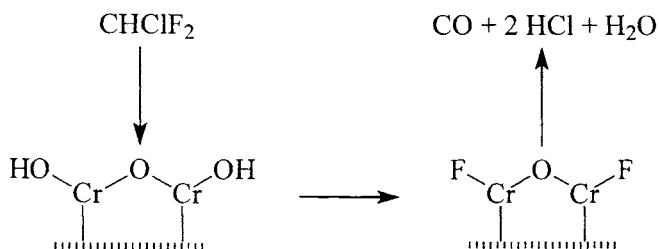


Fig. 1. TGA-MS spectra of products arising from conditioning of chromia using CHClF_2 $m/e_{(83)} = \text{CHCl}_3$; $m/e_{(69)} = \text{CHF}_3$; $m/e_{(67)} = \text{CHClF}_2$ (reproduced with permission from J. Catal., 140 (1993) 103 [38]).

due to the capture of halogen by the chromium oxide, was approximately 573 K. Simultaneously, the conversion of CHClF_2 to the dismutation products (CHF_3 and CHCl_3) was observed at ca 573 K, suggesting that the halogen uptake by the catalyst coincides with the onset of catalytic activity. Under isothermal conditions, the dismutation of CHClF_2 commences about 523 K [39]. The difference in the onset-temperatures of about 50 K is due largely to the different conditions used. Even under these conditions, the catalyst precursor requires a certain time of activation during its interaction with the CFC gas phase. Within only a few minutes, fundamental changes in the properties of the solid surface occur and it becomes catalytically active, resulting in a rapid establishment of the dismutation equilibrium. The increase of the catalytic activity is accompanied by a rapidly increasing liberation of HCl followed by a decrease in HCl concentration in the effluent. The process of HCl evolution is complete at nearly the same time as the catalyst reaches its full activity. Other gaseous fluoroalkanes exhibit similar behaviour, however the time required to obtain full catalytic activity and the extent of HCl evolution depend on the fluoroalkane used [39]. Although there is no indication for the formation of any chromium halides from XRD measurements, chemical analysis indicates the uptake of fluorine and chlorine by the solid, some few percent of fluoride and up to 0.4% chloride. Evidently halogenation of chromia, at least at the surface, is required for it to be catalytically active for fluorine/chlorine exchange reactions. Reaction between surface OH groups and a fluoroalkane molecule leads to destruction of the latter and the formation of hydrogen halides and CO_2 or CO (cf Scheme 1). This was demonstrated for the heterogeneously catalysed hydrolysis reaction of CFCs on γ -alumina and chromia surfaces [40]. As long as OH groups or adsorbed water molecules are present to act as Brønsted sites on the surface, a heterogeneous reaction between gaseous CFCs/HFCs and these Brønsted acid centres occurs, resulting in destruction of the halocarbon followed by fluorination of the solid surface.

Mechanistically different but resulting in a similar change of the surface, is the behaviour of C_2 hydrohalocarbons. In a study of $\text{CF}_3\text{CH}_2\text{Cl}$ fluorinated over unfluorinated chromias and chromias fluorinated to differing degrees it was observed that, in the absence of HF, the reaction of $\text{CF}_3\text{CH}_2\text{Cl}$ over fluorinated chromia led to large quantities of olefins in the effluent stream [41]. It is believed that



Scheme 1

Reaction of a CHClF_2 molecule with hydroxyl groups on a chromia surface

dehydrohalogenation/addition reactions play a key-role in the synthesis of $\text{CF}_3\text{CH}_2\text{F}$ starting from trichloroethene [42,43]. This leads to the suggestion that dehydrofluorination is an important reaction when a hydrofluorocarbon is allowed to react in the presence of an unfluorinated chromia.

The values of the free energies of selected heterogeneous reactions between stoichiometric Al_2O_3 or Cr_2O_3 and possible gaseous reactants (Table 2) illustrate the thermodynamic considerations involved. In the alumina system, formation of Al—F bonds is likely to be favoured strongly over that of Al—Cl bonds, however the values of the $\text{Cr}_2\text{O}_3 + \text{HX}$ reaction enthalpies are of the same order of magnitude and uptake of both halogens by chromia might be expected.

Since X-ray diffraction analysis is not helpful in detecting solid phases formed at the surface which may be catalytically active, other techniques were used to obtain information relating to the active surface sites of fluorinated chromia. Although using the tracer [^{18}F] it is possible to differentiate among three different surface fluoride species [12], these studies do not enable the nature of the solid phases formed during the activation process to be determined with certainty. Therefore, XPS studies have been performed by several groups [10,38,39] in order to follow the changes of the oxide surface arising from fluorination. Up to 10 w/w% surface fluoride was detected employing gaseous HF and about 8% using CHF_3 as the fluorinating agent. Surprisingly, the Cr $2p_{3/2}$ binding energy did not exhibit any significant changes as a result of surface fluorination. However, from the value for the F 1s binding energy, ca 684.2 eV, strong evidence for the formation of fluorinated chromia species was obtained [38]. Later, more extensive XPS measurements on chromia, fluorinated chromia, and chromium fluoride phases clearly demonstrated that these values are not characteristic of completely fluorinated chromia samples but are indicative of partly fluorinated chromia surfaces [39].

Figure 2 provides an overview of the characteristic changes resulting from the fluorination of the chromia surface [39], here given in so called “chemical state plots” according Wagner and Joshi [45]. In such plots, binding energies (BE) of the photoelectrons for an element are plotted vs the kinetic energy (KE) of the respective Auger electrons. The modified Auger parameter data (linear relationships), carrying

Table 2

Free energies for some selected gas/solid reactions [44]

Reaction	$\Delta G_F^\phi / \text{kJ mol}^{-1}$
$\text{Al}_2\text{O}_3 + 3\text{CHClF}_2 \rightarrow 2\text{AlF}_3 + 3\text{CO} + 3\text{HCl}$	−690
$\text{Al}_2\text{O}_3 + 3\text{CHCl}_2\text{F} \rightarrow 2\text{AlCl}_3 + 3\text{CO} + 3\text{HF}$	−193
$\text{Al}_2\text{O}_3 + 6\text{HF} \rightarrow 2\text{AlF}_3 + 3\text{H}_2\text{O}$	−329
$\text{Al}_2\text{O}_3 + 6\text{HCl} \rightarrow 2\text{AlCl}_3 + 3\text{H}_2\text{O}$	+211
$\text{Cr}_2\text{O}_3 + 3\text{CHClF}_2 \rightarrow 2\text{CrF}_3 + 3\text{CO} + 3\text{HCl}$	−460
$\text{Cr}_2\text{O}_3 + 3\text{CHCl}_2\text{F} \rightarrow 2\text{CrCl}_3 + 3\text{CO} + 3\text{HF}$	−429
$\text{Cr}_2\text{O}_3 + 6\text{HF} \rightarrow 2\text{CrF}_3 + 3\text{H}_2\text{O}$	−68
$\text{Cr}_2\text{O}_3 + 6\text{HCl} \rightarrow 2\text{CrCl}_3 + 3\text{H}_2\text{O}$	−56

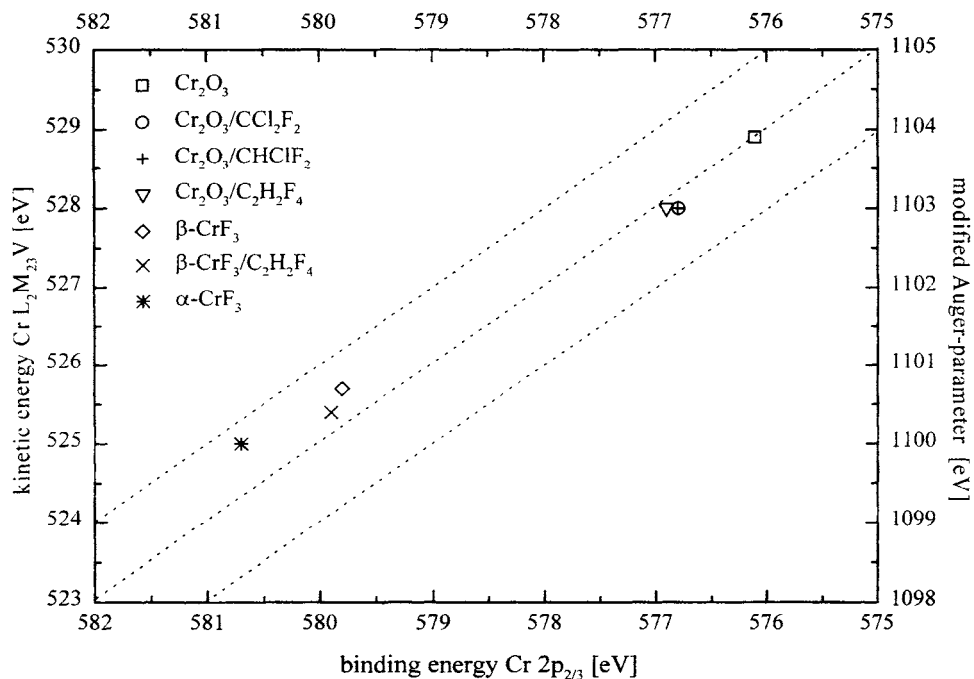


Fig. 2. Chromium chemical state plot for chromium oxide and fluoride samples before and after activation with halocarbons (static charge reference C 1s: 284.8 eV) (reproduced with permission from J. Catal., 159 (1996) 270 [39]).

additional analytical information, are included, and the chemical state plot of Cr data determined from untreated pure chromium compounds (used as reference samples) and the treated samples are given. Considering only pure untreated Cr_2O_3 and CrF_3 samples, two distinct regions of binding energy are apparent. One region is characteristic for chromium oxide bonds (about 576 eV) whereas the other one is due to chromium fluoride bonds (around 580 eV). Apparently, the activation of chromia results in nearly the same shift of the XPS data, even if different fluoroalkanes are used. However, neither $\text{Cr } 2p_{3/2}$ nor F1s binding energies (cf Fig. 3) of the treated samples are located in the regions expected for pure chromium fluorides but chromium can be described as being partially fluorinated. In agreement with the thermodynamic considerations above (Table 2), chromia is partially fluorinated. It is still uncertain whether there are domains of pure chromium fluoride at the surface of treated samples or larger areas of chromium oxofluoride species. The latter seems to be more likely.

Chromium can exist in several oxidation states and early EPR studies suggested that the catalytic activity of chromia is related strongly to the presence of different oxidation states on the surface [46]. Small amounts of $\text{Cr}^{>3+}$ in chromia can be attributed to high temperature synthesis procedures (e.g. incomplete thermolysis of ammonium dichromate), however, oxidized Cr-sites can also be formed in contact

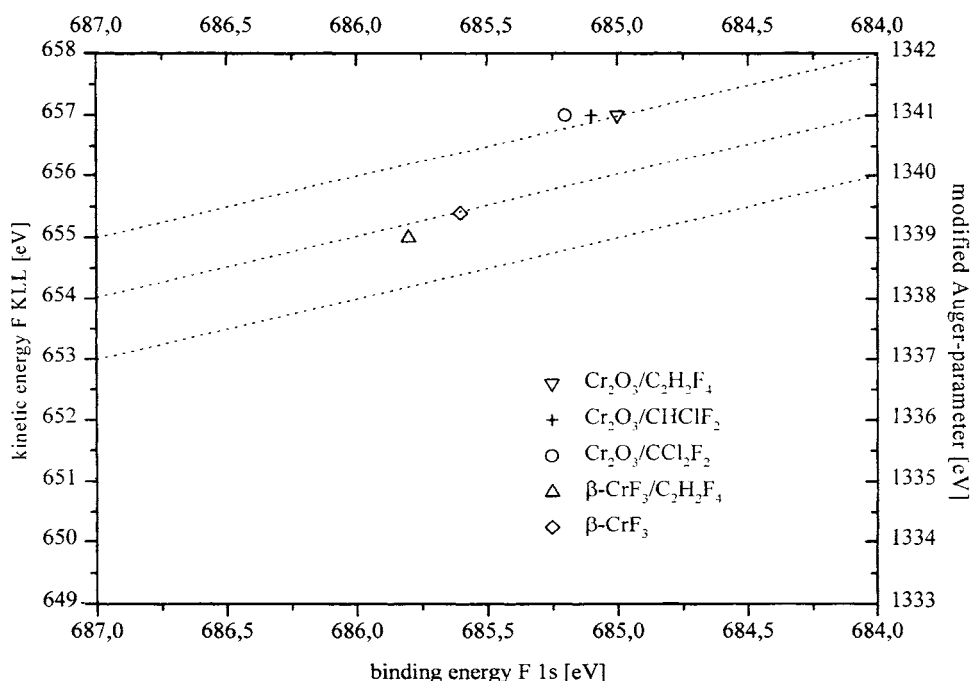


Fig. 3. Fluorine chemical state plot for chromium oxide and fluoride samples before and after activation with halocarbons (static charge reference C 1s: 284.8 eV) (reproduced with permission from J. Catal. 159 (1996) 270 [39]).

with air at slightly elevated temperatures. Hence, the influence of the oxidation state of chromium is a point of special interest. This facet of, nominally, Cr_2O_3 was observed by several workers concerned with different catalytic reactions of this oxide [11,47–49]. The interaction of chromia surfaces with dihydrogen was ascribed to the reduction of Cr^{4+} and Cr^{6+} surface sites [11]. Moreover, the activity of chromia for dismutation reactions of CHClF_2 was found to depend strongly on the oxidation state of chromium at the surface [38]. Employing different gases, e.g. air, N_2 , CO, for the final calcination step of chromia, results in different catalytic activities, even after surface fluorination, which led to the conclusion that the creation of active sites in this reaction involves a reduction of high-valent chromium ions.

On the basis of temperature programmed reduction and oxidation (TPR-TPO) measurements, it was proposed that the calcination of chromia used as a catalyst for the selective fluorination of $\text{CF}_3\text{CH}_2\text{Cl}$ into $\text{CF}_3\text{CH}_2\text{F}$ depends strongly on the gas used to calcine the precursor [50]. Furthermore, the fluorination of $\text{CF}_3\text{CH}_2\text{Cl}$ depends directly on the number of reversibly oxidizable chromium atoms in the catalysts. The oxidation/reduction properties are related closely to the atmosphere of pre-treatment and a linear relationship between the catalytic activity and the hydrogen uptake during the second reduction step has been found [51].

Fluorinated chromia used to catalyze the isomerization reaction of CHF_2CHF_2 to $\text{CF}_3\text{CH}_2\text{F}$, also exhibited evidence for the importance of chromium in higher oxidation states. FTIR spectroscopic measurements of CO adsorption confirmed the occurrence of Cr^{4+} and Cr^{5+} on the surface of chromia catalysts before being used [52]. During the activation, Cr^{4+} and Cr^{5+} sites were reduced and enhanced activity of the catalyst was observed. The reaction pathway proposed for isomerization involves the formation of hydrogen fluoride due to the degradation reaction of the fluoroalkane.

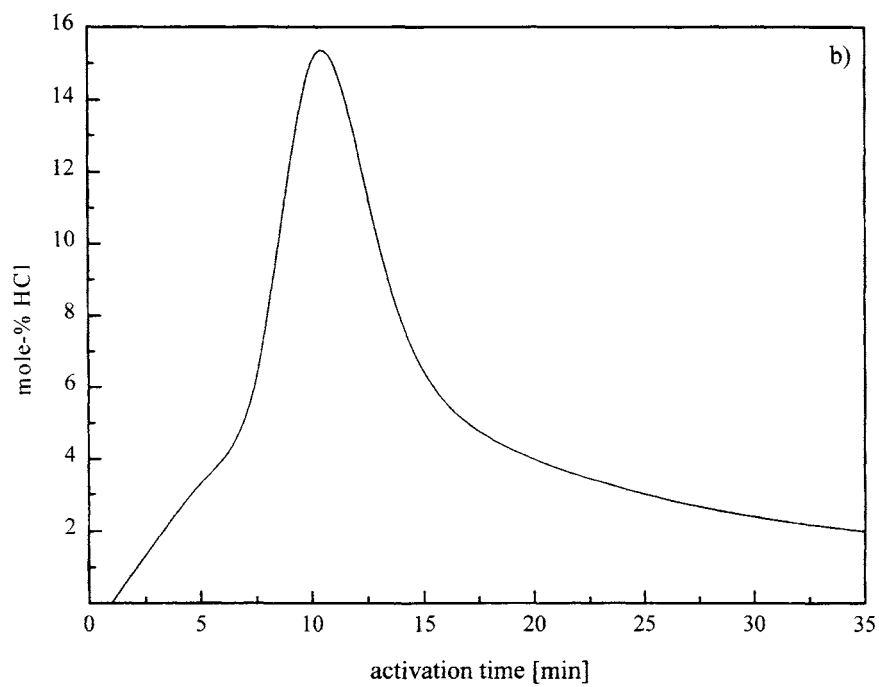
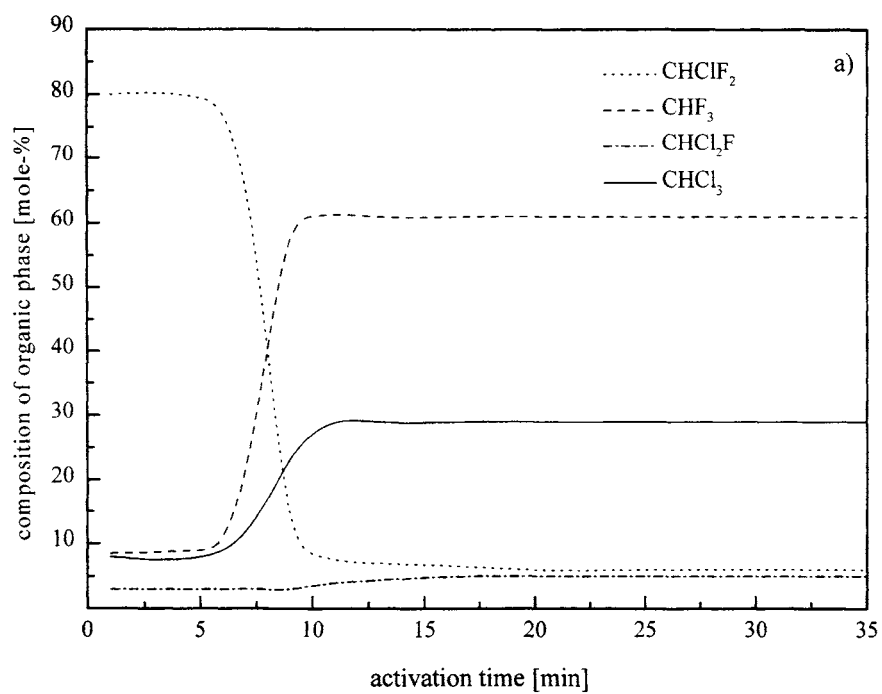
From these results, for the chromium system one may propose the following ideas regarding the catalytic active surface sites. In general, fluorination leads to a replacement of a less electronegative element (oxygen) by a more electronegative one (fluorine). This results in a higher positive charge at the metal sites and, therefore, in an increased Lewis acidity.

Secondly, treatment of precursor by "in situ" reduction of $\text{Cr}^{>3+}$ sites using suitable reductants, e.g. HFCs, CO, H_2 , results in Cr^{3+} sites which provide improved accessibility for nucleophilic gaseous molecules due to their lower co-ordination.

12.2.2 Fluorinated alumina

Commonly, non-corundum aluminium(III) oxide phases are used as heterogeneous catalysts for halogen exchange reactions. These metastable phases usually belong to the γ -alumina class including crystalline, pseudo-crystalline, and amorphous materials, too many to be described in detail here. γ -Alumina has a defect spinel lattice with cubic close packing and some distortion in the anionic sublattice. Due to non-occupied tetrahedral cation sites, a decreased density is observed and the ability to incorporate other cations is apparent. Large specific surface areas as well as large pore volumes usually cause high reactivity, enhanced sorption capacity, and good catalytic activity. All non-corundum phases contain varying amounts of water and/or hydroxyl groups at the surface. By calcination of alumina, surface hydroxyl groups acting as Brønsted centers can be removed as water, thus generating Lewis acid sites at the surface. These surface hydroxyl groups play a key role in the activation of aluminas used in heterogeneous fluorination reactions as will be shown below.

As with the chromia system, alumina must be activated before being used as a catalyst. Under isothermal conditions at 523 K, the activation of alumina prior to the dismutation reaction of CHCl_2F parallels the behaviour of chromia as discussed above [53]. As can be seen from Fig. 4, here too, within a short period, the catalyst becomes active resulting in a rapid establishment of the dismutation equilibrium (Fig. 4(a) and (c)). This is accompanied by the rapid liberation of HCl whereas only traces of HF are detected in the gas phase. Although XRD gives no indication for the formation of any aluminium halides, up to 13 mass% fluoride was found after 40 min. but only traces of chloride, ranging from 0.05 to 0.3%. Even higher degrees of fluorination were achieved using high surface area, highly reactive



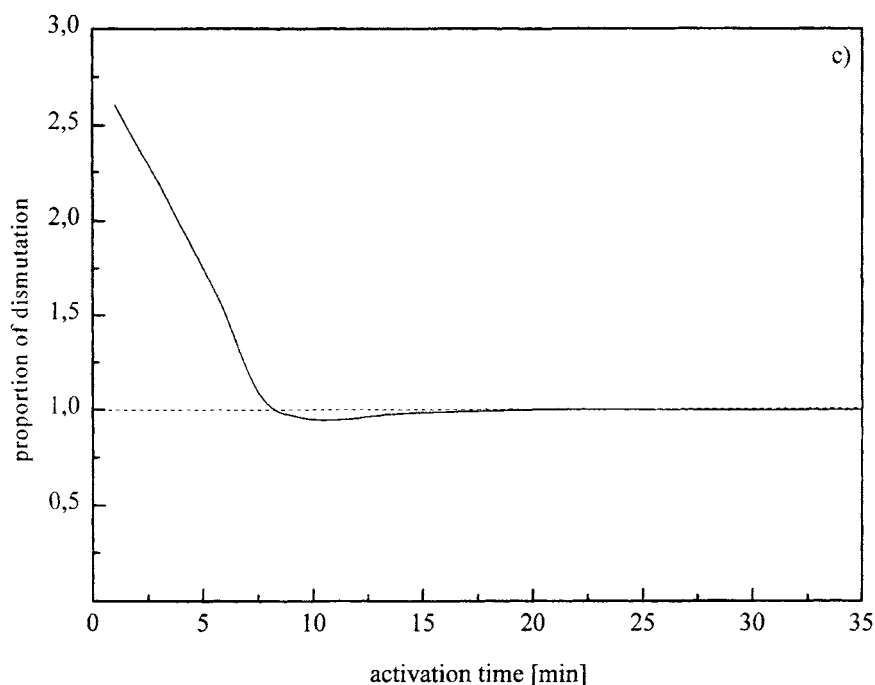


Fig. 4. Change of the gas phase composition during conditioning of γ -alumina using CHCl_2F at 532 K. (a) concentration of haloalkanes in the gas phase; (b) concentration of HCl released; (c) dismutation ratio ($\text{dm} = 1$ represents the theoretical ratio) (reproduced with permission from J. Prakt. Chem., 334 (1992) 591 [53]).

alumina aerogels [54,55]. Within a comparable time a significantly higher degree of fluorination was achieved using CHF_3 as the conditioning gas.

In contrast to the chromia system, the formation of AlF_3 is strongly favoured over that of AlCl_3 (Table 2), being in full agreement with experimental observation. In order to evaluate whether the alumina surface becomes partially or completely fluorinated, the formation of aluminium fluoride phases formed after impregnation of alumina with aqueous ammonium fluoride followed by calcination, was investigated employing ^{27}Al NMR spectroscopy [56]. In agreement with previous findings [57] the authors found that $\text{Al}(\text{OH},\text{F})_3$, $\text{AlF}_3 \cdot n\text{H}_2\text{O}$, and AlF_3 phases are formed and it was concluded that a transformation of alumina to AlF_3 via $\text{Al}(\text{OH},\text{F})_3$ had occurred. A simplified reaction pathway was described which includes the intermediate formation of several hydroxyfluorides.

Amorphous, fluorinated alumina catalysts were also investigated with respect to their potential to convert acetylene to high-octane fuel components [58]. The highest activity of fluorinated alumina samples was found for catalysts containing between 1.5 and 3% fluoride. However, no comment was made regarding the new solid phases formed but calcined $\text{AlF}_3 \cdot 3\text{H}_2\text{O}$, also tested for comparison, showed no catalytic activity. Fluorination of alumina catalysts with CHF_3 or C_2HF_5 at 773 K resulted

in a crystalline fluorinated product, α -AlF₃, and unreacted γ -alumina [59]. In agreement with the findings of others [60–64], there were no indications for the formation of β -AlF₃ or other fluoride phases. However, at these temperatures, the meta-stable β -AlF₃ would be converted to the stable α -AlF₃ phase [65–67].

Other fluorinating agents than CFCs were used such as SF₄, OSF₂, OCF₂, and HF. Under the experimental conditions employed, there was no evidence for the formation of bulk α -AlF₃ and the fluorination treatment was regarded as an efficient means of reducing significantly the surface hydroxyl groups present on the surface [68]. By analogy with earlier work [69], it was assumed that surface Al—F bonds were formed. However, there are differences among the four reagents used with respect to both the extent of fluorination achieved and the ability of the solid fluorine species to undergo [¹⁸F] exchange with HF. SF₄ was found to generate stronger Lewis acid sites at the γ -alumina surface than OSF₂. Although there is no observable exchange between HF and anhydrous aluminium(III) fluoride under similar conditions, addition of H₂O vapour which presumably results in hydroxylation and hydration of the surface, leads to substantial [¹⁸F] exchange.

Using an approach similar to that already described for chromia, the changes occurring on alumina surfaces during the activation stage were investigated by means of photoelectron spectroscopy [70]. Using Al 2p, O 1s, as well as F 1s photo peaks, comprehensive information relating to the surface changes can be obtained. Using CHClF₂ or CClF₂CH₃ to activate γ -alumina or Al(OH,F)₃·yH₂O led to a final surface product whose binding energies are higher (688.1–689.1 eV) than those of α -AlF₃ (687.5 eV), or β -AlF₃ (687.8 eV). Binding energies are w.r.t. aliphatic C 1s = 248.8 eV as the static charge reference. This study indicates that after long activation times (ca 6 h) conversion of alumina, at least in the surface region, to aluminium fluoride is complete. It must be remembered however that this conclusion is made from ex-situ XPS experiments.

More definitive information concerning changes in the surface that occur during activation [71] is possible using a new technique for referencing (Au 4f_{7/2}) [72] combined with in situ techniques. The Au 4f_{7/2} referenced chemical state plot of aluminium compounds, (Fig. 5) displays different binding energies (BE) for oxides, hydroxofluorides and fluorides. Most importantly, both aluminium(III) fluoride modifications (α - and β -) can be distinguished due to the high precision of this technique. After treatment of γ -alumina with CHF₃ under in situ conditions, two new aluminium species can be detected. The major phase (6a), at an Al 2p BE of 75.6 eV, was elucidated as an aluminium-(hydr)oxo-fluoride. The minor phase (6b, ca 20% of the aluminium content) has an Al 2p BE of 78.2 eV suggesting the presence of an AlF₃ phase. However, surprisingly, the BE is higher (by 0.7 and 1.0 eV respectively) than those measured for α - and β -AlF₃ reference samples.

In the chemical state plot of fluorine, only one species has been found for γ -alumina activated by CHF₃ (cf Fig. 6), and chemical states of fluorine in this material and in β -AlF₃ appear to be very similar. Exposure to air of the material leads to hydrolysis. The chemical state plots of fluorine, indicate that hydrolysis of Al—F surface bonds commences after 10 min and continues over a period of at least one month.

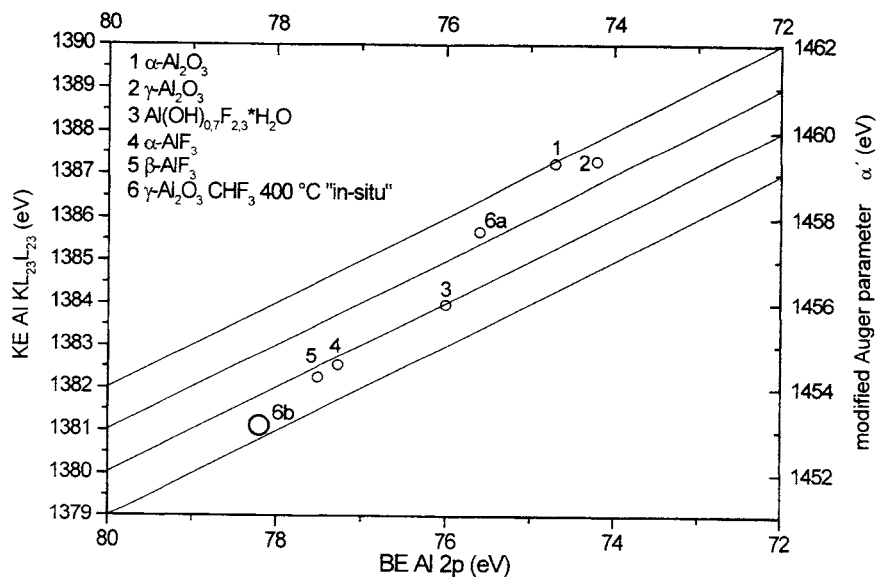


Fig. 5. Chemical state plot for Al in CHF_3 activated γ -alumina (circles give uncertainties of measurements). BE and KE data are referenced to Au $4f_{7/2}$ (84.0 eV). (a) majority species; (b) minority species [71].

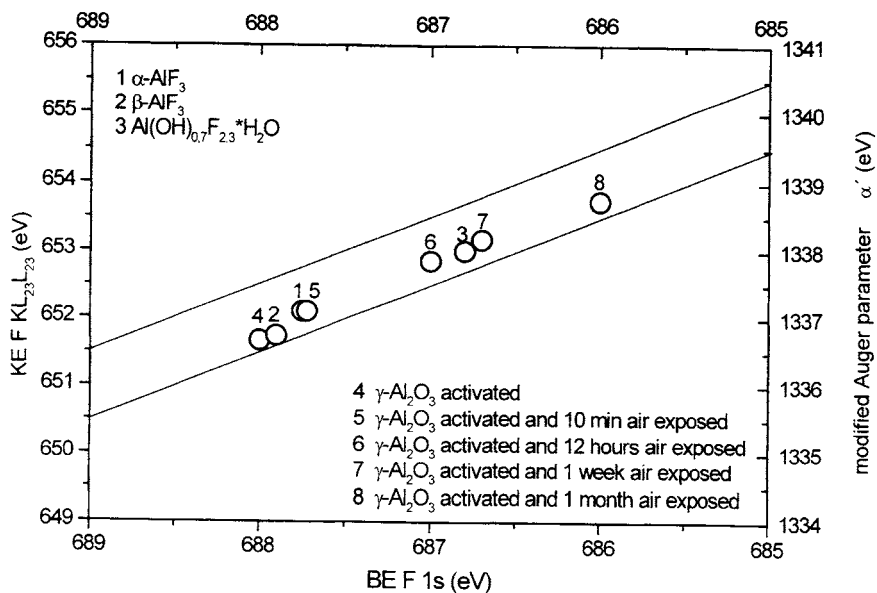


Fig. 6. Chemical state plot for F in CHF_3 activated γ -alumina before and after exposure to air (circles give uncertainties of measurements); BE and KE data are referenced to Au $4f_{7/2}$ (84.0 eV) [71].

There are two possible explanations for the higher BE compared with the pure (α - and β -) AlF_3 reference samples. Either, the activation of γ -alumina with a fluorocarbon results in a very active surface state which differs from the pure reference fluorides, possibly due to the presence of chemisorbed HF molecules at the surface, or that the difference is the result of partial hydrolysis of the ex situ prepared reference samples. However, the surface of AlF_3 samples, prepared by classical crystallization from HF solution, is not modified in such an extreme manner after exposure to air. Only small changes in the BE can be detected and this suggests that there are in fact real differences in the activity/states of the surface sites of fluorinated γ -alumina catalysts.

To obtain further information on this point, changes in the alumina catalyst during the dismutation of CHClF_2 , as shown in Fig. 4, were followed by combined in situ XPS measurements [73]. Figure 7 displays the Al 2p binding energies of several Al samples and in order to improve the sensitivity, the scale is expanded, hence, the pure AlF_3 phases are not included here. The X-ray amorphous alumina catalyst exhibits slightly higher binding energies than the γ -alumina reference samples, most probably due to the influence of particle size on the relaxation behaviour. The slight increase of the BE after calcination of this amorphous alumina starting material (sample 5) indicates the partial removal of surface OH-groups due to condensation. After 5 min treatment with CHClF_2 a significant change of the binding energy

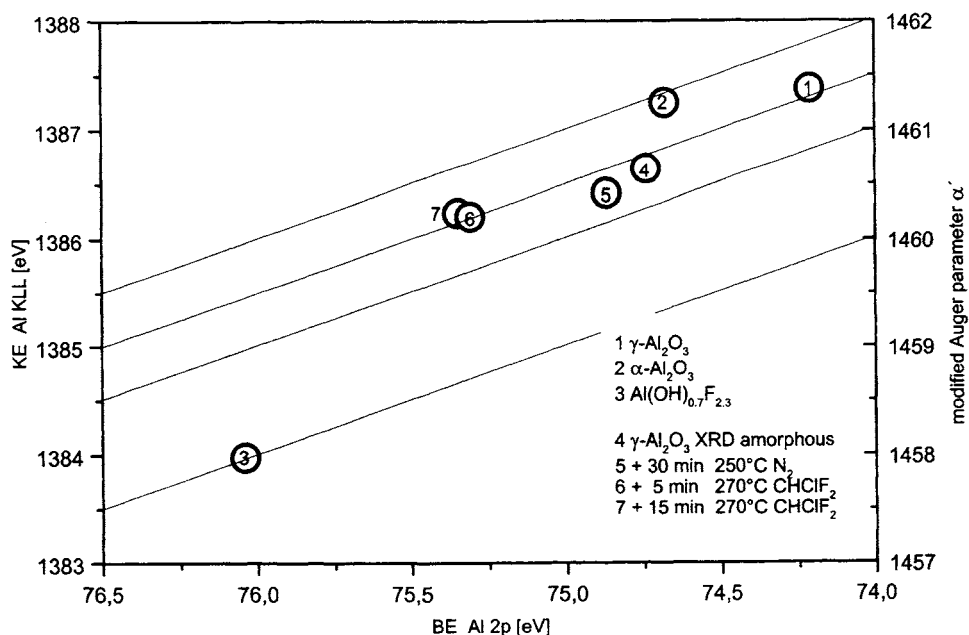


Fig. 7. Chemical state plot for Al in several aluminium oxide reference samples and in CHClF_2 activated γ -alumina (circles give uncertainties of measurements); BE and KE data are referenced to Au $4f_{7/2}$ (84.0 eV).

has occurred, consistent with the fluorination of the surface. Surprisingly, after 15 min, the binding energy of the surface phase is little different from that after 5 min activation, and is still significantly lower than for the pyrochlore, $\text{Al}(\text{OH})_{0.7}\text{F}_{2.3}$, reference phase. In contrast, the catalytic behaviour of the sample activated for 5 min and that activation for 15 min is completely different (cf Fig. 4). More informative are the F 1s binding energies which are shown in Fig. 8. The 15 min activated sample (6) exhibits significantly higher BE than the 5 min sample (5). Although the catalytically active phase (sample 6) has a BE similar to the pyrochlore $\text{Al}(\text{OH})_{0.7}\text{F}_{2.3}$ phase, the different position of the modified Auger parameter indicates quite different structural environments in the two phases. From additional TOF-SIMS measurements on these samples it is concluded that, "at this time there are no pure aluminium fluoride phases at the surface but the partially fluorinated, aluminium oxofluoride" related phases present are catalytically active [73].

Changes in the catalytic activity of activated alumina surfaces have also been probed by Temperature Programmed Desorption (TPD) and FTIR photoacoustic measurements [74]. Ammonia TPD allows a fast and convenient determination of the overall acidity of a solid surface. The desorption profiles provide information on the distribution, the amount and strengths of the acid surface sites, since molecules adsorbed at weaker sites desorb at lower temperatures than those adsorbed at stronger acidic sites. The activation of γ -alumina with CHClF_2 resulted in a sig-

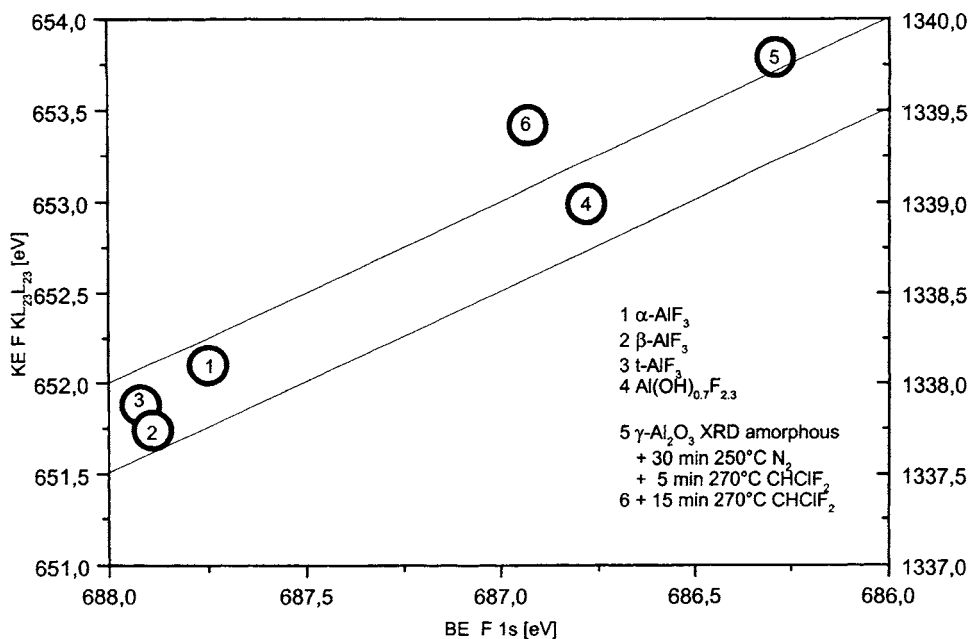


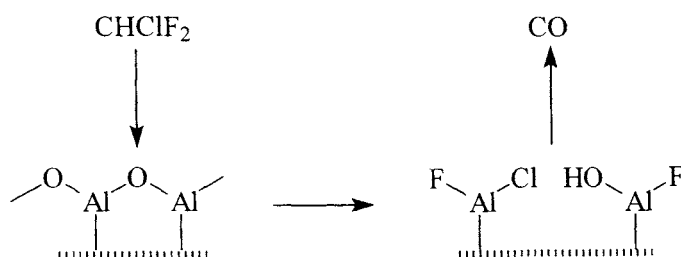
Fig. 8. Chemical state plot for F in different AlF_3 reference samples and in CHClF_2 activated γ -alumina (circles give uncertainties of measurements); BE and KE data are referenced to $\text{Au } 4f_{7/2}$ (84.0 eV) [73].

nificantly increased number and strength of the acidic surface sites, due to the replacement of OH and/or O by F.

On basis of pyridine FTIR photoacoustic spectroscopic measurements a differentiation between Lewis and Brønsted acid sites was achieved [74]. The FTIR photoacoustic spectra of calcined and activated γ -alumina samples before and after the adsorption of pyridine were compared. Brønsted acid sites were not found in the calcined sample, consistent with the findings of other studies [75,76]. Calcination of γ -alumina up to 973 K resulted in increased Lewis acidity whereas Brønsted acid sites were not formed. Comparing calcined samples with samples treated with CHClF_2 at 523 K noticeable differences were observed. The number of Lewis acid sites was not increased significantly, but from the 19b ring mode of pyridine at approximately 1450 cm^{-1} , it has been proved that a shift to higher wave numbers has occurred indicating a strengthening of the acid site. A further significant difference between the calcined and activated samples is the formation of Brønsted acid sites in case of the latter one, simply explained according to Scheme 2. However, these Brønsted sites, as well as surface chlorines, disappear as fluorination of the surface proceeds.

Combining the results of the studies described above enabled the following conclusions to be drawn:

- (i) Alumina surfaces react quickly with fluorine containing alkanes, for example, according to Scheme 2. Initially, surface hydroxyl groups are cleaved resulting in partially fluorinated Al-O species. The higher Al 2p BE-values determined from XPS indicate an increased electron deficiency (higher Lewis acidity) at the aluminium sites which is in agreement with the observed increased catalytic activity, with the increased ammonia adsorption (TPD), and with the shift in the pyridine 19b ring mode at 1450 cm^{-1} (Pa-FTIR). The electron deficiency at the aluminium site, however, is only slightly influenced by further fluorination. Lower BE values associated with fluorine as fluorination proceeds, indicate a higher electron density and consequently a higher basicity at the anionic part of the surface, due to electron density transfer from lattice oxygen to fluorine, while the electron density at the Al site remains unchanged. Further fluorination results in replacement of oxygen/hydroxyl by fluorine and consequently



Scheme 2

Reaction of a CHClF_2 molecule with an alumina surface originating Brønsted acid sites

electron transfer from the anion lattice is suppressed. The F 1s binding energy increases due to decreased electron density. This is confirmed, e.g. by X-ray excited Auger Electron Spectroscopy (XAES), which shows a decreased electron density at the oxygen side as a result of fluorination [73].

- (ii) While hydroxyl groups are present at the surface, the solid phases exhibit little or no catalytic activity but undergo further heterogeneous reactions with fluorocarbons resulting in continued fluorination of the surface until the catalytic dismutation reaction dominates. However, fluorination continues but is suppressed significantly and is diffusion limited. Finally a completely fluorinated, AlF_3 bulk phase is produced.
- (iii) The heterogeneously catalyzed chlorine for fluorine exchange occurs exclusively at Lewis acid sites on the surface, a similar situation to that for chromia catalysts. However, for alumina, due to the thermodynamic situation, the heterogeneous reaction between the solid and fluorine containing gaseous compounds results finally in the formation of pure bulk AlF_3 . For chromia this seems to stop at the chromium oxofluoride stage.

12.3 Chromium and aluminium fluorides

Catalytically active sites for Cl—F-exchange reactions are Lewis acidic in nature. Considering that fluorine is more electronegative than oxygen and is able to form a similar variety of different structures in its compounds which are often similarly chemically inert and thermally stable, one should expect even higher Lewis acidity in metal fluorides than in the respective metal oxides. Somewhat surprisingly however, until now less attention have been paid to the catalytic potential of metal fluorides in heterogeneous catalyzed reactions. The preceding sections have demonstrated that there is strong evidence that aluminium oxyfluoride phases are catalytically active in halogen exchange reactions and that further fluorination results in the formation of aluminium fluoride phases which are highly active catalysts. The situation for chromium as has been pointed out, is rather different.

Both metals form a series of MF_3 modifications which are isotypic to each other. In general, in these MF_3 compounds, the coordination number of the cation is 6, and the structural arrangement can be described in terms of a three dimensional array of corner-sharing octahedra.

Only the rhombohedral $\alpha\text{-MF}_3$ modification is thermodynamically stable, and occurs with the VF_3 -type-structure [77]. The anionic arrangement can be described as a compact stacking perpendicular to the ternary axis. The cations are located at the corners and at the center of the rhombohedron. All the other MF_3 phases are meta-stable. The $\beta\text{-MF}_3$ phases adapt a hexagonal tungsten bronze structure (HTB) having nanoporous openings defined by cornersharing rings of six $[\text{MF}_6]$ octahedra which run along the c axis. New modifications of aluminium fluoride, designated as η -, θ -, and $\kappa\text{-AlF}_3$, have been synthesized and structurally characterized recently [78–82]. Their structures are very similar to the HTB structure. Furthermore, both aluminium and chromium, form isotypic hydroxofluorides,

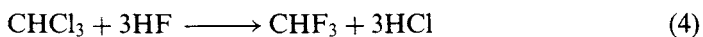
$\text{MF}_x(\text{OH})_{3-x}$ ($0.4 < x < 2.07$) [83] occurring in the pyrochlore structure. This is more open than the HTB-structure because slightly distorted hexagonal channels are located along all six plane diagonals of the cubic cell [84].

12.3.1 Aluminium fluoride catalysts

Many investigations have shown that $\text{Al}(\text{OH},\text{F})_3$, $\alpha\text{-AlF}_3$, and $\beta\text{-AlF}_3$ are formed as a result of the reaction of alumina with fluoroalkanes. Consequently, these fluoride phases have been synthesised and their catalytic behaviour and surface properties investigated. Among pyrochlore $\text{Al}(\text{F},\text{OH})_3$, $\alpha\text{-AlF}_3$ and $\beta\text{-AlF}_3$, only the latter one exhibits immediately catalytic activity in C_1 dismutations. As γ -alumina, also $\text{Al}(\text{F},\text{OH})_3$ requires an activation before it becomes catalytically active whereas pure $\alpha\text{-AlF}_3$ does not exhibit any catalytic activity, neither after a prolonged treatment with fluorocarbons nor at higher temperatures up to 873 K. Even employing a larger amount of $\alpha\text{-AlF}_3$, to obtain the same absolute surface area, did not result in a significantly enhanced catalytic activity. Only after introducing crystal disorder, e.g. by partial hydrolysis, a slight activity was observed [74].

The catalytic behaviour of the solid fluoride phases is consistent with their behaviour in Temperature Programmed Desorption (TPD) and pyridine FTIR photoacoustic measurements. Calcined $\beta\text{-AlF}_3$ already exhibits full catalytic activity without any activation. Characteristic for this phase is the appearance of two distinct regions of high concentrations of acid sites at the surface, one in the temperature region around 423 K representing weak acidity and one around 623 K representing strong acid surface sites. In contrast, $\alpha\text{-AlF}_3$ does not exhibit any potential for pyridine adsorption, thus showing that there are no acid sites at its surface.

All metastable AlF_3 phases have nanoporous openings defined by corner-shared rings of six $[\text{AlF}_6]$ octahedra. Whereas the $\beta\text{-AlF}_3$ phase has these channels aligned along the c -direction of the crystal, forming straight channels, the $\eta\text{-AlF}_3$ phase has adjacent rings tilted with respect to each other, producing an undulating channel along the ab -plane. The structure of the new tetragonal phase, $\theta\text{-AlF}_3$ [78] contains different rings formed from 5, 4, and 3 $[\text{AlF}_6]$ octahedra. The 5-rings form an undulating 3-D interconnected channel system around tetrahedral clusters of four $[\text{AlF}_6]$ octahedra. The microporous nature of this new phase is similar to that of the $\beta\text{-AlF}_3$ and $\eta\text{-AlF}_3$ phases. The new $\kappa\text{-AlF}_3$ phase, prepared by thermal decomposition of $\beta\text{-NH}_4\text{AlF}_4$ [80,81] has channels running through the crystal comprising 5, 4, and 3 rings of corner shared $[\text{AlF}_6]$ octahedra. The catalytic activities of these new phases in the fluorination of CHCl_3 and CCl_3CF_3 , Eqns (4) and (5) are compared in Table 3.



Both reactions were run under the same conditions at 623 K using a fixed bed of

Table 3

Catalytic activities of several AlF_3 phases in fluorination reactions of CHCl_3 or CCl_3CF_3 with HF at 623 K under gas flow conditions

Compound	Surface area/m ² g ⁻¹	Conversion to CHF_3 in %	Conversion to CCl_2FCF_3 in %
$\alpha\text{-AlF}_3$	3	2	4
$\beta\text{-AlF}_3$	53	49	10
$\eta\text{-AlF}_3$	58	4	12
$\theta\text{-AlF}_3$	64	10	11
$\kappa\text{-AlF}_3$	19	50	45

granulated material, $\beta\text{-AlF}_3$ and $\alpha\text{-AlF}_3$ being included for comparison [79] (cf Table 3).

From this, it can be deduced that open network structures of AlF_3 exhibit catalytic activity. Since the catalytic process occurs at the surface of these solids and taking into account the catalytic inactivity of the compact $\alpha\text{-AlF}_3$ phase, it can be concluded that the particular surface structure arising from the bulk MF_6 octahedra arrangement and the availability of the active centres, but not the size of the surface area, are of crucial importance for the catalytic process.

12.3.2 Structural differences between $\alpha\text{-AlF}_3$ and $\beta\text{-AlF}_3$ -related phases

The feature that $\alpha\text{-AlF}_3$, and the framework open structures of the other AlF_3 phases have in common is that aluminium is octahedrally co-ordinated by six fluoride anions. However, the kind of linkage of these $[\text{AlF}_6]$ octahedra differs fundamentally. In rhombohedral $\alpha\text{-AlF}_3$ the cations are located at the corners and at the centre of the rhombohedron [84]. Figure 9(a) shows the $[\text{AlF}_6]$ octahedra network in this structure. In contrast, $\beta\text{-AlF}_3$ adopts the hexagonal tungsten bronze (HTB) structure [85] which is presented in Fig. 9(b), where the $[\text{AlF}_6]$ octahedra form hexagonal channels along the *c*-axis. Owing to this open structure, the density of $\beta\text{-AlF}_3$ is significantly lower than that of $\alpha\text{-AlF}_3$. In $\beta\text{-AlF}_3$ the channel diameter is only about 2.46 Å, which is too small for incorporating haloalkane molecules. Moreover, only fluoride anions form the inner surface of these channels which cannot therefore act as Lewis acid sites. The same is true for η -, θ -, and $\kappa\text{-AlF}_3$ phases. On this basis, a simple model has been proposed combining the experimental data of the observed acidity and the catalytic activity of both phases [39]. According to this model, the activity differences between $\alpha\text{-AlF}_3$ and $\beta\text{-AlF}_3$ -related phases arise from differences of the surface structures arising from differences in their bulk structures. Thus, the surface derived from $\alpha\text{-AlF}_3$ is covered completely with large, basic fluoride anions, irrespective of its indices (cf Fig. 10(a)). In contrast, cleavage of the HTB-structure related AlF_3 -phases along the directions of channels results in a buckled surface structure with exposed metal atoms which are coordinatively

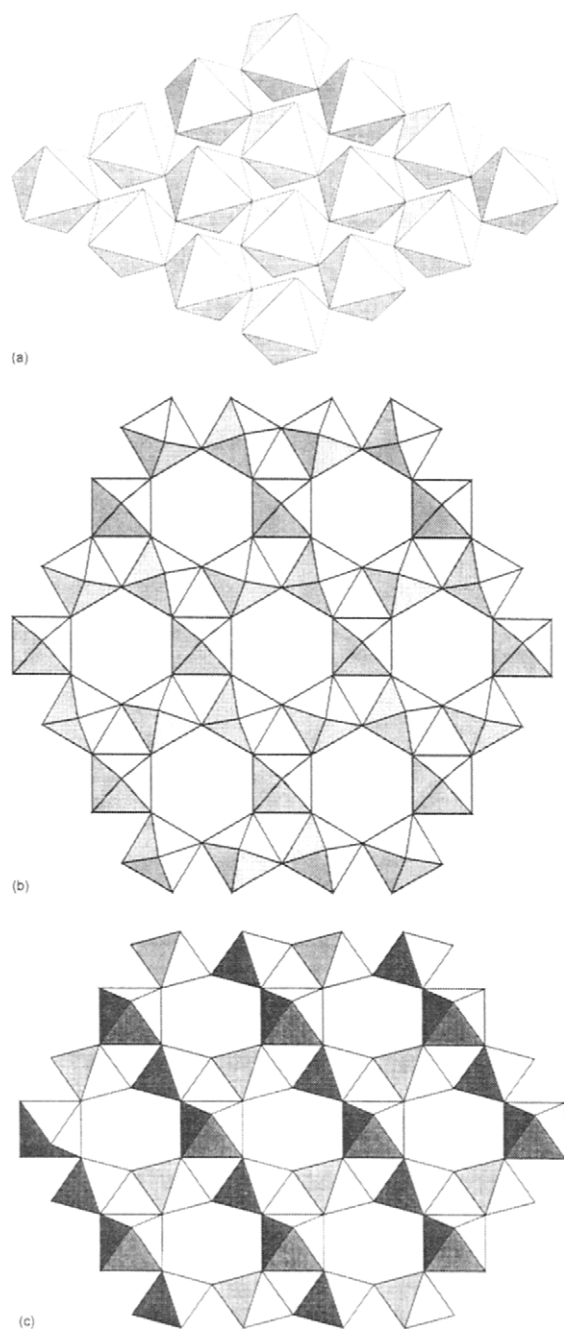


Fig. 9. Linking of MF₆ octahedra: (a) in the structure of $\alpha\text{-AlF}_3$; (b) in the HTB structure of $\beta\text{-AlF}_3$ in $[001]$ direction; and (c) in the pyrochlore structure of $\text{AlF}_{2.3}(\text{OH})_{0.7} \cdot \text{H}_2\text{O}$ in $[110]$ direction (one of six channel directions).

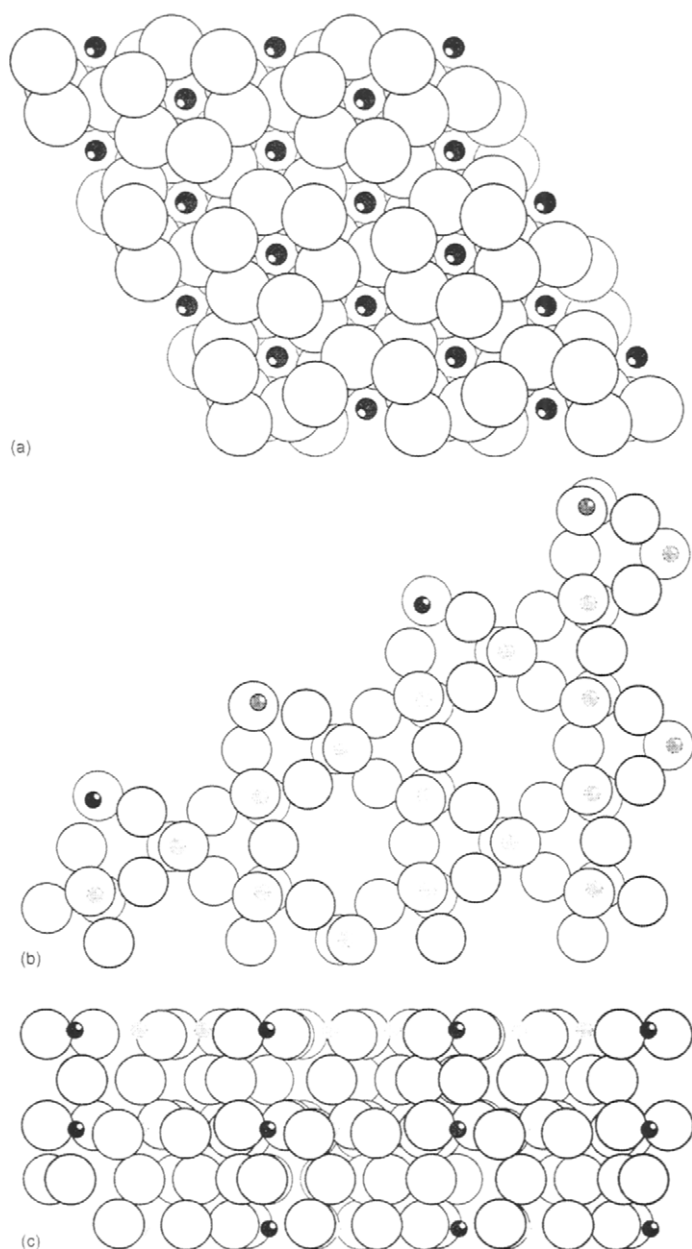


Fig. 10. Possible surface structures of MF₃ phases (M = Al, Cr): (a) Section of α -MF₃ in z -direction (big circles – F atoms; small circles – M atoms). All M atoms are imbedded in the surface oxygen layer at $c = 1/3$; (b) Section of the channels of β -MF₃ in c -direction (big circles – F atoms; small circles – M atoms); (c) View on the surface of β -MF₃ originated as shown in (b). Dark small circles represent M atoms on the top of the wave above the F surface atoms (reproduced with permission from J. Catal., 159 (1996) 270 [39]).

unsaturated and are sterically accessible by fluoroalkanes (cf Fig. 10(b)) thus explaining the observed Lewis acidity and catalytic activity of β - AlF_3 -related phases.

At first sight, the catalytic behaviour and the surface properties of pyrochlore $\text{Al}(\text{OH},\text{F})_3$ does not fit this model since the pyrochlore structure (cf Fig. 9(c)) is a more open one than the HTB- AlF_3 structure. However, since aluminium hydroxofluoride is susceptible to thermal decomposition, it is in fact no longer pyrochlore $\text{Al}(\text{OH},\text{F})_3$ under the temperature conditions employed for the catalytic reactions. Thus, the behaviour of this phase in heterogeneous catalytic halogen exchange can be explained by the presence of amorphous alumina which determines the surface characteristics at the initial stage. Consequently, this phase acts in a manner similar to alumina and not until the surface becomes completely fluorinated does it reach its full catalytic activity.

12.3.3 Chromium(III) fluoride phases

Due to the structural similarities of aluminium and chromium fluorides, one should expect similarities in their surface properties and catalytic behaviour. Thus, the well characterized pure chromium fluoride phases have been investigated in a similar way as described above for the aluminium systems [39,74]. From these results, $\text{Cr}(\text{OH},\text{F})_3$, α - CrF_3 , and β - CrF_3 follow approximately the behaviour described already for the aluminium system. However, there are several differences which have to be considered in more detail. In contrast to α - AlF_3 , the isotypic pure α - CrF_3 exhibits non-negligible catalytic activity. The thermodynamic situation for the competitive formation of metal fluorides and metal chlorides is fundamentally different for the aluminium and chromium systems (see Table 2). The small value of $\Delta G^\circ_{\text{F}}$ for the formation of CrF_3 is probably the reason why chromia becomes only partly fluorinated, whereas alumina in contact with gaseous fluoroalkanes forms a compact aluminium fluoride layer under the same conditions. Stable chromium(III) oxofluorides could be formed under the conditions discussed here but they are not well characterized at the present time.

12.4 Doped species in the oxide and fluoride families

Some years ago, a hypothesis regarding the acidity generation of binary oxides was proposed by Tanabe et al. [86], enabling the prediction of types of binary oxides that would show acidic properties (Brønsted or Lewis) and providing insights regarding the structure of the acid sites. However, this hypothesis has not been applied systematically to the development and evaluation of new metal mixed fluorination catalysts. Although numerous aluminas and chromias have been claimed in patents, only some few systems have been seriously investigated and described in the literature regarding their chemical, structural and surface properties. Consequently, this is still a field in which many questions remain unanswered.

12.4.1 The oxide family

Since most technical processes for manufacturing HFCs are likely to be based on chromia rather than alumina, related model catalysts comprising various supported and unsupported chromias have been evaluated. A new generation of fluorinated catalysts based on divalent metal chromites, $M(II)O-Cr_2O_3$ where $M(II) = Mg, Mn, Co, Ni$ or Zn has been claimed in several patents and zinc, nickel, and magnesium doped chromias have been investigated recently [87]. The doped chromias were obtained by impregnation of freshly precipitated $Cr_2O_3 \cdot xH_2O$ with aqueous solutions of respective $M(II)$ -salts or by co-precipitation with subsequent calcination. Doping, in general, affects the crystallinity of the chromia obtained. Thus, higher surface areas are characteristic for chromias of lower crystallinity and, since they offer more active sites, increased degrees of conversion are found. Generally, surface area decreases slightly upon fluorination. In the catalytic HF reaction of CF_3CH_2Cl to CF_3CH_2F , lightly zinc doped chromias have superior catalytic activities to undoped chromias while heavily zinc doped chromias are inferior to undoped materials. From X-ray studies, it was deduced that doping, to whatever extent, does not alter the bulk structure of chromia but the dopant leads to significant reductions in the apparent activation energy of the reaction.

Other transition $M(II)$ dopants do not produce promotional effect to match that of $Zn(II)$, although nickel(II) nor $Mg(II)$ doped catalysts have characteristics in common with the $Zn(II)$ analogues. These results are in accordance with other studies of $Ni(II)$ [88] and $Mg(II)$ [89] as dopants for chromia. Although lightly doped $Mg(II)$ chromias had inferior conversion of CF_3CH_2Cl , these catalysts had longer lifetimes than chromias which were undoped.

XPS and TEM measurements indicate that after fluorination, zinc and nickel, on the surface of these catalysts is present as ZnF_2 or NiF_2 , respectively and these findings support the idea that the $Zn(II)$ and $Ni(II)$ species on doped fluorinated chromias do not become integrated into the surface structure but are, in fact, distinct phases on the surface.

12.4.2 The fluoride family

Since phases related to $\beta-AlF_3$ exhibit pronounced catalytic activity, attempts have been made to promote activity in this phase by doping with other metals. The perceived advantage is that doped fluoride phases should not alter in contact with haloalkanes since they are already fluorinated. At the present time metals that have been seriously investigated as dopants for $\beta-MF_3$ phases are for $M = Al, Cr(III)$ and $Mg(II)$ and for $M = Cr, Fe(III)$ and $Mg(II)$.

The same synthesis procedure as that developed for the synthesis of pure $\beta-MF_3$ was employed for doped $\beta-MF_3$ phases. Hydrated, doped $\alpha-MF_3 \cdot 3H_2O$ samples were precipitated and then dehydrated under the atmosphere that originates from the dehydrate. Chromium(III) doping into AlF_3 , results in two distinct solid phases depending on the Cr-content [90]. For up to 50% Cr-doping, X-ray studies show exclusively the $\beta-MF_3$ related structure, however, with a decreased crystallinity which results in an almost amorphous region at high $Cr(III)$ levels of doping. This

is accompanied by an increase in the surface area reaching a maximum at about 34% Cr and 66% Al. Further increase in Cr(III) doping decreases the surface area. Under these synthesis conditions, the pure chromium phase is $\text{CrF}_{0.94}(\text{OH})_{2.06}$ occurring with the pyrochlore structure. In accordance with an increase in the concentration of Lewis acidic centers on the surface due to the increased surface area, samples containing up to 50% Cr(III) doped into $\beta\text{-AlF}_3$ exhibited somewhat higher catalytic activity in the dismutation reaction of CCl_2F_2 than pure $\beta\text{-AlF}_3$. The situation is rather different for Mg(II) doping. As in the oxide family, only at low levels of Mg(II) doping is a promotional effect observed. However, at levels up to 10% Mg(II) doping, very high catalytic activity (90% conversion) in the CCl_2F_2 dismutation is observed compared with $\beta\text{-AlF}_3$ (80%). At 20% Mg(II) doping, only 20% conversion was obtained, indicating the inhibited effect of Mg at higher dopant concentrations. From X-ray measurements, incorporation of Mg into the structure of $\beta\text{-AlF}_3$ was deduced and confirmed by later XANES investigations [91]. Consistent with this, XPS measurements [92] indicate the formation of Mg_xF_y clusters in the cavities of the open framework of the host structure which may act as strong Lewis acid sites. At higher concentrations of Mg(II) these clusters condense forming catalytically inactive MgF_2 as an isolated phase on the surface.

Doping of CrF_3 with Fe(III) or Mg(II), would be expected to result in the formation of solid solutions. However, depending on the Fe(III) concentration, there are two distinct regions, a concentration range from 0 to 41% Fe(III) with the pyrochlore structure and a second range from 65 to 100% Fe with the HTB structure [93]. The surface areas of the latter samples are about double those of the former. At about 65% Fe(III) a maximum in the acidity of the samples was observed, acidity decreases with further increase of Fe(III). These phases however, exhibit only average catalytic activity.

Magnesium doping into CrF_3 yields phases that are either amorphous or of low crystallinity on the basis of X-ray studies. Evidently, mutual substitution within the lattices does not occur. In agreement with chemical analysis of the product phases, weak reflections in the XRD patterns indicate the formation of pyrochlore-related hydroxofluorides rather than pure fluoride phases. However, at high Mg(II) concentrations there is a dramatic increase in the surface area with values up to one decade higher than in pure $\text{CrF}_{0.39}(\text{OH})_{2.61}$. The concentration of acidic centers as well as the catalytic activity in dismutation reaction of CCl_2F_2 and fluorination of $\text{CF}_3\text{CH}_2\text{Cl}$ mirror this increase, the highest degrees of conversion being obtained with samples having Mg(II) in the range 65–92% [93].

In summary, the development of doped catalysts, in both oxide and fluoride families, for catalytic fluorination is at an early stage. Much work remains to be done before a clear picture is obtained, however it is apparent that doping can perturb the crystalline nature of pure phases under some circumstances. When a substantially greater surface area results, a high concentration of acidic surface sites is also observed. There is considerable uncertainty regarding the selectivity and long term stability of doped catalysts and these aspects require further investigation.

12.5 Mechanistic studies

The derivation of a mechanism for a chemical reaction is by its very nature an uncertain process, being dependent critically on the nature and extent of the experimental evidence. Mechanisms that have at their heart a surface process or processes are even more uncertain and when the constraints imposed by the manipulation of HF are also taken into account, it is not surprising that there have been relatively few mechanistic studies made of heterogeneous catalytic fluorination. However a catalytic process cannot be said to be understood fully without a mechanism based on the experimental evidence available and such studies are helpful in the design of the next generation of catalysts. In most cases the work described below involves chromia or γ -alumina based catalysts that have been pretreated according to the methods described above. Studies involving C_2 and C_1 compounds are described in turn.

12.5.1 Catalytic fluorination of C_2 compounds

Using a combination of the radiotracers [^{18}F] and [^{36}Cl] has enabled the transformations under flow conditions of the chlorofluoroethane series $C_2Cl_{6-n}F_n$, $n=0$ and 2–5 inclusive which occur on chromia extensively fluorinated with HF, to be described in some detail [11,94,95]. Two key observations were made. Firstly, that [^{36}Cl] radioactivity could be deposited on fluorinated chromia by H^{36}Cl or [^{36}Cl]— CCl_2FCF_3 flow, 75–85% of which was removed by subsequent flow of $C_2Cl_2F_4$ isomers or $\text{CCl}_2\text{FCClF}_2$ [94]. Secondly, [^{18}F] or [^{36}Cl] activity incorporated into product mixtures by flow over previously labelled catalysts was distributed in a predictable fashion when the mixtures were separated into their components by radio G.C. — [95]. The probability of a radiolabel, [^{18}F] or [^{36}Cl], being observed in a given component, correlated directly with the degree to which that component had been fluorinated or chlorinated. This behaviour is not consistent with a series of dismutation reactions in which carbon-bound halogens, Cl or F, are redistributed among the components of the series $C_2Cl_{6-n}F_n$ but indicates the occurrence of an intermolecular halide transfer involving surface Cl or F at each step. There is no requirement for chlorination, Cl-for-F, and fluorination, F-for-Cl, reactions to be concerted, as would be required for a dismutation. In contrast the isomerization $\text{CCl}_2\text{FCClF}_2 \rightarrow \text{CCl}_3\text{CF}_3$ and possibly also $\text{CClF}_2\text{CClF}_2 \rightarrow \text{CCl}_2\text{FCF}_3$, involve no surface halide species and are regarded as intramolecular [95]. Interestingly, one of the first mechanistic studies involving CFCs, reported many years ago, resulted in a similar conclusion, that the isomerization of $\text{CCl}_2\text{FCClF}_2$ in the presence of aluminium(III) chloride was also intramolecular [96]. The halogen exchange and isomerization reactions are summarized in Scheme 3; mechanistic proposals for fluorination, chlorination and isomerization of $\text{CCl}_2\text{FCClF}_2$ [95] are shown in Fig. 11; they are speculative, particularly the suggestion that oligomeric $(\text{HF})_n$ species are present on the catalyst surface.

The possibility of catalytic fluorination and chlorination occurring in C_2 HCFCs has been demonstrated for CHClFCF_3 using the precursor CoCl_2 supported on alumina which is subsequently treated with HF [97]. Mechanisms based on

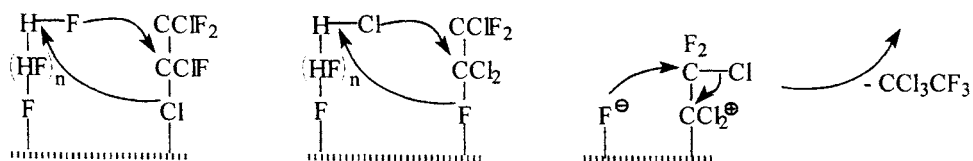
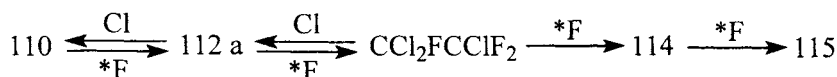
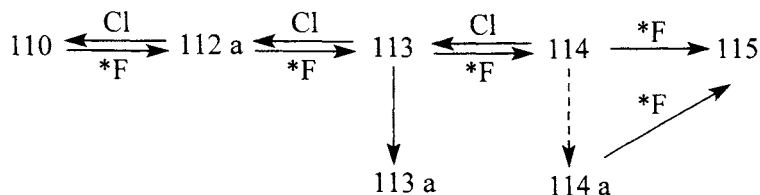


Fig. 11. Mechanistic proposals for (a) fluorination and chlorination; (b) isomerization (reproduced with permission from Appl. Catal., A79 (1991) 89 [95]).

(a)



(b)



Scheme 3. Halogen exchange and isomerization reaction scheme for chloro- fluoroethane behaviour on fluorinated chromia at 700 K. (a) Partial model deduced using CCl_2FCClF_2 as feedstock and catalyst labelled with $[^{18}F]$; CCl_3CF_3 and CCl_2FCF_3 are also identified products but the routes whereby they are formed are not defined. (b) Model deduced using all experimental data. F and Cl are catalytically active species; * = radioactive; 110, 112a, 113, 113a, 114, 114a and 115 are C_2Cl_6 , CCl_3CClF_2 , CCl_2FCClF_2 , CCl_3CF_3 , $CClF_2CClF_2$, CCl_2FCF_3 and $CClF_2CF_3$ (reproduced with permission from Appl. Catal., A79 (1991) 89 [95]).

dehydrohalogenation/hydrohalogenation steps are in principle possible for HCFCs and HFCs (see below) but labelling with 2H indicated that they are unlikely here. A detailed kinetic study led to a mechanistic scheme rather similar to the halogen exchange model for CFCs. In particular, the fluorination/chlorination reactions using HF or HCl involve active sites where at least two adsorbed species are involved in the rate determining step, i.e. a classical Langmuir–Hinshelwood mechanism, HF being strongly adsorbed and $CHClFCF_3$ weakly adsorbed relative to HX , $X = Cl$ or F . An identical double-site model results in the best fit to the kinetic data and is summarized as follows:

$R_F - X * S + HY * S \rightarrow R_F - Y * S + HX * S$ where for fluorination $X = Cl$ and $Y = F$ and, for chlorination, $X = F$ and $Y = Cl$. The reactants are chemi- or physisorbed at the active sites, S , where S is either a Lewis acid site, or, if a metal hydrido-halide complex, $H-S-X(Y)$, is formed, a low-oxidation state metal site [97].

in which all reacting species are in adsorbed states [43,98]. If chromia is conditioned with a chlorofluorocarbon rather than with a hydrofluorocarbon, additional reactions occur due to the intervention of adsorbed HCl [43], in harmony with the catalytic reactions described earlier.

A dehydrochlorination–hydrofluorination pathway appears to account for the *room temperature* conversion of C_2 and C_3 hydrochlorocarbons to HCFCs by HF in the presence of supported organic layer catalysts [99,100]. These catalysts are derived from SF_4 fluorinated or CCl_4 chlorinated γ -alumina; the surfaces are both highly Lewis acidic and contain labile surface halogen [68,101]. Treatment of the surfaces with CH_3CCl_3 results in dehydrochlorination and oligomerization of the latter to give a highly coloured organic layer on the Lewis acidic surface. The ability of the layer to trap hydrochlorocarbons and the presence of labile surface fluoride [100] are believed to be important factors in the catalysis of reactions between HF and CH_3CCl_3 or related compounds to give HCFCs [99]. Hydrochlorocarbons that do not undergo dehydrochlorination readily, exhibit little or no reactivity. Related behaviour is shown by catalysts derived from fluorinated Fe_3O_4 and Co_3O_4 [102].

Although the mechanistic picture for chlorofluoroethanes is now clear, considerable further work involving HCFCs and HFCs is required before definitive mechanisms may be said to be established.

12.5.2 Catalytic fluorination of C_1 compounds

Perhaps surprisingly, in view of the widespread use of halogenated C_1 compounds, there has been relatively little mechanistic activity in the heterogeneous context. One of the first mechanistic proposals for the catalytic fluorination of CCl_4 by HF over an aluminium(III) fluoride catalyst involved complexation of CCl_4 by an ill-defined HF- - AlF_3 surface complex [13], emphasising the very strong adsorption of HF on AlF_3 at the expense of CCl_4 . On the basis of a later kinetic modelling study, fluorination of CCl_4 over chromium(III) fluoride has been described as a stepwise process, yielding successively CCl_3F , CCl_2F_2 and $CClF_3$. In all cases a modified Langmuir–Hinshelwood mechanism is proposed, arising from the very different adsorption characteristics of HF and the halomethanes [103]. In contrast, fluorination of CCl_4 at an HF prefluorinated chromia surface from which adsorbed HF has been removed during the final pretreatment step, is proposed, in an elegant study, to occur by two simultaneous processes $CCl_4 \rightarrow CCl_3F$ and $CCl_4 \rightarrow CCl_2F_2$ having identical activation energies [104]. The intermediates postulated are shown in Fig. 13. Although the intermediate for di-exchange is geometrically possible on the (001) surface of α - CrF_3 [104], in view of the discussion in earlier parts of the chapter, the appropriateness of this description of the catalytic surface could be questioned.

There have been two recent kinetic studies of the dismutation behaviour of $CHCl_2F$, $CHClF_2$ and other members of the $CHCl_{3-n}F_n$ series, in one case over activated γ -alumina under conventional flow conditions [105] in the other, over activated chromia using plug-flow and temporal analysis of products (TAP) reactors

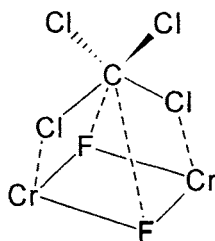
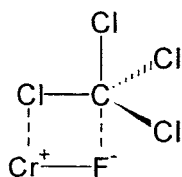


Fig. 13. Intermediates proposed for mono- and di-exchange of Cl by F in CCl_4 at a fluorinated chromia surface (reproduced with permission from J. Catal. 174 (1998) 219 [104]).

[38]. In neither case was it possible to propose definitive mechanisms due to the complexity of the systems; in the γ -alumina study, it is suggested that adsorption–desorption processes are slow relative to rapid dismutation between two adsorbed species [105], while from the chromia study mono-molecular halogen exchange reactions with metal halide surface sites are indicated [38]. The latter mechanism is reminiscent of the halogen exchange model proposed [95] for C_2 CFCs on fluorinated chromia.

12.5.3 Catalytic hydrogenolysis

Catalytic hydrogenolysis of CFCs has become very important in view of its relevance to the production of hydrofluoroalkanes, particularly CH_2F_2 and CH_2FCF_3 (Table 1). It is also a method whereby unwanted stocks of CFCs can be converted to useful compounds. Early work in this area was described in 12.1.2 but the past five years have seen an explosion of activity, particularly relating to hydrogenolysis of CCl_2F_2 and $\text{CCl}_2\text{FCClF}_2$. Most of the work is outside the scope of this chapter, since it does not involve fluoride catalysts, but we conclude the chapter with two aspects that are relevant.

There is now substantial evidence that hydrogenolysis of CCl_2F_2 on supported noble metal catalysts, which leads to mixtures of CH_2F_2 and CH_4 , occurs via a difluorocarbene intermediate [106,107,108], a pleasing parallel with one of the mechanisms proposed for CCl_4 fluorination [104]. A carbene intermediate is pro-

posed also for hydrogenolysis of CCl_2FCF_3 [109]. Deactivation of palladium catalysts during hydrogenolysis due to the formation of halide surface species that are implicated in Pd oxidation/sintering, is a characteristic of carbon or oxide supports; the surface reactions in the latter case are possibly related to the activation processes for fluorination catalysts. Deactivation can be minimized by working at high partial pressures of dihydrogen [109] but the use of metal fluorides, such as AlF_3 , TiF_4 and ZrF_4 as supports may be beneficial [106,110,111]. The situation to date appears to indicate that supports such as AlF_3 produce less active catalysts than those employing carbon or binary oxides but may they may be more resistant to deactivation. Here, as with other topics discussed in this chapter, there is considerable scope for catalyst development and undoubtedly fluorides and new fluorination methods will continue to feature prominently.

References

- [1] B.C. Gates, *Catalytic Chemistry*, John Wiley & Sons Ltd., NY, 1991, Chapter 1, p. 2.
- [2] L.E. Manzer, *Catal. Today*, 13 (1992) 13.
- [3] G. Webb, J.M. Winfield, In: *Chemistry of Waste Minimization*, J.H. Clark (Ed.), Blackie Academic and Professional, London, 1995, Chapter 8, pp. 222ff.
- [4] M. Veccho, G. Groppelli, J.C. Tatlow, *J. Fluorine Chem.*, 4 (1974) 117.
- [5] L. Kolditz, G. Kauschka, W. Schmidt, *Z. Anorg. Allg. Chem.*, 434 (1977) 41.
- [6] L. Kolditz, U. Calov, G. Kauschka, W. Schmidt, *Z. Anorg. Allg. Chem.*, 434 (1977) 55.
- [7] L. Kolditz, V. Nitzsche, G. Heller, T. Stösser, *Z. Anorg. Allg. Chem.* 476 (1981) 23.
- [8] L. Marangoni, C. Gervasutti, L. Conte, *J. Fluorine Chem.*, 19 (1981/82) 21.
- [9] L. Marangoni, D. Carmello, R. Passerini, *Chim. Ind. (Milan)*, 67 (1985) 467.
- [10] D. Bechadargue, M. Blanchard, P. Canesson, *Appl. Catal.*, 27 (1986) 179.
- [11] J. Kijowski, G. Webb, J.M. Winfield, *J. Fluorine Chem.*, 27 (1985) 213.
- [12] J. Kijowski, G. Webb, J.M. Winfield, *Appl. Catal.*, 27 (1986) 181.
- [13] G.P. Gambaretto, F. Auezzu, E. Gola, *J. Appl. Chem. Biotechnol.*, 23 (1973) 175.
- [14] S. Okazaki, H. Eriguchi, *Chem. Lett.*, (1980) 891.
- [15] J.R. Anacona, P.B. Davies, A.H. Ferguson, *Chem. Ind.*, (1986) 490.
- [16] E. Kemnitz, D. Hass, *Z. Phys. Chem. (Leipzig)*, 269 (1988) S1131; 270 (1989) S937.
- [17] C. Gervasutti, L. Marangoni, W. Marra, *J. Fluorine Chem.*, 19 (1981/82) 1.
- [18] J.R. Lacher, A. Kianpour, F. Oetting, J.D. Park, *Trans. Farad. Soc.*, 52 (1956) 1500.
- [19] J.R. Lacher, A. Kianpour, J.D. Park, *J. Phys. Chem.*, 60 (1956) 1454.
- [20] S.D. Witt, E.-C. Wu, K.-L. Loh, Y.-N. Tang, *J. Catal.*, 71 (1981) 270.
- [21] J.S. Campbell, C. Kemball, *Trans. Farad. Soc.*, 57 (1961) 809.
- [22] S.P. von Halasz, *Germ. Patent* 3,009,760, 1981 (to Hoechst) *Chem. Abstr.*, 95 (1981) 186620.
- [23] W.H. Gumprecht, *US Patent* 4,311,863, 1982 (to DuPont) *Chem. Abstr.*, 96 (1982) 180749.
- [24] M. Yoshizumi, Y. Yamashity, *Jp. Patent* 1-228925, 1989 (to Mitsubishi Metal Corp.) *Chem. Abstr.*, 112, (1981) 54966.
- [25] D. Carmello, G. Guglielmo, *Eur. Patent* 282005 1989 (to Ausimont) *Chem. Abstr.*, 110 (1981) 10080.
- [26] W.H. Gumprecht, L.E. Manzer, V.N.M. Rao, *US Patent* 4,843,181, 1989 (to DuPont) *Chem. Abstr.*, 111, (1989) 214116.

- [27] G.J. Moore, H.M. Massey, US Patent 4,950,815 (1990), assigned to E.I. duPont de Nemours & Co.
- [28] J.J. Lerou, US Patent 5,036,036 (1989), assigned to E.I. duPont de Nemours & Co.
- [29] H.J. Freund, *Angew. Chem.*, 109 (1997) 444.
- [30] C.Xu, M. Haßel, H. Kuhlenbeck, H.-J. Freund, *Surf. Sci.*, 258 (1991) 23.
- [31] C.Xu, B. Dillmann, H. Kuhlenbeck, H.-J. Freund, *Phys. Rev. Lett.*, 67 (1991) 3551.
- [32] F. Rohr, M. Bäumer, H.-J. Freund, J.A. Mejias, V. Stämmeler, S. Müller, L. Hammer, K. Heinz, *Surf. Sci.*, 372 (1997) 291.
- [33] H. Kuhlenbeck, Xu, B. Drillmann, M. Haßel, B. Adam, D. Ehrlich, S. Wohlrab, H.-J. Freund, U.A. Dittinger, H. Neddermeyer, M. Neuber, M. Neumann, *Ber. Bunsenges. Phys. Chem.*, 96 (1992) 15.
- [34] C.A. Ventrice, D. Ehrlich, E.L. Garfunkel, B. Dillmann, D. Heskett, H.-J. Freund, *Phys. Rev. B* 46 (1992) 12892.
- [35] M. Bender, D. Ehrlich, I.N. Yakovkin, F. Rohr, M. Bäumer, H. Kuhlenbeck, H.-J. Freund, V. Staemmler, *J. Phys. Condens Matter*, 7 (1995) 5289.
- [36] D. Bechadergue, M. Blanchard, P. Canesson, In: *Heterogeneous Catalysis and Fine Chemicals*, M. Guisnet et al. (Eds.), Elsevier, Amsterdam, 1980, pp. 257ff.
- [37] E. Kemnitz, D. Hass, B. Grimm, *Z. Anorg. Allg. Chem.*, 589 (1990) 228.
- [38] D.R. Coulson, P.W.J.G. Wijnen, J.J. Lerou, L.E. Manzer, *J. Catal.*, 140 (1993) 103.
- [39] E. Kemnitz, A. Kohne, I. Grohmann, A. Lippitz, W.E.S. Unger, *J. Catal.*, 159 (1996) 270.
- [40] E. Kemnitz, A. Kohne, E. Lieske, *J. Fluorine Chem.*, 81 (1996) 197.
- [41] D.M.C. Kavanagh, T.A. Ryan, B. Mile, *J. Fluorine Chem.*, 64 (1993) 167.
- [42] A. Kohne, E. Kemnitz, *J. Fluorine Chem.* 75 (1995) 103.
- [43] E. Kemnitz, K.-U. Niedersen, *J. Fluorine Chem.*, 79 (1996) 111.
- [44] E. Kemnitz, D.-H. Menz, *Progress in Solid State Chemistry*, 1998, in press.
- [45] C.D. Wagner, A. Joshi, *J. Electron Spectrosc. Relat. Phenom.*, 47 (1988) 283.
- [46] K. Jagannathan, A. Srinivasan, C.N.R. Rao, *J. Catal.*, 69 (1981) 418.
- [47] M. Shelef, K. Otto, H. Ghnadi, *J. Catal.*, 12 (1968) 361.
- [48] J.T. Gleaves, J.R. Ebner, T.C. Kuechler, *Catal., Rev. Sci. Eng.*, 30 (1989) 43.
- [49] V. Indovina, D. Cordischi, S. De Rossi, G. Ferrais, G. Ghiotti, A. Chirino, *J. Mol. Catal.*, 68 (1991) 53.
- [50] S. Brunet, B. Requieme, E. Matouba, J. Barrault, M. Blanchard, *J. Catal.*, 152 (1995) 70.
- [51] S. Brunet, B. Boussand, D. Martin, *J. Catal.*, 171 (1997) 287.
- [52] K.-U. Niedersen, E. Schreier, E. Kemnitz, *J. Catal.*, 167 (1997) 210.
- [53] E. Kemnitz, A. Hess, *J. Prakt. Chem.*, 334 (1992) 591.
- [54] T. Skapin, E. Kemnitz, *Catal. Lett.*, 40 (1996) 241
- [55] T. Skapin, *J. Mat. Chem.* 5 (1995) 1215.
- [56] E.C. DeCanio, J.W. Bruno, V.P. Nero, J.C. Edwards, *J. Catal.*, 140 (1993) 84.
- [57] F.P.J.M. Kerkhof, J.C. Oudejans, J.A. Moulijn, E.R.A. Matulewicz, *J. Colloid Interface Sci.*, 77 (1980) 120.
- [58] V.M. Allenger, C. Fairbridge, D.D. McLean, M. Ternan, *J. Catal.*, 105 (1987) 71.
- [59] R.I. Hedge, M.A. Barteau, *J. Catal.*, 120 (1989) 387.
- [60] G.B. McVicker, C.J. Kim, J.J., Eggert, *J. Catal.*, 80 (1983) 315.
- [61] H.J. Reitsma, C. Boelhouwer, *J. Catal.*, 33 (1974) 39.
- [62] P.O. Scokart, A. Selim, J.P. Damon, P.G. Rouxhet, *J. Colloid Interface Sci.*, 70 (1979).
- [63] A. Moerkerken, B. Behr, M.A. Noordeloos-Maas, C. Boelhouwer, *J. Catal.*, 24 (1972) 177.

- [64] F.P.J.M. Kerkhof, H.J. Reitsma, J.A. Moulijn, *React. Kinet, Catal. Lett.*, 7 (1977) 15.
- [65] J. Grobelny, *J. Fluorine Chem.*, 9 (1977) 187.
- [66] A. Baumer, R. Caruba, G. Turco, C.R. Hebd., *Seances Acad. Sci. Ser. D 271D* (1970) 1.
- [67] D.-H. Menz, Ch. Mensing, W. Hönle, H.G. v. Schnering, *Z. Anorg. Allg. Chem.*, 611 (1992) 107.
- [68] A. Bendada, G. Webb, J.M. Winfield, *Eur. J. Solid State Inorg. Chem.*, 33 (1996) 907.
- [69] J.R. Schlup, R.W. Vaughan, *J. Catal.*, 99 (1986) 304.
- [70] A. Hess, E. Kemnitz, A. Lippitz, W.E.S. Unger, D.-H. Menz, *J. Catal.*, 148 (1994) 270.
- [71] O. Boese, E. Kemnitz, A. Lippitz, W.E.S. Unger, 7th European Conference on Applications of Surface and Interface Analysis (ESCASIA 97), Goeteborg, Sweden, June 16–20, pp. 189–192.
- [72] O. Boese, E. Kemnitz, A. Lippitz, W.E.S. Unger, *Fresenius J. Anal. Chem.*, 358 (1997) 175.
- [73] O. Boese, E. Kemnitz, 12th European Symposium on Fluorine Chemistry, Berlin 1998, Germany, August 29–September 2, PI 50.
- [74] A. Hess, E. Kemnitz, *J. Catal.*, 149 (1994) 449.
- [75] M. Riseman, F.E. Massoth, G. Muralhi Dhar, E.M. Eyring, *J. Phys. Chem.*, 86 (1982) 184.
- [76] E.R.A. Matulewiz, F.P.J.M. Kerkhof, J.A. Moulijn, H.J. Reitsma, *J. Colloid Interface Sci.*, 77 (1980) 110.
- [77] R. Hoppe, D. Kissel, *J. Fluorine Chem.*, 24 (1984) 327.
- [78] U. Bentrup, *Eur. J. Solid State Inorg. Chem.*, 29 (1992) 51.
- [79] N. Herron, W.E. Farneth, *Adv. Mater.*, 8 (1996) 959.
- [80] N. Herron, D.L. Thorn, R.L. Harlow, F. Davidson, *J. Am. Chem. Soc.*, 115 (1993) 3028.
- [81] N. Herron, R.L. Harlow, D.L. Thorn, *Inorg. Chem.*, 32 (1993) 2985.
- [82] N. Herron, D.L. Thorn, R.L. Harlow, G.A. Jones, J.B. Parise, J.A. Fernandez-Baca, Th. Vogt, *Chem. Mat.*, 7 (1995) 75.
- [83] J.M. Cowle, T.R. Scott, *J. Am. Chem. Soc.*, 70 (1948) 105.
- [84] D. Babel, A. Tressaud, In: *Inorganic Solid Fluorides*, P. Hagemuller (Ed.), Academic Press Inc. NY, 1985 pp. 77–203.
- [85] A. Le Bail, C. Jacoboni, M. Leblanc, R. De Pape, H. Duroy, J.L. Fourquet, *J. Solid State Chem.*, 77 (1988) 96.
- [86] K. Tanabe, T. Sumiyoshi, K. Kiyoura, J. Kitagawa, *Bull. Chem. Soc. Jpn.* 47 (1974) 1064.
- [87] W.D.S. Scott, PhD Thesis, Glasgow University, 1997; P. Landon, G. Webb, J.M. Winfield, unpublished work.
- [88] S. Brunet, B. Boussand, J. Barrault, 11th Int. Cong. Catal., Baltimore 1996, Proc. pp. 433.
- [89] H. Kim, H.S. Kim, B.G. Lee, H- Lee, S. Kim, *J. Chem. Soc. Chem. Comm.*, (1995) 2383.
- [90] E. Kemnitz, A. Hess, G. Rother, S. Troyanov, *J. Catal.*, 159 (1996) 332.
- [91] I. Grohmann, A. Hess, E. Kemnitz, W. Fentrup, W.E.S. Unger, J. Wong, M. Rowen; T. Tanaka, M. Froeba, *J. Mater. Chem.*, 8 (1998) 1453.
- [92] O. Boese, E. Kemnitz, A. Lippitz, W.E.S. Unger, *Fresenius Appl. Surf. Sci.*, 120 (1997) 181.
- [93] B. Adamscyck, A. Hess, E. Kemnitz, *J. Mater. Chem.*, 6 (1996) 1731.
- [94] L. Rowley, G. Webb, J.M. Winfield, A. McCulloch, *Appl. Catal.*, 52 (1989) 69.
- [95] L. Rowley, J. Thomson, G. Webb, J.M. Winfield, A. McCulloch, *Appl. Catal. A*, 79 (1991) 89.

- [96] W.T. Miller Jr, E.W. Fager, P.H. Griswald, *J. Am. Chem. Soc.*, 72 (1950) 705.
- [97] D.R. Coulson, *J. Catal.*, 142 (1993) 289.
- [98] E. Kemnitz, K.-U. Niedersen, *J. Catal.*, 155 (1995) 283.
- [99] J. Thomson, G. Webb, J.M. Winfield, D. Bonniface, C. Shortman, N. Winterton, *Appl. Catal. A*, 97 (1993) 67.
- [100] A. Bendada, D.W. Bonniface, F. McMonagle, R. Marshall, C. Shortman, R.R. Spence, J. Thomson, G. Webb, J.M. Winfield, N. Winterton, *Chem. Commun.*, (1996) 1947.
- [101] J. Thomson, G. Webb, J.M. Winfield, *J. Mol. Catal.*, 67 (1991) 117.
- [102] J. Thomson, *J. Chem. Soc., Faraday Trans.*, 90 (1994) 3585.
- [103] E. Kemnitz, G. Hansen, A. Hess, A. Kohne, *J. Mol. Catal.*, 77 (1992) 193.
- [104] A. Farrokhia, B. Sakakini, K.C. Waugh, *J. Catal.*, 174 (1998) 219.
- [105] A. Hess, E. Kemnitz, *Appl. Catal. A*, 82 (1992) 247.
- [106] B. Coq, F. Figuéras, S. Hub, D. Tournigant, *J. Phys. Chem.*, 99 (1995) 11159.
- [107] B.S. Ahn, S.C. Lee, D.J. Moon, B.G. Lee, *J. Mol. Catal. A*, 106 (1996) 83.
- [108] A. Wiersma, E.J.A.X. van de Sandt, M.A. den Hollander, H. van Bakkum, M. Makkei, J.A. Moulijn, *J. Catal.*, 177 (1998) 29.
- [109] Z. Karpinski, K. Early, J.L. d'Itri, *J. Catal.*, 164 (1996) 378.
- [110] B. Coq, J.M. Cognion, F. Figuéras, D. Tournigant, *J. Catal.*, 141 (1993) 21.
- [111] D. Ju-Moon, M. Jo-Chung, K. You-Park, S. In-Hong, *Appl. Catal. A*, 168 (1998) 159.

CHAPTER 13

Chemistry in Perfluorinated Organic Solvents

Eric G. Hope and Alison M. Stuart

Department of Chemistry, University of Leicester, Leicester, LE1 7RH, UK

13.1 Introduction

Although the unique physical and chemical properties of perfluorinated inorganic solvents (e.g. HF, SbF₅, BrF₃, BrF₅, IF₅ etc.) have been exploited in synthetic chemistry for many years (see Refs [1–3] and also chapters 2, 4 and 12 in this text for recent highlights and reviews), highly fluorinated or perfluorinated organic solvents have received little attention until relatively recently. This neglect has occurred in spite of the extensive investigations into the physical properties of these solvents and the subsequent application of these unusual properties in areas as diverse as medicine, cosmetics and heavy industry [4–9]. In fact, the reluctance to utilise perfluorinated organic solvents in synthesis has probably arisen from their apolarity and miscibility behaviour (see Sec. 2). However, following the high profile publication of an application of these solvents which relies upon their miscibility properties, by Horváth and Rábai in 1994 [10,11], synthetic chemistry in perfluorinated organic solvents or mixed perfluorinated-conventional solvent systems represents one of the major growth areas in fluorine chemistry within the last four years which looks well-placed to continue into the next millenium (Fig. 1). Some of the early work in this area has been highlighted [12–15].

With hindsight, three groups have implemented research into synthetic chemistry utilising perfluorinated organic solvents, although Horváth and Rábai [10] were undoubtedly the most influential and coined the term “fluorous” for those solvents which exhibit the appropriate behaviour. Two synthetic directions have been outlined. In the first, the idea of *similia similibus solvuntur* (like dissolves like) has been exploited by Horváth and Rábai [10] and Vogt [16] by the derivatisation of homogeneous catalysts with long perfluoroalkyl sidechains (called “ponytails” by Horváth and Rábai) which offer the facile separation of product(s) from reactant/catalyst after catalysis in a fluorous solvent/organic solvent mixture; the so-called “fluorous biphasic system”, FBS (Fig. 2). In the second, Zhu [17] recognised that the physical and chemical properties of perfluorocarbons could be exploited to offer new and exciting reaction media.

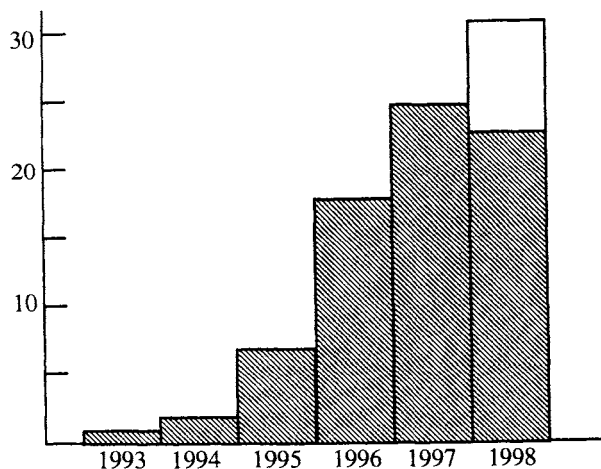


Fig. 1. The growth in the number of publications using perfluorocarbon solvents.

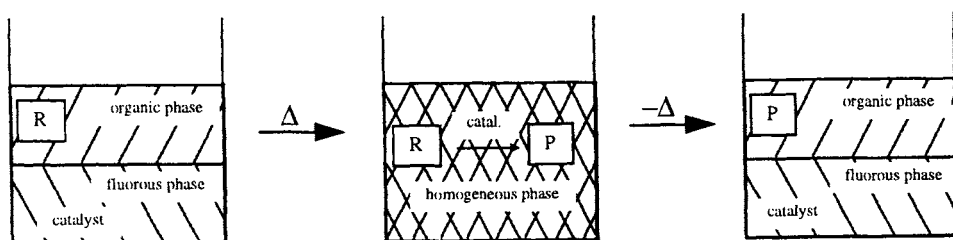


Fig. 2. Catalysis within the Fluorous Biphasic System (FBS).

In this chapter, following a brief introduction to the world of fluorous solvents, we detail the expanding array of synthetic chemistry utilising these unique media. The potential value of using fluorous solvents as vehicles for synthetic chemistry can only be estimated, however, it can only be augmented by the elegant simplicity of the concepts.

13.2 Physical and chemical properties of perfluorinated organic solvents

A wide range of fluids with similar physical and chemical properties, including linear and cyclic perfluoroalkanes, linear and cyclic perfluoroethers and polyethers, perfluorotertiary amines and, in a few instances, perfluoroalkylhalides, may be considered to be "perfluorinated" or "fluorous". Solvents within these categories are marketed around the world under a series of brandnames (Table 1). In certain instances, the commercial fluids represent mixtures of similar compounds with

Table 1

Brandnames and suppliers of perfluorinated fluids

Solvent Tradename	Supplier/Manufacturer	General Chemical Composition
FLUTEC [®]	F2 Chemicals Ltd	Perfluoro- <i>n</i> -alkanes Perfluoro-cycloalkanes
FLUORINERT [®]	3M	Perfluoro- <i>n</i> -alkanes Perfluorinated cyclic ethers Perfluorotrialkylamines
HOSTINERT [®]	Hoechst	Perfluoro- <i>n</i> -alkanes Perfluorinated cyclic ethers Perfluorotrialkylamines
KRYTOX [®]	DuPont	Homopolymers of hexafluoropropene oxide
FOMBLIN [®] GALDEN [®]	Montedison	Photooxidation products of hexafluoropropene or tetrafluoroethene
DEMNUM [®]	Daikins	Homopolymers of tetrafluorooxetane

comparable physical and chemical properties. Crucially, all these branded solvents behave similarly and, when taken as a set, offer an enormous breadth of liquid ranges.

It is well established that fluorination can dramatically alter the physical and chemical properties of organic molecules [18,19]. Nowhere are these effects more noticeable than in the area of perfluorinated hydrocarbons [4,5]. The high ionisation potential of fluorine [20] and its low polarisability [21] confer very weak intermolecular interactions (and, hence, low boiling points), low refractive indexes, low surface energies, low internal pressures and high compressibilities on perfluorocarbons. Hence, perfluorinated compounds are extremely non-polar and are poor solvents for all materials except those with similarly low cohesive energies (e.g. gases or other highly fluorinated materials) [4]. For example, the application of these solvents as oxygen carriers in medicine relies upon their unique ability to dissolve oxygen and CO₂ (more than 10 times greater than water) [22] and their very low toxicity [9,23]. It should be noted that other gases also have high solubilities. This high gas solubility does not arise from an attractive interaction between the solvent and the gas, but rather results from the gas molecules occupying large cavities within the perfluorocarbon [24]. Perfluorocarbons are practically insoluble in water but can dissolve some low molecular weight hydrocarbons (e.g. pentane, hexane) and are, crucially, immiscible with many common organic solvents (e.g. toluene, dichloromethane) at room temperature [25]. Heats of solution of perfluorocarbons are very different to those of "conventional" organic solvents [25] and, in terms of solvent-solute interactions, perfluorocarbons are more like liquid noble gases than hydrocarbons.

In addition to these physical properties, the extreme electronegativity of fluorine [20], which results in highly polarised C—F bonds, is manifest in the legendary

strength of the C—F bond [26]. Interestingly, fluorination also influences the strengths of adjacent bonds whence C—C bonds in poly(CF₂CF₂) are about 8 kcal mol⁻¹ stronger than those in polythene, and perfluoropolyethers are more thermally stable than perfluorocarbons owing to their especially strong C—O bonds [19]. When these thermodynamic properties are taken alongside the steric requirements of fluorination (the currently accepted van der Waals radius of F is 1.47 Å [27]), the outstanding chemical and thermal stabilities of perfluorocarbons are easy to understand. Typical maximum working temperatures for perfluorocarbon solvents are 400–450°C [5] and these solvents are inert to boiling acids and alkalis as well as oxidising or reducing agents under normal conditions; fusion with alkali metals converts many perfluorocarbons into carbon plus metal fluorides [28] whilst reaction with glass (or silica) above ca 500°C gives CO₂ + SiF₄ [4].

Hence, perfluorocarbons offer “environmentally-friendly” alternatives to common organic solvents with the potential for long lifetimes in industrial processes and are especially suitable for long, high temperature reactions. Furthermore, they are excellent substitutes for chlorinated solvents, like carbon tetrachloride, which are being phased out under the international agreement called the “Montreal Protocol on Substances that Deplete the Ozone Layer” and this has been demonstrated in their use as solvents in photooxidations [29] and brominations [30] of alkenes.

13.3 Coordination chemistry and fluorous biphasic catalysis

In order to utilise the specific properties of perfluorocarbon solvents in catalysis, it is necessary to make the catalyst soluble in these unusual solvents. Vogt [16] and Horváth and Rábai [10] recognised that this would only be possible by attaching highly fluorinated sidechains to a ligand for coordination to the active metal centre. Hence, the synthesis of suitably derivatised ligands, an evaluation of how these highly fluorinated substituents would influence the coordination chemistry of these ligands and their value in catalytic systems, are essential to the development of this field. A number of different types of ligand have been investigated and, for convenience, this section is subdivided by ligand class.

13.3.1 Phosphorus(III) ligands

Phosphorus(III) ligands, in particular phosphines, are the most widely studied ligand system in homogeneous catalysis. It is not surprising, therefore, that Horváth and Rábai chose the derivatisation of a phosphine in their seminal paper [10] and that this class of ligand (Fig. 3) has received significantly more attention than other ligands for fluorous biphasic catalysis.

13.3.1.1 Ligand synthesis

Horváth and Rábai prepared the fluorous-derivatised phosphine (**1a**) in 26% yield by a radical induced reaction of the commercially-available alkene (C₆F₁₃CH=CH₂) with PH₃ [10,11]; Gladys et al., by incorporating a second step, have improved

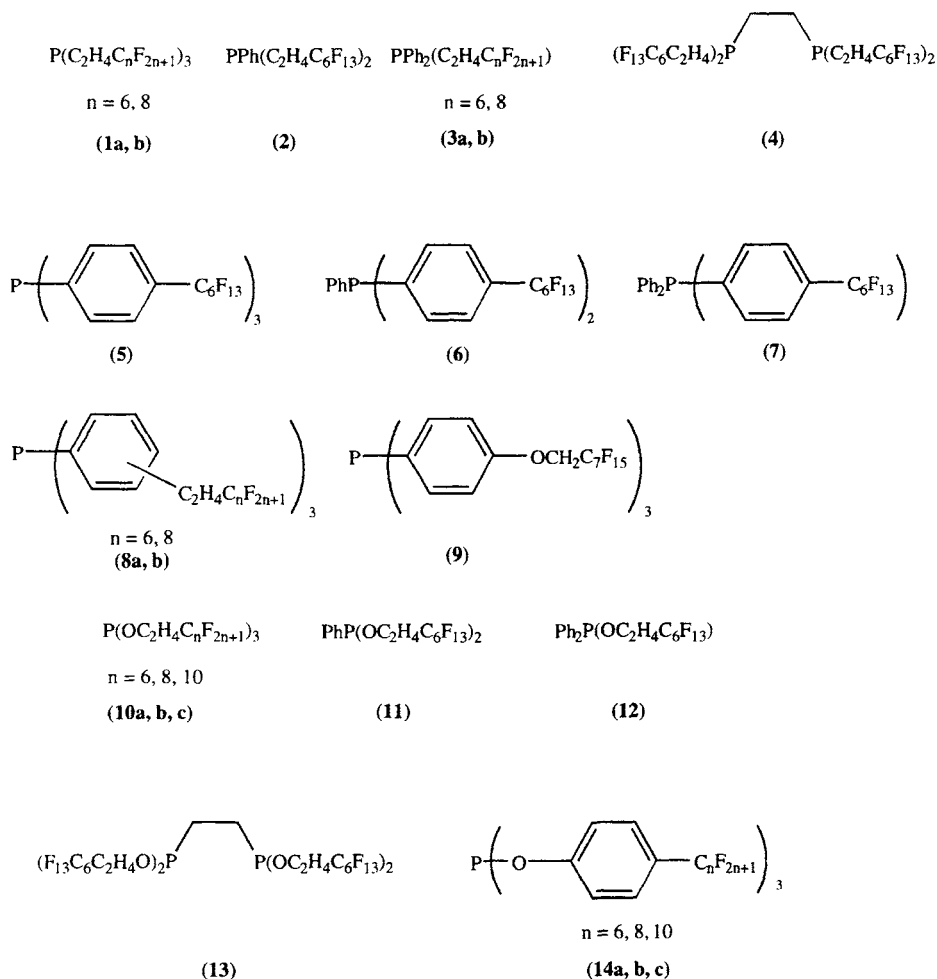


Fig. 3. Perfluoroalkyl-derivatised phosphorus(III) ligands.

the yield to 53% [31]. Interestingly, this ligand was first prepared in 1985 from the reaction of $\text{C}_6\text{F}_{13}\text{C}_2\text{H}_4\text{ZnI}$ with PCl_3 , but the potential scope of this ligand for coordination chemistry and catalysis was not recognised [32]. Alternative preparations via the Grignard reagent [33,34] or an alkyl zinc reagent [35] have subsequently been published which allow the synthesis of a series of related ligands with one, two, three or four ponytails (2–4). N.B. the Grignard route had previously been used by Horváth and Rábai [11] to prepare the trialkylphosphine (1b) with C_8F_{17} sidechains. Throughout this work, the C_2H_4 group has been included in an attempt to minimise the strongly electron-withdrawing influence of the perfluorinated alkyl chain. In the absence of a spacer group, e.g. for the simplest perfluoroalkyl-derivatised phosphine, $\text{P}(\text{CF}_3)_3$, the fluorine atoms reduce the

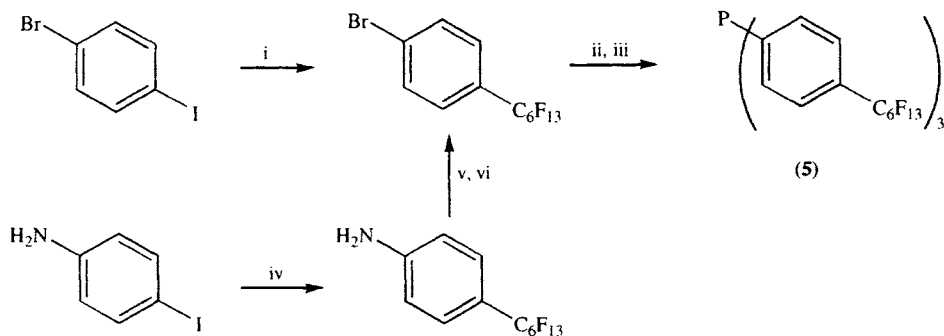
σ -donation properties of the phosphorus atom to such a large extent that this group of ligands do not coordinate strongly to metal centres and have little value in catalysis [36]. In an attempt to assess the effectiveness of the spacer group, Horváth has undertaken some theoretical calculations (Table 2) [37] which indicate that even very long hydrocarbon chains do not completely insulate the phosphorus atom from the fluorine atoms, but that beyond a C_3H_6 group the variation with additional CH_2 units is minimal. With this in mind, Gladysz et al. have recently reported [31,38] the elegant syntheses of a series of derivatised phosphine ligands with C_nH_{2n} ($n = 1, 2, 3, 4$) spacer groups for which the spectroscopic data confirm the earlier theoretical calculations, but which also demonstrate that longer perfluoroalkyl units are required to confer preferential perfluorocarbon solubility (a pre-requisite for FBS compatibility).

Various groups have prepared related phosphine ligands (**5–9**) with aryl- or derivatised-aryl-spacer groups as alternative electronic insulators. Interestingly, as with the trialkylphosphines, the first syntheses of ligands in this class can be traced back to a 1970 patent [39] for perfluorocarbon-soluble phosphorus(III) antioxidant oil additives but, again, the value of these compounds in coordination chemistry and catalysis was not recognised. In two parallel publications [33,40], the perfluoroalkyl-*para*-substituted triphenylphosphine ligand (**5**) was prepared using Cu-mediated coupling reactions and lithiation (Scheme 1). The extension to ligands with one or two perfluoroalkyl substituents or *meta*-derivatised ligands or chelating bidentate analogues of bis(diphenylphosphino)ethane (DPPE) is straightforward [33,41]. Empirically (see below) it has been shown that the C_6H_4 spacer group does not completely insulate the phosphorus atoms from the perfluoroalkyl ponytails and the inclusion of additional spacer groups has been investigated. Leitner et al. [42] have described triarylphosphines (e.g. **8**) with *meta*- or *para*-substituted $C_2H_4C_6F_{13}$ units. Gladysz et al. [31] have briefly introduced the derivatisation of aryl phosphines with $C_3H_6C_nF_{2n+1}$ ponytails using a Wittig-hydrogenation sequence whilst an $O(CH_2)_xC_nF_{2n+1}$ ($x = 1, 2$ or 3) unit (e.g. **9**) can be incorporated by the reaction of $Rf(CH_2)_xOTf$ (prepared from the commercially available alcohols and triflic anhydride) with *para*-hydroxy-arylphosphines or -arylphosphine oxides [43].

Table 2

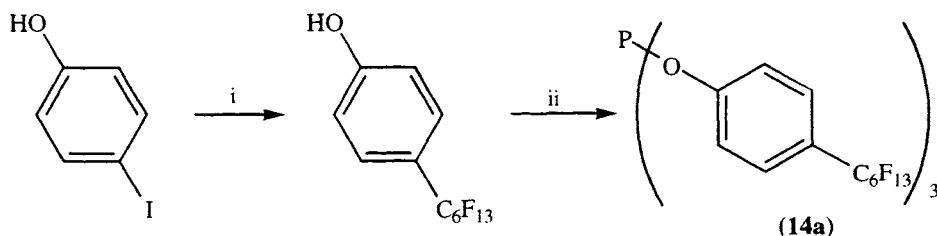
Calculated electronic properties of $P[(CH_2)_nCF_2CF_3]_3$ molecules

	Phosphorus lone-pair level, eV	Phosphorus Mulliken population (q)	Protonation Energy, eV
$P(CF_2CF_3)_3$	-11.7	0.83	-6.5
$P(CH_2CF_2CF_3)_3$	-10.6	0.62	-7.7
$P(C_2H_4CF_2CF_3)_3$	-9.9	0.48	-8.3
$P(C_3H_6CF_2CF_3)_3$	-9.5	0.40	-8.6
$P(C_4H_8CF_2CF_3)_3$	-9.3	0.38	-8.8
$P(C_5H_{10}CF_2CF_3)_3$	-9.2	0.36	-8.9



Scheme 1. Reagents and conditions: (i) $\text{C}_6\text{F}_{13}\text{I}$, Cu, bipy, dmso, C_6F_6 ; (ii) $n\text{BuLi}$, Et_2O , -78°C ; (iii) PCl_3 , Et_2O ; (iv) $\text{C}_6\text{F}_{13}\text{I}$, Cu, dmso; (v) NaNO_2 , HBr ; (vi) CuBr .

Alternatively, additional electronic insulation can be achieved by the incorporation of an oxygen spacer adjacent to the phosphorus atom. Again, this was conceived by Horváth and Rábai in their initial publication [11] with the synthesis of the highly moisture-sensitive trialkylphosphite (**10b**) obtained in 55% yield from the reaction of PCl_3 with the commercially available alcohol ($\text{HOCH}_2\text{CH}_2\text{C}_8\text{F}_{17}$) in the presence of base. The C_6F_{13} and $\text{C}_{10}\text{F}_{21}$ derivatised phosphites and the related phosphinites and phosphonites (**11,12**) (with one or two ponytails respectively) [33] and a potentially chelating bidentate bis-phosphonite (**13**) [44] have been prepared by analogous routes. Following the coupling of a perfluoroalkyl group to a phenol, similar condensations with phosphorus chlorides afford the triaryl-phosphinite, -phosphonite and phosphite ligands (**14**) which incorporate the OC_6H_4 group as a spacer unit (Scheme 2) [33].



Scheme 2. Reagents and conditions: (i) $\text{C}_6\text{F}_{13}\text{I}$, Cu, bipy, dmso, C_6F_6 ; (ii) PCl_3 , NEt_3 , Et_2O .

13.3.1.2 Transition metal complexes

The application of these perfluoroalkyl-derivatised ligands in FBS catalysis (see below) relies upon the generation, often *in situ*, of transition metal complexes. However, the potential impact of these perfluoroalkyl substituents is unknown, and there have been a growing number of publications directed towards identifying any physical or chemical consequences of these substitutions. Most importantly,

throughout these coordination studies, direct analogues of well-known metal-phosphine complexes have been prepared by established experimental procedures indicating that catastrophic variations in the ligand properties do not occur upon derivatisation with large numbers of perfluoroalkyl groups.

The first direct evaluations of the coordination properties of these derivatised ligands came from a series of communications from a number of groups. The syntheses, spectroscopic and structural characterisations of analogues of Vaska's complex $\text{trans}[\text{MCl}(\text{CO})\text{L}_2]$ $\{\text{M} = \text{Rh}, \text{L} = \text{P}(\text{C}_2\text{H}_4\text{C}_6\text{F}_{13})_3 \text{ or } \text{P}(4\text{-C}_6\text{H}_4\text{C}_6\text{F}_{13})_3; \text{M} = \text{Ir}, \text{L} = \text{P}(\text{C}_2\text{H}_4\text{C}_6\text{F}_{13})_3\}$ were contemporaneous [45–47]. For the rhodium complexes, $^1J_{\text{RhP}}$ offers little information on the electronic influence of the perfluoroalkyl substituents and similar conclusions can be drawn from similar data for $[\text{RhCl}\{\text{P}(\text{C}_2\text{H}_4\text{C}_6\text{F}_{13})_3\}_3]$ [48,49]. However, $\nu(\text{CO})$, by comparison with data for the triethyl- and triphenyl-phosphine complexes, clearly indicates that the spacer groups *do not* completely shield the metal centre(s) from the electronegative fluorine atoms. The aryl spacer appears to be slightly more effective as an insulator than its alkyl counterparts. As might be expected, single crystal structure determinations for the rhodium and iridium complexes with the trialkyl ligand (**1a**) are virtually identical. In both cases, the anticipated *trans*-phosphine geometry is confirmed and crucially there appears to be little variation in the metal coordination environment (bond lengths and angles) between these structures and related, structurally-characterised, Vaska's analogues. The most striking features of the structural determinations are the arrangements of the six perfluoroalkyl groups per metal centre. Four are essentially parallel and co-planar (allowing for the slight helical twist associated with the 1,3-repulsive fluorine-fluorine interactions) in what have been described as “rafts” [46,47] or “rugby posts” [45] depending on which side of the Atlantic Ocean the authors work. The crystal lattices are comprised of stacks of molecules in which these ponytails are paired back-to-back and end-on-end resulting in the maximisation of the number of short(ish) fluorine-fluorine interactions (Fig. 4). From a large number of structural determinations on perfluoroalkyl-derivatised metal complexes from our laboratory, it can be concluded that these fluorine-fluorine interactions are crucial in determining the intermolecular interactions in the solid state in these systems. The remaining perfluoroalkyl units in these structurally characterised Vaska's analogues radiate away from these rafts and kink, alternatively, above and below the metal-donor atom plane. EXAFS studies on the rhodium complexes in perfluorocarbon solution and in the solid state indicate that, within the accuracy of the technique, the metal coordination environment is unaffected by dissolution [45]. In a subsequent paper [50], the enthalpies of reaction of $[\text{RhCl}(\text{CO})_2]_2$ and $[\text{Cp}^*\text{RuCl}(\text{COD})]$ with the trialkylphosphine (**1a**) have been measured by anaerobic solution calorimetry in THF at 30.0°C and compared with those for the analogous substitution reactions with “conventional” monodentate phosphines. For the rhodium complex, where electronic effects are important, the authors conclude that the fluorine-derivatised ligand is a poorer σ -donor than PEt_3 , which is in agreement with the conclusions from the spectroscopic comparisons. From the ruthenium reaction, where ligand sterics dominate the thermodynamics, the authors conclude that sterically PEt_3 and the trialkyl phosphine (**1a**) are virtually identical.

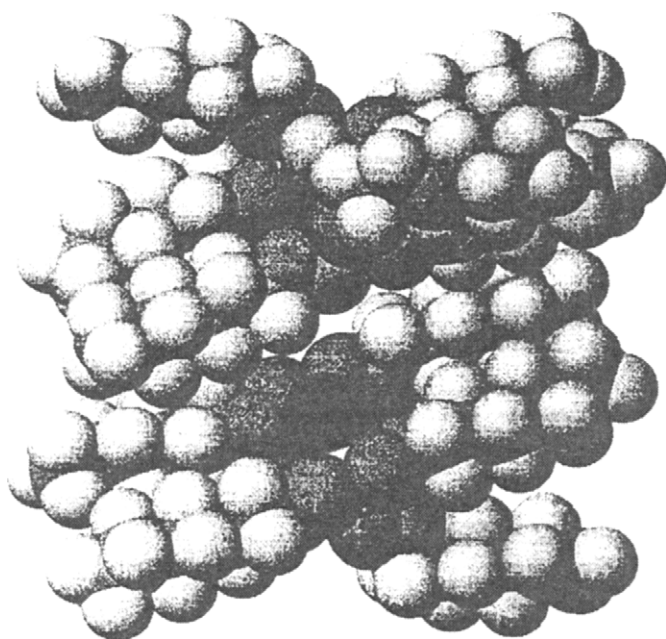


Fig. 4. Packing of two molecules of $[\text{IrCl}(\text{CO})\{\text{P}(\text{C}_2\text{H}_4\text{C}_6\text{F}_{13})_3\}_2]$; non-hydrogen atoms are given at the van der Waals radii (fluorine atoms light, chlorine atoms dark). (Reproduced by permission from *Angew. Chem., Int. Ed. Engl.*, 36 (1997) 1612).

In the first publication [49] on a comprehensive series of transition metal complexes, in this case containing the triarylphosphine ligands (**5,6,7**), the stepwise electronic influence on addition of each perfluoroalkyl unit is clear from $\nu(\text{CO})$ and NMR data. Here, structural characterisations of $[\text{Cp}^*\text{RhCl}_2\text{L}]$ and *cis-/trans*- $[\text{PtCl}_2\text{L}_2]$ $\{\text{L} = \text{P}(\text{4-C}_6\text{H}_4\text{C}_6\text{F}_{13})_3\}$ confirm that the perfluoroalkyl substituents have a negligible structural impact on the first coordination sphere at the metal centres and that interactions between the substituents determine how the metal complexes pack in the solid state. In a sister paper [51], the coordination chemistry of the bidentate ligand $(\text{4-C}_6\text{H}_4\text{C}_6\text{F}_{13})_2\text{PCH}_2\text{CH}_2\text{P}(\text{4-C}_6\text{H}_4\text{C}_6\text{F}_{13})_2$ mirrors that of the monodentate triarylphosphine ligands.

An alternative way to assess the impact of ligand substituents is to investigate the reaction chemistry of the metal complex. This is closely aligned with catalytic studies which are described in the next section. Two groups have briefly looked at oxidative addition reactions to *trans*- $[\text{IrCl}(\text{CO})\text{L}_2]$ $\{\text{L} = \text{trialkylphosphine (1a) or triarylphosphines (5,6,7)}\}$. In the case of the aryl phosphines, O_2 addition studies [49] indicate a sequential reduction in rate of reaction with the introduction of each ponytail. However, attempts to obtain definitive kinetic data indicated that these reactions do not follow the well-documented pseudo-first-order kinetics typical for O_2 addition to Vaska's analogues indicating that the perfluoroalkyl groups physically or chemically influence the mechanism in this system. Further kinetic

studies are under investigation. For **1a**, a more comprehensive range of oxidative addition reactions have been undertaken [47]. For the H₂ and O₂ additions, analogous reductions in rate between non-fluorous and fluorous derivatised ligands mirror the reduction in electron density at the metal centre. However, further solvent studies indicate that perfluorocarbons can *retard* the rate of hydrogenations and oxygenations when compared to those in other solvents, despite higher molar H₂ and O₂ solubilities. It is unclear whether solvent polarity or the existence of cavities within the solvent have the greatest influence but, undoubtedly, the metal complex and gas molecules are stabilised more than the transition state in perfluorocarbons than in conventional solvents. In the oxidative addition reactions of alkyl halides to the Vaska's analogue, the rate and mechanism are strongly affected by solvent. In particular, in perfluoromethylcyclohexane, CF₃C₆F₁₁, there is no evidence for the typical S_N2 oxidative addition pathway and the authors prefer a free radical chain reaction mechanism [47].

The value of perfluoroalkyl-derivatised ligands in FBS catalysis depends on the preferential solubility of the catalyst in a fluorous solvent. Initially, this was established, qualitatively, by ³¹P NMR spectroscopic studies [37,49], but very recently [52] the "fluorous partition coefficients" of metal complexes of the trialkyl phosphine (**1a**) have been measured analytically, from which both a fluorine content of > 60% and the number of perfluoroalkyl groups, which shield the hydrocarbon domain of the complex, are crucial for a high fluorous partition.

13.3.1.3 Catalysis

In recent years, there has been significant interest in attempting to design processes which can draw upon the key advantages of homogeneous and heterogeneous catalysis. The appeal of a system, which could offer the selectivity of a homogeneous solution process combined with the ease of separation of product(s) from catalyst typically found in heterogeneous processes, is obvious. A number of such processes have been developed, including polymer supported catalysts and aqueous/organic biphasic catalysis. The latest candidate for evaluation is catalysis in mixed perfluorocarbon/organic solvent two-phase systems (the so-called fluorous biphasic system, FBS). It should be noted that a number of perfluoroalkyl substituted ligands have been used for catalysis in supercritical CO₂ [34,42,53], but this work is outside the scope of this article.

The initial reports [10,11] details the hydroformylation of 1-octene in a toluene/CF₃C₆F₁₁ biphasic at 100°C under 10 atm CO/H₂ (1:1) using a catalyst generated *in situ* from [Rh(CO)₂(acac)] and P(C₂H₄C₆F₁₃)₃ (**1a**)(1:40) offering 85% conversion to aldehydes and an *n/i* ratio of 2.9. A further, in-depth, analysis of the merits of hydroformylation under FBS conditions makes a number of key conclusions [37]. Here, the hydroformylation of 1-decene and ethylene were investigated with the same catalyst (generated *in situ*) under batch and semi-continuous conditions at 100°C and 1.1 MPa CO/H₂ (1:1) in a 50/50 vol% toluene/CF₃C₆F₁₁ solvent mixture which is homogeneous under these conditions. The long-term stability of this catalyst is greater than that based on PPh₃, the selectivity (*n/i* ratio) is similar but the catalytic activity is an order of magnitude lower. The reaction, as expected, is first-order

in both rhodium and alkene and is inhibited by excess phosphine whereas selectivity increases with phosphine concentration and the best *n/i* ratio (7.84) was obtained at a ligand concentration of 0.3 mol dm^{-3} and a P:Rh ratio of ca 100. The semi-continuous experiments were highly successful with total turnovers of up to 35,000 during 9 cycles with only 1.18 ppm loss of Rh/mol of product(s) which arises from the low but finite solubility of the catalyst in the organic phase. Recent, preliminary, results on the hydroformylation of 1-hexene using a similar catalyst, generated *in situ* using the tris-derivatised aryl phosphine (**5**) indicate a marginally better activity and selectivity than that achieved with triphenylphosphine and with minimal catalyst loss (Table 3) [54,55]. The same ligand (**5**) has been used to generate (*in situ*) a Pd(0) catalyst for cross-coupling reactions between organozinc bromides and aryl iodides in a two-phase toluene/perfluorooctylbromide ($\text{C}_8\text{F}_{17}\text{Br}$) solvent system at 60°C [40]. Catalyst recovery is high and the fluorous phase was reused a number of times with minimal reductions in product yield. The catalytic activity is higher than that for the related Pd(0)— PPh_3 system which has been ascribed to the electronic influence of the perfluoroalkyl substituents.

The hydroboration of alkenes represents an ideal reaction to adapt for fluorous conditions since current methodology often involves the destruction of the metal catalyst and a perfluorocarbon-soluble analogue of Wilkinson's catalyst, $[\text{RhCl}\{\text{P}(\text{C}_2\text{H}_4\text{C}_6\text{F}_{13})_3\}_3]$, has been prepared and evaluated [48]. Good results were obtained using a toluene or THF/ $\text{CF}_3\text{C}_6\text{F}_{11}$ solvent system with the catalyst, alkene and catecholborane, however, this group established that their reactions were more rapid in the absence of the organic solvent. High catalyst recovery was established by recycling the fluorous phase with minimal reductions in yield or turnover frequencies. The rates of hydroboration with the fluorous-derivatised catalyst were lower than those using Wilkinson's catalyst under homogeneous conditions, although this may be a result of the heterogeneous conditions employed in this work.

A general assessment of the relative catalytic activity of a series of fluorous-derivatised ligands and their protio-congeners has been made using the hydrogenation of styrene as a model system (Table 4) [54,55]. In contrast to the results on hydroformylation, rates of hydrogenation are slower under fluorous biphasic conditions than in a conventional organic solvent. In line with well-established trends, the incorporation of perfluoroalkyl substituents causes a reduction in rate relative to their protio-congeners and this effect is most pronounced for the C_2H_4 spacer unit indicating that this is a poorer electronic insulator than the C_6H_4 group. The most promising results are found for the $\text{C}_6\text{H}_4\text{OCH}_2$ spacer group indicating that it is possible to completely insulate the metal centre from the electronic effects of the perfluoroalkyl substituents. Throughout this work, near-quantitative catalyst recovery was established using Rh-atomic absorption spectroscopy.

13.3.2 Macrocyclic ligands

The additional stability arising on the coordination of macrocyclic ligands has been exploited in many fields, including catalysis and, hence, the synthesis and coordination chemistry of macrocyclic ligands are areas of intense academic and

Table 3

Hydroformylation of hex-1-ene catalysed by rhodium complexes

Ligand	Hex-1-ene %	Isomerised hexenes %	2-ethyl- pentanal %	2-methyl- pentanal %	Heptanal %	Conversion %	Selectivity to aldehydes %	<i>n</i> : <i>i</i> ratio
PPh ₃ ^a	0.05	0.7	1.9	22.4	74.7	99.95	99.5	3.1
PPh ₃	0.07	0.3	trace	22.6	77.1	99.93	99.8	3.4
(5)	0.10	0.9	1.0	20.2	77.4	99.90	98.7	3.7

Conditions: [Rh(acac)(CO)₂] (0.001 mol dm⁻³) and phosphine (0.003 mol dm⁻³) dissolved in a degassed mixture of toluene (2 cm³) and PP3 (2 cm³) was heated to 70°C and the pressure of CO/H₂ adjusted to 20 bar. After equilibration, hex-1-ene (1 cm³) was injected and the pressure immediately adjusted to 20 bar. The solution was stirred at 400 rpm for 1 h and the pressure maintained by a mass flow controller. Qualitative analyses were by GCMS and quantitative analyses by glc using *n*-octanol as an internal standard. ^a Solvent system toluene (4 cm³).

Table 4

Hydrogenation of styrene catalysed by rhodium complexes

Ligand	Rate mmol dm ⁻³ h ⁻¹	Ligand	Rate mmol dm ⁻³ h ⁻¹
PPh ₃	155	P(4-C ₆ H ₄ CF ₃) ₃	139
PPh ₃ ^a	211	P(3-C ₆ H ₄ CF ₃) ₃	100
PPh ₃ ^b	160	PEt ₃	177
PPh ₃ ^c	276	P(C ₂ H ₄ C ₆ F ₁₃) ₃ (1a)	79
P(4-C ₆ H ₄ C ₆ F ₁₃) ₃ (5)	128	PEtPh ₂	105
P(4-C ₆ H ₄ C ₆ F ₁₃) ₃ (5) ^b	146	PEt(4-C ₆ H ₄ C ₆ F ₁₃) ₂	62
P(4-C ₆ H ₄ C ₆ F ₁₃) ₃ (5) ^c	86	P(4-C ₆ H ₄ OCH ₃) ₃	218
P(4-C ₆ H ₄ C ₆ F ₁₃) ₃ (5) ^d	115	P(4-C ₆ H ₄ OCH ₂ C ₇ F ₁₅) ₃ (9)	201
P(3-C ₆ H ₄ C ₆ F ₁₃) ₃	117		

Conditions: The ligand (1.257×10^{-4} mol dm⁻³) was dissolved in a degassed mixture of hexane (6 cm³), PP3 (10 cm³) and styrene (1.8 cm³), pressurised to 1 bar with H₂ and equilibrated with stirring at 63.5°C. A solution of [RhCl(C₂H₄)₂]₂ (1.571×10^{-5} mol dm⁻³) in toluene (2 cm³) was added and the mixture stirred for 1 h. Analyses were by glc. ^aSolvent system 18 cm³ toluene. ^bSolvent system 8 cm³ fluorobenzene/10 cm³ PP3. ^cSolvent system 8 cm³ toluene/10 cm³ PP3. ^dSolvent system 18 cm³ PP3 (product extracted at the end of the catalytic runs with toluene).

industrial interest. Three types of derivatised-macrocyclic ligand systems (Fig. 5) have been considered under fluorous biphasic conditions. As with the phosphorus(III) ligand systems, Horváth and Rábai undertook the first experiments in this area, derivatising phthalocyaninato-iron(II), -nickel(II) and -cobalt(II) complexes with four perfluorooctyl sidechains via pressurised, heated, reactions of the underivatised metal complexes with C₈F₁₇I [10,11]. It is interesting that the related copper(II) derivative had been disclosed in 1960 as a “Teflon compatible dye” [56]. The intense blue colour of the cobalt(II) complex was used in a clear representation of the ease of separation under FBS conditions [10] and in a preliminary study of catalytic oxygenation under an FBS regime [11].

Two groups have focused their attentions on perfluoroalkyl-derivatised porphyrin complexes as oxidation catalysts utilising not only the potential for facile separation of product(s)/catalyst and the high solubility of O₂ in perfluorocarbon solvents, but also the enhanced activity arising from the incorporation of the highly electron-withdrawing perfluoroalkyl groups in the *meso* positions of the porphyrin ring. In fact, the possibility of perfluorocarbon solubility was not considered during the synthesis, structural characterisation and electrochemical studies on the zinc complex of 5,10,15,20-tetrakis(heptafluoropropyl)porphyrin (**15**) [57]. Indeed, considering the relatively short perfluoroalkyl ponytails, the subsequent application [58] of this complex as a singlet-oxygen photosensitiser under FBS conditions (for details see Sec. 4.1) is somewhat surprising. An alternative ligand system is the perfluoroalkyl-substituted, tetra-*meso*-aryl porphyrin (**16,17,18**). In initial studies

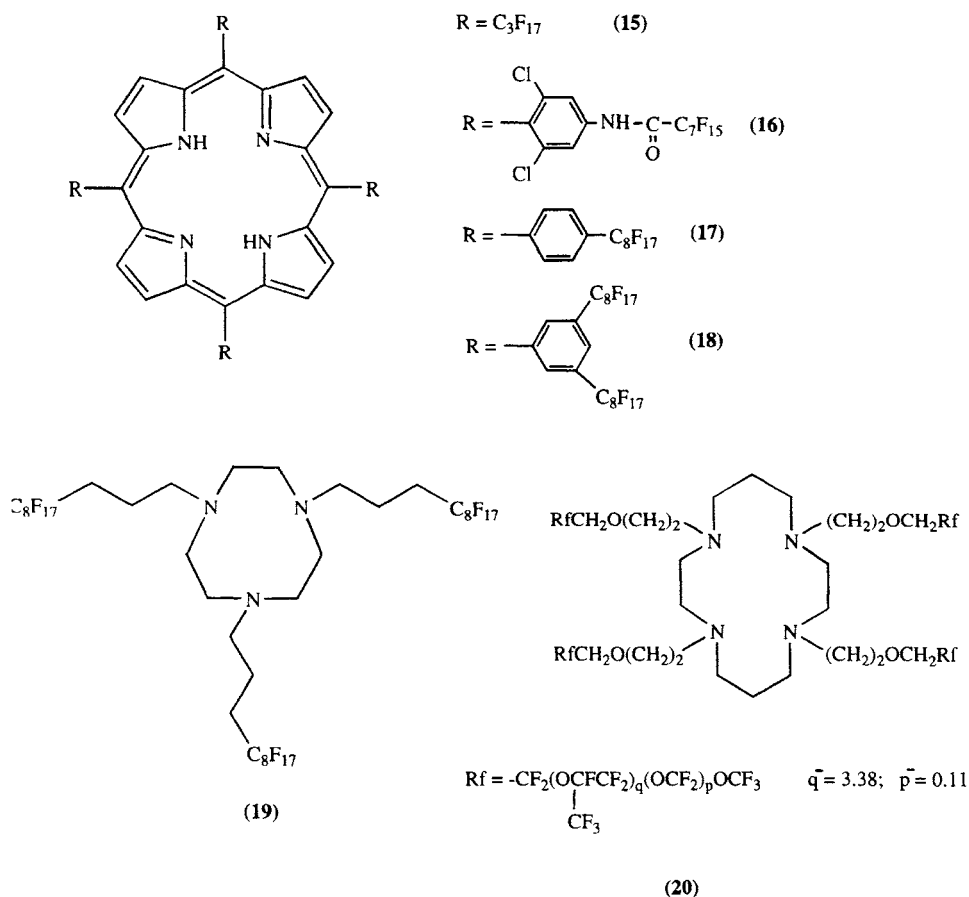
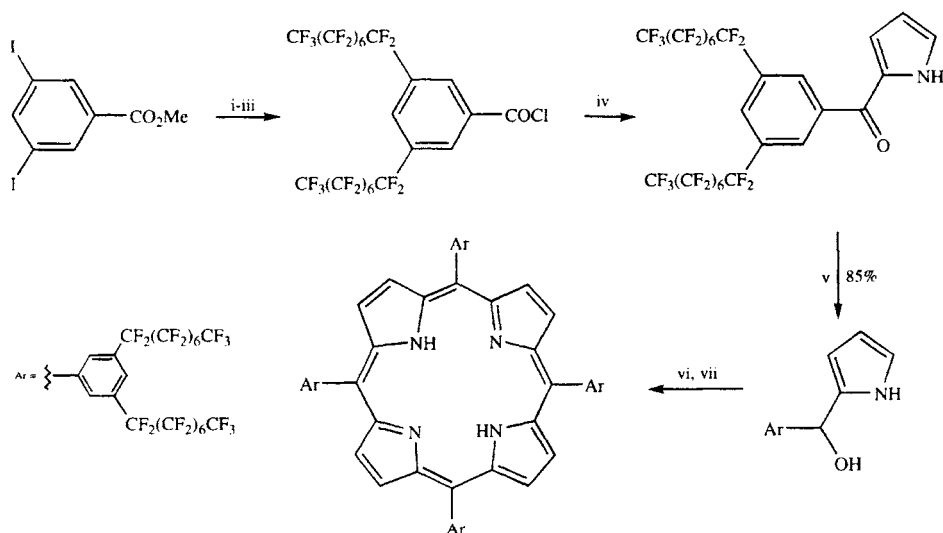


Fig. 5. Perfluoroalkyl-derivatised macrocyclic ligands.

[59,60], enhanced catalytic activity arising from the incorporation of C_8F_{17} units was not accompanied by perfluorocarbon solubility. Interestingly, these authors note a variation in organic solvent solubility with the site of the ponytail. Perfluorocarbon solubility was achieved by incorporating eight C_8F_{17} groups (two per *meso*-aryl ring) without additional spacer units [61]. This ligand (18) could only be prepared by what must be considered to be “non-standard” synthetic procedures (Scheme 3). The cobalt complex of (18) is an active catalyst for the two-phase (perfluorocarbon-acetonitrile) aerobic epoxidation of alkenes with 2-methylpropanal. The oxidations were performed in a rapidly-stirred, biphasic mixture. The conversions and selectivities achieved under this regime were high, catalyst recovery and re-use was illustrated and, most importantly, in comparison to related oxidations with cobalt-*meso*-tetraarylporphyrins, much higher substrate-catalyst ratios (1000:1 vs 20:1) could be employed [61].

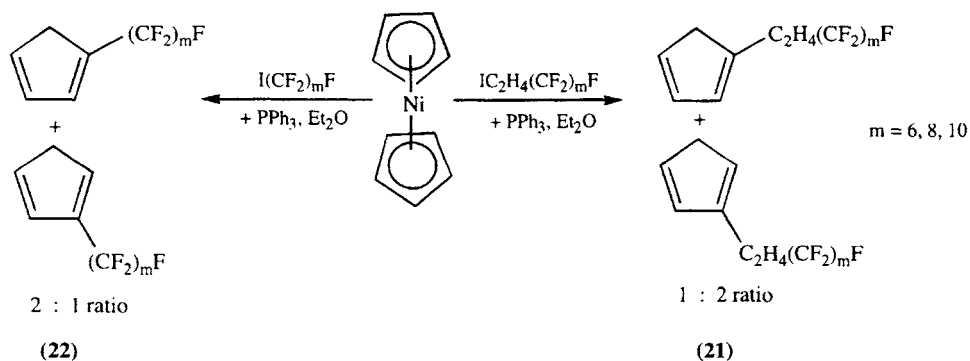


Scheme 3. Reagents and conditions: (i) $C_8F_{17}I$, Cu, DMF, $125^\circ C$; (ii) KOH, H_2O -MeOH, reflux; (iii) $SOCl_2$, reflux; (iv) pyrrole, EtMgBr, Et_2O , $0^\circ C$; (v) LAH, THF; (vi) $Zn(OAc)_2 \cdot 2H_2O$, propanoic acid, reflux, then 2,3-dichloro-5,6-dicyano-1,4-benzoquinone; (vii) CF_3CO_2H , reflux, then aqueous $NaHCO_3$.

The third type of macrocyclic ligand system investigated under the FBS regime are the azacycloalkanes. Fish et al. [62] describe the complexation of 1,4,7- $[C_8F_{17}(CH_2)_3]_3$ -1,4,7-triazacyclononane (**19**) with $[M(C_8F_{17}(CH_2)_2CO_2)_2]$ ($M = Mn, Co$) as alkane or alkene oxidation catalysts using a propyl group to insulate the nitrogen donors and an ethyl group to insulate the carboxylate donors (see Sec. 3.4) from the ponytails. Alternatively, Pozzi et al. [63] have employed a $CH_2OC_2H_4$ unit similarly in a comparable study using the tetraaza-macrocyclic metal complexes show good activity for the *t*-BuOOH/ O_2 oxidation of alkenes (particularly those with allylic hydrogens) under a two-phase system consisting of the complex in perfluoroheptane and the neat substrate [62]. The results are in agreement with the autooxidation mechanism involving alkoxy or alkylperoxy radicals and catalyst recovery and re-use was established. Similar results, using very similar conditions, were achieved for copper and cobalt complexes of the tetraaza-macrocyclic [63].

13.3.3 Cyclopentadienyl ligands

In view of the prevalence and industrial importance of delocalised organic ligands, such as $\eta^5-C_5H_5$ (Cp), it is not surprising that perfluoroalkylated analogues have been investigated. A series of perfluoroalkylated ferrocenes and ferrocenium salts, incorporating up to C_8F_{17} units, have been prepared by conventional synthetic methods to enhance the lipophilicity of these metal derivatives [64]. However, although these workers did not assess the perfluorocarbon solubility of their



Scheme 4. Derivatised cyclopentadienyl ligands.

derivatives, it is unlikely that they would be preferentially soluble in fluoruous solvents in view of their large hydrocarbon content.

Derivatised cyclopentadienes and their metal complexes with shorter or no hydrocarbon spacers have been elegantly detailed by Hughes et al. [52,65]. The parent ligands are formed as mixtures of double-bond isomers, although the exact ratio depends on the length of the ponytail and the presence/absence of the C_2H_4 spacer (Scheme 4). In neither series was the symmetric 5-alkylated isomer observed. Metal complexes of the ligands with the C_2H_4 spacer (**21**) can be prepared by deprotonation, at low temperature with butyllithium, followed by reaction with metal halides. Unfortunately, deprotonation of the cyclopentadienes without the C_2H_4 spacer (**22**) resulted in decomposition and the range of metal complexes with these ligands is, consequently, limited.

Ponytailed ferrocenes $[(\text{CpRf})_2\text{Fe}]$, manganese, rhenium and rhodium carbonyl complexes $\{[(\text{CpRf})\text{M}(\text{CO})_3] \text{ M} = \text{Mn, Re}; [(\text{CpRf})\text{Rh}(\text{CO})_2]\}$ have been prepared and fully characterised. Since none of these complexes are preferentially soluble in perfluorocarbon solvents (as determined gravimetrically) more than one perfluoroalkyl group per Cp ligand would be necessary for preferential solubility. Preferential solubility is achieved for the mixed derivatised-ligand complex $[(\text{CpRf})\text{Rh}(\text{CO})\{\text{P}(\text{C}_2\text{H}_4\text{C}_6\text{F}_{13})_3\}]$ [52]. Oxidation potentials for the ferrocene complexes, which show Nernstian behaviour, are very close to that for unsubstituted ferrocene indicating that the C_2H_4 spacer effectively insulates the metal from the perfluoroalkyl chain [65]. Similar conclusions are drawn from $\nu(\text{CO})$ data for the manganese and rhenium complexes. The electrochemical data also allow diffusion coefficients for the ferrocene derivatives to be calculated. Although the C_6F_{13} -derivatised complex has a similar diffusion coefficient to that for decamethylferrocene, the value for the $\text{C}_{10}\text{F}_{21}$ -derivatised compound is only 16% of that value indicating that the long perfluoroalkyl groups have a significant impact on the mobility of these complexes. Direct reaction of $[\text{Co}_2(\text{CO})_8]$ with the derivatised cyclopentadienes allows the synthesis of complexes $[(\text{CpRf})\text{Co}(\text{CO})_2]$ with and without the C_2H_4 spacer. The $\nu(\text{CO})$ data for these complexes confirm that

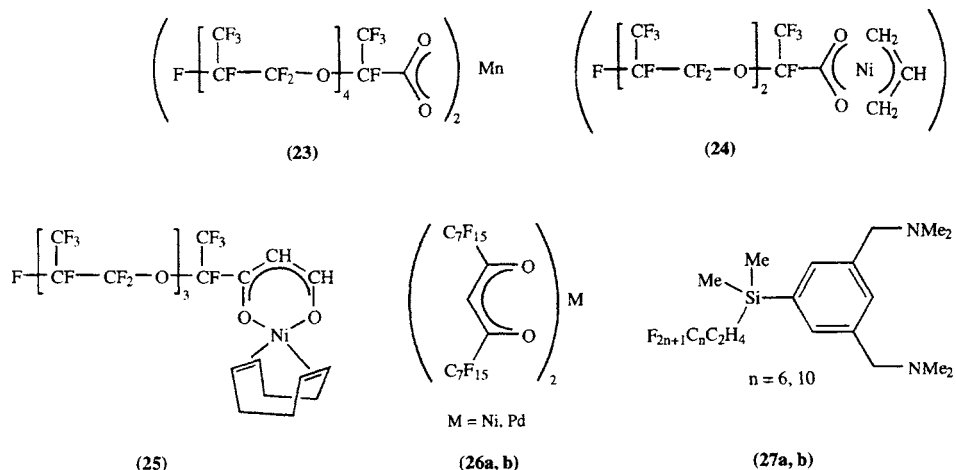


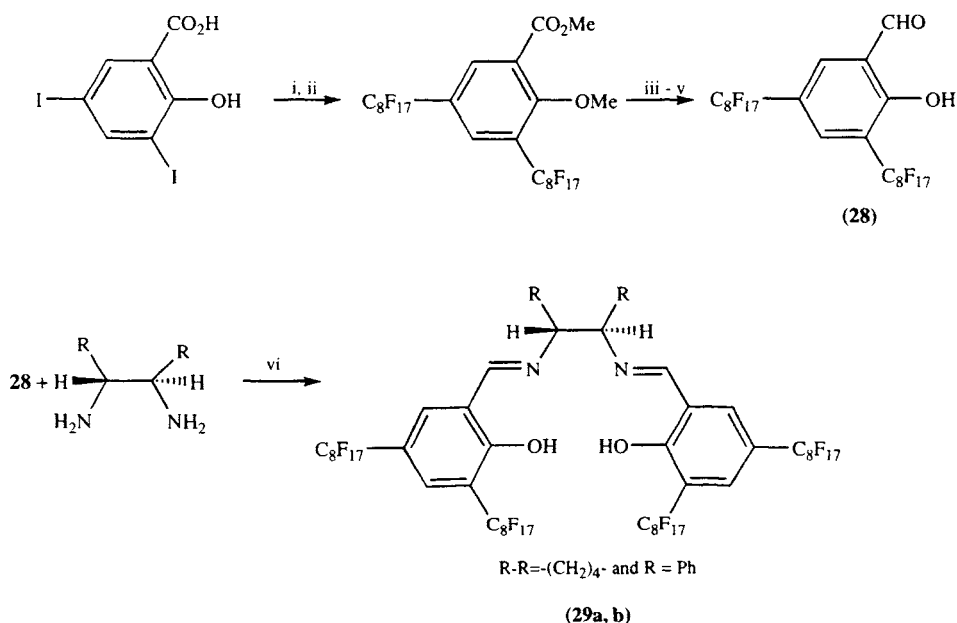
Fig. 6. Some perfluoroalkyl-derivatised chelating ligands and their metal complexes.

the C₂H₄ spacer adequately insulates the metal centre which is supported by the dramatic increase in $\nu(\text{CO})$ for the complexes without this spacer [65].

13.3.4 Other ligand systems

This section outlines the synthesis, coordination chemistry and catalytic studies using oxygen and nitrogen donor ligands. Vogt [16] prepared a series of carboxylate ligands based upon hexafluoropropylene oligomers. Coordination to cobalt(II), manganese(II) (23) and nickel(II) centres (24), using established procedures, gave metal complexes with preferential perfluorocarbon solubility which were tested as oxidation catalysts (Co, Mn) and as a catalyst for the polymerisation of butadiene (Ni) (Fig. 6). The results were reasonable, but complex stability and catalyst recovery were not good. Interestingly, the related straight-chain perfluorocarboxylate cobalt(II) and manganese(II) complexes [62,63] are only slightly-soluble in perfluorocarbon solvents indicating that either the oxygen linkers or the length of the perfluoroalkyl units are crucial for preferential perfluorocarbon solubility in these systems with only one or two ponytails.

Vogt [16] also prepared nickel-cyclooctadienyl ethene polymerisation catalysts using β -diketonate ligands with one perfluoroalkyl substituent (25), but again, although the species were active, catalyst decomposition was a problem. Related β -diketonate ligands with two C₇F₁₅ ponytails have been described by Knochel (Fig. 6) [66,67]. The nickel complex (26a) is an active catalyst for the oxidation of aldehydes with molecular oxygen or sulphides in the presence of isobutyraldehyde in a vigorously stirred toluene/perfluorodecalin two-phase system. The palladium complex (26b) has been used as a catalyst for the Wacker oxidation of alkenes using *t*-BuOOH in a similar benzene/C₈F₁₇Br system. In both processes, no leaching of the catalyst was observed and the catalysts could be re-used with modest decreases in



Scheme 5. Reagents and conditions: (i) Me₂SO₄, K₂CO₃, acetone, reflux; (ii) C₈F₁₇I, Cu, DMF, 125°C; (iii) LAH, Et₂O, 0°C; (iv) aq. NaOCl, KBr (10 mol%), TEMPO, PhCF₃, 5°C; (v) BBr₃, CH₂Cl₂, -78°C, then room temp.; (vi) EtOH, reflux.

yield. A related ruthenium catalyst, generated *in situ*, can be used for the epoxidation of alkenes in a toluene/C₈F₁₇Br two-phase system but up to 5%, by weight, of catalyst could be lost over a number of catalytic cycles [66].

van Koten has derivatised his aryldiamine ligand system with C_nF_{2n+1}C₂H₄Si(Me)₂ (*n* = 6, 10) ponytails (**27**) (Fig. 6) [68]. Coordination chemistry, a crystal structure of a nickel complex, and evaluation of these complexes as Kharasch catalysts (using the addition of CCl₄ to methylmethacrylate in dichloromethane as a model reaction) indicate that the C₂H₄SiMe₂ spacer completely insulates the aryl ring from the perfluoroalkyl substituents and that neither ligand system is preferentially soluble in perfluorocarbon solvents negating the application of these ligands as FBS catalysts.

The possibility of asymmetric induction under the fluorous biphasic conditions was first speculated upon by Horváth and Rábai [10], and this year has seen the first report of asymmetric catalysis in a fluorous biphasic [69]. Two, C₂ symmetric salen ligands (**29a, b**) with four C₈F₁₇ ponytails have been prepared (Scheme 5) and their Mn(II) complexes evaluated as chiral catalysts for the aerobic oxidation of alkenes under FBS-modified Mukaiyama conditions. Both complexes are active catalysts (isolated yields of epoxides up to 85%) under unusually low catalyst loadings (1.5% cf. the usual 12%). Although catalyst recovery and re-use was demonstrated, low enantioselectivities were observed in most cases.

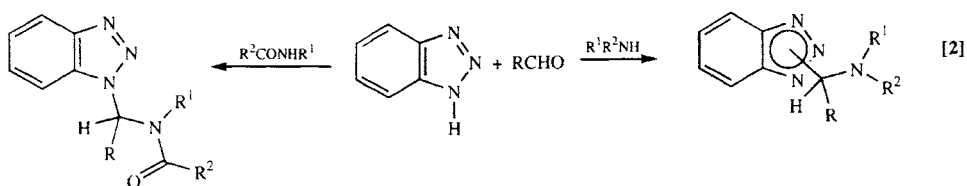
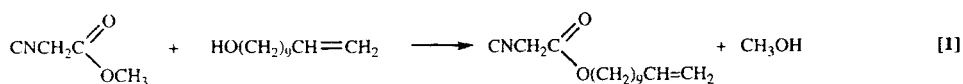
13.4 Synthesis in perfluorocarbon solvents

The properties of perfluorocarbons can be exploited to provide reaction media for organic and inorganic synthesis, where their attractions include their low reactivity, easy phase separation from organic reaction products without purification, their low toxicity and their broad liquid ranges.

13.4.1 One-phase systems

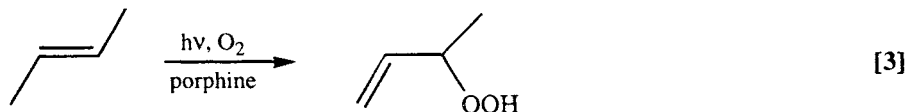
The first report of a perfluorocarbon as a solvent for synthesis pre-dates Horváth and Rábai's fluorous biphasic paper by 14 years. Kelly [70] investigated the flash photolysis of chromium hexacarbonyl in perfluoroheptane where the chromium pentacarbonyl (generated during photolysis) was shown to be more reactive in perfluorocarbon solvents than in hydrocarbon solvents. This effect, presumably, arises from the weak solvation of the unsaturated metal centre by the perfluorocarbon.

However, the widespread application of perfluorocarbons as immiscible solvents followed Zhu's 1993 paper [17] on transesterifications (Eqn. (1)). To shift the equilibrium in this reaction, it is essential that the resulting alcohol, e.g. methanol, is removed from the reaction mixture. Since the alcohols are miscible when normal reagents and solvents are used, this is not an easy task to perform. However, Zhu solved this problem by using a modified Dean–Stark trap and a perfluorocarbon as the solvent. The trap allowed the denser fluorous phase to be returned to the reaction mixture and after refluxing the reaction mixture for two hours, approximately three grams of methanol was separated off. It was also observed that in the esterification of $\text{CH}_2=\text{C}(\text{CH}_3)\text{CO}_2\text{H}$ with PhCH_2OH , quantitative amounts of water were separated in 3.5 h in perfluorocarbon fluid (82% yield) whilst it took 5 hours in toluene (81% yield). Similarly, Katritsky [71] also applied the same combination of a perfluorocarbon solvent and an inverse Dean–Stark trap to remove the water formed in the reaction between benzotriazole, aldehydes and either amines or amides (Eqn. (2)). The reactions were much faster and most yields were higher than using a normal Dean–Stark trap with benzene or toluene. An additional advantage of these reactions is the easy workup. The organic products were separated from the perfluorocarbon solvent by phase separation, allowing the solvent to be reused with minimal purification.



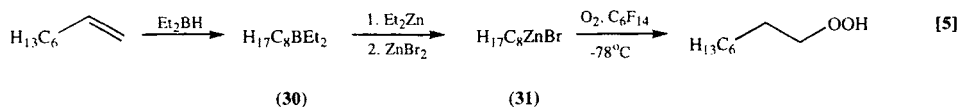
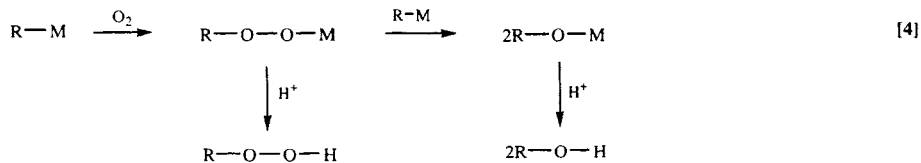
Zhu has subsequently shown that in addition to water, perfluorocarbons can also be used as media for suspension polymerisations [72]. Due to the lower surface tension of perfluorocarbons, organic monomers can be dispersed for the first time without using surfactants, however, the yields of regularly-sized beads were increased by using the right surfactants. The major advantage of using perfluorocarbons is that the scope of suspension polymerisations can be extended to monomers which were previously either too soluble in water or not stable in water. Consequently, monomers with a reactive functional group such as an acid chloride, a carboxylic acid, an isocyanate, a trimethoxysilane, an hydroxyl and an aziridine were polymerised in one step in perfluorocarbons to give the corresponding cross-linked copolymer beads. Similarly, perfluorocarbons can also be used for cationic suspension polymerisations where most cationic initiators, like TiCl_4 and $\text{BF}_3 \cdot \text{Et}_2\text{O}$, are moisture-sensitive.

Utilising the ability of perfluorocarbons to dissolve substantial amounts of gases, Chambers demonstrated that perfluorocarbons are good replacements for chlorinated solvents in the photooxidation of alkenes [29]. When an alkene and porphine sensitiser were irradiated with light, singlet oxygen ($^1\text{O}_2$) was introduced at a specific site and quantitative yields of peroxide products were obtained (Eqn. (3)). The perfluorocarbon fluids were recovered easily by phase separation and reused. However, the sensitiser often decomposes when either high concentrations of substrates are used or the substrate is not very reactive. DiMaggio increased the chemical stability of tetraphenylporphyrin (TPP) by the introduction of electron-withdrawing heptafluoropropyl groups (**15**) [57,58]. In parallel experiments when 0.1 M carbon tetrachloride solutions of allylic alcohol were photolysed for 22.5 h, only 11% of TPP was left at the end of the experiment whilst 85% of (**15**) remained. Unfortunately, both of the sensitisers degraded extensively when the substrate concentration was increased to 1 M, but it is possible to circumvent this problem by separating the sensitiser from the reaction substrates and products. A fluorous biphasic system was therefore set up by dissolving the substrate in the top acetonitrile layer and (**15**) in the lower perfluorocarbon phase. Under these conditions the amount of degradation of (**15**) was reduced significantly and at the end of the reaction the fluorous-sensitiser solution could be reused directly.

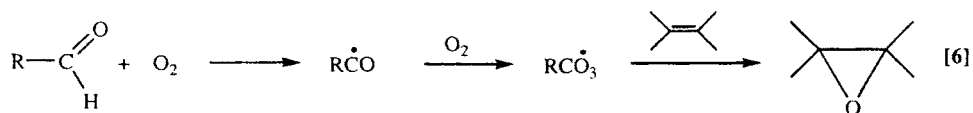


Knochel has championed the use of perfluorocarbons as the reaction media for performing oxidations of organometallics because of the high solubility of oxygen in these solvents and their non-flammability [73–76]. Hydroperoxides can be prepared by reacting organometallics (Li, Mg, Al, Cd, Zn) with oxygen but alcohols are often produced in this reaction pathway (Eqn. (4)). To obtain good yields of peroxides, the organometallic should be added slowly to a large excess of oxygen at low temperature and so large volumes of ether are normally required.

For example, a mixture of octyl hydroperoxide and octanol was obtained in the ratio of 80:20 (66% yield) in the oxidation of dioctylzinc (3 mmol) in ether (1000 cm³) at -90°C. By using perfluorohexane it was possible to reduce the volume of solvent required to 50 cm³ [73–76]. It was also discovered that better yields of peroxides were obtained from the less reactive alkylzinc bromides (31) than from dialkylzincs in perfluorohexane at -78°C and octylzinc bromide, which was prepared from octene (Eqn. (5)), was oxidised to octylhydroperoxide in 85% isolated yield. A range of functional groups, like chloro, bromo, OSi(Pr)ⁱ₃ and ester were tolerated under these conditions and good yields (58–85%) as well as good ratios of hydroperoxides : alcohols (>98:2) were achieved. The same method was also applied successfully to chiral and secondary alkenes. By using a reductive workup (2 N HCl, Zn) it was also possible to prepare terminal alcohols from alkenes [74,76]. Hence, octanol was prepared in 95% yield by adding dioctylzinc to an oxygen-saturated solution of perfluorohexane. Knochel [75] has extended this work further by showing that it is possible to oxidise diethylorganoboranes (30) in bromoperfluorooctane to give alcohols in good yields (61–95%). Not only does this save one step, but it also avoids using the pyrophoric diethylzinc reagent. The oxidations normally took less than 5 h and were faster than the reactions in THF, which gave lower yields. Again, functional groups like a halide, TIPS-ether, ester, malonate and sulfonamide were unaffected by the oxidations and most surprisingly, retention of configuration was observed in the oxidation of secondary diethylorganoboranes.



Pozzi has also shown that perfluorocarbons are excellent replacements for chlorinated solvents in the epoxidation of alkenes with sacrificial aldehydes in the absence of metal catalysts [77]. It is believed that the acylperoxy radical, which is formed by the reaction of oxygen with an aldehyde, is responsible for the epoxidation (Eqn. (6)).



13.4.2 Two-phase systems

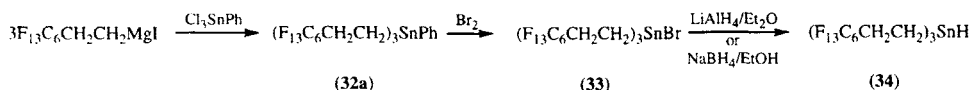
Synthesis in two-phase perfluorocarbon/organic solvent systems, similar to those used for catalysis with metal complexes, is limited. Beyond DiMagno's porphyrin-sensitised oxidation (detailed above), Nakamura [78] has reported a two-phase perfluorooctylation of aromatic compounds and Bégue [79] has used perfluoro-2-butyldihydrofuran and toluene as the reaction medium for the $\text{Mn}(\text{OAc})_3 \cdot 2\text{H}_2\text{O}$ catalysed aerobic epoxidations of unfunctionalised olefins. Here, oxygen gas was bubbled through a mixture of alkene, catalyst and pivaldehyde dissolved in the solvent system. At end of the reaction, 5% K_2CO_3 was added and the three phases were separated. The fluorous phase was reused and the product epoxide was recovered from the organic phase in good yields (75–100%). Again, fluorous solvents exhibited faster reaction times and simplified the purification of the final products.

Another potential application of perfluorocarbons is their use as “bulking agents” where the volume of “conventional” solvent is reduced by replacement with a perfluorocarbon. Although the “halex” reaction is a successful industrial process, there are problems recovering the toxic dipolar aprotic solvents. Chambers [80] has shown that, on a preparative scale, up to 75% of the sulfolane can be replaced in the halex reaction by an equivalent volume of perfluorohydrophenanthrene (b. pt. = 215°C). On cooling the reaction mixture, it is a simple matter to separate off the fluorous solvent at the end of the reaction for recycling.

13.5 Multi-phase purification using perfluorocarbon solvents

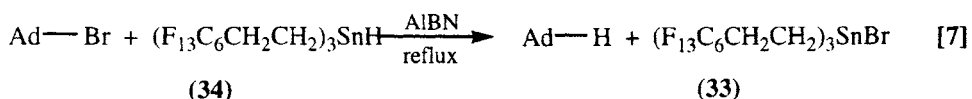
Curran has recently applied the fluorous biphas concept to develop cleaner and more efficient organic synthesis. One method for doing this is to attach a “fluorous-phase label”, which normally consists of long perfluoroalkyl groups, to the reagent to render it preferentially soluble in the fluorous phase in exactly the same way as Horváth and Rábai [10,11] synthesised fluorous-soluble catalysts. At the end of the reaction it is the fluorous-phase label which enables the simple purification of the reaction mixture by liquid–liquid extraction between organic and perfluorocarbon solvents. The desired product is retained in the organic phase whilst the spent reagent is extracted into the fluorous phase allowing it to be recycled and reused, after it has been regenerated in to its active form.

Curran [81–83] first demonstrated the value of this approach by the successful reduction of 1-bromoadamantane using the fluorous-soluble tin hydride reagent, tris(2-(perfluorohexyl)ethyl)tin hydride {**34**, $(\text{F}_{13}\text{C}_6\text{CH}_2\text{CH}_2)_3\text{SnH}$ }. The fluorous tin hydride reagent was synthesised in three steps from 2-perfluorohexyl-1-iodoethane in an overall yield of 65% (Scheme 6). In an attempt to mimic the



Scheme 6.

chemical reactivity of tributyltin hydride, the ethylene spacer group was deliberately included to try to insulate the tin hydride from the electron-withdrawing effect of the fluoros ponytails. When the reduction of 1-bromoadamantane was carried out in organic solvents, fluoros solvents or under fluoros biphasic conditions, the reaction was not very successful because the fluoros tin hydride reagent was not soluble in most organic solvents and the organic substrate was not soluble in the fluoros solvents. To provide a homogeneous reaction medium, Curran used the "hybrid" solvent, α,α,α -trifluorotoluene (sometimes called benzotrifluoride, BTF). In fact, 1-bromoadamantane was reduced, under reflux, with 1.2 equivalents of tin hydride (34) in 3 h (Eqn. (7)). After removal of the solvent, the reaction mixture was partitioned between $\text{CF}_3\text{C}_6\text{F}_{11}$ and dichloromethane. The organic phase provided adamantane in 90% yield and the fluoros phase recovered the fluoros tin bromide (33), which can be recycled after reduction with LiAlH_4 . The liquid-liquid extraction was successful because of the very high partition coefficient of the fluoros tin hydride reagent for fluoros solvents and no tin by-products were detected in the organic phase by ^1H NMR spectroscopy. Similarly, no adamantane was detected in the fluoros extract. Although tris(2-(perfluorohexyl)ethyl)tin hydride (34) also reduced some phenyl selenides, nitro compounds and xanthates in a similar fashion to Bu_3SnH , a detailed kinetic study revealed that the rate constants for trapping primary alkyl radicals with $(\text{F}_{13}\text{C}_6\text{CH}_2\text{CH}_2)_3\text{SnH}$ were actually about two times as great as those for Bu_3SnH [84], which was attributed to the electron-withdrawing effect of the perfluoroalkyl groups. However, the advantage of the fluoros tin hydride reagent lies in its simple but effective workup, which ensures that no toxic tin by-products contaminate the organic product (the main restraint on the commercial use of tributyltin hydride).



A catalytic method for the reduction of 1-bromoadamantane was developed using only 10% fluoros tin hydride reagent (34). Sodium cyanoborohydride (1.3 equivalents) was required as the co-reductant and *tert*-butanol was added to aid dissolution. At the end of the reaction the solvent was removed and the crude reaction mixture was purified by a three-phase liquid extraction. The top aqueous phase removed the inorganic salts, the tin reagents were extracted into the bottom fluoros phase and the adamantane was isolated in 92% yield from the organic phase. The same tin reagent was reused five times in this catalytic cycle with no decrease in yield. In fact, even with only 1% of the fluoros tin reagent, 1-bromoadamantane was reduced in 95% yield. A control experiment indicated that the tin reagent is essential for the reaction as 1-bromoadamantane was not reduced by sodium cyanoborohydride alone over 24 h. Under 80 atmospheres of CO pressure the same catalytic cycle was also used for the hydroxymethylation of organic halides [85].

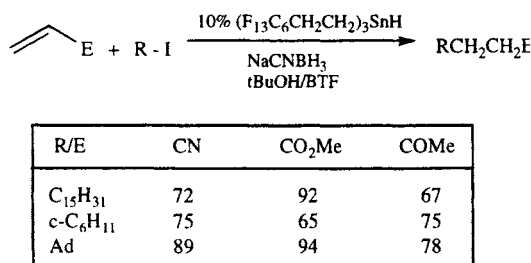


Fig. 7. Multiplex synthesis using a perfluoroalkyl-derivatised tin hydride reagent.

Following the successful application of these convenient purification procedures, Curran recognised the potential of this tin reagent for carrying out combinatorial synthesis [81–83,86]. The easy phase separation of organic products from fluorous reagents is comparable with solid phase synthesis where the polymer-bound product is separated from the soluble reagents by filtration. Curran showed that it is possible to conduct multiple, parallel organic synthesis, often called “multiplex syntheses”, using the fluorous tin hydride reagent by carrying out a series of radical additions in parallel. As shown in Fig. 7, three halides were crossed with three alkenes using the same catalytic method described for the reduction of 1-bromoadamantane. Excess alkene (5 equivalents) and sodium cyanoborohydride (1.3 equivalents) were used to make sure that all of the starting halide reacted. After evaporation of the solvents and excess alkenes, each of the nine products were isolated in good yields and purity by, just, three-phase liquid–liquid extraction.

From this work it is apparent that this approach has two distinct advantages over solid phase synthesis. Firstly, by using permanently fluorous-labelled reagents there is no need to attach and detach the substrate to the solid phase and this not only saves two steps of the reaction but also means that it is no longer necessary to have a functional group present on all the substrates for attachment to the solid phase. In addition, the fluorous extracts can be combined and evaporated to recover the fluorous reagent for reuse. The second major advantage is that the reactions can now be performed in homogeneous reaction media, but the immiscibility of fluorous solvents can still be used for the straightforward separation of products from reagents. However, one of the problems of fluorous chemistry is guaranteeing high enough partition coefficients of the fluorous reagents to allow their quantitative recovery.

As well as labelling reagents permanently fluorous, Curran has also labelled substrates temporarily fluorous for multiplex synthesis. For example, a series of fluorous aryl tin substrates were prepared (Fig. 8) and used as variable pieces of a small library of Stille couplings [86–88]. A mixture of tin reactant (**32a–d**, 1.2 equivalents), halide or triflate (**35a–e**, 2 mmol, 1 equivalent), PdCl₂(PPh₃)₂ (2 mol%) and LiCl (3 equivalents) in THF/DMF (1/1, 1 cm³) was heated at 80°C for 22 h. The reactions were carried out in groups of five by reacting one tin reactant with all five partners in separate vials simultaneously. After evaporation of the solvent, the crude

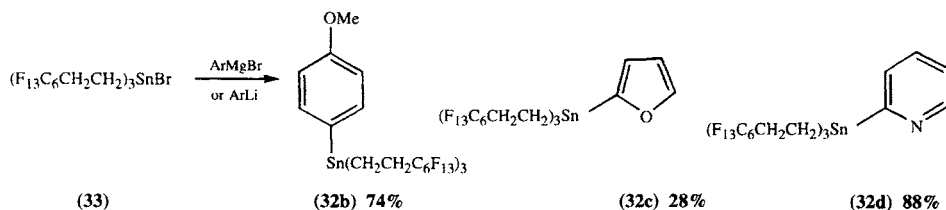
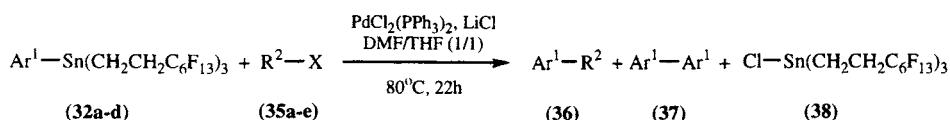


Fig. 8. Perfluoroalkyl-derivatised aryl tin reactants.



Substrate (35)	Tin Reactant ^a		
	(32a)	(32b)	(32c)
C ₆ H ₅ I	90	97(10)	45
p-CH ₃ COC ₆ H ₄ Br	90(7)	87(6)	72
p-NO ₂ C ₆ H ₄ Br	94(9)	98(8)	93
p-NO ₂ C ₆ H ₄ OTf	82(9)	86(8)	83
PhCH ₂ Br	77(5)	98(7)	32

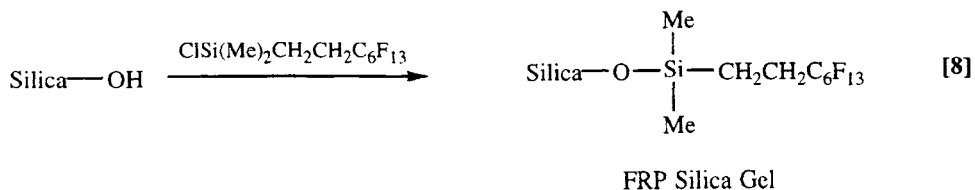
^aYields(%) of symmetrical biaryl (37) in parentheses

Fig. 9. Stille coupling reactions.

reaction mixtures were purified by three-phase extraction between water, dichloromethane and perfluorohexane. Although the fluorous phase recovered 80–90% of the tin chloride (38), which could be recycled to form more fluorous aryl tin substrates, further extractions were required to remove all of it from the organic phase. The dichloromethane extract provided a mixture of the major cross-coupled product (36) and the minor homocoupled biaryl by-product (37), and this mixture was finally purified by preparative TLC. All the results are reported in Fig. 9 and good yields were obtained, except for two reactions with the furyl tin reactant where the products were quite volatile. Isolated yields of the homocoupled by-products (37) ranged from 5 to 10%, although they were not observed for the furyl tin reactant due to the high volatility of its homocoupled product. Similar to the reactions with pyridyltributyl tin, those reactions with the fluorous pyridyl tin reactant (32d) were not very clean and so the reaction products were not fully purified or characterised. A similar result was also obtained when the reaction was carried out under microwave irradiation [89], but a good yield of the desired product (79%) was achieved when the LiCl was replaced by CuO.

Although the fluororous aryl tin reactants (**32a–d**) definitely have advantages over using aryltributylstannanes (easy and efficient separation of tin by-products from organic products, recycling the fluororous label), they are not as suitable for multiplex synthesis as the $(\text{F}_{13}\text{C}_6\text{CH}_2\text{CH}_2)_3\text{SnH}$ reagent (**34**). The major disadvantage of the Stille couplings is the production of the symmetrical homocoupled by-product which partitions into the organic phase with the desired cross-coupled product. This means that the two products still have to be separated by column chromatography which is labour intensive and, therefore, not ideal for rapid parallel synthesis. Another drawback is the long reaction times (22 h), but these times were reduced dramatically to 2 minutes by carrying out the reactions under microwave irradiation [89]. Fortunately, under these conditions, the amount of symmetrical biaryls were also reduced to less than 3%, except with electron-rich aryl halides (10–15%).

The tris(2-(perfluorohexyl)ethyl)stannane group has also been used to label an allyl substrate [90] and a Cp^* group [91] temporarily fluororous which were used in the thermal allylations of aldehydes and the synthesis of Cp^*MCl_4 ($\text{M} = \text{Nb}, \text{Ta}$) derivatives. As in the Stille couplings, the fluororous label was detached during the reaction to give the organic/organometallic product and fluororous tin by-products. As well as purifying the reactions by a two-phase extraction, a second set of thermal allylations were also purified by fluororous solid-phase extraction. For this technique “fluororous reverse phase (FRP) silica gel” [82,86,90] was prepared by silylating standard “flash chromatography” grade silica gel with commercially available $\text{ClSi}(\text{Me})_2\text{CH}_2\text{CH}_2\text{C}_6\text{F}_{13}$ (Eqn. (8)). The crude reaction mixture was loaded onto the FRP silica gel and eluted initially with acetonitrile. As the organic products do not interact with the column, the organic products were eluted immediately in the acetonitrile. On the other hand, the fluororous tin by-products are retained on the column by fluorine–fluorine interactions but, by eluting with a non-polar organic solvent like hexane or a fluororous solvent, these interactions are broken and the fluororous tin by-products can then be eluted. In essence, fluororous solid-phase extraction is more like a filtration which separates the organic products from the fluororous by-products. This technique is probably not only easier to carry out in parallel but also easier to automate than liquid–liquid extractions. It is especially advantageous if it is more selective than two-phase extractions and saves carrying out more than one organic-fluororous extraction.



13.6 Fluororous synthesis and fluororous-phase switches

Following these successes, Curran developed another new strategy for facile product/byproduct/reagent separation which he has called “fluororous synthesis” [82,86].

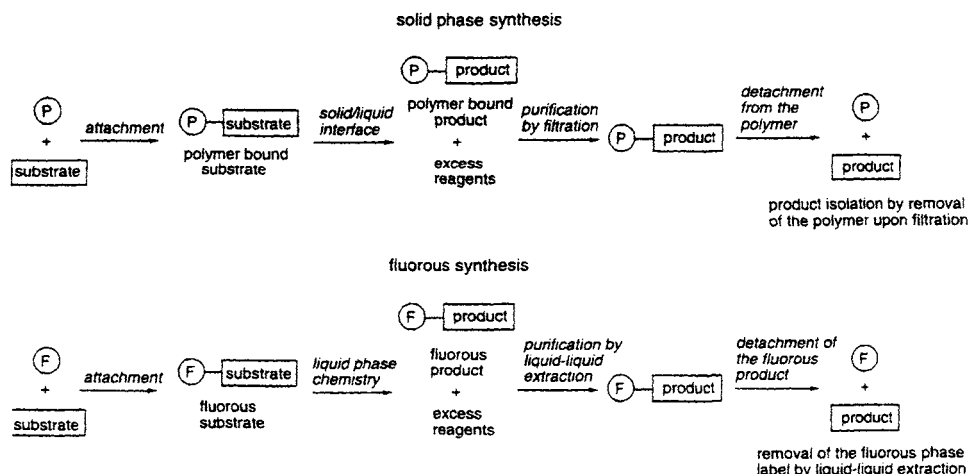
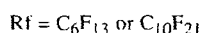
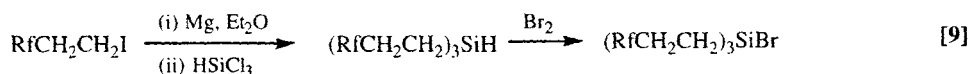


Fig. 10. A Comparison between the methodologies of solid phase synthesis and fluorous synthesis. (Reproduced by permission from J. Org. Chem., 36 (1998) 2917).

The methodology is very similar to solid-phase synthesis (Fig. 10) and involves (i) the attachment of a fluorous phase label to the substrate; (ii) subjecting the labelled substrate to one or more reactions and purifying the reaction mixtures at each stage only by three-phase extraction; (iii) detachment of the fluorous label to release the desired organic product into the organic phase. The main advantages of fluorous synthesis over solid-phase synthesis is that homogeneous reactions can be conducted under standard conditions and that the fluorous substrates are like “normal” organic molecules which can be identified and analysed by traditional methods (NMR, mass spectroscopy, TLC, chromatography, HPLC etc.).

Fluorous synthesis was first demonstrated by the 1,3-dipolar cycloaddition of nitrile oxides to alkenes and alkynes [82,86,92,93]. Although this reaction produces isoxazolines and isoxazoles in high yields, column chromatography is normally required to separate the furoxan dimer from the target product. Figure 11 is a multilayer scheme which shows both the preparative route to the isoxazolines in the horizontal dimension and the purifications at each stage in the vertical dimension. The synthesis of the desired product is highlighted in boldface. The fluorous phase labelling reagent, $\text{BrSi}(\text{CH}_2\text{CH}_2\text{C}_6\text{F}_{13})_3$, was easily prepared by brominating the corresponding silane, $\text{HSi}(\text{CH}_2\text{CH}_2\text{C}_6\text{F}_{13})_3$ (Eqn. (9)).



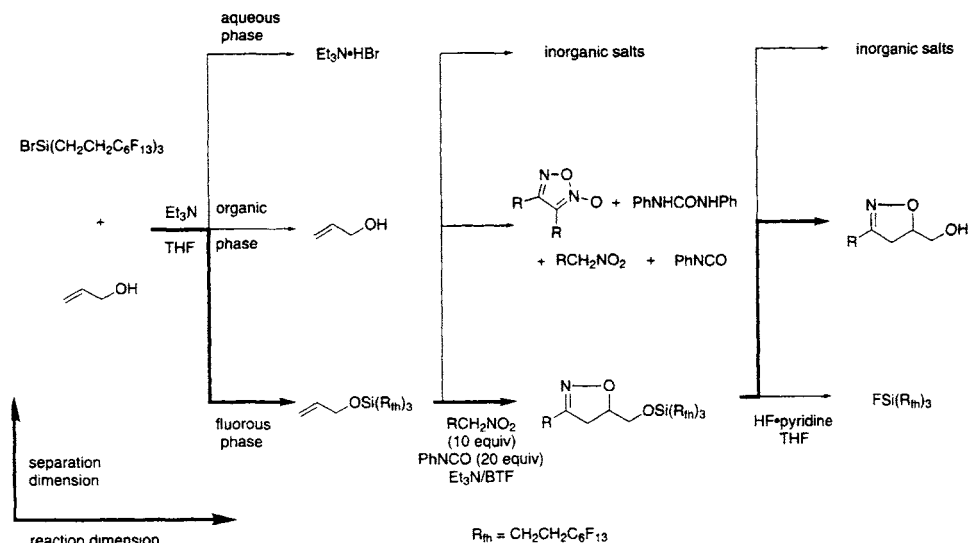


Fig. 11. Fluororous synthesis illustrated in a multilayer reaction scheme. (Reproduced by permission from *Angew. Chem., Int. Ed. Engl.*, 37 (1998) 1174).

Excess alcohol (2–4 equivalents) was used to ensure that all of this label was consumed in the silylation. A large excess of the nitrile oxide was prepared by the dehydration of a nitroalkane (10 equivalents) with phenylisocyanate (20 equivalents) and used to ensure a quantitative yield of the fluororous isoxazoline. Primary and secondary alcohols can not be used in this synthesis as they react with the isocyanate and so the fluororous silyl group was also acting as a protecting group. In the final step HF.pyridine was used to desilylate the isoxazoline and return it to the organic phase. Since HF.pyridine is very corrosive it is not the easiest reagent to handle and another disadvantage of this work is that the expensive fluororous label, $\text{FSi}(\text{CH}_2\text{CH}_2\text{C}_6\text{F}_{13})_3$ was not recycled. However, the isoxazolines were obtained from the final organic phase in reasonable yields (29–99%) and high purities (>94%), which is very impressive considering such large excesses of organic reagents were used in the cycloaddition. Although this preparation only demonstrated, essentially, a one-step synthesis, it is possible to envision this method being applied to multistep syntheses.

Fluororous synthesis has also been applied to multicomponent condensations [86,92,94] and oligosaccharide synthesis [95] which uses a fluororous benzyl protecting group. By reacting a substrate and two or more reactants in one step, multicomponent condensations facilitate the introduction of two or more variable side chains to the target compound. Consequently, these condensations, like the Ugi and Biginelli reactions (Fig. 12), are especially beneficial to combinatorial chemistry. Scheme 7 shows the long, six-step synthesis of a fluororous-phase labelled benzoic acid reactant. In the fluororous Ugi reaction a large excess (17 equivalents) of the aldehyde, amine and isonitrile were used to drive the reaction to completion

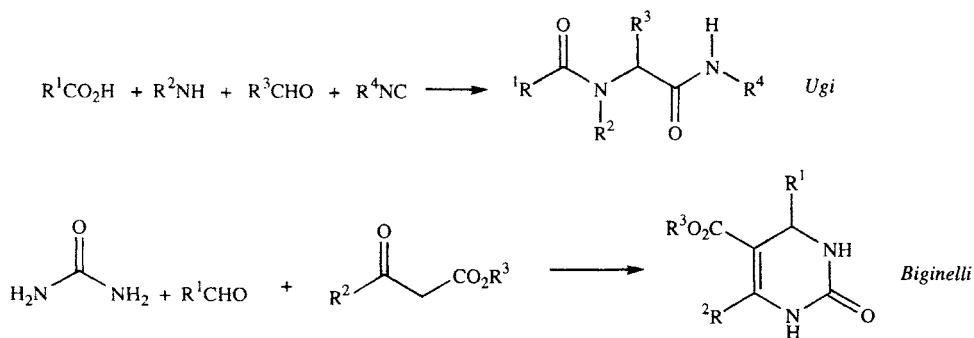
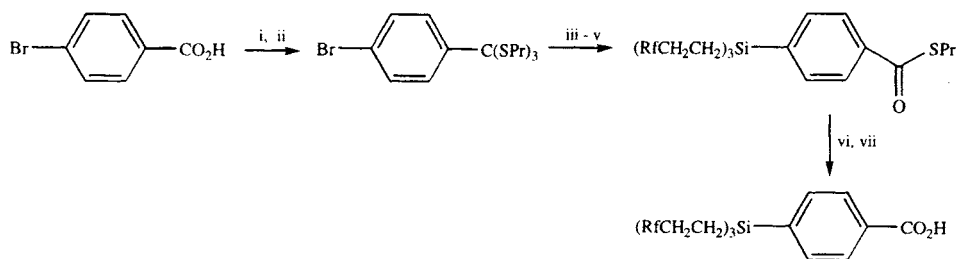


Fig. 12. Ugi and Biginelli reactions.

Scheme 7. Reagents and conditions: (i) SOCl_2 , reflux; (ii) Pr^iSH , AlCl_3 , 60°C , 48 h; (iii) $t\text{-BuLi}$, -78°C ; (iv) $(\text{RfCH}_2\text{CH}_2)_3\text{SiBr}$; (v) AgNO_3 , THF, H_2O , acetone, BTF; (vi) Br_2 , C_6F_{14} ; (vii) THF, BTF, H_2O .

and the fluoros benzoic acid was used to provide the fluoros label on the final product. However, it was essential that the fluoros label contained enough fluorine to render the product preferentially soluble in the fluoros phase. To do this effectively, it was necessary to substitute the C_6F_{13} group in the bromosilane with a $\text{C}_{10}\text{F}_{21}$ group. Good yields were obtained by heating the reaction mixture at 90°C for 48 h and a two-phase extraction separated the fluoros-labelled product from the excess reagents. Surprisingly, the fluoros silyl group was more difficult to cleave than expected. There was no reaction with LiOH in THF/ H_2O , HF.pyridine in THF, CsF in THF/ MeOH or trifluoroacetic acid in dichloromethane. Desilylation only occurred with TBAF (1.5 equivalents) in THF at room temperature and delivered the final organic product into the organic phase. To show the potential of the fluoros Ugi reaction in combinatorial synthesis, it was used to make a small library of amino acids. The results show that reasonable overall yields (32–99%) and good purities (81–95%) were obtained in this application. By synthesising a fluoros-labelled urea reactant, exactly the same fluoros methodology was also applied to the Biginelli reaction to prepare a series of dihydropyrimidines. Again, reasonable yields (47–71%) and excellent purities (>90%) were obtained showing that higher molecular weight products (up to 500) can be extracted successfully into the fluoros phase for easy purification without any tedious chromatography.

One of the problems observed in the above fluorous synthesis is that large excesses of reagents and reactants must be used to drive all of the reactions to completion because the substrate and product will both go into the same phase. An additional problem was observed in the Stille couplings where the by-product belonged to the same phase as the target organic compound. One method for solving these problems is to perform a "fluorous-phase" switch [86,92]. This involves either (i) switching the phase of the reactants, reagents or by-products by attaching or detaching a fluorine label; or (ii) switching the phase of the products/intermediates from all the other reaction components. For example, Fig. 13 shows how a fluorous azide reagent is transformed into a fluorous-labelled tetrazole and the chemoselective phase-switch, which detaches the fluorous label from the tetrazole releasing it into the organic phase, separates it from any unreacted fluorous azide. This means that the target organic product can now be separated from all the other reagents and by-products even if the reaction is not quantitative.

Alternatively, an organic-fluorous-organic "double switch" involves the reaction of a functional group in an organic molecule with a fluorous label to extract the organic product into the fluorous phase and hence separate it from all the other reaction components. This method is very effective because it also allows the detachment of the fluorous label to be utilised as demonstrated by the reaction of a simple Grignard reagent with an aldehyde (Fig. 13). When an excess of Grignard reagent was used, $R^2Si(CH_2CH_2C_6F_{13})_3$ was formed as well as the silyl ether and both compounds were extracted into the fluorous phase. By the reaction with either CsF or TBAF the fluorous label was removed only from the silyl ether permitting the desired alcohol

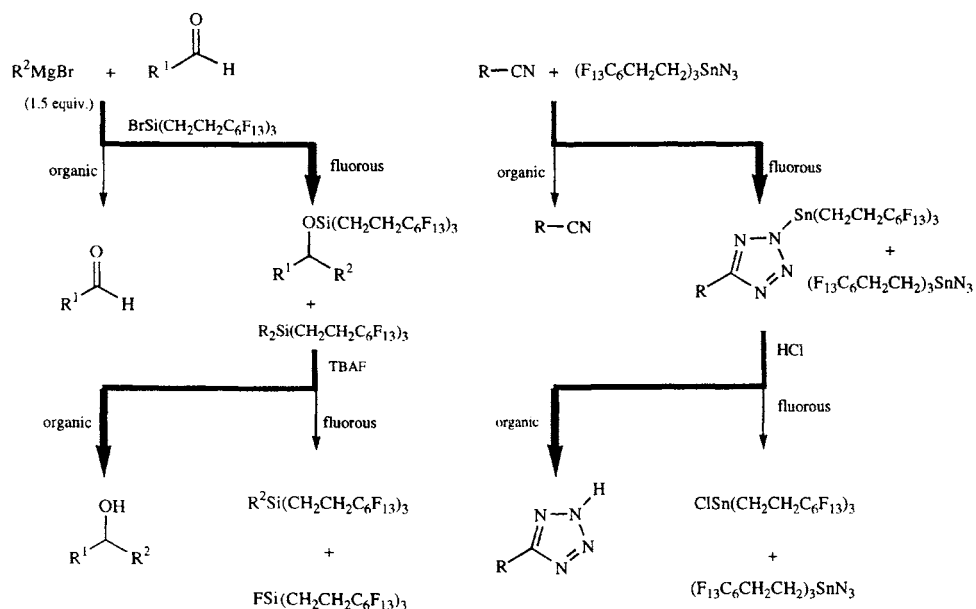


Fig. 13. Fluorous phase switches.

to return to the organic phase and be separated from both $R^2Si(CH_2CH_2C_6F_{13})_3$ and $FSi(CH_2CH_2C_6F_{13})_3$. Now it does not matter if the reaction does not go to completion because any unreacted aldehyde will be removed at the end of the first step. Another similar option would be to render the by-product preferentially soluble in the fluorous phase leaving the desired product in the organic phase.

13.7 Conclusions and future directions

From a surprisingly low level, using perfluorinated solvents for synthetic chemistry, separation technology and catalysis now represents one of the major growth areas in synthetic fluorine chemistry. The work to-date has given a firm foundation for progress in these areas and some clear indications about the directions new work should follow. Perfluorocarbon solvents and fluorous biphasic catalysis will not offer the solution to all preparative, catalytic or solvent problems, rather these systems should be considered and, where appropriate, applied. Currently, a large amount of effort has been directed towards minimising the influence of the perfluoroalkyl ponytail, whereas a number of groups have now illustrated that, for particular systems, these electronic effects could be beneficial and the appreciation of this fact should allow the design and development of systems which not only benefit from facile separation but also improvements in rate and selectivity. We await new developments with considerable interest.

Notes added in proof Following submission of this manuscript, a number of papers have appeared. Bringing the survey of the literature up to-date to the end of 1998, overviews on fluorous biphasic chemistry have appeared [96,97] summarising the work to-date and outlining the authors ideas for the future. A full paper [98] describing the synthesis of phosphinite and phosphite ligands, their metal complexes and the application of some of these species in hydrogenation catalysis, including a crystal structure of *trans*-[RhCl(CO)(PPh₂OC₂H₄C₆F₁₃)₂], elaborates on the earlier conference abstract [44]. A more detailed description of the preparation of **8a** has appeared [99] including purification over fluorous reverse phase silica (Eqn. (8)) [82,86,90] and methylperfluorooctanethionate has been outlined as a useful tool for the indirect perfluoroalkylmethylation of amines [100]. High enantioselectivities have been identified in the catalytic protonation of a samarium enolate in fluorous biphasic systems [101].

Acknowledgements

We thank the EPSRC (AMS) and the Royal Society (EGH) for financial support.

References

- [1] M.F.A. Dove, A.F. Clifford, In: Chemistry in Non-Aqueous Ionizing Solvents, Vol. 2.1, J. Jander, H. Spandau, C.C. Addison (Eds.), Vieweg, Wiesbaden, 1971, pp. 121–300.

- [2] G.A. Olah, G.K.S. Prakash, J. Sommer, *Superacids*, Wiley, NY, 1985.
- [3] F. Aubke, M.S.R. Cader, F. Mistry, In: *Synthetic Fluorine Chemistry*, G.A. Olah, R.D. Chambers, G.K.S. Prakash (Eds.), Wiley, NY, 1992, Chapter 4.
- [4] D.S.L. Slinn, S.W. Green, In: *Preparation, Properties and Industrial Applications of Organofluorine Compounds*, R.E. Banks (Ed.), Ellis Horwood, Chichester, 1982, Chapter 2.
- [5] S.W. Green, D.S.L. Slinn, R.N.F. Simpson, A.J. Woytek, In: *Organofluorine Chemistry. Principles and Commercial Applications*, R.E. Banks, B.E. Smart, J.C. Tatlow (Eds.), Plenum, NY, 1994, Chapter 4.
- [6] D. Sianesi, G. Marchionni, R.J. De Pasquale, In: *Organofluorine Chemistry. Principles and Commercial Applications*, R.E. Banks, B.E. Smart, J.C. Tatlow (Eds.), Plenum, NY, 1994, Chapter 20.
- [7] Y. Ohsaka, In: *Organofluorine Chemistry. Principles and Commercial Applications*, R.E. Banks, B.E. Smart, J.C. Tatlow (Eds.), Plenum, NY, 1994, Chapter 21.
- [8] G. May, *Chem. Br.*, 33 (1997) 34.
- [9] K.C. Lowe, In: *Organofluorine Chemistry. Principles and Commercial Applications*, R.E. Banks, B.E. Smart, J.C. Tatlow (Eds.), Plenum, NY, 1994, Chapter 26.
- [10] I.T. Horváth, J. Rábai, *Science*, 266 (1994) 72.
- [11] I.T. Horváth, J. Rábai, *US Patent*, 5,463,082 (1995).
- [12] J.A. Gladysz, *Science*, 266 (1994) 55.
- [13] B. Cornils, *Angew. Chem., Int. Ed. Engl.*, 34 (1995) 1575.
- [14] B. Cornils, *Angew. Chem., Int. Ed. Engl.*, 36 (1997) 2057.
- [15] D.E. Bergreiter, *Chemtracts — Organic Chemistry*, 8 (1995) 108.
- [16] M. Vogt, *Dissertation, Technische Hochschule Aachen*, August 26, 1991.
- [17] D.-W. Zhu, *Synthesis*, (1993) 953.
- [18] M. Hudlický, *Chemistry of Organic Fluorine Compounds: A Laboratory Manual with Comprehensive Literature Coverage*, Ellis Horwood, Chichester, 1992.
- [19] B.E. Smart, In: *Organofluorine Chemistry. Principles and Commercial Applications*, R.E. Banks, B.E. Smart, J.C. Tatlow (Eds.), Plenum, NY, 1994, Chapter 3.
- [20] K.D. Sen, C.K. Jorgensen, *Electronegativity*, Springer-Verlag, NY, 1987.
- [21] J.K. Nagel, *J. Am. Chem. Soc.*, 112 (1990) 4740.
- [22] J.G. Riess, M. Le Blanc, *Pure Appl. Chem.*, 54 (1983) 2383.
- [23] M.N. Gleason, R.E. Gosselin, H.C. Hodge, *Clinical Toxicology of Commercial Products*, Williams and Wilkins, Baltimore, 1963.
- [24] (a) M'H.A. Hamza, G. Seratrice, M.-J. Stébé, J.J. Delpuech, *J. Am. Chem. Soc.*, 103 (1981) 3733; (b) J. Afzal, S.R. Ashlock, B.M. Fung, E.A. O'Rear, *J. Am. Chem. Soc.*, 90 (1986) 3019; (c) S. Oikawa, M. Tsuda, N. Nagayama, *Theor. Chim. Acta.*, 64 (1984) 403; (d) H.G. Mack, H. Oberhammer, *J. Chem. Phys.*, 87 (1987) 2158.
- [25] A.M.F. Barton, *Handbook of Solubility Parameters and Other Cohesive Parameters*, CRC Press, Boca Raton, 1983.
- [26] B.E. Smart, In: *Molecular Structure and Energetics*, Vol. 3, J.F. Liebman, A. Greenberg (Eds.), VCH, Deerfield Beach, Florida, 1986.
- [27] A. Bondi, *J. Phys. Chem.*, 68 (1964) 441.
- [28] (a) C.Y. Yang, J.A. Tarter, *Anal. Chem.*, 55 (1983) 1775; (b) L. Kavan, F.P. Dousek, K. Micka, *J. Phys. Chem.*, 94 (1990) 5127.
- [29] R.D. Chambers, G. Sandford, A. Shah, *Synthetic Communications*, 26 (1996) 1861.
- [30] S.M. Pereira, G.P. Savage, G.W. Simpson, *Synthetic Communications*, 25 (1995) 1023.
- [31] J.A. Gladysz, *Abstracts of Papers of the American Chemical Society*, 216 (1998) Pt. 1 p. 20-FLUO.

- [32] S. Benefice-Malouet, H. Blancou, A. Commeyras, J. Fluorine Chem., 30 (1985) 171.
- [33] P. Bhattacharyya, D. Gudmunsen, E.G. Hope, R.D.W. Kemmitt, D.R. Paige, A.M. Stuart, J. Chem. Soc., Perkin Trans., 1, (1997) 3609.
- [34] M.A. Carroll, A.B. Holmes, Chem. Commun., (1998) 1395.
- [35] F. Langer, K. Püntener, R. Stürmer, P. Knochel, Tetrahedron: Asymmetry, 8 (1997) 715.
- [36] D.M. Roddick, R.C. Schnabel, In: Inorganic Fluorine Chemistry. Toward the 21st Century, J.S. Thrasher, S.H. Strauss (Eds.), ACS, Washington, 1994, Chapter 27.
- [37] I.T. Horváth, G. Kiss, R.A. Cook, J.E. Bond, P.A. Stevens, J. Rábai, E.J. Mozeleski, J. Am. Chem. Soc., 120 (1998) 3133.
- [38] L.J. Alvey, D. Rutherford, J.J.J. Juliette, J.A. Gladysz, J. Org. Chem., 63 (1998) 6302.
- [39] (a) C. Tamborski, US Patent, 3,499,041 (1970); (b) C. Tamborski, C.E. Synder Jr., US Patent 4,011,267 (1977); (c) C. Tamborski, C.E. Synder Jr., J.B. Christian, US Patent, 4,454,349; (d) P. Gavezotti, E. Strepparola, US Patent, 4,681,693 (1987).
- [40] B. Betzemeier, P. Knochel, Angew. Chem., Int. Ed. Engl., 36 (1997) 2623.
- [41] D.R. Paige, PhD Thesis, University of Leicester, 1998.
- [42] S. Kainz, D. Koch, W. Baumann, W. Leitner, Angew. Chem., Int. Ed. Engl., 36 (1997) 1628.
- [43] D. Sinuo, G. Pozzi, E.G. Hope, A.M. Stuart, Tetrahedron Letts., 40 (1999) 849.
- [44] C.M. Haar, S.P. Nolan, Abstracts of Papers of the American Chemical Society, 216 (1998) Pt. 2 p. 37-INOR.
- [45] J. Fawcett, E.G. Hope, R.D.W. Kemmitt, D.R. Paige, D.R. Russell, A.M. Stuart, D.J. Cole-Hamilton, M.J. Payne, Chem. Commun., (1997) 1127.
- [46] M.-A. Guillevis, A.M. Arif, I.T. Horváth, J.A. Gladysz, Angew. Chem., Int. Ed. Engl., 36 (1997) 1612.
- [47] M.-A. Guillevis, C. Rocaboy, A.M. Arif, I.T. Horváth, J.A. Gladysz, Organometallics, 17 (1998) 707.
- [48] J.J.J. Juliette, I.T. Horváth, J.A. Gladysz, Angew. Chem., Int. Ed. Engl., 36 (1997) 1610.
- [49] J. Fawcett, E.G. Hope, R.D.W. Kemmitt, D.R. Paige, D.R. Russell, A.M. Stuart, J. Chem. Soc., Dalton Trans., (1998) 3751.
- [50] C. Li, S.P. Nolan, I.T. Horváth, Organometallics, 17 (1998) 452.
- [51] E.G. Hope, R.D.W. Kemmitt, A.M. Stuart, J. Chem. Soc., Dalton Trans., (1998) 3765.
- [52] V. Herrera, P.J.F. de Rege, I.T. Horváth, T. Le Husebo, R.P. Hughes, Inorg. Chem. Commun., 1 (1998) 197.
- [53] A. Banet, D.R. Paige, A.M. Stuart, I.R. Chadbond, E.G. Hope, J. Xiao, Abstracts of 11th International Symposium on Homogeneous Catalysis, St. Andrews, Scotland (1998) p. P252.
- [54] E.G. Hope, R.D.W. Kemmitt, D.R. Paige, A.M. Stuart, Abstracts of 11th International Symposium on Homogeneous Catalysis, St. Andrews, Scotland, 1998, p. C7.
- [55] E.G. Hope, D. Gudmunsen, R.D.W. Kemmitt, D.R. Paige, A.M. Stuart, Abstracts of Papers of the American Chemical Society, 216 (1998) Pt. 1 p. 21-FLUO.
- [56] Minnesota Mining and Manufacturing Co., British Patent, 840,725 (1960).
- [57] S.G. DiMagno, R.A. Williams, M.J. Therien, J. Org. Chem., 59 (1994) 6943.
- [58] S.G. DiMagno, P.H. Dussault, J.A. Schultz, J. Am. Chem. Soc., 118 (1996) 5312.
- [59] G. Pozzi, S. Banfi, A. Manfredi, F. Montanari, S. Quici, Tetrahedron, 52 (1996) 11879.
- [60] G. Pozzi, I. Colombani, M. Miglioli, F. Montanari, S. Quici, Tetrahedron, 53 (1997) 6145.
- [61] G. Pozzi, F. Montanari, S. Quici, Chem. Commun., (1997) 69.

- [62] J.-M. Vincent, A. Rabion, V.K. Yachandra, R.H. Fish, *Angew. Chem., Int. Ed. Engl.*, 36 (1997) 2346.
- [63] G. Pozzi, M. Cavazzini, S. Quici, S. Fontana, *Tetrahedron Letts.*, 38 (1997) 7605.
- [64] C. Guillon, P. Vierling, *J. Organomet. Chem.*, 506 (1996) 211.
- [65] R.P. Hughes, J.A. Trujillo, *Organometallics*, 15 (1996) 286.
- [66] I. Klement, J. Lütjens, P. Knochel, *Angew. Chem., Int. Ed. Engl.*, 36 (1997) 1454.
- [67] B. Betzemeier, F. Lhermitte, P. Knochel, *Tetrahedron Letts.*, 39 (1998) 6667.
- [68] H. Kleijn, J.T.B.H. Jastrzebski, R.A. Gossage, H. Kooijman, A.L. Spek, G. van Koten, *Tetrahedron*, 54 (1998) 1145.
- [69] G. Pozzi, F. Cinato, F. Montanari, S. Quici, *Chem. Commun.*, (1998) 877.
- [70] J.M. Kelly, R. Bonneau, *J. Am. Chem. Soc.*, 102 (1980) 1220.
- [71] A.R. Katritzky, *Organic Preparations and Procedures Int.*, 27 (1995) 179.
- [72] D-W. Zhu, *Macromolecules*, 29 (1996) 2813.
- [73] I. Klement, P. Knochel, *Synlett*, 11 (1995) 1113.
- [74] I. Klement, H. Lütjens, P. Knochel, *Tetrahedron Lett.*, 36 (1995) 3161.
- [75] I. Klement, P. Knochel, *Synlett*, (1996) 1004.
- [76] I. Klement, H. Lütjens, P. Knochel, *Tetrahedron*, 53 (1997) 9135.
- [77] G. Pozzi, F. Montanari, M.T. Rispens, *Synthetic Communications*, 27 (1997) 447.
- [78] T. Nakamura, Y. Koga, *J. Chem. Soc., Perkin Trans.*, 2, (1998) 659.
- [79] K.S. Ravikumar, F. Barbier, J-P. Bégue, D. Bonnet-Delpon, *Tetrahedron*, 54 (1998) 7457.
- [80] R.D. Chambers, A.R. Edwards, *J. Chem. Soc., Perkin Trans. 1*, (1997) 3623.
- [81] D.P. Curran, S. Hadida, *J. Am. Chem. Soc.*, 118 (1996) 2531.
- [82] D.P. Curran, *Chemtracts: Org. Chem.*, 9 (1996) 75.
- [83] D.P. Curran, *Cancer Journal from Scientific American*, 4 (1998) S73.
- [84] J.H. Horner, F.N. Martinez, M. Newcomb, S. Hadida, D.P. Curran, *Tetrahedron Lett.*, 38 (1997) 2783.
- [85] I. Ryu, T. Niguma, S. Minakata, M. Komatsu, S. Hadida, D.P. Curran, *Tetrahedron Lett.*, 38 (1997) 7883.
- [86] D.P. Curran, *Angew. Chem. Int. Ed. Engl.*, 37 (1998) 1175.
- [87] D.P. Curran, M. Hoshino, *J. Org. Chem.*, 61 (1996) 6480.
- [88] M. Hoshino, P. Degenkolb, D.P. Curran, *J. Org. Chem.*, 62 (1997) 8341.
- [89] M. Larhed, M. Hoshino, S. Hadida, D.P. Curran, A. Hallberg, *J. Org. Chem.*, 62 (1997) 5583.
- [90] D.P. Curran, S. Hadida, M. He, *J. Org. Chem.*, 62 (1997) 6714.
- [91] N. Spetseris, S. Hadida, D.P. Curran, T.Y. Meyer, *Organometallics*, 17 (1998) 1458.
- [92] A. Studer, S. Hadida, R. Ferritto, S-Y. Kim, P. Jeger, P. Wipf, D.P. Curran, *Science*, 275 (1997) 823.
- [93] A. Studer, D.P. Curran, *Tetrahedron*, 53 (1997) 6681.
- [94] A. Studer, P. Jeger, P. Wipf, D.P. Curran, *J. Org. Chem.*, 62 (1997) 2917.
- [95] D.P. Curran, R. Ferritto, Y. Hua, *Tetrahedron Lett.*, 39 (1998) 4937.
- [96] F. Montanari, G. Pozzi, S. Quici, *Chim. Ind. (Milan)*, 80 (1998) 469.
- [97] I.T. Horváth, *Acc. Chem. Res.*, 31 (1998) 641.
- [98] C.M. Haar, J. Huang, S.P. Nolan, J.L. Peterson, *Organometallics*, 17 (1998) 5018.
- [99] S. Kainz, Z. Luo, D.P. Curran, W. Leitner, *Synthesis*, (1998) 1425.
- [100] L.E. Kiss, J. Rábai, L. Varga, I. Kövesdi, *Synlett*, (1998) 1243.
- [101] S. Takeuchi, Y. Nakamura, Y. Ohgo, D.P. Curran, *Tetrahedron Letts.*, 39 (1998) 8691.

CHAPTER 14

Surface Modification of Inorganic Materials by Fluorination Treatments

Christophe Cardinaud^a and Alain Tressaud^b

^a*Institut des Matériaux de Nantes (IMN-CNRS), 2, rue de la Houssinière, BP 3229, 44322 Nantes Cedex, France;* ^b*Institut de Chimie de la Matière Condensée de Bordeaux (ICMCB-CNRS), Avenue du Dr. Albert Schweitzer, 33608 Pessac Cedex, France*

14.1 Introduction

The surface characteristics of materials dominate the performance of the final products in many applications. For instance the mechanical behavior of composite materials are strongly dependent on the nature of the fiber/matrix interface, the lubricant properties are influenced by surface tribological effects, the success of bio-implants is mostly determined by biocompatibility, etc.

Surface treatments by exposure to very reactive atmospheres show several advantages when compared to more conventional methods:

- the chemical modification is limited to surface only and does not perturb the bulk properties,
- reaction temperature is very low and avoid thermal degradation of the material,
- non-equilibrium reactions are possible.

The exceptional reactivity of fluorine and fluorinating atmospheres has been demonstrated by the synthesis of a wide variety of inorganic fluorine compounds. Surface fluorination has been proposed for modifying and/or protecting the surface of various materials such as polymers, metal surfaces, tissues, biomaterials, carbon-based compounds (graphite, carbon blacks, diamond), inorganic ceramics (superconducting oxides, pigments). Depending on the expected properties of the treated materials, the fluorination can be carried out in plasma-enhanced conditions, for instance in radiofrequency plasmas of CF₄, NF₃, SF₆, or in F₂ or fluorinating gases under atmospheric pressure. In particular processing of materials by plasma techniques is being increasingly used in various areas of production and manufacturing. Plasma chemistry takes place under non-equilibrium conditions. This allows chemical reaction to occur at temperatures that are considerably lower than for thermal reactions taking place at thermodynamic equilibrium.

This chapter is organised as follows. Part I describes the basic concepts of plasma physics and chemistry, and successively presents the important parameters defining a cold plasma, some diagnostic techniques for plasma processing, then elements of fluorine-based plasma chemistry are given and finally a tentative to describe mechanisms of plasma fluorination of inorganic materials is made. Most of the notions describing the plasma and the interaction with the surface have been inspired from the following reference books: Grill [1], Manos and Flamm [2], Auciello and Flamm [3], Chapman [4], Lieberman and Lichtenberg [5]. In Part II, examples of surface modification of various classes of materials are presented in plasma conditions, then in various fluorinating media. It should be noted that the modification of surface properties by processes involving polymers, i.e. modification of surface polymers by fluorinated plasmas, surface polymerisation and deposition of metals on fluoropolymers, will not be considered in the following since they have been extensively treated in others [131].

14.2 Part I: Basic concepts of fluorine-based low pressure plasmas*

14.2.1 What is a cold plasma?

The word “plasma” has been used for the first time in 1928 by Langmuir [6] to describe ionised gases. The popular terminology “fourth state of matter”, often used to define the plasma state, refers to the energy of its constituents and truly applies when these are in thermodynamic equilibrium one with each other such as in stars or in interstellar medium. Plasmas used for materials processing are out of equilibrium. They are generated by electromagnetic excitation, and often also called “cold plasmas” or “low pressure plasmas”. A cold plasma can be described as a weakly ionised medium, which contains positive and negative charges in equal concentration moving in random directions among dominant neutral species.

One important feature is that this quasi-neutral gas of charged and neutral particles is characterised by a collective behaviour. The positive charges are atoms, molecules, or fragments of molecules which have lost electrons. The negative charges are generally electrons, but also in electronegative gases (and F-containing molecules such as SF_6 and CF_4 are among these) molecules or fragments to which are attached one or more electrons. To be maintained, the plasma needs to be fed with energy which replaces by some charge-generation mechanism the loss of charged particles by recombination or diffusion.

The second important feature about cold plasmas is that almost all the energy absorbed from the external electric field is gained by the electrons as they are by far the lightest of the charged constituents. This energy transfer proceeds through ohmic heating and stochastic heating. On the other hand the only efficient way the electrons can transfer their energy to the molecules of the gas is under inelastic collisions. As a result, even if the energy of the charged carriers and the neutral species tends to average by various collision processes and interactions, the system

*A list of symbols and subscripts that appear in this Part is given at the end of the chapter.

remains out of equilibrium and each plasma constituent (electrons, ions, neutral species) is characterised by a different energy distribution.

14.2.2 Important plasma parameters

The properties of the plasma, and the way the plasma interacts with the wall of the container or with any surface immersed in it (such as a sample) are described by a number of important parameters. A short review of some parameters is given hereafter, and typical values are reported in Table 1. In a first order approximation, parameters in the volume of the plasma control the formation of the active species and the chemical reactions in the gas phase, parameters at the plasma surface boundary control how these species interact with the surface. As described below this description is far too simple, and an important feedback exists between the plasma-surface interaction and the gas phase chemistry.

14.2.2.1 Parameters in the plasma volume

Densities and degree of ionisation. The neutral gas can be considered as in equilibrium with its container and described by the kinetic theory of gases. The neutral

Table 1

Typical range values for plasma parameters in rf diode and high density reactors, (calculation is done for a CF_4 plasma assuming Maxwell-Boltzmann distributions)

Plasma parameters (unity)	Rf diode (low density)	High density
P , pressure (Pa)	2.7–66.6	0.3–6.7
n_e , electronic density (m^{-3})	10^{16} – 10^{15}	10^{18} – 10^{16}
T_e , electron temperature (V)	5–8	3–5
n_n , neutral density (m^{-3})	$5 \cdot 10^{20}$ – $2 \cdot 10^{22}$	$5 \cdot 10^{19}$ – $2 \cdot 10^{21}$
α , degree of ionisation	10^{-5} – $5 \cdot 10^{-8}$	10^{-2} – $5 \cdot 10^{-6}$
λ_D , Debye length (m)	$2 \cdot 10^{-4}$ – $5 \cdot 10^{-4}$	10^{-5} – $2 \cdot 10^{-4}$
ν_{pe} , electron frequency (Hz)	10^9 – $2 \cdot 10^8$	10^{10} – 10^9
ν_{pi} , ion frequency (Hz)	$2 \cdot 10^6$ – $5 \cdot 10^5$	$2 \cdot 10^7$ – $2 \cdot 10^6$
$\lambda_{e/n}$, e^-/n mean free path (m) (elastic) [88]	10^{-2} – $2 \cdot 10^{-4}$	$2 \cdot 10^{-1}$ – $2 \cdot 10^{-3}$
$\nu_{e/n}$, e^-/n coll. frequency (s^{-1}) (elastic) [88]	$2 \cdot 10^9$ – 10^{10}	$5 \cdot 10^6$ – $5 \cdot 10^9$
$\lambda_{n/n}$, n/n mean free path (m) (hard sphere)	$5 \cdot 10^{-3}$ – $2 \cdot 10^{-4}$	$5 \cdot 10^{-2}$ – $2 \cdot 10^{-3}$
$\nu_{n/n}$, n/n coll. frequency (s^{-1}) (hard sphere)	$5 \cdot 10^4$ – $2 \cdot 10^6$	$5 \cdot 10^4$ – $2 \cdot 10^5$
$\lambda_{i/n}$, i/n mean free path (m) (in sheath-polarisation)	$5 \cdot 10^{-3}$ – $2 \cdot 10^{-4}$	$5 \cdot 10^{-2}$ – $2 \cdot 10^{-3}$
$\nu_{i/n}$, i/n coll. frequency (s^{-1}) (in sheath-polarisation)	$5 \cdot 10^5$ – 10^8	$5 \cdot 10^4$ – 10^6
Φ_i , Bohm ion flux ($\text{m}^{-2} \text{s}^{-1}$)	$6 \cdot 10^{19}$ – $6 \cdot 10^{18}$	$4 \cdot 10^{21}$ – $4 \cdot 10^{19}$
s , average sheath thickness (m)	$2 \cdot 10^{-3}$ – 10^{-2}	$5 \cdot 10^{-4}$ – $5 \cdot 10^{-3}$

density n_n is thus related to the pressure P and temperature T by the Avogadro relation. The electron density n_e , also called the plasma density, is the number of electron per volume unit. In electropositive plasmas, ions are positive charges and ion density n_i equals electron density, otherwise neutrality says that $n_i^+ = n_i^- + n_e$. The degree of ionisation α is given by the fraction of molecules which are ionised:

$$\alpha = \frac{n_i}{n_n + n_i}.$$

Energy distributions. Since the plasma density is generally low, the energy distribution of neutral species $f(E_n)$ is essentially controlled by the random collision processes among themselves and with the wall of the container. Then $f(E_n)$ follows a Maxwell-Boltzmann distribution (MBD), and the average energy for the neutral particles is: $\langle E_n \rangle = \frac{3}{2} \cdot k \cdot T_n$ with $T_n \sim T_{\text{wall}}$. However in a real case each neutral species population may or may not be in equilibrium with one another depending on the various generation and loss processes taking place. The electrons gain energy through acceleration by the electric field. This energy is spent in the plasma along two processes [5]. In the plasma volume, electrons accelerated by local fields (ohmic heating), loose their energy through momentum transfer with thermal electrons and in inelastic collisions with neutral species, and a random distribution is obtained. Stochastic heating occurs in the sheaths by the reflection of the electrons on the oscillating sheath edge (an image is that of the reflection of a ball on a moving wall). The latter is the main mode of energy transfer in low-pressure plasmas. Very little change occurs in the electron energy distribution function $f(E_e)$ by elastic collisions between electrons and heavy particles, as the kinetic energy transfer varies as:

$$\frac{m_e \cdot m_p}{(m_e + m_p)^2}.$$

The fraction of electrons which gain enough energy to induce excitation, ionisation or dissociation processes with the neutral species loose all or part of their energy through inelastic collisions. Therefore $f(E_e)$ varies from one plasma to another according to the nature of the gas and the various inelastic processes taking place. As the bulk of the plasma is quasi-neutral, instantaneous and time averaged fields are weak, and the assumption of an MBD shape for $f(E_e)$ is generally reasonable. In the plasma jargon the electron mean energy $\langle E_e \rangle$ is expressed in eV and using the relation $\langle E_e \rangle = \frac{3}{2} \cdot k \cdot T_e$, an "equivalent electron temperature" in eV corresponding to the product $k \cdot T_e$ is generally used. As an example, an MBD for 3 eV electrons is compared in Fig. 1 to the experimental $f(E_e)$ for a high density CHF_3 plasma obtained from Langmuir probe measurements. In reactive gases, the high energy part of the distribution may be depleted due to inelastic collisions with the neutral species, and $f(E_e)$ can differ significantly from an MBD. However considering reaction rates, only the fraction of the electron population above the reaction threshold is concerned. Then estimation of the rate is possible whenever this fraction behaves as an MBD.

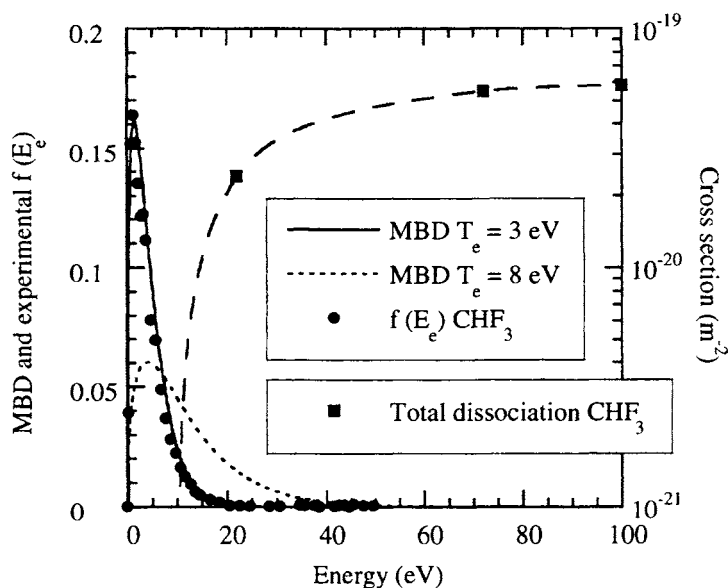


Fig. 1. Maxwell-Boltzmann electron energy distribution for 3 and 8 eV electrons, compared to experimental data for $f(E_e)$ in CHF_3 . Also shown is the total dissociation cross section of CHF_3 (reproduced with permission from Phys. Rev., A25 (1982) 1420 [7]).

Debye length and plasma frequencies. The Debye shielding is another important feature of the collective behaviour of a plasma. Debye shielding is the response of the charged particles to reduce the effect of local electric fields. The electrons are more mobile because they are lighter, and thus they react more rapidly than the ions to this perturbation. So, any local excess of positive or negative charged particles creates an electric field which induces a collective response from the electrons to cancel this field. Assuming an MBD, the electric field reduces as

$$\exp\left[-\frac{r}{\lambda_D}\right],$$

with

$$\lambda_D = \sqrt{\frac{\epsilon_0 \cdot k \cdot T_e}{e^2 \cdot n_e}}$$

the Debye length. The Debye length expresses the characteristic dimension of regions in which breakdown of charge neutrality can occur in a plasma. λ_D increases with decreasing n_e , so there is a low electron density limit for a ionised gas to be considered as a plasma, typically when λ_D is of the same order as the dimension of the discharge. This also means that the plasma cannot penetrate in parts or volumes of the process

chamber which have linear dimensions smaller than λ_D . Another important feature is that the Debye shielding is not complete. At a distance where the electrostatic potential is lower than $(k \cdot T_e/e)$ the charges can escape the charge cloud.

The response of the electrons to a potential perturbation induces oscillations of the electron cloud with a frequency

$$v_{pe} = \frac{1}{2 \cdot \pi} \sqrt{\frac{e^2 \cdot n_e}{m_e \cdot \epsilon_0}}.$$

The product $\omega_{pe} \cdot \lambda_D \approx \langle c_e \rangle$ indicates that the electrons are able to respond sufficiently fast to maintain the plasma neutrality if a perturbation of angular frequency $\omega < \omega_{pe}$ is occurring. Similarly, an ion plasma frequency can be defined:

$$v_{pi} = \frac{1}{2 \cdot \pi} \sqrt{\frac{e^2 \cdot n_i}{m_i \cdot \epsilon_0}}.$$

In rf driven plasmas at $v_{rf} = 13.56$ MHz, v_{pi} is usually below v_{rf} (except for very dense plasmas), whereas v_{pe} is well above. A simple picture of the plasma with respect to the excitation field is that of a fast electron cloud moving in a sea of static ions.

The charged particle collective behaviour (and thus the plasma) exists only if random collision processes do not smear out the coherence of the motion of the charged particles. This means in practice that the frequency of the electron-neutral collisions has to remain smaller than the electron plasma frequency.

Collision frequencies, mean free paths, and cross sections. Collision processes are central to the description of chemical reactions in the plasma. The mean free path $\lambda_{A/B}$ of particle A is the mean distance this particle travels before encountering particle B. $\lambda_{A/B}$ is related to the mean velocity of particle A and to the mean collision frequency between A and B.

In the case of neutral species at thermal equilibrium ($\langle c_A \rangle \approx \langle c_B \rangle$), the hard sphere approximation leads to

$$\lambda_{A/B} = \frac{1}{\sqrt{2}} \cdot \frac{1}{n_B \cdot \pi \cdot (r_A + r_B)^2}.$$

With respect to plasma chemistry, the most important collision processes in a weakly ionised plasma occur between charged particles and neutral particles. Elastic collisions concern principally coulombic and polarisation scattering processes. Coulombic scattering applies when the characteristic interaction time

$$\left(\approx \frac{2 \cdot a_0}{c_{A/B}} \right)$$

is shorter than the characteristic electron orbital time scale ($\sim 10^{-17}$ – 10^{-16} s). So it concerns particles with $c_A > 10^6$ m s⁻¹, that is fast electrons, which are very few

in the plasma. On the contrary, when the characteristic interaction time is greater than 10^{-17} s, the neutral particle has time enough to polarise. With respect to the $c_{A/B}$ condition, polarisation scattering concerns ion-neutral collisions and low energy electron-neutral collisions. For electrons of low energies, this simple picture is often complicated by quantum mechanical effects (Ramsauer minimum effect) and in some cases the cross section shows no dependency with a velocity just as in the hard sphere approximation.

Inelastic collisions between electrons and atoms or molecules are of particular interest as they lead to excitation and ionisation states, which often induce dissociation of the molecule or enhance chemical reactivity. The general behaviour for electron energy of the electron-atom or molecule dissociative excitation or ionisation cross section is given by:

$$\sigma_{e/n}^{\text{exc,ion}}(E_e) = \pi \cdot \left(\frac{e^2}{4 \cdot \pi \cdot \varepsilon_0} \right)^2 \cdot \frac{1}{E_e} \cdot \left(\frac{1}{E_{\text{th}}} - \frac{1}{U} \right),$$

for $E_e > E_{\text{th}}$ and with E_{th} the threshold energy for the process, and U the limit for the energy transfer in the process (that is $U = \min(E_e, E_{\text{ith}})$ for excitation and $U = E_e$ for ionisation).

Dissociative electron attachment collisions are important in electronegative gases, and the corresponding cross section has the following general shape:

$$\sigma_{e/n}^{\text{att}}(E_e) \propto \pi \cdot \left(\frac{e^2}{4 \cdot \pi \cdot \varepsilon_0} \right)^2 \cdot \frac{E_e - E_{\text{th}}}{E_{\text{th}}^3},$$

for $E_{\text{th}} < E < E_{\text{th}} + \Delta E$.

Reaction rates. For electron-neutral reactions such as dissociation: $\text{AB} + e \rightarrow \text{A} + \text{B} + e$, the reaction rates are generally of the second order and have the general expression:

$$\frac{dn_{\text{AB}}}{dt} = K_{e/\text{AB}} \cdot n_e \cdot n_{\text{AB}},$$

with

$$K_{e/\text{AB}} = \int_0^\infty c_{e/\text{AB}} \cdot \sigma_{e/\text{AB}}^{\text{diss}} \cdot f(c_{e/\text{AB}}) \cdot dc_{e/\text{AB}}$$

the rate constant.

Figure 1 also shows an MBD for 8 eV electrons and the typical variation with energy of the total electron impact dissociation cross section for CHF_3 [7]. This points out that the fraction of the electron population which has enough energy to initiate gas phase chemistry is extremely dependent upon T_e .

14.2.2.2 Parameters at the plasma-surface boundaries

Sheaths, Bohm criterion and floating potential. Sheaths are regions of positive space charge which are formed at the boundary of the plasma with any surface in contact with it. The plasma is quasi-neutral, so charged particles are not confined and easily lost to the wall. Electrons which have much higher thermal velocities than ions reach an immersed surface faster. This creates a negative potential at the surface which repels the electrons towards the plasma, and induces a positive space charge around the surface where $n_e < n_i$ (Fig. 2). The Debye shielding effect limits the extension of the sheath in the plasma to few λ_D .

Assuming an MBD for the electrons, conservation of energy and flux for the ions (no collisions) through the sheath leads to a condition known as the Bohm criterion for the energy with which the ions enter the sheath:

$$E_i > \frac{k \cdot T_e}{2}.$$

This criterion means that the ions enter the sheath with a velocity much greater than their thermal velocity, and only depending on the electron temperature. The ions are thus accelerated by a weak electric field in a pre-sheath region in which the charge neutrality exists ($n_e = n_i$) as it is part of the plasma (Fig. 2). If one neglects the ion initial energy, the voltage drop across this region with respect to the plasma

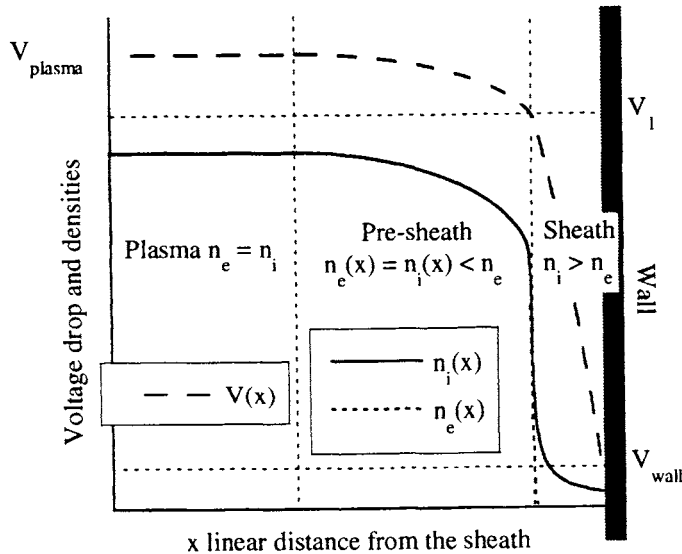


Fig. 2. Qualitative behaviour of the potential, and electron and ion densities drop in the sheath.

potential (V_p) is expressed by

$$V_1 - V_p = -\frac{k \cdot T_e}{2 \cdot e}$$

(Fig. 2). The plasma potential depends on the electron temperature, it will thus vary from one gas to another as a function of the ionisation threshold of the gas: the lower E_{ith} , the greater the electron fraction to be able to ionise the gas, and thus at equilibrium the lower T_e and V_p .

In the case of a floating surface, equilibrium corresponds to the situation where the ion and electron fluxes are equal at the surface, then

$$\Phi_e = \Phi_i = n_e \cdot \sqrt{\frac{k \cdot T_e}{m_i}} \cdot \exp\left[-\frac{1}{2}\right]$$

and the voltage drop across the sheath is

$$V_f - V_1 = \frac{k \cdot T_e}{2 \cdot e} \cdot \ln\left[2 \cdot \pi \cdot \frac{m_e}{m_i}\right]$$

(Fig. 2). As an important consequence, any surface immersed in the plasma is subjected during plasma processing to a positive ion bombardment.

As this ion assistance in the gas-surface chemistry may greatly influence the result of the plasma treatment, control of the ion flux and of the ion energy is a very important parameter in plasma processing. From the previous relation and the values of Table 1, one sees that the voltage drop across a floating sheath is typically 10–30 V. For processing purposes, it is often desirable to increase this bias and thus the ion energy. The most commonly encountered way to achieve this goal is to bias the surface under rf excitation as it allows processing of any materials: conductors, semiconductors, or insulators. In electronegative gases, formation of negative ions by electron attachment decreases the electron density, and replaces a fast and light negative charge by a slow and heavy one. This changes the properties of the sheath. The general trend is that the slow negative ions are more easily repelled into the plasma than the electrons would have been; this effect increases the importance of the electrons in the sheath, and reduces the voltage drop across the sheath. Negative ions which scarcely reach the surface are thus usually ignored in plasma-surface reaction schemes, but their indirect effect through the modification of the sheath characteristics may be important.

Ion flux and energy at a rf biased surface. In the most common experimental set-up this biased surface is insulated from the generator by a blocking capacitor. In rf diode reactors this electrode is also the one which excites the plasma; in rf triode plasma systems or in high density plasma reactors biasing allows to control the ion bombardment on the surface to be processed. In the presence of a blocking capacitor a situation very similar to the floating surface occurs. No current can

flow from the electrode to the external circuit, and the electrode is alternatively charged negatively and positively during an rf cycle. Due to the higher electron mobility, an average negative charge loads the electrode and equilibrium is obtained when ion and electron currents are cancelled on an average rf cycle. The voltage drop through the sheath is thus modulated along the rf cycle around a dc potential (V_{dc}) which is negative with respect to the plasma. The sheath thickness follows a similar rf modulation. Yet the general assumptions made in the previous section are still valid, and the time averaged ion flux on the surface is again given by the Bohm criterion:

$$\langle \Phi_i \rangle = n_e \cdot \sqrt{\frac{k \cdot T_e}{m_i}} \cdot \exp\left[-\frac{1}{2}\right]$$

So the ion flux on the surface is directly proportional to the plasma density.

The sheaths between the conductive plasma and the walls behave like capacitors, so a relation exists between the sheath voltages and the electrode areas A :

$$\frac{\langle V_p \rangle - V_{dc}}{\langle V_p \rangle} = \left[\frac{A_{\text{ground electrode}}}{A_{\text{rf electrode}}} \right]^n,$$

with $n \approx 1$ to 2.

The time taken by the ions to cross the sheath has a strong influence on their energy distribution when reaching the surface. If the ion average transit time is much longer than the rf period, then the ions feel only the average sheath voltage drop, whatever the instantaneous sheath potential when they enter the sheath. Their energy distribution is narrow and centred on $e \cdot (\langle V_p \rangle - V_{dc})$, this case is expected when $v_{pi} < v_{rf}$ and for collision-less sheaths. In the other case ($v_{pi} \gg v_{rf}$), the ion energy depends upon the instantaneous sheath potential at the moment the ion enter the sheath and the distribution can spread from the minimum to the maximum of the sheath voltage, that is between $\langle V_f \rangle$ and $2 \cdot (\langle V_p \rangle - V_{dc}) - \langle V_f \rangle$. Figure 3 reports a very clear interpretation of the shape of the ion energy distribution at the driven electrode in a low-pressure CF_4 plasma [8]. These results are in excellent agreement with theory which predicts a broadening of the distribution proportional to $\sqrt{m_i}$ [9]. Although the excitation frequency is larger than the ion plasma frequency, the ions follow partially the rf modulated field in the sheath. The common approximation that the ions are “frozen” and “see” only the average sheath voltage is practical to estimate the average ion energy but actually applies only for heavy ions and in the case of collision-less sheaths.

Effect of pressure: collisions in the sheath. The values reported in Table 1 suggest that the collision-less sheath is a weak approximation. In normal operating pressures, ion-neutral collisions occur in the sheath ($\lambda_{i/n} < \text{average sheath thickness}$). One can expect the average ion energy to decrease when increasing the pressure, and the ion energy distribution to be severely affected. The general trend given in Fig. 4 for the average ion energy on the grounded electrode [10] can be scaled on the

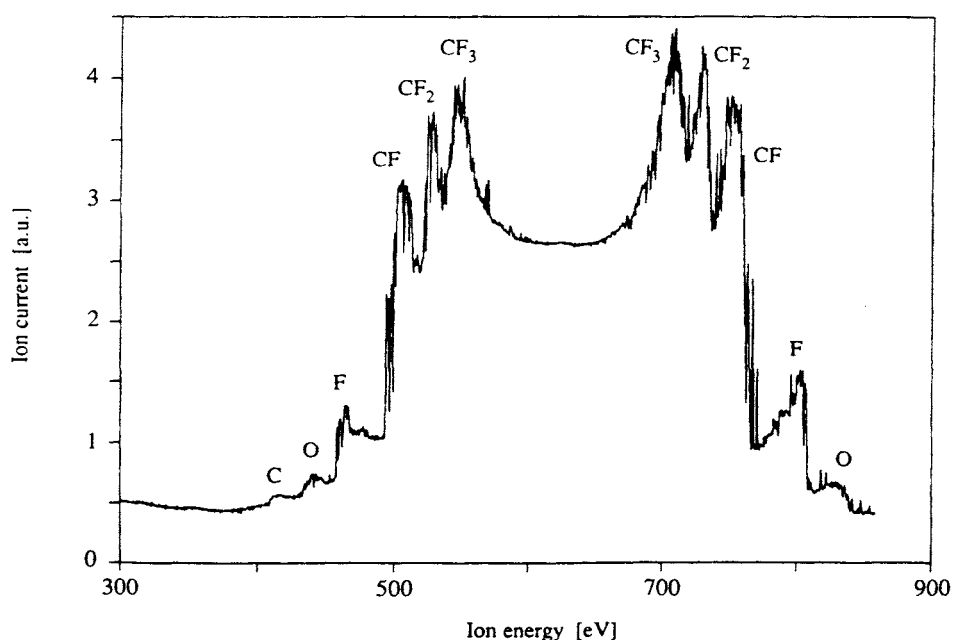


Fig. 3. Measured ion energy distribution in 3 mTorr CF_4 plasma (reprinted with permission from J. Appl. Phys., 67 (1990) 1229 [8]).

powered electrode. Charge exchange reactions, in which the ion becomes an energetic neutral and a thermal ion is created, and elastic scattering are the most probable processes for energy loss.

Figure 5 reports ion energy distributions at a rf-driven electrode in Cl_2 and SF_6 -He plasmas as a function of operating pressure [11]. In both cases the energy distribution is broadened on the low energy side when the pressure is increased. For Cl_2 the distribution spreads over a wide energy range at $P > 10$ Pa with low energy structures due to charge exchange collisions (just as in Ar). In the case of SF_6 /He, a large broadening is observed but no low energy features are present, possibly because of the occurrence of several ions in SF_6 plasmas [12]. Another important effect of collisions in the sheath is to random the direction of the ion velocities with respect to the surface (Fig. 4). Ions created via charge exchange processes have small incident angles, whereas ions suffering elastic collisions have a larger angle distribution.

14.2.3 Diagnostic techniques for plasma processing

The combination of analyses of both the plasma and the surface is probably the best strategy to improve the understanding of the plasma-surface interaction. A brief description of the most common techniques is given hereafter. Examples of applications are given here and later in Secs 14.2.4 and 14.2.5.

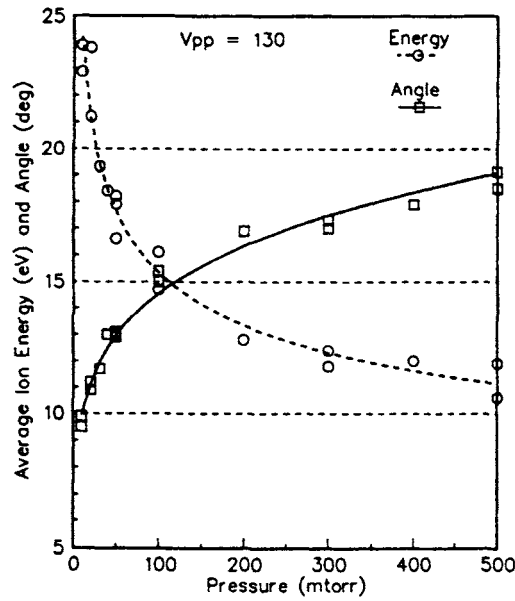


Fig. 4. Average ion energy and angle as a function of pressure (reprinted with permission from J. Appl. Phys., 68 (1990) 3916 [10]).

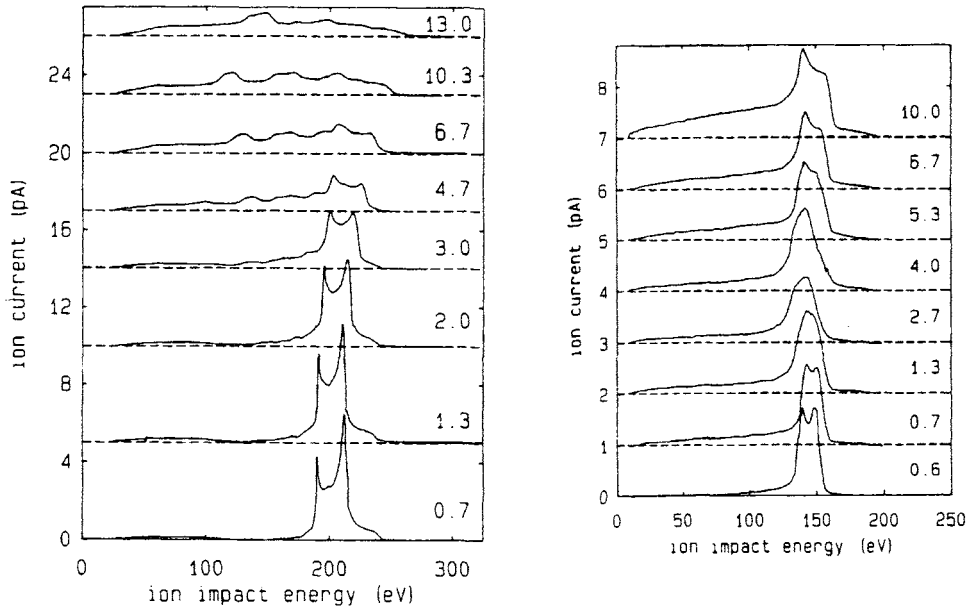


Fig. 5. Measured ion energy distribution in function of pressure (Pa), in Cl₂ (left) and SF₆-He (right) plasmas (reprinted with permission from J. Appl. Phys., 69 (1990) 1253 [11]).

14.2.3.1 Plasma diagnostics

Mass spectrometry. This technique is very attractive for in situ characterisation of plasma processing, as it can in principle detect all charged and neutral species. Sampling the plasma is achieved through a small orifice in the plasma reactor wall, the most efficient set-up are those where the extraction hood of the spectrometer itself is placed at the plasma boundary. The size of orifice should be less than λ_D so that the plasma does not get through. It should have an ideally “zero length” which means in practice that its length has to be shorter than $\lambda_{A/B}$ to minimise collision between the particles during their transport. In addition to the mass filter, modern mass spectrometers are frequently equipped with an energy analyser, which enables to obtain energy distributions of the plasma ions. Mass spectrometry has proven to be one of the most powerful techniques for the understanding of plasma processing. Reference data for inorganic fluorides gases can be found in Beattie [13]. If identification of gas phase molecular products is quite straightforward, as formation of C_xF_y ($x > 2$) species in C_2F_6 plasmas [14], detection of radicals or negative ions is less easy. Identification [15–17] and quantification [16] of radicals by the ionisation threshold method is possible. Figure 6 presents the intensity of CF_2^+ ions

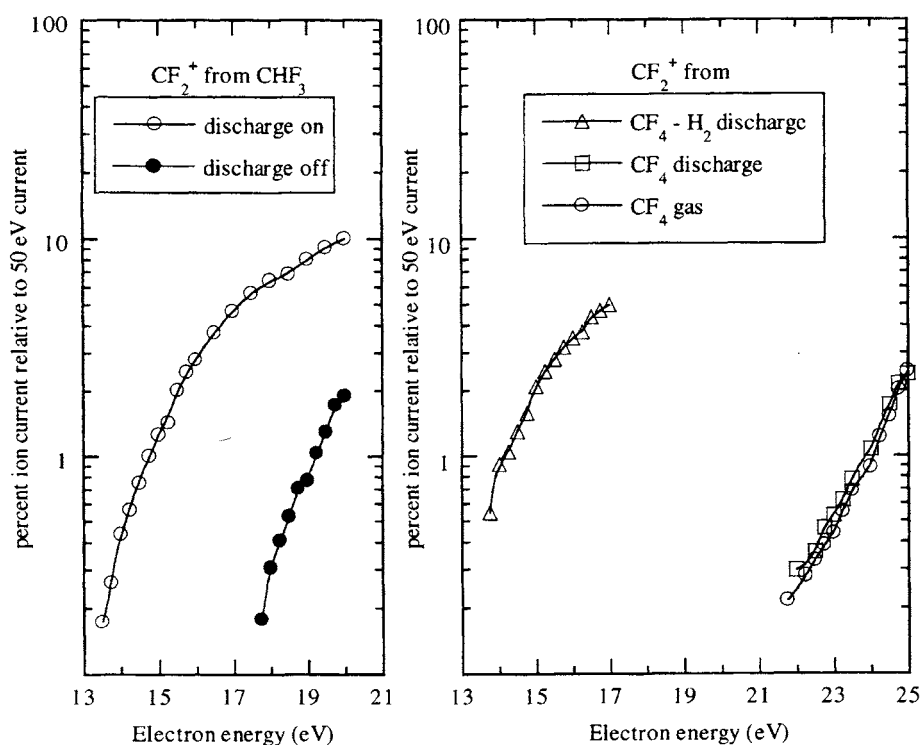


Fig. 6. Intensity of CF_2^+ as a function of electron energy in CHF_3 , CF_4 and CF_4 - H_2 plasmas (reprinted with permission from J. Appl. Phys. 50 (1979) 6594 [15]).

formed in the mass spectrometer ionisation chamber from direct ionisation or dissociative ionisation of neutral species vs the electron energy for CHF_3 , CF_4 and $\text{CF}_4\text{-H}_2$ plasmas. Knowing the ionisation potential of CF_2 (11.8 V), and the dissociative ionisation potential of CHF_3 (14.7 V) and CF_4 (21 V) into CF_2^+ , the results of Fig. 6 point out the presence of CF_2 radicals in CHF_3 and $\text{CF}_4\text{-H}_2$ plasmas and their absence in CF_4 . Detailed reactions discussing the formation of CF_2 in CF_4 upon addition of H_2 to CF_4 are presented in Sec. 15.2.4. Recently "polymerisation" reactions in fluorocarbon plasmas have been investigated by using an electron dissociative attachment technique [18], and have shown the formation of $\text{C}_n\text{F}_{2n-k}$ molecules up to $n = 9$.

Negative ions are expected to be in large concentration in fluorinated molecules discharges. These ions are generally confined in the discharge as very few of them have enough energy to cross the sheaths. Detection of negative ions can be achieved through modulation of the discharge at low frequency [19]: since the sheath vanishes immediately as the plasma is cut off, the negative ions are able to reach the orifice of the mass spectrometer during the "plasma off" period. An alternative method uses photodetachment processes [20].

An important feature of mass spectrometry is the detection of volatile plasma-surface interaction products. Figure 7 reports the evolution of the production rate of WF_6 and WOF_4 from a tungsten surface in $\text{SF}_6\text{-O}_2$ plasma upon plasma exposure time [21]. At a first glance, the rather surprising feature in these results is that during the surface oxide elimination the dominant product is WF_6

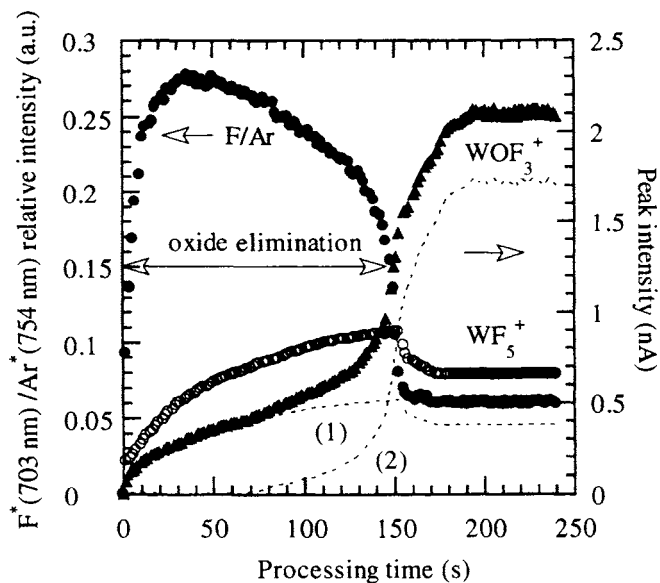


Fig. 7. Evolution of F/Ar , WF_5^+ , and WOF_3^+ with time during processing of tungsten in $\text{SF}_6\text{-O}_2$ (reprinted with permission from J. Electrochem. Soc., 140 (1993) 505 [21]).

and not WOF_4 , whereas the situation is reversed once the oxide is removed. The fluorination mechanism of W is discussed in Sec. 14.2.5.

Optical spectroscopies. These techniques are the least intrusive in situ plasma diagnostic methods. The most commonly used techniques are emission spectroscopy, absorption spectroscopy, laser-induced fluorescence.

Emission spectroscopy is the most popular since it is easy to implement. It is frequently used in industrial equipment for real-time control of a process. Very fine qualitative information of the plasma composition can be obtained. The drawback of this technique is that it provides information from excited species. These are only a small fraction of the total number of species, and they may be produced by more than one excitation pathway. Indeed the measured intensity I_{A^*} emitted by electron-excited species A^* from the ground state A can be expressed as:

$$I_{A^*} = C(\lambda) \cdot g(A^*, \lambda) \cdot n_A \cdot n_e \cdot \int_{E_{\text{th}}}^{\infty} \sigma_{e/A}^{\text{exc}}(E_e) \cdot f(E_e) \cdot \sqrt{2 \cdot \frac{E_e}{m_e}} \cdot dE_e$$

with $g(A^*, \lambda)$ the emission probability of radiation λ from A^* , and $C(\lambda)$ the apparatus response. As a result it is extremely difficult and usually impossible to correlate the measured intensity to the absolute concentration of the parent ground state species A. Yet in fluorine plasmas, emission spectroscopy combined with actinometry technique [21–24] allows to measure relative variations of the atomic fluorine concentration in the plasma, as a function of time, space, or experimental conditions. Examples are given in Secs 14.2.4 and 14.2.5. When the actinometry rules are not fully verified, the general trend in the evolution of emitting plasma species (and their ground state parents) can still be investigated through intensity normalisation to a reference line, which eliminates the dependency of I_{A^*} with electron density.

Absorption spectroscopy and laser induced fluorescence (LIF), give access to the concentration of molecules, atoms, and ions in the ground state. LIF is enable to achieve highly spatial and time resolved analyses. This technique is thus particularly suitable to investigate composition changes in the plasma, and obtain spatial or time concentration profiles. Published results in fluorine plasmas using absorption [25–27] and LIF [28–32] mainly concern temperature measurements [25] or the quantification of CF_x radicals [26–31] in fluorocarbon-based plasmas and SO_x in $\text{SF}_6\text{--O}_2$ discharges [32]. Recently LIF has been used to measure plasma-surface interaction products [33].

Langmuir probes. Electrostatic probe measurements give access in principle to n_e , n_i , $\langle V_p \rangle$, T_e , and to the electron energy distribution. If the implementation is easy (collection of the current using a biased conductor), it is much more difficult to obtain reliable measurements because the method is very intrusive. Most of the probes have a cylindrical geometry, but some probes are planar or spherical. The following conditions have to be fulfilled preferably. Ideally the probe dimension has to be smaller than λ_D , to limit perturbation of the plasma, also the sheath thickness around the probe has to stay smaller than $\lambda_{i/n}$ or $\lambda_{e/n}$ in order to limit

collisions [34]. These conditions are difficult to fulfil and thus the plasma is generally less dense around the probe. Another critical problem arises from the surface of collection: as it theoretically includes the sheath around the probe, the surface of collection may not be precisely defined. Moreover it varies with the probe bias and oscillates with the rf modulation of the plasma [35]. A way to correct the probe from the rf oscillation is to give it an oscillating reference, either using an external bias at the same frequency as the rf excitation (active correction), or using the plasma itself via a capacitor (passive correction) [36]. Although difficult to obtain, probe characterisation of a plasma is a nice complementary diagnostic to optical emission. As an example, Fig. 8 compares Ar (used as an actinometer) emission intensity I_{Ar^*} (750.4 nm) in a CHF₃-based plasma with calculation of

$$K_{e/\text{Ar}} \cdot n_e = n_e \cdot \int_{E_{\text{th}}}^{\infty} \sigma_{e/\text{Ar}}^{\text{exc}}(E_e) \cdot f(E_e) \cdot \sqrt{2 \cdot \frac{E_e}{m_e}} \cdot dE_e$$

deduced from Langmuir probe measurements.

14.2.3.2 Surface diagnostics

Surface diagnostics gives fine complementary information to plasma diagnostics, providing that the surface can be analysed in situ and possibly in real-time, or in a such a way that it does not suffer any dramatic chemical or structural modifications.

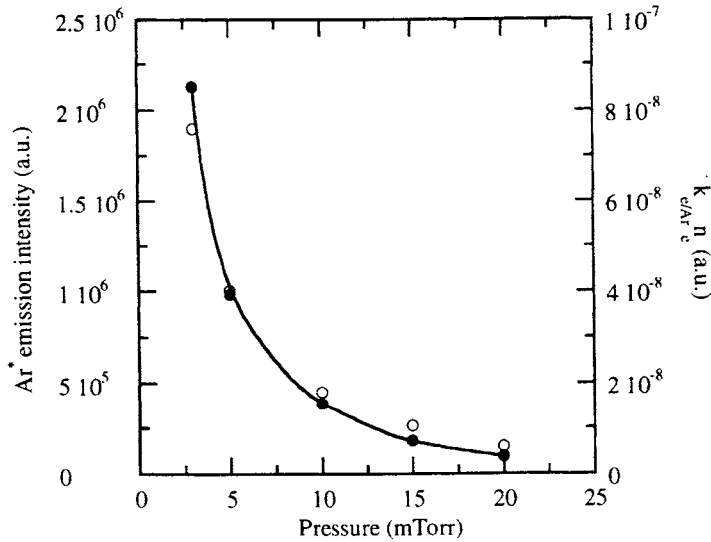


Fig. 8. Ar* optical emission intensity compared to $K_{e/\text{Ar}} \cdot n_e$ from Langmuir probe measurements as a function of pressure, the Ar* intensity being corrected for the variation of pressure.

X-ray photoelectron spectroscopy is probably the most commonly employed technique, as it gives information about the chemical species located in the first 15 nm below the surface. It is of particular interest if a vacuum transfer facility, from the processing chamber to the XPS, enables to avoid atmospheric contamination, as shown in Fig. 9. This experiment concerns W exposure to a SF_6 plasma. A sample transferred under vacuum is free of oxygen and carbon contamination as compared to a sample exposed to air between processing and analysis. In addition, the comparison of the surface chemistry in both cases gives some information on the nature of the chemical species. S is present on the W surface in the form of W-S species as in WS_2 compounds; these species are insensitive

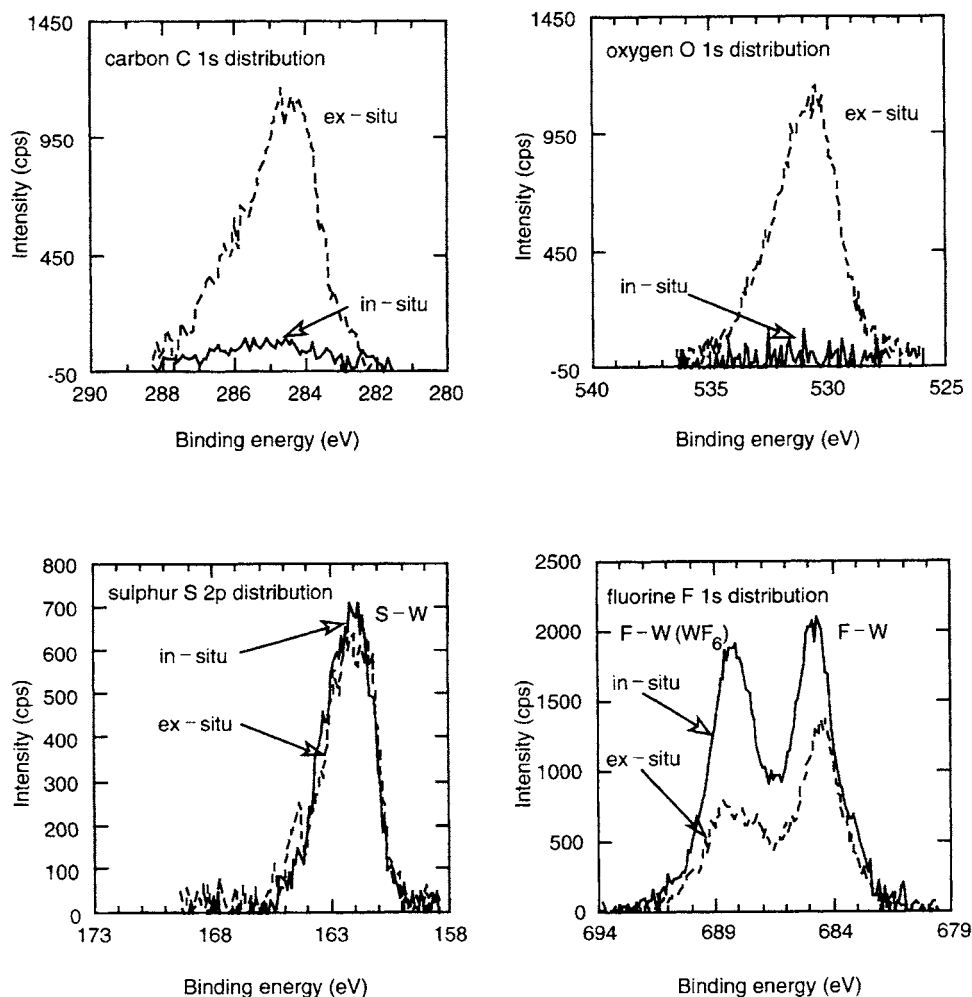


Fig. 9. XPS analysis of a W surface exposed to a SF_6 plasma, comparison between vacuum transfer (in situ) and air transfer (ex situ) from the process chamber to the XPS.

to atmospheric exposure. The F 1s distribution shows two contributions: one at 684.7 eV (F–W), results from the fluorination of the W surface, the second at 687.7 eV is very sensitive to atmospheric exposure and has been shown to decrease during the XPS analysis duration [21]: it is assigned to WF_6 molecules trapped on the surface [37]. XPS has been for a long time the only easy-to-use surface analysis method (with Auger spectroscopy). Since 1986, the development of ellipsometry and atomic force microscopy, have brought new surface analysis techniques.

Ellipsometry is probably the only easy-to-use surface analysis method which can be operated in situ and in real time. On the contrary, multiple internal reflection Fourier transform infrared spectroscopy is a very powerful technique [38] but it is rather tricky to implement. Ellipsometry allows real time studies of the surface modification during exposure to the plasma, and after the treatment. Figure 10 shows for example the variation of Ψ and Δ ellipsometry angles upon fluorination of Si in fluorine-based plasmas as a function of pressure and gas mixture [39], thus demonstrating the sensitivity of the technique. Infrared ellipsometry has also been used with success to investigate reaction layer composition and formation on Si in CF_4 -based plasmas [40,41], or to monitor patterning [42].

Atomic force microscopy has been up to now only scarcely used by the plasma processing community. Results mainly concern low-resolution measurements, that is modification of the surface roughness induced by the plasma [43,44]. Micro masking effects have been observed when processing Si with a SF_6 plasma beam at low temperature (Fig. 11) and correlated to the multi-layer adsorption of plasma species as observed by XPS [45]. Further development of vacuum techniques should allow high resolution surface probe microscopy measurements on plasma-treated samples, and possibly lead to complementary information on adsorption kinetics, surface density of states.

14.2.4 Fluorine-based plasma chemistry

14.2.4.1 Reactions in the gas phase

Electron impact processes are the main mechanisms for the production of active species.

Ionisation is simple: $\text{CF}_4 + e \rightarrow \text{CF}_4^+ + 2e$, or dissociative: $\text{CF}_4 + e \rightarrow \text{CF}_3^+ + \text{F} + 2e$ ($E_{\text{th}} \sim 15$ eV)

Excitation leads to dissociation: $\text{CF}_4 + e \rightarrow (\text{CF}_4)^* \rightarrow \text{CF}_3 + \text{F} + e$ $k_d \sim 10^{-16} \text{ m}^3 \text{ s}^{-1}$, the threshold energy for dissociative electronic excitation being always greater than that for thermal dissociation. In electronegative gases, dissociation is often attaching:



Electronic attachment: $\text{SF}_6 + e \rightarrow \text{SF}_6^-$ $k_a \sim 6.2 \cdot 10^{-18} \text{ m}^3 \text{ s}^{-1}$, is generally dissociative: $\text{SF}_6 + e \rightarrow \text{SF}_5^- + \text{F}$ $k_a \sim 2.3 \cdot 10^{-16} \text{ m}^3 \text{ s}^{-1}$. Negative ions formed by electron capture on complex molecules have long lifetimes, the lifetime of SF_6^- being estimated as 32 μs [46].

Neutral recombination: $\text{CF}_3 + \text{CF}_3 \rightarrow \text{C}_2\text{F}_6$ $k_{\text{nr}} \sim 8 \cdot 10^{-18} \text{ m}^3 \text{ s}^{-1}$, produces heavier molecules.

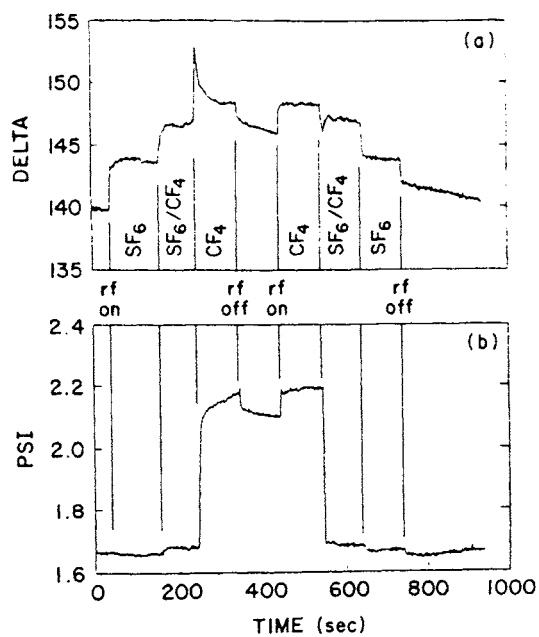
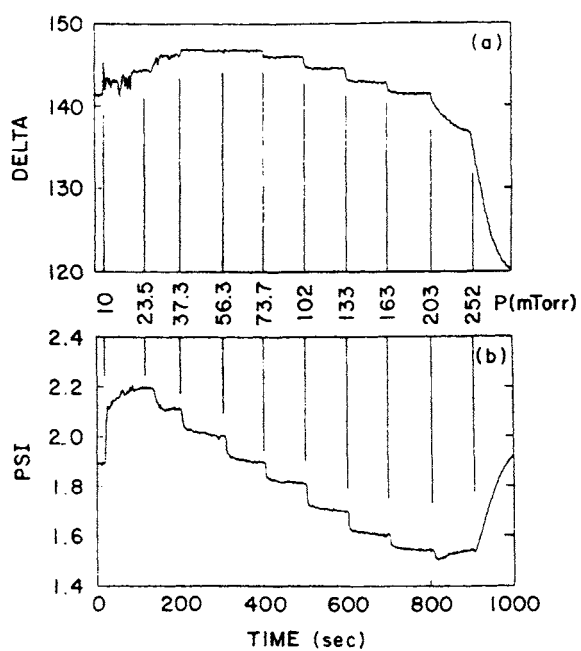


Fig. 10. Ellipsometry analysis in real-time of Si exposed to a CF_4 plasma, Ψ and Δ as a function of pressure or of gas mixture (reprinted with permission from J. Vac. Sci. Technol., A 11 (1993) 34 [39]).

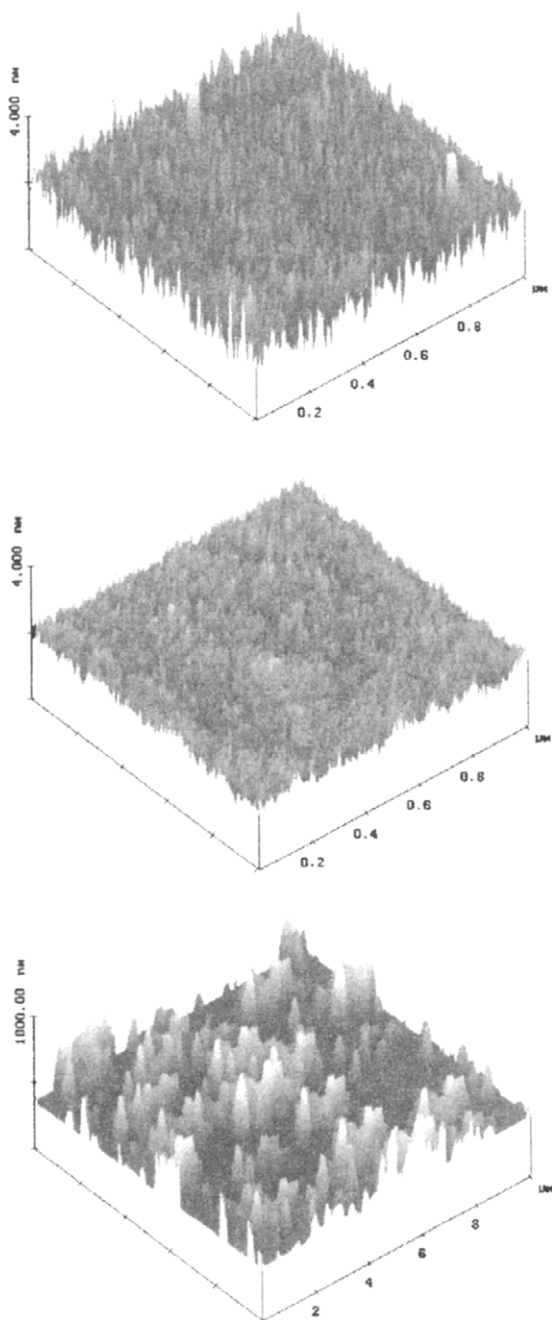


Fig. 11. Si surface aspect after exposure to an SF_6 plasma beam at various substrate temperatures, (top) non-exposed Si; (middle) $T = 230$ K; (bottom) $T = 200$ K. Beam energy is 360 eV, and ion current density 0.65 mA cm^{-2} .

Figure 12 reports electron impact cross sections for CF_4 [47] and SF_6 [48]. In the SF_6 data it should be noticed the very important attachment cross section for the formation of SF_6^- and SF_5^- with low energy electrons [49] which results from the comparable electron affinity of fluorine (3.40 eV) with respect to the dissociation energy of SF_6 (bond strength $\text{F}-\text{SF}_5 = 3.95$ eV), whereas the bond strength $\text{F}-\text{CF}_3$ is 5.56 eV.

In Table 2 is reported a set of the main reactions predicted to occur in a CF_4 rf plasma [50]. According to the authors, CF_2 radicals could outnumber CF_3 radicals: two fast reactions produce CF_2 from CF_4 (no 2) and CF_3 (no 3) with regard to CF_3 formation (no 1), whereas recombination processes for CF_2 (nos 7 and 8) have a much lower rate than for CF_3 (nos 5 and 6). Experimental results [51] as well as further modelling [52] temper this prediction and give typically a ratio of 1.2 for the relative density of CF_3 with respect to CF_2 . On the contrary, absorption spectroscopy analysis [30] is rather in agreement with Fig. 6 and gives a CF_3/CF_2 ratio varying between 5 and 10 with the source power.

14.2.4.2 Effect of additives

The use of gas mixtures enables to vary the composition of the plasma, and often gives more flexibility to optimise the process.

Addition of O_2 to CF_4 . Reactions in CF_4-O_2 plasmas have been extensively studied by several authors [53,54]. A well admitted set of reaction is reported in Table 3. Oxygen atoms produced in the discharge react rapidly with the CF_x radicals (reactions nos 21 to 23) by free radical exchange. The products of reaction are relatively stable species (CO , COF or COF_2) and atomic fluorine. This reaction scheme proceeds further (reaction nos 24 and 25) and gives stable molecules (CO_2) and more fluorine, whereas reaction between atomic fluorine and CO or CO_2 have smaller rates (reactions nos 30 and 31). The main effect upon addition of oxygen is thus a strong increase in the concentration of fluorine in the gas phase [55], and a drastic decrease in the CF_x radicals density [56,57] as confirmed by optical diagnostics. The interest for surface fluorination is obvious as it allows to increase the net fluorine flux onto the surface and prevents the formation of fluorocarbon films. A similar increase in the fluorine concentration is observed in the case of SF_6-O_2 mixtures [58].

Addition of H_2 to CF_4 . Addition of H_2 to CF_4 leads to the opposite result. The set of reactions given in Table 4 [59] indicates that hydrogen atoms react very rapidly with CF_3 (reaction no 9) and yield stable HF and CF_2 . Moreover, fluorine atoms are consumed in reaction nos 20 and 23 with H_2 and H to form HF . The effect of hydrogen addition is thus to decrease the concentration of fluorine (in the plasma jargon people refer to this as the scavenging effect of H_2 in fluorine chemistries) [60], and enhance the density of CF_2 which favours the formation of fluorocarbon films [61]. Many experimental results have confirmed this interpretation [62], examples are given in Figs 13 [63] and 14 [64]. In the particular case of Fig. 13, the authors have observed the F concentration to decrease as the Al electrode is progressively covered with a fluorocarbon layer when increasing the concentration of H_2 in

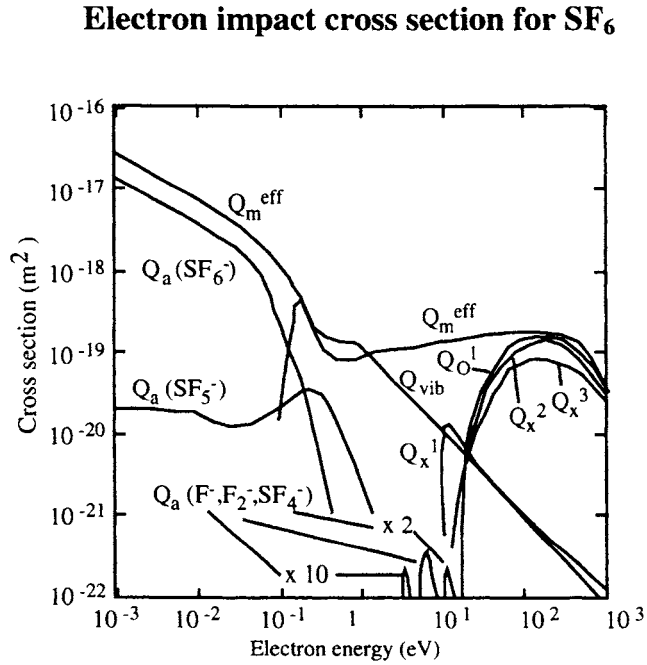
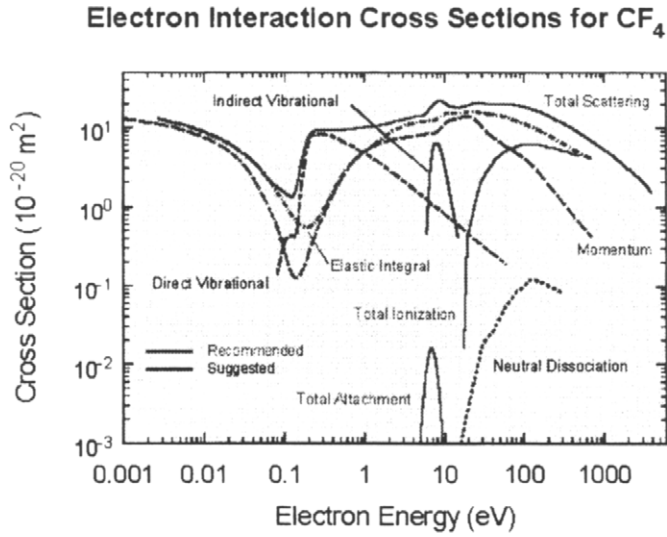


Fig. 12. Experimental cross sections for CF₄ and SF₆ (reprinted with permission from J. Appl. Phys., 64 (1988) 4269 [48] and J. Phys. Chem. Ref. Data, 25 (1996) 1341 [47]).

Table 2

Reaction set in CF₄ plasmas. (Reproduced with permission from Plasma Chem. Plasma Process., 6 (1986) 231 [50]).

Reaction number	Reaction	Rate coefficient at 0.5 Torr
1	$\text{CF}_4 \xrightarrow{e} \text{CF}_3 + \text{F}$	6 s^{-1}
2	$\text{CF}_4 \xrightarrow{e} \text{CF}_2 + 2 \text{ F}$	14 s^{-1}
3	$\text{CF}_3 \xrightarrow{e} \text{CF}_2 + \text{F}$	20 s^{-1}
4	$\text{CF}_2 \xrightarrow{e} \text{CF} + \text{F}$	20 s^{-1}
5	$\text{CF}_3 + \text{CF}_3 \xrightarrow{M} \text{C}_2\text{F}_6$	$8 \cdot 10^{-12} \text{ cm}^3 \text{ s}^{-1}$
6	$\text{CF}_3 + \text{F} \xrightarrow{M} \text{CF}_4$	$1.3 \cdot 10^{-11} \text{ cm}^3 \text{ s}^{-1}$
7	$\text{CF}_2 + \text{CF}_2 \xrightarrow{M} \text{C}_2\text{F}_4$	$5 \cdot 10^{-14} \text{ cm}^3 \text{ s}^{-1}$
8	$\text{CF}_2 + \text{F} \xrightarrow{M} \text{CF}_3$	$4.2 \cdot 10^{-13} \text{ cm}^3 \text{ s}^{-1}$
9	$\text{CF} + \text{F} \xrightarrow{M} \text{CF}_2$	$5 \cdot 10^{-15} \text{ cm}^3 \text{ s}^{-1}$
10	$\text{C}_2\text{F}_6 \xrightarrow{e} \text{CF}_3 + \text{CF}_3$	20 s^{-1}
11	$\text{C}_2\text{F}_4 \xrightarrow{e} \text{CF}_2 + \text{CF}_2$	20 s^{-1}
12	$\text{F} + \text{C}_2\text{F}_4 \longrightarrow \text{CF}_3 + \text{CF}_2$	$4 \cdot 10^{-11} \text{ cm}^3 \text{ s}^{-1}$
13	$\text{CF}_2 + \text{CF}_3 \xrightarrow{M} \text{C}_2\text{F}_5$	$8.8 \cdot 10^{-13} \text{ cm}^3 \text{ s}^{-1}$
14	$\text{C}_2\text{F}_5 + \text{F} \longrightarrow \text{CF}_3 + \text{CF}_3$	$1 \cdot 10^{-11} \text{ cm}^3 \text{ s}^{-1}$
15	$\text{CF} + \text{CF}_2 \longrightarrow \text{C}_2\text{F}_3$	$1 \cdot 10^{-12} \text{ cm}^3 \text{ s}^{-1}$
16	$\text{C}_2\text{F}_3 + \text{F} \longrightarrow \text{C}_2\text{F}_4$	$1 \cdot 10^{-12} \text{ cm}^3 \text{ s}^{-1}$

Table 3

Additional reaction set in CF₄—O₂ plasmas. (Reproduced with permission from Plasma Chem. Plasma Process., 6 (1986) 205 [53]).

Reaction number	Reaction	Rate coefficient at 0.5 Torr
17	$\text{O}_2 \xrightarrow{e} \text{O} + \text{O}$	6.5 s^{-1}
18	$\text{COF}_2 \xrightarrow{e} \text{COF} + \text{F}$	20 s^{-1}
19	$\text{CO}_2 \xrightarrow{e} \text{CO} + \text{O}$	40 s^{-1}
20	$\text{F}_2 \xrightarrow{e} \text{F} + \text{F}$	20 s^{-1}
21	$\text{CF}_3 + \text{O} \longrightarrow \text{COF}_2 + \text{F}$	$3.1 \cdot 10^{-11} \text{ cm}^3 \text{ s}^{-1}$
22	$\text{CF}_2 + \text{O} \longrightarrow \text{COF} + \text{F}$	$1.4 \cdot 10^{-11} \text{ cm}^3 \text{ s}^{-1}$
23	$\text{CF}_2 + \text{O} \longrightarrow \text{CO} + 2\text{F}$	$4 \cdot 10^{-12} \text{ cm}^3 \text{ s}^{-1}$
24	$\text{COF} + \text{O} \longrightarrow \text{CO}_2 + \text{F}$	$9.3 \cdot 10^{-11} \text{ cm}^3 \text{ s}^{-1}$
25	$\text{COF}_2 + \text{O} \longrightarrow \text{CO}_2 + \text{F}_2$	$2.1 \cdot 10^{-11} \text{ cm}^3 \text{ s}^{-1}$
26	$\text{F} + \text{O}_2 \longrightarrow \text{FO}_2$	$1.8 \cdot 10^{-16} \text{ cm}^3 \text{ s}^{-1}$
27	$\text{F} + \text{FO}_2 \longrightarrow \text{F}_2 + \text{O}_2$	$5.0 \cdot 10^{-11} \text{ cm}^3 \text{ s}^{-1}$
28	$\text{O} + \text{FO}_2 \longrightarrow \text{FO} + \text{O}_2$	$5.0 \cdot 10^{-11} \text{ cm}^3 \text{ s}^{-1}$
29	$\text{O} + \text{FO} \longrightarrow \text{F} + \text{O}_2$	$5.0 \cdot 10^{-11} \text{ cm}^3 \text{ s}^{-1}$
30	31 $\text{CO} + \text{F} \xrightarrow{M} \text{COF}$	

Table 4

Reaction set in $\text{CF}_4\text{—H}_2$ plasmas, at 0.5 Torr (Reproduced with permission from J. Electrochem. Soc., 137 (1990) 2280 [59]).

Reaction number	Reaction	Reaction number	Reaction
1	$\text{CF}_4 + e \longrightarrow \text{CF}_3 + \text{F} + e$	15	$\text{CHF}_3 + \text{F} \longrightarrow \text{CF}_3 + \text{HF}$
2	$\text{CF}_4 + e \longrightarrow \text{CF}_2 + 2 \text{F} + e$	16	$\text{CF}_3 + \text{HF} \longrightarrow \text{CHF}_3 + \text{F}$
3	$\text{CF}_3 + \text{CF}_3 + \text{M} \longrightarrow \text{C}_2\text{F}_6 + \text{M}$	17	$\text{CHF}_3 + \text{F} \longrightarrow \text{CF}_4 + \text{H}$
4	$\text{CF}_3 + \text{F} + \text{M} \longrightarrow \text{CF}_4 + \text{M}$	18	$\text{CF}_4 + \text{H} \longrightarrow \text{CHF}_3 + \text{F}$
5	$\text{CF}_2 + \text{F} + \text{M} \longrightarrow \text{CF}_3 + \text{M}$	19	$\text{CF}_3 + \text{H} + \text{M} \longrightarrow \text{CHF}_3 + \text{M}$
6	$\text{H}_2 + e \longrightarrow \text{H} + \text{H} + e$	20	$\text{F} + \text{H}_2 \longrightarrow \text{HF} + \text{H}$
7	$\text{CF}_4 + \text{H} \longrightarrow \text{CF}_3 + \text{HF}$	21	$\text{HF} + \text{H} \longrightarrow \text{F} + \text{H}_2$
8	$\text{CF}_3 + \text{HF} \longrightarrow \text{CF}_4 + \text{H}$	22	$\text{H} + \text{H} + \text{M} \longrightarrow \text{H}_2 + \text{M}$
9	$\text{CF}_3 + \text{H} \longrightarrow \text{CF}_2 + \text{HF}$	23	$\text{H} + \text{F} + \text{M} \longrightarrow \text{HF} + \text{M}$
10	14		$\text{CF}_2 + \text{HF} \longrightarrow \text{CHF}_3 + \text{H}$
11			$\longrightarrow \text{CHF}_3 + \text{H} \longrightarrow \text{CF}_3 + \text{H}_2$
12			$\text{CF}_3 + \text{H} \quad \text{CF}_2 + \text{HF} + \text{M} \longrightarrow \text{CHF}_3 + \text{M}$
13			$\text{CF}_3 + \text{H}_2 \quad \text{CHF}_3 + \text{M} \longrightarrow \text{CF}_2 + \text{HF} + \text{M}$

the gas, whereas there is no effect for a PTFE electrode. Moreover, when beginning at 40% H_2 and decreasing the H_2 concentration, the F signal starts at this lower value and stays constant for both materials. This different variation of the relative F concentration, depending on the way the plasma composition is modified reflects the real chemical nature of the electrode surface: Al in the first case, or a stable fluorocarbon layer in the other. This points out the important feedback of wall conditions on the plasma composition which is detailed in the next section.

14.2.4.3 Effect of materials surface

The chemistry of the gas phase is also strongly influenced by the nature of the surfaces (wall or sample) exposed to the plasma. As an example, Table 5 lists the probability of fluorine loss on various materials along different processes [2]. F recombines totally on zinc to form F_2 , is chemically inert on alumina, and reacts on Si or BN to form volatile products, thus inducing etching process.

Figure 15 reports experimental results obtained by emission spectroscopy on the relative evolution of the fluorine concentration in $\text{CF}_4\text{—O}_2$ and $\text{SF}_6\text{—O}_2$ mixtures in a rf diode reactor for various rf electrode materials (Al, Si, Ge) [55,65]. In the case of an electrode material inert with respect to the plasma (Al), addition of O_2 to SF_6 and CF_4 induces, as expected, an increase of the fluorine concentration until the dilution effect lowers the F density. The lower F concentrations observed in the case of Si and Ge electrodes are due to the consumption of fluorine on these surface to form volatile SiF_4 and GeF_4 . In the case of Si with SF_6 , from 0 to 40% O_2 addition reaction is so fast that it consumes all the additional fluorine produced in the plasma. Above 40% O_2 , the F concentration increases gradually to

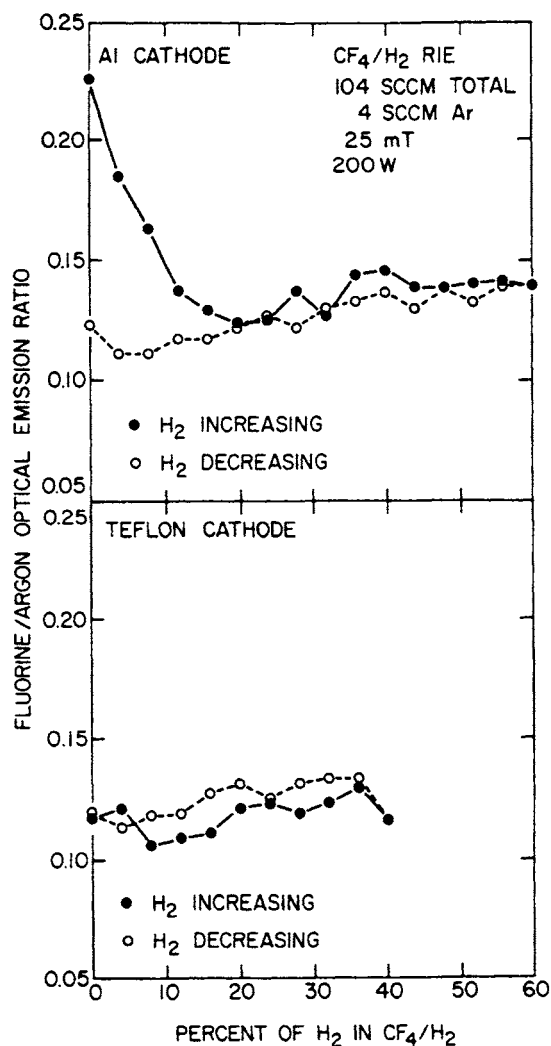


Fig. 13. Effect of fluorocarbon film deposition in CF₄—H₂ mixtures on the F concentration in the gas phase (reprinted with permission from J. Appl. Phys., 62 (1987) 662 [63]).

finally reach that observe for Al: this observation is a strong indication that the Si etching rate has decreased. On the contrary for Ge the evolution of the F density has a bell shape similar to that observed for Al, suggesting that the Ge etching rate remains high even in rich O₂ mixtures.

Gas phase reactions are highly sensitive to surface composition, and therefore processes on chamber material, wall contamination, and history use have an important effect on process chemistry.

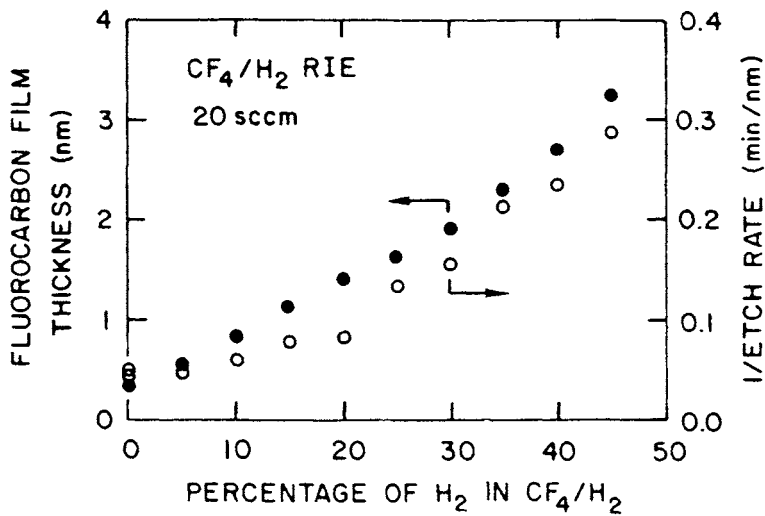


Fig. 14. Fluorocarbon film thickness on Si and Si etching rate as a function of the gas mixture in $\text{CF}_4\text{--H}_2$ plasmas (reprinted with permission from Mat. Res. Soc. Symp. Proc., 98 (1987) 229 [64]).

Table 5

Probability for F atom loss on various materials, from [2] p. 115

Material	Temperature, (K)	F atom loss probability	Process	Product
Alumina	300	$6.4 \cdot 10^{-5}$	Recombination	none
Quartz	300	$1.5 \cdot 10^{-4}$	Total loss	Si F_4
Quartz	300	$1.9 \cdot 10^{-5}$	Reaction	Si F_4
Pyrex	300	$1.6 \cdot 10^{-4}$	Recombination	
Steel	300–470	$2.8 \cdot 10^{-4}$	Recombination	
Molybdenum	300	$4.2 \cdot 10^{-4}$	Recombination	
Nickel	300	$7.2 \cdot 10^{-4}$	Recombination	
Aluminum (0.1% Cu)	300–560	$1.8 \cdot 10^{-3}$	Recombination	
Copper	300–570	> 0.011	Recombination	
Brass	300	> 0.05	Recombination	
Zinc	300	> 0.2	Recombination	F_2
Teflon	300	$< 7 \cdot 10^{-5}$	Recombination	
BN	300–500	~ 1	Reaction	BF_3, N_2
Silicon	300	0.0017	Reaction	SiF_4

14.2.5 Surface fluorination mechanisms: concepts and examples

Fluorine-based plasmas are currently employed in microelectronics industry for etching processes of metal (W), semiconductors (Si, Ge), or dielectrics (SiO_2 , Si_3N_4). Mechanistic studies have shown that the key parameters of the plasma-surface inter-

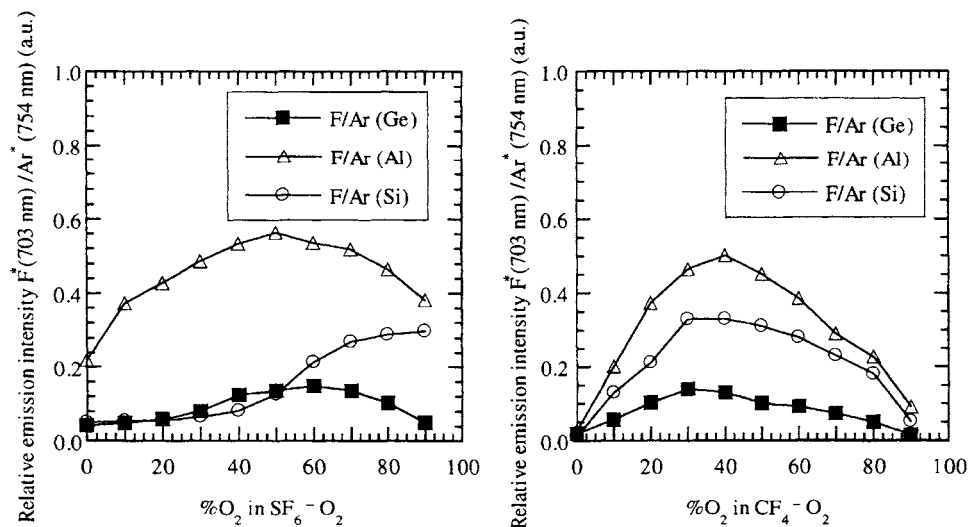


Fig. 15. Fluorine concentration in $\text{CF}_4\text{--O}_2$ and $\text{SF}_6\text{--O}_2$ mixtures for various electrode materials (reprinted with permission from Plasma Sources Sci. Technol., 4 (1995) 398 [55] and J. Vac. Sci. Technol., B 13 (1995) 235 [65]).

action varies for each material upon the gas mixture and the ion bombardment. Very often the ratio of the neutral flux to ion energy flux is the dominant parameter.

Ion-assisted gas-surface chemistry mechanism is probably the best terminology to describe the plasma processing of a surface. A remarkable illustration of the effect of ion bombardment is reported in Fig. 16 [66]. The reaction rate of XeF_2 with Si increases drastically upon the simultaneous combination of chemical species (XeF_2) and ions (Ar^+) on the surface. Obviously chemical reaction and some sputtering processes are expected to occur and to be responsible of the ablation of the material, but the combined effect of active neutral species and ion bombardment is more efficient than the sum of the individual processes.

14.2.5.1 General concepts of plasma-surface interaction

Spontaneous reactions. In this simple case the reaction rate is expected to be proportional to the flux of active neutral species on the surface. In plasma environment, this mechanisms truly occurs only in post discharge situation when the sample is located downstream with respect to the region where the plasma is created, and suffers no ion bombardment. Studies on the etching of Si and SiO_2 with F_2 plasmas [67] have shown that the reaction rate is proportional to the atomic fluorine density and obeys an Arrhenius law with temperature.

Sputtering. Sputtering is a purely physical process with a yield (atom ion^{-1}) given by the relation: $Y_i A \cdot (\sqrt{E_i} - \sqrt{E_{\text{th}}})$ with $E_i > E_{\text{th}}$, $\sim 20\text{--}50 \text{ eV}$ [68] for clean surfaces.

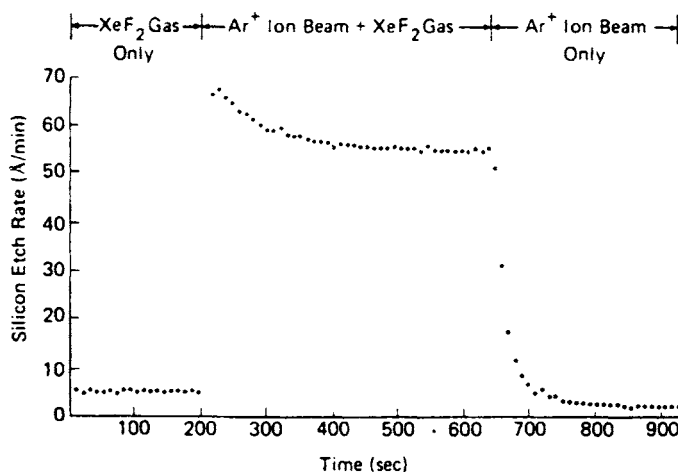


Fig. 16. Si etching rate in ion-assisted gas-surface chemistry mechanisms as compared to pure chemical reaction or ion sputtering (reprinted with permission from J. Appl. Phys., 50 (1979) 3189 [66]).

In plasma environment, the surface chemistry is modified with respect to the initial surface, and the threshold energy and the slope A are found to decrease [69,70]. In this case the terminology “chemical enhanced sputtering” is often used to distinguish this process from the sputtering of a clean surface. Sputtering leads to the ablation of the material, and can concern any surface exposed to the plasma, not only the surface to be processed.

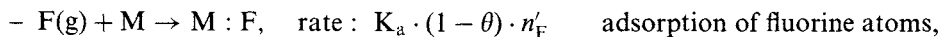
Surface activation. This term covers all processes in which ions essentially bring energy to the surface. This can lead to chemical damage such as broken bonds and create active sites for adsorption of neutral species. Another extremely important process is the activation of adsorbed species, or the activation of surface atoms under the impact of an ion, inducing a chemical reaction. This process is often called “chemical sputtering”, but a more correct term seems to be “ion-assisted reaction”. It leads to the formation of a weakly bound species which desorbs either spontaneously (spontaneous etching) or under the impact of another ion (chemical enhanced sputtering) [71,72]. It is this process which is responsible for the enhancement of the etching rate reported in the example of Fig. 16.

Damage. Energetic ions can cause damage well below the plasma-surface interaction layer. Structural damage concern mostly mono-crystalline materials, the damaged layer can reach 5–9 nm. Light atoms such as hydrogen can diffuse on several hundreds of Å. Materials can undergo strong modification of composition if the resulting product of the interaction is volatile for one element and unvolatile for another. A typical case is that of GaAs which exposed to SF₆ plasmas leads to the formation of volatile arsenic fluoride and leaves a GaF₃-rich layer on the surface [73,74].

14.2.5.2 Elements of surface kinetics

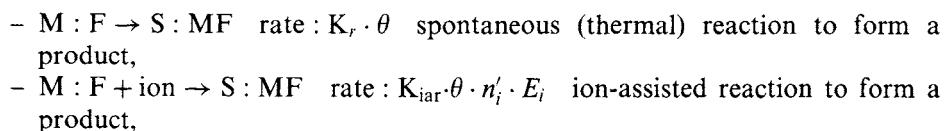
Let us consider the etching of a surface S of material M with F atoms and the volatile product to be MF. With the concepts defined above one can write the following set of reactions.

The first step is the adsorption of fluorine atoms:



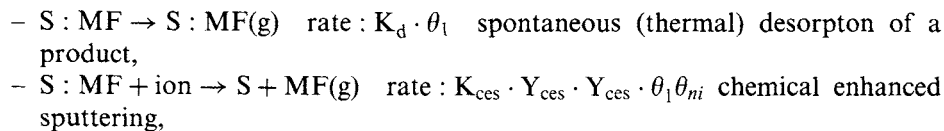
Adsorption of fluorine on the surface is supposed to obey Langmuir kinetics: θ the fraction of the surface covered with fluorine is smaller than one, with K_a ($\text{m}^3 \text{s}^{-1}$) being the adsorption rate constant per fluorine, and n'_F the fluorine concentration in the gas phase near the surface.

The second step is surface reactions:



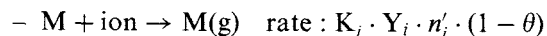
with K_{iar} ($\text{m}^3 \text{s}^{-1} \text{J}^{-1}$) the reaction rate constant per ion, and n'_i the ion concentration in the gas phase near the surface. The ion assistance is supposed to combine both ion energy and ion flux as the role of the ion bombardment is to bring energy to the surface.

The third step is product desorption:



with θ_1 the fraction of the surface covered with reaction products and K_{ces} the reaction constant per ion ($\text{m}^3 \text{s}^{-1}$).

Direct sputtering can be also considered:



In a steady state situation, the etching rate is expressed by:

$$\text{ER}(\text{atom s}^{-1}) = N_M \cdot S \cdot [K_i \cdot Y_i \cdot n'_i \cdot (1 - \theta) + K_d \cdot \theta_1 + K_{\text{ces}} \cdot Y_{\text{ces}} \cdot \theta_1 \cdot n'_i]$$

or,

$$\text{ER}(\text{m s}^{-1}) = \frac{N_M}{n_M} \cdot [K_i \cdot Y_i \cdot n'_i \cdot (1 - \theta) + K_d \cdot \theta_1 + K_{\text{ces}} \cdot Y_{\text{ces}} \cdot \theta_1 \cdot n'_i],$$

with n_M the atom density of material M and N_M the atom surface density.

Solving that $(\partial\theta/\partial t) = 0$ and $(\partial\theta_1/\partial t) = 0$ in a stationary regime gives:

$$ER = \frac{N_M}{n_M} \cdot (K_i \cdot Y_i \cdot n'_i + K_a \cdot n'_F) \cdot \left[\frac{1}{1 + \frac{K_a \cdot n'_F}{K_r + K_{iar} \cdot n'_i \cdot E_i}} \right].$$

This expression is unusable as it is, but it reduces to some interesting limits for some practical cases. Generally direct sputtering processes are negligible in reactive plasmas with respect to chemical processes, so one can omit the term $K_r \cdot Y_i \cdot n'_i$ and then:

$$ER = \frac{N_M}{n_M} \cdot \left[\frac{1}{\frac{1}{K_a \cdot n'_F} + \frac{1}{K_r + K_{iar} \cdot n'_i \cdot E_i}} \right].$$

This relation shows two interesting limits in the usual situation of plasma processing, that is when the sample is submitted to both ions and neutral species. When $K_a \cdot n'_F \ll K_r + K_{iar} \cdot n'_i \cdot E_i$, the etching is limited by the flux of fluorine atoms on the surface, then $\theta \ll 1$ and

$$ER = \frac{N_M}{n_M} \cdot K_a \cdot n'_F.$$

When $K_a \cdot n'_F \gg K_r + K_{iar} \cdot n'_i \cdot E_i$, the surface is saturated with fluorine, $\theta = 1$ and

$$ER = \frac{N_M}{n_M} \cdot [K_r + K_{iar} \cdot n'_i \cdot E_i].$$

In this latter case the etching rate is thus limited by the ion flux if $K_r \ll K_{iar} \cdot n'_i \cdot E_i$, or by the surface reaction rate in the absence of ion bombardment. Figure 17 shows the evolution of ER and these two limits. In addition, the above relation contains the reason why anisotropic etching (and thus pattern transfer for microelectronics) is achievable in plasma environment. Vertical etching (ER_v) is obtained by biasing the sample such as the ion-assistance prevails on thermal reactions: $K_{iar} \cdot n'_i \cdot E_i \gg K_r$. On another hand, the ion flux on the lateral sidewall of the trench is considered to be zero; this assumption is correct as long as the feature size is smaller than the Debye length so that the sheath edge stays parallel to the macroscopic surface and does not follow the pattern. Then the lateral etching rate (ER_l) corresponds to the case: $K_{iar} \cdot n'_i \cdot E_i \ll K_r$.

This model is quite universal providing that the ion-induced reaction rates prevail on the thermal reaction rates. It has been thoroughly discussed for Si and SiO₂ etching by means of beam experiments [75–77], and has been checked in plasma environment [78]. It is also verified for other systems: Si in Cl₂, [79], SiGe alloys in SF₆ [80], or InP in CH₄—H₂ [81].

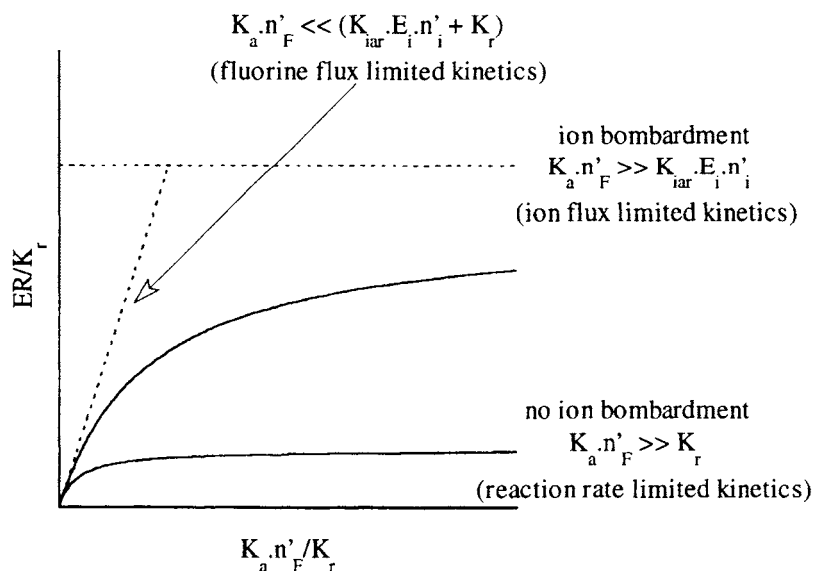


Fig. 17. Predicted evolution of the etching rate as a function of the fluorine density near the surface for a fixed ion energy flux on the surface.

14.2.5.3 Examples of fluorination mechanisms

Diffusion mechanism through a surface layer. A typical example of this situation is that of Si and SiO₂ in fluorocarbon plasmas. In this particular case, a competition exists at the surface between surface fluorination (which further leads to etching) and fluorocarbon film deposition. These systems have been extensively studied in the past years for their capability to give selective etching of SiO₂ over Si. A fluorocarbon film is present at the Si surface, and the reaction rate is inversely proportional to the layer thickness (Fig. 14). This indicates that a diffusion mechanism for the fluorine atoms takes place through this layer in order to account for the reaction with the material surface [64,82]. Moreover, for a given plasma chemistry, the layer thickness and competition is controlled by the ion energy flux on the surface [82,83] as described in Fig. 18. Such a diffusion mechanism is expected to control surface fluorination whenever the plasma phase contains precursors for film deposition. The key parameters which control the equilibrium between fluorination and deposition are two ratios: the F flux-to-CF_x flux ratio, and the ion energy flux-to-CF_x flux ratio. The above set of equation could probably be modified to express this situation with a competitive adsorption mechanism between F and CF_x.

Surface reactivity controlled mechanism. A common example is the fluorination of Si or Ge in SF₆—O₂ or CF₄—O₂ mixtures. As expected from Fig. 15, the reaction rate of Si and Ge increases upon addition of O₂ to SF₆ and CF₄ before decreasing in O₂ rich mixtures. In CF₄—O₂, the reaction mechanism is controlled by the compe-

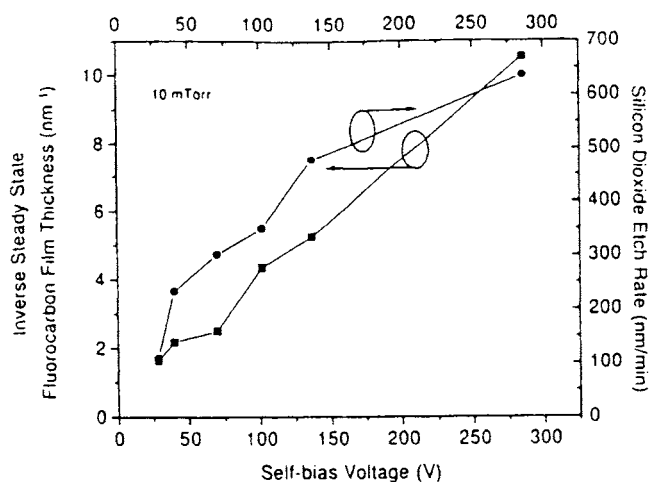


Fig. 18. Dependence of the fluorocarbon thickness on SiO_2 and SiO_2 etch rate with the sample bias voltage (ion energy) (reprinted with permission from J. Vac. Sci. Technol., A 15 (1997) 1881 [82]).

titution between F and O atoms for the occupancy of adsorption sites on the surface [84] with two key parameters: the F/O concentration ratio in the gas phase (n_F/n_O) and the surface reactivity to fluorine atoms. The latter is defined as proportional to the etching rate to fluorine concentration ratio (ER/n_F). Further experiments in $\text{SF}_6\text{--O}_2$ and $\text{CF}_4\text{--O}_2$, combining optical emission, X-ray photoelectron, and mass spectroscopies, have brought additional information [55,65]. The Si and Ge surface reactivities to fluorine have been determined from both mass spectrometry analysis and etch rates, and surface composition has been evaluated by XPS.

In the case of silicon, the surface reactivity and thus the effective etching rate is directly correlated to the surface chemistry: the formation of an oxyfluoride layer inhibits the reaction. In $\text{CF}_4\text{--O}_2$ mixtures, the inverse of the surface reactivity varies linearly with $[n_F/n_O]^{-1}$ as predicted by the model (Fig. 19), the slope being proportional to ratio of the adsorption-desorption rate constant of oxygen on the surface (K_a/K_d). In $\text{SF}_6\text{--O}_2$ mixtures a similar situation is observed with two slopes, indicating two regimes. The change of slopes corresponds to the formation of a "thick" oxyfluoride layer ($> 10 \text{ \AA}$). A further element is the difference in the ion energy flux onto the surface. For the same applied power, the sheath voltage drop on the driven electrode is much smaller ($\sim 30\text{--}70 \text{ V}$) in $\text{SF}_6\text{--O}_2$ mixtures than for $\text{CF}_4\text{--O}_2$ ($\sim 150\text{--}170 \text{ V}$), due to the much higher electron affinity of SF_6 -plasma products as compared to CF_4 . The following assumption can be proposed: the first slope in the (Si, SF_6) system is weak because fluorine flux is much larger than oxygen flux. The change of slope corresponds to a change of the chemical nature of the surface, adsorption mechanisms then concern an oxyfluoride layer not a clean Si surface. Such a behaviour is not encountered for (Si, CF_4) because

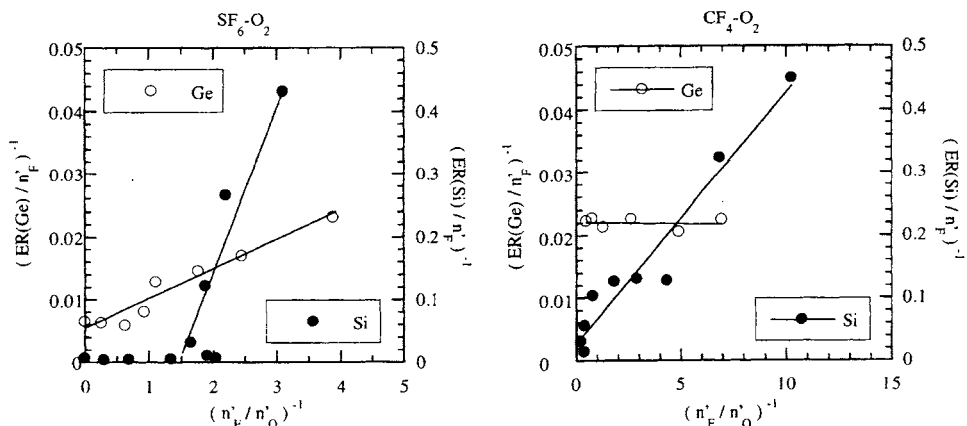


Fig. 19. Inverse of (ER/n_F) as a function of $[n_F/n_O]^{-1}$ for Si and Ge processes in CF_4 — O_2 and SF_6 — O_2 mixtures.

the ion energy flux is large enough to limit the formation of the oxyfluoride layer and allows surface damage or diffusion of fluorine to the underlying Si surface.

In the case of germanium, the formation of an oxyfluoride layer does not inhibit the etching in SF_6 — O_2 mixtures (only one slope), and for CF_4 — O_2 there is no dependency of the surface reactivity with the oxygen flux (null slope means $K_d \gg K_a$). Oxygen addition only provokes a modification of the fluorine concentration in the gas phase. Once more the energy brought by the ion bombardment explains these differences.

In conclusion Si etching is essentially controlled by the surface chemistry and diffusion of fluorine through the overlayer, as in the previous example, whereas germanium etching depends mainly on the fluorine flux with a weak effect of the surface chemistry.

Product desorption controlled surface chemistry. Plasma exposure of tungsten in SF_6 — O_2 mixtures results in two volatile products WF_6 and WOF_4 [85]. As indicated in Fig. 20 the dominant detected product varies with the nature of the electrode material that is with the atomic fluorine concentration [86] in the gas phase. WF_6 is the detected product in F-rich plasmas and WOF_4 that of F-poor plasmas. XPS analysis on a W plate exposed to SF_6 —40% O_2 shows the presence of WOF_4 compounds in addition to O—W, F—W, and SO_xF_y species. Moreover angular XPS analyses indicate that these WOF_4 species are located between the tungsten surface and the oxyfluoride external layer [87]. Reactions between the plasma species (F and O atoms) and the tungsten surface take place at the W-overlayer interface, after diffusion of these species through the overlayer.

Interpretation is that WOF_4 is probably the dominant product formed at the tungsten surface in SF_6 — O_2 . The nature of the final product desorbed in the gas phase depends on the fluorine and oxygen concentration in the gas phase. If these fluxes are high (as in the case of a plasma-insensitive electrode material, such as

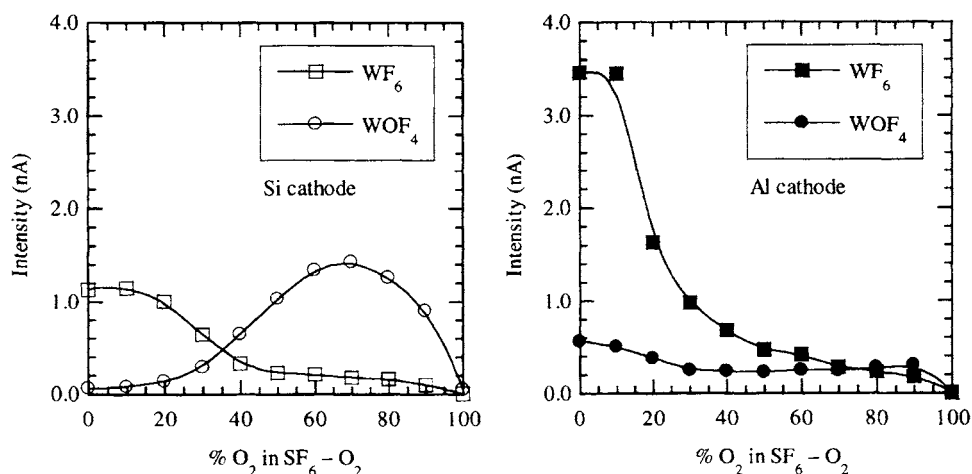


Fig. 20. Intensities of WF_5^+ (WF_6) and WOF_3^+ (WOF_4) signals detected in $\text{SF}_6\text{--O}_2$ plasmas.

Al), the slow desorbing WOF_4 species react with the incoming plasma species and the final product is dominantly WF_6 even though there is oxygen in the gas phase. This mechanism is accompanied by the formation of WO_xF_y species which maintains the overlayer. This explains the slow elimination of the oxide and the high fluorine concentration reported in Fig. 7 during oxide elimination. If these fluxes are low (as in the case of a plasma-reactive electrode material, such as Si or W), few reactions occur during the diffusion of WOF_4 in the overlayer, resulting in desorption of this product in the gas phase, and the overlayer is reduced to a minimum.

14.3 Part II: Examples of surface modification of inorganic materials

14.3.1 Surface modification in plasma-enhanced fluorination (PEF) conditions

14.3.1.1 Modification of surface properties of graphite

Graphite-based materials are nowadays involved in a very wide range of systems. They are used as bulk products or are combined with other components to form composite materials. The improvement of the properties of these systems mostly depends on the modifications that occur at the surface: for example, the mechanical behavior is dependent on the quality of the fiber/matrix interface and the water repellency is improved when the surface free-energy is reduced.

Graphite fluorides are solids of low surface energy and good thermal stability. They have been used as moisture resistant lubricants, water repellents and lithium battery cathodes [89]. Since many of the uses of graphite fluorides thus depend on their surface properties, surface fluorination of graphite materials has been expected to give rise to similar behavior. The methods that had been used in the past for implanting F-containing groups onto polymers through fluorinated

plasmas, have been therefore adapted to various type of graphite materials: bulk, flakes, fibers, powders. rf plasmas at 13.56 MHz and electron cyclotron resonance plasmas with rf-induced negative self-bias voltage have been mostly used with various fluorinated gases such as F_2 , NF_3 , CF_4 , SF_6 . It can be noted that depending on the experimental conditions, the fluorination could go to completion and bulk graphite fluoride could be obtained from graphite flakes treated in F_2 plasma at 20 MHz [90].

The hydrophobic nature of F-treated graphite can be evaluated from contact-angles of liquid droplets. The surface free-energy can be reduced from 50 mJ m^{-2} to as low as 7 mJ m^{-2} after exposure to NF_3 or SF_6 rf plasmas. A significant coverage of surface fluorination is achieved for exposure times of 10–15 min under an NF_3 plasma, yielding water contact angle of 115° [91]. In some case this value has been found to exceed that of PTFE [92].

In DC discharge plasmas, the sudden decrease of contact angle after 15 min treatment has been assigned by S. Okasaki et al. to a structural change of the material surface from crystallised graphite to an amorphous state [93]. It has been shown that the fluorination of PAN-based carbon fibers is more effective in the case of CF_4 -He plasmas than in 5% F_2 -He plasmas [94]. The study of the thermal stability of these F-treated fibers has shown however that a 70% loss of fluorine occurred when the samples were heated at 293°C for 10 min.

14.3.1.2 Influence of the morphology of carbon materials on the nature of C—F bonds

The nature of C—F bonds that are formed during the reaction between F species and C materials depends on two main factors: (i) the experimental conditions of fluorination (low-pressure plasmas, F_2 -gas, fluorinated media); and (ii) the physicochemical characteristics of the pristine materials (graphitisation level, morphology).

The influence of the experimental conditions has been extensively studied for the bulk fluorination of graphite by F_2 -gas in particular by N. Watanabe, T. Nakajima and H. Touhara [89,95]. When the thermal energy brought to the system is large enough ($T_{F_2} > 350^\circ\text{C}$), the fluorination gives rise to the formation of covalent C—F bonds with $sp^3\text{C}$, as for instance in the case of the graphite fluoride $(CF)_n$. On the other hand, when the fluorination is carried out at low-temperature ($T_{F_2} < 100^\circ\text{C}$), in the presence of additive or catalytic species, intercalation of F between the graphitic layers occurs, without modification of the sp^2 configuration of C [96]. In the corresponding graphite intercalation compounds (GICs) of C_xF formulation, the C—F bonds have been called “semi-ionic” after N. Bartlett et al. [97]: in the XPS spectra, these latter contributions take place at BE lower than those of covalent C—F bonds [98]. Fluorination of the internal surface of nanotubes has been recently achieved, the C atoms at the external surface retaining the sp^2 hybridization [132]. The influence of the physicochemical characteristics of the starting material on the surface modification will be illustrated below by two different types of carbon compounds: a highly graphitised material, i.e. exfoliated graphite, and a furnace carbon black (Corax N 115), in which the coherence length

of the ordered domains is limited to a few nm. Usual PEF conditions have been defined by F. Moguet [99]: inlet CF_4 flow = $8 \leq Q \text{ (cm}^3 \text{ min}^{-1}) \leq 16$; total pressure = $25 \leq p \text{ (mTorr)} \leq 200$; rf power = $40 \leq P \text{ (W)} \leq 110$; reaction duration = $10 \leq t \text{ (min)} \leq 300$. It can be noted that in these treatments O_2 was not added to CF_4 , because in several cases it might lead to an important etching of the materials.

PEF treatment of exfoliated graphite. The dependence of C_{1s} and F_{1s} XPS spectra of exfoliated graphite with the duration of plasma treatment is shown in Fig. 21 [99]. In the C_{1s} envelope of the XPS spectrum, the component that corresponds to the graphitic contribution (component 1) remains unchanged after plasma treatment. It is the majoritary component of the spectrum. Due to an asymmetry towards higher BE, this band can be fitted into two peaks at ca 284 and 285 eV [this asymmetry, which is common in metallic samples, is due to the interactions between the created positive core holes and the conduction electrons]. The second peak could also correspond to surface defect, C—H, and C—O groups. The components appearing for $285 < E_b \text{ (eV)} < 287$ can be assigned to the inductive effect of C—F bonds. They correspond to C atoms that are not directly bound to F atoms, but that are first neighbors of C— F_n groups. In the case of graphite, this contribution is weak because the number of reactive sites (i.e. surface defects and borders of graphitic domains) is limited. We will see that the results are totally different for carbon black samples.

The component at ca 287 eV (component 3) can be assigned to “semi-ionic” C—F bond of intercalated F species, and those at $E_b > 288$ eV to C atoms covalently bound to F atoms. The component at ca 289 eV (component 4) has been correlated to the fluorination of defects present at the surface or in the subsurface zone of the graphitic domains. In this case, the sp^2 configuration of C is maintained. The contribution at higher BE (component 5) may arise from different sources: fluorinated domains in which the graphene layers are buckled as in the covalent graphite fluoride $(\text{CF})_n$, or perfluoro groups CF_n with $n = 2$ or 3 present at the peripheral border of graphitic domains.

The evolution of XPS spectra, given in Fig. 21 shows that the contribution of pristine non-functionalised C atoms remains majoritary, whatever the duration of the plasma treatment. The most noticeable change is the increase of the component (4) corresponding to covalent C—F bonds which are formed by the interaction of F^\bullet radicals with the reactive sites of the material, i.e. surface defects, hydrogenated/oxygenated C atom, borders of the graphitic domains. When all these surface sites are fluorinated, the surface is saturated, what is accounted for by the value of C/F ratio of 3.2 obtained for $t \geq 120$ min [99].

The differences between surface fluorination, as obtained by PEF, and bulk fluorination, as obtained by F_2 -gas [experimental conditions: 10 bar F_2 + 0.2 bar HF; reaction temperature 25°C ; reaction duration: up to 3 d] are clearly evidenced in Fig. 22 and in Table 6. The latter route gives rise to a bulk stage-1 GIC of $\text{C}_{3.5}\text{F}$ formulation and a repeat distance $I_C \sim 0.55$ nm [100]. In both cases, the surface C-to-F ratio is more or less similar: 3.1 and 2.8 respectively. However, in the case of surface fluorination, F-intercalated contribution is almost absent, whereas it

is the main C—F contribution in the case of the GIC $C_{3.5}F$. The information deduced from $F1s$ spectra is also in good agreement with this result. The envelopes are formed in both cases of two contributions (Fig. 21): the ones at 685.6 eV correspond to F atoms intercalated between the graphene layers (GIC) and the ones

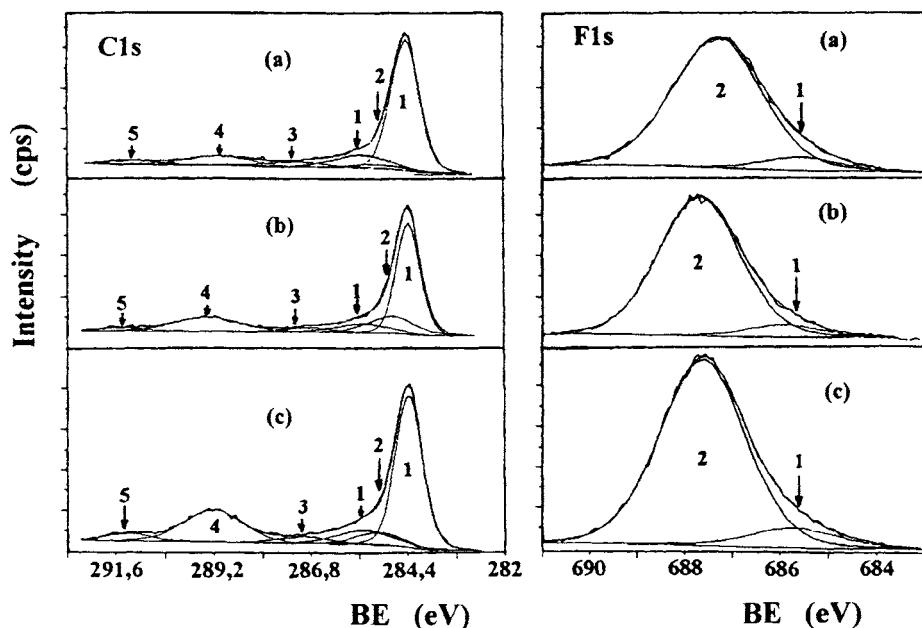


Fig. 21. $C1s$ and $F1s$ XPS spectra of CF_4 -plasma treated exfoliated graphite (Experimental conditions: $8\text{ cm}^3\text{ min}^{-1}$, 200 mTorr, 80 W, 15 min (a), 60 min (b), 120 min (c)).

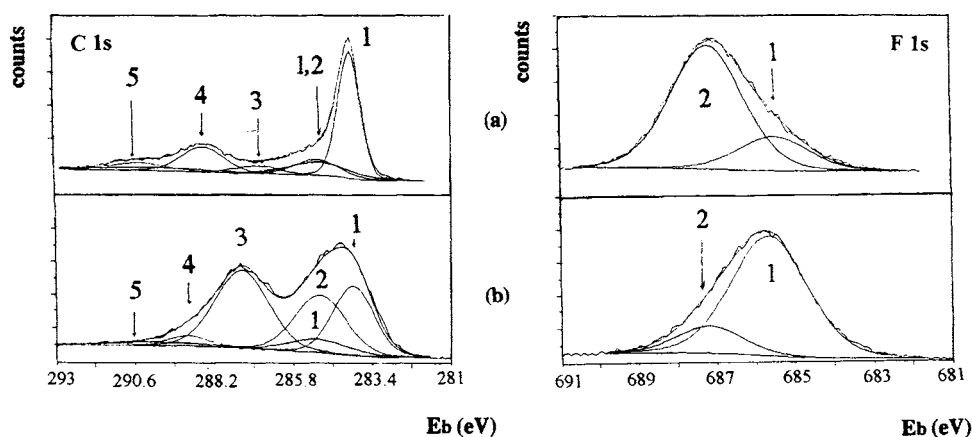


Fig. 22. Comparison of $C1s$ and $F1s$ XPS spectra of fluorinated exfoliated graphite: (a) surface-treated under PEF conditions; (b) GIC ($C_{3.5}F$) obtained under F_2 -gas conditions.

Table 6

C1s and F1s binding energies and relative amounts* of carbon and fluorine in fluorinated exfoliated graphite (1.7% O is also found at the surface)

Exp. Conditions	C1s binding energies (eV)	F1s binding energies (eV)	Assignment of the components
CF ₄ in rf plasma conditions	284.2 (42%)		Graphitic C
	285.2 (7%)		Asymmetric component
	287.0 (4%)	685.6 (6%)	"Semi-ionic" C—F bond
	288.7 (11%)		Covalent C—F bond (surface defects)
	290.6 (4%)	687.3 (24%)	Covalent C—F bond (similar to graphite fluorides)
F ₂ -gas under 10 bar pressure (+0.2 bar HF)	284.1 (25%)		Graphitic C
	285.1 (18%)		Asymmetric component + inductive effect of C—F bonds
	287.4 (26%)	685.7 (22%)	"Semi-ionic" C—F bond
	289.1 (3%)	687.3 (4%)	Covalent C—F bond

* The percentages are only indicative because of the uncertainty in the theoretical curve intensities due to the non-equivocal curve fitting.

at 687.3 eV to covalent F—C bonds. The PEF treatment concerns only a very thin layer of the surface of the sample, as shown by a rapid decrease of the F contribution after Ar sputtering. The type of bonds that are formed between C and F atoms is essentially covalent, and only a small amount of fluorine is intercalated. Compared to F₂-gas bulk fluorination, this method allows the formation of a covalent and insulating layer at the outermost surface only, which may act as an efficient protective coating.

PEF treatment of carbon blacks. Due to their important specific surface areas, that range from a few m²/g to several thousands m²/g, carbon blacks react thoroughly in PEF conditions. The reactivity of various types of carbon blacks with F₂-gas and other fluorinated reagents has been recently investigated by G. Nansé et al. [101–103].

We have chosen to present below the results obtained on furnace carbon black N115, because of its intermediate surface area of 145 m² g^{−1}. The fitted high resolution XPS spectra of C1s and F1s components are given in Fig. 23. Due to the complexity of the morphology of carbon blacks, ten components were required, in order to take into account the envelope of the C1s spectra. Details of the fitting procedure can be found in [101]. The different assignments for C and F atoms involved in each component are shown in Table 7. For C1s envelope, there are two major peaks. The peak at lower BE, located at 284.3 eV, can be assigned to the component C1s (1) which corresponds to non-functionalised sp² and sp³ C atoms that are not affected by fluorination. The area of component (1), which is noted

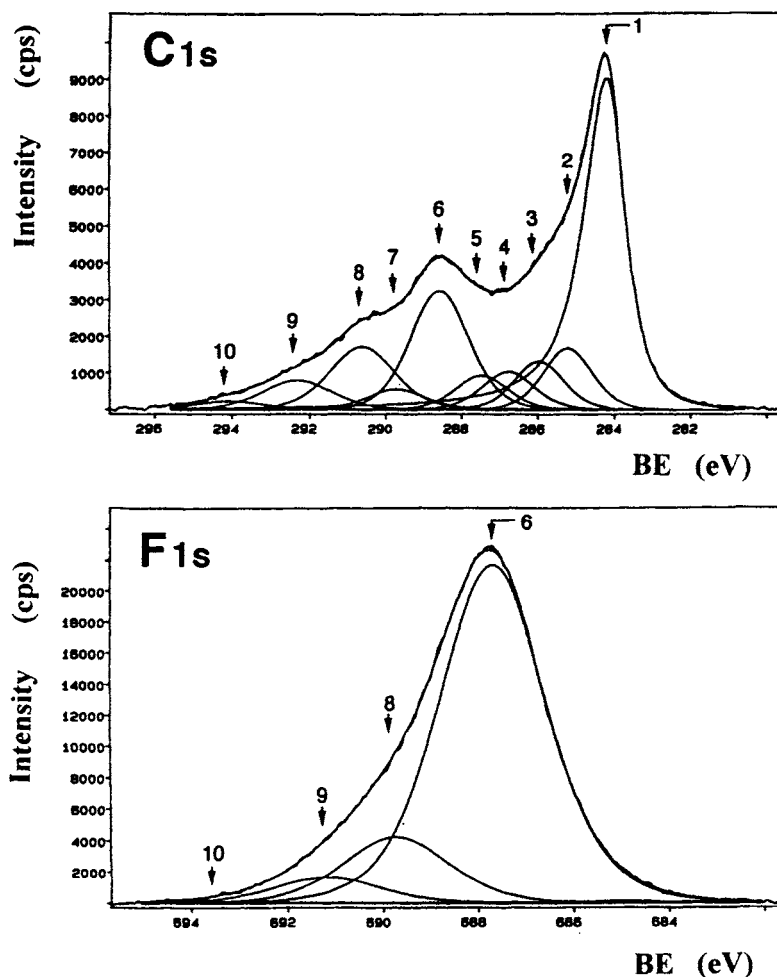


Fig. 23. Fitted high resolution C_{1s} and F_{1s} XPS spectra of plasma-fluorinated furnace carbon black (N115).

$AC\ 1s$ (1), represents 42% of the total area of the $C\ 1s$ envelope. This peak has been taken as an internal reference to define the energy separation with the other (i) components: ΔC_iC_1 . Areas of the different components and energy separation are collected in Table 8. The peak at higher BE, C_{1s} (6), which is located at 288.6eV and which is the most important component of C—F bonds, has been assigned to carbon atoms that are covalently linked to a fluorine atom at the surface and border of the graphitic domains of carbon blacks without any change in the sp^2 conformation of carbon in the bulk (Type I structure). Consequently, the C—C bond length does not differ significantly from that of the initial carbon. Between components (1) and (6) the envelope can be fitted into 4 components corresponding to C atoms that

are not directly bound to F atoms. The shift induced by the presence of F atoms in β position of a given C atoms, i.e. bound to its first neighbors, has been evaluated to about 0.6 ± 0.2 eV [102] and is roughly additive. The assignment of these components are given in Table 7.

Table 7

Energy shifts and assignments of the different components of C1s and F1s XPS spectra of PEF-treated N115 carbon black

Component	ΔC_1C_1 (eV)	Assignment
C ₁	–	Non-functionalised sp ² and sp ³ C atoms, not affected by fluorination
C ₂	1.0	Aliphatic non-functionalised sp ³ C in a non-fluorinated environment (areas modified by “plasma effect”)
C ₃	1.8	Non-functionalised sp ² C in β position to one F atom Non-functionalised sp ² C or sp ³ C in β position to one or two F atom(s), respectively
C ₄	2.6	sp ² C bound to an oxygen atom (phenol, phenyl ether) Non-functionalised sp ² C or sp ³ C in β position to two or three F atoms, respectively Oxygenated sp ³ C in a non-functionalised environment (CH _x —OH, or C—O—C)
C ₅	3.3 ± 0.1	Oxygenated sp ³ C in β position to a F atom Non-functionalised sp ³ C in β position to at least three F atoms sp ² C “semi-ionic”, bound to intercalated F atom (very weak contribution)
C ₆	4.2 ± 0.2	sp ² C covalently linked to an F atom in Type I structure
C ₇	5.4 ± 0.3	CF groups of Type I structure in β position of CF ₂ groups
C ₈	6.3 ± 0.4	CF ₂ groups of Type I structure CF groups of Type II structure
C ₉	7.9 ± 0.4	CF ₃ groups of Type I structure CF ₂ groups of Type II structure
C ₁₀	9.6 ± 0.4	CF ₃ groups of Type II structure Plasmon
Component	ΔF_1F_1 (eV)	Assignment
F ₆	–	F atoms in Type I structure
F ₈	2.0 ± 0.1	F atoms in Type II structure
F ₉	3.5 ± 0.1	F atoms in Type II structure with charge effect
F ₁₀	5.9 ± 0.1	F atoms in Type II structure with higher charge effect

Table 8

BE shifts of the different components of C1s and F1s
XPS spectra of PEF-treated N115 carbon black

Component	$\Delta C_i C_1$ (eV)	AC 1s (i) (%)
C ₁	–	43
C ₂	1.0	7
C ₃	1.8	6
C ₄	2.6	5
C ₅	3.3	4
C ₆	4.4	17
C ₇	5.5	2
C ₈	6.4	10
C ₉	8.1	5
C ₁₀	9.9	1

Component	$\Delta F_i F_6$ (eV)	AF1s (i) (%)
F ₆	–	79
F ₈	2.1	15
F ₉	3.5	5
F ₁₀	5.9	1

The components C1s (i), with $i \geq 6$, are attributed to carbon atoms that are covalently bound to F. The amount of such C in the layer explored by XPS can be evaluated from the ratio $\Sigma AC1s(i) (6 \leq i \leq 10) / \Sigma AC1s(\text{total})$. This ratio is equal to 36%. In order to identify the components shifted by the charge effect and to differentiate the various forms of fluorinated C that constitute the C1s (i) ($i \geq 6$) components, the F1s peak was taken as a reference. As a matter of fact, the chemical shift of F1s core level is less dependent on the x value of CF_x groups than the C core level. In Type I fluorinated structure [i.e. where F atoms are covalently bound to the C atoms of the surface or subsurface zones of particles which keep their graphitic character] F atoms belonging to either CF, CF₂ or CF₃ groups contribute to the same component of the spectrum. This component, F1s (6), is located at 687.6eV, and the difference in BE between corresponding components (6) of the F1s and C1s spectra is: $\Delta F_6 C_6 = 399.1$ eV. F atoms of CF, CF₂ and CF₃ groups belonging to polycyclic perfluorinated structures of Type II (see below) contribute to the same component, F1s (8). This component is shifted by 2.0 eV relative to F1s (6) in the direction of increasing BE. The corresponding fluorinated entities are those with the highest BE. Consequently, the components with even higher BE, i.e. with $i > 8$, can be attributed to fluorinated domains in which the charge effect is particularly important.

Covalent bonding which is formed between C and F atoms modifies locally the electrical conductivity of the sample. In other words, the key-point will be the extension of the thickness of the fluorinated islands. When the dimensions of these domain increase, the positive space charges that appear in these areas during the photoemission process can be only partially neutralised by photoelectrons and secondary electrons emitted from neighboring or underlying non-functionalised areas. The value of the BE separation between component (1) and high-energy components of C1s spectrum, i.e. $\Delta C_i C_1$, with $i \geq 6$, will thus depend on the degree of fluorination of the sample. The component C1s (7) at 289.8 eV corresponds mostly to CF groups of Type I with CF₂ groups as nearest neighbors. F atoms of these groups are assigned to component (6) of the F1s spectrum. The peak whose fitted component is located at 290.7 eV, C1s (8), can be attributed to CF₂ groups of fluorinated structure of Type I, whose F atoms contribute to F1s (6), and also to CF groups of polycyclic perfluorinated structures of *Type II, in which sp^3 C skeleton forms puckered layers similar to those of covalent graphite fluorides (CF)_n*. F atoms of this second type contribute to the component (8) of F1s envelope. Shoulder peak (9) and (10) correspond mostly to CF_n groups of Type II and are associated with components (9) and (10) of F1s [see Table 7]. The corresponding zones are strongly affected by charge effect. From the analysis of the XPS spectra of fluorinated, N115 carbon black samples we conclude that all fluorine atoms, fixed at the surface and in the subsurface zone of the carbon black particles, are covalently linked to carbon atoms. The majority of the structures of the fluorinated islands present at the surface is of Type I, a structure in which the planar conformation of the graphene layers is preserved. However fluorinated islands of Type II structure also exist at the surface and some of them show a significant charge effect.

As a concluding remark, it is possible to modify the nature of the fluorinated film which is formed on the surface of the carbon black by acting either on the nature of the host material or on the characteristics of the plasma. Concerning the physical properties, it can be expected that the formation of a fluorinated insulating layer on the surface of the carbon blacks increases the repulsion effect between the particles. The electrical contacts between the aggregates become therefore limited and the electrical permittivity, which primarily depends on the number of particles, should be increased.

14.3.1.3 Modification of surface properties of high T_C cuprate superconductors

In 1986, the discovery of high-temperature superconducting cuprates (HTSC) has led to unprecedented activities in numerous scientific fields, mainly because of the possible use of these materials for important technological achievements. Unfortunately the use of bulk HTSC was limited by their relatively low capacity for carrying high densities of electrical current, which is due to several serious material problems such as weak links that are generally present at grain boundaries. It has been shown that a fluorination treatment by F₂-gas contributes to remove impurities from grain boundaries [104], and to protect the material against moist air [105]; in addition the critical current density J_C could be increased. Unfortunately this process affords little indus-

trial adaptability due to drastic safety precautions. In addition, due to the extreme reactivity of F_2 , the treatment may easily proceed to a complete fluorination of the materials to insulating fluorides. In order to obtain a surface modification of these ceramics, rf-PEF has been proposed as an alternative processing [107].

Experimental procedures and XPS analysis. Pelletised samples of $YBa_2Cu_3O_{7-\delta}$ containing few residual carbonated species were heated at 920°C under an oxygen flow and slowly cooled under oxygen in order to achieve the optimum oxidation and to limit the cracks formation. The ceramics consisted of homogeneous grains of around $3\ \mu\text{m}$ diameter with an interconnected porosity of about 0.88. Even under these conditions, an amorphous layer was observed by TEM at the gas/solid interface that could be attributed to the presence of surface carbonate [106]. The superconducting properties of these materials have been shown to be improved by PEF treatments involving mixtures of CF_4 and O_2 gases [107,108]. Both values of the resistivity in the normal state (ρ) and of the superconducting transition width (ΔT_C) are reduced and the critical transition temperature (T_C) is increased of about 1 K. The investigation of the various experimental parameters of the process has shown that the improvement of the critical current density (J_C) mainly depends on the inlet precursor composition $CF_4 + x\% O_2$, on the total pressure, and on the reaction time. The experimental conditions have been optimised as follows: inlet precursor composition: $CF_4 + 25\% O_2$; CF_4 -gas flow: $60\ \text{cm}^3\ \text{min}^{-1}$; total pressure: 225 mTorr; rf power 50–100 W; reaction duration: 30 min. The improvement of the superconducting properties (Fig. 24(a)) is also supported by the decrease of the electrical resistivity in the high temperature domain (Fig. 24(b)).

Mechanisms of interaction between the reactive species of the plasma and $YBa_2Cu_3O_{7-\delta}$ ceramics have been proposed through detailed X-ray photoelectron spectroscopic analyses. Two different types of informations could be obtained from these experiments. The first one concerns the interaction of the reactive species (F_2 or F^*) with the grains at the external surface of the pellets. The second one deals

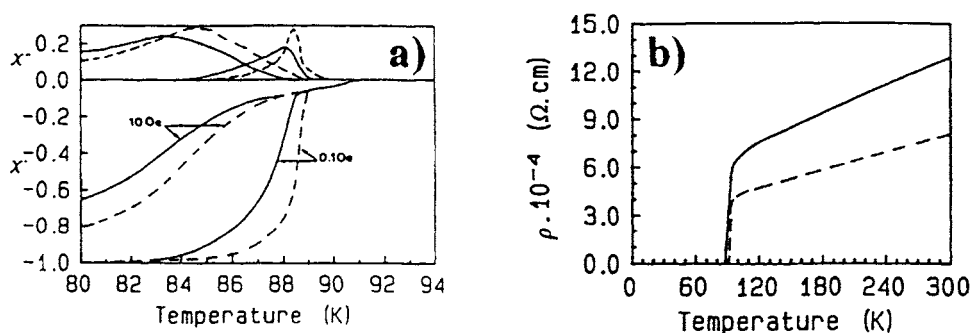


Fig. 24. Improvement of the superconducting properties of $YBa_2Cu_3O_{7-\delta}$ ceramics by PEF processing: (a) a.c. susceptibility curves before (—) and after (---) treatment; (b) temperature dependence of the resistivity before (—) and after (---) treatment.

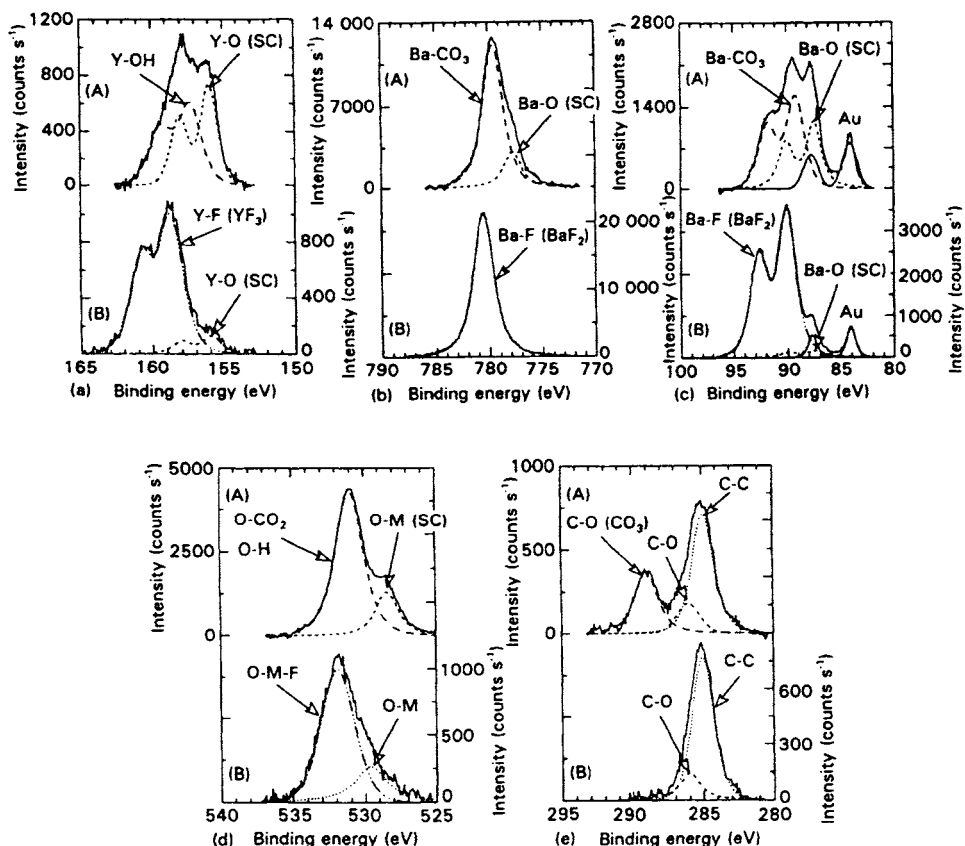


Fig. 25. Y 3d, Ba 3d_{5/2}, Ba 4d, O1s and C1s XPS spectra obtained at the surface of the outer grains of the YBa₂Cu₃O_{7-δ} ceramics before (A) and after (B) the CF₄ + 25% O₂ plasma treatment (the peaks of the superconducting phase are noted S.C.) (reproduced with permission from J. Mat. Sci., 29 (1994) 4260 [108]).

with the interaction between these species and the surface of the inner grains of the ceramics through the study of polished fractures. During the XPS measurement Cu is partly reduced to monovalent species, as already observed in other Cu-based superconductors [109]. Therefore the XPS study concerns only Y 3d, Ba 3d_{5/2}, Ba 4d, O 1s and F 1s levels.

Interaction of the reactive fluorinated species with the surface of outer grains of the YBa₂Cu₃O_{7-δ} ceramics. As shown in Fig. 25(a) before fluorination, Y and Ba XPS spectra of YBa₂Cu₃O_{7-δ} ceramics are currently characterised by two types of contributions. The binding energies of the so-called “superconducting peaks” are strongly shifted towards lower Eb values. They are attributed to metal–oxygen bonds corresponding to the YBa₂Cu₃O_{7-δ} lattice [110]. The second type of contribution corresponds to the degradation layer (Y—OH and Ba—CO₃) [111].

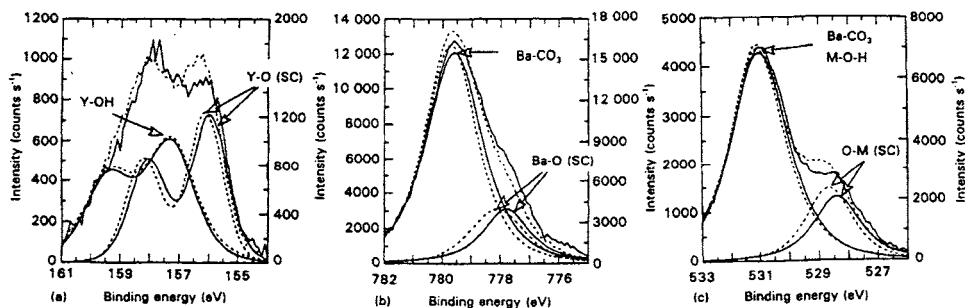


Fig. 26. Y 3d (a), Ba 3d_{5/2} (b) and O 1s (c) emission spectra obtained at the surface of the inner grains of the YBa₂Cu₃O_{7-δ} before (—) and after (---) the CF₄ + 25% O₂ plasma treatment (reproduced with permission from J. Mat. Sci., 29 (1994) 4260 [108]).

After plasma treatment both peaks of Y and Ba elements corresponding to the superconducting phase and to the degradation layer have disappeared from the surface of the outer grains of the ceramics (Fig. 25). New peaks are observed at 158.9 eV (Y 3d), 780.2 eV (Ba 3d_{5/2}) and 90.0 eV (Ba 4d). They can be unambiguously ascribed to metal–fluorine bonds (as already observed in the case of the F₂-gas treatment [112]). These observations are supported by the presence of a unique F 1s peak at 684.7 eV corresponding to fluorine–metal bonds. Contrary to the F₂-gas treatment, the PEF process removes the (OH)[−] and (CO₃)^{2−} species without getting (CF)_n and HF₂[−] species. The following assumption can be proposed: the interaction of F[•] species with the carbonate degradation layer would lead to the formation of volatile compounds like COF or COF₂.

Interaction of reactive fluorinated species with the surface of inner grains of YBa₂Cu₃O_{7-δ} ceramics. After the PEF treatment, the peaks corresponding in the Y 3d and Ba 3d_{5/2} spectra to the superconducting component and to the degradation layer do not change in intensity, and no new peak appears in the high BE domain, as shown in Fig. 26. These observations suggest that the PEF treatment does not decompose the surface of the inner grains, as observed for F₂-gas fluorination. Unfortunately the fluorine content that is distributed homogeneously in the sample has been previously determined by EPMA to be around 0.5 atm%, i.e. too small to be detected by XPS. However it can be pointed out that the peaks corresponding to the components of the superconducting phase are slightly shifted towards higher binding energy (+ 0.2 eV). These displacements cannot be attributed to a charge effect since the BE of the peaks corresponding to the degradation layer remains unchanged. The following assumption has been proposed to explain this behavior: metal–fluorine bonds would be present inside the superconducting phase and the slight shift observed (≈ 0.2 eV) towards higher BE for the superconducting components of the peaks Y 3d, Ba 3d_{5/2} and Ba 4d, would be assigned to an increase of ionicity of the corresponding bonds. The effect of PEF would thus correspond to an increase of the anion rate up to 6.83, which is the content required for optimised

superconducting properties (T_C and J_C) [107]. The treatment removes from the surface of outer grains the $(OH)^-$ and $(CO_3)^{2-}$ species located on the degradation layer of the materials and gives rise to the formation of an homogeneously fluorinated layer, about 7 nm. On the other hand, the PEF treatment does not seem to produce a fluorine rich layer at the surface of inner grains of the materials, but rather leads to the formation of metal-fluorine bonds inside the superconducting phase due to an oxidation process by F species. This effect results in an improvement of weak link behavior of the grain boundaries within the ceramics.

14.3.2 Surface modification in various fluorinating conditions

14.3.2.1 Passivation of metallic surfaces

In order to increase the protection and hydrophobicity of aluminum surfaces, a fluoride film having a high contact-angle and a smooth lustrous surface can be deposited using surface fluorination. The most effective method is to allow Al to react with graphite or graphite fluoride in the presence of F_2 -gas (0.1–1 bar) at high temperature (450–600°C). The film, which is 3 μm thick, contains large amounts of fluorine and aluminum and only small content of carbon. The contact angle of water on the film is 125° and the resistance is greater than $4 \times 10^{10} \Omega cm^{-1}$. In addition these films exhibit a good inertness with high resistance to acidic and alkaline corrosions and high thermal stability [89,113]. It can be added that in reactive ion etching reactions involving a mixture of fluorocarbon gases, a passivation layer (AlF_x) containing only small amount of carbon is also formed onto the reactor (Al) surface [114].

14.3.2.2 Adhesive properties of aluminum surfaces

One of the main inconvenience for the use of composite materials based on an Al matrix remains the difficulty to obtain interfaces of high quality because of the presence of an alumina layer which hinders the adhesion during the casting. Surface treatments by PEF or by low-temperature F_2 -gas fluorination lead to the formation of a very reactive aluminum fluoride film onto the metal [89,115]. Once fluorinated, the Al-based reinforcements can be set inside a mould in such a way that molten Al comes into contact with their surface. After casting, a noticeable increase of the tensile strength of the specimens reinforced by PEF-treated insets is observed, the rupture threshold being largely higher than that of bulky Al pieces [113]

14.3.2.3 Intermetallic compounds for hydrogen storage

A number of intermetallic compounds have been reported to absorb large amounts of hydrogen. However, large scale commercial applications of metal hydrides for the separation and purification of hydrogen have not been yet fully achieved because of the high sensitivity of the metal surface to gaseous impurities present in hydrogen, and also because of possible pyrophobicity in air.

The surface properties of such materials can be highly improved by a treatment in aqueous HF solutions. This processing has been applied to various series of alloys

and intermetallic compounds, such as $\text{La Ni}_{4.7}\text{Al}_{0.3}$ and Mg_2Ni , by S. Suda et al. [116]. The initial pH of the solution is set close to 5; during the experiment, a continuous consumption of F^- ions of the solution is caused by the formation of a solid fluoride film on the metal surface. Meanwhile the pH increases with several reaction steps that result from the decomposition of La oxide and hydroxide present on the surface and at the grain boundaries, that finally leads to the formation of a fluoride film rich in La, with the dissolution of Ni^{2+} ions in the solution. The complete reaction thus corresponds to the formation of a fluorinated layer, a few nm thick, and containing numerous catalytic Ni clusters instead of the originally oxide/hydroxide-contaminated material.

F-treated intermetallics exhibit extremely high reactivity and selectivity to H_2 , even in CO and CO_2 atmospheres. The treatment behaves as a curing effect of the external surface and creates a fluoride-rich layer with a Ni-enriched subsuperficial layer. The hydriding behavior is increased by the presence of microcracks running through the external layer: the initial activation process is enhanced, even for Mg-based alloys. In addition, a protective effect is observed since the samples can be safely stored in air for long time without degradation or surface reactivity [116].

14.3.2.4 Protection of diamond film coatings

The surface properties of many systems can be significantly improved by the use of coating exhibiting specific characteristics. Because of their outstanding properties, diamond films are involved in the coating of many products, such as cutting tools, optical items (disks, lenses, windows), biological implants.

It appeared decisive to modify chemically the outer surface of the diamond film itself, in order to create new surface properties. In particular when diamond is exposed to relatively high temperature or to varied stresses, its surface can easily transform to graphite in an irreversible process. Because of its reactivity, fluorine may act as a modifier which could improve some surface properties of diamond: lubricant properties, stability under oxidising conditions. In this scope, molecular F_2 , atomic F, or XeF_2 have been proposed as fluorinating media [117]. This improvement is particularly important since diamond can be grown at relatively low temperatures by CVD techniques. For instance, the exposition of a clean (111) surface of diamond to XeF_2 -gas leads to the dissociative chemisorption of fluorine, releasing Xe into the ambient. The clean surface had been prepared by heating the crystal in ultravacuum above the hydrogen desorption temperature. Around 80% of the surface of diamond is covered by C—F bonds as shown by the C1s photoemission spectra [118].

Similar results are obtained with microwave discharged (2450 MHz) SF_6 vapor at $P = 1$ mTorr during reaction durations ranging from a few min to several hours. After 20 min exposure, an average thickness of about 2 monolayers of diamond has been converted to fluorocarbon of CF formulation, in which CF_2 and CF_3 groups are also present [119]. Direct fluorination by F_2 -gas allows to replace hydrogen chemisorbed on the surface by fluorine at very low temperature, even at -10°C , whereas in the case of surface oxidised diamond, a complete replacement

of oxygen by fluorine is obtained for fluorination temperatures higher than 500°C [120].

14.3.2.5 PECVD of fluorinated diamond-like carbon films (hydrogenated amorphous films)

Interlayer dielectrics with a low dielectric constant are required to reduce the parasitic capacitance in ultralarge scale integration circuits. Although fluoropolymers such as PTFE have been for long time the lowest dielectric material, their low adhesive strength, low thermal stability and difficulty of manufacturing have limited their development in microelectronics. These films of fluorinated amorphous carbon (a-C:F) have been prepared for a similar purpose in a PECVD equipment using $\text{CF}_4\text{—CH}_4$ rf plasmas in 100–200 mTorr pressure at 50°C. The films that were grown at a 10 nm min^{-1} rate were deposited on $\text{SiO}_2/(100)\text{ Si}$ and $(100)\text{ p}^+\text{ Si}$ wafers previously covered by a thin film of hydrogenated amorphous carbon. Films with a dielectric constant as low as 2.1 were obtained [121]. In such systems, the leakage current is reduced to 10^{-8} A cm^{-2} by the use of (a-C:F) film. Since the electrical conduction in amorphous carbon takes place by hopping mechanism between localised states distributed in the mobility gap, the observed reduction of the leakage current can be assigned to the reduction of localised states by fluorination. It can be pointed out the decisive role of fluorinated DLC films for wear-resistant protective coatings [122,123]. The micro-tribological characteristics of Si-containing hard carbon films deposited on Si substrate are improved by CF_4 treatments: surface energy is reduced and so the micro-wear at an atomic scale [133,134].

14.3.2.6 Modification of wettability of materials

The modification of wettability of materials surfaces is in most cases a parameter of primary importance. Depending on the choice of application, the coating may exhibit either a high water repellency associated with lubricative and mold resealing properties or a high wettability, as in the case of carbon fibers to increase for instance their adhesion with the matrix in composites. We have seen in Sec. 14.3.1.1 that fluorination treatments of carbon materials using low-pressure plasmas or F_2 -gas generally lead to an enhancement of water repellency. This effect is due to the decrease of surface free energy that corresponds to the low polarisability of the covalent C—F bond, formed at the surface. The deposition of films formed of a metal/perfluoro compound composite on various types of substrates also leads to super repellent properties [124]. The metal is generally Ni and the perfluoro compound, such as PTFE or graphite fluoride $(\text{CF})_n$ should have been previously treated under F_2 -gas. This fluorination treatment is required to increase the number of CF_3 groups at the surface of the particles. The very high contact-angle of water droplets on Ni/ F_2 -treated PTFE ($\theta \sim 170^\circ$) is much higher than that observed on a PTFE plate ($\theta = 110^\circ$), as shown in Fig. 27.

These metal/ F_2 -treated PTFE composite films, with metals such as Ni, Au, Sn, Cr can also be prepared by electrodeposition in an electrolyte solution in which PTFE micrometric particles are suspended by using a cationic surfactant. In addition to their very high contact angle ($130 \leq \theta(^{\circ}) \leq 155$), the films show good corrosion

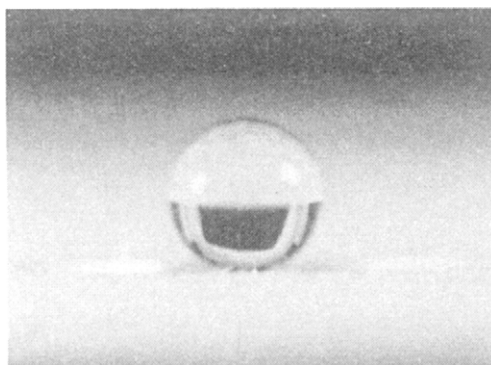


Fig. 27. Water droplet on an Ni/F₂-treated PTFE composite substrate, with contact angle of 173° (with courtesy of Y.B. Chong and N. Watanabe, Kyoto, (1991)).

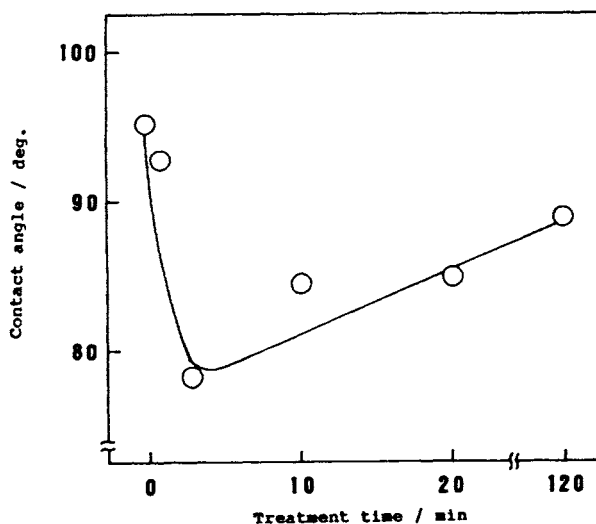


Fig. 28. Dependence of the contact angle upon the F₂-gas fluorination time (reproduced with permission from J. Fluorine Chem., 57 (1992) 169 [126]).

resistivity and thermal stability at 325°C in air [125]. On the other hand, improvement of wettability of various carbon surfaces fibers or powders has been achieved with very short fluorination times by F₂-gas. The minimum value of contact angle observed for water droplets ($\theta = 78^\circ$) is obtained for 3 min fluorination at 25°C under 10 Torr F₂-gas pressure, as shown in Fig. 28. The increase of wettability can be correlated with the increase of surface polar components and of oxygen content (C/O/F contents (%): 77.3/12.2/10.5) [126].

14.3.2.7 Electrochemical properties of cathode materials

LiMO_2 , with $M = \text{Co, Fe, Ni}$, are currently used as cathode in Li-ion secondary batteries. The electrochemical characteristics of these materials can be modified by surface fluorination. The fluorinating gases can be either NF_3 or ClF_3 in the following conditions: $p = 10$ mTorr; room temperature $< T < 200^\circ\text{C}$; reaction duration = 1 h. After the treatment with ClF_3 , the peaks of the cyclic voltammograms of LiCoO_2 become broad and the tailing below 3.5 V during the cathodic sweep disappears. The average charge/discharge potential of ClF_3 -treated LiCoO_2 is more anodic than those of untreated and NF_3 -treated samples [127].

14.3.2.8 Conversion of cuprate oxide thin films into superconductors

Pulsed laser ablation has been developed in many fields for the fabrication of thin films of oxide materials, in particular high T_C cuprate superconductors. In these materials, the increase of the carrier concentration can be obtained in many cases by chemical doping (cationic or anionic), in order to induce superconductivity.

In La_2CuO_4 thin films, the anionic modification of the carrier concentration has been achieved by annealing the films in an oxidising (F_2 -gas) atmosphere [128]. The films were prepared on (100) SrTiO_3 substrates by pulsed laser ablation from the oxide targets. Fluorine doping of La_2CuO_4 was then carried out by a treatment at $100\text{--}200^\circ\text{C}$ under 10% F_2 in N_2 . It is possible to control anionically the carrier concentration in the deposited thin films, in order to optimise the conditions, resulting in films with $T_C \sim 36$ K. From hysteresis cycles, critical current density (J_C) of 10^6 A cm^{-2} are observed at 10 K under zero field [128]. Thin films of $\text{YBa}_2\text{Cu}_3\text{O}_{7-\delta}$ prepared by the same method have been transformed into superconductors by NF_3 treatments [129,130]. The final T_C value, which can be as high as 89 K, depends on the initial oxygen deficiency. In addition, this fluorination treatment acts as a protection against moist air.

14.3.2.9 Fluorinated silicon dioxide films

Speed in Ultra Large Scale Integrated devices can be increased by reducing the capacitance of the interlayer insulators. Since SiO_2 is the material most used for such components, the replacement of oxygen by fluorine has attracted much interest this last decade. PECVD is generally used to elaborate these layers and it involves fluorinated gases such as CF_4 , SiF_4 , CCl_2F_2 , C_2F_6 [135,136].

14.4 Concluding remarks

Surface fluorination in various fluorinated media are currently used nowadays as processes that allow the modifications of many classes of materials, such as metals, intermetallics, semiconductors, carbons, superconductors, oxide ceramics. The above selected examples have illustrated some physical properties that can be drastically modified, including conduction, adhesion, passivation, superconductivity, hydrophobicity/wettability.

Acknowledgments

The authors would like to thank G. Turban and Mrs M.C. Peignon for comments, suggestions and encouragements. In Part II several examples (carbon materials and superconducting ceramics) have been taken from work carried out at ICMCB by F. Moguet and C. Magro during the course of their Doctorate theses. Messrs T. Shirasaki, L. Lozano (ICMCB-Bordeaux), C. Guimon (LPCM-Pau), G. Nansé, E. Papirer (ICSI-Mulhouse) are acknowledged for fruitful discussions and collaboration.

List of symbols of Part I

A^* : radiative activated species

a_0 : Bohr radius,

$$a_0 = \frac{4 \cdot \pi \cdot \epsilon_0 \cdot \hbar}{e^2 \cdot m_e} = 5.2918 \times 10^{-11} \text{ m}$$

c : velocity (m s^{-1}), $\langle c \rangle$ average velocity

e : electron charge (C)

E : energy (J), $\langle E \rangle$ average energy

ER : etch rate (m s^{-1}) or (atom s^{-1})

f : distribution function,

$$\text{MBD}(E_e) = \frac{2}{\sqrt{\pi}} \cdot \frac{1}{(k \cdot T_e)^{\frac{3}{2}}} \cdot \sqrt{E_e} \cdot \exp\left[-\frac{E_e}{k \cdot T_e}\right]$$

or,

$$f(c_e) = 4 \cdot \pi \cdot \left(\frac{m_e}{2 \cdot \pi \cdot k \cdot T_e}\right)^{\frac{3}{2}} \cdot c^2 \cdot \exp\left[-\frac{m_e \cdot c_e^2}{2 \cdot k \cdot T_e}\right]$$

I : emission intensity (au)

K : rate constant

k : Boltzmann constant

M : material

α_p : polarisability

ϵ_0 : permittivity of vacuum

λ : length (m), wavelength, mean free path, or Debye mean free path:

$$\lambda_{A/B} = \frac{\langle c_A \rangle}{\langle v_{A/B} \rangle}$$

σ : cross section (m^2), hard sphere:

$$\sigma_{A/B} = \pi \cdot (r_A + r_B)^2,$$

polarisation scattering:

$$\sigma_{A/B} = \sqrt{\frac{\pi \cdot e^2}{\epsilon_0} \cdot \alpha_p \cdot \frac{m_A + m_B}{m_A \cdot m_B} \cdot \frac{1}{c_{A/B}}}$$

Φ : flux density ($\text{m}^{-2} \text{ s}^{-1}$)

ν : frequency (Hz), radiation, plasma, or collision,

collision:

$$\langle v_{A/B} \rangle = \int_c n_B \cdot \sigma_{A/B} \cdot c_{A/B} \cdot f(c_{A/B}) \cdot dc_{A/B}$$

ω : angular frequency (Hz)

Signification of subscripts

a : adsorption

A/B : process between particle A (incident) and B (target)

ces : chemical enhanced sputtering

d : desorption (thermal)

m : mass (kg)	e : electron
n : density (m^{-3}), n' : density at the vicinity of a surface	i : ion
P : pressure (Pa)	iar : ion assisted reaction
r : particle radius in the hard sphere approximation (m)	n : neutral particle
S : surface (m^2)	p : heavy particle (ion or neutral)
T : temperature (K)	r : reaction (thermal)
V : potential (V)	s : sputtering
Y : sputtering yield	th : threshold

References

- [1] A. Grill, Cold Plasma in Materials Fabrication, IEEE Press, NY, 1993.
- [2] D.M. Manos, D.L. Flamm, Plasma Etching an introduction, Plasma-Materials Interaction Series, Academic Press, San Diego, 1989.
- [3] O. Auciello, D.L. Flamm, Plasma Diagnostics, Plasma-Materials Interaction Series, Academic Press, San Diego, 1989.
- [4] B. Chapman, Glow Discharge Processes, J. Wiley & Sons NY, 1980.
- [5] M.A. Lieberman, A.J. Lichtenberg, Principles of Plasma Discharges and Material Processing, J. Wiley & Sons NY, 1994.
- [6] I. Langmuir, Proc. Nat. Acad. Sci. U.S., 14 (1928) 627.
- [7] H. Winters, Phys. Rev., A 25 (1982) 1420.
- [8] A.D. Kuypers, H.J. Hopman, J. Appl. Phys., 67 (1990) 1229.
- [9] P. Benoit-Cattin, L-C. Bernard, J. Appl. Phys., 39 (1968) 5723.
- [10] J. Liu, L. Huppert, H.H. Sawin, J. Appl. Phys., 68 (1990) 3916.
- [11] A. Manenschijn, G.C.A.M. Janssen, E. van der Drift, S. Radelaar, J. Appl. Phys., 69 (1990) 1253.
- [12] A. Picard, G. Turban, B. Grolleau, J. Phys. D: Appl. Phys., 19 (1986) 991.
- [13] W.H. Beattie, Applied Spectroscopy, 29 (1975) 334.
- [14] G. Turban, B. Grolleau, P. Launay, P. Briaud, Rev. Phys. Appl., 20 (1985) 609.
- [15] E.A. Truesdale, G. Smolinsky, J. Appl. Phys., 50 (1979) 6594.
- [16] H. Sugai, H. Toyoda, J. Vac. Sci. Technol., A 10 (1992) 1193.
- [17] A. Tserepi, W. Schwarzenbach, J. Derouard, N. Sadeghi, J. Vac. Sci. Technol., A 15 (1997) 3120.
- [18] W.W. Stoffels, E. Stoffels, K. Tachibana, J. Vac. Sci. Technol., A 16 (1998) 87.
- [19] L.J. Overzet, J.H. Beberman, J.T. Verdeyen, J. Appl. Phys., 66 (1989) 1622.
- [20] E. Stoffels, W.W. Stoffels, D. Vender, G.M.W. Kroesen, F.J. de Hoog, J. Vac. Sci. Technol., A 13 (1995) 2051.
- [21] M-C. Peignon, Ch. Cardinaud, G. Turban, J. Electrochem. Soc., 140 (1993) 505.
- [22] J.W. Coburn, M. Chen, J. Appl. Phys., 51 (1980) 3134.
- [23] R. d'Agostino, F. Cramarossa, S. de Benedictis, G. Ferraro, J. Appl. Phys., 52 (1981) 1259.
- [24] V.M. Donnelly, D.L. Flamm, W.C. Dautremont-Smith, D.J. Ferder, J. Appl. Phys., 55 (1984) 242.
- [25] M. Haverlag, W.W. Stoffels, E. Stoffels, G.M.W. Kroesen, F.J. de Hoog, J. Vac. Sci. Technol., A 14 (1996) 384.

- [26] M. Haverlag, W.W. Stoffels, E. Stoffels, G.M.W. Kroesen, F.J. de Hoog, J. Vac. Sci. Technol., A 14 (1996) 380.
- [27] K. Miyata, M. Hori, T. Goto, J. Vac. Sci. Technol., A 15 (1997) 568.
- [28] B.K. McMillin, M.R. Zacharian, J. Vac. Sci. Technol., A 15 (1997) 230.
- [29] C. Suzuki, K. Sasaki, K. Kadota, J. Vac. Sci. Technol., A 16 (1998) 2222.
- [30] K. Miyata, M. Hori, T. Goto, J. Vac. Sci. Technol., A 14 (1996) 2343.
- [31] J-P. Booth, G. Hancock, N.D. Perry, M.J. Toogood, J. Appl. Phys., 66 (1989) 5251.
- [32] K.E. Greenberg, P.J. Hargis Jr, J. Appl. Phys., 68 (1990) 505.
- [33] G. Cunge, P. Chabert, J-P. Booth, Plasma Sources Sci. Technol., 6 (1997) 349.
- [34] V.A. Godyak, R.B. Piejak, B.M. Alexandrovich, Plasma Sources Sci. Technol., 1 (1992) 36.
- [35] N Hershkowitz, In: Plasma Diagnostics: Discharge Parameters and Chemistry, O. Auciello, D.L. Flamm (Eds.), Plasma-Materials Interaction Series, Academic Press, San Diego, 1989, p. 113.
- [36] M.B. Hopkins, J. Res. Nat. Inst. Stand. Technol., 100 (1995) 415.
- [37] M-C. Peignon, Ch. Cardinaud, G. Turban, J. Appl. Phys., 70 (1991) 3314.
- [38] D.C. Marra, E.S. Aydil, J. Vac. Sci. Technol., A 15 (1997) 2508.
- [39] G.S. Oehrlein, J. Vac. Sci. Technol., A 11 (1993) 34.
- [40] T. Shirafuji, W.W. Stoffels, H. Moriguchi, K. Tachibana, J. Vac. Sci. Technol., A 15 (1997) 209.
- [41] G.M.W. Kroesen, H-J Lee, H. Moriguchi, H. Motomura, T. Shirafuji, K. Tachibana, J. Vac. Sci. Technol., A 16 (1998) 225.
- [42] S. Vallon, O. Joubert, L. Vallier, F. Ferrieu, B. Drevillon, N. Blayo, J. Vac. Sci. Technol., A 15 (1997) 865.
- [43] M.J.M. Vugts, M.F.A. Eurlings, L.J.F. Hermans, H.G.W. Beijerinck, J. Vac. Sci. Technol., A 14 (1996) 2780.
- [44] R. Pétri, P. Brault, O. Vatel, D. Henry, E. André, P. Dumas, F. Salvan, J. Appl. Phys., 75 (1994) 1.
- [45] T. Chevolleau. Doctorate Thesis, Univ. Nantes-ISITEM, Nantes, France, 1998.
- [46] R.N. Compton, L.G. Christophorou, G.S. Hurst, P.W. Reinhardt, J. Chem. Phys., 45 (1966) 4634.
- [47] L.G. Christophorou, J.K. Olthoff, V.V.S. Rao, J. Phys. Chem. Ref. Data, 25 (1996) 1341.
- [48] A.V.P. Phelps, J. Appl. Phys., 64 (1988) 4269.
- [49] H.G. Lergon, M. Venugopalan, K.G. Müller, Plasma Chem. Plasma Process., 4 (1984) 107.
- [50] K.R. Ryan, I.C. Plumb, Plasma Chem. Plasma Process., 6 (1986) 231.
- [51] Y. Hikosaka, H. Toyoda, H. Sugai, Jpn. J. Appl. Phys. Part 2, 32 (1993) 353.
- [52] N.V. Mantzaris, E. Gogolides, A.G. Boudouvis, Plasma Chem. Plasma Process., 16 (1996) 301.
- [53] I.C. Plumb, K.R. Ryan, Plasma Chem. Plasma Process., 6 (1986) 205.
- [54] J.C. Martz, D.W. Hess, W.E. Anderson, Plasma Chem. Plasma Process., 10 (1990) 261.
- [55] A. Campo, Ch. Cardinaud, G. Turban, Plasma Sources Sci. Technol., 4 (1995) 398.
- [56] J-P. Booth, G. Hancock, N.D. Perry, Appl. Phys. Lett., 50 (1987) 318.
- [57] J-P. Booth, G. Hancock, N.D. Perry, D.C.W. Blaikeley, J.A. Cairn, R. Smailes, Mat. Res. Soc. Symp. Proc. 98 (1987) 135.
- [58] K.R. Ryan, I.C. Plumb, Plasma Chem. Plasma Process., 10 (1990) 207.
- [59] S.P. Venkatesan, I. Trachtenberg, T.F. Edgar, J. Electrochem. Soc., 137 (1990) 2280.
- [60] R.A.H. Heinecke, Solid-State Electron., 18 (1975) 1146.

- [61] J.W. Coburn, *J. Appl. Phys.*, 50 (1979) 5210.
- [62] H-H. Doh, J-H. Kim, K-W. Whang, S-H. Lee, *J. Vac. Sci. Technol.*, A 14 (1996) 1088.
- [63] G.S. Oehrlein, H.L. Williams, *J. Appl. Phys.*, 62 (1987) 662.
- [64] G.S. Oehrlein, *Mat. Res. Soc. Symp. Proc.*, 98 (1987) 229.
- [65] A. Campo, Ch. Cardinaud, G. Turban, *J. Vac. Sci. Technol.*, B 13 (1995) 235.
- [66] J.W. Coburn, H.F. Winters, *J. Appl. Phys.*, 50 (1979) 3189.
- [67] D.L. Flamm, V.M. Donnelly, J.A. Mucha, *J. Appl. Phys.*, 52 (1981) 3633.
- [68] P.C. Zalm, *J. Appl. Phys.*, 54 (1983) 2660.
- [69] J.L. Mauer, J.S. Logan, L.B. Zielinski, G.C. Schwartz, *J. Vac. Sci. Technol.*, 15 (1978) 1734.
- [70] T. Chevolleau, P-Y. Tessier, Ch. Cardinaud, G. Turban, *J. Vac. Sci. Technol.*, A 15 (1997) 2661.
- [71] M.E. Barone, D.B. Graves, *J. Appl. Phys.*, 77 (1995) 1263.
- [72] M.E. Barone, D.B. Graves, *J. Appl. Phys.*, 78 (1995) 6604.
- [73] P. Alnot, J. Olivier, F. Wyczisk, *J. Electron Spectrosc. Relat. Phenom.*, 43 (1987) 263.
- [74] A. Campo, Ch. Cardinaud, G. Turban, C. Dubon-Chevallier, V. Amarger, J. Etrillard, *J. Vac. Sci. Technol.*, A 11 (1993) 2536.
- [75] J.W. Butterbaugh, D.C. Gray, H.H. Sawin, *J. Vac. Sci. Technol.*, B 9 (1991) 1461.
- [76] D.C. Gray, I. Tepermeister, H.H. Sawin, *J. Vac. Sci. Technol.*, B 11 (1993) 1243.
- [77] M.J.M. Vugts, L.J.F. Hermans, H.G.W. Beijerinck, *J. Vac. Sci. Technol.*, A 14 (1996) 2138.
- [78] J. Ding, J-S. Jenq, G-H. Kim, H.L. Maynard, J.S. Hamers, N. Hershkowitz, J.W. Taylor, *J. Vac. Sci. Technol.*, A 11 (1993) 1283.
- [79] D. Dane, T.D. Mantei, *Appl. Phys. Lett.*, 65 (1994) 478.
- [80] M-C. Peignon, G. Turban, C. Charles, R.W. Boswell, *Surf. Coating Technol.*, 97 (1997) 465.
- [81] Y. Feurprier, Ch. Cardinaud, B. Grolleau, G. Turban, *J. Vac. Sci. Technol.*, A 16 (1998) 1552.
- [82] N.R. Rueger, J.J. Beulens, M. Schaepkens, M.F. Doemling, J.M. Mirza, T.E.F.M. Standaert, G.S. Oehrlein, *J. Vac. Sci. Technol.*, A 15 (1997) 1881.
- [83] Ch. Cardinaud, G. Turban, *Appl. Surf. Sci.*, 45 (1990) 109.
- [84] C.J. Mogab, A.C. Adams, D.L. Flamm, *J. Appl. Phys.*, 49 (1978) 3796.
- [85] A. Picard, G. Turban, *Plasma Chem. Plasma Process.*, 5 (1985) 333.
- [86] M-C. Peignon, Ch. Cardinaud, G. Turban, *J. Appl. Phys.*, 70 (1991) 3314.
- [87] M-C. Peignon. Doctorate Thesis, Univ. Nantes-ISITEM, Nantes, France, 1993.
- [88] U. Kortshagen, A. Shivarova, E. Tatrova, D. Zamfirov, *J. Phys. D: Appl. Phys.*, 26 (1994) 301.
- [89] N. Watanabe, T. Nakajima, H. Touhara, *Graphite Fluorides*, Elsevier, Amsterdam, 1988.
- [90] R.J. Lagow, L.A. Shimp, D.K. Lam, R.F. Baddour, *Inorg. Chem.*, 11 (1972) 2568.
- [91] G.D. Merfeld, M.A. Petrich, *J. Vac. Sci. Technol.*, A12 (1994) 365
- [92] K. Kotera, H. Tanaka, M. Uchida, T. Hirao, N. Iwamoto, *J. Japan Inst. Metals*, 60 (1996) 595.
- [93] S. Okazaki, M. Kogoma, S. Kanazawa, T. Moriwaki, *Proc. Jap. Symp. Plasma Chem.*, 1 (1988) 251.
- [94] I.H. Loh, R.E. Cohen, R.F. Baddour, *J. Mater. Sci.*, 22 (1987) 2937.
- [95] T. Nakajima, N. Watanabe, *Graphite Fluorides and Carbon-Fluorine Compounds*, CRC Press, Boca Raton, 1991.
- [96] A. Tressaud, *Mol. Cryst. Liq. Cryst.*, 244 (1994) 13.

- [97] T. Mallouk, N. Bartlett, *J. Chem. Soc. Chem. Commun.*, 103 (1983).
- [98] A. Tressaud, C. Guimon, V. Gupta, F. Moguet, *Mat. Sc. Engin.*, B30 (1995) 61.
- [99] F. Moguet, Doctorate Thesis, Univ. Bordeaux I, (1996).
- [100] A. Tressaud, V. Gupta, L. Piroux, L. Lozano, E. Marquestaut, S. Flandrois, A. Marchand, O.P. Bahl, *Carbon*, 32 (1994) 1485.
- [101] G. Nansé, E. Papirer, P. Fioux, F. Moguet, A. Tressaud, *Carbon*, 35 (1997) 175.
- [102] G. Nansé, E. Papirer, P. Fioux, F. Moguet, A. Tressaud, *Carbon*, 35 (1997) 371.
- [103] G. Nansé, E. Papirer, P. Fioux, F. Moguet, A. Tressaud, *Carbon*, 35 (1997) 515.
- [104] J.M. Dance, A. Tressaud, B. Chevalier, J. Darriet, J. Etourneau, *Solid State Ionics*, 32/33 1989 p 1188.
- [105] B. Lépine, Doctorate Thesis, Univ. Bordeaux I, 1990.
- [106] J.M. Heintz, C. Magro, A. Tressaud, P. Dordor, J.P. Bonnet, *J. Less-Comm. Metals*, 164-165 (1990) 1377.
- [107] C. Magro, Doctorate Thesis, Univ. Bordeaux I, 1992.
- [108] C. Magro, A. Tressaud, L. Lozano, J. Etourneau, N. Hudakova, C. Cardinaud, G. Turban, *J. Mat. Sci.*, 29 (1994) 4225; *ibid.* 4260.
- [109] W. Herzog, M. Schwarz, H. Sixl, R. Hoppe, *Z. Phys.*, B71 (1988) 19.
- [110] S. Myhra, J.C. Rivière, A.M. Stewart, P.C. Healy, *Z. Phys.*, B72 (1988) 413.
- [111] R.P. Vasquez, M.C. Foote, B.D. Hunt, *J. Appl. Phys.*, 66 (1989) 4866.
- [112] A. Tressaud, K. Amine, J.P. Chaminade, J. Etourneau, Tran Minh-Duc, A. Sartre, *J. Appl. Phys.*, 68 (1990) 248.
- [113] C. Briant, J.C. Da Rugna, A. Tressaud, F. Girot, French Patent no. 9501786 (1995).
- [114] J.F. Daviet, L. Peccoud, P. Lassagne, A. Ermolieff, S. Marthon, F. Pierre, Le Vide, *Les Couches Minces*, Suppl. No 256, Société Française du Vide, Paris, (1991) 365.
- [115] H. Yamada, T. Nakajima, N. Watanabe, *Angew. Chem. Int. Ed.*, 21 (1982) 378.
- [116] F.J. Lin, S. Suda, *J. Alloys Compounds*, 231 (1995) 742 (and several other contributions in the same issue).
- [117] D.E. Patterson, R.H. Hauge, J.L. Margrave, *Mat. Res. Soc. Symp. Proc.*, 140 (1989) 351.
- [118] J.F. Morar, F.J. Himpsel, G. Hollinger, J.L. Jordan, G. Hughes, F.R. McFeely, *Phys. Rev.*, B33 (1986) 1340; *ibid.* 1346.
- [119] P. Cadman, J.D. Scott, J.M. Thomas, *J. Chem. Soc., Chem. Commun.*, (1975) 654.
- [120] T. Ando, K. Yamamoto, M. Kano, Y. Sato, Y. Takamatsu, S. Kawasaki, F. Okino, H. Touhara, *J. Chem. Soc., Faraday Trans.*, 91 (1995) 3209.
- [121] K. Endo, T. Tatsumi, *J. Appl. Phys.*, 78 (1995) 1370.
- [122] J. Seth, S.V. Babu, *Thin Solid Films*, 230 (1993) 90.
- [123] A. Grill, V.V. Patel, U. S. Patent 5, 674, 638, (1997).
- [124] Y.B. Chong, N. Watanabe, *Proc. 13th Intern. Symp. Fluorine Chem.*, Contribution A-43, Bochum, Germany, 1991.
- [125] H. Kiyokawa, T. Kiyokawa, R. Ikeda, S. Yonezawa, Y.B. Chong, M. Takashima, *Proc. 3rd Conf. on High Performance Coating Materials: Fluorine in Coatings II*, (Contribution 12), Munich, Germany, 1997.
- [126] Y.B. Chong, H. Ohara, *J. Fluorine Chem.*, 57 (1992) 169.
- [127] S. Yonezawa, A. Hirano, T. Kimura, M. Takashima, *Proc. 12th Europ. Symp. Fluorine Chem.*, Contribution PI-83, Berlin, Germany, 1998.
- [128] S.T. Lees, I. Gameson, M.O. Jones, P.P. Edwards, C. Greaves, F. Wellhofer, P. Woodall, I. Langford, M. Slaski, *Physica*, C270 (1996) 305.
- [129] O. Peña, M. Mokhtari, C. Perrin, C. Thivet, M. Guilloux-Viry, A. Perrin, M. Sergent, *Physica*, C206 (1993) 6.

- [130] P. Massiot, Doctorate Thesis, Univ. Rennes I, 1998.
- [131] M.R. Wertheimer, L. Martinu and E.M. Liston, Handbook of Thin Film Process Technology, Chapter E3.0, IOP Publ., Bristol, 1996.
- [132] Y. Hattori, Y. Watanabe, S. Kawasaki, F. Okino, B.K. Pradhan, T. Kyotani, A. Tomita, H. Touhara, Carbon, 37 (1999) 1033.
- [133] S. Miyake, R. Kaneko, Y. Kikuya, I. Sugimoto, J. Tribology, Trans. ASME, 113 (1991) 384.
- [134] C. Donnet, Surf. Coatings Techn. 100–101 (1998) 180.
- [135] M. C. Paul, R. Sen, T. Bandyopadhyay, J. Mater. Sci. 32 (1997) 3511.
- [136] S. Hasegawa, T. Tsukaoka, T. Inokuma, Y. Kurata, J. Non-Cryst. Solids 240 (1998) 154.

CHAPTER 15

Fluorinated Carbon Materials for Energy Conversion

Tsuyoshi Nakajima

Department of Polymer Chemistry, Graduate School of Engineering, Kyoto University, Sakyo-ku, Kyoto, 606-8501, Japan

15.1 Introduction

Carbon materials have two dimensional layered structures which are suitable for intercalation of foreign molecule, atom or ion. It has been known that many substances such as alkali and alkaline earth metals with low ionization potentials, and halogens, halides or acids with high electron affinity are intercalated in graphene layers, yielding many kinds of graphite intercalation compounds. One of the important applications of graphite intercalation compounds is their use as electrode materials for batteries. The primary lithium/graphite fluoride batteries were developed by Matsushita Industries Ltd, in Japan [1,2]. It was the first battery which utilized metallic lithium as an electrode material and organic solvents as an electrolyte solution, showing a high discharge potential of 2–3 V with a discharge capacity of 600–800 mAhg⁻¹ [1–4]. Since the commercialization of lithium/graphite fluoride batteries, several alternative carbon fluorine compounds were proposed as cathode active masses. They are fluorine-graphite intercalation compounds prepared at room temperature [5–8], graphite fluorides prepared from the residual carbon obtained by decomposition of graphite oxide [9,10], fluorinated graphite oxides [8,11,12] and so on. Several groups are still working on the synthesis and electrochemical properties of carbon–fluorine compounds. After the primary lithium/graphite fluoride and lithium/manganese dioxide batteries were widely spread, main interests of researchers and industries moved to the development of lithium secondary batteries. Recently Sony Co. developed lithium ion secondary batteries using non-graphitizable carbon as an anode material for lithium ion intercalation with lithium cobalt oxide as a positive electrode and organic electrolyte solution [13]. Since then, lithium ion secondary batteries have been produced on an industrial scale by many battery companies. It should be noted that fluorine compounds such as LiPF₆ and poly(vinylidene fluoride), PVdF are now employed in the practical batteries as an electrolyte and binder, respectively. Some other fluoride electrolytes are also under development. The details are presented in the next chapter. Thus the importance of fluorine compounds in lithium secondary batteries

is increasing. On the synthesis and electrochemical characteristics of carbon–fluorine compounds, some books and reviews were already published [3,4,8,12,14,15].

The present chapter deals with recent advances in carbon–fluorine compounds, in particular focusing on their electrochemical properties.

15.2 Recent advances on fluorine-intercalated carbon materials

15.2.1 Fluorine–graphite intercalation compound

Several new attempts were recently conducted on the intercalation of fluorine into carbon materials. Fluorine-intercalated carbon fibers were synthesized at room temperature under fluorine pressures of $\sim 1 \times 10^5$ and $\sim 1 \times 10^6$ Pa in the presence of a small amount of HF [16–20]. Carbon hosts were polyacrylonitrile (PAN)- and pitch-based carbon fibers as-received and heat-treated at around 3000°C. Table 1 summarizes the synthetic conditions, compositions, stage numbers and repeat distances along *c*-axis (I_c) of fluorine-intercalated carbon fibers [16,20]. The composition and stage number depended on the basic structure and crystallinity of host fiber and the pressure of fluorine gas. The amounts of intercalated fluorine were higher for better graphitized fibers and higher fluorine pressures. The presence of a Lewis acid such as HF is known to be essential for fluorine intercalation in carbon materials below 100°C. When a trace of HF ($\leq 0.1\%$) is present in a reaction system (method A in Table 1), the resulting compounds were $C_{>8}F$ of higher stages than 2, in most cases. However, mixtures of Stage 1 and Stage 2 with compositions of C_4F to C_6F were obtained in the presence of 10% HF (method B) for both carbon fibers. The method C using 1×10^6 Pa fluorine gave C_3F of pure Stage 1 and C_4F of mixtures of Stage 1 and Stage 2. The Stage 1 C_3F with I_c value of 0.615 nm was obtained from graphitized pitch-based carbon fiber. X-ray photoelectron spectroscopy (XPS) study indicated the existence of semi-ionic and covalent C—F bonds around the surfaces of fluorinated fibers [17,20].

A high resolution transmission electron microscopy (TEM) study was also carried out on fluorine-intercalated carbon fibers [18,20]. A TEM image of a mixture of Stage 2 ($I_c = 0.94$ nm) and Stage 3 ($I_c = 1.27$ nm), $C_{10}F$ showed the same interlayer spacing as that of starting graphite and no domain of a stage number $n \geq 2$ was detected. The absence of long range alignment of graphene layers was attributed to the deintercalation of fluorine, which might have reacted with carbon atom, creating lattice defects. Fluorine-intercalated graphites of stage number $n \geq 2$ are less stable than the Stage 1. Deintercalation of fluorine therefore occurred under high vacuum. The complete deintercalation of fluorine was achieved within several hours. In case of a mixture of Stage 1 ($I_c = 0.5$ nm) and Stage 2 ($I_c = 0.94$ nm), C_7F , the TEM image showed the intercalated domains with d value of 0.5 nm and domains with d value close to that of graphite (~ 0.335 nm). A TEM image of Stage 1, C_3F gave only one type of interlayer spacing of 0.61 ± 0.02 nm as shown in Fig. 1. Thus Stage 1 C_xF was less affected in moist air or under high vacuum than those of higher stages, however, some structural changes were observed when the samples were left in the laboratory atmosphere for several months. After fluorination, C_3F exhibited

Table 1

Structural data for some fluorine-intercalated fibers (PAN-based IPCL and pitch-based): method A refers to $P_{F_2} \sim 1 \times 10^5$ Pa ($\leq 0.1\%$ HF); method B to $P_{F_2} \sim 1 \times 10^5$ Pa ($+1 \times 10^4$ Pa HF); method C to $P_{F_2} \sim 1 \times 10^6$ Pa ($+1 \times 10^4$ Pa HF)

Type of fiber(heat treatment)	Experi-mental conditions	Weight uptake (%)	Elemental compo-sition	Stage	X-ray analysis [() minor component]	
					I_c (± 0.01 nm)	L_c (after interc.)
						L_c (before interc.)
IPCL (as receiv.)	method A, B, or C	7–16	$C_{10-22}FH_\delta$		poorly crystallized	–
IPCL (3100°C)	method A	11	$C_{14}FH_\delta$	4	1.62	0.53
	method B	25	C_6FH_δ	2/1	0.94/0.47	0.45
	method C	38	C_4FH_δ	2/1	0.94/0.47+0.55	0.4
P55 (3100°C)	method A	16	$C_{10}FH_\delta$	3	1.27	0.4
P120 (as receiv.)		18	C_9FH_δ	3/2	1.27/0.94	0.5
P55 (as receiv.)		33	$C_{4.8}FH_\delta$	2/1	0.94/0.48	0.5
P75 (3100°C)	method B	29	$C_{5.4}FH_\delta$	2/1	0.94/0.48+0.53	0.35
P55 (3100°C)		33	$C_{4.9}FH_\delta$	2/1	0.94/0.48+0.53	0.35
P75 (3100°C)		37	$C_{4.3}FH_\delta$	(2)/1	(0.94)/(0.48)+0.53	–
P120 (as receiv.)	method C	39	$C_{4.1}FH_\delta$	(2)/1	(0.94)/(0.48)+0.545	0.3
P75 (3100°C)		54	C_3FH_δ	1	0.615	0.3

IPCL: PAN-based fibers produced by Indian Petro Chemicals Ltd. P55, P75, P120: pitch-based fibers from Amoco, USA. (Reproduced with permission from Carbon, 32 (1994) 1485 [16]).

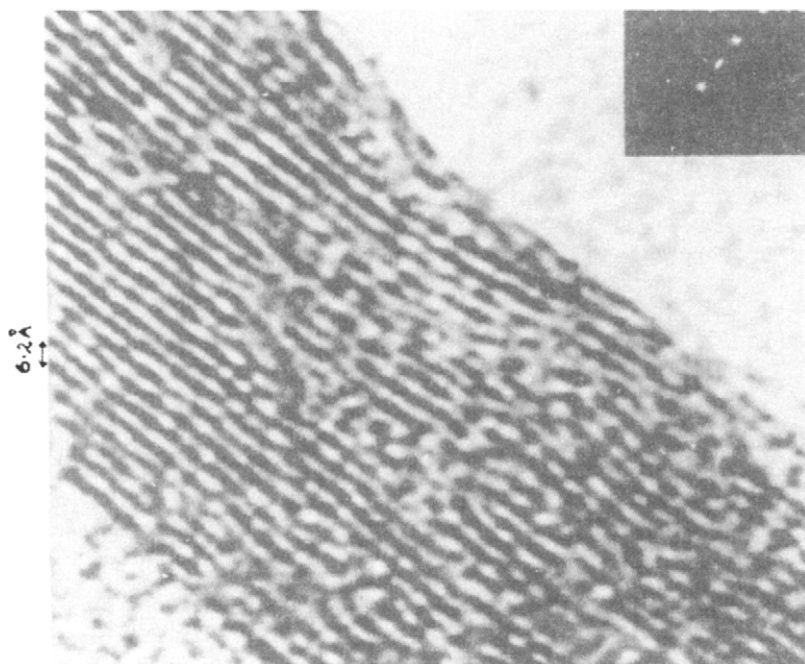


Fig. 1. TEM image of fluorinated pitch-based fiber (HTT-P75), C_3F (reproduced with permission from Carbon, 33 (1995) 1339 [18]).

an interlayer spacing of 0.61 nm as shown in Fig. 1, but after 8 months in air, a decrease in the interlayer spacing to 0.56 nm and an increase of disordering of parallel graphene layers were observed.

The thermal stability of fluorine-intercalated carbon fibers was examined by thermogravimetry (TG) and differential scanning calorimetry (DSC) [19,20]. A high stage $C_{22}F$ (sample 1), four mixtures of Stage 2 and Stage 1, C_4F – C_6F (samples 2–5) and a Stage 1 C_3F (sample 6) were subjected to the thermal analyses. In the temperature range of 50–200°C, a weight loss of about 2–3 wt% was observed except sample 1 of a high stage which showed a larger weight loss of about 9 wt%. The sample 1 gave the strongest exothermic peak in this temperature range ($\Delta H = 95 \text{ J g}^{-1}$). The enthalpy changes were smaller in the mixtures of Stage 2 and Stage 1 (samples 2–5) and the smallest value of 18 J g^{-1} in the Stage 1 compound (sample 6). Between 200°C and 500°C, stepwise decrease of weight to about 10 wt% was observed for samples 2–5, however, monotonous decrease in weight to about 10 wt% was also detected for Stage 1 compound (sample 6). Drastic decrease in weight occurred at about 500°C in all the samples except sample 1. X-ray diffraction measurements indicated that the compounds changed to the higher stages with increasing temperature and finally decomposed to carbon at about 500°C. In the DSC curves small endothermic peaks were observed at around 240°C except Stage 1 C_3F (sample 6), which could be due to deintercalation of fluorine at this temperature

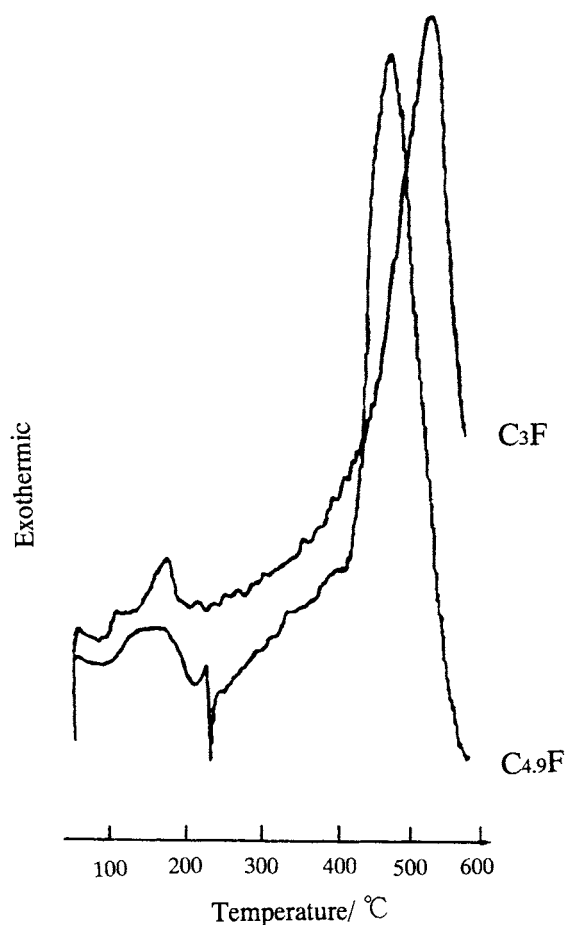


Fig. 2. DSC curves of fluorine-intercalated carbon fibers (Stage 2+1 C_{4.9}F and Stage 1 C₃F) in nitrogen atmosphere (heating rate 5 K min⁻¹) (reproduced with permission from Synth. Metals, 73 (1995) 69 [19]).

as shown in Fig. 2. The Stage 1 C₃F did not show such an endothermic peak because fluorine was more strongly bonded to carbon. A large exothermic peak was detected at about 370°C for the high stage C₂₂F (sample 1), and those for samples 2–6 were observed between 450°C and 540°C. These large exothermic peaks would correspond to the final decomposition of the samples.

Theoretical and experimental approaches were recently done using highly oriented pyrolytic graphite (HOPG) and natural graphite flake as host materials. The X-ray diffraction patterns of Stage 1 and Stage 2 C_xF samples prepared from HOPG and natural graphite flake were reproduced by intensity calculation of (00 ℓ) diffraction lines on the basis of almost ionic and semi-ionic fluorine-intercalated layers and bi-intercalation structure models [21].

C_xF was synthesized at room temperature and -78°C using elemental fluorine and high-oxidation state transition-metal fluorides such as AgF_3 and NiF_3 under a quite low HF contamination ($\text{HF} \leq 0.01\%$) [221]. The host materials were mainly HOPG chips. The products were Stage 1 to Stage 4 compounds with compositions of $C_{4.2}F$ to $C_{14.6}F$. The Stage 1 $C_{4.2}F$ had a large I_c value of 1.034 nm with a minor Stage 2 phase. The main products were stage 2–4 compounds with compositions of $C_{6.1}F$ – $C_{14.6}F$. To confirm the fluorinating ability of AgF_3 and NiF_3 , blank tests were performed at room temperature and -78°C without AgF_3 and NiF_3 . At room temperature, no fluorine was intercalated into such an HOPG as used in the study, although a small amount of fluorine was inserted into only a much thinner HOPG chip (weight: 3 mg). However, at -78°C , some fluorine was intercalated/absorbed even without catalysts into HOPG chips with the same dimensions as those usually used in the study. About half of the intercalated/absorbed fluorine was released several weeks after the samples obtained at -78°C without catalyst were sealed into ampules.

NMR study was also performed on C_xF compounds prepared at room temperature in the presence of a trace of HF [23,24]. Low field ($B_0 = 0.7\text{ T}$) ^{19}F NMR measurements showed that, for the samples except for diluted compounds with $x > 8$ in C_xF , ^{19}F NMR spectra obtained at room temperature consisted of two lines: a narrow line ($\sim 1\text{ kHz}$) from mobile fluorine species such as $\text{HF}_2^{\delta-}$ and a broad line (between ~ 11 and $\sim 18\text{ kHz}$ for $x = 8$ and 3.8 , respectively) from the “rigid lattice”. At high magnetic field, 7T, the room temperature spectra also consisted of broad and narrow lines except for the diluted samples with $x > 8$ in C_xF , which gave only narrow lines, as shown in Fig. 3. The broad lines in the range between -30 and -270 ppm are attributed to “rigid” C–F bonds in graphite galleries. The intensity ratios of broad to narrow lines decreased with decreasing fluorine content as shown in Fig. 4, in which the broad line disappeared at $x \approx 8.5$. Figure 4 indicates that electron localization, i.e. C–F bond formation starts at $x \approx 8.5$ in C_xF . The ^{19}F NMR spectra can be correlated with the inplane electrical conductivities previously obtained [3,15]. The electrical conductivity increases and reaches a plateau until the fluorine content increases to $x \approx 8.5$ in C_xF , and then starts to gradually decrease with further increase in fluorine concentration. This behavior of the electrical conductivity suggests that a number of positive holes would increase and become almost saturated with increase in fluorine content up to $x \approx 8.5$ in C_xF , after which the electron localization starts to occur and is enhanced with increase in fluorine content.

A new attempt to synthesize C_xF was done using transition fluorometallates, K_2MnF_6 in anhydrous hydrogen fluoride (aHF) at room temperature [25]. The results are given in Table 2. In these reactions, Mn^{4+} and Ni^{4+} oxidize graphite and yielded Stage 1 C_xF compounds with I_c values of 0.56–0.60 nm in the absence of elemental fluorine. A disadvantage is that the products are mixed with HF insoluble MnF_3 and NiF_2 , therefore the accurate compositions could not be determined.

Electrochemical fluorination of graphite sheet was also made in 47% HF aqueous solution [26]. Galvanostatic fluorination of graphite yielded a Stage 2 C_xF with I_c

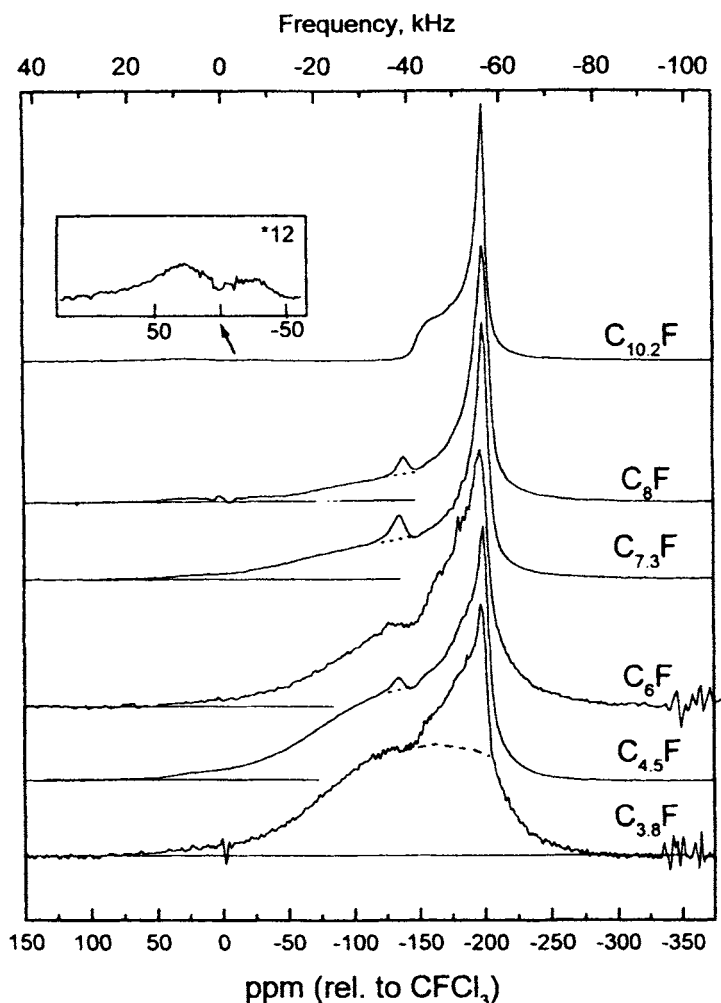


Fig. 3. Room temperature ^{19}F NMR spectra of fluorine-intercalated graphite at 282.4 MHz. In addition to an intensive broad line in the range between -30 , -270 ppm, weak broad peaks around $\delta \sim 0$ ppm (shown in inset) exist; for some fluorinated compounds the fine structure is not pronounced (reproduced with permission from *J. Phys.: Condens. Matter*, 10 (1998) 7633 [24]).

value of 0.89 – 0.90 nm, and the Stage 1 of the bi-intercalation structure with I_c of 1.14 – 1.18 nm. The saturated compositions were $\text{C}_{4.1}\text{F}$ for Stage 2 and $\text{C}_{2.8}\text{F}$ for Stage 1, respectively, from weight uptake. For the Stage 2 compound with I_c of ~ 0.90 nm, a structure model in which semi-ionic (semi-covalent) fluorine atoms were inserted in graphene layers in double rows was proposed.

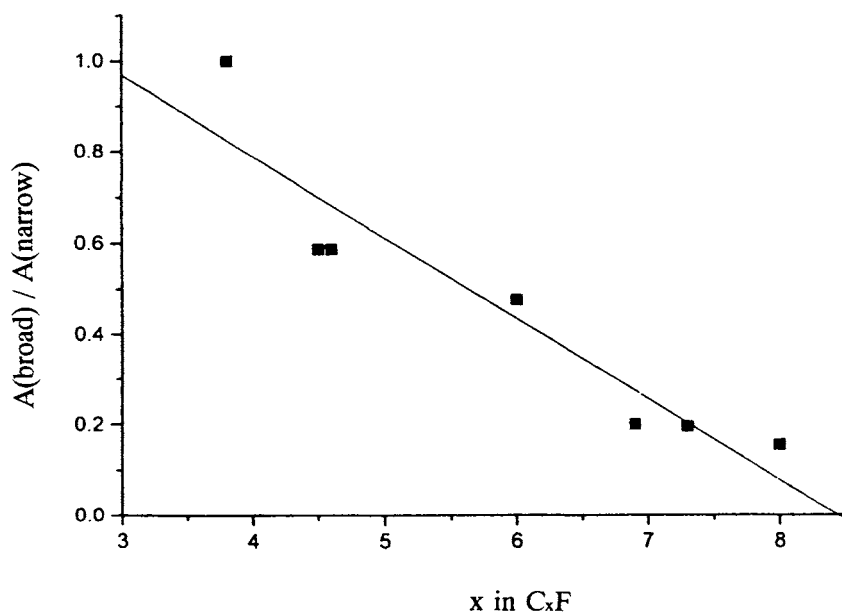


Fig. 4. The amplitude ratio of broad to narrow ^{19}F line in fluorine-intercalated graphite at room temperature ($\nu_0 = 282.4$ MHz) (reproduced with permission from J. Phys.: Condens. Matter, 10 (1998) 7633 [24]).

15.2.2 Fluorinated carbon nanotubes

Carbon nanotube is prepared by arc discharge of carbon electrodes or chemical vapor deposition at high temperatures. Reactivity of carbon nanotube with elemental fluorine is an interesting subject in comparison with that for graphite or fullerene. Carbon nanotube prepared by arc discharge was fluorinated by elemental fluorine between room temperature and 500°C [27]. A starting material was powdered cylinder core (MER corp.). The average length of nanotube was 964 nm, and average external and internal diameters were 18.4 nm and 3.6 nm, respectively. The diameters showed that carbon nanotube consisted of 22 rolled graphene layers on the average. TEM images indicated that small carbon particles (average diameter: 45 nm) were mixed with carbon nanotubes. Carbon nanotubes were fluorinated without any chemical pretreatment under a fluorine pressure of 1.0×10^5 Pa for 1–21 d. Reaction conditions and analytical data are summarized in Table 3. Color was black for the products obtained below 400°C while gray for that prepared at 500°C . The products obtained between room temperature and 60°C were Stage 1 compounds with compositions, C_4F – C_5F , and those obtained between 80°C and 100°C were the Stage 2, C_7F . For the products obtained at temperatures, 100°C or higher, no distinct stage structures were found from the X-ray diffraction patterns except graphite fluoride, $(\text{CF})_n$, obtained at 500°C . The fluorine contents of samples, 9–15 in Table 3 are much lower than those of others.

Table 2

Reactivity and X-ray diffraction data for reactions of graphite with K_2MnF_6 , K_2NiF_6 , Na_3FeF_6 , and CoF_3 in anhydrous HF at ambient temperature

Exp#	Reagent	C:M ratio	Insoluble product	Soluble product
1	K_2MnF_6	28	$C_{28}HF_2$ (2nd stage, $c=0.935$ nm) MnF_3	KHF_2 $K_2MnF_6(v.w.)$
2	K_2MnF_6	5–6	C_xF (1st stage, $c=0.59$ nm) MnF_3	K_2MnF_6
3	K_2MnF_6	4	C_xF (1st stage, $c=0.60$ nm) MnF_3	KHF_2 K_2MnF_6
4	K_2NiF_6	56	graphite, C_xF (1st stage, $c=0.57$ nm) $NiF_2(broad)$	KHF_2
5	K_2NiF_6	4	C_xF (1st stage, $c=0.59$ nm) NiF_2	KHF_2
6	K_2NiF_6	2	C_xF (1st stage, $c=0.59$ nm) NiF_2	KHF_2
7	Na_3FeF_6	28	graphite unindexed lines	$NaHF_2$
8	Na_3FeF_6	4	graphite C_xF (1st stage, $c=0.56$ nm)	unindexed lines
9	Na_3FeF_6	20	graphite C_xF (1st stage, $c=0.56$ nm) unindexed lines	$NaHF_2$ unindexed lines
10	CoF_3	4	graphite CoF_3	none

(Reproduced with permission from Carbon, 31 (1993) 437 [25]).

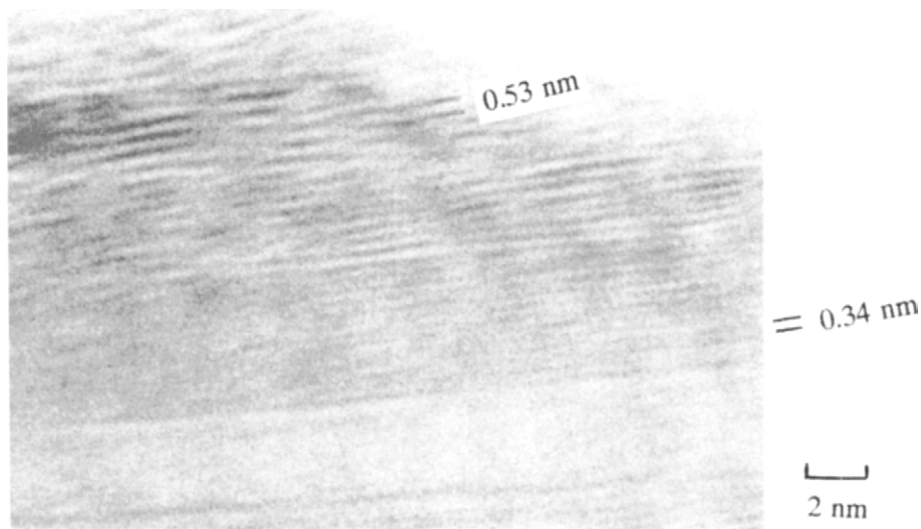
Intercalation of fluorine into carbon nanotube was confirmed by TEM observation. Figure 5 shows a TEM image of Stage 1 $C_{5.3}F$ prepared at room temperature. Fluorine is intercalated into outer part of nanotube and the interlayer spacing of inner part is nearly equal to that for original nanotube. The latter was indicated by the broad peaks at around 26.5° in 2θ observed in both Stage 1 and Stage 2 samples. It was also observed from low magnified images that the top of nanotube was still closed without destruction after fluorination. This was common for all the samples. A highly magnified TEM image of Stage 2 $C_{6.8}F$ prepared at $80^\circ C$ was not obtained because the Stage 2 compound with nearly ionic C—F bond was unstable under high vacuum and electron beam irradiation. TEM image of a sample obtained at $180^\circ C$ indicated that only the surface layers were expanded to 0.47 nm showing the semi-ionic fluorine-intercalated layers. When carbon nanotube was fluorinated between $300^\circ C$ and $400^\circ C$, fluorinated layers were also observed around the surface, however, being corrugated layers with I_c value of 0.65 nm, which suggests the formation of thin graphite fluoride layers ($2\text{--}3$ nm).

Table 3

Reaction conditions, compositions and XRD data of fluorinated carbon nanotubes

Sample	Tem./°C	Time/day	C/F	a_0 /nm	Stage	I_c /nm
Carbon nanotube	—	—	—	0.2460	—	0.3413
1	RT	3	5.3	0.2458	1	0.529
2	RT	14	3.9	0.2456	1	0.537
3	RT	14	3.8	0.2450	1	0.556
4	40	14	5.2	0.2460	1	0.528
5	60	14	3.9	0.2453	1	0.541
6	80	14	6.8	0.2454	2	0.951
7	100	21	7.3	0.2447	2	0.954
8	100	21	8.8	0.2444	—	0.319
9	100	14	18.0	0.2456	—	0.339
10	140	14	19.9	0.2456	—	0.336
11	180	14	22.6	0.2458	—	0.340
12	250	14	35.9	0.2455	—	0.339
13	300	5	30.7	0.2457	—	0.341
14	300	14	45.0	0.2459	—	0.340
15	400	7	15.8	0.2454	—	0.341
16	500	1	1.0	0.2552	(CF) _n	0.646

(Reproduced with permission from Eur. J. Solid State Inorg. Chem., 33 (1996) 831 [27]).

Fig. 5. TEM image of carbon nanotube fluorinated at room temperature, Stage 1 C_{5.3}F (reproduced with permission from Eur. J. Solid State Inorg. Chem., 33 (1996) 831 [27]).

with covalent C—F bond. TEM image of carbon nanotube fluorinated at 500°C showed no layered structure though the diameter of fluorinated nanotube was increased to about twice of that of pristine nanotube, i.e. ca. 40 nm.

In the IR absorption spectra, several absorptions due to stretching vibration of carbon-fluorine bond were observed between 1000 and 1300 cm^{-1} . Stage 1 $\text{C}_{5.2}\text{F}$ had three absorptions at 1080, 1125 and 1260 cm^{-1} , in which those observed at 1080 and 1125 cm^{-1} are attributed to semi-ionic (semi-covalent) C—F bond, and that at 1260 cm^{-1} is due to peripheral groups such as CF_2 and CF_3 [28]. The absorption at 1125 cm^{-1} observed for Stage 1 $\text{C}_{5.2}\text{F}$ shifted to higher wave numbers with increasing fluorination temperature, i.e. 1175 cm^{-1} at 180°C and 1220 cm^{-1} at 400°C and 500°C. X-ray photoelectron and Raman spectra also showed the change of C—F bonding from the semi-ionic to the covalent.

Fullerene C_{60} is easily fluorinated by elemental fluorine at temperatures less than 100°C [29,30] probably because of its nearly spherical surface and exposed π bonding. Direct fluorination of organic compounds by fluorine gas demonstrated that fluorine was preferentially bonded to a carbon atom with a high electron density [31,32]. This may be a main reason why fullerene C_{60} is more easily fluorinated than graphite. On the contrary, the fluorination behavior of carbon nanotube is similar to that of graphite as already shown.

Fluorination of carbon nanotube prepared by chemical vapor deposition was recently carried out [33]. Carbon nanotubes ($\sim 10\text{ }\mu\text{m}$ in length and 20–40 nm in outer diameter) were prepared by thermal decomposition of acetylene at 900°C using a cobalt catalyst supported on silica. Chemical treatments of carbon nanotubes with concentrated HF and dilute HNO_3 significantly reduced the amounts of silica and cobalt mixed in the samples. Carbon nanotubes as-prepared and graphitized at 2800°C were fluorinated at 500°C for 4 h and at room temperature for 10 h. Nanotubes fluorinated by elemental fluorine at 500°C were white graphite fluoride $(\text{CF})_n$ with $\text{F/C} = 1$ and $I_c = 0.69\text{ nm}$. IR absorption spectrum exhibited a very intense band at 1223 cm^{-1} as seen for graphite fluoride. The tubular structure was no more observed. Nanotubes fluorinated by a gaseous mixture of F_2 , HF and IF_5 at room temperature yielded CF_x samples with $x = 0.22\text{--}0.40$, mixed with unreacted phase. IR absorption spectrum gave a broad band centered at about 1100 cm^{-1} corresponding to semi-ionic C—F bond. TEM image of fluorinated graphitized nanotubes showed the perturbation of surface fluorinated layers.

15.3 New aspects on the electrochemical behavior of fluorine-intercalated graphite

15.3.1 Discharge characteristics of fluorine-graphite intercalation compounds

Fluorination of natural graphite powder ($\approx 4\text{ }\mu\text{m}$) by a gas mixture of F_2 , HF and IF_5 yielded high fluorine content samples, $\text{CF}_{0.8}$, $\text{CF}_{0.9}$ and $\text{CF}_{1.0}$ [34]. The structural parameters obtained by X-ray diffraction were $I_c = 0.59\text{ nm}$ and $a_0 = 0.246\text{ nm}$. XPS data indicated the existence of two C_{1s} peaks at 287.0 eV and 289.4 eV, and one F_{1s} peak at 688.0 eV, which are intermediate values between those for semi-ionic and covalent C—F bonds. Galvanostatic discharge of these CF_x samples was done

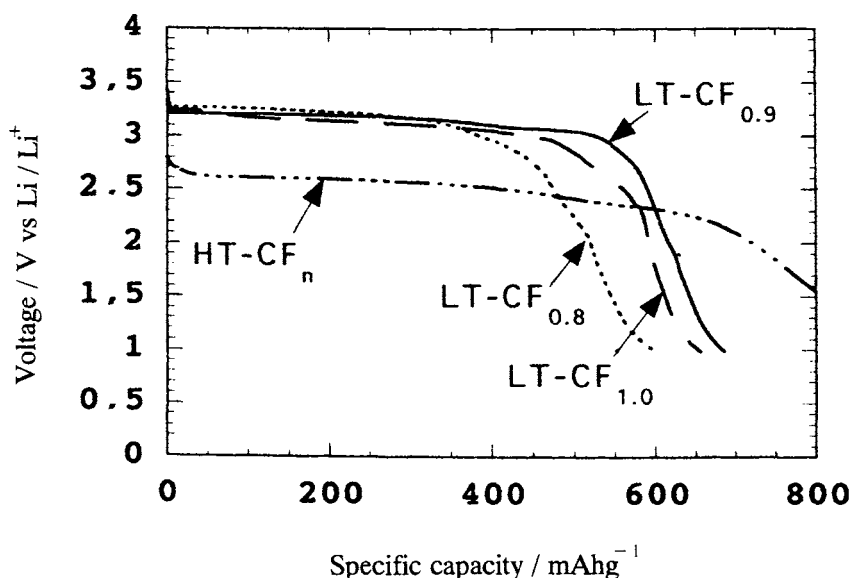


Fig. 6. Galvanostatic discharge curves of button-type cells Li/1 M LiClO₄ + EC : PC : DME/LT-CF_x, HT-CF_x at 40 mA g⁻¹. LT-CF_x: fluorine-graphite intercalation compound prepared at a low temperature, HT-CF_x: graphite fluoride prepared at a high temperature (reproduced with permission from J. Power Sources, 68 (1994) 708 [34]).

in organic solvent with metallic lithium anode and reference electrode. Discharge voltages varied from 3.26 V to 3.15 V with increasing x from 0.8 to 1.0 in CF _{x} at a current density of 40 mA g⁻¹ as shown in Fig. 6. Discharge capacities were 619–433 mA g⁻¹ for CF_{1.0} and 611–553 mA h g⁻¹ for CF_{0.9} in current densities of 27–267 mA g⁻¹ and 530–523 mA h g⁻¹ for CF_{0.8} in current densities of 27–160 mA g⁻¹. No large differences in the discharge capacities were found between current densities, 27 mA g⁻¹ and 160 mA g⁻¹.

Fluorination procedure was modified by employing two-step reactions [35]. Natural graphite powder and graphitized petroleum coke (10–30 μ m) were fluorinated by a gas mixture of F₂, HF and IF₅ at room temperature for 4 h, and further fluorinated by elemental fluorine at a temperature between 150°C and 350°C for 6 h. The main effect of the second fluorination was the progressive disappearance of (002) diffraction line associated with residual Stage 1 phase of iodine fluoride which was formed during the first step of fluorination. The interlayer spacing (I_c) varied between 0.62 nm and 0.63 nm with increasing second fluorination temperature. The a -axis parameter a_0 was 0.246 nm close to that of graphite. XPS study showed that C_{1s} peak indicating carbon atoms bound to fluorine shifted from 288.0 eV to 289.8 eV with increasing second fluorination temperature from 150°C to 354°C. This indicates that nature of C—F bonding changed from nearly semi-ionic to almost covalent. Figure 7 shows the galvanostatic discharge curves at different current densities. The discharge potentials were flat and between 3.15 V and 2.69 V

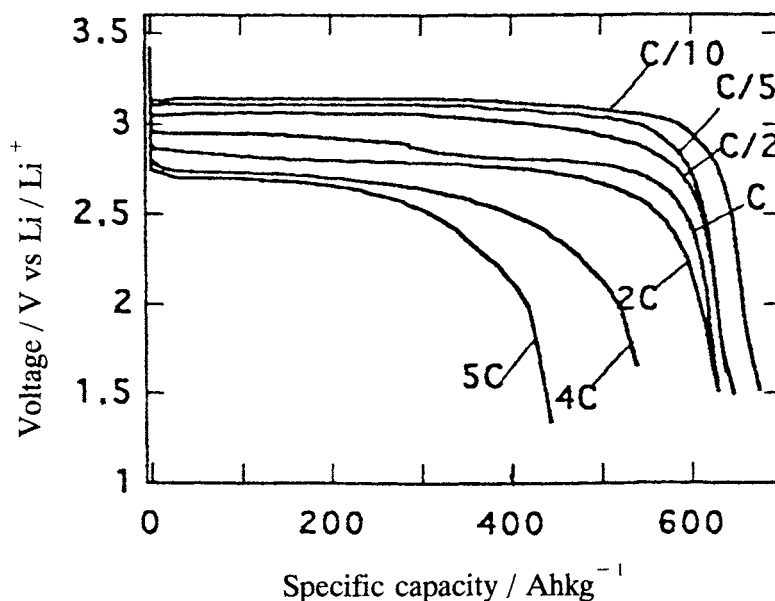


Fig. 7. Galvanostatic discharge curves of Li/LT- CF_x cells under different rates. LT- CF_x : fluorine-graphite intercalation compound prepared at a low temperature. C/10: 80 mA g^{-1} , C/5: 160 mA g^{-1} , C/2: 400 mA g^{-1} , C: 800 mA g^{-1} , 2C: 1600 mA g^{-1} , 4C: 3200 mA g^{-1} , 5C: 4000 mA g^{-1} (reproduced with permission from Mol. Cryst. Liq. Cryst., 310 (1998) 397 [35]).

in the range of current densities of 80–4000 mA g^{-1} . The discharge capacities were about 600 mAh g^{-1} except for at current densities, 3200 and 4000 mA g^{-1} . Impedance measurements were conducted on CF_x and graphite fluoride $(\text{CF})_n$ prepared from petroleum coke after 10% discharge. The results is shown in Fig. 8. At high frequency ($\approx 10^4$ Hz), the first intercepts of the Nyquist plots with real part axis of the impedance ($\text{Re}(Z)$) were the same for two curves ($\approx 2 \Omega$). The difference was more pronounced in the second intercepts at medium frequencies (1–10 Hz) which lay in 40 Ω for CF_x and 90 Ω for $(\text{CF})_n$. The frequency range is associated with the charge transfer reaction. The higher resistance of $(\text{CF})_n$ would be due to its larger C—F bond energy. In the low frequency range (1– 10^{-2} Hz), the diffusion is the dominant mechanism.

Discharge behavior of fluorinated carbon nanotubes were also examined in organic solvents [36,37]. Two types of carbon nanotubes mentioned in the previous section showed similar discharge behavior to each other. In nanotubes fluorinated at room temperature, their discharge potentials decreased almost linearly with time, giving rather small capacities. Those fluorinated at high temperatures, however, exhibited lower but flat discharge potentials which are similar to those of graphite fluoride with covalent C—F bond.

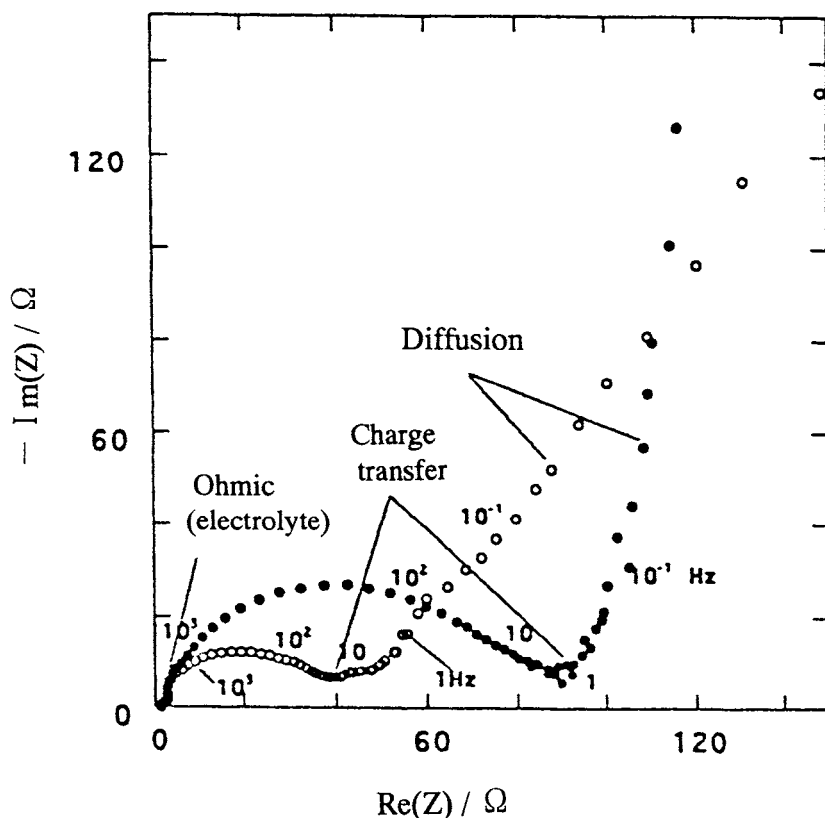


Fig. 8. Nyquist plots of Li/LT-CF_x, Li/HT-CF_x cells. LT-CF_x: fluorine-graphite intercalation compound prepared at a low temperature, HT-CF_x: graphite fluoride prepared at a high temperature (reproduced with permission from Mol. Cryst. Liq. Cryst., 310 (1998) 397 [35]).

15.3.2 Discharge characteristics of fluorinated graphite oxide

Graphite oxide and fluoride are classified into covalent type graphite intercalation compounds. Graphite oxide contains carbonyl and hydroxyl groups, and shows therefore hydrophilic nature different from graphite fluoride having high hydrophobicity [38]. Discharge of graphite oxide itself does not proceed well as shown later, compared with the discharge of graphite fluoride, probably because of higher instability of discharge products, Li₂O and LiOH than that of LiF. Partial fluorination of graphite oxide was, however, found to improve the discharge characteristics [11]. Graphite oxide was prepared by a modified Staudenmaier method using conc. H₂SO₄, fuming HNO₃ and KClO₃, and Brodie method using fuming HNO₃ and KClO₃. Fluorination of graphite oxide was conducted by flowing elemental fluorine over graphite oxide at a temperature between room temperature and 200°C. IR absorption spectra of graphite oxide and fluorinated ones suggested that main

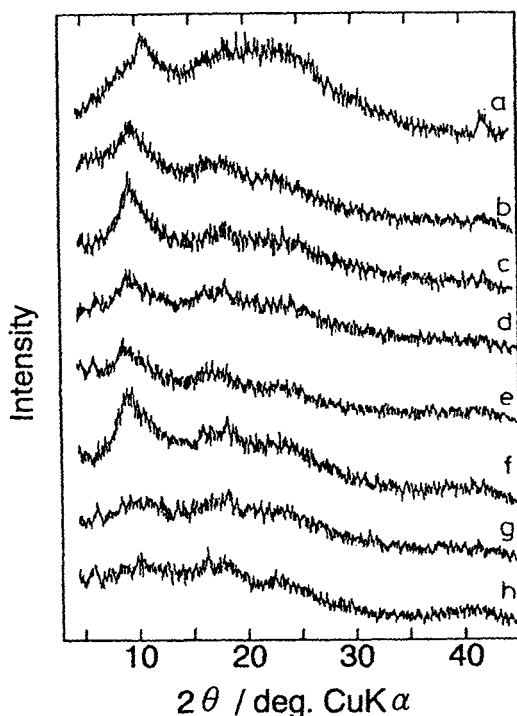


Fig. 9. X-ray diffraction patterns of graphite oxide and those fluorinated at various temperatures.

a: graphite oxide	$C_8O_{4.12}H_{2.81}$
b: fluorinated at 90°C	$C_8O_{2.53}F_{4.82}$
c: fluorinated at 100°C	$C_8O_{2.40}H_{0.90}F_{4.56}$
d: fluorinated at 110°C	$C_8O_{2.21}H_{0.62}F_{5.15}$
e: fluorinated at 120°C	$C_8O_{2.15}H_{0.22}F_{5.32}$
f: fluorinated at 150°C	$C_8O_{2.17}H_{0.63}F_{5.52}$
g: fluorinated at 175°C	$C_8O_{1.54}F_{6.80}$
h: fluorinated at 200°C	$C_8O_{1.28}F_{7.17}$

(reproduced with permission from *Denki Kagaku*, 61 (1993) 594 [11]).

fluorination reactions were the replacement of hydroxyl to fluorine and formation of $\rightarrow CF$ and $\rightarrow COF$ groups.

Fluorination of graphite oxide starts at room temperature, however, the main reaction is dehydration of graphite oxide at this temperature. When fluorination temperature was raised to around 100°C, fluorinated graphite oxide showed a strong (001) diffraction line at about 10° in 2θ (Cu-K α), i.e. ca 0.88 nm as shown in Fig. 9, which supports a Stage 2 type structure model of graphite oxide because fluorinated graphite oxide does not contain any water molecule in the hydrophobic fluorinated layers [39]. Fluorination converts the hydrophilic nature of graphite oxide to the hydrophobic and improves its thermal stability.

Initial discharge potentials of fluorinated graphite oxides, prepared by the modified Staudenmaier method, were in the range of 3.20–3.35 V at a current density

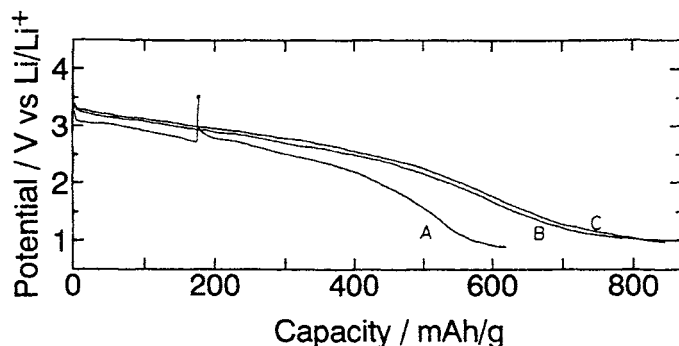


Fig. 10. Discharge characteristics of $C_8O_{2.17}H_{0.63}F_{5.52}$ obtained at 150°C at various current densities. A: 0.05 Adm^{-2} , B: 0.01 Adm^{-2} and C: 0.005 Adm^{-2} in 1 M LiClO_4 -PC solution at 25°C (reproduced with permission from *Denki Kagaku*, 61 (1993) 594 [11]).

of 0.05 Adm^{-2} . The potentials gradually decreased with discharge, and no initial drop in the potential was observed. The discharge capacities and energy densities were about 600 mAhg^{-1} and 1400 Whkg^{-1} respectively. In the case of graphite oxide prepared by the modified Staudenmaier method, those fluorinated in the range of 100 – 175°C showed high discharge potentials and large capacities. The sample fluorinated at 200°C gave a slightly lower discharge potential. Figure 10 shows the discharge curves of graphite oxide fluorinated at 150°C at different current densities. The discharge at a lower current density of 0.005 Adm^{-2} exhibited higher discharge capacity of 820 mAhg^{-1} and energy density of 1950 Whkg^{-1} than others.

Graphite oxide prepared by Brodie method has a higher crystallinity than that by Staudenmaier method [38]. Amounts of oxygen and hydrogen contained in graphite oxide prepared by Brodie method are smaller because of the lower degree of C—C bond rupture. Graphite oxide itself had a strong (001) diffraction line at 14° in 2θ , however, a fluorinated sample exhibited a broad (001) line at around 10° in the same manner as in the case of graphite oxide prepared by the modified Staudenmaier method. The thermal stability was also improved by fluorination. However, the dependency of fluorination temperature on the discharge behavior was different from graphite oxide prepared by the modified Staudenmaier method. Graphite oxide and that fluorinated at room temperature were not easy to discharge as shown in Fig. 11, however, discharge behavior was significantly improved with increasing fluorination temperature, and a discharge capacity of 675 mAhg^{-1} and energy density of 1420 Whkg^{-1} were obtained for graphite oxide fluorinated at 110°C . A sample fluorinated at 200°C showed a lower discharge potential which is close to that of graphite fluoride. At a decreased current density of 0.005 Adm^{-2} , a discharge capacity of 840 mAhg^{-1} and energy density of 1900 Whkg^{-1} were achieved.

Increase in fluorination temperature would enhance the covalency of C—F bond and destruction of the layered carbon skeleton by C—C bond rupture as indicated by X-ray diffraction profiles shown in Fig. 9. The C—C bond rupture leads to

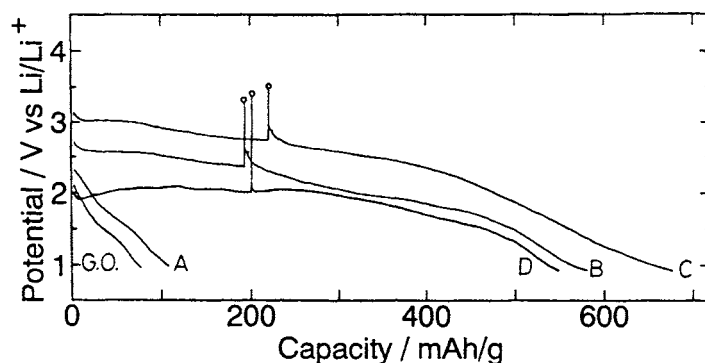


Fig. 11. Discharge characteristics of graphite oxide, those fluorinated at various temperatures in 1 M LiClO_4 -PC solution at 25°C (0.05 Adm^{-2}).

G.O.: graphite oxide	$\text{C}_8\text{O}_{2.99}\text{H}_{1.71}$
A: fluorinated at room temperature	$\text{C}_8\text{O}_{2.73}\text{H}_{2.08}\text{F}_{0.01}$
B: fluorinated at 100°C	$\text{C}_8\text{O}_{1.80}\text{H}_{0.84}\text{F}_{3.38}$
C: fluorinated at 110°C	$\text{C}_8\text{O}_{1.09}\text{F}_{5.47}$
D: fluorinated at 200°C	$\text{C}_8\text{O}_{0.71}\text{F}_{5.93}$

(reproduced with permission from *Denki Kagaku*, 61 (1993) 594 [11]).

the formation of covalently bonded CF_2 and CF_3 groups existing at the edge of graphene layers. These groups are difficult to discharge by electrochemical reduction [40]. Specific surface areas of fluorinated graphite oxides prepared by Brodie method also changed by fluorination from $77 \text{ m}^2\text{g}^{-1}$ of graphite oxide to 115, 147 and $99 \text{ m}^2\text{g}^{-1}$ for those fluorinated at 100°C, 110° and 200°C, respectively. Graphite oxide fluorinated at 110°C had the highest surface area. The discharge characteristics and structure changes by fluorination indicate that the optimum fluorination temperatures are in the range of 100–175°C for graphite oxide prepared by the modified Staudenmaier method and at around 110°C for that prepared by Brodie method.

15.4 Charge-discharge behavior of surface-fluorinated graphite

15.4.1 Composition and structure changes of graphite by surface fluorination

Several types of carbon materials are now used as anodes of lithium ion secondary batteries. As electrochemical reaction takes place at two-dimensional surface of an electrode, surface structure of the electrode material would be one of the important factors governing the cell performance. Oxygen species such as hydroxyl, carbonyl and carboxyl groups usually exist at the surface of a carbon material. They form lithium salts at the beginning of first charge, yielding a so-called solid electrolyte interface with decomposed products of organic solvents [41]. The surface species chemically interact with lithium ions, forming a potential barrier against the reversible intercalation and deintercalation of lithium ions into and from graphite.

In order to increase the reaction rate and capacity, some methods to modify the surface structure and composition were recently attempted [42–49]. They are surface oxidation [42–45] and surface fluorination [46–48] of graphite and carbon, and metal coating to carbon surface [49]. These show that surface modifications are useful techniques to improve the electrochemical characteristics of graphite and carbon.

It has been found that surface fluorination of graphite powder increases its reversible capacity to higher values than the theoretical one, 372 mAhg^{-1} which corresponds to Stage 1 lithium-intercalated graphite LiC_6 . Natural graphite powder ($\approx 7 \mu\text{m}$) was allowed to react with elemental fluorine ($3 \times 10^4 \text{ Pa}$) for 2 or 10 min at a temperature between 80°C and 520°C . In some cases, graphite samples were fluorinated at $100\text{--}130^\circ\text{C}$ for 2–15 min by elemental fluorine of $2 \times 10^4\text{--}1 \times 10^5 \text{ Pa}$, and the temperature of the reactor was successively raised to $300\text{--}380^\circ\text{C}$ under vacuum to make the partial decomposition of surface fluorinated layers.

Table 4 shows the compositions of surface-fluorinated graphite samples, obtained by elemental analysis, and surface compositions calculated from the peak areas of

Table 4

Compositions of surface-fluorinated graphite samples, obtained by elemental analysis, calculated from the peak areas of X-ray photoelectron spectra

Fluorination temperature($^\circ\text{C}$)	Elemental analysis (at%)			XPS (at%)		
	C	F	O ^c	C	F	O
128 ^a	98.2	1.3	0.5	91.3	6.4	2.3
194 ^a	99.4	0.6	0.0	86.9	10.4	2.7
256 ^a	99.2	0.5	0.3	92.0	6.0	2.0
328 ^a	99.1	0.6	0.3	90.4	8.2	1.4
390 ^a	99.4	0.6	0.0	83.1	14.6	2.3
454 ^a	99.0	1.0	0.0	87.0	11.4	1.6
497 ^a	98.4	1.2	0.4	87.4	11.3	1.3
522 ^a	97.7	2.2	0.1	84.8	13.9	1.3
84 ^b	95.4	1.9	2.7	87.7	7.9	4.4
120 ^b	95.2	2.3	2.5	86.3	9.6	4.1
151 ^b	96.1	2.1	1.8	87.9	8.6	3.5
189 ^b	98.6	1.2	0.2	85.4	11.8	2.8
258 ^b	99.1	0.6	0.3	86.4	11.3	2.3
302 ^b	99.2	0.7	0.1	82.0	15.9	2.1
400 ^b	99.2	0.8	0.0	91.5	7.1	1.4
446 ^b	98.1	3.7	0.2	80.6	18.1	1.3
492 ^b	98.9	1.0	0.1	88.9	9.9	1.2
513 ^b	98.5	1.2	0.3	85.7	13.1	1.2

^a fluorinated for 2 min, ^b fluorinated for 10 min, ^c calculated by subtracting the analytical values for carbon, fluorine from 100 wt% (reproduced with permission from *Electrochim. Acta*, 44 (1999) 2879 [48]).

X-ray photoelectron spectra. The total fluorine contents were only 0.5–2.2 at% for 2 min-fluorinated samples and 0.6–3.7 at% for 10 min-fluorinated ones, while the surface fluorine concentrations were much higher, i.e. 6.0–14.6 at% and 7.1–18.1 at%, respectively. Since only the surface regions of graphite samples were fluorinated, the fluorine concentrations obtained by XPS are much higher than those by elemental analysis in all the samples. Fluorination degree is slightly higher in 10 min-fluorinated samples than in 2 min-fluorinated ones. Not only fluorine but also small amounts of oxygen were detected by XPS in all the samples. The surface oxygen concentration decreased with increasing fluorination temperature and time. Since the surface oxygen content of original natural graphite powder is 1.5–2 at%, the samples fluorinated below 200°C had obviously the larger amounts of surface oxygen than pristine graphite. This may be because the hydrolysis of adsorbed fluorine took place by the exposure of fluorinated graphite samples to the air.

Figure 12 and Table 5 show typical X-ray photoelectron spectra and binding energies of surface-fluorinated samples, respectively. The C_{1s} spectra have four peaks as listed in Table 5. The peaks at 284.2–284.3 eV are observed at the same binding energy for graphite itself, indicating carbon atoms unbound to fluorine. The second peaks centered at 285.2–285.4 eV may include the contributions due to C—O bonding and carbon atoms adjacent to C—F bonds. The third peaks centered at 288.3–288.5 eV are intermediate between semi-ionic C—F bond, usually observed in highly fluorinated Stage 1, C_2F — $C_{2.5}F$, and covalent C—F bond [15,29,30]. These peaks were slightly shifted to higher binding energy, i.e. the covalency of C—F bond was increased with increasing fluorination temperature and time. Corresponding to the C_{1s} peaks, F_{1s} spectra provided their peaks centered at 687.8 eV. The last C_{1s} peaks centered at 291.0–291.2 eV may be the satellite plasmon peaks and contribution due to a small amount of covalent C—F bond. The O_{1s} peaks centered at 532.1–532.4 eV and 533.5–533.9 eV indicate carbonyl and hydroxyl groups, respectively.

X-ray diffraction measurements of surface-fluorinated graphite samples indicated almost no change in $d(002)$ values and crystallite sizes by surface fluorination except those fluorinated between 80°C and 150°C. In this temperature range, the intercalation of fluorine into surface region of graphite may take place. In fact, slight broadening of (002) diffraction line, i.e. the decrease of crystallite size along c -axis was observed.

Raman spectroscopy reveals mainly the surface structure of carbon materials to several tens nanometers. The typical Raman spectrum of graphite powder is shown in Fig. 13a. A strong band at 1580 cm^{-1} indicates an E_{2g2} vibration mode in the graphitic region of carbon materials (G-band) and a weak one at 1360 cm^{-1} shows an A_{1g} mode arising from the disordering in carbon (D-band) [50,51]. The upshift of G-band which is usually observed in fluorine-intercalated graphite was not detected probably because of the fluorination of thin surface of graphite. The D-band is observed in carbon materials with relatively low crystallinity and in fine powder of graphite. A graphite sheet such as highly oriented pyrolytic graphite shows only a strong band at 1580 cm^{-1} . However, pulverization of graphite causes a weak band to appear at 1360 cm^{-1} with a strong one at 1580 cm^{-1} because fine

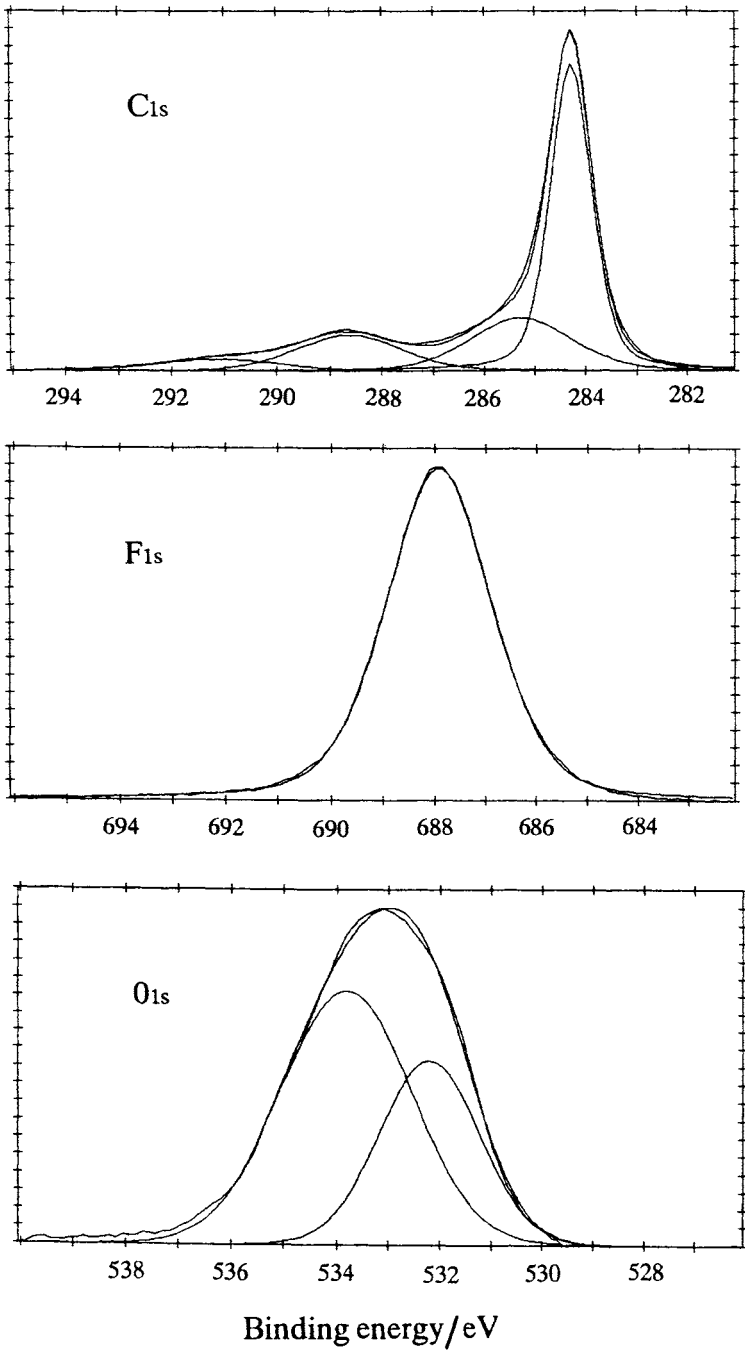


Fig. 12. X-ray photoelectron spectra of graphite fluorinated for 2 min at 390°C (reproduced with permission from *Electrochim. Acta*, 44 (1999) 2879 [48]).

Table 5

Binding energies of X-ray photoelectron spectra of surface-fluorinated graphite samples

Sample	C _{1s} (eV)	F _{1s} (eV)	O _{1s} (eV)
2 min fluorinated	284.25 ± 0.05 (56–62%)	687.8 ± 0.2 (100%)	532.4 ± 0.2 (36–58%) 533.9 ± 0.3 (42–62%)
	285.2 ± 0.1 (21–26%)		
	288.3 ± 0.4 (8–16%)		
	291.0 ± 0.3 (5–7%)		
10 min fluorinated	284.25 ± 0.05 (56–65%)	687.8 ± 0.2 (100%)	532.1 ± 0.3 (21–57%) 533.5 ± 0.4 (44–79%)
	285.4 ± 0.2 (10–23%)		
	288.5 ± 0.4 (10–22%)		
	291.2 ± 0.4 (4–6%)		

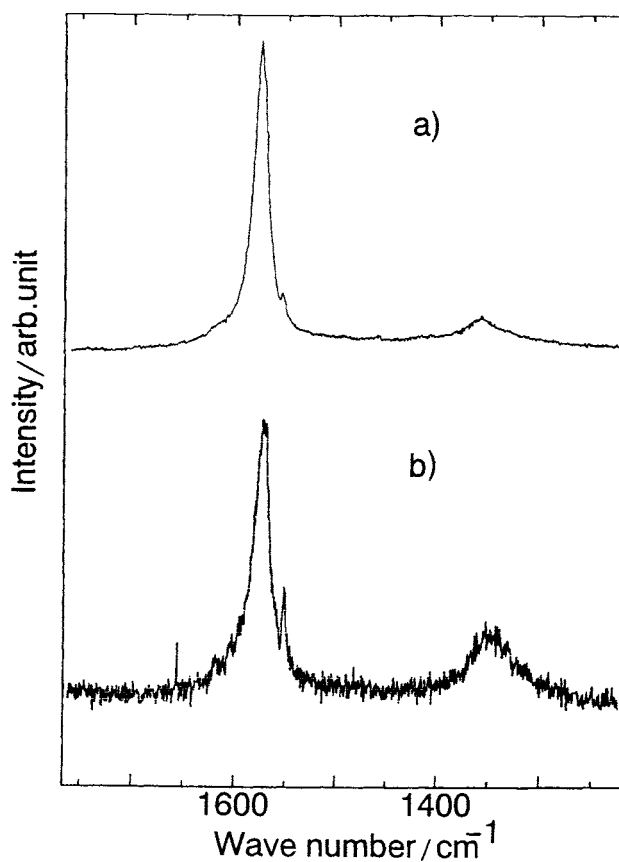
(Reproduced with permission from *Electrochim. Acta*, 44 (1999) 2879 [48]).Fig. 13. Raman spectra of original graphite (a), 2 min-fluorinated sample at 390°C (b) (reproduced with permission from *Electrochim. Acta*, 44 (1999) 2879 [48]).

Table 6

 $R (= I_D/I_G)$ values of Raman spectra of surface-fluorinated graphite samples

Temp. (°C)	2 min fluorinated	Temp. (°C)	10 min fluorinated
Original	0.083	Original	0.083
128	0.23	120	0.35
150	0.18	151	0.40
—	—	189	0.15
256	0.23	258	0.21
390	0.25	400	0.23
497	0.29	492	0.27

(Reproduced with permission from *Electrochim. Acta*, 44 (1999) 2879 [48]).

powdery graphite has a large disordered surface (edge planes). The ratio of D-band to G-band intensities, $R (= I_D/I_G)$ expresses the degree of surface disordering of graphite powder [50,51]. A small sharp band at around 1560 cm^{-1} is due to oxygen. As shown in Fig. 13(b), the intensity of D-band was enhanced by surface fluorination. The R values for 2 and 10 min-fluorinated graphite samples are given in Table 6, which indicates that R values increased from 0.083 to 0.15–0.40. In many cases, they were between 0.2 and 0.3. The results clearly show that the surface disordering of graphite powder takes place by short time fluorination.

15.4.2 Charge-discharge characteristics of surface-fluorinated graphite

Electrochemical behavior of surface-fluorinated graphite was examined by galvanostatic charge–discharge cycling at a current density of 60 mA g^{-1} and cyclic voltammetry at 0.1 mV s^{-1} in 1 M LiClO_4 ethylene carbonate (EC) /diethyl carbonate (DEC) (1:1) solution at 25°C . The counter and reference electrodes were metallic lithium. The typical charge–discharge curves of original graphite and surface-fluorinated samples are shown in Fig. 14. The profiles of the potential curves of fluorinated samples are nearly the same as that for original graphite. The potentials are low both in the intercalation and deintercalation processes of lithium ions. The difference is only the charge and discharge capacities. Figures 15 and 16 indicate charge capacities of 2 and 10 min-fluorinated graphite samples as a function of cycle number in comparison with those of original graphite powder. All the 2 min-fluorinated samples obviously showed the higher charge capacities than original graphite by about 5–10% while the 10 min-fluorinated samples gave slightly different results from the 2 min-fluorinated ones. The half of 10 min-fluorinated samples having high surface fluorine concentrations, relatively low total fluorine contents and middle values of $R (= I_D/I_G)$ showed the higher charge–discharge capacities than graphite powder, however, the others which did not satisfy all of these conditions possessed the similar capacities to that of original graphite or the less.

The electrochemical results can be correlated with total fluorine contents obtained by elemental analysis and surface fluorine concentrations by XPS given in Table 4.

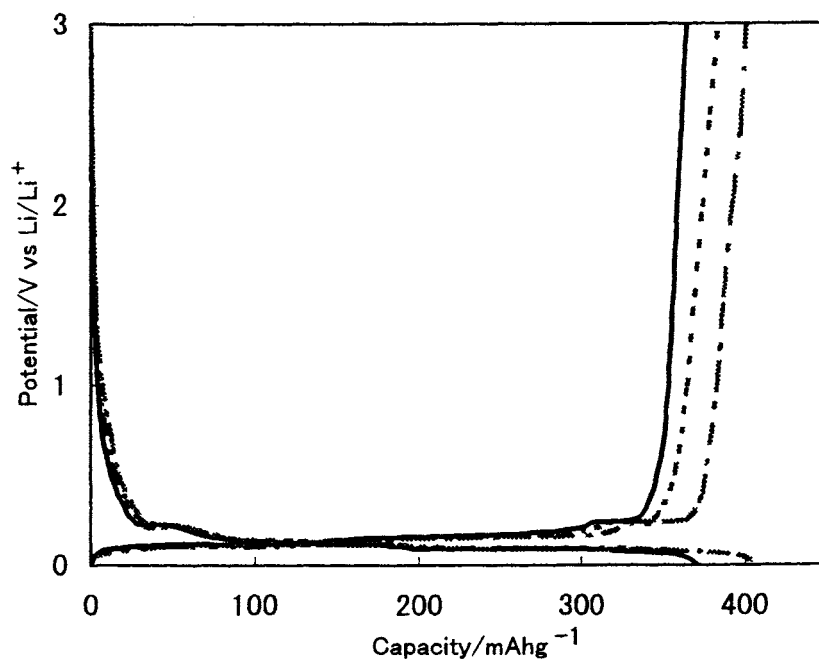


Fig. 14. Charge-discharge curves of original graphite, surface fluorinated samples (10th cycle). — : original graphite, - - - : 2 min-fluorinated at 128°C, — · — : 2 min-fluorinated at 390°C (reproduced with permission from *Electrochim. Acta*, 44 (1999) 2879 [48]).

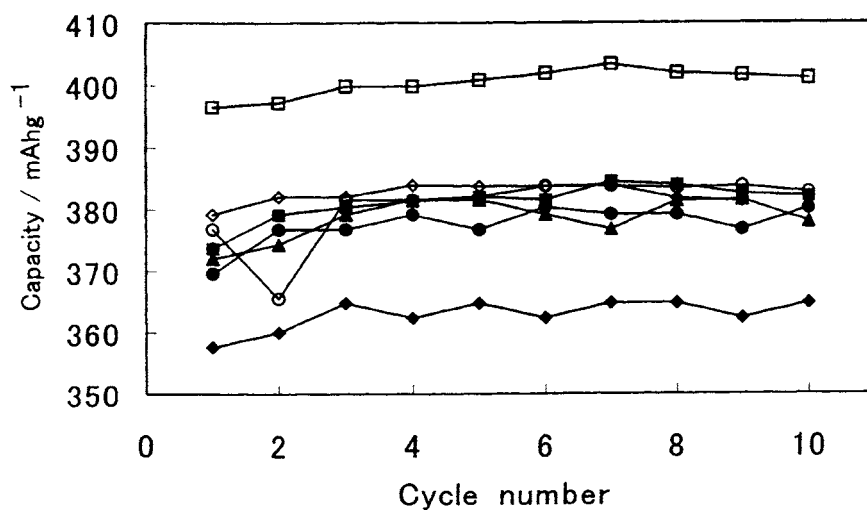


Fig. 15. Charge capacities of 2 min-fluorinated graphite samples as a function of cycle number. ♦: original, ■: 128°C, ◇: 150°C, ▲: 194°C, ●: 256°C, □: 390°C, ○: 497°C (reproduced with permission from *Electrochim. Acta*, 44 (1999) 2879 [48]).

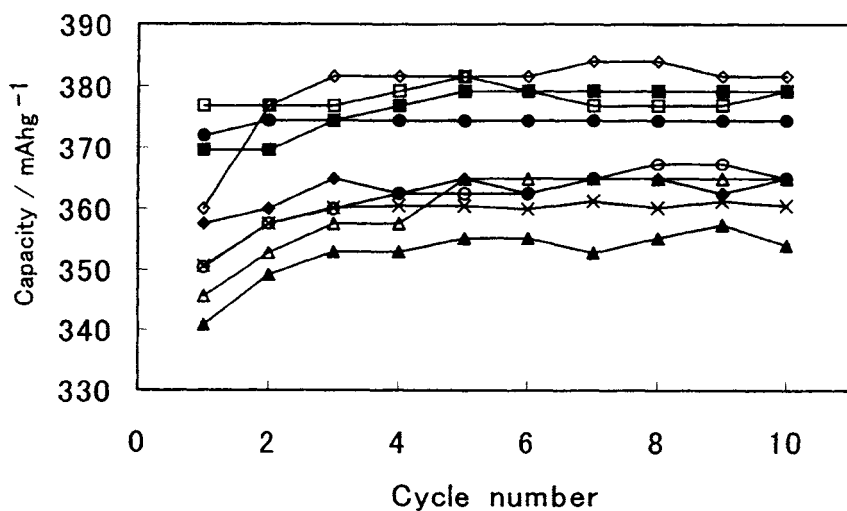


Fig. 16. Charge capacities of 10 min-fluorinated graphite samples as a function of cycle number. ◆: original, ■: 120°C, ▲: 151°C, ×: 189°C, ◇: 258°C, ●: 302°C, ○: 400°C, △: 446°C, □: 513°C (reproduced with permission from *Electrochim. Acta*, 44 (1999) 2879 [48]).

Table 7

Coulombic efficiencies (%) of graphite samples fluorinated for 2 min

Fluori- nation temp. (°C)	Cycle number									
	1	2	3	4	5	6	7	8	9	10
Original	79.7	94.3	96.2	96.8	97.4	96.2	96.8	98.1	97.4	98.1
128	71.1	94.5	95.5	96.9	96.8	96.4	97.6	98.2	98.2	98.8
150	77.0	93.7	94.8	95.6	96.3	96.3	96.5	96.4	96.3	—
194	77.7	94.7	96.4	97.6	98.1	98.0	97.2	99.1	98.7	98.4
256	79.0	—	97.8	98.1	97.7	98.6	98.9	99.3	99.1	98.3
390	75.4	95.1	96.3	96.9	97.1	97.8	98.4	98.5	98.7	98.9
497	72.0	92.9	95.9	97.1	97.1	97.8	98.2	98.6	98.6	99.1

(Reproduced with permission from *Electrochim. Acta*, 44 (1999) 2879 [48]).

Among 2 min-fluorinated samples, the first coulombic efficiencies were relatively lower in the samples with fluorine contents more than 1 at% (the samples fluorinated at 128°C and 497°C in Table 7), though their charge capacities were higher than that of original graphite powder. The samples having the lower fluorine contents than 1 at% showed the similar first coulombic efficiencies to that for original graphite. The sample fluorinated at 390°C gave the highest charge capacities of ca. 400 mAhg⁻¹, having the total fluorine content less than 1 at% and the highest surface fluorine concentration of 14.6 at%. The same trend was found on the 10

Table 8

Coulombic efficiencies (%) of graphite fluorinated for 10 min

Fluorination temp. (°C)	Cycle number									
	1	2	3	4	5	6	7	8	9	10
Original	79.7	94.3	96.2	96.8	97.4	96.2	96.8	98.1	97.4	98.1
120	61.8	91.7	92.7	94.6	96.3	96.9	97.5	98.1	98.1	98.8
151	57.8	93.2	96.1	96.8	98.0	98.7	98.6	99.3	99.1	99.7
189	65.8	94.3	96.8	97.6	98.0	98.0	98.4	100	99.0	98.8
258	76.5	94.0	96.4	97.5	97.5	97.5	98.8	98.8	98.1	98.1
302	78.7	95.7	96.9	97.5	98.1	98.7	98.1	98.7	99.4	99.4
400	76.4	93.7	95.5	96.8	96.8	97.4	98.1	98.1	99.4	98.7
446	75.0	94.2	96.1	96.8	98.1	98.1	98.7	98.7	99.3	98.7
513	71.7	94.6	95.7	96.9	98.1	98.1	97.5	97.5	98.1	98.1

(Reproduced with permission from *Electrochim. Acta*, 44 (1999) 2879 [48]).

min-fluorinated samples. The samples with the total fluorine contents higher than 1 at% (the samples fluorinated at 120, 151, 189 and 513°C in Table 8) had the low first coulombic efficiencies of 57.8–71.7%. The samples with fluorine contents less than 1 at% and relatively high surface fluorine concentrations (the samples fluorinated at 258°C and 302°C) showed the better results than graphite powder itself. Even if the total fluorine contents were higher than 1 at%, the samples gave the higher than or similar charge capacities to that of original graphite powder when their surface fluorine concentrations were relatively high (the samples fluorinated at 513°C and 446°C in Table 8). It is vice versa for the sample fluorinated at 400°C. The fluorine content of this sample was 0.84 at% less than 1 at%, however, the charge capacities were nearly the same as that of original graphite probably because the surface fluorine concentration was a relatively low value of 7.1 at%. In the 10 min-fluorinated samples, those with total fluorine contents less than 1 at% and relatively higher surface fluorine concentrations gave the preferable results of high capacities without decrease in first coulombic efficiencies. With respect to surface oxygen, no definite correlation between surface oxygen concentrations and charge–discharge characteristics of surface-fluorinated graphite was found. The results obtained suggest that graphite powder should be fluorinated for a short time so as to have a low fluorine content less than 1 at% as a whole and high surface fluorine concentration. To obtain surface-fluorinated graphite having high performance, the fluorination conditions such as fluorine pressure, fluorination temperature, and duration of fluorination should be carefully controlled. In addition, there would be another important factor on graphite: particle size distribution. Graphite powder with as homogeneous particle size distribution as possible would be preferable because the fluorination degree is changed depending on the particle size.

Table 9

Surface compositions of graphite samples before and after charge-discharge cycling, obtained by XPS

Sample	Before cycling (at%)			After cycling (at%)		
	C	F	O	C	F	O
1	94.3	3.6	2.1	98.2	0.2	1.6
2	91.5	6.9	1.5	98.3	0.2	1.5
3	94.7	3.1	2.2	98.6	0.3	1.1
4	93.8	4.5	1.7	98.2	0.2	1.6
5	96.1	1.5	2.4	98.2	0.2	1.6
6	95.9	0.9	3.2	98.9	0.1	1.0

Sample 1: fluorinated at 100°C for 2 min by 3×10^4 Pa F_2 .

Sample 2: fluorinated at 154°C for 2 min by 3×10^4 Pa F_2 .

Sample 3: fluorinated at 110°C for 15 min by 1×10^5 Pa F_2 , followed by temperature increase to 297°C.

Sample 4: fluorinated at 116°C for 15 min by 1×10^5 Pa F_2 , followed by temperature increase to 335°C.

Sample 5: fluorinated at 130°C for 2 min by 1×10^5 Pa F_2 , followed by temperature increase to 359°C.

Sample 6: fluorinated at 131°C for 5 min by 1×10^5 Pa F_2 , followed by temperature increase to 355°C.

(Reproduced with permission from *Electrochim. Acta*, 44 (1999) 2879 [48]).

Table 10

$R (= I_D/I_G)$ values of Raman spectra of surface-fluorinated graphite samples before and after charge-discharge cycling

Sample	Before cycling	After cycling
Original	0.083	0.16
1	0.15	0.29
2	0.17	0.34
3	0.20	0.29
4	0.15	0.24
5	0.15	0.24
6	0.13	0.26

Sample 1: fluorinated at 100°C for 2 min by 3×10^4 Pa F_2 .

Sample 2: fluorinated at 154°C for 2 min by 3×10^4 Pa F_2 .

Sample 3: fluorinated at 112°C for 15 min by 1×10^5 Pa F_2 , followed by temperature increase to 297°C.

Sample 4: fluorinated at 116°C for 15 min by 1×10^5 Pa F_2 , followed by temperature increase to 335°C.

Sample 5: fluorinated at 130°C for 2 min by 1×10^5 Pa F_2 , followed by temperature increase to 359°C.

Sample 6: fluorinated at 131°C for 5 min by 1×10^5 Pa F_2 , followed by temperature increase to 355°C.

(Reproduced with permission from *Electrochim. Acta*, 44 (1999) 2879 [48]).

15.4.3 Surface composition and structure changes by charge–discharge cycling

Tables 9 and 10 show the changes in surface compositions and surface roughness by charge–discharge cycling. The surface fluorine concentrations were significantly reduced to 0.1–0.3 at% by electrochemical reduction. Most of surface fluorine atoms would have been removed as lithium fluoride by first reduction because a fluorine reduction peak was observed only in the first reduction curve of cyclic voltammograms. The surface oxygen atoms were also reduced to 1.0–1.6 at%. Table 10 indicates that the *R* values obtained by Raman spectroscopy were increased by charge–discharge cycling both in graphite powder itself and surface-fluorinated samples. The results given in Tables 9 and 10 demonstrate that fluorine and oxygen atoms are significantly removed from graphite surfaces by electrochemical reduction, accompanying the increase of surface roughness. One can imagine the formation of naphthalene- and anthracene-like disordered carbon at the surface of graphite. Some disordered carbon materials can accommodate larger amounts of lithium ions than LiC_6 corresponding to Stage 1 lithium-intercalated graphite. Several intercalation/ doping mechanisms were recently proposed for these phenomena [52,53]. Formation of an ionic complex composed of lithium ions and aromatic rings with negative charges was suggested in disordered carbon anodes [52]. It is also known that alkali metals easily form charge transfer complexes with naphthalene and anthracene. These reactions are usually adopted for the synthesis of alkali metal-intercalated graphites in organic solvents. The higher charge capacities than LiC_6 , that is, 372 mAhg^{-1} obtained in the surface-fluorinated graphite samples may be attributed to such a mechanism as the formation of charge transfer complexes in disordered nanopores existing at the surface of graphite electrode.

References

- [1] M. Fukuda, T. Iijima, Proceedings of 9th International Power Sources Symposium, London, 1974, p. 713.
- [2] M. Fukuda, T. Iijima, Prog. Batteries Solar Cells, 1 (1978) 26.
- [3] N. Watanabe, T. Nakajima, H. Touhara, Graphite Fluorides, Elsevier Sci. Pub., Amsterdam, 1988.
- [4] T. Nakajima, N. Watanabe, Graphite Fluorides and Carbon-Fluorine Compounds, CRC Press, Inc., Boca Raton, FL, (1991).
- [5] T. Nakajima, M. Kawaguchi, N. Watanabe, Electrochim. Acta, 27 (1982) 1535.
- [6] R. Hagiwara, M. Lerner, N. Bartlett, T. Nakajima, J. Electrochem. Soc., 135 (1988) 2393.
- [7] A. Hamwi, M. Daoud, J.C. Cousseins, Synth. Metals, 30 (1989) 23.
- [8] A. Hamwi, J. Phys. Chem. Solids, 57 (1996) 677.
- [9] T. Nakajima, R. Hagiwara, K. Moriya, N. Watanabe, J. Electrochem. Soc., 133 (1986) 1761.
- [10] T. Nakajima, A. Mabuchi, R. Hagiwara, N. Watanabe, F. Nakamura, J. Electrochem. Soc., 135 (1988) 273.
- [11] T. Nakajima, Y. Matsuo, Y. Morino, Denki Kagaku, 61 (1993) 594.

- [12] R. Yazami, In: Fluorine-Carbon, Fluoride-Carbon Materials, by T. Nakajima (Ed.), Marcel Dekker, Inc., New York, NY, 1995, Chapter 7.
- [13] K. Tozawa, N. Nagaura, Prog. Batt. Solar Cells, 9 (1990) 209.
- [14] A. Tressaud, Mol. Cryst. Liq. Cryst., 244 (1994) 13.
- [15] T. Nakajima, In: Fluorine-Carbon, Fluoride-Carbon Materials, T. Nakajima (Ed.), Marcel Dekker, Inc., New York, NY, 1995, Chapter 1.
- [16] A. Tressaud, V. Gupta, L. Piraux, L. Lozano, E. Marquestaut, S. Flandrois, A. Marchand, Carbon, 32 (1994) 1485.
- [17] A. Tressaud, G. Guimon, V. Gupta, F. Moguet, Mater. Sci. Eng., B30 (1995) 61.
- [18] A. Tressaud, M. Chambon, V. Gupta, S. Flandrois, O.P. Bahl, Carbon, 33 (1995) 1339.
- [19] V. Gupta, R.B. Mathur, O.P. Bahl, A. Tressaud, S. Flandrois, Synth. Met., 73 (1995) 69.
- [20] Vinay Gupta, Ph. D. thesis of Maharshi Dayanand Saraswati University, Ajmer, India (1997).
- [21] T. Nakajima, T. Tamura, Synth. Met., 73 (1995) 63.
- [22] T. Nakajima, Y. Matsuo, B. Žemva, A. Jesih, Carbon, 34 (1996) 1595.
- [23] A.M. Panich, T. Nakajima, S. D. Goren, Chem. Phys. Lett., 271 (1997) 381.
- [24] A.M. Panich, T. Nakajima, H.-M. Vieth, A.F. Privalov, S.D. Goren, J. Phys.: Condens. Matter, 10 (1998) 7633.
- [25] J.P. Lemmon, M.M. Lerner, Carbon, 31 (1993) 437.
- [26] Y. Matsuo, M. Segawa, J. Mitani, Y. Sugie, J. Fluorine Chem., 87 (1998) 145.
- [27] T. Nakajima, S. Kasamatsu, Y. Matsuo, Eur. J. Solid State Inorg. Chem., 33 (1996) 831.
- [28] T. Mallouk, B.L. Hawkins, M.R. Conard, K. Zilm, G.E. Maciel, N. Bartlett, Phil. Trans. R. Soc. London Ser. A, 314 (1985) 179.
- [29] Y. Matsuo, T. Nakajima, Z. anorg. allg. Chem., 621 (1995) 1943.
- [30] Y. Matsuo, T. Nakajima, S. Kasamatsu, J. Fluorine Chem., 78 (1996) 7.
- [31] C. Gal, S. Rozen, Tetrahedron Lett., 25 (1984) 449.
- [32] S. Rozen, C. Gal, J. Fluorine Chem., 27 (1985) 143.
- [33] A. Hamwi, H. Alvergnat, S. Bonnamy, F. Beguin, Carbon, 35 (1997) 723.
- [34] P. Hany, R. Yazami, A. Hamwi, J. Power Sources, 68 (1997) 708.
- [35] R. Yazami, P. Hany, P. Masset, A. Hamwi, Mol. Cryst. Liq. Cryst., 310 (1998) 397.
- [36] A. Hamwi, P. Gendraud, H. Gaucher, S. Bonnamy, F. Beguin Mol. Cryst. Liq. Cryst., 310 (1998) 185.
- [37] T. Nakajima, S. Kasamatsu, Y. Matsuo, unpublished data.
- [38] W. Scholz, H.P. Boehm, Z. anorg. allg. Chem., 369 (1969) 327.
- [39] T. Nakajima, A. Mabuchi, R. Hagiwara, Carbon, 26 (1988) 357.
- [40] N. Watanabe, T. Nakajima, R. Hagiwara, J. Power Sources, 20 (1987) 87.
- [41] T. Zheng, W.R. Mckinnon, J.R. Dahn, J. Electrochem. Soc., 143 (1996) 2137.
- [42] E. Peled, C. Menachem, D. Bar-Tow, A. Melman, J. Electrochem. Soc., 143 (1996) L4.
- [43] M. Hara, A. Satoh, N. Takami, T. Ohsaki, Tanso, 165 (1994) 261.
- [44] J.S. Xue, J.R. Dahn, J. Electrochem. Soc., 142 (1995) 3668.
- [45] T. Takamura, M. Kikuchi, Denchi Gijusu, 7 (1995) 29.
- [46] T. Nakajima, K. Yanagida, Denki Kagaku, 64 (1996) 922.
- [47] T. Nakajima, K. Yanagida, Tanso, 174 (1996) 195.
- [48] T. Nakajima, M. Koh, R.N. Singh, M. Shimada, Electrochim. Acta, 44 (1999) 2879.
- [49] R. Takagi, T. Okubo, K. Sekine, T. Takamura, Denki Kagaku, 65 (1997) 333.
- [50] F. Tunistra, J.L. Koenig, J. Chem. Phys., 53 (1970) 1126.
- [51] D.S. Knight, W.B. White, J. Mater. Res., 4 (1989) 385.
- [52] M. Hara, A. Satoh, N. Takami, T. Ohsaki, J. Phys. Chem., 99 (1995) 16338.
- [53] Y. Matsumura, S. Wang, J. Mondori, Carbon, 33 (1995) 1457.

CHAPTER 16

Fluorine Compounds in Battery Applications

Kiyoshi Kanamura

*Department of Applied Chemistry, Graduate School of Engineering, Tokyo Metropolitan University,
1-1 Minami-ohsawa, Hachioji, Tokyo 192-0397, Japan*

16.1 Introduction

A lot of fluorine compounds have been widely used in various novel electrochemical devices, such as sensor, fuel cells, batteries, and so on. These compounds play an important key role in these application fields. Special nonmetal fluorides and fluorinated polymers have been often used in fuel cells and batteries. In this chapter, some interesting topics for fluorine materials in rechargeable lithium batteries and polymer electrolyte fuel cells are introduced. Both devices have been extensively studied for power sources of portable devices, electric vehicles, and load-leveling system [1–4]. In these electrochemical systems, highly oxidative atmosphere is used to realize a high energy density, which must be needed for the above new demands. Therefore, the materials concerned should be stable in such an oxidative atmosphere. For this purpose, fluorine materials are very suitable because of their strong bond energies in especially C—F bond and nonmetal fluorides. This is due to a high electronegativity of fluorine atom. Another important aspect is a hydrophobic nature of fluoropolymers. This is normally utilized for optimizing a circumstance of reaction site in fuel cells. In this chapter, these interesting properties of fluorine compounds used in energy conversion systems (electric energy \leftrightarrow chemical energy) will be reviewed.

16.2 Rechargeable lithium batteries

Many types of rechargeable batteries have been developed as portable power sources for small electronic devices, such as watch, calculator, video camera, computer and so on. Lead–acid battery, Ni–Cd battery, Ni–Metal hydride battery, and lithium battery are well known and used in some portable electronic devices. Lithium batteries are the most attractive with regard to energy density or power density. Recently, a new rechargeable lithium battery, that is a so-called “Lithium Ion Battery”, was proposed by “Sony Company” [5]. In this battery, carbon materials

and transition metal oxides are used as anode and cathode active materials, respectively. Electrochemical reactions occurring in this battery are explained by insertion and extraction (intercalation or deintercalation) of lithium ions into and from host matrixes of both active materials for anode and cathode. Figure 1 shows a schematic illustration of rechargeable lithium ion battery constructed by LiCoO_2 cathode, graphite anode, and non-aqueous electrolyte in separator [4]. During a charge process of the battery, lithium ions are extracted from LiCoO_2 to form Li_xCoO_2 ($x < 1$) and lithium ions are simultaneously inserted into graphite electrode to form Li_xC_6 ($x < 1$). During the discharge process, inverse reactions take place, leading to movement of lithium ions from graphite electrode to Li_xCoO_2 electrode. During discharge and charge cycles, lithium ions move from cathode to anode or from anode to cathode, which is so-called a rocking chair type reaction. Thus, electrochemical reactions occurring in rechargeable lithium ion batteries are very simple. However, many kinds of materials are used in practical batteries. Materials used in the rechargeable lithium battery are summarized in Table 1.

From this table, electrolytes, separators, and binders involve fluorine atoms more or less. Especially, many kinds of fluorine compounds have been synthesized as electrolyte salts in order to realize high solubilities and high ionic conductivities of

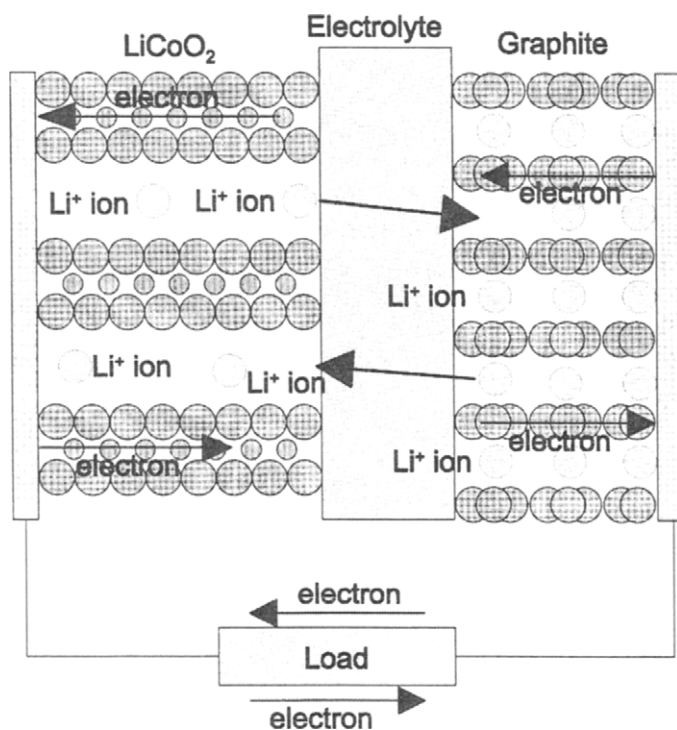


Fig. 1. Schematic illustration for a rechargeable lithium ion battery with LiCoO_2 cathode, graphite anode and nonaqueous electrolyte.

Table 1

Materials used in rechargeable lithium battery

Part	Material	Example
Cathode	Li^+ accepting material	LiCoO_2 , LiMn_2O_4 , LiNiO_3 , Polyaniline, Polypyrrole
Anode	Li^+ accepting material	Graphite, Lithium metal, SnO , Lithium alloy
Electrolyte salt	Inorganic and organic lithium compounds	<i>LiPF_6, LiBF_4, LiAsF_6, LiClO_4, LiCF_3SO_3, $\text{Li}(\text{CF}_3\text{SO}_2)_2\text{N}$</i>
Electrolyte solvent	Aprotic solvent	Propylene carbonate, Diethyl carbonate, Dimethyl carbonate, Dimethoxy ethane
Binding material	Polymer	<i>Teflon</i> , <i>PVdF</i>
Conducting material	Carbon	Acetylene black
Separator	Polymer	Polypropylene, Polyethylene (<i>partially fluorinated polymer</i>)
Cell case	Plastic, Stainless Steel	Mo rich Stainless Steel, Polyethylene

Italic: related to Fluorine Chemistry.

nonaqueous electrolyte solutions. In rechargeable lithium batteries, lithium intercalated graphite or carbons have been used as anode materials [6–9]. Their electrode potentials are enough negative to reduce H_2O , so that H_2O cannot be used as a solvent. Nonaqueous solvents, such as aprotic organic solvents and molten salts, have to be used to avoid a reduction of solvent on anode materials. Most of electrolyte salts used in aqueous solutions, such as Na_2SO_4 , NaCl , LiCl , and so on, cannot dissolve in nonaqueous solvents to high concentrations, which results in low ionic conductivities of nonaqueous electrolyte solutions due to low solubilities of the electrolyte salts. In order to obtain high ionic conductivities of nonaqueous electrolyte solutions, high solubilities of electrolyte salts are needed, so that new electrolyte salts have to be developed for rechargeable lithium batteries. Firstly, LiClO_4 was used as an electrolyte salt for nonaqueous electrolyte solutions. The solubilities of LiClO_4 in some organic solvents are much larger than those of NaCl , Li_2SO_4 , LiCl , and Na_2SO_4 . This is due to the large size of ClO_4^- anion. Lithium salts with large anions are suitable for electrolyte salts used in aprotic organic solvents. For this reason, various kinds of anions are proposed to realize high concentrations of lithium salts in nonaqueous solvents. In general, fluorine is suitable for synthesizing stable large anions due to its chemical bond characteristics [10]. In fact, LiBF_4 , LiAsF_6 , and LiPF_6 are very popular lithium salts used in rechargeable lithium batteries. LiPF_6 have been used in most of rechargeable lithium batteries.

16.2.1 Nonaqueous electrolytes for rechargeable lithium batteries

The anions mentioned in the previous section have been extensively investigated to make clear their electrochemical properties, such as stability, ionic conductivities, transference numbers, impurities, and so on. The most important property among

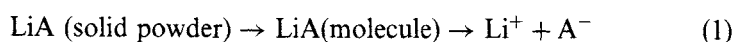
Table 2

Ionic conductivities of various aqueous and nonaqueous electrolytes used in rechargeable batteries

Electrolyte Salt	PC	GBL	PC/DME	GBL/DME	PC/EMC (1:1 mol)	H ₂ O
NaOH	–	–	–	–	–	330
HCl	–	–	–	–	–	180
LiBF ₄	3.4	7.5	9.7	9.4	3.3	–
LiClO ₄	5.6	10.9	13.9	15.0	5.7	–
LiPF ₆	5.8	10.9	15.9	18.3	8.8	–
LiAsF ₆	5.7	11.5	15.6	18.1	9.2	–
CF ₃ SO ₃ Li	1.7	4.3	6.5	6.8	1.7	–
(CF ₃ SO ₂) ₂ NLi	5.1	9.4	13.4	15.6	7.1	–
C ₄ F ₉ SO ₃ Li	1.1	3.3	5.1	15.3	1.3	–

PC: propylene carbonate, GBL: γ -butyrolactone, DME: dimethoxy ethane, EMC: ethyl methyl carbonate, Ionic conductivity 1.0 mol dm⁻³ Salt, mS/cm.

them is the ionic conductivity. Table 2 shows ionic conductivities of typical aqueous and nonaqueous electrolyte solutions. In general, nonaqueous electrolyte solutions of lithium salts have lower ionic conductivities compared with those of aqueous electrolyte solutions. It induced a serious problem when practical batteries using organic solvents are constructed. The low conductivity of nonaqueous electrolyte solution results in a large ohmic drop in batteries. This corresponds to generation of large current distributions in both cathode and anode materials. Under such undesirable large current distributions, both active materials can not be utilized at 100%. Therefore, the conductivity of electrolyte solution is very important. From Table 2, it can be seen that a conductivity of nonaqueous electrolyte solution depends on a kind of electrolyte salt. A relatively high conductivity is obtained by using LiPF₆ electrolyte salt. LiPF₆, LiBF₄, and LiAsF₆ are dissolved in organic solvent to form Li⁺ ion and anion. Li⁺ ion is usually solvated by organic solvents to form a large solvated cation, which is comparable with the size of an anion. Hence, the transference number of cation is smaller than that of anion, even though the original volume of cation is much smaller than that of anion. Therefore, the ionic conductivity of nonaqueous electrolyte solution strongly depends on the size and chemical structure of anion [11–13]. An ionic dissociation of lithium salt is also very critical for the ionic conductivity. The equilibrium is written by the following equation.



The conductivity of nonaqueous electrolyte solution increases with increasing concentration of lithium salt and then decreases through a maximum, as shown in Fig. 2. Such behavior has been explained by the ionic dissociation process of LiA (molecule in solution) as described by the equation. A high dissociation of

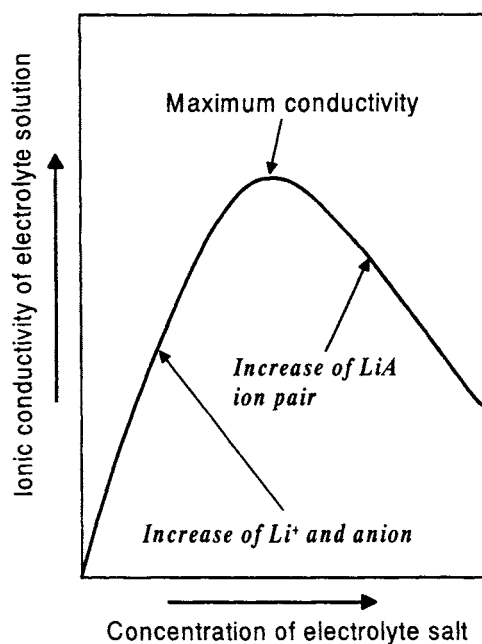


Fig. 2. General dependence of ionic conductivity on concentration of electrolyte salt (LiA) in nonaqueous electrolyte solution.

LiA molecule is attained by a strong acid characteristic of anion. PF_6^- is a more acidic anion, compared with BF_4^- and AsF_6^- ions. The strong dissociation leads to the high concentrations of Li^+ ion and anion, giving a high ionic conductivity of nonaqueous electrolyte solution containing LiPF_6 , as shown in Table 2 [12,14,15]. Therefore, more acidic anions are suitable for electrolyte salts of nonaqueous electrolyte solutions used in rechargeable lithium batteries. Most of compounds involving fluorine often show a strong acid nature, so that fluorides may be suitable for electrolyte salts of nonaqueous electrolyte solutions.

16.2.1.1 Stability of nonaqueous electrolyte solutions

Rechargeable lithium batteries with carbon materials and transition metal oxides have a high cell voltage, 4.0 V, which is very important to realize high energy and power densities of the batteries. Figure 3 shows a summary of energy densities of various types of batteries. From this figure, it is very clear that rechargeable lithium batteries have the highest energy density among various types of batteries. However, such a high voltage leads to some critical problems in safety and lifetime of rechargeable lithium batteries. The most serious problem is the decomposition of nonaqueous electrolyte solutions at both anode and cathode, that is, thermal stability of the nonaqueous electrolyte solutions when batteries are overheated by an unexpected accident.

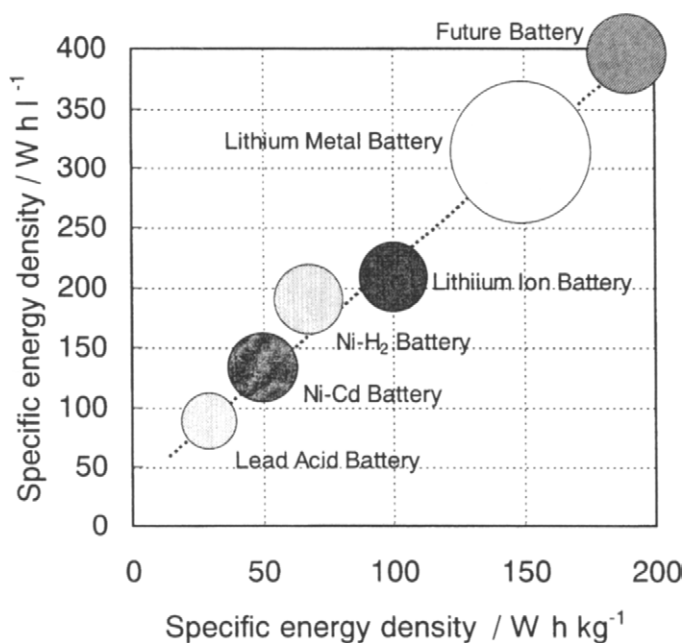


Fig. 3. Specific energy density (per unit volume and unit weight) of various kinds of rechargeable batteries.

Nonaqueous electrolyte solutions can be reduced at negative electrodes, because of an extremely low electrode potential of lithium intercalated carbon material. The reduction products have been identified with various kinds of analytical methods. Table 3 shows several products that detected by in situ or ex situ spectroscopic analyses [16–29]. Most of products are organic compounds derived from solvents used for nonaqueous electrolytes. In some cases, LiF is observed as a reduction product. It is produced from a direct reduction of anions or chemical reactions of HF on anode materials. Here, HF is sometimes present as a contaminant in nonaqueous solutions containing nonmetal fluorides. Such HF would be produced due to instability of anions. A direct reduction of anions with anode materials is a possible scheme for formation of LiF, but anode materials are usually covered with a surface film that prevents a direct contact of anode materials with nonaqueous electrolytes. Therefore, LiF formation is due to chemical reactions with HF [19]. Where does HF come from? Originally, there is no HF in nonaqueous electrolyte solutions. HF can be produced by decomposition of fluorides. For example, HF can be formed in nonaqueous electrolyte solutions by decomposition of PF_6^- ions through the reactions with H_2O [19,30].



Table 3

Various compounds formed on materials of rechargeable lithium batteries due to decomposition of nonaqueous electrolytes

Electrolyte or solvent	Compounds formed by reduction or oxidation of nonaqueous electrolytes	References
LiClO ₄ /PC	Li ₂ CO ₃	[16]
	Li ₂ CO ₃ , LiCl, partially chlorinated hydrocarbon	[17]
	Li ₂ CO ₃ , LiCl, LiOCO ₂ R (CH ₃ CHCH ₂ OCO ₂ Li, CH ₃ CHCHOCO ₂ Li, LiOCH ₂ (CH ₂)CHOCO ₂ Li)	[18]
	Li ₂ O, LiOH, Li ₂ CO ₃ , LiCl (minor)	[19]
LiAsF ₆ /PC	LiCO ₃ , LiF, LiOCO ₂ R	[18]
	Li ₂ CO ₃ , LiOH, Li ₂ O, LiF	[19]
DEC	CH ₃ CH ₂ OCO ₂ Li, CH ₃ CH ₂ OLi,	[18]
(LiClO ₄ /DEC)	Li ₂ CO ₃ , LiOH, Li ₂ O, LiOCO ₂ R, LiCl (minor)	[20]
(LiPF ₆ /DEC)	Li ₂ CO ₃ , LiOH, Li ₂ O, LiF	[20]
LiAsF ₆ /THF	BuOLi, LiF, —As—O—As—	[21]
	LiOCH ₂ CH ₂ CH ₂ CH ₃	[22]
	LiOR, LiF, Li _x AsF _y	[23]
	Li ₂ CO ₃ , LiOH, Li ₂ O, LiF (minor)	[24]
	—O(CH ₂) ₄ —THF, F ₂ —O—As—O—As—F ₂	[25]
	CH ₃ (CH ₂) ₄ OLi, CH ₃ CH(OLi)CH ₂ CH ₂ CH ₃	[26]
Li/AsF ₆ /2MeTHF	CH ₃ OLi, LiF	[21]
LiAsF ₆ /DME	CH ₃ CH ₂ CH ₂ CO ₂ Li, cyclic <i>b</i> -keto ester anion	[27]
LiClO ₄ /g-BL	LiOCO ₂ R, Li ₂ CO ₃ , LiOH, Li ₂ O, LiCl (minor)	[24]
LiClO ₄ /DOL	CH ₃ OLi, CH ₃ CH ₂ OLi, LiOCH ₂ CH ₂ (OCH ₂)OX (X=OLi, H, OR)	[28]
LiClO ₄ /MF	CH ₃ OLi, LiOOCH	[29]

Moreover, HF is generally used in the production process of LiPF₆, so that HF may remain in LiPF₆ as one of contaminant species. The HF concentration in a nonaqueous electrolyte solution has been suppressed to avoid undesirable corrosion of materials used in batteries. On the other hand, a small amount of HF sometimes works as a good inhibitor for suppressing undesirable reactions occurring on anode materials. Surface films, formed on anode materials, strongly depend on the presence of HF in nonaqueous electrolyte solutions, as discussed in the following section. However, the formation of HF by the decomposition of LiPF₆, LiBF₄, and LiAsF₆ should be completely suppressed to obtain a stable discharge and charge performance of rechargeable lithium batteries. Therefore, H₂O content have to be kept at less than 20 ppm in nonaqueous electrolyte solutions, which leads to negligible decomposition of electrolyte salts.

Another important point on electrolyte salts is an oxidative behavior at cathode materials in rechargeable lithium batteries. Probably, this subject is more important than reductive decomposition of electrolyte salts. The oxidation of nonaqueous electrolytes solutions containing various electrolyte salts has been investigated in

order to keep high performance and safety of rechargeable lithium batteries, because the oxidation of nonaqueous electrolyte solutions results in a low ionic conductivity and a production of high-pressure gas in batteries [31–34]. Both behaviors are very critical for performance and safety of batteries and must be suppressed in a practical battery. So far, many important efforts on this subject have been done to clarify an effect of electrolyte salt on the oxidation of nonaqueous electrolyte solutions. Figure 4 shows linear sweep voltammograms for propylene carbonate electrolytes containing 1.0 mol dm^{-3} LiClO_4 when using various types of electrodes. In most of publications, Pt electrode is used as a working electrode, which is a typical inert (non-catalytic) electrode [35–44]. On the other hand, Ni, Al, and LiCoO_2 are relatively catalytic materials [45–47]. From the comparison of current–potential curves on these electrodes, it is clear that the electrochemical oxidation is strongly affected by the kind of electrodes. Moreover, the on-set potentials for the oxidation of nonaqueous electrolyte solutions and the dependence of the oxidation of nonaqueous electrolyte solutions on kind of electrolyte salts have been extensively studied by several groups, as shown in Fig. 5 [44,45]. This means that anions are related to the oxidation process of nonaqueous electrolyte solution. In order to explain this effect, it has been suggested that the electrochemical oxidation of anion precedes the oxidation of solvent. In other words, the stability of anions is the key factor for the oxidation of electrolyte solvent. From this point of view, the theoretical calculation was performed to estimate the HOMO (Highest Occupied Molecular Orbital) levels of various anions, which correspond to oxidation potentials of anions [48–51]. Table 4 shows the calculated HOMO energy levels for some fluoride anions. The most stable anion is expected to be $\text{Li}((\text{CF}_3)_2\text{CHOSO}_2)_2\text{N}$, from this HOMO calculation. The result obtained by the calculation was in good agreement with the experimental result obtained by electrochemical techniques [48–51]. Therefore, a stable anion can be designed according to this simple calculation. Based on this calculation, several new electrolyte salts have been synthesized by Sonoda et al., as shown in Fig. 6. Imide type salts are very meaningful to obtain highly stable anions, because of high electron withdrawing property of fluorocarbon groups.

16.2.1.2 Thermal decomposition of electrolyte salts

The rechargeable lithium ion battery is very attractive in its high-energy density. However, this advantage induces a serious disadvantage in its safety at the same time. Therefore, many types of special issues are included in this battery to keep its safety. The chemical stability of original materials used in the batteries is essentially important to produce such a high energy density battery. Electrolyte salts should not be easily decomposed even if the battery temperature reaches more than 100°C . From this point of view, the thermal stability of electrolyte salt has been investigated. For example, when batteries with nonaqueous solvents containing LiClO_4 are heated at more than 100°C , batteries may explode, like a small bomb. More stable electrolyte salts are therefore necessary. A lot of fluorides are usually more stable than other electrolyte salts. Figure 7 shows the thermogravimetric

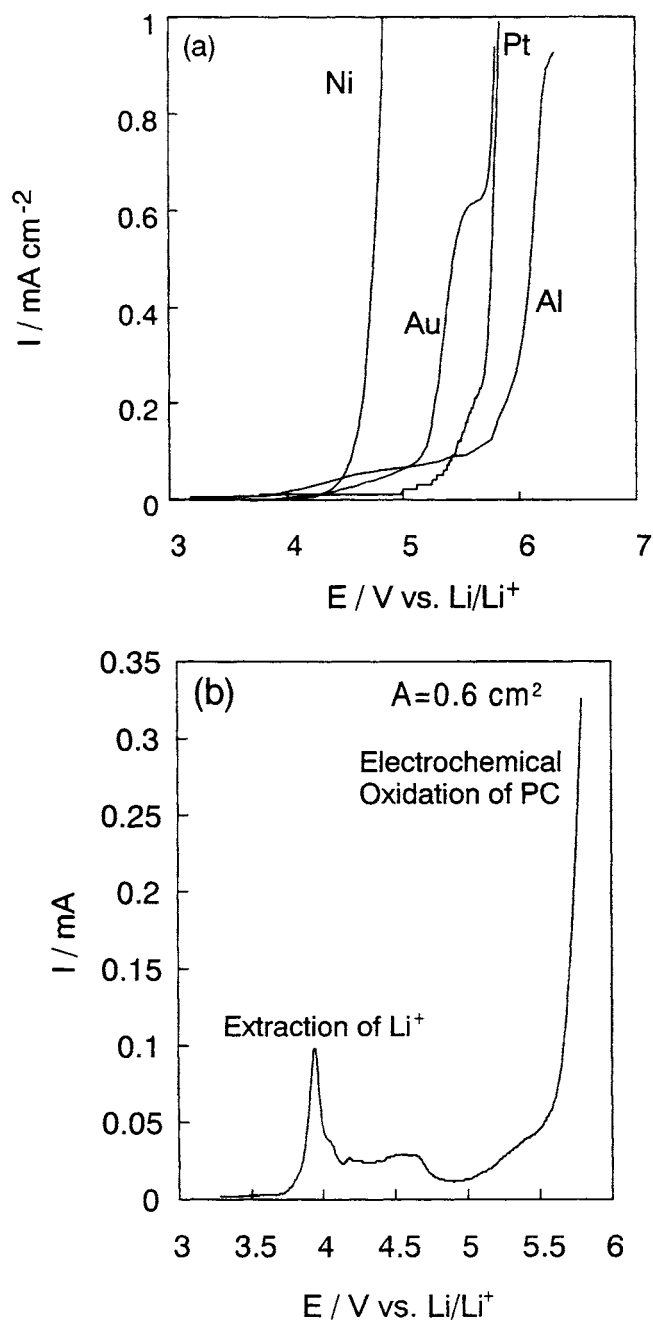


Fig. 4. Current-potential curves for electrochemical oxidation of propylene carbonate containing 1.0 LiClO₄ on various kinds of electrodes, (a) metal electrodes and (b) LiCoO₂ oxide electrode (reproduced with permission from J. Electroanal. Chem., 419 (1996) 77 [47], J. Electrochem. Soc., 142 (1995) 1383 [44], J. Power Sources, 57 (1995) 119 [46]).

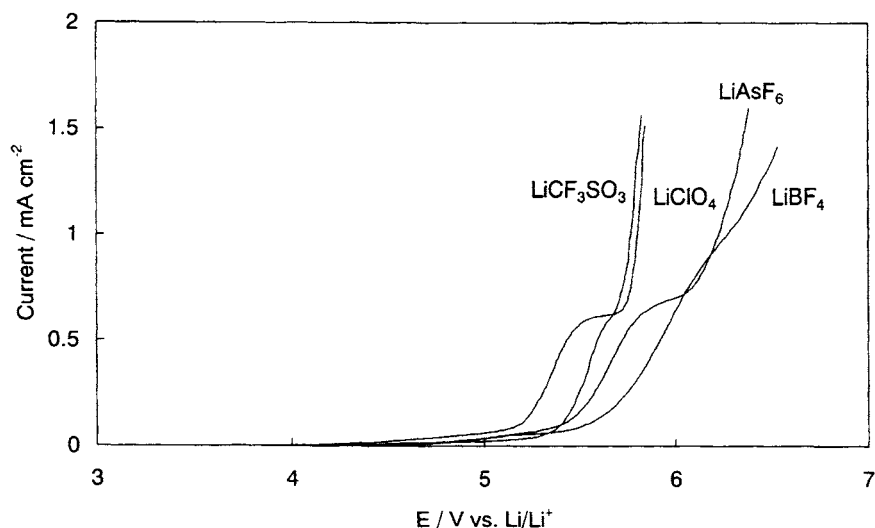


Fig. 5. Current-potential curves for various propylene carbonate electrolytes on Pt electrode (reproduced with permission from J. Electrochem. Soc., 143 (1996) 2548 [45]).

Table 4

Calculated energy for highest occupied molecular orbital (HOMO) of various anions

Anion	HOMO energy (eV)
CH_3SO_3^-	-5.7
$\text{CH}_2\text{FSO}_3^-$	-5.9
$\text{CHF}_2\text{SO}_3^-$	-6.2
CF_3SO_3^-	-7.0
$(\text{CF}_3\text{OSO}_2)_2\text{N}^-$	-8.6
$(\text{CF}_3\text{CH}_2\text{OSO}_2)_2\text{N}^-$	-8.3
$(\text{CF}_3\text{CF}_2\text{CH}_2\text{OSO}_2)_2\text{N}^-$	-8.4
$((\text{CF}_3)\text{CHOSO}_2)_2\text{N}^-$	-8.9
$(\text{CF}_3\text{SO}_2)_2\text{N}^-$	-8.2
$(\text{CF}_3\text{SO}_2)_2\text{C}^-$	-8.7

(Reproduced with permission from Denki Kagaku, 65 (1997) 909 [50], Battery Technol., 6 (1994) 45 [49], 10 (1998) 106 [51]).

analysis (TG) and Differential Thermal Analysis (DTA) curves for LiBF_4 and LiPF_6 [52,53]. Both electrolyte salts decompose at 200°C . The thermal decomposition process for each electrolyte salt has been proposed as follows:

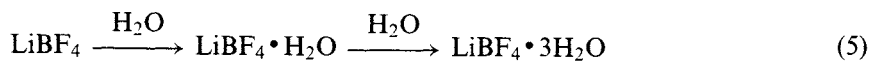
Decomposition at 200°C



$\text{B}(\text{Ph}(-\text{CF}_2)_2-3,5)_4^-$ (HOMO : -6.87 eV) (experimental : -----)	$\text{B}(\text{Ph}(-\text{CF}_2)_2-3)_4^-$ (HOMO : -6.52 eV) (experimental : 4.06 V)
$\text{BPh}_3(\text{Ph}(-\text{CF}_2)_2-3,5)^-$ (HOMO : -5.70 eV) (experimental : -----)	$\text{B}(\text{Ph}(-\text{CF}_2)_2-4)_4^-$ (HOMO : -6.87 eV) (experimental : 4.06 V)

Fig. 6. New developed electrolyte salts containing F element to obtain a high stability for electrochemical oxidation, and HOMO energy and experimentally determined oxidation potential (vs Li/Li^+) (reproduced with permission from J. Power Sources, 68 (1997) 307 [48], Denki Kagaku, 65 (1997) 909 [50], Battery Technol., 6 (1994) 45 [49], 10 (1998) 106 [51]).

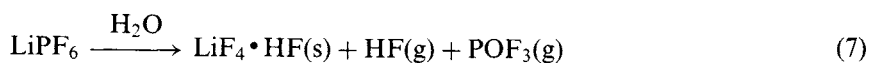
Reaction with moisture



Decomposition at 200°C



Reaction with moisture



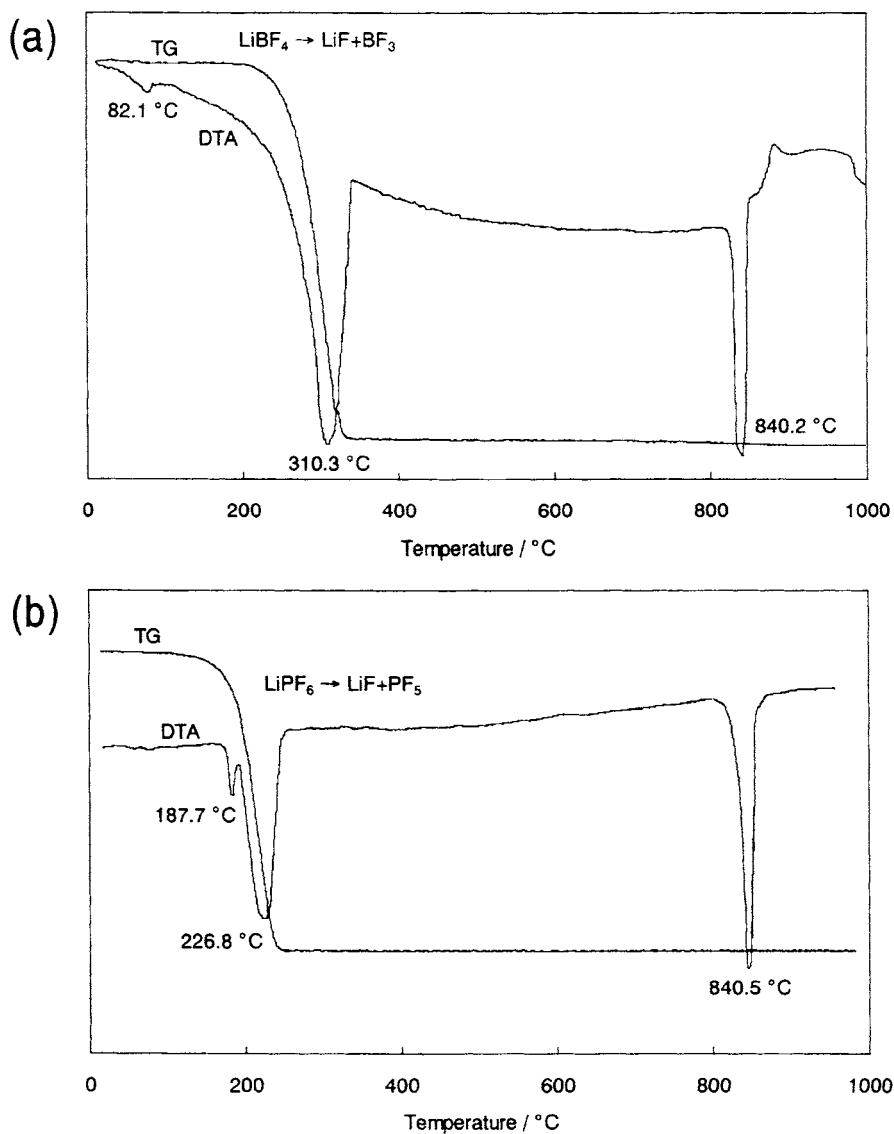


Fig. 7. TG and DTA data for (a) LiPF_6 and (b) LiBF_4 (reproduced with permission from Battery Technol., 8 (1996) 108 [52]).

In order to develop more stable salts, imide type salts, LiCF_3SO_3 and $\text{Li}(\text{CF}_3\text{SO}_2)_2\text{N}$ decomposing at higher temperature than 400°C, have been synthesized [52]. These salts are suitable for rechargeable lithium batteries due to their high thermal stability. Unfortunately, these electrolyte salts cannot be used in practical batteries, because of Al corrosion in nonaqueous electrolyte solutions with these electrolyte

salts [54]. Al is now used as a current collector of positive electrodes. Therefore, at this moment, LiPF_6 is the most suitable electrolyte salt for rechargeable lithium batteries.

16.2.1.3 Corrosion of Al in nonaqueous electrolyte solution with imide salts

An electrode potential of Al is so negative that Al might be dissolved by an anodic polarization. This means that Al current collector dissolves in electrolyte solutions when it is used at positive electrodes of rechargeable lithium batteries. However, Al is very stable because of a stable passivation film that mostly consists of Al oxides. In the case of aqueous electrolyte solutions, oxides or hydroxides are formed on Al under a stable condition, leading to a perfect passivation of Al. Oxide ions or hydroxide ions can be easily supplied from water molecule existing in aqueous electrolyte solutions. In the case of nonaqueous electrolyte solutions, organic solvents are used instead of H_2O . The stability of passivation films on Al electrode is affected by a kind of nonaqueous electrolyte solution. Several researches on the stability of Al in nonaqueous electrolyte solutions have been reported [46,48,56]. When inorganic fluorine compounds are used as electrolyte salts, most of nonaqueous electrolyte solutions are stable. However, when LiCF_3SO_3 or $\text{Li}(\text{CF}_3\text{SO}_2)_2\text{N}$ is used, Al electrode is not stable. Figure 8 shows the current–potential curves obtained by a linear sweep voltammetry in propylene carbonate containing various electrolyte salts. Anodic currents observed in all curves correspond to oxidation of nonaqueous electrolyte solutions or Al electrodes. Electrolyte solutions containing LiPF_6 or LiBF_4 showed a very low anodic current even in more anodic potential range [46]. This is because passivation films on Al electrode are stable in these electrolyte solutions. On the contrary, a large anodic current was observed in the electrolyte solutions containing LiCF_3SO_3 and $\text{Li}(\text{CF}_3\text{SO}_2)_2\text{N}$ [55,56]. This means that oxidation takes place on Al electrode in these electrolyte solutions. Moreover, the anodic current during the forward scan (indicated by arrow) was smaller than that during the back scan, at the first cycle. Such a phenomenon is usually related to a surface state change of electrode. The anodic current increased with the cycle of potential sweep. This also indicates the surface state change of the Al electrode. In order to confirm the surface state change of Al, the Al electrode was observed with scanning electron microscope. Figure 9 shows the scanning electron micrograph of the Al electrode after anodic polarization at 5.0 V vs. Li/Li^+ in propylene carbonate containing either LiCF_3SO_3 or $\text{Li}(\text{CF}_3\text{SO}_2)_2\text{N}$. In both cases, there are many holes on the Al electrode, indicating that electrochemical dissolution of Al occurred during the anodic polarization. From these micrographs, it can be concluded that the anodic currents observed in both electrolyte solutions correspond to the anodic oxidation of Al as well as the electrochemical oxidation of nonaqueous electrolyte solutions. The passivation film on the Al electrode may be broken by the anodic polarization in these electrolyte solution.

In the case of electrolyte solution with LiPF_6 or LiBF_4 , the surface film composition changed from Al oxide to Al oxide and fluoride [46]. Probably, the passivation film becomes more stable by these compositional changes. In nonaqueous electrolyte solutions containing LiCF_3SO_3 or $\text{Li}(\text{CF}_3\text{SO}_2)_2\text{N}$, the stability of the passivation

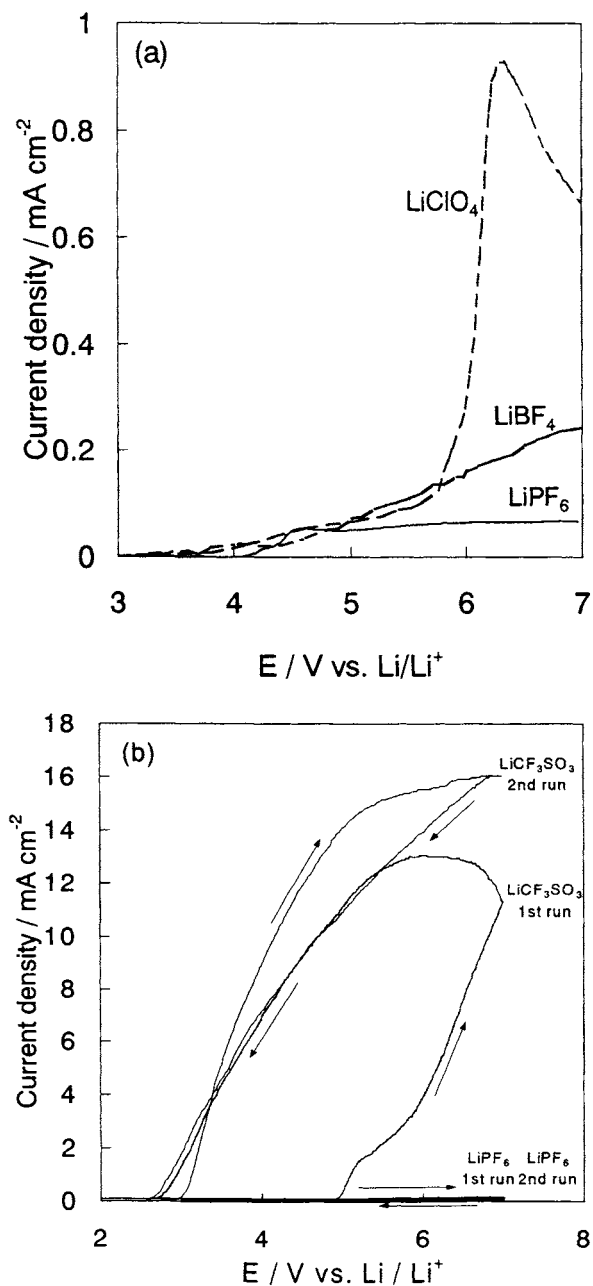


Fig. 8. Current-potential curves for various electrolytes on Al electrode, (a) propylene carbonate containing 1.0 mol dm⁻³ LiClO₄, LiBF₄, or LiPF₆; (b) propylene carbonate containing 1.0 mol dm⁻³ LiCF₃SO₃ (in (b), current-potential curve obtained in propylene carbonate containing 1.0 mol dm⁻³ LiPF₆ was also shown (reproduced with permission from J. Power Sources, 57 (1995) 119 [46], Battery Technol., 10 (1998) 85 [56]).

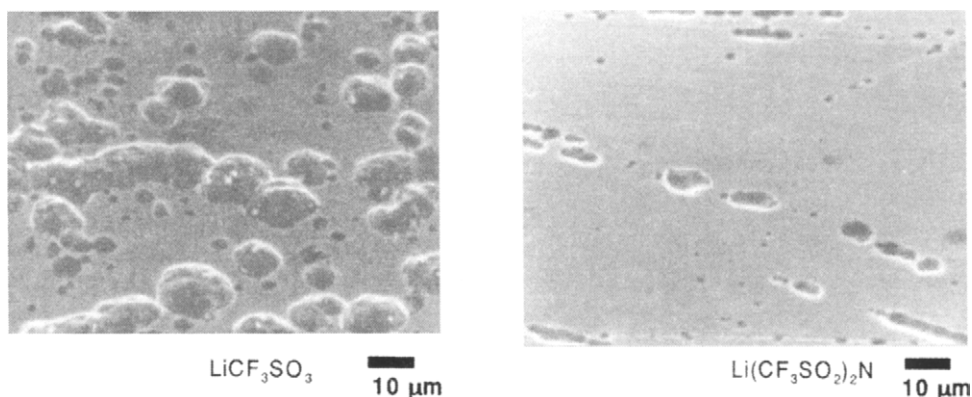


Fig. 9. Scanning electron micrographs for Al electrode polarized at 5.0 V vs Li/Li^+ for 1 h in propylene carbonate containing (a) $1.0 \text{ mol dm}^{-3} \text{ LiCF}_3\text{SO}_3$; and (b) $1.0 \text{ mol dm}^{-3} \text{ Li}(\text{CF}_3\text{SO}_2)_2\text{N}$ (reproduced with permission from J. Power Sources, in press [57], Battery Technol., 10 (1998) 85 [56]).

film decreases with the anodic polarization, resulting in the dissolution of Al electrode (the corrosion Al electrode). The difference in corrosion behaviors is due to the physical properties of the electrolyte salts. The oxidative decomposition of these anions can be explained by the molecular orbital calculation described above. According to this calculation, the stability of PF_6^- and BF_4^- are lower than those of CF_3SO_3^- and $(\text{CF}_3\text{SO}_2)_2\text{N}^-$ [48–51]. On the Al electrode, PF_6^- and BF_4^- may be oxidized to form some active species, such as fluorine atom or fluoride radicals reacting with the passivation film to form a new surface film having fluorine. This process provides a more stable passivation film to avoid a corrosion of Al electrode during anodic polarization. Decomposition of CF_3SO_3^- and $(\text{CF}_3\text{SO}_2)_2\text{N}^-$ also takes place on Al electrodes, but the decomposition potentials are more anodic than those for PF_6^- and BF_4^- . One of possible reasons for Al corrosion may be explained by this difference in oxidation potentials. A high stability of anion leads to a slow supply of some active species providing more stable chemical compositions of passivation films. Before formation of more stable passivation films, passivation films on Al electrodes are broken down by anodic polarization. This results in high dissolution of Al. The oxidation potential increased with increasing acidity of anions. From this point of view, several new fluoride compounds were synthesized and tested as the electrolyte salt for rechargeable lithium batteries [48,55,56]. In the case of imide salts, it is easy to change their acidity with changing fluorocarbon chain length binding to $-\text{SO}_2\text{NSO}_2-$, because fluorocarbon chain works as an electron acceptor and enhances softness of anions resulting in high dissociation constant of electrolyte salts. In fact, $(\text{C}_2\text{F}_5\text{SO}_2)_2\text{N}^-$ or $(\text{CF}_3\text{SO}_2)(\text{C}_4\text{F}_9\text{SO}_2)\text{N}^-$ ions are very strong acid and their lithium salts easily dissociate to ions in nonaqueous solvents. Dissolution of Al in nonaqueous electrolyte solutions strongly depends on a kind of anion, as stated above. When these new salts are used as electrolyte salts, Al corrosion might be suppressed by their highly soft character of anions (due to less formation of aluminum complexes). Figure 10 shows scanning electron micrographs

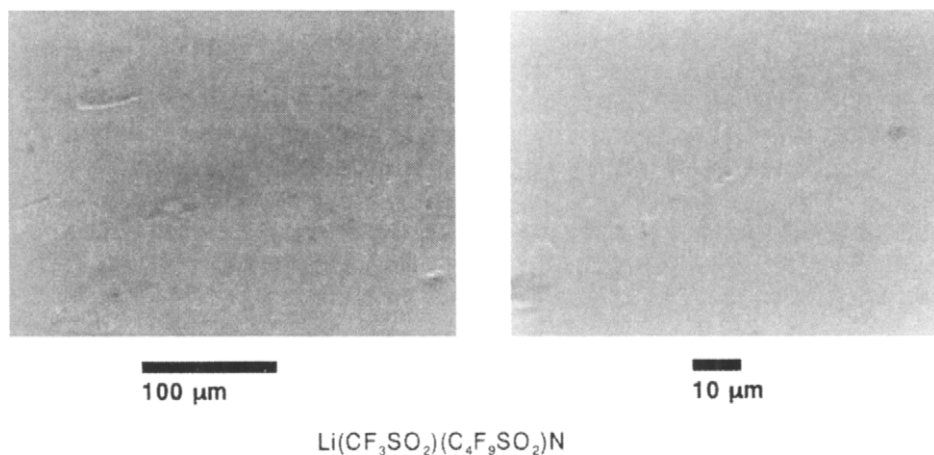


Fig. 10. Scanning electron micrographs for Al electrode polarized at 5.0 V vs Li/Li^+ for 1 h in propylene carbonate containing 1.0 mol dm^{-3} $\text{Li}(\text{CF}_3\text{SO}_2)(\text{C}_4\text{F}_9\text{SO}_2)\text{N}$ (reproduced with permission from Battery Technol., 10 (1988) 85 [56], J. Power Sources, in press [57]).

of Al surface after the anodic polarization at 5.0 V vs Li/Li^+ in propylene carbonate containing 1.0 mol dm^{-3} $\text{Li}(\text{CF}_3\text{SO}_2)(\text{C}_4\text{F}_9\text{SO}_2)\text{N}$. The corrosion of Al was not observed in these photographs. The similar result has been published by 3M group using $\text{Li}(\text{C}_2\text{F}_5\text{SO}_2)_2\text{N}$ imide salt [55]. This salt is also very acidic. In the case of $\text{Li}(\text{CF}_3\text{SO}_2)\text{N}$, there were a lot of pits on the Al electrode after the same anodic polarization. From the comparison of these two results, it can be said that imide salts having long fluorocarbon chains suppress the anodic dissolution of Al. After the anodic polarization, the passivation film was analyzed by X-ray Photoelectron Spectroscopy (XPS). The XPS spectra before the anodic polarization showed the presence of Al oxides on Al surface, and those after the anodic polarization in propylene carbonate with LiPF_6 indicated that aluminum oxide, fluorides, and oxyfluorides are present on Al electrode. On the other hand, the XPS spectra after the anodic polarization in propylene carbonate with $\text{Li}(\text{CF}_3\text{SO}_2)(\text{C}_4\text{F}_9\text{SO}_2)\text{N}$ indicated the presence of the same aluminum compounds on the Al as existed before the anodic polarization. These compounds were different from those observed for the Al electrode oxidized in the electrolyte solutions containing LiPF_6 , from which the difference in the chemical compositional changes of the passivation films was clearly observed. These results strongly suggest a special effect of imide salts having long chains with fluorocarbon groups. The explanation for this extremely interesting behavior has not been given, yet. However, we can easily expect an importance of a length of fluorocarbon chain involved in imide salts.

16.2.1.4 New imide salts for high voltage batteries

New imide salts have an interesting characteristic from the viewpoint of Al corrosion. Recently, much more important characteristics have been reported [57].

As described above, new imide salts have long chains of fluorocarbon group in its molecular structure. This provides a strong acid property and other interesting electrochemical behaviors. Probably, electrochemical stability of nonaqueous electrolyte solutions containing such new imide salts are influenced by an interaction between hydrocarbon part of solvents and fluorocarbon part of imide salts. What kind of effect can be deduced from this interaction? Figure 11 shows the SNIFTIR spectra for an electrochemical oxidation of a mixed solvent of diethyl carbonate and dimethoxy ethane containing 1.0 mol dm^{-3} $\text{Li}(\text{CF}_3\text{SO}_2)(\text{C}_4\text{F}_9\text{SO}_2)\text{N}$ or LiClO_4 on LiCoO_2 . The Fourier Transform Infrared (FTIR) spectra are differential ones between two different electrode potentials, so that the upward peaks correspond to consumption of compounds originally existing in a particular electrochemical system and the downward ones correspond to formation of new compounds due to decomposition of nonaqueous electrolyte solutions. When LiClO_4 was used as the electrolyte salt, this mixed solvent was oxidized at 4.0 V vs Li/Li^+ on LiCoO_2 cathode. This behavior has been observed for most of nonaqueous electrolyte systems. On the other hand, we could not see any decomposition of the electrolyte on LiCoO_2 when $\text{Li}(\text{CF}_3\text{SO}_2)(\text{C}_4\text{F}_9\text{SO}_2)\text{N}$ was used as the electrolyte salt. This difference is based on the kind of electrolyte salt used for nonaqueous electrolyte solutions. It must be noticed that such an excellent effect of the new imide is more pronounced by using ether-type solvent. When only ester solvents are used,

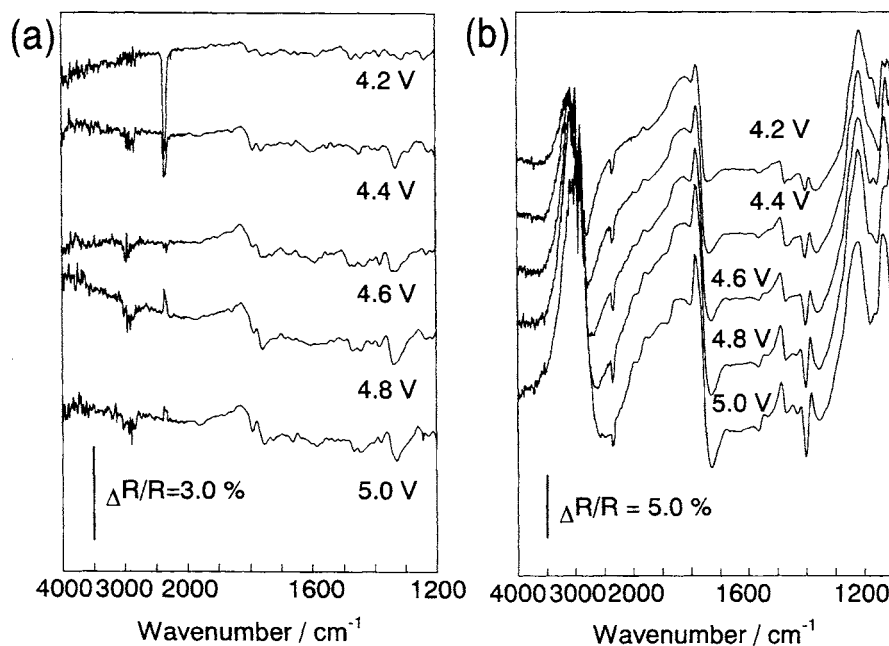


Fig. 11. Subtractively normalized interfacial fourier transform infrared spectra for electrochemical oxidation of propylene carbonate containing 1.0 mol dm^{-3} (a) $\text{Li}(\text{CF}_3\text{SO}_2)(\text{C}_4\text{F}_9\text{SO}_2)\text{N}$ and (b) LiClO_4 (reproduced with permission from J. Power Sources, in press [57]).

nonaqueous electrolyte solution decomposes at 4.2 V vs Li/Li⁺. These results suggest that an interaction between solvents and salts provides a surprising stability of nonaqueous electrolyte solutions. This type of solvent effect has not been proposed. The fluorocarbon chain of Li(CF₃SO₂)(C₄F₉SO₂)N may have excellent characteristics for physical properties of nonaqueous electrolyte solutions. Other kinds of new imide salts have to be developed to obtain ultra-high voltage rechargeable lithium batteries.

16.2.2 Surface modification of lithium metal using HF and HF complexes

As discussed above, LiPF₆ and LiBF₄ decompose to form HF in nonaqueous electrolyte solution. In addition, HF is often used as a fluorinated agent or a reaction medium when fluorine compounds are prepared. A trace of HF possibly remains in the salts and dissolved in nonaqueous electrolyte solution. Usually, HF was a typical undesirable species for battery system, but its function was not understood well before. Recently, a lot of reports have been published to discuss several chemical reactions of HF with the components contained in rechargeable lithium batteries. A very interesting behavior has been observed on lithium metal.

Lithium metal is the most promising anode material for rechargeable lithium batteries, however its rechargeability is not adequately high for practical use. This problem is caused by surface morphology of lithium metal deposited during charging process. In order to improve its rechargeability of lithium metal, many excellent researches have been done around the world. In an earlier stage of these studies, it was suggested that lithium metal was covered with a surface film having an ionic conductivity for Li⁺ ion. The surface film is very important to avoid chemical reactions of lithium metal with nonaqueous electrolyte solutions. If this type of surface film was not present on lithium metal surface, nonaqueous electrolyte solutions would be reduced by lithium which has an enough negative potential to reduce most polar organic solvents and electrolyte salts. Moreover, the presence of the surface film influences the morphology of lithium deposited during the charging process. In some cases, lithium dendrites are formed and possibly contact to a positive electrode. This situation is one of the typical failure modes of rechargeable lithium batteries with lithium metal [58–61]. Therefore, many research groups around the world have extensively studied chemical composition and structure of the surface film. The most popular model is ionically conductive solid film consisting of various organic and inorganic compounds, as shown in Fig. 12 [62]. The compounds in the surface film have been detected with in situ and ex situ FTIR measurement, X-ray photoelectron spectroscopy, and other various interfacial spectroscopic techniques. The most interesting feature of the surface film on lithium is deduced from a stability of electrolyte salt, which has been discussed in a previous section. LiPF₆, LiBF₄, LiAsF₆, LiCF₃SO₃ and Li(CF₃SO₂)₂N have been applied to rechargeable lithium batteries as electrolyte salts. Depending on the nature of the electrolyte salts, HF contents in nonaqueous electrolyte solutions change. For example, the electrolyte solution containing LiPF₆ usually has the highest HF content among those with other electrolyte salts [19]. A trace of HF strongly influences the nature

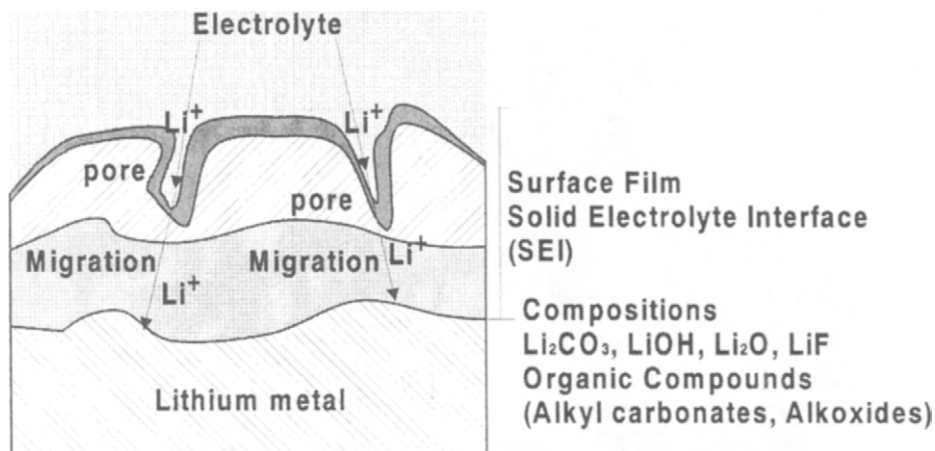


Fig. 12. Solid electrolyte interface (SEI) model for surface formed on lithium metal and graphite electrodes in nonaqueous electrolytes.

of the surface film formed on lithium metal. This phenomenon has been confirmed by X-ray photoelectron spectroscopy [24]. The XPS spectra in Fig. 13 were obtained for the surface of lithium deposited on Ni substrate in propylene carbonate containing $1.0 \text{ mol dm}^{-3} \text{ LiPF}_6$. The formation of LiF in the surface film on lithium was confirmed by the XPS spectra. This result clearly shows the effect of HF. Lithium foil is usually prepared from ingot using special equipment. An atmosphere for this preparation is a decisive factor for the chemical composition of the native surface film on lithium foil. This means that lithium foil is always covered with the native film consisting of various kinds of lithium compounds. For example, Li_2O , LiOH , and Li_2CO_3 have been identified as the main components of the native surface film, which can be confirmed by X-ray photoelectron spectroscopy. The model for the surface film is illustrated in Fig. 14. When LiClO_4 , LiCF_3SO_3 , $\text{Li}(\text{CF}_3\text{SO}_2)_2\text{N}$ and LiAsF_6 are used as electrolyte salts, the surface films are relatively stable in nonaqueous electrolyte solution. However, when LiPF_6 and LiBF_4 are used, the native surface films are changed by an effect of HF produced by decomposition of electrolyte salts. Figure 15 shows the X-ray photoelectron spectra for the surface films on lithium immersed in four kinds of propylene carbonate electrolyte solutions [19]. From these spectra, it can be seen that the chemical compositions and thickness of surface films are extremely influenced by the immersion in these electrolytes. This result clearly indicates that some chemical reactions proceed during the immersion of lithium foils in the solutions. In the case of propylene carbonate with LiClO_4 , the surface film on lithium does not change during the immersion. On the other hand, the surface films on lithium were completely changed during the immersion in propylene carbonate with LiBF_4 and LiPF_6 [63]. The changes in propylene carbonate with LiPF_6 that are expected from the X-ray photoelectron spectra, can be schematically illustrated

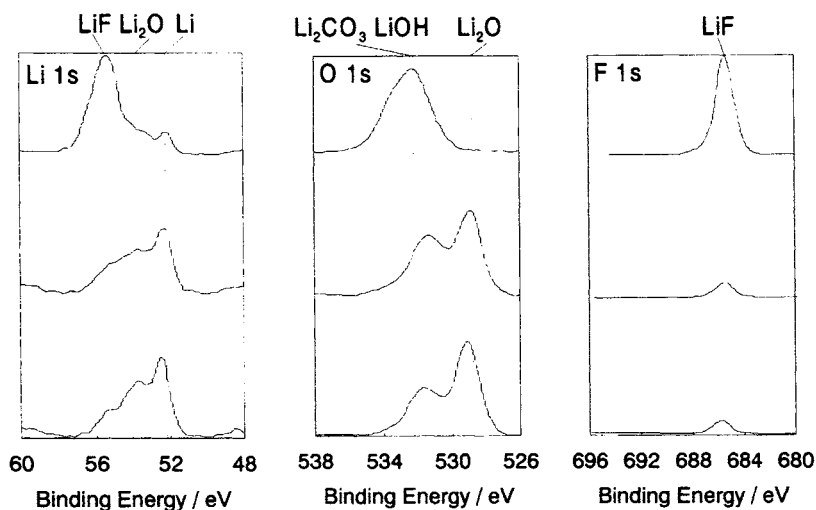


Fig. 13. XPS spectra for lithium metal deposited on Ni metal in propylene carbonate containing 1.0 mol dm^{-3} LiPF_6 (reproduced with permission from J. Electroanal. Chem., 394 (1995) 49 [24]).

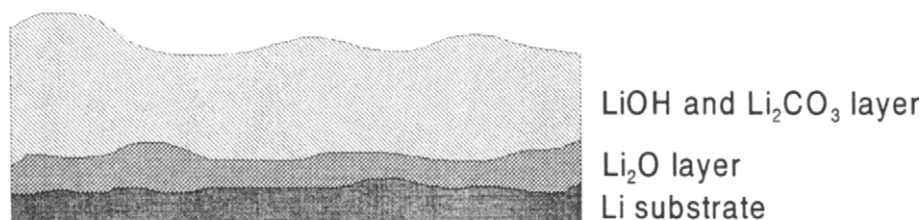
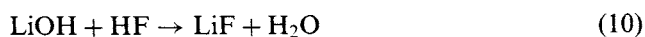
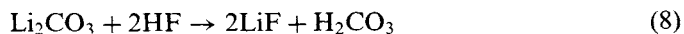


Fig. 14. Schematic illustration for native surface film on lithium foil.

in Fig. 16. As discussed above, though lithium metal has enough ability to reduce the solvents and electrolyte salts, large amounts of organic, phosphor and boron compounds were not observed on the lithium surfaces. This result means that chemical reactions of solvents or salts with lithium metal are not the main reactions for the surface film change. Therefore, it can be said that LiF is not formed by chemical reaction of anions with lithium metal, but is produced by the effect of HF . Possible chemical reactions of HF were proposed as follows, [19,63,64]:



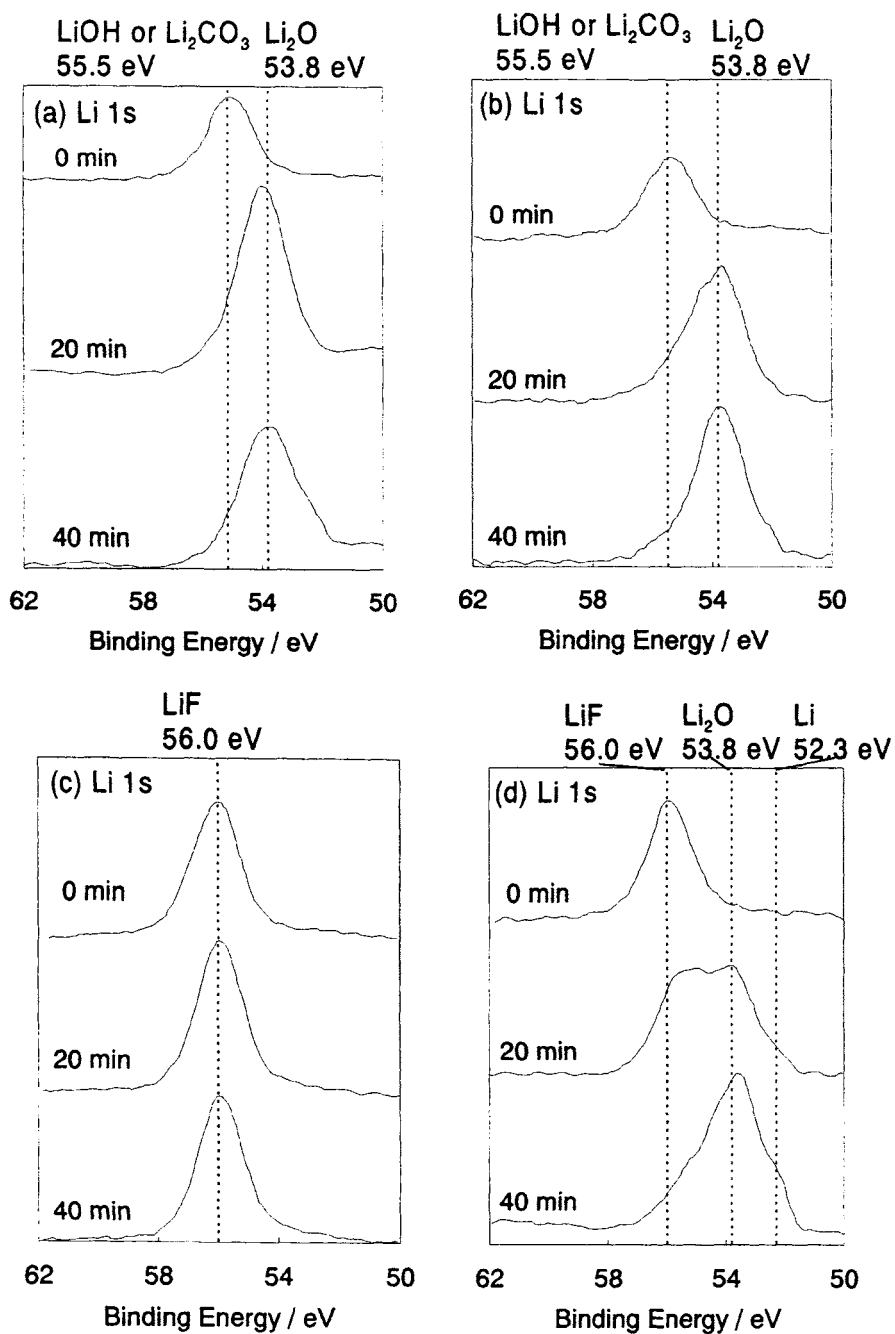


Fig. 15. XPS spectra for lithium metal surface after immersion in propylene carbonate containing 1.0 mol dm⁻³ (a) LiClO₄, (b) LiAsF₆, (c) LiBF₄, or (d) LiPF₆ (reproduced with permission from J. Electroanal. Chem., 333 (1992) 127 [19]).

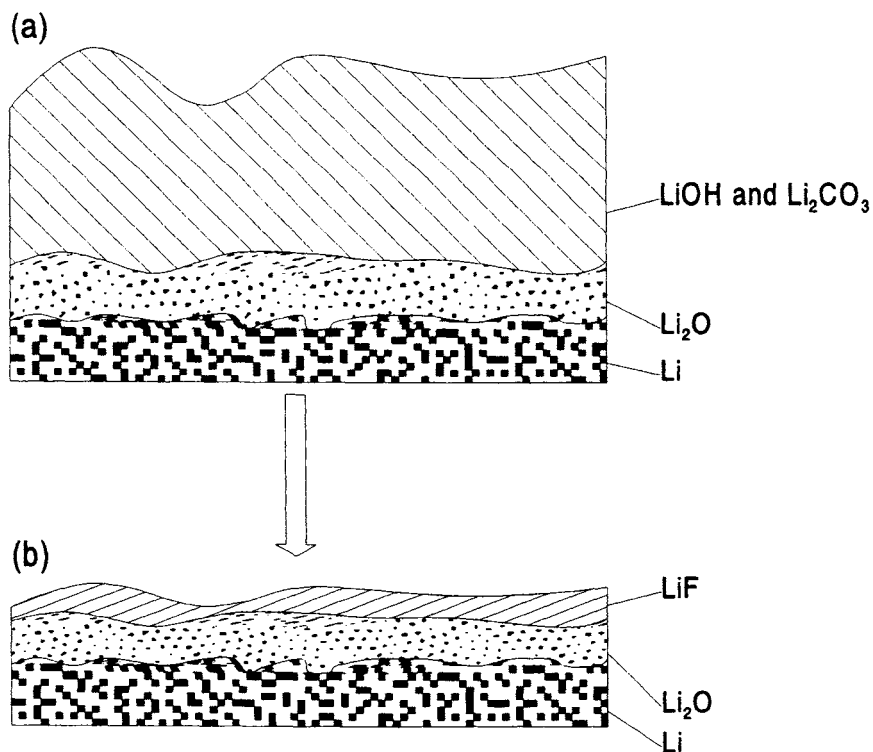


Fig. 16. Schematic illustration of surface film change in propylene carbonate containing 1.0 mol dm^{-3} LiPF_6 .

These reactions are typical acid-base reactions of lithium compounds with HF. In nonaqueous electrolyte solutions, HF works as a weak acid, however HF may strongly react with lithium compounds at the surface film on lithium. Through these reactions, the native surface film is converted to a new one. Here, a very interesting behavior of lithium metal deposition is observed when the native surface film is changed to the new one consisting of a very thin LiF/Li₂O layer, which is formed in propylene carbonate with LiPF_6 . Figure 17 shows scanning electron micrographs of lithium metal electrochemically deposited on a lithium foil immersed in propylene carbonate with LiClO_4 or LiPF_6 for 24 h. In propylene carbonate with LiPF_6 electrolyte, lithium was deposited in a hemispherical form, however, in propylene carbonate with LiClO_4 , lithium was deposited in a typical dendrite form. This difference is due to the nature of the surface films formed on the lithium foils in two electrolyte solutions. From these results, it can be concluded that HF plays an important role for morphology of lithium deposits. If propylene carbonate with LiClO_4 contains a trace of HF, lithium deposits will exhibit a hemispherical form. In fact, Fig. 18 shows that the hemispherical form of lithium can be obtained when a small amount of HF is added to propylene carbonate with LiClO_4 [65–67].

The surface film on such lithium particles have been analyzed with X-ray photoelectron spectroscopy, which shows that the surface film has the same chemical compositions and structure, as those obtained for lithium particles deposited in propylene carbonate with LiPF_6 . This means that HF works as a modification agent during the electrochemical deposition of lithium. The clear suppression of lithium dendrite is very important for rechargeability of lithium metal anode. In fact,

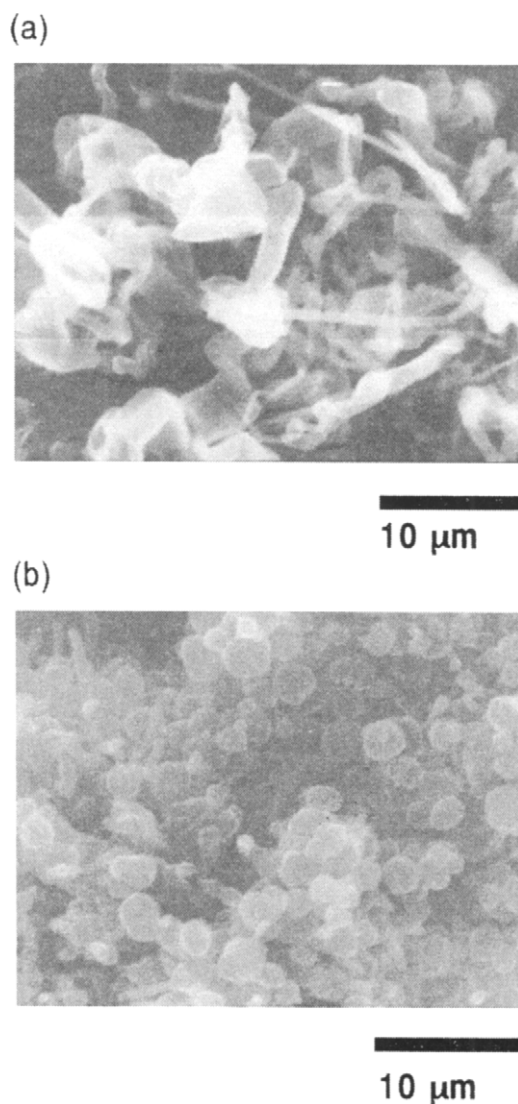


Fig. 17. Scanning electron micrographs of lithium deposited on lithium foil in propylene carbonate containing 1.0 mol dm^{-3} (a) LiClO_4 , or (b) LiPF_6 (deposition is performed after immersion for 24 h) (reproduced with permission from *Electrochim. Acta*, 40 (1995) 913 [64]).

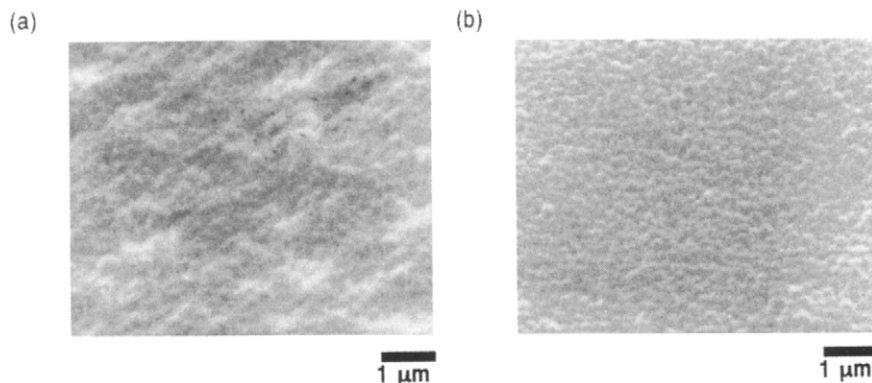


Fig. 18. Scanning electron micrographs of lithium deposited on Ni substrate in propylene carbonate containing $1.0 \text{ mol dm}^{-3} \text{ LiClO}_4$ and 100 ppm HF at 0.2 mA cm^{-2} and (b) 1.0 mA cm^{-2} (reproduced with permission from *J. Electrochem. Soc.*, 143 (1996) 2187 [66]).

the coulombic efficiency for lithium metal in the course of discharge and charge cycles is improved by addition of HF into nonaqueous electrolyte solution [68]. Probably, the surface film on lithium deposited in the electrolyte solution containing HF is so uniform that the electrochemical deposition of lithium takes place at entire surface of substrate electrode uniformly.

Thus, the addition of HF is very useful to obtain high discharge and charge cycleability. However, HF is a very dangerous compound for human beings. An alternative chemical compound should be needed for a practical use of HF addition. Recently, some complex compounds with HF were synthesized for electrochemical fluorination [69]. For example, organic anion complexes with HF are relatively safe compared with HF. In organic electrochemical fluorination, these types of electrolyte salts have been used to obtain active fluorine species. These complex compounds have been also used as additives to modify the surface conditions of lithium. Morphology of lithium deposited in nonaqueous electrolyte solution containing HF complex was very similar to that shown in Fig. 18 and the performance of lithium anode was clearly improved by the addition of such compounds. For example, EC+DME containing $1.0 \text{ mol dm}^{-3} \text{ LiClO}_4$ with $(\text{C}_2\text{H}_5)_4\text{NF}(\text{HF})_4$ has an excellent effect for improving rechargeability of lithium metal anode [70,71]. Figure 19 shows the utilization change of a cell having LiCoO_2 cathode and Ni substrate as an anode current collector. In this cell, no lithium was present on the Ni substrate at the initial stage of the battery. Lithium metal was deposited at the first charge process and then utilized in the following discharge and charge cycles. When no additive is contained in the nonaqueous electrolyte solution, the utilization of lithium anode decreased with cycling during 20 discharge and charge cycles and the efficiency was on a level at 80–70%. However, the cycle efficiency in the nonaqueous electrolyte solution with 100 ppm $(\text{C}_2\text{H}_5)_4\text{NF}(\text{HF})_4$ is much greater than that without any additive, and nearly equal to 100% except the initial three cycles. The surface state of lithium was also observed with X-ray photoelectron spectroscopic analysis after the first

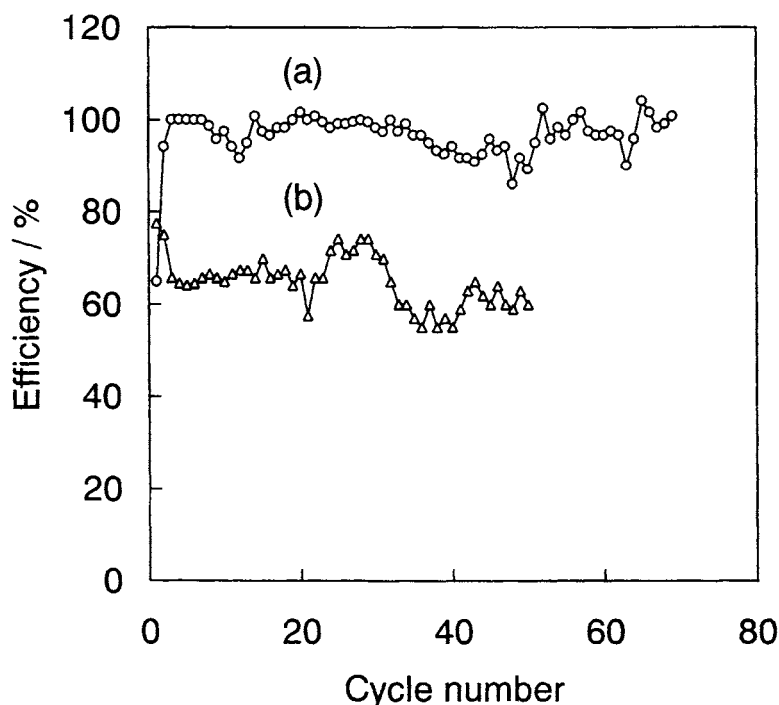


Fig. 19. Discharge and charge efficiency of lithium metal in a mixed solvent of ethylene carbonate and dimethoxy ethane containing $1.0 \text{ mol dm}^{-3} \text{ LiClO}_4$ (a) with and (b) without 100 ppm HF at 0.5 mA cm^{-2} .

charge process. The surface film on lithium involved LiF and Li_2O layers at outside and inside parts, respectively. The chemical compositions and structure show that the effect of $(\text{C}_2\text{H}_5)_4\text{NF}(\text{HF})_4$ additive is understood by the formation of HF in nonaqueous electrolyte solution. In this case, no water was added into the nonaqueous electrolyte solution. This makes possible the long cycle life of lithium metal anode.

Thus, the chemistry of HF in nonaqueous electrolyte solution is very important even though its content is in the order of 100 ppm. Therefore, much attention has to be paid on the synthesis and stability of fluoride compounds in nonaqueous electrochemistry and battery field. In particular, new compounds containing fluorine would be more and more important to realize more reliable nonaqueous electrolyte system and interface control in rechargeable lithium batteries.

16.2.3 Solid polymer electrolyte

Fluorine containing organic compound is also important to prepare solid polymer electrolyte, which is very attractive as a novel electrolyte system [72–74]. At the initial stage of polymer electrolyte development, simple electrolyte salts, such as LiPF_6 and LiClO_4 , are used in rechargeable lithium batteries. However, their

solubilities are low, leading to low conductivities of polymer electrolyte. Recently, imide salts are used in most of polymer electrolytes to attain high ionic conductivities. This type of polymer electrolyte exhibits a relatively high ionic conductivity and a high thermal stability [74]. In addition, gel electrolytes are also developed to obtain higher ionic conductivities. In this case, imide salts are also used to realize high conductivities. In Table 5, polymer and gel electrolytes developed in recent years are summarized [74]. These conductivities are smaller than those of liquid electrolytes used in rechargeable lithium batteries. However, polymer and gel electrolytes provide several advantages compared with liquid type electrolytes.

1. Electrolyte does not leak out from cells.
2. Flexible battery can be made.
3. Rectangular type battery manufacture is improved.
4. High thermal stability.
5. High safety.

Figure 20 shows a schematic illustration for polymer electrolyte batteries proposed by several research groups [74]. The positive electrode is made in a sheet shape consisting of a composite of conducting material, binder, solid polymer electrolyte, and active material. The negative electrode is also in a sheet consisting of lithium metal or a composite of carbon, conducting material, binder, and solid polymer electrolyte. As binders, several partially fluorinated organic compounds have been used in practical batteries. Usually, the kind of polymer is selected so as to obtain

Table 5

Conductivity of various types of solid polymer and gel electrolytes

Solid polymer electrolyte	Conductivity S cm ⁻¹
38 EC/33 PC/21 PAN/8 LiClO ₄	1.7×10^{-3}
62 EC/33 PC/16 PAN/PEGDA 8/LiClO ₄	1.2×10^{-3}
68 PC/16 PAN 16 LiClO ₄	8.6×10^{-4}
61 EC/13.2 PC 20.6 PAN/5.2 LiCF ₃ SO ₃	1.1×10^{-3}
61 EC/13.2 PC 20.6 PAN/LiBF ₄	0.3×10^{-3}
61 EC/13.2 PC 20.6 PAN/5.2 LiAsF ₆	0.77×10^{-3}
64.1 EC/13.8 PC/16.6 PAN/5.5 LN(SO ₂ CF ₃) ₂	0.74×10^{-3}
68 EC/15 PC/3 PEGDA/14 LiClO ₄	4×10^{-3}
24 EC/21 PC/10 Tetraglyme/27 PVP/18 LiClO ₄	8.0×10^{-4}
35 EC/30 PC/25 PVP/11 LCF ₃ SO ₃	4.0×10^{-4}
31 EC/26 PC/32 PVP/11 LCF ₃ SO ₃	2.4×10^{-4}
54 PC/35 PVP/11 LiCF ₃ SO ₃	1.5×10^{-4}
55 w/o MEEP/45 w/o PEO-[LiN(SO ₂ CF ₃) ₂] _{0.13}	6.7×10^{-5}
MEEP-[LiN(SO ₂ CF ₃) ₂] _{0.25}	6.5×10^{-5}
PEO-(LiClO ₄) _{0.13}	3.9×10^{-9}

38 EC/33 PC/21 PAN/8 LiClO₄ indicates that this polymer includes EC, PC, PAN, and LiClO₄ in weight ratio of 38:33:21:8 (reproduced with permission from "Application of Electroactive Polymers," B. Scrosati (ed.), Chapman & Hall, London (1993) [74]).

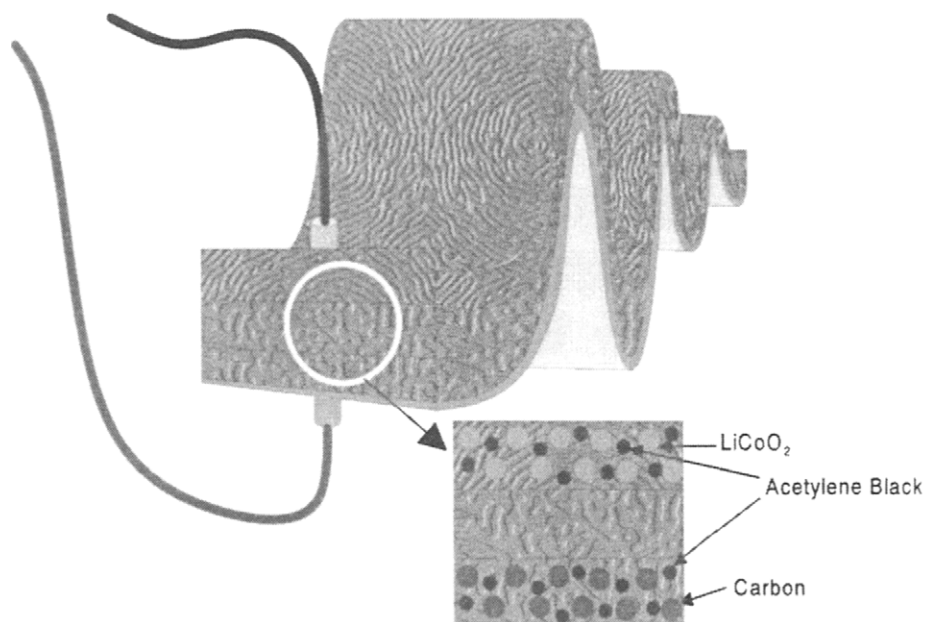


Fig. 20. Schematic illustration of polymer battery with LiCoO_2 cathode, carbon anode and polymer electrolyte.

a high mechanical strength of the positive and negative sheets and a high conductivity of agglomerate of active and conducting materials. The polymer electrolyte film was sandwiched by the positive and negative sheets to construct polymer batteries. When gel electrolyte was used as the electrolyte, the similar structure is adopted for manufacturing of polymer batteries. In those batteries, some problems are generated from interface properties. Figure 21 shows a schematic illustration for interfaces between solid polymer or gel electrolyte and active materials [75]. A part of polymer contacts well with active materials, but the other part loses contact with active materials. This contact problem leads to a low uniformity of current distribution in rechargeable polymer battery systems, giving rise to a difficulty for realizing a high performance (low polarization) and a high utilization of active materials. When lithium metal is used as anode material, the diversity in current distribution causes the dendritic lithium deposition during charging process of the battery which is a main problem for lithium metal anode as discussed above. In order to obtain a good contact between polymer electrolyte (or gel electrolyte) and active materials, a nature of polymer electrolyte is very important. Recently, an effect of polymers used in gel electrolytes has been investigated to control the interfacial problem of polymer batteries. For example, polyvinylidene fluorides have been used as a network polymer of gel electrolyte [76]. In this case, the interfacial problem with lithium metal anode is fairly improved to provide a high performance of polymer batteries. The most interesting point for this polymer, a

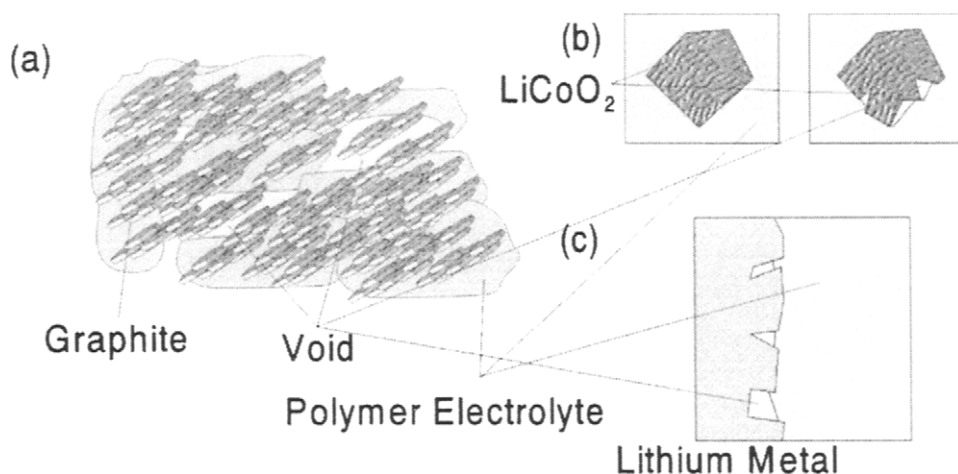


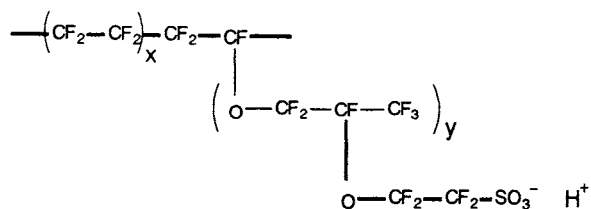
Fig. 21. Contact between active materials and polymer electrolyte, (a) graphite, (b) LiCoO_2 , and (c) lithium metal.

part of C—H bonds is converted to C—F bonds that are reactive with lithium metal. This may provide a good effect on the suitable formation of interface between lithium metal anode and polymer electrolyte. Various alternative polymers of polyvinylidene fluoride can be prepared. Such polymers may realize a better performance of rechargeable lithium battery. Therefore, it can be concluded that the preparation of various fluorinated polymers is one of important technology for producing high reliable rechargeable polymer batteries.

16. 3 Fuel cell

Polymer electrolytes have also been used in fuel cell field, as a novel electrolyte system providing high current densities for electric vehicles, load leveling systems, and electric power plant [77–83]. The most famous polymer is Nafion[®] produced by DuPont Chemical Co. The chemical structure of Nafion[®] is very unique as shown in Fig. 22. The main polymer chain is a fluorinated ether group with side chains, the end of which consists of ion exchange groups. The main chain is of course very hydrophobic, but the side chain is hydrophilic. This opposite nature causes an interesting structure of Nafion[®], which is regarded as an ion channel. In polymer electrolyte fuel cells, the Nafion[®] is used as an electrolyte membrane. At cathode and anode, oxygen and hydrogen are reduced and oxidized to form H_2O . The cell configuration and reactions for polymer electrolyte fuel cell (PEFC) are schematically illustrated in Fig. 23. Carbon with Pt catalyst is attached at both sides of perfluorinated ion exchange membrane. Hydrogen and air go through the fuel cell, in which the electrochemical reactions take place. At cathode, oxygen in air is reduced to O^{2-} . At anode, hydrogen is oxidized to H^+ . H^+ migrates in the ion

Nafion



Flemion

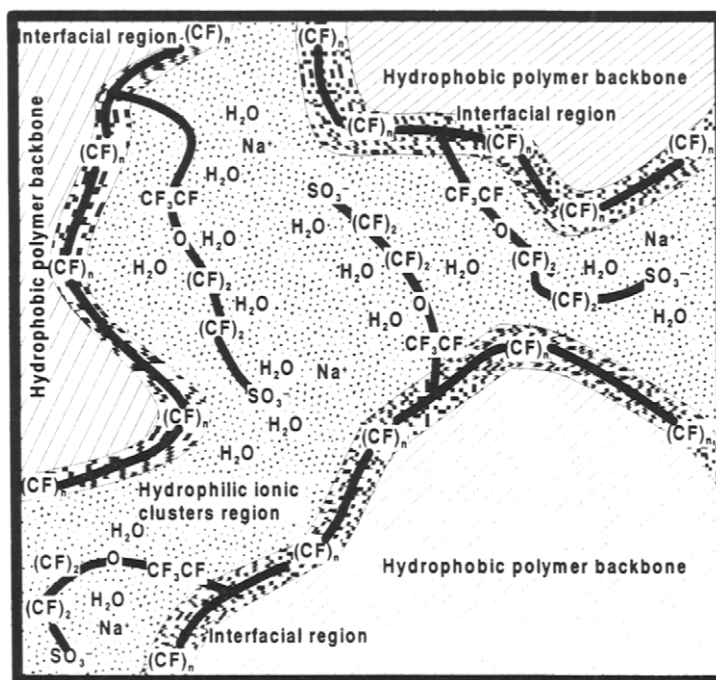
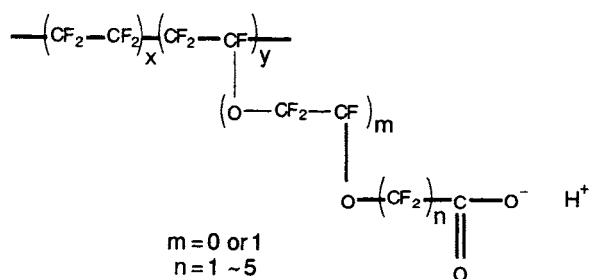


Fig. 22. Chemical structure of Nafion[®] and schematic illustration for microphase separation in Nafion[®] membrane.

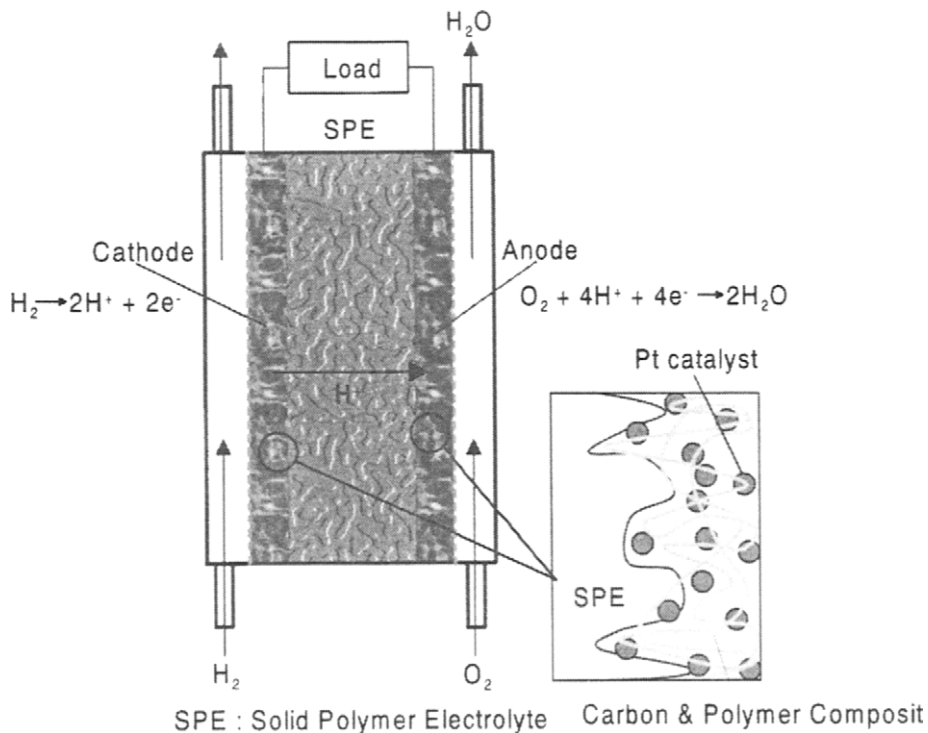


Fig. 23. Schematic illustrations for solid polymer electrolyte fuel cell and composite electrode with Pt catalyst, carbon conducting material, and binding polymer material.

exchange membrane and reaches to cathode. O^{2-} and two H^+ are combined to form H_2O . These electrochemical reactions occur at a three-phase boundary region of electrode, electrolyte, and gas. This region is illustrated as shown in Fig. 24. Polymer electrolyte works as a network to produce such a three-phase boundary [84–88]. Therefore, the structure and chemical composition of the exchange membrane is very important to keep the effective reaction interface region. For example, H_2O is formed at a cathode region and accumulated at a reaction site. This H_2O should be removed from the cathode immediately, otherwise the three-phase boundary is covered with H_2O to lose the high catalytic activity for the electrochemical reduction of O_2 . Therefore, interaction between H_2O and polymer electrolyte must be controlled to avoid such a process failure [89,90]. For this purpose, the fluorocarbon chain involved in solid polymer electrolyte plays an important role. Another good characteristic of solid polymer electrolyte is a solubility of oxygen [91,92]. In solid polymer fuel cells, the oxygen reduction is the slowest process, which induces a large polarization of the cell. In order to accelerate this process, the concentration of oxygen near the electrode should be increased by controlling the circumstance of the three-phase boundary region at the cathode, where the fluorocarbon chain also works as an effective component, because of high solubility

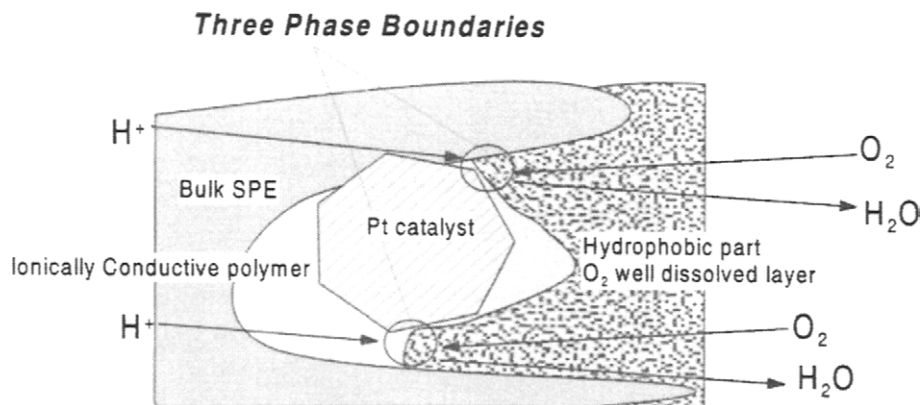


Fig. 24. Schematic illustration for three phase boundary for oxygen reduction in solid polymer electrolyte.

of oxygen in C—F compounds. This effect is so-called “dry cave effect” [93]. In this way, fluorocarbon chains in solid polymer electrolyte have an important effect on fuel cell construction and electrochemical reactions.

16.4 Summary

In this chapter, the importance of fluorine chemistry for electrochemical energy conversion and storage is demonstrated. Several key components in electrochemical energy conversion systems contain fluorine, which is due to the unique characteristics of fluorine. In the case of energy conversion systems, more severe circumstances will be generated to obtain high performance of the system, that is more oxidative and reductive situations may be used to realize a high energy density and a high energy conversion efficiency. Therefore, fluorine chemistry would become more and more important and attractive in energy conversion systems developed in near future.

References

- [1] J.P. Gabano, In: *Lithium Batteries*, J.P. Gabano (Eds.), Academic Press, London, 1983, Chapter 1.
- [2] Z. Takehara, K. Kanamura, *Electrochim. Acta*, 38 (1993) 1169.
- [3] J.R. Dahn, A.K. Sleight, H. Shi, B.M. Way, W.J. Weydanz, J.N. Reimers, Q. Zhong, U. von Sacken, In: *Lithium Batteries—New Materials, Developments and Perspectives*, G. Pistoia (Ed.), Elsevier Science, Amsterdam, 1994, Chapter 1.
- [4] S. Megahed, B. Scrosati, *Interface*, 4 (1995) 34.
- [5] K. Tozawa, N. Nagaura, *Prog. Batt. Solar Cells*, 9 (1990) 209.
- [6] D. Fauteux, R. Koksang, *J. Applied. Electrochem.*, 23 (1993) 1.
- [7] K. Kanamura, *Denki Kagaku*, 65 (1997) 722.

- [8] R. Fong, U. von Sacken, J.R. Dahn, *J. Electrochem. Soc.*, 137 (1990) 2009.
- [9] N. Imanishi, H. Kashiwagi, T. Ichikawa, Y. Takeda, O. Yamamoto, M. Inagaki, *J. Electrochem. Soc.*, 140 (1993) 315.
- [10] M. Ue, S. Mori, 95 Asian Conference of Electrochemistry, 3A-5, Suita, Japan, 1995.
- [11] M. Ue, *J. Electrochem. Soc.*, 141 (1994) 3336.
- [12] M. Ue, S. Mori, *J. Electrochem. Soc.*, 142 (1995) 2577.
- [13] Y. Mtsuda, M. Morita, F. Tachihara, *Bull. Chem. Soc. Jpn*, 59 (1986) 1967.
- [14] S. Tobishima, T. Oakada, *Electrochim. Acta*, 30 (1985) 1715.
- [15] L.G. Scanlon Jr, In: *Batteries and Fuel Cells for Stationary and Electric Vehicle Application*, A.R. Landgrebe, Z. Takehara (Eds.), PV 93-8, The Electrochemical Society Proceedings Series, Pennington, NJ, 1993, p. 36.
- [16] A.N. Dey, *Thin Solid Films*, 43 (1977) 131.
- [17] G. Nazri, R.H. Muller, *J. Electrochem. Soc.*, 132 (1985) 2050.
- [18] D. Aurbach, M.L. Daroux, P. Faguy, E. Yeager, *J. Electrochem. Soc.*, 134 (1987) 1611.
- [19] K. Kanamura, H. Tamura, Z. Takehara, *J. Electroanal. Chem.*, 333 (1992) 127.
- [20] K. Kanamura, H. Takezawa, S. Shiraishi, Z. Takehara, *J. Electrochem. Soc.*, 144 (1997) 1900.
- [21] V.R. Koch, *J. Electrochem. Soc.*, 126 (1979) 181.
- [22] D. Aurbach, M. Daroux, P.W. Faguy, E. Yeager, *J. Electrochem. Soc.*, 135 (1988) 1863.
- [23] D. Aurbach, O. Chusid (Youngman), *J. Electrochem. Soc.*, 140 (1993) L1.
- [24] K. Kanamura, H. Tamura, S. Shiraishi, Z. Takehara, *J. Electroanal. Chem.*, 394 (1995) 49.
- [25] M. Odziemkowski, M. Krell, D.E. Irish, *J. Electrochem. Soc.*, 139 (1992) 3052.
- [26] Y. Malik, D. Aurbach, P. Dan, A. Meitav, *J. Electroanal. Chem.*, 282 (1990) 73.
- [27] D. Aurbach, *J. Electrochem. Soc.*, 136 (1989) 1606.
- [28] D. Aurbach, O. Youngman, Y. Gofer, A. Meitav, *Electrochim. Acta*, 35 (1990) 625.
- [29] Y.E. Ely, D. Aurbach, *Langmuir*, 8 (1992) 1845.
- [30] D.W. Sharp, In: *Advances in Fluorine Chem.*, Vol. 1, M. Stacey, J.C. Tatlow, A.G. Sharpe (Eds.), Butterworths Scientific Pub., London, 1960, p. 69.
- [31] U. von Sacken, J.R. Dahn, *Extended Abstracts of Electrochemical Society Fall Meeting*, Abstract No.54, The Electrochem. Soc. Inc., New Jersey, 1990, p. 87.
- [32] M.A. Gee, F.C. Laman, *J. Electrochem. Soc.*, 140 (1993) L53.
- [33] F. C. Laman, Y. Sakurai, T. Hirai, J. Yamaki, S. Tobishima, *Extended Abstract of Sixth International Meeting on Lithium Batteries*, III-A-01 (1992).
- [34] D. Fouchard, L. Xie, W. Ebner, S. Megahead, *Rechargeable Lithium and Lithium Ion Batteries*, 94-28, The Electrochem. Soc. Inc., New Jersey, 1994, p. 348.
- [35] P. Novak, P.A. Christensen, T. Iwashita, W. Vielstich, *J. Electroanal. Chem.*, 263 (1989) 37.
- [36] B. Rasch, E. Cattaneo, P. Novak, W. Vielstich, *Electrochim. Acta.*, 36 (1991) 1397.
- [37] G. Eggert, J. Heitbaum, *Electrochim. Acta.*, 31 (1986) 1443.
- [38] G. Tourillon, J.E. Dubois, P.C. Lacaze, *J. Electroanal. Chem.*, 100 (1979) 247.
- [39] K.M. Abraham, *J. Electrochem. Soc.*, 137 (1990) 1856.
- [40] A.H. Maki, D.H. Geske, *J. Chem. Phys.*, 30 (1959) 1356.
- [41] S.A. Calmbell, C. Bowes, R.S. McMillan, *J. Electrochem. Soc.*, 284 (1990) 195,
- [42] M. Fleischmann, D. Pletcher, *Tetrahedron Lett.*, 60 (1968) 6255.
- [43] F. Ossola, G. Pistoia, R. Seeber, P. Ugo, *Electrochim. Acta*, 33 (1988) 47,
- [44] K. Kanamura, S. Toriyama, S. Shiraishi, Z. Takehara, *J. Electrochem. Soc.*, 142 (1995) 1383.

- [45] K. Kanamura, S. Toriyama, S. Shiraishi, Z. Takehara, *J. Electrochem. Soc.*, 143 (1996) 2548.
- [46] K. Kanamura, T. Okagawa, Z. Takehara, *J. Power Sources*, 57 (1995) 119.
- [47] K. Kanamura, S. Toriyama, S. Shiraishi, M. Ohashi, Z. Takehara, *J. Electroanal. Chem.*, 419 (1996) 77.
- [48] F. Kita, A. Kawakami, T. Sonoda, H. Kobayashi, *J. Power Sources*, 68 (1997) 307.
- [49] F. Kita, A. Kawakami, T. Sonoda, H. Kobayashi, *Battery Technology*, 6 (1994) 45.
- [50] F. Kita, A. Kawakami, T. Sonoda, *Denki Kagaku*, 65 (1997) 909.
- [51] T. Sonoda, J. Nie, H. Kobayashi, F. Kita, A. Kawakami, *Battery Technology*, 10 (1998) 106.
- [52] K. Momota, *Battery Technology*, 8 (1996) 108.
- [53] V.N. Plakhotnik, V.B. Tul'chinskii, V.K. Steba, *Russ. Inorg. Chem.*, 31 (1976) 451.
- [54] K. Murakami, F. Kita, A. Kawakami, Extended Abstract of 61st Electrochemical Society Meeting of Japan, Sendai, Japan, 1994, p. 44.
- [55] L.J. Krause, W. Lamanna, J. Summerfield, M. Engle, G. Korba, R. Loch, R. Atanasoski, *J. Power Sources*, 68 (1997) 320.
- [56] K. Kanamura, *Battery Technology*, 10 (1998) 85.
- [57] K. Kanamura, *J. Power Sources*, to be submitted.
- [58] R.D. Rauch, S.B. Brummer, *Electrochim. Acta*, 22 (1977) 75.
- [59] V.R. Koch, *J. Power Sources*, 6 (1981) 357.
- [60] I. Yoshimatsu, T. Hirai, J. Yamaki, *J. Electrochem. Soc.*, 135 (1988) 2422.
- [61] M. Arakawa, S. Tobishima, Y. Nemoto, M. Ichimura, J. Yamaki, *J. Power Sources*, 43-44 (1993) 27.
- [62] E. Peled, *J. Electrochem. Soc.*, 126 (1979) 2047.
- [63] K. Kanamura, H. Tamura, S. Shiraishi, Z. Takehara, *J. Electrochem. Soc.*, 142 (1995) 340.
- [64] K. Kanamura, H. Tamura, S. Shiraishi, Z. Takehara, *Electrochim. Acta*, 40 (1995) 913.
- [65] K. Kanamura, S. Shiraishi, Z. Takehara, *Chem. Lett.*, 1995 (1995) 209.
- [66] K. Kanamura, S. Shiraishi, Z. Takehara, *J. Electrochem. Soc.*, 143 (1996) 2187.
- [67] S. Shiraishi, K. Kanamura, Z. Takehara, *Langmuir*, 13 (1997) 3542.
- [68] S. Shiraishi, K. Kanamura, Z. Takehara, *J. Electrochem. Soc.*, in press.
- [69] K. Momota, M. Morita, Y. Mtauda, *Electrochim. Acta*, 38 (1993) 1123.
- [70] S. Shiraishi, K. Kanamura, Z. Takehara, *New Trends in Pure and Applied Chemistry*, 1 (1997) 45.
- [71] K. Kanamura, S. Shiraishi, Z. Takehara, *J. Fluorine Chemistry*, 87 (1998) 235.
- [72] A. Vallee, S. Besner, J. Prud'homme, *Electrochim. Acta*, 37 (1992) 1579.
- [73] S. Sylla, J.Y. Sanchez, M. Armand, *Electrochim. Acta*, 37 (1992) 1699.
- [74] K.M. Abraham, In: *Application of Electroactive Polymers*, B. Scrosati (Ed.), Chapman & Hall, London, 1993, pp. 75-112.
- [75] E. Peled, D. Golodnitsky, G. Ardel, C. Menachem, D. Bar Tow, V. Eshkenazy, *Materials Research Society Symposium Proceedings*, 393 (1995) 209.
- [76] Y. Uchida, M. Kitahara, S. Komaba, T. Osaka, Extended Abstract of The 38th Battery Symposium in Japan, 1997, p. 271.
- [77] How to be fair with CARB's ZEV mandate?, Interlink Report, (June 2, 1995).
- [78] P.G. Patil, The role of alternative fuels in the new generation of vehicles, SAE Paper No. 52379 (1995).
- [79] H. Creveling, *Proc. Automot. Tech. Dev. Contract. Coord. Meet.* 1992, 1993, pp. 485-492.
- [80] P. Howard, C. Greenhill, *SAE Tech. Pap. Ser.*, No. 931817, 1993, pp. 113-120.

- [81] H. Takenaka, et al., Proc. Int. Fuel Cell Conf. Feb., 3–6, 1992, pp. 414–420.
- [82] S. Ogino, Y. Kimura, Fuel Cell Powered Electric Vehicle 13th International Electric Vehicle, (October 1996), Vol. 1, Symposium (EVS 13), Osaka, Japan, 1996, pp. 671–674.
- [83] R. Laidley, Lt(N) T Wagner, Trans. Inst. Mar. Eng. C. Conf., Vol. 104, No. 2, 1992, pp. 245–251.
- [84] J.T. Hinatsu, M. Mizuhata, H. Takenaka, J. Electrochem. Soc., 141 (1994) 1493.
- [85] S. Gottesfeld, C. Lopez, J. Valerio, T. Zawodzinski, J. Electrochem. Soc., 140, (1993) 1981.
- [86] H.L. Yeager, Z. Twardowski, L.M. Clarke, J. Electrochem Soc., 129 (1982) 324.
- [87] R.B. Moore, C. Martin, Macromolecules, 22 (1989) 3594.
- [88] P.C. Rieke, N.E. Vanderborgh, J. Mem. Sci., 32 (1987) 313.
- [89] K. Yasuda, M. Mizuhata, Battery Technology, 10 (1998) 153.
- [90] K. Kawahara, T. Haga T. Suzuki, T. Asaoka, Battery Technology, 10 (1998) 159.
- [91] S. Gottesfeld, I.D. Raistrick, S. Srinivasan, J. Electrochem. Soc., 134 (1987) 1455.
- [92] D.R. Lawson, L.D. Whiteley, C.R. Martin, M.N. Szentirmay, J.I. Song, J. Electrochem. Soc., 135 (1988) 2247.
- [93] M. Razaq, A. Razaq, E. Yeager, D.D. DesMarteau, S. Singh, J. Electrochem. Soc., 136 (1989) 385.

CHAPTER 17

Fluorinated Fullerenes

Hidekazu Touhara and Fujio Okino

Department of Chemistry, Faculty of Textile Science and Technology, Shinshu University, Ueda 386-8567, Japan

17.1 Introduction

The chemistry of fullerenes, the third form of carbon after graphite and diamond, with fluorine is essentially limited to the formation of C—F covalent bonds. This makes a contrast with the fullerene/alkali metal system where fullerenes act as electron acceptors forming “fulleride” ions. This difference, of course, is attributed to the difference between fluorine and alkali metals. Graphite, another form of carbon, being amphoteric in its chemical properties, can readily form ionic intercalation compounds with donors and acceptors, whereas ionic compounds of C_{60} with cationic C_{60} , i.e. C_{60}^+ , are barely known. This difference is attributed to the electron accepting character of C_{60} rather than donating. Graphite fluoride, $(CF)_n$ with covalent C—F bonds, is formed under harsh conditions of 873–913 K, whereas fluorofullerenes $C_{60}F_x$ with covalent C—F bonds are formed relatively easily at room temperature to 573 K. These behavior differences are noteworthy since both fullerenes and graphite are made solely of carbon, and fullerenes are usually classified into carbon π conjugate system. The differences are mainly attributed to the difference in s–p hybridization of carbon atoms. The slight deviation from ideal sp^2 hybridization in C_{60} is significant enough to cause its electronic properties to differ from that of graphite. Once fluorinated, fluorinated fullerenes resemble graphite fluoride $(CF)_n$ in some aspects more than fullerenes resemble graphite. In a sense any deviation from pure planar sp^2 hybridization leads to the regime of three dimensions to which sp^3 belongs.

Since the knowledge of electronic structure is essential to the understanding of the chemical/electrochemical and physical behaviors of fullerenes and to their electrochemical applications, the electronic structures of molecular and solid C_{60} , and the changes in electronic structure upon fluorination are discussed extensively in this review. Emphasis is also placed on the selective syntheses of fluorinated fullerenes which are necessarily related to their molecular structures. The molecular structures have been essentially determined by NMR; determination of the molecu-

lar structures of fluorinated fullerenes by crystallographic method has been hindered by the spherical nature of fluorinated fullerenes, which results in rotational motion of the molecules even at low temperatures. It has also been hindered by the compound difficulty of forming single crystals of selectively synthesized fluorofullerenes. The difficulty in the selective syntheses lies in the non-regioselectivity of fluorination, which leads to the formation of a wide range of fluorinated fullerenes. Crystal structures of some of the selectively synthesized fluorofullerenes, however, have been determined and they are explained in detail including their phase transitions.

Several reviews on fluorinated fullerenes are available [1–4], and some of the sections of this review were written based on them including new and more detailed data. The authors wish that this review serves a reader as a compact but comprehensive source of information on the subjects dealt in this review.

17.2 Electronic structures and fluorination

17.2.1 *Electronic structures of molecular and solid C₆₀*

Although each carbon atom on fullerene C₆₀ molecule has essentially three electrons with sp² hybridization for σ -bonding and one 2p_z electron for π -bonding, the electronic structure and properties of C₆₀ are significantly different from those of other conjugated carbon π electron systems such as aromatic hydrocarbons and carbon materials. The characteristic aspect of C₆₀ electronic structure is the rehybridization of the carbon π atomic orbitals as a result of the curvature that is imposed on the conjugated carbon atoms by the spherical shape of the molecule [5]. The curvature in the conjugated C₆₀ molecule causes the sp² σ -bonds at the carbon atom to deviate from planarity; the hybridization of 2s and 2p orbitals is not pure sp² and, hence, the π -orbitals are no longer of pure p-orbital character, but include a finite 2s component [5,6]. C₆₀ molecule has, therefore, an intermediate hybridization between sp² and sp³, and the π -orbital axis vector theory analyses have shown that the average σ -bond hybridization for C₆₀ is sp^{2.28} and that its π -orbital fractional character is 0.081–0.085 [7].

Ultraviolet photoelectron spectroscopy (UPS) and photodetachment measurements have given an electron affinity E_a of 2.7 eV for the C₆₀ molecule [8,9]. The distorted sp² hybridization together with the topological character of C₆₀ accounts for the considerably larger E_a than those of planar conjugated hydrocarbons, and gives C₆₀ a wide range of abilities to act as an electron acceptor and a strong electrophile.

As for the ability of C₆₀ to function as an electron donor, it would be difficult to obtain acceptor-type fullerene salts or charge transfer complexes because of the higher ionization potential I_p of 7.6 eV [10] for the molecule. In fact, the electrochemical oxidation of C₆₀ in solutions is irreversible [11,12], in contrast to the reversible, six one-electron cathodic reduction in solutions [13,14].

Many studies and publications have been devoted to the electronic band structure of fullerenes in the solid state and subsequently several reviews have been published on this subject [15,16]. Here, a schematic diagram of energy levels relative to

the vacuum level for gaseous and solid state C_{60} is shown in Fig. 1 [3]. The lowest unoccupied molecular orbitals (LUMO) and the highest occupied molecular orbitals (HOMO) of C_{60} are triply and five-fold degenerate, respectively. In the condensed phase, the LUMO and HOMO degenerate orbitals each form LUMO-derived π^* and HOMO-derived π bands, respectively. The LUMO and the HOMO energies in Fig. 1 correspond to the experimentally observed E_a value [10] and ionization threshold energy I_{th} [17], respectively. For solid state C_{60} , UPS measurements by Sato et al. [18] gave $I_{th} = 6.2$ eV. Takahashi et al. [19] reported $I_{th} = 1.9$ eV relative to the Fermi level E_F . Benning et al. [20] reported the HOMO–LUMO separation of 2.6 eV from UPS and inverse photoelectron spectroscopy (IPES) measurements. From these reports, the energies of the LUMO, the E_F and the HOMO of solid state C_{60} are obtained to be 3.6 eV, 4.3 eV and 6.2 eV, respectively [21]. It should be noted that the energies of the LUMO and the HOMO are shifted in going from the vapor to the solid phase by 0.95 and 1.4 eV, respectively, due to the polarization of the surrounding molecules. The Fermi level is located closer to the bottom of the conduction band than to the top of the valence band in the energy gap, indicating that crystalline C_{60} is an n-type semiconductor.

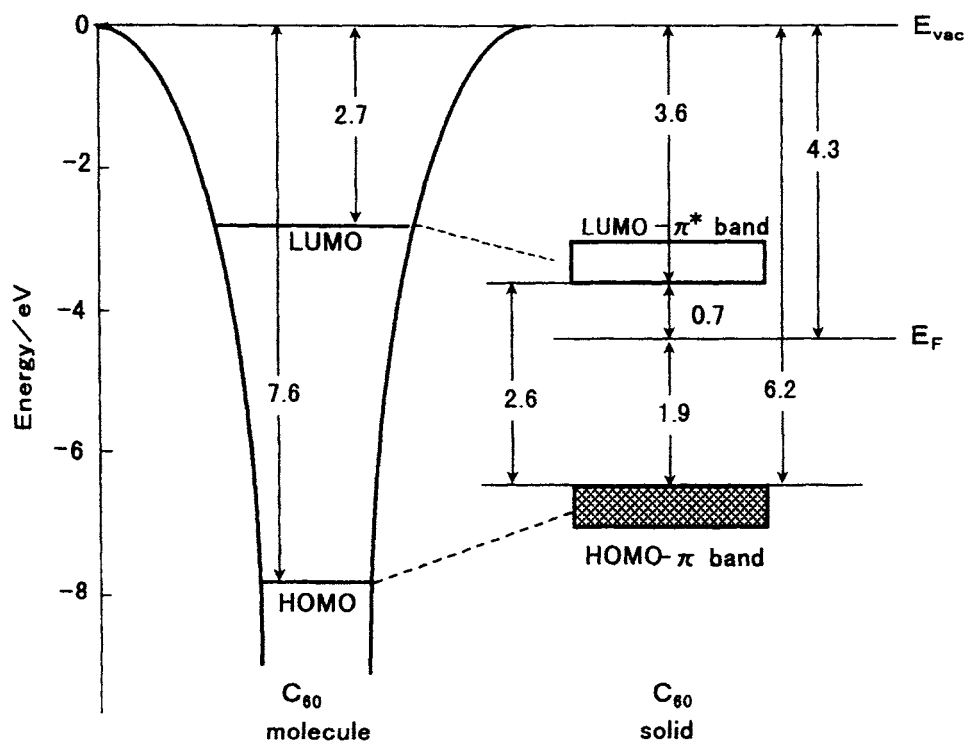


Fig. 1. Schematic diagram of energy levels for molecular and solid C_{60} (adapted by permission of Pergamon from Comprehensive Supramolecular Chemistry, Vol. 7, 1996 p. 29 [3]).

17.2.2 Fluorination of fullerenes C_{60} and C_{70}

The electronic state and properties of solid state C_{60} described above lead to very characteristic interactions and reactions of C_{60} with fluorine and fluorides. Although the E_F value (4.3 eV) of crystalline C_{60} is comparable to that (4.4 eV) of semi-metal graphite, the intercalation or doping behaviors of these materials are quite different from each other. Contrary to the great facility in preparations of fluorine- or fluoride-graphite intercalation compounds, oxidative fluorine or fluoride intercalation of C_{60} has not yet been established, and only preliminary results are available. The doping of C_{60} with SbF_5 and AsF_5 are reported [22,23]. SbF_5 - and AsF_5 -doped C_{60} were green and semiconducting. Preliminary results in our laboratory also indicate that C_{60} can be doped with AsF_6^- by the reaction of AsF_5/F_2 , and with F^- electrochemically using $(CH_3)_4NF \cdot 4HF$ as an electrolyte, both yielding blue compounds. These results suggest that C_{60} acceptor compounds could be prepared using a strong Lewis acid with a high electron affinity or electrochemical method.

By contrast, owing probably to radical reaction and stronger C—F bonds, fullerenes easily react with elemental fluorine to give a variety of C—F covalent compounds, $C_{60}F_x$ and $C_{70}F_x$, with a wide range of composition. The extent of fluorination and the time necessary for completion of reaction strongly depend on fluorination temperature and the crystallinity of fullerenes. The mechanism of halogen addition has been ambiguous, though it is reasonable to assume that radicals are involved. Recently, based on the reaction of C_{60} in CCl_4 solution with interhalogen compound IF_5 , Taylor and coworkers have proposed that halogenation of fullerenes is a radical process [24].

Comprehensive reviews have recently been published on fullerene fluorinations [1–4]. Direct fluorinations of C_{60} have so far been carried out using elemental fluorine at the temperatures ranging from room temperature up to 588 K. The fluorination even at room temperature yields $C_{60}F_{33-44}$ [1,2]. The higher temperature fluorinations up to 548 K give $C_{60}F_{44-48}$ with abundant species $C_{60}F_{46}$ [25,26], and $C_{60}F_{48}$ is the most highly fluorinated C_{60} -species so far obtained in bulk amounts [25,27,28]. Hyperfluorinated fullerenes $C_{60}F_{2n}$ ($n > 30$) indicates the rupture of C_{60} skeletal bonds [27].

Although the formation of fully fluorinated fullerene C_{60} was firstly reported in 1991 based on the sharp singlet of ^{19}F NMR spectrum of the product in tetrahydrofuran solution [29], the preparation in macroamount has not been confirmed in the late 1990s. The fully fluorinated $C_{60}F_{60}$ has been detected only in mass spectra of the products obtained by direct fluorination with elemental fluorine [30,31].

As for fluorination of C_{70} fullerene, it has been demonstrated that pure C_{70} is fluorinated more rapidly than C_{60} , because of the less dense molecular packing in the former [2]. Fluorinations at 343 and 473 K give $C_{70}F_{48}$ [32] and $C_{70}F_{58}$ [33] as the highest fluorinated species, respectively. The heat treatment at 663 K of the mixture of C_{70} and MnF_3 powders yields $C_{70}F_{36/38/40}$ with the most abundant species $C_{70}F_{38}$ [34].

By the direct fluorination with elemental fluorine, it is still difficult to prepare pure compounds $C_{60}F_x$ and $C_{70}F_x$ of specific fluorine content because the reaction between fluorine gas and solid state C_{60} and C_{70} proceeds under heterogeneous conditions and, therefore, lacks control. Attempts to prepare stoichiometrically pure compounds have become successful using solid phase reactions between fullerenes and metal fluorides. These are described in the next section. It has been unsuccessful so far, but efforts are being made to produce fluorinated fullerenes $C_{60}F_x$ of lower fluorine content ($x < 18$) [24].

17.3 Selective syntheses and molecular structures [4]

Contrary to the theoretical predictions [35,36] that perfluorofullerene, $C_{60}F_{60}$, will be stable and observable in the laboratory, and to the initial claim of the synthesis of $C_{60}F_{60}$ [29], perfluorinated C_{60} with intact skeleton has not been identified yet. Up until the late 1990s, $C_{60}F_{48}$ seems to be the most highly fluorinated C_{60} with intact skeleton [27,28]. Figure 2 shows the mass spectrum of the product of fluorination C_{60} —NaF mixture at 523 K followed by fluorination with

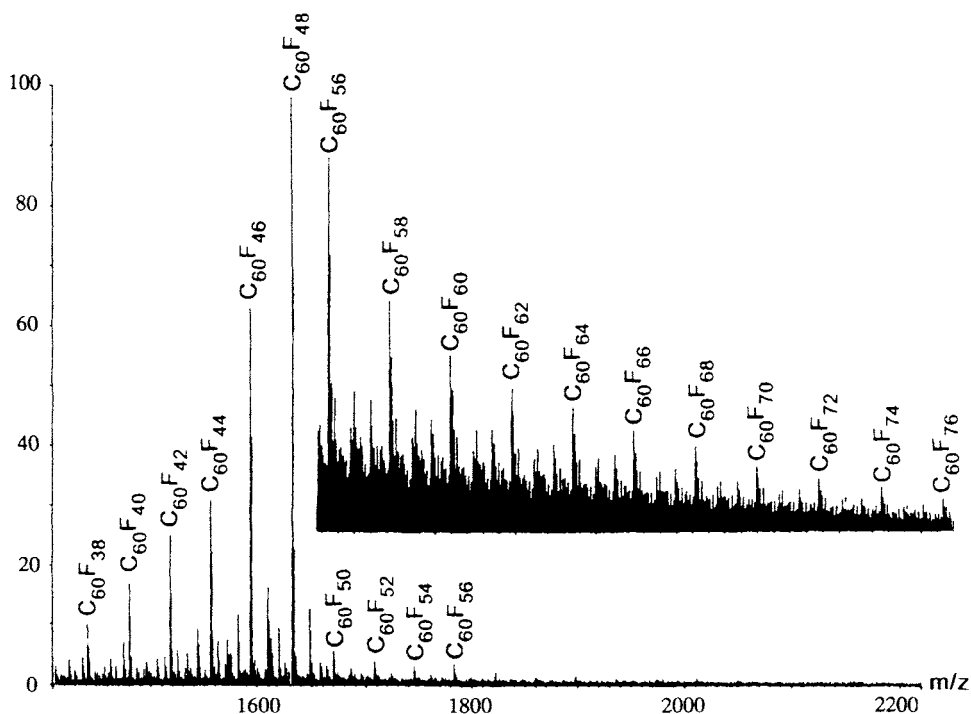


Fig. 2. EI mass spectrum of the product of fluorination C_{60} —NaF mixture at 523 K followed by fluorination with UV-irradiation at 358 K. The intensity of $C_{60}F_{60}^{++}$ is $\sim 1.3\%$ of $C_{60}F_{48}$ (reproduced by permission from J. Am. Chem. Soc., 115 (1993) 5886. Copyright 1993 American Chemical Society [27]).

UV-irradiation at 358 K, indicating $C_{60}F_{48}$ to be the major constituent with the abrupt intensity decline after $C_{60}F_{48}$ and the smooth decrease thereafter continuing beyond $C_{60}F_{76}$ [27]. This strongly suggests that $C_{60}F_{\geq 50}$ has a broken cage. If $C_{60}F_{60}$ maintained the intact skeleton, there should be a disruption in peak intensity between $C_{60}F_{60}$ and $C_{60}F_{62}$, since the latter necessarily has a broken cage.

Selective synthesis of $C_{60}F_x$ of specific fluorine content has encountered great difficulty, because fluorination usually proceeds under heterogeneous conditions and, therefore, lacks control. Up until the late 1990s, three stoichiometrical compounds, $C_{60}F_{48}$, $C_{60}F_{36}$ and $C_{60}F_{18}$, have been selectively synthesized and structurally characterized. Figure 3 summarizes their synthetic methods together with the formation of ca $C_{60}F_{46}$ single crystal described in Sec. 17.4.

17.3.1 Selective synthesis and molecular structure of $C_{60}F_{48}$

$C_{60}F_{48}$ was the first fluorinated fullerene molecule with specific fluorine content to be isolated and characterized [28,37].

A finely ground mixture of C_{60} and NaF was placed in a quartz tube and fluorinated in a flow of F_2 at 523 K for 20 h [28]. The sample was extracted with $CFCl_3$, mixed with NaF, and fluorinated additionally for 30 h at 548 K. Extraction with $CFCl_3$ gave fluorofullerenes in 56% chemical yield, of which >60% proved to be a single structural isomer (two chiral forms of D_3 symmetry) by ^{19}F NMR spectrum shown in Fig. 4(a-1) [28]. The structures and Schlegel diagrams of the $C_{60}F_{48}$ enantiomer pair are shown in Figs. 5 and 6(a), respectively [28]. In the NMR figure, the lines between peaks indicate connectivities established by COSY

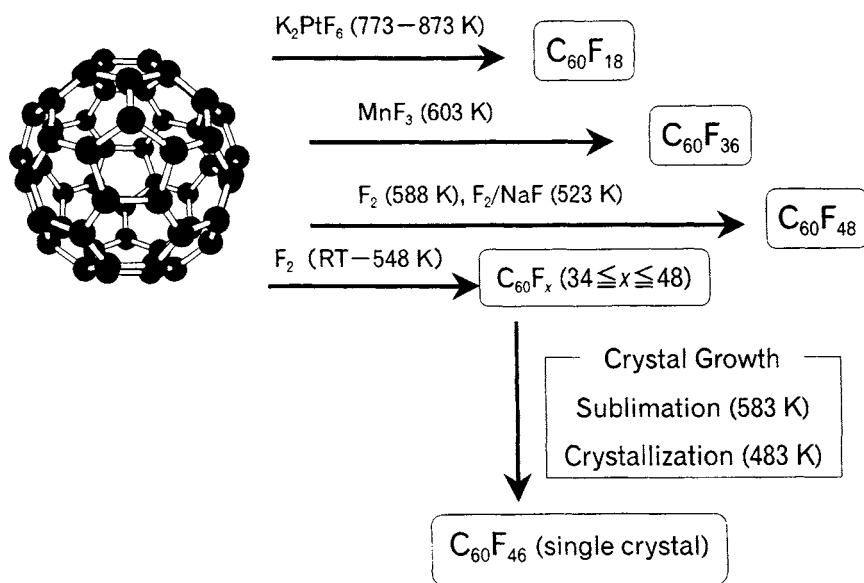


Fig. 3. Synthetic routes to $C_{60}F_{18}$, $C_{60}F_{36}$ and $C_{60}F_{48}$, and to the formation of ca $C_{60}F_{46}$ single crystal.

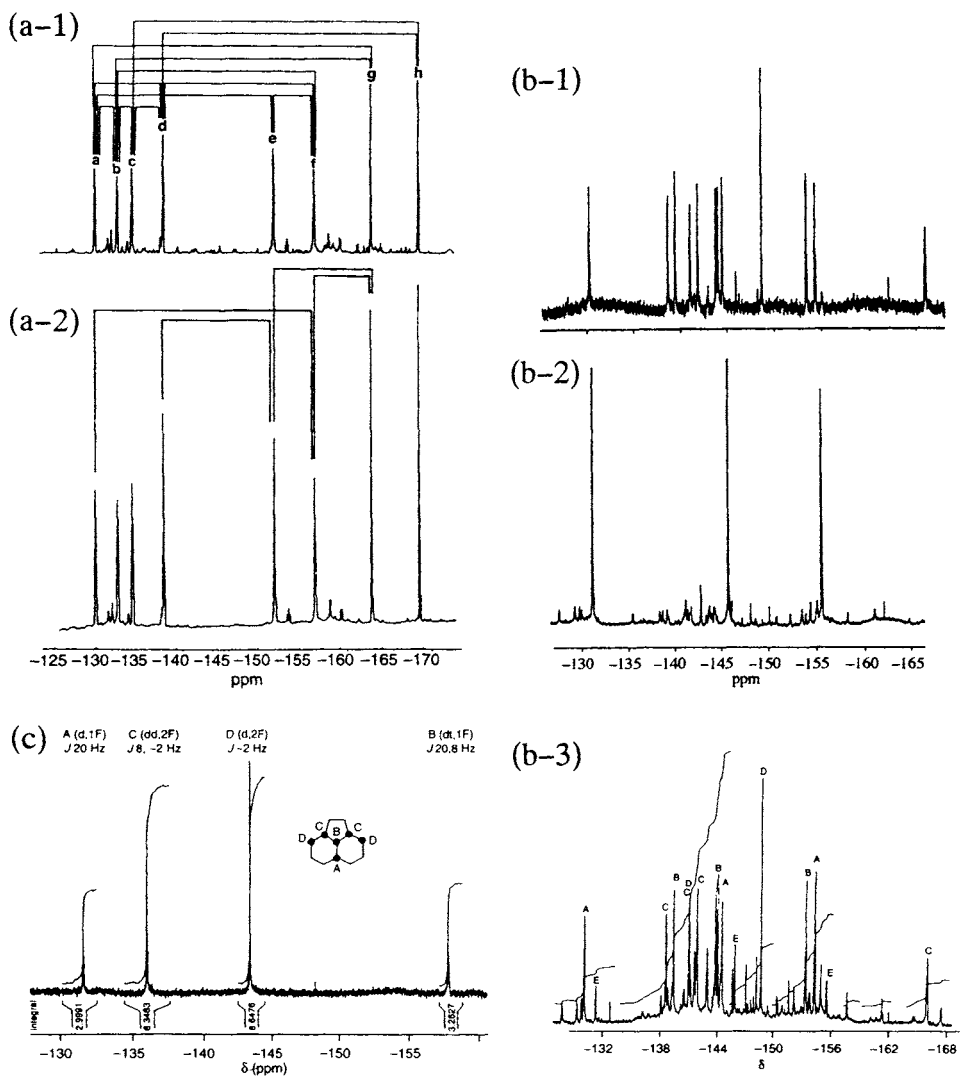


Fig. 4. ^{19}F NMR spectra of (a-1) and (a-2) $\text{C}_{60}\text{F}_{48}$, (b-1) $\text{C}_{60}\text{F}_{36}$ (C_3 isomer), (b-2) $\text{C}_{60}\text{F}_{36}$ (T isomer), (b-3) $\text{C}_{60}\text{F}_{36}$ (mixture of C_3 and T isomers) and (c) $\text{C}_{60}\text{F}_{18}$ ((a-1) reproduced with permission from J. Am. Chem. Soc., 116 (1994) 819 [28]; (a-2) reproduced with permission from J. Chem. Soc., Perkin Trans. 2, (1996) 2276 [37]; (b-1) and (b-2) reproduced with permission from J. Chem. Soc., Perkin Trans. 2, (1998) 651 [39]; (b-3) reproduced with permission from Chem. Commun., (1996) 530 [34]; (c) reproduced with permission from Chem. Commun., (1996) 2550 [42]).

experiments. However, of the eleven F—F 1,3 couplings predicted by the structure, only four couplings (a – b , a – d , b – c , c – d ; see Fig. 6(a) for F-atom designations) were observed, rendering the structure assignment less secure [4,37]. In this preparative method the role of NaF is not clear. However, NaF seems to play a role of disperser

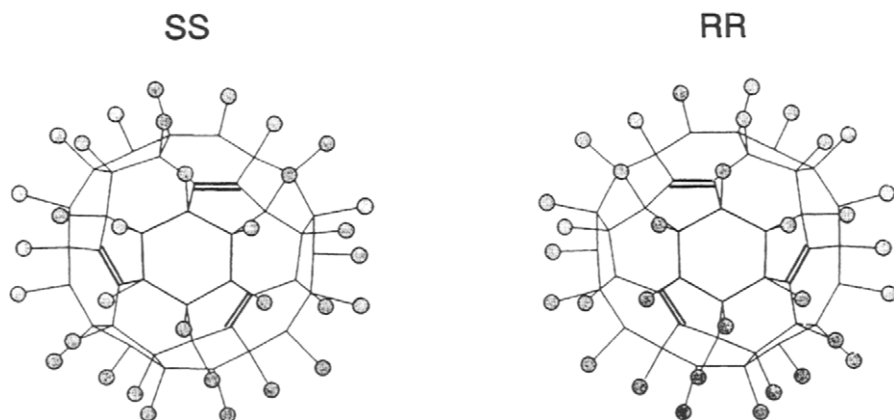


Fig. 5. Structure of the $C_{60}F_{48}$ enantiomer pair (reproduced with permission from J. Am. Chem. Soc., 116 (1994) 820 [28]).

of C_{60} and heat sink thus allowing a slower and more uniform fluorination than without NaF.

Boltalina et al. [37] fluorinated C_{60} with fluorine gas under increasingly vigorous consecutive conditions: (a) 343 K, 4 h; (b) a further 5 h at 493 K; (c) a further 11 h at 548 K, and (d) a further 3 h at 588 K. The electron ionization (EI) mass spectra for these samples are given in Fig. 7. The increasing extent of fluorination along this series is apparent. Sample (d) is $C_{60}F_{48}$ of high purity. Samples obtained by fluorination at 588 K for 16 h in a single run are essentially identical to sample (d). They were white and chemical analysis indicated the stoichiometric formula $C_{60}F_{48\pm 1}$. The field desorption (FD) mass spectrum for $C_{60}F_{48}$ is shown in Fig. 8(a) [38]. A strong peak of $C_{60}F_{48}$ at 1632 amu (atomic mass unit) is eminent. The IR spectrum shown in Fig. 9(a) has sharp bands at 1238, 1215, 1199, 1170, 1142, 1126, 771, 754, 724, 650 and 603 cm^{-1} , and is consistent with a single component [37]. Though not of a pure compound, shown in Fig. 9(d) for comparison is the IR spectrum for the product obtained by fluorination at 343 K, 4 h, whose mass spectrum is given in Fig. 7(a). It shows broad peaks typical of fluorofullerenes of mixed compositions and, probably, of mixed isomers for each $C_{60}F_x$ with specific fluorine content. The ^{19}F NMR spectrum for sample $C_{60}F_{48}$ using CDCl_3 as solvent is shown in Fig. 4(a-2) [37]. The 2D COSY spectrum shows the couplings $a-f$, $d-e$, $e-g$ and $f-g$ (see Fig. 6(a) for F-atom designations) in addition to the 4 couplings observed previously for the spectrum shown in Fig. 4(a-1), supporting the proposed structure. It is indeed remarkable that one enantiomer pair out of millions of possible isomers of $C_{60}F_{48}$ is obtained by a generally non-regioselective fluorination at elevated temperatures. It is also remarkable that a sample of this purity of specific fluorine content is obtained without separation by high performance liquid chromatography (HPLC). The formation of $C_{60}F_{48}$ by the reaction of C_{60} with F_2 at 588 K is likely to be thermodynamically controlled and this $C_{60}F_{48}$ enantiomer pair must be significantly, though slightly, more stable than the other $C_{60}F_{48}$ isomers and other $C_{60}F_x$ ($x < 48$).

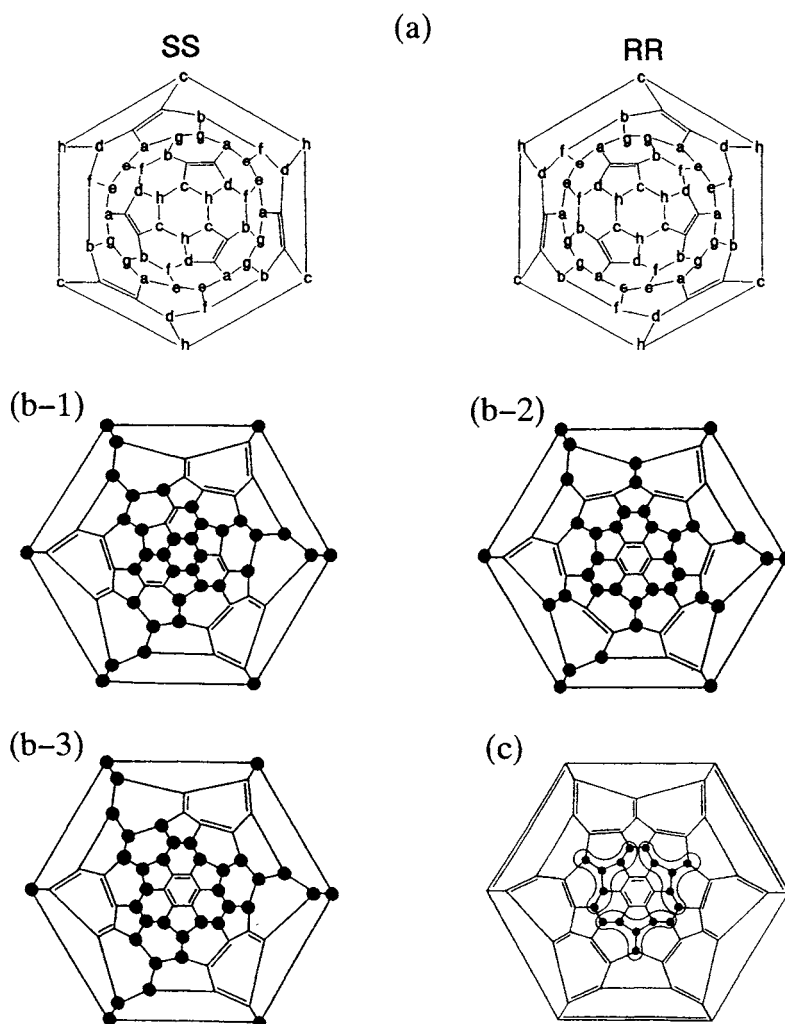


Fig. 6. Schlegel diagrams of (a) $C_{60}F_{48}$, (b-1) $C_{60}F_{36}$ (C_3 isomer I), (b-2) $C_{60}F_{36}$ (C_3 isomer II), (b-3); $C_{60}F_{36}$ (T isomer); and (c) $C_{60}F_{18}$ ((a) reproduced with permission from J. Am. Chem. Soc., 116 (1994) 820 [28]; (b) reproduced with permission from J. Chem. Soc., Perkin Trans. 2, (1998) 652 [39]; (c) reproduced with permission from Chem. Commun., (1996) 2550 [42]).

17.3.2 Selective synthesis and molecular structure of $C_{60}F_{36}$

Following the preliminary publication [34] on preparation of $C_{60}F_{36}$ and $C_{70}F_{36/38/40}$, Boltalina et al. reported the selective synthesis and characterization of $C_{60}F_{36}$ [39]. $C_{60}F_{36}$ was prepared by grinding together a mixture of C_{60} and MnF_3 which was placed in a nickel tube contained in a glass tube. This was evacuated and placed in a furnace such that part of the glass tube was protruded outside. The

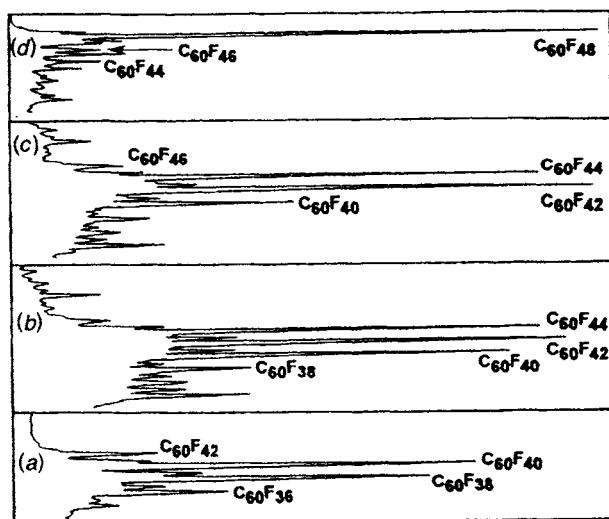


Fig. 7. EI mass spectra for the products of fluorination of C_{60} under increasingly vigorous consecutive conditions: (a) 343 K, 4 h; (b) a further 5 h at 493 K; (c) a further 11 h at 548 K, and (d) a further 3 h at 588 K (reproduced with permission from J. Chem. Soc., Perkin Trans. 2, (1996) 2276 [37]).

furnace was then heated to 623 K during 30 min and maintained at this temperature for 24 h during which material ranging from pale brown through orange–yellow to almost white deposited on the cold zone. This color change parallels that observed for fluorinated activated carbon fibers (ACF) [40]. It indicates that in both cases the electronic structures change as the degree of fluorination increases. This preparation method was effective since fluorinated fullerenes are more volatile than C_{60} ; although the volatility increases with the degree of fluorination, less fluorinated material sublimates as it is formed and lands at lower-temperature regions, thus evading further fluorination at high temperature. The deposit was purified by HPLC separation which involved elution first with toluene to separate highly polar $C_{60}F_{18}$, then with toluene–hexane mixtures, and finally hexane. Two main fractions of $C_{60}F_{36}$ were obtained. The main peak at 1404 amu in the mass spectra of these compounds shown in Fig. 8(b-1) and (2) corresponds to $C_{60}F_{36}$. The peak at 1335 amu is due to $C_{59}F_{33}^+$ arising from loss of CF_3^+ . The ^{19}F NMR of the first fraction shown in Fig. 4(b-1) consists of 12 lines of equal intensity showing it to have C_3 symmetry. The spectrum of the second fraction shown in Fig. 4(b-2) consists of three lines of equal intensity, indicating it to have T symmetry. This was confirmed by ^{13}C NMR spectroscopy which shows two lines of equal intensity in the sp^3 region. The ratio of the two fractions was ca 3:1 (C_3 : T). The Schlegel diagrams for possible two C_3 (I and II) and the T isomers are shown in Fig. 6(b-1), (2) and (3). The C_3 (II) and T isomers contain the $C_{60}F_{18}$ moiety as a subset, suggesting that $C_{60}F_{18}$ is the precursor of $C_{60}F_{36}$. Although there is no definitive way to distinguish between C_3 isomers I and II by ^{13}C NMR, for each will give eight lines in the sp^3 region, isomer II is favored because of its relationship to $C_{60}F_{18}$, and the relationship

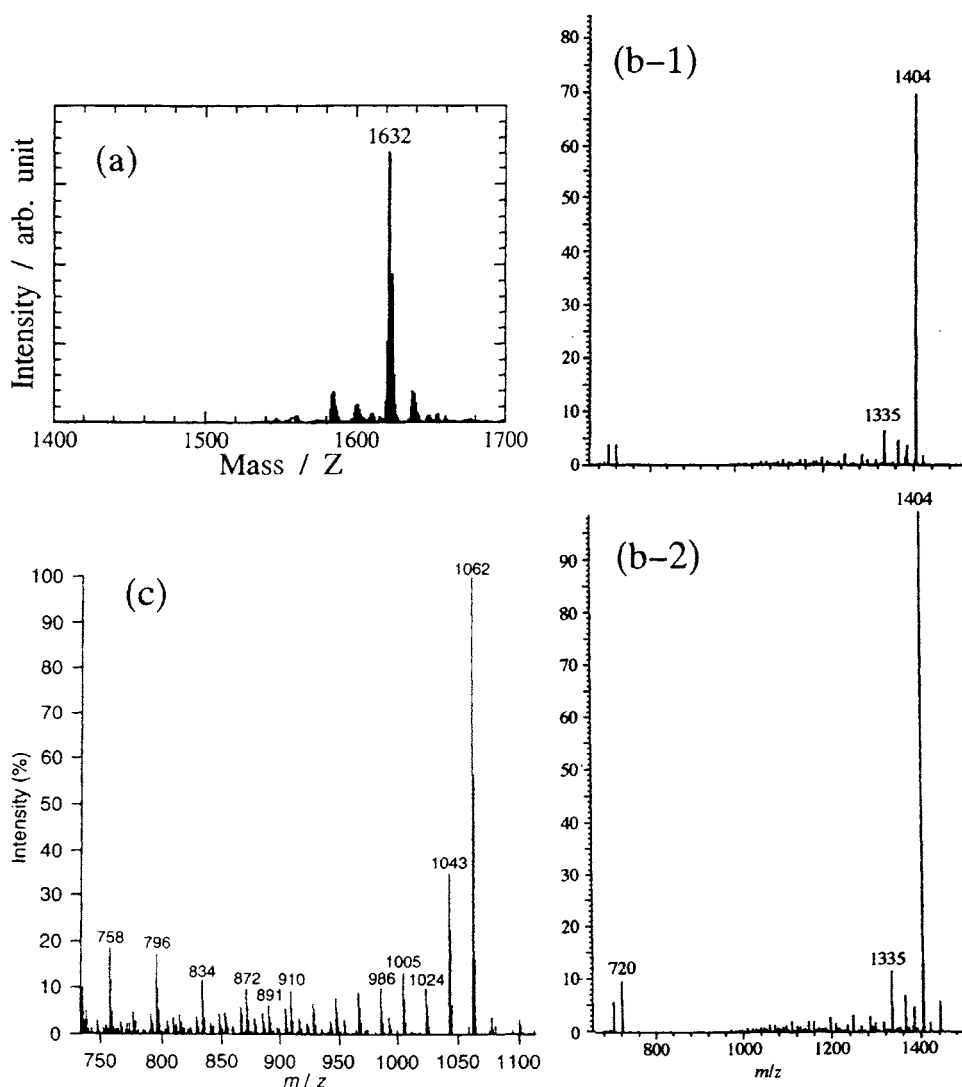


Fig. 8. FD mass spectrum of (a) $C_{60}F_{48}$, and EI mass spectra of (b-1) $C_{60}F_{36}$ (C_3 isomer), (b-2) $C_{60}F_{36}$ (T isomer) and (c) $C_{60}F_{18}$ ((a) reproduced with permission from J. Phys. Chem. B, in press [38]; (b-1) and (b-2) reproduced with permission from J. Chem. Soc., Perkin Trans. 2, (1998) 650 [39]; (c) reproduced with permission from Chem. Commun., (1996) 2549 [42]).

between $C_{60}H_{36}$ and $C_{60}H_{18}$ [41]. The IR spectrum of the C_3 isomer (Fig. 9(b-1)), probably isomer II, shows a main band at 1163 cm^{-1} , a secondary one at 1133 cm^{-1} and a weak feature at 1074 cm^{-1} [39]. The IR spectrum (Fig. 9 (b-2)) of the T isomer shows a main band at 1175 cm^{-1} , two smaller peaks at 1140 and 1127 cm^{-1} and a small but sharp band at 1060 cm^{-1} [39]. In the IR spectrum of the crude material

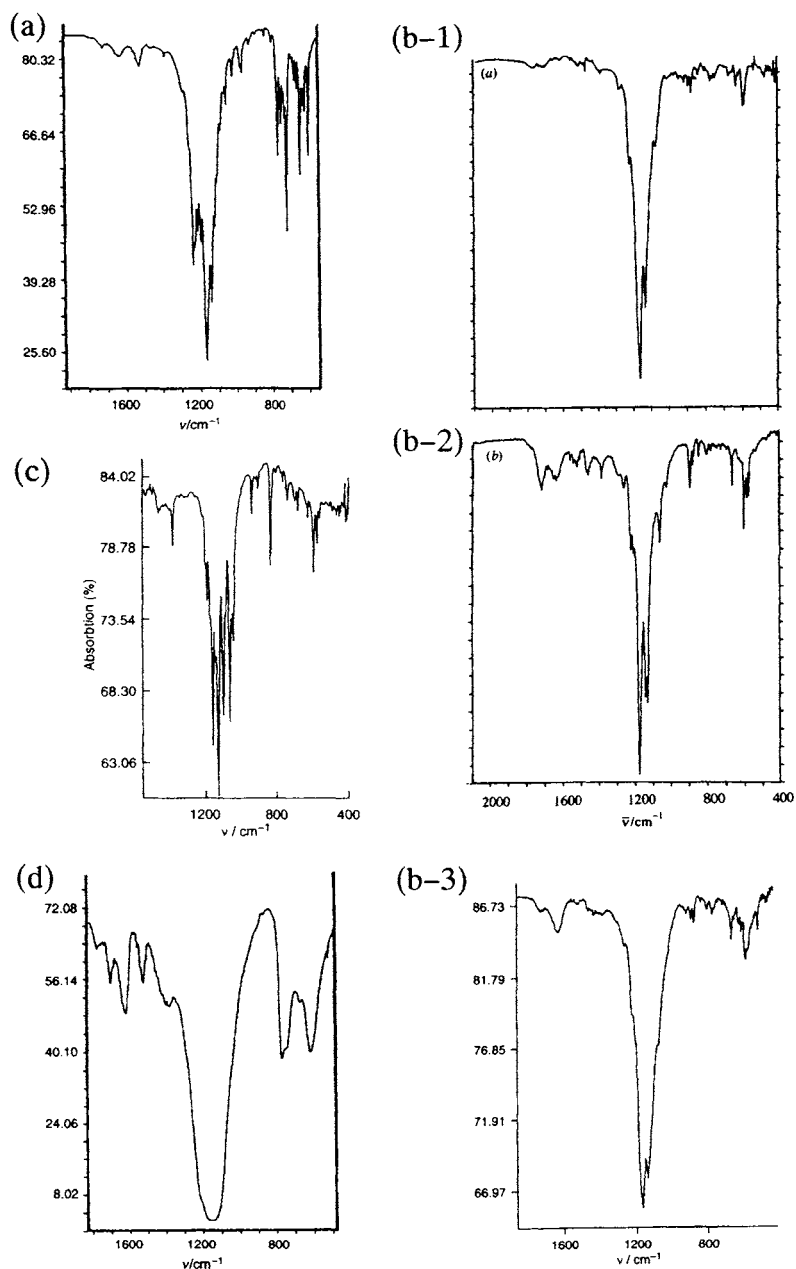


Fig. 9. IR spectra of (a) $\text{C}_{60}\text{F}_{48}$, (b-1) $\text{C}_{60}\text{F}_{36}$ (C_3 isomer), (b-2) $\text{C}_{60}\text{F}_{36}$ (T isomer), (b-3) $\text{C}_{60}\text{F}_{36}$ (mixture of C_3 and T isomers), (c) $\text{C}_{60}\text{F}_{18}$ and (d) Mixture of C_{60}F_n obtained by fluorination at 343 K, 4 h, whose mass spectrum is given in Fig. 7(a) ((a) and (d) reproduced with permission from J. Chem. Soc., Perkin Trans. 2, (1996) 2276 [37]; (b-1) and (b-2) reproduced with permission from J. Chem. Soc., Perkin Trans. 2, (1998) 651 [39]; (b-3) reproduced with permission from Chem. Commun., (1996) 529 [34]; (c) reproduced with permission from Chem. Commun., (1996) 2550 [42]).

before HPLC separation shown in Fig. 9(b-3) [34] the latter component is evident as a slight shoulder in the spectrum and was responsible for the main band appearing slightly shifted at 1166 cm^{-1} . The NMR spectrum of the crude material before HPLC separation is also given in Fig. 4(b-3) [34].

17.3.3 Selective synthesis and molecular structure of $C_{60}F_{18}$

$C_{60}F_{18}$ was prepared by grinding a mixture of C_{60} and K_2PtF_6 (potassium hexafluoroplatinate) intimately and placing it in a Knudsen cell incorporated within a magnetic sector mass spectrometer [42]. A collection plate was situated outside the outlet of the cell. The reaction was run for 8 h at 500–600 K. The mass spectrum of the deposit (ca 10% yield) indicated mainly the presence of C_{60} , $C_{60}F_{36}$ and $C_{60}F_{18}$. The fluorofullerenes were separated from the unreacted C_{60} by extraction with chloroform, and final purification was carried out by HPLC using toluene as eluent. The Schlegel diagram of $C_{60}F_{18}$ is given in Fig. 6(c). It has C_{3v} symmetry and is quite polar since the attachment of fluorine is limited only to a hemisphere. $C_{60}F_{18}$ is a green–yellow microcrystalline solid, readily soluble in hexane, toluene, chloroform, etc. The EI mass spectrum (Fig. 8(c)) of $C_{60}F_{18}$ at 1062 amu shows greater fragmentation compared to that for $C_{60}F_{36}$. This may be due to the use of higher probe temperatures owing to the lower volatility of $C_{60}F_{18}$ arising from its lower degree of fluorination and higher polarity. The ^{19}F NMR spectrum of $C_{60}F_{18}$ (Fig. 4(c)) shows four lines with intensity ratios 1:2:2:1. The positions of the resonances depend on two factors: the number of adjacent electron-withdrawing sp^2 -hybridized carbons, and the electronegativity of the elements attached to the adjacent sp^3 -hybridized atoms. The IR spectrum (Fig. 9(c)) consists of very sharp bands at 1385, 1196, 1163, 1133, 1103, 1067, 1045, 939, 833, 733, 683, 589 and 570 cm^{-1} , indicative of a single isomer.

17.3.4 Synthesis of $C_{70}F_x$

Effective selective synthesis of $C_{70}F_x$ with specific fluorine content has not been attained and none of the molecular structures of $C_{70}F_x$ has been determined in the late 1990s. Similar to C_{60} , direct fluorination of C_{70} with elemental fluorine yields a series of $C_{70}F_x$. However depending on reaction temperature and time, degree of fluorination varies with the maximum intensity observed at a certain $C_{70}F_x$ in mass spectra. The mass spectrum of the fluorinated mixture of C_{60}/C_{70} at a probe temperature of 573 K indicated the formation of fluorine compounds from $C_{70}F_{36}$ to $C_{70}F_{46}$ with the maximum intensity at $C_{70}F_{40}$ [43]. Fluorination of a 9/1 C_{60}/C_{70} mixture at 548 K for 4 h under F_2 flow produced $C_{70}F_{46-54}$, with $C_{70}F_{54}$ representing the highest degree of fluorination; longer reaction times did not produce detectable fluorination beyond $C_{70}F_{56}$ [25]. However, $C_{70}F_{58}$ was observed in the mass spectrum of the product obtained by the direct fluorination at 473 K for 7 days [33]. In the FD mass spectrum of this product shown in Fig. 10(a), $C_{70}F_{50-58}$ species were observed with the maximum-intensity peak at $C_{70}F_{54}$. In this case a relatively selective synthesis of $C_{70}F_{52/54/56}$ was attained. For less fluorinated C_{70} , a fairly selective synthesis of $C_{70}F_x$ was attained by the same method used to obtain $C_{60}F_{36}$

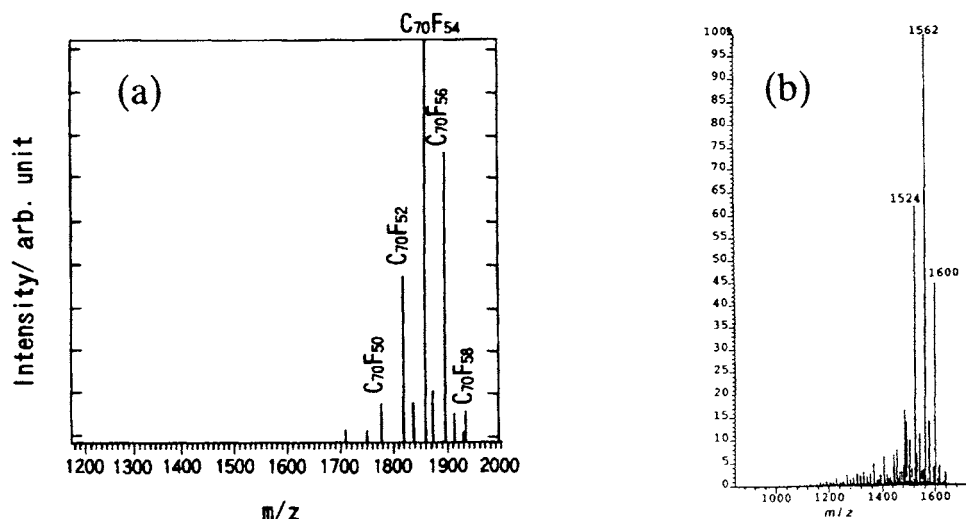


Fig. 10. Mass spectra of $C_{70}F_x$ obtained by (a) direct fluorination at 473 K for 7 d and (b) reaction with MnF_3 ((a) reproduced with permission from J. Electrochem. Soc., 143 (1996) L214 [33]; (b) reproduced with permission from Chem. Commun., (1996) 530 [34]).

described in Sec. 17.3.2 [34], except that higher temperature of 663 K was employed. The mass spectrum given in Fig. 10(b) shows main peaks at 1524, 1562 and 1600 amu corresponding to $C_{70}F_{36/38/40}$, with $C_{70}F_{38}$ as the major component. This parallels the behavior in the hydrogenation of C_{70} [41].

17.4 Crystal structures

The crystal structures of C_{60} and C_{70} are briefly reviewed first.

The structure of solid C_{60} has been determined by synchrotron-X-ray diffraction [44] and neutron diffraction on powder samples [45]. At room temperature C_{60} solid forms a face-centered cubic (fcc) lattice with lattice constant $a = 1.417$ nm (space group $Fm\bar{3}m$) [44]. Room temperature ^{13}C NMR measurements indicate that C_{60} molecules are rotating rapidly [46–48]. The shell radius is 0.352 nm and the van der Waals radius of the molecule is 0.501 nm [44]. The solid undergoes a first-order transition at ca 250 K [49], and below the transition temperature the molecules are orientationally ordered, forming a simple-cubic (sc) structure with a four-molecule basis (space group: $Pa\bar{3}$) [44,45,50,51]. Below the transition the motion becomes slower and the molecules execute jumps between symmetry-equivalent orientations [46–48]. A typical powder XRD pattern of C_{60} and its simulation are given in Fig. 11(a) [52].

Compared with C_{60} , the structures and phase diagram of C_{70} are less well understood [53–55]. This is because of the molecular anisotropy of C_{70} , which allows various degrees of rotational freedom, and of the presence of the impurities, which makes

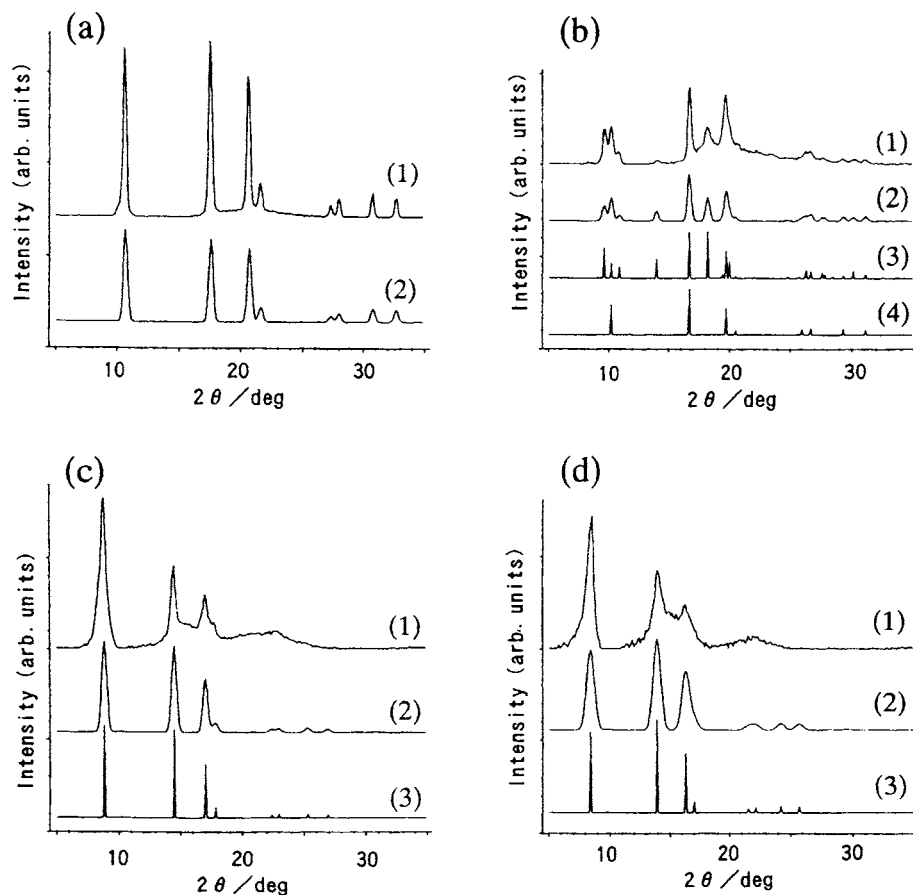


Fig. 11. Observed and simulated XRD patterns of (a) C_{60} , (b) C_{70} , (c) C_{60}F_x and (d) C_{70}F_x . (1), (2) and (3) are observed, simulated and calculated patterns, respectively (Cu- K_α). In (b), (3) is calculated for hcp and (4) for fcc. The simulation was attained by broadening calculated peaks (reproduced with permission from Trans. Mat. Res. Soc. Jpn., 14B (1994) 1206 [52]).

different phases appear under the same T - P conditions. Transition temperatures are often sample dependent owing probably to intrinsic or extrinsic hystereses. However, for purer solid C_{70} samples, the transition of fcc \leftrightarrow rhombohedral (rh) at around room temperature under ambient pressure has been firmly established. In the fcc structure, the molecules have random rotational freedom. The alignment of the long axes of C_{70} along the $[111]$ direction of fcc leads to the rh phase. As the temperature is further lowered, the rh phase may transform into a monoclinic (mncl) phase depending on samples. A hexagonal close-packed (hcp) lattice is usually observed for samples crystallized from solution. However, crystals obtained by sublimation sometimes have also the hcp structure. Upon heating, a shear transformation can occur and the rh phase appears followed by the fcc phase. When

an ideal hcp crystal with the c/a ratio of 1.63 is cooled, an hcp structure with the c/a ratio of >1.63 may appear. Further cooling can bring about an mncl phase. All of the structures are described as stacking sequences of close-packed monomolecular layers [55]. A typical powder XRD pattern of C_{70} and its simulation are given in Fig. 11(b) [52]. In this case the sample consists of the fcc and hcp phases.

17.4.1 Crystal structure of $C_{60}F_x$ with mixed x ($x = 40-48$)

When the control of fluorination of C_{60} is not rigorous or the following separation by, for example, HPLC is not applied, fluorination of C_{60} usually yields $C_{60}F_x$ powder containing molecules with various number of fluorine atoms. The powder X-ray diffraction pattern essentially consists of 3 lines and they are indexed as (111), (220) and (311) reflection lines of a cubic lattice with $a \approx 1.71$ nm. The lattice constant varies from sample to sample: 1.709 nm (nominal composition $C_{60}F_{45}$, fluorinated under 1 atm F_2 at 363 K for 11.5 d) [56], 1.709 nm ($C_{60}F_{40}$, 1 atm F_2 at 338 K for 27 d) [56], 1.707 [57] and 1.719 nm [52] (both $C_{60}F_{45}$, 1 atm F_2 at 473 K for 4 h). The observed and simulated XRD patterns are given in Fig. 11(c) [52]. The structure of $C_{60}F_x$ is described as an fcc cubic lattice with close-packing of rotating and/or orientationally disordered $C_{60}F_x$ molecules [52,57]. The structure was simulated by the spherical-shell model in which a $C_{60}F_x$ is represented by one inner spherical shell of carbon and one outer spherical shell of fluorine with the radii of 0.387 and 0.523 nm, respectively [52].

17.4.2 Single crystal structure of $C_{60}F_x$ ($x \approx 46$)

A more precise work was carried out on $C_{60}F_x$ using a single crystal of $C_{60}F_x$ ($x \approx 46$) [26], in which $C_{60}F_{44}$, $C_{60}F_{46}$ and $C_{60}F_{48}$ were determined to be the main components by the mass spectrum. C_{60} was fluorinated under 1 atm F_2 at 498 K for 2 d, and single crystals were grown in a sealed quartz tube by the sublimation of $C_{60}F_x$ from one of the ends controlled at 583 K to the other end at 483 K. The precession photographs indicate that the crystal has an fcc lattice with the cell constant of 1.716 nm. In fitting the collected data the intensities were calculated using the spherical-shell model with two spherical shells of carbon with $r_C = 0.313$ and 0.383 nm, and a spherical shell of fluorine with $r_F = 0.512$ nm. The carbon atoms with a C—F bond constitute the outer carbon shell, while the carbon atoms without fluorine attachment constitute the inner carbon shell. This structure is depicted schematically on the left side of Fig. 12.

This model is supported by the molecular structure of the D_3 $C_{60}F_{48}$ (RR isomer in Figs. 5 and 6(a)) optimized by PM3 calculations [26]. Figure 13 shows a part of the optimized structure of the $C_{60}F_{48}$ around the C—C double bond. The calculations show that the C atoms forming double bonds constitute the inner sphere of carbon atoms. There are two more C layers with slightly different radii made of the C atoms with F-atom attachment. They together form the outer sphere of C atoms observed by the single crystal work. The carbon atoms at $a-d$ have the smaller radius, and those at $e-h$ have the larger radius (see Fig. 6(a) for $a-h$ designations). These two spheres were not able to be discerned by the X-ray

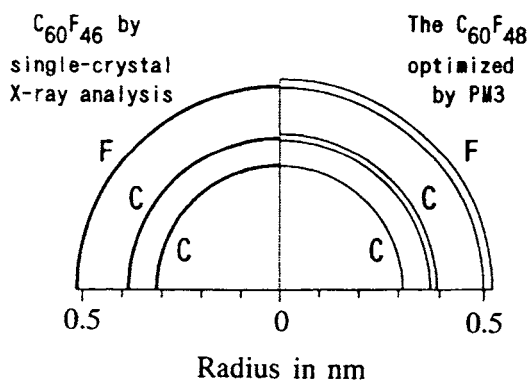


Fig. 12. Schematic diagram of the radial distributions of C and F atoms in $ca\ C_{60}F_{46}$ obtained by X-ray single crystal analysis and in $C_{60}F_{48}$ optimized by PM3 (reproduced with permission from Fullerene Sci. Technol., 4 (1996) 883 [26]).

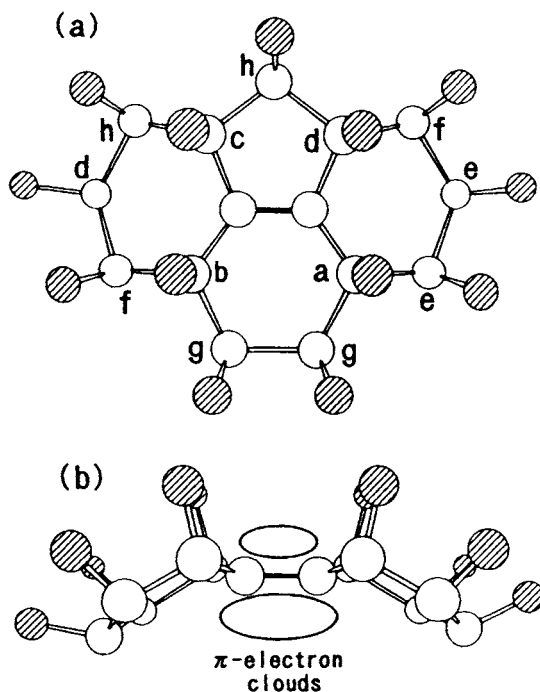


Fig. 13. Structure around the C—C double bond in $C_{60}F_{48}$ optimized by PM3. The C—C double bond is at the center. (a) Top view; (b) Side view indicating the larger π -electron cloud inside the sphere than outside. In (b), an h and two g sites shown in (a) are omitted. Site designations $a-h$ are the same as in Fig. 6(a) (reproduced with permission from Fullerene Sci. Technol., 4 (1996) 881 [26]).

structural analysis. Two fluorine spheres with a slight difference in radius are formed accordingly. The schematic diagram of the radial distribution of C and F atoms calculated for the $C_{60}F_{48}$ by PM3 is shown on the right side of Fig. 12.

The occurrence of the two spheres with a slight difference in radius for C and F is explained as follows. There are two kinds of carbon atoms with F attachment in the $D_3 C_{60}F_{48}$ molecule; those at *e-h* which are surrounded by three carbon atoms with fluorine attachment at *a, b, c* or *d*, and those at *a-d* which are surrounded by one of the double-bond forming carbon atoms and two carbon atoms with fluorine attachment at *e, f, g* or *h*. Although one is inclined to consider that fluorine attachment on any of the quasi- sp^2 ($sp^{2.28}$; see Sec. 17.2.1) hybridized carbon atoms in C_{60} will induce a pronounced sp^3 character on the C atom, it is not necessarily the case in $C_{60}F_{48}$ as Fig. 13 indicates. The sp^3 character of the carbon atoms at *e-h* is barely stronger than that of C atoms in C_{60} , whereas the carbon atoms at *a-d* have stronger sp^3 character. The weak sp^3 character or the strong sp^2 character of the *e-h* carbon atoms with fluorine attachment is easily visualized when one think of the hypothetical $C_{60}F_{60}$, where the curvature of the carbon sphere ought to be the same as in C_{60} , i.e., each carbon atom has to have $sp^{2.28}$ hybridization despite the fluorine attachment. The surroundings around the carbon atoms at *e-h* are similar to those in $C_{60}F_{60}$. The local geometry around the double-bonded carbon atoms in $C_{60}F_{48}$ allows the carbon atoms at *a-d* to have stronger sp^3 character with their larger part of π -electron cloud inside the sphere as indicated in Fig. 13(b). This may explain, kinetically, the non-existence or non-observation of $C_{60}F_{60}$ with intact cage which is predicted to be stable by some calculations [35,36]. Once $C_{60}F_{48}$ is formed, electronegative fluorine cannot attack $C_{60}F_{48}$ not only because of the dense coverage of the sphere by the 48 fluorine atoms but also because of the sought-after carbon π -electrons reside mainly inside the cage. The sphere needs to be broken in order for the 49th carbon atom to be attacked by fluorine. This suggests that perfluorinated fullerene $C_{60}F_{60}$ could only be formed by the simultaneous addition of 60 fluorine atoms to C_{60} or by the instantaneous formation of $C_{60}F_{60}$ in a similar way as C_{60} is formed.

17.4.3 Crystal structures of $C_{60}F_{48}$ and $C_{60}F_{36}$

The crystal structures of $C_{60}F_{48}$ and $C_{60}F_{36}$ each consisting of molecules of specific fluorine content have been determined recently [38]. They were prepared by the methods described in Secs 17.3.1 [37] and 17.3.2 [34,39], respectively. Powder samples of $C_{60}F_{48}$ and $C_{60}F_{36}$ at room temperature are indexed by body-centered tetragonal (bct) and body-centered cubic (bcc) lattices, respectively. The observed and simulated XRD patterns for $C_{60}F_{48}$ and $C_{60}F_{36}$ are given in Fig. 14. To simulate the observed patterns, a two-shell (one fluorine- and one carbon-atom shells) model was used as the three-shell model used for the single crystal work described above is too sophisticated to deal with the limited numbers of diffraction peaks observed in the powder XRD patterns. The radii r_F and r_C of the fluorine and carbon atom shells, respectively, were set equal to 0.51 and 0.37 nm for $C_{60}F_{48}$, and 0.49 and 0.35 nm for $C_{60}F_{36}$.

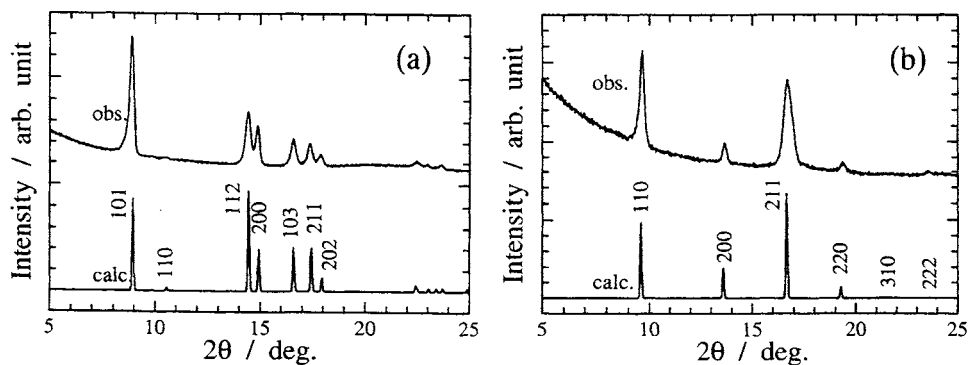


Fig. 14. Observed and calculated XRD patterns of (a) $C_{60}F_{48}$ and (b) $C_{60}F_{36}$ (Cu-K $_{\alpha}$) (reproduced with permission from J. Phys. Chem. B, 103 (1999) 1223 [38]).

Table 1

Lattice parameters, Z and V/Z of $C_{60}F_{48}$, $C_{60}F_{36}$ [38] and $C_{60}F_x$ [26]

	Lattice parameters (nm)		Z	V/Z (nm ³)
	a	b		
$C_{60}F_{48}$ (bct)	1.1852(8)	1.791(1)	2	1.257
$C_{60}F_{36}$ (bcc)	1.302(1)		2	1.104
$C_{60}F_x$ (fcc)	1.7158(3)		4	1.263

Table 1 summarizes the lattice parameters, number of molecules (Z) in a unit cell, and volume per molecule (V/Z) of $C_{60}F_{48}$ and $C_{60}F_{36}$ powder samples [38], and $C_{60}F_x$ ($x \approx 46$) single crystal [26]. The difference in V/Z values between $C_{60}F_{48}$ and $C_{60}F_x$ is small, suggesting the structural similarity of the two structures. The extended cell of bct can be treated as a face-centered tetragonal (fct) cell which is derived by the elongation of an fcc cell along the c -axis with the new choice of a -axis coinciding with the C -face diagonal of the initial bct cell. Indeed, the lattice parameters of this extended “fct” cell for $C_{60}F_{48}$ are $a = 1.675$ nm and $c = 1.79$ nm, which are close to the lattice constant $a = 1.716$ nm of $C_{60}F_x$, confirming the close structural resemblance in these two materials. These indicate that the fcc single crystal is a metastable phase quenched from high temperature.

In situ X-ray diffraction experiments at high temperatures indicate the bct to fcc phase transition of $C_{60}F_{48}$. Figure 15 shows the changes in the diffraction patterns of $C_{60}F_{48}$ and $C_{60}F_{36}$ with temperature. The diffraction pattern of $C_{60}F_{48}$ begins to change at about 353 K, whereas no remarkable change was observed in the diagrams of $C_{60}F_{36}$. The phase at high temperatures of $C_{60}F_{48}$ is fcc. This bct to fcc transition of $C_{60}F_{48}$ is reversible. As mentioned in the previous paragraph, the bct cell of $C_{60}F_{48}$ can be expressed as an extended “fct” cell which is a modified

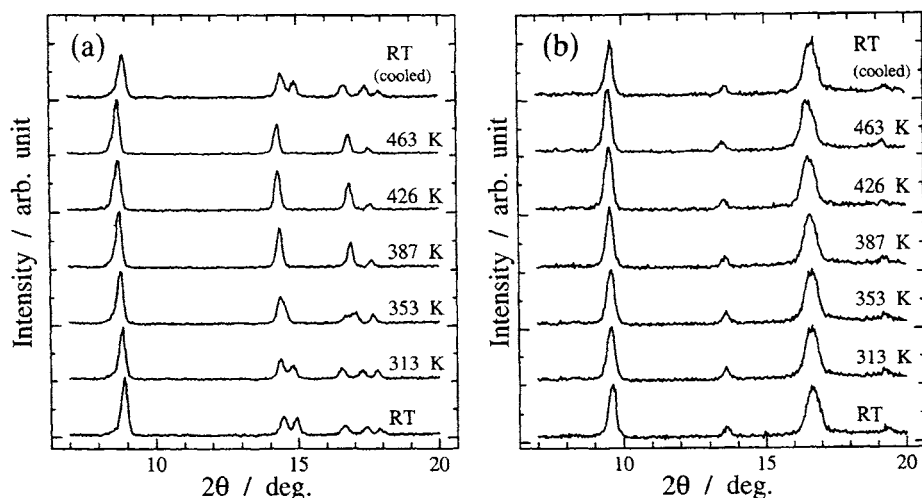


Fig. 15. Changes in XRD patterns of (a) $C_{60}F_{48}$ and (b) $C_{60}F_{36}$ with temperature (Cu- K_α) (reproduced with permission from J. Phys. Chem. B, 103 (1999) 1223 [38]).

fcc cell. The a/c ratio of the extended “fct” cell becomes close to 1 with increasing temperature and exactly 1 at the transition temperature. The mechanism of this transition can be explained as follows. The molecular structure of $C_{60}F_{48}$ is known as D_3 symmetry based on the NMR spectrum (see Sec. 17.3.1) [28,37]. Provided that all the unique axes (three-fold rotation axes) of the molecules lie parallel to the c -axis of the bct cell and that the molecules rotate around these axes, the a/c ratio should be different from 1. However, at high temperature, the more vigorous and random motion of the molecules will make the apparent molecular shape spherical and the fcc phase can appear. On the other hand, two isomers are known for $C_{60}F_{36}$ molecules having T and C_3 symmetries (see Sec. 17.3.2) [39]. The bcc crystal structure may have arisen owing to the T symmetry of the molecule, which belong to the cubic group, coupled with thermal motion. Mixing of the C_3 molecules can randomize molecular orientations resulting in apparent spherical shape on the average.

17.4.4 Crystal structure of $C_{70}F_x$

Fluorinated fullerenes, $C_{70}F_x$, are made of large bucky balls decorated with fluorine atoms. The $C_{70}F_x$ molecules are considered to be bonded to each other by weak van der Waals interactions. Although the molecular structures of $C_{70}F_x$ have not been determined so far, they are expected to be less spherical than $C_{60}F_x$, because of the elongated molecular structure of C_{70} . However, the crystal structure of $C_{70}F_x$ ($x \approx 32$) is described as an fcc lattice with close-packing of spherical $C_{70}F_x$ molecules [52]. The observed and simulated XRD patterns are given in Fig. 11(d). It is to be noted that the pristine C_{70} before fluorination exhibited two phases, fcc and hcp,

as shown in Fig. 11(b) while the fluorinated sample consisted of the fcc phase alone. This suggests that $C_{70}F_x$ is more spherical than C_{70} . This apparent spherical nature of $C_{70}F_x$ can be attributed to the following; facile rotation of the molecules owing to the weaker intermolecular attractions in $C_{70}F_x$ than in C_{70} , or orientational disorder of $C_{70}F_x$ molecules in combination with the differences in the number of fluorine atoms and in the site of C—F bonds. As in the case of $C_{60}F_x$ the structure can be simulated by the spherical-shell model. In this case, however, a $C_{70}F_x$ molecule is represented by five inner spherical shells of carbon and five outer spherical shells of fluorine as a first approximation owing to the five nonequivalent carbon atoms in C_{70} [52].

It has been found that the $C_{70}F_x$ transforms from a crystalline to an amorphous phase at about 5.5 GPa [58]. Figure 16 shows the change in XRD pattern of $C_{70}F_x$ with pressure. It indicates a discontinuous loss in the diffracted X-ray intensity between 3.8 and 5.5 GPa. The pressure–volume relation of $C_{70}F_x$ was also investigated and the bulk modulus and its pressure derivative were determined to be 26.6 GPa and 3.0, respectively (see Table 3).

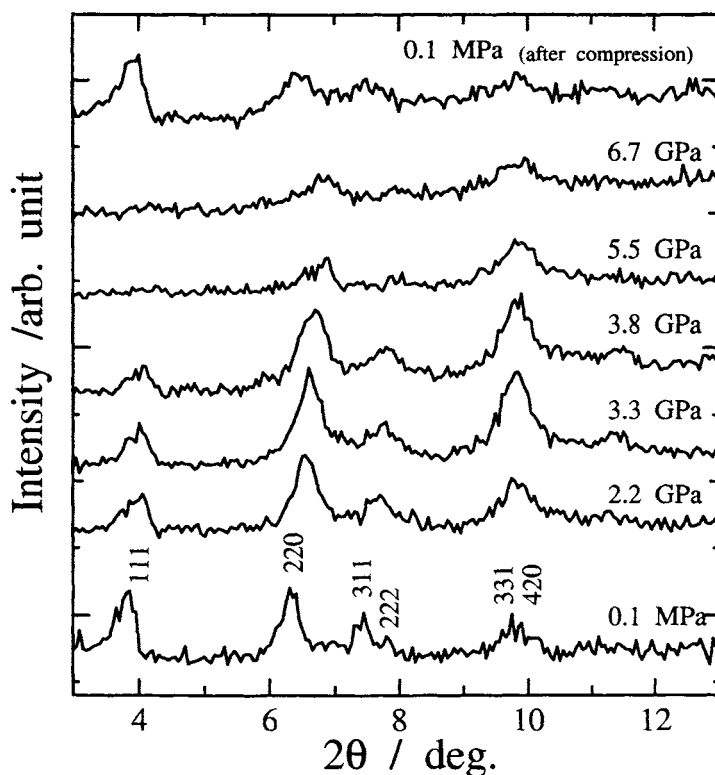


Fig. 16. Change in XRD pattern of $C_{70}F_x$ with pressure (Cu- K_α) (reproduced with permission from Solid State Commun., 108 (1998) 749 [58]).

17.5 Electronic structures and chemical bonding

17.5.1 Energy diagrams of $C_{60}F_x$

An attractive feature of fullerenes is the interaction of their π electrons with fluorine, which has given a very broad array of fullerene fluorides as is described in the previous section. Electronic properties of these new fluorides based on the third allotrope of carbon are of great interest and importance from the view points of materials science and potential use. In fact, as will be described in the next section, electrochemical properties such as electromotive force and reduction potential strongly reflect the changes in the C_{60} electronic structure through fluorination.

Studies on the electronic structure of fluorinated fullerenes have been carried out by using UPS [59], electron affinity estimation in gas phase reaction [60], and UV-visible absorption spectroscopy [25,61]. As for the core level electronic structure, X-ray photoelectron spectroscopy (XPS) measurements [56,62,63] have been performed. Seki and coworkers have systematically and extensively investigated the chemical bonding and the electronic structure of fluorinated fullerenes, $C_{60}F_x$ and $C_{70}F_x$, by near edge X-ray absorption fine structure (NEXAFS) spectroscopy, UPS and XPS [21,64]. They have derived a comprehensive energy diagram for $C_{60}F_x$ covering the wide energy range from the core to the unoccupied levels, and discussed the correlation of the electronic structures with those of C_{60} , as follows [21,64].

Figure 17 shows the energy diagrams of $C_{60}F_x$ ($x \geq 40$) together with those of C_{60} for comparison. Each diagram consists of C1s core, LUMO, HOMO and E_F , and covers the vapor and the solid phases [21,64]. The data are for the highly fluorinated $C_{60}F_x$ with x over 40, for which extensive information is available. It is of great interest that all the energy levels of $C_{60}F_x$ become stabilized from the corresponding levels of C_{60} . This change can be ascribed to the strong inductive effect of electronegative fluorine atoms. It should be noted that the HOMO and the LUMO levels of C_{60} are lowered by different amounts of 2.2 eV and 1.4 eV, respectively.

From the XPS measurements, the C1s binding energy relative to the vacuum level can be determined. The value for the double-bond carbon atoms without attached fluorine in $C_{60}F_x$ is higher than that of C_{60} by 2.6 eV. This change can be ascribed to the inductive effect of fluorine. The value for carbon atoms combined with fluorine is 293.8 eV which is higher than that of C_{60} by 4.8 eV, indicating that the C-F bonds are covalent in nature.

17.5.2 Changes in electronic structure of C_{60} by fluorination

Seki and coworkers have explained changes in electronic structure by taking account of the change of the π -conjugation and the inductive effect of fluorine atoms. In Fig. 18, it is quantitatively explained that how these two effects influence the HOMO and the LUMO levels in different ways [21,64]. The fluorination changes the double bonds of the fullerene into single bonds. The residual double bonds become isolated, and the size of the π -conjugated system on the C_{60} cage becomes reduced. The reduction of the π -conjugation leads to the narrowing of the π and π^* bands as shown

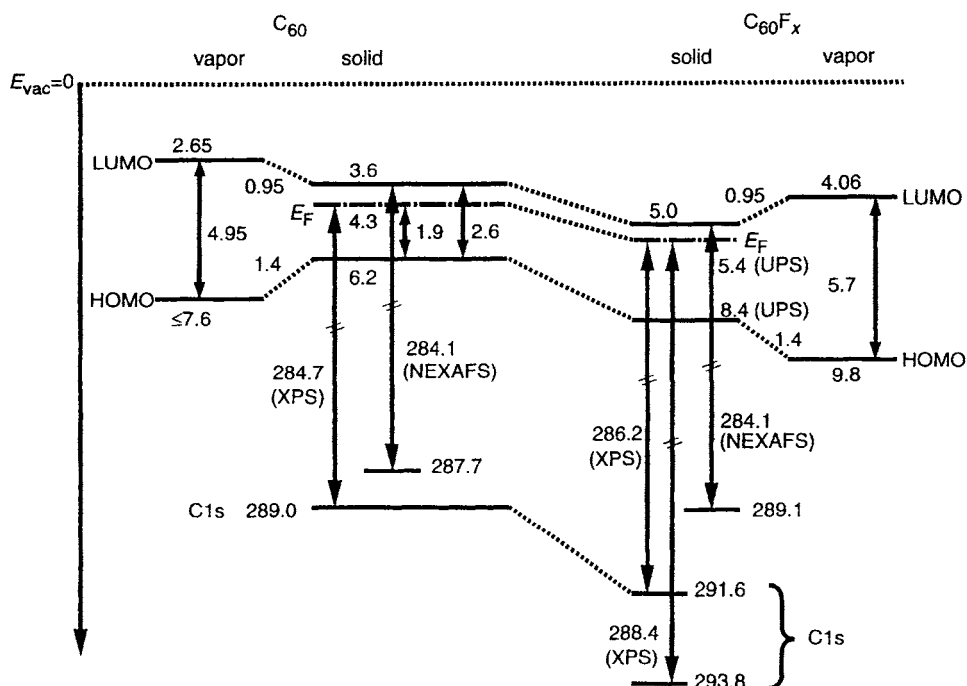


Fig. 17. The energy diagrams of C₆₀ and C₆₀F_x relative to the vacuum level (reproduced by permission of American Chemical Society from J. Phys. Chem. A, 102 (1998) 558 [21]).

in Fig. 18(b). At the same time, the inductive effect lowers the two bands as shown in Fig. 18(c). These two effects are estimated quantitatively by assuming a common magnitude for the narrowing of the π and π^* band widths by $2a$ and the lowering by the inductive effect by $b + a$ ($= 2.2$ eV). As for the LUMO, the two effects work in opposite directions. The inductive effect lowers the LUMO, while the narrowing of the π^* band width raises the LUMO. As a combined effect, the inductive effect dominates, and leads to the lowering of the LUMO by $b - a$ ($= 1.4$ eV). These relations find $a = 0.4$ eV and $b = 1.8$ eV.

The Fermi level is also lowered by 1.1 eV after fluorination in Fig. 17. The work functions of C₆₀F_x (5.6, 5.2 and 5.4 eV for $x = 30, 36$ and 48 , respectively) obtained by UPS are considerably larger than those (4.1–5.0 eV) of usual organic compounds. This suggests that C₆₀F_x is a very strong electron acceptor. From the estimated energies of the HOMO and the LUMO of C₆₀F_x molecule in gas phase, the HOMO–LUMO gap is estimated to be 5.7 eV.

In Fig. 19, it is shown how the energies of LUMO, Fermi and HOMO levels obtained in UPS measurements change depending on the degree of fluorination [21,64].

It is noteworthy that the ionization threshold energy gradually increases with fluorination. This change is consistent with the interpretation that fluorination

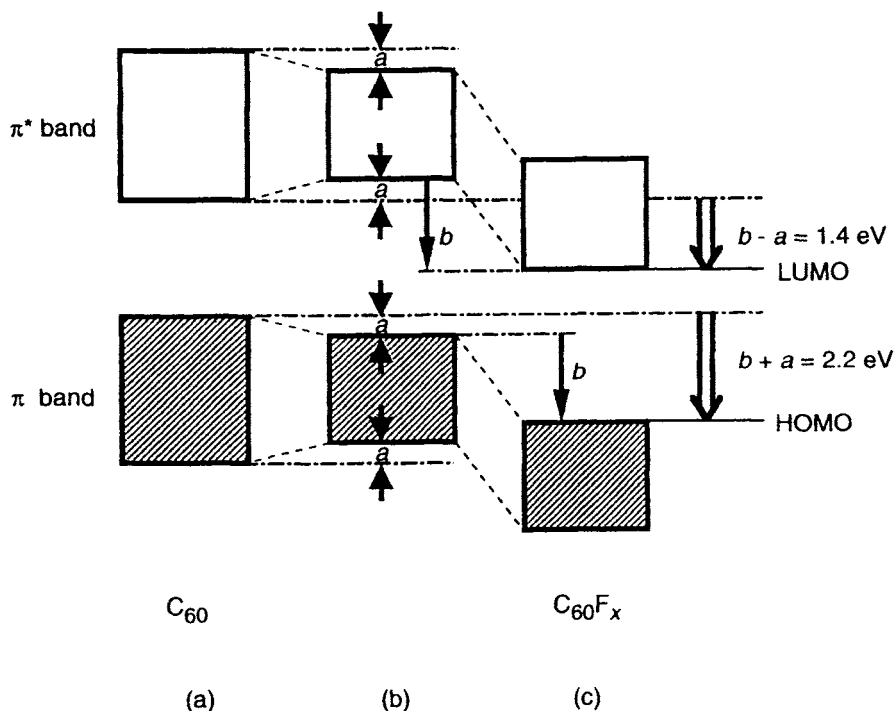


Fig. 18. Schematic diagram for the influences of fluorination upon the π and π^* bands of C_{60} . (a) The π and π^* bands of C_{60} . (b) The reduction of the π -conjugation leads to the narrowing of the π and π^* band width by $2a$. At the same time, (c) the inductive effect lowers the two bands by b (reproduced by permission of American Chemical Society from J. Phys. Chem. A, 102 (1998) 558 [21]).

makes the HOMO level of C_{60} deeper. On the other hand, the Fermi energies show no simple correlation with the degree of fluorination. One of the plausible reasons is that the $C_{60}F_{30}$ used in the experiment was not a pure compound with specific content of fluorine, and another reason is that $C_{60}F_x$ of specific content of fluorine can consist of several geometrical isomers. The different isomers will have various distribution of double bonds over the molecule, which will lead to a different electronic structure.

17.6 Electrochemical properties

Fluorinated fullerenes have drawn much attention because of their potential uses such as cathode material for a high energy density cell, electric devices, etc., and there have been several reports on the electrochemical behavior of fluorofullerenes $C_{60}F_x$ and $C_{70}F_x$. Electrochemical studies on these materials provide another way to understand the changes in electronic structures upon fluorination.

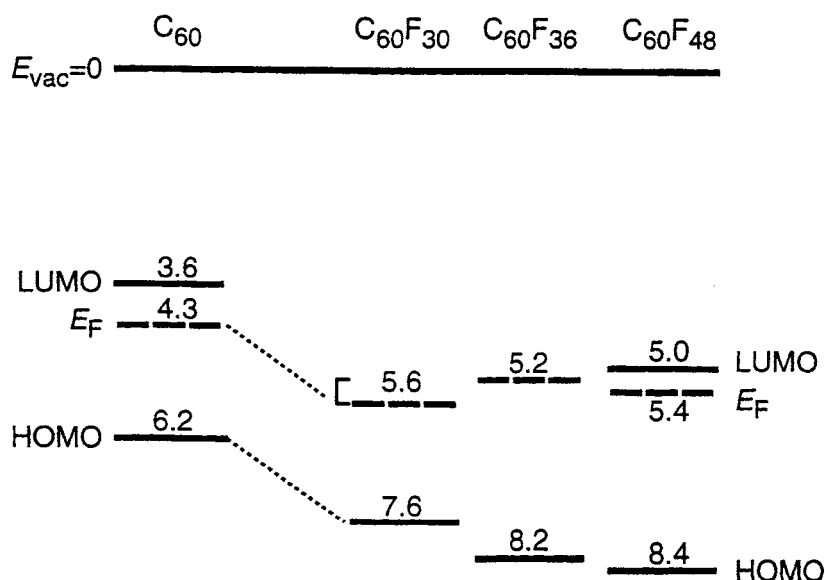
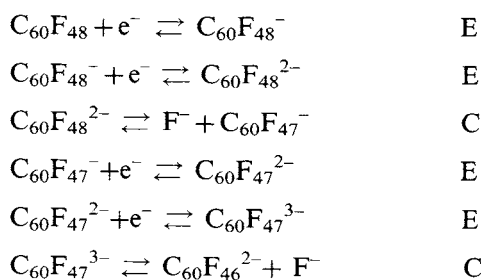


Fig. 19. The change of the energy of the LUMO and the HOMO levels of C₆₀F_x with x. (reproduced by permission of American Chemical Society from J. Phys. Chem. A, 102 (1998) 559 [21]).

17.6.1 Cyclic voltammetry and electron affinity of C₆₀F_x and C₇₀F_x

Zhou et al. reported the first cyclic voltammetric (CV) study of C₆₀F₄₈ in solution and showed that the reduction potential of C₆₀F₄₈ is more positive than that of the first reduction wave of C₆₀ by 1.38 V [65]. This shift reflects exactly the change of the LUMO level of C₆₀ upon fluorination as is shown in Fig. 19. Based on the CV behavior and electrospray mass spectroscopy, they proposed the following ECEEC mechanism for the first four reduction waves of C₆₀F₄₈.



where E represents a reversible one-electron transfer at the electrode, and C refers to an irreversible chemical reaction in the solution that is coupled to an electrode reaction.

Cyclic voltammograms of C₆₀F₄₆ in a CH₂Cl₂/0.1 M TBAPF₆ (tetrabutylammonium hexafluorophosphate) solution are shown in Fig. 20 [33]. The reduction of C₆₀F₄₆ to its anion radical occurs at the first half wave potential $E_{1/2} = 0.51$

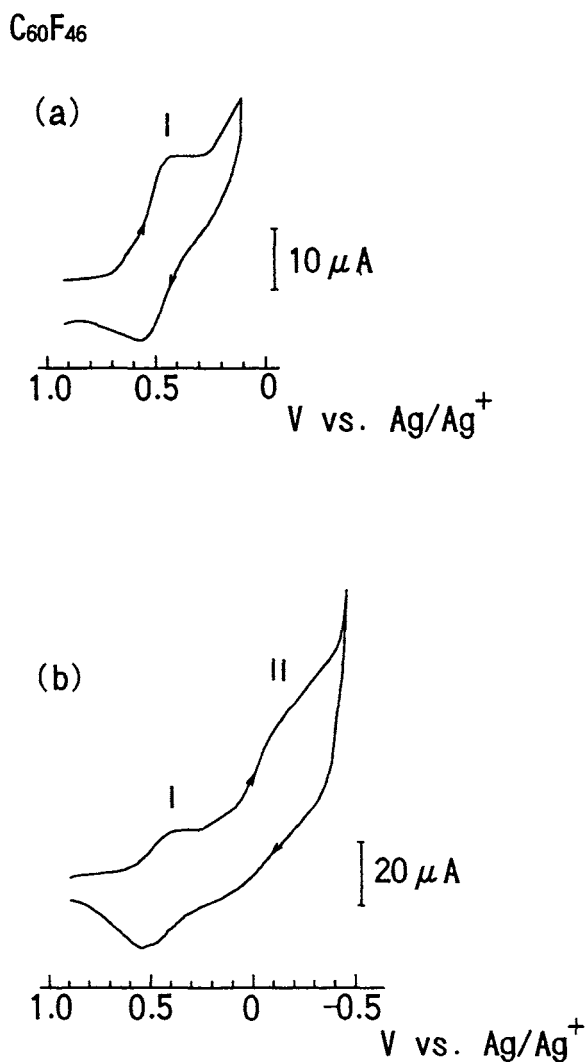


Fig. 20. Cyclic voltammograms of a 0.5 mM solution of $C_{60}F_{46}$ in $CH_2Cl_2/0.1$ M TBAPF₆, with the potential reversed at (a) 0.1 V and (b) -0.4 V vs Ag/Ag^+ . The scan rate is 0.02 V/s (reproduced by permission from the Electrochemical Society from J. Electrochem. Soc., 143 (1996) L215 [33]).

V with respect to the Ag/Ag^+ reference electrode. The separation of anodic and cathodic peak potentials is ca 70 mV, suggesting a reversible process.

A CV scan toward a more negative potential at a scan rate of 20 mV/s produces the second reduction wave of $C_{60}F_{46}$ (Fig. 20(b)) with a peak potential E_{pc} of -0.10 V vs Ag/Ag^+ . No evident anodic wave is observed at scan rates up to 0.5 V/s when the potential scan is reversed after wave II, indicating that $C_{60}F_{46}^{2-}$ is unstable, and that a following chemical reaction, perhaps a rapid loss of F^- to form $C_{60}F_{45}^-$

occurs. Since $C_{60}F_{45}^-$ formed from the chemical reaction of $C_{60}F_{46}^{2-}$ may be reduced at a potential very close to that of $C_{60}F_{46}^-$, a larger reduction current is observed for wave II. Thus an EEC process is indicated in the CV for $C_{60}F_{46}$.

Cyclic voltammograms of $C_{70}F_{54}$ in a CH_2Cl_2 solution are shown in Fig. 21 with different reversing potentials [33]. The differences in electrochemical properties

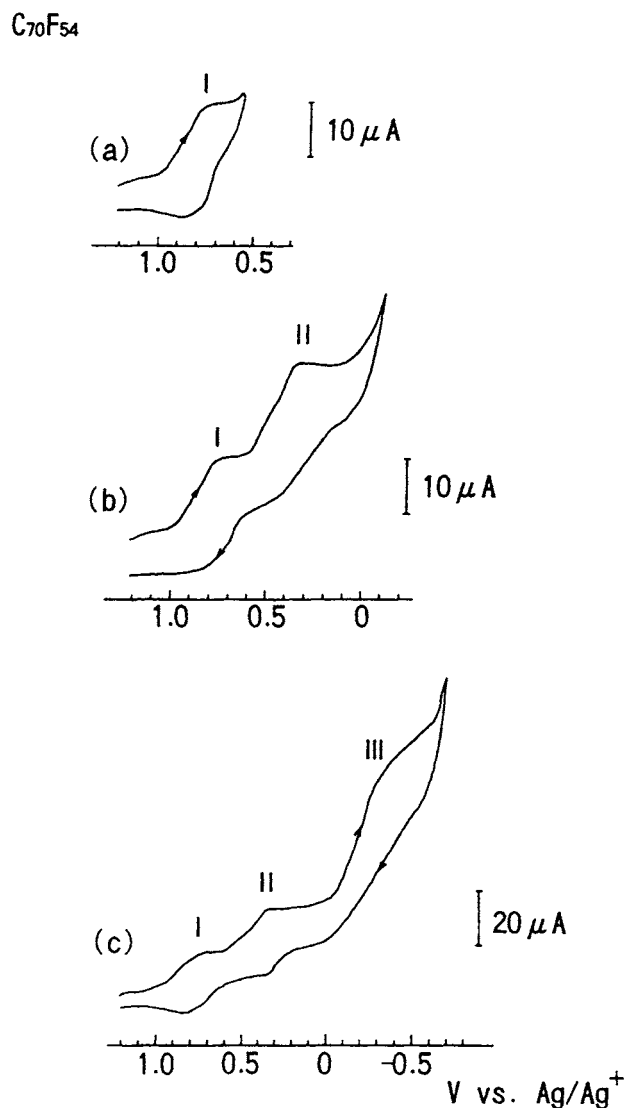
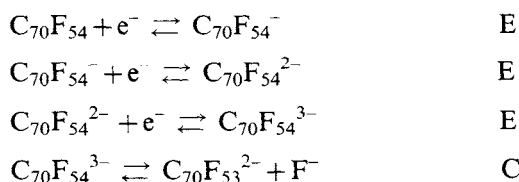


Fig. 21. Cyclic voltammograms of a 0.5 mM solution of $C_{70}F_{54}$ in $CH_2Cl_2/0.1$ M $TBAPF_6$, with the potential reversed at (a) 0.5 V, (b) -0.1 V and (c) -0.7 V vs Ag/Ag^+ . The scan rate is 0.02 V/s (reproduced by permission of the Electrochemical Society from J. Electrochem. Soc., 143 (1996) L215 [33]).

between $C_{70}F_x$ and C_{70} are parallel to those between $C_{60}F_x$ and C_{60} owing to the similar electrochemical properties of C_{60} and C_{70} . The $E_{1/2}$ of $C_{70}F_{54}$ is shifted positively by 0.25 V with respect to that of C_{70} and is more positive than that of $C_{60}F_{46}$, although the $E_{1/2}$ of C_{60} and C_{70} are almost the same. Moreover, two reversible one-electron-transfer steps are observed for $C_{70}F_{54}$, suggesting that $C_{70}F_{54}^{2-}$ is more stable than $C_{60}F_{46}^{2-}$ in the time scale of the voltammetry. This is similar to the fact that C_{70}^{2-} is less reactive in CH_2Cl_2 than C_{60}^{2-} . It is interesting to note that in Fig. 21 the 0.44 V separation between waves I and II corresponds approximately to the electron-by-electron reduction of C_{70} in solution. When scanned toward a more negative potential, $C_{70}F_x^{2-}$ can be further reduced yielding a broad irreversible wave at an E_{pc} of -0.3 V vs Ag/Ag^+ (Fig. 21(c)). However, no evident corresponding re-oxidation peak is observed, suggesting that a following chemical reaction occurs just as the case for $C_{60}F_x$. Therefore, an EEEC mechanism is proposed for the CV of $C_{70}F_{54}$.



Electron affinities for a series of fluorinated fullerenes have been evaluated using the relationships between E_a and half wave potential $E_{1/2}$ as follows.

A free energy of reduction ΔG_{red} bears the relation, $\Delta G_{red} = -nFE_0$, to the standard reduction potential E_0 , which is approximately identical to the first $E_{1/2}$. A combination of these relationships and Born's solvation model yields the following equation between the difference in electron affinity ΔE_a and the difference in the first half wave potential $\Delta E_{1/2}$ for two species [33].

$$\Delta E_a = F\Delta E_{1/2} - 0.5 e^2(1 - 1/\epsilon)(1/r_1 - 1/r_2) \quad (1)$$

Where e is the elementary electric charge, r is the radius of ions, and ϵ is the dielectric constant of solvent.

Using the observed $E_{1/2}$ values, the ΔE_a values between C_{60} and $C_{60}F_x$, C_{70} and $C_{70}F_x$ can be estimated by Eqn. (1). The estimated values are summarized in Table 2 together with the data necessary for calculations [33]. The ΔE_a of 0.08 eV between C_{60} and C_{70} , which is almost equal to the value, 0.073 ± 0.019 eV, reported by Burba using time-of-flight mobility measurements [66], is consistent with the more accurate values for E_a , 2.666 ± 0.001 eV for C_{60} and 2.676 ± 0.001 eV for C_{70} , obtained by Brink et al. using a new technique, laser photodetachment of C_{60}^- and C_{70}^- cooled in a heavy ion storage ring [67].

The E_a values of fullerenes increase as the degree of fluorination increases and, consequently, the electronic structures of fluorinated fullerenes varies as a function of the number of fluorine atoms attached to the fullerene molecules. These results

Table 2

First half-wave potentials, radii, half-wave potential differences and electron affinities of C_{60} , $C_{60}F_{36}$, $C_{60}F_{46}$, $C_{60}F_{48}$, C_{70} and $C_{70}F_{54}$. Half-wave potentials (V vs Ag/Ag⁺) for C_{60} , $C_{60}F_x$, C_{70} and $C_{70}F_x$ in CH_2Cl_2 containing 0.1 M TBAPF₆ at 0.02 V/s

	$E_{1/2}$ (V)	r (nm)	$\Delta E_{1/2}$ (V)	ΔE_a (eV)	E_a (eV)
C_{60}	−0.88	0.50	0	0	2.666 ± 0.001 [67]
$C_{60}F_{36}$	−0.05	0.61	0.83	1.06	3.48
$C_{60}F_{46}$	0.51	0.61	1.39	1.62	4.23
$C_{60}F_{48}$ [65]	0.53	—	—	—	4.06
C_{70}	−0.81	0.53	0.07	0.08	2.74
$C_{70}F_{54}$	0.76	0.63	1.57	1.76	4.42

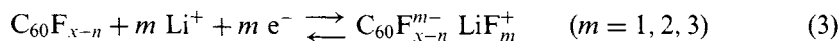
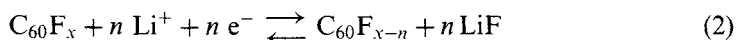
are quite consistent with the changes in electronic structures of C_{60} upon fluorination described in the former section.

17.6.2 Lithium cells with $C_{60}F_x$ and $C_{70}F_x$ cathodes

A primary battery based on fluorine and lithium is theoretically the optimum redox system for a high energy density power source, and such a battery has been realized commercially by the use of graphite fluoride (CF)_n as a cathode material for a lithium battery with an electrolyte-organic solvent system. In this context, the potential use of fluorinated fullerenes as high-density energy conversion materials has made it important and interesting to investigate the performances of lithium cells with fluorinated fullerene cathodes.

In the early stage of the studies on these subjects, several attempts have been made by using the fluorinated fullerenes as cathode materials of lithium cells in LiClO₄-propylene carbonate solution [68,69]. However, the interpretation of the electrochemical results and evaluations of cell performances were difficult because of the dissolution of reduced species of fullerenes and fluorinated fullerenes in the electrolytes during the electrochemical process. This difficulty has been overcome using solid-state lithium cells Li/Li⁺-MEP-7/A {A = C_{60} , C_{70} , $C_{60}F_x$, $C_{70}F_x$, Li⁺-MEP-7 = a polymer electrolyte which is Li⁺ doped polyphosphazene derivatives [—N=P(OC₂H₄OCH₃)₇—]_n}, and the electrochemical characteristics of Li/ $C_{60}F_x$ and Li/ $C_{70}F_x$ cells have fully been investigated [70]. Cyclic voltammograms of $C_{60}F_x$ and $C_{70}F_x$ each showed an irreversible reduction peak at a higher potential (ca 3.1 V vs Li⁺/Li for $C_{60}F_x$ and 3.4 V for $C_{70}F_x$). Since no corresponding re-oxidation peak appeared when the sweep direction was reversed after the reduction sweep, it is assigned to the irreversible reduction of C—F bonds. The irreversible C—F bond reduction peak of $C_{60}F_x$ appears at a potential more positive than that observed for (CF)_n by 0.5 V, indicating that the C—F bonds in fluorinated fullerene have higher activity and are reduced more easily than those in (CF)_n. When swept to more negative potentials (1.0 V vs Li⁺/Li), three and four redox peaks are observed

for $C_{60}F_x$ and $C_{70}F_x$, respectively. As the redox potentials are near those observed for pristine fullerenes, these are due to the doping of Li^+ into the reduced $C_{60}F_{x-n}$ and $C_{70}F_{x-n}$, the electronic structures of which have been recovered near those of pristine C_{60} and C_{70} by the reduction of C—F bonds. Therefore, the cathodic reactions during CV can be deduced as follows:



Parallel equations apply to $C_{70}F_x$.

The galvanostatic discharge curves of $C_{60}F_{45}$ and $C_{70}F_{50}$ at 298, 323 and 373 K are shown in Fig. 22, where the cathode utilities were calculated from the quantity of electricity passed. The discharge performances improve greatly by raising the temperature, and it is attributed to the temperature dependence of the ionic conductivity of the solid electrolyte. The cell discharges stably under a load of $10 \mu A/cm^2$, and a high utilization of 90% is obtained at 373 K. The potential decreases gradually and no plateau is observed, suggesting a continuous change in the E_F during the discharge. This is in contrast to the discharge characteristics of $(CF)_n$, where potential barely decreases until the end of discharge [71,72]. This is because of the heterogeneous electrochemical reduction of $(CF)_n$ as opposed to the homogeneous reduction of $C_{60}F_x$. The XPS analyses of the discharged products confirmed that the discharge reaction proceeds with the reduction of C—F bonds until the

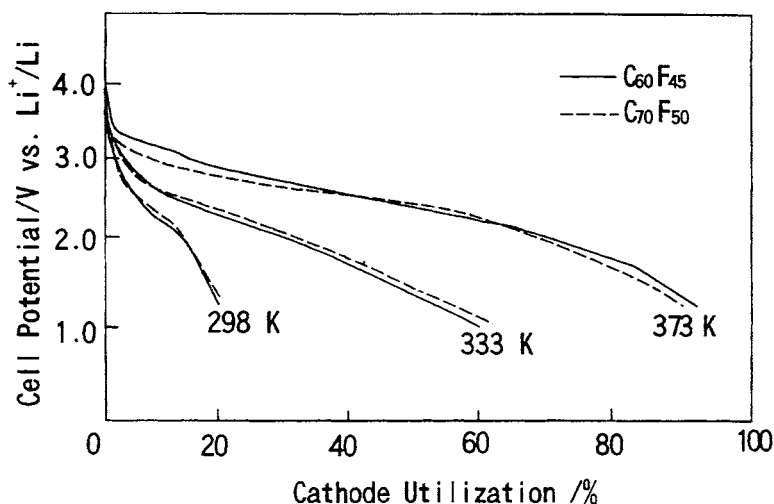


Fig. 22. Galvanostatic discharge curves of Li/Li^+ -MEP-7/ $C_{60}F_x$ and $C_{70}F_x$ cells at $10 \mu A/cm^2$ (reproduced by permission of the Electrochemical Society from J. Electrochem. Soc., 143 (1996) 2270 [70]).

C—F bonds in the $C_{60}F_x$ are completely reduced as follows:



The discharge properties of $C_{70}F_x$ is essentially the same as those of $C_{60}F_x$.

The discharge mechanism proposed above indicates that $C_{60}F_x$ with different degrees of fluorination are formed under the different cathode utilities (discharge percent of the cathode material). Hence, it is possible to investigate the change in E_F for $C_{60}F_x$ and $C_{70}F_x$ with different degrees of fluorination by determining

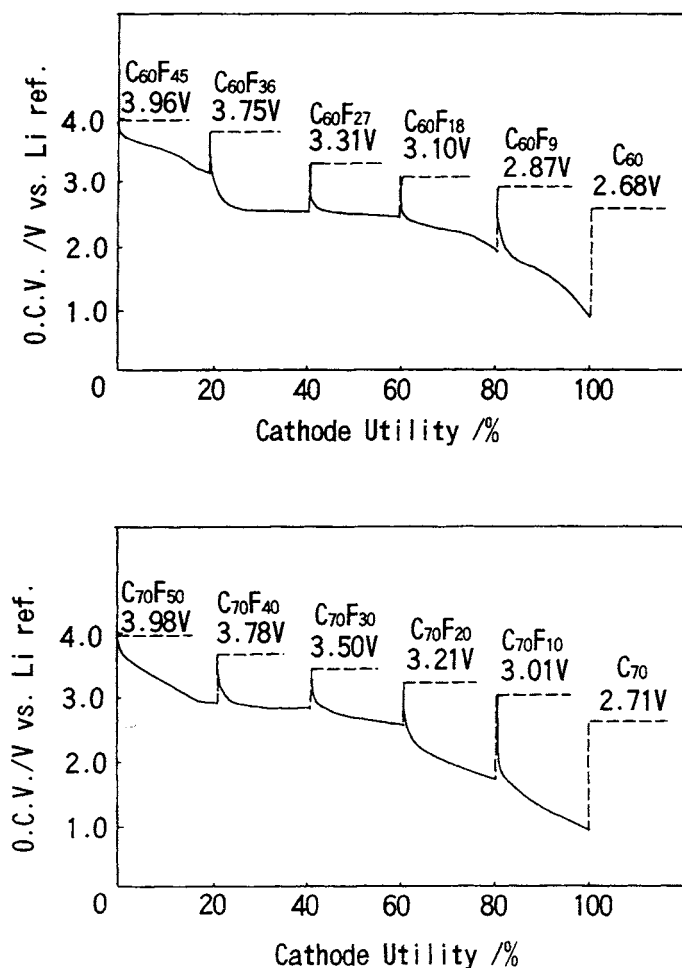


Fig. 23. Dependences of open circuit voltage (OCV) on cathode utility of discharge ($10 \mu\text{A}/\text{cm}^2$) at 373 K for $C_{60}F_x$ and $C_{70}F_x$ cells. Dashed line indicates recovery of OCV over 24 h. Time scale is not taken into account (reproduced by permission of the Electrochemical Society from J. Electrochem. Soc., 143 (1996) 2271 [70]).

the open circuit voltage (OCV) at various discharge utilities. The OCV at different cathode utilities are shown in Fig. 23. The values of x at different utilities of discharge have been calculated from the quantity of electricity passed. Compared with the OCV of pristine fullerenes, the OCV of the fluorinated fullerenes before discharge are higher by ca 1.0 V, suggesting the E_F energy of the fullerenes are lowered greatly by fluorination. It is noted that the OCV decreases as the value of x decreases during discharge, implying that a rise in E_F levels occurs through the transfer of electrons into the π -band and that the consequent recovery of the electronic band structure to those of pristine C_{60} and C_{70} has been achieved. This, again, is in contrast to the case of $(CF)_n$, where the OCV is recovered to the initial value until the end of discharge [71,72]. The OCV for $C_{60}F_x$ and $C_{70}F_x$ after discharge are 2.60 V and 2.71 V, respectively, which are approximately equal to those of pristine C_{60} and C_{70} , indicating that the electronic structures of $C_{60}F_x$ and $C_{70}F_x$ have recovered to those of C_{60} and C_{70} after discharge.

17.7 Properties and potential applications

Basic investigations such as selective syntheses, structural and electronic properties of fluorinated fullerenes have recently been much developed as was discussed earlier in this chapter. In general, however, research on applications is still at a very early stage. Potential applications of these materials would be related to their characteristic physical and chemical properties, some of which are summarized in Table 3.

The sublimation temperatures (under Ar gas flow) of fullerenes C_{60} and C_{70} drastically decrease by fluorination, and the sublimation enthalpy ΔH_s of C_{60} also decreases greatly. The changes in thermal properties upon fluorination suggest the weaker intermolecular bonding of $C_{60}F_x$ and $C_{70}F_x$ than that of pristine

Table 3

Some physical properties of C_{60} , $C_{60}F_x$ ($x \approx 46$), C_{70} and $C_{70}F_x$ ($x \approx 54$)

	C_{60}	$C_{60}F_x$	C_{70}	$C_{70}F_x$
Sublimation temperature (K) ^a	1050	700	1100	700
Sublimation enthalpy (kJ/mol)	186	113	180	122
Contact angle of water (deg.)	90	103.5	—	—
Fermi level (eV)	4.3	5.4	—	—
Electron affinity (eV)	2.67	4.06	2.68	4.33
OCV vs Li^+/Li ref. (V)	3.1	3.9	3.1	4.0
Theoretical capacity (Wh/kg)	—	2650	—	2360
Bulk modulus K_0 (GPa)	18.1 [76]	17.2 [77]	25 [54]	26.6 [58]
K_0' ($=dK_0/dP$)	5.7 [76]	10.7 [77]	10.6 [54]	3.0 [58]
Phase transition	sc \rightleftharpoons fcc at 260 K	No transition down to 10 K [73]	mncl (280 K) \rightleftharpoons rh \rightleftharpoons (330 K) fcc	No transition down to 80 K [77]

^a Under Ar flow.

fullerenes. These properties are consistent with the observation that, contrary to the crystalline C_{60} , no phase transformation due to rotational transition is observed down to 10 K for $C_{60}F_x$ crystals [73]. The C_{60} thin films (500 nm) prepared by the vacuum evaporation method has a hydrophobic surface for which the contact angle of a water droplet is 90° . The value increases more than 13° by the fluorine addition, indicating the lower surface energy of $C_{60}F_x$.

The bulk moduli K of $C_{60}F_x$ and $C_{70}F_x$ obtained by X-ray diffraction experiments under high pressure up to 7 GPa are almost comparable to those of C_{60} and C_{70} , indicating that the cage structures of molecules are maintained under the high pressure and that their "softness" are unchanged by fluorine addition [58].

The properties mentioned above would offer significant potential for selected mechanical and tribological applications. Ever since C_{60} was discovered, the possibility of using fluorinated fullerenes such as $C_{60}F_{60}$ as super-lubricants was considered. It has, however, been shown that highly fluorinated C_{60} lacks chemical stability under a certain circumstance; they hydrolyse rapidly in the presence of water and a cosolvent for the fluorinated species [74,75], and therefore has been considered to be unsuitable for application as a lubricant. Nevertheless it should be emphasized here that highly fluorinated fullerenes $C_{60}F_x$ ($x \approx 46$) obtained by high temperature fluorinations (473–503 K) are stable in moist air, even in water and the phase-pure compounds with a high symmetry obtained by recently developed selective synthesis will be more stable than mixtures used in the early stage of $C_{60}F_x$ chemistry in the first half-1990s.

Electronics and electrochemical applications are of great interest. As described in Secs 17.2, 17.5 and 17.6, the energies of E_F and E_a of C_{60} become larger as the degree of fluorination increases. These results suggest that the control of electronic structure of C_{60} are possible by the control the fluorine addition. Highly fluorinated $C_{60}F_x$ ($x > 40$) has a wide band gap larger than 3 eV, whereas, fluorinated fullerenes $C_{60}F_x$ of lower fluorine content ($x < 18$) which are being challenged to prepare, will have a narrower band gap suitable for potential electronics. The discharge reaction in the lithium cell with $C_{60}F_x$ or $C_{70}F_x$ cathode is irreversible and therefore the cells are of primary batteries. Nonetheless, the theoretical energy densities of both $C_{60}F_x$ and $C_{70}F_x$, based on their OCV values, are extremely large.

References

- [1] J.H. Holloway, In: Fluorine-Carbon and Fluoride-Carbon Materials, T. Nakajima (Ed.), Marcel Dekker, Inc., New York, NY, 1995, Chapter 6.
- [2] J.H. Holloway, E.G. Hope, In: The Chemistry of Fullerenes, R. Taylor (Ed.), World Scientific, Singapore, 1995, Chapter 6.
- [3] F. Okino, H. Touhara, In: Comprehensive Supramolecular Chemistry, Vol. 7, Solid State Supramolecular Chemistry: Two- and Three-Dimensional Inorganic Networks, J.L. Atwood, J.E.D. Davies, D.D. MacNicol, F. Vögtle (Ser. Eds.), G. Alberti, T. Bein (Eds.), Pergamon, Oxford, 1996, Chapter 2.
- [4] R. Taylor, Russ. Chem. Bull., 47 (1998) 823.
- [5] R.C. Haddon, Philos. Trans. R. Soc. Lond. A, 343 (1993) 53.

- [6] S. Saito, A. Oshiyama, *Phys. Rev. Lett.*, 66 (1991) 2637.
- [7] R.C. Haddon, *J. Am. Chem. Soc.*, 112 (1990) 3385.
- [8] L.-S. Wang, J. Conceicao, C. Jin, R.E. Smalley, *Chem. Phys. Lett.*, 182 (1991) 5.
- [9] S. Saito, A. Oshiyama, *Phys. Rev. B*, 49 (1994) 17413.
- [10] D.L. Lichtenberger, K.W. Nebesny, C.D. Ray, D.R. Huffman, L.D. Lamb, *Chem. Phys. Lett.*, 176 (1991) 203.
- [11] D. Dubois, K.M. Kadish, S. Flanagan, L. Wilson, *J. Am. Chem. Soc.*, 113 (1991) 7773.
- [12] P. Scharff, W. Bischof, S. Ebinal, C. Ehrhardt, R. Gerken, V. Kaiser, F. Menzel, C. Tanke, *Carbon*, 32 (1994) 709.
- [13] Q. Xie, E. Pérez-Cordero, L. Echegoyen, *J. Am. Chem. Soc.*, 114 (1992) 3978.
- [14] Y. Ohsawa, T. Saji, *J. Chem. Soc., Chem. Commun.*, (1992) 781.
- [15] *Electronic Properties of Fullerenes*, H. Kuzmany, J. Fink, Mehring, S. Roth (Eds.), Springer-Verlag, Berlin, 1993.
- [16] *The Fullerenes*, H.W. Kroto, J.E. Fischer, D.E. Cox (Eds.), Pergamon Press, Oxford, 1993.
- [17] S.H. Yang, C.L. Pettiette, J. Conceicao, O. Cheshnovsky, R.E. Smalley, *Chem. Phys. Lett.*, 139 (1987) 233.
- [18] N. Sato, Y. Saito, H. Shinohara, *Chem. Phys.*, 162 (1992) 433.
- [19] T. Takahashi, T. Morikawa, S. Sato, H. Katayama-Yoshida, A. Yuyama, K. Seki, H. Fujimoto, S. Hino, S. Hasegawa, K. Kamiya, H. Inokuchi, K. Kikuchi, S. Suzuki, K. Ikemoto, Y. Achiba, *Physica C*, 185-189 (1991) 417.
- [20] P.J. Benning, D.M. Poirier, T. Ohno, Y. Chen, M.B. Jost, F. Stepniak, G.H. Kroll, J.H. Weaver, J. Fure, R.E. Smalley, *Phys. Rev. B*, 45 (1992) 6899.
- [21] R. Mitsumoto, T. Araki, E. Ito, Y. Ouchi, K. Seki, K. Kikuchi, Y. Achiba, H. Kurosaki, T. Sonoda, H. Kobayashi, O.V. Boltalina, V.K. Pavlovich, L.N. Sidorov, Y. Hattori, N. Liu, S. Yajima, S. Kawasaki, F. Okino, H. Touhara, *J. Phys. Chem. A*, 102 (1998) 552.
- [22] W.R. Datars, P.K. Ummat, T. Olech, R.K. Nkum, *Solid State Commun.*, 86 (1993) 579.
- [23] W.R. Datars, P.K. Ummat, *Solid State Commun.*, 94 (1995) 649.
- [24] A.J. Adamson, J.H. Holloway, E.G. Hope, R. Taylor, *Fullerene Sci. Technol.*, 5 (1997) 629.
- [25] A.A. Tuinman, P. Mukherjee, J.L. Adcock, R.L. Hettich, R.N. Compton, *J. Phys. Chem.*, 96 (1992) 7584.
- [26] F. Okino, S. Kawasaki, Y. Fukushima, M. Kimura, T. Nakajima, H. Touhara, *Fullerene Sci. Technol.*, 4 (1996) 873.
- [27] A.A. Tuinman, A.A. Gakh, J.L. Adcock, R.N. Compton, *J. Am. Chem. Soc.*, 115 (1993) 5885.
- [28] A.A. Gakh, A.A. Tuinman, J.L. Adcock, R.A. Sachleben, R.N. Compton, *J. Am. Chem. Soc.*, 116 (1994) 819.
- [29] J.H. Holloway, E.G. Hope, R. Taylor, G.J. Langley, A.G. Avent, T.J. Dennis, J.P. Hare, H.W. Kroto, D.R.M. Walton, *J. Chem. Soc., Chem. Commun.*, (1991) 966.
- [30] S.K. Chowdhury, S.D. Cameron, D.M. Cox, K. Kniaz, R.A. Strongin, M.A. Cichy, J.E. Fischer, A.B. Smith, III, *Org. Mass. Spectr.*, 28 (1993) 860.
- [31] H. Selig, K. Kniaz, G.B.M. Vaughan, J.E. Fischer, A.B. Smith III, *Macromol. Symp.*, 82 (1994) 89.
- [32] R. Taylor, G.J. Langley, J.H. Holloway, E.G. Hope, A.K. Brisdon, H.W. Kroto, D.R.M. Walton, *J. Chem. Soc., Perkin Trans. 2*, (1995) 181.
- [33] N. Liu, H. Touhara, Y. Morio, D. Komichi, F. Okino, S. Kawasaki, *J. Electrochem. Soc.*, 143 (1996) L214.

- [34] O.V. Boltalina, A.Ya. Borschevskii, L.N. Sidorov, J.M. Street, R. Taylor, *Chem. Commun.*, (1996) 529.
- [35] G.E. Scuseria, *Chem. Phys. Lett.*, 176 (1991) 423.
- [36] J. Cioslowski, *Chem. Phys. Lett.*, 181 (1991) 68.
- [37] O.V. Boltalina, L.N. Sidorov, V.F. Bagryantsev, V.A. Seredenko, A.S. Zapol'skii, J.M. Street, R. Taylor, *J. Chem. Soc., Perkin Trans. 2*, (1996) 2275.
- [38] S. Kawasaki, T. Aketa, H. Touhara, F. Okino, O.V. Boltalina, I.V. Gol'dt, S.I. Troyanov, R. Taylor, *J. Phys. Chem. B*, 103 (1999) 1223.
- [39] O.V. Boltalina, J.M. Street, R. Taylor, *J. Chem. Soc., Perkin Trans. 2*, (1998) 649.
- [40] H. Touhara, N. Kadono, N. Watanabe, J.-J. Braconnier, *J. Electrochem. Soc.*, 134 (1987) 1071.
- [41] A.D. Darwish, A.K. Abdul-Sada, G.J. Langley, H.W. Kroto, R. Taylor, D.R.M. Walton, *J. Chem. Soc., Perkin Trans. 2*, (1995) 2359.
- [42] O.V. Boltalina, V.Yu. Markov, R. Taylor, M.P. Waugh, *Chem. Commun.*, (1996) 2549.
- [43] H. Selig, C. Lifshitz, T. Peres, J.E. Fischer, A.R. McGhie, W.J. Romanow, J.P. McCauley Jr, A.B. Smith III, *J. Am. Chem., Soc.*, 113 (1991) 5475.
- [44] P.A. Heiney, J.E. Fischer, A.R. McGhie, W.J. Romanow, A.M. Denenstein, J.P. McCauley Jr, A.B. Smith III, D.E. Cox, *Phys. Rev. Lett.*, 66 (1991) 2911.
- [45] W.I.F. David, R.M. Ibberson, J.C. Matthewman, K. Prassides, T.J.S. Dennis, J.P. Hare, H.W. Kroto, R. Taylor, D.R.M. Walton, *Nature*, 353 (1991) 147.
- [46] C.S. Yannoni, R.D. Johnson, G. Meijer, D.S. Bethune, J.R. Salem, *J. Phys. Chem.*, 95 (1991) 9.
- [47] R. Tycko, G. Dabbagh, R.M. Fleming, R.C. Haddon, A.V. Makhija, S.M. Zahurak, *Phys. Rev. Lett.*, 67 (1991) 1886.
- [48] R.D. Johnson, C.S. Yannoni, H.C. Dorn, J.R. Salem, D.S. Bethune, *Science*, 255 (1992) 1235.
- [49] P.A. Heiney, J.E. Fischer, A.R. McGhie, W.J. Romanow, A.M. Denenstein, J.P. McCauley Jr, A.B. Smith III, D.E. Cox, *Phys. Rev. Lett.*, 66 (1991) 2911.
- [50] R. Sachidanandam, A.B. Harris, *Phys. Rev. Lett.*, 67 (1991) 1467.
- [51] P.A. Heiney, J.E. Fischer, A.R. McGhie, W.J. Romanow, A.M. Denenstein, J.P. McCauley Jr, A.B. Smith III, D.E. Cox, *Phys. Rev. Lett.*, 67 (1991) 1468.
- [52] F. Okino, H. Fujimoto, R. Ishikawa, H. Touhara, *Trans. Mat. Res. Soc. Jpn.*, 14B (1994) 1205.
- [53] G.B.M. Vaughan, P.A. Heiney, J.E. Fischer, D.E. Luzzi, D.A. Ricketts-Foot, A.R. McGhie, Y.-W. Hui, A.L. Smith, D.E. Cox, W.J. Romanow, B.H. Allen, N. Coustel, J.P. McCauley Jr, A.B. Smith III, *Science*, 254 (1991) 1350.
- [54] C. Christides, I.M. Thomas, T.J.S. Dennis, K. Prassides, *Europhys. Lett.*, 22 (1993) 611.
- [55] M.A. Verheijen, H. Meekes, G. Meijer, P. Bennema, J.L. de Boer, S. van Smaalen, G. van Tendeloo, S. Amelinckx, S. Muto, J. van Landuyt, *Chemical Physics*, 166 (1992) 287.
- [56] T. Nakajima, M. Matsuo, *Carbon*, 30 (1992) 1119.
- [57] F. Okino, H. Touhara, K. Seki, R. Mitsumoto, K. Shigematsu, Y. Achiba, *Fullerene Sci. Technol.*, 1 (1993) 425.
- [58] S. Kawasaki, T. Aketa, F. Okino, H. Touhara, T. Hattori, T. Nagai, T. Yamanaka, *Solid State Commun.*, 108 (1998) 749.
- [59] P.J. Benning, T.R. Ohno, J.H. Weaver, P. Mukherjee, J.L. Adcock, R.N. Compton, B.I. Dunlap, *Phys. Rev. B*, 47 (1993) 1589.
- [60] C. Jin, R.L. Hettich, R.N. Compton, A. Tuinman, A. Derecskei-Kovacs, D.S. Marynick, B.I. Dunlap, *Phys. Rev. Lett.*, 73 (1995) 2821.

- [61] K. Kniaż, J.E. Fischer, H. Selig, G.B.M. Vaughan, W.J. Romanow, D.M. Cox, S.K. Chowdhury, J.P. McCauley, R.M. Strongin, A.B. Smith III, *J. Am. Chem. Soc.*, 115 (1993) 6060.
- [62] D.M. Cox, S.D. Cameron, A. Tuinman, A. Gakh, J.L. Adcock, R.N. Compton, E.W. Hagaman, K. Kniaż, J.E. Fischer, R.M. Strongin, M.A. Cichy, A.B. Smith III, *J. Am. Chem. Soc.*, 116 (1994) 1115.
- [63] S. Kawasaki, F. Okino, H. Touhara, T. Sonoda, *Phys. Rev. B*, 53 (1996) 16652.
- [64] R. Mitsumoto, Doctoral Thesis, Nagoya University (1998).
- [65] F. Zhou, G.J. Van Berkel, B.T. Donovan, *J. Am. Chem. Soc.*, 116 (1994) 5485.
- [66] M.E. Burba, S.K. Lim, A.C. Albrecht, *J. Phys. Chem.*, 99 (1995) 11839.
- [67] C. Brink, L.H. Anderson, P. Hvelplund, D. Mathur, J.D. Voldstad, *Chem. Phys. Lett.*, 233 (1995) 52.
- [68] F. Okino, S. Yajima, S. Suganuma, R. Mitsumoto, K. Seki, H. Touhara, *Synth. Metals*, 70 (1995) 1447.
- [69] Y. Matsuo, T. Nakajima, *Electrochem. Acta*, 41 (1996) 15.
- [70] N. Liu, H. Touhara, F. Okino, S. Kawasaki, Y. Nakacho, *J. Electrochem. Soc.*, 143 (1996) 2267.
- [71] N. Watanabe, T. Nakajima, H. Touhara, *Graphite Fluorides*, Elsevier, Amsterdam, 1988, p. 150.
- [72] R. Hagiwara, T. Nakajima, N. Watanabe, *J. Electrochem. Soc.*, 135 (1988) 3128.
- [73] F. Okino, S. Kawasaki, H. Touhara, unpublished data.
- [74] R. Taylor, J.H. Holloway, E.G. Hope, A.G. Avent, G.J. Langley, T.J. Dennis, J.P. Hare, H.W. Kroto, D.R.M. Walton, *J. Chem. Soc., Chem., Commun.*, (1992) 665.
- [75] R. Taylor, A.G. Avent, T.J. Dennis, J.P. Hare, H.W. Kroto, D.R.M. Walton, J.H. Holloway, E.G. Hope, G.J. Langley, *Nature*, 355 (1992) 27.
- [76] S.J. Duclos, K. Brister, R.C. Haddon, A.R. Kortan, F.A. Thiel, *Nature*, 351 (1991) 380.
- [77] S. Kawasaki, F. Okino, H. Touhara, unpublished data.

Text Quotation References

Text page 557, line 7–line 15; and page 576, line 10 – page 578, line 2: adapted with permission of American Chemical Society from *J. Phys. Chem. A*, 102 (1998) 552 [21].

CHAPTER 18

Fluorinated Pitch

Hiroyuki Fujimoto^a and Toshiyuki Maeda^b

^aResearch & Development Department, Osaka Gas Co. Ltd., Torishima 6-19-9, Konohana-ku, Osaka, 554-0051, Japan; ^bResearch & Development Department, Osaka Gas Co. Ltd., Hirano-cho 4-1-2, Chuo-ku, Osaka, 541-0046, Japan

18.1 Historical aspect

18.1.1 Direct fluorination of carbons and condensed polynuclear aromatic compounds

Graphite fluorides, $(\text{CF})_n$ and $(\text{C}_2\text{F})_n$, are well-known as the products by the direct fluorination of carbon material. Among them, $(\text{CF})_n$ has already been commercialized as the cathode material of lithium batteries [1–4]. These compounds are generally prepared from carbon or crystallized graphite at temperatures considerably higher than 300 or 350°C [5]. That is, $(\text{CF})_n$ is formed at around 600°C, and $(\text{C}_2\text{F})_n$ at around 350°C from graphite. Between these temperatures, a mixture of $(\text{CF})_n$ and $(\text{C}_2\text{F})_n$ is obtained. At temperatures less than 100°C, fluorine exclusively intercalates into graphite under the coexistence of hydrogen fluoride or metal fluorides [6–8].

On the other hand, Margrave et al. reported that the condensed polynuclear aromatic compounds such as anthracene, pyrene and coronene, were easily fluorinated even at ambient temperature and that the various perfluoro-derivatives were obtained depending upon the starting materials [9–12]. In their method, fluorine gas was introduced into the reactor at a slow rate such that the initial concentration of the fluorine was a mere trace and the concentration of fluorine was then gradually increased up to 100%. Such fluorination condition was quite different from that of the graphite in spite of the common feature of the existence of the graphite-like layers and π -bond.

18.1.2 Pitch as a raw material for direct fluorination

There is a compound called “pitch” which is regarded as an intermediate material between carbon and condensed polynuclear aromatic compounds from the structural and stoichiometric viewpoint. There is no clear definition as concerns pitch, but it is generally regarded as a mixture of a variety of aromatic hydrocarbons with various molecular weights and a solid at room temperature with a softening point. Though the pitch is classified into aromatic organic material, the average molecular

weight is considerably larger than those of aromatic hydrocarbons used for the fluorination by Margrave et al. Especially, the mesophase pitch is also considered as a precursor of graphite, because it is the starting material of carbon- or graphite-fiber and is the lamellar compound. The history of mesophase pitch traces back to the study done by Brooks and Taylor in 1961 [13–15]. They found a formation and enlargement of optical anisotropic fine spheres from within the melt of coal in the process of the heat treatment of coal. These spheres have single crystallographic orientation and swell until they begin to interfere with each other's growth. And finally, the mosaic-type solid structure called "bulk mesophase" forms. Brooks and Taylor firstly proposed "mesophase" as a technical term for this intermediate phase from liquid to solid, in which organic compounds are polymerized by the thermal decomposition or condensation reaction to give a optical anisotropic structure with regular orientation of molecules. Since then, the understanding of the carbonization phenomena has improved substantially.

Nowadays, it is widely known that mesophase transformation occurs in organic materials such as pitches during the pyrolysis at temperature between 350°C and 500°C [16]. During the heat treatment of pitch, polycondensed aromatic hydrocarbons are formed by the thermal decomposition, followed by the orientation of polycondensed aromatic hydrocarbons in a fixed direction and finally the mesophase spheres are formed by the stacking of the oriented polycondensed hydrocarbons. Once these spherules meet each other, the coalescence occurs to larger droplets leading eventually to bulk mesophase. Then, the further pyrolyzation of the coalesced mesophase produces the several textures such as fibrous or mosaic. This mesophase transformation is essential for the formation of precursors to be carbonized or graphitized. In 1985, Fujimoto et al. thought that the structural similarity of mesophase pitch to carbon would give the similar compound to graphite fluoride, and applied a mesophase pitch to a raw material for the direct fluorination [17–21]. The pitch used by them was prepared from a coal tar pitch by the heat treatment up to 450°C, so that the softening point was ca 300°C. They firstly obtained a yellowish white powdery compound with the composition of $\text{CF}_{1.16}$ and $\text{CF}_{1.27}$ by the direct fluorination of mesophase pitch at 0°C in 1985 [17,18] and reported their basic structure and physicochemical properties [17,18,21,23,24]. After that, they also obtained the other types of fluorinated pitches (transparent resin and liquid types) by controlling the fluorination conditions and revealed their structures [22,24]. Most of the basic studies concerning the fluorinated pitches were done by Fujimoto et al. and reported in detail [17–24]. Nowadays, three types of fluorinated pitches are known. In this chapter, the synthetic method, basic structures, physicochemical properties and promising applications of the fluorinated pitches will be given.

18.2 Synthesis and structure of fluorinated pitch

18.2.1 Synthetic method

As mentioned in the last section, three types of fluorinated pitches, yellowish white powdery solid (S-type), colorless transparent resin (R-type) and liquid (L-type),

are known. The first one is obtained by the direct fluorination of pitch at the temperature range of 0–250°C, and the others are by the heat treatment of the S-type fluorinated pitch under a fluorine atmosphere at the temperature range of 200–400°C. Hereafter, the materials will be abbreviated as S-type, R-type and L-type, respectively and followed by its fluorination or heat treatment temperature, for instance, “S-type90” for the specimen fluorinated at 90°C, and “R-type250” for the specimen heat-treated at 250°C. The detail synthetic conditions are as follows.

18.2.1.1 Direct fluorination of mesophase pitch

In general, the substitution of hydrogen by fluorine and addition of fluorine to C=C bond are such an exothermic reaction that they accompany the cleavage of C—C bond and the ring-opening reaction. Hence, for the first attempt of fluorination of pitch, Fujimoto et al. selected the lower reaction temperature of 0–250°C compared with that of graphite [17,18]. As a result, they found that the fluorine smoothly reacts with pitch to give the S-type of fluorinated pitch even at 0°C. After that, they investigated the relation between the fluorine gas volume for the reaction and yield in detail [21,24]. In Fig. 1 is plotted the weight ratio, $(W_p/W_s) \times 100$, where W_p and W_s denote the quantities of fluorinated pitch and mesophase pitch, respectively, as a function of the amount of supplied fluorine gas for the fluorination

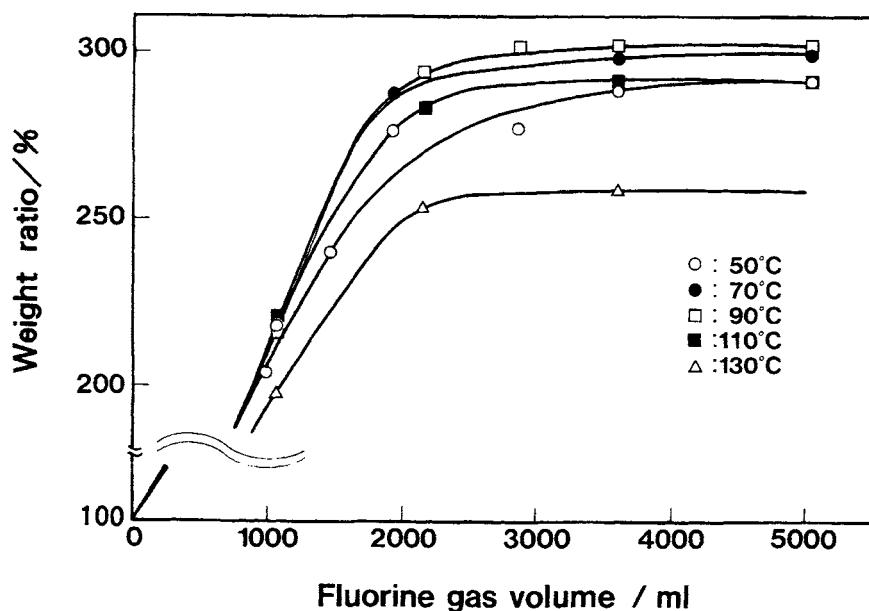
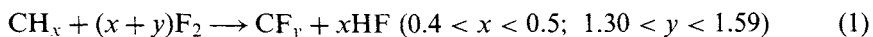


Fig. 1. Weight ratio of the solid type fluoride to the mesophase pitch as a function of the amount of supplied fluorine gas at several temperatures (quoted from H. Fujimoto, A. Mabuchi, T. Maeda, Y. Matsumura, N. Watanabe, H. Touhara, *Carbon*, 30 (1992) 851, with permission).

at the temperatures between 50°C and 130°C. As the reaction proceeds, the weight increases with increasing the introduced fluorine gas volume and finally goes up to 2.53–3.02 times that of the initial value, while the color of pitch changes from black to yellowish white. As the reaction temperature increases, the color of resulting compound becomes more white. This result correlates to the amount of the residual double-bonds in S-type fluoride. That is, the number of the double-bonds decreases with increasing the reaction temperature. It is supported by the result of elemental analysis. As is shown in Fig. 2, F/C atomic ratio of S-type fluoride increases with the reaction temperature. On the other hand, in Fig. 1, the maximum gain in weight firstly increases with increasing the temperature to become maximum at 90°C and then decreases with increasing temperature. It is considered that this is due to the increase of the decomposition of fluorinated product caused by the cleavage of C—C bond. Especially, above 150°C, the fluorinated pitch is hardly obtained because of the competition between the formation and decomposition reaction of fluorinated compound.

This fluorination reaction is basically caused by the addition of fluorine to carbon double-bond and the displacement of hydrogen by fluorine according to the equation.



However, the addition and displacement of fluorine are such exothermic reactions that they are accompanied by the ring-opening reaction and cleavage of methylene bridges, of which relative amounts are affected by the fluorination temperature. Therefore, in order to restrict the ring-opening reaction, the fluorination must be carried out at relatively low temperatures, for instance, 50°C and 70°C. On

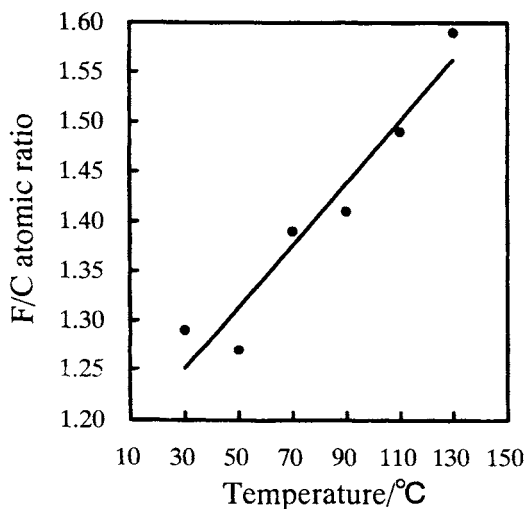


Fig. 2. F/C atomic ratio of solid type fluorinated pitch as a function of the fluorination temperature.

the other hand, it is also pointed out that the S-type fluoride is not fully perfluorinated below 70°C because of the insufficient diffusion energy of fluorine atoms. As a result, unreacted carbon atoms remain in the bulk in the form of double-bonded carbon and the color of the S-type fluoride is not white like graphite fluoride, (CF)_n, but yellowish white.

Maeda considered that the formation reaction of fluorinated pitch is kinetically written by

$$dx/dt = k \cdot (1 - x)^m \cdot P^n \quad (2)$$

where x , t , k , P are conversion rate, time, coefficient of reaction rate, partial pressure of F₂, respectively [25]. He experimentally determined the parameters of m and n to be 0.5, and estimated the activation energy to be 10.03 kJ/mol.

18.2.1.2 Heat treatment of the S-type fluoride in a fluorine atmosphere

Based on the results above mentioned, Fujimoto et al. developed a new fluorination procedure in order to prepare the perfluorinated pitch, and obtained two types of other fluorinated pitches [23,24]. The new process is by the heat treatment at 200–400°C of S-type of fluorinated pitch prepared at relatively low temperature in a fluorine atmosphere. They firstly fluorinated the mesophase pitch at 70°C for 10 h (first step for the preparation of S-type fluorinated pitch) and then heated up to a selected temperature between 200°C and 400°C, and maintained this temperature for 12 h (second step for the heat-treatment of fluorinated pitch). Thus, they obtained two kinds of fluorocarbons, a transparent resin (R-type) and a liquid (L-type). L-type is a viscous fluid containing some volatile materials and the viscosity gradually becomes higher when it is kept for a few weeks in an air atmosphere even at ambient temperature. They reported that the R-type was obtained in the nickel boat in the heating zone and L-type at the bottom of the vertical reaction vessel which was cooled down by the water. Therefore, it is likely that the liquid fluorocarbon is formed by the vaporization of some component contained in the S-type fluoride or decomposition reaction during the heat treatment of the S-type fluoride. The yields of these compounds depends on the heat treatment temperature. In Fig. 3, the yields of the R-type and L-type fluorocarbons are plotted as a function of the heat treatment temperature of the S-type fluoride. The yield of the former decreases with increase of the heat treatment temperature and finally, at 400°C, it can not be obtained at all. On the other hand, the yield of the latter increases with increase of temperature and it is selectively obtained at 400°C.

18.2.2 Structures

As mentioned in the last section, three types of fluorinated pitch are obtained by controlling the fluorination conditions. In this section, the basic structures of those compounds will be discussed based on the results of various analyses.

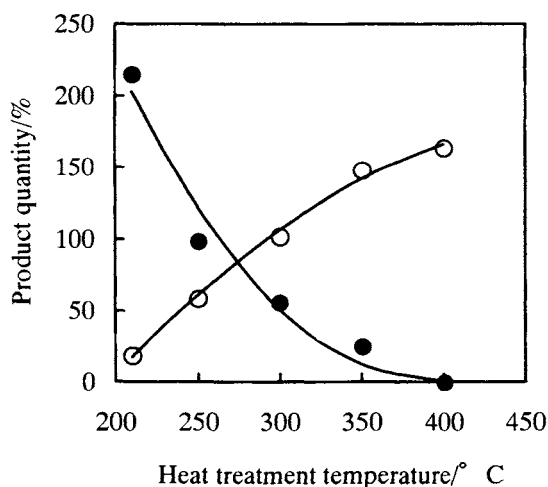


Fig. 3. The yields of the resin and liquid type fluorocarbons as a function of the heat treatment temperature

$$\text{Yield} = \frac{\text{Weight of products}}{\text{Weight of the pristine solid type fluorinated pitch}}$$

18.2.2.1 Powdery solid type of fluorinated pitch

Mesophase pitch is a precursor material of graphite. Accordingly, the X-ray diffraction pattern of the mesophase pitch, as is shown in Fig. 4(A), shows a peak at around 26° which is related to interlayer spacing between the graphite-like planes. In order to verify whether this basic structure come from the mesophase pitch is held before and after fluorination or not, it is important to measure the X-ray diffraction pattern of S-type fluoride. Figure 4(B) and (C) show a typical X-ray diffraction pattern of S-type fluoride and that of graphite fluoride prepared from petroleum coke, respectively. Graphite fluoride has two peaks at around 13° and 40° which are attributed to 001 and 100 line, respectively and the peaks appeared in the pattern of S-type fluoride seems to be closely related to these peaks. However, these two peaks of S-type fluoride are broader than those of graphite fluoride. Taking into consideration that the graphite fluoride is a covalent-bonded intercalation compound, the S-type fluoride is also a lamellar compound and its structure is similar to that of $(\text{CF})_n$ with a low crystallinity.

Fujimoto et al. analyzed S-type fluoride by extensive measurement of ESCA for the purpose to investigate whether hydrogen atoms are replaced by fluorine or not, and whether fluorine adds to double-bonds or not. Figure 5 shows the C_{1s} spectrum of typical S-type fluoride with those of graphite fluoride and polytetrafluoroethylene (PTFE). Concerning PTFE, as the structural formula is expressed by $-(\text{CF}_2)_n-$, the C_{1s} spectrum consists of the peak originating from CF_2 - group (292.4 eV) and the small shoulder peak observed at around 294 eV corresponding to CF_3 which exists at the end of linear structure of PTFE. On the other hand, C_{1s} spectrum of graphite fluoride is composed of the large amount of CF - group at 290 eV and very

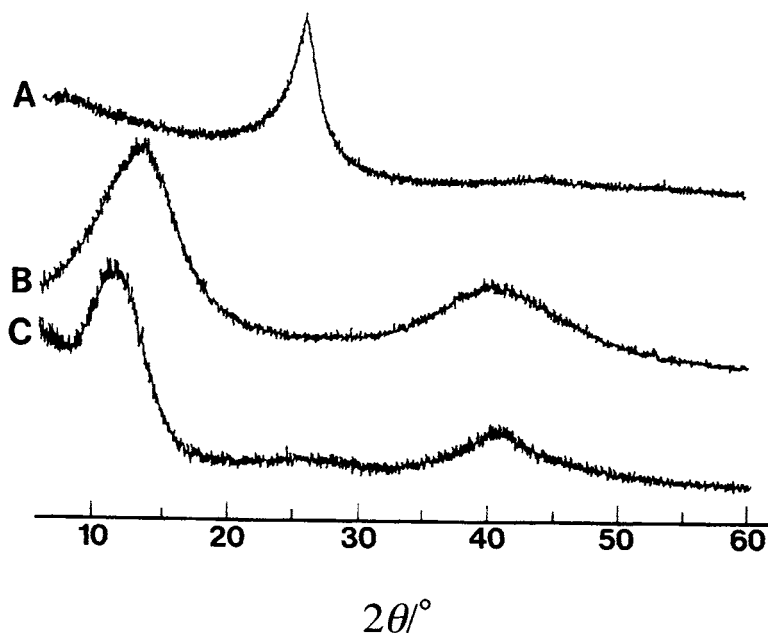


Fig. 4. Typical X-ray diffraction patterns of mesophase pitch, fluorinated pitch and $(CF)_n$: (A) mesophase pitch; (B) solid type fluorinated pitch prepared at 70°C; (C) graphite fluoride, $(CF)_n$. (Quoted from H. Fujimoto, A. Mabuchi, T. Maeda, Y. Matsumura, N. Watanabe, H. Touhara, *Carbon*, 30 (1992) 851, with permission).

small amount of CF_2 - group at 292 eV which exists in the periphery of a layer of hexagonal carbon network. By contrast, with respect to the S-type fluoride, it exhibits a peak at 290 eV due to CF - group, a peak at 292 eV, CF_2 - group and a peak at 294 eV, CF_3 -. It indicates that the CF_2 - groups are not merely peripheral groups, but constitute principal components of the S-type fluoride, as opposed to the CF_2 - groups in the graphite fluoride. Moreover, there was little trace of C—H group. Accordingly, all the hydrogen atoms are considered to be replaced by fluorine.

Although the graphite fluoride is not soluble in any solvent, the fluorinated pitch is soluble in some fluorosolvents such as C_6F_6 , which makes possible the further study by means of ^{19}F NMR to clarify the species of functional groups in fluorinated pitch. The ^{19}F NMR spectra of the S-type fluorides prepared from mesophase pitch at several temperatures are shown in Fig. 6. There exists 5 peaks centered at around -5 ppm, -17 ppm, -55 ppm, -75 ppm and -120 ppm, respectively. The first two peaks at -5 ppm and -17 ppm are assigned to CF_3CF - group and CF_3CF_2 - groups, respectively [26,27]. The third and fourth peaks broaden from -30 ppm to -80 ppm are attributed to $-CF_2$ - groups. The last peak at -120 ppm corresponds to CF - group. The most noticeable feature is that the intensity of CF_3CF_2 - group increases with increasing fluorination temperature. This functional group can

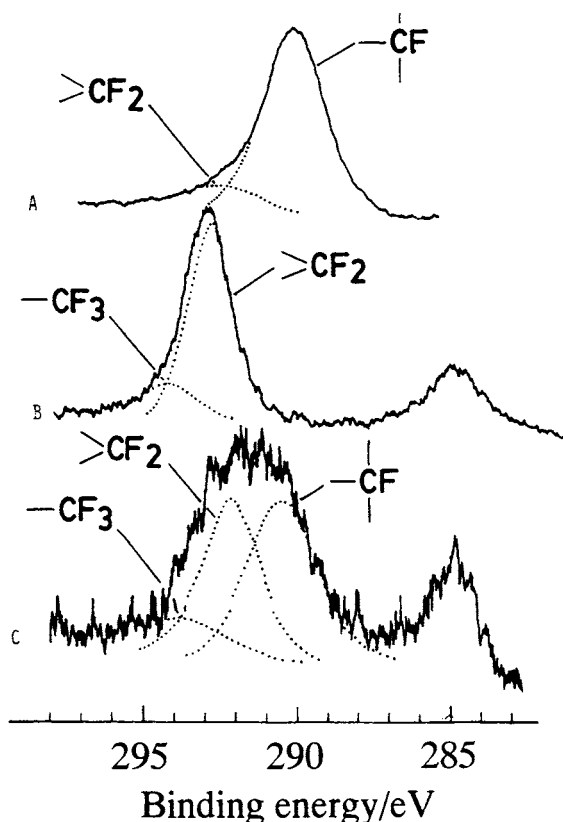


Fig. 5. C_{1s} ESCA spectra of solid type fluorinated pitch, $(CF)_n$ and PTFE: (A) solid type fluoride prepared at 70°C ; (B) graphite fluoride, $(CF)_n$; (C) PTFE. (Quoted from the poster material of Ref. [18]).

not be formed without the ring-opening reaction. Consequently, it is considered that the decomposition of the S-type fluoride simultaneously occurs with the fluorination reaction at relatively higher temperatures.

Pitch consists of a variety of aliphatic and aromatic molecules with molecular weights ranging between about 400 and 4000. Mochida et al. analyzed the extracted quinoline insoluble (QI) component which exhibits the liquid crystal and proposed the structure called "Spider web model" [28]. According to their model, the relatively small condensed-ring compounds in QI component which have the molecular weight of 150–800 are connected by methylene bridges so as to increase its molecular weight. Such polymeric substances with various molecular weights interact with others by van der Waals force to form lamellar structure. On the basis of this proposed structure of pitch, if it is postulated that all the hydrogen atoms in pitch are displaced by fluorine and that the additional reaction of fluorine proceeds completely, the average structure of S-type fluoride will be schematically illustrated as Fig. 7. The fluorine atoms add to the double-bonds from above and below the carbon ring

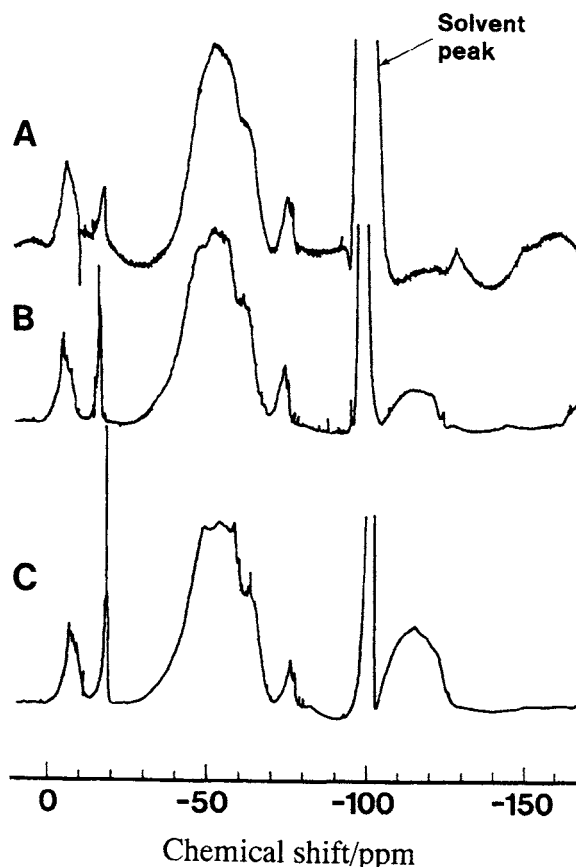


Fig. 6. ^{19}F NMR spectra of solid type fluoride: (A) prepared at 50°C ; (B) prepared at 90°C ; (C) prepared at 110°C . (Quoted from H. Fujimoto, A. Mabuchi, T. Maeda, Y. Matsumura, N. Watanabe, H. Touhara, *Carbon*, 30 (1992) 851, with permission).

network to form the chair-type condensed cyclohexane ring and displace hydrogen atoms which exist in the periphery of the aromatic condensed ring. Such a structure of the condensed ring is identical to that of $(\text{CF})_n$. However, $(\text{CF})_n$ is wholly composed of such a structure, whereas the S-type fluoride is composed of the condensed ring compounds crosslinked by perfluorocarbon bridges which are formed by the substitution of the hydrogen atoms of the methylene bridges crosslinking the aromatic condensed rings in a pitch by fluorine atoms.

Considering the H/C atomic ratio of pitch, the F/C ratio of such a perfluorinated pitch must be approximately expressed as follows; [24]

$$\text{F/C} = f_a + \text{H/C} \dots \quad (3)$$

where H/C is an atomic ratio and f_a is the aromaticity index. As the H/C and f_a

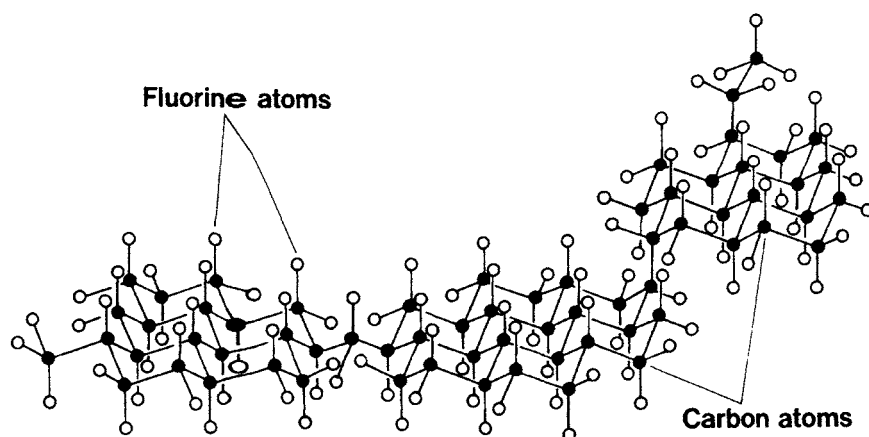


Fig. 7. An average structure model of solid type fluoride (quoted from H. Fujimoto, M. Yoshikawa, A. Mabuchi, T. Maeda, *J. Fluorine Chem.*, 57 (1992) 65, with permission).

Table 1

Physical and chemical properties of S-type fluoride

Sample	F/C atomic ratio	Molecular weight	Interlayer Spacing/nm	Specific gravity	Refractive index	Dielectric constant
S-type30	1.29	4300	0.685	—	—	—
S-type50	1.27	—	0.686	—	1.390	1.93
S-type70	1.39	2700	0.674	1.98	1.380	1.90
S-type90	1.41	—	0.651	2.03	1.373	1.89
S-type110	1.49	2070	0.642	2.07	1.368	1.87
S-type130	1.59	—	0.641	2.07	1.365	1.86
(CF) _n	1.00	—	0.585 ¹	2.68 ²	—	—
PTFE	2.00	—	—	2.1	1.35 ³	< 2.1

¹ The value of (CF)_n prepared from natural graphite, quoted from the Ref. [31]; ² The value of (CF)_n prepared from natural graphite, quoted from the Ref. [32]; ³ Quoted from the Ref. [33].

values of the pitch used in the study by Fujimoto et al. are 0.48 and 0.9–1.0, respectively, the F/C atomic ratios is estimated to be between 1.38 and 1.48. As shown in Table 1, the F/C ratios of S-type90 and S-type110 coincide with the values estimated from Eqn. (3), while those of the samples prepared at relatively lower temperature, for instance, S-type30 or S-type50 show the lower values, 1.29 and 1.27, respectively. This result indicates that there are some carbons which does not bond with fluorine in it. Considering that the color of the S-type fluoride is not white, but yellowish-white, unreacted carbons might be double-bonded each other. Such double-bonded carbons probably exist mainly inside of the con-

densed-cyclohexane rings. On the other hand, F/C ratio of S-type130 is higher than the value estimated from Eqn. (3). This is due to the formation of CF_3CF_2 - group by the ring-opening reaction, which is supported by the result of ^{19}F NMR.

18.2.2.2 Transparent resin type and liquid type of fluorinated pitch

Figure 8(A), (B) and (C) show the ^{19}F NMR spectra of L-type and R-type compounds prepared by the heat treatment at 210°C and the S-type fluoride prepared at 70°C , respectively. Both R and L compounds have basically the same peaks as those of the original S-type fluoride. Consequently, the fundamental structures can be considered to be almost the same as that of the original S-type fluoride. The most noticeable point is that the peak centered at -18 ppm, which is assigned to a CF_3CF_2 - group, of the R-type and L-type are more intense than in the original S-type fluoride. This functional group can only be formed by the ring-opening of the cyclohexane ring in S-type fluoride. Accordingly, the formation of R- and

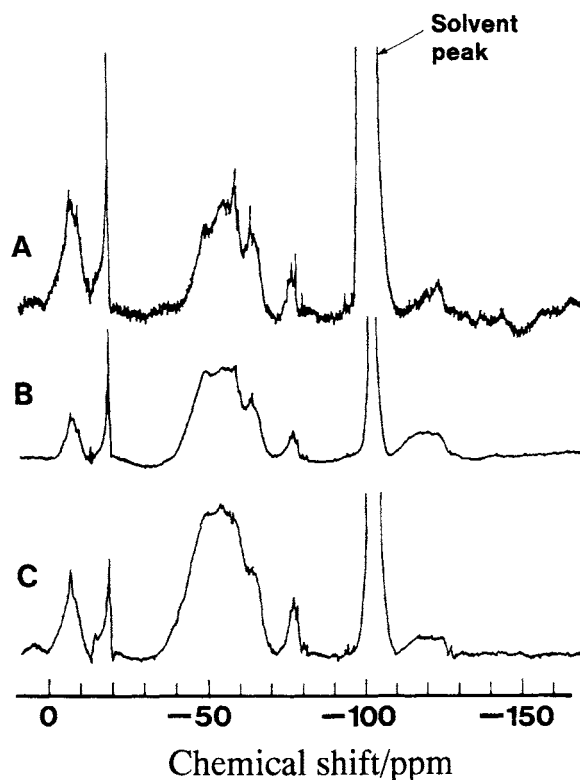


Fig. 8. The ^{19}F NMR spectra of liquid and resin type fluorinated pitches prepared by the heat treatment at 210°C together with the original fluorinated pitch; (A) Liquid type fluorinated pitch; (B) Resin type fluorinated pitch; (C) Solid type fluorinated pitch prepared at 70°C . (Quoted from H. Fujimoto, M. Yoshikawa, A. Mabuchi, T. Maeda, J. Fluorine Chem., 57 (1992) 65, with permission).

L-type compounds are considered to be caused by the ring-opening reaction and the cleavage of C—C bonds.

As the amount of CF_3CF_2 - group relatively increases by the ring-opening reaction during heat-treatment, it is expected that the F/C atomic ratio of both R and L compounds are higher than that of the original S-type fluoride. Figure 9 shows the results of the elemental analysis of the resulting compounds. The F/C atomic ratio of the solid R-type increases up to 1.51 with increasing heat treatment temperature. This is consisted with the increase of the number of CF_3CF_2 - group during the perfluorination of the S-type fluoride. On the other hand, for the L-type, such a relation between F/C and the temperature is not observed. This is presumably due to the vaporization of volatile materials contained in the L-type compound. Since such volatile matters had already vaporized before elemental analysis, the measured atomic ratios are for the residual non-volatile L-type compound. Molecular weights measured for the R-type heat-treated at 210°C and L-type treated at 400°C are 2070 and 850, respectively. Considering that the molecular weight of the original S-type fluoride is about 2700. It is obvious that the S-type fluoride was excessively fluorinated and decomposed by the heat-treatment accompanying the ring-opening reaction, the cleavage of the C—C bonds and the addition of fluorine atoms to double-bonds which remain in the bulk of S-type fluoride.

Based upon the results of elemental analysis, the molecular weights and the structure of the original S-type fluoride, the average structure of the liquid fluorocarbon is concluded as in Fig. 10. The fluorine atoms bond to the carbon atoms from above and below the carbon ring network to form 2 or 3 condensed cyclohexane rings and the periphery of the network consists of the CF_2 , CF_3CF_2 -, CF_3CF - groups

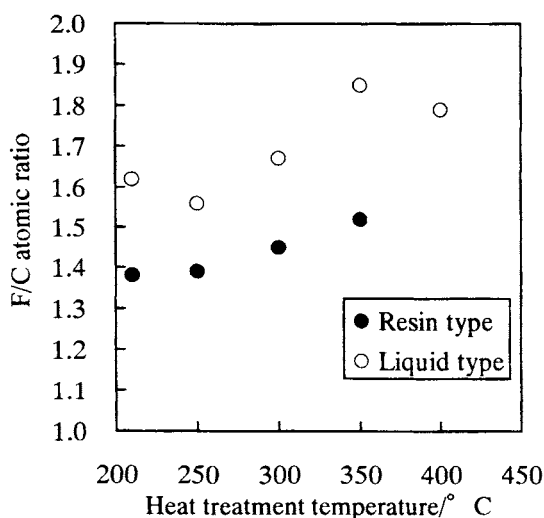


Fig. 9. Relation between the F/C atomic ratio of resin and liquid type fluoride and heat treatment temperature.

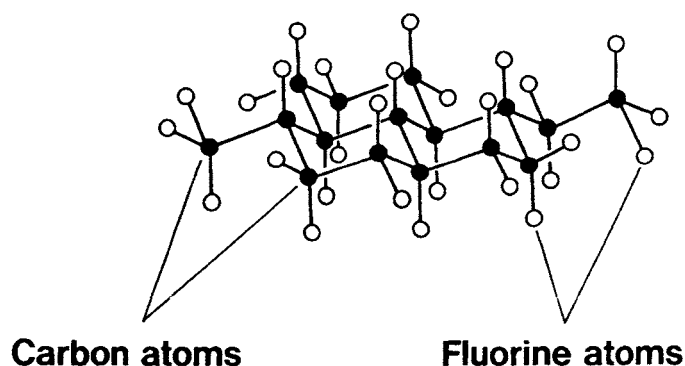


Fig. 10. An average structure of the liquid fluorocarbon (quoted from H. Fujimoto, M. Yoshikawa, A. Mabuchi, T. Maeda, *J. Fluorine Chem.*, 57 (1992) 65, with permission).

etc. The R-type's structure is also considered to be similar, and the difference between the compounds is mainly due to molecular weight. Accordingly, R-type will have a structure such that the condensed cyclohexane ring compounds are crosslinked by perfluorocarbon bridges or the presence of more cyclohexane rings is than in the L-type.

18.3 Physical and chemical properties of solid type fluorinated pitch

The fluorocarbons have unique properties such as low surface energy, low refractive index, excellent insulating ability, not observed in hydrocarbons with similar carbon skeleton structure, because of the strong C—F bond, and the large electro-negativity, the small van der Waals radii, and the small polarizability of fluorine atom. These unique properties are applied to many fields such as a surface coating material, a solid lubricant etc. [29,30]. Since the S-type fluoride is regarded as an intermediate compound between graphite fluoride, $(\text{CF})_n$ and PTFE from the viewpoint of stoichiometry, such common properties of fluorocarbons are also expected for the S-type fluoride. In the present section, physical and chemical properties of S-type fluoride will be introduced.

18.3.1 Chemical composition, molecular weight and specific gravity

Table 1 shows the data of chemical compositions, molecular weights, interlayer spacing and specific gravities of S-type fluorides. As concerns the composition, there is a clear tendency that the F/C atomic ratio increased from 1.29 to 1.59 with increasing the fluorination temperature. Contrary, the molecular weight decreases from 4300 to 2070 with increasing the reaction temperature. As the fluorination temperature increases, the reactivity of elemental fluorine with pitch increases. As a result, the CF_2 bridges crosslinking the condensed cyclohexane rings are cleaved at higher temperatures accompanying the lowering of the molecular weight and the distortion

caused by the structural change from sp^2 carbon to sp^3 carbon is broken off. As a result, the interlayer spacing decreases from 0.685 nm to 0.641 nm with increasing the fluorination and the specific gravity increases.

18.3.2 Refractive index and dielectric constant

In general, the refractive index decreases with the increment of the fluorine content in a polymer because of the small polarizability of fluorine. Column 6 in Table 1 shows refractive indexes of S-type fluorides. As the reaction temperature increases, the refractive index tends to decrease. This tendency is in good agreement with that of F/C atomic ratio. On the basis of the Maxwell's theory of electro-magnetism, the dielectric constant, ϵ is equal to the square of refractive index, n under a fixed frequency. The dielectric constants of the S-type fluoride calculated based on the relation are also shown in Table 1, Column 7. The dielectric constant slightly decreased with increasing the fluorination temperature.

18.3.3 Water- and oil-repellency

Since the F/C atomic ratio and the amount of CF_3 - group of S-type fluoride increase with increasing the fluorination, the water- and oil-repellencies are expected to be improved with increasing the reaction temperature considering the surface tension of CF_3 -. However, as shown in Table 2, the contact angles are independent from the reaction temperature. The surface condition would be almost the same, even the composition is altered. The dominant appearance of CF_3 - group on the surface would be necessary for the improvement of the oil-repellency. The surface free energy of S-type fluoride, $(CF)_n$ and PTFE calculated according to the theory by Owens and Wendt [35–37] are listed in Table 3. Calculation give the surface free energy of 0.95–2.02 mJ/m² for S-type fluoride, 7.01 mJ/m² for $(CF)_n$ and 15.88 mJ/m² for PTFE. The surface energy of S-type fluoride is much lower than those

Table 2

Contact angles for solid type fluoride and other samples at 30°C

Samples	Water	17% NaOH	Glycerol	Formamide	1,4-Butanediol
S-type30	143.3	139.3	146.3	135.2	penetrate
S-type50	142.4	136.7	142.9	138.5	115.9
S-type70	142.1	137.9	142.3	137.2	115.6
S-type90	143.6	137.4	141.1	135.2	115.8
S-type110	143.2	138.6	143.5	138.3	120.6
S-type130	141.3	139.1	140.2	137.1	117.2
$(CF)_n$	143 ± 3^1	139 ± 2^1	151 ± 2^1	128 ± 3^1	103 ± 2^1
PTFE	109 ± 2^1	114 ± 3^1	105 ± 2^1	95 ± 1^1	86 ± 2^1

¹ Quoted from Ref. [34].

Table 3

Components of surface energy of solid type fluoride

Samples	γ^d mJ/m ²	γ_s^h mJ/m ²	γ_s mJ/m ²
S-type30	2.02	6.75×10^{-3}	2.02
S-type50	0.67	0.28	0.95
S-type70	0.95	0.19	1.14
S-type90	2.12	1.87×10^{-3}	2.12
S-type110	0.89	0.16	1.05
S-type130	0.79	0.29	1.08
(CF) _n	6.59	0.43	7.02
PTFE	15.07	0.81	15.88

of (CF)_n and PTFE. As the graphite fluoride and PTFE have little CF₃ groups, their surface energy would be larger than that of S-type fluoride.

18.3.4 Oxidizing ability of fluorine and chemical resistance

When the S-type fluoride is kept in a glass ampule for a few weeks, the inside of the glass tube become frosted. It indicates that a small amount of fluorine species having oxidizing ability are contained in the S-type fluoride. Fujimoto et al. measured the oxidizing ability of fluorine in S-type fluoride by the iodometry. The samples prepared at more than 70°C have little oxidizing ability, while S-type30 and S-type50 contain 0.1 wt% and 0.09 wt% of fluorine species having the oxidizing ability, respectively.

The S-type fluoride shows an excellent resistance against HCl and HNO₃ solutions, while it reacts with alkaline solutions such as aq. NH₃ and NaOH and the colors of samples immersed and solution turn to black and brown, respectively. Especially, the change in aq. NH₃ occurs rapidly just after immersion. The resistance against the organic solvents is also excellent concerning the samples prepared above 70°C. However, in the case of S-type30 and S-type50, the color of the organic solvent turned to yellow by the immersion. This would be due to the attack by the absorbed fluorine species having the oxidizing ability which is detectable by iodometry.

18.3.5 Thermal behavior

Thermal behavior of S-type fluoride is quite different from that of (CF)_n in spite of the structural analogue to (CF)_n. That is, (CF)_n exothermically decomposes to gaseous fluorocarbons such as CF₄, C₂F₆, etc. and amorphous carbon at temperatures higher than 500°C, while the S-type fluoride decomposes up to about 450°C to form the fluorocarbons having a sublimative property. Fujimoto et al. applied this feature of S-type fluoride to vacuum vapor deposition method in order to pre-

pare a thin film of fluorinated pitch on the aluminum plate using the S-type fluoride prepared at 0°C [17–21]. Figure 11 shows the result of characterization of the obtained film by C_{1s} ESCA [17,18,24]. The thin film is also composed of CF_3 -, CF_2 - and CF - groups as well as the original S-type fluoride and has another new peak at 287–288 eV. It would be formed by the cleavage of CF_2 bridges which combine the units of the condensed-cyclohexane rings each to each in S-type fluoride. Figure 12 shows water drops on the S-type fluoride, its derived film and PTFE, respectively. As shown in Fig. 12, the thin film as well as the S-type fluoride has contact angles (113° and 145°) larger than PTFE (109°) indicating the lower surface energy.

Properties investigated so far are summarized in Table 4 together with those of $(CF)_n$ and PTFE. The properties such as composition, molecular weight, specific gravity, interlayer spacing, which reflect the characteristics of the bulk, changes as a function of the fluorination temperature and there is no inconsistency with the proposed structure shown in Fig. 7. On the other hand, surface energy, water-

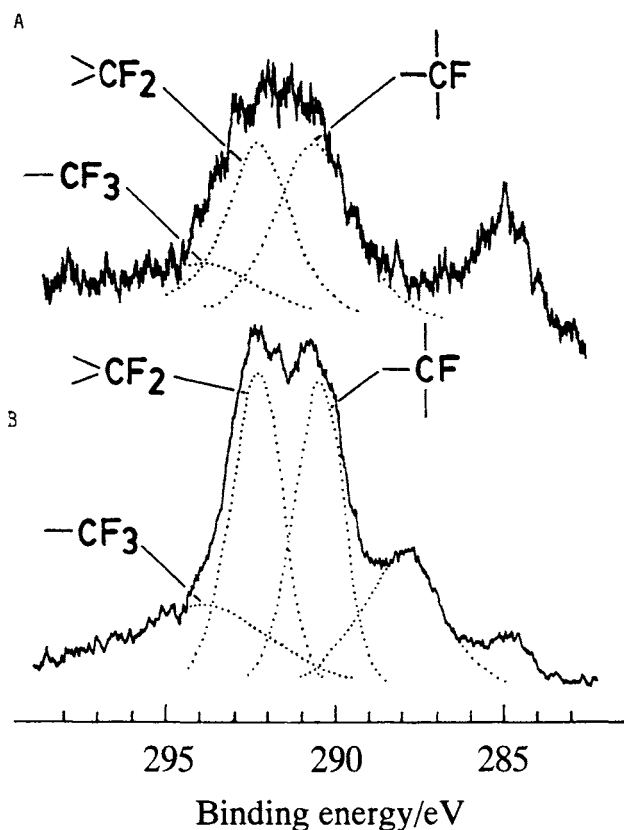


Fig. 11. C_{1s} ESCA spectra of solid type fluoride and derived thin film: (A) solid type fluorinated pitch prepared at 0°C; (B) Thin film derived from fluorinated pitch. (Quoted from the poster material of Ref. [18] and also quoted in p. 104 of Ref. [25]).

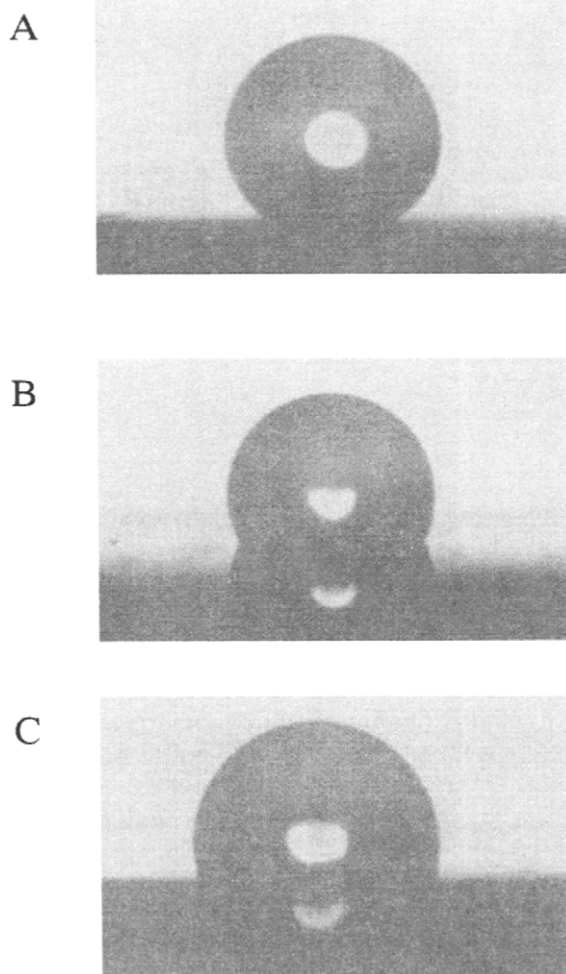


Fig. 12. Water drop on solid type fluoride, derived thin film and PTFE: (A) on solid type fluoride; (B) on thin film derived from solid type fluoride; (C) on PTFE. (Quoted from H. Fujimoto, A. Mabuchi, T. Maeda, Y. Matsumura, N. Watanabe, H. Touhara, *Carbon*, 30 (1992) 851, with permission).

and oil-repellencies which reflect the surface condition do not depend on the fluorination temperature.

18.4 Applications of fluorinated pitch

The characteristics of fluorinated pitch (Pitch Fluoride) [20–25,38–44] include high water repellency, high solubility in fluorine-containing solvents and ease of micronization. We examined the characteristics of solid, glassy and liquid

Table 4

Various physical and chemical properties of solid type fluoride, graphite fluoride and PTFE

	Solid type fluorinated pitch	(CF) _n	PTFE
F/C atomic ratio	1.15–1.59	1.00	2.00
Molecular weight	4300–2070	–	–
Specific gravity	ca 2.0	2.68	2.1
Interlayer spacing/nm	0.64–0.69	0.585	–
Color	Yellowish white or almost white	White	White
Contact angles°			
Water	141–143	143	109
17% NaOH	137–140	139	114
Glycerol	140–146	151	105
Formamide	135–139	128	95
1,4-butandiol	115–121	103	86
Surface energy/mJm ⁻²	1.0–2.0	7.01	15.88
Refractive index	1.36–1.39	–	1.35
Dielectric constant	ca 1.9	–	< 2.1
Acid resistance	Excellent	Excellent	Excellent

fluorinated pitches to find their applications. The possible applications of fluorinated pitch are shown in Fig. 13. The latter part of the chapter describes the applications of various types of fluorinated pitches, focusing on composite plating.

18.4.1 Composite plating

18.4.1.1 Conventional composite plating [45,46]

18.4.1.1.1 Outline of composite plating. The purpose of electroplating or electroless plating is to deposit a metallic coating on a substrate surface. If particles are suspended in a plating solution, they may be incorporated in a coating during deposition. This phenomenon is called codeposition. Generally, incorporation of such particles is regarded as a plating failure. Composite plating utilizes such codeposition to form a new coating. Figure 14 shows the outline of the codeposition mechanism of nickel composite plating using fluoroplastic particles. The fluoroplastic particles are dispersed in the plating solution using cation surfactants, and then codeposited with nickel ions on the substrate surface. Accordingly, micro-composite consisting of metal and fluoroplastic is formed on the substrate by composite plating. Theoretically there are an infinite number of combinations of a deposited metal with codeposited particles. Composite plating has been studied extensively since 1960. However, its use was limited due to the difficulty in quality control method and high cost. Surface treatment techniques to provide various functional characteristics have attracted much attention, and improvements in various

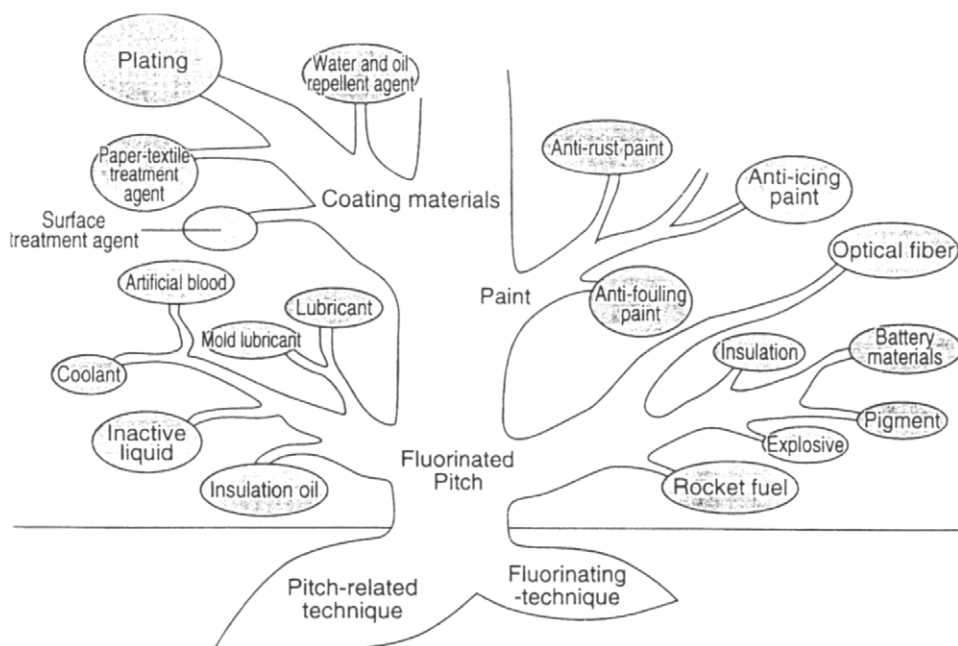


Fig. 13. Application fields of fluorinated pitch.

surface properties for decoration, corrosion prevention, wear resistance and so on, have been demanded. Composite plating is now applied widely to various fields to provide surfaces with functional characteristics that could not be realized by conventional surface treatment techniques. A composite with water repellency would be valuable as a material giving specific and excellent functional characteristics. In Japan, Takeuchi et al. applied for a patent on a composite plating method using graphite fluoride $[(CF)_n]$ in 1970 [47]. Preparation of a composite with water-repellent powder finely dispersed in a high-melting point metal is difficult by metallurgical methods.

18.4.1.1.2 Combination of metal to be deposited with water repellent powder. In composite plating, the characteristics of particles to be codeposited are the most important. Water repellent fluoroplastic powder represented by Polytetrafluoroethylene (PTFE) has various unique and interesting characteristics such as non-adhesiveness, self-lubricity and chemical resistance, as well as water repellency. Incorporation of such powder into the composite plating would give a surface with quite different characteristics from those obtained by conventional surface treatments. Representative water repellent powders used in this study of composite plating are graphite fluoride $[(CF)_n]$ and PTFE.

1. $Ni/(CF)_n$ composite electroplating.

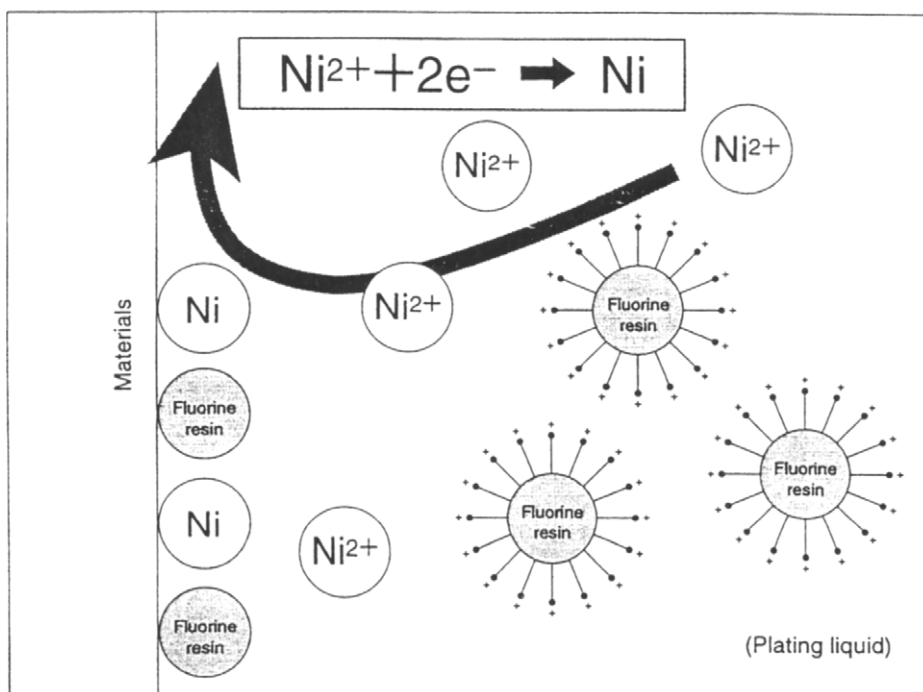


Fig. 14. Codeposition mechanism.

(CF)_n obtained by direct fluorination of graphite, shows extremely high water repellency. Its properties have been widely known and applied to solid lubricants, battery materials and releasing agents. Patents and papers on composite plating using (CF)_n were published since 1970. Yamaguchi et al. [48] proposed a method of dispersing (CF)_n in a plating solution using a cation surfactant. They reported the maximum amount of codeposition of the order of 10 wt%. However, composite plating has not yet been industrialized.

2. Ni/PTFE composite electroplating.

One of the representative fluoroplastics, PTFE, excels in heat and chemical resistance, having specific characteristics such as water repellency and self-lubricity. Matsumura et al. [49,50] reported on Ni/PTFE composite electroplating using a Watts nickel bath and a nickel sulfamate plating bath, and developed a technique to codeposit PTFE sub-micron particles up to 40 vol%. Recently, research is being done by focusing on composite plating with ultra-high water repellency, using tetrafluoroethylene oligomer (TFEO) with lower molecular weight [51–54].

3. Electroless Ni/PTFE composite plating [55].

PTFE composite plating by the electroless plating method excels in its workability for producing hard coatings. Accordingly, plating material manufacturers generally

use this method rather than the electroplating. Chiba et al. developed a plating solution giving such a high concentration of codeposited metal as 15–35% [56,57]. However, there were a number of problems such as plating cost and stability of the plating solutions. Therefore, this plating method could not be used, for example, in the appliance industry, which requires a certain level of appearance and consumes a large amount of plating materials. However, Osaka Gas Co. Ltd and Matsushita Electric Industrial Co. Ltd have jointly developed its application to electric iron bases [58], and have produced several hundred thousand units per year since 1996. Application of the Ni/PTFE composite plating will be expanded in the future.

18.4.1.1.3 Physical properties of metallic coating formed by composite plating. The coating with codeposited water repellent particles has a lower hardness than that prepared by only metal deposition, showing the improved sliding characteristics and wear resistance. The coating is provided with characteristics such as water repellency and non-adhesiveness which the usual metallic coatings do not have. As the amount of codeposited PTFE increases, the contact angle becomes larger, and water repellency higher. PTFE has a high contact angle, 110° of a water drop. The composite plating with PTFE ensures water repellency as high as that of PTFE when the amount of codeposited PTFE is 10 wt% or more.

18.4.1.2 Composite plating using fluorinated pitch [59–63]

As stated above, this composite plating method is very interesting because it gives new composites that could not be manufactured by conventional methods. Some composite plating materials using PTFE as a fluoroplastic have been commercialized, and their practical uses are still being developed. However, many fields require the higher water repellency. Accordingly, the composite plating was attempted using fluorinated pitch as a fluorine compound to obtain the coatings with higher water repellency. Using the experimental equipment shown in Fig. 15 and fluorinated pitch micronized to $D_{50} = 1.3 \mu\text{m}$ shown in Fig. 16 as a codeposition material, the fluorinated pitch-nickel composite plating on a SUS 430 substrate was examined under the following conditions.

1. Plating bath composition
 - Fluorinated pitch: 50 g/l
 - Nickel sulfamate: 360 g/l
 - Nickel chloride: 45 g/l
 - Boric acid: 30 g/l
 - pH: 4.2
2. Plating conditions
 - Current density: 1, 3, 5, or 7 A/dm^2
 - Plating bath temperature: 50°C
 - Coating thickness: $25 \mu\text{m}$
3. Plated substrate heat treatment temperature: 285°C , $1.8 \times 10^3 \text{ s}$.

Figure 17 shows the relationship between current density and amount of codeposited fluorinated pitch (vol%). As the current density increased, the amount of

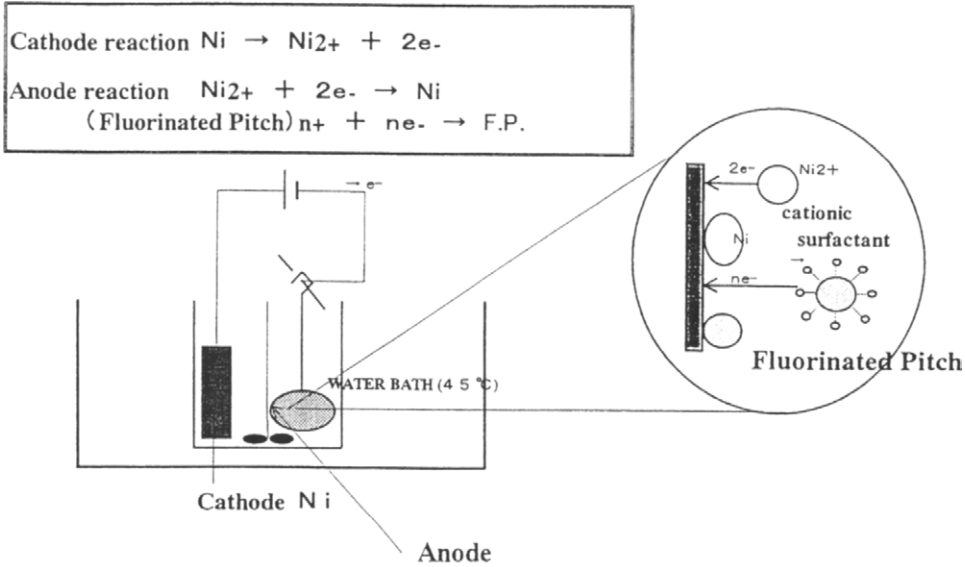


Fig. 15. Illustration of electro-composite plating of nickel and fluorinated pitch particles.

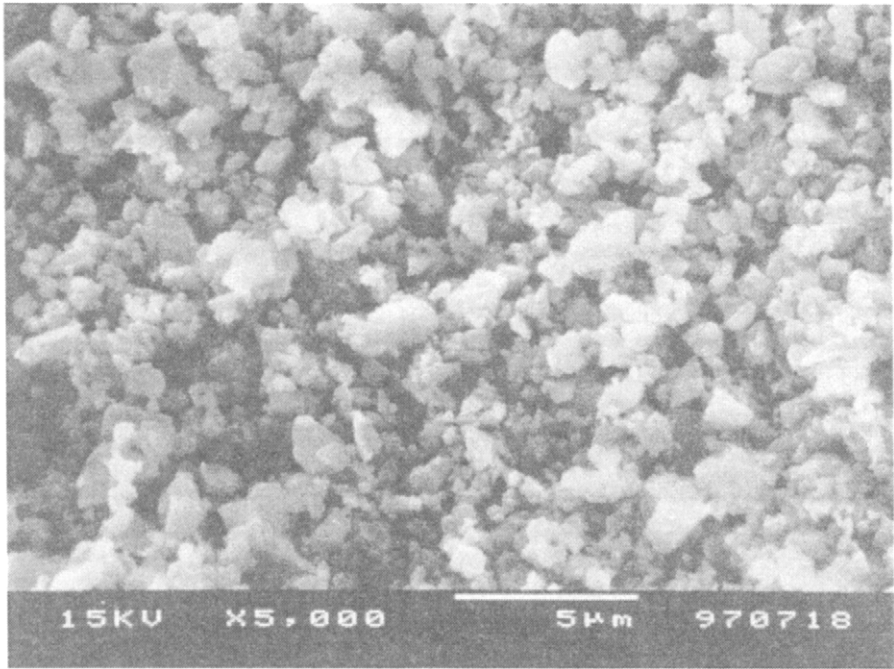


Fig. 16. SEM images of fluorinated pitch after powdering for composite film.

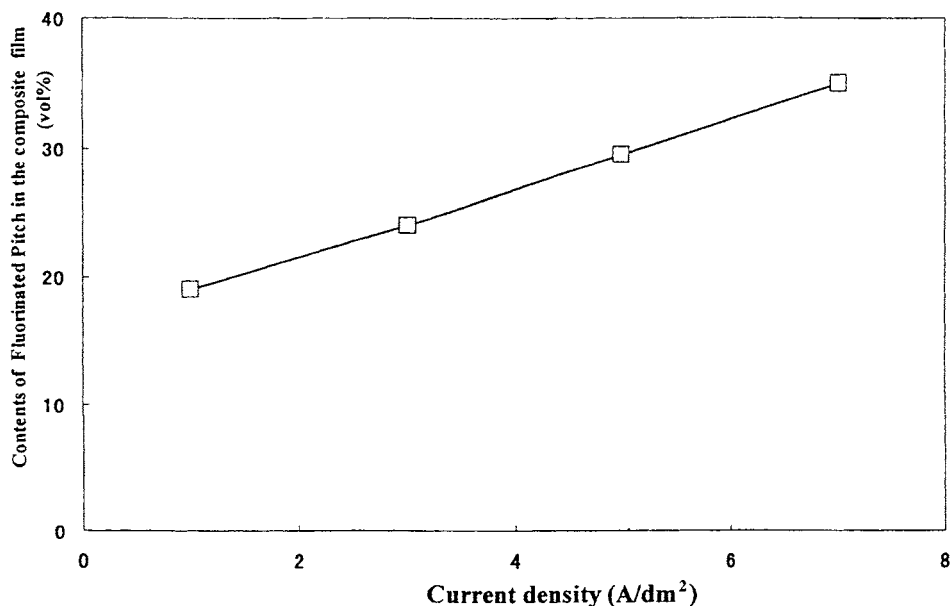


Fig. 17. Dependence of current density on the contents of fluorinated pitch in the composite film.

codeposition increased linearly from 18% to 35%. Observation of the metallic coating surface and cross section by scanning electron microscopy (SEM), revealed that the fluorinated pitch was dispersed uniformly in the nickel coating in the same manner as in PTFE codeposition (Fig. 18). This finding shows that composite plating with fluorinated pitch is possible. Figure 19 shows the relationship between the amount of codeposited fluorinated pitch in the coating and the contact angle of a water drop on the fluorinated pitch-codeposited coating. When the amount of deposited fluorinated pitch is 18% or more, the contact angle is 145° or larger. The contact angle for nickel-plated substrate is 75°. Thus, the addition of a small amount of fluorinated pitch can increase water repellency. Table 5 shows the characteristics of the coatings obtained by fluorinated pitch composite plating and PTFE composite plating, and conventional fluorine coating (paint). Fluorinated pitch composite plating would be used in consequence of its improved durability and possible applications, based on its high water repellency.

18.4.2 Oxygen permeability

Fluorine compounds have an oxygen affinity. Accordingly, application of the fluorinated pitch-deposited film to an oxygen enrichment membrane material was examined. The compound was deposited on a porous substrate under the following deposition conditions.

Sample: Fluorinated pitch (fluorinated at 70°C)

Heating temperature: room temperature to 500°C

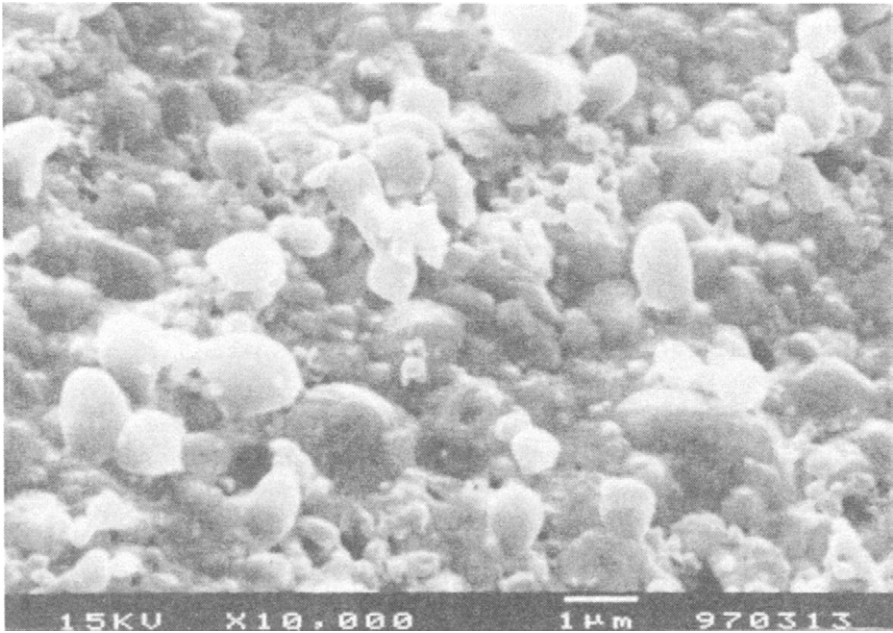


Fig. 18. SEM images of Ni-fluorinated pitch composite film.

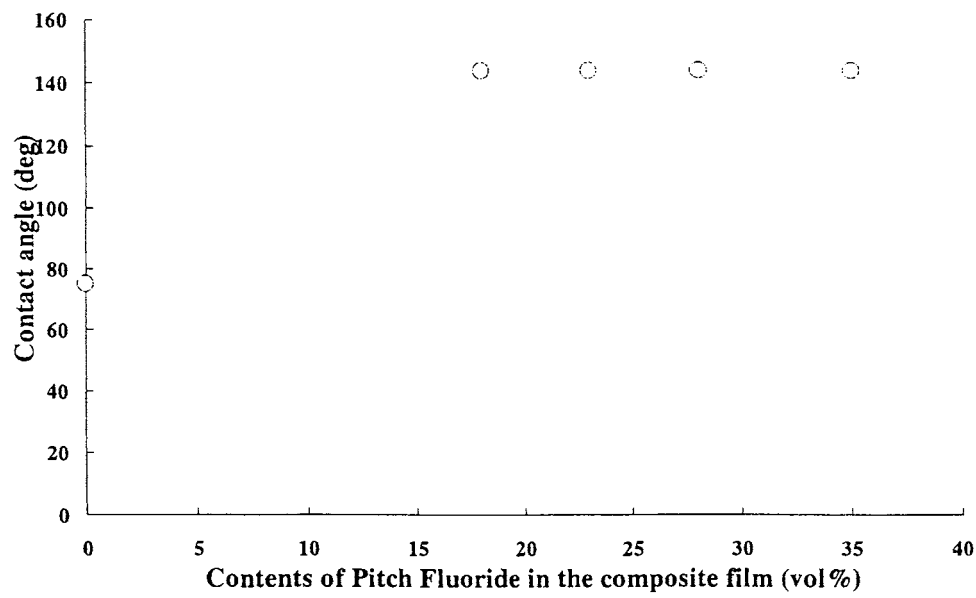


Fig. 19. Dependence of contact angle with water on the contents of co-deposited fluorinated pitch in the composite films.

Table 5

Characteristics of composite plating films

Coating method	Fluorine resin	Anit-fouling	Heat resistance (short time)	Water repellency	Heat conductivity	Film strength (scratch-free)	Coloring	Anti-corrosion
Composite plating	PTFE	PTFE (Polytetra fluoroethylene)	⊙	⊙	⊙	⊙	×	Corrosion of plating metal
	Fluorinated Pitch	Fluorinated Pitch	⊙	⊙	⊙	⊙	(⊙)	
Conventional coating (paint)		PTFE, FEP	⊙	△	×	×	×	Pinhole, corrosion by peeling

Heating rate: 5°C/min, maintained at 500°C for 10 min.

Pressure: 1.33×10^{-4} to 1.33×10^{-3} Pa

Substrate: porous substrate (ceramic filter)

Substrate temperature: 30–50°C

Film thickness: 1.575 μm

The permeating speed was obtained by the experiments using oxygen and nitrogen gases. The permeability constant and the permeating speed were determined as shown below.

Permeability constant $\text{PO}_2 = 8.5 \times 10^{-9}$, $\text{PN}_2 = 3.45 \times 10^{-9}$,

α (permeability constant ratio) = $(\text{PO}_2/\text{PN}_2) = 2.46$

Permeating speed $\text{RO}_2 = 7.17 \times 10^{-4}$ [$\text{m} \cdot \text{m}^{-2} \cdot \text{s}^{-1} \cdot \text{Pa}$],

$\text{RN}_2 = 2.91 \times 10^{-4}$ [$\text{m} \cdot \text{m}^{-2} \cdot \text{s}^{-1} \cdot \text{Pa}$]

Compared with PTFE, fluorinated pitch has a higher oxygen transmission constant, but a lower separation ratio α .

18.4.3 Humidity sensor

Conventional humidity sensors of the electric resistance variable type use hydrocarbon polyelectrolyte as a moisture sensing material. Therefore, the sensors usually have insufficient heat resistance, and cannot be used at temperatures of 60°C or more. Another problem is that they deteriorate when in contact with cigarette smoke and oil contained in the air [64,65]. When the fluorinated pitch-deposited coating was breathed upon, the electrical resistance quickly decreased, but electrical resistance quickly recovered when this action was stopped. Then, how to develop a humidity sensor excelling in humidity response sensitivity, heat resistance and durability was attempted [66]. Two kinds of comb-like electrodes with different electrode gaps were made, and a thin film was formed on the surfaces by vacuum deposition of fluorinated pitch. The obtained fluorinated pitch sensors were left at rest in a thermostatic chamber, and electrical resistance was determined under the following conditions.

Sensor temperature: 50°C

Relative humidity range: 10–90 (RH%)

Applied voltage: 10 V DC

Figure 20 shows the relationship between relative humidity and resistance of the fluorinated pitch sensors, determined by comb-like electrodes having electrode gaps of 10 μm and 200 μm . As relative humidity increases, the resistance becomes lower. Particularly the sensor with an electrode gap of 10 μm showed a change in electrical resistance of the order of more than 10,000 while relative humidity changed from 10% to 85%, and exhibited an acceptable resistance reduction curve. However, since the absolute value of the resistance is high, to industrialize the sensor, it must be improved by using fluorinated pitch with a low fluorine–carbon ratio (F/C) or IAD (ion-beam assisted deposition) or by decreasing the electrode gap to reduce the electrical resistance.

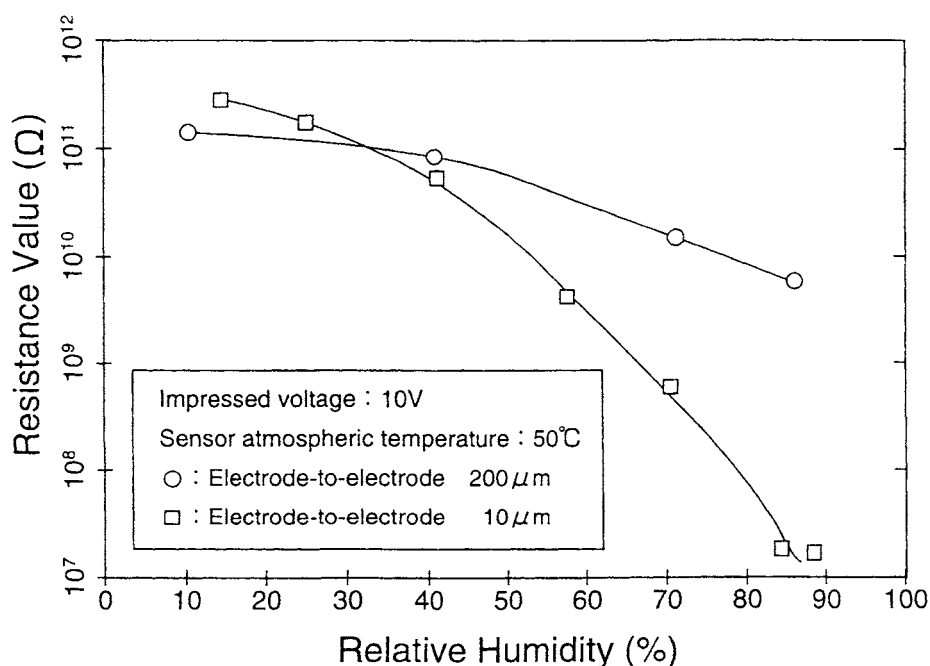


Fig. 20. Humidity sensibility characteristics of fluorinated pitch films.

18.4.4 Applications using reactivity of fluorinated pitch

18.4.4.1 Colored fluorinated pitch [67]

Carbon-carbon double bonds and hydrogen atoms remain in fluorinated pitch with a low fluorination degree, i.e. in incompletely fluorinated pitch in the solid state. Accordingly, fluorinated pitch may maintain its chemical reactivity. Utilizing this chemical reactivity to create a reaction between incompletely fluorinated pitch and a dye containing amino groups, the colored fluorinated pitch with chemical stability was synthesized without losing the original characteristics, such as water repellency and lubricity. The synthetic method of colored fluorinated pitch is as follows:

1. A dye suspended in 500 ml of THF in 10 wt% is added to 30.0 g of fluorinated pitch. The mixture is intensively agitated for 3 h at room temperature.
2. After completion of the reaction, solid matter is separated from the reaction mixture by filtration, and then washed with water.
3. Colored fluorinated pitch is extracted by using hexafluorobenzene (C_6F_6).
4. The extract is concentrated through vacuum distillation and dried to obtain colored fluorinated pitch.

This reaction yielded colored fluorinated pitch from white powdery solid fluorinated pitch. Various products produced in this manner have such large contact angles of water drops as 145° or more. Figure 21 shows the results of ^1H NMR measurement

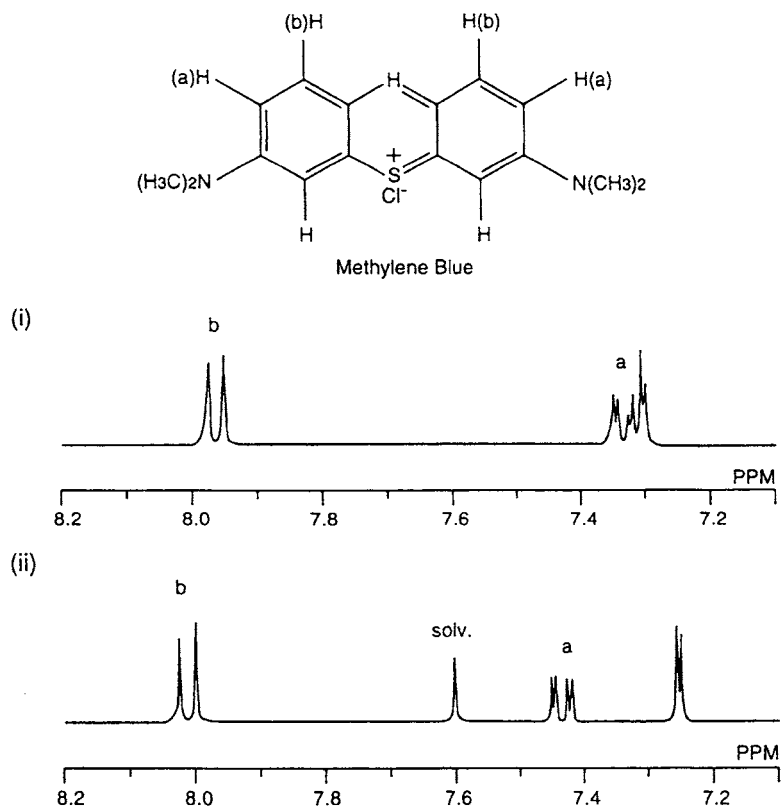


Fig. 21. ¹H NMR spectra of methylene blue before (i) and after (ii) reaction with fluorinated pitch.

performed before and after the reaction between the fluorinated pitch and methylene blue which is used as a dye. The proton "a" of the product shifted to a magnetic field 0.10 ppm lower than that of the proton "a" of the raw material. Also, the proton "b" of the product shifted to a magnetic field 0.08 ppm lower than that of the proton "b" of the raw material. The colored fluorinated pitch was soluble in fluoride solvents. It is presumed from these results that the nitrogen atoms in the methylene blue structure and the fluorinated pitch are bonded in molecular level. It is suggested that the nitrogen atom of the dye acts as a nucleophilic agent to introduce unsaturated carbon into the fluorinated pitch molecules in the reaction (Fig. 22). It was verified that a dye, and fluorinated pitch as a raw material could be bonded to synthesize a new fluorine-containing material with high coloring stability and ultra-high water repellency.

18.4.4.2 Application as a catalyst [67,68]

The additional reaction of fluoroalkyl iodide to alkynes is important as a method of introducing fluoroalkyl groups into organic molecules. The reaction methods to emit

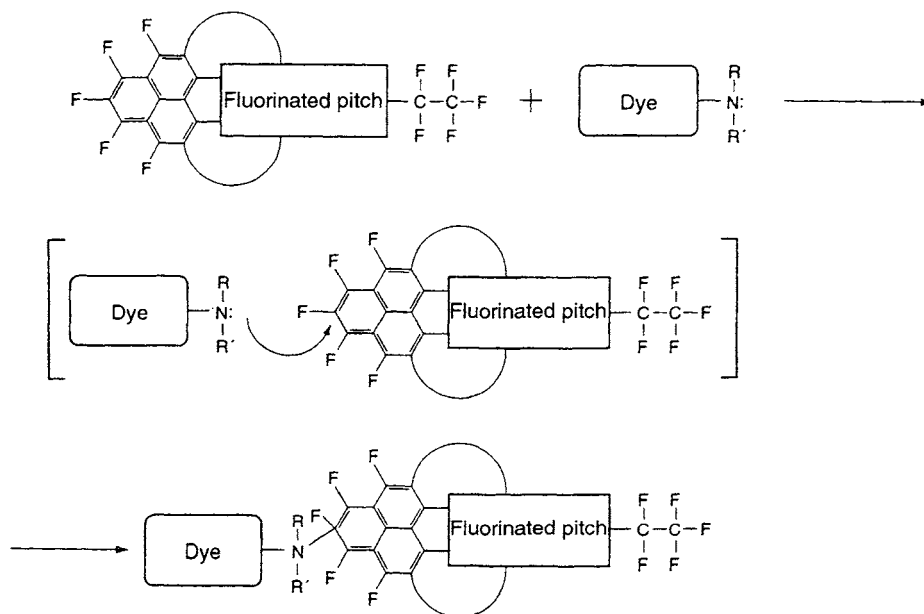


Fig. 22. Reaction mechanism of fluorinated pitch with dye.

light at high temperatures and to use an organo metallic catalyst were reported. The present experiments showed that the addition reaction of fluoroalkyl iodide to alkynes was efficiently carried out even at room temperature in the presence of a fluorinated pitch catalyst. The additional reaction was performed according to the following procedure. Fluorinated pitch of 10 wt% to the substrate was added to the THF solution of alkynes having an equivalent weight to that of fluoroalkyl iodide. The solution was agitated at room temperature for 5 h. After completion of the reaction, fluorinated pitch was separated by filtration, and the resulting filtrate was concentrated by vacuum distillation. The product was isolated by column chromatography, and the structure was analyzed based on the spectral data. As a result, it was found that the use of fluorinated pitch facilitates the introduction of fluoroalkyl groups into alkynes and the generation of alkene iodide having fluoroalkyl groups. This reaction seems to be carried out by the mechanism shown in Fig. 23. The use of fluorinated pitch as a catalyst facilitates the addition of fluoroalkyl iodide to alkynes at room temperature, and therefore, is a remarkably effective method of obtaining alkene iodides having various fluoroalkyl groups. Moreover, fluorinated pitch is insoluble in the reaction medium, and can be recycled by filtration.

18.4.5 Other applications

In addition to the above-mentioned applications, we have examined and developed other applications based on the physical properties of fluorinated pitch. First, its

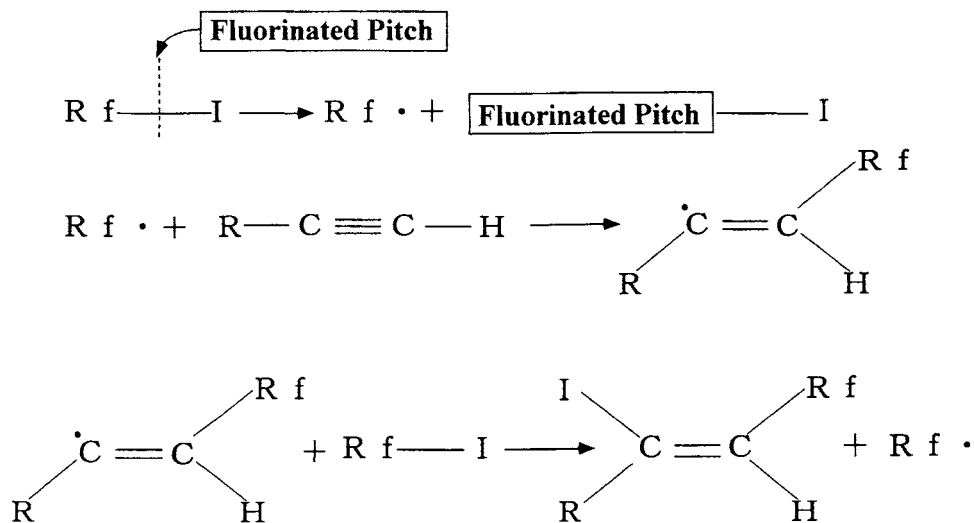


Fig. 23. Reaction mechanism.

application to paint to utilize the high water repellency of solid fluorinated pitch was examined [69–71]. Fluorinated pitch excels other fluoroplastics in dispersion ability, and water repellency is realized by adding only a small quantity of fluorinated pitch. Fluorinated pitch is soluble in fluoride solvents, therefore it can be applied to emulsion type liquid wax. And then use of fluorinated pitch as a water- and oil-repellent agents for fibers was examined [72,73]. It is expected that fluorinated pitch will be used to treat fibers, and electrode materials (carbon materials) for fuel cells having fine pores. In addition, fluorinated pitch might be used as a colored pencil lead material because it has a high dispersing ability, slidability and low-temperature fusibility [74,75]. Fluorinated pitch was found to have an affinity for fluoroplastics, and improved sliding effects when used as a binder for producing a composite material with carbon fiber and fluoroplastic [76]. Addition of fluorinated pitch to lube oil improved the seizing limit point [77]. The application of glassy fluorinated pitch to the fields where its transparency will be utilized is under examination. Liquid fluorinated pitch can be used as inactive fluid or fluorine oil that is different from conventional fluids in structure, and there is a possibility of its use as insulating oil in large transformers [78]. As stated in this chapter, fluorinated pitch is an attractive new material that has excellent characteristics with the possibility of various applications. However, fluorinated pitch differs from conventional fluoroplastics in structure and characteristics. The development of a low-cost manufacturing method is very important in order to find commercial uses for fluorinated pitch.

References

- [1] N. Watanabe, M. Fukuda, US Patent 3536532 (1970).
- [2] M. Fukuda, T. Iijima, *Prog. Batt. Solar Cells*, 1(1978) 26.
- [3] J. Watanabe, H. Ogawa, R. Okazaki, *Prog. Batt. Solar Cells*, 1(1978) 39.
- [4] J. Watanabe, E. Kawakubo, T. Shinagawa, Y. Kajikawa, *Prog. Batt. Solar Cells*, 1 (1978) 39.
- [5] Y. Kita, N. Watanabe, Y. Fujii, *J. Am. Chem. Soc.*, 101(1979) 3832.
- [6] T. Nakajima, M. Kawaguchi, N. Watanabe, *Carbon*, 20 (1982) 287.
- [7] T. Mallouk, N. Bartlett, *J. Chem. Soc. Chem. Commun.*, (1983) 103.
- [8] T. Mallouk, B.L. Hawkins, M.P. Conrad, K. Zilm, G.E. Maciel, N. Bartlett, *Phil. Trans. R. Soc. Lond.*, A314 (1985) 179.
- [9] J.L. Margrave, R.J. Lagow, US Patent 3775489 (1973).
- [10] *Chem. Eng. News*, 48 (1970) 40.
- [11] J.L. Adcock, R.A. Beh, R.J. Lagow, *J. Org. Chem.*, 40 (1975) 3271.
- [12] J.L. Margrave, R.J. Lagow, *J. Fluorine Chem.*, 33 (1986) 133.
- [13] G.H. Taylor, *Fuel*, 40 (1961) 465.
- [14] J.D. Brooks, G.H. Taylor, *Carbon*, 3 (1965) 185.
- [15] *Chemistry and Physics of Carbon*, 4, P.L. Walker Jr. (Ed.), Marcel Dekker, NY, 1968, p. 248.
- [16] H. Honda, *Carbon*, 26 (1988) 139.
- [17] H. Fujimoto, Y. Matsumura, N. Watanabe, H. Touhara, Abstract of the 12th Annual meeting on carbon materials in Japan, 1985, p.16.
- [18] Y. Matsumura, H. Fujimoto, N. Watanabe, H. Touhara, Poster figure in Poster Session S25 of Centenary of the discovery of fluorine, International fluorine symposium, Paris, 1986.
- [19] Y. Matsumura, H. Fujimoto, N. Watanabe, H. Touhara, JPN Patent JP-A-62-275190 (1986).
- [20] Y. Matsumura, H. Fujimoto, N. Watanabe, H. Touhara, US Patent 916073 (1986).
- [21] H. Fujimoto, A. Mabuchi, T. Maeda, Y. Matsumura, N. Watanabe, H. Touhara, *Carbon*, 30 (1992) 851.
- [22] H. Fujimoto, T. Maeda, M. Yoshikawa, N. Watanabe, *J. Fluorine Chem.*, 60 (1993) 69.
- [23] H. Fujimoto, M. Yoshikawa, A. Mabuchi, T. Maeda, *J. Fluorine Chem.*, 57 (1992) 65.
- [24] H. Fujimoto, Doctoral thesis, Kyoto University, Kyoto, 1992.
- [25] T. Maeda, Doctoral thesis, Osaka University, Osaka, 1997.
- [26] T. Shimizu, M. Hatano, *J. Synth. Org. Chem. Jpn.*, 43 (1985) 371.
- [27] T. Ando, F. Namigata, Y. Shimokawa, *Kagaku No Ryoiki*, 21 (1967) 379.
- [28] I. Mochida, K. Maeda, K. Takeshita, *Carbon*, 15 (1977) 17.
- [29] T. Satogawa, JPN Patent JP-A-54-24302 (1978).
- [30] S. Yoshizawa, N. Watanabe, JPN Patent JP-A-43-25012 (1968).
- [31] Y. Kita, N. Watanabe, Y. Fujii, *J. Am. Chem. Soc.*, 101 (1979) 3832.
- [32] Y. Kita, Doctoral thesis, Kyoto University, Kyoto, 1977, p. 48.
- [33] T. Satogawa, Kinosei gan fussokobunshi, *Nikkan Kogyo Shinbunsha*, Tokyo, 1982, p. 3.
- [34] N. Watanabe, T. Nakajima, N. Ohsawa, *Bull. Chem. Soc. Jpn.*, 55 (1982) 2029.
- [35] D.K. Owens, R.C. Wendt, *J. App. Poly. Sci.*, 13 (1969) 1741.
- [36] F.M. Fowkes, *J. Phys. Chem.*, 66 (1962) 382.
- [37] L.J. Hayes, *J. Fluorine Chem.*, 8 (1976) 69.
- [38] T. Maeda, A. Mabuchi, H. Fujimoto, US Patent 427419.

- [39] T. Maeda, H. Fujimoto, M. Yoshikawa, N. Watanabe, H. Touhara, J. Fluorine Chem., 54 (1991) 40.
- [40] Y. Matsumura, Kagaku to Kogyo, 44 (1991) 1501.
- [41] T. Maeda, H. Fujimoto, M. Yoshikawa, M. Saito, Aromatikkusu, 44 (1992) 273.
- [42] T. Maeda, H. Fujimoto, M. Saito, Y. Hirata, Kagaku Kougaku Ronbunshu, 22 (1996) 728.
- [43] T. Maeda, A. Mabuchi, M. Saito, Y. Hirata, Kagaku Kougaku Ronbunshu, 22 (1996) 1334.
- [44] T. Maeda, M. Yoshikawa, M. Yamada, H. Matsuyoshi, Y. Hirata, Kagaku Kougaku Ronbunshu, 23 (1997) 323.
- [45] T. Chiba, T. Maeda, Hyomengijyutu, 47 (1996) 584.
- [46] S. Matsumura, Kinzokuhyomengijutsu, 36 11 (1985) 442.
- [47] H. Takeuchi, Y. Okamoto, Japan Patent, S49-20459
- [48] F. Yamaguchi, S. Kurosaki, N. Watanabe, Denki Kagaku, 42 (1975) 57.
- [49] S. Matsumura, T. Otake, Kagaku to Kogyo, 57 (1983) 138.
- [50] S. Matsumura, Shikizai Kyokanshi, 56 (1983) 328.
- [51] N. Watanabe, Y. Chong, Kagaku to Kogyo, 66 (1992) 11
- [52] N. Watanabe, Y. Chong, Nikkeimaterial & Technology, 135 (1993) 296.
- [53] H. Kiyokawa, R. Ikeda, Y. Chong, S. Yonezawa, M. Takashima, Hyomen, 48 (1997) 939.
- [54] H. Kiyokawa, T. Ibe, R. Ikeda, Y. Chong, S. Yonezawa, M. Takashima, Program and Abstracts of 15th International Symposium on Fluorine Chemistry, P(2) 160 (1997).
- [55] S. Matsumura, S. Sanchez, Summary of Electroness Nickel '91 Conference, 4-1 (1991).
- [56] T. Chiba, T. Nakamura, S. Matsumura et al., Summary of the 79th Conference of Hyomengijutsu Kyokai, 1989, p. 202.
- [57] T. Chiba, T. Nakamura, S. Matsumura et al., Summary of the 79th Conference of Hyomengijutsu Kyokai, 1989, p. 200.
- [58] N. Kanazawa, T. Maeda et al., US Patent, 08/718940.
- [59] T. Maeda, Kagaku to Kogyo, 69 (1995) 178.
- [60] M. Saito, M. Yamada, T. Maeda, T. Chiba, Summary of the 93rd Conference of the Surface Finishing Society of Japan, Chiba, 1996, p. 188.
- [61] M. Saito, M. Yamada, T. Maeda, T. Chiba, Summary of the 95th Conference of the Surface Finishing Society of Japan, Tokyo, 1997, p. 145.
- [62] M. Saito, M. Yamada, T. Maeda, T. Chiba, Summary of the 97th Conference of the Surface Finishing Society of Japan, Tokyo, 1998, p. 133.
- [63] T. Maeda, M. Yamada, H. Matsuyoshi, Y. Hirata, N. Watanabe, Program and Abstracts of 15th International Symposium on Fluorine Chemistry, Vancouver, Ad. Mat. C-5 (1997).
- [64] T. Tanaka, Keiryo Kanri, 36 (1987) 654.
- [65] A. Yamanaka, T. Kodera, K. Fujigawa, H. Kita, Dennki Kagaku, 56 (1988) 200.
- [66] T. Maeda, M. Saito, H. Fujimoto, Japan Patent H02-296140.
- [67] J. Sun, T. Maeda, M. Yamada, Abstracts of 12th European Symposium on Fluorine Chemistry, Berlin, C19 (1998).
- [68] J. Sun, M. Yamada, T. Maeda, Abstracts of The 22nd Fluorine Conference of Japan, Osaka, 1998, p. 249.
- [69] H. Fujimoto, T. Maeda, M. Sasabe, Japan Patent H05-093260.
- [70] T. Maeda, M. Yoshikawa, M. Saito, K. Onoe, Japan Patent H03-1929.
- [71] M. Yoshikawa, T. Maeda, Japan Patent H05-135625.
- [72] H. Fujimoto, M. Yoshikawa, Y. Arai, M. Sasabe, Japan Patent H04-194096.

- [73] T. Maeda, H. Fujimoto, M. Yoshikawa, Y. Arai, Japan Patent H03-237929.
- [74] T. Maeda, H. Fujimoto, M. Saito, Y. Arai, M. Sasabe, Japan Patent H04-027600.
- [75] K. Kitazawa, Nishimoto, T. Maeda, M. Saito, U.S. Patent 5318622.
- [76] N. Masuya, J. Nakazono, K. Mizobe, T. Maeda, Japan Patent H04-034143.
- [77] T. Maeda, H. Fujimoto, M. Yoshikawa, M. Saito, Y. Okita, Japan Patent H05-194972.
- [78] T. Maeda, M. Saito, Y. Makino, A. Miyamoto, Japan Patent H05-255526.

CHAPTER 19

Applications of Fluorides to Semiconductor Industries

Fuyuhiko Ishii¹ and Yasushi Kita²

¹Fluorine Chemistry Laboratory, New Products Development Division, Kanto Denka Kogyo Co. Ltd, 1497, Shibukawa, Gunma, 377-8513, Japan; ²Fine Chemicals Department, Central Glass Co. Ltd, 7-1 Kanda-Nishikicho 3-chome, Chiyoda-ku, Tokyo, 101-0054, Japan

19.1 Carbon tetrafluoride (CF₄) and hexafluoroethane (C₂F₆)

19.1.1 Introduction

Attempts to synthesize CF₄ and C₂F₆ were made quite early nearly at the same time when elemental fluorine was isolated by Moissan in 1886 [1]. Moissan attempted the reaction of fluorine with hydrocarbons, however, this resulted in violent explosions. In 1926, the first fluoride of carbon was obtained by P. Lebeau and A. Damien who succeeded in synthesis and isolation of CF₄ by combustion of carbon in fluorine [2].

The fluorinated carbon compounds are stable with low boiling points, and in addition, innocuous to human and incombustible, therefore various applications were investigated. But, due to their high prices, the utilization was limited to special low-temperature refrigerants or insulating gas of transformers (presently SF₆ is primarily used), or medium of wind tunnel tests [3]. However, since the latter half of the 1970s, as the application of CF₄ and C₂F₆ to etching/cleaning gas began in the semiconductor industry, the fluorinated carbon compounds suddenly came into the limelight, and production of a large volume of gases began in Japan and United States.

19.1.2 Physical and chemical properties of CF₄ and C₂F₆

Table 1 shows physical properties of CF₄ and C₂F₆ [4,5]. Each compound is colorless stable gases and is tasteless and odorless.

CF₄ and C₂F₆ are extremely stable and do not react with almost any substance except alkali metal, etc. [3]. Consequently, the toxicity of these gases is quite low, and what must be taken care of is only suffocation due to lack of oxygen.

Table 1

Physical properties of CF₄ and C₂F₆

Item	Carbon tetrafluoride	Hexafluoroethane
Formula	CF ₄	C ₂ F ₆
Molecular weight	88.005	138.012
Boiling point (101.325 kPa)	−128.0°C	−78.2°C
Freezing point (101.325 kPa)	−186.8°C	−100.6°C
Density, gas (101.325 kPa)	3.946 kg/m ³ (at 0°C)	5.734 kg/m ₃ (at 23.9°C)
Density, liquid (101.325 kPa)	1.317 kg/l (at −80°C)	1.611 kg/l (at −80°C)
Critical temperature	−45.6°C	19.7°C
Critical pressure	3.739 kPa	2.980 kPa
Critical volume	1.590 dm ³ /kg	1.6448 dm ³ /kg
Molar specific heat, gas, (101.325 kPa 25°C)		
Constant pressure	61.271 J/(mol·° K)	105.094 J/(mol·° K)
Constant volume	52.949 J/(mol·° K)	92.385 J (mol·° K)

19.1.3 Industrial manufacturing method of CF₄ and C₂F₆

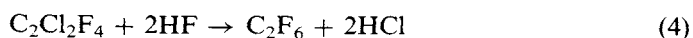
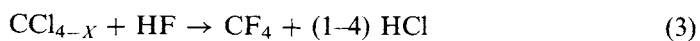
CF₄ and C₂F₆ are produced by the similar methods. The main manufacturing methods disclosed to date and their characteristics are summarized as follows:

1. Direct fluorination of carbon by fluorine.



This is the oldest method which has been practiced since isolation of fluorine was succeeded [2,6], but the heat generation is large and control of the reactions is difficult. In particular, in order to manufacture C₂F₆, moderate conditions must be selected. Under these conditions, reactions do not take place smoothly and there is a possibility of resulting explosions. Consequently, a method for adding a salt of Hg to the reaction system to allow the reactions to take place under relatively moderate conditions [7], or a method for adding halogen fluoride [8], etc. have been designed. According to a literature [7], there is no difference by the kind of carbon used, but our experiments indicate that fluorine is difficult to react with carbon having high crystallinity (for example, graphite) [9]. This method is primarily used for manufacturing CF₄ and high-purity CF₄ which do not contain any chlorine. However, expensive pure fluorine is required and thorough experience is necessary in its handling.

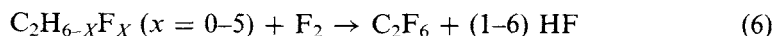
2. Halogen exchange by HF.



The most popular manufacturing methods of CF_4 and C_2F_6 are the fluorine-halogen exchange using catalysts such as chromium oxide, aluminum fluoride, iron fluoride, etc. [10–13]. These reactions are inexpensive manufacturing methods, but separation of by-product CF_3Cl from CF_4 is difficult, and a large volume of HF/HCl mixed acid is generated because two or more equivalents of HF are used. The key of this process lies in the life of the catalyst, and each manufacturer has made various improvements. Typical manufacturing conditions are given in Table 2 [11,13].

These halogen exchange reactions primarily depend on the reaction temperatures; at 200°C or lower, the reactions proceed only up to CClF_3 , and 400°C or a higher temperature is required for obtaining CF_4 at a high yield, and 500°C or the higher for C_2F_6 . With respect to the catalyst life, the yield of CF_4 lowers to 62% after 98 h. However, recycling of the catalyst is possible, and the initial performance can be recovered by activation [13]. Presently, procurement of raw materials, CCl_4 or CCl_3F , has become difficult as a result of discontinuation of production of flons.

3. Gas phase fluorination of methane or ethane and their derivatives by fluorine.



The basis of these reactions was developed by Bigelow et al. [14]. It is a key point to quickly remove the large reaction heat generated. They tried gas phase fluorination using Cu gauze as catalysts, and the desired substance was successfully obtained. By scrutinizing the technique further, they manufactured a reactor that can fluorinate at a high efficiency under moderate conditions (about 64°C) by spouting high-speed ethane and N_2 streams into the fluorine stream [15]. They pro-

Table 2
Typical reaction conditions

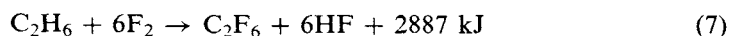
Manufacturer	E.I. du Pont de Nemours and Company			Daikin Industries
Catalyst	Cr_2O_3	Cr_2O_3	Cr_2O_3	chromium oxyfluoride
Reaction temperature	400°C	500°C	550°C	400°C
Raw material	CCl_4	CCl_2F_2	$\text{CCl}_2\text{FCClF}_2$	CClF_3
$\text{HF}/\text{raw material}$ ratio	8/1	4/1	4 ~ 5/1	4/1
Feed rate	CCl_4 0.6 g/g cat./h	CCl_2F_2 0.6 g/g cat./h	$\text{CCl}_2\text{FCClF}_2$ 0.5 g/g cat./h	space velocity $40-10 \text{ h}^{-1}$
CF_4	94.5	92	—	99.9
C_2F_6	—	—	94	—
CClF_3	5.2	8	—	0.06
CClF_2CF_3	—	—	4	—

duced C_2F_6 from C_2H_6 at a yield of 83% by this method. However, high-boiling point compounds which seemed to be partially fluorinated are generated as by-products.

This method is a simple process, but side reactions such as explosion sometimes occur when temperature, material feed ratio, and other reaction conditions are not well controlled.

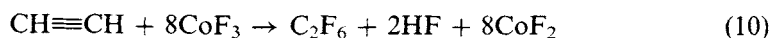
In recent years, several improved methods have been proposed. One is a method proposed by Allied Chemical Corporation, using SF_6 , CF_4 , C_2F_6 , etc. for a diluent of F_2 , in which the diluent is allowed to spout out from the inconel porous tube and reactions are allowed to take place at a relatively low temperature (max. $76^\circ C$) [16].

The other is a method released by Kanto Denka Kogyo Co., Ltd. A compound containing CF_3 group is fluorinated with diluted F_2 under the presence of a metal catalyst [17]. CF_3 containing substances significantly reduces the heat of reaction and the cleavage of the C—C bond is prevented. When C_2H_6 and CH_2FCF_3 are compared, the reaction heat of the latter is about 33% of that of the former.

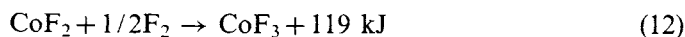
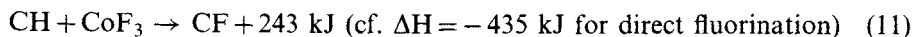


The clear difference in these two methods lies in the reaction temperature, which is as low as about $70^\circ C$ for the former, whereas the latter is carried out at a high temperature of $200^\circ C$ or higher.

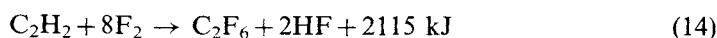
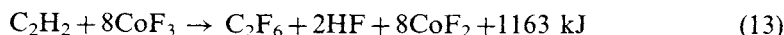
4. Fluorination of C_1 or C_2 compounds by the high valency metallic fluoride.



This is an indirect fluorination method by high valency metallic fluoride (CoF_3 , MnF_3 , etc.) at a high temperature. In particular, the reactions using CoF_3 have been extensively investigated since during World War II and technical reports covering details are available [18]. In this method, because the calorific value is divided in fluorinating of metal fluoride and organic compounds, the reactions become considerably moderate compared with direct gas-phase fluorination [19].



In addition, when compounds containing a multiple bond such as acetylene are used as raw materials, the consumption of F_2 can be reduced and the heat of reaction is also lowered. Because this method prevents the cleavage of C—C bond, it is particularly suitable for the manufacture of C_2F_6 . In our experiment, C_2F_6 can be obtained at a yield as high as 90% or more [20].



However, because this is based on the gas–solid reaction, the release of heat of reaction is difficult. High temperature portions (hot spots) are likely to be formed, and handling of fluoride powders is somewhat difficult.

In addition to these, various unique manufacturing methods of perfluorocarbon are available, though the industrial applications seem to be difficult. Those who are interested in these techniques should refer to the literatures [21].

Nowadays, CF_4 and C_2F_6 are produced on an industrial scale by the methods described above. However, the application of these gases is primarily to the semiconductor process, and the required gas purity is extremely high. The purity of regularly marketed gases is 4–5 N (99.99–99.999%). Consequently, much effort has been done on the purification method than on the manufacturing method.

Though the purification method of each company has not been disclosed, it is supposed that the gas generated is purified by adsorption method or the use of precision distilling columns after alkali washing and drying.

19.2 Nitrogen trifluoride (NF_3)

19.2.1 Introduction

NF_3 was synthesized by Ruff et al. for the first time in 1928 by the molten salt electrolysis [22]. Unlike the fluorinated carbons, the nitrogen trifluoride is easy to decompose due to relatively low bond energy in N—F bond, and therefore can be a fluorine source. Consequently, at first, many researches were made as a rocket fuel oxidizer. The utilization as cleaning/etching gas was developed in the semiconductor industry as in the case of fluorinated carbon [23].

19.2.2 Physical and chemical properties of NF_3

NF_3 is a colorless, stable gas with a characteristic musty smell at room temperature. At an elevated temperature, NF_3 exhibits strong oxidizing properties. Because it provides a low bond energy ($\text{F}_2\text{N—F}$) of 238.9 kJ/mol, and in addition, it is smaller than that of the remaining N—F bond, therefore the oxidation ability increases as a temperature rises. And NF_3 not only acts as a fluorinating agent but also serves as a supply source of NF_2 radical [24]. Table 3 shows physical properties of NF_3 [25,26].

NF_3 does not react with water at ambient temperature, however slowly hydrolyzed by basic solution at 100°C [25,27]. NF_3 reacts with metals, such as Cu, Bi, stainless steel, etc. at over 300°C, and form metal fluorides and N_2F_4 [25,28]. NF_3 also reacts with organic compounds, such as hexafluoropropene at 320°C in the presence of CsF, to give $(\text{CF}_3)_2\text{CFCF}(\text{CF}_3)_2$, $(\text{CF}_3)\text{CFNF}_2$, and $(\text{CF}_3)_2\text{C=NF}$ [25,29].

NF_3 is assumed to moderate acute inhalation toxicity when there is a possibility to cause anoxic deaths due to methemoglobinemia because it has a strong oxidation ability and methemoglobin is generated by oxidizing hemoglobin when inhaled [25]. In the acute inhalation, slight histolysis is observed in the liver and kidneys of some

Table 3

Physical properties of NF_3

Item	Nitrogen trifluoride
Formula	NF_3
Molecular weight	71.002
Boiling point (101.325 kPa)	-129.0°C
Freezing point (101.325 kPa)	-206.8°C (triple point)
Density, gas (101.325 kPa)	2.96 kg/m^3 (at 20°C)
Density, liquid (101.325 kPa)	1.531 kg/l (at -129.0°C)
Critical temperature	-39.3°C
Critical pressure	4.530 kPa
Critical volume	$1.915 \text{ dm}^3/\text{kg}$
Molar specific heat, gas,	(101.325 kPa 25°C)
Constant pressure	$53.371 \text{ J}/(\text{mol} \cdot ^\circ\text{K})$
Constant volume	—

rats, and enlargement and darkening of spleen are also observed [25]. In addition, mutagenesis is suspected (there is an assertion that it is an influence of impurities in NF_3) [30]. The Threshold Limit Value (TLV) is specified to be 10 ppm (30 mg/m^3) by ACGIH (1979) [25].

19.2.3 Industrial manufacturing methods of NF_3

The industrial manufacturing methods of NF_3 are classified in three categories: electrolysis method, reactions of F_2 with liquid phase ammonium-acid fluoride, and reactions of F_2 with metal fluoride ammonium complex.

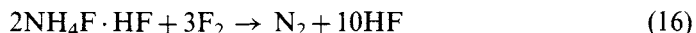
The electrolysis method is an effective method to synthesize NF_3 at one stage without using highly reactive fluorine. In a low-temperature method, anhydrous HF is used as the electrolyte and pyridine or its derivative is used as the nitrogen source [31]. A medium-temperature method uses NH_4F —HF [32] or NH_4F —HF—KF system [33]. The low-temperature method has many disadvantages that the electrolysis temperature must be held to the vicinity of 0°C because anhydrous HF with a low boiling point (bp 19.5°C) is used, and a condenser must be installed to reflux HF accompanying NF_3 into the electrolysis cell. The medium-temperature method called the Glemser process employs a nickel anode in NH_4 —HF electrolyte at 130°C , producing NF_3 with 62% current efficiency and 30–42% yield [32]. In the NH_4F —HF—KF system developed by Tasaka et al., molten KF 2HF is used as the electrolyte [24,33]. Since the HF vapor pressure is relatively low and the surface tension of the electrolyte is relatively large, carbon electrode and iron cell can be used. With 30–50 mol% of NH_4F , the operating conditions: temperature of 130°C , current density of $100\text{--}200 \text{ A/m}^2$, and cell voltage of 6–7 V achieved the 70% or higher current efficiency. The problem of the electrolysis method is that the anodic dissolution of nickel occurs. Therefore the electrode must be replaced

frequently. On the other hand, the cost of carbon electrode is low and the electrode is not needed to be frequently replaced, but carbon-fluorine compound is formed on the electrode surface which increase the polarization and a trace of CF_4 is also mixed. If a trace of water exists in the molten salt, N_2 , O_2 , ozone, N_2O and so on are generated at the anode. Consequently, a trace of water in the melt must be thoroughly removed by preliminary electrolysis.

The second NF_3 manufacturing method is the reaction of F_2 with liquid phase ammonium-acid fluoride, being developed by Air Products & Chemical Inc. [34]. In this method, NF_3 is obtained by the reaction of F_2 gas with molten $\text{NH}_4\text{F} \cdot \text{HF}$ kept at $127\text{--}160^\circ\text{C}$.



NH_4F immediately reacts with HF , giving $\text{NF}_4\text{F} \cdot \text{HF}$. Consequently, from 4 moles of a raw material $\text{NH}_4\text{F} \cdot \text{HF}$, 1 mole of desired NF_3 is produced with 5 moles of HF as by-products. The most important point in this reaction is the removal of heat of reaction. Local temperature rise induces the decomposition of NF_3 to N_2 and HF .



In order to prevent the local temperature rise, various contrivances have been made. For example, fluorine gas is bubbled into the bath from a sparger with a 1/64 to 1/4-inch holes, or a packed column is installed in the reactor to disperse fluorine gas and to facilitate heat transfer. Neat fluorine or fluorine diluted with N_2 is used for such a purpose. At around 150°C , 58% NF_3 can be obtained on the basis of fluorine.

The third method is a process developed by Central Glass Co. Ltd using the gas-solid reaction of ammonium complex of metal fluoride with fluorine [35]. Metal fluorides of Fe, Ti, Al, Cr, Mn, and so on can be used, however, aluminum fluoride seems the best from the viewpoints of cost and ease of handling. The reactions are supposed to take place at two stages as described below.



The reaction (17) begins at about 100°C and as the reaction proceeds, temperature rises to a suitable reaction temperature but the reaction finishes before temperature reaches 150°C . The reaction (18) begins at 150°C , and finishes before the temperature reaches 250°C . The yield is about 76% for reaction (17) and 65% for reaction (18). In this method, the control of the reaction temperature is essentially important, and it seems that thermal decomposition of complex may occur.

Requested purity of NF_3 is also very high (99.999%). The method of purification is almost the same as those for CF_4 and C_2F_6 , but the separation of a trace of CF_4 from NF_3 is very difficult, because both compounds have similar physical properties. Generally, the production of NF_3 is performed under the condition that no CF_4 is generated or NF_3 is purified by absorbing a trace of CF_4 by Molecular Sieves 5A under 10°C [36].

19.3 Applications of CF_4 , C_2F_6 , and NF_3 to plasma etching/cleaning in semiconductor industries

19.3.1 Introduction

Main industrial applications of these fluorides are uses as plasma etching/cleaning gases in the semiconductor industry. Hydrofluoric, phosphoric or nitric acid were used as etchant until the middle of the 1970s, however, as the IC integration was improved, the layer thickness and line-width remarkably decreased, and it became difficult to process by isotropic, wet etching. The dry etching using fluorinated gas such as CF_4 then appeared as a new technology. Two kinds of dry etching processes are available, i.e. isotropic plasma etching and anisotropic reactive ion etching. The mechanisms of these processes were explained by Abe [37].

In plasma etching, high-frequency glow discharge plasma using the capacitive coupling type or inductively coupled type external high-frequency electrode is employed. In general, the high frequency is 13.56 MHz and gas pressure is about 13 Pa. The basic reaction species in this etching is supposed to be a radical in plasma. Because the radical makes random movements in the plasma and is independent of the sheath potential generated on the substrate surface, etching is free of directionality, and consequently, isotropic etching becomes possible. This is used for etching Si, Si_3N_4 , and poly Si.

In the reactive ion etching (RIE), the reaction species contributing to etching is a reactive ion with directionality. By the potential in the sheath layer formed on the electrode or formed in the vicinity of the electrode surface, the positive ions in the plasma are forced to flow to the cathode by the acceleration voltage. The accelerated reactive ions (F^+ , CF_3^+) etch the substrate with directionality by a chemical reaction as well as physical collision effects. Because anisotropic etching is carried out by this method, fine patterns with high accuracy are formed. The parallel flat plate type equipment is used, and low frequencies such as 400 kHz are used in addition to 13.56 MHz. The gas pressure is lower than that of plasma etching. Recently, equipment using an electron cyclotron resonance is also available.

19.3.2 The role of perfluorocompounds (PFCs) in plasma etching

For etching of silicon, CF_4 is primarily used. NF_3 is normally used for cleaning of Si system, and C_2F_6 for cleaning of SiO_2 system because carbon-based gas is advantageous for cleaning of SiO_2 system as described below.

In plasma etching, various factors such as kinds of gases, level of power used, electrode-to-electrode distance and so on should be taken into account. For the gas used, fluorocarbon gas such as CF_4 is rarely used alone. O_2 , H_2 , CO and other gases are generally added in accordance with the etching/cleaning objectives. Of these, the most typical addition gases are O_2 and H_2 . The mechanisms were described by Coburn et al. [38] and Mogab et al. [39].

19.3.2.1 Etching for Si [38,39]

It is known that the silicon etching rate increases when O_2 is added to CF_4 , because carbon is oxidized by O_2 , and the fluorine concentration increases. CF_4 is unable to react with oxygen, therefore the mechanism for increase in the fluorine concentration may be attributed to the reaction of a radical species generated by dissociation of CF_4 with oxygen. The following reaction mechanism was proposed [39,40].

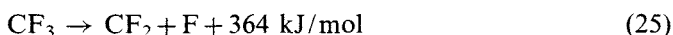
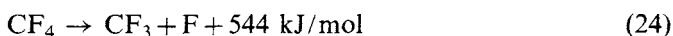
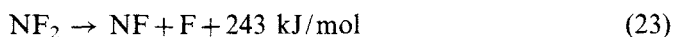
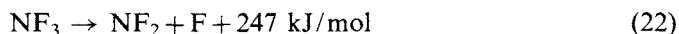


19.3.2.2 Etching for SiO_2 [38]

When H_2 is added to CF_4 , the Si etching rate increases selectively with respect to SiO_2 (for example, 30 times or more for Si). The reason is that fluorine concentration is decreased as fluorine is combined with hydrogen as HF and carbon is deposited on the substrate. The precipitated carbon reacts with oxygen in SiO_2 lattice, being removed from the surface by generating volatile CO, CO_2 and COF_2 . In the case of Si, fluorine is consumed to remove carbon, so the etching rate may be decreased.

19.3.2.3 Advantages of NF_3 in etching/cleaning [41]

As compared to CF_4 , the etching rate by NF_3 for Si is said to be about one or two order of magnitude higher. A factor to raise the etching rate is that the dissociation energy of NF_3 is significantly low as compared to that of CF_4 . The dissociation energy of NF_3 is about half of that for CF_4 .



In addition, NF_3 prepares no deposited layers on the substrate. Formation of such deposited layers cannot be avoided in case of CF_4 . To remove the deposited film, atomic fluorine is required. NF_3 gives no deposit and etching proceeds well without any contamination on the silicon surface. NF_3 thus has an advantage of being free from contamination by carbon atom.

19.4 Prevention of global warming (techniques for decomposition or recovery of PFC gases)

19.4.1 Introduction

In recent years, various countermeasures against global warming effects are discussed and are implemented in all the countries of the world. On the restriction

of greenhouse effect gas having global warming effects, the following decision was made in the 1997 Kyoto Conference for Global Warming Prevention. That is, aiming at 2008 to 2012, the reduction ratio of the whole global warming gas is set to 6% in Japan, 7% in the US, and 8% in Europe with the 1990 level as a reference. These PFC gases discharged in an extremely small amount as compared to CO_2 , CH_4 , etc., but they exhibit a strong absorption to wavelength in the vicinity of $1000\text{--}1200\text{ cm}^{-1}$, which is called the atmosphere window. As shown in Table 4, they are chemically stable and have an extremely long life in atmosphere from thousands to 10,000 years [42]. Consequently, GWP_{100} (global warming potential: ratio of influence of each gas to influence of the same volume of CO_2 after 100 years is set to 1, Table 4) determined from the absorption of infrared ray and atmospheric life is great, and long-term influences are particularly concerned.

With the current technique, the ratio of PFC gas used in the process is only the order of %, and more than one half of the gas is discharged to the outside. Consequently, semiconductor manufacturers, equipment manufacturers, and gas manufacturers are trying to take various countermeasures to reduce the discharge. The methods fall into the following four broad general categories:

1. Improvement in decomposition ratio of PFC gas,
2. Decomposition and removal of PFC gas discharged,
3. Recovery and recycling of discharged PFC gas, and
4. Use of alternative gas.

Presently, all the methods lack clinchers, but some have already been put into practical use on a small scale or experimentally. These techniques will be discussed as follows.

19.4.2 Improvement in decomposition ratio of PFCs in the semiconductor process

Researches are carried out by equipment manufacturers, for example, remote plasma cleaning method was presented by Applied Materials Inc. at the 1997 Semicon West [43]. This method improved the usual decomposition ratio of NF_3 , ca 50% to more than 99%. Plasma is normally generated in a chamber, however,

Table 4
The value of GWP_{100} for CF_4 , C_2F_6 , and NF_3

	Life (year)	GWP_{100}
CF_4	50,000	6500
C_2F_6	10,000	9200
NF_3	740	9700
CO_2	50–200	1

GWP_{100} : global warming potential; ratio of influence of each gas to influence of the same volume of CO_2 after 100 years is set to 1.

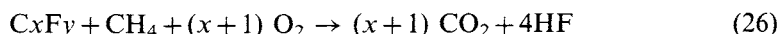
in the new method, an applicator with the microwave source is newly installed. High-density plasma is generated there to decompose almost all NF_3 and the fluorine radical formed is introduced into the cleaning chamber. In this method, the NF_3 decomposition ratio approaches to 100%, and improvement of the cleaning efficiency and reduction of damage to the furnace seem to take place at the same time. Even in the C_2F_6 cleaning equipment, the decomposition ratio can be improved by optimizing the conditions.

19.4.3 Decomposition and removal of PFC gas

The PFC gas decomposition and removal method is classified into two methods: combustion method and chemical decomposition method.

19.4.3.1 Combustion method

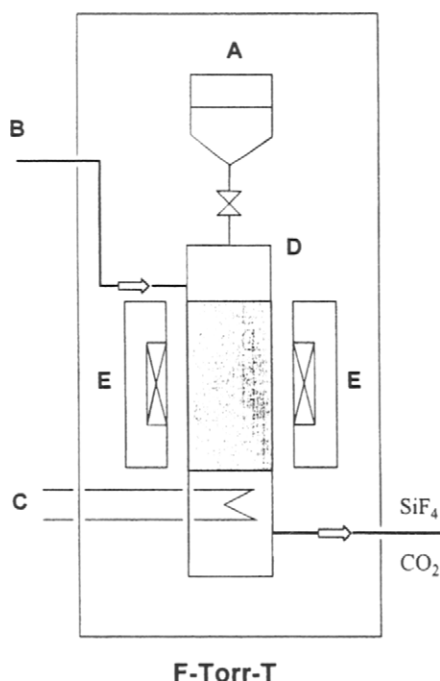
The principle of this method is to mix PFC gas with fuel (for example, H_2 , CH_4 , propane, etc.) and air, to oxidize and combust at a high temperature of over 900°C and to convert PFC gas into CO_2 and HF .



Various contrivances (material, for example, the use of porous ceramics, combustion furnace, burner profile, etc.) were made in the combustion method, and generation of NO_x , CO , etc. was suppressed. The combustion method is characterized by continuous and efficient removal of a large volume of PFC gas and simultaneous treatment of hydrides (SiH_4 , etc.), however, produces a large volume of CO_2 as a by-product, or requires a large volume of air and a large amount of energy for heating. According to the reports of various companies, the method seems to possess industrial pretreatment capabilities of 60–90% or more for C_2F_6 and 90% or more for NF_3 . However, in the case of CF_4 , the decomposition is difficult and the industrial pretreatment capability decreases to about 50%, requiring further contrivances to raise the reaction temperatures.

19.4.3.2 Chemical decomposition method

The chemical decomposition method employs the reactions of PFC with some chemical reagents (for example, metal or silicon compounds) packed in the equipment. Since no fuel is required, only a trace of CO_2 is generated. In addition, in the semiconductor plant where combustibles are frequently used, it has an advantage of no use of any fire. On the contrary, there are some cases that require treatment of acidic gas (industrial treatment by dry/wet scrubber) or fluorides generated by the reactions. Since the treated amount is small compared with the combustion method, there is a possibility for improvement in the future. With respect to the chemical decomposition method, the equipment (F-Torr SeriesTM) marketed by Kanto Denka Kogyo Co. Ltd, is shown in Fig. 1 [44]. PFC from the semiconductor process is introduced through B and is allowed to react with the SiO_2 filled in the reactor D which is heated with the heater E at 900 – 1200°C . In the reaction zone, PFC is completely decomposed and converted into SiF_4 and CO_2 . These can be



- (A) Storage vessel of the SiO_2
- (B) Fluoride waste gases from etching process or CFCs etc.
- (C) Cooling water
- (D) Decomposition reactor
- (E) Heater

1. Fluoride waste gases (or CFCs) (B) are delivered from the top of the decomposition reactor (D).
2. Gases (B) are encountered with the reagent at the controlled elevated temperature, and are converted to SiF_4 , CO_2 , etc.
3. Thus decomposed gases at a high temperature are cooled and exhausted from the equipment (C).
4. The reagent is supplied periodically from the storage vessel (A) to the reactor (D) according to the amount of fluoride waste gases or CFCs.
5. There is no residue from the reactor (D).

Fig. 1. The outline of decomposition equipment (F-Torr-TTM)

detoxified easily by an alkali scrubber, etc. The reagent gradually decreases as the reaction proceeds, however, is automatically replenished from the tank A. Figure 2 shows the relationship between the reaction temperature and decomposition ratio with respect to various PFCs. For NF_3 with a low bond energy, the equipment provides the 99% decomposition ratio at 800°C and 100% at 900°C . However, for CF_4 and C_2F_6 with a high C—F bond energy, the equipment provides only 50% and 87% decomposition ratios, respectively, even at 1100°C , requiring a high temperature of 1200°C to complete the industrial treatment. For such a high temperature treatment, the reactor materials become very expensive. A new reagent lowering the reaction temperature is now under development. The present equipment has an ability for decomposing 100% PFC gas at 15 l/min at maximum.

In the case of NF_3 , the reaction temperature can be lowered to 300°C by replacing the reagent with a certain metal or its oxide (F-Torr R SeriesTM).

19.4.4 PFC recovery and recycling technique

For the PFC recovery and recycling technique, the most popular concept is to concentrate and recover PFC on site and to purify off-site.

The most important problem in organizing the PFC recovery and recycling system is the PFC concentration technique. In the semiconductor process, inflammable toxic

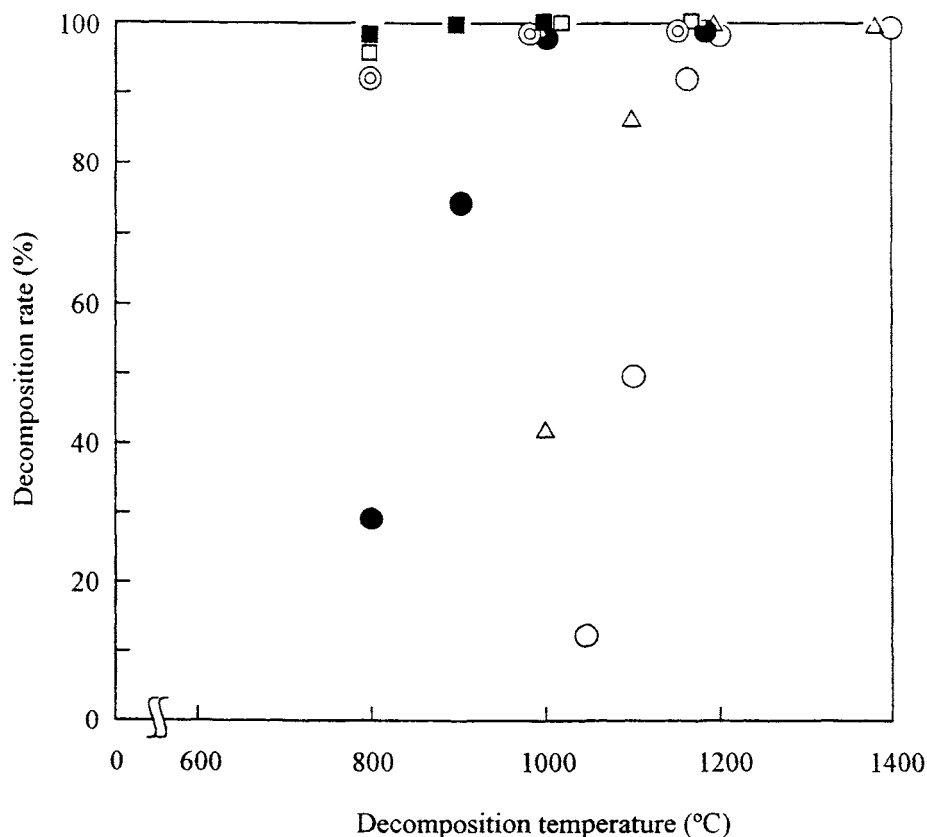


Fig. 2. Relationship between decomposition temperature and decomposition rate for various fluorinated gases. ○ CF₄, △ C₂F₆, ● SF₆, ⊙ CHF₃, □ CCl₂F₂, ■ NF₃.

gases such as silane (SiH₄), arsine (AsH₃), etc. are used. To prevent their backflow to the system or to protect pumps, a large volume of N₂ gas (ballast N₂) is added to the upstream side of the vacuum pump. The concentration of PFC discharged from the process is as low as several % and the concentration is not constant. Consequently, the recovered gas must be concentrated to a high value. For the recovering and concentrating of the gas discharged from the process, the following three techniques are presently disclosed.

1. Membrane separation method.
2. Low-temperature absorption process.
3. Pressure Swing Absorption (PSA) process.

All the processes are now under the investigation. The processes attracting a great attention as practical methods are: 1. Membrane separation method; and 2. Low-temperature absorption process.

19.4.4.1 Membrane separation method (membrane method)

As a typical example, a membrane method developed by Air Liquide Co. will be introduced [45]. The membrane method separates and recovers N_2 gas for dilution and PFC, utilizing the difference in permeability coefficients which are determined by the diffusivity and solubility depending on the dynamic diameter of molecule in polymer membrane. The choice of membrane is a key point. Figure 3 shows the conceptual drawing of the whole system and Fig. 4 outlines the separation of PFC by membrane. The exhaust gas from the semiconductor manufacturing equipment is discharged to the exhaust duct by a vacuum pump after diluting with ballast N_2 gas. Acidic gas such as HF or toxic gas such as silane in the exhaust gas are removed with the industrial pretreatment equipment for discharge (dry and wet alkali scrubber) which has been installed in the semiconductor plant. A large volume of N_2 or gas that does not affect the separation membrane, and PFC are obtained. By this process, N_2 and H_2O are removed by the membrane and only PFC is recovered. The recovered PFC gas is filled in the gas filling facilities and transferred to the purifying plant. In the gas purifying plant, CF_4 and C_2F_6 gases are purified and recycled to the semiconductor plant again.

The experimental results using a model gas as an exhaust gas from the cleaning equipment (total concentration of C_2F_6 and CF_4 : about 0.5–4%; flow rate: about 150–250 l/min.) indicate that both PFC recovery ratio and recovery concentration exceed 98%.

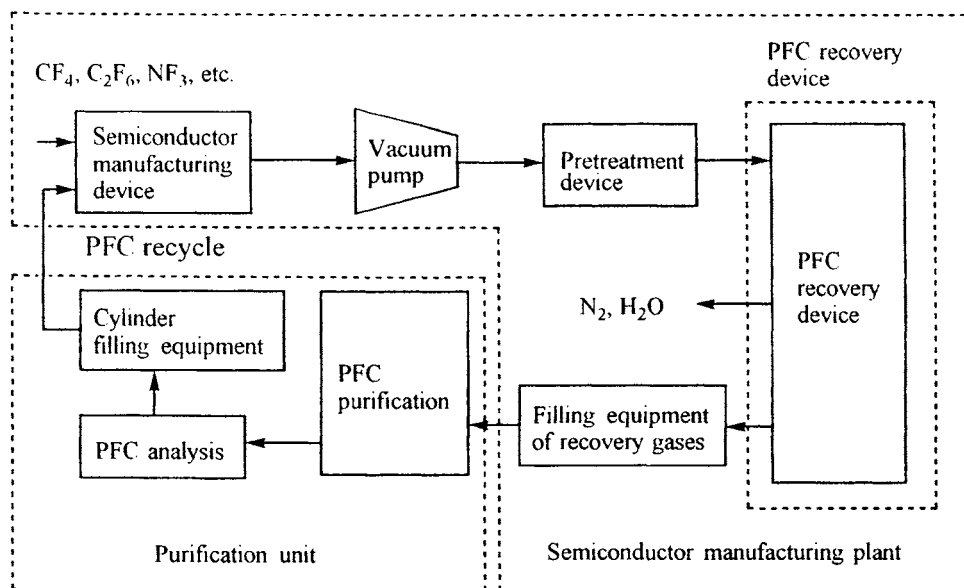


Fig. 3. Conceptual drawing of PFC recycle (reproduced with permission from abstracts of 14th semi-conductor technology seminar [45]).

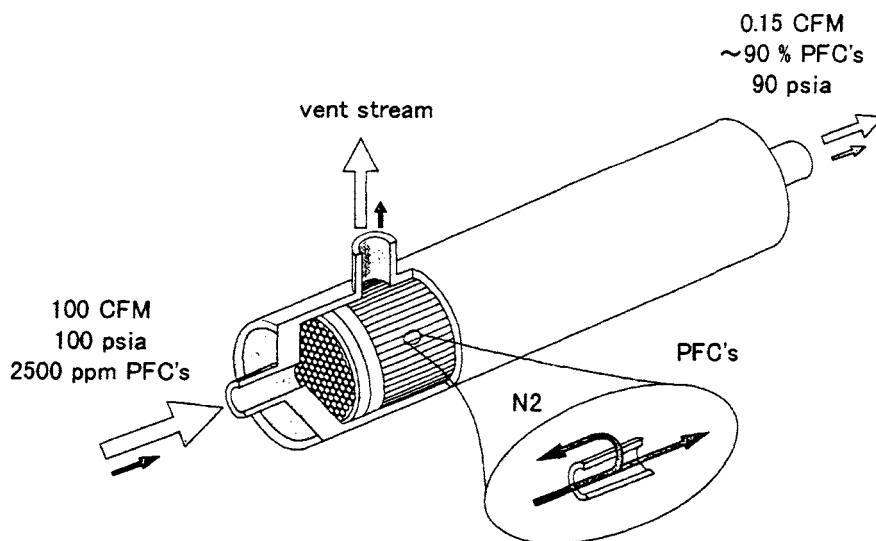


Fig. 4. PFC separation by membrane (reproduced with permission from abstracts of 14th semi-conductor technology seminar [45]).

19.4.4.2 Absorption separation method at a low temperature

One potential method for dealing with this issue is absorption followed by separation using low temperature (Cryogenic) distillation. One system is a “Cryogenic Rectification System”, which uses octafluoropropane (C_3F_8) as the wash liquid, published by Praxair Technology, Inc. [46]. Figure 5 shows the vapor pressure of CF_4 , C_2F_6 , and NF_3 [4,5,25]. Attempt to recycle these components by direct condensation or distillation encounters several problems:

1. The vapor pressure of CF_4 or NF_3 is extremely high at $-150^\circ C$. If these compounds are present in the exhaust stream, their condensation is very difficult.
2. The vapor pressure of C_2F_6 is also fairly high at $-150^\circ C$ while the freezing point is $-100^\circ C$, therefore C_2F_6 may be frozen if its condensation is attempted.

The system is operated in two steps; a continuous cryogenic absorption and a batch distillation which will overcome these issues. In this approach, C_3F_8 is utilized as a wash fluid in a continuous system. C_3F_8 , which has a high boiling point ($-36.7^\circ C$) and a low freezing point ($-183^\circ C$), is used to wash the other fluorochemicals from the inlet stream. This process yields a very high purity of nitrogen leaving the wash system. The captured PFCs are then stripped from the wash fluid and stored as a liquid mixture until sufficient amounts of the materials are accumulated, at which a batch cryogenic distillation will be performed to separate and purify the PFCs.

19.4.5 Alternative gases

In addition to the improvement of decomposition ratio and recovery and recycling of discharged PFC stated above, the use of an alternative gas is being investigated. The

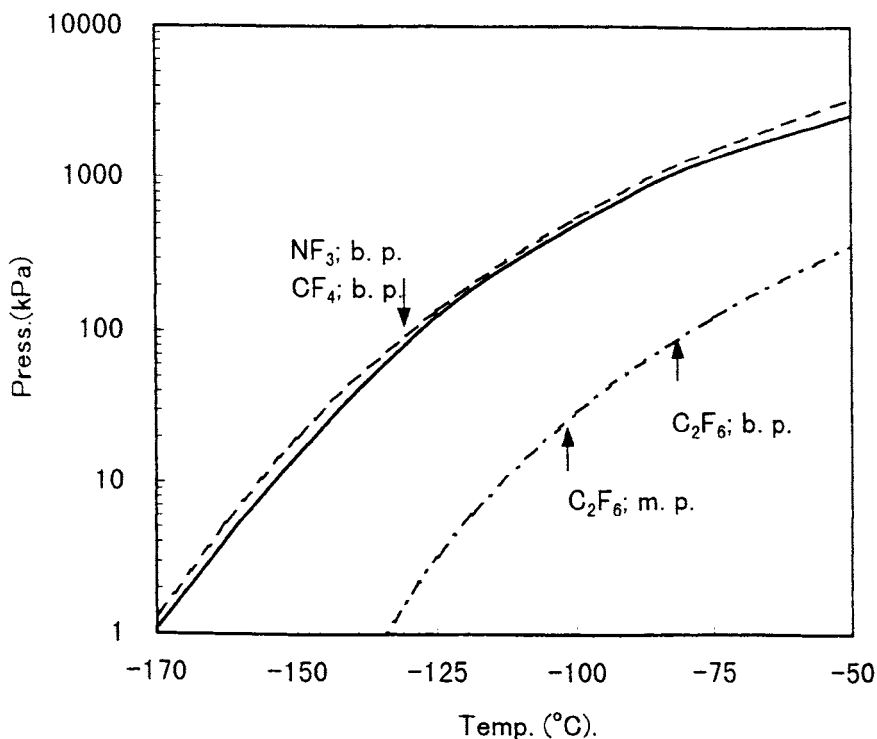


Fig. 5. Vapor pressure of CF₄, C₂F₆, and NF₃. — CF₄, — — C₂F₆, - - - NF₃

gases officially proposed now are hydrofluoroethers (Ex. HFE-227: CF₃OCHF CF₃; HFE-216: CF₃OCF=CF₂) [47] and (CF₃CO)₂CO [48], FC(O)C(O)F [49], etc. as etching gases. For the cleaning gas, chlorine trifluoride (ClF₃) has been proposed. The details on this material will be presented in Sec. 19.6.

Applications of semiconductors will increase more and more in the future, and both quality and quantity would be expanded. For the material, silicon will also be used extensively in the future, and for etching and cleaning, fluorine compounds are essential. However, protection of the global environment is an urgent and serious problem. For the effective utilization of fluorine resources, the combination of the improvement of PFC gas decomposition ratio with PFC recovery and recycling would be the most environmentally compatible method.

19.5 Tungsten hexafluoride, WF₆

19.5.1 Introduction

Among many metals, tungsten has the highest melting point of 3695 K, a very low vapor pressure and the highest tensile strength above 1650°C [50]. It is widely used

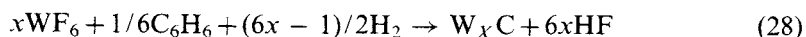
as lamp filaments, abrasion-resistant tools, forming and drawing dies, superalloys and other high-temperature applications. Because of its high melting point, however, the molding of tungsten is usually processed by powder metallurgy techniques. Small quantities of the rod are produced by arc or electron-beam melting. Its usefulness is limited because of the difficulty in processing it into varied and complex shapes. Additionally, grinding is also difficult because of its high hardness.

For these reasons, many studies have been made using chemical vapor deposition (CVD) techniques for obtaining coatings of any desired thickness and producing various shapes of tungsten metal and tungsten compounds. CVD is a convenient formation process of a nonvolatile solid film on a substrate by the reaction of vapor-phase chemicals that contain the required constituents. Tungsten hexafluoride is the most suitable source gas for CVD of tungsten because it is gaseous at room temperature and readily reduced by hydrogen at around 350°C to form tungsten films.



(Temperature: 350–600°C, Pressure: 101.3 kPa)

The CVD of tungsten by tungsten hexafluoride forms a dense and high-purity coating of tungsten on both metallic and nonmetallic substrates. It is used to fabricate solid tungsten pieces such as tubes or crucibles. In addition, tungsten hexafluoride is also used to form hard tungsten carbide coatings on steel [51].



(Temperature: 350–600°C, Pressure: 101.3 kPa)

Composite coatings of tungsten and rhenium are produced by the simultaneous chemical vapor deposition from their hexafluorides [52,53], and the addition of rhenium improves the ductility and high-temperature properties of the deposit.



(Temperature: 600–900°C, Pressure: <13.3 kPa)

Consequently, most of tungsten hexafluoride production had been used as a source gas in the CVD processes, but was quantitatively in small amounts.

In the fabrication of semiconductors, CVD is an important technique for the thin-film formations with an increase in device intensity performance. Tungsten hexafluoride has been widely used as a source gas of tungsten silicide (WSi_x) and tungsten metal for electrodes and interconnects.

19.5.2 Physical and chemical properties

The physical properties of tungsten hexafluoride are given in Table 5 [54–57].

Tungsten hexafluoride is a colorless gas at room temperature and is ten times as heavy as air. It condenses into a pale yellow liquid at 17.5°C and forms a white solid below 2.3°C [54]. The vapor pressure is given by the following equations [56]:

Table 5

Physical properties of tungsten hexafluoride

Property	Value	Reference
Boiling point (°C)	17.5	[54]
Melting point (°C)	2.3	[54]
Transition point (°C)	−8.2	[55]
Liquid density (kg/dm ³)	3.500(5°C), 3.441(15°C), 3.419(19°C)	[54]
Vapor pressure (kPa)	50.6(0°C), 113.7(20°C), 225.5(40°C)	[56]
Latent Heat of vaporization (kJ/mol)	26.49	[55]
Heat of fusion (kJ/mol)	1.76	[55]
Latent Heat of Sublimation (kJ/mol)	32.43 (above transition point) 38.28 (below transition point)	[55] [55]
Heat of transition (kJ/mol)	5.86	[55]
Heat capacity (J/K · mol)	119.026 (gas, 298.15 K)	[57]
Enthalpy of formation (kJ/mol)	−1721.716 (gas, 298.15 K)	[57]
Entropy of formation (J/K · mol)	341.013 (gas, 298.15 K)	[57]
Free energy of formation (kJ/mol)	−1632.346 (gas, 298.15 K)	[57]

$$\log_{10}P = 9.22616 - 2042.658/T \quad (187\text{--}265.55 \text{ K}) \quad (30)$$

$$\log_{10}P = 7.53130 - 1591.655/T \quad (265.55\text{--}273.63 \text{ K}) \quad (31)$$

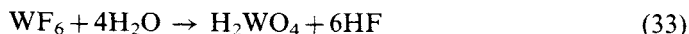
$$\log_{10}P = 19.85531 - 2745.200/T - 0.0416469T + 0.0000439111T^2 \quad (273.63\text{--}314 \text{ K}) \quad (32)$$

$$P = \text{kPa}, \quad T = \text{K}.$$

The solubility in anhydrous hydrogen fluoride is 3.14 mol/1000 g of HF [58].

Tungsten hexafluoride, as well as other transition-metal hexafluorides, exists as a symmetrical octahedral structure with the symmetry point group O_h near room temperature and in a phase of lower symmetry below the transition point [59,60]. The Raman and infrared spectra [61], infrared spectra [62] and NMR [63] were measured.

Tungsten hexafluoride is extremely unstable in the presence of moisture and completely hydrolyzes to tungstic acid [64].



Tungsten hexafluoride is a powerful fluorinating agent and reacts with many metals at room temperature. It reacts readily with ionic halides and other electron donors or bases to form complex ions or addition compounds [65]. It combines with KF, RbF and CsF but not NaF to form K_2WF_8 , Rb_2WF_8 and Cs_2WF_8 , respectively [66]. Tungsten hexafluoride reacts with alkali iodides in liquid sulfur dioxide to form NaWF_6 , KWF_6 , RbWF_6 and CsWF_6 which are all stable up to 250°C but are decomposed by water [67], it also reacts with KF in liquid IF_5 react to produce K_2WF_8 [68].

Tungsten hexafluoride dissolves in benzene or cyclohexane to give a bright red color; in dioxane it becomes pale red, and in ether it is a violet-brown [64].

19.5.3 Synthesis

Tungsten hexafluoride is commercially produced by the direct fluorination of tungsten. Though tungsten tetrafluoride (WF_4) is known as one of the compounds of tungsten and fluorine, tungsten hexafluoride is usually obtained by the reaction of pure tungsten metal with gaseous fluorine in a flow system under atmospheric pressure between 200 and 400°C.



It is swept away from the reaction zone in a stream of fluorine or nitrogen, condensed in traps and purified by distillation or sublimation. The surface oxide of the metal reacts with fluorine to form nonvolatile tungsten oxytetrafluoride, WOF_4 (bp = 185.9°C [69]). This may cause serious problems such as a blocking of the exhaust line. Accordingly it is preferable to use rods and blocks of tungsten as raw materials for the synthesis. When using a finely divided metallic powder, it is necessary to remove the surface oxide by hydrogen reduction at a high temperature.

For application to semiconductors, especially, tungsten hexafluoride is required to be of high purity because the impurities in tungsten hexafluoride significantly affect the reliability of the devices. High-purity product is currently available with total metallic impurity levels of less than 1 ppm and overall tungsten hexafluoride content of greater than 99.999%. Tungsten hexafluoride is shipped as a liquid under its own vapor pressure in stainless steel cylinders. It is classified as a corrosive liquid by the Department of Transportation (DOT) [70].

Nickel, monel, aluminum, copper, stainless steel and carbon steel are suitable metals for handling tungsten hexafluoride. Nickel and monel are more suitable at high temperatures of 100–400°C. Packing and gasketing can be made of polytetrafluoroethylene (PTFE). System components should be thoroughly clean and dry before use.

Tungsten hexafluoride is an irritating and corrosive gas. In the presence of moisture, hydrogen fluoride may be formed. Special care should be taken to avoid inhalation of the vapors or contact with skin. For disposal of tungsten hexafluoride, it can be diluted with an inert gas and scrubbed in water and a caustic solution. Small amounts of tungsten hexafluoride can be decomposed by passing through columns of soda lime or slaked lime.

19.5.4 Applications to semiconductor industries

Metal oxide semiconductor integrated circuit (MOS IC) has advanced to ultra-large-scale integration (ULSI), where an IC chip contains over 10 million semiconductor devices. In the early 21st Century, IC chips will move into the gigabit range. The most important factor in achieving the ULSI complexity is the continued reduction of the minimum device-feature size (linewidth). The minimum feature size of dynamic random access memory (DRAM) will decrease from its present linewidth of 0.35 μm in 64 Mb to 0.18 μm in 1 Gb. Another key requirement of submicron technology is the manufacture of multilevel interconnects which provide greater

flexibility in circuit design. At present, the number of interconnect layers is two and more than five levels in memory and logic circuits, respectively. The schematic cross section of MOS structure is given in Fig. 6. The IC devices are fabricated by many processing steps such as lithography, etching, metallization, and so on. Furthermore, they are repeated many times.

One of the important processing steps is the metallization process that connects individual devices together by microscopic wires to form circuits. For the metallization, the most widely used materials are polycrystalline silicon (polysilicon) and aluminum. Both materials form low-resistance ohmic contacts with p-type and heavily doped n-type silicon and also have the advantage of excellent adhesion both to silicon and silicon dioxide. Polysilicon is used as the conductor, semiconductor or resistor by proper doping with different impurities. Aluminum has a high conductivity and is readily deposited by physical vapor deposition (PVD) techniques such as evaporation and sputtering. While component density has increased, polysilicon has the disadvantage of low conductivity. The low melting temperature of aluminum correlates with a low resistance for electro-migration, and its high thermal expansion coefficient compared to silicon induced stress.

Accordingly, refractory metals have been extensively investigated for gate and interconnect metals in ULSI because of their low resistivities, high melting points, and high resistance to stress-migration and electro-migration. Table 6 shows the properties of refractory metal silicides and refractory metals compared with those of polysilicon and aluminum [71,72]. Among them, tungsten silicide and tungsten metal have several advantages such as thermal expansion coefficients close to that

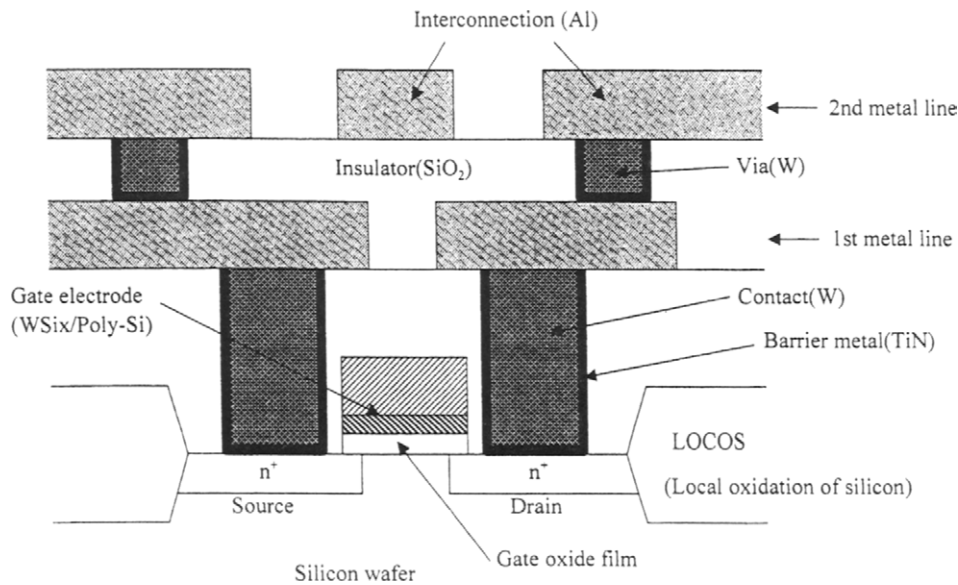


Fig. 6. Schematic cross section of MOS structure.

Table 6

Properties of refractory metal silicides and refractory metals

	Melting point (°C)	Electrical resistivity ($\times 10^{-8} \Omega \cdot \text{m}$)	Thermal expansion coefficient (ppm/°C, at 25°C)
Silicon			
Si ¹	1412	500	3.0
Alloys			
Al/Si	660–570	2.6–3.7	24
Silicides			
TiSi ₂	1540	13–17	10.5
MoSi ₂	1980	22–100	8.2
TaSi ₂	2400	8–45	8.8
WSi ₂	2050	14–70	6.2
Metals			
Ti	1677	43–47	8.5
Mo	2620	5	5.0
Ta	2996	13–16	6.5
W	3377	5.3	4.5
Cu	1083	1.69	16.6

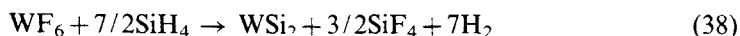
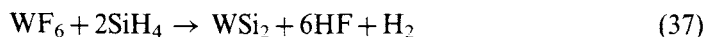
¹ For heavily doped polysilicon.

of silicon, low reactivity and high resistance to electro-migration. They have higher resistivities than that of aluminum, but much lower values than that of polysilicon.

On the other hand, deposition technologies play an increasingly important role in the fabrication of ULSI devices. For many years, the PVD techniques such as sputtering have been commonly used for depositing thin metal, metal alloy or metal silicide layers. For designs with high aspect ratio contact and via holes, however, the conventional metal sputtering results in inadequate step coverage, so that a technique that provides conformal films, such as CVD, is needed. A completely uniform or conformal step coverage means that the film thickness is constant along the walls and at the bottom of the step. CVD techniques have other advantages such as the control of film purity and layer stoichiometry in the case of silicides, and the ability to achieve spatially selective deposition. The most common CVD methods are atmospheric-pressure CVD (APCVD), low-pressure CVD (LPCVD) and plasma-enhanced CVD (PECVD, or plasma-CVD). A comparison of APCVD with LPCVD, called thermal-CVD, shows that the LPCVD makes possible the conformal step coverage and delicate control of composition and structure.

Tungsten hexafluoride is readily reduced to the metal by CVD as seen from Eqn. (27). Accordingly, it has been widely used for the formation of tungsten metal and tungsten silicide films. Besides Eqn. (27), the basic chemical reactions for

CVD-W and CVD-WSi_x, though the practical reactions are more complex, are as follows:



Tungsten silicide is used for a gate electrode and a local interconnect, and tungsten metal is used as a conducting material to fill in the contact and via holes. Tungsten hexafluoride was first employed as a source gas of WSi_x for the gate electrode and recently also as that of tungsten metal for the contact and via fillings. For this reason, the production of tungsten hexafluoride has gradually increased.

19.5.4.1. Gate electrode

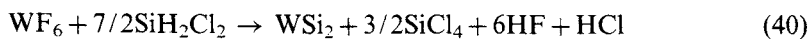
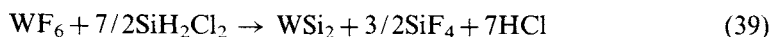
Tungsten silicide has been widely used as a gate electrode for the following reasons:

- lower resistance than that of polysilicon (up to one order of magnitude),
- high thermal stability and low reactivity against chemicals used in IC manufacturing processes,
- more excellent adhesion both to silicon and silicon dioxide than that of tungsten metal.

At present, tungsten silicide is usually used on the top of gate polysilicon as polycide structure which is an abbreviated name for polysilicon-silicide as shown in Fig. 6.

Tungsten silicide is readily deposited by the monosilane (SiH₄) reduction of tungsten hexafluoride at a temperature of 300–400°C [73]. The reactants in Eqns. (35–38) are the same. As can be expected, a higher SiH₄/WF₆ ratio results in WSi_x deposition. Tungsten silicide does not form at a SiH₄/WF₆ ratio below 3. Instead, tungsten is deposited at low flow rates with silicon incorporated in the grain boundaries. In fact, a SiH₄/WF₆ ratio greater than 10 is used to ensure the deposition of WSi_x ($x = 2.2\text{--}2.6$).

- Tungsten silicide can be also deposited by dichlorosilane (SiH₂Cl₂, or DCS) reduction at higher temperatures of 500–600°C [73].



Tungsten silicide deposited by DCS reduction contains much less fluorine than that by monosilane reduction, and the chlorine content is also low. Consequently, DCS is replacing monosilane in the CVD-WSi_x process because of good step coverage, good adhesion to polysilicon and SiO₂ and low resistivity.

With the continuing scale-down of ULSI features, the demand on the electrical resistivity of the electrode material is reduced. Many researchers have studied new conductor materials such as W/WN_x/poly-Si film.

19.5.4.2 Contacts and vias

With more stringent requirements on alignment tolerances and planarization in multilevel designs, it is important to fill in the contact and via holes with metal to maintain acceptable step coverage. The step coverage by sputtered aluminum rapidly decreases with increasing aspect ratio. Instead of the sputtered aluminum, tungsten metal has been widely used to fill in the contacts and vias by the CVD technique.

The formation of CVD-W plug was studied by a nonselective or blanket CVD-W and a selective CVD-W. Blanket CVD-W is deposited by the hydrogen or monosilane reduction of tungsten hexafluoride as shown in Eqns. (27), (35) and (36). At present, monosilane is mainly used as a reducing agent because of its high rates even at a low temperature.

When a tungsten plug is formed by blanket CVD-W, a barrier metal layer such as titanium nitride (TiN) is almost always used to prevent silicon migration into tungsten before CVD-W deposition. In addition, this barrier metal layer also provides adhesion of the CVD-W on SiO₂ and prevents the generation of particles from poorly grown CVD-W on SiO₂. Although titanium nitride can be deposited by sputtering from the compound target or by reactive sputtering (sputtering of titanium metal target in nitrogen atmosphere), it was also recently deposited by the CVD technique because of a better step coverage. Blanket CVD-W can be deposited not only in the contact windows, but also on the wafer. Excess tungsten on the wafer is then etched back or planarized by a reactive ion etching (RIE) system, leaving only the thicker tungsten in the contacts. Recently, chemical mechanical polishing (CMP) was applied to polishing metal for tungsten plug formation. If all contacts and vias on a chip have equal diameters, a blanket CVD-W is sufficient to fill even unequal depths simultaneously, because metal may be deposited on sidewalls as well as on horizontal surfaces. Additionally, blanket tungsten deposition is easily formed compared with selective tungsten deposition. Consequently, blanket CVD-W is most commonly applied to both memory and logic circuits.

On the other hand, a selective CVD-W makes good use of the selective nature of the deposition chemistry, i.e. tungsten can be selectively deposited on silicon, but not on SiO₂.



This process is necessary to use both the silicon and hydrogen or silane reduction reactions. Tungsten hexafluoride initially reacts with silicon to yield thin limited layers of tungsten, which reduces the transport of tungsten to silicon, passivating the WF₆—Si reaction phase. When tungsten hexafluoride reacts with silicon from the source/drain region, it may cause junction leakage. In this process, it is very difficult to maintain the perfect selectivity. The mechanism of the loss of selectivity has been studied, but no technique can still guarantee the total selectivity. Thus the selective CVD-W has many technical problems, but has the possibility of the filling in of the contact and via holes with high aspect ratios and reducing the number of steps required for metallization processes such as additional mask and etchback.

In the future, the continued scale-down in ULSI features will need more stringent requirements with respect to the electrical conductivity of materials for the contacts and vias. Copper has higher electrical conductivity than aluminum. The future demand for tungsten hexafluoride will be affected by the improvement in tungsten metallization and the progress in the technology of copper metallization.

19.6 Chlorine trifluoride, ClF_3

19.6.1 Introduction

Fluorine reacts exothermally with other halogens to form many halogen fluorides such as ClF , ClF_3 , ClF_5 , BrF , BrF_3 , BrF_5 , IF_3 , IF_5 , IF_7 , and so on. Halogen fluorides have similar chemical properties to those of fluorine, but commonly lower reactivity than elemental fluorine because of higher thermodynamic stability. Chlorine trifluoride is the most reactive compound among the halogen fluorides.

Many studies on chlorine trifluoride were carried out to develop atomic energy technologies. Chlorine trifluoride has been widely used for the preparation of uranium hexafluoride, and the process was thus developed for separating uranium from plutonium and fission products in used nuclear fuels [74]. Uranium metal and oxides are converted by chlorine trifluoride to volatile uranium hexafluoride, anhydrous hydrogen fluoride being used to accelerate the reaction with chlorine trifluoride. Hence, plutonium is converted to the involatile tetrafluoride, and most fission products also form involatile fluorides, which remain in the reaction vessel when uranium hexafluoride is volatilized. Uranium hexafluoride is then separated from other volatile components by distillation. Chlorine trifluoride was also studied as an oxidizer for such rocket fuels as hydrazine and its derivatives, since it shows high performance with the advantage over cryogenic systems that both the fuel and oxidizer may be stored as liquids at ambient temperature [74]. Most of the chlorine trifluoride production has been used in the processing of nuclear fuel to convert uranium to gaseous uranium hexafluoride.

Thus chlorine trifluoride has high reactivity and is somewhat easier to handle, to store and to transport than elemental fluorine because it is liquid at room temperature. These properties have been recognized to be attractive as an effective cleaning gas for some CVD processes in the semiconductor industries.

19.6.2 Physical and chemical properties

The physical properties of chlorine trifluoride are given in Table 7 [75–83].

Chlorine trifluoride is a colorless gas at room temperature. It condenses to colorless liquid at 11.75°C and freezes to a white solid below -76.32°C [75]. The vapor pressure is given by the following equations [75,76]:

$$\log_{10}P = 6.49201 - 1096.917/(T/\text{K} - 40.41) \quad (226.16\text{--}303.16 \text{ K}) \quad (42)$$

$$\log_{10}P = 6.38984 - 1048.94/(T/\text{K} - 45.5987) \quad (300\text{--}317 \text{ K}) \quad (43)$$

$$P = \text{kPa}, T = \text{K}.$$

Table 7

Physical properties of chlorine trifluoride

Property	Value	Reference
Boiling point (°C)	11.75	[75]
Melting point (°C)	-76.32	[75]
Transition point (°C)	-82.66	[75]
Vapor pressure (kPa)	60.1 (0°C), 141.9 (20°C), 294.7 (40°C)	[75,76]
Liquid density (kg/dm ³)	1.8555 (10°C), 1.8249 (20°C)	[77]
Solid density (kg/dm ³)	2.53 (-120°C)	[78]
Critical temperature (°C)	174	[75]
Critical pressure (kPa)	5776	[75]
Heat of vaporization (kJ/mol)	27.53	[75]
Heat of fusion (kJ/mol)	7.61	[75]
Heat of transition (kJ/mol)	1.51	[75]
Specific heat (J/K·mol)	65.2 (gas)	[79]
Viscosity (kg/m·s)	0.435 (20°C)	[80]
Surface tension (mN/m)	26.7 (0°C)	[80]
Specific conductivity (ohm ⁻¹ cm ⁻¹)	4.9 × 10 ⁻⁹ (25°C)	[81]
Dielectric constant	4.754 (0°C)	[82]
Heat capacity (J/K·mol)	63.848 (gas, 298.15 K)	[83]
Enthalpy of formation (kJ/mol)	-158.866 (gas, 298.15 K)	[83]
Entropy of formation (J/K·mol)	281.495 (gas, 298.15 K)	[83]
Free energy of formation (kJ/mol)	-118.901 (gas, 298.15 K)	[83]

The liquid density [77] is represented by the equation:

$$D = 1.8853 - 2.942 \cdot 10^{-3} t - 3.79 \cdot 10^{-5} t^2 \quad (-5 \text{ to } 46^\circ\text{C}) \quad (44)$$

$$D = \text{g/cm}^3, \quad t = ^\circ\text{C}.$$

Chlorine trifluoride deviates from ideal gas behavior. The divergence has been explained quantitatively by its association to a dimer [84]. The relationship between the equilibrium constant, $K_p = P_{\text{ClF}_3} / P_{\text{Cl}_2\text{F}_6}^{1/2}$, and the temperature from 9.5–24.2°C is derived as follows [85]:

$$\log_{10} K_p = -333.3 / T + 1.8932 \quad (45)$$

$$K_p = \text{atm}^{1/2}, \quad T = \text{K}.$$

The ClF₃ molecule has a planar distorted T-shaped structure with one short (0.1598 nm) and two long (0.1698 nm) Cl—F bonds. The angle between the two different kinds of Cl—F bonds is 87.48° [86,87]. The infrared and Raman spectra [88] and NMR [89] were measured. Gas chromatography was applied and data were obtained using a polytetrafluoroethylene-packed stainless steel column [90–92].

Chlorine trifluoride undergoes dissociation at elevated temperatures to chlorine monofluoride and fluorine: $\text{ClF}_3 = \text{ClF} + \text{F}_2$ [93]. The degree of dissociation is given

as 1.75%, 4.9% and 11.9% at 250, 300 and 350°C, respectively [94]. The dissociation increases to 50% at 460°C according to the following equation:

$$\begin{aligned}\log_{10}K_p &= 5570/T + 7.06 \\ K_p(\text{atm}) &= P_{\text{ClF}} \cdot P_{\text{F}_2} / P_{\text{ClF}_3}, \quad T = \text{K}.\end{aligned}\quad (46)$$

Liquid chlorine trifluoride is soluble in all proportions in liquid hydrogen fluoride. The phase equilibria of the system, chlorine trifluoride–hydrogen fluoride, were investigated by McGill et al. [95].

Chlorine trifluoride is a powerful oxidizing and fluorinating agent. Under the proper conditions, it reacts with all organic materials, metals and non-metals, except helium, argon, nitrogen and oxygen. Especially, a high concentration of chlorine trifluoride reacts violently and sometimes explosively with many organic and inorganic materials at room temperature. Chlorine trifluoride interacts violently with water unless precautions are taken to moderate the process, for example, by a decrease in temperature and/or by dilution.

Some metals such as nickel, copper and aluminum yield fluoride films of low permeability which prevent further reactions. However, this protective capacity is lost at elevated temperatures. Metals such as molybdenum, tungsten and titanium form volatile metal fluorides.

Such representative non-metal elements as boron, silicon, phosphorus, sulfur, arsenic, antimony, selenium and tellurium react with chlorine trifluoride at room temperature or on very slight warming to produce the corresponding fluorides. These reactions are generally vigorous and are accompanied by heat and light [96].

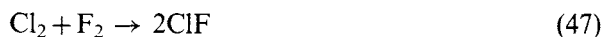
In general, oxides are converted to fluorides and oxyfluorides, while no reaction has been reported with ZnO, HgO, SiO₂, ZrO₂, ThO₂ and Fe₂O₃. At elevated temperatures or in the presence of a trace of water, these oxides also react with chlorine trifluoride. Under the conditions employed, no reaction was observed with NaCl, K₂SO₄, KNO₃, HgSO₄ or HgCl₂ [97].

Solvolysis reactions of alkali metal fluorides in ClF₃ at 100°C result in the formation of the corresponding alkali metal tetrafluorochlorates: KClF₄, RbClF₄ and CsClF₄. The tetrafluorochlorates of lithium and sodium are not obtained [98].

Many hydrogen-containing compounds, both organic and inorganic, inflame or explode when mixed with chlorine trifluoride. Some of the reactions may be moderated by diluting chlorine trifluoride with an inert gas, by dissolving the reagent in a relatively inert solvent such as carbon tetrachloride or a fluorocarbon, or by lowering the temperature. Some researches were carried out on chlorine trifluoride for the fluorination of organic compounds, though the reactions are commonly difficult to control. Ellis and Musgrave investigated the reactions between chlorine trifluoride and benzene derivatives in carbon tetrachloride solution, and both addition- and substitution-products were formed [99,100]. Muray [101] and Brower [102] reported the fluorination of tetrachlorobutadiene and alkanes, respectively.

19.6.3 Synthesis

The known compounds of fluorine and chlorine are chlorine monofluoride, ClF(bp = -100.8°C [74]), chlorine trifluoride and chlorine pentafluoride, ClF₅(bp = -13.1°C [74]). These compounds are synthesized by the direct fluorination of chlorine.



Chlorine trifluoride is commercially produced by the continuous gas-phase reaction of fluorine and chlorine in a nickel reactor between 250 and 300°C. The ratio of fluorine to chlorine is maintained slightly in excess of 3:1 to promote the conversion of chlorine monofluoride to chlorine trifluoride. Sufficient time is necessary to attain a high conversion rate to chlorine trifluoride. Temperature control is also critical since the disproportionation of chlorine trifluoride to chlorine monofluoride and fluorine occurs at elevated temperatures [79].

Chlorine monofluoride is prepared by the reaction of the stoichiometric mixture of chlorine and fluorine at temperatures ranging from 130 to 170°C [103]. The mixing of chlorine trifluoride and chlorine leads almost completely to the formation of chlorine monofluoride [86].

Chlorine pentafluoride is prepared by the combination of chlorine trifluoride with fluorine at high temperatures under high pressure. For example, a 14:1 mixture of fluorine and chlorine trifluoride is heated to 350°C for 1 h at a pressure of about 25.3 MPa [104].

In the application to semiconductors, especially, chlorine trifluoride should be a high-purity product. Such a product is commercially available with a chlorine trifluoride content of 99.9%–99.99%. Chlorine trifluoride is shipped as a liquid under its own vapor pressure in stainless steel cylinders. It is classified as an oxidizer and poison by DOT [79].

Nickel, monel, aluminum, copper, stainless steel and carbon steel are suitable metals for handling chlorine trifluoride. Nickel and monel are more suitable at elevated temperatures. Fluorinated polymers, such as polytetrafluoroethylene (PTFE) and polychlorotrifluoroethylene (PCTFE) exhibit good compatibility with gaseous chlorine trifluoride under static conditions. The calcium fluoride-filled PTFE shows better temperature stability. Caution must be used when these polymers are used under flowing conditions of chlorine trifluoride. In addition, these polymers should have smooth surfaces, and the surfaces should be free from organic greases and embedded impurities, which may ignite in the presence of chlorine trifluoride. Such non-fluorinated polymers as polyethylene and polyvinylchloride (PVC) should not be used as a material for apparatus. Equipment should be carefully and completely degreased and passivated with low concentration fluorine and chlorine trifluoride before use.

Chlorine trifluoride has a somewhat sweet odour and is highly irritating even in low concentrations. The time-weighted average (TWA) concentration for chlorine

trifluoride, established by the American Conference of Governmental Industrial Hygienists (ACGIH) in 1977, is 0.4 mg/m^3 for daily exposure for 8 h/d [79]. The National Institute for Occupational Safety and Health (NIOSH) reports the following toxicity levels for chlorine trifluoride: LC_{50} rats = 96 ppm/h, LC_{50} mice = 176 ppm/h and LC_{50} monkeys = 227 ppm/h [79]. Special care should be taken to avoid inhalation of vapors or contact with skin.

The disposal of chlorine trifluoride should be carried out by diluting with an inert gas until the concentration is less than 5% and scrubbing in water, followed by in a caustic solution. Small amounts of chlorine trifluoride can be decomposed by passing through columns of soda lime or activated alumina.

In the air, chlorine trifluoride may decompose to ClF , Cl_2 , ClOF , ClO_2F , ClO_3F , ClO_2 and HF , depending on the relative concentration of water and chlorine trifluoride [105,106]. Among them, chlorine dioxide (ClO_2) was reported to explode at a partial pressure greater than 6.7 kPa [107]. Therefore, a high concentration of ClF_3 should not be allowed to be in contact with water, and a cold trap should not be placed to condense it after the disposal of chlorine trifluoride. If chlorine trifluoride leaks out of the cylinder or chamber into the atmosphere, no explosion is expected to occur. Assuming that all of ClF_3 are converted to ClO_2 under 100% relative humidity at 25°C , the following reaction is anticipated:



As the partial pressure of water in air is 3.2 kPa at 25°C , that of ClO_2 leads to 1.3 kPa less than 6.7 kPa.

19.6.4 Applications to semiconductor industries

In the semiconductor industries, a number of materials are deposited on silicon wafers using CVD technologies such as plasma-CVD and thermal-CVD as described in the previous section. As the CVD process is repeated, a thick film is inevitably deposited on the various parts of the chamber and the internal walls of the exhaust tubes. This thick film generates contamination particles that affect the electrical resistance of the devices. Accordingly, cleaning of the apparatus is periodically necessary to eliminate the deposits and to improve the reliability of the device.

One of the conventional cleaning techniques is the wet cleaning method such as a chemical cleaning using strong acids or strong bases, or a mechanical cleaning by sand blasting or the like. These cleaning operations are troublesome and require the interruption of the operation of the equipment for a relatively long period because of the opening of the chamber. Additionally these methods cannot clean the inside of the chamber and, in particular, the fine parts of the apparatus to avoid the damage.

Another conventional cleaning technique is the dry cleaning method by plasma etching using a halogen-containing compound as the etching gas. The plasma cleaning methods are based on the generation of plasma by a radio frequency (RF)

discharge in a gas at a low pressure and comprise chemical, ion-sputtering and ion-enhanced plasma etching. The typical cleaning gases are CF_4 , C_2F_6 , SF_6 and NF_3 . This plasma cleaning method can be operated without opening the chamber. The in situ cleaning in the actual production line is extremely important for production efficiency. Therefore, extensive applications have been made in IC manufacturing processes. However, the plasma cleaning method also involves various problems as follows:

- it is necessary to attach a plasma-generation system to the equipment; so this is not suitable to clean the thermal CVD systems.
- it cannot clean the deposits on the backside of the RF electrode and on the internal walls of the exhaust tubes.
- it causes serious plasma-induced damage to the parts.

In addition, it was recently pointed out that the plasma cleaning gases such as CF_4 , C_2F_6 and SF_6 have a large Global Warming Potential (GWP) and a long life span in the atmosphere. As the unreactive gases in the chamber are released into the atmosphere, the abating and recycling technologies must be established in the near future.

Therefore, a plasma-less cleaning method using the highly reactive fluorine-containing gases such as chlorine trifluoride is noted and developed as a new dry cleaning material. The first report on the use of chlorine trifluoride as a cleaning gas was published by Lovelock in 1968 [108]. He employed a cleaning gas in order to remove contaminants such as grease and animal and vegetable matters from metal and other surfaces. In 1987, Aramaki et al. started to use a plasma-less cleaning gas for equipments of thin-film formation [109].

It is necessary for a cleaning gas of the CVD systems to satisfy the following conditions:

- no damage to the materials and parts used in the CVD systems,
- sufficient etching rate,
- abatement of gases including the by-products,
- safe handling, etc.

As chlorine trifluoride is a corrosive gas, suitable conditions must be selected in each cleaning process from a sufficient study on the corrosion-resistances of materials used in the CVD system, the characteristics of the semiconductor materials etched by chlorine trifluoride and so on.

Mouri et al. measured the reactivity against the various materials used in CVD systems and many kinds of the deposited products or by-products for the development of chemical-thermal cleaning techniques using reactive fluorine-containing gases [110–114]. The recommended temperatures for common materials in gaseous chlorine trifluoride and the typical etching rates of various deposits with chlorine trifluoride are shown in Tables 8 and 9, respectively. By choosing proper conditions, chlorine trifluoride is allowed to react with the deposits to form volatile products without corrosion of the materials. The compounds formed also must have a high vapor pressure and must be inert toward the materials, so that they might be pumped

Table 8

Recommended temperatures for common materials in gaseous ClF_3

Materials	Temperature
Metal	
SUS430	<70°C
SUS304	<150°C
SUS316	<150°C
HASTELLOY C-22	<190°C
INCONEL 600	<200°C
Ni201	<450°C
Al5052 (Al-Mg alloy)	<400°C ¹
Al6061 (Al-Si alloy)	<400°C ¹
Carbon	
Graphite	200–300°C
Glassy Carbon	<300°C
Ceramics	
SiC	<250°C
Al_2O_3	<500°C
AlN	<500°C
Quartz glass	<430°C
Polymer²	
PTFE (Polytetrafluoroethylene)	<150°C
PCTFE (Polychlorotrifluoroethylene)	<100°C
ECTFE (Ethylene-chlorotrifluoroethylene)	<100°C
VDF-HFP (Vinylidene fluoride-hexafluoropropylene)	not usable ³
TFE-PMVE (Tetrafluoroethylene-perfluoromethylvinylether)	not usable ⁴
PVC (Polyvinylchloride)	not usable
Polyethylene	not usable
Polypropylene	not usable
Polyimide	not usable
Silicone rubber	not usable

¹ Aluminum's are not measured over 400°C.² Polymers are measured in 10% of ClF_3 diluted with nitrogen gas, and should not be used in high concentration of ClF_3 .³ Sealants are usable below 100°C when partial pressure of ClF_3 is below 1.3×10^3 Pa.⁴ Sealants are usable below 180°C.

out of the reactor. For example, poly-Si and Si_3N_4 deposits can be removed by the following reactions:

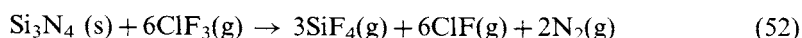
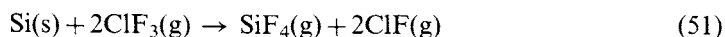


Table 9

Typical etching rate of deposited materials with ClF_3

Materials	Etch rate(nm/s)
a-Si:H	113 (100°C, 3.2×10^4 Pa, 10% ClF_3)
poly-Si	32 (100°C, 6.7×10^3 Pa, 50% ClF_3)
Single crystal-Si	11 (100°C, 1.3×10^2 Pa, 2.2% ClF_3)
Th-SiO ₂	9.8×10^{-2} (600°C, 2.7×10^2 Pa, 50% ClF_3)
TEOS-SiO ₂	0.39 (600°C, 2.7×10^2 Pa, 50% ClF_3)
	1.7×10^{-2} (520°C, 2.7×10^2 Pa, 50% ClF_3)
a-SiN _x :H	3.85 (187°C, 9.3×10^4 Pa, 2% ClF_3)
Si ₃ N ₄	0.43 (380°C, 73Pa, 100% ClF_3)
SiC	5.3×10^{-2} (421°C, 2.0×10^2 Pa, 100% ClF_3)
W	131 (420°C, 31 × Pa, 100% ClF_3)
TiN	3.07 (230°C, 9.3×10^4 Pa, 2% ClF_3)
Ti	3.07 (132°C, 9.3×10^4 Pa, 2% ClF_3)
Ta ₂ O ₅	2.5 (500°C, 1.3×10^2 Pa, 13% ClF_3)

In general, the composition and crystallinity of the deposits greatly vary according to the CVD conditions. The final products are also dependent on the formation conditions of the deposits and the cleaning conditions.

Consequently, the advantages of the chemical–thermal cleaning technique using chlorine trifluoride are summarized as follows:

- plasma-less process,
- wide variety of deposits etched,
- high etching rate,
- full chamber and exhaust line cleaning,
- easy abatement,
- compatible with environment (GWP, Life time = 0).

In the semiconductor industries, many kinds of flammable gases such as monosilane are used for filming, doping, epitaxial growth, etc. Accidental mixing of these flammable gases with an oxidizing gas such as chlorine trifluoride could cause an explosion. Lee et al. investigated the flammability limits of dichlorosilane, monosilane, tetraethyl orthosilicate (TEOS, $\text{Si}(\text{OC}_2\text{H}_5)_4$), ammonia, hydrogen and methane with chlorine trifluoride [115–117]. For dichlorosilane, monosilane, TEOS and ammonia, spontaneous ignition occurs above the flammability limit, and below this limit no reaction takes place even if electric sparks occur. For hydrogen and methane, no spontaneous ignition occurs, but an electric spark induces the ignition.

Chlorine trifluoride is a promising gas not only as the new cleaning gas but also as the replacement gas for global warming. On the other hand, Ibottoson et al. reported on plasma-less etching of single crystal silicon and some tantalum compounds with chlorine trifluoride [118,119]. The purpose of their studies was to apply chlorine

trifluoride to the etching processes of metallization such as circuit formation on silicon wafers. Besides the applications to the semiconductor industries, chlorine trifluoride has been also investigated in the manufacture of devices using similar thin films such as thin film transistors (TFT) and solar cells.

References

- [1] R.E. Banks, D.W.A. Sharp, J.C. Tatlow (Eds.), *Fluorine — The first hundred years (1886–1986)*, Elsevier Sequoia S.A., 1986, p. 81.
- [2] (a) P. Lebeau, A. Damiens, *Compt. Rend.*, 183 (1926) 1340; (b) P. Lebeau, A. Damiens, *Compt. Rend.*, 191 (1930) 939.
- [3] Kirk-Othmer, *Encyclopedia of Chemical Technology*, 3rd Edn, John Wiley & Sons, Inc., 10 (1978) p. 856.
- [4] W. Braker, A.L. Mossman, *Matheson Gas Data Book*, 6th Edn, (1980) p. 139, p. 356.
- [5] L'Air Liquide Division Scientifique, *Encyclopedie Des Gaz*, Elsevier Science Publishing Company, Inc., (1976) p. 215, p. 393.
- [6] J.H. Simons, L.P. Block, *J. Am. Chem. Soc.*, 59 (1937) 1407.
- [7] J.H. Simons, L.P. Block, *J. Am. Chem. Soc.*, 61 (1939) 2962.
- [8] (a) J. Nakamura T. Niinuma, H. Tomioka, M. Fukushima, (Kanto Denka Kogyo Co. Ltd), *Kokai Tokkyo Koho, Sho.* 58-162536 (1983); (b) J. Nakamura T. Niinuma, H. Tomioka, M. Fukushima, H. Hosoya, (Kanto Denka Kogyo Co. Ltd), *Kokai Tokkyo Koho, Sho.* 58-203924 (1983).
- [9] M. Fukushima, (Kanto Denka Kogyo Co. Ltd), unpublished data.
- [10] A.F. Benning, J.D. Park, S.E. Krahler, (E.I. Du Pont de Nemours & Company), US Patent 2,458,551 (1949).
- [11] Y. Osaka, H. Sonoyama, (Daikin Industries, Ltd.), *Kokai Tokkyo Koho, Sho.* 55-113728 (1980).
- [12] (a) H. Nakayama, H. Fujita, (Showa Denko K.K.), *Kokai Tokkyo Koho, Sho.* 56-73031 (1981); (b) K. Katamura, S. Tomada, H. Nakayama (Showa Denko K.K.), *Kokai Tokkyo Koho, Sho.* 61-134330 (1986).
- [13] F.W. Swamer, B.W. Howk, (E.I. Du Pont de Nemours & Company), US Patent 3,258,500 (1966).
- [14] (a) J.D. Calfee, L.A. Bigelow, *J. Am. Chem. Soc.*, 59 (1937) 2072; (b) J.D. Calfee, N. Fukuhara, D.S. Young, L.A. Bigelow, *J. Am. Chem. Soc.*, 62 (1940) 267; (c) D.S. Young, N. Fukuhara, L.A. Bigelow, *J. Am. Chem. Soc.*, 62 (1940) 1171; (d) E.H. Hadley, L.A. Bigelow, *J. Am. Chem. Soc.*, 62 (1940) 3302; (e) J.A. Cuculo, L.A. Bigelow, *J. Am. Chem. Soc.*, 74 (1952) 710.
- [15] E.A. Tyczkowski, L.A. Bigelow, *J. Am. Chem. Soc.*, 77 (1955) 3007.
- [16] (a) M.A. Robinson, H.R. Nychka, J.B. Hino, R.E. Eibeck, J.I. Brauman, (Allied Chemical Corporation), European Patent Application 0,032,210 (1981); (b) H.R. Nychka, J.B. Hino, R.E. Eibeck, M.A. Robinson, (Allied Chemical Corporation), European Patent Application 0,031,519 (1981).
- [17] H. Okajima, T. Nakano, F. Ishii, S. Sato, (Kanto Denka Kogyo Co. Ltd), Japanese Patent 2,513,758 (1996).
- [18] W.J. Murphy (Ed.), *Ind. and Eng. Chem. (Industrial Scale Development of Fluorocarbon process)*, 39 (1947) 289.
- [19] R.E. Banks. *Fluorocarbons and their Derivatives*, 2nd Edn, Macdonald Technical & Scientific, London, 1970, p. 10.

- [20] (a) H. Okajima, H. Tomioka, F. Ishii, M. Sato, S. Sato, (Kanto Denka Kogyo Co. Ltd), Japanese Patent 2,739,763 (1998); (b) M. Morioka, M. Sato, N. Takechi, H. Okajima, S. Sato, *J. Fluorine Chem.*, 58 (1992) 186.
- [21] (a) P.K. Baumgarten, H. Hills, (E.I. Du Pont de Nemours & Company), US Patent 3,386,989 (1968); (b) M.J. Couture, D. Hayashi, (E.I. Du Pont de Nemours & Company), US Patent 4,365,102 (1982); (c) J. Webster, J.J. Lerou, (E.I. Du Pont de Nemours & Company), WO 94/25418 (1994); (d) Y. Yamaguchi, T. Otuka, T. Hirata, (Daikin Industries, Ltd), Kokai Tokkyo Koho, Hei. 9-183743 (1997); (e) M. Fukushima, J. Nara, C. Shiobara, S. Sato, (Kanto Denka Kogyo Co. Ltd), Kokai Tokkyo Koho, Hei. 1-180839 (1989); (f) A.F. Benning, J.D. Park, (Kinetic Chemicals, Inc.), US Patent 2,351,390; (g) J.P. Manion, J.A. Philosophos, M.B. Robinson, British Patent 1,122,558 (1968); (h) J.H. Simons, R.L. Bond, R.E. McArthur, *J. Am. Chem. Soc.*, 62 (1940) 3477; (i) A.D. Krishenbaum, A.G. Streng, M. Hauptschein, *J. Am. Chem. Soc.*, 75 (1953) 3141.
- [22] O. Ruff, J. Fisher, F. Luft, *Z. Anorg. Allg. Chem.*, 172 (1928) 417.
- [23] (a) A.J. Woytek, J.T. Lileck, J.A. Barkanic, *Solid State Technology*, 27 (1984) 172; (b) C.S. Korman, T.P. Chow, D.H. Bower, *Solid State Technology*, 26 (1983) 115; (c) D.H. Bower, *J. Electrochem. Soc.*, 129 (1982) 795.
- [24] (a) C.J. Hoffman, R.G. Neville, *Chem. Rev.*, 62 (1962) 1; (b) M. Stacey, J.C. Tatlow, A.G. Sharpe (Eds.), *Advances in Fluorine Chemistry*, Butterworth, London, 4 (1965) p. 189.
- [25] W. Braker, A.L. Mossman, *Matheson Gas Data Book*, 6th Edn, (1980) p. 538.
- [26] L'Air Liquide Division Scientifique, *Encyclopedie Des Gaz*, Elsevier Science Publishing Company, Inc., 1976, p. 833.
- [27] G.L. Hurst, S.J. Khayat, *Adv. Chem. Ser.*, 54 (1966) 245.
- [28] C.B. Colburn, A. Kennedy, *J. Am. Chem. Soc.*, 80 (1958) 5004.
- [29] R.D. Dresdner, F.N. Tlumac, J.A. Young, *J. Am. Chem. Soc.*, 82 (1960) 5831.
- [30] B.Z. Drozdowicz, (Air Products and Chemicals, Inc.), *Genetic Toxicity Evaluation of NF₃*, Proceedings of the PFC Technical Update (SEMICON West 96), San Francisco, CA, 1996, p. 39.
- [31] (a) J.H. Simons, *J. Electrochem. Soc.*, 95 (1949) 47; (b) T.C. Simmons, F.W. Hoffmann, *J. Am. Chem. Soc.*, 79 (1957) 3429.
- [32] O. Glemser, J. Schröder, J. Knaak, *Chem. Ber.*, 99 (1966) 371.
- [33] (a) N. Watanabe, I. Ishigaki, S. Yoshizawa, *Denki Kagaku*, 32 (1964) 674; (b) N. Watanabe, A. Tasaka, K. Nakanishi, *Denki Kagaku*, 36 (1968) 685; (c) A. Tasaka, N. Watanabe, *Yoyuen*, 13 (1970) 152.
- [34] A.J. Woytek, J.T. Lileck, (Air Products and Chemicals, Inc.), US patent 4,091,081 (1978).
- [35] M. Aramaki, Y. Kobayashi, T. Nakamura, H. Nakano, T. Suenaga, (Central Glass Co. Ltd.), US Patent 4,543,242 (1985).
- [36] T. Suenaga, T. Fujii, Y. Kobayashi, (Central Glass Co. Ltd.), Kokai Tokkyo Koho, Hei. 3-208806 (1991).
- [37] H. Abe, *Oyo Butsuri*, 51 (1982) 348.
- [38] J.W. Coburn, H.F. Winters, *J. Vac. Sci. Technol.*, 16 (1979) 391.
- [39] C.J. Mogab, A.C. Adams, D.L. Flamm, *J. Appl. Phys.*, 49 (1978) 3796.
- [40] G. Valyi, V. Schiller, J. Gyimesi, J. Gyulai, *Thin Solid Films*, 76 (1981) 215.
- [41] J.A. Barkanic, D.M. Reynolds, R.J. Jaccodine, H.G. Stenger, J. Parks, H.L. Vedage, *Solid State Technology*, (1989) 109.

- [42] T. Takaichi, (Showa Denko K. K.), Activities in Gas Manufacturing Industry, Proceedings of PFC Forum 97 (SEMICON Japan 97), Makuhari, Japan, 1997, E-1.
- [43] T. Deacon, (Applied Materials Inc.), Chamber Cleaning: PFC Reduction, Proceedings of the Perfluorocompound (PFC) Technical Update (SEMICON West 97), San Francisco, CA, 1997.
- [44] (a) M. Fukushima, A. Baba, H. Suzuki, M. Yoshihara, Y. Omote, (Kanto Denka Kogyo Co. Ltd), Development of a System for Cleaning Environmentally Hazardous Fluorinated Waste Gases, Proceedings of The 14th International Symposium on Fluorine Chemistry, Yokohama, Japan, 1994, p. 260; (b) M. Fukushima, A. Baba, S. Yamashita, M. Yoshihara, Y. Omote, (Kanto Denka Kogyo Co. Ltd), Kokai Tokkyo Koho, Hei. 7-132211 (1995); (c) M. Fukushima, A. Baba, M. Yoshihara, Y. Omote, (Kanto Denka Kogyo Co. Ltd), Kokai Tokkyo Koho, Hei. 7-116466 (1995).
- [45] T. Fukuoka, Y. Osaki, T. Tukamoto, The 14th Semiconductor Technical Seminar (Air Liquide Japan, Ltd.), Makuhari, Japan, 1997, p. 31.
- [46] (a) Y. Jin, T.F. Fisher, (Praxair Technology, Inc.), US Patent 5,502,969 (1996); (b) T.F. Fisher, Y. Jin, (Praxair Technology, Inc.), US Patent 5,626,023 (1997).
- [47] Y. Yoshida, Japan's Research on Alternative Etching Gases, Proceedings of the Global Semiconductor Industry Conference on Perfluorocompound Emissions Control, Monterey, CA, 1998.
- [48] J. Langan, S. Rogers, R. Ciotti, B. Felker, (Air Products and Chemicals, Inc.), Investigation of Alternative Chamber Clean Chemistries for PFC Emission Reduction in the Novellus Concept One Reactor, Proceedings of the Perfluorocompound (PFC) Technical Update (SEMICON West 97), San Francisco, CA, 1997, H-1.
- [49] M. Luly, (Allied Signal Inc.), Low GWP Alternatives for the Semiconductor Industry, Proceedings of the Global Semiconductor Industry Conference on Perfluorocompound Emissions Control, Monterey, CA, 1998.
- [50] J.A. Mullendore, Encyclopedia of Chemical Technology, Vol. 23, 3rd Edn, H.F. Mark, D.F. Othmer, C.G. Overberger, G.T. Seaborg (Eds.), John Wiley & Sons, 1983, p. 413.
- [51] N.J. Archer, K.K. Yee, *Wear*, 48 (1978) 237.
- [52] L.W. Roberts, Proceeding of the 6th Plansee Seminar of High Temperature Materials, Reutte, 1969, p. 880.
- [53] F.J. Huegel, W.R. Holman, Proceeding of the 2nd International Conference of Chemical Vapor Deposition, NY, 1970, p. 171.
- [54] O. Ruff, E. Ascher, *Z. anorg. allg. Chem.*, 196 (1931) 413.
- [55] G.H. Cady, G.B. Hargreaves, *J. Chem. Soc.* (1961) 1563.
- [56] D. Meixner, A. Heintz, R.N. Lichtenthaler, *Ber. Bunsenges. Phys. Chem.*, 82 (1978) 220.
- [57] D.R. Stull, H. Prophet, JANAF Thermochemical Tables, 2nd Edn, National Bureau of Standards (Ed.), Washington, D.C., 1971, p. 772.
- [58] B. Frlac, H.H. Hyman, *Inorg. Chem.*, 6 (1967) 1596.
- [59] S. Siegel, D.A. Northrop, *Inorg. Chem.*, 5 (1966) 2187.
- [60] G. Nagarajan, D.C. Brinkley, *Z. Naturforsch.*, 26a (1971) 1658.
- [61] T.G. Burke, D.F. Smith, A.H. Nielsen, *J. Chem. Phys.*, 20 (1952) 447.
- [62] J. Gaunt, *Trans. Faraday Soc.*, 49 (1953) 1122.
- [63] I. Ursu, M. Bogdan, P. Fitori, A. Darabont, D.E. Demco, *Mol. Phys.*, 56 (1985) 297.
- [64] M.B. MacInnis, T.K. Kim, Encyclopedia of Chemical Technology, Vol. 23, 3rd Edn, H.F. Mark, D.F. Othmer, C.G. Overberger, G.T. Seaborg (Eds.), John Wiley & Sons, 1983, p. 426.
- [65] A.B. Burg, *Fluorine Chemistry*, Vol. 1, J.H. Simons (Ed.), 1950, p. 112.
- [66] B. Cox, D.W. Sharp, A.G. Sharpe, *J. Chem. Soc.* (1956) 1242.

- [67] G.B. Hargreaves, R.D. Peacock, *J. Chem. Soc.* (1957) 4212.
- [68] G.B. Hargreaves, R.D. Peacock, *J. Chem. Soc.* (1958) 2170.
- [69] G.H. Cady, G.B. Hargreaves, *J. Chem. Soc.* (1961) 1568.
- [70] A.J. Woytek, *Encyclopedia of Chemical Technology*, Vol. 10, 3rd Edn, H.F. Mark, D.F. Othmer, C.G. Overberger, G.T. Seaborg (Eds.), John Wiley & Sons, 1980, p. 823.
- [71] N.E. Miller, I. Beinglass, *Solid State Technol.*, 23 (1980) 79.
- [72] R.S. Blewer, *Solid State Technol.*, 29 (1986) 117.
- [73] R. Liu, *ULSI Technology*, C.Y. Chang, S.M. Sze (Eds.), McGraw-Hill Co., 1996, p. 371.
- [74] A.J. Downs, C.J. Adams, *Comprehensive Inorganic Chemistry*, Vol. 2, J.C. Bailar Jr, H.J. Emeleus, Sir Ronald Nyholm, A.F. Trotman-Dickenson (Eds.), Pergamon Press, 1973, Chapter 26, p. 1528.
- [75] J.W. Grisard, H.A. Bernhardt, G.D. Oliver, *J. Amer. Chem. Soc.*, 73 (1951) 5725.
- [76] T. Sato, S. Horiguchi, H. Ichimaru, S. Nakagawa, *J. Chem. Eng. Data*, 42 (1997) 169.
- [77] A.A. Banks, A.J. Rudge, *J. Chem. Soc.* (1950) 191.
- [78] R.D. Burbank, F.N. Bensey, *J. Chem. Phys.*, 21 (1953) 602.
- [79] A.J. Woytek, *Encyclopedia of Chemical Technology*, Vol. 10, 3rd Edn, H.F. Mark, D.F. Othmer, C.G. Overberger, G.T. Seaborg (Eds.), John Wiley & Sons, 1980, p. 722.
- [80] A.A. Banks, A. Davies, A.J. Rudge, *J. Chem. Soc.* (1953) 732.
- [81] M.T. Rogers, J.L. Speirs, M.B. Panish, *J. Phys. Chem.*, 61 (1957) 366.
- [82] M.T. Rogers, H.B. Thompson, J.L. Speirs, *J. Amer. Chem. Soc.*, 76 (1954) 4841.
- [83] D.R. Stull, H. Prophet, *JANAF Thermochemical Tables*, 2nd Edn, National Bureau of Standards, Washington, D.C., 1971, p. 511.
- [84] H. Heinz, H.J. Schumacher, *Z. Naturforsch.*, 2A (1947) 363.
- [85] H.H. Claassen, B. Weinstock, J.G. Maln, *J. Chem. Phys.*, 28 (1958) 285.
- [86] D.F. Smith, *J. Chem. Phys.*, 11 (1953) 609.
- [87] E.L. Muetterties, W.D. Phillips, *J. Amer. Chem. Soc.*, 79 (1957) 322.
- [88] H. Selig, H.H. Claassen, J.H. Holloway, *J. Chem. Phys.*, 52 (1970) 3517.
- [89] A.N. Hamer, *J. Inorg. Nucl. Chem.*, 9 (1959) 98.
- [90] J.F. Ellis, C.W. Forrest, P.L. Allen, *Anal. Chim. Acta*, 22 (1960) 27.
- [91] I. Lysyj, P.R. Newton, *Anal. Chem.*, 35 (1963) 90.
- [92] A.G. Hamlin, G. Iveson, T.R. Phillips, *Anal. Chem.*, 35 (1963) 2037.
- [93] H. Heinz, H.J. Schumacher, *Z. Naturforsch.*, 2A (1947) 362.
- [94] H.R. Leech, *A Comprehensive Treatise on Inorganic and Theoretical Chemistry*, Supplement II, Part I, J.W. Mellor (Ed.), Longmans, Green and Co., 1956, Chapter I, p. 147.
- [95] R.M. McGill, W.S. Wendolkowski, E.J. Barber, *J. Phys. Chem.*, 61 (1957) 1101.
- [96] H.S. Booth, J.T. Pinkston, *Fluorine Chemistry*, Vol. 1, J.H. Simons (Ed.), Academic Press Inc., 1950, p. 189.
- [97] H.S. Booth, J.T. Pinkston, *Chem. Revs.*, 41 (1947) 421.
- [98] E.D. Whitney, R.O. Maclaren, C.E. Fogle, T.J. Hurley, *J. Amer. Chem. Soc.*, 86 (1964) 2583.
- [99] J.F. Ellis, W.K.R. Musgrave, *J. Chem. Soc.* (1950) 3608.
- [100] J.F. Ellis, W.K.R. Musgrave, *J. Chem. Soc.* (1953) 1063.
- [101] J. Muray, *J. Chem. Soc.* (1959) 1884.
- [102] K.R. Brower, *J. Org. Chem.*, 52 (1987) 798.
- [103] E.A. Fletcher, B.E. Dahneke, *J. Amer. Chem. Soc.*, 91 (1969) 1603.
- [104] D.F. Smith, *Science*, 141 (1963) 1039.
- [105] R. Bougon, M. Carles, J. Aubert, *C.R. Acad. Sci. Paris*, t.265 (1967) 179.

- [106] F.N. Dost, D.J. Reed, V.N. Smith, C.H. Wang, *Toxicol. Appl. Pharmacol.*, 27 (1974) 527.
- [107] J.A. Wojtowicz, *Encyclopedia of Chemical Technology*, Vol. 5, 3rd Edn, H.F. Mark, D.F. Othmer, C.G. Overberger, G.T. Seaborg (Eds.), John Wiley & Sons, 1979, p. 580.
- [108] J.E. Lovelock, *Brit. Pat.*, 1,268,377 (1972).
- [109] M. Aramaki, K. Nakano, T. Suenaga, K. Yagii, H. Arai, Japan Tokkyo Kokai, 64-17857 (1989).
- [110] I. Mouri, T. Fujii, Y. Kobayashi, *Proceedings of the 7th Regular Meeting of Japanese-Soviet Fluorine Chemists*, Fukuoka, Japan, 7 (1991) 1.
- [111] I. Mouri, T. Fujii, Y. Kobayashi, S. Nakagawa, Y. Kita, *Extended Abstracts of 14th International Symposium on Fluorine Chemistry*, Yokohama, Japan, 1994, p. 3.
- [112] I. Mouri, S. Hayakawa, *J. Agric. Meteorol.*, 52 (1997) 849.
- [113] I. Mouri, S. Hayakawa, *J. Agric. Meteorol.*, 52 (1997) 853.
- [114] I. Mouri, PhD Thesis, United Graduate School of Yamaguchi University, Tottori University and Shimane University, 1998.
- [115] S.G. Lee, H. Ohtani, Y. Uehara, M. Aramaki, *J. Loss Prev. Process Ind.*, 5 (1992) 192.
- [116] S.G. Lee, T. Enomoto, H. Ohtani, Y. Uehara, *Combustion Sci. Tech. (Japan Edn)*, 1 (1993) 129.
- [117] S.G. Lee, H. Ohtani, Y. Uehara, *Jpn. Soc. Safety Eng.*, 33 (1994) 82.
- [118] D.E. Ibbotson, J.A. Mucha, D.L. Flamm, J.M. Cook, *J. Appl. Phys.*, 56 (1984) 2939.
- [119] D.E. Ibbotson, J.A. Mucha, D.L. Flamm, J.M. Cook, *Appl. Phys. Lett.*, 46 (1985) 794.

CHAPTER 20

Industrial Applications of Inorganic Fluorides

Dayaldas T. Meshri

Advance Research Chemicals Inc., 1110 W. Keystone Ave., Catoosa, OK 74015-3033, USA

20.1 Introduction

As we approach the millennium, it is inspiring and appropriate to review the applications of inorganic fluorine compounds and their impact on our modern life. Fluorine as an element does not exist alone in nature. The abundance of this unique element in the continental crust is 0.065% and 0.1% in metamorphic, igneous and sedimentary rocks. The greenish-blue, bluish-yellow, purple color of calcium fluoride crystals may have even attracted the attention of Indus Valley civilization, 5000 BC. An initial use of the mineral as a flux to lower the melting point of other minerals, by earlier civilizations, has expanded globally into hundreds of inorganic fluorides of Aluminum to Zirconium. In the modern age, many industrial and academic institutes are laboring each day to come up with new applications or the products for the betterment and comforts of our generation and the future of mankind.

Although it is beyond the scope of this article to cover all the applications of inorganic fluorine compounds, the author being on both the sides, Industry as well as Academic, has chosen to discuss from basic to advanced materials, which have or will have an economical and social impact on our lives.

20.2 Fluorspar

20.2.1 History

The two naturally occurring minerals containing fluorine are fluorspar: CaF_2 , and fluoroapatite: $\text{CaF}_2 \cdot 3\text{Ca}_3(\text{PO}_4)_2$. Fluorspar is found in many parts of the world. The world reserves are estimated in the range of 40–45 million metric tons, with nearly one-third located in South Africa. An additional 35 million metric tons are considered to be of sub-economic nature. The major fluorspar mining countries are China, Mexico, Mongolia, Russia, Republic of South Africa, France, Czechoslovakia, Spain, Italy, United Kingdom, Brazil, USA, Germany, Thailand, India, Romania and Turkey [1]. The fluorspar is classified on the basis of its purity and uses.

20.2.2 Classification

20.2.2.1 Blue Johns

This class of mineral is rarely or accidentally found while mining the other grades of fluorspar. It is a naturally occurring mineral which has huge crystals or lumps containing a variety of colors such as green, blue, yellow and purple. It also has a very shiny appearance. No human being would ever dare to destroy the beauty of these crystals by crushing them into a fine powder for their use as flux or in the production of HF.

Fortunately, these crystals eventually ended up in the hands of artists who converted them into vases, cups, holders and other ornamental objects which magnify our show rooms, living rooms or conference tables. These objects are popularly known as “Blue Johns”, named after the Blue John mine in Derbyshire, England which operated in the 18th Century.

20.2.2.2 Metallurgical grade

This material is also known as Met-spar. It is the most impure grade and the least expensive. It contains 60–85% CaF_2 . It is primarily used by the aluminum, steel, magnesium and non-ferrous industries as a fluxing agent to refine alloys and dephosphorize and desulphurize metals. It is also used by the brick industry as an antiscumming agent, by abrasive wheel manufacturers as a bonding agent and in portland cement to lower the clinkering temperature.

20.2.2.3 Ceramic-grade

This fluorspar contains 85–95% CaF_2 and is used as a flux in the steel industry, production of enamel glass to control refractive index and obtain desired opacity. It is also used in coatings of welding rods.

20.2.2.4 Acid-grade

This is the highest purity natural CaF_2 source which contains over 97% CaF_2 and is primarily used for the production of hydrogen fluoride, the basic raw material for organic and inorganic fluorine compounds. Low metallic impurities in fluorspar are required by the producers of anhydrous hydrogen fluoride.

20.2.2.5 New applications

Recently, several small scale applications have been developed such as removal of lead in flotation waste [2], in phosphate glasses [3], to obtain clean steel without deoxidation with aluminum [4], preparation of lanthanum [5], high purity CaF_2 (99.99%) is used in thermal plasma for purification of silicon [6], in the manufacturing of optical compounds for high energy lasers and infrared transmission systems [7].

20.2.2.6 Economics

The world production of calcium fluoride remains between 4 to 5 million metric tons and the market price is \$97–\$110/ton. Currently, over 33% of the world's requirement of fluorspar comes from China.

20.2.2.7 Fluoroapatite, $\text{CaF}_2 \cdot 3\text{Ca}_3(\text{PO}_4)_2$

This mineral is also known as a phosphate rock. It contains variable amounts of fluorine (3–4%). This rock also contains silica. When heated with sulfuric acid to produce phosphoric acid, it also gives fluorosilicic acid, H_2SiF_6 , as a by-product (commercially known as fluosilicic acid).

20.3 Hydrogen fluoride

20.3.1 History

The most important and basic raw material, hydrogen fluoride, used for the production of inorganic and organic fluorine compounds, alkylation catalyst and fluorinating reagent, was first discovered when Schwankhard of Nurnberg, in 1670, etched glass with fluorspar and sulfuric acid. Subsequent work by Marggraf, Sheele, and Davy identified the new compound as hydrofluoric acid [8–10]. Fremy was the first to produce anhydrous hydrogen fluoride, (AHF) from concentrated H_2SO_4 and fluorspar [11].

Although fully known in the early nineteenth century, commercial production was limited to aqueous HF for use in glass etching, foundry scale removal, polishing and metal surface finishing, and manufacturing of chemicals such as NaF, NaHF_2 , AlF_3 and fluoroborate salts. In 1931, the first bulk shipment of anhydrous hydrogen fluoride was made by Sterling Products Company (later merged with Pennsalt Mfg, which became Pennwalt Corp. and now Elf Atochem). It was used in the manufacturing of chlorofluorocarbons to be introduced as new refrigerants Freons[®]. The first producer of Freons[®] was Kinetic Chemicals, a joint venture between Frigidaire (General Motors) and DuPont. The new refrigerants were developed by the team of Midgley and Henne.

A revolution in the field of HF chemistry was created by World War II demand for high-octane aviation fuels, UF_6 for the developing nuclear industry and high molecular weight fluorinated polymers as fluorinated lubricant oils. New industrial applications increased the demand for anhydrous hydrogen fluoride. Whereas earlier production of anhydrous hydrogen fluoride had been by distillation of aqueous HF, new technology was developed to produce anhydrous hydrogen fluoride by direct route. The successful growth in the hydrofluorocarbons and other developments have resulted in the consumption of hydrogen fluoride about one million metric tons per year [12].

20.3.2 Fluorocarbons

Over 60% of AHF produced is used in the manufacturing of fluorocarbons used as refrigerants, blowing agents, solvents, anesthetics, fire extinguishants, and fluoropolymers. Fluorohalocarbons are considered unfriendly to the environment and have been replaced by hydrofluorocarbons. These also have some negative impact on the environment and their replacement by non-fluorine containing products could be imminent, particularly in single use applications such as foam blowing agents and solvents.

20.3.3 Alkylation

Anhydrous hydrogen fluoride and sulfuric acid are the two most common catalysts used by refineries in petroleum alkylation processes to produce a very high octane and low volatility gasoline.

The relative location of refinery and acid plant is one of the most important factors in the economic decision between sulfuric acid and anhydrous hydrogen fluoride as a catalyst for alkylation. Besides the distance, other factors such as regeneration of spent acid, energy costs, the nature of the feed and increasingly stringent regulatory constraints play an important role in the selection of alkylation catalyst. Sulfuric acid is selected for alkylation if feed is rich in pentenes or n-butene. HF is selected if the feed is rich in propenes or isobutane.

HF is intimately contacted with isobutane and mixed with light olefins (ethylenes, propenes, etc.) under pressure at 40–45°C to produce branch chain fuel which has very high octane value. HF, being only slightly soluble in hydrocarbons, is easily separated, recycled and regenerated. The alkylate is water washed and dried. The consumption of hydrofluoric acid per barrel of alkylate varies from 0.09 to 0.23 kg.

The major drawback of the use of anhydrous hydrogen fluoride is its lower boiling point and volatility at ambient temperatures. Some of the state governments believe that storage of AHF is highly risky in populated areas and creates life and environmental threats. As a result, some refineries have been forced to switch from AHF to H₂SO₄ alkylation process.

The other important alkylation, but on a much smaller scale, in which AHF is used is the manufacturing of detergents. This alkylation process produces environmental friendly, biodegradable detergent intermediates. Although HF is used as a catalyst in these processes, it is slowly consumed because of side reactions due to the impurities present in the feedstocks.

20.3.4 Nuclear industry

This industry is on the decline due to the peace-time agreements and Comprehensive Test Ban Treaty, (CTBT). Under this agreement, enrichment of UF₆ is restricted to lower grade U²³⁵ for reactor fuel to be used in commercial electric power generation. In North America, there is an antinuclear atmosphere, hence it is less likely to see the expansion or additions of nuclear power plants in the USA. Whereas China, India, and East European countries may require additional nuclear fuel for their fast growing industries and electrification of the rural areas.

Due to CTBT and other agreements between Russia and the USA to reduce nuclear arsenals, there is a surplus stock of enriched uranium. Enriched uranium can be processed and diluted to produce reactor fuel, displacing natural UF₆ manufactured from uranium oxides. As a result, fluorine plants in Russia, France, UK, South Africa and the USA have drastically reduced their fluorine production and attendant consumption of AHF. The nuclear industry is expected to use only 2–3% of total world production of AHF. It is first used in the conversion of U₃O₈ to UF₄ and also in the manufacture of fluorine to convert UF₄ to UF₆.

20.3.5 Aqueous HF

Only 4–5% of the world production of AHF is converted into 50–70% aqueous HF. Any concentration above 50% has substantial vapor pressure and requires fully ventilated areas to work with it. Aqueous HF is sold in drums as well as in tank cars. Drums are made of polyethylene and the tanks are rubber lined. The aqueous solutions of HF are used in the pickling of stainless steel, glass etching, quartz purification, chemical milling, metal coatings and production of electroplating salts such as fluoroborates and metal cleaning acids H_2TiF_6 , H_2ZrF_6 , alkali metal fluorides, LiF, NaF, KF, RbF, CsF and other specialty inorganic fluorides. A very high purity, 99.9999% aqueous HF is used in the electronic industry as an etchant for silicon wafers.

20.4 Aluminum fluoride

Substantial quantities of commercial and captive HF are used in the production of aluminum trifluoride and sodium cryolite, both used by the aluminum industry. The electrolytic process for the production of aluminum involves fused Al_2O_3 , AlF_3 , and Na_3AlF_6 . About 8–10% of the world production of HF is consumed by aluminum industry which serves the World's two largest industries; automotive and building construction. Due to the recent economic upturn, there is a large demand for aluminum metal in the market. As a result, the aluminum industry has opted for the least expensive source of fluoride ions such as hexafluorosilicic acid.

Today over half of the fluoride ions required by aluminum industry for NaF, AlF_3 , or Na_3AlF_6 comes from H_2SiF_6 . The latter is produced as a by-product of the fertilizer industry. At one time, fluorosilicic acid was considered a nuisance, environmentally unfriendly by-product. Today, however, this nuisance product has become a precious commodity.

20.5 Specialty chemicals

Hydrofluoric acid is very important and the basic ingredient for the preparation of highly specialized organic and inorganic fluorides. Organic fluorides, fluorinated herbicides, pharmaceutical intermediates, elastomers and inert liquids are prepared with anhydrous HF. Total HF consumption by organic fluorine compounds is 1–1.5% of world production.

20.6 Inorganic salts and acids

Alkali metal fluorides and ammonium bifluorides, fluoroborates, fluorophosphates, fluoroarsenates, fluoroantimonates, fluorotitanates, fluorozirconates, etc. require either anhydrous HF or aqueous HF for their preparations. Similarly, alkaline earth metals, transition metals, rare earth metal fluorides or their fluorosalts require

hydrogen fluoride. These salts are produced in multi-ton quantities and have a wide range of applications.

20.6.1 Ammonium bifluoride

NH_4HF_2 is prepared from ammonia and excess anhydrous hydrogen fluoride. Millions of pounds are used in flux for deoxidizing, in pickling of stainless steel, in wood preservation compounds, casein glues, manufacturing of coated papers, as a component of laundry sours, in vitreous enamels and dissolving silica in oil wells to regenerate oil flow, a process known as “acidization” [12]. Ammonium bifluoride is also used in dissolving silicate scales from boiler tubes that cannot be washed by usual mineral acids [13], rapid frosting of glass, low specular-reflecting finish on television face plate and on glass for picture framing [14], cleaning of optical lenses [15], in galvanizing and anodizing formulations, metal surface preparation prior to painting and making it abrasion resistant.

20.6.2 Alkali metal fluorides

The alkali metal fluorides, LiF, NaF, KF, CsF, and RbF are made by the action of hydroxide or carbonate on hydrofluoric acid. These are very important compounds and are produced in several hundred ton quantities.

20.6.2.1 Lithium fluoride

The primary use of lithium fluoride is in the ceramic industry. It reduces the firing temperature and improves the resistance to abrasion, acid attack and thermal shocks. It is essential component of the fluorine cell electrolyte. An addition of small amount (1–1.5%) to $\text{KHF}_2 : \text{HF}$ electrolyte improves the wettability of the carbon anodes and lowers the tendency of the cell to polarize. Another important use of LiF is in flux compositions containing chlorides, borates and other fluorides. Lithium fluoride windows made from high purity crystals are used for X-ray monochromators, UV, visible or IR regions [18].

20.6.2.2 Sodium fluoride

Its major applications are in preparing fluxes, fluoridation of drinking water to reduce dental cavities in children and adults, active ingredient of the major brand toothpastes in the manufacturing of $\text{Na}_2\text{PO}_3\text{F}$, vitreous enamels, pickling of stainless steel, in wood preservation compounds, casein glues, in the manufacturing of coated paper and in laundry sours. Worldwide production is over one million pounds.

20.6.2.3 Potassium, cesium and rubidium fluorometallates

These fluorides play an important role in the formation of flux components [19] such as K_3AlF_6 , KAlF_4 , CsAlF_4 , Cs_3AlF_6 , RbAlF_4 , Rb_3AlF_6 , RbCsSiF_6 , Cs_2SiF_6 , K_2SiF_6 , Rb_2SiF_6 , CsRbSiF_6 , CsKSiF_6 , $\text{NH}_4\text{CsSiF}_6$ and their combinations. These flux components seem to help the brazing of aluminum alloys up to 7000 series. All three fluorides KF, RbF, CsF, when dry and in fine powder form, are excellent

fluorinating reagents in the presence of polar solvents such as acetonitrile, dimethyl sulfoxide, formamide, etc. These metal fluorides displace chlorine, and bromine with fluorine in alkyl or aromatic halocarbons [20].

20.6.3 Lithium fluorosalts

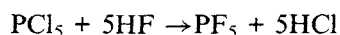
Lithium tetrafluoroborate, (LiBF_4), lithium hexafluorophosphate, (LiPF_6), lithium hexafluoroarsenate, (LiAsF_6), lithium trifluoromethane sulfonate, (LiSO_3CF_3), are the electrolyte salts of the 21st Century. The performance of lithium ion cells, primary and secondary lithium cells depends on the purity of these compounds. Several hundred tons of these materials have been produced and many more tons — and perhaps thousands of tons — will be required in the near future. One of the largest automotive producers predicts that there may be a market for 10–15 million pounds of these salts. The demand for Lithium ion primary cells is also very huge in electronics, computers, communication systems and military applications.

20.6.3.1 Preparation

Anhydrous lithium fluorosalts are very difficult to prepare and store in anhydrous form due to their strong affinity for water. Electrolyte containing HF and or H_2O is seriously objectionable to lithium ion battery system. As a result, a great precaution is required in selecting a system which is capable of removing both HF and H_2O from these salts.

Lithium tetrafluoroborate, LiBF_4 , is prepared by dissolving LiF in AHF and then BF_3 gas is passed until precipitation is complete. After the reaction is over, excess HF is decanted and LiBF_4 is dried under nitrogen until HF and H_2O contents are reduced below 100 ppm level. Reaction is carried out in Teflon[®], polyethylene or polypropylene lined reactors to avoid metallic contamination.

Lithium hexafluorophosphate, LiPF_6 , is prepared by dissolving LiF in AHF and passing PF_5 as pure gas or generated in situ as shown below:



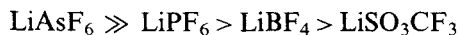
Hydrogen chloride generated in situ is insoluble in AHF and leaves the reactor spontaneously. After the reaction is over, excess anhydrous HF is decanted and LiPF_6 salt is dried very carefully as the dry salt has PF_5 vapor pressure at ambient temperature. Exposure of the salt to air or moisture produces white smokes due to a reaction between PF_5 and water present in the air. Phosphorus pentafluoride reacts with water and produces POF_3 and HF. A continuous vacuum drying of LiPF_6 above 100°C fully decomposes LiPF_6 to LiF and PF_5 .

Lithium hexafluoroarsenate, LiAsF_6 , can be prepared by passing AsF_5 gas into LiF-AHF solution or by the neutralization of $\text{HAsF}_6 \cdot 6\text{H}_2\text{O}$ with LiOH or Li_2CO_3 . Commercially, the neutralization of $\text{HAsF}_6 \cdot 6\text{H}_2\text{O}$ and removal of three moles of water is a more economical process. Extreme precautions must be taken in removing water of hydration of $\text{LiAsF}_6 \cdot 3\text{H}_2\text{O}$. Any substantial increase in temperature will result into the hydrolysis of the salt as shown below:



Also, the intermediate species such as LiAsF_5OH , $\text{LiAsF}_4(\text{OH})_2$, and $\text{LiAsF}_3(\text{OH})_3$ are observed if the drying temperature is raised above 70°C .

Lithium trifluoromethane sulfonate; LiSO_3CF_3 , can be easily prepared by the neutralization process. Commercially available trifluoromethane sulfonic acid is distilled and neutralized with either LiOH or Li_2CO_3 and the hydrated salt is obtained. Water of hydration is removed under vacuum without any difficulty. This salt is more stable at higher temperatures than LiBF_4 and LiPF_6 . The order of performance as an electrolyte in lithium batteries is as follows:



All these salts are available in commercial quantities. Major producers of LiPF_6 and LiBF_4 are Hashimoto, Central Glass, Morita of Japan and Advance Research Chemicals, Inc. of the USA; LiSO_3CF_3 is produced by Central Glass of Japan, 3M and Advance Research Chemicals, Inc. of the USA. While LiAsF_6 is produced by Advance Research Chemicals, Inc. only.

20.6.4 Metal fluoroborates

These salts are produced by reacting metal oxides, carbonates or hydroxides with fluoroboric acid. Copper, nickel, lead, zinc, tin fluoroborate solutions are used in electroplating baths. Fluoroboric acid is used in printed circuit for tin-lead plating [16] and as a stripping solution for removal of solder and plating metals from less active substances. A low grade fluoroboric acid or spent acid is used in the manufacturing of cryolite Na_3AlF_6 [17] for the production of aluminum. The worldwide production of fluoroboric acid is between 700–900 metric tons per year.

20.6.5 Fluoroacids

Acids within this group include: hexafluoroarsenic acid, $\text{HAsF}_6 \cdot x \text{H}_2\text{O}$, hexafluoroantimonic acid, $\text{HSbF}_6 \cdot x \text{H}_2\text{O}$, difluorophosphoric acid, HPO_2F_2 ; hexafluorophosphoric acid, $\text{HPF}_6 \cdot x \text{H}_2\text{O}$, fluoroboric acid, $\text{HBF}_4 \cdot x \text{H}_2\text{O}$, hexafluorotitanic acid, $\text{H}_2\text{TiF}_6 \cdot x \text{H}_2\text{O}$; hexafluorozirconic acid, $\text{H}_2\text{ZrF}_6 \cdot x \text{H}_2\text{O}$, and fluorosulfonic acid, HSO_3F . Except the first two acids, there is a very large demand for industrial applications. These acids are produced from oxides and 70% HF in monel or rubber lined reactors. A typical batch size is 10–12 tons. Hexafluorotitanic, hexafluorozirconic acids and their salts are used by metal surface cleaning and metal finishing industries. Acid salts are also used in the manufacturing of ceramics, glasses, fluxes, as fire retardants to treat wool garments, children's clothes and aviation upholstery. Sodium and potassium salts of HAsF_6 , HSbF_6 , HPF_6 are used for cationic polymerization [21–24]. Hexafluoroarsenic acid and its salts are being withdrawn from the market (except for limited use) due to known carcinogenic nature of arsenic compounds, even though AsF_6^- ion is very stable and has low toxicity. Difluorophosphoric acid HPO_2F_2 is used in the synthesis of tetraacetyldiamines, excellent yields are obtained when acetylation of AcNHNHAc ($\text{X} = \text{alkylene, cycloalkylene or arylene}$) with $\text{H}_2\text{C}=\text{C}=\text{O}$ is carried out in the presence of difluorophosphoric acid [25].

20.6.6 Fluorosulfonic acid

It is prepared by passing HF and SO₃ in fluorosulfonic acid which acts as a solvent as well as heat transfer media. Over 20,000 metric tons of HSO₃F are produced per year. It is mostly used as catalyst in the alkylation of branch chain paraffins [26–29], in the polymerization [30–31]. Fluorosulfonic acid is a very strong acid and when added to olefins, it remarkably increases the acidity of the system and enhances its catalytic activity similar to SbF₅, TaF₅ and NbF₅ [32–35]. It is also used in a chemical process to produce SiF₄ [36,37] and BF₃ [38].

20.7 Fluorine

Fluorine, F₂, a diatomic molecule is a non-metallic element and is a pale yellowish gas. It has a highly pungent irritating odour which can be commonly detected at concentration as low as 0.05 ppm. The odor resembles an ozone and chlorine mixture. Because of its very high reactivity, it does not occur freely in nature except for trace amounts in synthetic radioactive species. It is widely found in combination with other elements in the earth's crust. Fluorine being the most electronegative element, it can oxidize other elements to their highest valency level. Also, being very small in atomic size, several atoms of fluorine can surround another element and form simple or complex fluorides in which the other element achieves the highest oxidation state. At ambient temperature, fluorine reacts vigorously with most metals to form fluorides. Some metals and alloys such as aluminum, copper, iron, nickel, monel, Hastelloy-C, when exposed to fluorine, form an adherent and protective surface film of metal fluoride which retards further reaction, thus allowing the metals to be used in the storage and handling of elemental fluorine as well as halogen fluorides.

Fluorine liquefies at –188°C and solidifies at –220°C. Additional handling techniques, physical or thermodynamic properties are described in [39]. Although commercial production of elemental fluorine started 50 years after its discovery in 1886 by Henri Moissan, its production remained at laboratory level until the era of World War II. The latter required very large supplies of fluorine for the conversion of UF₄ to UF₆ and separation of U²³⁸ from U²³⁵ by gas diffusion process. The highly enriched U²³⁵ is also known as weapon grade U²³⁵ while 93–94% enriched U²³⁵ is used as a fuel in the mobile nuclear power reactors industry. For over 40 years, the nuclear industry, while enriching uranium in a variety of methods, always employed UF₆ as a feedstock. Vast amounts of UF₆ depleted in U²³⁵ are held in government and private reserves and represent an enormous, untapped fluoride reservoir.

Before and during World War II, the only countries producing fluorine on a commercial scale were the United States of America, United Kingdom and Germany. Post World War II period brought the involvement of the Soviet Union, Japan, France, Canada, Italy, South Africa and expansions of the United States, Germany and the United Kingdom operations.

Due to the disappearance of the cold war era, and disintegration of the Soviet Union States, demand for weapon grade U^{235} has decreased substantially which has created surpluses of commercial fluorine in the western industrial nations, Commonwealth of Independent Russian States (CIRS countries) and South Africa. Only the developing countries such as India and China have started new fluorine production facilities. It is estimated that world-wide production of elemental fluorine remains at 7000–9000 metric tons. A major portion of this production, (65–70%), is consumed by the UF_6 industry while the remaining 30–35% is used for the manufacture of IF_5 , SbF_5 , WF_6 , NF_3 , ClF_3 , CF_x , BrF_3 , ReF_6 , CoF_3 , fluorinating reagents, fluoropolymers and in the fluorination of polyolefin containers.

The fluorine industry, traditionally belonging to governments or large corporate interests, has recently experienced a new trend, especially in the USA. Smaller organizations with specialty product considerations, have embraced manufacturing of fluorine on a small scale. Very recently, the industries involved in the surface fluorination of polyolefin containers, in the synthesis of fluoropolymers, or manufacturing of NF_3 , WF_6 , ClF_3 and other high value specialty applications, have started new fluorine producing plants or have expanded their facilities.

20.8 Sulfur hexafluoride

Another one of the 21st Century's most important industrial chemicals prepared from elemental fluorine is sulfur hexafluoride. It is prepared by combining sulfur vapors and pure elemental fluorine [40,41]. After preparation, the gaseous mixture is scrubbed with hydroxide to remove HF, F_2 and other impurities and then it is heated to $400^\circ C$ to decompose any disulfur decafluoride, S_2F_{10} , to give SF_4 and SF_6 . The gaseous mixture is again passed through hydroxide tower followed by H_2SO_4 , BaO, P_2O_5 and activated alumina towers to remove any remaining residue of SF_4 , moisture and entrained sulfuric acid.

20.8.1 Properties

Sulfur hexafluoride is a nonflammable, colorless, odorless, tasteless, nontoxic and relatively unreactive gas which has been described quite often as an inert gas [42]. The current OSHA standard for allowable maximum concentration for human exposure in air is 6000 mg/m^3 (1000 ppm) TWA [43]. However, it must be noted that breakdown products, SF_4 , SOF_4 , SOF_2 from electric decomposition are toxic and are often scrubbed by passing over activated alumina, soda lime, or molecular sieves during maintenance [44].

Sulfur hexafluoride melts at $-50.5^\circ C$ and sublimates at $-63.9^\circ C$, critical pressure 3.759 mpa (37.2 atm), critical temperature, $45.55^\circ C$, liquid density 2.863 g/cm^3 , gas density 1.336 g/cm^3 , dielectric constant 1.00204 (gas), 1.81 (liquid). It is very good dielectric because a high gas density can be maintained at low temperatures and all the electrons are tightly bound. It is a very good electron scavenger as well as having strong breakdown strength. During electrical breakdown, it

captures primary electrons resulting in the formation of SF_5^- or SF_6^- ions and F atoms [45].

In sulfur hexafluoride, the sulfur atom is shielded by six fluorine atoms which impede kinetically any reaction with water, alkali hydroxides, ammonia or strong acids; as a result it remains inert to these reagents.

20.8.2 Uses

Due to a ban on polychlorinated biphenols, which were used in power substations and transformers as liquid dielectrics, an increased demand for electric power in the developing countries as well as in the industrialized nations during the last four years created a short supply of SF_6 in the market and price went up from \$8/kg to \$66/kg! This inflated price opportunity encouraged Chinese, Russian, German, South African and American producers to increase their capacity. Recently, because of the current over supply of SF_6 , price has come down to \$15/kg. The present worldwide production is over ten million pounds per year. It is extensively used by the electrical power industries in circuit breakers, high voltage coaxial cables, mini-power stations and transformers. Its non-electrical applications are as a tracer to study air flow patterns [46], underground pipe leak detection [47], dispersion of air pollutants [48], in loud speakers to improve pitch [49], in chemical laser [50,51], etching of semiconductor surfaces [52–55], casting of magnesium [56,57], removal of hydrogen and other gases from aluminum melts [58], filling enclosed space in double-pane windows [58,59], pressurizing tennis balls [61] and Nike tennis shoes.

20.9 Halogen fluorides

Fluorine reacts with other halogens and forms seven stable fluorides, ClF , ClF_3 , ClF_5 , BrF_3 , BrF_5 , IF_5 , and IF_7 . Chlorine pentafluoride is more reactive than elemental fluorine itself and iodine pentafluoride is least reactive among all the binary fluorides and is classified as a mild fluorinating reagent. Only three halogen fluorides, BrF_3 , ClF_3 and IF_5 , are of industrial importance as fluorinating reagents. The high reactivity of halogen fluorides with hydrocarbons leads to a spontaneous release of energy which is sufficient to attack the carbon skeleton and breaks C—C bonds. The excess energy thus released can result in explosion, fire and destruction of equipment and building structure. Another drawback in the use of halogen fluorides in the fluorination of hydrocarbons is that they often introduce both halogens into the substrate and produce a mixture of a variety of compounds which are difficult to separate.

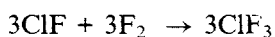
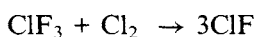
20.9.1 Bromine trifluoride

Bromine trifluoride is produced on a commercial scale by the reaction of elemental fluorine with bromine in a continuous gas-phase process. The ratio of bromine to fluorine is maintained close to 1:3. It can also be produced on a batch scale

by adding fluorine to liquid bromine and maintaining reaction temperature between 15°C and 50°C by circulating cold water around the reaction. It is mostly used in oil-well cutting tools. Worldwide production is less than 50 tons per year.

20.9.2 Chlorine trifluoride

Chlorine trifluoride is produced by a continuous gas-phase reaction of fluorine with chlorine. The manufacturing of chlorine trifluoride is somewhat complicated due to the formation of chlorine monofluoride. To eliminate the formation of chlorine monofluoride in chlorine trifluoride, reaction temperature is kept at 290°C and the ratio of fluorine to chlorine is maintained slightly more than 3:1 to promote a conversion of ClF to ClF₃. Excess Cl₂ will produce ClF while excess F₂ will convert ClF to ClF₃, as shown below:



There should be a high enough retention time in the reactor so that excess fluorine converts chlorine monofluoride to chlorine trifluoride. The current worldwide production of ClF₃ is less than 50 metric tons per year, which is much smaller than it was during World War II. It was reported that a German plant had a capacity of 5 tons/day during World War II [62].

The major use of ClF₃ is in the nuclear industry which converts unclean spent fuel reprocessing, uranium metal into gaseous uranium hexafluoride. Other applications are low temperature etchant for single crystalline silicon [63,64]. It is also used as a fluorinating reagent and in the synthesis of ClF and conversion of metals to metal fluorides such as tantalum and niobium metals to tantalum pentafluoride and niobium pentafluoride, respectively.

Chlorine trifluoride is a colorless gas, pale yellow or white liquid. Its melting and boiling points are -76.3°C and 11.75°C, respectively. It is easier to handle than elemental fluorine due to its low vapor pressure at room temperature. Chlorine trifluoride offers some advantages over NF₃ as an etchant. It is thermally activated rather than by plasma and can remove deposits simultaneously with process chamber cleaning. The process is free from manual labor and does not localize hot spots, as is the case with NF₃ plasma. Hot spots generated react with etchant and cause damage or breakdown of the protective surface coatings. Plasma zones produce nooks and crannies within the chamber which do not get cleaned thoroughly. NF₃ process cleans the chamber area only which is exposed to plasma, while ClF₃ thoroughly cleans the whole chamber. Because of these advantages over NF₃, ClF₃ has emerged in Japan as an in situ method for cleaning semiconductor process tools and this technology is also spreading in the USA.

20.9.3 Iodine pentafluoride

It is produced by the action of elemental fluorine on iodine which has a low melting point. The reaction is performed either in solvent or heating iodine to maintain

its liquid state. In a commercial preparation about one percent iodine is dissolved in IF_5 and brought into fluorination chamber where iodine reacts with fluorine and produces more IF_5 which is returned to the receiving vessel. Only a small portion of IF_5 is withdrawn from the receiving vessel as product, while the major portion of IF_5 is used for dissolving more iodine. This process goes on and on until all iodine is converted into IF_5 [65].

In another industrial process, iodine is heated above its melting point (113°C) and reacted with elemental fluorine under three atmosphere of pressure. A precaution is taken not to heat iodine above 150°C to avoid the formation of another product, IF_7 . Fluorine is added continuously until all iodine has reacted and converted to IF_5 [66].

20.9.3.1 Properties

Iodine pentafluoride is a pale yellow liquid at room temperature. Its melting point is 8.5°C , boiling point is 102°C , and liquid density 3.252 g/cm^3 . It is a very stable compound and produces little storage hazard. It could be stored in a closed container for a long time. It is the least reactive of the halogen fluorides and classified as a soft fluorinating reagent. It is used as a mildest, selective fluorinating reagent in the fluorination of organic molecules. It adds iodine and fluorine when reacted with unsaturated compounds. The fluorination reaction is easily controlled and losses due to oxidation fragmentation are minimized. The most important industrial use which requires several hundred thousands kilograms is with perfluoro-olefins in the presence of SbF_5 which acts as a catalyst [67]. It adds both fluorine and iodine to tetrafluoroethylene and produces a commercially important telomer [68]. It is also used for nucleophilic fluorine-aryl substitution reaction [69], plasma-free etching of Si, SiO_2 and Si_3N_4 in IF_5 [70]. Without a plasma the reactivity sequence of the interhalogen gases is of the following order: $\text{ClF}_3 > \text{IF}_5 > \text{F}_2$. The current worldwide production is about 300 tons per year.

20.10 Nitrogen trifluoride

20.10.1 Introduction

Among the several existing binary nitrogen-fluorine gaseous compounds, NF_3 , N_2F_4 , N_2F_2 , N_3F , nitrogen trifluoride NF_3 , is the only compound which has achieved an industrial importance. As a matter of fact, it is one of the fourth largest inorganic fluorides and the fastest growing compound in inorganic fluorine industry. The semiconductor industry has developed in situ cleaning process to remove residual materials from low pressure chemical vapor depositions (LPCVD), ion implantations, physical vapor depositions (PVD), and plasma etching, by flushing the chambers with perfluoro compounds (PFCs) such as CF_4 , C_2F_6 , C_3F_8 . As perfluorocarbon compounds pose a global warming potential threat to our environment, the semiconductor industry is reducing their consumption voluntarily and switching to ClF_3 and NF_3 cleaning processes.

20.10.2 Preparation

Although nitrogen trifluoride can be prepared by several chemical procedures, only two methods are technically and economically feasible for a large-scale production: The electrolysis of molten ammonium acid fluoride; and the direct fluorination of NH_3 in the presence of molten NH_4F [71]. The direct fluorination is carried out in specially designed reactor [72] in which NF_3 is produced by the reaction of F_2 with NH_3 in the presence of molten ammonium fluoride. As no hydrogen is generated in the direct fluorination process, it is considered safer than electrolytic process. In the later process, NF_3 is produced at the anode and H_2 at the cathode.

20.10.3 Purification

The electronic industry has established tough standards for gases and other chemicals. As a result, several methods have been developed for the purification of NF_3 . An impurity, such as N_2F_2 , is removed by pyrolysis over heated metal fluorides [73] or heated metal turnings [74], between 200–300°C to avoid conversion of NF_3 to N_2F_4 . The other impurities, such as N_2O , CO_2 , H_2O , are removed by adsorption on zeolites [75]. The most difficult impurity to remove is CF_4 which has nearly identical physical properties of NF_3 [76,77].

20.10.4 Economics

There are four major producers of NF_3 in the world. Air Products and Chemicals, Inc., Mitsui Toatsu, Central Glass and Kanto Denka Kogyo. Very recently, Advance Specialty Gases has announced production of NF_3 on a much smaller scale. Total worldwide production of NF_3 is between 600 and 800 tons per year and its demand is continuously on the rise, although it has seen some challenge from ClF_3 .

20.10.5 Properties

Nitrogen trifluoride, NF_3 , is a colorless gas. It melts at -129°C and boils at -206°C . It has a musty, pungent odor. It can be a potent oxidizer at an elevated temperature. Nitrogen trifluoride is a toxic substance and is most hazardous by inhalation. It induces the production of methemoglobin which reduces oxygen levels in the body tissues, but exposure to fresh air or breathing oxygen reverts it back to hemoglobin. The OSHA permissible exposure limits are set TLV-TWA 10 ppm or 29 mg/kg. It is non-corrosive gas to steel, stainless steel and nickel, provided the metal surface has been properly cleaned, passivated and kept free from moisture.

20.11 Antimony fluorides

20.11.1 Antimony trifluoride

Antimony trifluoride and antimony pentafluoride are the only two antimony compounds of commercial significance. Although antimony forms stable mixed halides such as SbCl_4F , SbCl_3F_2 , SbCl_2F_3 , SbClF_4 , Sb_2F_{11} and polymer $(\text{SbCl}_4\text{F})_4$, these

forms have remained a laboratory curiosity. In the early stage of chlorofluorocarbons and fluorocarbons production, antimony trifluoride was used on a very large scale in a process known as Swarts reaction [88]. The effectiveness of SbF_3 as a fluorinating agent is increased substantially by addition of Cl_2 , Br_2 , or SbCl_5 to the reaction mixture [89]. However, the modern hydrocarbon or fluorocarbon industry does not use such large quantities of SbF_3 . The major use of SbF_3 is in the manufacturing of SbF_5 . Small quantities of SbF_3 are also being used in selective fluorination processes and recently it is being used in the manufacturing of fluoride glass, fluoride glass optical fiber preform [96], and transparent conductive films [97]. The total worldwide consumption of SbF_3 is about 15 tons/year.

20.11.2 Preparation

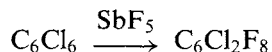
Antimony trifluoride is easily prepared by dissolving Sb_2O_3 in aqueous HF or in an excess anhydrous hydrogen fluoride. The aqueous HF solutions are carefully evaporated to dryness.

20.11.3 Properties

Antimony trifluoride is a very hygroscopic, white, crystalline powder. To keep it dry, it is always kept packaged under the atmosphere of nitrogen or argon. Its solubility in water is 384.7 g/100 g at 0°C and 492.4 g/100 g at 25°C [91]. It is also soluble in methanol (154 g/100 ml) and acetone 55.3g/100 ml at 25°C. It goes under hydrolysis in water slower than SbCl_3 .

20.11.4 Antimony pentafluoride

It is a very active fluorinating reagent which is generally used in the fluorination of completely halogenated compounds or as a catalyst in the manufacturing of telomers [92], epoxy silicon coatings [93], polymerization of ethylene and propylene hydrocarbons [94], isomerization, alkylation, oligomerization [95] etc. Fluorination of halogenated olefins or halogenated aromatic compounds with SbF_5 , results in an addition and substitution reactions simultaneously. For example, when hexachlorobenzene is reacted with SbF_5 it gives dichlorooctafluoro cyclohexene.



It is also used in the preparation of magic acids HSbF_6 and $\text{HSbF}_6 \cdot x \text{H}_2\text{O}$.

20.11.5 Economics

The worldwide market for SbF_5 is about 15–20 tons/year.

20.11.6 Properties

Antimony pentafluoride is a colorless, very viscous, fuming liquid. Its viscosity is 460 mpa which is very close to the value of glycerol. The polymerization of SbF_5 can be

prevented by addition of trace amount of anhydrous hydrogen fluoride. It melts at 7°C and boils at 142.7°C [98]. It has specific gravity 3.145 g/cm³ at 15.5°C. It can be stored in carbon steel, aluminum and Teflon[®] containers. It should not be handled in polyethylene or glass containers.

20.12 Tungsten hexafluoride

Tungsten hexafluoride is emerging as one of the most important inorganic fluoride compounds. It is playing a highly critical role in very large scale integration devices (VLSI) industry. Its consumption as a tungsten source in chemical vapor deposition is growing at the rate of approximately 20% annually and it is expected to grow continuously at this rate until 2005. Tungsten, when reacted with fluorine forms three binary fluorides: WF₄, WF₅, and WF₆. The first two forms were observed only in a high-energy system [99]. The last form, WF₆, is of the most important commercial interest. At present, the worldwide production of WF₆ is an estimated half million pounds. Each manufacturer, Air Products, Advance Research Chemicals, Inc., Bendgap/Matheson, are trying to improve the purity of the product for the VLSI market.

20.12.1 Physical and chemical properties

Tungsten hexafluoride is a colorless gas and water white liquid. If colored, it may be due to the presence of metallic impurities such as nickel, chromium, iron and copper, etc. It melts at 2°C and boils at 17.1°C. It reacts with water spontaneously and produces WO₃ and HF. It also reacts with alkali metal fluorides and forms M₂WF₈ where (M = K, Rb, Cs) [100]. Tungsten hexafluoride reacts with hydrogen or hydrogen containing compounds such as GeH₄ [101], SiH₄ [102], (C₂H₅)₂ SiH₂ [103], SiH₂F₂ [104] between 450–750°C at pressure <100 kpa (1 atm) [105] and produces tungsten metal and hydrogen fluoride. This characteristic makes WF₆ suitable for CVD processes. Tungsten hexafluoride is corrosive to the respiratory tract, eyes and skin. It produces burns similar to HF.

20.12.2 Manufacturing

Tungsten hexafluoride is manufactured commercially by reacting tungsten powder in gaseous fluorine at 250–300°C range. The reaction between tungsten and elemental fluorine is exothermic. In the beginning of the reaction, one has to heat the reactor, but once the reaction starts, most of the heat is being provided by the fluorination process. The product is collected in cold traps and metallic impurities are removed by distillation. The volatile impurity, HF, which has similar vapor pressure as WF₆ is separated by adsorption process. Tungsten hexafluoride can be stored in steel, monel or nickel cylinders and is shipped as a corrosive liquid.

20.13 Dentifrice materials

Both sodium monofluorophosphate $\text{Na}_2\text{PO}_3\text{F}$ and stannous fluoride SnF_2 have played an important role in fighting dental decay for the past half century. Whether it is fluoridation of water, or toothpaste or the oral rinse formulations that have been responsible for improved dental health of the population worldwide. The major toothpastes used around the globe contain one of the fluorides NaF , SnF_2 , or $\text{Na}_2\text{PO}_3\text{F}$. Each major toothpaste producer is using NaF and/or $\text{Na}_2\text{PO}_3\text{F}$ due to their lower costs. Procter and Gamble (P & G Group) substituted SnF_2 with NaF and called it Advanced Formula Crest[®] under the trademark Fluoristat[®]. The earlier SnF_2 formulation was known as Fluoristan[®]. It was a matter of economics. Price of tin was going up and SnF_2 has only 24% fluoride ion value. The price of stannous fluoride varies from \$22 to \$40/lb where as NaF dental grade has 45% available fluoride ion and a price is less than \$3/lb. Currently, stannous fluoride is used in special formulations and gels which are recommended by dentists or used in their offices.

As a result, the need for SnF_2 has decreased from 500,000 lbs/year to less than 20,000 lbs/year. While sodium monofluorophosphate still being comparatively less expensive, it has a worldwide market of over two million pounds/year. The comparative study of Hayden shows that sodium monofluorophosphate is approximately twice as effective as NaF in inhibiting acid production in a saliva-glucose mixture [105]. It is believed that the cavity prevention provided by fluoride ions is due to the replacement of hydroxyle group in hydroxyapatite, $\text{Ca}_5(\text{PO}_4)_3\text{OH}$ of the tooth by fluoride ions to forms more insoluble fluoroapatite, $\text{Ca}_5(\text{PO}_4)_3\text{F}$ [106].

20.13.1 Stannous fluoride

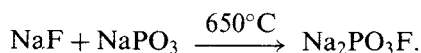
Commercial production of stannous fluoride is carried out by a reaction between mossy tin and anhydrous HF . It is also prepared by dissolving stannous oxide, SnO , in aqueous HF .

20.13.2 Properties

Stannous fluoride, SnF_2 , is a white crystalline compound which has its melting point at 219°C and boiling point at 850°C . It is readily soluble in water, aqueous HF and anhydrous HF .

20.13.3 Sodium monofluorophosphate

Sodium monofluorophosphate is produced commercially by fusion of sodium fluoride with sodium metaphosphate.



20.13.4 Properties

Sodium monofluorophosphate is highly soluble in water (42 g $\text{Na}_2\text{PO}_3\text{F}$ per 100 g solution). Dilute aqueous solutions of $\text{Na}_2\text{PO}_3\text{F}$ can be stored indefinitely and its melting point is 625°C .

20.14 Polycarbon monofluoride: CF_x

20.14.1 Introduction

Polycarbon monofluoride is also known as carbon fluoride or graphite fluoride. This material is of strategic importance for the industrialized nations. It plays a very important role due to its unique properties which have been responsible for its large industrial demand. The chemists have not settled their scores to confirm whether it is inorganic or organic compound but one thing is sure that the industry is exploring this compound continuously.

20.14.2 History

Direct fluorination of carbon was started by Moissan who obtained a variety of fluorocarbons. In 1934, Ruff and his associates while reacting carbon with fluorine, obtained a white solid product, $\text{CF}_{0.92}$ [78] and volatile fluorocarbons. No attention was paid to this non-volatile white solid residue. This work was further explored independently by Rüdorff and Rüdorff in Germany [79] and Palin in the United Kingdom [80]. They discovered that when carbon was fluorinated at $420\text{--}500^\circ\text{C}$, it produced polymeric material, CF_x , a grayish, off-white powder (where $x = 0.992$). In the early sixties, an extensive work was carried out by Margrave [81] and Watanabe [82]. In 1969, Meshri and White et al. [83] produced the first commercial samples of carbon fluoride and graphite fluoride, where they reported composition that ranged from $\text{CF}_{0.23}$ to $\text{CF}_{1.26}$. Subsequently, various institutes or corporations in Russia, Japan, USA and France have persuaded commercial markets. Currently, the only commercial quantities are available from Advance Research Chemicals, Inc., Central Glass Co., Osaka Gas Co. and Daikin Kogyo of Japan. The easy availability of these materials on a commercial scale has started a new era in the field of high energy density batteries, super lubricants, and many other unique applications.

20.14.3 Preparation

Any kind of carbon, such as natural graphite, petroleum coke, carbon black, carbon fiber, exfoliated graphite, natural or synthetic graphite and fullerenes can be fluorinated under controlled conditions. Each carbon has unique crystalline properties. To achieve a desired degree of fluorination — or carbon fluorine ratio — numerous experiments are conducted in specialized TGFA reactors to determine the operating conditions such as fluorination temperature, fluorine flow rate, and fluorination duration.

In a typical experiment, once the fluorination temperature and flow rate is determined, a finely divided carbon powder is loaded into the reactor. The tempera-

ture of the reactor is raised gradually and the contents of the reactor is flushed with N_2 to remove volatile impurities from carbon as well as the reactor. Fluorine diluted with N_2 or Ar is passed over the bed of carbon at temperatures ranging from 350–600°C for a few hours to 48 h or longer period, depending upon the type of carbon to be fluorinated, degree of fluorination required and fluorine flow rate used. The material typically used for aggressive lubrication applications are fluorinated for longer hours to reach fluorine concentrations of at least 63+%, while the one required for primary lithium batteries requires 61–63% of fluorine concentration in CF_x .

20.14.4 Chemical and physical properties

Fully fluorinated carbons with empirical formula CF_x , ($x > 1$) are snow white in color, inert to acids and alkalis and even to nascent hydrogen. These materials are hydrophobic and insoluble in any solvents. Polycarbon monofluoride with formula $CF_{1.0}$ is cream colored material and a poor conductor. Partially fluorinated carbons vary in color from gray to dark blue–black. Thermally less stable are those in which the fluoride content is between 24–45%, or the x value is in the range of 0.2–0.5. These materials hydrolyze in the presence of moisture and release HF when heated above 150°C. They are also susceptible to the attack of strong acids and alkalis. Fully fluorinated materials are stable from 400 to 600°C depending upon the degree of fluorination and the origin of the starting material.

20.14.5 Applications

The largest commercial application of CF_x is for primary non-aqueous, high energy, density lithium batteries. The origin of carbon for this application has historically been petroleum coke or synthetic carbon fiber. Worldwide production of battery grade material is between 40 and 50 tons/year. The other applications include lubrication in dry or moist air up to 400°C. In the atmosphere of N_2 it can be used up to 600°C according to NASA Lewis Research Center [83]. In certain applications it is a better lubricating agent than molybdenum sulfide, graphite or Teflon[®] PTFE [84,85]. Fussaro and Sliney also studied the lubrication properties of polyimide-bonded CF_x ($x = 1.1$) films and compared them with those polyimide films and MoS_2 -bonded films [86,87]. It is also used as a water or an oil repellent or a wettability controlling agent. It is mixed with various resins and rubbers to produce composites with low surface tension and then molded into the desired configuration or parts.

References

- [1] M.M. Miller, Fluorospa, Annual Report, US Department of Interior, Bureau of Mines, Washington D.C., 1991.
- [2] A.G. Nimchik, Kh. L. Usmanov, N.A. Sirzhiddinov Uzb, Khim. Zh. 6 (1991) 68–70.
- [3] V.D. Khlilev and co-workers, Masame, T. Matsuo, (Heisei) JPN Patent, 03291324 A2 (Dec. 20, 1991).
- [4] K. Masame, T. Matsuo, (Heisei) JPN Patent 03291324 a2 (Dec. 20, 1991).

- [5] Y. Bertaud et al., FR Patent, 2661425 A1 (Oct. 31, 1991).
- [6] P. Humbert and co-workers E.C. Photovoltaic-Sol. Energy Conference, Proc. Int. Conf., (1991) 261-266.
- [7] C.B. Willingham, R.T. Newberg, Exploratory Development of Fusion Cost Calcium Fluoride for 1.06 micrometer pulsed laser optics, Progress Report (Sept. 25 to Dec. 25, 1976) NTIS Document C00-4029-2 Raychem Co. For US Energy Research and Development Administration, (Jan. 1977).
- [8] A.S. Marggraf, Hist. Acad. Royale Sci. Berlin, 1768, p. 3.
- [9] K. Sheele, Srens. Vents. Acad. (1771) 120.
- [10] H. Davy, Philos. Trans. 103 (1813) 263.
- [11] E. Fremy, Ann. Chim. Phys., 47 (1856) 5.
- [12] H.K. Van Poolen, Oil gas J., 65 (1967) 93.
- [13] W.S. Midkiff, H.P. Foyt, Mater-Perform, 17(2) (1978) 17.
- [14] E.E. Junge, J. Chabal, (PPG Industries) US Patent, 3,373,130 (Mar. 19, 1968).
- [15] R.L. Parkens, M.R. Browne, Appl. Opt., 17 (1978) 1845.
- [16] M. Beckwith, G.F. Hau, US Patent, 3,888,778 (Mar. 13, 1973).
- [17] H.W. Heiser, Chem. Eng. Prog., 45(3) (1949) 169.
- [18] Harshaw Optical Crystals, Harshaw Chemical Co., Solm, Ohio, 1967, pp. 32-33.
- [19] D.T. Meshri, S.D. Meshri, D. B. Contractor et al., (Advance Research Chemicals, Inc.) US Patent, 5,785,770 (July 28, 1998).
- [20] M. Miller, J. Am. Chem. Soc., 99 (1977) 498.
- [21] Kin-Tai Chang, (American Can Company) US Patent, 4,197,174, (April 8, 1980).
- [22] James. V. Crivello, (General Electric Co.) US Patent, 4,136,102 (Jan. 23, 1979).
- [23] Larry A. Lien, J. Lamar Zollinger, (3M Co.) US Patent, 4,130,690 (Dec. 19, 1978).
- [24] Frances Joan Bergess et al., (UK Sec. of State for Defense) UK Patent, 1,561,968 (Mar. 5, 1980).
- [25] Gerhard Kuenstle, H. Spes, H. Siegel, (Walker-Chemie G.M.b.H) Ger. Offen #2,308,119 (Sept. 19, 1974).
- [26] P.T. Parker, I. Mayer, (Esso Research and Engineering Co.) US Patent, 3,778,489 (Dec. 11, 1973).
- [27] J.W. Brockington, (Texaco, Inc.) US Patent, 3,922,319 (Nov. 25, 1975).
- [28] D.A. McCauley, (Standard Oil Co.) US Patent, 3,928,487 (Dec. 23, 1975).
- [29] J.W. Brockington, (Texaco, Inc.) US Patent, 4,008,178 (Feb. 15, 1977).
- [30] C.A. Braidwood, A.G. Hovey, (Reichold Chemicals) US Patent, 2,419,185 (Apr. 15, 1947).
- [31] V.N. Ipatieff, C.B. Linn, (Universal Oil Products Co.) US Patent, 2,421,946 (June 10, 1947).
- [32] G.A. Olah, (Esso Research and Engineering Co.) US Patent, 3,708,553 (Jan. 2, 1973).
- [33] D.A. McCauley, (Standard Oil Co.) US Patent, 3,819,734 (June 25, 1974).
- [34] P.G. Rodewald, (Mobil Oil Co.) US Patent, 3,925,495 (Dec. 9, 1975).
- [35] P.G. Rodewald, (Mobil Oil Co.) US Patent, 3,984,352 (Oct. 5, 1976).
- [36] A.C. Hopkins, W.E. Watson, (Allied Corp.) Can Patent, 448, 662 (May 25, 1948).
- [37] A.J. Edwards, (National Smelting Co., Ltd.) Brit Patent, 775, 692 (Aug. 22, 1956).
- [38] D. Young, J. Pearson, (Allied Chemical Corp.) US Patent, 2,416,133 (Feb. 18, 1947).
- [39] J.F. Tompkins and co-workers, The Properties and Handling of Fluorine, Report No. ASD-TDR-62-273, Air Products and Chemicals, Inc. Allentown, PA, 1963.
- [40] W.E. Watson, H.G. Tepp et al., (Allied Signal) US Patent, 3,336,111 (Aug. 15, 1967).
- [41] M. Jaccoud, A.J.F. Ducouret, (Produits Chimiques Ugine Kuhlmann-Atochem) Eur. Patent, 87338 (Aug. 31, 1983).

- [42] C.L. Thomas, (Universal Oil Products Co.) US Patent, 2,313,103 (Mar. 9, 1943).
- [43] P.T. Parker, I. Mayer, (Esso Research and Engineering Co.) US Patent, 3,778,489 (Dec. 11, 1973).
- [44] W.C. Schumb, J.G. Trump, G.L. Priest, *Ind. Eng. Chem.*, 41 (1949) 1348.
- [45] R.L. Champion, Gaseous Dielectric-6, *Proceedings of the 6th International Symposium*, 1990, pp. 1–8.
- [46] P.J. Drivas, F.H. Shair, *Atmos. Environ.*, 8, (1974) p. 1155.
- [47] G.M. Thompson, (Tracor Research Corp.) US Patent, 5,046,353 (Sept. 10, 1991).
- [48] B.K. Lamb, D.E. Stock, *HTD, Am. Soc. Mech. Eng.*, 152 (1990) 55–59.
- [49] H.W. Sullivan, (D. Bogen and Co.) US Patent, 2,797,766 (July 2, 1957).
- [50] D.N. Kaye, *New Sci.*, 14 (1971) 65.
- [51] D.J. Spenser and co-workers, *Int. J. Chem. Kinet.*, 1 (1969) 493.
- [52] S.M. Bobbio, (Allied Signal) US Patent, 4,680,087 (July 14, 1987).
- [53] Mu Xiao-Chun, Multani Jagin, (Intel Corp.) US Patent, 4,980,018 (Dec. 25, 1990).
- [54] O. Hirokazu, K. Michihisa, *NEC Res. Dev.*, 37(2) (1996) 191–197.
- [55] F. Ren, J.M. Grow, M. Bhaskaran et al., *Mater. Res. Soc. Symp. Proc.*, 421 (1996) 251–255.
- [56] J.W. Fruhling, J.D. Hanawalt, *Am. Foundry Soc. Trans.*, 16 (1969) 159.
- [57] O. Schlem, *Giesserei*, 19 (1971) 558.
- [58] R.R. Corns et al., (AGA AB) US Patent, 4,959,010 (Sept. 25, 1990).
- [59] I. Fasth, J. Karlsen, (Barrier HB) US Patent, 4,800,693 (Jan. 31, 1989).
- [60] M. Rehfeld, (Saint-Grobain Vitrage) *Fr Patent*, 2,529,609 (Jan. 6, 1984).
- [61] J.J. Oransky et al., (Air Products and Chemicals) US Patent, 4,358, 111 (Nov. 11, 1982).
- [62] H.R. Neumark, *Trans. Electrochem. Soc.*, 91 (1947) 367.
- [63] Y. Saito, O. Yamaoka, A. Yoshida, *J. Vac. Sci. Technol.*, B9 (1991) 2503.
- [64] Y. Saito, M. Hirabaru, A. Yoshida, *J. Vac. Sci., Technol.*, B10 (1992) 175.
- [65] H.G. Tepp, (Allied Corp.) US Patent, 3,367,745 (1968).
- [66] J.T. Lileck, (Air Products and Chemicals, Inc.) US Patent, 4,108,966 (Aug. 22, 1978).
- [67] R.E. Parsons, (DuPont) US Patent, 3,123,185 (1964).
- [68] H.C. Fielding, In: *Organo fluorine Chemicals and their Industrial Applications*, R.E. Banks (Ed.), Ellis Horwood Publishers, Chichester UK, 1979.
- [69] H.J. Frohn, S. George, G. Henkel et al., *Z. Anorg. Allg. Chem.*, 621(7), (1995) 1251–56.
- [70] A. Guber; U. Koehler; et al., *Proc. SPIE — Int. Soc. Opt. Eng.*, 1993, p. 2089.
- [71] A.J. Woytek, J.T. Lileck, (Air Products and Chemicals, Inc.) US Patent, 4,091,081 (May 23, 1978).
- [72] A.J. Woytek, J.T. Lileck, *Chem. Eng.*, 84(26) (1977) 16.
- [73] I. Harads, H. Hokonohare, T. Yamaguchi, (Mitsui Toatsu Chemicals, Inc.) US Patent, 4,948,571 (Dec. 3, 1988).
- [74] J.T. Lileck, J. Papinsik, E.J. Steigenwalt, (Air Products and Chemicals, Inc.) US Patent, 4,193,976 (Mar. 18, 1980).
- [75] A.J. Woytek, P.B. Henderson, In: *Proceedings of the Institute of Environmental Science 37th Annual Meeting*, IES, Mount Prospect, 1990, p. 570.
- [76] T. Suenaga, T. Fuji, Y. Kobayashi, (Central Glass) US Patent, 5,069,887 (Dec. 3, 1991).
- [77] P.B. Henderson, C.G. Coe et al., (Air Products and Chemicals, Inc.) US Patent, 5,069,690 (Dec. 3, 1991).
- [78] O. Ruff, O. Bretschneider, F. Ebert *Z. Anorg. Allg. Chem.*, 217 (1934) 1.
- [79] W. Rüdorff, G. Rüdorff, *Z. Anorg. Chem.*, 253 (1947) 281.
- [80] D.E. Palin, K.D. Wadsworth, *Nature Allg.*, 162 (1948) 929.
- [81] J.L. Margrave et al. *J. Phy. Chem.*, 68 (1964) 290.

- [82] N. Watanabe, Y. Koyama, S.J. Yoshigawa, *J. Electrochem Soc.*, 1 (1964) 17.
- [83] R.L. Fusaro, H.E. Sliney, NASA Technical Note D-6714, March 1972.
- [84] R.L. Fusaro, H.E. Sliney, Preliminary investigation of graphite fluoride (CF_x)_n as a solid lubricant, NASA Tech, Note D-5097, March 1969.
- [85] R.L. Fusaro, H.E. Sliney, graphite fluoride (CF_x)_n, a new solid lubricant, ASLE/ASME Lubrication Conf.; Houston, Texas, ALSE Preprint 69 LC-9, (October 14–16, 1969).
- [86] R.L. Fusaro, H.E. Sliney, Lubricating characteristics of polyimide bonded graphite fluoride and polyimide thin films, *ASLE Trans.*, 16 (1973) 189.
- [87] R.L. Fusaro, H.E. Sliney, Effect of thermal aging on the tribological properties of polyimide films and polyimide bonded graphite fluoride films, *Lubr. Eng.*, 36 (1980) 143.
- [88] F. Swarts, *Bull. Acad. Roy Belg.*, 24 (1892) 309.
- [89] R.E. Banks, *Fluorocarbons and their Derivatives*, MacDonald, London, 1970, p. 1.
- [90] E.T. McBee, P.A. Wiseman, G.B. Bachman, *Ind. Eng. Chem.*, 39 (1947) 415–417.
- [91] A. Rosenheim, H. Grunbaum, *Z. Anorg. Chem.*, 61 (1909) 187.
- [92] R.E. Parsons, (DuPont) US Patent, 3,123,185 (1964).
- [93] L.A. Lien, J.L. Zollinger, (3M Co.) US Patent, 4,130,690 (Dec. 19, 1978).
- [94] S.K. Brownstein, (Canadian Patents and Development Ltd) US Patent, 3,631,002 (Dec. 28, 1971).
- [95] G.A. Olah, (Produits Chimiques Ugine Kuhlmann) US Patent, 4,116,880 (Sept. 26, 1978).
- [96] K. Fujiura, Y. Ohishi et al., *Eur. Patent*, 331,483 (Sept. 6, 1989).
- [97] N. Sonoda, N. Sato, *JPN Patent*, 63314713 (Dec. 22, 1988).
- [98] O. Ruff et al., *Chem. Ber.*, 42 (1909) 4021.
- [99] A. Bensaoula, E. Grossman, A. Ignatiev, *J. Appl. Phys.*, 62 (1987) 4587.
- [100] B. Cox, D.W. Sharp, A.G. Sharpe, *J. Chem. Soc.*, (1956) 1242.
- [101] C.A. Van der Jeugd, G.J. Leusink, et al., *Appl. Phys. Lett.*, 57 (1990) 354.
- [102] H.L. Park et al., *J. Electrochem Soc.*, 137 (1990) 3213.
- [103] D.A. Roberts et al., *Advanced Metallization for VLSI Applications*, Materials Research Society, Pittsburg, PA, 1992, pp. 127.
- [104] T. Kusumoto et al., (ULVAC Corp.) *JPN Patent*, J63250463 (Oct. 18, 1988).
- [105] J.B. Hayden et al., *J. Dent. Res.*, 30 (1951) 466.
- [106] E.J. Duff, *Caries Res.*, 7 (1973) 79.

Index

- absorption separation method, 639
 acetonitrile, 23
 acid-base reactions, 542
 acidic aHF, 105
 acidic surface sites, 384
 acidity of NiF_4 , 101
 acidobasic character, 218, 224
 actinide fluorides, 125
 activation, 377, 380
 activation energies, 187, 204
 active surface sites, 374, 376
 addition reaction, 593, 619
 adhesion, 482
 ADN sequences, 318
 adsorption-desorption, 397
 advantages of NF_3 in etching/cleaning, 633
 aerogels, 37
 Ag^{2+} salts, 80
 $\text{Ag}^{2+}(\text{MF}_6^-)_2$, 96
 $\text{Ag}^1\text{Ag}^{11}\text{F}_{21}$, 21
 $\text{Ag}_{(\text{solv})}^{2+}$, 80, 86
 Ag_2F_5 , 79, 84
 Ag_3F_8 , 79, 83
 $\text{Ag}(\text{AuF}_4)_2$, 92, 97
 $\text{Ag}(\text{BiF}_6)_2$, 96
 $(\text{AgF})_2\text{AgF}_4\text{AsF}_6$, 80
 $(\text{AgF})_2\text{AgF}_4\text{MF}_6$ ($\text{M}=\text{Sb}, \text{Au}, \text{Pt}$), 90
 $(\text{AgF})_n^{n+}$ chains, 91
 $(\text{AgF})_n^{n+}(\text{IrF}_6)_n^{n-}$, 92
 $\text{Ag}(\text{II})\text{Ag}(\text{III})\text{F}_5$, 84
 $\text{Ag}(\text{III})$ electron affinity, 85
 $\text{Ag}(\text{MF}_6)_2$, $\text{M}=\text{Sb}, \text{Nb}, \text{Ta}$ and Bi , 92
 $\text{Ag}(\text{NbF}_6)_2$, 96
 $\text{Ag}(\text{SbF}_6)_2$, 96
 $\text{Ag}(\text{TaF}_6)_2$, 96
 $\text{Ag}[\text{AuF}_4]_2$, 97
 AgAsF_6 , 90
 AgF^+ salts, 80
 $\text{AgF}^+\text{BF}_4^-$, 84
 AgF_2 monofluoro base, 84
 AgF_2^+ , 85
 AgF_3 bright red diamagnetic solid, 20–21, 81, 498
 AgFAgF_4 , 84
 AgFAsF_6 , 83
 AgFAuF_4 , 84
 AgFIrF_6 , 94
 AgFMF_4 with $\text{M}=\text{B}, \text{Au}$, 91
 AgFMF_6 with $\text{M}=\text{As}, \text{Au}, \text{Ir}, \text{Ru}, \text{Sb}, \text{Bi}$, 91
 AgFRuF_6 , 94
 $\text{AgRuF}_6\text{BiF}_6$, 93
 air- and moisture-stable ruthenium and osmium(II) fluoride, 59
 Al , 606, 644
 Al corrosion, 532
 Al surface, 482
 $\text{Al}(\text{OH}, \text{F})_3$, 379
 $\text{Al}(\text{OH}, \text{F})_3\text{yH}_2\text{O}$, 380
 Al-F bonds, 380
 AlCl_3 , 379, 393
 AlF_3 , 7, 379, 385, 398, 665
 $\text{AlF}_3 \alpha$, 380, 386, 387
 $\text{AlF}_3 \beta$, 380, 386, 387
 AlF_3 film, 482
 $\text{AlF}_3\text{nH}_2\text{O}$, 379
 AlF_3 -based glasses, 239
 alkali metal fluorides, 666
 alkaline, 605
 alkylation, 664
 alkylation catalyst, 663
 alkynes, 619
 alternative gases, 639
 alumina, 9, 37, 377
 alumina aerogels, 379
 aluminium fluoride catalysts, 386
 aluminium hydroxy-oxyfluoride, 380
 aluminium hydroxyfluorides, 379
 aluminium oxyfluoride, 383
 aluminophosphates, 210
 americium (III) cations in HF and HSO_3F , 348
 amine copper fluorides, 72
 amines, 211
 amino acids, 431
 ammonia adsorption (TPD), 384
 ammonium bifluoride, 666
 amorphous alumina, 382, 390
 amorphous layer, 479
 amorphous phase, 575
 amplification, 255, 268
 amplifiers, 261, 269
 an aromatic C–F bond, 56

- anhydrous $(\text{CH}_4\text{N})^+\text{F}^-$, 24
 anhydrous FeF_3 crystals, 17
 anhydrous hydrogen fluoride (aHF), 1, 79
 anionic species in superacids, 346
 anisotropic structure, 592
 anisotropic ion: Co^{2+} , 306
 anodes, 509
 anodic oxidation of Al, 533
 anthracene, 591
 antiferromagnetic coupling, 104
 antimony, 674
 antimony (V) fluoride: Lewis acidity in $\text{CF}_3\text{SO}_3\text{H}$, 343
 antimony (V) fluoride: Lewis acidity in HF, 338–340, 362
 antimony (V) fluoride: Lewis acidity in HSO_3F , 341, 342, 353
 antimony fluorides, 674
 antimony OTeF_5 derivatives, 134
 antimony oxide fluorides, 124
 antimony pentafluoride, 675
 antimony trifluoride, 674
 apatite, 36
 applications of CF_4 , C_2F_6 and NF_3 , 632
 aprotic organic solvents, 523
 aqueous HF, 665
 Arrhenius plots, 204
 arsenic (V) fluoride: Lewis acidity in HF, 337
 arsenic (V) fluoride: Lewis acidity in HSO_3F , 341
 arsenic OTeF_5 derivatives, 136
 arsenic oxide fluorides, 124
 arsenic pentafluorides, 80, 134, 558
 AsF_3 , 24
 $\text{AsOCl}_3\cdot\text{XeF}_4$, 26
 asymmetric induction, 420
 atomic force spectroscopy, 454
 atomization energy of KrF_2 , 105
 attenuation, 262
 Au^{II} -compounds, 21
 AuF_3 , 80
 Auger spectroscopy, 454
 automotive industry, 665
 azacycloalkanes, 417
 azide, 432

 $\text{B}(\text{OTeF}_5)_3$, 139
 $\text{Ba}_{12}\text{Cl}_5\text{F}_{19}$, 325
 $\text{Ba}_5\text{Nb}_3\text{O}_3\text{F}_{18}(\text{HF}_2)_2$, 16
 $\text{Ba}_7\text{Cl}_2\text{F}_{12}$, 325
 $\text{BaBrF}\cdot\text{Eu}$, 324
 BaClF , 323
 BaF_2 , 320
 BaLiF_3 , 318

 BaThF_6 , 320
 BaY_2F_8 , 317
 BeF_2 , 239
 Berry-style pseudorotation, 122
 BF_3 , 80, 669
 Bi_3NF_6 , 12
 bi-intercalation structure, 497, 499
 BiF_5 , 86, 134
 BiF_7^{2-} , 24
 Biginelli reactions, 430
 binary and complex fluorides of nickel, 100
 binary and complex fluorides of silver, 79
 binary anion conductive solid electrolyte, 185
 binary fluorides, 20
 binary fluorides of the transition metals, 79
 binary rare-earth compounds, 178
 binary rare-earth oxide fluorides, 177
 binary solids, solubility in superacids, 346
 binding energy (BE), 472, 480
 bis(fluorosulfonyl)imide, $\text{HN}(\text{SO}_2\text{F})_2$, 126
 bis(fluorosulfonyl)peroxide, $\text{S}_2\text{O}_6\text{F}_2$, 128
 bismuth, homopolyatomic cations, 357
 bismuth OTeF_5 derivatives, 134
 bismuth oxide fluorides, 124
 blanket CVD-W, 647
 blue emission, 255, 259
 Blue Johns, 662
 BOF, 117
 boron (III) fluoride; Lewis acidity in HF, 340
 boron (III) triflate: Lewis acidity in $\text{CF}_3\text{SO}_3\text{H}$, 343
 bond valence method, 149, 157
 boron OTeF_5 derivatives, 133
 branching ratios, 243, 253
 BrF_3 , 671
 BrF_5 , 25, 671
 Bridgman-Stockbarger, 31
 BrO_2F , 142
 Brodie method, 506
 BrOF_3 , 142
 BrOF_4^- , 142
 bromine, homopolyatomic cations, 354
 Brønsted acids in superacids, 332, 335
 Brønsted bases in superacids, 335–336
 Brønsted acid sites, 367, 373, 384
 built-in casting, 260
 bulk modulus, 575
 bulking agents, 424

 $(\text{C}_2\text{F}_5\text{SO}_2)_2\text{N}^-$, 535
 $(\text{C}_2\text{H}_5)_4\text{NF}(\text{HF})_4$, 544
 $(\text{CF}_3\text{SO}_2)(\text{C}_4\text{F}_9\text{SO}_2)\text{N}^-$, 535
 $(\text{CH}_3)_4\text{NF}$, 16
 C_2F_6 plasmas, 449

- C_3 symmetry, 564
 C_{60} , 555, 582
 C_{60} electronic structure, 556
 $C_{60}F_{48}$, 558–560, 579
 $C_{60}F_{60}$, 558–559, 572
 $C_{60}F_x$, 555
 C_{70} , 568, 582
 $C_{70}F_{36/38/40}$, 568
 $C_{70}F_{38}$, 568
 $C_{70}F_{56}$, 567
 $C_{70}F_{58}$, 567
 $C_{70}F_x$: higher pressure transformation, 575
C–F bond, 503
C–F bond activation, 52
CIs binding energy, 576
 $Ca_5(PO_4)_3F$, 661
 CaF_2 , 36, 323, 661
 CaF_2 substrates, 35
calcination, 376
capped-Archimedean-antiprism, 88
carbon blacks, 474
carbon dioxide, 119
carbon fibers, 494
carbon nanotubes, 500
carbon tetrafluoride, 625
carbon-fluorine compounds, 493
carbonate degradation, 481
carbonization, 592
carbonyl cations in HSO_3F , 352–353
carbonyl complexes, 22
carbonyl fluorides in HF, 352
carboxylate ligands, 419
catalysis, 37, 209, 406, 412
catalyst, 420, 618
catalytic fluorination, 368
catalytic hydrogenolysis, 367, 397
catalytic influence of AgF_2 , 86
catalytic properties, 182
cathode materials, 37, 486
cathodic reactions, 584
cationic $Ag(II)$, 85
cationic $Ag(III)$, 85
cationic $Ag(III)_{sol}$, 85, 105
cationic $Ni(IV)_{sol}$, 104
cationic polymerization, 668
cationic species, 21
cationic species in superacids, 348
 CCl_2F_2 , 369, 392
 CCl_2FCClF_2 , 393
 CCl_3CF_3 , 386
 CCl_4 chlorinated alumina, 396
 CeF_3 , 319
ceramic material, 11, 479
 $CF_2(NO)_2$, 29
 CF_3 radicals in stratospheric chemistry, 119
 CF_3CH_2Cl , 376, 391–392
 CF_3CH_2F , 369, 377, 391
 CF_4 plasmas, 437, 446, 457, 472
 CF_4-H_2 plasmas, 457
 CF_4-He plasmas, 450, 471
 CF_4-O_2 plasmas, 457, 468, 479
 CF_x radicals, 449, 451, 457
 CH_2ClCCl_2F , 395
 CH_2F_2 , 397
 CH_2FCF_3 , 395, 397
chain polymer, 84
chair-type, 599
chalcogens, 25
chalcogens, homopolyatomic cations, 355
channel waveguides, 272
charge capacities, 514, 516
charge density, 221
charge effect, 477
charge transfer complexes, 519
charge–discharge cycling, 514
 $CHCl_3$, 386
 $CHClF_2$, 376, 383
 $CHClFCF_3$, 394
chemical decomposition method, 635
chemical mechanical polishing (CMP), 647
chemical oxygenation, 120
chemical reactivity, 617
chemical sensors, 35
chemical vapor deposition, 36, 503, 641
chemical–thermal cleaning techniques, 653, 655
 CHF_2CF_3 , 395
 CHF_2CHF_2 , 377
 CHF_3 , 380, 386
 CHF_3 plasmas, 452
chimie douce, 7, 19, 37
chlorine dioxide, 652
chlorine monofluoride, 651
chlorine pentafluoride, 125, 651
chlorine trifluoride, 648–649, 651, 653, 672
chloro-fluoride glasses, 243
chlorocarbon hydrogenolysis, 370
chlorocarbons, 368
chlorofluorocarbons (CFCs), 367, 369, 397, 663
chlorofluoroethane, 393
chromia, 371
chromium (II) cations in HF, 349
chromium (III) cations in HF, 348
chromium penta carbonyl, 421
chromium fluoride, 375
chromium fluoride catalysts, 390
chromium oxidation states, 375
chromium oxide, 375
chromium oxide fluorides, 154, 375, 385

- chromium, molybdenum and tungsten, 54
 chromium-doped AlF_3 , 391
cis- N_2F_2 , 15
cis/trans- HOIF_4O , 143
 Cl_2 plasmas, 447
 Cl/F exchange, 369, 385, 395
 ClF , 671
 ClF_3 , 486, 648–649, 670–672
 ClF_5 , 13, 671
 ClO_2F , 14, 141–142
 ClO_3F , 141
 ClOF , 141
 ClOF_3 , 141
 ClOF_4^- , 142
 closed-packed F-atom array, 103
 cloverite, 215
 clusters, 224
 co-precipitation, 16, 391
 coatings: wear resistant, 484
 cobalt, 416, 419
 cobalt (II) cations in HF, 348
 cobalt fluoro N-donor complexes, 60
 CoCl_2 supported on alumina, 393
 COF , 457, 481
 COF_2 , 119–120, 457, 481
 color displays, 273
 colored fluorinated pitch, 617
 color centers, 324
 comb-like electrodes, 616
 combination of a flow system with a static pressure reaction, 13
 combinatorial synthesis, 426, 430
 combustion method, 635
 complex compounds, 544
 complex fluorides, 79
 complex fluorides of nickel (IV), 105
 complex fluorides of silver(III), 86
 composite coatings of tungsten and rhenium, 641
 composite materials, 482
 composite materials: metal/perfluoro compounds, 484
 composite materials: organic-inorganic frameworks, 230
 composite plating, 608, 611, 613
 compositions of surface-fluorinated graphite, 510
 condensation, 224
 condensed-cyclohexane, 601
 conductivity of H-NiF_3 , 103
 conproportionation reactions: iodine cations in $\text{CF}_3\text{SO}_3\text{H}$, 357
 conproportionation reactions: iodine cations in HF, 357
 contact angle, 471, 587, 611, 613
 contacts, 647
 cooperative effect, 259
 coordination chemistry, 406
 coordination compound of XeF_2 to a metal ion, 98
 copper, 648
 copper(III) and copper(IV) fluorides, 108
 coronene, 591
 corrosion Al electrode, 535
 corrosion problems, 10
 corundum, 371
 covalency of C–F bond, 508
 covalent C–F bonds, 494, 503, 511
 Cr^{2+} , 8
 Cr^{4+} , 377
 Cr^{4+} , Cr^{6+} surface sites, 376
 Cr^{5+} , 377
 $\text{Cr}(\text{OH},\text{F})_3$, 390
 CrF_3 , 8
 critical conditions for water, 17
 critical current density, 478, 486
 CrO_2F_2 , 154–155
 CrOF_3 , 155
 CrOF_4 , 154
 cross sections, 457
 cross-coupling, 413
 cross-relaxation, 244, 250, 254, 257
 cross-linking, 599
 cryolite, 665
 crystal field, 316
 crystal growth, 30, 224
 crystal structure of $(\text{AgF})_2\text{AgF}_4\text{AsF}_6$, 91
 crystal structure of $(\text{Xe}_2\text{F}_{11})_2\text{NiF}_6$, 106
 crystal structure of $(\text{XeF}_5)_2\text{NiF}_6$, 106
 crystal structure of $[\text{Ag}(\text{XeF}_2)_2]\text{AsF}_6$, 98
 crystal structure of AgF_3 , 81
 crystal structure of C_{60}F_x with mixed $x=(40-48)$, 570
 crystal structure of C_{70}F_x , 574
 crystal structure of KAgF_4 , 89
 crystal structure of MnF_4 , 111
 crystal structure of XeF_5AgF_4 , 87
 crystal structure parameters, 197
 crystal structures, 410, 568, 572
 crystal structures of Ag^{2+} salts, 96
 crystal structures of $\text{C}_{60}\text{F}_{48}$ and $\text{C}_{60}\text{F}_{36}$, 572
 crystallinity, 596
 Cs_2FeF_6 , 110
 Cs_2PdF_6 , 111
 Cs_2SiF_6 , 666
 Cs_3AlF_6 , 666
 CsAlF_4 , 666
 CsGd_2F_7 , 320
 CsKSiF_6 , 666
 CsPdF_6 , 111
 CsRbSiF_6 , 666

- $\text{CsY}_2\text{F}_7\text{:Ce}$, 320
 cubic stabilized zirconia, 202
 cubic phase, 181
 $\text{CuF}^+\text{AuF}_4^-$, 84
 CuF_4 , 108
 CuF_6^{2-} salts, 108
 current collector, 533
 current density, 611
 cutting tools, 483
 CVD, 483, 645, 647, 652, 676
 cyclic voltammograms of $\text{C}_{60}\text{F}_{46}$, 579
 cyclic voltammograms of $\text{C}_{70}\text{F}_{54}$, 581
 cyclohexane, 599
 cyclopentadienes, 418
 Czochralski, 31

 1D ferrimagnets, 290
 Dawson structure, 159
 decompose in a stepwise fashion, 12
 decomposition and removal of PFC gas, 635
 decomposition of NiF_4 , 101
 decomposition of nonaqueous electrolyte solutions, 525
 decomposition of PF_6^- ions, 526
 decomposition of precursors, 8
 dehydrochlorination, 395
 dehydrofluorination, 374, 395
 deintercalation of fluorine, 494
 dentifrice materials, 677
 desorption (TPD), 383
 detergents, 664
 deuteration, 30
 dialkylzincs, 423
 diamond films, 483
 diamond-like carbon (DLC) films, 484
 dielectric, 604
 dielectric spacers, 101
 diffusion, 272, 595
 difluorophosphate, 123
 difluorophosphoric acid HPO_2F_2 , 668
 dihydropyrimidines, 431
 dimeric rings of $(\text{XeF}_5)_2\text{PdF}_6$, 107
 dinitramide anion, $\text{N}(\text{NO}_2)_2^-$, 142
 dioxygen difluoride, 124
 dioxygenyl salt, 29
 direct fluorination, 178, 558, 626
 discharge behavior of fluorinated carbon nanotubes, 505
 discharge characteristics, 503, 508
 discharge mechanism, 584, 585
 dismutation, 368, 373, 377, 392, 396
 dismutation energy, 122
 disordered carbon, 519
 disposal, 643, 652

 disproportionation to NiF_2 and NiF_6^{2-} , 102
 disproportionation reactions: homopolyatomic cations, 359
 disproportionation reactions: transition metal cations in "low" oxidation states, 360
 dissociation energy, 457
 dissociation enthalpy for CoF_4 , 109
 doped catalysts, 390
 doping, 8
 double 4-rings, 213
 double-bonds, 594
 dry cave effect, 551
 dry cleaning method, 652
 dynamic random access memory (DRAM), 643

 $E_{1/2}$, 582
 E_a , 587
 E_F , 557, 576, 587
 EDFA, 269
 EI mass spectrum, 567
 elastomers, 665
 electrical circuit breaker, 671
 electrical conductivity, 185–186
 electro-magnetism, 604
 electrochemical devices, 521
 electrochemical fluorination of graphite, 498
 electrochemical oxidation of anion, 528
 electrochemical properties, 418, 578
 electrolysis, 187, 630
 electrolyte salts, 523
 electron affinity, 92, 556, 579, 582
 electron affinity of $\text{CoF}_4(\text{g})$, 109
 electron capture, 92
 electron density, 384
 electron ionization (EI) mass spectra, 562
 electron localization, 498
 electron probe microanalysis (EPMA), 481
 electron transport number, 189
 electron-oxidize PtF_6^- , 101
 electronegativity, 1, 3, 603
 electronegativity of OTeF_5 , 132
 electronic structures, 556
 electroplating, 609–610
 elemental fluorine, diluted or undiluted, 9, 178
 ellipsometry, 454
 elpasolite, 325
 enantioselectivities, 420
 energy conversion systems, 521
 energy densities, 508, 525
 energy diagrams, 576
 energy diagrams of C_{60}F_x , 576
 energy gap, 245
 energy levels, 556
 energy storage phosphors, 315, 323

- energy transfer, 252, 254, 257–258
 energy transfer up-conversion, 245
 enthalpies of reaction, 410
 environmentally-friendly, 406
 epitaxial growth, 35
 epoxidations, 416, 424
 EPR, 300, 324, 375
 Er^{3+} , 254, 263, 266–267, 270
 etched back, 647
 etching for Si, 633
 etching for SiO_2 , 633
 ether type solvent, 537
 europium (II) cations in HF, 357
 EXAFS, 162, 410
 excited state absorption, 244, 258, 268
 exothermic peak, 496
 extrusion, 261
 eye-safe, 265
- F^- acceptors, 80, 86
 F^- donors, 92
 F_2 -He plasmas, 471
 F^\bullet radicals, 472, 479
 F-bridged $(\text{Ag-F})_n^{n+}$ chains, 93
 F-bridges, 93
fac- $[\text{IrF}_3(\text{CO})_3]$, 52
 FBS, 417
 ^{36}Cl isotope, 393
 FD mass spectrum, 567
 ^{57}Fe Mössbauer, 139
 Fe-doped CrF_3 , 392
 FeF_3 , 7–8
 FEP plastics, 1
 Fermi level E_F , 557, 577
 ferrimagnetic trimers, 313
 ferrimagnetism, 286
 ferrocenes, 418
 ferromagnetic coupling, 104
 ferromagnets, 227
 fertilizer industry, 665
 fiber amplifiers, 265
 fiber laser, 262–263
 fibers, 239, 260, 264
 field desorption (FD) mass spectrum, 562
 field-independent magnetic moment, 104
 first coulombic efficiencies, 516
 first half wave potential, 579
 first Kr-N bond, 26
 first purely chemical synthesis of elemental fluorine, 20
 ^{18}F isotope, 368, 374, 393
 Fls electron, 193
 flammability limits, 655
 flow system, 9
- fluid, 595
 fluorescence properties, 182
 fluoride borates, 17
 fluoride carbonates, 17
 fluoride catalysts, 367
 fluoride derivatives of palladium(II) and platinum(II), 69
 fluoride glasses, 3
 fluoride glasses: beryllium-based, 236
 fluoride glasses: BIG, 236, 239, 271
 fluoride glasses: channel waveguides, 236
 fluoride glasses: corrosion, 236
 fluoride glasses: $\text{Cr}^{3+}:\text{Nd}^{3+}$ codoped, 247
 fluoride glasses: crystallization temperature, 236
 fluoride glasses: divalent fluoride-based, 239
 fluoride glasses: Eu^{3+} ions, 250
 fluoride glasses: fibers, 235, 262, 273
 fluoride glasses: fluoroaluminates, 241, 246, 251
 fluoride glasses: fluoroindates, 241, 246, 255, 258, 268
 fluoride glasses: fluorophosphates, 243, 259
 fluoride glasses: fluorozirconates, 241, 246, 251, 255, 258, 266
 fluoride glasses: Ho^{3+} , 251, 265
 fluoride glasses: indium-based, 236
 fluoride glasses: lasers, 235
 fluoride glasses: MF_2 -based, 239
 fluoride glasses: Nd^{3+} ions, 246, 248, 262
 fluoride glasses: optical properties, 235
 fluoride glasses: planar waveguides, 241
 fluoride glasses: Pr^{3+} ions, 243, 263, 268
 fluoride glasses: rare-earth activated, 235
 fluoride glasses: rare-earth-doped, 241, 242, 262
 fluoride glasses: telecommunication windows, 235
 fluoride glasses: transition temperature, 236
 fluoride glasses: ZBLAN, 236, 242, 268, 271
 fluoride glasses: zirconium-based, 236
 fluoride glasses: ZnF_2 -based, 238, 243
 fluoride ion affinity, 85
 fluoride phosphates, 17
 fluoride salts, 6
 fluoride silicates, 17
 fluoride solvents, 620
 fluoride glasses: AlF_3 -based, 253
 fluoride glasses: aluminozirconate fibers, 266
 fluoride glasses: amplifiers, 267
 fluoride glasses: BeF_3 -based, 239
 fluoride glasses: Bragg gratings, 266
 fluoride glasses: Dy^{3+} ions, 259
 fluoride glasses: Er^{3+} ions, 254
 fluoride glasses: fluorohafnates, 246
 fluoride glasses: gain coefficients, 268
 fluoride glasses: Gd^{3+} ions, 258
 fluoride glasses: InF_3 -based, 253

- fluoride glasses: low-phonon energy, 251
- fluoride glasses: microsphere, 265
- fluoride glasses: multiphonon relaxations, 254
- fluoride glasses: PZG, 271
- fluoride glasses: Sm^{3+} ions, 258
- fluoride glasses: Tb^{3+} ions, 259
- fluoride glasses: Tm^{3+} ions, 255, 257–258, 263
- fluoride glasses: Yb^{3+} ions, 257, 259, 265
- fluoride glasses: ZBLAN fibers, 263, 266, 273
- fluoride glasses: ZBLAN Nd^{3+} doped, 272
- fluoride glasses: ZBLAN: Ho^{3+} -doped fibers, 266
- fluoride glasses: ZBLAN: Pr^{3+} -doped fibers, 268
- fluoride glasses: ZBLAN: Tm^{3+} -doped fibers, 267
- fluoride glasses: ZrF_4 -based, 240, 253
- fluorinated alumina, 367, 377
- fluorinated carbon nanotubes, 500
- fluorinated chromia, 367, 371
- fluorinated Fe_3O_4 , 396
- fluorinated film, 478
- fluorinated gallophosphate, 215
- fluorinated graphite oxide, 506
- fluorinated lubricant oils, 663
- fluorinated oxide surface, 371
- fluorinated phosphates, 210
- fluorinated pitch (Pitch Fluoride), 607, 611, 613
- fluorinated pitch catalyst, 619
- fluorinated polymers, 663
- fluorinating reagents, 663, 667, 670, 671
- fluorination, 556, 591, 628
- fluorination behavior of carbon nanotube, 503
- fluorination of C_{70} , 558
- fluorination of fullerenes C_{60} and C_{70} , 558
- fluorination of graphite oxide, 506–507
- fluorination of organic compounds, 21, 107
- fluorination of organic substrates by higher nickel fluorides, 107
- fluorination of rare-earth oxides, 177
- fluorinator NiF_4 , 101
- fluorine, 669
- fluorine atom source, 85
- fluorine perchlorate, ClO_4F , 125
- fluorine-aryl substitution, 673
- fluorine-graphite intercalation compound, 494, 503
- fluorine-intercalated carbon fibers, 494, 496
- fluorite structure, 181, 194, 323
- fluorite-like cluster, 196
- fluorite-related structures, 181
- fluoro acid character of AgF_3 , 84
- fluoro acid GeF_4 , 81
- fluoro acidity of AgF_3 , 87
- fluoro acidity of PF_5 , 87
- fluoro base properties of AgF_2 , 84
- fluoroacyl derivative, 63
- fluoroalkanes, 373
- fluoroalkyl iodide, 618–619
- fluoroapatite, 661, 663
- fluoroborates, 668
- fluoroboric acid, 668
- fluoroboric acid $\text{HBF}_4 \cdot x\text{H}_2\text{O}$, 668
- fluorocarbon chain, 535
- fluorocarbons, 467, 595, 663
- fluorocoatings, 2
- fluorohalides, 324
- fluoroindate PDFA, 269
- fluoropentacarbonyl anions, 54–55
- fluoroperoxophosphate, 124
- fluorophlogopite, 6
- fluorophosphates, 123
- fluoroplastic, 609
- fluoropolymers, 670
- fluorosolvents, 597
- fluorosulfate, 127–129
- fluorosulfate derivatives, 128–129
- fluorosulfite, 125
- fluorosulfuric acid: experimental manipulation, 332
- fluorosulfuric acid: Hammett acidity function, 330
- fluorosulfuric acid: self-ionization (autoprotolysis), 332
- fluorous solvents, 403, 412
- fluorous biphasic system, 403, 412
- fluorous partition coefficients, 412
- fluorous synthesis, 428
- fluorous-phase label, 424
- fluorovanadophosphate, 226
- fluoroxysulfate ion, O_3SOF^- , 125
- fluorozirconate fibers, 257
- fluorspar, 661
- flux, 31
- fluxional behavior, 138, 150
- ^{19}F NMR spectrum, 105, 498, 560, 562, 564, 567
- ^{19}F NMR spectrum for sample $\text{C}_{60}\text{F}_{48}$, 562
- formation of HF , 10
- formula unit volume of AgF_3 , 81
- FOSO_2F , 129
- Fourier Transform Infrared (FTIR) spectra, 377, 537
- free energy, 374
- Freons[®], 663
- FTIR photoacoustic, 383
- fuel cell, 189
- fullerene C_{60} , 503
- fullerenes, 3
- gadolinium compounds, 320
- gallophosphates, 211
- galvanostatic discharge curves, 503, 504, 584

- gas phase fluorination, 627
- gas sensors, 272
- gas-solid reactions, 374, 631
- gate electrode, 646
- GeF_4 , 460
- gel electrolytes, 546
- gels, 16
- germanium (IV) fluoride: Lewis acidity in HF, 362
- germanium fluorosulfate derivatives, 129
- glass etching, 663, 665
- glass laser, 266
- glass stability, 236
- glassy fluorinated pitch, 620
- Global Warming Potential, 653
- gold, 130
- gold (II) carbonyl cations: in HF, 363
- gold (II) carbonyl cations: in HSO_3F , 352
- gold (II) cations: disproportionation in HF, 361
- gold (II) cations: generation in HF, 351
- gold (II) cations: generation in HSO_3F , 357
- gold derivative OTeF_5 , 139
- gold (III) fluorosulfate: Lewis acidity in HSO_3F , 343
- grain boundaries, 478, 482
- graphite, 471
- graphite (exfoliated), 472
- graphite fluoride $(\text{CF})_n$, 471
- graphite fluoride electrodes, 3
- graphite fluorides, 470, 478, 484, 591, 609, 678
- graphite intercalation compounds (GICs), 471
- graphite oxide, 506
- graphite-based materials, 470
- great solvating properties, 26
- group 4 organometallic fluorides, 53
- group 5 fluorides, 54
- group 9 carbonyl fluoride derivatives, 61
- $(\text{HF})_n$ oligomer, 393
- $\text{H}_2\text{NSO}_2\text{F}$, 127
- H_2O content, 527
- $\text{H}_2\text{PO}_3\text{F}$, 123
- H_2SiF_6 , 665
- hafnium oxide fluorides, 147
- halex, 424
- half wave potential $E_{1/2}$, 582
- halogens: homopolyatomic cations, 354
- halogen exchange, 373, 385, 626
- halogen fluorides, 648, 671
- halogen oxide fluorides, 117
- halons, 369
- Hammett acidity function scale: "single value" determinations, 330
- Hammett acidity function scale: experimental determination, 330
- heat evolved, 10
- herbicides, 665
- heterogeneous, 367
- hexafluoroantimonic acid $\text{HSbF}_6 \cdot x\text{H}_2\text{O}$, 668
- hexafluoroarsenates, 25
- hexafluoroarsenic acid $\text{HAsF}_6 \cdot x\text{H}_2\text{O}$, 668
- hexafluoroethane, 625
- hexafluorophosphates, 124
- hexafluorophosphoric acid $\text{HPF}_6 \cdot x\text{H}_2\text{O}$, 668
- hexafluorosilicic acid, 665
- hexafluorotitanic acid $\text{H}_2\text{TiF}_6 \cdot x\text{H}_2\text{O}$, 668
- hexafluorozirconic acid $\text{H}_2\text{ZrF}_6 \cdot x\text{H}_2\text{O}$, 668
- hexagonal tungsten bronze, 385, 387
- hexagonal tungsten bronze form (H-NiF_3), 100
- hexameric SBU-6, 216
- HF, 526
- HF adsorbed on AlF_3 , 396
- HF as a fluorinating agent, 10
- HF-fluorinated chromia, 395–396
- HgF_2 , 13
- hierarchy of powerful oxidizers, 93
- high oxidation states, 1, 20, 79, 85
- high T_c superconductors, 478, 486
- high valency metallic fluoride, 628
- high-oxidation state transition-metal fluorides, 498
- high-valent chromium ions, 376
- higher cobalt and iron fluorides, 109
- higher rhenium fluorides, 112
- higher iron fluorides, 110
- higher manganese fluorides, 110
- higher palladium fluorides, 111
- highly explosive XeO_3 , 28
- hole burning, 31, 315, 321–322
- HOMO, 528, 557, 576
- HOMO-derived π bands, 557
- homogeneous catalysts, 403
- homopolyatomic cations: disproportionation, 359
- homopolyatomic cations, metallic elements, 357
- homopolyatomic cations: non-metallic elements, 354
- homopolyatomic cations: stability in oleums, 355
- 'hot-wire' reactor, 28
- HOTeF_5 , 132, 137–141
- HPO_2F_2 , 122–123
- HPO_2F^- , 121
- HSO_3F , 128–131
- humidity sensor, 616
- hybridization for C_{60} , 556
- hydrazinium- or ammonium-compounds, 11
- hydrido-halide, 394
- hydroboration, 413
- hydrochlorofluorocarbons (HCFCs), 367, 369, 373

- hydrofluorination, 369, 395
hydrofluorocarbons (HFCs), 367, 369, 663
hydroformylation, 412
hydrogen bonding, 122–123
hydrogen fluoride, 663
hydrogen fluoride: experimental manipulation, 332, 349
hydrogen fluoride: Hammett acidity function, 330
hydrogen fluoride: self-ionisation (autoprotolysis), 332
hydrogen storage, 482
hydrogenation, 413
hydrogenolysis, 369–370
hydrophilic, 548
hydrophobicity, 482, 548
hydrothermal, 153, 211
hydrothermal growth, 118
hydrothermal method, 16
hydrothermal synthesis, 146, 149–150
hydroxyapatite, $\text{Ca}_5(\text{PO}_4)_3\text{OH}$, 677
hydroxyl groups, 372
hydroxymethylation, 425
- IAD, 616
 IF_5 , 25, 671, 673
 IF_7 , 671, 673
imide type salts, 528
imidodisulfuryl derivatives, 126
inductive effect, 472, 476
industrial applications, 4
infrared, 235, 238, 254
infrared emission, 254
infrared multiphonon edge, 238
infrared transmission, 235, 238
InP, 466
in situ measurements, 212, 223, 380
in-situ preparation of reactants, 14
integrated optics, 273
intensity calculation, 497
interatomic distance Ag-F, 88
intercalation, 493, 596
intercalation and deintercalation of lithium ions, 509
intercalation of fluorine, 494, 501
interlayer, 606
intermetallic compounds, 482
interstitial site, 194
intramolecular exchange, 122, 135, 138
intrinsic scattering losses, 239
 IO_2F_3 , 143
 IO_2F_4^- , 145
iodine, homopolyatomic cations: disproportionation, 357
iodine, homopolyatomic cations: generation and stability, 354, 355
iodine OTeF_5 derivatives, 136
iodine pentafluoride, 672
iodometry, 605
 IOF_5 , 142
 IOF_6^- , 132, 142–143
ion channel, 548
ion conductivity, 6
ion cyclotron resonance spectrometry, 117, 120, 121–122, 124, 131
ionic conductivities, 524
ionic exchange, 236, 241, 271–272
ionic solids, solubility in superacids, 346
ionically conductive solid film, 538
ionization energies, 319, 322
ionization potential, 93, 556
ionization processes, 315, 322
ionization threshold energy I_{th} , 557
ionizing radiation, 319
IR edge, 239
IR spectrum, 562, 567
IR spectrum of T and C_3 isomer, 565
Ir(III) trifluoride chemistry, 65
 IrF_6 , OsF_6 electron affinities of the gases, 92
iridium, 130
iridium and rhodium carbonyl fluoride phosphines, 62
iridium(I) or iridium(III) carbonyl phosphine cations, 66
iridium(III) carbonyl fluoride, 65
iron bases, 611
iron oxide fluorides, 161
irradiation, 27
irradiation of Kr/ F_2 mixtures immersed in liquid nitrogen, 28
iridium: carbonyl cations in superacidic media, 353
iridium: carbonyl compounds in HF, 352
isomerization, 367–369, 393
isoxazolines, 429
- jacketing, 260–261
Jahn-Teller distortion, 128, 298, 310
Jander's equation, 191
jarlite, 283
Judd-Ofelt theory, 242, 258, 259
- $2\text{KrF}_2 \cdot \text{MnF}_4$, 110
 $\text{K}^+ \text{AgF}_4^-$, 85
 $\text{K}_{0.12}\text{NiF}_3$, 101
 K_2GeF_6 , 81
 K_2NiF_6 , 105
 K_2SiF_6 , 666

- K₃AlF₆, 666
- K_xNiF₃, 103
- KF-halogen exchange, 369
- Kharasch catalysts, 420
- kinetics, 411
- kinetics of formation, 222
- KPF₆, 87
- KrF⁺Sb₂F₁₁[−], 112
- KrF⁺SbF₆[−], 112
- KrF⁺, 86
- KrF₄PtF₆[−], 86
- KrF₂, 28, 80
- KrF₂-MnF₄ adducts, 110
- KrF₂.MnF₄, 110

- La₂CuO₄, 486
- La(HF)₂(AsF₆)₃, 35
- labile surface fluoride, 396
- LaF₃, 35
- lamellar, 596
- Langmuir-Hinshelwood mechanism, 394
- LaNi_{4.7}Al_{0.3}, 483
- lanthanide (II) cations: in CF₃SO₃H, 352
- lanthanide (II) cations: in HF, 351
- lanthanide (III) cations: in HF, 348
- lanthanide contraction, 175
- lanthanide fluorides, 175
- lanthanide glutarates, 230
- lanthanides, 175
- Laplacian, 145
- laser crystals, 315, 317
- laser hosts, 31
- laser sources, 271, 273
- laser transition, 246
- laser-induced cooling, 273
- lasers, 260–266
- lasers: emitting in the infrared, 317
- lasers: emitting in the ultraviolet, 318
- lasers: emitting in the visible, 318
- lasers: tunable emission, 318
- lasers: up-conversion, 318
- lattice constant, 570
- lattice parameters, 573
- levitation technique, 240
- Lewis acid, 19, 494
- Lewis acid sites, 367, 377, 380, 384, 385, 392
- Lewis acids in superacids, 336
- Lewis bases in superacids, 336
- Lewis fluoro acid (BF₃, AsF₅, SbF₅), 105
- Li₂NiF₆, 103, 106
- Li((CF₃)₂CHSO₂)₂N, 528
- Li(C₂F₅SO₂)₂N, 536
- Li(CF₃SO₂)₂N, 533
- Li(CF₃SO₂)(C₄F₉SO₂)N, 536

- Li-ion batteries, 486
- LiAgF₄, 87
- LiCaAlF₆, 318
- LiCF₃SO₃, 533
- LiCoO₂, 486
- LiF, 666
- LiF formation, 526
- lifetime, 243, 253
- ligands, 407
- light scattering, 260
- light yield, 320
- linkage of the metal coordination polyhedra, 197
- LiPF₆, LiBF₄ and LiAsF₆, 524
- liquid fluorinated pitch, 620
- liquid wax, 620
- liquid-liquid extraction, 424
- LiSrAlF₆, 318
- lithium cells, 583
- lithium fluoride, 666
- lithium hexafluoroarsenate LiAsF₆, 667
- lithium hexafluorophosphate LiPF₆, 667
- lithium insertion, 19
- lithium ion, 667
- lithium ion batteries, 37, 493, 521, 679
- lithium salts with large anions, 523
- lithium tetrafluoroborate LiBF₄, 667
- lithium trifluoromethane sulfonate LiSO₃CF₃, 667–668
- LiYF₄ substrate, 35
- LiYF₄: Nd, 317
- low oxidation state, 2
- low pressure chemical vapor depositions, 673
- low-phonon energy, 235
- 'low valent', 51
- lubricant, 483, 484, 603
- lubrication, 679
- luminescent properties, 3, 30, 315
- luminescent properties: bandgap, 316
- luminescent properties: core-valence luminescence, 321
- luminescent properties: cross-luminescence, 316, 320
- luminescent properties: decay time, 325
- luminescent properties: excitonic emission, 322
- luminescent properties: Fano resonance, 322
- luminescent properties: fast decay, 319
- luminescent properties: lifetimes, 316
- luminescent properties: light yield, 321
- luminescent properties: trapped exciton, 322
- luminescent properties: ultrabroadband, 318
- LUMO, 557, 576
- LUMO-derived π* bands, 557

- [M(CO)₅X][−], 54

- $[\text{MF}_2(\text{CO})_2\text{L}_2]$, 59
 $\text{MF}_3\text{-}\alpha$: rhombohedral, 385
 M_2WF_8 , 676
 macrocyclic ligands, 413
 magnetic behaviour of R-, H- and P-NiF₃, 104
 magnetic coupling, 104
 magnetic dipolar interactions, 306
 magnetic moment, 284
 magnetic properties, 3, 182, 226
 magnetic properties of Ag⁺ salts, 97
 magnetic susceptibilities, 182
 magnetic susceptibility of (AgF)₂AgF₄AsF₆, 91
 magnetic susceptibility of Ag₃F₈, 83
 magnetic susceptibility of Cs₂CuF₆, 109
 magnetic susceptibility of MnF₄, 111
 magnetism: 2D correlation, 294
 magnetism: 3D ordering, 294
 magnetism: alternating chain, 298
 magnetism: antiferromagnetic chains, 296
 magnetism: axial anisotropy, 300
 magnetism: classical spins, 298
 magnetism: Curie constants, 288
 magnetism: Curie temperatures, 284
 magnetism: Curie-Weiss law, 288, 294
 magnetism: ferromagnetic interactions, 286
 magnetism: Fisher's model, 295
 magnetism: Heisenberg spins, 301
 magnetism: Ising spins, 301
 magnetism: isolated trimers, 310
 magnetism: lozenge chains, 304
 magnetism: mean-field approach, 313
 magnetism: metamagnetic transition, 308
 magnetism: paramagnetic state, 294
 magnetism: partition function, 289, 301
 magnetism: quantum spins, 298
 magnetism: spherical harmonics, 289
 magnetism: transfer matrix, 301
 magnetism: Van Vleck's formula, 290
 main-group element derivatives of the OTeF₅ group, 133
 main-group oxide fluorides, 117
 manganese, 130, 418–419
 manganese carbonyl cations in superacidic media, 353
 manganese (II) cations in HF, 348
 manganese (IV) fluoro-anions, 361
 manganese oxide fluorides, 159
 mass spectra, 564
 mass spectrum, 564, 568
 material of the reaction vessel, 10
 materials surface: adsorption, 465
 materials surface: diffusion, 467
 materials surface: ion-assisted reaction, 465
 materials surface: spontaneous desorption, 465
 materials surface: sputtering, 465
 materials used in the rechargeable lithium battery, 522
 Me₃SnF, 52
 mechanistics, 393
 mechanochemical reactions, 9
 membrane separation method, 638
 mercury, 131
 mercury(I),(II) carbonyl cations, 353
 mercury(II) fluoride, 75
 mercury, homopolyatomic cations, 357
 mesophase, 592
 metal carbonyl, 130
 metal coordination polyhedra, 195
 metal deposition, 611
 metal fluorides, 385
 metal fluoroacyl complexes, 59
 metal hydrides, 482
 metal–metal bonds, 38
 metallic surfaces, 482
 methane dehydrogenation, 182
 methemoglobin production, 674
 methylene, 599
 methylene blue dye, 618
 Mg₂Ni, 483
 Mg_xF_y clusters, 392
 Mg-doped AlF₃, 392
 Mg-doped chromia, 391
 Mg-doped CrF₃, 392
 MgF₂, 36
 microelectronics, 462, 466
 microporous compounds, 16, 212
 microwaves, 17
 Mie scattering, 239
 mild reaction conditions, 38
 mineral talc, 6
 mineralizer, 211
 mineralizing agent, 210
 minimum loss, 239
 mixed halides, 674
 mixed solvent, 537
 mixed valence iron fluorides, 17
 mixed valence NiF₃, 103
 mixed valence material, Ag(II)Ag(III)₂F₈, 83
 MnF₄: α , β , 111
 [Mn₄F₂₀] rings, 111
 MnO₃F, 159
 molecular C₆₀, 556
 molecular sieves, 209
 molecular solids, solubility in superacids, 341
 molecular structure of C₆₀F₁₈, 567
 molecular structure of C₆₀F₃₆, 563
 molecular structure of C₆₀F₄₈, 560
 molecular structures, 559

- molybdenum oxide fluorides, 155
- monophase of cubic stabilized zirconia, 202
- monoclinic lattice, 197
- monofluorophosphate, 123
- monofluoroselenites, 131
- monophosphate complexes, 220
- Montreal Protocol, 367, 369
- MoO_2F_2 , 155
- MoOF_4 , 156
- morphology of lithium, 542
- MOS structure, 644
- mosaic, 592
- multiphonon, 238–239, 262
- multiphonon relaxations, 259
- multiphonon transitions, 317
- multiplex syntheses, 426
- Mössbauer spectroscopy, 103, 226, 296
- $[\text{NiF}_3(\text{HF})_x]^+$, 104
- $\text{N}_2\text{F}^+\text{AsF}_6^-$, 15
- N_2F_2 , 673
- N_2F_4 , 673
- $\text{N}(\text{SO}_2\text{F})_2$ ligand, 127
- $\text{Na}_2\text{PO}_3\text{F}$, 677
- Na_3AlF_6 , 665
- NaF , 677
- Nafion[®], 548
- “naked” cations in superacids, 353
- “naked” fluoride ion, 119, 143
- nanoparticles, 36
- nanopores, 519
- nanoporous channels, 385–386
- native surface film, 539
- NaYF_4 : Yb, 317
- NbF_5 , 669
- NbO_2F , 152
- NbO_3F , 152
- NbOF_5^{2-} , 152
- NbOF_6^{3-} , 153
- Nd^{3+} , 246, 265, 267, 271
- near-field analysis, 272
- negative corona discharges, 125
- negative hyperconjugation, 119
- neodymium (III) cations in HF, 348
- neodymium containing compounds, 186
- nephelauxetic effect, 316
- neutron diffraction, 193, 284, 295
- NF_3 , 486, 670, 673
- NF_3 plasmas, 437, 486, 672
- $\text{NH}_4\text{CsSiF}_6$, 666
- NH_4HF_2 , 666
- NH_4MnF_3 , 36
- Ni clusters, 483
- Ni_2F_5 , 102
- Ni_4F_4 rings, 103
- $\text{Ni}(\text{BiF}_6)_2$, 101
- $\text{Ni}(\text{II})\text{Ni}(\text{IV})\text{F}_6$, 103
- nickel(II) cations in HF, 348
- nickel complexes, 419–420
- nickel chloride, 611
- nickel(IV) fluoride, 362
- nickel(IV) fluoro-anions, 361, 362
- nickel oxide fluorides, 161
- nickel oxyfluorophosphate, 231
- nickel sulfamate, 611
- nickel(II) fluoride, 69
- NiF_3 , 20, 100, 498
- $\text{NiF}_3/\text{NiF}_4$, 21
- NiF_4 , 20, 100
- NiF_6^{2-} , 106
- Nike[®] tennis shoes, 671
- niobium, 129, 134
- niobium (V) fluoride: Lewis acidity in HF, 339
- niobium (V) fluorosulfate: Lewis acidity in HSO_3F , 343
- niobium (V) triflate: Lewis acidity in $\text{CF}_3\text{SO}_3\text{H}$, 344
- niobium OTeF_5 derivatives, 137–138
- niobium oxide fluorides, 151
- nitrilium, 123
- nitrogen trifluoride, 629, 673
- nitrosyl fluoride, 120
- nitryl salts, 120
- NMR, 223, 379, 412, 498
- NO_2F , 120, 141–143, 161
- noble metal catalysts, 397
- noble-gas anions, 143
- noble-gas cations, 143
- NOF, 144, 154
- NOF_3 , 15, 120
- non-adhesiveness, 611
- non-catalytic fluorination, 369
- non-radiative, 235, 260
- non-radiative properties, 242
- non-radiative relaxation, 255
- non-VSEPR molecules, 145
- nuclear industry, 663–664, 669
- nucleation, 224
- Nyquist plots, 505
- $[\{\text{Os}(\text{CO})_3\text{F}_2\}_4]$, 58
- $(\text{O}_2^+)_2\text{PdF}_6^{2-}$, 111
- Olah's reagent, 52
- $\text{O}_2^+\text{AsF}_6^-$, 29
- O_2F , 124
- $\text{O}_2\text{F}_{(\text{soln})}$ in aHF, 87
- O_2F_2 , 28, 124
- O_2PdF_6 , 111

- O_4F_2 , 28, 124
 O1s electron, 192
 $\text{O}=\text{IF}_4\text{O}$, 143
 OCF_2 , 380
 OCV, 586
 OIF_4O ligand, 143
 olation, 221
 oligomeric condensation, 220
 oligosaccharide, 430
 one-electron oxidation, 93
 open circuit voltage (OCV), 586
 open framework, 209
 open networks, 387
 optical amplification, 241, 248, 254, 258–259, 267, 269, 272
 optical amplifiers, 235, 267, 269, 271
 optical fibers, 260, 262, 273
 optical loss, 260
 optical memories, 323, 325
 optical transmission, 236
 order-disorder arrangement, 194
 ordering temperatures, 104
 organometallic, 422
 organometallic and co-ordination chemistry
 group 11 and 12 fluorides, 72
 $\text{Os}_2\text{O}_4\text{F}_7^+$, 163
 OsCl_5 , 14
 OsF_5 groups, 132
 OSF_2 , 380
 OSF_5^- , 131
 osmium, 130
 osmium carbonyl compounds in HF, 352
 osmium cations in superacidic media, 353
 osmium dioxide tetrafluoride, 363
 osmium tetrafluoride, 361
 osmium oxide fluorides, 162
 OSO_2F , 143
 OsO_2F_3 , 163
 OsO_2F_3^+ , 163
 OsO_2F_4 , 162–163
 OsO_3F_2 , 162–163
 OsO_3F_3^- , 162
 $\text{OsO}_4\text{F}_2^{2-}$, 162
 OsOF_5 , 162–163
 OsOF_5^+ , 163
 OsOF_6 , 163
 OTeF_5 , 143
 OTeF_5 derivatives, 132, 137–141
 OTeF_5^- , 133
 oxidation/reduction, 376
 oxidation, 419–420, 422
 oxidative addition, 56, 411
 oxidative behavior, 527
 oxidative fluorinating agents, 124
 oxide fluorides, 2, 6, 117, 536
 oxide fluorides of aluminum, 117
 oxide fluorides of boron, 117
 oxide fluorides of carbon, 119
 oxide fluorides of gallium, 117
 oxide fluorides of indium, 117
 oxide fluorides of nitrogen, 120
 oxide fluorides of phosphorus, 120
 oxide fluorides of silicon, 119
 oxide fluorides of thallium, 117
 oxide fluorides of tin, 119
 oxide ion mobile structure, 195
 oxide ion transport number, 189, 204
 oxide ion-conducting solid electrolyte, 177, 189
 oxide peroxide fluoride, 151
 oxide-doped chromia, 391
 oxidizing capability, 85, 87
 oxidizing capability of Ag(III), 85
 oxidizing properties of R-, H- and P-NiF₃, 102
 oxolation, 221
 oxonium compounds, 19
 oxyfluoride glass ceramics, 246
 oxygen enrichment membrane, 613
 oxygen sensor, 189
 oxygenation, 415
 ozone shield, 2

 $[\text{PtF}(\text{PPh}_3)_3]^+$, 72
 $p_\pi-d_\pi$ bonding, 145
 $\text{P}_2\text{O}_3\text{F}_4$, 123
 Pa-FTIR, 386
 palladium, 130, 419
 palladium bisphosphine fluoro-bridged dimer, 71
 palladium(II) carbonyl compounds, 353
 palladium(II) phosphine fluoride derivatives, 70
 paramagnetic impurity, 91
 paramagnetism of Ag₃F₈, 83
 partition coefficient, 425, 426
 passivation film, 482, 533
 Pd catalysts, 370, 398
 Pd fluorides, 2
 Pd/C catalysts, 370
 PDFA, 268
 pentafluorides, 15
 pentafluorooxosulfate, 131
 pentafluorotellurates(VI), 132, 133
 perfluorinated organic solvents, 403
 perfluorination, 602
 perfluoro compounds, 673
 perfluoroalkanes, 404
 perfluoroalkyl, 410
 perfluoroalkylhalides, 404
 perfluoroethers, 404
 perfluoroolefins, 93, 673

- perfluoropropane, 93
- perfluoropropene, 93
- perfluorotertiary amines, 404
- periphery, 597
- permeability constant, 616
- permeating speed, 616
- perovskite, 30
- perovskite KMgF_3 , 318
- peroxide fluoride, 148
- peroxide fluorides, 146–147, 151–152
- perxenates, 117
- PF_2HO , 122
- PF_5 , 14, 80
- PFC recovery and recycling, 636
- pH range, 221
- pharmaceutical intermediates, 665
- phase diagram, 568
- phase transition of $\text{C}_{60}\text{F}_{48}$, 573
- phonon energies, 241, 267, 316
- phonon-side bands, 243, 250
- phosphine-supported copper(II) fluoride, 74
- phosphines, 406, 408
- phosphine oxides: π -bonding, 121
- phosphinites, 409
- phosphites, 409
- phosphonates, 230
- phosphors, 8
- phosphorus (V) fluoride: Lewis acidity in HF, 339
- photo-induced reactions, 272
- photochemical activation, 27
- photochemical dissociation of XeF_6 , 28
- photochemical equilibrium, 28
- photoconductivity, 322
- photodissociating F_2 , 87
- photodissociation of F_2 in the presence of basic aHF, 29
- photoionization, 321
- photooxidation, 422
- photostimulable phosphors, 323
- phthalocyaninato complexes, 415
- physical properties of tungsten hexafluoride, 641
- physical vapor deposition, 236, 271, 644, 673
- pitch, 591
- pitch-based carbon fiber, 494
- planar waveguide, 271, 273
- plasma cleaning gases, 653
- plasma cleaning methods, 652
- plasma constituents, 439
- plasma etching/cleaning, 632
- plasma-CVD, 652
- plasma-enhanced fluorination, 470
- plasma-less cleaning method, 653
- plasma-less etching, 655
- plasmas: floating potential, 444
- plasmas: ion flux, 445
- plasmas: cross sections, 442
- plasmas: damage, 464
- plasmas: Debye length, 441
- plasmas: degree of ionisation, 439
- plasmas: density, 439
- plasmas: diagnostic techniques, 447
- plasmas: energy distribution, 440
- plasmas: frequency, 441
- plasmas: Langmuir probes, 451
- plasmas: laser-induced fluorescence, 451
- plasmas: mass spectrometry, 449
- plasmas: mean free paths, 442
- plasmas: optical spectroscopies, 451
- plasmas: plasma-surface boundary, 444
- plasmas: reaction rates, 443
- plasmas: sheaths, 444
- plasmas: sputtering, 463
- plasmas: surface activation, 464
- platinum, 128, 130
- platinum (II) carbonyl compounds in superacids, 353
- platinum (IV) fluorosulfates: Lewis acidity in HSO_3F , 343
- platinum bisphosphine fluoro-bridged dimer, 72
- platinum metals, 15
- platinum trisphosphine monofluoro cation, 71
- plutonium (III) cations in HF and HSO_3F , 348
- PM3 calculations, 570
- pnictogens, 21
- PO_2F_2 groups, 123
- PO_2F_2^- , 121–122
- POF, 120
- POF_2 group, 121
- POF_2^- , 121
- POF_3 , 121, 123, 144
- POF_4^- , 121
- polarizability, 603
- polycarbon monofluoride: CF_x , 678
- polycrystalline silicon, 644
- polymer electrolyte, 545
- polymer electrolyte fuel cell (PEFC), 548
- polymeric $(\text{CuF})_n^{n+}$, 84
- polymeric binary fluorides, 104
- polymeric solids, solubility in superacids, 347
- polymerisation, 419, 422, 450
- polytetrafluoroethylene, 596, 609
- polyvinylidene fluorides, 547
- ponytails, 403
- pore volumes, 377
- porous antiferromagnets, 226
- porous materials, 210
- porphyrin, 118, 139, 415
- positive holes, 189

- powder X-ray diffraction pattern, 570
 powder XRD pattern of C_{60} , 568
 powerful oxidizer NiF_4 , 101, 105
 Pr^{3+} , 243, 265, 267
 praseodymium (III) cations in HF, 348
 precipitation of binary fluorides in anhydrous HF, 16
 precursors, 596
 preforms, 260
 preparation of very pure elemental fluorine, 28
 pressure systems, 6, 9
 prevention of global warming, 633
 primary batteries, 3
 'pseudofluoride' $[\text{OTeF}_5]^-$, 26
 pseudorotation, 138
 PtF_6^- , 86
 PTFE, 613
 pulsed laser ablation, 486
 purification method, 629, 631
 Pyr-FeF_3 , 19
 pyrene, 591
 pyridine adsorption (Pa-FTIR), 384
 pyro-hydrolysis, 175
 pyro-hydrolysis of rare-earth fluorides, 177
 pyrochlore, 7
 pyrochlore $\text{Al}(\text{OH})_{0.7}\text{F}_{2.3}$, 383
 pyrochlore $\text{Al}(\text{OH},\text{F})_3$, 390
 pyrochlore $\text{CrF}_{0.94}(\text{OH})_{2.06}$, 392
 pyrochlore form (P-NiF_3), 100
 pyrochlore $\text{MF}_x(\text{OH})_{3-x}$, 386
 PZG, 266
- quantum efficiencies, 241, 246, 268, 272
 quasi-stable intermediate, 191
 quenching, 181
 quinoline insoluble, 598
- $[\{\text{Ru}(\text{CO})_3\text{F}_2\}_4]$, 58
 $[\text{ReF}(\text{CO})_3(\text{PPh}_3)_2]$, 57
 radiative properties, 242
 radiofrequency (rf) plasmas, 437
 radiotracer studies, 368, 393
 Raman spectroscopy, 511
 Raman spectrum of $[\text{Ag}(\text{XeF}_2)_2]\text{AsF}_6$, 98
 rapid metathesis reactions, 38
 rare earth fluoroaurates, 13
 rare-earth fluoride-stabilized zirconia, 177, 198
 rare-earth fluorides, 175, 177, 316
 Rayleigh scattering, 239, 262
 $\text{Rb}_3\text{KInF}_6:\text{Ce}^{3+}$, 325
 Rb_2SiF_6 , 666
 Rb_3AlF_6 , 666
 RbAlF_4 , 666
 RbCsSiF_6 , 666
 $\text{Re}^{\text{VI}}\text{OF}_4$, 161
 $\text{Re}^{\text{VII}}\text{O}_3\text{F}$, 161
 reaction media, 403
 reaction of anhydrous HF with a metal hydride, 59
 reaction of F_2 with liquid phase ammonium-acid fluoride, 631
 reaction of metal carbonylmethyls with HF or HOTeF_5 , 58
 reaction with chalcogen fluorides, 64
 reactive sites, 472
 rechargeable batteries, 521
 recovery, 413
 red CuF_3 , 108
 reduction product, 526
 reduction steps, 13
 $\text{ReF}_6^+\text{ReF}_7\text{AuF}_6^-\text{AuF}_5$, 112
 ReF_6^+ salts, 112
 $\text{ReF}_6^+\text{ReF}_7\text{MF}_6^-\text{MF}_5$, 26, 112
 ReF_7 , 112
 refractive, 603
 refractive index dispersion, 241
 refrigerants, 369, 663
 ReO_2F , 161
 ReO_2F_3 , 138, 160
 ReO_2F_4^- , 161
 ReO_3F , 160
 ReOF_2 , 161
 ReOF_4 , 160
 ReOF_5 , 138, 160–161
 ReOF_6^- , 161
 repellency, 604
 resin, 592
 resistance, 616
 rf electrode, 460
 Rh-atomic absorption spectroscopy, 413
 rhenium carbonyl compounds in HF, 352
 rhenium carbonyl cations in superacidic media, 353
 rhenium complexes, 130, 418
 rhenium oxide fluorides, 159
 RhF_6 , 15
 rhodium complexes, 410, 418
 rhombohedral form of FeF_3 , 19
 rhombohedral NiF_3 (R-NiF_3), 100
 rhombohedral phase, 181, 184
 Rietveld analysis, 193, 196, 293
 ring-opening, 594
 rings Ni_3F_3 , 103
 rotational casting, 260
 RuF_6 , 15
 RuF_6^- , 86
 RuOF_3 , 162
 RuOF_4 , 162

- ruthenium carbonyl cations in superacidic media, 353
 ruthenium complexes, 410, 420
 ruthenium hydride fluoride, 59
 ruthenium oxide fluorides, 162
 ruthenium tetrafluoride, 362

 $[\{\text{ScF}(\text{Cp})_2\}_3]$, 53
 $(\text{SbCl}_4\text{F})_4$, 674
 S_2F_{10} , 670
 $\text{S}_2\text{O}_5\text{F}_2$, 129
 $\text{S}_2\text{O}_6\text{F}_2$, 127, 129–130
 salen, 420
 sapphire, 10
 Sb_2F_{11} , 674
 SbCl_2F_3 , 674
 SbCl_3F_2 , 674
 SbCl_4F , 674
 SbCl_5 , 367
 SbClF_4 , 674
 SbF_3 , 675
 SbF_5 , 86, 558, 669, 673, 675
 SbF_7^{2-} , 24
 samarium (II) cations in HF, 351
 scandium fluoride derivatives, 53
 scattering, 262
 Schlegel diagrams, 560, 564, 567
 scintillator crystals, 31, 315, 319
 secondary building units, 214
 selective CVD-W, 647
 selective syntheses, 559, 560, 563, 567
 selectivity, 392, 483
 selenium fluorosulfate derivatives, 128
 selenium, homopolyatomic cations, 355
 selenium oxide fluorides, 131
 semi-ionic C–F bond, 494, 503, 504, 511
 semiconductor industries, 643, 652
 SeO_2F^- , 131
 SeOF_2 , 131
 SeO_2F_2 , 143
 SF_4 , 380, 670
 SF_4 -fluorinated alumina, 396
 SF_5OCl , 131
 SF_5OOSF_5 , 131
 SF_5OSF_5 , 131
 SF_6 , 670
 SF_6 plasmas, 437, 447, 454
 SF_6 -He plasmas, 446
 SF_6 - O_2 plasmas, 450, 468
 shape of the amine, 218
 Si etching, 463, 466
 Si_3N_4 , 462
 SiF_4 , 460, 669
 SiGe , 466
 silicon wafers, 665
 silver carbonyls, 134, 140
 silver fluoride, 51
 silver OTeF_5 derivatives, 133
 silver(III), AgF_3 , 79, 80, 362
 silver(III) fluoro-anion, 361, 362
 Simons electrochemical fluorination process, 29, 107
 simple rare-earth oxide fluorides, 177, 178, 181
 SiNF , 11
 single crystal structure of C_{60}F_x , 570
 single-mode fibers, 260, 261
 SiO_2 , 462
 SiO_2 etching, 463, 466
 site occupancy, 196
 site symmetry, 250
 site-selective spectroscopy, 250
 slope efficiency, 248, 265–266
 Sm^{2+} ions, 258
 ^{119}Sn Mössbauer, 127–128
 SnF_2 stannous fluoride, 677
 SO_2 , 24
 SO_2ClF , 25, 125
 SO_2F group, 126
 SO_2F_2 , 122, 129, 131
 SO_3F groups, 127, 129
 SO_3F^- , 129, 131
 SO_4F^- , 125
 SO_xF_y , 469
 sodium fluoride, 666
 sodium monofluorophosphate, 677
 SOF_2 , 125
 SO_2F_2 , 125
 SOF_4 , 122, 131
 SOF_4^- , 131
 soft character of anions, 535
 sol-gel process, 6
 solid C_{60} , 556
 solid surface, 373
 solid-gas reaction, 178
 solid-phase extraction, 428
 solid polymer electrolyte, 545
 solid-state fuel battery, 189
 solid-state lithium cells, 583
 solid-state reaction, 177
 solid-state reaction path, 183
 solubility of KBiF_6 , 101
 solubility of oxygen, 550
 solvated $\text{Ag}^{2+}_{(\text{soln})}$, 92
 solvated complex cation $[\text{Ag}(\text{XeF}_2)_2]^+$, 98
 solvation of $\text{Ag}(\text{II})$, 90
 solvolysis by aHF, 90
 solvothermal, 31
 sorption capacity, 377

- spark discharge, 125
- specific surface areas, 377, 509
- spherical amines, 219
- spherical-shell model, 570
- spinel, 377
- square planar AgF_4^- , 89
- SrClF , 323
- SrF_2 , 323
- SrF_2 : Ag^+ , 318
- stabilizing reagents, 201
- stabilizing treatment, 201
- stacking, 592
- standard molar enthalpy of the formation of $\text{CoF}_4(\text{g})$, 109
- standard redox potential, 175
- stannous fluoride, 677
- Staudenmaier method, 506
- stepwise decomposition reaction, 12
- stereochemical activity, 124
- Stille couplings, 428
- strong acid characteristic of anion, 525
- strongest oxidizers KrF_2 , O_2F , 21
- structural features of R-, H- and P- NiF_3 , 103
- structure of Cs_2CuF_6 , 109
- structures of solid C_{60} and C_{70} , 568
- structure transition, 181
- structure of $\text{C}_{60}\text{F}_{48}$, 560
- sublimation temperatures, 586, 605
- sulfanuric fluoride, 126
- sulfur hexafluoride, 670
- sulfur, homopolyatomic cations, 354
- sulfuric acid: Hammett acidity function, 330
- sulfuric acid: self-ionisation (autoprotolysis), 332
- sunlight, 87
- super acids, 2, 19, 21, 329–331, 334–336, 341, 343, 345–346, 348–349, 358
- superconducting copper oxides, 37
- supercooling, 31
- supercritical media, 31
- superexchange, 104
- supersaturation, 224
- suppression of lithium dendrite, 543
- surface activation, 372
- surface area, 7
- surface catalytic activity, 383
- surface compositions of graphite, 519
- surface disordering of graphite, 514
- surface film, 538, 669
- surface fluorination, 509
- surface fluorine concentrations, 511, 514, 517, 519
- surface hydroxyl groups, 377, 384
- surface modifications, 470, 510
- surface OH, 373
- surface oxygen content, 511, 519
- surface roughness, 519
- surface sites, 382
- surface structure of carbon, 511
- surface-fluorinated graphite, 509, 514
- Swarts catalyst, 371
- switch, 432
- syntheses of Ag^{2+} salts, 91
- syntheses of AgF^+ salts, 91
- synthesis of chlorine fluorides, 651
- syntheses of fluorocobaltates(IV), 109
- syntheses of nickel(III) fluorides, 100
- syntheses of nickel(IV) fluoride, 100
- synthesis of WF_6 , 643, 651
- synthesis and crystal structure of Cs_2CuF_6 , 109
- synthesis of $(\text{AgF})_2\text{AgF}_4\text{MF}_6$, 90
- synthesis of $[\text{Ag}(\text{XeF}_2)_2]\text{AsF}_6$, 98
- synthesis of Ag_2F_5 , 84
- synthesis of Ag_3F_8 , 83
- synthesis of AgF_3 , 80
- synthesis of C_{70}F_x , 567
- synthesis of cobalt(IV) fluoride, 109
- synthesis of CuF_3 , 108
- synthesis of MnF_4 , 110
- synthesis of fluorinated pitch, 617
- (TAOS⁺), 38
- (TAS⁺), 38
- (TREAT-HF), 52
- T symmetry, 564
- TaF_5 , 669
- 'tailor made' solids, 224
- tantalum (V) fluoride: Lewis acidity in $\text{CF}_3\text{SO}_3\text{H}$, 344
- tantalum (V) fluoride: Lewis acidity in HF, 339
- tantalum (V) fluoride: Lewis acidity in HSO_3F , 343
- tantalum (V) fluorosulfate: Lewis acidity in HSO_3F , 344
- tantalum oxide fluorides, 151
- TaO_2F , 152
- TaOF_3 , 152
- TaOF_6^- , 153
- TAS fluoride, 119, 125, 127, 131
- TcO_2F_3 , 160
- TcO_2F_4^- , 160
- TcO_3F , 160
- TcOF_4 , 160
- TcOF_5 , 160
- $\text{Te}_2\text{O}_3\text{F}_2$, 132
- technetium (VII) dioxide trifluoride, 363
- technetium oxide fluorides, 159
- telecommunication, 245, 258, 267, 269
- telecommunication window, 269
- tellurium OTeF_5 derivatives, 135–136

- tellurium oxide fluorides, 131
 TEM image, 391, 494, 501
 temperature independent paramagnetism, 91
 templates, 211, 219
 TeOF_2 , 132
 TeOF_5^- , 132, 142
 tetrafluoroethylene oligomer, 610
 tetragonal phases, 181, 184
 tetrahalonium salts, 135
 tetrahedral clustering, 104
 tetrameric SBU-4, 219
 tetrazole, 432
 tetroxides, 117
 thallium OTeF_5 derivatives, 133–134
 theoretical calculations, 408
 thermal decomposition, 12
 thermal decomposition of R-NiF_3 , 102
 thermal decomposition of electrolyte salt, 530
 thermal stability, 496, 507
 thermal stability of electrolyte salt, 528
 thermal-CVD, 652
 thermally unstable fluorides, 27
 thermodynamically unstable binary fluorides, 79
 three-phase boundary region, 550
 threshold, 265–266
 TiF_4 , 398
 time-resolved spectroscopy, 250
 tin, 426
 tin hydride reagent, 424–425
 TiOF_2 , 146
 titanium (II) cations: generation in HF, 350
 titanium (II) cations: disproportionation in HF, 360
 titanium fluorophosphates, 228
 titanium nitride, 647
 titanium oxide fluorides, 145
 Tm^{3+} , 265, 267
 TOF-SIMS, 383
 toothpaste, 677
 TPD, 386
 traces of oxygen, 14
 traces of water, 12
 transesterifications, 421
 transference number, 524
 transition fluorometallates, 498
 transition metal complexes, 409
 transition metal cations in superacids: in “low”
 oxidation states, 352, 348
 transition metal cations in superacids: in normal
 oxidation states, 348
 transition metal element derivatives of the OTeF_5
 group, 137
 transition metal element fluorosulfates, 129
 transition metal fluorides, 51
 transition temperatures, 181
 transition-metal fluoro manganese and rhenium,
 57
 transmission electron microscopy, 494
 tribological applications, 587
 trifluoromethyl sulfate, 127
 trifluoromethylsulfuric (“Triflic”) acid, 349, 354
 trifluoromethylsulfuric (“Triflic”) acid: Hammett
 acidity function, 330
 trifluoromethylsulfuric (“Triflic”) acid:
 self-ionisation (autoprotolysis), 332
 trimethyl silyl reagents, 59, 67
 trithionate, 125
 tungsten bronzes, 3
 tungsten carbide coatings, 641
 tungsten hexafluoride, 640, 676
 tungsten metal vias, 644–645
 tungsten oxide fluorides, 156
 tungsten oxytetrafluoride, 643
 tungsten silicide, 644–646
 tungsten tetrafluoride, 643
 tungsten(II) fluoride carbonyl systems, 57

 UF_4 , 664, 669
 UF_6 , 663, 669
 UF_6 enrichment, 664
 Ugi reactions, 430
 ULM-n, 213
 ultra-high voltage rechargeable lithium batteries,
 538
 ultra-large-scale integration (ULSI), 643
 ultra-violet emission, 255
 unfluorinated chromia, 374
 up-conversion, 31, 235, 244, 251, 254–255, 257,
 259, 262, 272–273, 316–317
 up-conversion amplifier, 269
 up-conversion luminescence, 271
 uranium (III) cations: disproportionation in HF,
 360
 uranium (III) cations: generation in $\text{CF}_3\text{SO}_3\text{H}$,
 352
 uranium (III) cations: generation in HF, 349
 uranium fluorides, 231
 uranium hexafluoride, 648
 urea, 431
 usovite, 291
 UV irradiation, 87
 UV transparency, 31

 vanadium (II) cations in HF, 349
 vanadium oxide fluorides, 149
 vapor pressure, 648

- vaporization, 595
- Vaska's complex, 61, 410
- VF₃ type, 385
- vias, 647
- vibration modes, 243
- viscosity, 595
- vitroceramics, 246
- VLSI, 676
- VOF₃, 151
- VSEPR (valence shell electron repulsion), 122, 128–129, 135–137, 144
- waste SiF₄, 38
- water repellency, 470, 609, 611, 617
- water- and oil-repellent agents, 620
- Watts nickel bath, 610
- weakly coordinating anions, 26, 134
- weakly coordinating pnictogen anions, 134
- wet cleaning method, 652
- wettability coatings: lubricant, 484
- WF₄, 676
- WF₅, 676
- WF₆, 450, 469, 670, 676
- WO₂F₂, 157
- WO_xF_y, 470
- WOF₄, 157–158, 451, 469
- work functions, 577
- WS₂, 453
- (Xe₂F₁₁)₂MnF₆, 110, 100
- (XeF₅⁺CrF₅⁻)₄·XeF₄, 27
- (XeF₅)₂MnF₆, 110
- (XeF₅)₂NiF₆, 100
- X-ray imaging, 323
- X-ray photoelectron spectroscopy, 453, 536
- XAES, 385
- XANES, 392
- Xe₂⁺Sb₄F₂₁⁻, 21
- Xe₂F₁₁ groups, 106
- Xe₂F₁₁AuF₆, 106
- Xe-C bond, 24
- XeF₂, 27, 52, 80, 463, 483
- XeF₂ as a ligand for a metal ion, 98
- XeF₂, XeF₄, XeF₆, and KrF₂, 27
- XeF₄, 28
- XeF₅⁺, 20, 88, 106
- XeF₅AgF₄, 87
- XeF₅MF₆ salts, 89
- XeF₆, 27–28
- XeF₆ moderately good fluoride-ion donor, 86
- Xe(II) derivative, 132
- XeO₂F⁺, 137, 144
- XeO₂F₂, 144
- XeO₂F₃⁻, 144
- XeOF₂, 137, 143
- XeOF₃⁺, 137, 144
- XeOF₄, 143–144
- XeOF₅⁻, 144
- XPS, 192, 374, 380, 391, 472, 479
- XPS: binding energy (BE), 374, 380, 382, 384
- XPS: in situ, 380, 382
- XRD pattern of C₇₀F_x with pressure, 575
- XRD patterns, 570, 574
- XRD patterns for C₆₀F₄₈ and C₆₀F₃₆, 572
- YAG, 317
- Yb³⁺, 259
- YBa₂Cu₃O_{7-δ}, 480, 486
- YF₃: Yb³⁺, 317
- ytterbium (II) cations in HF, 351
- yttria-stabilized zirconia, 187, 204
- ZBLA, 272
- ZBLAN, 238–239, 262
- zeolites, 209
- zero-charged ammonium-SBU, 220
- zinc complexes, 134
- zinc fluoride, 74
- zirconium fluorophosphates, 228
- zirconium oxide, 198
- zirconium oxide fluorides, 147
- zirconium tetrafluoride, 201
- Zn-doped chromia, 391
- zone melting technique, 31
- ZrF₄, 398
- ZrNF, 11